

Hermann Schlichting (Deceased)
Klaus Gersten

Boundary- Layer Theory

Ninth Edition

Boundary-Layer Theory

Hermann Schlichting (Deceased)
Klaus Gersten

Boundary-Layer Theory

With contributions
from Egon Krause and Herbert Oertel Jr.

Translated by Katherine Mayes

Ninth Edition



Springer

Hermann Schlichting (Deceased)
Institute of Fluid Mechanics
Technical University of Braunschweig
Braunschweig
Germany

Klaus Gersten
Institute of Thermodynamics and Fluid
Mechanics
Ruhr-University Bochum
Bochum, Nordrhein-Westfalen
Germany

ISBN 978-3-662-52917-1
DOI 10.1007/978-3-662-52919-5

ISBN 978-3-662-52919-5 (eBook)

Library of Congress Control Number: 2016944848

1st edition: © McGraw-Hill New York 1955

2nd edition: © Pergamon London 1955

4th edition: © McGraw-Hill New York 1960

6th edition: © McGraw-Hill New York 1968

7th edition: © McGraw-Hill New York 1975

8th edition: © Springer-Verlag Berlin Heidelberg 2000

9th edition: © Springer-Verlag Berlin Heidelberg 2017

This work is subject to copyright. All rights are reserved by the Publisher, whether the whole or part of the material is concerned, specifically the rights of translation, reprinting, reuse of illustrations, recitation, broadcasting, reproduction on microfilms or in any other physical way, and transmission or information storage and retrieval, electronic adaptation, computer software, or by similar or dissimilar methodology now known or hereafter developed.

The use of general descriptive names, registered names, trademarks, service marks, etc. in this publication does not imply, even in the absence of a specific statement, that such names are exempt from the relevant protective laws and regulations and therefore free for general use.

The publisher, the authors and the editors are safe to assume that the advice and information in this book are believed to be true and accurate at the date of publication. Neither the publisher nor the authors or the editors give a warranty, express or implied, with respect to the material contained herein or for any errors or omissions that may have been made.

Typesetting: Katherine Mayes, Darmstadt and LE-TEX, Leipzig
Cover design: de'blik, Berlin

Printed on acid-free paper

This Springer imprint is published by Springer Nature
The registered company is Springer-Verlag GmbH Berlin Heidelberg

Preface to the Ninth English Edition

For this edition corrections have been carried out and additional important literature published in recent years have been included (66 additional references). Section 22.8 on plane turbulent wall jets has been completely rewritten. I am very thankful for valuable assistance to Prof. Dr. E. Krause, Prof. Dr. H. Oertel, Prof. Dr. W. Schneider, Prof. Dr. M. Breuer, Prof. Dr. H.-D. Papenfuß and last but not least Gertraude Odemar.

Bochum, March 2016

Klaus Gersten

Preface to the Eighth English Edition

According to the tradition of this book, a German edition has always been soon followed by the English translation. I am very grateful to Springer-Verlag for undertaking this version and for securing a translator. My particular thanks go to Katherine Mayes for this excellent translation. In the course of the translation, some errors in the German edition were corrected and a number of additions carried out. In this connection I am very thankful to Prof. Dr. W. Schneider, Vienna, for several suggestions and improvements. I would like to thank Ursula Beitz again for her careful checking of the bibliography. I hope that the English edition will attain the same positive resonance as the ninth German edition.

Bochum, May 1999

Klaus Gersten

Preface to the Ninth German Edition

There is no doubt that *Boundary-Layer Theory* by Hermann Schlichting is one of most important books within the sphere of fluid mechanics to appear in the last decade. Shortly before his death, Hermann Schlichting brought out the eighth edition which he revised together with his friend and former colleague Wilhelm Riegels.

When this edition went out of print and a new edition was desired by the publishers, I was very glad to take on the task. During the fifteen years I spent at the institute of my highly respected teacher Hermann Schlichting, I had already been involved with earlier editions of the book and had revised some chapters. The burden was also eased by the fact that boundary-layer theory in its widest sense has been my preferred direction of research for many years.

It quickly became clear that a complete revision was necessary; indeed this was also known to Hermann Schlichting. In the preface to the eighth edition he wrote: “Noting the systematic of our knowledge of today, it would have been desirable to fully revise this work; however such a process would have pushed back the appearance of this book by years.” Compared to the eighth edition, the literature of the last 15 years had to be taken into account and recent developments, in turbulence models for example, had to be incorporated. In order to keep the size of the book tractable, some results – those which no longer seem so important with today’s computing potential – had to be curtailed, or in some cases, left out altogether.

Thus the necessity to completely rewrite the text emerged. The fundamental divisions within the book were retained; as before it consists of the four major sections: basic laws of the flows of viscous fluids, laminar boundary layers, the onset of turbulence, turbulent boundary layers. However a new fifth section on numerical methods in boundary-layer theory has been added.

The partition into chapters had to be somewhat modified in order to improve the style of presentation of the material. Because of the necessary restrictions on the material, the aim was to concentrate on boundary-layer theory as the theory of high Reynolds number flows. Accordingly the chapter on “creeping flows”, that is flows at very small Reynolds numbers, was omitted.

It seemed natural to steer towards the style and level of presentation with the same target audience as with Hermann Schlichting.

The research area of boundary-layer theory is continuously growing, and it has become so extensive that no single person can possess a complete overview. Consequently I am extremely grateful to two colleagues who supported me actively. Professor E. Krause wrote the new additional chapter on numerical methods in boundary-layer theory, and Professor H. Oertel provided the revision of the section on the onset of turbulence (stability theory).

Further assistance was furnished from different sources. I am indebted to Dr.-Ing. Peter Schäfer and Dr.-Ing. Detlev Vieth for a great many new sample calculations. Dr. Vieth also read the entire text discerningly. I am grateful to him for numerous improving suggestions. Renate Gölzenleuchtnar deserves particular thanks for generating the figures which almost all had to be newly drawn up. I would like to thank Ursula Beitz particularly for her careful and exhaustive checking of the bibliography, while Marianne Ferdinand and Eckhard Schmidt were of first class assistance. It was by far impossible to adopt all citations, so that it may be necessary to revert to the eighth edition for specific references to earlier pieces of work.

The printing firm of Jörg Steffenhagen is due particular praise for an extremely fruitful collaboration. My thanks also go to Springer-Verlag for our most agreeable work together.

I hope we have been able to carry on the work of Hermann Schlichting as he would have wished.

Bochum, October 1996

Klaus Gersten

Contents

Introduction	XXI
--------------------	-----

Part I. Fundamentals of Viscous Flows

1. Some Features of Viscous Flows	3
1.1 Real and Ideal Fluids	3
1.2 Viscosity	4
1.3 Reynolds Number	6
1.4 Laminar and Turbulent Flows	12
1.5 Asymptotic Behaviour at Large Reynolds Numbers	14
1.6 Comparison of Measurements Using the Inviscid Limiting Solution	14
1.7 Summary	26
2. Fundamentals of Boundary-Layer Theory.....	29
2.1 Boundary-Layer Concept	29
2.2 Laminar Boundary Layer on a Flat Plate at Zero Incidence ..	30
2.3 Turbulent Boundary Layer on a Flat Plate at Zero Incidence ..	33
2.4 Fully Developed Turbulent Flow in a Pipe	36
2.5 Boundary Layer on an Airfoil	38
2.6 Separation of the Boundary Layer	39
2.7 Overview of the Following Material	48
3. Field Equations for Flows of Newtonian Fluids	51
3.1 Description of Flow Fields	51
3.2 Continuity Equation	52
3.3 Momentum Equation	52
3.4 General Stress State of Deformable Bodies	53
3.5 General State of Deformation of Flowing Fluids	57
3.6 Relation Between Stresses and Rate of Deformation	62
3.7 Stokes Hypothesis	65
3.8 Bulk Viscosity and Thermodynamic Pressure	66
3.9 Navier-Stokes Equations	68

3.10	Energy Equation	69
3.11	Equations of Motion for Arbitrary Coordinate Systems (Summary)	73
3.12	Equations of Motion for Cartesian Coordinates in Index Notation	76
3.13	Equations of Motion in Different Coordinate Systems	79
4.	General Properties of the Equations of Motion	83
4.1	Similarity Laws	83
4.2	Similarity Laws for Flow with Buoyancy Forces (Mixed Forced and Natural Convection)	86
4.3	Similarity Laws for Natural Convection	90
4.4	Vorticity Transport Equation	91
4.5	Limit of Very Small Reynolds Numbers	93
4.6	Limit of Very Large Reynolds Numbers	94
4.7	Mathematical Example of the Limit $Re \rightarrow \infty$	96
4.8	Non-Uniqueness of Solutions of the Navier–Stokes Equations .	99
5.	Exact Solutions of the Navier–Stokes Equations	101
5.1	Steady Plane Flows	101
5.1.1	Couette–Poiseuille Flows	101
5.1.2	Jeffery–Hamel Flows (Fully Developed Nozzle and Diffuser Flows)	104
5.1.3	Plane Stagnation–Point Flow	110
5.1.4	Flow Past a Parabolic Body	115
5.1.5	Flow Past a Circular Cylinder	115
5.2	Steady Axisymmetric Flows	116
5.2.1	Circular Pipe Flow (Hagen–Poiseuille Flow)	116
5.2.2	Flow Between Two Concentric Rotating Cylinders . .	117
5.2.3	Axisymmetric Stagnation–Point Flow	118
5.2.4	Flow at a Rotating Disk	119
5.2.5	Axisymmetric Free Jet	124
5.3	Unsteady Plane Flows	126
5.3.1	Flow at a Wall Suddenly Set into Motion (First Stokes Problem)	126
5.3.2	Flow at an Oscillating Wall (Second Stokes Problem)	129
5.3.3	Start–up of Couette Flow	130
5.3.4	Unsteady Asymptotic Suction	131
5.3.5	Unsteady Plane Stagnation–Point Flow	131
5.3.6	Oscillating Channel Flow	137
5.4	Unsteady Axisymmetric Flows	139
5.4.1	Vortex Decay	139
5.4.2	Unsteady Pipe Flow	139
5.5	Summary	141

Part II. Laminar Boundary Layers

6. Boundary–Layer Equations in Plane Flow;	
Plate Boundary Layer	145
6.1 Setting up the Boundary–Layer Equations	145
6.2 Wall Friction, Separation and Displacement	150
6.3 Dimensional Representation of the Boundary–Layer Equations	152
6.4 Friction Drag	155
6.5 Plate Boundary Layer	156
7. General Properties and Exact Solutions of the Boundary–Layer Equations for Plane Flows	165
7.1 Compatibility Condition at the Wall	166
7.2 Similar Solutions of the Boundary–Layer Equations	167
7.2.1 Derivation of the Ordinary Differential Equation	167
A Boundary Layers with Outer Flow	169
B Boundary Layers Without Outer Flow	172
7.2.2 Wedge Flows	172
7.2.3 Flow in a Convergent Channel	174
7.2.4 Mixing Layer	175
7.2.5 Moving Plate	177
7.2.6 Free Jet	177
7.2.7 Wall Jet	180
7.3 Coordinate Transformation	182
7.3.1 Görtler Transformation	182
7.3.2 v. Mises Transformation	183
7.3.3 Crocco Transformation	184
7.4 Series Expansion of the Solutions	184
7.4.1 Blasius Series	184
7.4.2 Görtler Series	186
7.5 Asymptotic Behaviour of Solutions Downstream	187
7.5.1 Wake Behind Bodies	187
7.5.2 Boundary Layer at a Moving Wall	190
7.6 Integral Relations of the Boundary Layer	191
7.6.1 Momentum–Integral Equation	191
7.6.2 Energy–Integral Equation	192
7.6.3 Moment–of–Momentum Integral Equations	194
8. Approximate Methods for Solving the Boundary–Layer Equations for Steady Plane Flows	195
8.1 Integral Methods	196

8.2	Stratford's Separation Criterion	202
8.3	Comparison of the Approximate Solutions with Exact Solutions	202
8.3.1	Retarded Stagnation-Point Flow	202
8.3.2	Divergent Channel (Diffuser)	204
8.3.3	Circular Cylinder Flow	205
8.3.4	Symmetric Flow past a Joukowsky Airfoil	207
9.	Thermal Boundary Layers	
	without Coupling of the Velocity Field	
	to the Temperature Field	209
9.1	Boundary-Layer Equations for the Temperature Field	209
9.2	Forced Convection for Constant Properties	211
9.3	Effect of the Prandtl Number	215
9.4	Similar Solutions of the Thermal Boundary Layer	218
9.5	Integral Methods for Computing the Heat Transfer	223
9.6	Effect of Dissipation; Distribution of the Adiabatic Wall Temperature	226
10.	Thermal Boundary Layers	
	with Coupling of the Velocity Field	
	to the Temperature Field	231
10.1	Remark	231
10.2	Boundary-Layer Equations	231
10.3	Boundary Layers with Moderate Wall Heat Transfer (Without Gravitational Effects)	233
10.3.1	Perturbation Calculation	233
10.3.2	Property Ratio Method (Temperature Ratio Method) .	237
10.3.3	Reference Temperature Method	240
10.4	Compressible Boundary Layers (Without Gravitational Effects)	241
10.4.1	Physical Property Relations	241
10.4.2	Simple Solutions of the Energy Equation	244
10.4.3	Transformations of the Boundary-Layer Equations .	246
10.4.4	Similar Solutions	249
10.4.5	Integral Methods	258
10.4.6	Boundary Layers in Hypersonic Flows	263
10.5	Natural Convection	265
10.5.1	Boundary-Layer Equations	265
10.5.2	Transformation of the Boundary-Layer Equations .	270
10.5.3	Limit of Large Prandtl Numbers ($T_w = \text{const}$) .	271
10.5.4	Similar Solutions	273
10.5.5	General Solutions	277
10.5.6	Variable Physical Properties	278
10.5.7	Effect of Dissipation	280

10.6 Indirect Natural Convection	281
10.7 Mixed Convection	284
11. Boundary-Layer Control (Suction/Blowing)	291
11.1 Different Kinds of Boundary-Layer Control	291
11.2 Continuous Suction and Blowing	295
11.2.1 Fundamentals	295
11.2.2 Massive Suction	297
11.2.3 Massive Blowing	299
11.2.4 Similar Solutions	302
11.2.5 General Solutions	307
1. Plate Flow with Uniform Suction or Blowing	307
2. Airfoil	309
11.2.6 Natural Convection with Blowing and Suction	310
11.3 Binary Boundary Layers	311
11.3.1 Overview	311
11.3.2 Basic Equations	312
11.3.3 Analogy Between Heat and Mass Transfer	316
11.3.4 Similar Solutions	317
12. Axisymmetric and Three-Dimensional Boundary Layers	321
12.1 Axisymmetric Boundary Layers	321
12.1.1 Boundary-Layer Equations	321
12.1.2 Mangler Transformation	323
12.1.3 Boundary Layers on Non-Rotating Bodies of Revolution	324
12.1.4 Boundary Layers on Rotating Bodies of Revolution	327
12.1.5 Free Jets and Wakes	331
12.2 Three-Dimensional Boundary Layers	335
12.2.1 Boundary-Layer Equations	335
12.2.2 Boundary Layer at a Cylinder	341
12.2.3 Boundary Layer at a Yawing Cylinder	342
12.2.4 Three-Dimensional Stagnation Point	344
12.2.5 Boundary Layers in Symmetry Planes	345
12.2.6 General Configurations	345
13. Unsteady Boundary Layers	349
13.1 Fundamentals	349
13.1.1 Remark	349
13.1.2 Boundary-Layer Equations	350
13.1.3 Similar and Semi-Similar Solutions	351
13.1.4 Solutions for Small Times (High Frequencies)	352
13.1.5 Separation of Unsteady Boundary Layers	353
13.1.6 Integral Relations and Integral Methods	354
13.2 Unsteady Motion of Bodies in a Fluid at Rest	355

13.2.1 Start-Up Processes	355
13.2.2 Oscillation of Bodies in a Fluid at Rest	362
13.3 Unsteady Boundary Layers in a Steady Basic Flow	365
13.3.1 Periodic Outer Flow	365
13.3.2 Steady Flow with a Weak Periodic Perturbation	367
13.3.3 Transition Between Two Slightly Different Steady Boundary Layers	369
13.4 Compressible Unsteady Boundary Layers	370
13.4.1 Remark	370
13.4.2 Boundary Layer Behind a Moving Normal Shock Wave	371
13.4.3 Flat Plate at Zero Incidence with Variable Free Stream Velocity and Wall Temperature	373
14. Extensions to the Prandtl Boundary-Layer Theory	377
14.1 Remark	377
14.2 Higher Order Boundary-Layer Theory	379
14.3 Hypersonic Interaction	389
14.4 Triple-Deck Theory	392
14.5 Marginal Separation	403
14.6 Massive Separation	408

Part III. Laminar-Turbulent Transition

15. Onset of Turbulence (Stability Theory)	415
15.1 Some Experimental Results on the Laminar-Turbulent Transition	415
15.1.1 Transition in the Pipe Flow	415
15.1.2 Transition in the Boundary Layer	419
15.2 Fundamentals of Stability Theory	424
15.2.1 Remark	424
15.2.2 Fundamentals of Primary Stability Theory	425
15.2.3 Orr-Sommerfeld Equation	427
15.2.4 Curve of Neutral Stability and the Indifference Reynolds Number	434
a Plate Boundary Layer	436
b Effect of Pressure Gradient	445
c Effect of Suction	457
d Effect of Wall Heat Transfer	460
e Effect of Compressibility	463
f Effect of Wall Roughness	467
g Further Effects	472
15.3 Instability of the Boundary Layer for Three-Dimensional Perturbations	473

15.3.1 Remark	473
15.3.2 Fundamentals of Secondary Stability Theory	476
15.3.3 Boundary Layers at Curved Walls	481
15.3.4 Boundary Layer at a Rotating Disk	485
15.3.5 Three-Dimensional Boundary Layers	487
15.4 Local Perturbations	493

Part IV. Turbulent Boundary Layers

16. Fundamentals of Turbulent Flows	499
16.1 Remark	499
16.2 Mean Motion and Fluctuations	501
16.3 Basic Equations for the Mean Motion of Turbulent Flows	504
16.3.1 Continuity Equation	504
16.3.2 Momentum Equations (Reynolds Equations)	505
16.3.3 Equation for the Kinetic Energy of the Turbulent Fluctuations (k -Equation)	507
16.3.4 Thermal Energy Equation	510
16.4 Closure Problem	511
16.5 Description of the Turbulent Fluctuations	512
16.5.1 Correlations	512
16.5.2 Spectra and Eddies	513
16.5.3 Turbulence of the Outer Flow	515
16.5.4 Edges of Turbulent Regions and Intermittence	515
16.6 Boundary-Layer Equations for Plane Flows	516
17. Internal Flows	519
17.1 Couette Flow	519
17.1.1 Two-Layer Structure of the Velocity Field and the Logarithmic Overlap Law	519
17.1.2 Universal Laws of the Wall	524
17.1.3 Friction Law	536
17.1.4 Turbulence Models	538
17.1.5 Heat Transfer	541
17.2 Fully Developed Internal Flows ($A = \text{const}$)	543
17.2.1 Channel Flow	543
17.2.2 Couette-Poiseuille Flows	544
17.2.3 Pipe Flow	549
17.3 Slender-Channel Theory	554
18. Turbulent Boundary Layers without Coupling of the Velocity Field to the Temperature Field	557
18.1 Turbulence Models	557

18.1.1 Remark	557
18.1.2 Algebraic Turbulence Models	559
18.1.3 Turbulent Energy Equation	560
18.1.4 Two-Equation Models	562
18.1.5 Reynolds Stress Models	565
18.1.6 Heat Transfer Models	568
18.1.7 Low-Reynolds-Number Models	570
18.1.8 Large-Eddy Simulation and Direct Numerical Simulation	571
18.2 Attached Boundary Layers	572
18.2.1 Layered Structure	572
18.2.2 Boundary-Layer Equations Using the Defect Formulation	574
18.2.3 Friction Law and Characterisitic Quantities of the Boundary Layer	577
18.2.4 Equilibrium Boundary Layers	580
18.2.5 Boundary Layer on a Plate at Zero Incidence	582
18.3 Boundary Layers with Separation	589
18.3.1 Stratford Flow	589
18.3.2 Quasi-Equilibrium Boundary Layers	591
18.4 Computation of Boundary Layers Using Integral Methods	594
18.4.1 Direct Method	594
18.4.2 Inverse Method	597
18.5 Computation of Boundary Layers Using Field Methods	598
18.5.1 Attached Boundary Layers	598
18.5.2 Boundary Layers with Separation	601
18.5.3 Low-Reynolds-Number Turbulence Models	603
18.5.4 Additional Effects	604
18.6 Computation of Thermal Boundary Layers	607
18.6.1 Fundamentals	607
18.6.2 Computation of Thermal Boundary Layers Using Field Methods	609
19. Turbulent Boundary Layers with Coupling of the Velocity Field to the Temperature Field	611
19.1 Fundamental Equations	611
19.1.1 Time Averaging for Variable Density	611
19.1.2 Boundary-Layer Equations	613
19.2 Compressible Turbulent Boundary Layers	617
19.2.1 Temperature Field	617
19.2.2 Overlap Law	619
19.2.3 Skin-Friction Coefficient and Nusselt Number	621
19.2.4 Integral Methods for Adiabatic Walls	623

19.2.5 Field Methods	625
19.2.6 Shock–Boundary–Layer Interaction	625
19.3 Natural Convection	627
20. Axisymmetric and Three–Dimensional	
Turbulent Boundary Layers	631
20.1 Axisymmetric Boundary Layers	631
20.1.1 Boundary–Layer Equations	631
20.1.2 Boundary Layers without Body Rotation	632
20.1.3 Boundary Layers with Body Rotation	635
20.2 Three–Dimensional Boundary Layers	637
20.2.1 Boundary–Layer Equations	637
20.2.2 Computation Methods	641
20.2.3 Examples	643
21. Unsteady Turbulent Boundary Layers	645
21.1 Averaging and Boundary–Layer Equations	645
21.2 Computation Methods	648
21.3 Examples	649
22. Turbulent Free Shear Flows	653
22.1 Remark	653
22.2 Equations for Plane Free Shear Layers	655
22.3 Plane Free Jet	659
22.3.1 Global Balances	659
22.3.2 Far Field	660
22.3.3 Near Field	665
22.3.4 Wall Effects	665
22.4 Mixing Layer	667
22.5 Plane Wake	669
22.6 Axisymmetric Free Shear Flows	671
22.6.1 Basic Equations	671
22.6.2 Free Jet	672
22.6.3 Wake	673
22.7 Buoyant Jets	675
22.7.1 Plane Buoyant Jet	675
22.7.2 Axisymmetric Buoyant Jet	676
22.8 Plane Wall Jet	677

Part V. Numerical Methods in Boundary–Layer Theory

23. Numerical Integration of the Boundary–Layer Equations	683
23.1 Laminar Boundary Layers	683
23.1.1 Remark	683
23.1.2 Note on Boundary–Layer Transformations	684
23.1.3 Explicit and Implicit Discretisation	685
23.1.4 Solution of the Implicit Difference Equations	689
23.1.5 Integration of the Continuity Equation	691
23.1.6 Boundary–Layer Edge and Wall Shear Stress	691
23.1.7 Integration of the Transformed Boundary–Layer Equations Using the Box Scheme	692
23.2 Turbulent Boundary Layers	695
23.2.1 Method of Wall Functions	695
23.2.2 Low–Reynolds–Number Turbulence Models	700
23.3 Unsteady Boundary Layers	701
23.4 Steady Three–Dimensional Boundary Layers	703
List of Frequently Used Symbols	709
References and Index of Authors	717
Index	799

Introduction

Short historical review

At the end of the 19th century, fluid mechanics had split into two different directions which hardly had anything more in common. On one side was the science of *theoretical hydrodynamics*, emanating from Euler's equations of motion and which had been developed to great perfection. However this had very little practical importance, since the results of this so-called classical hydrodynamics were in glaring contradiction to everyday experience. This was particularly true in the very important case of pressure loss in tubes and channels, as well as that of the drag experienced by a body moved through a fluid. For this reason, engineers, on the other side, confronted by the practical problems of fluid mechanics, developed their own strongly empirical science, *hydraulics*. This relied upon a large amount of experimental data and differed greatly from theoretical hydrodynamics in both methods and goals.

It is the great achievement of Ludwig Prandtl which, at the beginning of this century, set forth the way in which these two diverging directions of fluid mechanics could be unified. He achieved a high degree of correlation between theory and experiment, which, in the first half of this century, has led to unimagined successes in modern fluid mechanics. It was already known then that the great discrepancy between the results in classical hydrodynamics and reality was, in many cases, due to neglecting the *viscosity effects* in the theory. Now the complete equations of motion of viscous flows (the Navier Stokes equations) had been known for some time. However, due to the great mathematical difficulty of these equations, no approach had been found to the mathematical treatment of viscous flows (except in a few special cases). For technically important fluids such as water and air, the viscosity is very small, and thus the resulting viscous forces are small compared to the remaining forces (gravitational force, pressure force). For this reason it took a long time to see why the viscous forces ignored in the classical theory should have an important effect on the motion of the flow.

In his lecture on “Über Flüssigkeitbewegung bei sehr kleiner Reibung” (On Fluid Motion with Very Small Friction) at the Heidelberg mathematical congress in 1904, L. Prandtl (1904) showed how a theoretical treatment could be used on viscous flows in cases of great practical importance. Using theoretical considerations together with some simple experiments, Prandtl

showed that the flow past a body can be divided into two regions: a very thin layer close to the body (*boundary layer*) where the viscosity is important, and the remaining region outside this layer where the viscosity can be neglected. With the help of this concept, not only was a physically convincing explanation of the importance of the viscosity in the drag problem given, but simultaneously, by hugely reducing the mathematical difficulty, a path was set for the theoretical treatment of viscous flows. Prandtl supported his theoretical work by some very simple experiments in a small, self-built water channel, and in doing this reinitiated the lost connection between theory and practice. The theory of the *Prandtl boundary layer* or the *frictional layer* has proved to be exceptionally useful and has given considerable stimulation to research into fluid mechanics since the beginning of this century. Under the influence of a thriving flight technology, the new theory developed quickly and soon became, along with other important advances – airfoil theory and gas dynamics – a keystone of modern fluid mechanics.

One of the most important applications of boundary-layer theory is the calculation of the friction drag of bodies in a flow, e.g. the drag of a flat plate at zero incidence, the friction drag of a ship, an airfoil, the body of an airplane, or a turbine blade. One particular property of the boundary layer is that, under certain conditions, a reverse flow can occur directly at the wall. A *separation* of the boundary layer from the body and the formation of large or small eddies at the back of the body can then occur. This results in a great change in the pressure distribution at the back of the body, leading to the *form or pressure drag* of the body. This can also be calculated using boundary-layer theory. Boundary-layer theory answers the important question of what shape a body must have in order to avoid this detrimental separation. It is not only in flow past a body where separation can occur, but also in flow through a duct. In this way boundary-layer theory can be used to describe the flow through blade cascades in compressors and turbines, as well as through diffusers and nozzles. The processes involved in maximum lift of an airfoil, where separation is also important, can only be understood using boundary-layer theory. The boundary layer is also important for heat transfer between a body and the fluid around it.

Initially boundary-layer theory was developed mainly for the laminar flow of an incompressible fluid, where Stokes law of friction could be used as an ansatz for the viscous forces. This area was later researched in very many pieces of work, so that today it can be considered to be fully understood. Later the theory was extended to the practically important turbulent incompressible boundary-layer flows. Around 1890, O. Reynolds (1894) had already introduced the fundamentally important concept of apparent turbulent stresses, but this did not yet permit the theoretical treatment of turbulent flows. The introduction of the concept of the Prandtl mixing length, cf. L. Prandtl (1925), contributed considerable advances and, together with systematic experiments, allowed turbulent flows to be treated theoretically

with the help of boundary-layer theory. Even today a rational theory of fully developed turbulent flows remains to be found. Thanks to the great increase of velocities in flight technology, boundary layers in compressible flows were subsequently also thoroughly examined. As well as the boundary layer in the velocity field, a thermal boundary layer also forms; this is of great importance for the heat transfer between the flow and the body. Because of internal friction (dissipation) at high Mach numbers, the body surface heats up greatly. This causes many problems, particularly in flight technology and satellite flights ("thermal barrier").

The transition from laminar to turbulent flow, important for all of fluid mechanics, was first examined in pipe flow at the end of the last century by O. Reynolds (1883). Using the flow about a sphere, in 1914 Prandtl was able to show experimentally that the boundary layer also can be both laminar or turbulent and that the process of separation and thus the drag problem are controlled by this laminar-turbulent transition, cf. L. Prandtl (1914). The theoretical investigations into this transition assume Reynolds' idea of the instability of the laminar flow. This was treated by Prandtl in 1921. After some futile attempts, W. Tollmien (1929) and H. Schlichting (1933) were able to theoretically calculate the indifference Reynolds number for the flat plate at zero incidence. However it took more than ten years before the theory could be confirmed by careful experiments by H.L. Dryden (1946–1948) and his coworkers. The effect of other parameters on the transition (pressure gradient, suction, Mach number, heat transfer) were clarified using the stability theory of the boundary layer. This theory has found important application with, among other things, airfoils with very low drag (laminar airfoils).

An important characteristic of modern research into fluid mechanics in general and more specifically into the branch of boundary-layer theory is the close connection between theory and experiment. The most crucial advances have been achieved through a few fundamental experiments together with theoretical considerations. Many years ago, A. Betz (1949) produced a review of the development of boundary-layer theory, with particular emphasis on the mutual fructification of theory and experiment. Research into boundary layers, inspired by Prandtl from 1904, were, in the first 20 years up until Prandtl's Wilbur Wright memorial lecture at the Royal Aeronautical Society in London, (L. Prandtl (1927)) almost exclusively confined to Prandtl's institute in Göttingen. It is only since 1930 that other researchers have been involved in the further expansion of boundary-layer theory, initially in England and the USA. Today boundary-layer theory has spread over the whole world; together with other branches it forms one of the most important pillars of fluid mechanics.

In the mid-fifties, mathematical methods into singular perturbation theory were being systematically developed, cf. S. Kaplun (1954), S. Kaplun; P.A. Lagerstrom (1957), M. Van Dyke (1964b), also W. Schneider (1978).

It became clear that the boundary-layer theory heuristically developed by Prandtl was a classic example of the solution of a singular perturbation problem. Thus boundary-layer theory is a rational asymptotic theory of the solution of the Navier–Stokes equations for high Reynolds numbers, cf. K. Gersten (2000). This opened the possibility of a systematic development to higher order boundary-layer theory, cf. M. Van Dyke (1969), K. Gersten (1972), K. Stewartson (1974), K. Gersten; J.F. Gross (1976), V.V. Sychev et al. (1998), I.J. Sobey (2000). The asymptotic methods which were first developed for laminar flows were then, at the start of the seventies, carried over to turbulent flows, cf. K.S. Yajnik (1970), G.L. Mellor (1972). Reviews of asymptotic theory of turbulent flows are to be found in K. Gersten (1987), K. Gersten (1989c), A. Kluwick (1989a), as well as W. Schneider (1991). K. Gersten; H. Herwig (1992) have presented a systematic application of asymptotic methods (regular and singular perturbation methods) to the theory of viscous flows. The book by P.A. Libby (1998) also gives preferential treatment to asymptotic methods. Most of the characteristics of the asymptotic theory for high Reynolds-number flows can already be found in Prandtl's work, cf. K. Gersten (2000).

In turbulence modelling, the mixing length hypothesis developed by L. Prandtl (1925) led to an algebraic turbulence model. Twenty years later, L. Prandtl (1945) showed how transport equations for turbulent quantities such as the kinetic energy of the random motion, the dissipation and the Reynolds shear stress could be applied to improve to turbulence models. Calculation methods for turbulent boundary layers with highly refined turbulence models have been developed by, for example, P. Bradshaw et al. (1967), W.P. Jones; B.E. Launder (1973), K. Hanjalić; B.E. Launder (1976), as well as J.C. Rotta (1973). Overviews on turbulence modelling are presented by W.C. Reynolds (1976) and V.C. Patel et al. (1985). In two extremely noteworthy events at Stanford University in the years 1968 and 1980/81, the existing methods for calculating boundary layers were compared and examined in specially chosen experiments; see the reports by S.J. Kline et al. (1968) and S.J. Kline et al. (1981). A review on Reynolds number effects in wall-bounded turbulent flows by M. Gad-el-Hak; P.R. Bandyopadhyay (1994) is also worth mentioning.

The following tendency is emerging from the rapid developments in the area of supercomputing: the future will consist more of direct numerical solutions of the Navier–Stokes equations without any simplifications, and also of the computation of turbulent flows using direct numerical simulation (DNS), i.e. without using a turbulence model or by modelling only high frequency turbulent fluctuations (“large-eddy simulations”), cf. D.R. Chapman (1979). However numerical methods in computing flows at high Reynolds numbers only become efficient if the particular layered structure of the flow, as given by the asymptotic theory, is taken into account, as occurs if a suitable grid

is used for computation. Boundary-layer theory will therefore retain its fundamental place in the calculation of high Reynolds number flows.

The first summary of boundary-layer theory is to be found in two short articles by W. Tollmien (1931) in the *Handbuch der Experimentalphysik*. Some years later Prandtl's comprehensive contribution appeared in *Aerodynamic Theory*, edited by W.F. Durand, L. Prandtl (1935). In the six decades since then, the extent of this research area has become extraordinarily large. cf. H. Schlichting (1960) and also I. Tani (1977), A.D. Young (1989), K. Gersten (1989a), A. Kluwick (1998) and T. Cebeci; J. Cousteix (2005). According to a review by H.L. Dryden (1955), about 100 articles appeared in the year 1955, and 45 years later this number has grown to about 800 per year.

About the year 2000 the numerical methods in fluid mechanics had reached a standard that made it possible to solve the full Navier-Stokes equations. So-called Navier-Stokes/RANS methods (**R**eynolds **A**veraged **N**avier-**S**tokes) were in wide use at universities, research establishments and industry. Reynolds-stress models came into use, which in principle take into account non-isotropy of turbulence. Turbulence flow separation still remains to be a major issue. Maybe hybrid RANS-LES methods (**L**arge-**E**ddy **S**imulation, LES) are the ultimate industrial methods for the simulation of flow fields past realistic vehicle configurations, see E.H. Hirschel et al. (2014).

In spite of these developments concerning the numerical solutions of the full Navier-Stokes equations it can also be noticed that in recent years the extensions of boundary layer theory received increasing attention. Several textbooks have been published recently.

The Interactive Boundary Layer Theory by I.J. Sobey (2000) and the Asymptotic Theory of Separated Flows by V.V. Sychev et al. (1998) refer to laminar flows. The books by E.H. Hirschel et al. (2014), T. Cebeci (1999, 2004), M. Hallbäck et al. (Eds.) (1996) and T.K. Sengupta (2012) are concentrated on turbulent and transitional flows. The state of research can also be found in H. Steinrück (Ed.) (2010), A. Kluwick (Ed.) (1998) and G.E.A. Meier et al. (Eds.) (2006). These new developments of the asymptotic methods for high Reynolds number flows will be discussed in the appropriate Chapters 14 and 18.

Abstract

The nonlinear partial differential equations describing all general flow fields are called *Navier-Stokes equations*. In non-dimensional form these equations depend on the Reynolds number, which determines the effect of the viscosity in the flow. The higher the Reynolds number, the lower are the viscosity effects on the flow.

The boundary-layer theory is the *asymptotic theory of the Navier-Stokes equations for high Reynolds numbers*. This theory has been developed by Ludwig Prandtl (1904). Although this theory is now more than 110 years old, it is nowadays still being applied in industry and research, because many important fields of fluid mechanics (i.e. aeronautics, ship hydrodynamics, automobile aerodynamics) refer to flows at high Reynolds numbers.

The book has 23 Chapters and is divided into 5 Parts:

- I Fundamentals of Viscous Flows
- II Laminar Boundary Layers
- III Laminar-Turbulent Transition
- IV Turbulent Boundary Layers
- V Numerical Methods in Boundary Layer Theory

The boundary-layer theory is a *perturbation method*, because it starts from the limiting solution for infinitely large Reynolds number (solution for inviscid fluid) and is then perturbed by viscosity effects. Since the inviscid flow solution does not satisfy the no-slip condition at the wall, boundary-layer theory is called a singular perturbation method. For high Reynolds numbers the entire flow field consists of two different regions. In the larger of these two regions the flow is inviscid. The second region is a very narrow layer close to the wall called the *boundary layer*. The complete solution can be found by the *method of matched asymptotic expansions* as long as the boundary layer keeps attached to the wall.

When the boundary layer leads to separation, the limiting inviscid solution (as starting solution) is generally not known a priori. In this case a dimensionless length parameter (for instance: a step height compared to a flat plate) must be taken into the analysis. The two dimensionless parameters (geometrical parameter and Reynolds number) lead to a three-layer structure of the resulting flow field called

XXVIII Abstract

triple deck theory or asymptotic interaction theory. Within this theory boundary layers with separation and reattachment can be calculated without any singularities (Chapter 14.4). Where separation occurs in a flow, the limiting solution can often be chosen to be that flow where the geometry is changed just so that there is no separation (*marginal separation*: laminar: Chapter 14.5; turbulent: Chapter 18.5.2).

Part I

Fundamentals of Viscous Flows

1. Some Features of Viscous Flows

1.1 Real and Ideal Fluids

Theoretical investigations into fluid mechanics in the last century were mainly based on the ideal fluid, i.e. a fluid which is inviscid and incompressible. It is only since this century that the effects of viscosity and compressibility have been taken into account in any great way. In the flow of inviscid fluids, no tangential forces (shear stresses) exist between adjacent layers; only normal forces (pressures) do. This is equivalent to saying that an ideal fluid does not oppose a change in its shape with any internal resistance. The theory of flows of ideal fluids is mathematically very highly developed and indeed in many cases gives a satisfactory description of real flows, as for example, in the cases of wave motion and the formation of liquid jets. On the other hand, the theory of ideal fluids is useless when faced with the problem of calculating the drag of a body. It predicts that a body moving subsonically and uniformly through an infinitely extended fluid will experience no drag (D'Alembert's paradox).

This unacceptable result of the theory of ideal fluids is due to the fact that in a real fluid, in addition to the normal forces, tangential forces also occur both between layers in the fluid and between the fluid and the walls. These tangential or friction forces of real fluids are connected to a physical property called the *viscosity of the fluid*.

In the ideal fluid, there is a difference in the tangential velocities on the boundary between a solid body and the fluid, that is, the fluid slips along the side of the body. This is due to the absence of tangential forces. In a real fluid, on the other hand, because the fluid adheres to a solid wall, tangential forces do act.

The presence of tangential stress (shear stress) and the *no-slip condition* produces the essential difference between ideal and real fluids. Some particularly important fluids in practice, such as water and air, have a very low viscosity. In many cases the flows of such very low friction fluids are like the flows of ideal fluids, because in general the tangential forces are very small. In the theory of ideal fluids, the viscosity is ignored because by doing this such considerable simplifications of the equations of motion are reached that an extended mathematical theory is possible. However it is important to note that the no-slip condition does hold good even for very low viscosity fluids.

In some cases this no-slip condition leads to great discrepancies between the laws of motion for real and ideal fluids. In particular, the great difference in the drag laws between real and ideal fluids mentioned above originates from the no-slip condition.

This book is concerned with the laws of motion of low viscosity fluids because these are of great importance in practice. It will become clear how the behaviour of real fluids, sometimes consistent with the behaviour of ideal fluids and sometimes utterly different, can be explained.

1.2 Viscosity

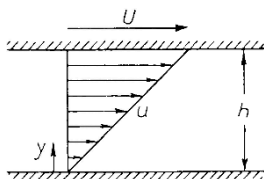


Fig. 1.1. Velocity distribution of a viscous fluid between two parallel flat walls (Couette flow)

The nature of viscosity of a fluid can be understood most easily by the following experiment. Consider the flow between two long parallel plane plates, one of which is at rest while the other moves with constant velocity U in its own plane. The distance between the plates is h (Fig. 1.1). We assume that the pressure in the entire fluid is constant. From experiment it is seen that the fluid adheres to both plates so that the velocity at the lower plate is zero, while at the upper plate the fluid moves with velocity U . In addition, we assume the simplest case (Newtonian fluid, constant temperature), i.e. there is a linear velocity distribution between the plates. Therefore the velocity is proportional to the distance y from the lower plate, and we have

$$u(y) = \frac{y}{h}U. \quad (1.1)$$

In order to maintain the state of the motion, a tangential force in the direction of motion must act on the upper plate. This keeps the friction forces of the fluid in equilibrium. According to experimental results, this force (force per unit surface area of the plate = shear stress τ) is proportional to U/h . In the general case, this can be replaced by du/dy . The constant of proportionality between τ and du/dy , which we will denote by μ^1 , depends on the nature of the fluid, i.e. it is a physical property of the fluid. It is very small for so-called mildly viscous fluids like water, alcohol and air, and is very large for very viscous fluids like oil or glycerine.

¹ According to DIN norm 1342 (viscosity of Newtonian fluids), the viscosity is denoted η . Since η is used here to denote a dimensionless coordinate, this book will differ from the DIN norm and denote the viscosity as μ .

Therefore, we have the elementary law of fluid friction in the form

$$\boxed{\tau = \mu \frac{du}{dy}} . \quad (1.2)$$

The value μ is a physical property of the fluid which is strongly dependent on the temperature and is called the *viscosity* of the fluid. The friction law given by Eq. (1.2) is called *Newton's law of friction*. Equation (1.2) can be interpreted as the defining equation for the viscosity. However it must be noted that the motion discussed here is a very simple special case. The flow in Fig. 1.1 is also called simple shear flow or Couette flow. The generalisation of this simple friction law yields Stokes law of friction (cf. Chap. 3). The physical unit of viscosity can be read straight off Eq. (1.2)¹. The shear stress has the units $\text{kg}/\text{m s}^2$ or N/m^2 and the velocity gradient du/dy the units s^{-1} . Therefore μ has the units

$$[\mu] = \frac{\text{kg}}{\text{m s}} = \frac{\text{Ns}}{\text{m}^2} = \text{Pa s} .$$

In all flows where friction forces act together with inertial forces, there is considerable importance attached to the ratio formed by the viscosity μ and the density ϱ , denoted the *kinematic viscosity*² ν :

$$\nu = \frac{\mu}{\varrho} \quad [\nu] = \frac{\text{m}^2}{\text{s}} . \quad (1.3)$$

Fluids where there is a nonlinear relation between the shear stress τ and the velocity gradient du/dy are called non-Newtonian fluids. Since all gases and many technically important liquids, e.g. water, demonstrate Newtonian behaviour (i.e. Eq. (1.2) holds), we will consider only Newtonian fluids in this book.

As already stated, the viscosity is a physical property. Since it establishes the momentum transport perpendicular to the main flow direction, viscosity is also called a transport property of the fluid. There are also corresponding physical properties of the fluid for heat and mass transport, and these will be discussed in Sects. 3.10 and 3.11.

The viscosity is in general a function of the temperature and pressure, although the temperature dependence is dominant. As the temperature increases, the viscosity of gases generally increases whereas that of liquids decreases. Numerical values for the viscosity of various materials are given in Sect. 3.11.

¹ The SI international system of units is used, i.e. the meter (m), the second (s), the kilogram (kg) for mass, the Newton (N) for force and the Pascal (Pa) for pressure. We have $1\text{Pa} = 1\text{N/m}^2 = 1\text{kg/m s}^2$. A legal unit of pressure is still $1\text{bar} = 10^5\text{Pa}$. The common system of measurement in the past was $1\text{kP} = 9.80665\text{ N}$ and $1\text{at} = 0.980665\text{ bar}$

² Another unit for the viscosity is the *Poise* $P = 0.1\text{Ns/m}^2$. The kinematic viscosity is also measured in *Stokes* $S = 10^{-4}\text{m}^2/\text{s}$.

1.3 Reynolds Number

We now have to deal with the fundamentally important question of when flows with the same flow direction past two geometrically similar bodies are geometrically similar to one another, i.e. when there is a geometrically similar development of the streamlines. Such flows with geometrically similar boundaries and streamline portraits are called *mechanically similar flows*. In order that the flows past two geometrically similar bodies (e.g. past two spheres) are mechanically similar for different fluids, different velocities and different body sizes, we clearly need to satisfy the condition that the forces acting on volume elements situated in similar positions are in the same ratio to each other.

The following forces generally act on a volume element: friction forces (proportional to the viscosity μ), inertial forces (proportional to the density ϱ), pressure forces and volume forces (e.g. gravitational force). In what follows we shall consider only the ratio of the inertial forces to the friction forces. For mechanically similar flows this must be equal for similarly positioned volume elements. For motion which is mainly in the x direction, the inertial force per unit volume is $\varrho du/dt$, where u is the velocity component in the x direction, and d/dt is the substantial derivative. For steady flow this can also be written as $\varrho \partial u / \partial x \cdot dx/dt = \varrho u \partial u / \partial x$, where $\partial u / \partial x$ is the change in velocity with position. The inertial force per unit volume is therefore $\varrho u \partial u / \partial x$. An expression for the friction force can easily be derived from Newton's law of friction Eq. (1.2). For a volume element whose x direction is in the direction of motion, Fig. 1.2 gives rise to the following expression for the shear forces:

$$\left(\tau + \frac{\partial \tau}{\partial y} dy \right) dx dz - \tau dx dz = \frac{\partial \tau}{\partial y} dx dy dz .$$

The friction force per unit volume is thus $\partial \tau / \partial y$, which, according to Eq. (1.2), is equal to $\mu \partial^2 u / \partial y^2$.

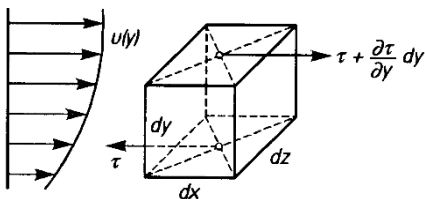


Fig. 1.2. Friction forces on a volume element

In this way we reach the condition of mechanical similarity, that the ratio of inertial to friction forces must be the same at similarly situated points:

$$\frac{\text{inertial force}}{\text{friction force}} = \frac{\varrho u \partial u / \partial x}{\mu \partial^2 u / \partial y^2} = \text{const.}$$

We shall now consider how these forces change as the characteristic quantities of the flow change. These are the density ϱ , the viscosity μ , a characteristic

velocity such as the free stream velocity V and a characteristic length dimension of the body such as the sphere's diameter d . The velocity at any point in the flow field u is proportional to the free stream velocity V , the velocity gradient $\partial u / \partial x$ to V/d and similarly $\partial^2 u / \partial y^2$ to V/d^2 . Thus the ratio of inertial force to friction force becomes

$$\frac{\text{inertial force}}{\text{friction force}} = \frac{\varrho u \partial u / \partial x}{\mu \partial^2 u / \partial y^2} \sim \frac{\varrho V^2 / d}{\mu V / d^2} = \frac{\varrho V d}{\mu}.$$

Since the constant of proportionality must be equal at similarly positioned points, the mechanical similarity of the flows is satisfied when the quantity $\varrho V d / \mu$ has the same value for both flows. Using $\mu / \varrho = \nu$ this dimensionless number can be written in the form Vd/ν . It is called the Reynolds number Re. Therefore mechanical similarity of the flows exists if the Reynolds number

$$\boxed{\text{Re} = \frac{\varrho V d}{\mu} = \frac{V d}{\nu}}$$

(1.4)

is equal for both flows. This relation was discovered by O. Reynolds (1883) while investigating flows in pipes and is named after him as *the similarity principle with respect to the Reynolds number*.

When the different quantities are replaced by their units, the dimensions of the Reynolds number can be seen immediately:

$$[\varrho] = \frac{\text{kg}}{\text{m}^3}, \quad [V] = \frac{\text{m}}{\text{s}}, \quad [d] = \text{m}, \quad [\mu] = \frac{\text{kg}}{\text{ms}}.$$

We have

$$\left[\frac{\varrho V d}{\mu} \right] = \frac{\text{kg}}{\text{m}^3} \cdot \frac{\text{m}}{\text{s}} \cdot \text{m} \cdot \frac{\text{ms}}{\text{kg}} = 1,$$

and thus the Reynolds number is dimensionless.

Dimensional considerations. Instead of starting off from the mechanical similarity of flows, the similarity principle with respect to the Reynolds number can be derived from dimensional considerations. We begin with the principle that all physical quantities can be expressed in a form which is not dependent on the chosen system of units. In the case at hand, the relevant quantities are the free stream velocity V , a characteristic length of the body d , the density ϱ and the viscosity μ . Using dimensional considerations we can pose the question: is there a combination of these four quantities in the form

$$V^\alpha d^\beta \varrho^\gamma \mu^\delta$$

which is dimensionless? If K is the symbol for force, L the symbol for length and T that for time, we obtain a dimensionless combination of the above quantities when

$$V^\alpha d^\beta \varrho^\gamma \mu^\delta = K^0 L^0 T^0.$$

Without loss of generality, we can choose one of the four numbers $\alpha, \beta, \gamma, \delta$ to be equal to 1, since any power of a dimensionless quantity is also dimensionless. If we choose $\alpha = 1$ we get

$$V^\alpha d^\beta \varrho^\gamma \mu^\delta = \frac{L}{T} L^\beta \left(\frac{KT^2}{L^4} \right)^\gamma \left(\frac{KT}{L^2} \right)^\delta = K^0 L^0 T^0 .$$

By setting the exponents of L, T, K equal left and right we get the three equations:

$$K : \quad \gamma + \delta = 0$$

$$L : \quad 1 + \beta - 4\gamma - 2\delta = 0$$

$$T : \quad -1 + 2\gamma + \delta = 0 .$$

The solution is

$$\beta = 1, \quad \gamma = 1, \quad \delta = -1 .$$

Therefore the only possible dimensionless combination of V, d, ϱ, μ is the ratio

$$\frac{\varrho V d}{\mu} = Re .$$

Dimensionless coefficients. These dimensional considerations can be extended even further when we look at the velocity field and the forces (normal forces and tangential forces) of flows with geometrically similar boundaries but different Reynolds numbers. The position of a point close to the geometrically similar body is given by the spatial coordinates x, y, z ; the dimensionless spatial coordinates are then $x/d, y/d, z/d$. The velocity components u, v, w are made dimensionless with the free stream velocity V and therefore the dimensionless velocities are $u/V, \dots$. In addition the normal and tangential stresses p and τ can usefully be made dimensionless with twice the stagnation pressure ϱV^2 , leading to the dimensionless stresses $p/\varrho V^2$ and $\tau/\varrho V^2$. The law of mechanical similarity discussed above can therefore be stated as follows: for two geometrically similar systems with the same Reynolds number, the dimensionless quantities $u/V, \dots, p/\varrho V^2$ and $\tau/\varrho V^2$ are only dependent on the dimensionless spatial coordinates $x/d, y/d, z/d$. If the two systems are not mechanically similar but only geometrically similar, the above dimensionless quantities also depend on the quantities V, d, ϱ, μ of both systems. From the principle that physical laws are independent of systems of units, it follows that the dimensionless quantities $u/V, \dots, p/\varrho V^2, \tau/\varrho V^2$ can only be dependent on a dimensionless combination of V, d, ϱ, μ . However the only dimensionless combination of these four quantities is the Reynolds number $Re = V d \varrho / \mu$. This leads us to the result that, for two geometrically similar systems whose Reynolds number is different, the dimensionless quantities of the flow field are only dependent on the dimensionless spatial coordinates $x/d, y/d, z/d$ and the Reynolds number Re .

These dimensional considerations are important in discussing the total force which acts on the body by the fluid flowing past it. This total force

consists of the normal pressures and the shear stresses acting on the surface of the body. If F is a component of the total force in any given direction, we can form a dimensionless force coefficient of the form $F/d^2 \rho V^2$. Instead of choosing the area d^2 it is usual to choose another characteristic surface S of the body, e.g. the face of the body in the free stream direction, which in the case of the sphere is $\pi d^2/4$. The dimensionless force coefficient is therefore $F/S \rho V^2$. Using the above considerations, we see that this dimensionless force coefficient, which represents the integral of $p/\rho V^2$ and $\tau/\rho V^2$ over the surface of the body, can, in the case of geometrically similar systems, only depend on the combination V, d, ρ, μ , and thus on the Reynolds number. The component of the resulting force parallel to the unperturbed free stream direction is denoted the drag D and the component perpendicular to the free stream direction is called the lift L . If, instead of choosing ρV^2 as the reference value, we choose the stagnation pressure $\rho V^2/2$, we find the dimensionless coefficients for the lift and the drag to be

$$c_L = \frac{L}{\frac{\rho}{2} V^2 S} \quad \text{and} \quad c_D = \frac{D}{\frac{\rho}{2} V^2 S}. \quad (1.5)$$

We are led to this result: in the case of geometrically similar systems, i.e. geometrically similar bodies which have the same orientation to the free stream direction, the dimensionless lift and drag coefficients are only dependent on the Reynolds number Re :

$$c_L = f_1(Re); \quad c_D = f_2(Re). \quad (1.6)$$

At this point we emphasise that these important conclusions which have been drawn from the similarity principle with respect to the Reynolds number in this simple form are only valid as long as gravitational forces and elastic forces (in the case of compressible fluids) are not taken into account. Otherwise additional dimensionless coefficients have to be included in the relations. For example, in flows of liquids with a free surface, where the gravitational force is important, the dimensionless Froude number appears:

$$Fr = \frac{V}{\sqrt{gd}}. \quad (1.7)$$

Correspondingly, in the case of high velocity flows, where additional elastic forces occur because of the compressibility of the fluid, the Mach number

$$Ma = \frac{V}{c}, \quad (1.8)$$

where c is the speed of sound, is an important additional dimensionless coefficient.

There is great importance for all of theoretical and experimental fluid mechanics attached to the similarity law given by Eq. (1.6). First of all, the dimensionless coefficients c_L , c_D and Re are independent of the system of units used. Calculating the functions $f_1(Re)$ and $f_2(Re)$ is, in many cases, impossible theoretically, and we have to turn to experiments to determine

them. If we wished, for example, to experimentally determine the drag coefficient c_D of a body, such as a sphere, without knowing the similarity principle with respect to the Reynolds number, we would have four independent parameters V, d, ϱ, μ , leading to an extraordinarily large number of measurements required. But by taking note of the similarity principle with respect to the Reynolds number we find that the dimensionless coefficients of spheres of different diameters d , in flows of different velocities V , in different flowing media with values ϱ and μ are ultimately only dependent on the one variable Re . The way in which Reynolds' similarity law has been confirmed by experiment is shown in Fig. 1.3, where the dependence of the drag coefficient of a flat plate at zero incidence on the Reynolds number is depicted. The

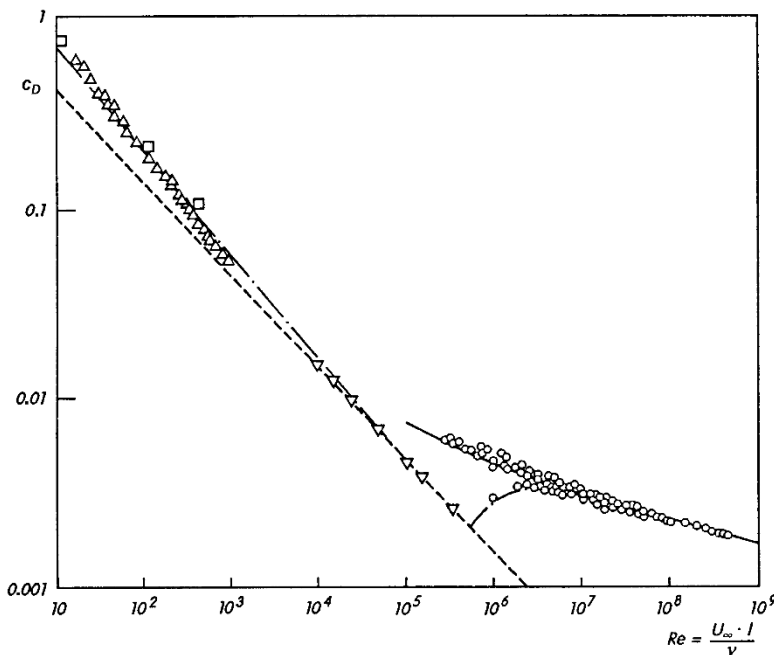


Fig. 1.3. Dependence of drag coefficients of flat smooth plates at zero incidence on the Reynolds number (friction drag of *one* plate side). c_D given in Eq. (1.5), $S = l \cdot b$, l : plate length, b : plate width

measurements:	○	different authors, cf. H. Schlichting (1982), p. 653
	△	Z. Janour (1951)
	▽	K.E. Schoenherr (1932)
theory:	- - -	laminar asymptote, from Eq. (2.10) (Blasius)
	—	turbulent asymptote, from Eq. (2.14)
	- - - -	asymptotic development for laminar flow, from Eq. (14.62)
numerical:	□	solution of Navier–Stokes equations by S.C.R. Dennis, cf. A.E.P. Veldman (1976)

drag coefficients measured for plates of quite different lengths all fit very well along one curve.

The dimensionless coefficients c_L and c_D introduced in Eq. (1.5) are related to flows *past* bodies (e.g. airfoils). But *internal flows* (flows through pipes, diffusers, etc.) are also characterised by dimensionless coefficients. For example, in the case of flows through circular pipes, where x is the coordinate in the flow direction, the pressure gradient dp/dx is characterised by the dimensionless pipe friction factor

$$\lambda = -\frac{d}{\frac{\rho}{2} u_m^2} \frac{dp}{dx}. \quad (1.9)$$

Here d is the diameter of the pipe, ρ is the density and u_m is velocity averaged over the cross-section. When the inner surface of the pipe is smooth, λ is again only a function of the Reynolds number Re , where this is now formed as

$$Re = \frac{\rho u_m d}{\mu} = \frac{u_m d}{\nu} \quad (1.10)$$

with the pipe diameter d and the average velocity u_m . The function $\lambda(Re)$ has been noted from numerous measurements and is shown in Fig. 1.4. As in the case of the flat plate, again here the points are all ordered onto one curve.

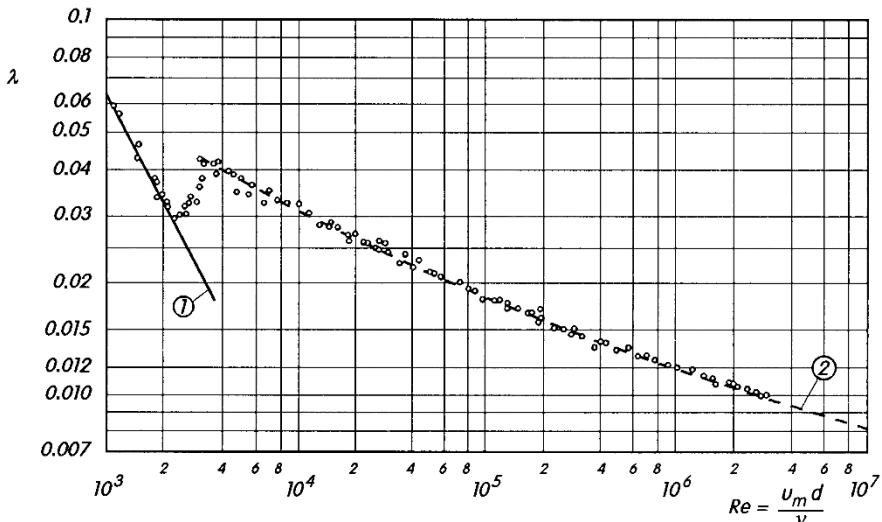


Fig. 1.4. Pipe friction factor for smooth pipes, dependent on the Reynolds number. Definition of λ from Eq. (1.9). Measurements by different authors, cf. H. Schlichting (1982), p. 611.

Curve 1 from Eq. (1.14), laminar, after G. Hagen (1839) and J.L.M. Poiseuille (1940).

Curve 2 from Eq. (2.18), turbulent

Figure 1.5 shows the results of measurements of the drag coefficients of spheres as a function of the Reynolds number and the Mach number by A. Naumann (1953). Here it is interesting to note that the effect of the Reynolds number vanishes for spheres in supersonic flows. This is because the pressures on the back of the sphere, which are more strongly affected by the Reynolds number, lose their influence on the drag compared to the pressures on the front.

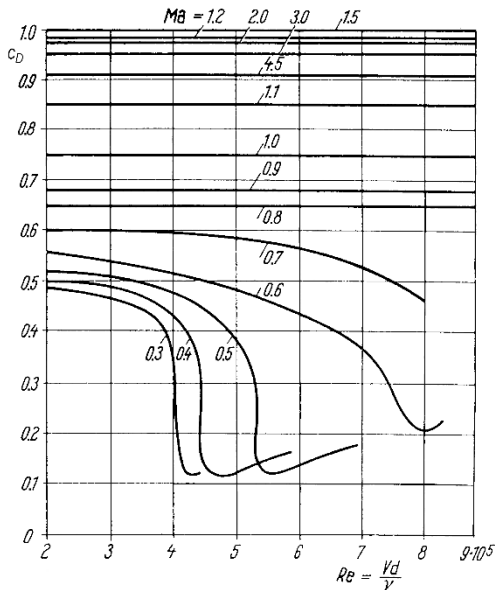


Fig. 1.5. Dependence of the drag coefficient of spheres on the Reynolds number and the Mach number, from measurements by A. Naumann (1953)

1.4 Laminar and Turbulent Flows

In Fig. 1.4, which shows the dependence of the pipe friction factor λ on the Reynolds number, there are clearly two different regions to be seen. Note that both the vertical and horizontal scales are logarithmic. At small Reynolds numbers, λ decreases in a straight line with increasing Re . At the “critical Reynolds number”

$$Re_{\text{crit}} = 2300 \quad (1.11)$$

this decrease stops abruptly, and a sharp increase in λ occurs. As Re increases further, λ then again decreases, but not with as large a slope as before, and no longer in a straight line.

The different behaviour of the curves $\lambda(Re)$ for $Re < Re_{\text{crit}}$ and $Re > Re_{\text{crit}}$ is due to the fact that there are two different kinds of flows. This

knowledge goes back to O. Reynolds (1883), where, in his famous *coloured filament experiment*, he showed the two different flow forms in pipe flow, see Fig. 1.6.

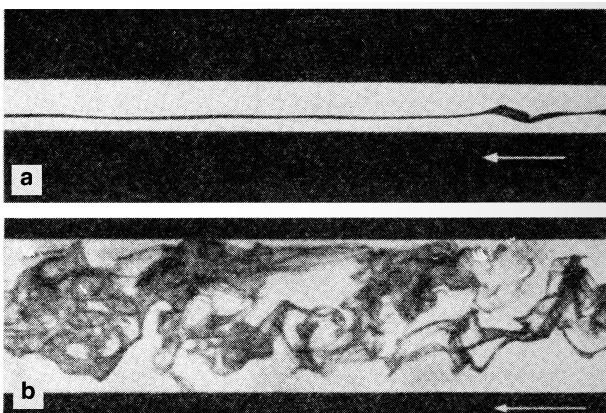


Fig. 1.6. Coloured filament experiment by O. Reynolds (1883). Flow in water made visible by a coloured filament, by W. Dubs (1939)
 (a) laminar flow, $Re=1150$ (b) turbulent flow, $Re = 2520$

A narrow tube is used to add coloured liquid to flowing water. This forms a thin filament of colour which can be viewed through the transparent walls of the pipe and gives an indication of the behaviour of the flow. At low flow velocities, or more precisely, at Reynolds numbers below the critical Reynolds number, straight coloured filaments form and move with the flow parallel to the axis of the pipe. This is a *layered flow*, where layers of fluid move with different velocities without great exchange of fluid particles perpendicular to the flow direction. It is also called *laminar flow*. If the velocity in the pipe flow is increased so that the critical Reynolds number is exceeded, the flow portrait changes dramatically. As in Fig. 1.6b, the coloured filaments carry out highly irregular transverse motions, which quickly lead to a complete scattering and squalling of the colour. This is now *turbulent flow*, characterised by a high irregular, random, *fluctuating motion*. It is superimposed on the regular basic flow and leads to large amounts of mixing perpendicular to the flow direction in the pipe.

There is also a critical Reynolds number visible in the drag coefficient $c_D(Re)$ of a flat plate at zero incidence, see Fig. 1.3. It is

$$Re_{\text{crit}} = 5 \cdot 10^5 . \quad (1.12)$$

For Reynolds numbers which are smaller than Re_{crit} , the flow past the plate is laminar; above Re_{crit} the importance of the turbulence becomes ever greater. The dramatic decrease in the c_D value of spheres at small Mach numbers (e.g. $Ma=0.3$), seen in Fig. 1.5, is also due to a transition from laminar to

turbulent flow. The treatment of laminar and turbulent flows is very different, and they are therefore dealt with in separate parts of this book. The transition from laminar to turbulent flow is also discussed in a chapter of its own. The book is thus subdivided into Parts I to V as follows: introductory chapters on fundamentals (Chaps. 1 to 5), laminar flows (Chaps. 6 to 14), the laminar–turbulent transition (Chap. 15), turbulent flows (Chaps. 16 to 22) and numerical methods (Chap. 23).

1.5 Asymptotic Behaviour at Large Reynolds Numbers

Since many technically important fluids have very low viscosity (e.g. air or water, see Table 3.1 in Chap. 3), the majority of flows in practice are flows with high Reynolds number. Therefore the asymptotic behaviour of dimensionless coefficients at high Reynolds numbers, as seen in Figs. 1.3 and 1.5, is very important. Boundary-layer theory, the topic of this book, deals with precisely this asymptotic behaviour. In other words, boundary-layer theory is a theory to determine the asymptotic behaviour of flows at large Reynolds numbers (i.e. $\text{Re} \rightarrow \infty$).

The limiting case $\text{Re} = \infty$ corresponds to the flow of an ideal fluid, i.e. a fluid with vanishing viscosity. Real flows which have finite but very large Reynolds numbers will then be only slightly different from this limiting case, and they can be considered to be small perturbations from the limiting case. Within the framework of boundary-layer theory, the flow equations are calculated using perturbation theory, where the starting point used is the solution for inviscid flow. Because of the no-slip condition, which in general cannot be satisfied by inviscid flows, we have to deal with *singular* perturbation theory. Boundary-layer theory is the original and classic example of the use of singular perturbation methods. L. Prandtl was the first person to apply a singular perturbation calculation to a partial differential equation. Since then, singular perturbation methods have been applied in many other areas of physics and technology, see e.g. J. Kevorkian; J.D. Cole (1981).

The main difficulty in boundary-layer theory today is that the solution for inviscid flows is not unique. Therefore the starting point for the perturbation theory, the limiting solution, can frequently a priori not be chosen.

1.6 Comparison of Measurements Using the Inviscid Limiting Solution

It can be expected of high Reynolds number flows that they will differ only slightly from the limiting case of inviscid flow. The following examples will be used to demonstrate this.

Pipe flow. The graph of $\lambda(\text{Re})$ in Fig. 1.4 shows quite clearly that λ tends to zero as the Reynolds numbers increases. It emerges from Fig. 1.7 that the velocity profiles become ever more flat, until, at the limit $\text{Re} = \infty$, a homogeneous velocity distribution is reached.

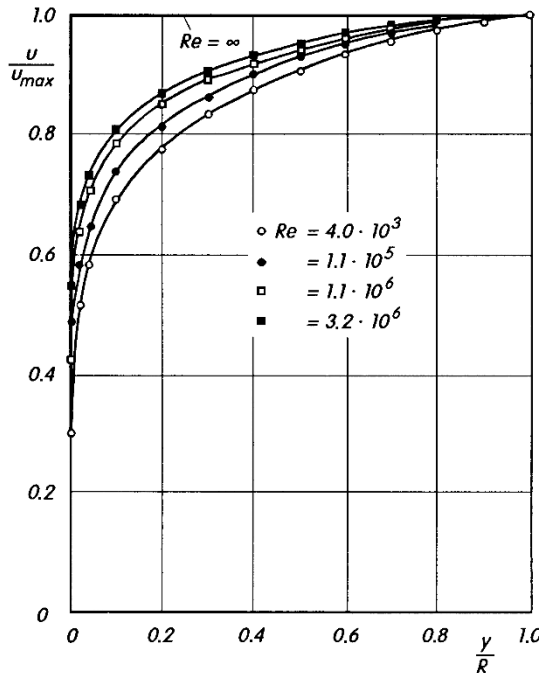


Fig. 1.7. Velocity distribution in a smooth pipe at different Reynolds numbers, from J. Nikuradse (1932)

In principle, one might like to know the asymptotic behaviour for the hypothetical case of what would happen if the pipe flow were to remain laminar for arbitrarily large Reynolds numbers above Re_{crit} . However there is no inviscid limiting solution for laminar pipe flows. When the pipe flow is fully laminar, only the pressure forces and the friction forces are in equilibrium, and inertial forces (proportional to ϱ) do not contribute. Therefore there is no dependence at all on the Reynolds number, which also contains ϱ . The Reynolds number dependence in Fig. 1.4 has been artificially generated. As will be shown in Sect. 5.2.1, the relation

$$-\frac{d^2}{\mu u_m} \frac{dp}{dx} = 32 \quad (1.13)$$

holds for fully developed laminar pipe flow. From dimensional analysis it follows that the dimensionless combination of dp/dx , d , μ and u_m must be a constant. By multiplying the numerator and the denominator in Eq. (1.13) by the density ϱ , we obtain the Hagen–Poiseuille pipe drag law for laminar pipe flows

$$\lambda = \frac{64}{\text{Re}} . \quad (1.14)$$

In Fig. 1.4, where both scales are logarithmic, this law is depicted as a straight line with a negative slope of one.

In contrast to laminar pipe flows, in the case of turbulent pipe flows there is also a contribution from the inertial forces. This is due to the turbulent fluctuating motion. Here a real Reynolds number dependence occurs, cf. Sect. 2.4.

Plate. According to Fig. 1.3, the c_D value for a flat plate at zero incidence tends to zero for large Reynolds numbers, both for the turbulent case and for the hypothetical purely laminar case. In both cases the inviscid boundary solution is therefore a simple translation flow (homogeneous velocity distribution).

Airfoil. Figure 1.8 shows the pressure distribution measured for a symmetric airfoil at zero angle of incidence and compares it to the inviscid solution. Setting aside what happens at the trailing edge, the differences are small. Because of the finite angle at the trailing edge, the inviscid solution gives rise to a stagnation point there, and, compared to viscous flows, to a sharply increased pressure.

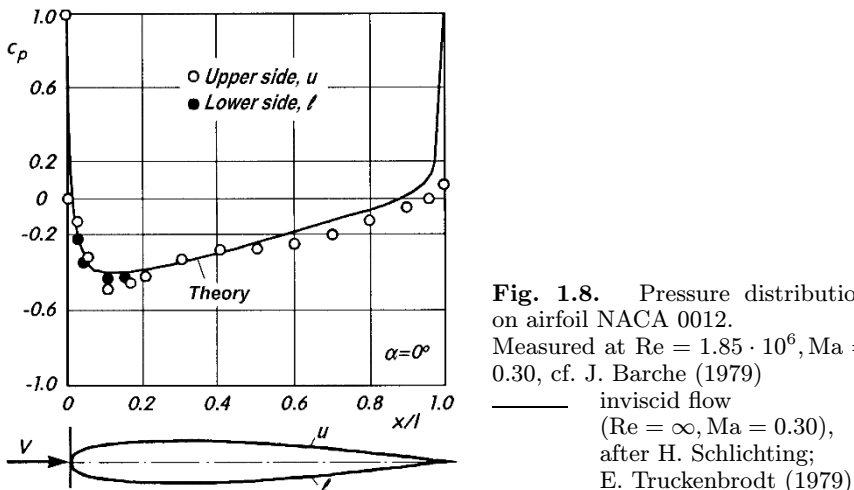


Fig. 1.8. Pressure distribution on airfoil NACA 0012.
Measured at $Re = 1.85 \cdot 10^6$, $Ma = 0.30$, cf. J. Barche (1979)

— inviscid flow
($Re = \infty, Ma = 0.30$),
after H. Schlichting;
E. Truckenbrodt (1979)

In Fig. 1.9 we find similarly good agreement for a cambered NACA airfoil with angle of attack $\alpha = 8^\circ$. In this example there are actually infinitely many inviscid limiting solutions. The solution where there is no flow around the trailing edge is the one which was chosen. This requirement of smooth flow past the trailing edge, known as the *Kutta condition*, follows from a physical property of viscous flows, where flow around a cusp at infinitely large velocities is impossible.

The dependence of the lift coefficient c_L on the angle of attack α is shown for the same NACA airfoil at the same Reynolds number in Fig. 1.10. Whereas the limiting solution $Re = \infty$ leads to vanishing drag (D'Alembert's paradox), the lift curve shows good approximation to the flow at $Re = 3 \cdot 10^6$.

The pressure distribution on an airfoil in a transonic flow is shown in Fig. 1.11. Both the measurements and the limiting solution show a sudden increase in the pressure on the upper side. This is due to a shock wave which occurs there. However, because of the effects of viscosity (displacement effect), the shock wave lies somewhat upstream compared to its position in the limiting case $Re = \infty$. Otherwise the limiting solution is a very good approximation. In contrast to the case of incompressible inviscid flows, the limiting solution $Re = \infty$ gives rise

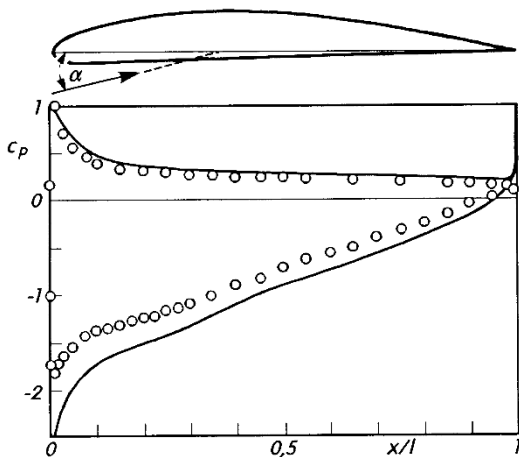


Fig. 1.9. Pressure distribution on airfoil NACA 4412 at angle of attack $\alpha = 8^\circ$, after R.M. Pinkerton (1936)

○ measurement, $Re = 3 \cdot 10^6$
 — theory, $Re = \infty$

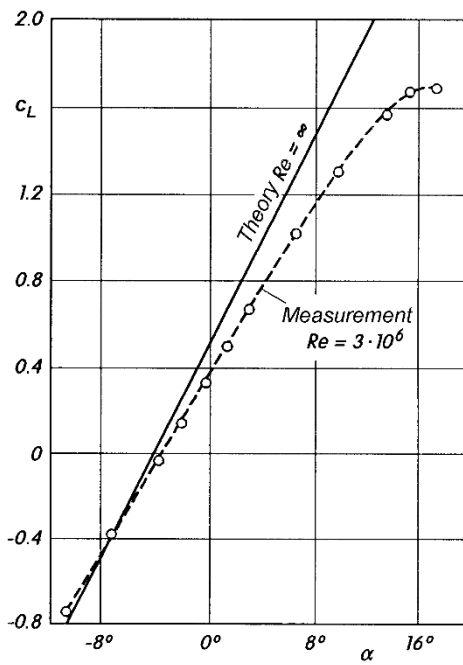


Fig. 1.10. Lift on the NACA 4412 airfoil, after R.M. Pinkerton (1936)
 Airfoil as in Fig. 1.9

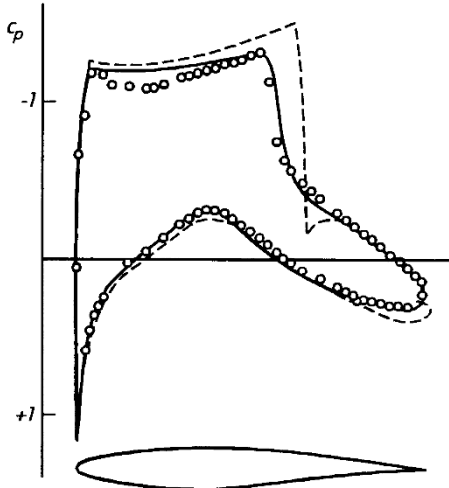


Fig. 1.11. Pressure distribution on airfoil RAE 2822 in transonic flow, after M.A. Schmatz (1986)
 $Ma = 0.73, \alpha = 2.8^\circ$
○ measurements, $Re = 6.5 \cdot 10^6$,
after J. Barche (1979),
 $c_D = 0.013; c_L = 0.72$
--- limiting solution for $Re = \infty$
— theory for $Re = 6.5 \cdot 10^6$,
see Sect. 19.2.6

to a finite drag in the case of transonic and supersonic flows. The shock waves which occur in these flows are connected with dissipation and the resulting loss in energy leads to a finite form drag, although small close to the speed of sound.

Circular cylinder. Figure 1.12 shows the drag coefficient $c_D = 2D/(\rho V^2 bd)$ as a function of the Reynolds number for a circular cylinder placed transversely in a flow. As in the similar case of the sphere at $Ma = 0.3$ shown in Fig. 1.5, there is a dramatic drop in the c_D value to be seen at the critical Reynolds number

$$Re_{\text{crit}} = 4 \cdot 10^5. \quad (1.15)$$

For subcritical Reynolds numbers $Re < Re_{\text{crit}}$, the flow past the cylinder is laminar. For large subcritical Reynolds numbers a constant drag coefficient of $c_D = 1.2$ is seen. This could possibly hint at an asymptotic state for the hypothetical case if the flow were to remain laminar at arbitrarily high Reynolds numbers. A typical pressure distribution from this Reynolds number regime ($Re = 10^5$) is shown in Fig. 1.13.

From the pressure distribution of inviscid flow past a circular cylinder, seen in Fig. 1.14a to be symmetric (the front and back are the same), we find that this flow is clearly unsuitable as a limiting solution. However there are other inviscid flows past a circular cylinder, and the well-known Kirchhoff–Helmholtz solution in Fig. 1.14b seems more reasonable. A particular characteristic of this flow is that it has two lines of discontinuity. These so-called free streamlines leave the contour of the cylinder tangentially with an angle of $\Theta_S = 55^\circ$ (the Brillouin–Villat condition) and separate the outer area with the total pressure of the free stream from the so-called “dead water” region, where the fluid is at rest and the pressure is that of the free stream. At the free streamlines, the total pressure, i.e. the difference of the total pressure inside and outside the free streamlines, is equal to the stagnation pressure of the free stream. The pressure distribution here is shown in Fig. 1.13. By integration, a non-zero form drag with a coefficient $c_D = 0.5$ is obtained for this inviscid flow. This value deviates considerably from the measured value of $c_D = 1.2$. To understand this deviation, we can look at an investigation by A. Roshko (1967). The essential result is recorded in Fig. 1.15. By introducing a splitter plate behind the cylinder the negative pressure at the back could be reduced considerably, i.e. the

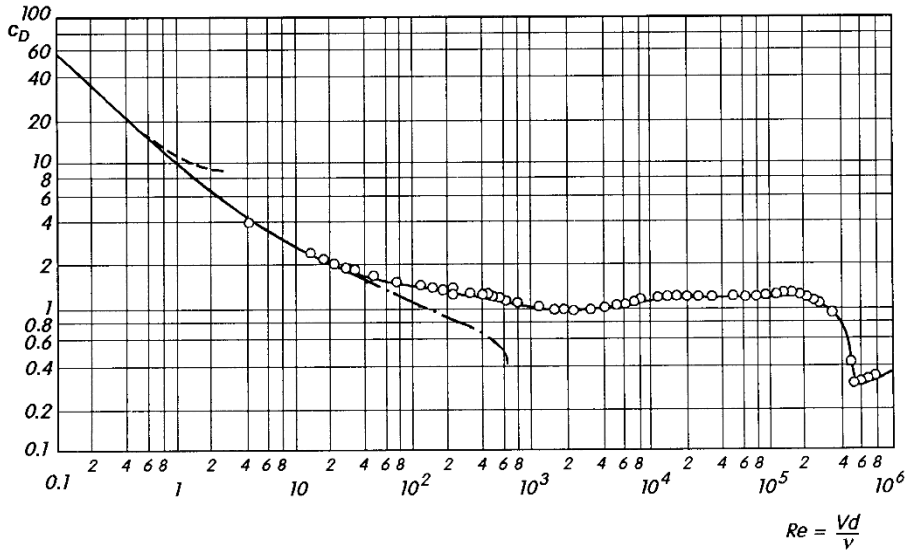


Fig. 1.12. Circular cylinder: drag coefficient vs. Reynolds number
 ○ measurements by C. Wieselsberger, see H. Schlichting (1982), p. 17
 - - - asymptotic formula for $Re \rightarrow 0$: $c_D = \frac{8\pi}{Re} [\Delta - 0.87 \Delta^3 + \dots]$,
 with $\Delta = [\ln(7.406/Re)]^{-1}$, $Re = Vd/\nu$, $c_D = 2D/(\rho V^2 bd)$
 - - - numerical results by A.E. Hamielec; J.D. Raal (1969) and
 B. Fornberg (1985) for steady flow
 $Re = 300$: steady: $c_D = 0.729$, after B. Fornberg (1985)
 unsteady: $c_D = 1.32$, after R. Franke; B. Schönung (1988)

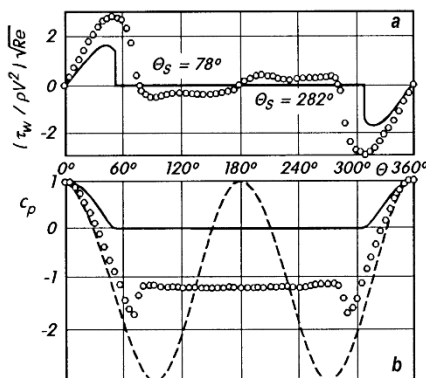


Fig. 1.13. Subcritical flow at a circular cylinder,
 ○ measurements at $Re = 10^5$,
 after E. Achenbach (1968)
 - - - symmetric limiting solution,
 from Fig. 1.14a
 — limiting solution by Kirchhoff-Helmholtz, see Fig. 1.14b
 Θ: peripheral angle,
 Θ_S : separation angle
 (a) distribution of wall shear stress,
 (b) distribution of wall pressure
 $c_p = 2(p - p_\infty)/(\rho V^2)$

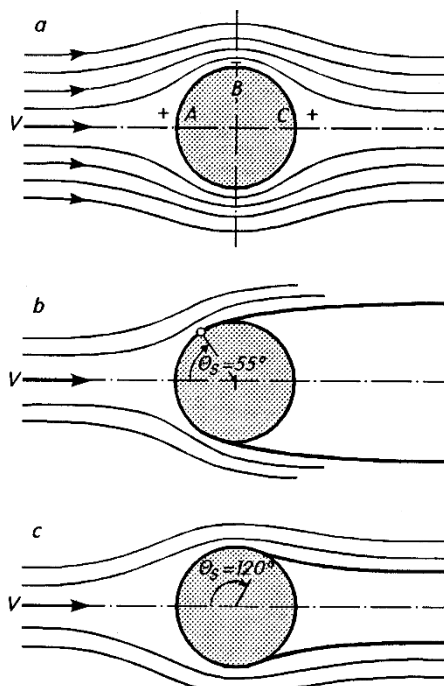


Fig. 1.14. Limiting solution ($Re = \infty$) for incompressible flow at a circular cylinder

- (a) symmetric flow
- (b) Kirchhoff-Helmholtz solution for subcritical flow
- (c) "fictitious body" solution for supercritical flow

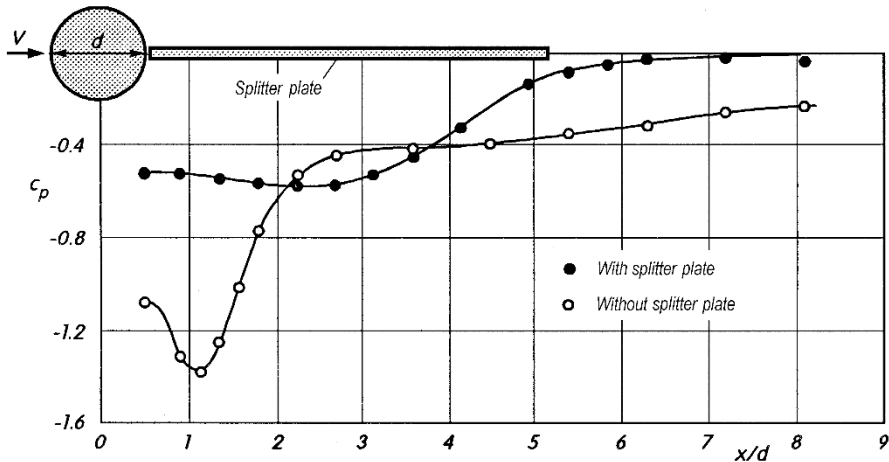


Fig. 1.15. Effect of a splitter plate in the wake of a circular cylinder, after A. Roshko (1967). $Re = 14\,500$, the laminar-turbulent transition takes place immediately after laminar separation

pressure coefficient at the back of the cylinder was changed from $c_p = -1.1$ to $c_p = -0.5$. This effect comes from the fact that, in spite of steady free stream, the flow at these high subcritical Reynolds numbers is not steady at all. Rather, there is a strongly oscillating flow due the alternating formation of vortices on the upper and lower halves of the back of the cylinder. Figure 1.16 shows an instantaneous picture of this flow.

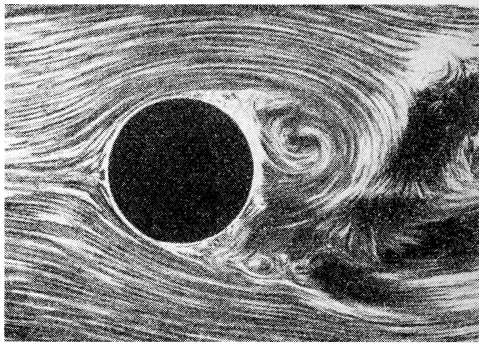


Fig. 1.16. Snapshot of the completely separated flow behind a circular cylinder, after L. Prandtl; O. Tietjens (1929, 1931)

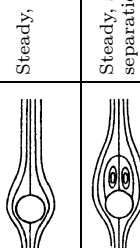
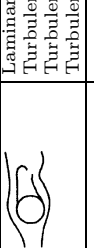
Table 1.1 by M.V. Morkovin (1964) summarises the different regions in cylinder flow. In the subcritical Reynolds number region we find periodic flow whose frequency is independent of the Reynolds number. The dimensionless frequency is called the *Strouhal number*

$$\text{Sr} = \frac{fd}{V}. \quad (1.16)$$

In the subcritical region it has the value $\text{Sr} = 0.21$. The measurement points for this region in Figs. 1.12 and 1.13 are therefore mean values of periodically oscillating values. The vortices which can clearly be seen in Fig. 1.16 obviously produce an increased negative pressure at the back of the cylinder. By introducing the splitter plate, the periodic production of vortices is halted, or at least drastically reduced, and the dead water pressure which governs the form drag is considerably lowered. In this manner, the drag coefficient of a flow, hypothetically assumed to be steady and laminar, at high Reynolds number past a cylinder would be $c_D = 0.5$. Thus the Kirchhoff–Helmholtz solution with the free streamlines depicted in Fig. 1.14b comes into play as a limiting solution. This idea is also supported by numerical results, cf. K. Gersten (1982b) and A.P. Rothmayer (1987). However, according to more recent investigations by B. Fornberg (1987), D.H. Peregrine (1985) and F.T. Smith (1985), the flow seems to be more complicated than this.

Table 1.1. Flow regimes at a circular cylinder (incompressible flow)

Reynolds number $\text{Re} = V d / \nu$
 Strouhal number $\text{Sr} = f d / V$

Reynolds number regime	Flow regime	Flow form	Flow characteristic	Strouhal number Sr_f	Drag coefficient c_D	Separation angle Θ_S
$\text{Re} \rightarrow 0$	Creeping flow		Steady, no wake	—	see Fig. 1.12	—
$3 - 4 < \text{Re} < 30 - 40$	Vortex pairs in wake		Steady, symmetric separation	—	$1.59 < c_D < 4.52$ ($\text{Re} = 30$) ($\text{Re} = 40$)	$130^\circ < \Theta_S < 180^\circ$ ($\text{Re} = 35$) ($\text{Re} = 5$)
$30 - 40 < \text{Re} < 80$	Onset of Karman vortex street		Laminar, unstable wake	—	$1.17 < c_D < 1.59$ ($\text{Re} = 100$) ($\text{Re} = 30$)	$115^\circ < \Theta_S < 130^\circ$ ($\text{Re} = 90$) ($\text{Re} = 35$)
$80 - 90 < \text{Re} < 150$	Pure Karman vortex street		Karman vortex street	$0.14 < \text{Sr} < 0.21$	$c_D \approx 1.2$	$\Theta_S \approx 80^\circ$
$150 < \text{Re} < 300$	Subcritical regime		Laminar, with vortex street instabilities	$\text{Sr} = 0.21$	$c_D \approx 1.2$	$\Theta_S \approx 80^\circ$
$300 < \text{Re} < 1.3 \cdot 10^5$	Critical regime		Laminar separation Turbulent reattachment Turbulent separation Turbulent wake	No preferred frequency	$0.2 < c_D < 1.2$	$80^\circ < \Theta_S < 140^\circ$
$1.3 \cdot 10^5 < \text{Re} < 3.5 \cdot 10^6$	Supercritical regime (transcritical)		Turbulent separation	$0.25 < \text{Sr} < 0.30$	$c_D \approx 0.6$	$\Theta_S \approx 115^\circ$

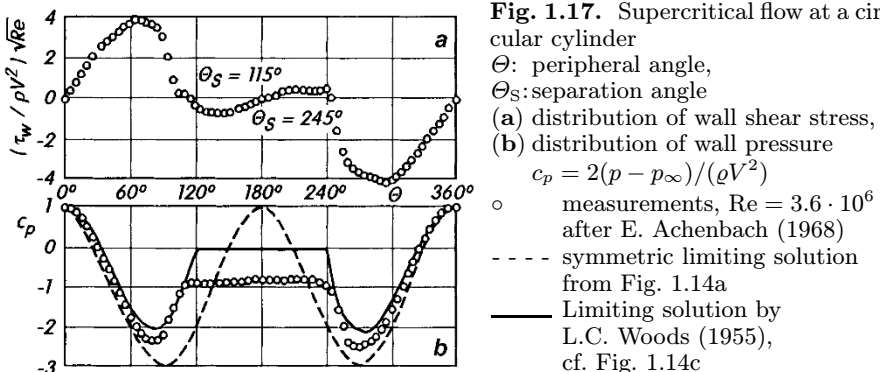


Fig. 1.17. Supercritical flow at a circular cylinder

Θ : peripheral angle,

Θ_S : separation angle

(a) distribution of wall shear stress,
(b) distribution of wall pressure

$$c_p = 2(p - p_\infty) / (\rho V^2)$$

- measurements, $Re = 3.6 \cdot 10^6$
after E. Achenbach (1968)
- - - symmetric limiting solution
from Fig. 1.14a
- Limiting solution by
L.C. Woods (1955),
cf. Fig. 1.14c

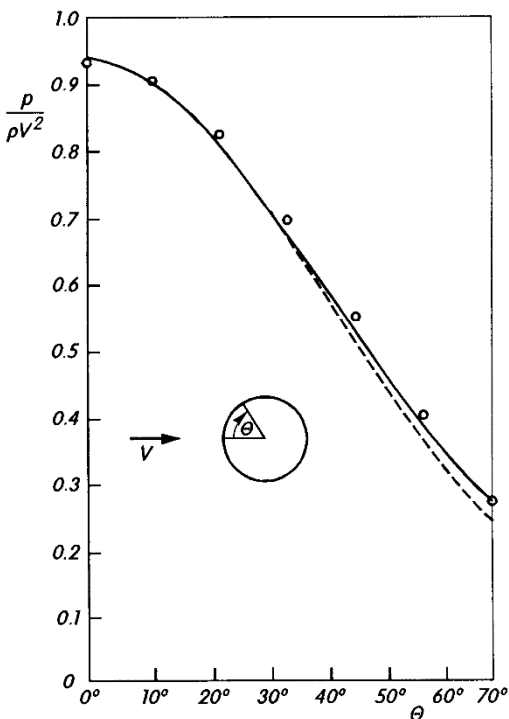


Fig. 1.18. Pressure at a circular cylinder at $Ma = 4.02$

- measurements at
 $Re = 1030$, cool
model, after O.K. Tewfik; W.H. Giedt (1959)

Theory by K. Oberländer
(1974):

- - - limiting solution
($Re = \infty$)

— solution for $Re = 1030$

For supercritical Reynolds numbers $Re > Re_{crit}$ there are also indications of an asymptotic limiting value of $c_D = 0.6$ (see Fig. 1.12 and Table 1.1). Here also the limiting solution is an inviscid flow with free streamlines corresponding to Fig. 1.14c, cf. L.C. Woods (1955) and R.V. Southwell; G. Vaisey (1948). A comparison of the pressure distribution of a possible limiting solution by L.C. Woods (1955) with measurements at $Re = 3.6 \cdot 10^6$ is shown in Fig. 1.17. Although the agreement is very good, it must be explicitly pointed out that the supercritical flows past

a circular cylinder are periodic flows and therefore the measured values oscillate periodically about an average pressure coefficient. On the other hand a steady solution was assumed for the limiting solution.

For further investigations on flows past circular cylinders see H. Schlichting (1982), R. Franke; B. Schönung (1988), E. Achenbach (1968), E. Achenbach (1971) as well as E. Achenbach; E. Heinecke (1981).

As in the case of the sphere in Fig. 1.15, the effect of the Reynolds number becomes less the higher the Mach number, i.e. the form drag predominates, cf. A. Naumann; H. Pfeiffer (1962). Figure 1.18 shows a comparison of the pressure distributions at a circular cylinder at Mach number $Ma = 4$ by K. Oberländer (1974). Here too there are only small deviations between measurements at $Re = 1030$ and the limiting solution. The perturbed limiting solution also shown will be treated in Sect. 14.2.

As seen in Fig. 1.5, the critical Reynolds number in flow past a sphere increases with increasing Mach number, so that for subsonic flows, subcritical conditions exist up to $Re = 10^6$. The form drag is then independent of the Reynolds number and agrees well with the limiting solution $Re = \infty$, as shown by, for example, W.D. Hayes; R.F. Probstein (1959).

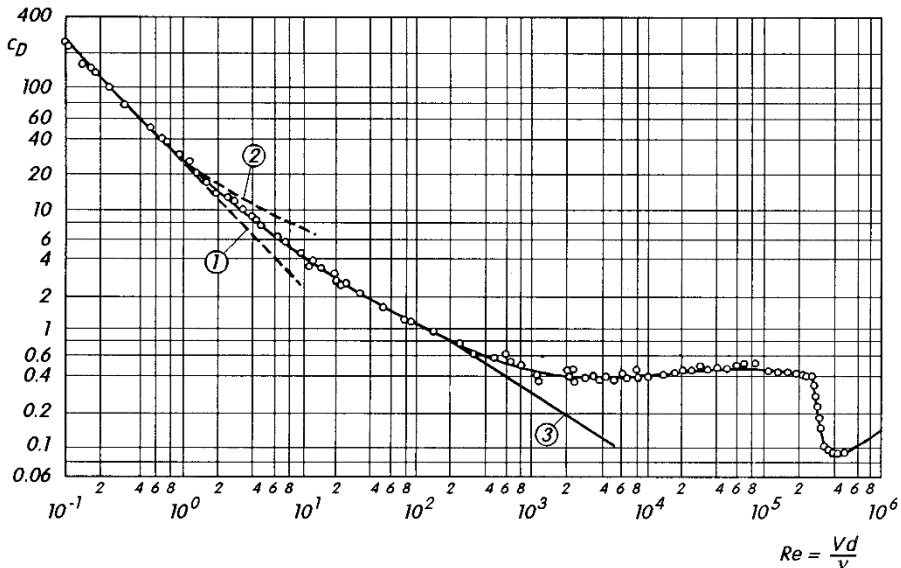


Fig. 1.19. Dependence of the drag coefficient of spheres on the Reynolds number
 Curve 1: theory, after G.G. Stokes (1856), $c_D = 24/Re$
 Curve 2: theory, after C.W. Oseen (1911), $c_D = 24/Re[1 + 3Re/16]$
 For the extension of this theory for higher Reynolds numbers,
 cf. M. Van Dyke (1964b)
 Curve 3: numerical results, after B. Fornberg (1988)
 Onset of unsteady flow at $Re = 200$, cf. U. Dallmann et al. (1993)

Sphere. The flow past a sphere is very similar to the flow past a cylinder. The drag diagram for the sphere in Fig. 1.19 corresponds to Fig. 1.12 for the cylinder. Again the subcritical and the supercritical states can be distinguished at high Reynolds numbers. Figure 1.20 shows two typical experimentally determined pressure distributions for these two states, cf. E. Achenbach (1972). At high Reynolds numbers there are deviations from the axial symmetry and unsteady processes occur, as shown by U. Dallmann et al. (1993) and B. Schulte-Werning; U. Dallmann (1991), and also E. Achenbach (1974a). The effect of the Mach number on the sphere's drag has already been shown in Fig. 1.5. E. Achenbach (1974b) has shown how the flow past a sphere depends on the roughness of the surface.

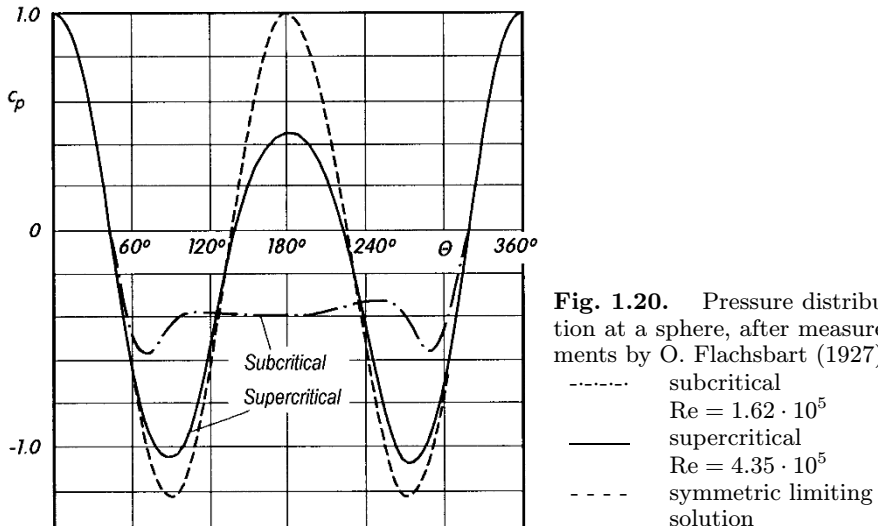


Fig. 1.20. Pressure distribution at a sphere, after measurements by O. Flachsbart (1927)

- - - subcritical
 $Re = 1.62 \cdot 10^5$
- supercritical
 $Re = 4.35 \cdot 10^5$
- · - symmetric limiting solution

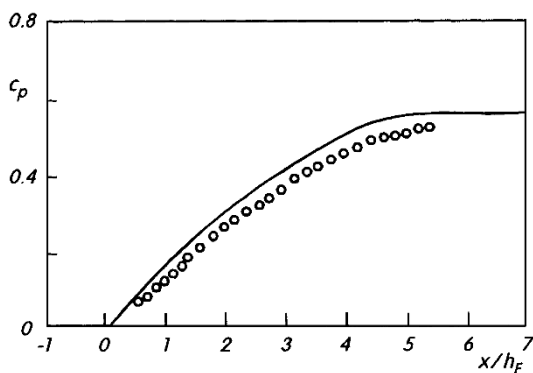


Fig. 1.21. Wall pressure in a plane diffuser $AR = 1.6$; $l/h_E = 6$, after K. Gersten; H.G. Pagen-darm (1983)

- measurements at
 $Re = 10^5$, $B = 0.061$
- limiting solution
($Re = \infty$, $B = 0$)

Diffuser. Apart from the pipe flow, all the flows above were *external* flows. Another example of an *internal* flow is the case of the technically extremely important diffuser. Figure 1.21 compares the pressure distribution at the wall of a plane diffuser with the limiting solution. For a given geometry, the diffuser flow is characterised by two dimensionless fluid mechanical coefficients. As well as the Reynolds number $\text{Re} = u_{mE} h_E / \nu$, the *blockage*

$$B = \left(1 - \frac{\bar{u}}{\bar{u}_{\max}}\right)_E \quad (1.17)$$

also appears as a measure of the lack of uniformity of the velocity distribution of the free stream. The index E implies the entrance conditions. In the limiting case, both coefficients reach their limiting values $\text{Re} = \infty$ and $B = 0$. The pressure distributions at the wall for the measurements at $\text{Re} = 10^5$ and for the limiting solution are very similar, and the differences are due to the viscosity and the blockage. The desired pressure rise in the diffuser is decreased by these effects, and optimum diffusers have a relative reduction in the pressure rise of about 10%.

1.7 Summary

In internal and external flows, the action of the flow can be divided into pressure forces (normal forces) and shear forces (tangential forces). As the examples have shown, the pressure distributions at bodies in flows at high Reynolds numbers and in the limiting case of inviscid flows are quite similar. Therefore, it seems obvious to begin with these limiting solutions and to deal with the differences from real (viscous) flows through corrections to the limiting solution. This is the basic idea of boundary-layer theory. Naturally the inviscid limiting solution cannot provide the shear forces, i.e. friction forces, which are important in determining the friction drag and friction losses (dissipation). The object of boundary-layer theory is to determine this force in particular. One of the main difficulties in the theory is that the limiting solution is sometimes a priori unknown for a given flow. This is because the inviscid solutions are not unique. Frequently the limiting solution is obvious, for example, for symmetry reasons (fully turbulent pipe flows, symmetric flow past thin airfoils, diffusers with moderate pressure increase). In many cases however the uniqueness of the limiting solution must be produced through additional conditions, for example, the Kutta condition (smooth flow-off at trailing edge of thin airfoils with small angle of attack). Difficulties then arise when no definite statement is possible about the limiting solution (circular cylinder, sphere, airfoil with large angle of attack, diffuser with strong pressure increase). Frequently the concept of a hypothetical limiting solution must be used. Then, for example, purely laminar or purely steady flows are assumed for high Reynolds numbers, even though the real flow has different behaviour.

The drag of bodies in flows consists of the pressure or form drag (integral of the pressure or normal forces over the body's surface) and the friction drag (integral of the shear or tangential forces). In the case of blunt bodies,

like cylinders and spheres, the form drag dominates. This is given to good approximation by the inviscid limiting case. Boundary-layer theory can be used to determine the friction drag and corrections to the form drag due to the viscosity.

A further possibility to determine the limiting solutions a priori consists of coupling the limiting process $\text{Re} \rightarrow \infty$ with a variation in the geometry considered. This can be used in the case of, for example, the flow at a rounded backward-facing step, where separation occurs for finite Reynolds numbers. This can be developed from the limiting solution of a plate at zero incidence, providing the step height goes to zero as $\text{Re} \rightarrow \infty$. Both limiting processes must, however, be suitably coupled to each other. Where separation occurs in a flow, the limiting solution can often be chosen to be that flow where the geometry is changed just so that there is no separation (*marginal separation*). These more recent further developments in boundary-layer theory will be discussed in Chap. 14.

2. Fundamentals of Boundary–Layer Theory

2.1 Boundary–Layer Concept

Flows of fluids with low viscosity values and thus very high Reynolds numbers occur in many technical applications. As was shown in the examples from the last chapter, the limiting solution $\text{Re} = \infty$ is often a good approximation. A notable shortcoming of this limiting solution is that the no-slip condition is not satisfied, i.e. the velocities at the wall are not zero but are finite. The viscosity must be taken into account in order to satisfy the no-slip condition. This takes care of the velocity transition from the limiting solution's finite value close to the wall to the value of zero directly at the wall. At large Reynolds numbers this transition takes place in a thin layer close to the wall, called by L. Prandtl (1904) the *boundary layer* or *frictional layer*. As will be shown, the boundary layer is thinner the higher the Reynolds number, i.e. the smaller the viscosity.

The concept of the boundary layer, therefore, implies that flows at high Reynolds numbers can be divided up into two unequally large regions. In the bulk of the flow region, the viscosity can be neglected, and the flow corresponds to the inviscid limiting solution. This is called the inviscid outer flow. The second region is the very thin boundary layer at the wall where the viscosity must be taken into account.

Within the boundary layer the two different flow forms mentioned in the previous chapter can both occur, that is, the flow can be laminar or turbulent. One then speaks of laminar boundary–layer flows, or laminar boundary layers for short, and equivalently of turbulent boundary layers.

It will be seen later that the division of the flow field into the inviscid outer flow and the boundary layer leads to considerable simplifications in the theoretical treatment of high Reynolds number flows. In fact it is only due to this idea of Prandtl that any theoretical headway could be made on these flows at all.

Before coming to the focus of this book, the mathematical theory, this chapter will be used to explain the main concepts of boundary layers purely physically, without using any mathematical methods.

2.2 Laminar Boundary Layer on a Flat Plate at Zero Incidence

Figure 2.1 is a snapshot of the flow along a thin flat plate which is being dragged through water. Aluminium particles have been sprinkled on the surface of the water to make the streamlines visible. The length of each particle streak is proportional to the flow velocity. It can be seen that directly at the wall is a thin layer where the velocity is considerably lower than it is at some distance from the wall. The thickness of this layer increases along the plate from front to back. In Fig. 2.2 the velocity distribution in this boundary layer on the plate is shown schematically, where the dimension in the transverse direction is enlarged greatly. At the leading edge there is a constant velocity distribution perpendicular to the plate. As the distance from the leading edge gets larger, the layer of particles slowed down by the friction becomes ever larger, since more and more fluid particles are caught up by the retardation. The thickness of the boundary layer $\delta(x)$ is therefore a monotonically increasing function of x . Here, however, it must be made absolutely clear that the concept of boundary-layer thickness δ has been artificially introduced. The transition from boundary-layer flow to outer flow, at least in the case of laminar flows, takes place continuously, so that a precise boundary cannot, in principle, be given. Since the concept of boundary-layer thickness is so vivid, it is very often used in practice. Frequently the boundary is arbitrarily given as being at the point where the velocity reaches a certain percentage of the outer velocity, e.g. 99%. For clarity, an index is often used, e.g. δ_{99} .

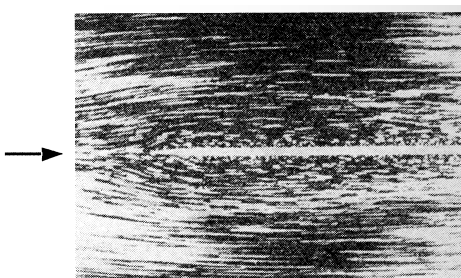


Fig. 2.1. Flow along a thin flat plate, after L. Prandtl; O. Tietjens (1931)

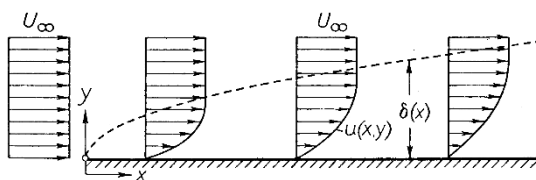


Fig. 2.2. Boundary layer at a flat plate at zero incidence (schematic)

Estimation of the boundary-layer thickness. For laminar plate boundary layers the boundary-layer thickness can easily be estimated as follows: in the boundary layer the inertial forces and the friction forces are in equilibrium. As was explained in Sect. 1.3, the inertial force per unit volume is equal to $\varrho u \partial u / \partial x$. For a plate of length x , $\partial u / \partial x$ is proportional to U_∞ / x , where U_∞ is the velocity of the outer flow. Thus the inertial force is of the order of magnitude $\varrho U_\infty^2 / x$. On the other hand, the friction force per unit volume is equal to $\partial \tau / \partial y$, and in laminar flows this is equal to $\mu \partial^2 u / \partial y^2$, by assumption. The velocity gradient perpendicular to the wall $\partial u / \partial y$ is of order U_∞ / δ , so that for the friction force per unit volume $\partial \tau / \partial y \sim \mu U_\infty / \delta^2$. Setting the inertial and friction forces equal we reach the relation

$$\mu \frac{U_\infty}{\delta^2} \sim \frac{\varrho U_\infty^2}{x}$$

or, solved for the boundary-layer thickness δ :

$$\delta \sim \sqrt{\frac{\mu x}{\varrho U_\infty}} = \sqrt{\frac{\nu x}{U_\infty}} . \quad (2.1)$$

The unknown numerical factor remaining in this equation can be determined from the exact solution of H. Blasius (1908) which is fully treated in Chap. 6. For the laminar boundary layer at a plate at zero incidence we have:

$$\delta_{99}(x) = 5 \sqrt{\frac{\nu x}{U_\infty}} . \quad (2.2)$$

The dimensionless boundary-layer thickness related to the plate length l is then

$$\frac{\delta_{99}(x)}{l} = \frac{5}{\sqrt{\text{Re}}} \sqrt{\frac{x}{l}} , \quad (2.3)$$

where $\text{Re} = U_\infty l / \nu$ is the Reynolds number formed with the plate length l . We see from Eq. (2.3) that the boundary-layer thickness decreases with increasing Reynolds number, so that in the limiting case $\text{Re} = \infty$ the boundary layer does indeed vanish. In addition we see from Eq. (2.3) that the boundary-layer thickness grows in proportion to \sqrt{x} .

Displacement thickness. As already stated, the boundary-layer thickness has been introduced arbitrarily. A correct and fluid mechanically interpretable measure for the thickness of the boundary layer is the *displacement thickness* δ_1 . It is defined by

$$U \delta_1(x) = \int_{y=0}^{\infty} (U - u) dy . \quad (2.4)$$

U is the velocity on the outer edge of the boundary layer at the position x . From this, the two shaded areas in Fig. 2.3 must be equal. The displacement

thickness tells us how far the streamlines of the outer flow are displaced by the boundary layer. For a plate at zero incidence we have

$$\frac{\delta_1(x)}{l} = \frac{1.721}{\sqrt{\text{Re}}} \sqrt{\frac{x}{l}}, \quad (2.5)$$

i.e. the displacement thickness δ_1 is about 1/3 of the boundary-layer thickness δ_{99} .

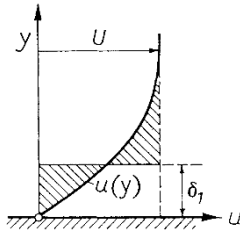


Fig. 2.3. Displacement thickness δ_1 of the boundary layer

Estimation of the friction forces. As with the boundary-layer thickness, the wall shear stress τ_w and thus the entire friction drag of the plate can also be estimated. According to Newton's law of friction, Eq. (1.2), we have:

$$\tau_w(x) = \mu \left(\frac{\partial u}{\partial y} \right)_w, \quad (2.6)$$

where the index w denotes the value at the wall. Using $\partial u / \partial y \sim U_\infty / \delta$ we find $\tau_w \sim \mu U_\infty / \delta$, and inserting the value of δ from Eq. (2.1),

$$\tau_w(x) \sim \mu U_\infty \sqrt{\frac{\rho U_\infty}{\mu x}} = \sqrt{\frac{\mu \rho U_\infty^3}{x}}. \quad (2.7)$$

Therefore the wall shear stress is proportional to $U_\infty^{3/2}$, and, particularly worth emphasising, to $1/\sqrt{x}$. The wall shear stress of a flat plate is therefore not a constant, but a function which decreases monotonically with x . The shear stresses are particularly large close to the leading edge of the plate. Using $\tau_w \sim \mu U_\infty / \delta$ it follows that the wall shear stress is inversely proportional to the boundary-layer thickness, i.e. the thinner the boundary layer the higher the wall shear stress. The constant of proportionality in Eq. (2.7) can again be determined from the exact solution, see Chap. 6. Therefore the *skin-friction coefficient* is

$$c_f = \frac{\tau_w(x)}{\frac{1}{2} \rho U_\infty^2} = \frac{0.664}{\sqrt{\text{Re}}} \sqrt{\frac{l}{x}}. \quad (2.8)$$

Knowing the relation of the wall shear stress to position $\tau_w(x)$, integration can be used to determine the entire friction drag. A plate wetted on one side with breadth b and length l has a friction drag of

$$D = b \int_0^l \tau_w(x) dx . \quad (2.9)$$

With Eq. (2.8), the drag coefficient related to the wetted surface $S = b \cdot l$ follows as

$$c_D = \frac{D}{\frac{\rho}{2} U_\infty^2 \cdot b \cdot l} = \frac{1.328}{\sqrt{\text{Re}}} . \quad (2.10)$$

This drag law is depicted in Fig. 1.3. The asymptotic character of this law can be seen, and for Reynolds numbers $\text{Re} > 10^4$ the measurements are very close to the theory.

2.3 Turbulent Boundary Layer on a Flat Plate at Zero Incidence

As was already mentioned in connection with Fig. 1.3, in reality the boundary layer on a plate does not always remain laminar. After a certain distance $x = x_{\text{crit}}$ (from the leading edge of the plate), the boundary layer becomes turbulent. In analogy to Eq. (1.12), the *critical* Reynolds number formed with the distance to the transition point is

$$\text{Re}_{x \text{ crit}} = \left(\frac{U x}{\nu} \right)_{\text{crit}} = 5 \cdot 10^5 \quad (\text{plate}) . \quad (2.11)$$

The boundary layer on a plate is laminar close to the leading edge and becomes turbulent further downstream, whereby the position of the transition point x_{crit} can be determined by the critical Reynolds number $\text{Re}_{x \text{ crit}}$ given. Although the transition from laminar to turbulent is a region of finite length, a transition point is used for simplicity and it is frequently assumed that the transition is sudden (see the footnote on p. 437). The numerical value of Re_{crit} is strongly dependent on how free from perturbation the outer flow is. In strongly perturbed flow $\text{Re}_{\text{crit}} = 3 \cdot 10^5$ is typical, whereas for particularly smooth flow values of $\text{Re}_{\text{crit}} = 3 \cdot 10^6$ have been reached, cf. Chap. 15.

The first investigations into the laminar–turbulent transition in the boundary layer were carried out by B.G. Van der Hegge Zijnen (1924), J.M. Burgers (1924) and M. Hansen (1928). The transition from laminar to turbulent flow forms is most noticeable by a great increase in the boundary-layer thickness and in the wall shear stress. Figure 2.4 shows the dimensionless combination $\delta_{99}/\sqrt{\nu x/U_\infty}$ depicted as a function of the dimensionless distance $\text{Re}_x = U_\infty x / \nu$ according to measurements by M. Hansen (1928). From Eq. (2.2), in laminar boundary layers this combination has approximately the constant value 5. For $\text{Re}_x = \text{Re}_{x \text{ crit}} = 3 \cdot 10^5$, the measurements demonstrate

a strong sudden increase. As will be shown later in Sect. 18.2.5, the thickness of the turbulent boundary layer on the plate is:

$$\frac{\delta U_\infty}{\nu} = 0.14 \frac{Re_x}{\ln Re_x} G(\ln Re_x) . \quad (2.12)$$

The function $G(\ln Re_x)$ is only weakly dependent on $\ln Re_x$. It has a limiting value of 1 for $\ln Re_x \rightarrow \infty$; this will be discussed more fully in Sect. 17.1.3. In the region of interest here $10^5 < Re_x < 10^6$, $G \approx 1.5$. The dependence on $\ln Re_x$ which appears in Eq. (2.12) is typical for turbulent boundary layers, and has to do with an asymptotic formula for large Reynolds numbers. According to this formula, the boundary-layer thickness grows as $\delta \sim x/\ln x$ for large x . At a given x , the boundary-layer thickness decreases with increasing Reynolds number, but only very slowly with $\delta/x \sim 1/\ln Re$. The combination corresponding to Eq. (2.12) shown in Fig. 2.4 shows good agreement with the measurements of M. Hansen. Since Eq. (2.12) holds for the case where a turbulent boundary layer is already present at the leading edge of the plate, a virtual origin of the boundary layer was assumed at $Re_x = 1.5 \cdot 10^5$ in drawing the curve of Eq. (2.12). This means that precisely at the transition point $Re_x = 3 \cdot 10^5$, the value of the combination is approximately 5.0, and therefore a continuous transition of the boundary layer from laminar to turbulent follows. The boundary-layer thicknesses for typical cases of water and air flows have been calculated from Eq. (2.12) and are given in Table 2.1.

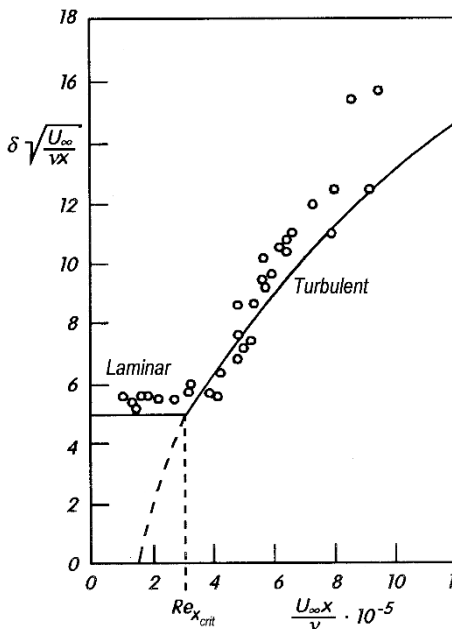


Fig. 2.4. Dependence of the boundary-layer thickness on the distance along a plate at zero incidence, after M. Hansen (1928)
 laminar: Eq. (2.2)
 turbulent: Eq. (2.12) with fictitious origin at $Re_x = 1.5 \cdot 10^5$

Friction forces. As will also be shown in Sect. 18.2.5, the formula analogous to Eq. (2.8) for the skin-friction coefficient of a turbulent boundary layer reads

$$c_f = 2 \left[\frac{\kappa}{\ln Re_x} G(\ln Re_x) \right]^2, \quad (2.13)$$

where $G(\ln Re_x)$ is again the function mentioned in connection with Eq. (2.12). The quantity $\kappa = 0.41$, called the Karman constant, is of fundamental importance for all turbulent wall boundary layers. It is a universal constant. From Eq. (2.13), the skin-friction coefficient for turbulent plate boundary layers decreases with increasing Reynolds number, but it does this extremely slowly, even more slowly than any small negative power of the Reynolds number. Assuming a turbulent boundary layer from the leading edge of the plate on, integration of the skin-friction coefficient over the length of the plate l gives the drag coefficient for a plate wetted on one side:

$$c_D = 2 \left[\frac{\kappa}{\ln Re} G(\ln Re) \right]^2, \quad (2.14)$$

where the Reynolds number Re is now formed with the plate length l . This function is shown in Fig. 1.3. The drag coefficient also decreases extremely slowly with increasing Reynolds number. Note that the functions G in Eqs. (2.13) and (2.14) are different, cf. Sect. 18.2.5.

Viscous sublayer. A peculiarity of turbulent boundary layers will be indicated at this point. In laminar boundary layers, the boundary layer is the region in the flow field affected by the viscosity, but this is not the case in turbulent boundary layers. The entire flow field is now divided into the outer flow, free from turbulence (or at least lacking in turbulence), and the turbulent flow, characterised by random fluctuating motion, inside the boundary layer. Since “apparent” friction forces occur in the turbulent boundary layer, as will be shown in Chap. 18, a turbulent boundary layer is also called a frictional layer. Within this turbulent frictional layer, the effect of the viscosity is restricted to a layer directly at the wall which is much thinner than the boundary layer. This is called the *viscous sublayer* or *viscous wall layer*. Therefore the turbulent boundary layer has a double layered structure. The larger part is a frictional layer only because of the “apparent friction” due to the turbulent fluctuating motion, and is unaffected by the viscosity. In the very thin viscous sublayer, the effects of the viscosity are in the form of “true” friction forces.

Although the transition between the two layers is continuous here too, in practice the concept of the thickness of the viscous sublayer δ_v is used. As will be shown in Sect. 17.1.2

$$\frac{\delta_v}{x} = \frac{50}{Re_x \sqrt{\frac{c_f}{2}}}, \quad (2.15)$$

where the skin-friction coefficient c_f is given by Eq. (2.13). From this, $\delta_v \sim \ln x$ grows very slowly with distance from the leading edge. It also decreases with increasing Reynolds number at a fixed x as $\delta_v \sim \ln \text{Re}_x/\text{Re}_x$.

The ratio of the sublayer thickness δ_v to the total thickness δ follows from Eqs. (2.12) and (2.15)

$$\frac{\delta_v}{\delta} = 680 \frac{\ln^2 \text{Re}_x}{\text{Re}_x}. \quad (2.16)$$

As Re_x increases, the part of the total frictional layer that makes up the viscous sublayer gets ever smaller.

Numerical examples of the absolute thickness of the sublayer are given in Table 2.1.

Table 2.1. Boundary-layer thickness δ and thickness of the viscous sublayer δ_v at the end of a flat plate at zero incidence in turbulent flow according to Eqs. (2.12) and (2.15). l : plate length, U_∞ : free stream velocity, ν : kinematic viscosity

	$\frac{U_\infty}{\text{m/s}}$	$\frac{l}{\text{m}}$	$\text{Re} = \frac{U_\infty l}{\nu}$	$\frac{\delta}{\text{mm}}$	$\frac{\delta_v}{\text{mm}}$
air $\nu = 15 \cdot 10^{-6} \frac{\text{m}^2}{\text{s}}$	50	1	$3.3 \cdot 10^6$	8	0.4
	100	1	$6.6 \cdot 10^6$	8	0.2
	100	5	$3.3 \cdot 10^7$	36	0.2
	200	10	$1.3 \cdot 10^8$	69	0.1
water $\nu = 10^{-6} \frac{\text{m}^2}{\text{s}}$	1	2	$2 \cdot 10^6$	17	1
	2	5	$1 \cdot 10^7$	39	0.6
	5	50	$2.5 \cdot 10^8$	321	0.4
	10	200	$2 \cdot 10^9$	1122	0.1

2.4 Fully Developed Turbulent Flow in a Pipe

In Chap. 1, in connection with Fig. 1.4., mention has already been made of fully developed turbulent flow in a pipe. This case of an internal flow is initially not a flow with typical boundary-layer character. However it has, just like the turbulent frictional layer described in the previous section, a double layer structure with a turbulent core and a viscous sublayer. As the Reynolds number increases, the thickness of the sublayer decreases, so that the final limiting solution is of a flow with homogeneous velocity. In this manner this flow can also be treated using the methods of boundary-layer theory.

Pipe friction factor. The pipe friction factor λ depicted in Fig. 1.4 is defined as follows:

$$\lambda = -\frac{d}{\frac{\rho}{2} u_m^2} \frac{dp}{dx} = \frac{4\bar{\tau}_w}{\frac{\rho}{2} u_m^2}. \quad (2.17)$$

As will be shown in Sect. 17.2.3, in the case of a smooth surface, the dependence on the Reynolds number $Re = u_m d / \nu$ is given by:

$$\lambda = 8 \left[\frac{\kappa}{\ln Re} G(\ln Re) \right]^2. \quad (2.18)$$

Here $G(\ln Re)$ is again a function which monotonically decreases with increasing $\ln Re$, and which has a limit of 1 for $Re \rightarrow \infty$. In the region of interest in practice, $2300 < Re < 10^7$, its value is about $G = 1.35$. The law of friction in Eq. (2.18) is shown in Fig. 1.4, and agrees well with experimental results.

Thickness of the viscous sublayer. The thickness of the viscous sublayer can also be determined approximately (see Chap. 17):

$$\frac{\delta_v}{d} = 122 \frac{\ln Re}{Re G(\ln Re)}. \quad (2.19)$$

As already mentioned, the thickness of the viscous sublayer decreases to zero with increasing Reynolds number. Numerical values of δ_v are given for practical examples of turbulent pipe flows of air and water in Table 2.2.

Table 2.2. Thickness of the viscous sublayer δ_v in fully developed turbulent pipe flow (smooth surface), according to Eq. (2.19)

	$\frac{u_m}{m/s}$	$\frac{d}{m}$	Re	G	$\frac{\delta_v}{mm}$
air $\nu = 15 \cdot 10^{-6} \frac{m^2}{s}$	3	0.01	$2 \cdot 10^3$	1.47	3.2
	3	0.1	$2 \cdot 10^4$	1.38	4.4
	3	1.0	$2 \cdot 10^5$	1.33	5.6
	30	0.01	$2 \cdot 10^4$	1.38	0.4
	30	0.1	$2 \cdot 10^5$	1.33	0.6
	30	1.0	$2 \cdot 10^6$	1.39	0.7
water $\nu = 10^{-6} \frac{m^2}{s}$	0.2	0.01	$2 \cdot 10^3$	1.47	3.2
	0.2	0.1	$2 \cdot 10^4$	1.38	4.4
	0.2	1.0	$2 \cdot 10^5$	1.33	5.6
	20	0.01	$2 \cdot 10^5$	1.33	0.06
	20	0.1	$2 \cdot 10^6$	1.29	0.07
	20	1.0	$2 \cdot 10^7$	1.26	0.08

2.5 Boundary Layer on an Airfoil

The boundary layers on flat plates at zero incidence treated in Sects. 2.2 and 2.3 were particularly simple, since the inviscid outer flow and thus the limiting solution were translation flows with constant pressure in the entire field. However, in the case of flow past an arbitrarily shaped body, additional pressure forces occur. Figure 2.5 shows the boundary layer on an airfoil, where, for reasons of clarity, the dimension in the transverse direction is enlarged greatly. As with the plate, a laminar boundary layer begins to develop at the nose of the airfoil. After a certain distance x_{crit} along the contour of the body, the laminar-turbulent transition occurs, so that the boundary layer is turbulent for $x > x_{\text{crit}}$. Because of the geometry of the body, the invis-

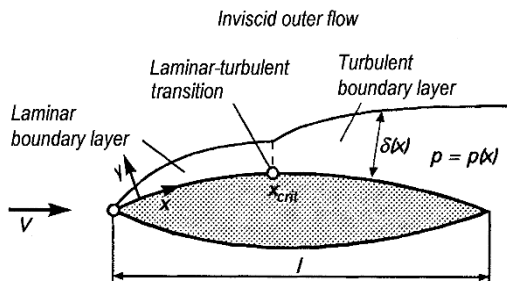


Fig. 2.5. Development of the boundary layer at an airfoil

cid outer flow gives rise to a pressure distribution on the outer edge of the boundary layer. This pressure distribution is “imposed” onto the boundary layer, i.e. at every point x , the pressure in the boundary layer perpendicular to the wall is constant. Therefore the pressure distribution on the outer edge of the boundary layer is identical to the pressure distribution at the wall. Any differences between these two pressure distributions could only arise from streamline curvature and the resulting pressure gradients perpendicular to the main flow direction as a compensation for centrifugal forces. Since boundary layers are very thin compared to the radius of curvature of the body’s contour at high Reynolds numbers, to first order, pressure gradients perpendicular to the wall do not occur. The pressure is imposed on the boundary layer by the outer flow and is only a function of x . Additionally, the dependencies mentioned in the case of the plate boundary layer are also valid: as the boundary layer develops along the contour of the body, in general the boundary-layer thickness $\delta(x)$ increases and the wall shear stress τ_w decreases. The increase in boundary-layer thickness downstream is greater in the case of turbulent boundary layers than laminar. As the Reynolds number formed with the free stream velocity V and a characteristic length of the body l increases, the thickness of the boundary layer decreases to zero in the limiting case $\text{Re} \rightarrow \infty$. The pressure distribution imposed by the outer flow is of considerable importance in the formation of the boundary layer. For

example, the position of the laminar-turbulent transition depends strongly on it. If the pressure greatly increases in the flow direction, as can occur in the region towards the back of the airfoil, or on the back of blunt bodies, it is possible that the boundary layer can separate from the wall. This extremely important phenomenon of boundary-layer separation will be treated in more detail in the next section.

2.6 Separation of the Boundary Layer

In order to explain the important phenomenon of boundary-layer separation, let us consider the flow past a blunt body, e.g. past a circular cylinder as in Fig. 2.6. In inviscid symmetric flow (Fig. 1.14a), an accelerated flow with pressure drop is present on the front half from D to E; from E to F on the back there is a decelerated flow with pressure increase. After setting the flow in motion, as long as the boundary layer remains very thin, an almost inviscid flow first forms. For a particle in the outer flow moving from D to E, pressure is transformed into kinetic energy, and moving from E to F, kinetic energy is transformed into pressure. A fluid particle directly at the wall in the

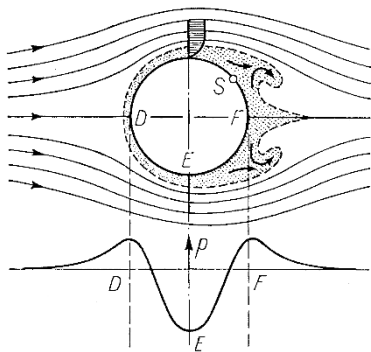


Fig. 2.6. Separation of the boundary layer and vortex formation at a circular cylinder (schematic). S = separation point

boundary layer is also acted on by the same pressure distribution as in the outer flow, since this is imposed on the boundary layer. Because of the strong friction forces in the thin frictional layer, a boundary-layer particle loses so much of its kinetic energy that it cannot manage to get over the “pressure mountain” from E to F. Such a particle cannot make much headway into the region of increasing pressure from E to F. It comes to a standstill, and is pushed backwards into motion by the pressure distribution of the outer flow. The flow portraits in Fig. 2.7 are a time sequence of this process on the back of a blunt body. The pressure increases along the contour of the body from left to right. The flow has been made visible by little particles of aluminium which have been sprinkled onto the surface of the water. The

boundary layer is easily seen in the figures by the short streaklines of the particles. In Fig. 2.7a (shortly after starting) the reversed motion has just begun at the trailing edge. In Fig. 2.7b, the boundary layer has thickened, and the start of the reversed motion has moved forward considerably. It can be seen from Fig. 2.7c that a large vortex has formed from the backflow, and this is even larger in Fig. 2.7d. This vortex then soon separates from the body and moves on downstream. This process changes the flow portrait at the back of the body fully and the pressure distribution is drastically changed compared to that of inviscid flow. The final flow state for the cylinder can be seen in Fig. 1.16. As the pressure distribution in Fig. 1.13 shows, there is quite a strong negative pressure in the region filled with vortices. This negative pressure is the origin of the large form drag of the body.

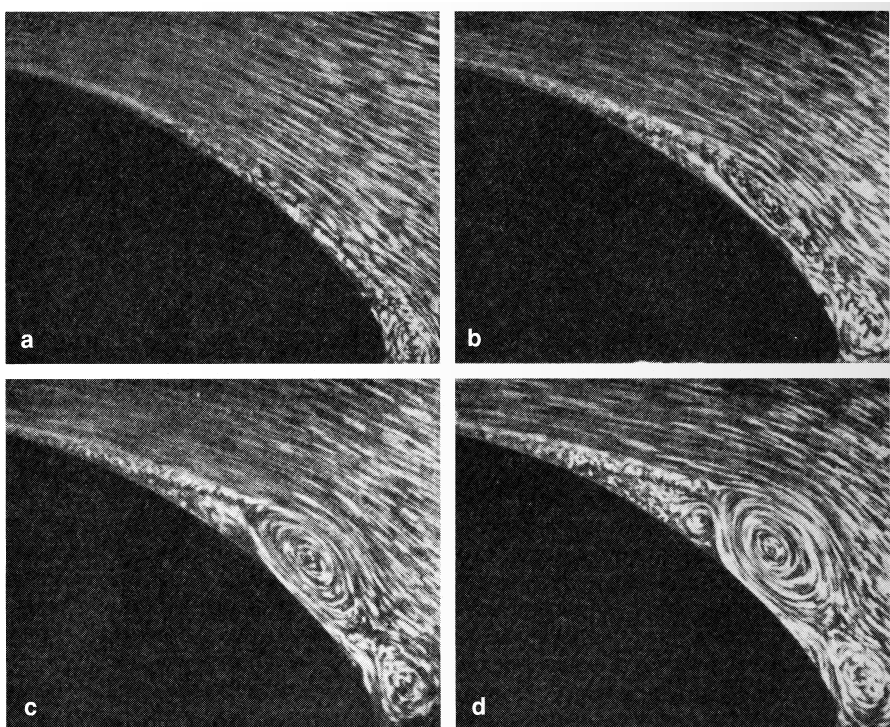


Fig. 2.7 a-d. Development in time of the separation at the back of a blunt body, after L. Prandtl; O. Tietjens (1931)

Separation condition. As well as the friction drag, boundary-layer theory is also able, via the separation process, to explain the form drag (pressure drag). There is always danger of separation in regions where the pressure increases, and it is even greater the larger the increase, particularly for bodies with blunt rear sides. We can now understand why the pressure distribution

observed in Fig. 1.8 for the slender airfoil agrees so well with the theoretical inviscid flow. The pressure increase at the back is so weak that the boundary layer does not separate. As a result, not much form drag occurs and the total drag consists mainly of the friction drag and remains therefore small.

The flow portrait of boundary-layer flow close to separation is of the kind depicted in Fig. 2.8. As a result of the backflow close to the wall, a strong thickening of the boundary layer takes place and with this, boundary-layer mass is transported away into the outer flow. At the point of separation, the streamlines leave the wall at a certain angle. The position of separation is given by the condition that the velocity gradient perpendicular to the wall vanishes at the wall, i.e. the wall shear stress τ_w vanishes:

$$\tau_w = \mu \left(\frac{\partial u}{\partial y} \right)_w = 0 \quad (\text{separation}). \quad (2.20)$$

The position of separation can only be determined by exact calculation (integration of the boundary-layer differential equations).

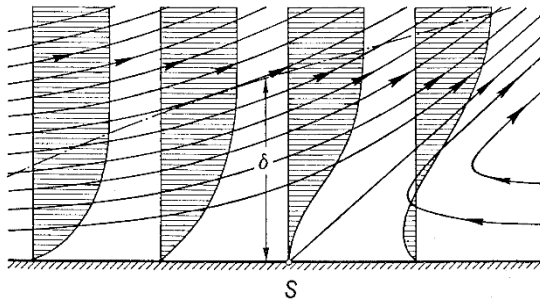


Fig. 2.8. Boundary-layer flow close to the separation point (schematic). S = separation point

The same process of separation discussed for flow past a circular cylinder also occurs in a channel which widens in the direction of flow (diffuser) (Fig. 2.9a). Up until the narrowest cross-section the pressure drops in the direction of flow. Here the flow is right along the walls, just as in inviscid flow. After the narrowest point, the expansion is so great and therefore the pressure increase so large that the boundary layer separates from both walls. The flow now only fills a small part of the cross-section of the channel. However, if the boundary layer is sucked away at the walls (Figs. 2.9b and 2.9c), the separation comes to a stop.

The flow portraits in Fig. 2.10 show that the pressure gradient along the wall acts together with the friction along the wall to govern the separation process. The picture on the left shows the flow against a wall placed perpendicular to it (plane stagnation-point flow). On the streamline of symmetry which leads to the stagnation point, there is a strong pressure increase in the direction of flow. However, there is no separation here because there is

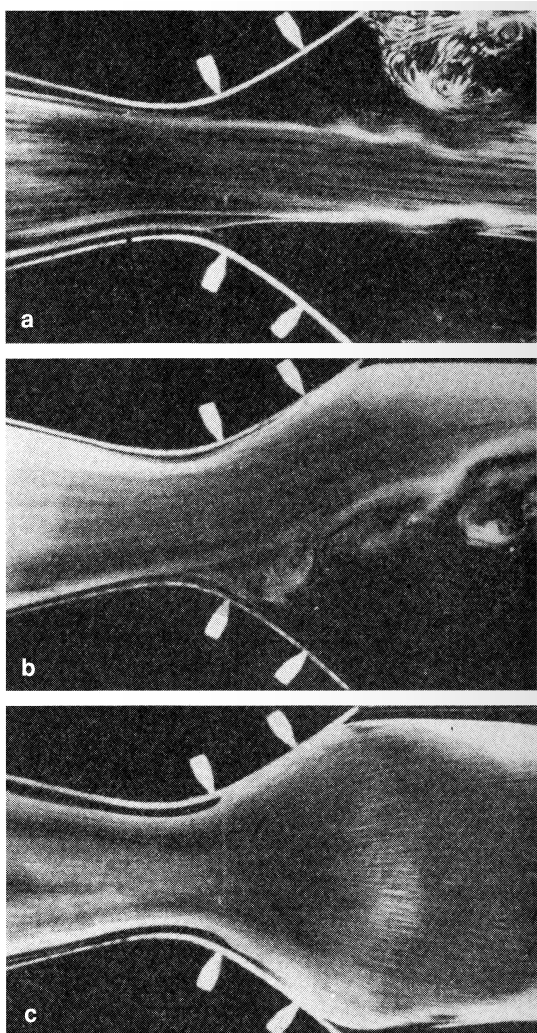


Fig. 2.9. Flow in a widening channel (diffuser) (a) separation at both diffuser walls, (b) suction of the boundary layer at the upper diffuser wall, (c) suction at both diffuser walls (after L. Prandtl; O. Tietjens (1931))

no wall friction present. There is even no separation at the wall itself, because here the boundary layer in both directions flows in the direction of falling pressure. If a very thin wall is now placed at right angles to the first wall at the stagnation point (Fig. 2.10b), it now has on it a boundary layer with increasing pressure in the flow direction. Because of this, the boundary layer here separates from the flat wall.

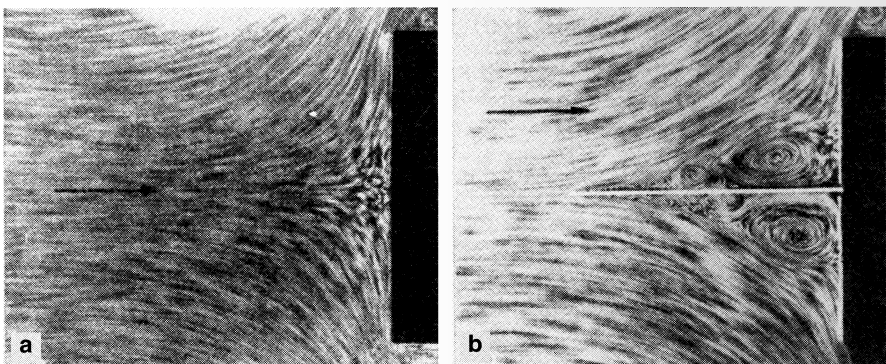


Fig. 2.10. Stagnation point flow, after H. Föttinger (1939), (a) free stagnation-point flow without separation, (b) retarded stagnation-point flow, with separation

The flow separation is frequently quite sensitive to small changes in the shape of the body, particularly if the pressure distribution is strongly affected by the change of shape of the body.

Other examples of separation. An instructive example is to be found in the flow portraits of the model of a motor vehicle (a VW–van) shown in Fig. 2.11 (E. Möller (1951), H. Schlichting (1954)). If the front of the van is square (a), the flow past the sharp front edge produces strong negative pressures and therefore a strong increase in pressure along the side walls. This leads to a complete separation of the boundary layer along the whole side wall and therefore to a large “dead water” area behind the body. The drag coefficient for this van with a square front is $c_D = 0.76$. For a rounded front (b), on the other hand, the strong negative pressures at the front edge are avoided and a flow attached to the entire side wall is achieved. There is a considerable reduction in the drag coefficient to $c_D = 0.42$. Further detailed investigations on such vehicles, also for asymmetric free streams, have been carried out by W.H. Hucho (1972, 1981).

Separation is also important in the production of lift on an airfoil. At small angles of attack (up to about 10°), the flow moves along both sides without separation, so that, to good approximation, an inviscid lift-producing flow is found. This pressure distribution was given in Fig. 1.9 (attached flow, Fig. 2.12a). As the angle of attack is increased, there is danger of separation

on the suction side. This is because the pressure increase is greater here. At a certain angle of attack, about 15° , separation occurs. The position of separation is quite close to the nose of the airfoil. The separated flow (Fig. 2.12b) has a large area of “dead water”. The inviscid lift-producing flow has been destroyed and the drag is now very high. The start of separation coincides approximately with the maximum lift of the airfoil.

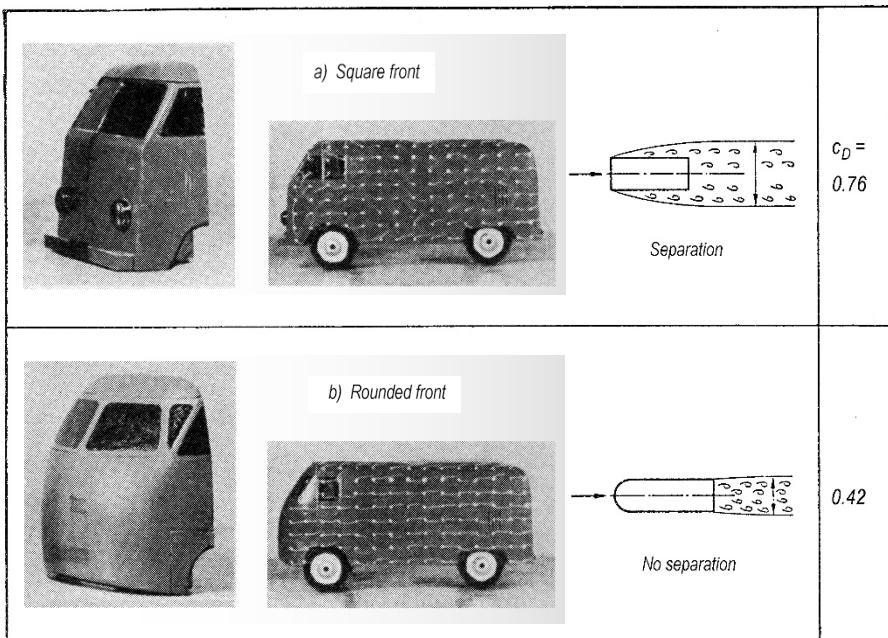


Fig. 2.11. Flow past a model of a vehicle (Volkswagen van), after E. Möller (1951). (a) Square front with fully separated flow along the entire side walls and large drag coefficient $c_D = 0.76$. (b) Rounded front with attached flow along the entire side wall and small drag coefficient $c_D = 0.42$.

Boundary-layer separation can even play a role when the angle of attack on an airfoil is moderate, if flow close to the speed of sound is considered. As already explained in Fig. 1.11, a shock generally forms on the suction side of the airfoil. If the shock is strong enough, the pressure distribution it causes can lead the boundary layer to separate. Because of the additional form drag occurring, a drastic increase of the drag can take place close to the speed of sound; this is frequently called the “sound barrier”.

Finally we present a particularly instructive example of how the drag of a body can be dramatically decreased if the separation of the boundary layer is completely avoided and additionally if the shape is suitably chosen. Figure 2.13 shows the effect of a suitable shaping (streamline form) on the drag: the

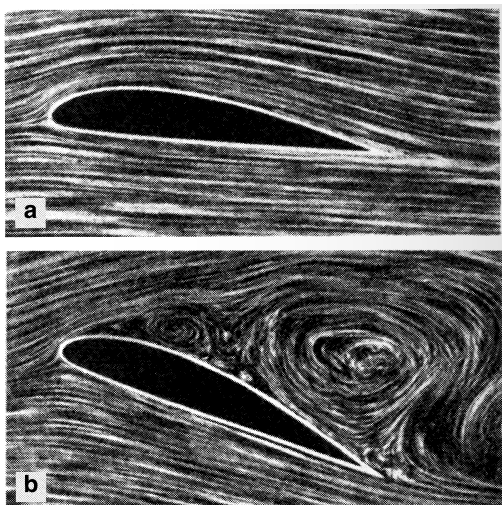


Fig. 2.12. Flow past an airfoil, (a) attached flow, (b) separated flow, after L. Prandtl; O. Tietjens (1931)

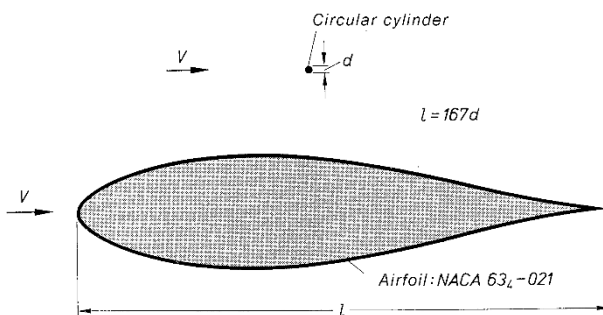


Fig. 2.13. Relative sizes of an airfoil and a circular cylinder at equal free stream velocities (parallel to the symmetry axis of the airfoil) which have the same drag.
 Airfoil: laminar airfoil NACA 63₄ - 021 with laminar boundary layer.
 Drag coefficient $c_D = 0.006$ at $Re_l = 10^6$ to 10^7
 Circular cylinder: drag coefficient $c_D = 1.0$ at $Re_l = 10^4$ to 10^5 (Fig. 1.12)
 The ratio of the chord of the airfoil l to the diameter of the cylinder d has the value $l/d = 1.0/0.006 = 167$

relative sizes of a symmetric airfoil and a circular cylinder (a thin wire) are sketched such that they have the same drag at the same free stream velocity. The cylinder has a drag coefficient of about $c_D \approx 1$, related to its frontal area, cf. Fig. 1.12. The airfoil has a very small drag coefficient of $c_D \approx 0.006$, related to its outline area. This extremely small drag coefficient was achieved by the fact that, because of suitable shaping, the boundary layer remains laminar almost along the entire length (laminar airfoil); see also Chap. 15, in particular Fig. 15.27.

Difference between laminar and turbulent boundary-layer separation. A particularly remarkable phenomenon connected with the laminar-turbulent transition in boundary layers occurs at blunt bodies, such as cylinders and spheres. It can be seen from Figs. 1.12 and 1.19 that, for Reynolds numbers Vd/ν of about $5 \cdot 10^5$ and $3 \cdot 10^5$ respectively, a sudden large drop in the drag coefficient takes place. This was first noted for spheres by G. Eiffel (1912), and has to do with the fact that the boundary layer becomes turbulent. The point of separation thus is moved further backwards, since, because of the turbulent mixing motion, the energizing action of the outer flow on the turbulent boundary layer is much greater than in the laminar case. The separation point for laminar flow lies approximately at the equator, but when the boundary layer becomes turbulent, the point is moved some distance downstream. Thus the “dead water” area behind the body becomes considerably narrower, and the pressure distribution becomes closer to that of inviscid flow (Fig. 1.17). As the dead water area shrinks, a considerable lessening of the form drag takes place, seen as a jump in the curve $c_D = f(\text{Re})$. L. Prandtl (1914) was able to show that this is the correct explanation by placing a thin wire ring around the sphere just in front of the equator (a “trip wire”). This artificially makes the laminar flow turbulent at a lower Reynolds number, and the same drop in drag which normally only happens at higher Reynolds numbers occurs. Figure 2.14 shows flow portraits where the flows have been made visible with smoke. On the left is a sphere in subcritical flow state, with a large dead water area and drag, and on the right, the supercritical state with small dead water area and drag. The second state has been produced using Prandtl’s trip wire. This experiment shows clearly that the jump in the resistance curve of the sphere and cylinder can only be understood as a boundary-layer effect.

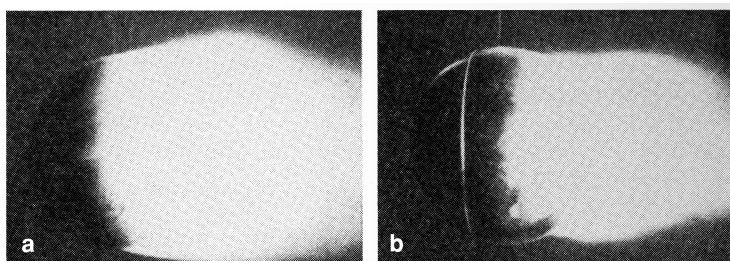


Fig. 2.14. Flow past a sphere, according to C. Wieselsberger (1914). (a) subcritical flow in subcritical Reynolds number regime, (b) supercritical flow in subcritical Reynolds number regime. Applying a thin trip wire enforces the subcritical flow

Other bodies which have a blunt rounded back side (e.g. elliptic cylinders) show in principle a similar drag coefficient dependence on the Reynolds number. For ever narrower bodies, the jump in the drag curve moves back further and further. In the case of a slender airfoil (Fig. 1.8), where basically

no boundary-layer separation takes place, there is also no jump in the c_D curve. The smooth increase in pressure on the back of this body is overcome by the boundary layer without separation. As we will see more clearly later, the pressure in the outer flow has an important effect on the position of the laminar-turbulent transition. In the area from the nose to the pressure minimum where the pressure decreases, the boundary layer is laminar, whereas from then on, in the region of rising pressure, it is mostly turbulent. It is important to note that separation can in general only be prevented if the flow in the boundary layer is turbulent. As will be seen later, a laminar boundary layer can tolerate only an extremely small pressure rise, so that separation occurs even if the body is very slender. This is particularly true even for airfoil flow with a pressure distribution as in Fig. 1.9. The danger of separation is largest here on the suction side. Here too, smooth, separation-free, lift-producing flow is only possible if the boundary-layer flow is turbulent. This can be summarised by saying that both the small drag of slender bodies as well as the lift of airfoils are generally due to the turbulence in the boundary layer.

One particular difference between laminar and turbulent boundary-layer separation should also be mentioned here. After the boundary layer has separated and left the body, it develops into so-called *free shear layers* further downstream, and forms the wake. In the limiting case $Re = \infty$, the laminar free shear layers reduce to lines and surfaces of discontinuity, cf. Fig. 1.14b. In contrast, the turbulent free shear layers have a finite thickness at $Re = \infty$. If turbulent free shear layers form from separation, the limiting solution at $Re = \infty$ has no viscosity, but does have friction: an apparent friction, due to the turbulent fluctuating motion, exists.

Unsteady wakes. As already discussed in Chap. 1 in connection with the flow past a cylinder (Figs. 1.15 and 1.16 and Table 1.1), in spite of steady free stream conditions, the flow after separation is in no way steady. By this we mean varying processes in the mean motion, which move slowly compared to any turbulent fluctuating processes. This phenomenon does not only occur in the case of a circular cylinder, but also in the cases of blunt bodies of arbitrary shape and airfoils at large angles of attack. Sometimes a regular arrangement of vortices rotating clockwise and anticlockwise appears behind the body; this is known as the *Karman vortex street*. The unsteady character of the wake clearly has a great effect on the drag of the body, cf. Fig. 1.15. Understandably, in particular cases it is extremely difficult to establish whether unsteady flow takes place, and how it is to be determined. Research into this is still very much underway: see the summaries by L. Rosenhead (1931/32), M.V. Morkovin (1964), R. Wille (1966), E. Berger; R. Wille (1972), T. Sarpkaya (1975), W.J. McCroskey (1977), H.W. Försching (1978) and D.P. Telionis (1981), as well as H. Schlichting (1982).

Measures to prevent separation. The separation of the boundary layer is generally undesirable, since it leads to great losses in energy. Certain measures have been devised to artificially prevent separation of the boundary layer.

It is physically easiest to *move the wall* in the flow direction too and thus to remove the velocity difference between wall and outer flow, the origin of boundary-layer formation. Of course, technically this is very difficult to realise. However L. Prandtl; O. Tietjens (1931) used a *rotating cylinder* to show that this method does work: on the side where the motion of the wall and the outer flow are the same there is no boundary-layer separation at all.

Another useful method to prevent boundary-layer separation is *suction*. The slowed boundary-layer material is sucked into the inside of the body through narrow slits on the wall. If the suction is strong enough, boundary-layer separation can be prevented. Boundary-layer suction was applied by L. Prandtl in 1904 in his first fundamental work on boundary layers on a circular cylinder. Separation can almost be completely prevented by suction through a slit on the back of the cylinder. Figure 2.9 shows an example of boundary-layer suction on the flow in a greatly diverging channel. Without suction there is strong separation (Fig. 2.9a). When suction is applied only on one side, the flow moves along this wall (Fig. 2.9b) and when suction is set in motion on both sides, the flow fills up the entire channel (Fig. 2.9c). We then obtain the flow portrait for inviscid flow. Suction has been used effectively to increase the lift on airfoils too. Applied to the back of the upper side, suction can be used to keep the flow along side the airfoil at much larger angles of attack than otherwise. This leads to a considerable increase in the maximum lift, O. Schrenk (1935).

Separation of the boundary layer can also be prevented by *blowing* tangentially into the boundary layer. Using a “wall jet” blown through a slit on the contour of the boundary layer parallel to the main flow direction, the boundary layer can be given enough kinetic energy to prevent separation. The maximum lift can be considerably increased using this principle.

In principle, a *slat* can be used on airfoils to prevent separation. In this case the pressure distribution on the airfoil is suitably influenced by the presence of the slat. Positive pressure gradients are avoided and thus separation prevented.

A summary of flow separation and its control may be found in P.K. Chang (1970), P.K. Chang (1976).

2.7 Overview of the Following Material

Now that we have briefly presented the essential physical fundamentals of flows with very low viscosity, the rational theory of these phenomena will be developed from the fluid-dynamic equations of motion of viscous fluid flows. This will be organised as follows: in Part I the general Navier-Stokes equations are derived. From these, in Part II Prandtl's boundary-layer equations

will be derived, based on the simplifications which follow from the smallness of the viscosity. The theory of integrating the boundary-layer equations for laminar flows will follow this. The problem of the onset of turbulence (laminar-turbulent transition) will be treated in Part III. Part IV will consist of the boundary-layer theory of fully developed turbulent flows. While the theory of laminar boundary layers can be treated purely by deduction from the Navier-Stokes differential equations, this has not been possible in the case of turbulent flows. Because they are so complicated, a purely theoretical approach is not possible. The theoretical treatment of turbulent flows therefore must depend on experimental results, and it is therefore a semi-empirical theory. The numerical methods of boundary-layer theory are treated in Part V.

3. Field Equations for Flows of Newtonian Fluids

3.1 Description of Flow Fields

The equations of motion for a general (Newtonian) fluid will now be established. In doing so the fluid will be considered to be a *continuum*. In a continuum the smallest volume element considered dV is still homogeneous, i.e. the dimensions of dV are still very large compared to the average distance between the molecules in the fluid. In gases the assumption of a continuum is valid if the Knudsen number $\text{Kn} = l_0/l$ is very small, where l_0 is the mean free path and l a characteristic length of the flow field, see S.A. Schaa (1958).

In three-dimensional motion the flow field is given by the velocity vector

$$\vec{v} = \vec{e}_x u + \vec{e}_y v + \vec{e}_z w \quad (3.1)$$

with the three components u , v , w in a Cartesian coordinate system with unit vectors \vec{e}_x , \vec{e}_y , \vec{e}_z , and also by the pressure p and the temperature T . To determine these five quantities, there are five equations available:

continuity equation (conservation of mass)

(conservation of mass)

three momentum equations (conservation of momentum)

(conservation of momentum)

energy equation (conservation of energy,
i.e. first law of thermodynamics)

It will become clear later that the angular momentum equation also must be taken into account, cf. Eq. (3.14). These generally valid balance laws are joined by the transport equations. For the isotropic Newtonian fluids considered here, there is a linear relation between the stress tensor and the rate of deformation, and the Fourier heat conduction law holds too. The completed five balance laws therefore contain physical properties for which the dependencies on temperature and pressure must be given: the density $\varrho(T, p)$, the isobaric specific heat capacity $c_p(T, p)$, as well as the transport properties viscosity $\mu(T, p)$ and thermal conductivity $\lambda(T, p)$. In what follows the conservation laws for mass, momentum and energy will be set up.

3.2 Continuity Equation

The continuity equation is a statement about the conservation of mass. It expresses the fact that, per unit volume, the sum of all mass flowing in and out per unit time must be equal to the change in mass due to change in density per unit time. For unsteady flows of a general fluid, this yields

$$\boxed{\frac{D\varrho}{Dt} + \varrho \operatorname{div} \vec{v} = 0} \quad (3.2)$$

or using alternative notation

$$\frac{\partial \varrho}{\partial t} + \operatorname{div}(\varrho \vec{v}) = 0. \quad (3.3)$$

Here $D\varrho/Dt$ is the *total* or *substantial* derivative of the density with respect to time, which as

$$\frac{D\varrho}{Dt} = \frac{\partial \varrho}{\partial t} + \vec{v} \cdot \operatorname{grad} \varrho \quad (3.4)$$

is composed of the *local* part $\partial \varrho / \partial t$ (in unsteady flow) and the *convective* part (as a consequence of the change in position) $\vec{v} \cdot \operatorname{grad} \varrho$.

The continuity equation can now be used to formulate the concept of the incompressible fluid more precisely, using the following definition:

For incompressible fluids the substantial derivative of the density with respect to time vanishes ($D\varrho/Dt = 0$).

It then immediately follows from the continuity equation Eq. (3.2) that incompressible flows, i.e. flows of incompressible fluids, are *source free*. We have:

$$\frac{D\varrho}{Dt} = 0, \quad \operatorname{div} \vec{v} = 0 \quad (\text{incompressible fluid}). \quad (3.5)$$

Constant density in the whole flow field is a sufficient but not a necessary condition for incompressible flow. In the case of flows in *density stratification*, for example in oceans, the density in the flow field is variable, but each fluid particle retains its density. See the following summaries: C.S. Yih (1965), O.M. Phillips (1966). *Internal gravity waves* are examples of incompressible flows with locally variable density, see J. Lighthill (1978), R.R. Long (1972).

3.3 Momentum Equation

The momentum equation is the basic law of mechanics which states that mass times acceleration is equal to the sum of the forces. Both body forces and surface forces (pressure and friction forces) act. If \vec{f} is the body force per

unit volume (e.g. $\vec{f} = \varrho \vec{g}$ where \vec{g} is the vector of gravitational acceleration) and \vec{P} the surface force per unit volume, the momentum equation reads as follows in vector notation:

$$\varrho \frac{D\vec{v}}{Dt} = \vec{f} + \vec{P}. \quad (3.6)$$

Here

$$\frac{D\vec{v}}{Dt} = \frac{\partial \vec{v}}{\partial t} + \frac{d\vec{v}}{dt} \quad (3.7)$$

is the substantial acceleration made up of the local acceleration $\partial \vec{v} / \partial t$ (in unsteady flows) and the convective acceleration $d\vec{v} / dt$ (as a consequence of change in position).

In general for convective acceleration we have

$$\frac{d\vec{v}}{dt} = \text{grad} \left(\frac{1}{2} \vec{v}^2 \right) - \vec{v} \times \text{curl} \vec{v}. \quad (3.8)$$

The (pseudo–vectorial) abbreviation

$$\frac{d\vec{v}}{dt} = (\vec{v} \cdot \text{grad}) \vec{v} \quad (3.9)$$

is frequently chosen.

The body forces are considered to be prescribed external forces. On the other hand the surface forces depend on the state of deformation (state of motion) of the fluid. All the surface forces on a volume element determine the *state of stress*¹. We now have to determine the relation between the state of stress and the state of deformation (transport equation). This relation can ultimately only be empirical. Statements which are generally valid come from the *thermodynamics of irreversible processes*, see the summaries by J. Meixner; H.G. Reik (1959), S.R. De Groot; P. Mazur (1962), J. Kestin (1966b) and I. Prigogine (1947).

Further considerations will be restricted to *isotropic Newtonian fluids*. All gases and many liquids, in particular water, are members of this category. A fluid is called isotropic if the relation between the stress tensor and the rate of deformation tensor is the same in all directions. If this relation is linear, we are dealing with a Newtonian fluid. We then speak of Newton's or Stokes's law of friction, an equation for the transport of momentum. As will be shown in Sect. 3.8, these transport equations contain only *one* transport quantity (the viscosity) as long as no relaxation processes occur in the fluid.

3.4 General Stress State of Deformable Bodies

In order to determine the surface forces, consider a volume element $dV = dx \cdot dy \cdot dz$ as in Fig. 3.1, whose front lower left corner has the coordinates x ,

¹ The concept of *surface stress* will not be explicitly used since it serves to describe free surfaces of liquids which are not treated here.

y, z . The following stresses (stress vectors = surface forces per unit surface area) act on the two surfaces normal to the x axis of size $dy \cdot dz$:

$$\vec{p}_x \text{ and } \vec{p}_x + \frac{\partial \vec{p}_x}{\partial x} dx . \quad (3.10)$$

The index x implies that the stress vector acts on a surface element whose normal is in the x direction. Similar terms are obtained for the surface elements $dx \cdot dz$ and $dx \cdot dy$ perpendicular to the y and z axes respectively. Thus we have the resulting surface forces in the three coordinate directions:

$$\text{plane } \perp x\text{-direction : } \frac{\partial \vec{p}_x}{\partial x} \cdot dx \cdot dy \cdot dz$$

$$\text{plane } \perp y\text{-direction : } \frac{\partial \vec{p}_y}{\partial y} \cdot dx \cdot dy \cdot dz$$

$$\text{plane } \perp z\text{-direction : } \frac{\partial \vec{p}_z}{\partial z} \cdot dx \cdot dy \cdot dz .$$

The total surface force \vec{P} per unit volume dV resulting from the stress state is therefore

$$\vec{P} = \frac{\partial \vec{p}_x}{\partial x} + \frac{\partial \vec{p}_y}{\partial y} + \frac{\partial \vec{p}_z}{\partial z} . \quad (3.11)$$

Here \vec{p}_x , \vec{p}_y and \vec{p}_z are vectors which can be decomposed into components. This decomposition will be carried out by denoting the components perpendicular to each surface element, that is the normal stresses, by σ , and by giving the direction of the normal stresses as an index.

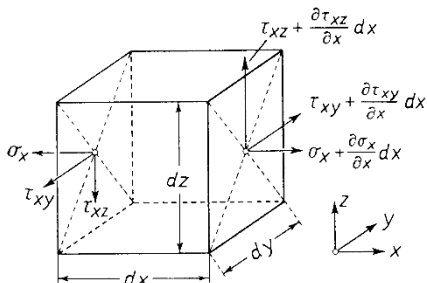


Fig. 3.1. Stresses on a volume element

The components in the plane of the surface elements are called tangential stresses τ . They acquire a double index: the first position indicates to which axis the surface element is perpendicular, and the second position states in which direction the stress τ is pointing.

Using this notation we have

$$\begin{aligned}\vec{p}_x &= \vec{e}_x \sigma_x + \vec{e}_y \tau_{xy} + \vec{e}_z \tau_{xz} \\ \vec{p}_y &= \vec{e}_x \tau_{yx} + \vec{e}_y \sigma_y + \vec{e}_z \tau_{yz} \\ \vec{p}_z &= \vec{e}_x \tau_{zx} + \vec{e}_y \tau_{zy} + \vec{e}_z \sigma_z.\end{aligned}\quad (3.12)$$

The state of stress is therefore determined by nine scalar quantities and these form the *stress tensor*. The nine components together of the stress tensor are also called the *stress matrix*:

$$\boldsymbol{\sigma} = \begin{pmatrix} \sigma_x & \tau_{xy} & \tau_{xz} \\ \tau_{yx} & \sigma_y & \tau_{yz} \\ \tau_{zx} & \tau_{zy} & \sigma_z \end{pmatrix}. \quad (3.13)$$

The stress tensor and its matrix are symmetric: thus two tangential forces whose indices only differ in their order are equal. This will be shown by considering the equation of motion of a fluid element. In general this motion can be decomposed into a translation and a rotation. For our aims we only need to consider the latter. Denoting the instantaneous angular acceleration of the fluid element by $\vec{\omega}$ ($\dot{\omega}_x, \dot{\omega}_y, \dot{\omega}_z$), we can write down the following for the rotation about the y axis:

$$\dot{\omega}_y dI_y = (\tau_{xz} dy dz) dx - (\tau_{xz} dx dy) dz = (\tau_{xz} - \tau_{zx}) dV.$$

Here dI_y is the moment of inertia of the element about the y axis. Now the moment of inertia dI is proportional to the fifth power of the linear dimension of the parallelepiped, while the volume element is proportional to the third power. Making the transition to a very small volume element, the left hand side of the above equation vanishes faster than the right hand side. Therefore we have

$$\tau_{xz} - \tau_{zx} = 0,$$

if $\dot{\omega}_y$ is not to become infinitely large. Analogous equations are obtained for the other two axes, thus proving the symmetry of the stress tensor. It is seen from above that the stress tensor would no longer be symmetric if the fluid had a local torque proportional to the volume dV . This can arise in, for example, an electrostatic field, cf. I. Müller (1973), p. 32.

Because of the relations

$$\begin{aligned}\tau_{xy} &= \tau_{yx} \\ \tau_{xz} &= \tau_{zx} \\ \tau_{yz} &= \tau_{zy}\end{aligned}\quad (3.14)$$

the stress matrix Eq. (3.13) has only six different stress components and is symmetric about the main diagonal:

$$\boldsymbol{\sigma} = \begin{pmatrix} \sigma_x & \tau_{xy} & \tau_{xz} \\ \tau_{xy} & \sigma_y & \tau_{yz} \\ \tau_{xz} & \tau_{yz} & \sigma_z \end{pmatrix}. \quad (3.15)$$

Using Eqs. (3.11), (3.12) and (3.14) we find the surface force per unit volume

$$\begin{aligned}\vec{P} = & \vec{e}_x \left(\frac{\partial \sigma_x}{\partial x} + \frac{\partial \tau_{xy}}{\partial y} + \frac{\partial \tau_{xz}}{\partial z} \right) \quad x\text{-comp.} \\ & + \vec{e}_y \left(\frac{\partial \tau_{xy}}{\partial x} + \frac{\partial \sigma_y}{\partial y} + \frac{\partial \tau_{yz}}{\partial z} \right) \quad y\text{-comp.} \\ & + \vec{e}_z \left(\underbrace{\frac{\partial \tau_{xz}}{\partial x}}_{\substack{\text{s'face} \\ yz}} + \underbrace{\frac{\partial \tau_{yz}}{\partial y}}_{\substack{\text{s'face} \\ zx}} + \underbrace{\frac{\partial \sigma_z}{\partial z}}_{\substack{\text{s'face} \\ xy}} \right) \quad z\text{-comp.}\end{aligned}\quad (3.16)$$

If we introduce this expression into the equation of motion (3.6), it reads, in component form

$$\begin{aligned}\varrho \frac{Du}{Dt} = & f_x + \left(\frac{\partial \sigma_x}{\partial x} + \frac{\partial \tau_{xy}}{\partial y} + \frac{\partial \tau_{xz}}{\partial z} \right) \\ \varrho \frac{Dv}{Dt} = & f_y + \left(\frac{\partial \tau_{xy}}{\partial x} + \frac{\partial \sigma_y}{\partial y} + \frac{\partial \tau_{yz}}{\partial z} \right) \\ \varrho \frac{Dw}{Dt} = & f_z + \left(\frac{\partial \tau_{xz}}{\partial x} + \frac{\partial \tau_{yz}}{\partial y} + \frac{\partial \sigma_z}{\partial z} \right).\end{aligned}\quad (3.17)$$

The first invariant of the stress tensor will “initially” be denoted as the pressure p :

$$p = -\frac{1}{3}(\sigma_x + \sigma_y + \sigma_z). \quad (3.18)$$

We will go into why we have used the reservation “initially” in Sect. 3.8.

In the *hydrostatic stress state* ($\vec{v} = 0$), all tangential forces vanish. Only the normal stresses remain, and these are all equal to each other and to the negative pressure from Eq. (3.18). Since measurements to determine the thermodynamic quantities can (in principle) be carried out in a fluid at rest, the pressure introduced via Eq. (3.18) is, in the hydrostatic case, identical to the thermodynamic pressure. This also holds for the case of a flowing fluid if, as will be shown in Sect. 3.8, there are no relaxation processes in the flow.

It is useful to separate the pressure from the normal stresses:

$$\tau_{xx} = \sigma_x + p, \quad \tau_{yy} = \sigma_y + p, \quad \tau_{zz} = \sigma_z + p. \quad (3.19)$$

Here the stresses have been decomposed additively into a part with the normal stress $-p$ that is the same in all directions, and a part which deviates from this (*deviator stresses*).

The momentum equations (3.17) then read

$$\begin{aligned}\varrho \frac{Du}{Dt} = & f_x - \frac{\partial p}{\partial x} + \left(\frac{\partial \tau_{xx}}{\partial x} + \frac{\partial \tau_{xy}}{\partial y} + \frac{\partial \tau_{xz}}{\partial z} \right) \\ \varrho \frac{Dv}{Dt} = & f_y - \frac{\partial p}{\partial y} + \left(\frac{\partial \tau_{yx}}{\partial x} + \frac{\partial \tau_{yy}}{\partial y} + \frac{\partial \tau_{yz}}{\partial z} \right) \\ \varrho \frac{Dw}{Dt} = & f_z - \frac{\partial p}{\partial z} + \left(\frac{\partial \tau_{zx}}{\partial x} + \frac{\partial \tau_{zy}}{\partial y} + \frac{\partial \tau_{zz}}{\partial z} \right)\end{aligned}\quad (3.20)$$

or in vector notation

$$\varrho \frac{D\vec{v}}{Dt} = \vec{f} - \text{grad } p + \text{Div } \boldsymbol{\tau} . \quad (3.21)$$

Here $\boldsymbol{\tau}$ is the *viscous stress tensor*. It contains only the deviator stresses and is likewise symmetric. Its matrix reads:

$$\boldsymbol{\tau} = \begin{pmatrix} \tau_{xx} & \tau_{xy} & \tau_{xz} \\ \tau_{xy} & \tau_{yy} & \tau_{yz} \\ \tau_{xz} & \tau_{yz} & \tau_{zz} \end{pmatrix} . \quad (3.22)$$

The system of three equations (3.20) contains the six components of the viscous stress tensor. The next exercise is to determine the relation between these six stress quantities and the rate of deformation, and in this way to introduce the three velocity components u, v, w or their derivatives into the right hand side of Eq. (3.20). Before deriving this relation in Sect. 3.6, we shall first examine these deformations more closely.

3.5 General State of Deformation of Flowing Fluids

If a flow takes place in a fluid, as time goes by each fluid element will be found at a new position. Throughout this motion the fluid element undergoes a deformation. Since the fluid motion is completely determined if the velocity vector is known as a function of place and time, $\vec{v} = \vec{v}(x, y, z, t)$, there exist kinematic relations between the rate of deformation and this function. The rate of deformation for a fluid element depends on the relative motion of two of its points. Therefore we consider two neighbouring points A and B as in Fig. 3.2. As a consequence of the velocity field, point A is moved to the position A' in the time dt , where $\vec{s} = \vec{v} dt$.

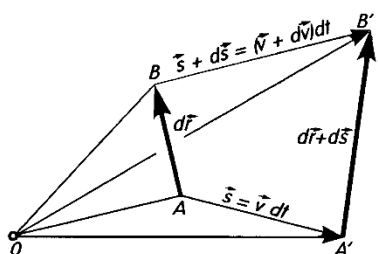


Fig. 3.2. Moving AB to $A'B'$

Since the velocity at point B , a distance $d\vec{r}$ from A , is different from that at A , B is moved to point B' , which is a distance $\vec{s} + d\vec{s} = (\vec{v} + d\vec{v})dt$ from B . To be precise: if the velocity components are u, v, w at point A , the velocity

components at point B can be found by expansion in a Taylor series to first order to get

$$\begin{aligned} u + du &= u + \frac{\partial u}{\partial x} dx + \frac{\partial u}{\partial y} dy + \frac{\partial u}{\partial z} dz \\ v + dv &= v + \frac{\partial v}{\partial x} dx + \frac{\partial v}{\partial y} dy + \frac{\partial v}{\partial z} dz \\ w + dw &= w + \frac{\partial w}{\partial x} dx + \frac{\partial w}{\partial y} dy + \frac{\partial w}{\partial z} dz . \end{aligned} \quad (3.23)$$

The motion of the point B relative to that of point A is therefore described by the following matrix of the nine partial derivatives of the local velocity:

$$\begin{pmatrix} \frac{\partial u}{\partial x} & \frac{\partial u}{\partial y} & \frac{\partial u}{\partial z} \\ \frac{\partial v}{\partial x} & \frac{\partial v}{\partial y} & \frac{\partial v}{\partial z} \\ \frac{\partial w}{\partial x} & \frac{\partial w}{\partial y} & \frac{\partial w}{\partial z} \end{pmatrix} . \quad (3.24)$$

It is useful to arrange the expressions for the relative velocity components du , dv , dw in Eq. (3.23) in the following manner:

$$\begin{aligned} du &= (\dot{\varepsilon}_x dx + \dot{\varepsilon}_{xy} dy + \dot{\varepsilon}_{xz} dz) + (\omega_y dz - \omega_z dy) \\ dv &= (\dot{\varepsilon}_{xy} dx + \dot{\varepsilon}_y dy + \dot{\varepsilon}_{yz} dz) + (\omega_z dx - \omega_x dz) \\ dw &= (\dot{\varepsilon}_{xz} dx + \dot{\varepsilon}_{zy} dy + \dot{\varepsilon}_z dz) + (\omega_x dy - \omega_y dx) . \end{aligned} \quad (3.25)$$

It can easily be shown that the newly introduced quantities have the following meaning:

$$\begin{aligned} \dot{\varepsilon} &= \begin{pmatrix} \dot{\varepsilon}_x & \dot{\varepsilon}_{xy} & \dot{\varepsilon}_{xz} \\ \dot{\varepsilon}_{yx} & \dot{\varepsilon}_y & \dot{\varepsilon}_{yz} \\ \dot{\varepsilon}_{zx} & \dot{\varepsilon}_{zy} & \dot{\varepsilon}_z \end{pmatrix} \\ &= \begin{pmatrix} \frac{\partial u}{\partial x} & \frac{1}{2} \left(\frac{\partial v}{\partial x} + \frac{\partial u}{\partial y} \right) & \frac{1}{2} \left(\frac{\partial w}{\partial x} + \frac{\partial u}{\partial z} \right) \\ \frac{1}{2} \left(\frac{\partial u}{\partial y} + \frac{\partial v}{\partial x} \right) & \frac{\partial v}{\partial y} & \frac{1}{2} \left(\frac{\partial w}{\partial y} + \frac{\partial v}{\partial z} \right) \\ \frac{1}{2} \left(\frac{\partial u}{\partial z} + \frac{\partial w}{\partial x} \right) & \frac{1}{2} \left(\frac{\partial v}{\partial z} + \frac{\partial w}{\partial y} \right) & \frac{\partial w}{\partial z} \end{pmatrix} \end{aligned} \quad (3.26)$$

and

$$\omega_x = \frac{1}{2} \left(\frac{\partial w}{\partial y} - \frac{\partial v}{\partial z} \right); \omega_y = \frac{1}{2} \left(\frac{\partial u}{\partial z} - \frac{\partial w}{\partial x} \right); \omega_z = \frac{1}{2} \left(\frac{\partial v}{\partial x} - \frac{\partial u}{\partial y} \right). \quad (3.27)$$

The matrix $\dot{\varepsilon}$ is symmetric, so that

$$\dot{\varepsilon}_{yz} = \dot{\varepsilon}_{xy}; \quad \dot{\varepsilon}_{xz} = \dot{\varepsilon}_{zx}; \quad \dot{\varepsilon}_{zy} = \dot{\varepsilon}_{yz} \quad (3.28)$$

and $\omega_x, \omega_y, \omega_z$ are the components of the *angular velocity* vector $\vec{\omega}$, which is connected to the *vorticity vector* $\text{curl } \vec{v}$ by¹

$$\vec{\omega} = \frac{1}{2} \text{curl } \vec{v} . \quad (3.29)$$

The tensor belonging to the matrix (3.26) is called the *rate of deformation tensor* or *strain-rate tensor*.

Let us now discuss the kinematic interpretation of each of the quantities in Eq. (3.26). Since our attention is on the direct neighbourhood of point A , and since the motion of point B relative to point A is of interest, we set the origin to A and interpret dx, dy, dz as the coordinates of point B in a Cartesian coordinate system. In this manner, the expressions in Eq. (3.25) can be read as the components du, dv, dw of the relative velocity, which are linear functions of the spatial coordinates. In order to understand the meaning of the different terms in the matrices (3.26) and the equations (3.27), we will consider them individually.

Volume dilatation. The diagram in Fig. 3.3a portrays the field of the relative velocities for the case where all the terms in Eq. (3.26) vanish, except for $\partial u / \partial x$ which we assume is positive. The velocity of each point B relative to A is

$$du = \left(\frac{\partial u}{\partial x} \right) dx .$$

The field consists of planes $x = \text{const}$ which move smoothly with a velocity which is proportional to the distance dx from the plane $x = 0$. An elementary parallelepiped with A and B on the vertical edges in such a velocity field is deformed in the longitudinal direction by shifting the side BC with increasing velocity. Thus $\dot{\varepsilon}_x$ is the extension velocity for the volume element in the x direction. Similarly, the terms $\dot{\varepsilon}_y = \partial v / \partial y$ and $\dot{\varepsilon}_z = \partial w / \partial z$ are extension velocities in the y and z directions respectively.

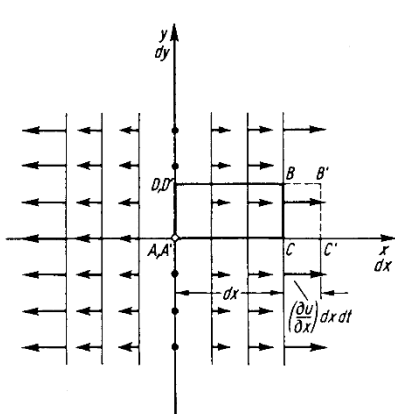
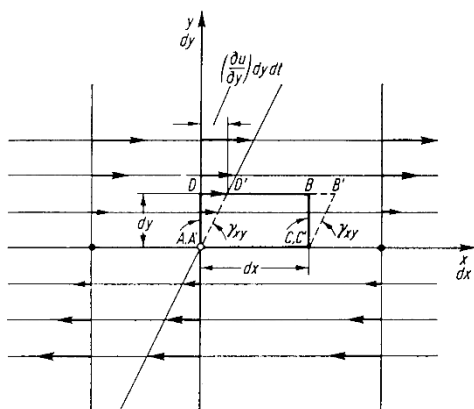
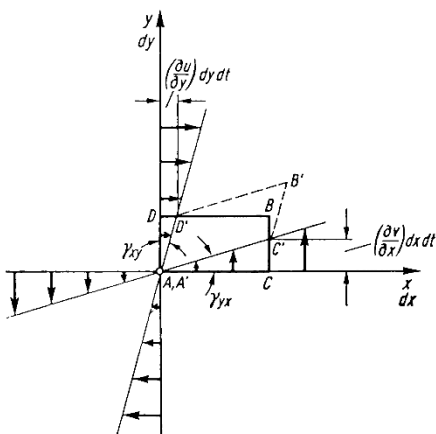
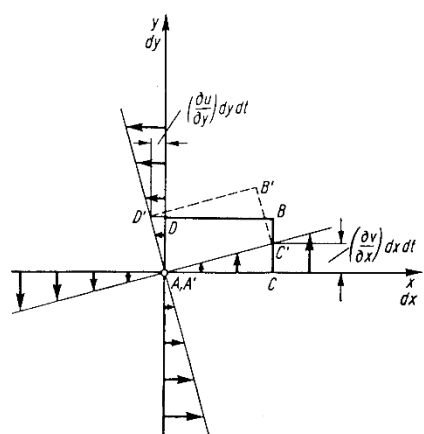
Now it is easy to write down the deformation experienced by a fluid element by simultaneous action of all three diagonal elements of the matrices (3.24) or (3.26). The element is stretched in all three directions, and there is a relative change in volume due to the change in length of the three sides:

$$\begin{aligned} \dot{\varepsilon} &= \frac{\{dx + \frac{\partial u}{\partial x} dx dt\} \{dy + \frac{\partial v}{\partial y} dy dt\} \{dz + \frac{\partial w}{\partial z} dz dt\} - dx dy dz}{dx dy dz dt} \\ &= \frac{\partial u}{\partial x} + \frac{\partial v}{\partial y} + \frac{\partial w}{\partial z} \\ &= \text{div } \vec{v} . \end{aligned} \quad (3.30)$$

Throughout this deformation the shape of the element, described by the angles at the sides, remains unchanged since all right angles are conserved. Thus $\dot{\varepsilon}$ describes the local instantaneous *volume dilatation* of the fluid element. If the fluid is incompressible we have $\dot{\varepsilon} = 0$, as would be expected. For a compressible fluid, Eq. (3.2) yields

$$\dot{\varepsilon} = \text{div } \vec{v} = -\frac{1}{\varrho} \frac{D\varrho}{Dt} . \quad (3.31)$$

¹ Note that in the English-speaking world the symbol $\vec{\omega}$ frequently stands for $\text{curl } \vec{v}$, that is, for twice the angular velocity.

Fig. 3.3. Different kinds of motion of a fluid element**Fig. 3.3a.** Uniform extension in the \$x\$ direction, if \$\partial u / \partial x > 0\$ and the remaining components of \$\dot{\epsilon}\$ vanish**Fig. 3.3b.** Uniform shear deformation, if \$\partial u / \partial y > 0\$ and the remaining components of \$\dot{\epsilon}\$ vanish**Fig. 3.3c.** Uniform deformation, if \$\dot{\epsilon}_{xy} = \dot{\epsilon}_{yx} = [(\partial u / \partial y) + (\partial v / \partial x)] / 2 > 0\$ and the remaining components of \$\dot{\epsilon}\$ vanish (here \$\partial u / \partial y = \partial v / \partial x\$)**Fig. 3.3d.** Rigid body rotation, if \$\omega_z = [(\partial v / \partial x) - (\partial u / \partial y)] / 2 \neq 0\$ and the remaining components of \$\dot{\epsilon}\$ vanish (here \$\partial v / \partial x = -\partial u / \partial y\$)

This implies that the volume dilatation, i.e. the relative change in volume, is equal to the negative relative change of the local density.

Shear deformation. The relative velocity field has a completely different form if one of the off-diagonal terms of the matrix (3.24), e.g. $\partial u / \partial y$, does not vanish but is, for example, positive. The field corresponding to this case is sketched in Fig. 3.3b; it is a pure shear deformation. The original right angle at point A changes by $d\gamma_{xy} = [(\partial u / \partial y) dy dt] / dy$; therefore the shear angular velocity is $d\gamma_{xy} / dt = \dot{\gamma}_{xy} = \partial u / \partial y$. If both derivatives $\partial u / \partial y$ and $\partial v / \partial x$ are positive, the right angle at point A is changed by a superposition of these two motions, as is shown in Fig. 3.3c. It is obvious that the right angle at point A is changed by twice the absolute value of

$$\dot{\varepsilon}_{yx} = \dot{\varepsilon}_{xy} = \frac{1}{2} \left(\frac{\partial u}{\partial y} + \frac{\partial v}{\partial x} \right).$$

This is given by the two off-diagonal terms in matrix (3.26). In general the three off-diagonal terms $\dot{\varepsilon}_{xy} = \dot{\varepsilon}_{yx}$, $\dot{\varepsilon}_{xz} = \dot{\varepsilon}_{zx}$ and $\dot{\varepsilon}_{zy} = \dot{\varepsilon}_{yz}$ describe the deformation of a right angle lying in a plane normal to the axis whose index does not appear. In these deformations, the volume of the element is retained and only its shape is changed.

Rigid body rotation. The motion is again different if $\partial u / \partial y = -\partial v / \partial x$ as is shown in Fig. 3.3d. From the considerations above, and from the fact that now $\dot{\varepsilon}_{xy} = 0$, we can conclude that in this case the right angle at point A is not altered. This is also obvious from the diagram which shows that the fluid element rotates about the point A. This rotation takes place without deformation and can be described as the rotation of a rigid body. The instantaneous angular velocity is

$$\frac{(\partial v / \partial x) dx dt}{dx dt} = \frac{\partial v}{\partial x} = -\frac{\partial u}{\partial y}.$$

We can now easily see that the component ω_z of $\frac{1}{2} \operatorname{curl} \vec{v}$ in Eq. (3.27), known as the angular velocity of the velocity field, represents the instantaneous angular velocity of the rigid body rotation and that $\omega_z \neq 0$.

In the general case when $\partial u / \partial y \neq -\partial v / \partial x$, the fluid element rotates and is simultaneously deformed. We can interpret the term

$$\dot{\varepsilon}_{xy} = \dot{\varepsilon}_{yx} = \frac{1}{2} \left(\frac{\partial u}{\partial y} + \frac{\partial v}{\partial x} \right)$$

as a deformation and

$$\omega_z = \frac{1}{2} \left(\frac{\partial v}{\partial x} - \frac{\partial u}{\partial y} \right)$$

as a rigid body rotation.

Because Eqs. (3.23) and (3.25) are linear, it can be concluded that the general case can be obtained by superposition of the two simple cases mentioned. Therefore, for two neighbouring points A and B in a fluid with velocity field $\vec{v}(x, y, z)$, we can decompose their motion uniquely into four components as follows:

- (a) a pure translation, described by the velocity components u, v, w of \vec{v} ;
- (b) a rigid body rotation, described by the components $\omega_x, \omega_y, \omega_z$ of $\frac{1}{2} \operatorname{curl} \vec{v}$;
- (c) a volume dilatation, described by $\dot{\epsilon} = \operatorname{div} \vec{v}$, with linear dilatations $\dot{\varepsilon}_x, \dot{\varepsilon}_y, \dot{\varepsilon}_z$ in the directions of the three axes;
- (d) a deformation, given by the three components $\dot{\varepsilon}_{xy}, \dot{\varepsilon}_{xz}, \dot{\varepsilon}_{yz}$ with mixed indices.

Only the final two motions lead to a deformation of the fluid element about the reference point A ; the first two merely lead to a change in position.

The elements of the matrix (3.26) represent the components of a symmetric tensor called the *rate of deformation tensor*; its mathematical properties are analogous to the similarly symmetric stress tensor. It is known from the theory of elasticity, cf. L. Hopf (1927), A.E.H. Love (1952), and from general tensor algebra that three orthogonal axes which determine three perpendicular planes and thus a preferred Cartesian coordinate system can be assigned to every symmetric tensor. In this coordinate system, the stress vector (or the rate of deformation vector) is perpendicular to one plane, i.e. parallel to one axis. When such a coordinate system is chosen, the matrices (3.15) or (3.26) retain only their diagonal elements. Using a bar ($\bar{\cdot}$) to denote the values of the components affected, we obtain the matrices

$$\begin{pmatrix} \bar{\sigma}_x & 0 & 0 \\ 0 & \bar{\sigma}_y & 0 \\ 0 & 0 & \bar{\sigma}_z \end{pmatrix} \quad \text{and} \quad \begin{pmatrix} \bar{\varepsilon} & 0 & 0 \\ 0 & \bar{\dot{\varepsilon}}_y & 0 \\ 0 & 0 & \bar{\dot{\varepsilon}}_z \end{pmatrix}. \quad (3.32)$$

Recall that such a coordinate transformation does not change the trace of the matrix, so that

$$\sigma_x + \sigma_y + \sigma_z = \bar{\sigma}_x + \bar{\sigma}_y + \bar{\sigma}_z \quad (= -3p) \quad (3.33)$$

and

$$\dot{\varepsilon}_x + \dot{\varepsilon}_y + \dot{\varepsilon}_z = \bar{\dot{\varepsilon}}_x + \bar{\dot{\varepsilon}}_y + \bar{\dot{\varepsilon}}_z \quad (= \dot{\varepsilon} = \operatorname{div} \vec{v}). \quad (3.34)$$

As has already been mentioned, these quantities are invariants of the tensors. In two such coordinate systems (both denoted with a bar), stresses occur in the fluid in two perpendicular directions and the surface elements are displaced in two perpendicular directions, as shown in Figs. 3.4a and 3.4b. This of course does not imply that there are no shear stresses in some other plane, or that the element remains undeformed.

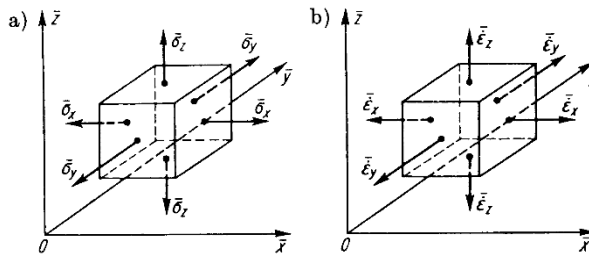


Fig. 3.4. Main axes for the stresses (a) and for the rate of deformation (b)

3.6 Relation Between Stresses and Rate of Deformation

We emphasise again here that the equations which couple the surface forces to the flow field can only be obtained from the interpretation of experimental results and that here we treat only isotropic Newtonian fluids. The ideas of the previous section have given us the necessary mathematical tools to allow these relations to be stated precisely.

If a fluid is at rest, there are no tangential stresses and the normal stresses are equal to the negative pressure, which is identical to the thermodynamic

pressure. If the fluid is in motion, the equation of state still determines the pressure at every point (“principle of local state”, cf. J. Kestin (1966a)). It was therefore useful to introduce the viscous stress tensor corresponding to Eq. (3.19), cf. Eq. (3.22), since its components are due only to the motion and vanish at rest.

From the explanations in the previous section, we can assume that the components of the viscous stress tensor only depend on the components of the rate of deformation tensor and not explicitly on the velocity components u, v, w , or on the components of the angular velocity vector $\omega_x, \omega_y, \omega_z$. This is the same as saying that the instantaneous translation (components of motion (a)) as well as the instantaneous rigid body rotation (components of motion (b)) of a fluid element do not generate any surface stresses apart from the pressure components already stated. This statement is a precise formulation of the local conditions observed when a finite fluid volume carries out a general motion which is the same as that of an equivalent rigid body. Therefore, we conclude from this that the components of the viscous stress tensor τ_{ij} can only depend on the velocity gradients $\partial u / \partial x, \dots, \partial w / \partial z$ in suitable combinations.

These relations must be linear. They must remain unchanged when the coordinate system is rotated, and, because of the isotropy, when the axes are exchanged. The isotropy also requires that the main axes of the stress tensor coincide with the axes of the rate of deformation tensor at all points in the field. In order to achieve this, an arbitrary point in the field is chosen and the local coordinate system $\bar{x}, \bar{y}, \bar{z}$ so chosen that its axes lie along the main axes of the stress tensor. Let the velocity components in this system be $\bar{u}, \bar{v}, \bar{w}$.

From this we see that the isotropy can only be conserved if each of the three normal stresses $\bar{\tau}_{xx}, \bar{\tau}_{yy}, \bar{\tau}_{zz}$ depend only on those components of the rate of deformation tensor in the same directions, and on the sum of these three components. Therefore we obtain the following ansatz, with expressions which only contain the spatial derivatives of the velocity components:

$$\begin{aligned}\bar{\tau}_{xx} &= \lambda \left(\frac{\partial \bar{u}}{\partial \bar{x}} + \frac{\partial \bar{v}}{\partial \bar{y}} + \frac{\partial \bar{w}}{\partial \bar{z}} \right) + 2\mu \frac{\partial \bar{u}}{\partial \bar{x}} \\ \bar{\tau}_{yy} &= \lambda \left(\frac{\partial \bar{u}}{\partial \bar{x}} + \frac{\partial \bar{v}}{\partial \bar{y}} + \frac{\partial \bar{w}}{\partial \bar{z}} \right) + 2\mu \frac{\partial \bar{v}}{\partial \bar{y}} \\ \bar{\tau}_{zz} &= \lambda \left(\frac{\partial \bar{u}}{\partial \bar{x}} + \frac{\partial \bar{v}}{\partial \bar{y}} + \frac{\partial \bar{w}}{\partial \bar{z}} \right) + 2\mu \frac{\partial \bar{w}}{\partial \bar{z}}.\end{aligned}\quad (3.35)$$

The quantities $\bar{u}, \bar{v}, \bar{w}$ and $\omega_x, \omega_y, \omega_z$ do not appear in these equations, for reasons explained earlier. The final term in each expression is the linear dilatation, i.e. a change in shape, and the first term is the volume dilatation, i.e. a change in volume; this is equivalent to a change in density. The factor 2 in the final term has been introduced in order to identify μ with the viscosity introduced in Chap. 1 (cf. Fig. 1.1). The proportionality factors μ and λ

must, because of the isotropy, have the same values in each of the equations (3.35). It can easily be seen that swapping any of the three pairs of axes of the quantities (\bar{u}, \bar{x}) , (\bar{v}, \bar{y}) , (\bar{w}, \bar{z}) leaves these equations unchanged. Indeed this has to be the case for an isotropic medium. In addition, Eq. (3.35) is the only combination of the spatial derivatives which has the required properties. If the reader cannot see this immediately, the proof can be found using tensor calculus, or from W. Prager (1961), p. 88.

The relations in Eq. (3.35) can be written down for any system of coordinates by applying a general rotation using a suitable linear transformation. The explicit calculation will not be given here. It is tedious to carry out directly, but it becomes simple if tensor calculus is used. Useful formulae for the direct calculation are to be found in L. Hopf (1927), H. Lamb (1932), A.E.H. Love (1952), while the calculation using tensor calculus is given by W. Prager (1961).

This calculation transforms the system (3.35) to

$$\begin{aligned}\tau_{xx} &= \lambda \operatorname{div} \vec{v} + 2\mu \frac{\partial u}{\partial x} \\ \tau_{yy} &= \lambda \operatorname{div} \vec{v} + 2\mu \frac{\partial v}{\partial y} \\ \tau_{zz} &= \lambda \operatorname{div} \vec{v} + 2\mu \frac{\partial w}{\partial z},\end{aligned}\tag{3.36}$$

$$\begin{aligned}\tau_{xy} = \tau_{yx} &= \mu \left(\frac{\partial v}{\partial x} + \frac{\partial u}{\partial y} \right) \\ \tau_{yz} = \tau_{zy} &= \mu \left(\frac{\partial w}{\partial y} + \frac{\partial v}{\partial z} \right) \\ \tau_{zx} = \tau_{xz} &= \mu \left(\frac{\partial u}{\partial z} + \frac{\partial w}{\partial x} \right).\end{aligned}\tag{3.37}$$

The abbreviation $\operatorname{div} \vec{v}$ has been used here. Note that the indices x, y, z , the velocity components u, v, w and the coordinates x, y, z undergo cyclic exchange.

If we apply these equations to the simple flow in Fig. 1.1, we obtain Eq. (1.2), thus confirming that the general equations above reduce to Newton's law of friction and are indeed a suitable generalisation. Here we note that the factor μ is identical to the viscosity of the fluid discussed in Sect. 1.2; in fact this also justifies the factor 2 introduced into Eq. (3.35). The physical justification of the second factor λ requires further discussion. We note, however, that it can only be meaningful for compressible fluids, since, for incompressible fluids, $\operatorname{div} \vec{v} = 0$ means that the terms proportional to λ vanish identically.

3.7 Stokes Hypothesis

Even though the problem we are discussing now arose more than one and a half centuries ago, the physical interpretation of the factor λ in Eq. (3.35) and (3.36) for flows where $\operatorname{div} \vec{v}$ is non-zero is still being discussed today. In the equations of motion its value is determined using a hypothesis by G.G. Stokes (1849). We shall first of all not concern ourselves with the physical laws on which the Stokes hypothesis is based, but merely state the result. We assume that the following relation exists between the two physical properties:

$$3\lambda + 2\mu = 0 \quad \text{or} \quad \lambda = -\frac{2}{3}\mu . \quad (3.38)$$

This sets the value of λ in relation to the viscosity μ . Thus the number of physical properties which characterise the stress field in a compressible fluid is reduced from two to one, hence to the same number as for an incompressible fluid.

If we introduce this value of λ into Eq. (3.19) and Eq. (3.36), we obtain the normal components of the stress tensor to be

$$\begin{aligned} \sigma_x &= -p - \frac{2}{3}\mu \operatorname{div} \vec{v} + 2\mu \frac{\partial u}{\partial x} \\ \sigma_y &= -p - \frac{2}{3}\mu \operatorname{div} \vec{v} + 2\mu \frac{\partial v}{\partial y} \\ \sigma_z &= -p - \frac{2}{3}\mu \operatorname{div} \vec{v} + 2\mu \frac{\partial w}{\partial z} . \end{aligned} \quad (3.38a)$$

The components τ_{xy} , τ_{xz} and τ_{yz} of the stress tensor are unaffected by the Stokes hypothesis, cf. Eq. (3.37).

Although Eq. (3.38) must be viewed as a pure hypothesis, or even as an educated guess, the equations of motion arising from inserting Eq. (3.38) can be accepted because they have been confirmed by an exceedingly large number of experiments, sometimes in extreme conditions, as will be realised by the reader on completing this book. These equations of motion are a very good description of actual physical processes.

The components of the viscous stress tensor represent those stresses which lead to dissipation in an isothermal flow, whereas other aspects of dissipation in the temperature field are due to heat conduction, cf. Sect. 3.10. Further, since the factor λ only appears in the normal stresses τ_{xx} , τ_{yy} , τ_{zz} which also contain the thermodynamic pressure Eq. (3.19), it is clear that the physical meaning of the factor λ is connected with the mechanism of dissipation if the fluid volume is changed by a finite amount, and with the relation between the stress tensor and the thermodynamic pressure.

At this point it should be noted that if λ and μ are proportional, all terms containing λ as a factor can be neglected in boundary-layer theory. As M. Van Dyke (1962c) showed, these terms do not even play any role in second order boundary-layer theory, cf. Chap. 14.

3.8 Bulk Viscosity and Thermodynamic Pressure

We shall now return to the earlier general discussion without assuming that the Stokes hypothesis Eq. (3.38) is valid. We shall restrict ourselves to the case without shear stresses, since their physical interpretation and origin are clear.

Consider a fluid system where a normal stress $\bar{\sigma}$ acts equally on all its boundaries, e.g. a sphere as in Fig. 3.5a.

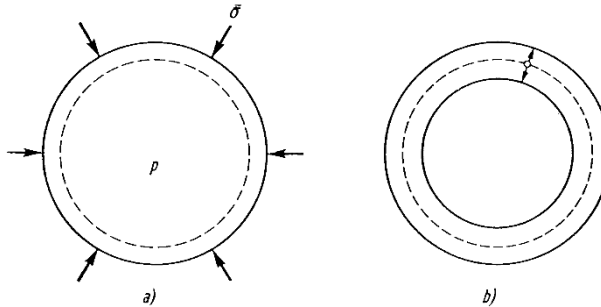


Fig. 3.5. (a) Quasi-static compression; (b) oscillatory motion of a spherically shaped fluid mass

If there is no motion, the normal stress is equal to but in the opposite direction to the thermodynamic pressure p . In the case of motion, adding the three equations (3.35), and using Eq. (3.19) yields

$$\bar{\sigma} = -p + \left(\lambda + \frac{2}{3}\mu \right) \operatorname{div} \vec{v}, \quad (3.39)$$

reiterating the fact explained earlier. Now we have assumed a quasi-static motion whose velocity is small compared to the spreading velocity of pressure perturbations, so that there is uniform pressure in the spherical fluid element. The question now arises of what this relation implies in a general flow field. If the system is compressed quasi-statically and reversibly the previous case again holds, since asymptotically $\operatorname{div} \vec{v} = 0$. In such a case, the work per unit time and unit volume in a thermodynamic reversible process, cf. Sect. 3.10, Eq. (3.54), becomes

$$\frac{\dot{W}}{dV} = -p \operatorname{div} \vec{v}. \quad (3.40)$$

For finite values of $\operatorname{div} \vec{v}$ and in the case of compression, expansion or oscillation at finite amplitudes, the average stress $\bar{\sigma}$ and the pressure $-p$ are equal only if the coefficient

$$\mu' = \lambda + \frac{2}{3}\mu \quad (3.41)$$

vanishes identically (the Stokes hypothesis). If this is not the case, $\bar{\sigma}$ and $-p$ are not equal. If $\mu' \neq 0$, the oscillatory motion of the spherically symmetric system in Fig. 3.5b leads to dissipation, even if the temperature in the volume of gas remains constant. The same is true of finite expansion and compression too. For this reason, the coefficient μ' is called the *bulk viscosity*: it is the property which (in analogy to the normal viscosity μ in the case of deformation) is responsible for the energy dissipation in a fluid of smooth temperature distribution due to a finite change in volume. The bulk viscosity is therefore a second physical property of a compressible,

isotropic Newtonian fluid. It appears in the constitutive relations (3.36) and must be measured in addition to the coefficient μ . It is clear that

$$\begin{aligned}\mu' = 0 \quad &\text{requires that } p = -\bar{\sigma}, \\ \mu' \neq 0 \quad &\text{requires that } p \neq -\bar{\sigma}.\end{aligned}$$

The assumption of the Stokes hypothesis is equivalent to the assumption that the thermodynamic pressure is equal to the value of the invariant “one third of the sum of the normal stresses”, even if finite compression and expansion take place. In addition it is equivalent to the assumption that the oscillatory motion of a large spherical system is reversible as long as it is isothermal. More about the thermodynamics of irreversible processes in a continuous system can be found in work by J. Meixner; H.G. Reik (1959), I. Prigogine (1947) and S.R. De Groot; P. Mazur (1962).

In order to determine under what conditions the bulk viscosity of a compressible fluid vanishes, experimental investigations must be carried out, or else the methods of statistical thermodynamics which allow the transport coefficients to be worked out from fundamentals must be used. Direct measurement of the bulk viscosity is difficult to carry out, and to this end there are as yet no reliable results. Statistical methods for high density gases are not yet so well developed that they yield useful insights into these problems. It is probable that the bulk viscosity vanishes for low density gases, i.e. under conditions where only binary collisions occur. In dense gases, the numerical value of the bulk viscosity seems to be very small. This means that Eq. (3.40) describes the work done in a continuous system without shear stresses exceedingly well even here, and that dissipation at constant temperature, even in the general case, only arises via the deviator stresses. Thus we are again led to the Stokes hypothesis, and to Eq. (3.39). This does not hold for fluids where the relaxation processes are due to local deviations from chemical equilibrium, cf. S.R. De Groot; P. Mazur (1962), J. Meixner, H.G. Reik (1959) and L.D. Landau; E.M. Lifschitz (1966). Such relaxation processes occur when, for example, chemical reactions take place, or, in gases with complex structures, when a relatively slow energy transition takes place between the translation and rotation degrees of freedom on the one hand and the oscillation degrees of freedom on the other. If relaxation processes occur, the thermodynamic pressure is no longer equal to one third of the sum of the main diagonal elements of the stress tensor.

It is occasionally objected that the assumption of the Stokes hypothesis, i.e. the assumption that the bulk viscosity of the Newtonian fluid vanishes, does not agree with the intuitive idea that a fluid sphere whose boundary oscillates as a result of compression and expansion (Fig. 3.5b) dissipates energy. This would indeed be true because, as is easily seen from above, the dissipative part of the stress field vanishes under such conditions. However we must not forget that such a conclusion is only valid if the temperature of the gas sphere is kept constant throughout the oscillation. Normally this is impossible. Because of this, an oscillating gas sphere will soon develop a temperature field and energy will be dissipated in the direction of the temperature gradient, cf. J. Kestin (1966b).

Sound absorption is one of those processes where the bulk viscosity plays a role (cf. L.D. Landau; E.M. Lifschitz (1966), J. Meixner, H.G. Reik (1959)), as is the shock wave (cf. F.M. White (1974)). The question of whether the bulk viscosity vanishes for monatomic gases has been dealt with in the work of C. Truesdell (1954).

3.9 Navier–Stokes Equations

If the transport equations (constitutive relations) corresponding to Eqs. (3.36) and (3.37) are inserted into the momentum equation Eq. (3.20), and the Stokes hypothesis Eq. (3.38) taken into account, we find the following equations of motion in Cartesian coordinates:

$$\begin{aligned} \varrho \frac{Du}{Dt} &= f_x - \frac{\partial p}{\partial x} + \frac{\partial}{\partial x} \left[\mu \left(2 \frac{\partial u}{\partial x} - \frac{2}{3} \operatorname{div} \vec{v} \right) \right] \\ &\quad + \frac{\partial}{\partial y} \left[\mu \left(\frac{\partial u}{\partial y} + \frac{\partial v}{\partial x} \right) \right] + \frac{\partial}{\partial z} \left[\mu \left(\frac{\partial w}{\partial x} + \frac{\partial u}{\partial z} \right) \right] \\ \varrho \frac{Dv}{Dt} &= f_y - \frac{\partial p}{\partial y} + \frac{\partial}{\partial y} \left[\mu \left(2 \frac{\partial v}{\partial y} - \frac{2}{3} \operatorname{div} \vec{v} \right) \right] \\ &\quad + \frac{\partial}{\partial z} \left[\mu \left(\frac{\partial v}{\partial z} + \frac{\partial w}{\partial y} \right) \right] + \frac{\partial}{\partial x} \left[\mu \left(\frac{\partial u}{\partial y} + \frac{\partial v}{\partial x} \right) \right] \\ \varrho \frac{Dw}{Dt} &= f_z - \frac{\partial p}{\partial z} + \frac{\partial}{\partial z} \left[\mu \left(2 \frac{\partial w}{\partial z} - \frac{2}{3} \operatorname{div} \vec{v} \right) \right] \\ &\quad + \frac{\partial}{\partial x} \left[\mu \left(\frac{\partial w}{\partial x} + \frac{\partial u}{\partial z} \right) \right] + \frac{\partial}{\partial y} \left[\mu \left(\frac{\partial v}{\partial z} + \frac{\partial w}{\partial y} \right) \right]. \end{aligned} \quad (3.42)$$

These differential equations are known as the Navier–Stokes equations. Using symbolic notation, they can be given in a form which is valid in all coordinate systems:

$$\varrho \frac{D\vec{v}}{Dt} = \vec{f} - \operatorname{grad} p + \operatorname{Div} \boldsymbol{\tau} \quad (3.43)$$

with

$$\boldsymbol{\tau} = \mu \left(2 \dot{\boldsymbol{\epsilon}} - \frac{2}{3} \boldsymbol{\delta} \operatorname{div} \vec{v} \right), \quad (3.44)$$

where $\boldsymbol{\delta}$ is the Kronecker unit tensor ($\delta_{ij} = 1$ for $i = j$, $\delta_{ij} = 0$ for $i \neq j$).

The above equations were first set up by M. Navier (1827) and S.D. Poisson (1831) on the basis of considerations on the action of the intermolecular forces. Later the same equations were derived without such hypotheses by B. De St.Venant (1843) and G.G. Stokes (1849), using, as a basis, the same assumptions made here, that the normal and shear stresses are linear functions of the rate of deformation, as had already been introduced via Newton's law of friction.

Since the Stokes assumption for the friction forces is purely empirical, one cannot be a priori sure that the Navier–Stokes equations correctly describe the motion of a fluid. Therefore they must be checked, something that can only be done experimentally. It must, however, be taken into account that the great mathematical difficulty of these equations means that only very few

solutions are known where the convective terms interact quite generally with the friction terms. However, known particular solutions, such as laminar pipe flow and the boundary-layer solutions which will be discussed later, agree so well with the experimental results that there is hardly any doubt about the general validity of the Navier–Stokes equations.

As a consequence of the Navier–Stokes equations, an equation for the mechanical energy can be derived. If the Navier–Stokes equation in the x direction is multiplied by u , that in the y direction by v and that in the z direction by w , and the sum of these equations formed, the energy equation for the mechanical energy is found. This reads, in vector notation:

$$\varrho \frac{D(\frac{1}{2}\vec{v}^2)}{Dt} = \vec{v} \vec{f} - \vec{v} \operatorname{grad} p + \vec{v} \operatorname{Div} \boldsymbol{\tau}. \quad (3.45)$$

If we assume that a steady potential ψ (i.e. independent of t) exists for the volume force \vec{f} , with

$$\vec{f} = -\varrho \operatorname{grad} \psi, \quad (3.46)$$

then it follows from Eq. (3.45) that

$$\varrho \frac{D(\frac{1}{2}\vec{v}^2 + \psi)}{Dt} = -\vec{v} \operatorname{grad} p + \vec{v} \operatorname{Div} \boldsymbol{\tau}. \quad (3.47)$$

As stated at the start of Chap. 3, in addition to the continuity equation and the Navier–Stokes equations, the (thermal) energy equation containing the first law of thermodynamics is also required for a complete description of flow fields. This will be derived in the following section.

3.10 Energy Equation

In order to set up the equation for the energy balance in a flow, we consider a fluid particle of mass $dM = \varrho dV$ and volume $dV = dx dy dz$ in a Cartesian coordinate system and follow it on its path in the flow. According to the first law of thermodynamics, the gain in total energy DE_t (the index t stands for *total energy*) in unit time Dt is equal to the heat supplied to the mass element $\dot{Q} Dt$ and the work done on the element $\dot{W} Dt$. Therefore we have:

$$\frac{DE_t}{Dt} = \dot{Q} + \dot{W} \quad \left[\frac{\text{J}}{\text{s}} \right]. \quad (3.48)$$

energy change heat flux power

DE_t/Dt is the substantial change in E_t , and this generally has both a local part and a convective part, cf. Eq. (3.4). Heat can be supplied both by heat conduction and by heat radiation. For small temperature differences, however, the radiation is generally not considerable, and will thus not be taken into account in this book. See summaries of gas radiation dynamics by S.I. Pai (1965), E.M. Sparrow; R.D. Cess (1966), W. Schneider (1968), W.G. Vincenti;

S.C. Traugott (1971). In principle, heat could also be supplied via heat sources in the mass element. Such heat sources could occur in the form of chemical reactions (combustion) or of Joule's heat in electromagnetic gas dynamics, cf. the following literature: J.A. Shercliff (1965), P.A. Libby; F.A. Williams (1980), F. Barthmä (1975). These heat sources will also not be taken into account in this book.

The heat transferred per unit surface area and per unit time is denoted by the heat flux vector $\vec{q}(q_x, q_y, q_z)$, ($[\vec{q}] = \text{J/m}^2 \text{s}$). Therefore the heat entering the volume element (Fig. 3.1) through the surface element perpendicular to the x direction per unit time is $q_x dy dz$, while that exiting per unit time is $[q_x + (\partial q_x / \partial x) dx] dy dz$. Therefore the supply of heat in the x direction in time Dt is

$$\dot{Q}_x = -\frac{\partial q_x}{\partial x} dx dy dz = -\frac{\partial q_x}{\partial x} dV.$$

Thus the total supply of heat is

$$\dot{Q} = -dV \left(\frac{\partial q_x}{\partial x} + \frac{\partial q_y}{\partial y} + \frac{\partial q_z}{\partial z} \right) \quad (3.49)$$

or

$$\dot{Q} = -dV \operatorname{div} \vec{q}. \quad (3.50)$$

Hence the supply of heat is proportional to the divergence of the heat flux vector \vec{q} . Since the divergence is a measure for the source strength of the vector field in question, the term \dot{Q} is strictly speaking also a source term.

The total energy E_t generally consists of three parts: the internal energy $dM \cdot e$, the kinetic energy $\frac{1}{2}dM \cdot \vec{v}^2$ and the potential energy $dM \cdot \psi$. The following statement holds:

$$dE_t = dM e_t = dV \varrho e_t = dV \varrho \left(e + \frac{1}{2} \vec{v}^2 + \psi \right). \quad (3.51)$$

Here e ($[e] = \text{m}^2/\text{s}^2$) is the specific internal energy. Thus the substantial change of the total energy follows as

$$\frac{DE_t}{Dt} = dV \varrho \frac{De_t}{Dt} = dV \varrho \frac{D(e + \frac{1}{2} \vec{v}^2 + \psi)}{Dt}. \quad (3.52)$$

To determine the power \dot{W} we first consider, for example, the work done on the mass element within the time Dt by σ_x . From Fig. 3.1 we have

$$\begin{aligned} \dot{W}_{\sigma_x} &= dy dz \left[-u \sigma_x + \left(u + \frac{\partial u}{\partial x} dx \right) \left(\sigma_x + \frac{\partial \sigma_x}{\partial x} dx \right) \right] \\ &= dV \frac{\partial}{\partial x} (u \sigma_x). \end{aligned}$$

Thus the total rate of work done by all normal and tangential stresses on the mass element of volume dV is:

$$\dot{W} = dV \left[\frac{\partial}{\partial x}(u\sigma_x + v\tau_{xy} + w\tau_{xz}) + \frac{\partial}{\partial y}(u\tau_{yx} + v\sigma_y + w\tau_{yz}) + \frac{\partial}{\partial z}(u\tau_{zx} + v\tau_{zy} + w\sigma_z) \right]. \quad (3.53)$$

Here $\sigma_x, \sigma_y, \dots, \tau_{xy}$ are the total stresses in Eqs. (3.13) and (3.15). In symbolic form (vector notation) this can also be written as

$$\dot{W} = dV \operatorname{div}(\boldsymbol{\sigma} \vec{v}). \quad (3.54)$$

If we insert Eqs. (3.50), (3.52) and (3.54) into Eq. (3.48), we find the energy equation

$$\varrho \frac{D(e + \frac{1}{2}\vec{v}^2 + \psi)}{Dt} = -\operatorname{div} \vec{q} + \operatorname{div}(\boldsymbol{\sigma} \vec{v}). \quad (3.55)$$

The change in total energy, i.e. the sum of the internal, kinetic and potential energies, is equal to the energy supplied by heat conduction and the work done by the surface forces.

If we take the relation between the stress tensor $\boldsymbol{\sigma}$ and the viscous stress tensor $\boldsymbol{\tau}$ into account, cf. Eq. (3.19),

$$\boldsymbol{\sigma} = -\boldsymbol{\delta}p + \boldsymbol{\tau}, \quad (3.56)$$

then Eq. (3.55) can also be written as follows:

$$\frac{\partial(\varrho e_t)}{\partial t} = -\operatorname{div}[(p + \varrho e_t)\vec{v} - \boldsymbol{\tau}\vec{v} + \vec{q}]. \quad (3.57)$$

Therefore the local change in the total energy can be identified as the divergence of a vector field. A balance law formulated in this way has, it is said, a *divergence* form or a *strictly conservative* form.

The energy equation Eq. (3.55) can also be formulated as a balance equation for the specific total enthalpy

$$h_t = e_t + \frac{p}{\varrho} \quad (3.58)$$

as follows

$$\varrho \frac{Dh_t}{Dt} = -\operatorname{div} \vec{q} + \frac{\partial p}{\partial t} + \operatorname{div}(\boldsymbol{\tau} \vec{v}). \quad (3.59)$$

By subtracting the energy equation (3.47) for the mechanical energy derived in the previous section from Eq. (3.55) for the specific total energy e_t , the balance law for the internal energy can be found:

$$\varrho \frac{De}{Dt} = -\operatorname{div} \vec{q} - p \operatorname{div} \vec{v} + \Phi. \quad (3.60)$$

Here the *dissipation function* is:

$$\Phi = \operatorname{div}(\boldsymbol{\tau} \vec{v}) - \vec{v} \operatorname{Div} \boldsymbol{\tau} \quad (3.61)$$

Taking the transport equations Eq. (3.36) and Eq. (3.37) and the Stokes hypothesis Eq. (3.38) into account, we find in Cartesian coordinates

$$\begin{aligned} \frac{\Phi}{\mu} = & 2 \left[\left(\frac{\partial u}{\partial x} \right)^2 + \left(\frac{\partial v}{\partial y} \right)^2 + \left(\frac{\partial w}{\partial z} \right)^2 \right] \\ & + \left(\frac{\partial v}{\partial x} + \frac{\partial u}{\partial y} \right)^2 + \left(\frac{\partial w}{\partial y} + \frac{\partial v}{\partial z} \right)^2 \\ & + \left(\frac{\partial u}{\partial z} + \frac{\partial w}{\partial x} \right)^2 - \frac{2}{3} \left(\frac{\partial u}{\partial x} + \frac{\partial v}{\partial y} + \frac{\partial w}{\partial z} \right)^2 \end{aligned} \quad (3.62)$$

or

$$\begin{aligned} \frac{\Phi}{\mu} = & \frac{2}{3} \left[\left(\frac{\partial u}{\partial x} - \frac{\partial v}{\partial y} \right)^2 + \left(\frac{\partial v}{\partial y} - \frac{\partial w}{\partial z} \right)^2 + \left(\frac{\partial w}{\partial z} - \frac{\partial u}{\partial x} \right)^2 \right] \\ & + \left(\frac{\partial v}{\partial x} + \frac{\partial u}{\partial y} \right)^2 + \left(\frac{\partial w}{\partial y} + \frac{\partial v}{\partial z} \right)^2 + \left(\frac{\partial u}{\partial z} + \frac{\partial w}{\partial x} \right)^2 . \end{aligned} \quad (3.63)$$

Other forms of the energy equation are also possible. As a balance of the specific enthalpy

$$h = e + \frac{p}{\varrho} \quad (3.64)$$

it reads

$$\varrho \frac{Dh}{Dt} = -\operatorname{div} \vec{q} + \frac{Dp}{Dt} + \Phi . \quad (3.65)$$

If we use the generally valid relation, cf. J. Kestin (1966a),

$$\frac{Dh}{Dt} = c_p \frac{DT}{Dt} + \frac{1 - \beta T}{\varrho} \frac{Dp}{Dt} \quad (3.66)$$

with the *isobaric specific heat capacity* c_p , ($[c_p] = \text{J/kg K}$) and the *coefficient of thermal expansion*

$$\beta = -\frac{1}{\varrho} \left(\frac{\partial \varrho}{\partial T} \right)_p , \quad (3.67)$$

the energy equation can be formulated as a balance for the temperature field:

$$\varrho c_p \frac{DT}{Dt} = -\operatorname{div} \vec{q} + \beta T \frac{Dp}{Dt} + \Phi . \quad (3.68)$$

This form of the energy equation will be used in preference in what follows.

Finally, because

$$T \frac{Ds}{Dt} = \frac{Dh}{Dt} - \frac{1}{\varrho} \frac{Dp}{Dt}$$

a balance equation for the specific entropy s can also be derived from the energy equation Eq. (3.65):

$$\varrho \frac{Ds}{Dt} = -\operatorname{div} \left(\frac{\vec{q}}{T} \right) - \frac{\vec{q}}{T^2} \operatorname{grad} T + \frac{1}{T} \Phi. \quad (3.69)$$

Apart from the divergence term, there are also two source terms on the right hand side of this equation which imply entropy production. According to the second law of thermodynamics, the entropy of an adiabatic system ($\vec{q} = 0$ at the boundary of the system) cannot decrease. Therefore the terms Φ/T and $-(\vec{q}/T^2) \operatorname{grad} T$ are not negative. Because of Eq. (3.63) it therefore follows that the viscosity μ must be positive. It follows from the second condition that the thermal conductivity λ , which is still to be introduced, must also be positive.

One more transport equation which connects the heat flux vector \vec{q} with the temperature field must now be added to the balance equation for the energy. From J.B. Fourier (1822) we have for the heat conduction

$$\vec{q} = -\lambda \operatorname{grad} T, \quad (3.70)$$

where the *thermal conductivity* λ ($[\lambda] = \text{J/m s K}$) is a positive physical property. Therefore the energy equation finally reads

$$\boxed{\varrho c_p \frac{DT}{Dt} = \operatorname{div}(\lambda \operatorname{grad} T) + \beta T \frac{Dp}{Dt} + \Phi}. \quad (3.71)$$

For plane flows this is written in Cartesian coordinates as:

$$\begin{aligned} \varrho c_p \left(\frac{\partial T}{\partial t} + u \frac{\partial T}{\partial x} + v \frac{\partial T}{\partial y} \right) &= \frac{\partial}{\partial x} \left(\lambda \frac{\partial T}{\partial x} \right) + \frac{\partial}{\partial y} \left(\lambda \frac{\partial T}{\partial y} \right) \\ &\quad + \beta T \left(\frac{\partial p}{\partial t} + u \frac{\partial p}{\partial x} + v \frac{\partial p}{\partial y} \right) + \Phi \end{aligned} \quad (3.72)$$

with the dissipation function Φ as in Eq. (3.62) or Eq. (3.63).

3.11 Equations of Motion for Arbitrary Coordinate Systems (Summary)

The derivation of the equations of motion will first be carried out for Cartesian coordinate systems. By using symbolic notation (vector notation), the equations of motion can be written in general terms as follows:

$$\frac{D\varrho}{Dt} = -\varrho \operatorname{div} \vec{v}, \quad (3.73)$$

$$\varrho \frac{D\vec{v}}{Dt} = \vec{f} - \operatorname{grad} p + \operatorname{Div} \left[\mu \left(2\dot{\epsilon} - \frac{2}{3} \delta \operatorname{div} \vec{v} \right) \right], \quad (3.74)$$

$$\varrho c_p \frac{DT}{Dt} = \operatorname{div}(\lambda \operatorname{grad} T) + \beta T \frac{Dp}{Dt} + \Phi. \quad (3.75)$$

We have

$$\frac{Da}{Dt} = \frac{\partial a}{\partial t} + \vec{v} \cdot \text{grad } a \quad (3.76)$$

with $a = \varrho, T$ or p and

$$\frac{D\vec{v}}{Dt} = \frac{\partial \vec{v}}{\partial t} + \text{grad} \left(\frac{1}{2} \vec{v}^2 \right) - \vec{v} \times \text{curl } \vec{v}. \quad (3.77)$$

Frequently the operators div and grad are written using the Nabla operator ∇ , as, e.g. $\nabla \vec{v} \equiv \text{div } \vec{v}$, $\nabla p \equiv \text{grad } p$.

There are therefore five equations for the five unknowns: p, T and the three components of \vec{v} . They are valid providing the following conditions hold:

- a) The fluid is a continuum.
- b) The stress tensor is symmetric. (The fluid has no local torque proportional to the volume, as would be possible in an electric field.)
- c) The fluid is isotropic. (There is no locally preferred direction, i.e. the main axes of the stress and rate of deformation tensors are the same.)
- d) The fluid is Newtonian. (There is a linear relation between the stress tensor and the rate of deformation tensor.)
- e) The Stokes hypothesis is valid, i.e. the bulk viscosity vanishes. (No relaxation processes may occur, i.e. the relaxation times for internal transfer processes must be very small compared to the deformation times.)
- f) The “principle of the local state” is valid. (At each point in the flow field the same equations of state hold as in a system at rest, i.e. there are no local or time gradients of the state variables present in the equations of state, cf. J. Kestin (1968).)
- g) The local thermodynamic state can be described using two state variables. If we choose p and T as these state variables, multi-phase flows are then not possible. Further, diffusion processes are not taken into account, since more than two state variables are required for their description. Diffusion processes will be discussed briefly in Sect. 11.3.
- h) The Fourier law for the heat flux vector holds.
- i) Heat sources (e.g. radiation, chemical reactions, Joule’s heat) are neglected.

The following boundary conditions at the walls are used with the equations of motion:

a) No-slip condition:

The velocity component v_t tangential to the wall vanishes at the wall. This is a condition which was discovered empirically, and which is satisfied very well within the framework of continuum mechanics. S. Goldstein (1965) has presented details of the no-slip condition, also from a historical point of view. At extremely low gas densities the no-slip condition is no longer satisfied: these are then *slip flows*, cf. S.A. Schaaf; P.L. Chambré (1958). The equations of motion are still valid for these flows, but the boundary conditions have to be changed appropriately.

b) Normal component of the velocity

The velocity component v_n normal to the wall generally vanishes where the walls are impermeable. However they are non-zero if the wall is permeable and fluid is either sucked or blown through it, cf. Chap. 11. The normal components of the velocity can also be non-zero in the case of non-porous walls if mass transfer processes are taken into account, as in the case of binary or multi-fluid flows. For example, condensation corresponds to suction and evaporation to blowing, cf. Chap. 11.

c) Temperature field

The number of different possible boundary conditions for the temperature field is much greater than the number for the velocity field. The principal different types of boundary conditions follow:

Boundary conditions of the first kind:

The wall temperature is prescribed. In the continuum regime, the fluid takes on the wall temperature at the wall. In flows of very low density gases (*slip flows*), however, there is a jump in temperature, cf. S.A. Schaaf; P.L. Chambré (1958).

Boundary conditions of the second kind:

The heat flux at the wall $q_w = (\vec{q} \cdot \vec{n})_w$, where \vec{n} is the normal unit vector at the wall, is prescribed.

Boundary conditions of the third kind:

These can be a coupling of the wall temperature and the heat flux at the wall. However, such boundary conditions could also be coupling conditions with the temperature field inside the wall.

The equations of motion make up a system of five partial differential equations for p , T and the three components of the velocity vector \vec{v} . In order to complete the system, the equations of state for the density $\varrho(p, T)$ and the

isobaric specific heat capacity $c_p(p, T)$, as well as relations for the viscosity $\mu(p, T)$ and the thermal conductivity $\lambda(p, T)$ must all be at hand. The coefficient of thermal expansion β which is also in the energy equation is found by partial differentiation of the equation of state for $\varrho(p, T)$.

The physical properties mentioned are summarised for some technically important fluids in Table 3.1. More data for water can be found in W. Wagner; A. Kruse (1998). The table (for $p_R = 1$ bar) also gives an overview of the changes in the physical properties with respect to temperature and pressure. The dependencies of the quantities μ , λ and c_p on the pressure are generally very small and can mostly be neglected. This table also shows that, in the case of liquids, the temperature dependence of the viscosity is important. Note that the changes in the physical properties close to the critical point can take on considerable values.

The historical development of the Navier-Stokes equations has been described by E. Krause (2014).

3.12 Equations of Motion for Cartesian Coordinates in Index Notation

In order to simplify the equations of motion, index notation is frequently used for vectors and tensors in Cartesian coordinates. Here Einstein's summation convention must be taken into account: if a given index appears twice, then it must be summed from one to three. The position vector has the components x_i and the velocity vector the components u_i .

The equations of motion read:

continuity equation:

$$\frac{\partial \varrho}{\partial t} + \frac{\partial}{\partial x_i}(\varrho u_i) = 0 . \quad (3.78)$$

momentum equation:

$$\frac{\partial}{\partial t}(\varrho u_i) + \frac{\partial}{\partial x_j}(\varrho u_i u_j) = f_i - \frac{\partial p}{\partial x_i} + \frac{\partial \tau_{ij}}{\partial x_j} \quad (3.79)$$

with

$$\tau_{ij} = \mu \left(\frac{\partial u_i}{\partial x_j} + \frac{\partial u_j}{\partial x_i} - \frac{2}{3} \delta_{ij} \frac{\partial u_\ell}{\partial x_\ell} \right) . \quad (3.80)$$

energy equation:

$$\begin{aligned} \frac{\partial}{\partial t}(\varrho c_p T) + \frac{\partial}{\partial x_j}(\varrho c_p u_j T) \\ = \beta T \left(\frac{\partial p}{\partial t} + u_j \frac{\partial p}{\partial x_j} \right) + \tau_{ij} \frac{\partial u_i}{\partial x_j} + \frac{\partial}{\partial x_j} \left(\lambda \frac{\partial T}{\partial x_j} \right) . \end{aligned} \quad (3.81)$$

The most concise way of writing the equations of motion is the strictly conservative form. With $f_i = -\varrho \partial \psi / \partial x_i$ they read:

$$\frac{\partial U}{\partial t} + \frac{\partial F_j}{\partial x_j} = Q_j \quad (3.82)$$

Table 3.1. Physical properties, temperature dependence Eq. (4.30), pressure dependence Eq. (10.26), of air, water, oil, sodium at $p_R = 1\text{bar}$

Fluid	Air	Water	Oil (Shell Voluta 919)			Sodium (liquid)
T/K	293	473	273	293	343	473
$T/^\circ\text{C}$	20	200	500	0	20	70
$\rho/\frac{\text{kg}}{\text{m}^3}$	1.188	0.736	0.450	999.8	998.2	977.8
$\mu/\frac{10^{-9}\text{kg}}{\text{ms}}$	18.185	25.850	35.800	1791.5	1001.6	403.9
$\nu/\frac{10^{-6}\text{m}^2}{\text{s}}$	15.307	35.122	79.556	1.792	1.004	0.413
$\lambda/\frac{10^{-3}\text{W}}{\text{mK}}$	25.721	38.660	56.346	561.1	598.5	663.1
$c_p/\frac{\text{kJ}}{\text{kgK}}$	1.014	1.048	1.096	4.219	4.185	4.188
\Pr	0.717	0.702	0.696	13.47	7.00	2.55
$-\beta T = K_q$	-1.000	-1.000	-1.000	0.018	-0.061	-0.200
K_μ	0.775	0.696	0.633	-9.264	-7.239	-4.758
K_λ	0.891	0.809	0.726	0.924	0.872	0.404
K_c	0.068	0.076	0.108	-0.226	-0.050	0.052
\tilde{K}_ϱ	1	1	1	$5 \cdot 10^{-5}$	$5 \cdot 10^{-5}$	$5 \cdot 10^{-5}$
\tilde{K}_μ	$6 \cdot 10^{-4}$	$3 \cdot 10^{-4}$	$1 \cdot 10^{-4}$	$-1 \cdot 10^{-4}$	$-5 \cdot 10^{-5}$	$6 \cdot 10^{-5}$
\tilde{K}_λ	$2 \cdot 10^{-3}$	$9 \cdot 10^{-4}$	$4 \cdot 10^{-4}$	$1 \cdot 10^{-4}$	$8 \cdot 10^{-5}$	$8 \cdot 10^{-5}$
\tilde{K}_c	$2 \cdot 10^{-3}$	$5 \cdot 10^{-4}$	$2 \cdot 10^{-4}$	$-1 \cdot 10^{-4}$	$-7 \cdot 10^{-5}$	$-5 \cdot 10^{-5}$
temperature dependence						
pressure dependence						

with the matrices

$$U = \begin{pmatrix} \varrho \\ \varrho u_i \\ \varrho e_t \end{pmatrix}, \quad F_j = \begin{pmatrix} \varrho u_j \\ \varrho u_i u_j + \delta_{ij} p - \tau_{ij} \\ u_j (\varrho e_t + p) - u_\ell \tau_{\ell j} - \lambda \frac{\partial T}{\partial x_j} \end{pmatrix}, \quad Q_j = \begin{pmatrix} 0 \\ f_i \\ 0 \end{pmatrix}, \quad (3.83)$$

where the viscous stress tensor τ_{ij} is given by Eq. (3.22) and the specific total energy e_t by Eq. (3.51).

With a general coordinate transformation from x_j to $\xi_j(x_j)$ of the form

$$\begin{aligned} \xi_1 &= \xi_1(x_1, x_2, x_3) \\ \xi_2 &= \xi_2(x_1, x_2, x_3) \\ \xi_3 &= \xi_3(x_1, x_2, x_3) \end{aligned} \quad (3.84)$$

the equations of motion can again be brought to strictly conservative form. H. Vi-viand (1974) and M. Vinokur (1974) have shown that, for $Q_j = 0$, Eq. (3.82) becomes

$$\frac{\partial U^*}{\partial t} + \frac{\partial F_j^*}{\partial \xi_j} = 0 \quad (3.85)$$

with

$$U^* = \frac{1}{J} U, \quad (3.86)$$

$$F_j^* = \frac{1}{J} F_i \frac{\partial \xi_j}{\partial x_i}, \quad (3.87)$$

where J is the Jacobi determinant:

$$J = \frac{\partial(\xi_1, \xi_2, \xi_3)}{\partial(x_1, x_2, x_3)} = \begin{vmatrix} \frac{\partial \xi_1}{\partial x_1} & \frac{\partial \xi_1}{\partial x_2} & \frac{\partial \xi_1}{\partial x_3} \\ \frac{\partial \xi_2}{\partial x_1} & \frac{\partial \xi_2}{\partial x_2} & \frac{\partial \xi_2}{\partial x_3} \\ \frac{\partial \xi_3}{\partial x_1} & \frac{\partial \xi_3}{\partial x_2} & \frac{\partial \xi_3}{\partial x_3} \end{vmatrix}. \quad (3.88)$$

3.13 Equations of Motion in Different Coordinate Systems

Cylindrical coordinates

position vector

$$r, \varphi, z$$

velocity vector

$$\vec{v}(v_r, v_\varphi, v_z)$$

angular velocity vector

$$\begin{aligned} \vec{\omega} &= \frac{1}{2} \operatorname{curl} \vec{v} \\ \omega_r &= \frac{1}{2} \left(\frac{1}{r} \frac{\partial v_z}{\partial \varphi} - \frac{\partial v_\varphi}{\partial z} \right) \\ \omega_\varphi &= \frac{1}{2} \left(\frac{\partial v_r}{\partial z} - \frac{\partial v_z}{\partial r} \right) \\ \omega_z &= \frac{1}{2r} \left[\frac{\partial}{\partial r} (rv_\varphi) - \frac{\partial v_r}{\partial \varphi} \right] \end{aligned} \quad (3.89)$$

continuity equation

$$\frac{\partial \rho}{\partial t} + \frac{1}{r} \frac{\partial (\rho r v_r)}{\partial r} + \frac{1}{r} \frac{\partial (\rho v_\varphi)}{\partial \varphi} + \frac{\partial (\rho v_z)}{\partial z} = 0 \quad (3.90)$$

momentum equations

$$\begin{aligned} \rho \left(\frac{\partial v_r}{\partial t} + v_r \frac{\partial v_r}{\partial r} + \frac{v_\varphi}{r} \frac{\partial v_r}{\partial \varphi} - \frac{v_\varphi^2}{r} + v_z \frac{\partial v_r}{\partial z} \right) \\ = f_r - \frac{\partial p}{\partial r} + \frac{1}{r} \frac{\partial (r \tau_{rr})}{\partial r} + \frac{1}{r} \frac{\partial \tau_{r\varphi}}{\partial \varphi} + \frac{\partial \tau_{rz}}{\partial z} - \frac{\tau_{\varphi\varphi}}{r} \end{aligned} \quad (3.91)$$

$$\begin{aligned} \rho \left(\frac{\partial v_\varphi}{\partial t} + v_r \frac{\partial v_\varphi}{\partial r} + \frac{v_\varphi}{r} \frac{\partial v_\varphi}{\partial \varphi} + \frac{v_r v_\varphi}{r} + v_z \frac{\partial v_\varphi}{\partial z} \right) \\ = f_\varphi - \frac{1}{r} \frac{\partial p}{\partial \varphi} + \frac{1}{r^2} \frac{\partial}{\partial r} (r^2 \tau_{r\varphi}) + \frac{1}{r} \frac{\partial \tau_{\varphi\varphi}}{\partial \varphi} + \frac{\partial \tau_{\varphi z}}{\partial z} \end{aligned} \quad (3.92)$$

$$\begin{aligned} \rho \left(\frac{\partial v_z}{\partial t} + v_r \frac{\partial v_z}{\partial r} + \frac{v_\varphi}{r} \frac{\partial v_z}{\partial \varphi} + v_z \frac{\partial v_z}{\partial z} \right) \\ = f_z - \frac{\partial p}{\partial z} + \frac{1}{r} \frac{\partial (r \tau_{rz})}{\partial r} + \frac{1}{r} \frac{\partial \tau_{\varphi z}}{\partial \varphi} + \frac{\partial \tau_{zz}}{\partial z} \end{aligned} \quad (3.93)$$

energy equation

$$\begin{aligned} \varrho c_p & \left(\frac{\partial T}{\partial t} + v_r \frac{\partial T}{\partial r} + \frac{v_\varphi}{r} \frac{\partial T}{\partial \varphi} + v_z \frac{\partial T}{\partial z} \right) \\ & = \frac{1}{r} \frac{\partial}{\partial r} \left(\lambda r \frac{\partial T}{\partial r} \right) + \frac{1}{r} \frac{\partial}{\partial \varphi} \left(\lambda \frac{1}{r} \frac{\partial T}{\partial \varphi} \right) + \frac{\partial}{\partial z} \left(\lambda \frac{\partial T}{\partial z} \right) \\ & + \beta T \left(\frac{\partial p}{\partial t} + v_r \frac{\partial p}{\partial r} + \frac{v_\varphi}{r} \frac{\partial p}{\partial \varphi} + v_z \frac{\partial p}{\partial z} \right) + \Phi \end{aligned} \quad (3.94)$$

viscous stresses

$$\begin{aligned} \tau_{rr} & = \mu \left(2 \frac{\partial v_r}{\partial r} - \frac{2}{3} \operatorname{div} \vec{v} \right) \\ \tau_{\varphi\varphi} & = \mu \left[2 \left(\frac{1}{r} \frac{\partial v_\varphi}{\partial \varphi} + \frac{v_r}{r} \right) - \frac{2}{3} \operatorname{div} \vec{v} \right] \\ \tau_{zz} & = \mu \left(2 \frac{\partial v_z}{\partial z} - \frac{2}{3} \operatorname{div} \vec{v} \right) \\ \tau_{r\varphi} & = \mu \left[r \frac{\partial}{\partial r} \left(\frac{v_\varphi}{r} \right) + \frac{1}{r} \frac{\partial v_r}{\partial \varphi} \right] \\ \tau_{rz} & = \mu \left(\frac{\partial v_z}{\partial r} + \frac{\partial v_r}{\partial z} \right) \\ \tau_{\varphi z} & = \mu \left(\frac{\partial v_\varphi}{\partial z} + \frac{1}{r} \frac{\partial v_z}{\partial \varphi} \right) \end{aligned} \quad (3.95)$$

dissipation function

$$\begin{aligned} \frac{\Phi}{\mu} & = 2 \left[\left(\frac{\partial v_r}{\partial r} \right)^2 + \left(\frac{1}{r} \frac{\partial v_\varphi}{\partial \varphi} + \frac{v_r}{r} \right)^2 + \left(\frac{\partial v_z}{\partial z} \right)^2 \right] \\ & + \left[r \frac{\partial}{\partial r} \left(\frac{v_\varphi}{r} \right) + \frac{1}{r} \frac{\partial v_r}{\partial \varphi} \right]^2 + \left(\frac{1}{r} \frac{\partial v_z}{\partial \varphi} + \frac{\partial v_\varphi}{\partial z} \right)^2 \\ & + \left(\frac{\partial v_r}{\partial z} + \frac{\partial v_z}{\partial r} \right)^2 - \frac{2}{3} (\operatorname{div} \vec{v})^2 \end{aligned} \quad (3.96)$$

divergence

$$\operatorname{div} \vec{v} = \frac{1}{r} \frac{\partial(r v_r)}{\partial r} + \frac{1}{r} \frac{\partial v_\varphi}{\partial \varphi} + \frac{\partial v_z}{\partial z} . \quad (3.97)$$

Natural coordinates for plane flows (cf. Fig. 3.6)

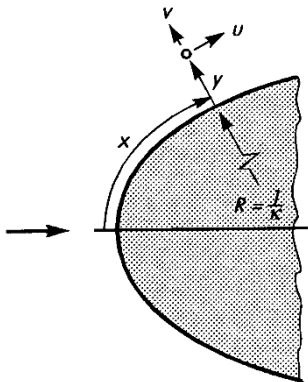


Fig. 3.6. Natural coordinate system for plane flows

contour curvature

$$\kappa(x) = 1/R(x)$$

coordinates

$$x, y$$

velocity vector

$$\vec{v}(u, v)$$

angular velocity

$$\omega = \frac{1}{2} \left\{ \frac{1}{1 + \kappa y} \frac{\partial v}{\partial x} - \frac{1}{1 + \kappa y} \frac{\partial}{\partial y} [(1 + \kappa y) u] \right\} \quad (3.98)$$

continuity equation

$$\frac{\partial \varrho}{\partial t} + \frac{1}{1 + \kappa y} \frac{\partial (\varrho u)}{\partial x} + \frac{1}{1 + \kappa y} \frac{\partial}{\partial y} [(1 + \kappa y) \varrho v] = 0 \quad (3.99)$$

momentum equations

$$\begin{aligned} \varrho & \left(\frac{\partial u}{\partial t} + \frac{u}{1 + \kappa y} \frac{\partial u}{\partial x} + v \frac{\partial u}{\partial y} + \frac{\kappa}{1 + \kappa y} u v \right) \\ & = f_x - \frac{1}{1 + \kappa y} \frac{\partial p}{\partial x} + \frac{1}{1 + \kappa y} \frac{\partial \tau_{xx}}{\partial x} + \frac{1}{(1 + \kappa y)^2} \frac{\partial}{\partial y} [(1 + \kappa y)^2 \tau_{xy}] \end{aligned} \quad (3.100)$$

$$\begin{aligned} \varrho & \left(\frac{\partial v}{\partial t} + \frac{u}{1 + \kappa y} \frac{\partial v}{\partial x} + v \frac{\partial v}{\partial y} - \frac{\kappa}{1 + \kappa y} u^2 \right) \\ & = f_y - \frac{\partial p}{\partial y} + \frac{1}{1 + \kappa y} \frac{\partial \tau_{xy}}{\partial x} + \frac{1}{1 + \kappa y} \frac{\partial}{\partial y} [(1 + \kappa y) \tau_{yy}] - \frac{\kappa}{1 + \kappa y} \tau_{xx} \end{aligned} \quad (3.101)$$

energy equation

$$\begin{aligned}
 & \varrho c_p \left(\frac{\partial T}{\partial t} + \frac{u}{1+\kappa y} \frac{\partial T}{\partial x} + v \frac{\partial T}{\partial y} \right) \\
 &= \frac{1}{1+\kappa y} \frac{\partial}{\partial x} \left(\frac{\lambda}{1+\kappa y} \frac{\partial T}{\partial x} \right) + \frac{\partial}{\partial y} \left(\lambda \frac{\partial T}{\partial y} \right) \\
 &+ \beta T \left(\frac{\partial p}{\partial t} + \frac{u}{1+\kappa y} \frac{\partial p}{\partial x} + v \frac{\partial p}{\partial y} \right) \\
 &+ \Phi
 \end{aligned} \tag{3.102}$$

viscous stresses

$$\begin{aligned}
 \tau_{xx} &= \mu \left[\frac{2}{1+\kappa y} \left(\frac{\partial u}{\partial x} + \kappa v \right) - \frac{2}{3} \operatorname{div} \vec{v} \right] \\
 \tau_{yy} &= \mu \left(2 \frac{\partial v}{\partial y} - \frac{2}{3} \operatorname{div} \vec{v} \right) \\
 \tau_{xy} &= \mu \left(\frac{\partial u}{\partial y} - \frac{\kappa u}{1+\kappa y} + \frac{1}{1+\kappa y} \frac{\partial v}{\partial x} \right)
 \end{aligned} \tag{3.103}$$

dissipation function

$$\begin{aligned}
 \frac{\Phi}{\mu} &= 2 \left\{ \left[\frac{1}{1+\kappa y} \left(\frac{\partial u}{\partial x} + \kappa v \right) \right]^2 + \left(\frac{\partial v}{\partial y} \right)^2 \right\} \\
 &+ \left[\frac{\partial u}{\partial y} + \frac{1}{1+\kappa y} \left(\frac{\partial v}{\partial x} - \kappa u \right) \right]^2 - \frac{2}{3} (\operatorname{div} \vec{v})^2
 \end{aligned} \tag{3.104}$$

divergence

$$\operatorname{div} \vec{v} = \frac{1}{1+\kappa y} \frac{\partial u}{\partial x} + \frac{\partial}{\partial y} [(1+\kappa y)v]. \tag{3.105}$$

Other coordinate systems

The following coordinate systems may also be found in the literature:

- a) General orthogonal coordinates: H.S. Tsien (1958),
- b) Spherical polar coordinates: R.L. Panton (1984),
- c) Natural coordinates in axisymmetric flows: M. Van Dyke (1962c),
- d) Surface orientated monoclinic coordinate system (two non-orthogonal coordinates on the surface and the normal to the surface):
E.H. Hirschel; W. Kordulla (1981),
- e) Moving (accelerated and rotating) coordinate system:
G.K. Batchelor (1974), J.H. Spurk (1997).

4. General Properties of the Equations of Motion

4.1 Similarity Laws

Before we discuss solutions of the equations of motion in the next chapter, some general properties of these equations shall first be discussed.

First we will examine which quantities enter into the solutions of the equations of motion. If we relate the desired values to suitably chosen *reference values*, then the dimensionless solution can only depend on dimensionless position coordinates and on other dimensionless values. These are called *similarity parameters*. Two flows in similar geometries are called physically similar when all their similarity parameters are equal. Apart from the surrounding walls, in this case the streamlines and the lines of constant pressure are similar. The knowledge of the relevant coefficients for a flow problem is of fundamental importance in carrying out *modelling*. Often a geometrically similar but smaller model is made of the actual object about which the flow processes need to be known. This model is then examined in a wind or water tunnel. Thus the question of the *physical similarity of flows* arises, and with it the question of whether the results from modelling can be carried over to full-scale constructions.

Already in Chap. 1 we considered the question of the dynamic similarity of two flows in which inertial forces and friction forces act, and found that their Reynolds numbers must be the same (*similarity principle with respect to the Reynolds number*). This was reached by estimating the forces, and will now, along with other similarity laws, be derived from the equations of motion.

We start out from the equations of motion Eq. (3.73) to Eq. (3.77). The reference quantities chosen are a length l (a typical dimension of the body), a velocity V (e.g. the free stream velocity), and a thermodynamic state, denoted by the reference temperature T_R and the reference pressure p_R . The associated physical properties are ϱ_R , μ_R , c_{pR} , λ_R and β_R . For the body force per unit volume we set

$$\vec{f} = \varrho \vec{g} = \varrho g \vec{e}_g , \quad (4.1)$$

where \vec{e}_g is the unit vector in the direction of gravitational acceleration, and g is taken to be a constant.

The following dimensionless quantities are introduced:

$$\begin{aligned}
 x^* &= \frac{x}{l}, & y^* &= \frac{y}{l}, & z^* &= \frac{z}{l}, \\
 t^* &= \frac{tV}{l}, & \vec{v}^* &= \frac{\vec{v}}{V}, & p^* &= \frac{p - p_R}{\rho_R V^2}, \\
 T^* &= \frac{T}{T_R}, & \varrho^* &= \frac{\varrho}{\varrho_R}, & \mu^* &= \frac{\mu}{\mu_R}, \\
 c_p^* &= \frac{c_p}{c_{pR}}, & \lambda^* &= \frac{\lambda}{\lambda_R}, & \beta^* &= \frac{\beta}{\beta_R}, \\
 \dot{\varepsilon}^* &= \frac{l}{V} \dot{\varepsilon}, & \text{grad}^* .. &= l \text{ grad}.., & \text{div}^* .. &= l \text{ div}.., \\
 \text{Div}^* .. &= l \text{ Div}.., & \text{curl}^* .. &= l \text{ curl}.., & \Phi^* &= \frac{l^2}{\mu_R V^2} \Phi.
 \end{aligned} \tag{4.2}$$

The pressure p only appears in the equations of motion in its derivatives, and thus it is permissible to use only the difference from the reference pressure.

If the dimensionless quantities in Eq. (4.2) are inserted into the equations of motion (3.73) to (3.77), we find:

$$\frac{D\varrho^*}{Dt^*} = -\varrho^* \text{div}^* \vec{v}^*, \tag{4.3}$$

$$\varrho^* \frac{D\vec{v}^*}{Dt^*} = \frac{1}{Fr^2} \varrho^* \vec{e}_g - \text{grad}^* p^* + \frac{1}{Re} \text{Div}^* \left[\mu^* \left(2\dot{\varepsilon}^* - \frac{2}{3} \delta \text{div}^* \vec{v}^* \right) \right], \tag{4.4}$$

$$\varrho^* c_p^* \frac{DT^*}{Dt^*} = \frac{1}{Re Pr} \text{div}^* (\lambda^* \text{grad}^* T^*) - K_\varrho Ec \beta^* T^* \frac{Dp^*}{Dt^*} + \frac{Ec}{Re} \Phi^*. \tag{4.5}$$

Here the following five dimensionless characteristic numbers appear:

$$\text{Reynolds number} \quad Re = \frac{\varrho_R V l}{\mu_R}, \tag{4.6}$$

$$\text{Froude number} \quad Fr = \frac{V}{\sqrt{gl}}, \tag{4.7}$$

$$\text{Prandtl number} \quad Pr = \frac{\mu_R c_{pR}}{\lambda_R} = \frac{\nu_R}{a_R}, \tag{4.8}$$

$$\text{Eckert number} \quad Ec = \frac{V^2}{c_{pR} T_R}, \tag{4.9}$$

$$\text{thermal expansion number} \quad K_\varrho = -\beta_R T_R. \tag{4.10}$$

In addition

$$\nu = \frac{\mu}{\varrho} \tag{4.11}$$

the *kinematic viscosity* ($[\nu] = \text{m}^2/\text{s}$) and

$$a = \frac{\lambda}{\varrho c_p} \quad (4.12)$$

the *thermal diffusivity* ($[a] = \text{m}^2/\text{s}$), are used here in the reference state.

Of these five characteristic numbers, Pr and K_ϱ are pure fluid properties which are in general dependent on the reference state.

It follows from these considerations that flows past geometrically similar bodies are physically similar when the five numbers above are the same. This assumes, of course, that the initial and boundary conditions are analogous.

It is seldom that all five characteristic numbers agree in model flows and full-scale experiments. If only some of the characteristic numbers are the same, we have *partial similarity*. In these cases one attempts to adhere to the important similarity laws for that flow, i.e. to make the corresponding similarity parameters agree. Certain corrections have to be carried out in going from the model flow results to full-scale constructions for those numbers which remain unequal. Here the dependence of the solution on these similarity parameters must be known.

The main concern of fluid mechanics is to determine the dependence of the solutions of the equations of motion on the characteristic numbers. In particular cases, additional quantities could be added to this list through the effects of the initial and boundary conditions prescribed. If, for example, a frequency f is given, maybe by a body in a flow which carries out forced oscillations, then the Strouhal number given in Eq. (1.16) appears too. A temperature difference, e.g. $T_w - T_R$, is often given in heat transfer problems. Then $(T_w - T_R)/T_R$ would be a further characteristic number.

Other characteristic numbers related to those given here are often found in the literature. In Eq. (4.5) there is the combination

$$\text{Pe} = \text{Re} \cdot \text{Pr} \quad (4.13)$$

which is called the Peclet number. The Mach number already mentioned in Chap. 1 (cf. Eq. (1.8)) is related to Eckert number as follows:

$$\text{Ec} = \text{Ma}^2 \frac{c_R^2}{c_{pR} T_R} = \text{Ma}^2 \hat{K}_c . \quad (4.14)$$

Here the *speed of sound number* $\hat{K}_c = c_R^2/(c_{pR} T_R)$ is again a pure physical property. (For the ideal gas, i.e. $p/\varrho = RT$, we have $\hat{K}_c = \gamma - 1$ and $K_\varrho = -1$.)

In order to reduce the number of characteristic numbers it is usual to investigate the asymptotic behaviour of the solutions for very large or very small values. This means, to first approximation, a reduction in the number of characteristic numbers. The boundary-layer theory treated in this book is precisely such an asymptotic theory, for the case of very large Reynolds numbers ($\text{Re} \rightarrow \infty$).

If we go over to the limit $\text{Re} = \infty$, the equations (4.3) to (4.5) reduce to those for inviscid flows, and, apart from the physical characteristic numbers,

K_ϱ and \hat{K}_c , only the Froude number and the Mach number remain. However the inviscid solutions cannot satisfy the no-slip condition at the walls. Therefore, they can be used everywhere for $Re \rightarrow \infty$ with the exception of a thin layer close to the wall, the boundary layer, whose computation is the main topic of this book.

In the limit $Fr \rightarrow \infty$, the effect of gravity vanishes. This can indeed be assumed in many areas of application, e.g. flight technology, motor vehicle aerodynamics, and flows in compressors and gas turbines.

If we assume that the density and viscosity are constant (i.e. $\varrho^* = \mu^* = 1$), then the flow is incompressible (cf. Eq. (3.5)) and the velocity and pressure fields are independent of the temperature field (one-sided decoupling). In the limit $Fr \rightarrow \infty$, they can then only be dependent on the Reynolds number. This demonstrates the central importance of the similarity principle with respect to the Reynolds number for all of fluid mechanics.

Not only the velocity, pressure and temperature fields are of interest, but also the wall shear stress τ_w and the heat flux at the wall q_w . Dimensionless quantities are introduced for these too:

the *skin-friction coefficient*

$$c_f = \frac{\tau_w}{\frac{\varrho_R}{2} V^2} \quad (4.15)$$

and the *Nusselt number* at a given temperature difference $T_w - T_\infty$

$$Nu = \frac{q_w l}{\lambda_R (T_w - T_\infty)} . \quad (4.16)$$

Denoting the position vector with \vec{r} , the general solution of the equations of motion in three-dimensional form read

$$\begin{aligned} \vec{v}^* &= \vec{f}_1(\vec{r}^*, Re, Fr, Pr, Ec, K_\varrho) \\ p^* &= f_2(\vec{r}^*, Re, Fr, Pr, Ec, K_\varrho) \\ T^* &= f_3(\vec{r}^*, Re, Fr, Pr, Ec, K_\varrho) \\ c_f &= f_4(\vec{r}_w^*, Re, Fr, Pr, Ec, K_\varrho) \\ Nu &= f_5(\vec{r}_w^*, Re, Fr, Pr, Ec, K_\varrho) . \end{aligned} \quad (4.17)$$

4.2 Similarity Laws for Flow with Buoyancy Forces (Mixed Forced and Natural Convection)

If the buoyancy forces ($\sim 1/Fr^2$) of a flow are of importance, it is useful to consider only the difference of pressure and temperature fields from the

corresponding static fields. For a static field independent of time ($\vec{v} = 0$), it follows from Eq. (3.74) and Eq. (4.1) that

$$\varrho_{\text{stat}} \vec{g} \vec{e}_g = \text{grad } p_{\text{stat}} . \quad (4.18)$$

Subtracting this equation from Eq. (3.74), and using

$$p = p_{\text{stat}} + p_{\text{mot}} \quad (4.19)$$

leads to a relation, which, when written in dimensionless form corresponds to Eq. (4.4) and reads

$$\begin{aligned} \varrho^* \frac{D\vec{v}^*}{Dt^*} &= \frac{1}{\text{Fr}^2} (\varrho^* - \varrho_{\text{stat}}^*) \vec{e}_g - \text{grad}^* p_{\text{mot}}^* \\ &\quad + \frac{1}{\text{Re}} \text{Div}^* \left[\mu^* \left(2\dot{\varepsilon}^* - \frac{2}{3} \boldsymbol{\delta} \text{div}^* \vec{v}^* \right) \right] . \end{aligned} \quad (4.20)$$

Here p_{mot} is the pressure due only to the motion of the fluid.

For flows with buoyancy, it is usual to consider only small deviations of the temperature and pressure from their reference values. We can use a Taylor expansion for the density $\varrho(T, p)$ about the reference state as an approximation for the equation of state:

$$\varrho(T, p) = \varrho_R + \left(\frac{\partial \varrho}{\partial T} \right)_R (T - T_R) + \left(\frac{\partial \varrho}{\partial p} \right)_R (p - p_R) + \dots . \quad (4.21)$$

Now in general we have

$$\left(\frac{\partial \varrho}{\partial p} \right)_T = \gamma \left(\frac{\partial \varrho}{\partial p} \right)_s = \frac{\gamma}{c_v^2} \quad \text{with} \quad \gamma = \frac{c_p}{c_v} . \quad (4.22)$$

Therefore Eq. (4.21) can be brought to the following dimensionless form:

$$\varrho^*(T^*, p^*) = 1 + K_\varrho(T^* - 1) + \gamma \text{Ma}^2 p^* + \dots . \quad (4.23)$$

We see from this equation that incompressible flow ($\varrho^* = 1$) requires a double limit to be formed:

$$\left. \begin{aligned} \text{Ma} &\rightarrow 0 \\ T &\rightarrow T_R \end{aligned} \right\} \quad \text{incompressible flow} . \quad (4.24)$$

The single limit $\text{Ma} \rightarrow 0$ is in general *not* sufficient for an incompressible flow.

The Mach numbers in actual flows with buoyancy are very small. Therefore, in what follows, only the limit $\text{Ma} \rightarrow 0$ will be considered. Then the pressure terms in Eq. (4.23) fall away, as do the two terms proportional to Ec in the energy equation (because of Eq. (4.14)). From the reduced equation for the density, Eq. (4.23), it follows that the static field is

$$\varrho_{\text{stat}}^* = 1 + K_\varrho(T_{\text{stat}}^* - 1) . \quad (4.25)$$

Therefore the momentum equation Eq. (4.20) reads

$$\begin{aligned} \varrho^* \frac{D\vec{v}^*}{Dt^*} &= \frac{K_\varrho}{Fr^2} (T^* - T_{\text{stat}}^*) \vec{e}_g - \text{grad}^* p_{\text{mot}}^* \\ &\quad + \frac{1}{Re} \text{Div}^* \left[\mu^* \left(2\dot{\varepsilon}^* - \frac{2}{3} \boldsymbol{\delta} \text{div}^* \vec{v}^* \right) \right]. \end{aligned} \quad (4.26)$$

Here $T_{\text{stat}}^*(r^*)$ can still depend on the position, as, for example, in the earth's atmosphere. Because of the limit $\text{Ma} \rightarrow 0$, only the derivative of the temperature appears in the energy equation. The energy equation can thus be interpreted as an equation for $T^* - 1$ instead of for T^* .

In heat transfer problems, there are two cases which are of particular importance: when a temperature difference e.g. $T_w - T_R$, is given, or when a heat flux q_w at the wall is given.

If a temperature difference $T_w - T_R$ is given, the following dimensionless temperature is introduced:

$$\vartheta = \frac{T - T_R}{T_w - T_R} = \frac{T^* - 1}{T_w^* - 1}. \quad (4.27)$$

With this, the momentum equation and the energy equation read

$$\begin{aligned} \varrho^* \frac{D\vec{v}^*}{Dt^*} &= \frac{K_\varrho(T_w^* - 1)}{Fr^2} \vartheta \left[1 - \frac{T_{\text{stat}}^* - 1}{T_w^* - 1} \right] \vec{e}_g \\ &\quad - \text{grad}^* p_{\text{mot}}^* + \frac{1}{Re} \text{Div}^* \left[\mu^* \left(2\dot{\varepsilon}^* - \frac{2}{3} \boldsymbol{\delta} \text{div}^* \vec{v}^* \right) \right], \end{aligned} \quad (4.28)$$

$$\varrho^* c_p^* \frac{D\vartheta}{Dt^*} = \frac{1}{Re Pr} \text{div}^* (\lambda^* \text{grad}^* \vartheta). \quad (4.29)$$

If Taylor expansions are used for the physical properties μ^* , c_p^* and λ^* , just as was done with the density, we obtain

$$\begin{aligned} \varrho^*(T^*) &= 1 + K_\varrho(T_w^* - 1)\vartheta \\ \mu^*(T^*) &= 1 + K_\mu(T_w^* - 1)\vartheta \\ c_p^*(T^*) &= 1 + K_c(T_w^* - 1)\vartheta \\ \lambda^*(T^*) &= 1 + K_\lambda(T_w^* - 1)\vartheta. \end{aligned} \quad (4.30)$$

Numerical values of K_α ($\alpha = \varrho, \mu, c, \lambda$) for various fluids are to be found in Table 3.1.

The following important limiting process is known in the literature as the *Boussinesq approximation*:

$$T_w \rightarrow T_R, \quad V \rightarrow 0, \quad T_{\text{stat}} \rightarrow T_R, \quad (4.31)$$

ensuring, however, that

$$\text{Ar} = \frac{K_\varrho(1 - T_w^*)}{\text{Fr}^2} = \frac{\beta_R(T_w - T_R)gl}{V^2} \quad (4.32)$$

and

$$\vartheta_{\text{stat}} = \frac{T_{\text{stat}} - T_R}{T_w - T_R} \quad (4.33)$$

remain finite. The first number is the coupling parameter for the double limiting processes and is called the *Archimedes number*. In this limiting case the flow is incompressible, and the equations of motion are considerably simplified:

$$\text{div } \vec{v}^* = 0, \quad (4.34)$$

$$\frac{D\vec{v}^*}{Dt^*} = \text{Ar} \vartheta(1 - \vartheta_{\text{stat}}) \vec{e}_g - \text{grad}^* p_{\text{mot}}^* + \frac{2}{\text{Re}} \text{Div}^* \boldsymbol{\varepsilon}^*, \quad (4.35)$$

$$\frac{D\vartheta}{Dt^*} = \frac{1}{\text{RePr}} \text{div}^*(\text{grad}^* \vartheta). \quad (4.36)$$

Formally, this system of equations arises as follows: using Eqs. (4.3) to (4.5), with $\text{Ma} \rightarrow 0$, all physical properties are taken to be constant, with the exception of those in the buoyancy term where a linear relation between density and temperature is introduced.

If, instead, a wall heat flux q_w is given at the wall, formally the same system of equations is found. Here ϑ , Ar and ϑ_{stat} have the following meanings:

$$\vartheta = \frac{T - T_R}{q_w l / \lambda_R}, \quad (4.37)$$

$$\text{Ar} = \frac{\beta_R gl^2 q_w}{V^2 \lambda_R}, \quad (4.38)$$

$$\vartheta_{\text{stat}} = \frac{T_{\text{stat}} - T_R}{q_w l / \lambda_R}. \quad (4.39)$$

Again these quantities remain fixed in the limiting process

$$q_w \rightarrow 0, \quad V \rightarrow 0, \quad T_{\text{stat}} \rightarrow T_R. \quad (4.40)$$

In analogy to Eq. (4.30) we find

$$\varrho^*(T^*) = 1 + K_\varrho \frac{q_w l}{\lambda_R T_R} \vartheta \quad (4.41)$$

and equivalent expressions for the remaining physical properties.

These limiting processes are called the Boussinesq approximation after J. Boussinesq (1903). However, A. Oberbeck (1876) apparently also worked on this earlier, so that some authors speak of the Oberbeck–Boussinesq

approximation, cf. D.D. Joseph (1976), G.P. Merker (1987). For both cases, the general solution reads

$$\begin{aligned}\frac{\vec{v}}{V} &= \vec{f}_1(\vec{r}^*, \text{Re}, \text{Ar}, \text{Pr}, \vartheta_{\text{stat}}) \\ \frac{p_{\text{mot}} - p_{\text{R}}}{\rho_{\text{R}} V^2} &= f_2(\vec{r}^*, \text{Re}, \text{Ar}, \text{Pr}, \vartheta_{\text{stat}}) \\ \vartheta &= f_3(\vec{r}^*, \text{Re}, \text{Ar}, \text{Pr}, \vartheta_{\text{stat}}).\end{aligned}\quad (4.42)$$

4.3 Similarity Laws for Natural Convection

Flows arising solely from the differences in density caused by temperature differences are called *natural convection flows* or *free convection flows*. In such cases, the free stream velocity falls away; indeed, a reference velocity V does not a priori exist.

The similarity laws for natural convection flows will be derived from the equations of motion for mixed convection, with the special case $V = 0$.

If ν_{R}/l is chosen as a reference velocity instead of V , the momentum equation Eq. (4.26) leads to

$$\begin{aligned}\rho^* \frac{D\vec{v}^*}{Dt^*} &= \text{Ga} K_{\rho}(T^* - T_{\text{stat}}^*) \vec{e}_g - \text{grad}^* p_{\text{mot}}^* \\ &\quad + \text{Div}^* \left[\mu^* \left(2\dot{\varepsilon}^* - \frac{2}{3} \delta \text{div}^* \vec{v}^* \right) \right].\end{aligned}\quad (4.43)$$

A new characteristic number is now the *Galilei number*

$$\text{Ga} = \frac{\text{Re}^2}{\text{Fr}^2} = \frac{gl^3}{\nu_{\text{R}}^2}. \quad (4.44)$$

It contains no reference velocity. The two equations (4.26) and (4.43) are equivalent. Both are valid for mixed convection, while the latter is also valid for natural convection. Boussinesq approximations can also be given for Eq. (4.43). In the limit of small temperature differences or else small heat fluxes at the wall we obtain:

$$\frac{D\vec{v}^*}{Dt^*} = \text{Gr} \vartheta (1 - \vartheta_{\text{stat}}) \vec{e}_g - \text{grad}^* p_{\text{mot}}^* + 2 \text{Div}^* \dot{\varepsilon}^*. \quad (4.45)$$

Here again, note the differences in the two cases:

With a given temperature difference $T_{\text{w}} - T_{\text{R}}$:

Limiting process:

$$T_{\text{w}} \rightarrow T_{\text{R}}, \quad \nu_{\text{R}} \rightarrow 0, \quad T_{\text{stat}} \rightarrow T_{\text{R}}, \quad (4.46)$$

so that

$$\vartheta = \frac{T - T_R}{T_w - T_R}, \quad (4.47)$$

the *Grashof number*

$$Gr = Ar \cdot Re^2 = \frac{gl^3 \beta_R (T_w - T_\infty)}{\nu_R^2} \quad (4.48)$$

and ϑ_{stat} from Eq. (4.33) all remain finite.

With a given heat flux q_w :

Limiting process:

$$q_w \rightarrow 0, \quad \nu_R \rightarrow 0, \quad T_{\text{stat}} \rightarrow T_R, \quad (4.49)$$

so that

$$\vartheta = \frac{T - T_R}{q_w l / \lambda_R}, \quad (4.50)$$

the Grashof number

$$Gr = Ar \cdot Re^2 = \frac{gl^4 \beta_R q_w}{\lambda_R \nu_R^2} \quad (4.51)$$

and ϑ_{stat} from Eq. (4.39) all remain finite.

The general solutions are now formally the same for both cases:

$$\begin{aligned} \frac{\vec{v}l}{\nu_R} &= \vec{f}_1(\vec{r}^*, Gr, Pr, \vartheta_{\text{stat}}) \\ \frac{(p_{\text{mot}} - p_R)l^2}{\rho_R \nu_R^2} &= f_2(\vec{r}^*, Gr, Pr, \vartheta_{\text{stat}}) \\ \vartheta &= f_3(\vec{r}^*, Gr, Pr, \vartheta_{\text{stat}}). \end{aligned} \quad (4.52)$$

We emphasise for these limiting cases that very small viscosities have already been assumed here. However, we are generally not yet dealing with a flow with boundary-layer character. This only appears when the Grashof number becomes very large ($Gr \rightarrow \infty$); then the effect of the pressure gradient frequently vanishes, as will be shown in more detail in Chap. 11.

4.4 Vorticity Transport Equation

As has already been shown, the velocity and pressure fields become independent of the temperature if the density and viscosity are constant and the buoyancy force (a consequence of the weight) can be neglected. The flow is then incompressible. The momentum equation can then be transformed into an equation for the angular velocity vector in Eq. (3.27)

$$\vec{\omega} = \frac{1}{2} \operatorname{curl} \vec{v}, \quad (4.53)$$

cf. R.L. Panton (1984), p. 327. It reads

$$\frac{D\vec{\omega}}{Dt} = (\vec{\omega} \cdot \text{grad})\vec{v} + \nu \Delta \vec{\omega} \quad (4.54)$$

and is called the *vorticity transport equation*. According to this equation, the angular velocity of a fluid particle is changed due to the two different mechanisms shown in the two terms on the right hand side of Eq. (4.54). The first term describes vortex stretching and bending of vortex lines. Vortex lines are, by definition, always parallel to the angular velocity vector and correspond to streamlines in the velocity field. The mechanism denoted by $(\vec{\omega} \cdot \text{grad})\vec{v}$ does not exist in plane flows. The second term describes the diffusion of angular velocity which is a result of the viscosity and it is in this way in which the viscosity can be understood as a transport coefficient for the angular velocity. It should be noted that the vorticity transport equation does not contain the pressure. However this is understandable, since normal stresses can have no effect on the angular velocity of the particles.

The vorticity transport equation becomes particularly simple for *plane flows*. In Cartesian coordinates it reads

$$\frac{\partial \omega}{\partial t} + u \frac{\partial \omega}{\partial x} + v \frac{\partial \omega}{\partial y} = \nu \left(\frac{\partial^2 \omega}{\partial x^2} + \frac{\partial^2 \omega}{\partial y^2} \right) \quad (4.55)$$

with

$$\omega = \omega_z = \frac{1}{2} \left(\frac{\partial v}{\partial x} - \frac{\partial u}{\partial y} \right) . \quad (4.56)$$

In this case there is a far-reaching analogy to the energy equation:

$$\frac{\partial T}{\partial t} + u \frac{\partial T}{\partial x} + v \frac{\partial T}{\partial y} = a \left(\frac{\partial^2 T}{\partial x^2} + \frac{\partial^2 T}{\partial y^2} \right) , \quad (4.57)$$

where a is the thermal diffusivity given in Eq. (4.12). The transport processes are analogous here. The thermal diffusivity a in the temperature field corresponds to the kinematic viscosity in the angular velocity field. For $a = \nu$ (i.e. $\text{Pr} = 1$), and with the same boundary conditions, the solutions for temperature and angular velocity would be identical.

By eliminating the pressure, the three equations (continuity equation, two momentum equations) for u , v and p are reduced to two equations for u and v . By introducing a *stream function* $\psi(x, y)$ the number of equations can be reduced even further. Setting

$$u = \frac{\partial \psi}{\partial y}, \quad v = -\frac{\partial \psi}{\partial x} , \quad (4.58)$$

the continuity equation is automatically satisfied. For the angular velocity we have

$$\omega = -\frac{1}{2} \Delta \psi \quad (4.59)$$

and therefore the vorticity transport equation is

$$\frac{\partial(\Delta\psi)}{\partial t} + \frac{\partial\psi}{\partial y} \frac{\partial(\Delta\psi)}{\partial x} - \frac{\partial\psi}{\partial x} \frac{\partial(\Delta\psi)}{\partial y} = \nu \Delta \Delta \psi . \quad (4.60)$$

In this form the vorticity transport equation only contains one unknown ψ . We now have a (still nonlinear) fourth order differential equation.

Special case $\omega = \text{const}$. It is obvious that flows of constant angular velocity ($\omega = \text{const}$) and particularly irrotational flows ($\omega = 0$) are solutions of the plane vorticity transport equation. Unfortunately, apart from a very few exceptions, these solutions do not satisfy the no-slip condition at the wall, and so generally have no importance in practice.

Flows at constant angular velocity, which include the Couette flows treated in Chap. 1, are however important in connection with separated flows, cf. G.K. Batchelor (1956).

Irrotational flows are called potential flows. In spite of having non-zero viscosity (viscous potential flows), these are solutions of the Navier-Stokes equations. Physically sensible solutions can be found from all two-dimensional potential flows past cylindrical bodies by interchanging the meanings of the streamlines and the potential lines. The case is then that of bodies with suction or blowing on the surface where the no-slip condition is indeed satisfied.

Frequently the no-slip condition can be satisfied by moving the wall along with the flow. The simplest example is the flow at a rotating cylinder in a fluid otherwise at rest. The potential flow with pure circumferential velocity $\sim 1/r$ (*potential vortex*) is a solution of the Navier-Stokes equations. More on this can be found in the work by G. Hamel (1941) and J. Ackeret (1952).

Viscous potential flows have a non-zero dissipation function Φ (from Eq. (3.62)). This has been discussed by J. Zierep (1983). It corresponds to the total power of the wall shear stress on the “moving” surface.

4.5 Limit of Very Small Reynolds Numbers

In the case of very slow motion or where the viscosity is very large, the friction forces are considerably larger than the inertial forces, since the latter are proportional to the square of the velocity while the former are linear. To first order, the inertial terms can therefore be completely neglected compared to the friction terms, and with Eq. (4.60), we obtain

$$\Delta \Delta \psi = 0 . \quad (4.61)$$

This is now a linear differential equation, to which a solution can far more easily be found than to the complete equation (4.60). Flows which satisfy Eq. (4.61) are called *creeping flows*. Cancelling out the inertial terms in the limit of very slow motion is mathematically permissible because the order of the differential equation is not reduced and therefore the solutions of the simplified differential equation (4.61) can satisfy just as many boundary conditions as the full equation (4.60).

Creeping motion can be interpreted as solutions of the Navier–Stokes equations in the *limit of very small Reynolds numbers* ($\text{Re} \rightarrow 0$).

Creeping motion solutions of Eq. (4.61) were given by G.G. Stokes (1856) for the sphere. The Stokes solution can be applied, for example, to the cases of fog droplets in the air or of very small spheres in thick oil, where the velocities are always so small that the inertial terms can validly be neglected. *Hydrodynamic lubrication theory*, which is concerned with the flow of lubrication oil in the narrow gap between shaft and bearing, also emerges from the simplified equations of creeping motion. Even though the velocities are not small here, the small gap heights and the relatively high oil viscosity ensure that the friction forces are much larger than the inertial forces. Summaries of the flow at small Reynolds numbers have been given by W.E. Langlois (1964) and J. Happel; H. Brenner (1973), cf. also K. Gersten; H. Herwig (1992), p. 233.

4.6 Limit of Very Large Reynolds Numbers

Of considerably greater importance in practical application is the other limiting case, where, in Eq. (4.60), the friction terms are appreciably larger than the inertial terms. Since the technically important fluids, water and air, have small viscosities, it is this case which usually arises whenever the velocities are at all large. This is the *limit of very large Reynolds numbers* ($\text{Re} \rightarrow \infty$). In this case, however, considerably more care has to be taken with the mathematical simplifications resulting from the differential equation (4.60). It is not permitted simply to delete the friction terms on the right hand side of Eq. (4.60). Doing this would reduce the order of the differential equation from four to two, and not all the boundary conditions of the full differential equation could be satisfied by the simplified differential equation. This question is central to *boundary-layer theory*. We will now first of all discuss in detail what general statements can be made about the solutions of the Navier–Stokes equations in the limit of large Reynolds numbers.

The character of the solutions of the Navier–Stokes equations in this limit can be illustrated using the analogy between the vorticity and temperature fields already mentioned (Eqs. (4.55) and (4.57)). Consider the flow past a body in Fig. 4.1, whose wall temperature is higher than the surrounding temperature T_∞ .

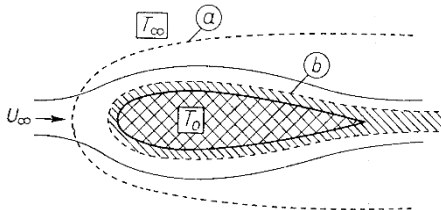


Fig. 4.1. Analogy between the temperature distribution and the distribution of the angular velocity close to a body in a flow, $T_0 = T_w > T_\infty$.
 (a), (b): limits of the heated region
 (a) for small flow velocities
 (b) for large flow velocities

From the analogy between Eqs. (4.55) and (4.57) we expect that the solutions for the angular velocity ω and the temperature difference $T - T_\infty$ will have similar character.

Now the character of the temperature field is somewhat obvious, purely by illustration. In the limit that the flow velocity goes to zero (rest), the higher temperature of the body will act equally on its surroundings on all sides. Even at very small flow velocities, the surroundings of the body will be affected by the heating in all directions. However if the flow velocity is increased, it is obvious that the region affected by the heating will be drawn together to a narrow zone directly at the body and a tail of heated fluid behind it (Fig. 4.1).

The character of the solution of Eq. (4.55) for the angular velocity ω is the same. At small velocities (friction forces large compared to inertial forces), we find angular velocity in the entire surroundings of the body. On the other hand, at large velocities (friction forces small compared to inertial forces), we expect a flow field where angular velocity is only present in a narrow zone along the surface of the body and in a tail behind it, while the rest of the surroundings remains practically irrotational (cf. Fig. 4.1). Thus we expect that, in the limit of very small friction forces, i.e. very large Reynolds numbers, the solutions of the Navier–Stokes equations will be such that the entire flow field can be divided up into an irrotational outer flow, which obeys the laws of inviscid flow and can be dealt with as potential flow, and a thin layer close to the body as well as a wake behind the body, where there is angular velocity and where the Navier–Stokes equations have to be used. It is only in this layer that the friction forces are appreciable, i.e. the same size as the inertial forces. This layer is called the *frictional* or *boundary layer*. This idea of the frictional layer was first introduced to fluid mechanics by L. Prandtl (1904) at the beginning of this century, and it has proved to be very productive. It is only the division of the entire flow field into the inviscid outer flow and the frictional boundary-layer flow that has allowed the mathematical difficulty of the Navier–Stokes equations to be eased so greatly that it became possible to integrate them for many cases. This forms the contents of the boundary-layer theory in the following chapters.

In certain simple cases it can be shown by direct calculation from the Navier–Stokes equations that, in the limit of very large Reynolds numbers, a thin layer close to the body exists, to which the action of the viscosity is restricted. These cases will be discussed in Chap. 5.

The limiting case discussed above, where the friction forces prevail over the inertial forces (*creeping flows*, Reynolds number very small), introduces considerably simplifications mathematically, because neglecting the inertial forces in the Navier–Stokes equations does not lower their order, but does make them *linear*. The other limiting case, where the inertial forces prevail over the friction forces (*frictional layer*, Reynolds number very high) is mathematically more difficult than the creeping flow. If we were simply to set μ to

zero in the Navier–Stokes equations, the highest order derivative would drop out of both the original Navier–Stokes equations (3.42) and the equation for the stream function (4.60). All the boundary conditions of the original complete differential equations could then no longer be satisfied by the lower order differential equations resulting from this (so-called *Euler differential equations*). Now this does not imply that the solutions of an equation simplified by elimination of the friction terms would be physical meaningless. Further, it is possible to prove that these solutions agree with the complete solution of the full Navier–Stokes equations almost everywhere in the limit of very large Reynolds numbers. The exception is restricted to a thin layer close to the wall, namely the boundary layer. Therefore we can imagine that the complete solution of the Navier–Stokes consists of different parts: the so-called “outer” solution, obtained with the help of the Euler equations of motion, and a so-called “inner” solution, or boundary–layer solution, which only exists in a thin layer directly at the wall. This emerges from the Navier–Stokes equations by coordinate transformation and taking the limit $\text{Re} \rightarrow \infty$, as will be shown in Chap. 6. The outer and inner solutions should be matched onto one another in such a way that both solutions are valid in an overlap region.

4.7 Mathematical Example of the Limit $\text{Re} \rightarrow \infty$

Since the discussion above deals with some of the most important fundamentals of boundary–layer theory, let us elucidate these ideas further with a very simple mathematical example given by L. Prandtl¹.

We consider the oscillation of a point mass with damping, given by the differential equation

$$m \frac{d^2x}{dt^2} + k \frac{dx}{dt} + cx = 0 . \quad (4.62)$$

Here m is the oscillating mass, k the damping constant, c the spring constant, x the distance of the mass from the position of rest, and t the time.

The initial conditions are given as

$$t = 0 : \quad x = 0 . \quad (4.63)$$

In analogy to the Navier–Stokes equations with very small kinematic viscosity ν , we consider the limit of very small mass m , since then in Eq. (4.62) too the highest order term becomes very small.

The complete solution of (4.62) with initial condition (4.63) reads

$$x = A[e^{-(ct/k)} - e^{-(kt/m)}] \quad m \rightarrow 0 , \quad (4.64)$$

where A is a free constant which could be fixed by a second initial condition.

¹ L. Prandtl, *Anschauliche und nützliche Mathematik*, lectures Winter semester 1931/32, Göttingen.

If we set $m = 0$ in Eq. (4.62) we obtain the simplified differential equation

$$k \frac{dx}{dt} + cx = 0, \quad (4.65)$$

which is now a first order differential equation with solution

$$x_o(t) = Ae^{-(ct/k)}. \quad (4.66)$$

By choosing the initially arbitrary constant A suitably, this solution agrees with the first term of the complete solution. However it cannot satisfy the initial condition (4.63). Therefore it is a solution for large times ("outer" solution).

A simplified differential equation can also be derived from Eq. (4.62) for the solution for small times ("inner" solution). To this end a new "inner" variable is introduced by "stretching" the time coordinate t :

$$t^* = \frac{t}{m}. \quad (4.67)$$

Using this, Eq. (4.62) reads

$$\frac{d^2x}{dt^{*2}} + k \frac{dx}{dt^*} + m c x = 0. \quad (4.68)$$

For $m = 0$ we obtain the differential equation for the "inner solution":

$$\frac{d^2x}{dt^{*2}} + k \frac{dx}{dt^*} = 0. \quad (4.69)$$

with the solution

$$x_i(t^*) = A_1 e^{-kt^*} + A_2. \quad (4.70)$$

In spite of the simplification, this equation remains second order, and it can satisfy the initial condition (4.63). We then have

$$A_1 = -A_2. \quad (4.71)$$

Determining the constant A_2 is carried out by matching up the "inner" solution and the "outer" solution corresponding to Eq. (4.66). The solutions in Eq. (4.66) and (4.70) must be equal in an overlap region, i.e. for intermediate times. It must hold that:

$$\lim_{t^* \rightarrow \infty} x_i(t^*) = \lim_{t \rightarrow 0} x_o(t). \quad (4.72)$$

In words the conforming condition says: the "outer" limit of the inner solution is equal to the "inner" limit of the outer solution. From Eq. (4.72) it immediately follows that

$$A_2 = A \quad (4.73)$$

and thus for the inner solution

$$x_i(t^*) = A(1 - e^{-kt^*}). \quad (4.74)$$

This solution can also be obtained from the complete solution in Eq. (4.64) if the first term is expanded for small t and only the first term of the expansion is taken into account, i.e. setting

$$\lim_{t \rightarrow 0} e^{-(ct/k)} = 1. \quad (4.75)$$

The two solutions, the outer solution from Eq. (4.66) and the inner solution from Eq. (4.74) represent the entire solution if each is applied in its region of validity.

At a given t , Eq. (4.64) for $m \rightarrow 0$ passes over to the outer solution. We obtain the entire solution valid for the whole t region (the composite solution) from the partial solutions by adding both solutions. Here the part in common to both solutions may only be taken into account once, i.e. it must be subtracted:

$$x(t) = x_o(t) + x_i(t^*) - \lim_{t^* \rightarrow \infty} x_i(t^*) = x_o(t) + x_i(t^*) - \lim_{t \rightarrow 0} x_o(t). \quad (4.76)$$

In this manner, the composite solution in Eq. (4.64) follows from the two separate solutions.

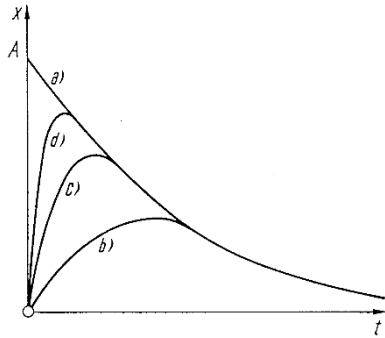


Fig. 4.2. Solution of the oscillator equation (4.62) for $m \rightarrow 0$.

(a) Solution of the simplified differential equation (4.65), $m = 0$;
 (b), (c), (d) Solutions of the complete differential equation (4.62) for different values of m . For small values of m , curve (d) depicts a solution with “boundary-layer character”

The composite solution in Eq. (4.64) is shown graphically in Fig. 4.2 for $A > 0$. Curve a is the outer solution. Curves b , c and d are the composite solution, where the value of m decreases as we go from b to d .

If we compare this solution with the Navier–Stokes differential equations, the complete differential equation (4.62) corresponds to the Navier–Stokes differential equations of a viscous fluid; the simplified differential equation (4.65) to the outer solution of the Euler differential equation of an inviscid fluid; and the simplified differential equation (4.69) to the inner solution of the boundary–layer equations which have still to be derived. The initial condition (4.63) corresponds to the no-slip condition of the viscous fluid, which can be satisfied by the solutions of the Navier–Stokes equations but not by the solutions of the Euler equations. The outer solution corresponds to the inviscid outer flow (potential flow) which does not satisfy the no-slip condition at the wall. The inner solution corresponds to the boundary–layer flow which is determined by the viscosity and which is only valid in a narrow zone attached to the wall (boundary layer or frictional layer). However it is only by including this boundary–layer solution that the no-slip condition at the wall can be satisfied, and thus the entire solution make sense physically.

Therefore this simple example has again confirmed the same mathematical idea we saw in the previous section, namely that taking the limit to very small viscosities (very large Reynolds numbers) in the Navier–Stokes equations cannot be carried out by simply eliminating the friction terms in the differential equation. It is performed by first obtaining the solution and then allowing the Reynolds number to become very large.

Later we will see that it is not necessary to retain the complete Navier–Stokes equations when taking the limit $\text{Re} \rightarrow \infty$. For reasons of mathematical simplicity, we will be able to assume a number of terms in these equations, in particular friction terms, are small enough to be neglected. However it is important that not all the friction terms are neglected, since this would reduce the order of the Navier–Stokes equations.

4.8 Non-Uniqueness of Solutions of the Navier–Stokes Equations

The solutions of the Navier–Stokes equations do not have to be unique for given initial and boundary conditions. Primarily because of the nonlinearity of the differential equations, variation of geometric or fluid mechanical parameters can lead to bifurcations in the solution and thus to multiple solutions. Thus, in spite of steady initial conditions, the solutions can also become unsteady. The transition from laminar to turbulent flow is in principle a series of such solution bifurcations which lead to ever more complex structures of the solutions, cf. Chap. 15.

In steady flows there are frequently multiple solutions when flow separation or backflow occur. One of the solutions is frequently a flow attached to the body, whereas the other solutions describe flow with separation. Such lack of uniqueness can also occur in boundary layers, as will be shown in later chapters. In particular, it will be shown in Chap. 14 that hysteresis can also occur.

5. Exact Solutions of the Navier–Stokes Equations

The task of finding exact solutions of the Navier–Stokes equations is generally extremely difficult. The nonlinearity of these equations forbids the use of the principle of superposition which served so well in the case of inviscid incompressible potential flows. In spite of this, there are some special cases where exact solutions can be given, and this is most often true when the nonlinear inertial terms vanish in a natural way.

The possibilities nowadays to exploit supercomputers and highly developed numerical methods for nonlinear partial differential equations allow us to determine even the general solutions to the Navier–Stokes equations, cf. B.E. Schönung (1990). However the difficulties become greater with increasing Reynolds number. This has to do with the particular structure of the solutions at high Reynolds numbers.

In this chapter we will discuss some exact solutions of the Navier–Stokes equations for incompressible flow. We will see that in the limiting case of high Reynolds numbers, most of these exact solutions have a *boundary-layer character*.

Comprehensive overviews of the solutions of the Navier–Stokes equations have been given by R. Berker (1963) and C.Y. Wang (1989, 1991).

The solutions discussed here can be classified as follows:

- steady plane flows,
- steady axisymmetric flows,
- unsteady plane flows,
- unsteady axisymmetric flows.

Each category can be further subdivided into flows with and without nonlinear inertial terms and into internal and external flows.

The following selection of examples aim to depict foremost the boundary-layer character of flows at high Reynolds numbers.

5.1 Steady Plane Flows

5.1.1 Couette–Poiseuille Flows

Parallel flows constitute a particularly simple class of solution. A flow is called parallel if only *one* velocity component is different from zero, all fluid particles

moving in the same direction. If, for example, only the velocity component u is non-zero, and thus v is everywhere zero, it follows immediately from the continuity equation that $\partial u / \partial x = 0$ and therefore u cannot be dependent on x . Thus for parallel flows we have:

$$u = u(y); \quad v = 0. \quad (5.1)$$

From the Navier–Stokes equations (3.42) for the y direction, it then follows immediately that $\partial p / \partial y = 0$ ($p = p_{\text{mot}}$ is here the pressure due to the motion only, cf. Eq. (4.19)). The pressure is therefore only dependent on x . In addition all the convective terms in the equation in the x direction vanish. This leaves

$$\frac{dp}{dx} = \mu \frac{d^2u}{dy^2}. \quad (5.2)$$

What remains is thus a linear differential equation, with two unknowns $u(y)$ and $p(x)$. However since the left hand side of Eq. (5.2) can only depend on x and the right hand side only on y , both sides must be equal to a constant. In this way Eq. (5.2) is actually two equations, namely $dp/dx = C$ and $d^2u/dy^2 = C/\mu$.

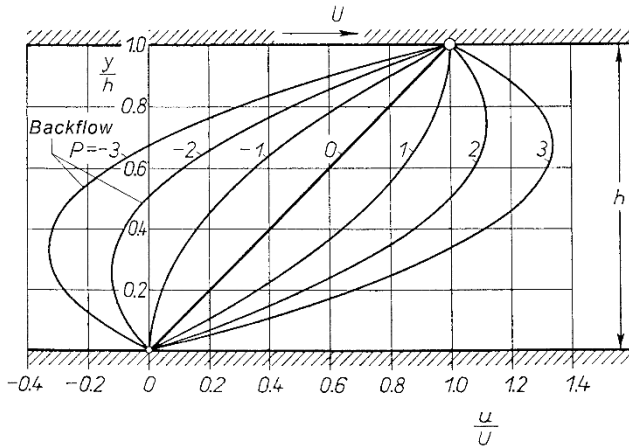


Fig. 5.1. Couette–Poisseille flows between two parallel flat walls
 $P > 0$ pressure drop in direction of wall motion
 $P < 0$ pressure increase in direction of wall motion

As in Fig. 5.1, we consider the flow between two parallel flat plates a distance h apart and with a pressure gradient dp/dx , where the upper plate moves in its own plane with velocity U . The boundary conditions are

$$y = 0 : \quad u = 0; \quad y = h : \quad u = U. \quad (5.3)$$

The corresponding solution to Eq. (5.2) is:

$$u = \frac{y}{h}U - \frac{h^2}{2\mu} \frac{dp}{dx} \frac{y}{h} \left(1 - \frac{y}{h}\right) \quad (5.4)$$

or

$$\frac{u}{U} = \frac{y}{h} + P \frac{y}{h} \left(1 - \frac{y}{h}\right) \quad (5.5)$$

with the dimensionless pressure gradient

$$P = \frac{h^2}{2\mu U} \left(-\frac{dp}{dx} \right). \quad (5.6)$$

The solution of Eq. (5.3), with P as parameter, is depicted in Fig. 5.1. For $P > 0$, i.e. for pressure drop in the direction of motion of the upper plate, the velocity is positive over the whole width of the channel. For $P < -1$, negative velocities (*backflow*) can also occur in a part of the cross-section. In this case the dragging action of the faster neighbouring layers on the fluid close to the moving wall is not enough to overcome the influence of the adverse pressure gradient.

Let us discuss two special cases of the general solution (5.4). The case of no pressure gradient $dp/dx = 0$ leads to

$$u = \frac{y}{h} U. \quad (5.7)$$

This pure shearing flow is called Couette flow after the Frenchman M. Couette, cf. also Fig. 1.1.

The second special case is pure channel flow with $U = 0$, and is called Poiseuille flow after the Frenchman J.L.M. Poiseuille (1846). The general flows given by Eq. (5.4) are a combination of these two flows and are called Couette–Poiseuille flows. From Eq. (5.4), the channel flow has a parabolic velocity distribution with a maximum velocity in the plane of symmetry given by

$$u_{\max} = -\frac{h^2}{8\mu} \frac{dp}{dx} \quad (5.8)$$

and an average velocity of

$$u_m = \frac{Q}{hb} = -\frac{h^2}{12\mu} \frac{dp}{dx} = \frac{2}{3} u_{\max}. \quad (5.9)$$

It is usual to express the relation between the pressure drop and the average velocity with the dimensionless *friction factor* λ . This is defined by

$$-\frac{dp}{dx} = \frac{\lambda}{d_h} \frac{\rho}{2} u_m^2 \quad (5.10)$$

where

$$d_h = \frac{4A}{U_P} = 2h \quad (5.11)$$

is the *hydraulic diameter* of the channel cross-section (U_P is the wetted circumference of the flow cross-section of area A). If the Reynolds number is formed with the average velocity u_m and the hydraulic diameter d_h , Eqs. (5.9) and (5.10) can be combined to form the drag law

$$\lambda = \frac{96}{Re} \quad (5.12)$$

with

$$Re = \frac{u_m d_h}{\nu}. \quad (5.13)$$

Couette–Poiseuille flows are important in considering flows in bearings. The special case of vanishing volume flux ($P = -3$) also has practical application, e.g. in the case of wind-driven flows of flat stretches of “standing” water. Couette–Poiseuille flows are laminar as long as the Reynolds number remains under a certain limit,

the so-called critical Reynolds number. It has been shown by experiment that the critical Reynolds number in Couette flow is about

$$\text{Re}_{\text{crit}} = \left(\frac{hU}{\nu} \right)_{\text{crit}} = 1300 \quad (5.14)$$

and in the case of channel flow is about

$$\text{Re}_{\text{crit}} = \left(\frac{u_m d_h}{\nu} \right)_{\text{crit}} = 3000 . \quad (5.15)$$

For $\text{Re} > \text{Re}_{\text{crit}}$ the flows become turbulent. Turbulent Couette–Poiseuille flows are treated in Sect. 17.2.2.

5.1.2 Jeffery–Hamel Flows (Fully Developed Nozzle and Diffuser Flows)

We now consider an extension to channel flows: plane flows between straight non-parallel walls, as in Fig. 5.2. Whereas in channel flows the inertial terms vanish, in the cases of nozzles and diffusers, accelerations and decelerations occur. For a source at $r = 0$, a diffuser (divergent channel) occurs; in the case of a sink, a nozzle (convergent channel).

From the Navier–Stokes equations in polar coordinates, Eq. (3.91), we use the ansatz

$$\frac{u(r, \varphi)}{u_{\max}(r)} = F(\eta), \quad \eta = \frac{\varphi}{\alpha} \quad (5.16)$$

and obtain an ordinary differential equation for the normalised velocity profile $F(\eta)$:

$$F''' + 2\alpha \text{Re} F F' + 4\alpha^2 F' = 0 \quad (5.17)$$

with the boundary conditions

$$F(-1) = 0, \quad F(0) = 1, \quad F(+1) = 0 . \quad (5.18)$$

The Reynolds number

$$\text{Re} = \frac{u_{\max} r \alpha}{\nu} \quad \begin{cases} \text{diffuser: } \alpha > 0, & u_{\max} > 0 \\ \text{nozzle: } \alpha < 0, & u_{\max} < 0 \end{cases} \quad (5.19)$$

is always positive and, since $u_{\max} \sim 1/r$, it is independent of r . The streamlines are therefore straight lines through the origin. The circumferential component of the velocity is thus equal to zero everywhere. The solution of the differential equation (5.17) was given by G.B. Jeffery (1915) and G. Hamel (1916), and allows $F(\eta)$ to be written in terms of elliptical functions, cf. e.g. F.M. White (1974), p. 184.

Without going into the details of the calculation, let us sketch the character of the solution briefly. A family of velocity distributions at different Reynolds numbers for the diverging channel $\alpha = 5^\circ$ and for the converging channel $|\alpha| = 5^\circ$ is depicted in Fig. 5.2. The velocity distributions are very

different for the convergent and divergent channels, and in the latter case vary greatly with Reynolds number, cf. K. Millsaps; K. Pohlhausen (1953).

In the *convergent* channel (nozzle), for large Reynolds numbers, the velocity is almost constant for a large section in the centre, and only close to the walls does it drop off sharply to zero. In this case it has a pronounced “*boundary-layer character*”.

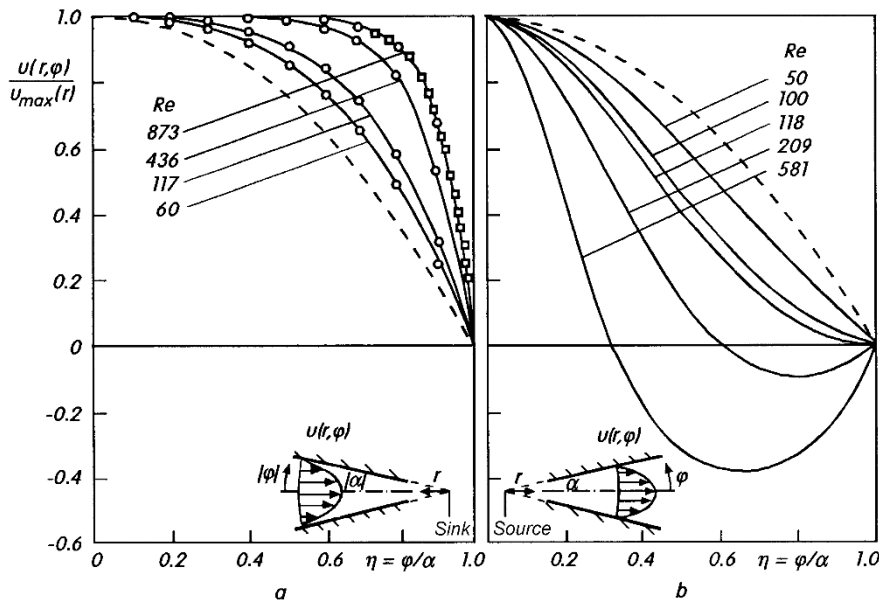


Fig. 5.2. Jeffery–Hamel flows in convergent and divergent channels
(a) velocity profiles in a convergent channel (nozzle), opening angle $2\alpha = -10^\circ$.

- exact solution
- ○ ○ slender-channel solution
- □ □ boundary-layer solution
- - - quasi-Poiseuille flow (parabolic profile)

(b) velocity profiles in a divergent channel (diffuser), opening angle $2\alpha = 10^\circ$.

- exact solution
- - - quasi-Poiseuille flow (parabolic profile)

In the *divergent* channel (diffuser), depending on the Reynolds number, very different forms of velocity distributions are obtained. Each of these profiles is much more sharply curved in the middle than the (dashed) parabola found for the channel with parallel walls. The velocity distributions for the two largest Reynolds numbers are characterised in that they have two regions of backflow. The velocity distributions have four roots. Since the wall can be at any of these points, two different flows can be determined for each of these distributions. Thus for an opening angle of $2\alpha = 10^\circ$, these distributions have *two* symmetric regions of backflow, and with opening angles of 6.6° or

8.0° , there is an antisymmetric distribution with *one* region of backflow. Such antisymmetric velocity distributions are indeed observed in diffusers.

As can be seen from the differential equation (5.17), the Jeffery–Hamel solutions depend on the two parameters α and Re . From the solution $F(\eta)$ we obtain the following results:

(a) volume coefficient (width b)

$$c_V = \frac{\dot{V}}{2r\alpha u_{\max} b} = \frac{u_m}{u_{\max}} = \frac{1}{2} \int_{-1}^{+1} F(\eta) d\eta , \quad (5.20)$$

(b) skin-friction coefficient

$$c_f = \frac{2|\tau_w|}{\varrho u_{\max}^2} = \frac{2|F'(1)|}{\text{Re}} , \quad (5.21)$$

(c) pressure coefficient ($p_\infty = p(r \rightarrow \infty)$)

$$c_p = \frac{p_\infty - p(r, \eta)}{\varrho u_{\max}^2 / 2} = \frac{1}{\alpha \text{Re}} [F''(1) - 4\alpha^2 F(1)] , \quad (5.22)$$

(d) wall pressure coefficient

$$c_{pw} = \frac{p_\infty - p(r, 1)}{\varrho u_{\max}^2 / 2} = \frac{F''(1)}{\alpha \text{Re}} . \quad (5.23)$$

The results for nozzle flow with $\alpha = -\pi/4$ are shown in Fig. 5.3. In addition the asymptotes for $\text{Re} \rightarrow 0$ (creeping flow) and $\text{Re} \rightarrow \infty$ (boundary-layer flow) are given. For this case ($\alpha = -\pi/4$), the differential equation (5.17) for creeping flow $\text{Re} \rightarrow 0$ reduces to

$$F''' + \frac{\pi^2}{4} F' = 0 \quad (5.24)$$

with the simple solution $F(\eta) = \cos(\pi\eta/2)$.

We will consider the limiting case $\text{Re} \rightarrow \infty$ in some more detail, since it can be used to demonstrate the basic concept of boundary-layer theory easily.

Boundary-layer theory. We look for the solutions of the differential equation (5.17) at a given $\alpha < 0$ (nozzles) for large Reynolds numbers $\text{Re} \rightarrow \infty$. Dividing Eq. (5.17) by Re and then forming the limit $\text{Re} \rightarrow \infty$, this equation reduces to $FF' = 0$ with the non-trivial solution $F = 1$. Now this solution satisfies the boundary condition at the axis ($\eta = 0$), but not the no-slip condition at the walls. The solution $F = 1$ corresponds to inviscid sink flow. It is valid everywhere except in a very thin region directly at the wall, the boundary layer. There the solution breaks down, since the original differential equation becomes too strongly degenerate and its order is reduced, so that all the boundary conditions can no longer be satisfied.

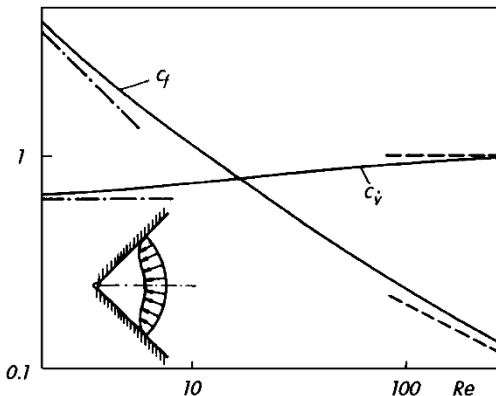


Fig. 5.3. Volume and skin-friction coefficients of the Jeffery–Hamel solution for a nozzle flow with opening angle $2\alpha = -90^\circ$.

Asymptotes:

$\text{Re} \rightarrow 0$, creeping flow:

$$c_V = 2/\pi, c_f = \pi^3/(4\text{Re})$$

$\text{Re} \rightarrow \infty$, boundary-layer theory:

$$c_V = 1, c_f = 2\sqrt{\pi/(3\text{Re})}$$

In the wall region, the so-called boundary layer, a further solution must be found which satisfies the no-slip condition and which passes over to the solution $F = 1$ in the core with increasing distance from the wall. Instead of η a new *stretched coordinate* is introduced:

$$\xi = (1 - \eta)\sqrt{-\alpha \text{Re}} . \quad (5.25)$$

This can be thought of as a stretched distance from the wall. Denoting derivatives with respect to ξ with a dot, the differential equation for $F(\xi)$ reads

$$\ddot{F} - 2F\dot{F} - \frac{4\alpha}{\text{Re}}\dot{F} = 0 . \quad (5.26)$$

In the limit $\text{Re} \rightarrow \infty$ this equation reduces to

$$\ddot{F} - 2F\dot{F} = 0 . \quad (5.27)$$

The order of the original equation is not lowered. The stretching with the factor $\sqrt{-\alpha \text{Re}}$ in Eq. (5.25) was indeed chosen that a degeneration of the differential equation was avoided. The boundary conditions of Eq. (5.27) are:

$$\xi = 0 : \quad F = 0; \quad \xi \rightarrow \infty : \quad F = 1, F' = 0 . \quad (5.28)$$

One analytical solution exists:

$$F(\xi) = 3 \tanh^2 \left(\frac{\xi}{\sqrt{2}} + \operatorname{artanh} \sqrt{\frac{2}{3}} \right) - 2 \quad (5.29)$$

with

$$\dot{F}(0) = 2/\sqrt{3} \quad \text{and} \quad \ddot{F}(0) = -1 . \quad (5.30)$$

For $\xi = 3.3$, $F(\xi) = 0.99$. If the edge of the boundary layer is fixed at the point where the velocity is 99% of the velocity at the axis, then we have

$$1 - \eta_{99} = \frac{3.3}{\sqrt{-\alpha \text{Re}}} . \quad (5.31)$$

Thus the boundary-layer thickness decreases with increasing Reynolds number, in inverse proportion to the square root of the Reynolds number, a characteristic result for laminar boundary layers. For the skin-friction coefficient, Eq. (5.21) yields

$$c_f \sqrt{\text{Re}} = 4 \sqrt{\frac{-\alpha}{3}}. \quad (5.32)$$

The combination $c_f \sqrt{\text{Re}}$ is also typical for laminar boundary layers. Finally, from Eq. (5.23) we find $c_{pw} = 1$, i.e. the pressure distribution at the wall corresponds to the pressure distribution in the inviscid core flow. In other words, the pressure distribution of the inviscid core flow is imposed on the wall boundary layer.

In conclusion, it can be established that the flow in nozzles ($\alpha < 0$) at large Reynolds numbers has a layered structure. The flow field consists of two regions: the larger core region with inviscid flow, and the boundary layer close to the wall, where the viscosity plays a role and ensures that the velocity passes over from its full value in the core to the value zero at the wall (the no-slip condition). The thickness of the boundary layer and the skin-friction coefficient are proportional to $1/\sqrt{\text{Re}}$, and thus tend to zero with increasing Reynolds number. In both regions, equations are to be solved which are simpler than the full Navier–Stokes equations. The solutions which are determined separately have to be matched up in an overlap region. Such boundary-layer solutions for $\text{Re} \rightarrow \infty$ do not exist for diffusers ($\alpha > 0$).

Slender-channel theory. Not all solutions of Jeffery–Hamel flows have a boundary-layer character for $\text{Re} \rightarrow \infty$. As can be seen from the initial equation (5.17), another limiting value is possible for $\text{Re} \rightarrow \infty$. This is a double limit, where, as well as $\text{Re} \rightarrow \infty$, the limit $\alpha \rightarrow 0$ is also taken, so that the product αRe remains constant. At fixed αRe , the opening angle α decreases with increasing Reynolds number, i.e. the geometric configuration becomes “more slender”. The solutions for this double limit, where there is a coupling of fluid mechanical and geometrical quantities, are determined using *slender-channel theory*. In considering the limit, here too there is a simplification of the flow equation, but no degeneration. In this case, using $\alpha \rightarrow 0$, Eq. (5.17) reduces to

$$F''' + 2\alpha \text{Re} F' F'' = 0 \quad (5.33)$$

with the unchanged boundary conditions as in Eq. (5.18). The solutions of this (still) nonlinear differential equation do not have boundary-layer character, and they exist for both nozzles ($\alpha < 0$) and diffusers ($\alpha > 0$). There is now a single-parameter family of solutions with the slender-channel parameter αRe . In Fig. 5.4, the quantity $[F'(1)]^2$ of these slender-channel solutions is given as a function of αRe , where $F'(1)$, from Eq. (5.21), is a measure for

the skin-friction coefficient. The value $[F'(1)] = 4$ at $\alpha Re = 0$ corresponds to the solution for the channel made up of two parallel walls in Eq. (5.12). The numbers on the curves are the Reynolds numbers of some examples from Fig. 5.2. The asymptote to the curve for $\alpha Re \rightarrow -\infty$ (nozzles) corresponds to the boundary-layer solution already discussed. The solutions for diffusers ($\alpha Re > 0$) are of interest. At $\alpha Re = 10.3$ the skin-friction coefficient vanishes, and for $\alpha Re > 10.3$ backflow takes place close to the wall. With increasing αRe the volume flux of the backflow increases, so that at $\alpha Re = 50.73$ the total volume flux finally vanishes. The curve sketched in the figure corresponds to symmetric solutions. However for $\alpha Re > 10.3$ antisymmetric solutions, where there is backflow only at one wall, are also possible. At $\alpha Re = 10.3$ the solution bifurcates, and for $\alpha Re > 10.3$ the solution is non-unique.

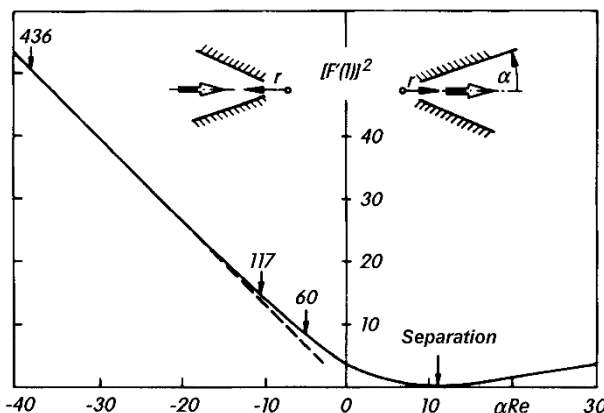


Fig. 5.4. Jeffery–Hamel solutions for $\alpha \rightarrow 0$, $Re \rightarrow \infty$ with $\alpha Re = O(1)$, slender-channel theory
--- asymptote
 $[F'(1)]^2 = -\frac{4}{3}\alpha Re$ according to boundary-layer theory

This non-uniqueness of solutions is a characteristic frequently seen in high Reynolds number flows.

The energy equation, with correspondingly chosen boundary conditions, also leads to an ordinary differential equation, and thus to similar temperature profiles. Temperature distributions due only to dissipation have been calculated by K. Millsaps; K. Pohlhausen (1953). Even without taking account of the dissipation, temperature distributions at the wall dependent on the coordinate r (power laws) lead to self-similar temperature profiles, as B.L. Reeves; Ch.J. Kippenhan (1962) have shown. Because of the linearity of the energy equation, both effects can be superimposed.

The Jeffery–Hamel solutions were used by L.E. Fraenkel (1962, 1963) to approximately compute the flow in symmetric plane channels with weakly curving walls. Perturbations to the Jeffery–Hamel flows have been comprehensively examined by W.H.H. Banks et al. (1988).

5.1.3 Plane Stagnation–Point Flow

The previous examples were concerned with internal flows where only one velocity component was present.

A simple example of a flow past a body where both velocity components appear will now be discussed: the plane stagnation–point flow in Fig. 5.5.

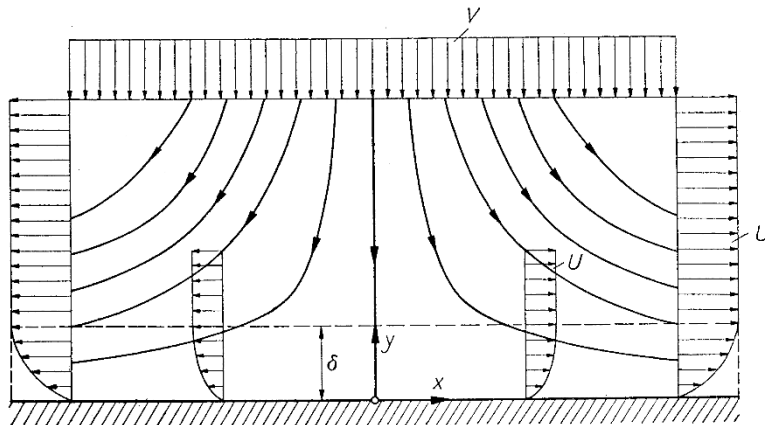


Fig. 5.5. Plane stagnation–point flow

The velocity distribution of the inviscid flow (potential flow) in the neighbourhood of the stagnation point reads

$$U = ax; \quad V = -ay,$$

where a denotes a constant. Using the Bernoulli equation, the corresponding pressure distribution follows as

$$P_0 = P + \frac{\rho}{2}(U^2 + V^2) = P + \frac{\rho}{2}a^2(x^2 + y^2),$$

where P is the pressure at an arbitrary position, and P_0 is the pressure at the stagnation point ($x = 0, y = 0$). Now this inviscid flow satisfies the Navier–Stokes equations but not the no-slip condition at the wall ($y = 0$).

In order to satisfy this too, the effect of the viscosity must be taken into account. To do this we use the ansatz for the velocity and pressure distributions:

$$u = U f'(\eta) = axf'(\eta); \quad v = -\sqrt{a\nu}f(\eta), \quad (5.34)$$

$$P_0 = p + \frac{\rho}{2}a^2 \left[x^2 + \frac{2\nu}{a}F(\eta) \right] \quad (5.35)$$

with the transformed coordinate

$$\eta = \sqrt{\frac{a}{\nu}} y . \quad (5.36)$$

Since flows of fluids with low values of the kinematic viscosity ν are of greatest interest to us, the new coordinate can be thought of as a “stretched” distance from the wall. The continuity equation is identically satisfied by the trial solutions (5.34) to (5.36). From the Navier–Stokes equation in the x direction, we find an ordinary differential equation for the function $f(\eta)$ which can also be thought of as the dimensionless stream function $\psi = x\sqrt{\alpha\nu}f(\eta)$:

$$f''' + f f'' + 1 - f'^2 = 0 \quad (5.37)$$

with the boundary conditions

$$\eta = 0 : f = 0, f' = 0; \quad \eta \rightarrow \infty : f' = 1 . \quad (5.38)$$

These follow from the impermeability of the wall (from $v(x, 0) = 0$ it follows that $f(0) = 0$) and from the no-slip condition (from $u(x, 0) = 0$ it follows that $f'(0) = 0$). At large distances from the wall ($\eta \rightarrow \infty$) the velocity $u(x, \eta)$ should pass over smoothly into that for inviscid flow $U(x, y)$. Using Eq. (5.34), this leads to the condition $f'(\infty) = 1$.

Since Eq. (5.37) is a third order differential equation, precisely those three boundary conditions in (5.38) can be satisfied. Therefore the condition that $v(x, \eta)$ should pass over to $V(x, y)$ for $\eta \rightarrow \infty$ can no longer be prescribed. As the solution of Eq. (5.37) shows, this condition is indeed not satisfied.

From Eq. (5.34) it follows that

$$\lim_{\eta \rightarrow \infty} (v - V) = \sqrt{a\nu} \beta_1 \quad (5.39)$$

with the non-zero value

$$\beta_1 = \lim_{\eta \rightarrow \infty} [\eta - f(\eta)] . \quad (5.40)$$

Because of the effect of viscosity, the velocity is directed away from the wall in the outer region of flow. The boundary layer has a *displacement effect*, and the flow in the outer region behaves as potential flow, displaced from the wall by the thickness

$$\delta_1 = \sqrt{\frac{\nu}{a}} \beta_1 . \quad (5.41)$$

The quantity δ_1 , defined using the original variables as

$$\delta_1 = \frac{1}{U} \int_0^{\infty} (U - u) dy \quad (5.42)$$

is therefore called the *displacement thickness*. It is a measure of the difference in volume flux between the inviscid and viscous flow, cf. Fig. 2.3. The

“displacement effect” is a typical boundary–layer effect which vanishes with decreasing viscosity.

The integration of the Navier–Stokes equation in the y direction leads to the solution

$$F(\eta) = \frac{1}{2}f^2(\eta) + f'(\eta). \quad (5.43)$$

This leads to the pressure distribution on the stagnation line ($x = 0$) from Eq. (5.35):

$$P_0 = p + \frac{\rho}{2}v^2 + a\mu f'. \quad (5.44)$$

The total pressure on the stagnation line $g = p + \rho v^2/2$ is then

$$g = P_0 - a\mu f'(\eta). \quad (5.45)$$

This interesting relation implies that the total pressure on the stagnation line increases as we move closer to the wall (!). Because of the boundary condition $f'(\infty) = 1$, the difference between the total pressure $(g)_{\text{outer}} = g(\eta \rightarrow \infty)$ at large distances from the wall (i.e. in the inviscid outer region) and the total pressure at the stagnation point $(g)_{\text{stag}} = P_0$ is

$$(g)_{\text{outer}} - (g)_{\text{stag}} = -a\mu. \quad (5.46)$$

Measuring the total pressure with a Pitot–tube therefore gives rise to a measurement error. The total pressure measured is too high, since, because of the effects of viscosity, the value $(g)_{\text{stag}}$ is measured at the probe and is not the desired total pressure of the outer flow, which, from (5.46), is somewhat smaller. The correction is proportional to μ , and thus is very small for large Reynolds numbers. This error effect of the viscosity is called the *Barker effect* in the literature, cf. M. Barker (1922).

The solution of the differential equation (5.37) was first presented by K. Hiemenz (1911), and therefore plane stagnation–point flow is sometimes also called Hiemenz flow. Hiemenz’s solution was later improved upon by L. Howarth (1935). It is shown in Fig. 5.6, cf. also Table 5.1. At about $\eta = \eta_\delta = 2.4$, we have $f' = 0.99$, i.e. $u = 0.99U$. There the velocity has come to within 1% of its final value. If we denote that distance from the wall $y = \delta$ as the boundary–layer thickness (or the frictional–layer thickness), we have

$$\delta = \eta_{99} \sqrt{\frac{\nu}{a}} = 2.4 \sqrt{\frac{\nu}{a}}. \quad (5.47)$$

For these flows too, the layer affected by the viscosity is thin, and it is proportional to $\sqrt{\nu}$. Equation (5.35) shows that the pressure gradient $\partial p/\partial y$ is proportional to $\rho a \sqrt{\nu a}$ and is therefore also very small at small viscosities. It should be noted that the dimensionless velocity distribution u/U is, from Eq. (5.34), independent of the length x , and thus this is a *similar solution*. This means that the partial Navier–Stokes equation can be reduced to an ordinary differential equation, Eq. (5.37). The boundary–layer thickness δ

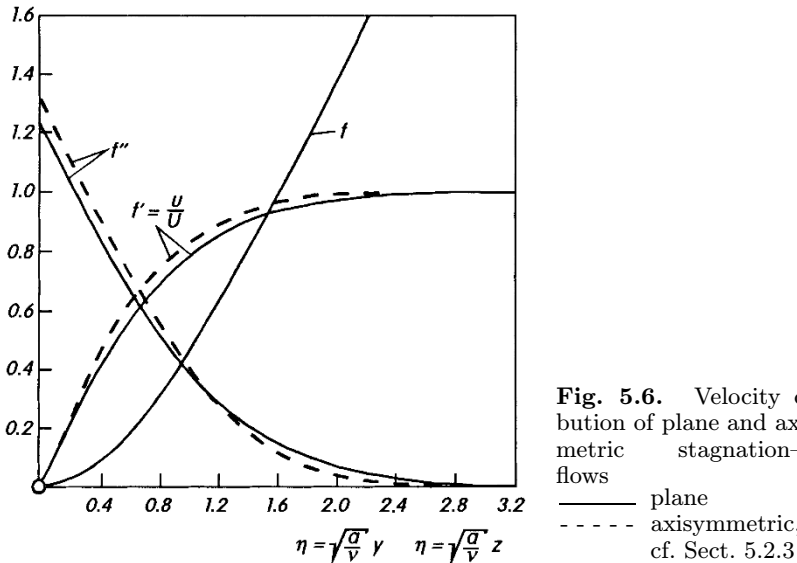


Fig. 5.6. Velocity distribution of plane and axisymmetric stagnation-point flows

— plane
- - - axisymmetric,
cf. Sect. 5.2.3

from Eq. (5.47), i.e. the limit between the frictional boundary layer and the inviscid outer flow, is independent of x for these particular flows.

The solutions found here for the viscous flow close to a stagnation point do not only occur at a plane wall, but also in plane flow past any cylindrical body with a blunt nose at the stagnation point. In such cases, this solution is restricted to a small region around the stagnation point, as long as the curved surface there can be replaced by the tangential plane in the stagnation point.

Suction or blowing. The solution discussed until now can easily be extended to the case where the wall is porous, and where fluid is blown or sucked through it. The boundary conditions for $v(x; 0)$ at the wall in Eq. (5.38) have to be changed to

$$\eta = 0 : \quad f = f_w \quad \begin{cases} f_w > 0 : & \text{suction} \\ f_w < 0 : & \text{blowing} \end{cases} . \quad (5.48)$$

The no-slip condition is retained, but cf. G.J. Hokenson (1985). Solutions at different values f_w can be found in, for example, K. Gersten et al. (1972). As expected, the displacement effect is heightened by blowing, and reduced by suction. For suction of $f_w = 0.54$, the displacement effect just vanishes ($\beta_1 = 0$), and for $f_w > 0.54$ a reversal of the displacement effect occurs: “entrainment”. Both the limiting cases of very strong suction and massive blowing are treated in the work mentioned above. In the case of strong suction ($f_w \rightarrow \infty$), the ansatz

$$f(\eta) = f_w + \frac{1}{f_w} \varphi(\eta_i), \quad \eta_i = \eta f_w \quad (5.49)$$

is used, along with Eqs. (5.37) and (5.38) in the limiting case $f_w \rightarrow \infty$ to get

$$\ddot{\varphi} + \ddot{\varphi} = 0 \\ \eta_i = 0 : \quad \varphi = 0, \dot{\varphi} = 0; \quad \eta_i \rightarrow \infty : \quad \dot{\varphi} = 1, \quad (5.50)$$

where the dots imply differentiation with respect to the “stretched” coordinate η_i . The solution

$$\varphi(\eta_i) = \eta_i - 1 + e^{-\eta_i} \quad (5.51)$$

corresponds to the velocity distribution known as the “*asymptotic suction profile*”

$$\frac{u(x, y)}{U(x)} = 1 - e^{\frac{v_w y}{\nu}} \quad (v_w < 0), \quad (5.52)$$

which is independent of the parameter $a(!)$.

In the case of massive blowing ($f_w \rightarrow -\infty$) a simple solution can be given. With the ansatz

$$f(\eta) = f_w - f_w \varphi(z), \quad z = \frac{\eta}{-f_w} \quad (5.53)$$

Eqs. (5.37) and (5.38) reduce to

$$(\varphi - 1)\ddot{\varphi} + 1 - \dot{\varphi}^2 = 0 \\ z = 0 : \quad \varphi = 0, \dot{\varphi} = 0; \quad z = \frac{\pi}{2} : \quad \dot{\varphi} = 1. \quad (5.54)$$

Dots here imply differentiation with respect to the “*compressed*” coordinate z . It is worth noting that, in this limiting case, the term describing the friction forces f''' or $\ddot{\varphi}$ vanishes and thus the order of the differential equation is reduced. Then the external boundary condition is satisfied not for $z \rightarrow \infty$ but for the finite value of $z = \pi/2$. The solution of Eq. (5.54) $\varphi = 1 - \cos z$ leads to the simple velocity distribution

$$\frac{u(x, y)}{U(x)} = \sin \frac{ay}{v_w} \quad 0 \leq y \leq \frac{\pi v_w}{2a}. \quad (5.55)$$

The zero streamline ($\varphi = 1, f = 0$) is at a distance $z = \pi/2$ from the wall. This is the *dividing streamline* which separates the fluid blown out of the wall from the fluid of the outer flow. At this point there is a singularity in the velocity distribution: the curvature is not continuous. This is due to the fact that Eq. (5.56) corresponds to an *inviscid* solution. In spite of this, the wall shear stress can be computed from Eq. (5.55) as

$$\tau_w(x) = \frac{\mu a U(x)}{v_w} = \frac{\mu a^2 x}{v_w}. \quad (5.56)$$

At finite Reynolds numbers a “*frictional*” layer forms around the dividing streamline, and here the viscosity ensures the continuous progress of the velocity curvature across the dividing streamline. This frictional “transition

solution" can be written in terms of *parabolic cylinder functions*, as shown by K. Gersten et al. (1972).

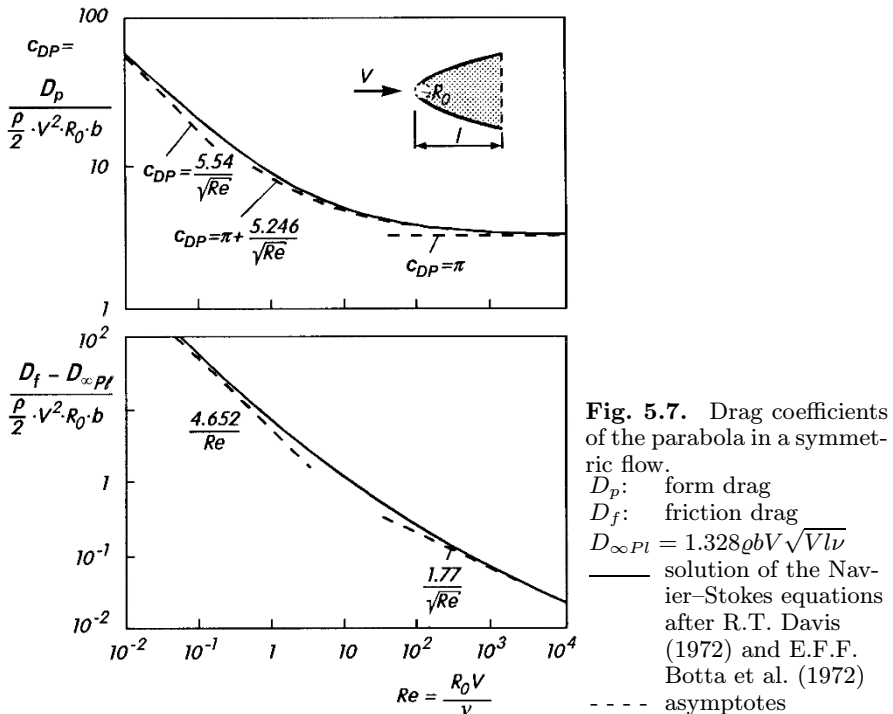
The solutions of the energy equation without taking the dissipation into account are also given in this work. The temperature is then independent of x , i.e. the case $T_w = \text{const}$ is then identical to the case $q_w = \text{const}$. The effect of dissipation was investigated by K. Gersten; H. Körner (1968). For adiabatic walls, the dissipation leads to a distribution of the wall temperature proportional to x^2 , the so-called "*adiabatic wall-temperature distribution*", which depends both on the Prandtl number and on the suction or blowing.

5.1.4 Flow Past a Parabolic Body

A characteristic of the solutions of the Navier–Stokes equations discussed until now was that the velocity profiles were similar and therefore the partial differential equations could be reduced to ordinary differential equations. In the case of symmetric flow past a parabola, such a reduction is no longer possible and so the partial differential equations have to be solved numerically. Numerical solutions of the Navier–Stokes equations for symmetric flows past a parabola have been given by R.T. Davis (1972) and by E.F.F. Botta et al. (1972). Drag coefficients resulting from these calculations, broken down into form drag (pressure drag) and friction drag, are shown as a function of the Reynolds number in Fig. 5.7. Here the Reynolds number is formed with the free-stream velocity V and the radius of curvature R_0 of the parabola at its apex (the stagnation point). The asymptotes for $\text{Re} \rightarrow 0$ correspond to *creeping* flow past a parabola. More interesting are the asymptotes for $\text{Re} \rightarrow \infty$. In this limiting case, the form drag follows from the potential theory solutions. In contrast to D'Alembert's paradox, potential theory yields a non-zero value, since here we are dealing with a *half-body* which continuously expands backwards. The asymptote for $\text{Re} \rightarrow \infty$ for the friction drag corresponds to the boundary-layer solution at a parabola. This will be discussed in Chap. 14. The figure clearly shows the excellent agreement between the exact solution of the Navier–Stokes equations and the asymptotic solutions for values of the Reynolds number above $\text{Re} > 10^3$. The flow past a parabola is comparatively simple, since the pressure on the contour always decreases downstream and therefore the shear stress at the wall never vanishes. There is no separation leading to backflow. This is different in the following case.

5.1.5 Flow Past a Circular Cylinder

The discussions in Chap. 1 showed that the flow past a circular cylinder is unsteady above about $\text{Re} = Vd/\nu > 90$. Thus steady flow past a cylinder in reality does not exist for the limit $\text{Re} \rightarrow \infty$. In spite of this, the steady Navier–Stokes equations have been solved numerically for Reynolds numbers $\text{Re} > 90$, by, for example, B. Fornberg (1980, 1985) and J.C. Wu;



U. Gulcat (1981). It can clearly be seen from these calculations that, with increasing Reynolds number, regions where the vorticity is finite which are a measure of the effects of the viscosity cling to the body ever more closely, and thus assume boundary-layer character. The steady solutions also tend towards a limiting solution for $\text{Re} \rightarrow \infty$. As already mentioned in Chap. 1, the Kirchhoff–Helmholtz solution of so-called *free streamlines* is a possible limiting solution. However more recent work, cf. F.T. Smith (1979a, 1985), has shown that the limiting solution may not be so simple.

5.2 Steady Axisymmetric Flows

5.2.1 Circular Pipe Flow (Hagen–Poiseuille Flow)

The axisymmetric flow corresponding to plane channel flow is the fully developed flow through a straight pipe with circular cross-section (radius $R = d/2$). Let the axis of the pipe lie along the x axis, and r be the radial coordinate measured outwards from the axis. The velocity components in the radial and tangential directions are zero, and the velocity component in the axial direction is denoted by u and is only dependent on r . The pressure is constant in every cross-section. Of the three

Navier–Stokes equations in cylindrical coordinates, Eq. (3.93), only the equation in the x direction remains. This reduces to

$$\mu \left(\frac{d^2 u}{dr^2} + \frac{1}{r} \frac{du}{dr} \right) = \frac{dp}{dx} \quad (5.57)$$

with the boundary condition (the no-slip condition) $u = 0$ for $r = R$. The solution of Eq. (5.57) is a velocity distribution of parabolic form

$$u(r) = u_{\max} \left(1 - \frac{r^2}{R^2} \right) \quad (5.58)$$

and

$$u_{\max} = 2u_m = \frac{R^2}{4\mu} \left(-\frac{dp}{dx} \right). \quad (5.59)$$

The relation between pressure drop and average velocity $u_m = Q/\pi R^2$ is expressed by the dimensionless pipe friction factor λ , which is defined using the following relation:

$$-\frac{dp}{dx} = \frac{\lambda \rho}{d} u_m^2. \quad (5.60)$$

From (5.59) it then follows that

$$\lambda = \frac{64}{Re} \quad (5.61)$$

with

$$Re = \frac{u_m d}{\nu}. \quad (5.62)$$

This relation agrees extremely well with measurements, as long as the Reynolds number lies below the critical Reynolds number $Re_{\text{crit}} = 2300$. The pipe flow becomes turbulent above this value, cf. Sect. 17.2.3.

An extension of simple pipe flow to flows in a *weakly diverging pipe* has been given by H. Blasius (1910). It was seen that the laminar flow can only tolerate a very small rise in pressure before separation occurs. Backflow is just prevented at the wall (the separation condition) for $dR/dx \leq 12/Re$.

An exact solution of the Navier–Stokes equations can be given for a pipe of concentric circular cross-section (a so-called *annulus*), see W. Müller (1936).

The computation of full pipe flows for *arbitrary cross-sectional shapes* is based on the solution of the Poisson differential equation. Solutions for different cross-sections are to be found in the work by R.K. Shah; A.L. London (1978).

5.2.2 Flow Between Two Concentric Rotating Cylinders

The flows between two concentric rotating cylinders which rotate with different but steady rotational speeds also lead to simple exact solutions of the Navier–Stokes equations, cf. H. Schlichting (1982), p. 88. Since these solutions do not take on boundary-layer character for small viscosities, we will not consider them here further and will only mention two special cases. If one of the cylinders stands still, the solution in the limit $(R_2 - R_1)/R_1 \rightarrow 0$ reduces to the Couette flow discussed above. In the second limiting case, the inner cylinder rotates, while the radius of the outer (motionless) cylinder tends towards infinity. This is now the flow at a

single rotating cylinder in surroundings at rest. The solution is that of a potential vortex with velocity profile

$$u(r) = \frac{\Gamma}{2\pi r} . \quad (5.63)$$

Because of the moving wall, this is one example where inviscid flow also satisfies the no-slip condition. In spite of the lack of viscosity, the wall shear stress and the moment M transmitted to the fluid can be determined. For a cylinder with height H , radius R and angular velocity ω we have

$$M = 4\pi\mu H R^2 \omega . \quad (5.64)$$

5.2.3 Axisymmetric Stagnation-Point Flow

In a similar manner to the case of plane stagnation-point flow, an exact solution of the Navier–Stokes equation can also be obtained for axisymmetric stagnation-point flow. Fluid flow impinges on a wall at right angles and flows along this wall radially in all directions. This kind of flow is also found close to the stagnation point on bodies of revolution whose axes lie at zero incidence. We will use cylindrical coordinates r, φ, z , and, unlike in Sect. 3.13, velocity components U, V, W (inviscid) or u, v, w (viscous). It can easily be shown that the inviscid flow

$$\begin{aligned} U &= ar; \quad V = 0; \quad W = -2az ; \\ P_0 &= P + \frac{\rho}{2}(U^2 + W^2) = P + \frac{\rho}{2}a^2(r^2 + 4z^2) \end{aligned}$$

satisfies the Navier–Stokes equation, but not the no-slip condition at the wall ($z = 0$). In order to satisfy this too, the effect of the viscosity must be taken into account. We use the ansatz

$$u = U f'(\eta) = ar f'(\eta); \quad w = -2\sqrt{a\nu} f(\eta) , \quad (5.65)$$

$$P_0 = p + \frac{\rho}{2}a^2 \left[r^2 + \frac{4\nu}{a} F(\eta) \right] \quad (5.66)$$

with

$$\eta = \sqrt{\frac{a}{\nu}} z . \quad (5.67)$$

For the function $f(\eta)$ we find

$$f''' + 2f f'' + 1 - f'^2 = 0 \quad (5.68)$$

with the boundary conditions

$$\eta = 0 : \quad f = 0, \quad f' = 0; \quad \eta \rightarrow \infty : \quad f' = 1 . \quad (5.69)$$

This differential equation is identical to Eq. (5.37), up to the factor 2 in the second term. For $F(\eta)$ we obtain

$$F(\eta) = f^2 + f' .$$

Equation (5.68) was first solved by F. Homann (1936), and later by N. Frössling (1940). The function $u/U = f'(\eta)$ is given in Fig. 5.6, while Table 5.1 contains some important numerical values. The Barker effect also holds for this solution, although with the term $-2a\mu$ on the right hand side of Eq. (5.46). In analogy to Eq. (5.47) we find the boundary-layer thickness is

$$\delta = 2.8 \sqrt{\frac{\nu}{a}} . \quad (5.70)$$

Using the transformation

$$f(\eta) = \frac{1}{\sqrt{2}} \varphi(\bar{\eta}) , \quad \eta = \frac{1}{\sqrt{2}} \bar{\eta} , \quad (5.71)$$

instead of Eqs. (5.68) and (5.69) we find the differential equation

$$\ddot{\varphi} + \varphi \ddot{\varphi} + \frac{1}{2}(1 - \dot{\varphi}^2) = 0 \quad (5.72)$$

with the boundary conditions

$$\bar{\eta} = 0 : \quad \varphi = 0, \dot{\varphi} = 0; \quad \bar{\eta} \rightarrow \infty : \quad \dot{\varphi} = 1 . \quad (5.73)$$

This equation has frequently been solved in the literature, cf. Sect. 7.2 for the case of suction and blowing, i.e. with the boundary condition $\varphi(0) = \varphi_w$, e.g. by K. Gersten; H. Körner (1968) and W.E. Stewart; R. Prober (1962). K. Gersten (1973b) has discussed the limiting cases of massive suction and massive blowing. The solutions of the energy equations corresponding to each case are also given in the above works.

The extension to the three-dimensional stagnation point has been treated by K. Gersten (1973a).

The flow at a paraboloid of revolution has been computed by R.T. Davis; M.J. Werle (1972).

Table 5.1. Function values at the wall and at a large distance from the wall used in describing stagnation-point flow

plane				axisymmetric			
η	f	f'	f''	η	f	f'	f''
0	0	0	1.2326	0	0	0	1.3120
∞	$\eta - 0.648$	1.0	0	∞	$\eta - 0.569$	1.0	0

5.2.4 Flow at a Rotating Disk

A further example of an exact solution of the Navier-Stokes equations is the flow close to a flat disk rotating in a fluid which is otherwise at rest

with constant angular velocity ω about an axis perpendicular to its plane. Because of the no-slip condition and the viscosity, the layer of fluid directly at the disk is carried along with it and driven outwards by the centrifugal force. New fluid particles are then continuously pulled onto the disk in the axial direction and then ejected centrifugally again. This is therefore a fully three-dimensional flow which acts as a pump. Figure 5.8 shows this flow in perspective. There are velocity components present in all three directions, which, again deviating from Sect. 3.13, are denoted u , v , w (with cylindrical coordinates r , φ , z).

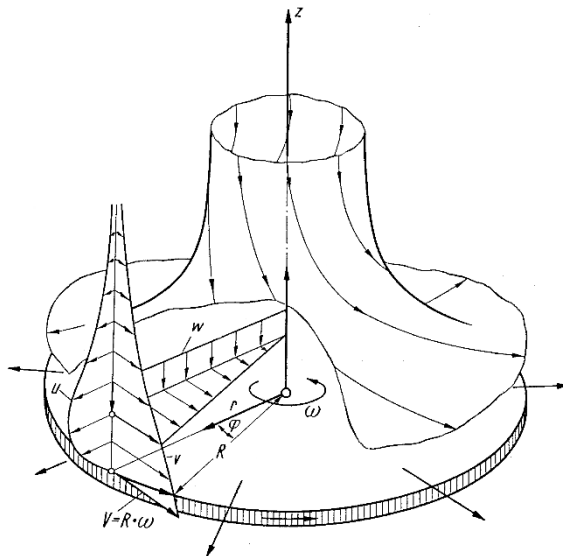


Fig. 5.8. Flow close to a rotating disk in a fluid at rest, velocity components:
 u : radial
 v : azimuthal
 w : axial

First let us calculate the thickness δ of the layer “carried” along with the disk. There must be a relation

$$\delta = f(\nu, \omega)$$

for this thickness. According to the Π theorem of dimensional analysis, it follows that

$$\delta \sim \sqrt{\frac{\nu}{\omega}} . \quad (5.74)$$

The thickness of the layer set into rotation by the viscosity is therefore smaller the smaller the viscosity ν .

For the solution of the Navier–Stokes equations it is useful to relate the distance from the wall z to the quantity $\sqrt{\nu/\omega}$, i.e. to introduce a dimensionless wall distance

$$\zeta = \sqrt{\frac{\omega}{\nu}} z . \quad (5.75)$$

Using the trial solutions

$$\begin{aligned} u &= r\omega F(\zeta); \quad v = r\omega G(\zeta); \quad w = \sqrt{\omega\nu}H(\zeta); \\ p &= p_0 + \varrho\nu\omega P(\zeta) \end{aligned} \quad (5.76)$$

and the continuity equation and the Navier–Stokes equations in cylindrical coordinates from Sect. 3.13, we obtain the following system of ordinary differential equations:

$$\begin{aligned} 2F + H' &= 0 \\ F^2 + F'H - G^2 - F'' &= 0 \\ 2FG + HG' - G'' &= 0 \\ P' + HH' - H'' &= 0 \end{aligned} \quad (5.77)$$

with the boundary conditions

$$\begin{aligned} \zeta = 0 : \quad F &= 0, \quad G = 1, \quad H = 0, \quad P = 0 \\ \zeta \rightarrow \infty : \quad F &= 0, \quad G = 0. \end{aligned} \quad (5.78)$$

The solution of this system was first given approximately by Th. v.Kármán (1921); later a more precise calculation was presented by W.G. Cochran (1934). This is depicted in Fig. 5.9, cf. also Table 5.2.

As before with the stagnation-point flow, the velocity field is first to be determined from the continuity equation and the equations of motion close to the wall, and subsequently the pressure distribution perpendicular to the wall is worked out. For the pressure it is found

$$P(\zeta) = H' - \frac{1}{2}H^2. \quad (5.79)$$

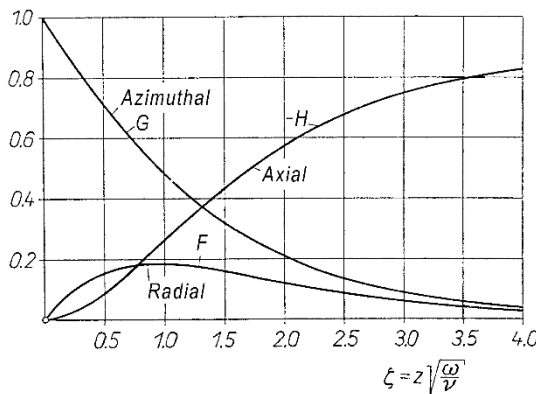


Fig. 5.9. Velocity distributions at a rotating disk in a fluid at rest, cf. Table 5.2

Table 5.2. Function values at the wall and at a large distance from the wall used in describing the flow at a rotating disk in a fluid at rest after M.H. Rogers; G.N. Lance (1960)

$\zeta = z\sqrt{\omega/\nu}$	F'	$-G'$	$-H$	P
0	0.51023	0.61592	0	0
∞	0	0	0.88446	0.39113

It emerges that the circumferential velocity has dropped to within 1% of the disk velocity at $\zeta = 5.5$. Therefore the thickness of the layer is

$$\delta = 5.5 \sqrt{\frac{\nu}{\omega}} . \quad (5.80)$$

The slope of the streamlines at the wall to the circumferential direction is

$$\tan \varphi_0 = - \left(\frac{\partial u / \partial z}{\partial v / \partial z} \right)_w = - \frac{F'(0)}{G'(0)} = 0.828 \quad (\varphi_0 = 39.6^\circ) . \quad (5.81)$$

Although the calculation is strictly speaking applicable to an infinitely extended disk only, the results will now be applied to a circular disk of finite radius R . This is certainly allowable if the radius R is large compared to the thickness δ of the layer carried with the disk, so that the edge effects on the entire circular area are restricted to a small ring shaped area.

The moment of such a disk will now be determined. The contribution of an annular of thickness dr with radius r is $dM = -2\pi r^2 dr \tau_{z\varphi}$. Here $\tau_{z\varphi}$ is the circumferential component of the wall shear stress, cf. Eq. (3.95). From Eq. (5.76) this is

$$\tau_{z\varphi} = \mu \left(\frac{\partial v}{\partial z} \right)_w = \varrho r \omega \sqrt{\nu \omega} G'(0) . \quad (5.82)$$

The moment of a disk wetted on *one* side then follows as

$$M = -2\pi \int_0^R r^2 \tau_{z\varphi} dr = -\frac{\pi}{2} \varrho R^4 \sqrt{\nu \omega^3} G'(0) . \quad (5.83)$$

It is customary to introduce the following dimensionless coefficient for the moment for a disk wetted on *both* sides:

$$c_M = \frac{2M}{\varrho \omega^2 R^5 / 2} . \quad (5.84)$$

With the Reynolds number

$$\text{Re} = \frac{R^2 \omega}{\nu} \quad (5.85)$$

and the value $G'(0) = -0.6159$ from Table 5.2 we find

$$c_M = \frac{3.87}{\sqrt{\text{Re}}} . \quad (5.86)$$

This formula for the moment coefficient is depicted in Fig. 5.10 as curve (1), and is compared with experimental results from Th. Theodorsen; A. Regier (1944), G. Kempf (1924), W. Schmidt (1921) as well as D. Riabouchinsky (1935, 1951). Up to Reynolds numbers of about $\text{Re} = 3 \cdot 10^5$ the agreement of the theory of Eq. (5.86) with the measurements is very good. Turbulence occurs for higher Reynolds numbers. Turbulent flow at a rotating disk is treated in Sect. 20.1.3; it yields the law sketched in Fig. 5.10 as curve (2).

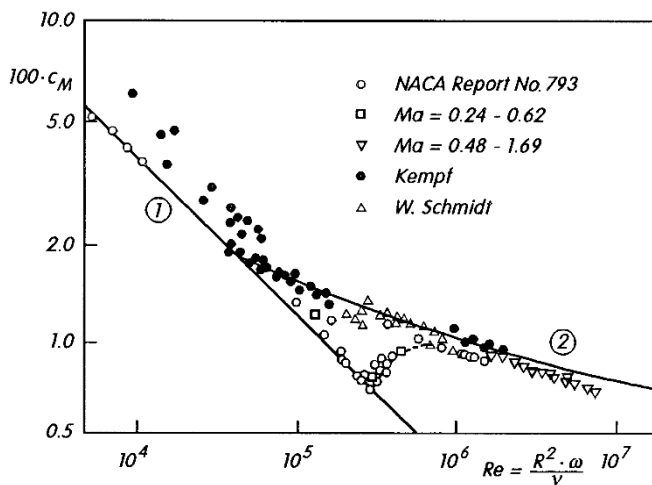


Fig. 5.10. Moment coefficients of a rotating disk wetted on both sides.
(1) laminar, from Eq. (5.86). (2) turbulent, from Eq. (20.18)

The volume flux which is axially drawn towards the plate and radially driven outwards by the centrifugal force on *one* side of a disk of radius R is

$$Q = 2\pi R \int_0^\infty u dz = -H(\infty)\pi R^2 \sqrt{\nu \omega} = 0.885\pi R^3 \omega / \sqrt{\text{Re}} . \quad (5.87)$$

It is also worth noting that the pressure difference over the thickness of the disk is proportional to $\rho v \omega$, i.e. it is very small at low viscosities. The pressure depends only on the distance from the wall, and is therefore independent of the radius R .

As has already been mentioned, the rotating disk acts as a pump. In this flow the fluid experiences an increase in the total pressure. The increase in

the mechanical energy in the flow is

$$\begin{aligned} P_M &= \int_0^\infty \left[p + \frac{\rho}{2}(u^2 + v^2 + w^2) \right] 2\pi R u dz \\ &= \pi \rho R^4 \omega \sqrt{\frac{\nu}{\omega}} \left[\int_0^\infty (F^2 + G^2) F d\zeta - \frac{4}{Re} \int_0^\infty F^2 d\zeta \right]. \end{aligned} \quad (5.88)$$

With the numerical value

$$\int_0^\infty (F^2 + G^2) F d\zeta = 0.088$$

we find for $Re \rightarrow \infty$ that

$$P_M = 0.088 \pi \rho R^4 \sqrt{\nu \omega^5} = 0.29 |M| \omega. \quad (5.89)$$

At high Reynolds numbers the pump efficiency has a value of 29%.

The extension to the case of homogeneous suction has been considered by J.T. Stuart (1954) and E.M. Sparrow; J.L. Gregg (1960b). The latter work also contains the case of homogeneous blowing. The limiting case of massive blowing has been treated by H.K. Kuiken (1971). The solutions of the corresponding energy equations are dealt with in the work of E.M. Sparrow; J.L. Gregg (1960b) and, in the case of massive blowing, by K. Gersten; W.P. Cosart (1980).

A generalisation of the problem at hand to the case where the fluid at infinity moves with angular velocity $\Omega = s\omega$ has been treated by M.G. Rogers; G.N. Lance (1960). It turns out that, for a rotation in the opposite direction, with $s < -0.2$, a physically sensible solution only exists when homogeneous suction is applied.

A further generalisation is the flow between two disks rotating in opposite directions, cf. G.K. Batchelor (1951); see also K. Stewartson (1953) and G.L. Mellor et al. (1968). A good summary has been given by P.J. Zandbergen; D. Dijkstra (1987).

5.2.5 Axisymmetric Free Jet

An interesting *similar* solution of the Navier–Stokes equations in spherical polar coordinates is due to L. Landau (1944) and H.B. Squire (1951), namely the flow of the axisymmetric free jet. For details of the calculation, see the original work, or the presentations by G.K. Batchelor (1974) and F.S. Sherman (1990). A typical example of the streamline field is given in Fig. 5.11. The edge of the free jet can be defined as the position where the streamlines are the smallest distance away from the axis. It emerges from the figure that the edge of the jet is a cone with semi opening angle Θ_0 . Integrating the momentum flux on the spherical surface about the origin yields the momentum

of the free jet. The solution for small values of ν only is given here. The free jet momentum flux is

$$\dot{I} = \frac{64\pi}{3} \frac{\varrho\nu^2}{\Theta_0^2} \quad (\nu \rightarrow 0). \quad (5.90)$$

For a given momentum flux \dot{I} , the semi opening angle $\Theta_0 \sim \nu$ gets smaller with decreasing viscosity. For small values of ν , the jet flow of the actual jet is therefore concentrated in a small region close to the axis. In this limit $\nu \rightarrow 0$

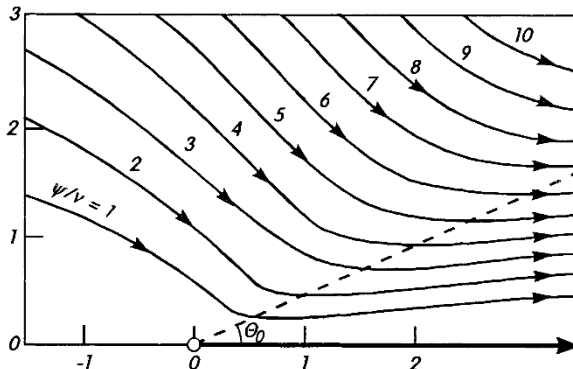


Fig. 5.11. Streamlines of the axisymmetric free jet flow, after G.K. Batchelor (1974), $\Theta_0 = 24.6^\circ$

we can therefore talk of a boundary-layer flow. In the limiting case $\nu = 0$ the momentum flux \dot{I} would have infinitely large velocity, but vanishing volume flux Q , so that the product of velocity and volume flux gives the desired finite momentum. This singular velocity distribution in the form of a Dirac function is then *blurred* by the effect of the viscosity, so that the radius of the jet is proportional to ν . This boundary-layer solution is fully dealt with in Sect. 12.1.5. It will be seen that the volume flux Q of the free jet in the axial direction increases linearly with the distance from the origin. Because of the viscosity, fluid at the edge of the jet is continually carried along from the surroundings at rest; this “entrainment” means that the jet gets continually wider. The side suction of the fluid from the surroundings is easily seen from Fig. 5.11.

If the axisymmetric jet exits a wall as shown in Fig. 7.7, then there is no similar solution to the Navier-Stokes equations which also satisfies the no-slip condition at the wall; this has been shown by K. Potsch (1981), see also W. Schneider (1981).

An extension to *radial jets*, where the outlet is a peripheral slit in a tube, has been described by H.B. Squire (1955).

5.3 Unsteady Plane Flows

Frequently exact solutions of the unsteady Navier–Stokes equations exist when there are already exact solutions of the corresponding steady flow at hand. Examples of unsteady flows are “*start-up*” flows from rest, or “*shut-down*” flows where the flow dies away in time. Unsteady flows can also be produced by periodic boundary conditions (oscillating wall, periodic conditions for the velocity or pressure). A characteristic of the flows considered in what follows is that the unsteady parts of the velocity are independent of the coordinate x parallel to the wall. Because of this, the simplifications to the Navier–Stokes equations are so great that exact solutions can be determined. Because $\partial u / \partial x = 0$ and $\partial v / \partial x = 0$, it follows from the continuity equation that $v(t) = v_w(t)$. Either there is suction ($v_w < 0$) or blowing ($v_w > 0$), or the v component of the velocity vanishes. Because of the independence from the x coordinate, the Navier–Stokes equations reduce to the two following *linear* differential equations

$$\varrho \left(\frac{\partial u}{\partial t} + v_w \frac{\partial u}{\partial y} \right) = - \frac{\partial p}{\partial x} + \mu \frac{\partial^2 u}{\partial y^2}, \quad (5.91)$$

$$\varrho \frac{dv_w}{dt} = - \frac{\partial p}{\partial y}. \quad (5.92)$$

The pressure is therefore only dependent on y if there is time dependent suction or blowing at hand.

5.3.1 Flow at a Wall Suddenly Set into Motion (First Stokes Problem)

We now treat a *start-up* flow, i.e. motion from rest. We consider the flow close to a wall which is suddenly set into motion with a constant velocity U_0 in its own plane. This problem was first solved by G.G. Stokes (1856) in his famous treatment of the pendulum. Since Lord Rayleigh (1911) also treated this flow, it is often called the *Rayleigh problem* in the literature. Let the wall lie along the x axis. Since the pressure is constant in the whole space, Eq. (5.91) reduces to

$$\frac{\partial u}{\partial t} = \nu \frac{\partial^2 u}{\partial y^2} \quad (5.93)$$

with the boundary conditions

$$\begin{aligned} t \leq 0 : \quad y \geq 0 : \quad u &= 0 \\ t > 0 : \quad y = 0 : \quad u &= U_0 \\ y \rightarrow \infty : \quad u &= 0. \end{aligned} \quad (5.94)$$

As can be seen from the energy equation (3.72), Eq. (5.93) is identical to the heat conduction equation for one-dimensional unsteady temperature fields $T(y, t)$. There are therefore many solutions to this differential equation in the literature on heat conduction. e.g. U. Grigull; H. Sandner (1986) and H.S. Carslaw; J.C. Jaeger (1959).

The desired solution of Eq. (5.93) has the general form $u/U_0 = f(y, t, \nu)$. From the Π theorem in dimensional analysis it follows that $u/U_0 = F(y/\sqrt{t\nu})$. Indeed, by introducing the dimensionless similarity variable

$$\eta = \frac{y}{2\sqrt{\nu t}} \quad (5.95)$$

for the function $u/U_0 = f(\eta)$, Eq. (5.93) yields the ordinary differential equation

$$f'' + 2\eta f' = 0 \quad (5.96)$$

with the boundary conditions $f(0) = 1$ and $f(\infty) = 0$. The solution is

$$\frac{u}{U_0} = \operatorname{erfc} \eta = 1 - \operatorname{erf} \eta, \quad (5.97)$$

where

$$\operatorname{erf} \eta = \frac{2}{\sqrt{\pi}} \int_0^\eta e^{-\eta^2} d\eta \quad (5.98)$$

is the error function, and $\operatorname{erfc} \eta$ is the complimentary error function.

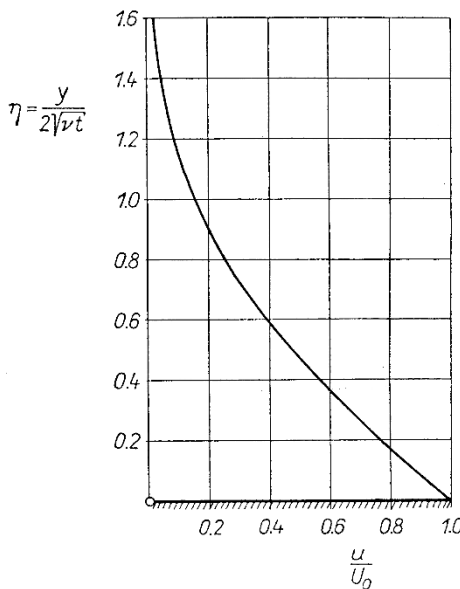


Fig. 5.12. Velocity distribution close to a wall suddenly set into motion (first Stokes problem)

The velocity distribution is shown in Fig. 5.12. The velocity profiles at different times are “similar” to one another, i.e. they can map onto each other by changing the scale on the y axis. The complimentary error function has the value 0.01 at $\eta_{99} = 1.8$. By taking the definition of δ into account, the thickness of the layer carried along is therefore

$$\delta = 2\eta_{99}\sqrt{\nu t} = 3.6\sqrt{\nu t}. \quad (5.99)$$

It is proportional to the square root of the kinematic viscosity and the square root of the time. For large times, δ tends towards infinity, i.e. the entire field above the plate eventually takes on the velocity of the plate. From (5.97) we find the wall shear stress to be

$$\tau_w = \mu \left(\frac{\partial u}{\partial y} \right)_w = -\varrho U_0 \sqrt{\frac{\nu}{\pi t}}. \quad (5.100)$$

At the initial instant ($t = 0$) the wall shear stress is infinite, and it decreases to zero in proportion to $1/\sqrt{t}$. It is also proportional to $\sqrt{\nu}$.

This solution can easily be extended to cases where the wall velocity is an arbitrary function of the time $U(t)$. Since the differential equation (5.93) is linear, new solutions can be produced by superposition of solutions. If we take the given function $U(t)$ to be a *multi-step function* with small steps dU , the entire solution consists of elementary solutions for the step function treated here with the velocity step dU as follows

$$u(y, t) = \int_{-\infty}^t dU \operatorname{erfc} \left(\frac{y}{2\sqrt{\nu(t-\tau)}} \right). \quad (5.101)$$

Because of the time difference $t - \tau$ in the argument of the complimentary error function, it is ensured that the velocity distribution at time t only depends on the velocities $U(t)$ at earlier times. By integration of Eq. (5.101) we are led to the general solution known as *Duhamel's folding integral*

$$u(y, t) = \frac{y}{2\sqrt{\pi\nu}} \int_{-\infty}^t \frac{U(\tau)}{(t-\tau)^{3/2}} e^{-\frac{y^2}{4\nu(t-\tau)}} d\tau. \quad (5.102)$$

Since the partial derivatives of u are functions of both y and t , which are also solutions of Eq. (5.93), solutions for the cases when the wall shear stress is a step function, or an arbitrary function of time, can immediately be written down.

An extension of these flows taking the compressibility into account is given by E. Becker (1960).

There is a certain affinity between the first Stokes problem and the free convection flow set suddenly into motion at a vertical flat wall whose temperature changes abruptly, cf. C.R. Illingworth (1950).

5.3.2 Flow at an Oscillating Wall (Second Stokes Problem)

Consider an infinitely extended flat wall carrying out harmonic oscillations in its own plane. This problem was first treated by G.G. Stokes (1856) and later by Lord Rayleigh (1911). Because of the no-slip condition, the flow velocity at the wall is

$$y = 0 : \quad u(0, t) = U_0 \cos nt. \quad (5.103)$$

For thus boundary condition, the solution of Eq. (5.93) reads

$$u(y, t) = U_0 e^{-\eta_s} \cos(nt - \eta_s) \quad (5.104)$$

with

$$\eta_s = \sqrt{\frac{n}{2\nu}} y. \quad (5.105)$$

The velocity distribution is therefore an oscillation with amplitude $U_0 \exp(-\eta_s)$ decreasing outwards, where the layer at a distance y from the wall has a phase lag of $y\sqrt{n/2\nu}$ compared to the motion of the wall. The velocity distribution for different times is shown in Fig. 5.13. Two layers at a distance $2\pi\sqrt{2\nu/n}$ from each other oscillate in phase. This distance can be considered to be a kind of wavelength of the oscillation; it is called the *depth of penetration* of the viscous wave. The layer which oscillates has a thickness $\delta_s = 4.6\sqrt{2\nu/n}$ (the envelope $u/U_0 = \exp(-\eta_s)$ shown in Fig. 5.13 has the value 0.01 at $\eta_s = 4.6$). The layer is therefore thinner the higher the frequency and the smaller the kinematic viscosity.

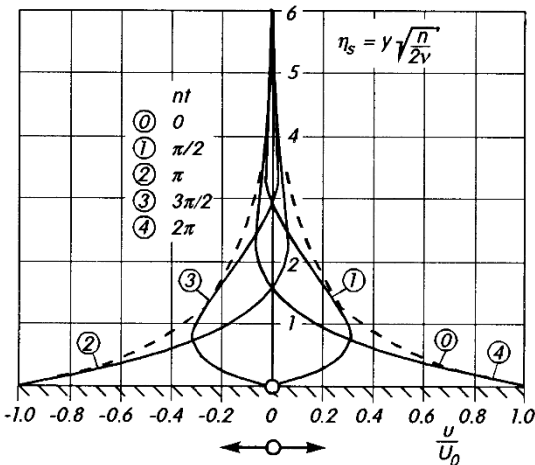


Fig. 5.13. Velocity distribution close to an oscillating wall (second Stokes problem)
---- envelope
 $u/U_0 = \exp(-\eta_s)$

The solution in Eq. (5.104) and Fig. 5.13 also represents an analogous solution of the thermal energy equation, e.g. the temperature distribution beneath the surface of the earth due to seasonal periodic temperature oscillations at the surface.

5.3.3 Start-up of Couette Flow

The formation of the frictional layer at a wall suddenly set into motion treated in Sect. 5.3.1 can also be solved for the case where the moving wall is at a distance h from a wall at rest. We will now deal with the time development of Couette flow, which, for large times, leads to the linear velocity distribution in Fig. 1.1. The solution of Eq. (5.93) for the corresponding boundary conditions can be given as the following series:

$$\begin{aligned} \frac{u}{U_0} = F(\eta, \eta_h) &= \operatorname{erfc} \eta - \operatorname{erfc}(2\eta_h - \eta) \\ &\quad + \operatorname{erfc}(2\eta_h + \eta) - \operatorname{erfc}(4\eta_h - \eta) \\ &\quad + \operatorname{erfc}(4\eta_h + \eta) - + \dots \end{aligned} \quad (5.106)$$

with

$$\eta = \frac{y}{2\sqrt{\nu t}}, \quad \eta_h = \frac{h}{2\sqrt{\nu t}}. \quad (5.107)$$

This is shown in Fig. 5.14. Here only the first profiles are at all similar (for about $t < 0.05h^2/\nu$). This is true as long as the layer carried along is not very much retarded by the opposite fixed wall, i.e. as long as the layer thickness δ from Eq. (5.99) is smaller than the distance between the plates. The later profiles ($t > 0.05h^2/\nu$) are no longer “similar”, and approach the linear distribution of the steady state asymptotically. A series expansion of the solution, which converges well for large times, is given by R.L. Panton

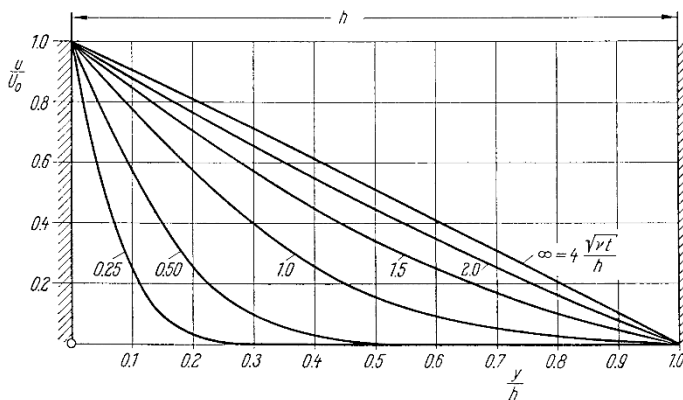


Fig. 5.14. Start-up of Couette flow

(1984), p. 277. Exact solutions of unsteady Couette flow have been computed by J. Steinheuer (1965) for the case where the wall at rest in the steady state is abruptly brought to a constant velocity. A special case of these solutions is the case of the sudden halting of the moving wall, i.e. the *shut-down* of Couette flow.

5.3.4 Unsteady Asymptotic Suction

If the velocity $u(y \rightarrow \infty, t) = U(t)$ is non-zero at a large distance from the wall ($y = 0$), Eq. (5.91) can also be written as

$$\frac{\partial u}{\partial t} + v_w \frac{\partial u}{\partial y} = \frac{dU}{dt} + \nu \frac{\partial^2 u}{\partial y^2}. \quad (5.108)$$

The differential equation is simpler for a constant “outer flow” U_0 , and we obtain the simple solution

$$u(y, t) = U_0 \left(1 - e^{-\frac{v_w y}{\nu}} \right). \quad (5.109)$$

Since the boundary condition for $y \rightarrow \infty$ is only satisfied for negative v_w (i.e. suction), Eq. (5.109) is called the *asymptotic suction profile*.

According to J.T. Stuart (1955), for any outer velocity

$$U(t) = U_0[1 + f(t)], \quad (5.110)$$

there is an exact solution of Eq. (5.108) of the form

$$u(y, t) = U_0[1 - e^{-\eta} + g(\eta, T)] \quad (5.111)$$

with

$$\eta = -\frac{v_w y}{\nu} \quad \text{and} \quad T = \frac{v_w^2 t}{4\nu}. \quad (5.112)$$

The function $g(\eta, T)$ must satisfy the partial differential equation

$$\frac{\partial g}{\partial T} = f'(T) + 4 \left(\frac{\partial g}{\partial \eta} + \frac{\partial^2 g}{\partial \eta^2} \right) \quad (5.113)$$

with the boundary conditions:

$$\eta = 0 : \quad g = 0; \quad \eta \rightarrow \infty : \quad g = f(T).$$

The solutions of Eq. (5.113) have been determined by J. Watson (1958) for some particular functions $f(T)$. The following outer flows were examined: undamped and damped oscillations, and sudden changes from one value to another.

Accelerated and decelerated plate motion in a fluid at rest with homogeneous suction has been investigated by J. Zierep; K. Bühler (1993).

5.3.5 Unsteady Plane Stagnation-Point Flow

Oscillating wall. A simple generalisation of the steady stagnation-point flow discussed in Sect. 5.1.3 arises when the wall oscillates. In this case the

total solution is a superposition of the known steady solution and a periodic part. With the trial solution, cf. Eq. (5.34) to (5.36)

$$\begin{aligned} u(x, y, t) &= ax f'(\eta) + U_0[g(\eta) \cos nt + h(\eta) \sin nt] \\ v(x, y, t) &= -\sqrt{a\nu}f(\eta) \\ p(x, y, t) &= p_0 - \frac{\varrho}{2}a^2 \left[x^2 + \frac{2\nu}{a}F(\eta) \right] \\ \eta &= \sqrt{\frac{a}{\nu}}y \end{aligned} \quad (5.114)$$

and the Navier–Stokes equations together with Eq. (5.37), we obtain the following linear system of equations for the functions $g(\eta)$ and $h(\eta)$

$$\begin{aligned} g'' + f'g' - f'g - kh &= 0 \\ h'' + fh' - f'h + kg &= 0 \end{aligned} \quad (5.115)$$

with the boundary conditions

$$\eta = 0 : \quad g = 1, \quad h = 0; \quad \eta \rightarrow \infty : \quad g = 0, \quad h = 0$$

and the dimensionless frequency $k = n/a$.

The wall velocity $u_w(t) = U_0 \cos nt$ is therefore a harmonic function of frequency n .

Since the steady solution $f(\eta)$ is contained in the Eqs. (5.115), it influences the oscillating part of the flow. On the other hand, the steady part is independent of the wall motion.

The solution functions $g(\eta)$ and $h(\eta)$ have been computed by N. Rott (1955), cf. also M.B. Glauert (1956a) and J. Watson (1959). In general they still depend on k . For the limiting cases $k \rightarrow 0$ and $k \rightarrow \infty$ simple asymptotic solutions can be written down. In the limit $k \rightarrow 0$ it follows from Eq. (5.115) that

$$g = \frac{f''}{f''_w}, \quad h = 0. \quad (5.116)$$

This solution is a *quasi-steady* solution.

If, for the limit $k \rightarrow \infty$, we introduce the new coordinate

$$\eta_s = \sqrt{\frac{k}{2}}\eta = \sqrt{\frac{n}{2a}}\eta = \sqrt{\frac{n}{2\nu}}y = \frac{y}{\delta_s} \quad (5.117)$$

the equations for $k \rightarrow \infty$ reduce to

$$\ddot{g} - 2h = 0, \quad \ddot{h} + 2g = 0,$$

where the dots imply derivatives with respect to η_s . In this limiting case, the unsteady motion becomes independent of the steady basic flow. The solutions are

$$g = e^{-\eta_s} \cos \eta_s, \quad h = e^{-\eta_s} \sin \eta_s \quad (5.118)$$

and the velocity field is

$$u(x, y, t) = ax f'(\eta) + U_0 e^{-\eta_s} \cos(nt - \eta_s) \quad (k \rightarrow \infty). \quad (5.119)$$

The unsteady part is therefore identical to the solution for the oscillating wall, as in Eq. (5.104).

In this high frequency limit the flow then has a *two-layer structure*. The thickness of the (steady) frictional layer is given by Eq. (5.47) as $\delta = 2.4\sqrt{\nu/a}$, whereas the layer affected by the wall motion has the thickness $\delta_s = 4.6\delta/\sqrt{k}$, and is thus smaller than the frictional layer thickness δ at high frequencies. Since the solution in Eq. (5.104) was given by Stokes, this thin layer close to the wall is called the *Stokes layer*.

A generalisation of this solution to arbitrary motions of the wall has been given by J. Watson (1959). If the wall oscillates perpendicular to the plane of the stagnation-point flow, a three-dimensional unsteady flow occurs. This has been treated by W. Wuest (1952).

Oscillating outer flow (amplitude independent of x).

For the outer velocity

$$U(x, t) = ax + U_0 \cos nt \quad (5.120)$$

we can again choose the ansatz (5.114). Instead of Eq. (5.115) we now obtain a set of equations extended by terms for the pressure gradient

$$\begin{aligned} g'' + f'g' - f'g - kh + 1 &= 0 \\ h'' + fh' - f'h + kg - k &= 0 \end{aligned} \quad (5.121)$$

with the boundary conditions

$$\eta = 0 : \quad g = 0, \quad h = 0; \quad \eta \rightarrow \infty : \quad g = 1, \quad h = 0.$$

The system of equations (5.121) has been computed by K. Gersten (1965) for different frequency parameters k . Again simple limiting solutions can be given. The quasi-steady solution ($k = n/a \rightarrow 0$) reads

$$g = f', \quad h = 0 \quad (k \rightarrow 0), \quad (5.122)$$

while the Stokes limiting solution ($k \rightarrow \infty$) reads

$$g = 1 - e^{-\eta_s} \cos \eta_s, \quad h = -e^{-\eta_s} \sin \eta_s. \quad (5.123)$$

This flow also has the two-layer structure mentioned above.

With knowledge of the periodic solutions, the Laplace transform can be used to determine solutions for outer flows of the form

$$U(x, t) = ax + U(t)$$

with an arbitrary function $U(t)$, cf. K. Gersten (1967).

Oscillating outer flow (amplitude proportional to x).

For the outer flow we now have:

$$U(x, t) = \bar{U}(x) + U_1(x, t) = ax + \varepsilon ax \cos nt . \quad (5.124)$$

The inviscid outer flow pulsates as a whole, i.e. $V(y, t) = -ay(1 + \varepsilon \cos nt)$ also.

Since the outer flow consists of a steady part and an unsteady part, u , v and p are decomposed as

$$\begin{aligned} u(x, y, t) &= \bar{u}(x, y) + u_1(x, y, t) \\ v(x, y, t) &= \bar{v}(x, y) + v_1(x, y, t) \\ p(x, y, t) &= \bar{p}(x, y) + p_1(x, y, t) . \end{aligned} \quad (5.125)$$

The bar means the time average over one period, so that $\bar{u}_1 = \bar{v}_1 = \bar{p}_1 = 0$.

At large distances from the wall the Navier–Stokes equation in the x direction yields

$$\frac{\partial U}{\partial t} + U \frac{\partial U}{\partial x} = -\frac{1}{\rho} \frac{\partial p}{\partial x} . \quad (5.126)$$

If we insert Eq. (5.124) into this equation and form the time average, we obtain:

$$\bar{U} \frac{d\bar{U}}{dx} + \overline{U_1 \frac{\partial U_1}{\partial x}} = -\frac{1}{\rho} \frac{\partial \bar{p}}{\partial x} . \quad (5.127)$$

Subtracting this equation from Eq. (5.126) produces

$$\frac{\partial U}{\partial t} + \bar{U} \frac{\partial U_1}{\partial x} + U_1 \frac{d\bar{U}}{dx} + U_1 \frac{\partial U_1}{\partial x} - \overline{U_1 \frac{\partial U_1}{\partial x}} = -\frac{1}{\rho} \frac{\partial p_1}{\partial x} \quad (5.128)$$

as the equation to determine the pressure gradient $\partial p_1 / \partial x$.

In a similar way we find the following equations for the average motion in the flow field

$$\frac{\partial \bar{u}}{\partial x} + \frac{\partial \bar{v}}{\partial y} = 0 , \quad (5.129)$$

$$\bar{u} \frac{\partial \bar{u}}{\partial x} + \bar{v} \frac{\partial \bar{u}}{\partial y} = \bar{U} \frac{d\bar{U}}{dx} + \nu \frac{\partial^2 \bar{u}}{\partial y^2} + F(x, y) \quad (5.130)$$

with

$$F(x, y) = \overline{U_1 \frac{\partial U_1}{\partial x}} - \left(\overline{u_1 \frac{\partial u_1}{\partial x} + v_1 \frac{\partial u_1}{\partial y}} \right) . \quad (5.131)$$

Equations (5.129) and (5.130) for the average motion agree with the equation for steady flows up to the function $F(x, y)$ in Eq. (5.131). Because of the oscillation velocities, the average flow is different from the flow found when the oscillation is omitted. This difference is easily seen in the additional function

$F(x, y)$. It is a consequence of the nonlinearity of the differential equation. The additional function can physically be construed as an additional imposing force, similar to the friction force of a steady flow. It is therefore called an “apparent friction force”, cf. also Sect. 16.2.

In order to work out $F(x, y)$, the functions $u_1(x, y, t)$ and $v_1(x, y, t)$ have to be determined. These are solutions of the following system of equations:

$$\frac{\partial u_1}{\partial x} + \frac{\partial v_1}{\partial y} = 0, \quad (5.132)$$

$$\begin{aligned} \frac{\partial u_1}{\partial t} &+ \left(\bar{u} \frac{\partial u_1}{\partial x} + \bar{v} \frac{\partial u_1}{\partial y} \right) + \left(u_1 \frac{\partial \bar{u}}{\partial x} + v_1 \frac{\partial \bar{u}}{\partial y} \right) \\ &+ \left(u_1 \frac{\partial u_1}{\partial x} + v_1 \frac{\partial u_1}{\partial y} \right) - \left(\overline{u_1 \frac{\partial u_1}{\partial x}} + \overline{v_1 \frac{\partial u_1}{\partial y}} \right) \\ &= \frac{\partial U_1}{\partial t} + \bar{U} \frac{\partial U_1}{\partial x} + U_1 \frac{\partial \bar{U}}{\partial x} + U_1 \frac{\partial U_1}{\partial x} - \overline{U_1 \frac{\partial U_1}{\partial x}} + \nu \frac{\partial^2 u_1}{\partial y^2}. \end{aligned} \quad (5.133)$$

As is to be expected, this system of equations is considerably simplified for the limiting case of high frequencies $n \rightarrow \infty$, as shown by C.C. Lin (1957). Introducing the two new coordinates

$$T = nt, \quad \eta_s = \sqrt{\frac{n}{2\nu}}y \quad (5.134)$$

and then forming the limit $n \rightarrow \infty$, (5.133) reduces to

$$\frac{\partial u_1}{\partial T} = \frac{\partial U_1}{\partial T} + \frac{1}{2} \frac{\partial^2 u_1}{\partial \eta_s^2}. \quad (5.135)$$

Only three terms remain from the complicated equation (5.133), namely the local accelerations and the friction term. In this way, as in the previous examples for high frequency flows, the oscillation becomes independent of the average motion. In addition Eq. (5.135), in contrast to Eq. (5.133), is linear. For an outer flow of the form

$$U(x, t) = \bar{U}(x) + U(x) \cos nt \quad (5.136)$$

we find from Eq. (5.135) that

$$u_1(x, y, t) = U(x) [\cos T - e^{-\eta_s} \cos(T - \eta_s)]. \quad (5.137)$$

It is characteristic here that the phase shift of the oscillation velocity $u_1(x, y, t)$ unlike the outer flow is dependent on the wall distance y or η_s . From the continuity equation (5.132) we obtain the component $v_1(x, y, t)$ which also shows this typical phase shift. Using $u_1(x, y, t)$ and $v_1(x, y, t)$, the additional function $F(x, y)$ from Eq. (5.131) can now be computed. We find

$$F(x, y) = \frac{1}{2} U \frac{dU}{dx} \bar{F}(\eta_s), \quad (5.138)$$

where

$$\bar{F}(\eta_s) = e^{-\eta_s} [(2 + \eta_s) \cos \eta_s - (1 - \eta_s) \sin \eta_s - e^{-2\eta_s}] \quad (5.139)$$

is a universal function independent of the outer flow $U(x)$. It is shown in Fig. 5.15. It has its greatest value at the wall.

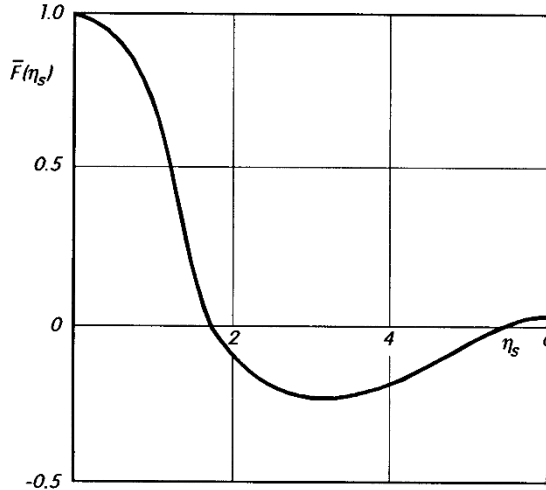


Fig. 5.15. The function $\bar{F}(\eta_s)$ from Eq. (5.139) for a simple harmonic oscillation of the outer flow

According to Eq. (5.138), the function $F(x, y)$ vanishes for constant U , and therefore so does the effect of the oscillation on the average motion, as the previous example has also shown. For an outer flow of general form

$$U(x, t) = \bar{U}(x) + \sum_{j=1} U_j(x) \cos(jnt) \quad (5.140)$$

we find

$$F(x, y) = \frac{1}{2} \sum_{j=1} U_j \frac{dU_j}{dx} \bar{F}(\eta_{sj}) \quad (5.141)$$

with

$$\eta_{sj} = \sqrt{\frac{jn}{2\nu}} y. \quad (5.142)$$

From Eq. (5.130), for stagnation-point flow with $\bar{u} = axf'(\eta, k, \varepsilon)$, we get the following differential equation

$$f''' + f f'' + 1 - f'^2 + \frac{1}{2} \varepsilon^2 \bar{F}(\eta_s) = 0$$

with $\eta_s = \sqrt{k/2}\eta$ and the boundary conditions Eq. (5.38). This equation was first solved for small values of ε^2 by K. Gersten (1965). The first two terms in the series expansion of the solution function $f = f_0 + \varepsilon^2 f_1 + \dots$ were

determined, as was the corresponding temperature field. It turns out that the average wall shear stress increases due to the oscillation of the outer flow, while the heat transfer at the wall decreases.

Oscillating velocity and temperature fields were also investigated in detail. The oscillations of the wall shear stress and the wall heat flux generally show a phase shift compared to the oscillation of the outer velocity. At very high frequencies, the wall shear stress leads by 45° , while the heat flux lags by 90° . It is particularly worth noting that the unsteady part proportional to ε^2 also oscillates with double the frequency, i.e. with $2n$. This is a consequence of the nonlinearity of the Navier–Stokes equations.

It has also been shown by K. Gersten (1967) how, using the Laplace transform, solutions can be found for the oscillating stagnation-point flow for cases where a steady stagnation-point flow goes over to a slightly different steady stagnation-point flow via an arbitrary time transition function.

5.3.6 Oscillating Channel Flow

An example of an unsteady *internal flow* is that occurring in a channel when the fluid is acted on by periodic drops in the pressure. This flow is realised by a periodically moving piston. We assume an infinitely long channel, with the x axis lying in the centre. Since the motion is independent of x , again the greatly simplified and linear equation (5.91) is valid, with $v_w = 0$ and the boundary conditions $u(y = \pm h/2) = 0$. Let the pressure gradient produced by the piston motion be harmonic

$$-\frac{1}{\varrho} \frac{\partial p}{\partial x} = K \sin nt ,$$

where K is a constant. Because of the linearity of the differential equation to be solved, complex notation recommends itself, thus

$$-\frac{1}{\varrho} \frac{\partial p}{\partial x} = -i K e^{int} ,$$

where, since $\exp(int) = \cos nt + i \sin nt$, only the real part has any physical significance. Writing the velocity in the form $u(y, t) = f(y) \exp(int)$, we obtain the following differential equation for the amplitude distribution $f(y)$:

$$f'' - \frac{i n}{\nu} f = i \frac{K}{\nu} . \quad (5.143)$$

This leads to the solution

$$u(y, t) = -\frac{K}{n} e^{int} \left\{ 1 - \frac{\cosh[y \sqrt{in/\nu}]}{\cosh[(h/2) \sqrt{in/\nu}]} \right\} . \quad (5.144)$$

This can be used to obtain quite simple results for the limits of very small and very large frequencies.

For very small values of n , we expand $\cosh \varphi = 1 + \varphi^2/2 + \dots$ up to the quadratic term and Eq. (5.144) becomes

$$u(y, t) = \frac{K}{2\nu} \left(\frac{h^2}{4} - y^2 \right) \sin nt \quad (n \rightarrow 0),$$

where the complex notation has now been dropped. This is the *quasi-steady* case, i.e. for slow oscillations the velocity distribution has the same phase as the pressure gradient which excites it, while the distribution of the amplitude is parabolic, as in the steady case.

For very large values of n we use the asymptotic formula $\cosh \varphi \rightarrow e^\varphi/2$ to obtain the solution

$$u(y, t) = \frac{K}{n} [\cos nt - e^{-\eta_s} \cos(nt - \eta_s)] \quad (n \rightarrow \infty) \quad (5.145)$$

with

$$\eta_s = \sqrt{\frac{n}{2\nu}} \left(\frac{h}{2} - y \right). \quad (5.146)$$

For large values of n , the second term decreases very fast with increasing distance from the wall ($h/2 - y$), so that only the first term which is independent of the distance from the wall remains. Therefore this solution has a *boundary-layer character*. The fluid in the core oscillates inviscidly, with a phase shift of 90° . A comparison of Eq. (5.145) and Eq. (5.137) shows that this is the Stokes solution for an oscillating “outer flow”. Therefore, in the high frequency case, the flow consists of two layers: the inviscid “*piston flow*” in the core, and the frictional Stokes wall layer. From this solution it follows that the time squared average is

$$\overline{\frac{u^2(\eta_s)}{K^2/2n^2}} = 1 - 2e^{-\eta_s} \cos \eta_s + e^{-2\eta_s}. \quad (5.147)$$

This distribution is shown in Fig. 5.16. Its maximum is not in the centre of the channel ($\eta_s \rightarrow \infty$), but is within the Stokes layer ($\eta_s < 4.6$) at $\eta_s = 2.28$.

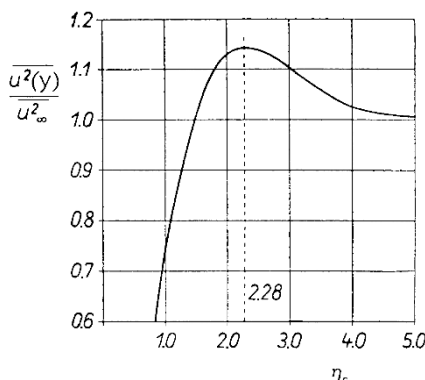


Fig. 5.16. Distribution of the time squared average of the velocity in the case of periodic channel flow from Eq. (5.147),
 $\overline{\frac{u^2}{u^2_\infty}} = K^2/(2n^2)$: time average of the velocity at a large distance from the wall

This effect has been found experimentally in oscillating pipe flows, and is called the “*annular effect*”, cf. E.G. Richardson; E. Tyler (1929), see also Sect. 5.4.2. There we discuss the affinity between oscillating channel flow and start-up or shut-down flow occurring from suddenly shutting off the pressure drop.

5.4 Unsteady Axisymmetric Flows

5.4.1 Vortex Decay

It has already been shown that the potential vortex solution is an exact solution of the Navier–Stokes equations for the flow at a rotating circular cylinder in a fluid at rest. The time–decay of such a vortex as a consequence of the viscosity can also be described as an exact solution, as shown by C.W. Oseen (1911) and G. Hamel (1916). If the circular cylinder stops rotating at time $t = 0$, the distribution of the circumferential velocity as a function of the radius r and the time t reads

$$u(r, t) = \frac{\Gamma_0}{2\pi r} \left(1 - e^{-\frac{r^2}{4\nu t}} \right). \quad (5.148)$$

This velocity distribution is shown in Fig. 5.17. Here Γ_0 is the circulation of the vortex at time $t = 0$.

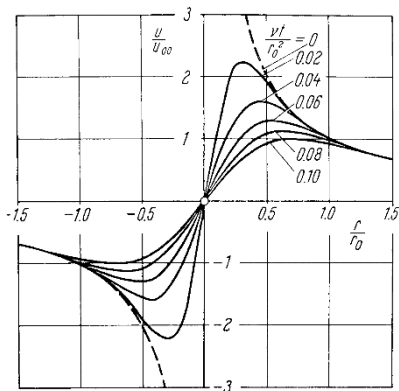


Fig. 5.17. Change in time of the velocity distribution close to a vortex filament as a consequence of the action of the viscosity Γ_0 : circulation of the vortex filament at time $t = 0$, at the start of the action of viscosity, $u_\infty = \Gamma_0/(2\pi r_0)$, r_0 is any chosen radius

Experimental investigations into this process have been carried out by A. Timme (1957).

The case where the initial velocity distribution of the vortex is different from that of potential theory has been theoretically and experimentally investigated by K. Kirde (1962).

5.4.2 Unsteady Pipe Flow

In analogy to the unsteady channel flows mentioned in the previous section, there also exist corresponding solutions for circular pipes. Let x be the coordinate along the axis of the pipe and r the radial distance from the centre.

Since we assume that the pipe is long, the solution will be independent of x . Using the Navier–Stokes equations in Eq. (3.93) and neglecting no other terms we have

$$\frac{\partial u}{\partial t} = -\frac{1}{\varrho} \frac{\partial p}{\partial x} + \nu \left(\frac{\partial^2 u}{\partial r^2} + \frac{1}{r} \frac{\partial u}{\partial r} \right) \quad (5.149)$$

with the boundary condition $u(r = R, t) = 0$ (no-slip condition). For the harmonically oscillating pressure gradient

$$-\frac{1}{\varrho} \frac{\partial p}{\partial x} = K \sin nt, \quad (5.150)$$

one obtains the solution

$$u(r, t) = -\frac{K}{n} e^{int} \left[1 - \frac{J_0(r\sqrt{-in/\nu})}{J_0(R\sqrt{-in/\nu})} \right]. \quad (5.151)$$

Here J_0 is the zeroth order Bessel function. For very low frequencies we thus find the *quasi-steady* solution

$$u(r, t) = \frac{K}{4\nu} (R^2 - r^2) \sin nt \quad (n \rightarrow 0). \quad (5.152)$$

At very high frequencies we have

$$u(r, t) = \frac{K}{n} \left[\cos nt - \sqrt{\frac{R}{r}} e^{-\eta_s} \cos(nt - \eta_s) \right] \quad (n \rightarrow \infty) \quad (5.153)$$

with

$$\eta_s = \sqrt{\frac{n}{2\nu}} (R - r). \quad (5.154)$$

This is again a solution with a two-layer structure: the inviscid core flow and the Stokes layer close to the wall.

Figure 5.18 shows the velocity profile of the oscillating pipe flow for an intermediate frequency ($\sqrt{n/\nu}R = 5$) at different times during one period of oscillation. Comparing the pressure gradient depicted below this, we can clearly see the phase lag of the flow in the centre of the pipe behind that in the layer close to the wall, cf. M.J. Lighthill (1954). As has already been mentioned in Sect. 5.3.6, the *annular effect* predicted for high frequencies has also been experimentally confirmed here. Since Eq. (5.149) is linear, the solutions from Eq. (5.151) for different frequencies can be additively combined with each other.

Pipe start-up flow is closely related to oscillating pipe flow. Here the fluid in the infinitely long pipe is initially at rest. At time $t = 0$, a time-independent pressure drop is suddenly switched on. Because of the friction and inertial forces, a pipe start-up flow forms which asymptotically passes over to the Hagen–Poiseuille parabolic velocity distribution. The solution to this problem has been given by F. Szymansky (1932). It is characteristic here that the velocity in the centre of the pipe initially remains locally

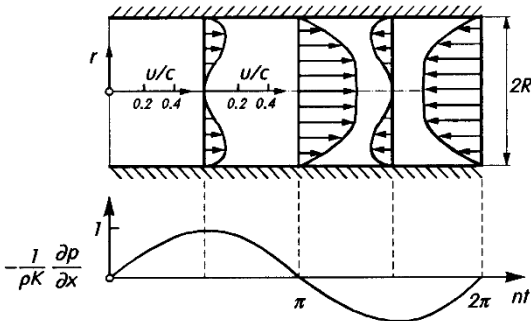


Fig. 5.18. Velocity distribution of an oscillating pipe flow at different times within one period, after S. Uchida (1956),
pressure gradient $-\partial p/\partial x = \varrho K \sin nt$,
 $k = R\sqrt{n/\nu} = 5$
 $c = Kk^2/(8n) = 3.125K/n$

almost constant, and that the viscosity only has any effect in a thin layer close to the wall. Only later does the action of the viscosity reach the centre of the pipe. The corresponding flow occurring when a pressure drop is suddenly switched off (“*pipe shut-down flow*”) has been computed by W. Gerbers (1951). W. Müller (1936) has considered the start-up flow in an annulus.

5.5 Summary

The following results should be recalled from the study of the exact solutions of the Navier–Stokes equations, since these are the ones which will be of greatest importance in what follows later:

1. If a solution tends to an inviscid solution in the limit $\nu \rightarrow 0$, the solution has a *boundary-layer character* for small values of ν . In this case, the effects of viscosity are restricted to a thin layer close to the wall, the *frictional layer* or *boundary layer*. The flow can be considered to be a perturbation to the inviscid limiting solution.
2. The thickness δ of the boundary layer can be estimated as follows. As a consequence of the viscosity from the wall, the transport of momentum over this layer takes place with velocity $U_V(\nu, \delta)$, which, from dimensional considerations, is $U_V = \nu/\delta$. If t_B is a typical time spent by a fluid particle in the layer, we have $\delta = U_V t_B$, or, since $U_V = \nu/\delta$,

$$\delta \sim \sqrt{\nu t_B} .$$

The boundary-layer thickness is therefore proportional to the square root of the kinematic viscosity. The time spent in the boundary layer depends on the flow under consideration, e.g. $t_B = t$ (a flat plate suddenly set in motion), $t_B = 1/n$ (oscillating flow), $t_B = r/u_{\max}$ (nozzle flow).

3. Flows with two different characteristic times t_B have a *two-layer structure*. An example of this is stagnation-point flow oscillating at high frequency $k = n/a \rightarrow \infty$. As well as the layer of thickness $\delta \sim \sqrt{\nu/a}$ from

the steady case (Prandtl layer), there is also the much thinner Stokes layer of thickness $\delta_s \sim \sqrt{\nu/n}$ which is a consequence of the oscillations affected by the viscosity.

4. Because of the nonlinearity of the Navier–Stokes equations, in the case of oscillating flows there is a change in the average motion compared to the non-oscillating case. For the same reason, as well as the fundamental frequency of the oscillations in the flow field, higher harmonics of this frequency also occur. At high frequencies, the kinetic energy of the oscillation close to the wall is particularly high, and a phase shift of -45° arises between the oscillations of the wall shear stress and the outer velocity, i.e. the velocity lags behind the wall shear stress.

Part II

Laminar Boundary Layers

6. Boundary-Layer Equations in Plane Flow; Plate Boundary Layer

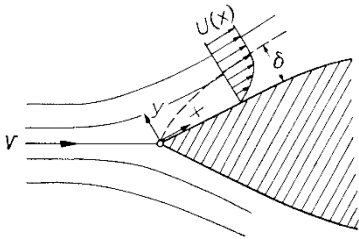
6.1 Setting up the Boundary-Layer Equations

We now wish to treat flows with very small viscosity or very high Reynolds numbers. An important contribution to the science of fluid motion was made in 1904 by L. Prandtl (1904). Prandtl showed the manner in which the viscosity has its effect for high Reynolds number flows and how the Navier-Stokes differential equations can be simplified to yield approximate solutions for this limiting case. We shall now derive the simplifications which arise for the Navier-Stokes equations in the case of very small friction forces in a physically illustrative manner.

For simplicity we consider the plane flow of a fluid with very low viscosity past a slender cylindrical body, Fig. 6.1. The velocities are of the order of magnitude of the free stream velocity V apart from in the immediate neighbourhood of the surface of the body. Both the streamline picture and the velocity distribution are almost identical to those of inviscid flow (potential flow). More precise investigations show, however, that the fluid on the surface does not slip along the wall, as in the case of potential flow, but *adheres* to it. There is a transition from zero velocity at the wall to the full velocity which is present at a certain distance from the wall. This transition takes place in a very thin layer called the *boundary layer* or *frictional layer*. We now have to distinguish between two regions, between which there is actually no sharp division:

1. A very thin layer right beside the body where the velocity gradient normal to the wall $\partial u / \partial y$ is very large (*boundary layer*). A very small viscosity μ can play an important role here since the viscous shear stress $\tau = \mu \partial u / \partial y$ can reach considerable values.
2. The remaining region outside this layer. Here there are no large velocity gradients, so the action of the viscosity is unimportant. In this region the flow is frictionless and potential.

Altogether it may be said that the boundary layer is thinner the smaller the viscosity, or, more generally, the higher the Reynolds number. It was seen for some exact solutions of the Navier-Stokes equations in Chap. 5 that the

**Fig. 6.1.** Boundary-layer flow along a wall

boundary-layer thickness is proportional to the square root of the kinematic viscosity:

$$\delta \sim \sqrt{\nu} .$$

In the simplifications of the Navier-Stokes equations which follow, it will be assumed that this boundary-layer thickness is very small compared to a still unspecified linear dimension of the body l :

$$\delta \ll l .$$

Thus the solutions of the boundary-layer equations have an asymptotic character for very high Reynolds numbers.

If we use the free stream velocity V and a characteristic dimension of the body l as reference values, the relation $\delta \sim \sqrt{\nu}$ leads to the dimensionally correct representation

$$\frac{\delta}{l} \sim \frac{1}{\sqrt{\text{Re}}} \quad \text{with} \quad \text{Re} = \frac{Vl}{\nu} . \quad (6.1)$$

That is, the boundary-layer thickness tends to zero with increasing Reynolds number.

We now want to establish what simplifications of the Navier-Stokes equations arise if (only) the asymptotic solutions at high Reynolds number are to be determined. Instead of going along the path of Chap. 5, by first solving the complete Navier-Stokes equations and then determining the asymptotic solution for $\text{Re} \rightarrow \infty$, the asymptotic solution will now be ascertained directly from correspondingly simplified differential equations. Consider first the two-dimensional problem in Fig. 6.1, assuming the wall is flat. Let the x axis lie along the wall, and the y axis be perpendicular to it. We now want to write the continuity equation and the Navier-Stokes equations in dimensionless form. All lengths will be referred to the characteristic length l already introduced and all velocities to the free stream velocity V . The pressure is made dimensionless with ρV^2 and the time with l/V . Furthermore, the Reynolds number, which is very large by assumption, is

$$\text{Re} = \frac{\rho V l}{\mu} = \frac{Vl}{\nu} . \quad (6.2)$$

Thus the equations read, in dimensionless notation:

momentum equation in the x direction:

$$\frac{\partial u^*}{\partial t^*} + u^* \frac{\partial u^*}{\partial x^*} + v^* \frac{\partial u^*}{\partial y^*} = -\frac{\partial p^*}{\partial x^*} + \frac{1}{\text{Re}} \left(\frac{\partial^2 u^*}{\partial x^{*2}} + \frac{\partial^2 u^*}{\partial y^{*2}} \right), \quad (6.3)$$

$$1 \quad 1 \quad 1 \quad \delta^* \quad \frac{1}{\delta^*} \quad \delta^{*2} \quad 1 \quad \frac{1}{\delta^{*2}}$$

momentum equation in the y direction:

$$\frac{\partial v^*}{\partial t^*} + u^* \frac{\partial v^*}{\partial x^*} + v^* \frac{\partial v^*}{\partial y^*} = -\frac{\partial p^*}{\partial y^*} + \frac{1}{\text{Re}} \left(\frac{\partial^2 v^*}{\partial x^{*2}} + \frac{\partial^2 v^*}{\partial y^{*2}} \right), \quad (6.4)$$

$$\delta^* \quad 1 \quad \delta^* \quad \delta^* \quad 1 \quad \delta^{*2} \quad \delta^* \quad \frac{1}{\delta^*}$$

continuity equation:

$$\frac{\partial u^*}{\partial x^*} + \frac{\partial v^*}{\partial y^*} = 0. \quad (6.5)$$

$$1 \quad 1$$

If the limit $\text{Re} \rightarrow \infty$ is taken in Eq. (6.3) and (6.4), these equations reduce to those for inviscid flows and, in the case of a uniform free stream, describe potential flow. These would already be the asymptotic solutions were it not for the no-slip condition which, except for some special cases, is not satisfied by potential flows.

The desired asymptotic solutions which should also satisfy the no-slip condition will therefore only differ from the potential flow solutions at and close to the wall. Therefore different equations from those for inviscid flow must hold in this layer close to the wall, the boundary layer. Since the friction forces play an important role in this layer, the friction terms in the equations describing the flow here may not all be neglected. The simplification of the Navier-Stokes equations will be carried out using this idea. The order of magnitude of the separate terms in these equations will first be estimated. The length x^* and the velocity u^* have the order of magnitude $O(1)$. However the length y^* has the order of magnitude of the boundary-layer thickness, $O(\delta^*)$. Since for $\text{Re} \rightarrow \infty$, i.e. $\delta^* \rightarrow 0$, see Eq. (6.1), the continuity equation should not become degenerate, it follows that $v^* = O(\delta^*)$. The orders of magnitude of the various terms in Eq. (6.3) to (6.5) have been written underneath each equation. Here it was assumed that the local accelerations (e.g. $\partial u^* / \partial t^*$) are of the same order of magnitude as the convective accelerations (e.g. $u^* \partial u^* / \partial x^*$). This means that there are no sudden accelerations, as could happen in the case of, for example, strong pressure waves. In order that at least one friction term does not vanish in the x -momentum equation, the factor $1/\text{Re}$ must be of the order of magnitude $O(\delta^{*2})$. This is again the result $\delta^* \sim 1/\sqrt{\text{Re}}$, known already from Chap. 5, in Eq. (6.1).

Since the ordinate $y^* = O(\delta^*)$ assumes very small values in the boundary layer for $\delta^* \rightarrow 0$, it is not suitable to describe boundary-layer flow. Therefore the coordinate $y^* = O(\delta^*)$ and the velocity component $v^* = O(\delta^*)$ are transformed using the *boundary-layer transformation* as follows:

$$\bar{y} = y^* \sqrt{\text{Re}} \sim \frac{y^*}{\delta^*}, \quad \bar{v} = v^* \sqrt{\text{Re}} . \quad (6.6)$$

The new variables \bar{y} and \bar{v} are, like x^* and u^* , of order of magnitude $O(1)$. If we introduce these variables \bar{y} and \bar{v} into Eq. (6.3) to (6.5) and form the limit $\text{Re} \rightarrow \infty$, we obtain the *Prandtl boundary-layer equations*:

$$\frac{\partial u^*}{\partial x^*} + \frac{\partial \bar{v}}{\partial \bar{y}} = 0 , \quad (6.7)$$

$$\frac{\partial u^*}{\partial t^*} + u^* \frac{\partial u^*}{\partial x^*} + \bar{v} \frac{\partial u^*}{\partial \bar{y}} = - \frac{\partial p^*}{\partial x^*} + \frac{\partial^2 u^*}{\partial \bar{y}^2} , \quad (6.8)$$

$$0 = - \frac{\partial p^*}{\partial \bar{y}} . \quad (6.9)$$

From Eq. (6.6), the quantities y^* and v^* have been *stretched* by a power of the Reynolds number. The exponent $1/2$, i.e. the square root of the Reynolds number, was so chosen that forming the limit leaves at least one friction term $\partial^2 u^* / \partial \bar{y}^2$.

The simplifications in these equations formed after taking the limit are considerable compared to the Navier-Stokes equations. The drastic reduction in the momentum equation in the y direction to Eq. (6.9) implies that the pressure is independent of \bar{y} , and thus is constant across a cross-section in the boundary layer. Therefore it can be taken from the pressure at the edge of the boundary layer where it is determined by the inviscid flow. It is as if the pressure is “imposed” onto the boundary layer by the outer flow. The pressure can be taken as a known function in the boundary layer, only dependent on the length coordinate x^* and the time t^* . The number of unknowns has now been reduced by one. Instead of the three functions u^* , v^* , p^* , now only the functions u^* , \bar{v} are to be determined. At the outer edge of the boundary-layer flow, the longitudinal velocity u^* passes over to the velocity in the outer flow $U^*(x^*, t^*)$. Since the velocity gradients $\partial u^* / \partial \bar{y}$ and $\partial^2 u^* / \partial \bar{y}^2$ vanish there, Eq. (6.8) reduces to

$$\frac{\partial U^*}{\partial t^*} + U^* \frac{\partial U^*}{\partial x^*} = - \frac{\partial p^*}{\partial x^*} . \quad (6.10)$$

Using this to eliminate the pressure gradient in Eq. (6.8), Eq. (6.9) is no longer required. We obtain two equations for the two desired functions $u^*(x^*, \bar{y}, t^*)$ and $\bar{v}(x^*, \bar{y}, t^*)$ in the boundary layer:

$$\frac{\partial u^*}{\partial t^*} + u^* \frac{\partial u^*}{\partial x^*} + \bar{v} \frac{\partial u^*}{\partial \bar{y}} = \frac{\partial U^*}{\partial t^*} + U^* \frac{\partial U^*}{\partial x^*} + \frac{\partial^2 u^*}{\partial \bar{y}^2} , \quad (6.11)$$

and

$$\frac{\partial u^*}{\partial x^*} + \frac{\partial \bar{v}}{\partial \bar{y}} = 0 \quad (6.12)$$

with the boundary conditions:

$$\begin{aligned} \bar{y} = 0 : \quad u^* &= 0, \quad \bar{v} = 0 \\ \bar{y} \rightarrow \infty : \quad u^* &= U^*(x^*, t^*) . \end{aligned} \quad (6.13)$$

The aim of boundary-layer theory (for plane, incompressible flows) is to solve the system Eq. (6.11) to (6.13) for a given outer flow velocity distribution $U^*(x^*, t^*)$.

For *steady* flows the system reads

$$u^* \frac{\partial u^*}{\partial x^*} + \bar{v} \frac{\partial u^*}{\partial \bar{y}} = - \frac{dp^*}{dx^*} + \frac{\partial^2 u^*}{\partial \bar{y}^2}, \quad (6.14)$$

$$\frac{\partial u^*}{\partial x^*} + \frac{\partial \bar{v}}{\partial \bar{y}} = 0, \quad (6.15)$$

$$\begin{aligned} \bar{y} = 0 : \quad u^* &= 0, \quad \bar{v} = 0 \\ \bar{y} \rightarrow \infty : \quad u^* &= U^*(x^*) . \end{aligned} \quad (6.16)$$

Using $dp^*/dx^* = -U^* dU^*/dx^*$, the pressure gradient can again be eliminated.

As well as the reduction of the number of equations, there is also a further simplification in the momentum equation in the longitudinal direction. There is a term absent in Eq. (6.14) compared to Eq. (6.3). The mathematical consequences of this are far-reaching. Whereas the system Eq. (6.3) to (6.5) is elliptic, Eq. (6.14) to (6.16) is a parabolic system. The latter has the rather attractive property that the effects of the function $U^*(x^*)$ on the solution functions $u^*(x^*, \bar{y})$, $\bar{v}(x^*, \bar{y})$ can only act downstream. Therefore when two functions $U^*(x^*)$ are the same up to the point x_0^* and only differ for $x^* > x_0^*$, then their solutions are also identical for $x^* \leq x_0^*$.

The numerical solution of the system (6.14) to (6.16) which will be discussed in Chap. 23 can, because of the parabolic system type, be carried out using a *marching procedure*.

It clearly emerges from the derivation of the Prandtl boundary-layer equations that they and their solutions are independent of the Reynolds number. It is only when the boundary-layer transformation in Eq. (6.6) is inverted that the dependence of the original velocities $u^* = f_1(x^*, y^*\sqrt{\text{Re}})$, $v^*\sqrt{\text{Re}} = f_2(x^*, y^*\sqrt{\text{Re}})$ on the Reynolds number is found. Only *one* calculation, valid for all high Reynolds numbers, has to be carried out.

6.2 Wall Friction, Separation and Displacement

The solution of the boundary-layer equations is often used to determine the technically important *wall shear stress* and *displacement thickness*. We shall now discuss these quantities briefly.

Skin-friction coefficient. For the dimensionless wall shear stress we introduce the *skin-friction coefficient*

$$c_f(x^*) = \frac{\tau_w(x^*)}{\frac{\rho}{2} V^2}. \quad (6.17)$$

From the boundary-layer solutions this becomes

$$c_f(x^*) = \frac{2\mu(\partial u/\partial y)_w}{\rho V^2} = \frac{2}{\sqrt{\text{Re}}} \left(\frac{\partial u^*}{\partial y} \right)_w. \quad (6.18)$$

Therefore the skin-friction coefficient is determined from the velocity gradient at the wall ($\bar{y} = 0$). The skin-friction coefficients for *all* laminar boundary layers tend to zero with increasing Reynolds number as $1/\sqrt{\text{Re}}$. One exception is the wall jet, cf. Sect. 7.2.7.

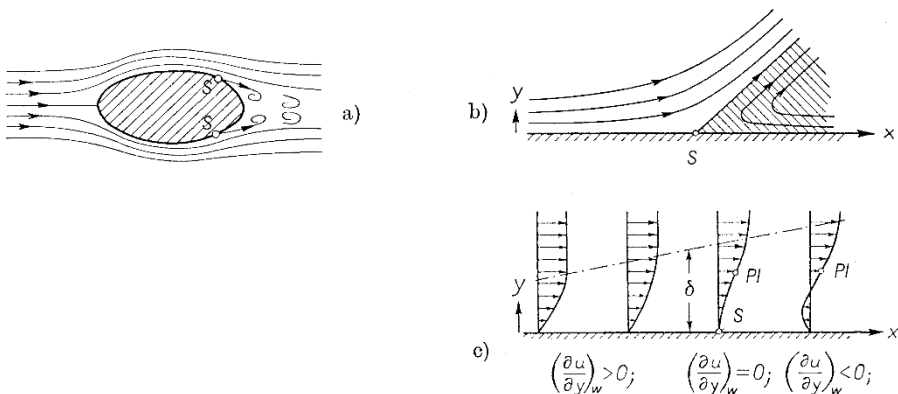


Fig. 6.2. Separation of the boundary layer
 (a) flow past a body with separation (*S* = separation point)
 (b) streamlines close to the separation point
 (c) velocity distributions close to the separation point (*PI* = point of inflection)

Separation point. One case of particular importance is that where the skin-friction coefficient reaches the value zero. This point at which the wall shear stress vanishes is called the *separation point*. It will be seen that separation occurs in the region where the pressure increases (adverse pressure gradient). Whereas a pressure increase corresponds to a drop in the kinetic energy in

the outer flow, within the boundary layer the fluid which is retarded by friction cannot, because of its lower kinetic energy, move very much into the high pressure region. It therefore deviates away from the high pressure area, separating from the body and is drawn right into the main flow (Fig. 6.2). This then leads to a case where the fluid close to the wall, which follows the pressure gradient, flows in the opposite direction to the outer flow. The separation point is defined as the boundary between the forwards and backflow in the layer closest to the wall, i.e.

$$\left(\frac{\partial u}{\partial y} \right)_{y=0} = 0 \quad (\text{separation point}) . \quad (6.19)$$

It follows from the derivation of the boundary-layer equations that the position of the separation point is *independent* of the Reynolds number.

Displacement. If we consider the boundary conditions in Eq. (6.13) and Eq. (6.16) we notice that at the outer edge of the boundary layer, the velocity component u^* passes over to that of the outer flow U^* . However there is no corresponding condition for the v^* component. In fact the v^* component does *not* become the corresponding component V^* of the outer flow, and a finite difference remains between these two quantities. This will now be determined. The velocity components of the outer flow, denoted in dimensionless form by $U^*(x^*, y^*)$ and $V^*(x^*, y^*)$, satisfy the continuity equation

$$\frac{\partial U^*}{\partial x^*} + \frac{\partial V^*}{\partial y^*} = 0 . \quad (6.20)$$

The Taylor expansion of the velocity components $U^*(x^*, y^*)$ for small dimensionless distances from the wall y^* reads

$$U^*(x^*, y^*) = U^*(x^*, 0) + \left(\frac{\partial U^*}{\partial y^*} \right)_w y^* + \left(\frac{\partial^2 U^*}{\partial y^{*2}} \right)_w \frac{y^{*2}}{2} + \dots . \quad (6.21)$$

If the velocity field of the the outer flow is also subjected to the boundary-layer transformation in Eq. (6.6), that is, to

$$\bar{y} = y^* \sqrt{\text{Re}}; \quad \bar{V} = V^* \sqrt{\text{Re}}, \quad (6.22)$$

it follows that

$$\frac{\partial U^*}{\partial x^*} + \frac{\partial \bar{V}}{\partial \bar{y}} = 0 , \quad (6.23)$$

$$U^*(x^*, \bar{y}) = U^*(x^*, 0) + \left(\frac{\partial U^*}{\partial y^*} \right)_w \frac{\bar{y}}{\sqrt{\text{Re}}} + O \left(\frac{1}{\text{Re}} \right) . \quad (6.24)$$

Subtracting the two continuity equations (6.15) and (6.23) leads to

$$\frac{\partial \bar{v}}{\partial \bar{y}} - \frac{\partial \bar{V}}{\partial \bar{y}} = \frac{\partial U^*}{\partial x^*} - \frac{\partial u^*}{\partial x^*}$$

or else, after integrating over the thickness of the boundary layer (and using $\bar{v}(x^*, 0) = \bar{V}(x^*, 0) = 0$)

$$\lim_{\bar{y} \rightarrow \infty} (\bar{v} - \bar{V}) = \frac{d}{dx^*} \int_0^\infty [U^*(x^*, 0) - u^*(x^*, \bar{y})] d\bar{y}. \quad (6.25)$$

Here we exchanged the order of integration and differentiation on the right hand side and, because $\text{Re} \rightarrow \infty$, used Eq. (6.24) to replace $U^*(x^*, \bar{y})$ with $U^*(x^*, 0)$. Equation (6.24) also provides the justification for the functions $U^*(x^*, 0, t^*)$ and $U^*(x^*, 0)$ in the boundary conditions (6.13) and (6.15) respectively. The boundary layer is so thin that, in asymptotic approximation, $U^*(x^*, t^*)$ does not change. This is particularly true at straight walls, where, since potential flow is irrotational ($\partial V^*/\partial x^* = \partial U^*/\partial y^* = 0$), the quantity $(\partial U^*/\partial y^*)_w$ vanishes.

Since the integral in Eq. (6.25) is positive and increases with x^* , at the edge of the boundary layer we have $\bar{v} > \bar{V}$. The difference is called the *displacement velocity*. The boundary layer has a displacement effect on the outer flow, but in the case of large Reynolds numbers this is very small and can be neglected within the framework of the Prandtl boundary-layer theory. The boundary-layer solution can be improved upon by a higher order boundary-layer theory, discussed in Chap. 14, where the outer flow is modified as a consequence of the displacement velocity.

As well as the displacement action, there is also a second higher order effect, namely the *wall curvature*. As will also be shown in Chap. 14, the wall curvature has no effect on the Prandtl boundary-layer equations as long as the radius of curvature is of the order of magnitude of the reference length l , and thus much larger than the “boundary-layer thickness” δ . Flows which have comparatively sharp corners are therefore excluded. Since the wall curvature has no effect, the coordinate system x^*, \bar{y} can be considered to be a “curved” Cartesian coordinate system, where the x^* axis follows the contour of the wall and the \bar{y} direction is perpendicular to the local x^* direction. Therefore the geometry of the body under consideration does not enter into the boundary-layer computation, and the effects of the geometry are only seen via the velocity distribution $U^*(x^*, t^*)$ or $U^*(x^*)$ at the wall ($\bar{y} = 0$).

6.3 Dimensional Representation of the Boundary-Layer Equations

Although the dimensionless representation is actually required for a mathematically correct derivation of the boundary-layer equations, we shall now and in what follows retract the boundary-layer transformation and again use the dimensional representation of the boundary-layer equations. At first glance this does not seem particularly sensible. Our justification is that later we will consider boundary layers which start off laminar and then become

turbulent. Since the boundary-layer transformation which we have discussed makes no sense for turbulent boundary layers, the dimensional representation seems most appropriate for both flow forms in the boundary layer.

We find from Eqs. (6.11) and (6.12) that the boundary-layer equations in dimensional form are

$$\frac{\partial u}{\partial t} + u \frac{\partial u}{\partial x} + v \frac{\partial u}{\partial y} = -\frac{1}{\varrho} \frac{\partial p}{\partial x} + \nu \frac{\partial^2 u}{\partial y^2}, \quad (6.26)$$

$$\frac{\partial u}{\partial x} + \frac{\partial v}{\partial y} = 0 \quad (6.27)$$

with the boundary conditions:

$$y = 0 : \quad u = 0, \quad v = 0; \quad (6.28)$$

$$y \rightarrow \infty : \quad u = U(x, t).$$

In the outer flow we have:

$$\frac{\partial U}{\partial t} + U \frac{\partial U}{\partial x} = -\frac{1}{\varrho} \frac{\partial p}{\partial x}. \quad (6.29)$$

For *steady* flows this system of equations simplifies to

$$u \frac{\partial u}{\partial x} + v \frac{\partial u}{\partial y} = -\frac{1}{\varrho} \frac{dp}{dx} + \nu \frac{\partial^2 u}{\partial y^2} \quad (6.30)$$

$$\frac{\partial u}{\partial x} + \frac{\partial v}{\partial y} = 0 \quad (6.31)$$

with the boundary conditions

$$y = 0 : \quad u = 0, \quad v = 0; \quad (6.32)$$

$$y \rightarrow \infty : \quad u = U(x)$$

and the relation in the outer flow

$$U \frac{dU}{dx} = -\frac{1}{\varrho} \frac{dp}{dx}. \quad (6.33)$$

Although the kinematic viscosity ν explicitly appears in the system of equations in this representation, it must always be recalled that, because of the boundary-layer transformation, ν is not a *real* parameter of the boundary-layer solution.

A further lack of elegance in the dimensional representation is the way of denoting the outer edge of the boundary layer. While denoting $\bar{y} = (y/l)\sqrt{\text{Re}} \rightarrow \infty$ made good sense, since for a fixed y , \bar{y} tended to infinity for $\text{Re} \rightarrow \infty$, this is no longer the case for y . In fact y is a very small quantity at the edge of the boundary. In spite of this we will use $y \rightarrow \infty$ here, since no problems arise as long as we continue to recall the meaning of this representation (that y be large enough to cover the boundary-layer region).

Wall shear stress. The wall shear stress can be determined from the solution function $u(x, y)$ by differentiation as follows:

$$\tau_w(x) = \mu \left(\frac{\partial u}{\partial y} \right)_w . \quad (6.34)$$

Displacement thickness. In dimensional form, Eq. (6.25) reads

$$\lim_{y \rightarrow \infty} (v - V) = \frac{d(U\delta_1)}{dx} , \quad (6.35)$$

where the length

$$\delta_1 = \int_0^\infty \left[1 - \frac{u(x, y)}{U(x)} \right] dy \quad (6.36)$$

is called the *displacement thickness*, since, from Eq. (6.35) it is a measure of the displacement action. In Fig. 6.3 δ_1 is indicated geometrically. Since, from Eq. (6.36), both shaded regions must have the same area, the volume flux in the boundary layer given by the profile $u(x, y)$ is identical to the volume flux which the outer flow with velocity $U(x)$ *displaced* away from the wall by displacement thickness δ_1 would have.

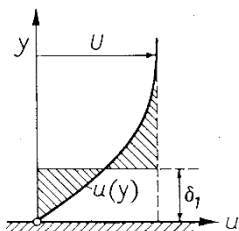


Fig. 6.3. Displacement thickness δ_1 of the boundary layer

Stream function. By introducing the *stream function* ψ , the system of two equations (6.26) and (6.27) for two functions u and v can be reduced to one equation for one function ψ . This function is defined by

$$u = \frac{\partial \psi}{\partial y}, \quad v = -\frac{\partial \psi}{\partial x} . \quad (6.37)$$

It satisfies the continuity equation (6.27), and Eq. (6.26) becomes

$$\frac{\partial^2 \psi}{\partial y \partial t} + \frac{\partial \psi}{\partial y} \frac{\partial^2 \psi}{\partial x \partial y} - \frac{\partial \psi}{\partial x} \frac{\partial^2 \psi}{\partial y^2} = -\frac{1}{\varrho} \frac{\partial p}{\partial x} + \nu \frac{\partial^3 \psi}{\partial y^3}. \quad (6.38)$$

This is a third order differential equation. The boundary conditions then read $(\partial \psi / \partial y)_w = 0$, $(\partial \psi / \partial x)_w = 0$, $(\partial \psi / \partial y)_\infty = U$. If we compare Eq. (6.38) with the equation (4.60) for the stream function which arose from the complete Navier–Stokes equations, we see that the approximation of the boundary–layer theory has reduced the order of the differential equation from four to three. We can now understand why only three boundary conditions can be given, i.e. why there is no boundary condition for v at the outer edge of the boundary layer.

6.4 Friction Drag

From the distribution of the wall shear stress $\tau_w(x)$ in Eq. (6.34), the friction drag can be easily computed by integration of $\tau_w(x)$ over the surface of the body. If b is the width of the body and l its length, then the friction drag on the upper side of the body shown in Fig. 6.4 is

$$D_f = b \int \tau_w(x) \cos \varphi dx, \quad (6.39)$$

where the coordinate x , as is usually the case in boundary–layer theory, follows the contour of the body. We integrate over the entire length of the surface in the flow, from the nose to the trailing edge. Introducing \hat{x} as the coordinate along the chord of the body, and using $dx \cdot \cos \varphi = d\hat{x}$, we see from (6.39) that

$$D_f = b \int_0^l \tau_w(\hat{x}) d\hat{x}. \quad (6.40)$$

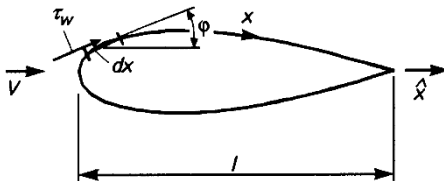


Fig. 6.4. Computing the friction drag

If the boundary layer is thick, or if separation occurs, then considerable displacement effects can appear. In such cases, the pressure distribution of the outer flow must be modified using higher order boundary–layer theory, as treated in Chap. 14. The difference from the pressure distribution computed for the given body contour leads to a *pressure* or *form drag*. In this way the form drag is in fact a friction effect. Details may be found in Chap. 14.

6.5 Plate Boundary Layer

Before we discuss a whole series of general properties of the boundary-layer differential equations in the next chapter, we shall look at a few examples here already, to familiarise ourselves further with the boundary-layer equations. The simplest example of application of the boundary-layer equations is the flow along a very thin flat plate. This case was the first example of the Prandtl boundary-layer equations treated by H. Blasius (1908) in his doctoral thesis in Göttingen. Let the plate start at $x = 0$, extend parallel to the x axis and be of semi-infinite length (Fig. 6.5). We will treat the steady flow parallel to the x axis with free stream velocity U_∞ . In this case the velocity of the potential flow is constant, that is $dp/dx = 0$. The boundary-layer equations (6.30) to (6.32) become

$$u \frac{\partial u}{\partial x} + v \frac{\partial u}{\partial y} = \nu \frac{\partial^2 u}{\partial y^2}, \quad (6.41)$$

$$\frac{\partial u}{\partial x} + \frac{\partial v}{\partial y} = 0, \quad (6.42)$$

$$\begin{aligned} y = 0 : \quad & u = 0, \quad v = 0; \\ y \rightarrow \infty : \quad & u = U_\infty. \end{aligned} \quad (6.43)$$

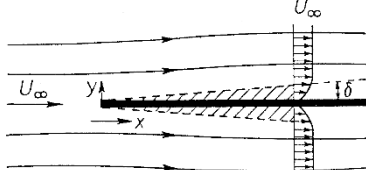


Fig. 6.5. Boundary layer on a flat plate at zero incidence

Since the system has no characteristic length, we can assume that the velocity profiles at different distances from the leading edge are *affine* or *similar* to one another, i.e. that the velocity profiles $u(y)$ at different distances x can be mapped onto each other by suitable choice of scaling factors for u and y . A suitable scaling factor for u could be the free stream velocity U_∞ , while for y , the “boundary-layer thickness” $\delta(x)$, which increases with distance x , could be used. Strictly speaking, $\delta(x)$ is not the boundary-layer thickness, but rather a scaled measure of the boundary-layer thickness which is equal to the boundary-layer thickness up to some numerical factor, cf. Eq. (6.60). The similarity law of the velocity profile can thus be written as $u/U_\infty = \varphi(\eta)$ with $\eta = y/\delta(x)$, where the function $\varphi(\eta)$ is independent of x .

The x dependence of $\delta(x)$ can be seen rather easily as follows. The quantity δ is proportional to the thickness of the layer which is affected by the friction, i.e. by viscous effects. The viscosity causes a momentum transport

moving outwards from the wall. The characteristic transport velocity U_V is dependent on ν and δ . From dimensional considerations we have $U_V \sim \nu/\delta$. The quantity $\delta(x)$ is thus dependent on which fluid particles close to the wall are displaced away from the wall by this momentum transport and which have already passed by the position x via their translational motion with velocity U_∞ . The length of time required for a particle with velocity U_∞ to move past position x is x/U_∞ . On the other hand, for the momentum transport, the time $\delta/U_V = \delta^2/\nu$ is needed to move over the thickness δ at velocity $U_V \sim \nu/\delta$. Setting these two times equal it follows that $\delta^2/\nu \sim x/U_\infty$ or

$$\delta(x) \sim \sqrt{\frac{x\nu}{U_\infty}} . \quad (6.44)$$

This is exactly the same as Eq. (6.1) if we replace l there by x and V by U_∞ . The *similarity variable* $\eta \sim y/\delta(x)$ is set as

$$\eta = y \sqrt{\frac{U_\infty}{2\nu x}} . \quad (6.45)$$

This initially arbitrary choice of the factor $\sqrt{2}$ for $\delta(x)$ will be seen to be useful since the resulting differential equation then assumes a particularly simple form.

The continuity equation can be integrated introducing a stream function $\psi(x, y)$ as in Eq. (6.37). We set

$$\psi = \sqrt{2\nu x U_\infty} f(\eta) , \quad (6.46)$$

where $f(\eta)$ is the dimensionless stream function. For the velocity components we then obtain

$$u = \frac{\partial \psi}{\partial y} = \frac{\partial \psi}{\partial \eta} \frac{\partial \eta}{\partial y} = U_\infty f'(\eta) , \quad (6.47)$$

$$v = -\frac{\partial \psi}{\partial x} = -\left(\frac{\partial \psi}{\partial x} + \frac{\partial \psi}{\partial \eta} \frac{\partial \eta}{\partial x} \right) = \sqrt{\frac{\nu U_\infty}{2x}} (\eta f' - f) , \quad (6.48)$$

where the dash on the f implies differentiation with respect to η . If we use this to form the individual terms in Eq. (6.41) we finally obtain the following ordinary differential equation for the stream function

$$f''' + f f'' = 0 \quad (\text{Blasius equation}) . \quad (6.49)$$

The boundary conditions from Eq. (6.43) are

$$\begin{aligned} \eta = 0 : \quad & f = 0, \quad f' = 0 , \\ \eta \rightarrow \infty : \quad & f' = 1 . \end{aligned} \quad (6.50)$$

In this case the two partial differential equations (6.41) and (6.42) have been transformed by the similarity transformations (6.45) and (6.46) to lead to one ordinary differential equation for the stream function. This is nonlinear

and third order. The three boundary conditions Eq. (6.50) are thus sufficient to completely determine this solution.

The numerical solution of this differential equation can be found using, for example, a Runge-Kutta method called the “shooting” method. Instead of solving the boundary value problem, the initial value problem with values $f(0) = 0$, $f'(0) = 0$ and an estimated value $f''(0) = f_w''$ is solved. The estimated value f_w'' is changed until the boundary condition $f'(\infty) = 1$ is satisfied. In practice this condition is satisfied at a position with finite but large enough η value (here e.g. $\eta = 5$ gives a deviation from 1 of less than 10^{-4}). Some important numerical values for the solution are given in Table 6.1. A more comprehensive table is to be found in the work by L. Howarth (1938).

Table 6.1. Characteristic values for the boundary layer on a flat plate at zero incidence

f_w''	0.4696
$\beta_1 = \lim_{\eta \rightarrow \infty} [\eta - f(\eta)]$	1.2168
$\beta_2 = \int_0^\infty f'(1 - f')d\eta$	0.4696
$\beta_3 = \int_0^\infty f'(1 - f'^2)d\eta$	0.7385

Velocity distribution. The distribution of the longitudinal velocity $u/U_\infty = f'(\eta)$ is shown in Fig. 6.6a. The curvature close to the wall is very little. Directly at the wall, the curvature vanishes exactly because of $f'''(0) = 0$. This follows from the differential equation since $f(0) = 0$. The transverse component of the velocity in the boundary layer from Eq. (6.48) is also given in Fig. 6.6b. It is worth noting here that at the outer edge of the boundary layer, i.e. for $\eta \rightarrow \infty$, the transverse component is non-zero. This is again the *displacement velocity* which was already mentioned in Sect. 6.2. We find

$$v_\infty(x) = \sqrt{\frac{\nu U_\infty}{2x}} \beta_1 = 0.8604 U_\infty \sqrt{\frac{\nu}{x U_\infty}} \quad (6.51)$$

with

$$\beta_1 = \lim_{\eta \rightarrow \infty} [\eta - f(\eta)] = 1.2168 . \quad (6.52)$$

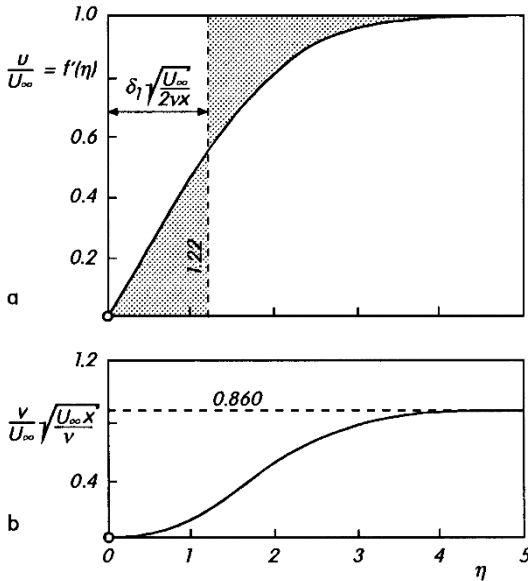


Fig. 6.6. Velocity distribution in the boundary layer at a flat plate, after H. Blasius (1908)

(a) velocity component parallel to the wall
 (b) transverse component of the velocity

Friction drag. The drag experienced by a plate is purely friction drag. This can easily be determined from the solution given above. From Eq. (6.40) the drag of *one* side of the plate is

$$D = b \int_0^l \tau_w(x) dx , \quad (6.53)$$

where b is the width of the plate and l its length. Now the local wall shear stress is

$$\tau_w(x) = \mu \left(\frac{\partial u}{\partial y} \right)_w = \mu U_\infty \sqrt{\frac{U_\infty}{2\nu x}} f''_w = 0.332 \mu U_\infty \sqrt{\frac{U_\infty}{\nu x}} , \quad (6.54)$$

where the numerical value for f''_w was taken from Table 6.1. The skin-friction coefficient in Eq. (6.17) with the reference velocity U_∞ then becomes

$$c_f(x) = \frac{\tau_w(x)}{\frac{\rho}{2} U_\infty^2} = \frac{0.664}{\sqrt{Re_x}} , \quad (6.55)$$

where the Reynolds number formed with the length x has been used:

$$Re_x = \frac{U_\infty x}{\nu} . \quad (6.56)$$

Combining Eqs. (6.53) and (6.54) we find the drag on *one* side of the plate:

$$D = f''_w \mu b U_\infty \sqrt{\frac{U_\infty}{2\nu}} \int_0^l \frac{dx}{\sqrt{x}} = f''_w b U_\infty \sqrt{2\mu \rho l U_\infty} . \quad (6.57)$$

The drag of the plate is therefore proportional to $U_\infty^{3/2}$ and to $l^{1/2}$, i.e. not proportional to l . This has to do with the fact that the parts of the plate at the rear contribute a relatively lower amount to the total drag than those at the front. This is because they are located in a region which has a thicker frictional layer and thus a smaller wall shear stress. If we introduce a dimensionless *drag coefficient* in the usual manner using the equation

$$c_D = \frac{D}{\frac{\rho}{2} U_\infty^2 bl} \quad (6.58)$$

where the wetted area bl serves as a reference area, we can use Eq. (6.57) to find the drag formula

$$c_D = \frac{1.328}{\sqrt{Re}} \quad (6.59)$$

with the Reynolds number $Re = U_\infty l / \nu$. This formula, called the Blasius drag law, is valid for laminar flows, that is for Reynolds numbers under the critical Reynolds number $Re_{crit} = 5 \cdot 10^5$ to 10^6 . The formula in Eq. (6.59) is depicted in Fig. (1.3) and Fig. (18.3). In regions where the flow is turbulent, to be discussed in Sect. 18.2.5, the drag is considerably greater than that in Eq. (6.59).

Boundary-layer thickness. There is no unique boundary-layer thickness, since the effect of the viscosity in the boundary layer decreases asymptotically as we move outwards from the wall. The component of velocity parallel to the wall u passes over asymptotically to the velocity U_∞ of the outer flow (the function $f'(\eta)$ goes asymptotically to 1). If we define the boundary-layer thickness to be the position where $u = 0.99U_\infty$, we find that $\eta_{99} = 3.6$. Therefore the boundary-layer thickness defined in this way is

$$\delta_{99} \approx 5.0 \sqrt{\frac{\nu x}{U_\infty}} . \quad (6.60)$$

Displacement thickness. A physically sensible measure for the thickness of the boundary layer is the displacement thickness which was already introduced in Eq. (6.36) (Fig. 6.3). By this we understand the thickness by which the inviscid outer flow is displaced outwards by the drop in velocity in the boundary layer. The reduction of the volume flux due to the action of viscosity is

$$\int_0^\infty (U_\infty - u) dy ,$$

and therefore the defining equation for δ_1 is

$$U_\infty \delta_1 = \int_0^\infty (U_\infty - u) dy$$

or

$$\delta_1 = \int_0^\infty \left(1 - \frac{u}{U_\infty}\right) dy \quad (\text{displacement thickness}) . \quad (6.61)$$

Using u/U_∞ from Eq. (6.47) this becomes

$$\delta_1 = \sqrt{\frac{2\nu x}{U_\infty}} \int_0^\infty [1 - f'(\eta)] d\eta = \beta_1 \sqrt{\frac{2\nu x}{U_\infty}} = 1.7208 \sqrt{\frac{\nu x}{U_\infty}} , \quad (6.62)$$

where the definition of β_1 is taken from Eq. (6.52). The distance from the wall $y = \delta_1$ is also shown in Fig. 6.6a. The viscosity displaces the streamlines of the outer flow outwards from the wall by this amount. The displacement thickness is approximately one third of the boundary-layer thickness δ_{99} in Eq. (6.60).

Momentum thickness. At this point we will also mention the value for the *momentum thickness* δ_2 which will be made use of later. The smaller amount of momentum flowing in the boundary layer relative to that in the inviscid outer flow is $\varrho \int_0^\infty u(U_\infty - u) dy$, and therefore the momentum thickness can be defined by

$$\varrho U_\infty^2 \delta_2 = \varrho \int_0^\infty u(U_\infty - u) dy$$

or

$$\delta_2 = \int_0^\infty \frac{u}{U_\infty} \left(1 - \frac{u}{U_\infty}\right) dy \quad (\text{momentum thickness}) . \quad (6.63)$$

Computing this for a plate at zero incidence gives:

$$\delta_2 = \sqrt{\frac{2\nu x}{U_\infty}} \int_0^\infty f'(1 - f') d\eta = \beta_2 \sqrt{\frac{2\nu x}{U_\infty}}$$

which, using the numerical value for β_2 in Table 6.1 is

$$\delta_2 = 0.664 \sqrt{\frac{\nu x}{U_\infty}} . \quad (6.64)$$

Energy thickness. Along with the momentum thickness, we will later also use the *energy thickness* δ_3 . The lower kinetic energy in the boundary layer relative to that in the inviscid outer fluid is $\varrho \int_0^\infty u(U_\infty^2 - u^2) dy$, and therefore an energy thickness can also be defined as

$$\varrho U_\infty^3 \delta_3 = \varrho \int_0^\infty u(U_\infty^2 - u^2) dy$$

or

$$\delta_3 = \int_0^\infty \frac{u}{U_\infty} \left(1 - \frac{u^2}{U_\infty^2} \right) dy \quad (\text{energy thickness}) . \quad (6.65)$$

Computing this for a plate at zero incidence gives:

$$\delta_3 = \sqrt{\frac{2\nu x}{U_\infty}} \int_0^\infty f'(1 - f'^2) d\eta = \beta_3 \sqrt{\frac{2\nu x}{U_\infty}} = 1.0444 \sqrt{\frac{\nu x}{U_\infty}} . \quad (6.66)$$

Here is a summary of the three different relations:

$$\text{displacement thickness: } \delta_1 = 0.34 \delta_{99}$$

$$\text{momentum thickness: } \delta_2 = 0.13 \delta_{99}$$

$$\text{energy thickness: } \delta_3 = 0.20 \delta_{99} .$$

Leading edge singularity. It is seen from Eqs. (6.51) and (6.54) that the displacement velocity $v_\infty(x)$ and the wall shear stress $\tau_w(x)$ become infinite at the leading edge $x = 0$. This singularity is an indication that the boundary-layer theory is invalid directly at the leading edge. This singularity can be got rid of using a higher order theory, as will be discussed in Chap. 14.

Experimental investigations. Measurements to confirm the existing theory were first carried out by both B.G. Van der Hegge Zijnen (1924) and J.M. Burgers (1924), and afterwards by M. Hansen (1928). Particularly illuminating measurements were also later presented by J. Nikuradse (1942). It turned out that the frictional layer is strongly affected by the shape of the nose on the leading edge of the plate and also by weak pressure gradients in the outer flow which may be present. These circumstances were taken into account in the measurements of J. Nikuradse which were carried out on a plate in a flow of air. Figure 6.7 shows Nikuradse's measurements on the velocity distribution in the laminar boundary layer for different distances from the leading edge of the plate. The similarity in velocity profiles at different distances x from the leading edge predicted by the theory are well confirmed by the measurements, and the shape of the measured velocity profiles also agrees well with the theory. Figure 2.4 already depicted the dimensionless boundary-layer thickness $\delta_{99} \sqrt{U_\infty / \nu x}$ versus the Reynolds number formed with the length x . As long as the boundary layer remains laminar, this dimensionless value remains constant and its numerical value is approximately equal to that in Eq. (6.60). For large Reynolds numbers $U_\infty x / \nu$, the boundary layer no longer remains laminar and it is replaced by the turbulent boundary layer. This can be seen in Fig. 2.4 in the manner in which, in the turbulent boundary layer, the boundary-layer thickness grows much faster with the length x . The measurements of B.G. Van der Hegge Zijnen (1924) and

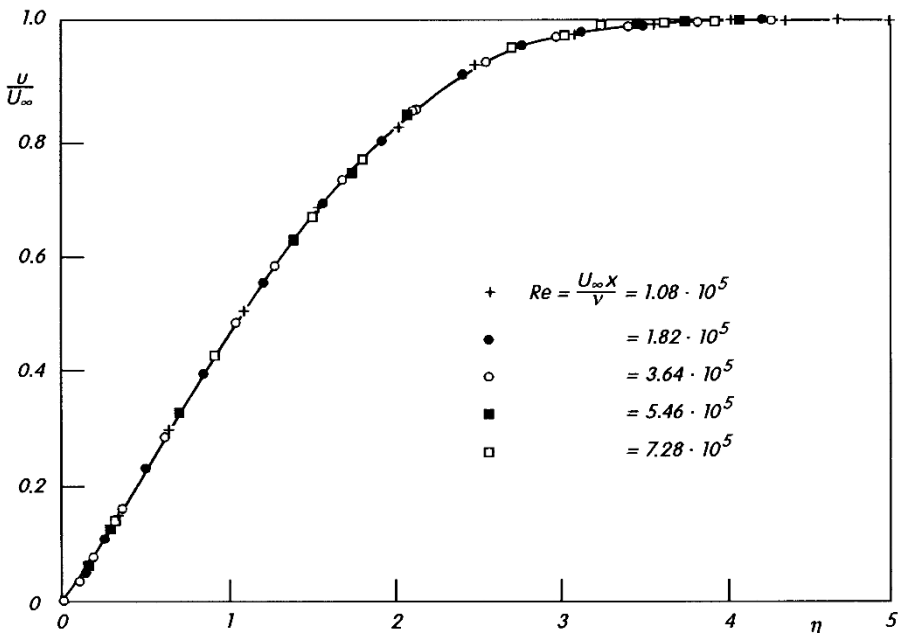


Fig. 6.7. Velocity distribution in the laminar boundary layer on a flat plate at zero incidence, after measurements by J. Nikuradse (1942)

M. Hansen (1928) show that the transition from the laminar to the turbulent flow state takes place at Reynolds number $U_\infty x/\nu = 3 \cdot 10^5$. From Eq. (6.62) this corresponds to a Reynolds number formed with the displacement thickness of $U_\infty \delta_1/\nu = 950$. More recent measurements have shown that this so-called “critical” Reynolds number can take on even higher values of up to $U_\infty x/\nu = 3 \cdot 10^6$ in an air flow which is particularly free of perturbations.

The laminar friction law of the flat plate has also been put to the test exhaustively. On the one hand the local wall shear stress can be determined *indirectly* using Eq. (6.34) from the slope of the velocity profile. On the other hand, *direct* shear stress measurements can be carried out using a small section of the plate arranged in a flexible manner in the wall (floating element). The result of these careful measurements by H.W. Liepmann and S. Dhawan (1951) is depicted in Fig. 6.8. Here the local skin-friction coefficient $c_f = \tau_w / \frac{1}{2} \rho U_\infty^2$ is drawn against the Reynolds number formed with the length x , i.e. $Re_x = U_\infty x/\nu$. In Reynolds number regions of $Re_x = 2 \cdot 10^5$ to $6 \cdot 10^5$, both the laminar and the turbulent flow states are possible. In this region, the latter can be enforced by suitable measures, e.g. a trip wire.

The indirect and direct shear stress measurements are in excellent agreement. For laminar flows, the Blasius drag law from Eq. (6.55), which states $c_f = 0.664/\sqrt{Re_x}$, is confirmed extremely well by the measurements. Even in

the turbulent case, the measurements agree well with the theoretical formula which will be dealt with in Sect. 18.2.5.

The complete agreement of theoretical and experimental results for the velocity distribution and the wall shear stress of the laminar boundary layer on a flat plate at zero incidence in the region $Re_x > 5 \cdot 10^4$ shown in Figs. 6.7 and 6.8 gives us, from a physical point of view, definite proof of the admissibility of the boundary-layer simplifications. As will be shown in Chap. 14, the results of boundary-layer theory can even be used for smaller Reynolds numbers.

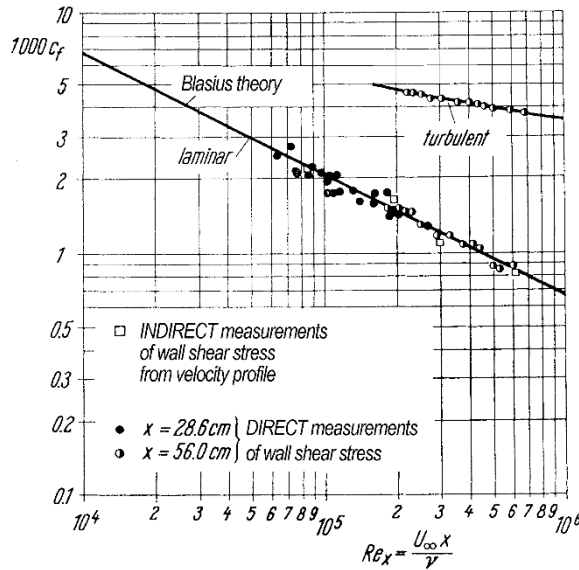


Fig. 6.8. Local skin-friction coefficient of a flat plate at zero incidence determined from indirect and direct wall shear stress measurements by H.W.Liepmann; S. Dhawan (1951) and S. Dhawan (1953)
 $c_f = 2\tau_w/\rho U_\infty^2$
 Theory: laminar,
 from Eq. (6.55),
 turbulent,
 from Eq. (2.13)
 or (18.96)

7. General Properties and Exact Solutions of the Boundary-Layer Equations for Plane Flows

Before further examples of the calculation of boundary layers are treated in the next chapter, some general properties of boundary-layer equations will be discussed. We will confine ourselves to steady, two-dimensional, incompressible boundary layers.

Although the boundary-layer equations are considerably simplified compared to the Navier-Stokes equations, their nonlinearity means that they are mathematically still so difficult that few general statements can be made about their solutions. First of all it is important to note that the Navier-Stokes equations are *elliptic* equations while Prandtl's boundary-layer equations are *parabolic*. The simplifications used led us to see that the pressure can be assumed to be constant at right angles to the boundary layer, while along the wall the pressure can be regarded as being "imposed" by the outer flow and thus is a given function. This omission of the equations of motion perpendicular to the direction of flow can also be taken physically to mean that a particle in the boundary layer moving in the transverse direction has neither mass nor experiences any deceleration due to friction. It is obvious when the character of the equations of motion is changed so fundamentally, that their solutions must also exhibit certain mathematical attributes.

The considerable simplifications of the boundary-layer equations compared to the Navier-Stokes equations were the result of considering the asymptotic limit $\text{Re} \rightarrow \infty$. The solutions of the boundary-layer equations are therefore better approximations the higher the Reynolds number, providing the critical Reynolds number is not exceeded (transition to turbulence). Generalisations of the theory for moderately large Reynolds numbers will be treated in Chap. 14.

The rapid development of computers and with it of advances in numerical methods in solving nonlinear partial differential equations in the last decades has meant that in practice boundary-layer equations are often solved numerically. The standard numerical methods for this are treated in Chap. 23.

7.1 Compatibility Condition at the Wall

The boundary-layer equation reads, cf. Eq. (6.30)

$$u \frac{\partial u}{\partial x} + v \frac{\partial u}{\partial y} = -\frac{1}{\rho} \frac{dp}{dx} + \nu \frac{\partial^2 u}{\partial y^2}. \quad (7.1)$$

If this equation is specified for the wall ($y = 0$), since $u(x, 0) = 0$, $v(x, 0) = 0$ we obtain the *compatibility condition at the wall*

$$\mu \left(\frac{\partial^2 u}{\partial y^2} \right)_w = \frac{dp}{dx}. \quad (7.2)$$

Relations can also be derived for the higher derivatives at the wall when we differentiate Eq. (7.1) partially by y and then specify it at the wall. The third derivative then follows as

$$\left(\frac{\partial^3 u}{\partial y^3} \right)_w = 0. \quad (7.3)$$

From Eq. (7.2) we see that the curvature of the velocity profile at the wall is indeed determined by the pressure gradient, and that the curvature changes its sign with the pressure gradient. Figure 7.1 shows the velocity profiles for the two cases for pressure drop and pressure increase. For flows with pressure drop (accelerated flows, favourable pressure gradient $dp/dx < 0$), Eq. (7.2) yields $(\partial^2 u / \partial y^2)_w < 0$ and therefore $\partial^2 u / \partial y^2 < 0$ over the entire boundary-layer thickness. For flows with pressure increase (retarded flows, adverse pressure gradient $dp/dx > 0$), we find $(\partial^2 u / \partial y^2)_w > 0$. Since at a large distance from the wall it is certainly true that $\partial^2 u / \partial y^2 < 0$, in this case there must be a point inside the boundary layer where $\partial^2 u / \partial y^2 = 0$, i.e. a *point of inflection* of the velocity profile.

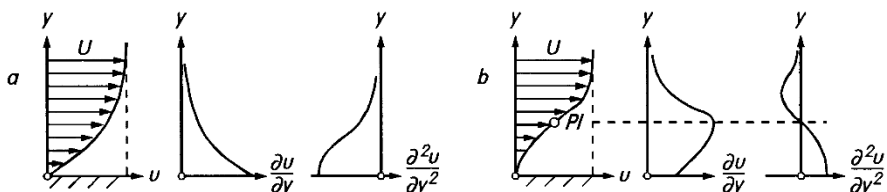


Fig. 7.1. Velocity distribution in the boundary layer and its derivatives.
PI: point of inflection; (a) pressure drop; (b) pressure increase

It therefore follows from this that the velocity profile always has a point of inflection in the case of retarded outer flows. This has important consequences for the flow separation. Since the velocity profile in the separation point must have a point of inflection, because of the vertical wall tangent (in the $y-u$

representation), it follows that separation can only occur when the outer flow is retarded (pressure increase, adverse pressure gradient).

The presence of a point of inflection in the velocity profile of the boundary layer is also of great importance for the stability (the laminar–turbulent transition) of the boundary layer, as will be shown in Chap. 15.

7.2 Similar Solutions of the Boundary–Layer Equations

7.2.1 Derivation of the Ordinary Differential Equation

In the example of the boundary layer at a plate at zero incidence in Sect. 6.4, we were able to reduce the boundary–layer equations (two partial differential equations) to one ordinary differential equation. This was possible because we were dealing with a so-called similar solution, where the velocity profiles at different points are *affine* or *similar*, i.e. they can be mapped onto one another by choosing suitable scaling factors.

In what now follows we shall examine whether further similar solutions exist in addition to the plate boundary layer and for which outer flows with distributions $U(x)$ these are to be found. These questions have been discussed comprehensively by S. Goldstein (1939) and later by W. Mangler (1943). We shall begin with the boundary–layer equations for plane steady incompressible flow, given by Eqs. (6.30) to (6.32) as:

$$u \frac{\partial u}{\partial x} + v \frac{\partial u}{\partial y} = U \frac{dU}{dx} + \nu \frac{\partial^2 u}{\partial y^2}, \quad (7.4)$$

$$\frac{\partial u}{\partial x} + \frac{\partial v}{\partial y} = 0 \quad (7.5)$$

with the boundary conditions

$$y = 0 : \quad u = 0, \quad v = 0; \quad y \rightarrow \infty : \quad u = U.$$

The continuity equation can be integrated by introducing the stream function $\psi(x, y)$ with

$$u = \frac{\partial \psi}{\partial y}, \quad v = -\frac{\partial \psi}{\partial x}.$$

Thus Eq. (7.4) becomes

$$\frac{\partial \psi}{\partial y} \frac{\partial^2 \psi}{\partial x \partial y} - \frac{\partial \psi}{\partial x} \frac{\partial^2 \psi}{\partial y^2} = U \frac{dU}{dx} + \nu \frac{\partial^3 \psi}{\partial y^3}. \quad (7.6)$$

We now carry out a coordinate transformation from the variables x, y to the new dimensionless variables

$$\xi = \frac{x}{l}, \quad \eta = \frac{y}{l} \frac{\sqrt{\text{Re}}}{\delta(\xi)} = \frac{\bar{y}}{\bar{\delta}(\xi)}. \quad (7.7)$$

Here the Reynolds number

$$\text{Re} = \frac{Vl}{\nu} \quad (7.8)$$

is formed with the reference velocity V and the reference length l . Since $\bar{y} = (y/l)\sqrt{\text{Re}}$ corresponding to Eq. (6.6) is the distance from the wall after the boundary-layer transformation, $\bar{\delta}(\xi)$ can be interpreted as the boundary-layer measure (proportional to the boundary-layer thickness) in this scale.

With the trial solution for the stream function:

$$\psi(\xi, \eta) = \frac{lU_N(\xi)}{\sqrt{\text{Re}}} \bar{\delta}(\xi) f(\xi, \eta) \quad (7.9)$$

it follows that the longitudinal component of the velocity is

$$\frac{u(\xi, \eta)}{U_N(\xi)} = f'(\xi, \eta), \quad (7.10)$$

where the dash implies differentiation with respect to η .

If we identify $U_N(\xi)$ as the velocity of the outer flow $U(\xi)$, we would have found all *similar* solutions, as long as $f'(\eta)$ only depended on η . Instead of the partial differential equation for $f(\xi, \eta)$ we would then have an ordinary differential equation for $f(\eta)$. The orthogonal component of the velocity is then found from Eq. (7.9) to be

$$-v(\xi, \eta)\sqrt{\text{Re}} = \frac{d}{d\xi}(U_N \bar{\delta}) f + U_N \left(\bar{\delta} \frac{\partial f}{\partial \xi} - \frac{d\bar{\delta}}{d\xi} \eta f' \right). \quad (7.11)$$

If we now insert the trial solutions Eqs. (7.7) and (7.9) into Eq. (7.6), we obtain the following differential equation for the dimensionless stream function $f(\xi, \eta)$:

$$f''' + \alpha_1 f f'' + \alpha_2 - \alpha_3 f'^2 = \bar{\delta}^2 \frac{U_N}{V} \left(f' \frac{\partial f'}{\partial \xi} - f'' \frac{\partial f}{\partial \xi} \right). \quad (7.12)$$

Here $\alpha_1, \alpha_2, \alpha_3$ are defined as:

$$\alpha_1 = \frac{\bar{\delta}}{V} \frac{d}{d\xi}(U_N \bar{\delta}), \quad \alpha_2 = \frac{\bar{\delta}^2}{V} \frac{U}{U_N} \frac{dU}{d\xi}, \quad \alpha_3 = \frac{\bar{\delta}^2}{V} \frac{dU_N}{d\xi}. \quad (7.13)$$

Since Eq. (7.7) is a formal transformation, Eq. (7.12) initially remains a partial differential equation for the function $f(\xi, \eta)$. However in this new form it can immediately be seen when similar solutions occur, i.e. when Eq. (7.12) reduces to an ordinary differential equation for the function $f(\eta)$. If the quantities $\alpha_1, \alpha_2, \alpha_3$ are constants, solutions for $f(\eta)$ which are independent of ξ can be found. The right hand side of Eq. (7.12) then vanishes and the boundary-layer equations reduce to the ordinary differential equation

$$f''' + \alpha_1 f f'' + \alpha_2 - \alpha_3 f'^2 = 0. \quad (7.14)$$

For prescribed constants α_1 , α_2 and α_3 , the equations (7.13) can be interpreted as defining equations for the remaining unknown functions $U(\xi)$, $U_N(\xi)$ and $\bar{\delta}(\xi)$. The solutions of these three differential equations yield, in particular, the distribution $U(\xi)$ of the outer flow for which similar solutions exist.

Depending on the choice of the constants α_1 to α_3 , we can differentiate between the following two classes of similar solutions:

A Boundary layers with outer flow ($U(\xi) \neq 0$)

In these cases we set $U_N(\xi) = U(\xi)$. Therefore $\alpha_2 = \alpha_3$. For α_1 we have to differentiate between the cases where it is positive, negative or zero.

A.1 Wedge flows ($\alpha_1 = 1$)

If α_1 is positive, then without loss of generality we can set $\alpha_1 = 1$, since, in the relation between α_1 and $\bar{\delta}$ from Eq. (7.13), the thickness scale $\bar{\delta}$ is only fixed up to a numerical factor. With $\alpha_2 = \alpha_3 = \beta$ it then follows that

$$f''' + ff'' + \beta(1 - f'^2) = 0 \quad (7.15)$$

with the boundary conditions

$$\eta = 0 : \quad f = 0, f' = 0; \quad \eta \rightarrow \infty : \quad f' = 1. \quad (7.16)$$

Equation (7.15) was first stated by V.M. Falkner; S.W. Skan (1931) and for this reason is also called the Falkner–Skan equation. The solutions and their dependence on β were also later examined by D.R. Hartree (1937). We will come back to this in the next section. As it is easy to see by insertion, the two equations from Eq. (7.13)

$$\frac{\bar{\delta}}{V} \frac{d}{d\xi}(U\bar{\delta}) = 1; \quad \frac{\bar{\delta}^2}{V} \frac{dU}{d\xi} = \beta \quad (7.17)$$

have the solutions

$$\frac{U}{V} = B\xi^m; \quad \bar{\delta} = \sqrt{\frac{2}{B(m+1)}} \xi^{\frac{1-m}{2}} \quad (7.18)$$

with the following relation between m and β :

$$m = \frac{\beta}{2-\beta}; \quad \beta = \frac{2m}{m+1}. \quad (7.19)$$

Here the case for $\beta = 2$ was excluded. For this it is found that

$$\frac{U}{V} = B \exp(2p\xi); \quad \bar{\delta} = \sqrt{\frac{1}{Bp}} \exp(-p\xi) \quad (\beta = 2, m \rightarrow \infty). \quad (7.20)$$

If we combine Eqs. (7.7) and (7.8), we acquire the dimensional representation of the *similarity variable* η

$$\eta = y \sqrt{\frac{m+1}{2} \frac{U}{\nu x}} = y \sqrt{\frac{1}{2-\beta} \frac{U}{\nu x}} \quad (\beta \neq 2). \quad (7.21)$$

By choosing the constant B in Eq. (7.18), we fix the reference velocity V . For instance, with $B = 1$, V is equal to the velocity U at the position $\xi = 1$, i.e. at $x = l$. Since the origin of the coordinate system can be chosen arbitrarily, we could have set $\xi - \xi_0$ (where ξ_0 is an arbitrary constant) instead ξ into Eq. (7.18).

The result of these considerations is therefore that *similar* solutions of the boundary-layer equations are obtained if the velocity distribution $U(x)$ of the inviscid outer flow is a *power law*. Such potential flows do indeed occur at wedge shaped bodies, and are thus called *wedge flows*. From Fig. (7.2) we see that we must differentiate between positive and negative powers. The flows past a flat plate at zero incidence ($m = 0, \beta = 0$) and close to a stagnation point ($m = 1, \beta = 1$) which we have already treated are special cases of wedge flows. In the plate boundary layer the Falkner-Skan equation reduces to Eq. (6.49); in the stagnation-point flow to Eq. (5.37).

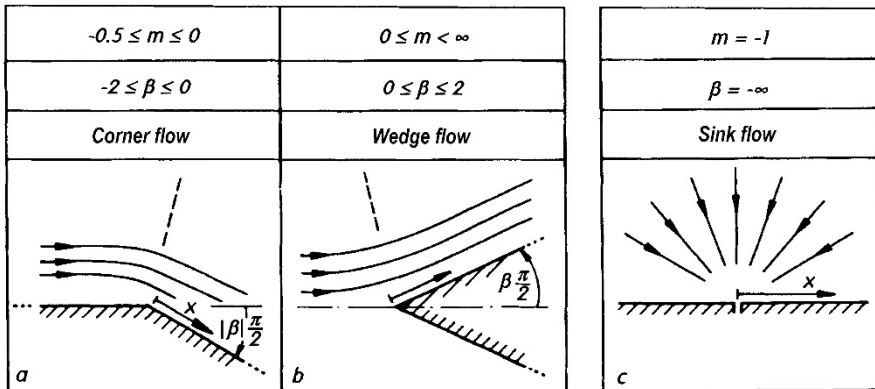


Fig. 7.2 a-c. Different potential flows with $U \sim \xi^m$ at the wall; $m = \beta/(2-\beta)$; $\beta\pi/2 \equiv$ half wedge angle for wedge flows

A.2 Reversed wedge flows ($\alpha_1 = -1$)

With $\alpha_2 = \alpha_3 = -\beta$ it follows from Eq. (7.14) that

$$f''' - f f'' - \beta(1 - f'^2) = 0.$$

Therefore from Eq. (7.13) we find

$$\frac{U}{V} = -B\xi^m; \quad \bar{\delta} = \sqrt{\frac{2}{B(m+1)}} \xi^{\frac{1-m}{2}},$$

where β and m again have the same relation as in Eq. (7.19). The flow now moves towards the origin $\xi = 0$. The outer flow is a wedge flow where the sign of the velocity is changed. Such flows arise as secondary flows at walls in the neighbourhood of moving plates ($m = -1/2$), free jets ($m = -2/3$), wall jets ($m = -3/4$) or sink flows ($m = -1/3$), cf. S. Haas; W. Schneider (1997), as well as in nozzles with contoured walls. It is mainly accelerated flows ($m < 0$) which are physically important. In the case of retarded flows ($m > 0$), velocity profiles with backflow generally occur, see F.M. White (1974), p. 284.

A.3 Flow in a convergent channel (sink flow), $\alpha_1 = 0$

If $\alpha_1 = 0$, we can, without loss of generality, set $\alpha_2 = \alpha_3 = 1$. Thus it follows from Eq. (7.14) that

$$f''' + 1 - f'^2 = 0. \quad (7.22)$$

In this case, we obtain from Eq. (7.13)

$$U(x) = -\frac{a}{x}; \quad \bar{\delta} \sqrt{\frac{V}{al}} x; \quad \eta = y \sqrt{\frac{-U}{\nu x}} = \frac{y}{x} \sqrt{\frac{a}{\nu}}. \quad (7.23)$$

This $U(x)$ distribution is, for $a > 0$, that of the flow in a convergent channel (nozzle) with flat walls (*sink flow*), cf. Fig. 7.2.

With the stream function

$$\psi(x, y) = -\sqrt{\nu a} f(\eta) \quad (7.24)$$

we find the velocity components

$$u = U f'(\eta); \quad v = -\sqrt{\nu a} \frac{\eta}{x} f'(\eta). \quad (7.25)$$

The boundary conditions to Eq. (7.22) are

$$\eta = 0 : \quad f' = 0; \quad \eta \rightarrow \infty : \quad f' = 1, \quad f'' = 0. \quad (7.26)$$

The condition $f''(\infty) = 0$ is in principle unnecessary since Eq. (7.22) can be considered as a second-order differential equation for the function $f'(\eta)$. This case can be interpreted as a wedge flow with the particular exponent $m = -1$ ($\beta \rightarrow -\infty$). If we differentiate Eq. (7.22) with respect to η and set $f'(\eta) = F(\eta)$, it follows that

$$F''' - 2FF' = 0 \quad (7.27)$$

with the boundary conditions

$$\eta = 0 : \quad F = 0; \quad \eta \rightarrow \infty : \quad F = 1, \quad F' = 0. \quad (7.28)$$

This differential equation has already been treated when we considered the exact solutions of the Navier-Stokes equations in Sect. 5.1.2. In this case a closed solution can be given, cf. Eq. (5.29). This solution was first presented by K. Pohlhausen (1921).

B Boundary layers without outer flow ($U(\xi) = 0$)

It may at first seem unusual to consider the boundary-layer equations when there is no outer flow. However, in Chap. 5 we already met cases of frictional layers which, in the limiting case $\text{Re} \rightarrow \infty$ ($\nu \rightarrow 0$), yield outer flows which are at rest: the frictional layers then arise via the motion of the wall (a rotating disk, a wall suddenly set into motion or an oscillating wall) or through the injection of momentum in the form of a Dirac delta function (free jet). In cases such as these, the complete Navier-Stokes equations are again reduced to the boundary-layer equations for $\text{Re} \rightarrow \infty$. Similar solutions are then obtained from a differential equation which comes from setting $\alpha_2 = 0$ (since $U = 0$) and $\alpha_1 = 1$ (fixing the thickness scale $\bar{\delta}$) in Eq. (7.14):

$$f''' + f f'' - \alpha_3 f'^2 = 0. \quad (7.29)$$

The following examples are worth mentioning:

$\alpha_3 = 0$: boundary layer at the moving flat plate ($U_N = U_w$)

$\alpha_3 = -1$: free jet ($U_N \sim u_{\max}$, $V \sim K/\nu$)

$\alpha_3 = -2$: wall jet ($U_N \sim u_{\max}$, $V \sim KQ_b/\nu^2$).

The meaning of the function U_N is given in each case in brackets. Note in particular that the reference velocity V for the latter two examples also depends on the viscosity, so that $V \rightarrow \infty$ for $\nu \rightarrow 0$, a point which will be discussed in more detail in the next sections.

7.2.2 Wedge Flows

As mentioned in the last section, the flows at wedges lead to an important class of *similar* solutions of the boundary-layer equations. The velocities of wedge flows obey the power law

$$U(x) = a x^m. \quad (7.30)$$

Using the trial solutions

$$u = a x^m f'(y) = U(x) f'(\eta), \quad (7.31)$$

$$v = -\sqrt{\frac{m+1}{2} \nu a x^{m-1}} \left(f + \frac{m-1}{m+1} \eta f' \right), \quad (7.32)$$

$$\eta = y \sqrt{\frac{m+1}{2} \frac{a}{\nu} x^{m-1}} = y \sqrt{\frac{m+1}{2} \frac{U}{\nu x}} \quad (7.33)$$

we obtain the ordinary differential equations (7.15) with the boundary conditions (7.16) for the dimensionless stream function $f(\eta)$. Equation (7.19) defines the free parameter β .

Some important numerical values of these solutions are given in the next chapter in Table 8.1. Velocity profiles $f'(\eta)$ for different values of β (or equivalently m) are given in Fig. 7.3. These solutions were examined in great detail by D.R. Hartree (1937) and hence are called *Hartree profiles*. For accelerated flows ($m > 0$, $\beta > 0$),

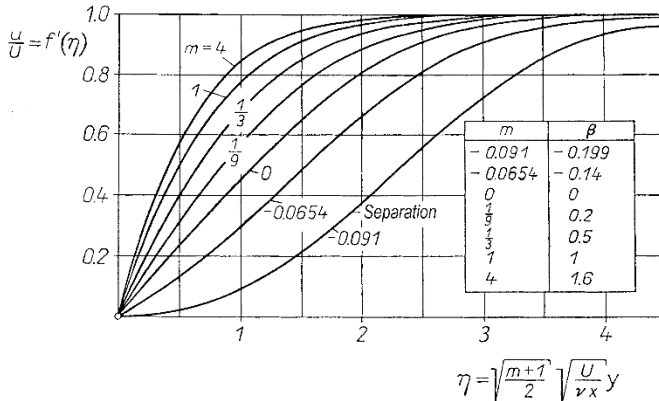


Fig. 7.3. Velocity distribution in the laminar boundary layer of the wedge flow $U(x) = ax^m$. Relation (7.19) holds between the wedge angle β (Fig. 7.2) and m

we obtain velocity profiles without a point of inflection; for retarded flows ($m < 0, \beta < 0$), profiles with a point of inflection. Some important special cases are the flat plate flow ($m = 0$) and the stagnation-point flow ($m = 1$).

Another case worth pointing out is that where $m = 1/3, \beta = 1/2$. Applying the transformation $f(\eta) = \sqrt{2}\varphi(\xi)$, $\eta = \sqrt{2}\xi$ to Eq. (7.15) we find the differential equation

$$\varphi''' + 2\varphi\varphi'' + 1 - \varphi'^2 = 0 \quad (7.34)$$

for $\varphi(\xi)$. This is in agreement with Eq. (5.68) for the axisymmetric stagnation-point flow. Computing the boundary layer of the axisymmetric stagnation-point flow allows us to work back to that for the plane wedge flow with wedge angle $\pi\beta = \pi/2$ (right-angled wedge). We will look at a more general relation between plane and axisymmetric boundary layers in Sect. 12.1.2.

The case $m = -0.091, \beta = -0.199$ corresponds to the velocity profile with vanishing wall shear stress (separation). From the small numerical value $m = -0.091$ we see that the laminar boundary layer can only withstand a very small retardation of the flow (or equivalently a very small adverse pressure gradient) before separation takes place.

A comprehensive discussion of the solution manifold of Eq. (7.15) has been carried out by K. Stewartson (1954). He showed that there exists a further solution as well as the Hartree solution within the region of pressure increase ($-0.199 < \beta < 0$). In this solution, the velocity profile demonstrates backflow, see Fig. 10.3 and Fig. 11.8. A detailed look at the solutions with backflow for $\beta \rightarrow 0$ is given by S.N. Brown; K. Stewartson (1966) and S.N. Brown (1966).

The equations (7.15) and (7.16) have an even larger manifold of solutions if a velocity excess is allowed into the velocity profile, cf. P.A. Libby; T.M. Liu (1967) and F.M. White (1974), p. 280. K. Nickel (1973) showed that such velocity excesses cannot arise naturally in the boundary layer, but they can be generated by, for example, injecting a jet into the boundary layer. Similar solutions for such *wall jets with outer flow* have been given by J. Steinheuer (1968b). It is seen there that, in the limiting case of vanishing outer flow, the simple wall jet flow appears. This will be treated in Sect. 7.2.7.

7.2.3 Flow in a Convergent Channel

The velocity distribution $U = -a/x$ is found in the case of sink flow, cf. Fig. 7.2c. A sector from the sink flow can be interpreted as a potential flow in a convergent channel (wedge nozzle). The flow at a channel wall with the boundary layer which it forms is shown in Fig. 7.4. The dimensionless stream function $f(\eta)$ has to satisfy Eq. (7.22) and the boundary conditions (7.26). After differentiation with respect to η , and using $f'(\eta) = F(\eta)$, we obtain the differential equation (5.27) which possesses a closed solution corresponding to Eq. (5.29). Therefore the velocity profile is

$$\frac{u}{U} = f'(\eta) = 3 \tanh^2 \left(\frac{\eta}{\sqrt{2}} + \operatorname{artanh} \sqrt{\frac{2}{3}} \right) - 2 \quad (7.35)$$

with

$$\eta = \frac{y}{x} \sqrt{\frac{a}{\nu}} = y \sqrt{\frac{-U}{x\nu}} . \quad (7.36)$$

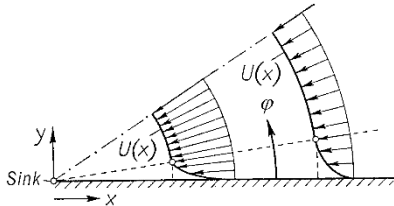


Fig. 7.4. Flow in a convergent channel (nozzle); sink flow

From $f''_w = 2/\sqrt{3}$ we can determine the wall shear stress. At $\eta_{99} = 3.3$ we find $f' = 0.99$. The boundary-layer thickness

$$\delta_{99} = \eta_{99} \sqrt{\frac{\nu}{a}} x = 3.3 \sqrt{\frac{\nu}{a}} x \quad (7.37)$$

is proportional to the coordinate x . In this case we can use Eq. (7.25) to determine the displacement velocity

$$v_\infty(x) = \sqrt{\nu a} \frac{\eta}{x} = U \sqrt{\frac{\nu}{a}} \eta = U \frac{y}{x} , \quad (7.38)$$

that is, a negative quantity. However, along with the $U(x)$ distribution, it forms precisely the radial velocity field of the inviscid sink flow. Here the lines $\eta = \text{const}$ are straight lines through the origin ($y/x = \text{const}$). Therefore in this example the inviscid flow outside the boundary layer remains unaffected, i.e. there is *no* displacement effect. If, instead of Cartesian coordinates, we had used polar coordinates (r, φ) as in Sect. 5.1.2, the circumferential component would always have been zero. As will be shown in Sect. 14.2, there are *optimal coordinates* which present the displacement effect of boundary layers in a particularly skillful manner. In the case of the boundary layer in a convergent channel, those optimal coordinates are polar coordinates.

7.2.4 Mixing Layer

Another flow not yet discussed which does not take place at a wall and where the boundary-layer equations are valid for high Reynolds numbers is the laminar *mixing layer* between two parallel flows with different velocities. The problem is sketched in Fig. 7.5: two initially unperturbed parallel flows with velocities U and λU interact, as a consequence of friction, with one another from the position $x = 0$ downstream. For low values of the viscosity ν , the transition from the velocity U to the velocity λU takes place in a thin mixing zone, in which the transverse component v of the velocity is small compared to the longitudinal velocity u . Thus the boundary-layer equation without the pressure term is valid. Since there is no characteristic length in this problem, *similar* solutions are found. If we specialise the equations (7.30) to (7.33) for $m = 0$, we find the same differential equation for $f(\eta)$ as for the boundary layer at a flat plate at zero incidence:

$$f''' + ff'' = 0. \quad (7.39)$$

However the boundary conditions are different. Initially we find

$$\eta \rightarrow +\infty : \quad f' = 1; \quad \eta \rightarrow -\infty : \quad f' = \lambda. \quad (7.40)$$

A third necessary boundary condition is missing. J.B. Klemp; A. Acrivos (1972) have shown that the location of the dividing streamline remains indeterminate if both streams are subsonic and semi-infinite in extent. The only exception is the case $\lambda = 0$.

In spite of this result, however, the problem is not necessarily ill posed, because it might still be possible to consider the flow within the leading-edge region in close proximity of the origin. This will then lead to a third boundary condition for the asymptotic solution far downstream.

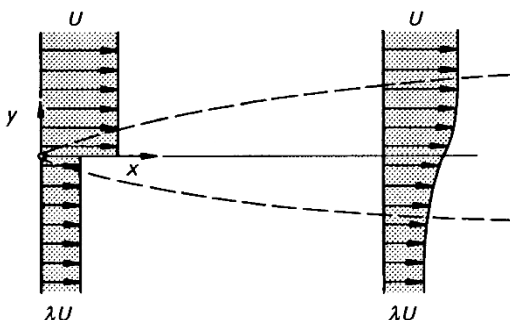


Fig. 7.5. Velocity profile in the mixing layer

The special case of the mixing layer with $\lambda = 0$ is also called the *jet boundary* or *half jet*, since it describes the transition to surroundings at rest. The third boundary condition for the differential equation (7.39) is

$$f''(\eta \rightarrow \infty) = 0. \quad (7.41)$$

Numerical results for this jet-boundary solution are given in Table 7.1. It turns out that the v -component is zero at the upper edge and therefore the approaching parallel flow remains unaffected. This means, however, that the zero streamline, i.e. the dividing streamline, must be displaced ever further downwards with increasing distance x , since more and more fluid is retarded above the dividing streamline. Because of condition (7.41) the position of the dividing streamline (DS) is given by

$$y_{DS} = -0.3740 \sqrt{\frac{2vx}{U}}. \quad (7.42)$$

The entrainment velocity in surroundings at rest is found by setting $f(-\infty) = -0.8757$ to be

$$v(\eta \rightarrow -\infty) = 0.8757 \sqrt{\frac{\nu U}{2x}}. \quad (7.43)$$

In Section 11.2.4 it is mentioned that this special solution corresponds to the flat plate solution with very high blowing such that the boundary layer lifts off the plate (see Fig. 11.9).

The first solutions for the mixing layer have been given by D.R. Chapman (1949) and R.C. Lock (1951). This solution is of importance for the computation of separated flows behind blunt bodies, cf. M. Tanner (1973).

Table 7.1. Numerical results for the jet-boundary solution (mixing layer with $\lambda = 0$), position of the dividing streamline at $\eta = -0.3740$

η	f	f'	f''
$\rightarrow \infty$	η	1	0
0	0.2392	0.6914	0.2704
-0.3740	0	0.5872	0.2825
$\rightarrow -\infty$	-0.8757	0	0

7.2.5 Moving Plate

The boundary layer at a moving plate was already mentioned in the last section. If a flat plate in surroundings at rest is moved with constant velocity U_w as in Fig. 7.6, the no-slip condition means that a boundary layer exists close to the wall.

Since there is no characteristic length, there are similar solutions. Again Eq. (7.39) is valid, this time with the boundary conditions

$$\eta = 0 : f = 0, f' = 1; \quad \eta \rightarrow \infty : f' = 0. \quad (7.44)$$

Here it is important that the moving plate emerges from a wall, see Fig. 7.6. This fixes the origin of the coordinate system and has an analog function to the leading edge of a flat plate at zero incidence in a flow. Both permit only then a steady solution in a spatially fixed coordinate system

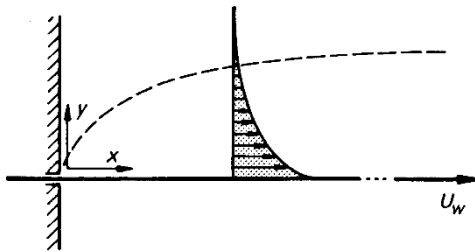


Fig. 7.6. Velocity profile at a moving plate

From the solution of Eq. (7.39) we find:

$$f''_w = -0.6276; f(\infty) = 1.1426. \quad (7.45)$$

The wall shear stress thus follows as

$$-\frac{\tau_w}{\rho U_w^2} = 0.44375 \sqrt{\frac{\nu}{U_w x}}. \quad (7.46)$$

In addition, as in the case of the mixing layer, there is an *entrainment* effect with the velocity

$$v_\infty = -0.808 \sqrt{\frac{\nu U_w}{x}}. \quad (7.47)$$

This entrainment velocity ensures that the volume flux increases downstream in the boundary layer.

7.2.6 Free Jet

A further example of a flow without an outer flow to which the boundary-layer theory can be applied is the flow of a free jet in surroundings at rest. Since there is also no bounding wall, this is a free boundary layer or free shear layer. Thence comes the name *free jet*, cf. Fig. 7.7.

The *similar* solutions which exist satisfy the equation, see Eq. (7.29)

$$f''' + ff'' - \alpha_3 f'^2 = 0 \quad (7.48)$$

with the boundary conditions

$$\eta \rightarrow -\infty : f' = 0; \quad \eta = 0 : f = 0; \quad \eta \rightarrow +\infty : f' = 0. \quad (7.49)$$

We first observe that, in this example, the differential equation and all the boundary conditions are *homogeneous*, and thus $f(\eta) = 0$ is a solution of the system. This *trivial solution* is obviously not the desired solution, and so at least one other non-trivial solution must exist, as a so-called *eigen-solution* of the system. For this to exist, α_3 must take on a particular value, the *eigenvalue*. If we integrate Eq. (7.48) with respect to η from $\eta \rightarrow -\infty$ to $\eta \rightarrow +\infty$, and use the boundary conditions Eq. (7.49) we obtain

$$(1 + \alpha_3) \int_{-\infty}^{+\infty} f'^2 d\eta = 0$$

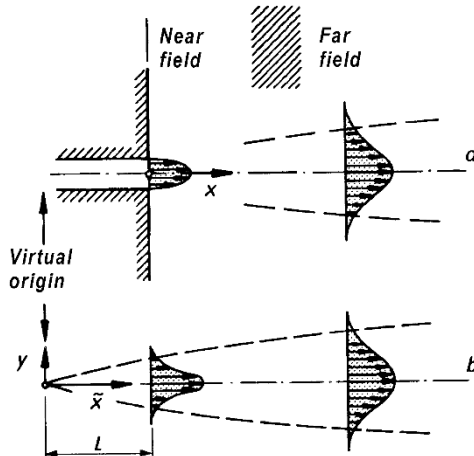


Fig. 7.7. Velocity profile of the free jet, $\tilde{x} = x + L$
 (a) parabola shaped profile at the outlet
 (b) fictitious replacement flow with virtual origin

and therefore the eigenvalue $\alpha_3 = -1$. The equation thus given by $f''' + ff'' + f'^2 = 0$ has the simple analytic solution

$$f(\eta) = 2 \tanh \eta; \quad f'(\eta) = 2(1 - \tanh^2 \eta). \quad (7.50)$$

With the constants $\alpha_1 = 1$ and $\alpha_3 = -1$, the functions $U_N(\xi)$ and $\bar{\delta}(\xi)$ can be determined from Eq. (7.13), and thus η from Eq. (7.7). We find

$$\frac{U_N}{V} = 3 \left(\frac{\nu}{Vx} \right)^{1/3}, \quad \eta = \frac{y}{x} \left(\frac{Vx}{\nu} \right)^{1/3}. \quad (7.51)$$

The reference velocity V must now be worked out. Since, at first, there exists no prescribed velocity for this flow, a connection will have to be ascertained between V and the characteristic quantities for the flow under consideration. In the case of the free jet flow this is the *jet momentum*. Since the pressure is the same everywhere in the flow field, the momentum flux \dot{I} in the jet must be independent of the length x . The *kinematic momentum flux* referred to the width b is found to be

$$K = \frac{\dot{I}}{\varrho b} = \int_{-\infty}^{+\infty} u^2 dy = 9\nu V \int_{-\infty}^{+\infty} f'^2(\eta) d\eta = 48\nu V. \quad (7.52)$$

We emphasise that the reference velocity

$$V = \frac{K}{48\nu} \quad (7.53)$$

is dependent on the kinematic viscosity and tends to infinity for $\nu \rightarrow 0$. Equation (7.53) can also be determined, up to a numerical constant, through dimensional analysis.

With this reference velocity, Eqs. (7.7), (7.10) and (7.11) are used to obtain the velocity distribution

$$\begin{aligned} u &= 0.4543 \left(\frac{K^2}{\nu x} \right)^{1/3} (1 - \tanh^2 \eta) \\ v &= 0.5503 \left(\frac{K\nu}{x^2} \right)^{1/3} [2\eta(1 - \tanh^2 \eta) - \tanh \eta] \\ \eta &= 0.2753 \left(\frac{K}{\nu^2} \right)^{1/3} \frac{y}{x^{2/3}} . \end{aligned} \quad (7.54)$$

The “entrainment velocity” of the jet has the value

$$v_\infty = -v_{-\infty} = -0.5503 \left(\frac{K\nu}{x^2} \right)^{1/3} . \quad (7.55)$$

The volume flux referred to the width b

$$Q_b(x) = \frac{Q(x)}{b} = \int_{-\infty}^{+\infty} u dy = 3.302(K\nu x)^{1/3} \quad (7.56)$$

increases, due to the entrainment effect, continually with the length coordinate x . On the other hand, the (“kinematic”) kinetic energy referred to the width

$$E = \frac{1}{2} \int_{-\infty}^{+\infty} u^3 dy = 0.0086 \left(\frac{K^5}{\nu x} \right)^{1/3} \quad (7.57)$$

decreases with the length x , precisely so much that

$$EQ_b = 0.028 K^2 . \quad (7.58)$$

The “width” of the free jet is often taken to be the distance of the points with half the maximum velocity (“half-value width”). Using $\tanh^2 0.881 = 0.5$, Eq. (7.54) yields the half-value width of

$$y_{0.5} = 3.20 \left(\frac{\nu^2}{K} \right)^{1/3} x^{2/3} . \quad (7.59)$$

This increases with the length x and is proportional to $\nu^{2/3}$.

This last result is particularly worth taking note of because previously all thicknesses of boundary layers have been proportional to $\nu^{1/2}$. This difference between the free jet “boundary layer” and all the other boundary layers has to do with the fact that in the case of the free jet there is no prescribed velocity, rather a prescribed jet momentum. Therefore the *boundary-layer transformation* described in Chap. 6 will now also transform the velocity u^* . Instead of Eq. (6.6) the boundary-layer transformation for the free jet now reads

$$\bar{y} = y^* \text{Re}^p, \quad \bar{u} = u^* \text{Re}^q, \quad \bar{v} = v^* \text{Re}^r . \quad (7.60)$$

Inserting this into Eq. (6.3) and comparing the highest powers of Re delivers

$$p = r - q; \quad 2p = 1 - q. \quad (7.61)$$

Since the jet momentum is independent of the length x , it follows from Eq. (7.52) that

$$2q + p = 1 \quad (7.62)$$

with the results $p = q = 1/3$, $r = 2/3$.

The similar solution given here describes the *far field* of a free jet. The free jet flow is sketched in Fig. 7.7a. Here it has been assumed that the jet has approximately the profile of a fully developed channel flow at the outlet in the wall, that is, does not yet possess the profile it demonstrates further downstream. However, in the far field, similar profiles are to be expected, since the effect of the start of the jet dies away. Therefore the similar solution shown is a fictitious flow, although one which does describe a real flow in the far field. Now the origin of this fictitious flow will in general not be at $x = 0$, but rather at the *virtual origin* at $x = -L$ as shown in Fig. 7.7b. In all formulae x must thus be replaced by $\tilde{x} = x + L$.

Measurements by E.N. Andrade (1939) have confirmed the theoretical results very well. The jet is laminar up until about $\text{Re} = 30$, where the Reynolds number is referred to the average outlet velocity and the slit height.

7.2.7 Wall Jet

A wall jet occurs when a jet flows along a wall on one side, while on the other side mixing takes place with the surroundings at rest, Fig. 7.8. Here there is also a *similar* solution, which again satisfies Eq. (7.48), this time with the boundary conditions

$$\eta = 0 : \quad f = 0, \quad f' = 0; \quad \eta \rightarrow \infty : \quad f' = 0. \quad (7.63)$$

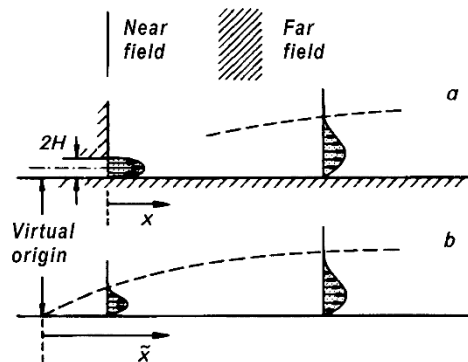


Fig. 7.8. Velocity profile of the wall jet, $\tilde{x} = x + L$
 (a) parabola shaped profile at the outlet
 (b) fictitious replacement flow with virtual origin

This is again an *eigenvalue* problem. In order to determine the eigenvalue α_3 we first integrate Eq. (7.29) from η to ∞ . This yields

$$f'' + ff' + (1 + \alpha_3) \int_{\eta}^{\infty} f'^2 dy = 0. \quad (7.64)$$

We now multiply this equation by f' and then integrate from 0 to ∞ . Similarly, Eq. (7.29) is multiplied by f and then integrated from 0 to ∞ . The combination of these two equations leads to the relation

$$(2 + \alpha_3) \int_0^\infty f f'^2 d\eta = 0. \quad (7.65)$$

Since the integral is positive, it follows that the eigenvalue is $\alpha_3 = -2$. The following implicit analytic solution of Eq. (7.48) with $\alpha_3 = -2$ and the boundary conditions Eq. (7.63) was given by N.I. Akamnov (1953) and M.B. Glauert (1956b):

$$\eta = \ln \frac{\sqrt{1 + \sqrt{f} + f}}{1 - \sqrt{f}} + \sqrt{3} \arctan \frac{\sqrt{3f}}{2 + \sqrt{f}}. \quad (7.66)$$

Here the function $f(\eta)$ has been normalised with $f(\infty) = 1$. Because the boundary conditions are homogeneous, the solution is initially not unique, since for any solution $f(\eta)$, arbitrarily many other solutions of the form $Af(A\eta)$ exist. Applying this norm ensures that the function $f(\eta)$ lies in the interval $0 \leq f(\eta) \leq 1$. Important numerical values pertaining to this solution are

$$f'_{\max} = 2^{-5/3} = 0.315 \quad \text{for } \eta = 2.029; \quad f''_w = \frac{2}{9}. \quad (7.67)$$

With the constants $\alpha_1 = 1$ and $\alpha_3 = -2$, the functions $U_N(\xi)$ and $\bar{\delta}(\xi)$ can be determined from Eq. (7.13) and hence η from Eq. (7.7):

$$\frac{U_N}{V} = 4 \left(\frac{\nu}{Vx} \right)^{1/2}; \quad \eta = \frac{y}{x} \left(\frac{Vx}{\nu} \right)^{1/4}. \quad (7.68)$$

We now have to determine the reference velocity V . In contrast to the free jet, in the case of the wall jet the jet momentum is no longer independent of the length x , rather, because of the wall shear stress, it decreases with increasing x . However it turns out that in the case of the wall jet the product of the jet momentum flux and the volume flux is a constant. We obtain

$$KQ_b = \left(\int_0^\infty u^2 dy \right) \left(\int_0^\infty u dy \right) = \frac{128}{9} \nu^2 V = \frac{20}{9} F. \quad (7.69)$$

The wall jet constant F introduced by M.B. Glauert is given by

$$F = \frac{32}{5} \nu^2 V = \int_0^\infty u \left(\int_y^\infty u^2 dy \right) dy. \quad (7.70)$$

Thus the following results for the wall jet flow are found:

$$\tau_w = 0.221 \varrho \left(\frac{F^3}{\nu x^5} \right)^{1/4}, \quad (7.71)$$

$$u_{\max} = 0.498 \left(\frac{F}{x\nu} \right)^{1/2}, \quad (7.72)$$

$$y_{u_{\max}} = 3.23 \left(\frac{\nu^3 x^3}{F} \right)^{1/4}, \quad (7.73)$$

$$v_\infty = -0.629 \left(\frac{F\nu}{x^3} \right)^{1/4}, \quad (7.74)$$

$$Q_b = 2.51(F\nu x)^{1/4}. \quad (7.75)$$

$$K = 0.884 \left(\frac{F^3}{\nu x} \right)^{1/4}, \quad (7.75a)$$

7.3 Coordinate Transformation

7.3.1 Görtler Transformation

The following coordinate transformation was applied to the boundary-layer equations Eqs. (7.4) and (7.5) by H. Görtler (1952b):

$$\xi = \frac{1}{\nu} \int_0^x U(x) dx; \quad \eta = \frac{U(x)}{\nu \sqrt{2\xi}} y; \quad \psi(x, y) = \nu \sqrt{2\xi} f(\xi, \eta), \quad (7.76)$$

thus leading to the following partial differential equation for the dimensionless “referred” stream function $f(\xi, \eta)$:

$$f_{\eta\eta\eta} + f f_{\eta\eta} + \beta(\xi)(1 - f_\eta^2) = 2\xi(f_\eta f_{\xi\eta} - f_\xi f_{\eta\eta}) \quad (7.77)$$

with the so-called *principal function*

$$\beta(\xi) = 2 \frac{U'(x)}{U^2(x)} \int_0^x U(x) dx. \quad (7.78)$$

The boundary conditions here are

$$\eta = 0 : \quad f = 0, \quad f_\eta = 0; \quad \eta \rightarrow \infty : \quad f_\eta = 1.$$

The numerical values pertaining to the outer flow now no longer appear in the boundary conditions, but only in the principal function $\beta(\xi)$. For the wedge function with $U(x) \sim x^m$, the principal function is reduced to the constant $\beta = 2m/(m+1)$ from Eq. (7.19), whereby Eq. (7.77) becomes the Falkner-Skan equation Eq. (7.15) for similar solutions.

One considerable advantage in using Eq. (7.77) instead of Eq. (6.38) for the boundary-layer computation has to do with the fact that in general the transformation Eq. (7.76) gets rid of the singularity at the leading edge. A second is that, to first order, the coordinate η takes the growth of the boundary-layer thickness in the longitudinal direction into account, a point of immense advantage in numerical computation. Therefore many numerical methods for the computation of laminar boundary layers use Eq. (7.77), cf. H. Schlichting (1982), p. 188.

7.3.2 v. Mises Transformation

One remarkable transformation of the boundary-layer equations worth taking note of was given by R. v. Mises (1927). Instead of the Cartesian coordinates x and y , the independent variables used are x and the stream function ψ . Substituting

$$u = \frac{\partial \psi}{\partial y}, \quad v = -\frac{\partial \psi}{\partial x}$$

into Eqs. (7.1) and (7.5), and introducing, instead of x , y , the new coordinates $\xi = x$, $\eta = \psi$, we obtain

$$\begin{aligned} \frac{\partial u}{\partial x} &= \frac{\partial u}{\partial \xi} \frac{\partial \xi}{\partial x} + \frac{\partial u}{\partial \eta} \frac{\partial \eta}{\partial x} = \frac{\partial u}{\partial \xi} - v \frac{\partial u}{\partial \psi}, \\ \frac{\partial u}{\partial y} &= \frac{\partial u}{\partial \xi} \frac{\partial \xi}{\partial y} + \frac{\partial u}{\partial \eta} \frac{\partial \eta}{\partial y} = 0 + u \frac{\partial u}{\partial \psi}. \end{aligned}$$

Thus from Eq. (7.1) we then acquire

$$u \frac{\partial u}{\partial \xi} + \frac{1}{\varrho} \frac{dp}{d\xi} = \nu u \frac{\partial}{\partial \psi} \left(u \frac{\partial u}{\partial \psi} \right).$$

Introducing the “total head”

$$g = p + \frac{1}{2} \varrho u^2, \quad (7.79)$$

where the small amount $\varrho v^2/2$ can be neglected, we find, reverting to the symbol x for ξ

$$\frac{\partial g}{\partial x} = \nu u \frac{\partial^2 g}{\partial \psi^2}. \quad (7.80)$$

Here we can also set

$$u = \sqrt{\frac{2}{\varrho} [g - p(x)]}.$$

Equation (7.80) is now a differential equation for the total head $g(x, \psi)$. The boundary conditions are:

$$g = p(x) \text{ for } \psi = 0 \quad \text{and} \quad g = p(x) + \frac{\varrho}{2} U^2 = \text{const} \text{ for } \psi = \infty.$$

The flow representation in the x - y plane can be found if we use the equation

$$y = \int \frac{d\psi}{u} = \sqrt{\frac{\varrho}{2}} \int_{\psi=0}^{\psi} \frac{d\psi}{\sqrt{g - p(x)}}$$

to transform from ψ to y . Equation (7.80) is related to the heat conduction equation. The one-dimensional heat conduction equation (e.g. for a bar where

T denotes the temperature, t the time, x the length coordinate and a the thermal diffusivity, cf. Chap. 3) is

$$\frac{\partial T}{\partial t} = a \frac{\partial^2 T}{\partial x^2}. \quad (7.81)$$

However, the transformed boundary-layer equation, unlike Eq. (7.81), is nonlinear, because the thermal diffusivity is replaced by νu , which depends on the independent variable x , as well as on the dependent variable g .

At the wall with $\psi = 0$, $u = 0$, $g = p$, Eq. (7.80) exhibits a rather unpleasant singularity. The left hand side becomes $\partial g / \partial x = dp / dx \neq 0$. On the right hand side we have $u = 0$ and thus $\partial^2 g / \partial \psi^2 = \infty$. This is troublesome for the numerical evaluation and is intimately connected to the compatibility condition at the wall, Eq. (7.2). L. Prandtl (1938), who deduced this transformation long before the appearance of v. Mises work, presented an incisive discussion of Eq. (7.80), but never published it¹.

Practical examination of Eq. (7.80) was carried out by H.J. Luckert (1933) when he investigated the example of the Blasius plate boundary layer. A critical discussion of these results is to be found in L. Rosenhead; J.H. Simpson (1936).

For the boundary layer with pressure increase, the v. Mises equation (7.80) has been integrated numerically by A.R. Mitchell; J.Y. Thomson (1958). Here the singularity at the wall was supported by a suitable series expansion of the velocity profile close to the wall, taking the compatibility conditions at the wall into account.

7.3.3 Crocco Transformation

It was suggested by L. Crocco (1946) that the quantity $\partial u / \partial y$ could be used instead of y as an independent variable. This has the advantage that the region of integration is then finite. However here again singularities appear, cf. W. Schönauer (1963).

7.4 Series Expansion of the Solutions

7.4.1 Blasius Series

The “similar” solutions of the boundary-layer equations dealt with up to now comprise only a relatively small class of solutions. It is already a long time ago that H. Blasius (1908) presented a computation method for general boundary layers with arbitrary velocity distributions $U(x)$ of the outer flow. This was based on a series expansion of the solution in powers of x . It is thus called

¹ See the footnote in L. Prandtl (1938) on p. 79 as well as the letter by L. Prandtl to ZAMM Vol. 8 (1928, p. 249).

the Blasius series. This method was later further developed by K. Hiemenz (1911) and L. Howarth (1935). Here the velocity distribution $U(x)$ of the outer flow is given as a power series in x , where x is the coordinate measured along the contour of the body. The velocity distribution in the boundary layer is then also written down as such a power series, where the coefficients are still functions of the y coordinate measured at right angles to the wall. L. Howarth succeeded in finding a trial solution for the velocity distribution in the boundary layer such that the y dependent coefficient functions have a universal character, i.e. they are independent of the specific data of the body in the flow. In this manner it was possible to compute these functions "provisionally". The boundary layer of a given body can then be determined quite simply using these once and for all tabulated functions, assuming that the functions have been expanded up to a high enough power.

Nowadays the importance of numerical methods for boundary-layer computation has expanded so much that this has led to the decline of the practical importance of computation via the Blasius series. Therefore we will only present a few results, while for a more complete discussion we recommend H. Schlichting (1965a), p. 145.

For a *symmetric* external flow, let the velocity distribution of the outer flow be given by the series expansion

$$U(x) = u_1 x + u_3 x^3 + u_5 x^5 + \dots . \quad (7.82)$$

The coefficients u_1, u_3, \dots only depend on the geometry of the body and can be assumed to be known. The continuity equation is satisfied by introducing a stream function $\psi(x, y)$. It seems obvious, in analogy to Eq. (7.76), to expand $\psi(x, y)$ too as a power series in x , with coefficients which are dependent on y . The series ansatz is carried out so that the functions which are dependent on y no longer depend on the coefficients u_1, u_3, \dots of the outer flow, and are thus universal. These functions have been computed by A.N. Tifford (1954) up to power x^{11} , cf. H. Schlichting (1965a), p. 148. Using these functions we find the wall shear stress to be

$$\begin{aligned} \tau_w(x) = \varrho u_1 \sqrt{\nu u_1} & \left[x \cdot 1.2326 + 4x^3 \frac{u_3}{u_1} 0.7244 \right. \\ & + 6x^5 \left(\frac{u_5}{u_1} 0.6347 + \frac{u_3^2}{u_1^2} 0.1192 \right) \\ & + 8x^7 \left(\frac{u_7}{u_1} 0.5792 + \frac{u_3 u_5}{u_1^2} 0.1829 + \frac{u_3^3}{u_1^3} 0.0076 \right) \\ & \left. + \dots \right]. \end{aligned} \quad (7.83)$$

Corresponding formulae can also be written down for the displacement thickness $\delta_1(x)$ and other global boundary-layer characteristic quantities.

The region of application of the Blasius series is greatly restricted, because precisely for bodies of interest in practice (e.g. airfoils) many terms in

the series are required, far more than can be tabulated with reasonable computational effort. This has to do with the fact that, for slender bodies, the outer velocity initially increases sharply close to the front stagnation point and then changes only a little beyond this point. Such a function can only be poorly represented by a power series with just a few terms.

A further disadvantage of the Blasius series has to do with the computation of the separation point. i.e. the point where $\tau_w = 0$. If the function $U(x)$ is given, a *singularity* occurs at the separation point. As S. Goldstein (1948b) showed, close to separation we have

$$\lim_{x \rightarrow x_S} \tau_w(x) \sim \sqrt{x_S - x}, \quad (7.84)$$

where x_S denotes the separation point. Therefore the wall shear stress tends to zero with a vertical tangent, and a continuation of the boundary-layer computation beyond the separation point is not possible. The singular behaviour of Eq. (7.84) is impossible to represent via a power series, and thus the Blasius series is imprecise close to the separation point.

The Blasius series has also been extended to unsymmetric cases, i.e. where $U(x)$ also retain the even powers, by L. Howarth (1935). The class of outer flows with

$$U(x) = U_0 - ax^n \quad (n = 1, 2, 3, \dots) \quad (7.85)$$

has been treated by L. Howarth (1938) and I. Tani (1949) with power series expansions. In the simplest case $n = 1$ this can be interpreted as flow in a channel, in which one part has parallel walls (velocity U_0) and the next section is convergent ($a < 0$) or divergent ($a > 0$). If we write Eq. (7.85) for $n = 1$ in the form $U(x) = U_0(1 - x/l)$, this can be construed as a flow along a flat wall which begins at $x = 0$ and which meets a second infinitely extended wall at right angles at $x = l$. This is a kind of “retarded stagnation-point flow” as shown in Fig. 2.10b, with the stagnation point at $x = l$. Worked examples will be discussed in Chap. 8.

7.4.2 Görtler Series

A series expansion for the solution of the boundary-layer equations based on Eq. (7.77) was presented by H. Görtler (1952b) and (1957a). Here it is assumed that the principal function $\beta(\xi)$ can be represented as a power series in ξ . Here too it is possible to give the solution in the form of universal functions, and these have been collected by H. Görtler (1957b). Compared to the Blasius series, the Görtler series demonstrates much better convergence behaviour. Even the first term of the series gives a useable approximation of the boundary layer from the leading edge to much further downstream. This first term is a Hartree profile ($\beta_0 = \beta(\xi = 0)$) from the family of wedge flows. Again worked examples will be presented in Chap. 8.

7.5 Asymptotic Behaviour of Solutions Downstream

In what follows we shall investigate the asymptotic behaviour of boundary-layer solutions far downstream. Here again we deal with series expansions of the solutions, but in this case for large values of x . The main term under consideration in this expansion is the leading term which reflects the asymptotic behaviour of the solution for $x \rightarrow \infty$.

7.5.1 Wake Behind Bodies

As the examples of the mixing layer and the free jet showed, the application of the boundary-layer equations is not necessarily restricted to the presence of fixed walls. They can also be applied when there is a layer with dominating frictional effects in the interior of a flow.

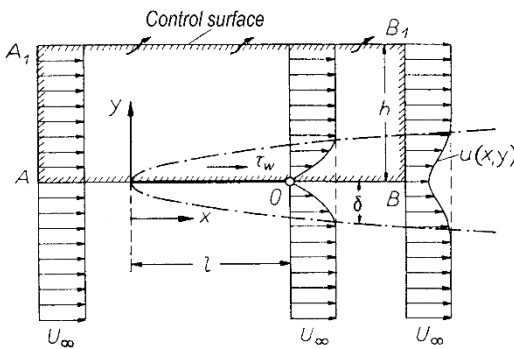


Fig. 7.9. Wake behind a two-dimensional body

The wake flow behind a flat plate of length l as in Fig. 7.9 is also such an example. The two boundary layers on the upper and lower sides coalesce at the trailing edge and further downstream produce a *wake profile*, whose width increases with increasing distance from the body, while the *velocity defect* decreases. On the whole, as we will see later, the shape of the velocity profile in the wake, also called *wind shadow*, is independent of the shape of the body for $x \rightarrow \infty$, up to a scaling factor. The asymptotic development for $x \rightarrow \infty$ has been given by W. Tollmien (1931). Since the magnitude of the velocity defect continually decreases with increasing x , it can be assumed for $x \rightarrow \infty$ that the velocity defect

$$u_1(x, y) = U_\infty - u(x, y) \quad (7.86)$$

is small compared to U_∞ , so that quadratic terms of u_1 and equivalently of v_1 can be neglected. Since the pressure is constant far downstream, we use the

boundary-layer equation (7.4) and insert Eq. (7.86), neglecting the quadratic terms in u_1 and v_1 to obtain

$$U_\infty \frac{\partial u_1}{\partial x} = \nu \frac{\partial^2 u_1}{\partial y^2} \quad (7.87)$$

with the boundary conditions

$$y = 0 : \quad \frac{\partial u_1}{\partial y} = 0; \quad y \rightarrow \infty : \quad u_1 = 0.$$

This equation is a *linear* partial differential equation. This linearity is characteristic for the computation of *small perturbations*. The differential equation is, as Eq. (7.80), again identical to the unsteady heat conduction equation. With the trial solution

$$u_1 = U_\infty C \left(\frac{x}{l} \right)^{-m} F(\eta), \quad \eta = \frac{y}{2} \sqrt{\frac{U_\infty}{\nu x}} \quad (7.88)$$

we obtain the following differential equation for the function $F(\eta)$:

$$F'' + 2\eta F' + 4mF = 0 \quad (7.89)$$

with the boundary conditions

$$\eta = 0 : \quad F' = 0; \quad \eta \rightarrow \infty : \quad F = 0.$$

Table 7.2. Balance of volume flux and x momentum on the control surface in Fig. 7.9

cross-section	volume flux	x momentum
AB	0	0
AA_1	$b \int_0^h U_\infty dy$	$\varrho b \int_0^h U_\infty^2 dy$
BB_1	$-b \int_0^h u dy$	$-\varrho b \int_0^h u^2 dy$
A_1B_1	$-b \int_0^h (U_\infty - u) dy$	$-\varrho b \int_0^h U_\infty (U_\infty - u) dy$
$\sum = \text{control surface}$	$\sum \text{volume flux} = 0$	$\sum \text{momentum flux} = \text{drag}$

The still unknown exponent m (*eigenvalue*) can be determined via a global momentum balance around the body in Fig. 7.9. The rectangular control surface AA_1B_1B is placed far enough away from the body that the pressure on it is unperturbed. The pressure is constant over the whole of the control surface and so there is no contribution to the momentum balance from the pressure forces. In calculating the momentum flux across the control surface, we must note that for continuity reasons fluid must flow out across the upper and lower surfaces. The quantity of fluid leaving through A_1B_1 is equal to

the difference between that entering through AA_1 and leaving through BB_1 . The momentum balance is given in Table 7.2, where inflowing volume fluxes are counted positive and outflowing volume fluxes negative. Then the drag corresponds to the total momentum flux, thus giving us

$$D = b\varrho \int_{-\infty}^{+\infty} u(U_\infty - u) dy . \quad (7.90)$$

Here the limits of integration may be set to $y = \pm\infty$ instead of $y = \pm h$, since the integrand in Eq. (7.90) vanishes for $|y| > h$. With the trial solution (7.88), Eq. (7.90) yields

$$D \approx b\varrho \int_{-\infty}^{+\infty} U_\infty u_1 dy = 2b\varrho U_\infty^2 C \left(\frac{x}{l}\right)^{-m} \sqrt{\frac{\nu x}{U_\infty}} \int_{-\infty}^{+\infty} F(\eta) d\eta . \quad (7.91)$$

Since this balance must be independent of x , it follows that $m = 1/2$. Equation (7.89) thus determined becomes

$$F'' + 2\eta F' + 2F = 0 \quad (7.92)$$

which, after integrating once, yields

$$F' + 2\eta F = 0$$

with the solution

$$F(\eta) = e^{-\eta^2} . \quad (7.93)$$

Using the integral

$$\int_{-\infty}^{+\infty} F(\eta) d\eta = \int_{-\infty}^{+\infty} e^{-\eta^2} d\eta = \sqrt{\pi}$$

it follows from Eq. (7.91) that the drag coefficient is

$$c_D = \frac{D}{\frac{\varrho}{2} U_\infty^2 bl} = \frac{4\sqrt{\pi}C}{\sqrt{\frac{U_\infty l}{\nu}}} . \quad (7.94)$$

Therefore the final solution for the defect velocity in the wake of a body with drag coefficient c_D is

$$\frac{u_1(x, y)}{U_\infty} = \frac{c_D}{4\sqrt{\pi}} \sqrt{\frac{U_\infty l}{\nu}} \left(\frac{x}{l}\right)^{-\frac{1}{2}} \exp\left(-\frac{y^2 U_\infty}{4x\nu}\right) . \quad (7.95)$$

From Eq. (7.88) it then follows that the half-value width of the wake is

$$y_{0.5} = 1.7 \sqrt{\frac{\nu x}{U_\infty}} \quad (7.96)$$

i.e. here too the width of the frictional layer is proportional to $\sqrt{\nu}$.

It is worth noting that, in spite of the widening of the wake, the defect volume flux in the wake is independent of x , i.e. no side entrainment occurs in this flow. The compensating volume flux which flows out through the sides of the control surface does so already in the *near field* of the body, and not in the *far field* described by the solution (7.95). This solution may be used at about $x > 3l$.

For the extension of this solution to smaller x values, see the work by S.A. Berger (1971), p. 237.

In most practical cases, wake flows are turbulent, since the velocity profiles in the wake possess points of inflection and are thus particularly unstable. Consequently the transition to turbulent flow takes place at relatively low Reynolds numbers, cf. Chap. 15.

Note (Jet in parallel flow)

The wake solution is also valid for the asymptotic decay of a free jet flow in an equally directed parallel flow. Instead of the drag coefficient c_D , the analogously defined *jet momentum coefficient* c_μ appears, and $u_1(x, y)$ is interpreted as an excess velocity.

7.5.2 Boundary Layer at a Moving Wall

If a body moves in surroundings which are at rest close to an infinitely extended ground (e.g. motor vehicle, airfoil close to the ground), a frictional layer forms at the ground. This was comprehensively investigated by E. Beese (1984). In a coordinate system fixed to the body, the flow is parallel far behind the body, since the ground moves with the velocity of the free stream U_∞ . Small deviations of the velocity from the constant velocity U_∞ therefore again obey the differential equation (7.87) as the ground boundary layer decays for $x \rightarrow \infty$. This time the boundary conditions are

$$y = 0 : \quad u_1 = 0, \quad y \rightarrow \infty : \quad u_1 = 0.$$

With the trial solution Eq. (7.88), we again obtain Eq. (7.89), now with the eigenvalue $m = 1$. The differential equation

$$F'' + 2\eta F' + 4F = 0$$

with the boundary conditions

$$\eta = 0 : \quad F = 0; \quad \eta \rightarrow \infty : \quad F = 0$$

has the solution

$$F = C\eta e^{-\eta^2},$$

where the factor C depends on the history of the boundary layer further upstream.

Note (Start of the ground boundary layer)

It has been shown by E. Beese (1984) that the start of the ground boundary layer under a body with lift can be computed as a small deviation from the parallel flow, using a linearised boundary-layer equation analogous to Eq. (7.87), which however also contains a pressure term.

7.6 Integral Relations of the Boundary Layer

In many practical cases it is not the details of the velocity field inside the boundary layer which are of interest, but rather certain *integral values* of the boundary layer, which do depend on the length x , but are “*global values*” with respect to any dependence on y . Such suitable integral values for the global description of the boundary layer are obtained from an integration of the boundary-layer equations with respect to y over the boundary-layer thickness.

7.6.1 Momentum–Integral Equation

To derive the momentum–integral equation of the boundary layer, we start out from Eqs. (7.4) and (7.5), i.e. we restrict ourselves initially to plane, steady, incompressible flow. Integrating Eq. (7.5) from $y = 0$ (wall) to $y = h$, where the layer $y = h$ is everywhere outside the boundary layer, we obtain

$$\int_{y=0}^h \left(u \frac{\partial u}{\partial x} + v \frac{\partial u}{\partial y} - U \frac{dU}{dx} \right) dy = -\frac{\tau_w}{\varrho}. \quad (7.97)$$

Here the wall shear stress τ_w has been used to replace $\mu(\partial u / \partial y)_w$. From the continuity equation, the normal velocity v can be replaced by $v = -\int_0^y (\partial u / \partial x) dy$, so that we find:

$$\int_{y=0}^y \left(u \frac{\partial u}{\partial x} - \frac{\partial u}{\partial y} \int_0^y \frac{\partial u}{\partial x} dy - U \frac{dU}{dx} \right) dy = -\frac{\tau_w}{\varrho}.$$

Integrating the second term by parts yields

$$\int_{y=0}^h \left(\frac{\partial u}{\partial y} \int_0^y \frac{\partial u}{\partial x} dy \right) dy = U \int_0^h \frac{\partial u}{\partial x} dy - \int_0^h u \frac{\partial u}{\partial x} dy,$$

so that we obtain

$$\int_0^h \left(2u \frac{\partial u}{\partial x} - U \frac{\partial u}{\partial x} - U \frac{dU}{dx} \right) dy = -\frac{\tau_w}{\varrho}.$$

This can be summarised as

$$\int_0^h \frac{\partial}{\partial x} [u(U - u)] dy + \frac{dU}{dx} \int_0^h (U - u) dy = \frac{\tau_w}{\rho}.$$

Since in both integrals the integrand vanishes outside the boundary layer, we can also set $h \rightarrow \infty$.

We now introduce the displacement thickness δ_1 and momentum thickness δ_2 first used in Chap. 6, using the equations

$$\delta_1 U = \int_{y=0}^{\infty} (U - u) dy \quad (\text{displacement thickness}) \quad (7.98)$$

and

$$\delta_2 U^2 = \int_{y=0}^{\infty} u(U - u) dy \quad (\text{momentum thickness}) . \quad (7.99)$$

In the first term of the equation above, the order of the differentiation with respect to x and the integration with respect to y may be interchanged, since the upper limit h is independent of x . This leads to

$$\boxed{\frac{d}{dx} (U^2 \delta_2) + \delta_1 U \frac{dU}{dx} = \frac{\tau_w}{\rho}} . \quad (7.100)$$

This is the *momentum-integral equation for plane, incompressible boundary layers*. In this form it is valid for both laminar and turbulent boundary layers. It was first presented in the notation used here by E. Gruschwitz (1931). It is used in the approximate methods for computing both laminar and turbulent boundary layers, cf. Chap. 8 and Sect. 18.4.

7.6.2 Energy–Integral Equation

Using a similar approach to that used for the momentum–integral equation, an *energy–integral equation* was also given for the laminar boundary layer by K. Wieghardt (1948). It is obtained by first multiplying the equation of motion by u and then integrating from $y = 0$ to $y = h > \delta(x)$. Again replacing v by using the continuity equation, this yields

$$\varrho \int_0^h \left[u^2 \frac{\partial u}{\partial x} - u \frac{\partial u}{\partial y} \left(\int_0^y \frac{\partial u}{\partial x} dy \right) - u U \frac{dU}{dx} \right] dy = \mu \int_0^h u \frac{\partial^2 u}{\partial y^2} dy .$$

The second term can be integrated by parts to give

$$\int_0^h \left[u \frac{\partial u}{\partial y} \left(\int_0^y \frac{\partial u}{\partial x} dy \right) \right] dy = \frac{1}{2} \int_0^h (U^2 - u^2) \frac{\partial u}{\partial x} dy ,$$

while combining the first and third terms yields:

$$\int_0^h \left[u^2 \frac{\partial u}{\partial x} - uU \frac{dU}{dx} \right] dy = \frac{1}{2} \int_0^h u \frac{d}{dx} (u^2 - U^2) dy .$$

If we also integrate the right hand side by parts, we obtain

$$\frac{1}{2} \rho \frac{d}{dx} \int_0^\infty u(U^2 - u^2) dy = \mu \int_0^\infty \left(\frac{\partial u}{\partial y} \right)^2 dy . \quad (7.101)$$

Here again the upper limit of the integral could be replaced by $h \rightarrow \infty$, since outside the boundary layer the integrands are equal to zero. The quantity $\mu(\partial u / \partial y)^2$ gives the energy transformed to heat per unit volume and time by the friction (dissipation, cf. Sect. 3.10). On the left hand side the term $\rho(U^2 - u^2)/2$ is the loss of mechanical energy (kinetic energy) which the boundary layer suffers compared to potential flow. Therefore $(\rho/2) \int_0^\infty u(U^2 - u^2) dy$ is the energy loss flux, and the left hand side is the change in the energy loss flux per unit length in the x direction.

If we introduce the *energy thickness* δ_3 via

$$U^3 \delta_3 = \int_0^\infty u(U^2 - u^2) dy \quad (\text{energy thickness}) \quad (7.102)$$

we then obtain from Eq. (7.101):

$$\frac{d}{dx} (U^3 \delta_3) = 2\nu \int_0^\infty \left(\frac{\partial u}{\partial y} \right)^2 dy \quad (7.103)$$

or, since $\tau = \mu(\partial u / \partial y)$,

$$\frac{d}{dx} (U^3 \delta_3) = \frac{2}{\rho} \int_0^\infty \tau \frac{\partial u}{\partial y} dy = \frac{2}{\rho} \mathcal{D} . \quad (7.104)$$

The integral \mathcal{D} defined by Eq. (7.104) is called the *dissipation integral*. This is the *energy-integral equation for plane, incompressible boundary layers*. In the form of Eq. (7.104) it is also valid for turbulent boundary layers.

K. Wieghardt (1948) has shown that further integral equations can be written down for the boundary layer if the boundary-layer equation is multiplied by some power u^n ($n = 0, 1, 2, \dots$) and then the integration over the

boundary layer is carried out. However the strength of the statements contained in integral equations found in this manner decreases with increasing n , so that mostly only the two integral equations mentioned for $n = 0$ (momentum-integral equation) and $n = 1$ (energy-integral equation) are used in practice, cf. A. Walz (1966), p. 78.

7.6.3 Moment-of-Momentum Integral Equations

A family of n integral equations can be produced by first multiplying the boundary-layer equation by the power y^n and then integrating over the thickness of the boundary layer. If we further eliminate the v component using the continuity equation, we obtain

$$\int_0^\infty \left[u \frac{\partial u}{\partial x} - \frac{\partial u}{\partial y} \int_0^y \frac{\partial u}{\partial x} dy - U \frac{dU}{dx} \right] y^n dy = \frac{1}{\rho} \int_0^\infty \frac{\partial \tau}{\partial y} y^n dy . \quad (7.105)$$

The case $n = 0$ corresponds to the momentum-integral equation. For $n = 1$ we obtain the moment-of-momentum-integral equation in the following form:

$$\begin{aligned} \frac{d}{dx} \left[\int_0^\infty u(U-u)y dy \right] + \int_0^\infty \left[(U-u) \frac{\partial}{\partial x} \left(Uy + \int_0^y u dy \right) \right] dy \\ = \frac{1}{\rho} \int_0^\infty \tau dy . \end{aligned} \quad (7.106)$$

In practice this integral equation is often favoured above the energy-integral equation, since in general the integral appearing in Eq. (7.106) is more easy to determine using the shear stress than the dissipation integral in Eq. (7.104). For laminar flows the right hand side of Eq. (7.106) is simply νU .

The integral equations introduced here will be used in the integral methods discussed in Chap. 8 and Sect. 18.4.

8. Approximate Methods for Solving the Boundary-Layer Equations for Steady Plane Flows

Remark. In order to calculate the flow in the boundary layer, in general partial differential equations must be solved. Today there are many very effective and precise numerical methods available, as will be shown in Chap. 23.

In many practical applications it is not necessary to determine the “exact” solutions of the boundary equations: it is enough to know the result to “within a few percent”.

Approximate solutions to the boundary-layer equations can be obtained in the following manner. The integral relations of the boundary layer derived in Sect. 7.6 are used as a foundation here. They can be read as ordinary differential equations for, for example, the displacement thickness δ_1 or the momentum thickness δ_2 , as well as for the wall shear stress τ_w and the dissipation integral \mathcal{D} . Now each equation initially contains more than one unknown, so these integral relations themselves are not enough to calculate the characteristic values in the boundary layer. In order to acquire further equations of motion, we need an approximation assumption: we suppose that the velocity profiles all come from one “profile family”, i.e. they are from a given number of possible profiles. They differ from other members of the family by one or more parameters, hence the expressions *single-parameter* or *multi-parameter profile family*. These assumptions lead to relations between the boundary characteristic values and the profile parameters, which thus remain as functions along the boundary layer needing to be found. The number of equations which then need to be added to the integral relations therefore depends directly on the number of profile parameters.

The approximate methods based on this are called *integral methods*. The essential differences between the various methods which have arisen in the past are contained in the differences in the profile family and in the use of the different integral relations.

In what follows an integral method which uses a single parameter profile family will be presented in concrete terms.

8.1 Integral Methods

As we have already mentioned, the various integral methods differ mainly in the profile family prescribed. Frequently a power ansatz is used to describe the velocity profile. In the first integral method ever used, a fourth order polynomial was applied. When the boundary conditions were taken into account this leads to a single-parameter profile family. This first integral method is based on two articles by Th. v.Kármán (1921) and K. Pohlhausen (1921) and for this reason is often referred to as the Karman-Pohlhausen method.

Here we choose a different profile family, namely that used by A. Walz (1966) in his integral method. It is assumed that the profile corresponds locally to a Hartree profile; this is known as “*local similarity*”. These profiles are solutions of the single-parameter Falkner-Skan equation (7.15) and thus represent a single-parameter profile family with parameter β .

The integral method is based on the momentum-integral equation, Eq. (7.100):

$$\frac{d}{dx}(U^2 \delta_2) + \delta_1 U \frac{dU}{dx} = \frac{\tau_w}{\varrho}. \quad (8.1)$$

With the similarity variables from Eq. (7.21)

$$\eta = \frac{y}{\delta_N(x)}, \quad \delta_N = \sqrt{\frac{2\nu x}{U(m+1)}} \quad (8.2)$$

we find the following relations for the boundary-layer characteristic quantities appearing in Eq. (8.1) with the parameter β :

Displacement thickness from Eq. (7.98):

$$\delta_1 = \beta_1 \delta_N, \quad \beta_1 = \int_0^\infty (1 - f') d\eta = \lim_{\eta \rightarrow \infty} (\eta - f) \quad (8.3)$$

Momentum thickness from Eq. (7.99):

$$\delta_2 = \beta_2 \delta_N, \quad \beta_2 = \int_0^\infty (1 - f') f' d\eta = \frac{f''_w - \beta \beta_1}{1 + \beta} \quad (8.4)$$

Wall shear stress:

$$\frac{\tau_w}{\varrho} = \nu \left(\frac{\partial u}{\partial y} \right)_w = \frac{\nu U}{\delta_N} f''_w. \quad (8.5)$$

Here the quantities $\beta_1(\beta)$, $\beta_2(\beta)$ and $f''_w(\beta)$ are all functions of the parameter β , as can also be seen from Table 8.1. The quantity δ_N is a measure of the boundary-layer thickness. It is proportional to the thickness δ_{99} , where the constant of proportionality β_{99} still depends on β , cf. Table 8.1. We have

$$\delta_{99} = \beta_{99} \delta_N. \quad (8.6)$$

Table 8.1. Characteristic quantities of the solutions of the Falkner–Skan equation (7.15) with the boundary conditions (7.16), the so-called Hartree profiles.

Using the following relations:

$$\begin{aligned} m &= 2/(2 - \beta) & F &= \beta\beta_2^2 \\ \beta_1 &\text{ from Eq. (8.3)} & \beta_2 &\text{ from Eq. (8.4)} & F_1 &= 2\beta_2 f_w'' \\ &&&& \beta_2 = (f_w'' - \beta\beta_1)/(1 + \beta) & F_2 \text{ from Eq. (8.19a)} \\ &&&& \beta_D = (\beta + 0.5)\beta_3 & H_{12} = \beta_1/\beta_2 \\ &&&& \beta_{99} \text{ from Eq. (8.11)} & H_{32} = \beta_3/\beta_2 \end{aligned}$$

β	m	F	F_1	F_2	H_{12}	H_{32}	β_2	f_w''	β_D	β_{99}	Notes
-0.199	-0.090	-0.0681	0.000	0.754	4.029	1.515	0.585	0.000	0.267	4.8	Separation
-0.1	-0.048	-0.0265	0.329	0.557	2.801	1.552	0.515	0.319	0.319	3.8	
0.0	0.000	0.0000	0.441	0.441	2.591	1.573	0.470	0.470	0.369	3.6	Constant pressure
0.1	0.053	0.0190	0.511	0.360	2.481	1.586	0.435	0.587	0.415	3.4	
0.2	0.111	0.0333	0.561	0.300	2.411	1.595	0.408	0.687	0.455	3.2	
0.3	0.176	0.0439	0.593	0.253	2.373	1.602	0.386	0.775	0.491	3.1	
0.4	0.250	0.0538	0.627	0.215	2.325	1.607	0.367	0.854	0.530	3.0	
0.5	0.333	0.0612	0.649	0.184	2.297	1.611	0.350	0.928	0.564	2.9	
0.6	0.429	0.0677	0.669	0.158	2.274	1.615	0.336	0.996	0.597	2.8	
0.7	0.538	0.0725	0.682	0.137	2.261	1.618	0.322	1.059	0.625	2.7	
0.8	0.666	0.0778	0.699	0.117	2.241	1.621	0.312	1.120	0.657	2.6	
0.9	0.818	0.0816	0.709	0.101	2.228	1.623	0.301	1.178	0.684	2.5	
1.0	1.000	0.0855	0.721	0.085	2.216	1.626	0.292	1.233	0.713	2.4	Stagnation point

If we insert the results from Eq. (8.3) to (8.5) into Eq. (8.1), it follows that

$$\frac{d(\beta_2 \delta_N)}{dx} + \left(2 + \frac{\beta_1}{\beta_2}\right) \frac{\beta_2 \delta_N}{U} \frac{dU}{dx} = \frac{\nu}{U \delta_N} f_w'' . \quad (8.7)$$

Now this equation still contains two unknowns, namely the scale function $\delta_N(x)$ and the parameter $\beta(x)$. Therefore a further equation will be required. Here the compatibility condition at the wall in Eq. (7.2) is used, which, taking the Bernoulli equation for the outer flow from Eq. (6.33) into account, reads:

$$\nu \left(\frac{\partial^2 u}{\partial y^2} \right)_w = -U \frac{dU}{dx} . \quad (8.8)$$

It follows from this that for the Hartree profile it is

$$f_w''' = -\frac{\delta_N^2}{\nu} \frac{dU}{dx} = -\beta . \quad (8.9)$$

If the function $U(x)$ is given, Eqs. (8.7) and (8.9) are then two equations to determine the two desired functions $\delta_N(x)$ and $\beta(x)$. With these functions, we can then determine further characteristic quantities for the boundary layer from Eqs. (8.3) to (8.5). The energy thickness from Eq. (7.102)

$$\delta_3 = \beta_3 \delta_N, \quad \beta_3(\beta) = \int_0^\infty (1 - f'^2) f' d\eta , \quad (8.10)$$

and the dissipation integral

$$\mathcal{D} = \beta_{\mathcal{D}} \mu \frac{U^2}{\delta_N}, \quad \beta_{\mathcal{D}}(\beta) = \int_0^\infty f''^2 d\eta \quad (8.11)$$

and finally the different velocity profiles can all be determined from $\delta_N(x)$ and $\beta(x)$.

Instead of determining $\delta_N(x)$ and $\beta(x)$, A. Walz (1966) introduced two new functions $Z(x)$ and $\Gamma(x)$ as independent variables, defined as follows:

$$Z(x) = \frac{\delta_2^2}{\nu} U , \quad (8.12)$$

$$\Gamma(x) = -\frac{\delta_2^2}{U} \left(\frac{\partial^2 u}{\partial y^2} \right)_w . \quad (8.13)$$

The quantity $Z(x)$ has the dimensions of a length and represents a thickness parameter, while $\Gamma(x)$ is dimensionless and has the property of a profile parameter.

For the *Hartree profiles* it follows from Eq. (8.13) that

$$\Gamma(\beta) = -\beta_2^2(\beta) f_w'''(\beta) = \beta \beta_2^2(\beta) , \quad (8.14)$$

i.e. there is a fixed relation between Γ and β for the Hartree profile family. Since Γ thus determines the form of the velocity profile just as β does, Γ is therefore also called the *shape factor*.

The equations (8.7) and (8.9) can now be written down as defining equations for the unknown functions $Z(x)$ and $\Gamma(x)$:

$$\frac{dZ}{dx} + (3 + 2H_{12}) \frac{Z}{U} \frac{dU}{dx} = F_1(\Gamma), \quad (8.15)$$

$$\frac{Z}{U} \frac{dU}{dx} = \Gamma \quad (8.16)$$

with

$$H_{12}(\Gamma) = \frac{\delta_1}{\delta_2} = \frac{\beta_1}{\beta_2} \quad (8.17)$$

and

$$F_1(\Gamma) = \frac{2\tau_w \delta_2}{\rho v U} = 2\beta_2 f_w'' . \quad (8.18)$$

In summary, it follows that

$$\frac{dZ}{dx} = F_2(\Gamma) \quad (8.19)$$

with

$$F_2(\Gamma) = F_1(\Gamma) - [3 + 2H_{12}(\Gamma)]\Gamma . \quad (8.19a)$$

The functions $F_1(\Gamma)$, $H_{12}(\Gamma)$ and in particular $F_2(\Gamma)$ are all tabulated for the Hartree profiles in Table 8.1. Equations (8.16) and (8.19) form a coupled system of two equations for the two unknown functions $Z(x)$ and $\Gamma(x)$, whereby the combination $(dU/dx)/U$ is given. This is the solution of an ordinary differential equation of first order, whose numerical solution is considerably more simple than the solution of the partial differential equation for the velocity field. The integral method formulated in this manner has the particular advantage that it yields *exact* solutions for all wedge flows.

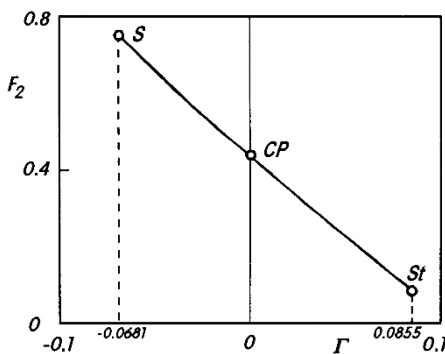


Fig. 8.1. Function $F_2(\Gamma)$ from Eq. (8.19a), cf. Table 8.1
 St: stagnation point
 CP: constant pressure
 S: separation point

The decisive advantage of introducing the functions $Z(x)$ and $\Gamma(x)$ lies in the fact that the function $F_2(\Gamma)$ is almost linear, as seen in Fig. 8.1. If the curve $F_2(\Gamma)$ is approximated by the linear relation

$$F_2(\Gamma) = a - b\Gamma, \quad (8.20)$$

Eqs. (8.16) and (8.19) yield the differential equation

$$\frac{dZ}{dx} + \frac{b}{U} \frac{dU}{dx} Z = a. \quad (8.21)$$

The solution of this equation can be written down explicitly. We obtain the following *quadrature formula*

$$Z(x) = Z(x_i) \left[\frac{U(x_i)}{U(x)} \right]^b + \frac{a}{[U(x)]^b} \int_{x_i}^x [U(x)]^b dx, \quad (8.22)$$

where $Z(x_i)$ is the value of $Z(x)$ at the position x_i . For $x_i = 0$ and $Z(0) = 0$ it follows that

$$Z(x) = \frac{a}{[U(x)]^b} \int_0^x [U(x)]^b dx. \quad (8.23)$$

The condition $Z(0) = 0$ implies that the calculation of the boundary layer at $x = 0$ commences either with a stagnation point ($U(0) = 0$) or with a leading edge ($\delta_2(0) = 0$).

The linear approximation of $F_2(\Gamma)$ corresponding to Eq. (8.20) is now carried out in two sections:

$$\Gamma > 0 : \quad a = 0.441 \quad b = 4.165 \quad (8.24)$$

$$\Gamma < 0 : \quad a = 0.441 \quad b = 4.579.$$

Here the constants a and b have been so chosen that the plate flow ($\Gamma = 0$), the stagnation-point flow ($\Gamma = 0.0855$) and the separation flow ($\Gamma = -0.0681$) are still exactly described by Eq. (8.23). Therefore the integral method described is not an approximate method with respect to these three flows.

If $Z(x)$ and $\Gamma(x)$ are known, the desired variables can be determined by inverse transformation:

$$\delta_2 = \left(\frac{Z\nu}{U} \right)^{1/2}, \quad (8.25)$$

$$\delta_1 = \delta_2 H_{12}(\Gamma), \quad (8.26)$$

$$\delta_3 = \delta_2 H_{32}(\Gamma), \quad (8.27)$$

$$\delta_N = \frac{\delta_2}{\beta_2(\Gamma)}, \quad (8.28)$$

$$\tau_w = \frac{\mu U}{2\delta_2} F_1(\Gamma), \quad (8.29)$$

$$\mathcal{D} = \beta_{\mathcal{D}}(\Gamma) \beta_2(\Gamma) \frac{\mu U^2}{\delta_2}. \quad (8.30)$$

The functions $H_{12}(\Gamma)$, $H_{23}(\Gamma)$, $\beta_2(\Gamma)$, $F_1(\Gamma)$ and $\beta_{\mathcal{D}}(\Gamma)$ can be read off from Table 8.1.

In this manner Eq. (8.22) can be used to reduce the calculation of laminar boundary layers to the evaluation of a quadrature formula.

To evaluate Eq. (8.22) numerically, the function $U(x)$ is approximated in the interval x_i to x_{i+1} by the linear relation

$$U(x) = U_i + \frac{U_{i+1} - U_i}{x_{i+1} - x_i} (x - x_i), \quad (8.31)$$

where $U_i = U(x_i)$. The integration in Eq. (8.22) can then be carried out and we obtain the simple computation rule:

$$Z_{i+1} = \left(\frac{U_i}{U_{i+1}} \right)^b Z_i + \frac{a}{1+b} \frac{1 - (U_i/U_{i+1})^{b+1}}{1 - (U_i/U_{i+1})} (x_{i+1} - x_i). \quad (8.32)$$

From Eq. (8.16) it follows that

$$\Gamma_{i+1} = \frac{Z_{i+1}}{U_{i+1}} \frac{U_{i+1} - U_i}{x_{i+1} - x_i}. \quad (8.33)$$

In general the calculation commences at $Z = 0$ and ends at the latest when the value $\Gamma = -0.0681$ for the separation point has been reached. In practice, the boundary layer in the region of pressure increase ($\Gamma < 0$) frequently changes over to the turbulent state.

Practical application has shown that the integral method due to A. Walz delivers very good approximate solutions when the flow is not in a region of extreme pressure gradient dp/dx . Therefore we would have to exclude flows which are greatly retarded or greatly accelerated. For such flows, it is not that the integral method yields fundamentally wrong results, but that care has to be taken that the chosen profile family approximates the expected velocity profiles as well as possible.

For multi-parameter profile families, further integral equations are required. In addition to the momentum-integral equation, the energy-integral equation from Eq. (7.100) is frequently also chosen, cf. A. Walz (1966) pp. 93, 131 and 230. A similar integral method for compressible boundary layers is described in Sect. 10.4.5, and this also comprises the incompressible boundary layer for $Ma_e \rightarrow 0$ as a special case, see example 1. For other integral methods, see H. Schlichting (1982), p. 209 and 221.

Nowadays integral methods are mainly of practical importance for turbulent boundary layers. If an integral method is used for a turbulent boundary layer, it is generally sensible for simplicity to compute the initial laminar region using an integral method too.

8.2 Stratford's Separation Criterion

A separation criterion has been given by B.S. Stratford (1957) with which the position of the separation point can be determined essentially directly from the given velocity distribution $U(x)$. To this end, we consider an outer flow which has the constant velocity U_0 from $x = x_f$ to $x = x_0$ and from then on is a retarded flow ($dU/dx < 0$). According to Stratford, this flow separates at the position where

$$\left[1 - \left(\frac{U(x)}{U_0}\right)^2\right]^{1/2} (x_S - x_f) \frac{d}{dx} \left[\left(\frac{U(x)}{U_0}\right)^2\right] = -0.102. \quad (8.34)$$

For given values $U(x)$, U_0 and x_f , this is an equation for the position of the separation point x_S .

This separation criterion can be applied to all flows where a velocity maximum occurs before separation. There (at $x = x_0$) the momentum thickness δ_{20} must be known. We now assume that it corresponds to a plate boundary layer of length $x_0 - x_f$, i.e. x_f is a fictitious leading edge of this imagined plate. Since from Eq. (6.64), $\delta_{20} = 0.664\sqrt{\nu(x_0 - x_f)/U_0}$ holds, we use the following relation in Eq. (8.34):

$$x_S - x_f = x_S - x_0 + \frac{\delta_{20}^2 U_0}{0.441\nu}. \quad (8.35)$$

The combination of Eqs. (8.34) and (8.35) can be used to determine the position $x_S - x_0$ of the separation point behind the velocity maximum, providing $U(x)$, U_0 and δ_{20}/ν are given. Examples are presented in the following section.

8.3 Comparison of the Approximate Solutions with Exact Solutions

In what follows, some examples of the solutions for boundary–layer flow as determined using the integral method (quadrature method) in the previous section will be presented and compared with solutions resulting from numerical computation of the boundary–layer equations. Since, in principle, numerical methods can produce solutions with arbitrary precision, we can consider these to be “exact” solutions.

8.3.1 Retarded Stagnation–Point Flow

We consider the flow first calculated by L. Howarth (1935), see also Eq. (7.85), with a linearly decreasing velocity of the form

$$\frac{U(x)}{U_0} = 1 - \frac{x}{l}. \quad (8.36)$$

From Fig. 2.10b, this can be interpreted as a retarded stagnation-point flow. However it can also be interpreted as the flow at a plate in a diverging channel (diffuser).

For this velocity distribution $U(x)$ the quadrature formula (8.23) yields the closed solution

$$Z(x) = \frac{a}{b+1} \frac{1 - (1 - \frac{x}{l})^{b+1}}{(1 - \frac{x}{l})^b}, \quad (8.37)$$

and from Eq. (8.16) it follows that

$$\Gamma(x) = -\frac{a}{b+1} \frac{1 - (1 - \frac{x}{l})^{b+1}}{(1 - \frac{x}{l})^{b+1}}. \quad (8.38)$$

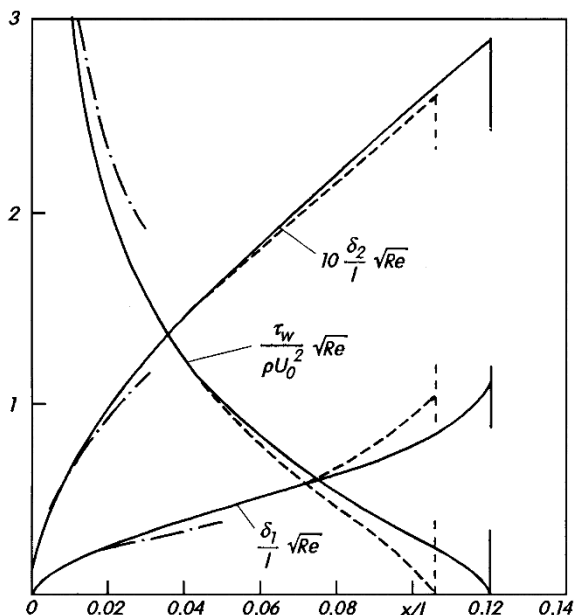


Fig. 8.2. Boundary-layer characteristic values $\delta_1(x)$, $\delta_2(x)$ and $\tau_w(x)$ for the retarded stagnation-point flow, with $U(x)$ from Eq. (8.36), $Re = U_0 l / \nu$

- exact solution, after W. Schönauer (1963)
- - - integral method
- · — plate solution for $U = U_0$

Figure 8.2 shows some important boundary-layer characteristic values plotted against the length x . The exact solution is due to W. Schönauer (1963). The flow commences as a plate flow at $x = 0$, so that there is initially no difference between the solutions. Because of the retarded flow, separation occurs further downstream. The position of the separation point delivered by

the integral method is $x_S/l = 0.105$, while the exact value lies at $x_S/l = 0.120$. The separation criterion of Stratford yields $x_S/l = 0.121$. It can be seen from Fig. 8.2 that the wall shear stress of the exact solution attains the value zero with a vertical tangent (*Goldstein singularity*, cf. Eq. (7.84)). Considerably better agreement with the exact solution can be achieved with an integral method which uses the energy-integral equation instead of the compatibility condition at the wall, cf. A. Walz (1966), p. 184.

8.3.2 Divergent Channel (Diffuser)

The flow in a divergent channel (diffuser) is a further example of a retarded flow. It is very similar to the previous example, and it is the counterpart of the boundary layer in the convergent channel given in Sect. 7.2.3. From Fig. 8.3, the outer flow is a source flow, for which potential theory yields the velocity distribution

$$U(x) = \frac{U_0}{1 + \frac{x}{l}}, \quad (8.39)$$

independent of the opening angle of the diffuser.

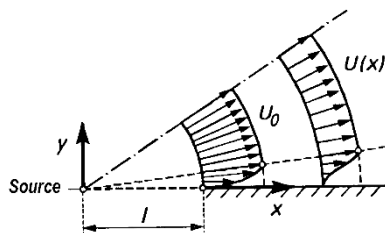


Fig. 8.3. Boundary layer in a divergent channel (diffuser) with the outer flow $U(x)$, from Eq. (8.39)

According to the separation criterion of Stratford, Eq. (8.34), the position of the separation point is $x_S/l = 0.16$. The exact value is at $x_S/l = 0.15$, while the integral method delivers $x_S/l = 0.13$.

An expansion of $U(x)$ from Eq. (8.39) for small values of x/l yields

$$\frac{U}{U_0} = 1 - \frac{x}{l} + \left(\frac{x}{l}\right)^2 - + \dots$$

showing the similarity to the previous example. Supplying the “acceleration term” $(x/l)^2$, the separation point at $x_S/l = 0.12$ is shifted downstream to $x_S/l = 0.15$. Wedge diffusers with laminar boundary layers without separation can, in the most favourable case (homogeneous free stream), have an area ratio of 1.15.

The position of the separation point is only independent of the opening angle of the diffuser as long as the displacement effect of the boundary layer is small enough to be neglected. However, for very small opening angles this is not the case. There is then an interaction between the outer flow and the boundary layer, which will be discussed in detail in Chap. 14.

8.3.3 Circular Cylinder Flow

We consider the velocity distribution which potential theory yields for the flow past a circular cylinder. It reads

$$U(x) = 2V \sin \frac{x}{R} = 2V \sin \varphi . \quad (8.40)$$

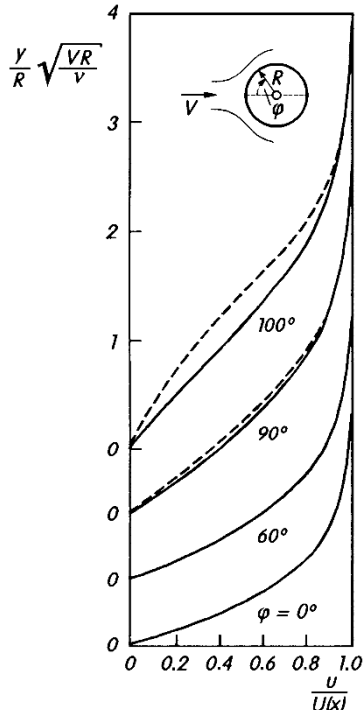
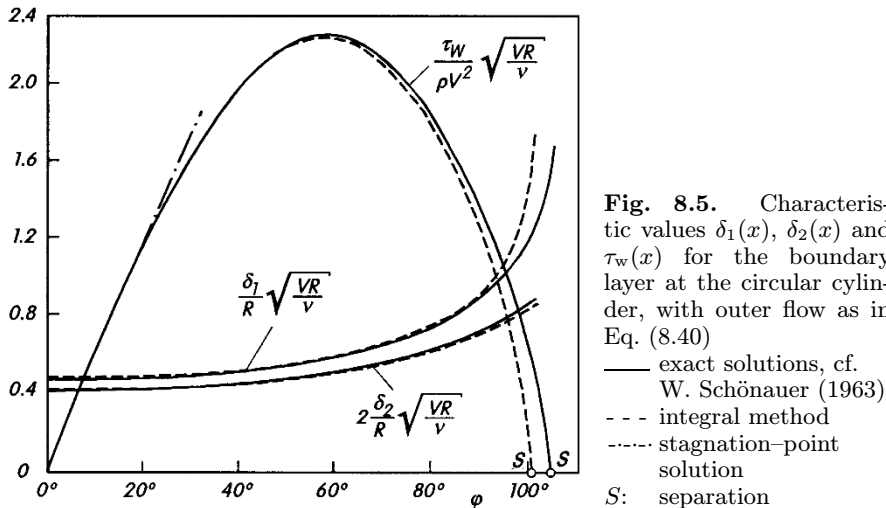


Fig. 8.4. Velocity distributions in the boundary layer of the circular cylinder with outer flow as in Eq. (8.40)
 — exact solutions, cf. W. Schönauer (1963)
 - - - - integral method

Figure 8.4 shows the velocity profiles for different peripheral angles φ . The approximations from the integral method are compared with the exact distribution from W. Schönauer (1963). In the region of accelerated outer flow, $0^\circ < \varphi < 90^\circ$, there is almost complete agreement, while beyond the pressure minimum as we approach the separation point, the deviations grow quickly.

Figure 8.5 depicts the following boundary-layer characteristic values: the displacement thickness δ_1 , the momentum thickness δ_2 and the wall shear stress τ_w . Here too we can see the growth of the deviations between the exact solution and the approximation as we approach the separation point. The exact value for the position of the separation point is at $\varphi_S = 104.5^\circ$, cf. R.M. Terrill (1960) or W. Schönauer (1963).

The exact solution shows the singularity of S. Goldstein (1948b), which can be seen from the vertical tangents of $\delta_1(x)$ and $\tau_w(x)$ at the separation



point $x_S = R\varphi_S$. The integral method yields $\varphi_S = 100.7^\circ$, while the criterion of Stratford gives the surprisingly precise value of $\varphi_S = 105^\circ$, if the approximate value for the momentum thickness is taken for x_0 (i.e. $\varphi = 90^\circ$). However, this value for δ_{20} is only about 1.7% smaller than the exact value.

Experiments on circular cylinders in the subcritical region show, however, that the position of the separation point is at about $\varphi_S = 80^\circ$. According to E. Achenbach (1968), the flow separates for a Reynolds number of $Re = Vd/\nu = 10^5$ at $\varphi_S = 78^\circ$. This could give us the impression that the flow separates already before the pressure minimum and that the separation point is in a region of accelerated flow. This apparent contradiction between theory and experiment was solved by K. Hiemenz (1911). He found that the experimentally determined pressure distribution deviates considerably from the theoretical distribution in Eq. (8.40), and that the pressure minimum is in fact to be found at $\varphi = 70^\circ$. Thus the separation point of about $\varphi_S = 80^\circ$ is indeed well within the region of retarded outer flow. For the Reynolds number $Re = Vd/\nu = 1.9 \cdot 10^4$, K. Hiemenz determined the experimental velocity distribution to be

$$\frac{U(x)}{V} = 1.814 \frac{x}{R} - 0.271 \left(\frac{x}{R}\right)^3 - 0.0471 \left(\frac{x}{R}\right)^5. \quad (8.41)$$

The experiments demonstrated separation at about $\varphi_S = 81^\circ$. The computation of the boundary layer for $U(x)$ in Eq. (8.41) yields the global boundary-layer characteristic values shown in Fig. 8.6. The position of the separation point is shown from the exact solution to be $\varphi_S = 78.7^\circ$, from the integral method $\varphi_S = 76.5^\circ$ and from the Stratford criterion $\varphi_S = 80^\circ$.

For the “real” velocity distribution $U(x)$ of the outer flow, the boundary-layer flow is correctly described by the boundary-layer equations. A comparison with other integral methods can be found in A. Walz (1966), p. 189. The

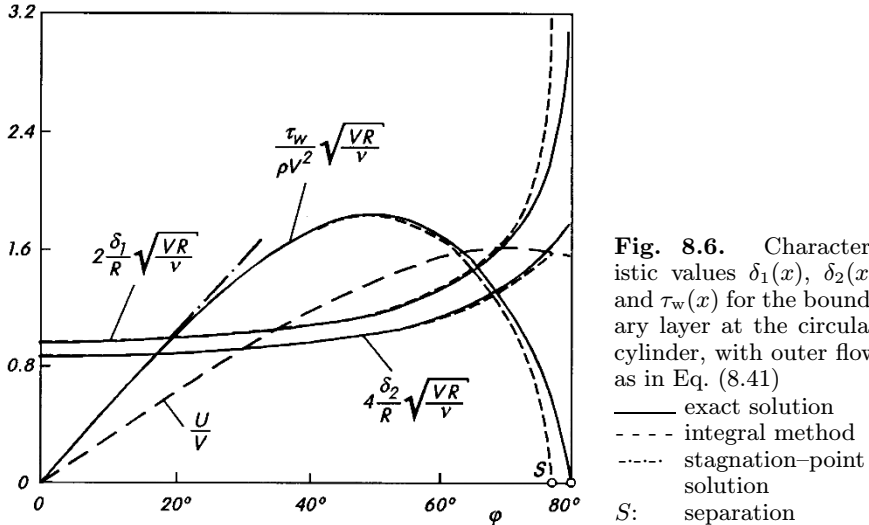


Fig. 8.6. Characteristic values $\delta_1(x)$, $\delta_2(x)$ and $\tau_w(x)$ for the boundary layer at the circular cylinder, with outer flow as in Eq. (8.41)

- exact solution
- - - integral method
- · - stagnation-point solution
- S: separation

deviations between the experimentally determined distribution $U(x)$ and the potential theory distribution in Eq. (8.40) come from the strong “displacement effect”, to be discussed in detail in Chap. 14. This effect is particularly noticeable in the case of blunt bodies, where the flow is characterised by large separation regions behind the body.

Details of experimentally determined velocity distributions corresponding to Eq. (8.41) for other Reynolds numbers can be found in H.L. Evans (1968), p. 180.

All examples treated up to now led to separation. From a given $U(x)$, a singularity formed in the separation point so that no further computation beyond this point was possible. As will be shown in detail in Chap. 14, this singularity does not appear if we do not prescribe $U(x)$, but rather allow an interaction between the boundary layer and the outer flow, and in this manner determine the function $U(x)$ as part of the solution when computing the boundary layer.

8.3.4 Symmetric Flow past a Joukowsky Airfoil

Finally, we consider one more flow without separation. This is the flow past a symmetric Joukowsky airfoil at angle of attack $\alpha = 0^\circ$. The airfoil has a relative thickness of $d/l = 0.044$, and is thus slender enough that no separation occurs. According to T. Cebeci; A.M.O. Smith (1974), p. 33, it is only for the Joukowsky airfoil with $d/l = 0.046$ that the wall shear stress vanishes just at the trailing edge. Figure 8.7 shows the outer flow $U(x)$ and the dimensionless wall shear stress. The calculation with the integral method exhibits good agreement with the exact solution. Although the integral method yields a separation point, it is situated just in front of the trailing edge.

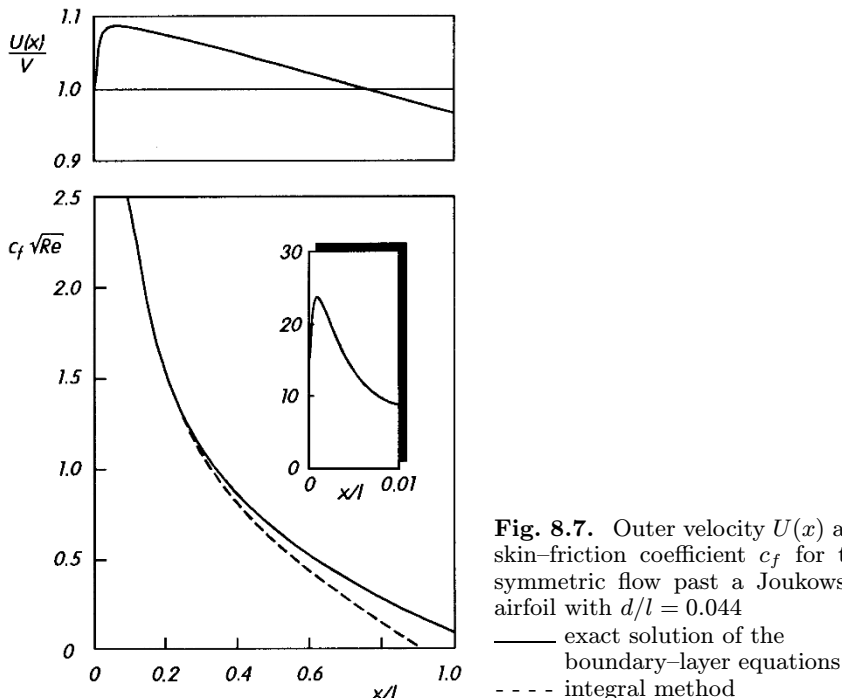


Fig. 8.7. Outer velocity $U(x)$ and skin-friction coefficient c_f for the symmetric flow past a Joukowsky airfoil with $d/l = 0.044$

— exact solution of the boundary-layer equations
- - - integral method

For the drag coefficient c_D (taking both sides into account) we find $c_D = 2.32\sqrt{Re}$ (exact) and $c_D = 2.16\sqrt{Re}$ (approximation). It is interesting to note that, because of the thickness distribution of the airfoil, the drag is lower than that of the flat plate $c_D = 2.66\sqrt{Re}$. This comes from the low wall shear stresses in the back region of the airfoil, since there the boundary layer tends towards the separation point with $\tau_w = 0$.

9. Thermal Boundary Layers without Coupling of the Velocity Field to the Temperature Field

9.1 Boundary-Layer Equations for the Temperature Field

Our considerations of boundary-layer flows up until now have referred only to the velocity field. These will now be correspondingly extended to include the temperature field. It will be assumed that heat is transferred to the flow field through the surrounding walls, so that a temperature field forms together with the velocity field. It will be seen that the temperature field also has a boundary-layer character at high Reynolds numbers, i.e. the temperature field can also be divided into two regions: in the region close to the wall, where the thermal conductivity λ plays a role, and a region where λ can be neglected. If both a velocity field and a temperature field exist, there is generally also a mutual coupling between these two fields.

In this chapter we will first discuss those particular flows with heat transfer for which the velocity field is decoupled from the temperature field. This is the case if the physical properties ϱ and μ are constant, i.e. can be assumed to be independent of the temperature and pressure. This assumption is certainly justified as long as the temperature and pressure differences within the boundary layer are small. Then all statements about the velocity boundary layers in Chaps. 6 to 8 remain valid. In order to describe the temperature field, the (thermal) energy equation must be taken into account. If the thermal conductivity λ and the isobaric specific heat capacity c_p can also be assumed to be constant, the energy equation from Eq. (3.72), in Cartesian coordinates, for a (steady) two-dimensional flow reads

$$\varrho c_p \left(u \frac{\partial T}{\partial x} + v \frac{\partial T}{\partial y} \right) = \lambda \left(\frac{\partial^2 T}{\partial x^2} + \frac{\partial^2 T}{\partial y^2} \right) + \Phi, \quad (9.1)$$

where the dissipation function from Eq. (3.62) is

$$\frac{\Phi}{\mu} = 2 \left[\left(\frac{\partial u}{\partial x} \right)^2 + \left(\frac{\partial v}{\partial y} \right)^2 \right] + \left(\frac{\partial v}{\partial x} + \frac{\partial u}{\partial y} \right)^2. \quad (9.2)$$

Equation (9.1) shows that a (convective) change in the temperature (i.e. in the internal energy) is possible via conduction and dissipation. Since the velocity components $u(x, y)$ and $v(x, y)$ appear in Eq. (9.1), the calculation

of the temperature field requires that we know what the velocity field is. The velocity field will now be assumed to be that of a flow at high Reynolds number, i.e. the flow will have boundary-layer character.

With the reference quantities l , V and ΔT , the following dimensionless quantities are introduced:

$$x^* = \frac{x}{l}, \quad y^* = \frac{y}{l}, \quad u^* = \frac{u}{V}, \quad v^* = \frac{v}{V} \quad \vartheta = \frac{T - T_\infty}{\Delta T}. \quad (9.3)$$

Here ϑ is defined as the dimensionless temperature exceeding the temperature T_∞ of the outer flow. ΔT is some suitable reference temperature difference, which will be determined later.

Introducing the variables y^* and v^* from the boundary-layer transformation Eq. (6.6)

$$\bar{y} = y^* \sqrt{\text{Re}}, \quad \bar{v} = v^* \sqrt{\text{Re}}, \quad \text{Re} = \frac{\rho V l}{\mu} = \frac{V l}{\nu}, \quad (9.4)$$

the energy equation (9.1) together with (9.2) becomes

$$\begin{aligned} \frac{\rho c_p V \Delta T}{l} \left(u^* \frac{\partial \vartheta}{\partial x^*} + \bar{v} \frac{\partial \vartheta}{\partial \bar{y}} \right) &= \frac{\lambda \Delta T}{l^2} \left(\frac{\partial^2 \vartheta}{\partial x^{*2}} + \text{Re} \frac{\partial^2 \vartheta}{\partial \bar{y}^2} \right) \\ &+ \frac{\mu V^2}{l^2} \left\{ 2 \left[\left(\frac{\partial u^*}{\partial x^*} \right)^2 + \left(\frac{\partial \bar{v}}{\partial \bar{y}} \right)^2 \right] + \left(\frac{1}{\sqrt{\text{Re}}} \frac{\partial \bar{v}}{\partial x^*} + \sqrt{\text{Re}} \frac{\partial u^*}{\partial \bar{y}} \right)^2 \right\}. \end{aligned} \quad (9.5)$$

If we now take the limit for large Reynolds numbers ($\text{Re} \rightarrow \infty$), we obtain the equation for the thermal boundary layer (in dimensionless form):

$$u^* \frac{\partial \vartheta}{\partial x^*} + \bar{v} \frac{\partial \vartheta}{\partial \bar{y}} = \frac{1}{\text{Pr}} \frac{\partial^2 \vartheta}{\partial \bar{y}^2} + \text{Ec} \left(\frac{\partial u^*}{\partial \bar{y}} \right)^2. \quad (9.6)$$

Here we have introduced the following two dimensionless numbers:

$$\text{Prandtl number} \quad \text{Pr} = \frac{\mu c_p}{\lambda}, \quad (9.7)$$

$$\text{Eckert number} \quad \text{Ec} = \frac{V^2}{c_p \Delta T}. \quad (9.8)$$

We assume that these two characteristic numbers remain finite in taking the large Reynolds number limit.

The Prandtl number is a pure physical property, see Table 3.1. The Eckert number is a measure of the dissipation effects in the flow. Since this grows in proportion to the square of the velocity, it can be neglect for small velocities. In an air flow ($c_p = 1000 \text{ m}^2/\text{s}^2 \text{ K}$) with $V = 10 \text{ m/s}$ and a reference temperature difference of $\Delta T = 10 \text{ K}$, we find $\text{Ec} = 0.01$. Because of the dissipation, a temperature field emerges even if there is no heat transfer, i.e. in the case of so-called adiabatic (insulating) walls. The walls then have a higher temperature than the temperature T_∞ of the outer flow. This wall temperature is called the *adiabatic wall temperature*, and will be discussed in more detail in Sect. 9.6.

At the outer edge of the velocity boundary layer, where $\partial u^*/\partial \bar{y} = 0$ holds, $\vartheta = 0$ satisfies the differential equation (9.6). Thus at large distances from the wall, the temperature is that of the outer flow T_∞ , i.e. we have $\vartheta(x^*, \bar{y} \rightarrow \infty, \text{Pr}) = 0$. There are more different kinds of boundary conditions possible for thermal boundary layers than for velocity boundary layers, since these latter are fixed by the no-slip condition and the impermeability of the wall. The different kinds of boundary conditions for thermal boundary layers will be discussed in the next section.

Equation (9.1) is a linear differential equation, and thus its general solution can be written down as a superposition of the solution without dissipation and the solution which is due to the dissipation:

$$\vartheta(x^*, \bar{y}, \text{Pr}, \text{Ec}) = \vartheta_1(x^*, \bar{y}, \text{Pr}) + \text{Ec} \vartheta_2(x^*, \bar{y}, \text{Pr}) . \quad (9.9)$$

The following equations therefore hold:

$$u^* \frac{\partial \vartheta_1}{\partial x^*} + \bar{v} \frac{\partial \vartheta_1}{\partial \bar{y}} = \frac{1}{\text{Pr}} \frac{\partial^2 \vartheta_1}{\partial \bar{y}^2} , \quad (9.10)$$

$$u^* \frac{\partial \vartheta_2}{\partial x^*} + \bar{v} \frac{\partial \vartheta_2}{\partial \bar{y}} = \frac{1}{\text{Pr}} \frac{\partial^2 \vartheta_2}{\partial \bar{y}^2} + \left(\frac{\partial u^*}{\partial \bar{y}} \right)^2 . \quad (9.11)$$

In what follows these two equations will be investigated separately. First of all the thermal boundary layer without dissipation will be treated, i.e. we will look for solutions $\vartheta_1(x^*, \bar{y}, \text{Pr})$. This is permissible because either the velocity is small enough that the dissipation may be neglected (i.e. $\text{Ec} \rightarrow 0$), or, else the partial solution due to dissipation can always be added on later, cf. Sect. 9.6.

For completeness we also present Eq. (9.6) for the thermal boundary layer in dimensional form (constant properties):

$$\varrho c_p \left(u \frac{\partial T}{\partial x} + u \frac{\partial T}{\partial y} \right) = \lambda \frac{\partial^2 T}{\partial y^2} + \mu \left(\frac{\partial u}{\partial y} \right)^2 . \quad (9.12)$$

9.2 Forced Convection for Constant Properties

If the dissipation is neglected, the temperature field in the thermal boundary layer is described by Eq. (9.10). In dimensional form this equation reads

$$u \frac{\partial T}{\partial x} + v \frac{\partial T}{\partial y} = a \frac{\partial^2 T}{\partial y^2} , \quad (9.13)$$

where

$$a = \frac{\lambda}{\varrho c_p} \quad (9.14)$$

is denoted the *thermal diffusivity*. In order to determine the temperature field $T(x, y)$ in the boundary layer, we need to know the velocity field $u(x, y), v(x, y)$. Therefore since the motion of the fluid is forced, we speak of *forced convection* and, in connection with the calculation of the temperature field using Eq. (9.13), of *forced convective heat transfer*.

Let us turn our thoughts to the boundary conditions for Eq. (9.13) or (9.10). As already explained, at great distances from the wall, the temperature is that of the outer flow T_∞ ($\vartheta_1 = 0$). The following types of boundary conditions at the wall can be prescribed:

1. the wall temperature distribution $T_w(x)$,
2. the heat flux distribution at the wall $q_w(x) = -\lambda(\partial T / \partial y)_w$,
3. a relation between T_w and q_w . This so-called *boundary condition of the third kind* or *mixed boundary condition* occurs particularly when both the temperature field in the flow and the temperature field at the body (heat conduction problem) are to be computed simultaneously.

Frequently it is sufficient to restrict oneself to the two *standard boundary conditions* $T_w = \text{const}$ and $q_w = \text{const}$. Since the energy equation (9.13) is linear, the solutions found with the standard boundary conditions can be used to generate the general solutions for arbitrary distributions $T_w(x)$ or $q_w(x)$ via *superposition*.

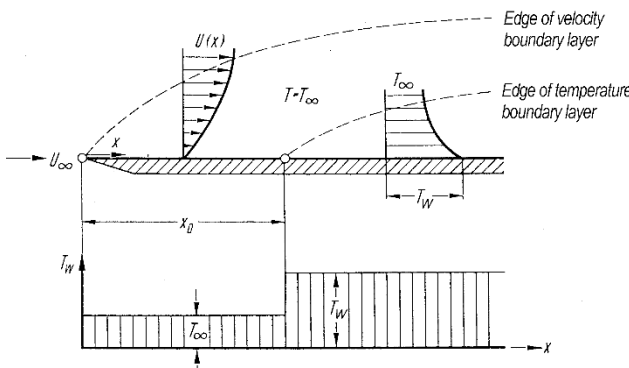


Fig. 9.1. Development of the velocity and temperature boundary-layer distribution for a discontinuous jump in the wall temperature at position $x = x_0$ (standard problem)

Such a standard solution for the case of constant wall temperature is shown in Fig. 9.1. Here the wall temperature is initially equal to the outer temperature T_∞ between $x = 0$ and $x = x_0$, and at position $x = x_0$ it suddenly jumps to the constant value T_w . If the solution of this problem is

$$\vartheta_1(x, y, x_0) = \frac{T(x, y, x_0) - T_\infty}{T_w - T_\infty} , \quad (9.15)$$

then for any arbitrary temperature distribution at the wall $T_w(x_0)$ the solution is

$$T(x, y) - T_\infty = \int_0^x \vartheta_1(x, y, x_0) dT_w(x_0), \quad (9.16)$$

For a known temperature field $T(x, y)$ we obtain the distribution of the heat flux

$$q_w(x, x_0) = -\lambda \left(\frac{\partial T}{\partial y} \right)_w = \alpha(x, x_0)(T_w - T_\infty), \quad (9.17)$$

where α is the *coefficient of heat transfer*. It has the units $[\alpha] = \text{W/m}^2\text{K}$. If $\alpha(x, x_0)$ is the distribution of the coefficient of heat transfer for the standard problem in Fig. 9.1, the wall heat flux for a general temperature distribution $T_w(x)$ emerges as

$$q_w(x) = \int_0^x \alpha(x, x_0) dT_w(x_0). \quad (9.18)$$

Equations (9.16) and (9.18) are Stieltjes integrals and they permit discontinuities in the temperature distribution $T_w(x_0)$. For continuous and differentiable distributions $T_w(x)$, the wall heat flux is found to be

$$q_w(x) = \int_0^x \alpha(x, x_0) \frac{dT_w}{dx_0} dx_0. \quad (9.19)$$

A corresponding expression also holds for Eq. (9.16).

In analogy, the standard solution for constant q_w ($0 \leq x < x_0 : q_w = 0$, $x_0 \leq x : q_w = \text{const}$) also yields the wall temperature for arbitrary distributions $q_w(x_0)$:

$$T_w(x) - T_\infty = \int_0^x g(x, x_0) \frac{dq_w(x_0)}{dx_0} dx_0, \quad (9.20)$$

where

$$g(x, x_0) = \frac{T_w(x) - T_\infty}{q_w} \quad (9.21)$$

is the distribution of the reciprocal coefficient of heat transfer for the corresponding standard solution.

The numerical computation of temperature fields with discontinuous functions as boundary conditions naturally provides difficulties. Frequently the jump function is replaced by a steep but continuous transition function, cf. T. Cebeci; P. Bradshaw (1984), p. 98.

In applications it is in most cases not necessary to know all the details of the temperature field. The first point of interest is the heat flux q_w at the wall, or else the coefficient of heat transfer α from Eq. (9.17).

The dimensionless characteristic number for heat transfer is the *Nusselt number*

$$\text{Nu}(x) = \frac{\alpha(x)l}{\lambda} = \frac{q_w(x)l}{\lambda[T_w(x) - T_\infty]} . \quad (9.22)$$

This can be used to formulate the boundary conditions at the wall from Eq. (9.10) and the desired results as follows:

1. $T_w = \text{const}$

$$\Delta T = T_w - T_\infty, \quad \vartheta_1 = \frac{T - T_\infty}{T_w - T_\infty}, \quad (9.23)$$

$$y = 0 : \quad \vartheta_1 = 1 . \quad (9.24)$$

Result:

$$\frac{\text{Nu}(x^*)}{\sqrt{\text{Re}}} = - \left(\frac{\partial \vartheta_1}{\partial y} \right)_w = f(x^*, \text{Pr}) . \quad (9.25)$$

2. $q_w = \text{const}$

$$\Delta T = \frac{q_w l}{\lambda \sqrt{\text{Re}}}, \quad \vartheta_1 = \frac{T - T_\infty}{q_w l} \lambda \sqrt{\text{Re}}, \quad (9.26)$$

$$y = 0 : \quad \left(\frac{\partial \vartheta_1}{\partial y} \right)_w = -1 . \quad (9.27)$$

Result:

$$T_w(x) - T_\infty = \frac{q_w l}{\lambda \sqrt{\text{Re}}} \vartheta_{1w}(x^*, \text{Pr}) \quad (9.28)$$

or

$$\frac{\sqrt{\text{Re}}}{\text{Nu}} = \vartheta_{1w}(x^*, \text{Pr}) . \quad (9.29)$$

We see that in *all* thermal boundary layers, the Nusselt number only appears in combination with the Reynolds number as $\text{Nu}/\sqrt{\text{Re}}$. (One exception is the wall jet, cf. Table 9.1.) This follows from the boundary-layer simplifications and yields the asymptotic behaviour of the heat transfer at large Reynolds numbers.

If the distribution of the wall temperature $T_w(x)$ is dependent on x , one must be careful in applying the coefficient of heat transfer $\alpha = q_w/(T_w - T_\infty)$, since at positions with $T_w = T_\infty$, α will in general become singular. Therefore the formation of the Nusselt number with the local temperature difference is not recommended for variable $T_w(x)$. A fixed temperature difference (at one reference point) or the outer flow temperature T_∞ would then be suitable reference quantities, cf. K. Gersten; H. Herwig (1992), p. 16 and the example in Sect. 9.4 (linear wall temperature distribution at a flat plate at zero incidence).

9.3 Effect of the Prandtl Number

It is seen from Eq. (9.10) that the Prandtl number is the salient characteristic number for thermal boundary layers and heat transfer in forced convection. The Prandtl number is a physical property, and, from its definition $\text{Pr} = \nu/a$, is the ratio of two quantities which characterise the transport properties of the fluid with respect to the momentum (kinematic viscosity) and with respect to the heat (thermal diffusivity). If the transport property with respect to the momentum, i.e. the viscosity, is particularly large, the momentum decreasing effect of the wall (no-slip condition) will extend well into the flow, i.e. the thickness δ of the velocity boundary layer will be relatively large. The same holds for the thickness δ_{th} of the thermal boundary layer. Thus it is understandable that the Prandtl number for forced convection is a direct measure of the ratio of the thicknesses of the two boundary layers.

For the plate at zero incidence, with $\text{Pr} = 1$ (i.e. $\nu = a$) and $T_w = \text{const}$, the differential equations for $u^* = u/U_\infty$ (Eq. (6.14)) and for $1 - \vartheta_1$ (Eq. (9.10)) including the boundary conditions are identical. In this case the velocity boundary layer and the thermal boundary layer have the same thickness ($\delta = \delta_{th}$). For $\text{Pr} = 1$ for any other flow, the two boundary-layer thicknesses are of the same order of magnitude.

The two limiting cases of very small and very large Prandtl numbers are of particular interest since they lead to greatly simplified calculations of the heat transfer. Here only the standard case $T_w = \text{const}$ will be considered.

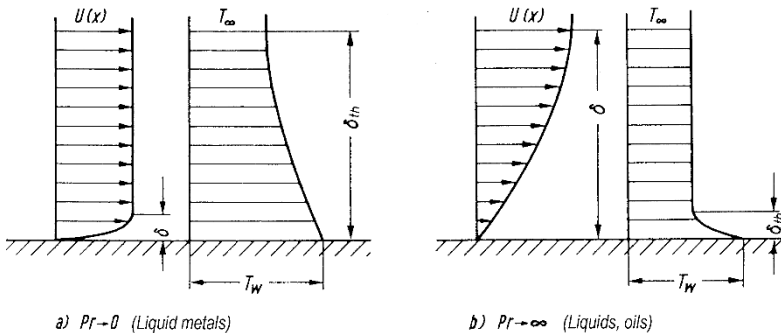


Fig. 9.2 a,b. Comparison of the distributions of velocity and temperature for boundary-layer flows with very small and with very large Prandtl numbers

Small Prandtl numbers. As can be seen from Fig. 9.2a, for small Prandtl numbers, such as those which occur in liquid metals (e.g. mercury), because $\delta_{th} \gg \delta$, the velocity boundary layer can be disregarded when calculating the thermal boundary layer. Therefore the velocities $u(x, y)$ and $v(x, y)$ can be replaced by the corresponding velocities at the outer edge of the velocity boundary layer $u(x, y) = U(x)$ and $v(x, y) = -(dU/dx)y$ (this follows from

the continuity equation). The energy equation (9.13) then assumes the simple form

$$U(x) \frac{\partial T}{\partial x} - y \frac{dU}{dx} \frac{\partial T}{\partial y} = a \frac{\partial^2 T}{\partial y^2} . \quad (\text{Pr} \rightarrow 0) \quad (9.30)$$

By introducing the similarity variable

$$\eta = y \frac{U(x)}{2 \sqrt{a \int_{x_0}^x U(x) dx}} \quad (9.31)$$

with the meaning of x_0 as in Fig. 9.1, we obtain the following *ordinary* differential equation for $\vartheta_1(x, y, x_0) = \vartheta(\eta) = (T - T_\infty)/(T_w - T_\infty)$

$$\vartheta'' + 2\eta\vartheta' = 0, \quad \vartheta(0) = 1, \quad \vartheta(\eta \rightarrow \infty) = 0 . \quad (9.32)$$

The solution is the Gaussian error function, cf. Eq. (5.98). This reduction to a similar solution is only possible for the standard case $T_w = \text{const}$.

Thus we obtain the following universal quadrature formula for the local Nusselt number:

$$\text{Nu} = \frac{\alpha l}{\lambda} = \frac{U(x)l}{\sqrt{\pi\nu \int_{x_0}^x U(x) dx}} \text{Pr}^{1/2} \quad (\text{Pr} \rightarrow 0, T_w = \text{const}) . \quad (9.33)$$

The formulae resulting from this for the flat plate at zero incidence ($U = U_\infty$) and the stagnation-point flow ($U(x) = ax$) are given in Table 9.1 for $x_0 = 0$.

For the flat plate at zero incidence it is found from Eq. (9.33) that the coefficient of heat transfer $\alpha(x, x_0)$ in Eq. (9.17) for the standard problem in Fig. 9.1 is

$$\alpha(x, x_0) = \sqrt{\frac{U_\infty \lambda^2}{\pi\nu(x - x_0)}} \text{Pr}^{1/2} \quad (x > x_0) . \quad (9.34)$$

As an example of the application of Eq. (9.18), let us consider the flat plate at zero incidence with a power function for the wall temperature distribution: $T_w(x) - T_\infty = bx^n$. This delivers the result, cf. K. Gersten; H. Körner (1968):

$$\frac{\text{Nu}}{\sqrt{\text{Re}}} = \frac{\Gamma(1+n)}{\Gamma(\frac{1}{2}+n)} \left(\frac{x}{l} \right)^{-1/2} \text{Pr}^{1/2} \quad (\text{Pr} \rightarrow 0) . \quad (9.35)$$

Since Nu is formed with respect to $T_w(x) - T_\infty = bx^n$, for $n = 1/2$ the heat flux q_w is constant, see Table 9.1.

An overview of the solutions for small Prandtl numbers can be found in S.R. Galante; S.W. Churchill (1990).

Large Prandtl numbers. The other limiting case of $\text{Pr} \rightarrow \infty$ was first solved many years ago by M.A. Lévêque (1928). The thickness of the thermal boundary layer δ_{th} is very small compared to the thickness of the velocity boundary layer δ , cf. Fig. 9.2b. In the limiting case $\text{Pr} \rightarrow \infty$, the entire thermal boundary layer lies within that region where the velocity profile still depends linearly on y . The same circumstances can also occur for intermediate Prandtl numbers if, for somewhat more fully developed boundary layers, the thermal boundary layer as in Fig. 9.1 starts with a temperature jump at the wall at the position $x = x_0$. If we take the following solutions for the velocity components close to the wall

$$u(x, y) = \frac{\tau_w(x)}{\mu} y, \quad v(x, y) = -\frac{d\tau_w}{dx} \frac{y^2}{2\mu}, \quad (9.36)$$

the resulting energy equation (9.13) can be reduced to an ordinary differential equation by means of a similarity transformation. Introducing the similarity variable

$$\eta = y \sqrt{\frac{\tau_w}{\mu}} \left(9a \int_{x_0}^x \sqrt{\frac{\tau_w(x)}{\mu}} dx \right)^{-1/3} \quad (9.37)$$

with the jump position x_0 as in Fig. 9.1, for the standard case $T_w = \text{const}$ we obtain the following differential equation:

$$\frac{d^2 T}{d\eta^2} + 3\eta^2 \frac{dT}{d\eta} = 0. \quad (9.38)$$

The solution of this equation can be given in terms of the incomplete gamma function. The following quadrature formula then holds for the Nusselt number:

$$\boxed{\text{Nu} = \frac{\alpha l}{\lambda} = 0.5384 l \left(\frac{\varrho}{\mu^2} \right)^{1/3} \sqrt{\tau_w} \left(\int_{x_0}^x \sqrt{\tau_w} dx \right)^{-1/3} \text{Pr}^{1/3}} \quad (9.39)$$

$$(\text{Pr} \rightarrow \infty, T_w = \text{const}),$$

where $0.5384 = 3^{1/3}/\Gamma(1/3)$.

These formulae are given for the particular cases of the flat plate at zero incidence ($\tau_w = 0.332\mu U_\infty \sqrt{U_\infty/\nu x}$) and the stagnation-point flow ($\tau_w = 1.2326\sqrt{\varrho\mu a^3 x}$) in Table 9.1 (for $x_0 = 0$). By using Eq. (9.18), the wall heat flux can also be determined for arbitrary temperature differences, cf. M.J. Lighthill (1950), H.W. Liepmann (1958) and F.M. White (1974), p. 334. As will be shown when we consider Fig. 9.3, the asymptotic formulae for $\text{Pr} \rightarrow \infty$ are also good approximations for moderate Prandtl numbers.

Table 9.1. Asymptotic formulae for the heat transfer at the plate, stagnation point and wall jet. The (“heated”) wall jet has the temperature T_∞ at $x = 0$

	$\text{Pr} \rightarrow 0$	$\text{Pr} \rightarrow \infty$
flat plate $T_w = \text{const}$	$\frac{\text{Nu}}{\sqrt{\text{Re}}} = \frac{1}{\sqrt{\pi}} \left(\frac{x}{l}\right)^{-1/2} \text{Pr}^{1/2}$	$\frac{\text{Nu}}{\sqrt{\text{Re}}} = 0.339 \left(\frac{x}{l}\right)^{-1/2} \text{Pr}^{1/3}$
flat plate $q_w = \text{const}$	$\frac{\text{Nu}}{\sqrt{\text{Re}}} = \frac{\sqrt{\pi}}{2} \left(\frac{x}{l}\right)^{-1/2} \text{Pr}^{1/2}$	$\frac{\text{Nu}}{\sqrt{\text{Re}}} = 0.464 \left(\frac{x}{l}\right)^{-1/2} \text{Pr}^{1/3}$
stagnation point $V = U(x)l/x$	$\frac{\text{Nu}}{\sqrt{\text{Re}}} = \sqrt{\frac{2}{\pi}} \text{Pr}^{1/2}$	$\frac{\text{Nu}}{\sqrt{\text{Re}}} = 0.661 \text{Pr}^{1/3}$
heated wall jet $T_w = \text{const}$	$\frac{\text{Nu}}{\text{Re}^{3/4}} = 0.629 \left(\frac{x}{l}\right)^{-3/4} \text{Pr}$	$\frac{\text{Nu}}{\text{Re}^{3/4}} = 0.235 \left(\frac{x}{l}\right)^{-3/4} \text{Pr}^{1/3}$
heated wall jet $q_w = \text{const}$	$\frac{\text{Nu}}{\text{Re}^{3/4}} = 0.629 \left(\frac{x}{l}\right)^{-3/4} \text{Pr}$	$\frac{\text{Nu}}{\text{Re}^{3/4}} = 0.422 \left(\frac{x}{l}\right)^{-3/4} \text{Pr}^{1/3}$

The formula (9.39) breaks down in the separation point because $\tau_w = 0$. An expansion of the solution for the velocity distribution up to the quadratic term

$$u(x, y) = \frac{\tau_w(x)}{\mu} y + \frac{1}{2\mu} \frac{dp}{dx} y^2 \quad (9.40)$$

can yield some improvement, cf. D.B. Spalding (1958). We will look at this special case in the following section (for $\tau_w = 0$ we find $\text{Nu} \sim \text{Pr}^{1/4}$).

9.4 Similar Solutions of the Thermal Boundary Layer

Since the temperature field is dependent on the velocity field, a necessary condition for the occurrence of similar temperature profiles is that there are similar solutions for the velocity field. In Sect. 7.2 we treated those flows where the velocity field leads to similar solutions. We now look at the problem of determining for which thermal boundary conditions these flows also lead to similar solutions for the temperature field. An analysis similar to that in Sect. 7.2 will show that similar temperature profiles in the boundary layer arise when the distribution of the wall temperature obeys a power law.

Introducing the dimensionless temperature difference

$$\vartheta(\eta) = \frac{T(x, y) - T_\infty}{\Delta T_R \cdot \xi^n} \quad (9.41)$$

with $\xi = x/l$, and using the following trial solutions from Sect. 7.2.1:

$$u(x, y) = U_N(\xi) f'(\eta), \quad (9.42)$$

$$-v(x, y) = \frac{1}{\sqrt{\text{Re}}} \left[f(\eta) \frac{d}{d\xi} (U_N \bar{\delta}) - U_N \frac{d\bar{\delta}}{d\xi} \eta f' \right], \quad (9.43)$$

$$\eta = \frac{y}{l} \frac{\sqrt{\text{Re}}}{\bar{\delta}(\xi)}, \quad (9.44)$$

we can use the momentum equation, cf. Eq. (7.14) to obtain

$$f''' + \alpha_1 f f'' + \alpha_2 - \alpha_3 f'^2 = 0 \quad (9.45)$$

and from the energy equation (9.13)

$$\vartheta'' + \text{Pr} (\alpha_1 f \vartheta' - \alpha_4 f' \vartheta) = 0. \quad (9.46)$$

Here the constants α_1 to α_3 have the same meanings as in Eq. (7.13). The additional constant α_4 is

$$\alpha_4 = n \frac{U_N(\xi) \bar{\delta}^2(\xi)}{V\xi}. \quad (9.47)$$

If we choose the following boundary conditions for Eq. (9.46):

$$\eta = 0 : \quad \vartheta = 1; \quad \eta \rightarrow \infty : \quad \vartheta = 0, \quad (9.48)$$

it follows from Eq. (9.41) that

$$T_w(x) - T_\infty = \Delta T_R \xi^n. \quad (9.49)$$

Therefore $\Delta T_R = T_w(x = l) - T_\infty$.

From the gradient at the wall ϑ'_w we obtain the Nusselt number from $\text{Nu} = q_w l / [\lambda(T_w(x) - T_\infty)]$ as

$$\frac{\text{Nu}}{\sqrt{\text{Re}}} = - \frac{\vartheta'_w}{\bar{\delta}(\xi)}. \quad (9.50)$$

The two standard boundary conditions are

$$\begin{aligned} T_w &= \text{const} : \quad n = 0 \\ q_w &= \text{const} : \quad \xi^n / \bar{\delta}(\xi) = \text{const}. \end{aligned} \quad (9.50a)$$

A comparison of Eqs. (9.45) and (9.46) shows that for $\text{Pr} = 1$, $\alpha_2 = 0$ and $\alpha_3 = \alpha_4$ and for appropriate boundary conditions we find

$$\vartheta = 1 - f', \quad \vartheta'_w = -f''_w. \quad (9.51)$$

In the literature, this special case is called the *Reynolds analogy*. It can only occur at constant pressure ($\alpha_2 = 0$), that is, either for the flat plate ($\alpha_3 = 0$) or for the wall jet ($\alpha_3 = -2$).

In the special case of $\alpha_4 = -\alpha_1$, Eq. (9.46) may be integrated to give the result $\vartheta'_w = 0$; i.e. heat is only transferred to the flow at the singular origin (leading edge).

As in Sect. 7.2.1, we can differentiate between the following cases:

1. Boundary layers with a wall

1.1 Wedge flow ($\alpha_1 = 1, \alpha_2 = \alpha_3 = \beta, \alpha_4 = n(2 - \beta)$)

From Eq. (9.46) the energy equation reads

$$\vartheta'' + \text{Pr} \left(f\vartheta' - \frac{2n}{m+1} f'\vartheta \right) = 0 \quad (9.52)$$

with the boundary conditions from Eq. (9.48). Because $U \sim \xi^m$ and $\bar{\delta} \sim \xi^{(1-m)/2}$ from Eq. (7.18), instead of Nu and Re, the following characteristic numbers are used for wedge flow:

$$\text{Nu}_x = \frac{q_w x}{\lambda[T_w(x) - T_\infty]}, \quad \text{Re}_x = \frac{U(x)x}{\nu}. \quad (9.53)$$

Thus instead of Eq. (9.50) we obtain

$$\frac{\text{Nu}_x}{\sqrt{\text{Re}_x}} = -\sqrt{\frac{m+1}{2}} \vartheta'_w(m; n; \text{Pr}). \quad (9.54)$$

For the standard boundary conditions $q_w = \text{const}$, Eq. (9.50a) yields

$$n = \frac{1-m}{2} \quad (q_w = \text{const}). \quad (9.55)$$

Some numerical values for ϑ'_w can easily be determined from Table 9.2:

plate, $T_w = \text{const}$	$\vartheta'_w = -\text{Pr}\sqrt{a_T/2}$
plate, $q_w = \text{const}$	$\vartheta'_w = -\text{Pr}\sqrt{2a_T}$
stagnation point	$\vartheta'_w = -\text{Pr}\sqrt{a_T/(1+b_T)}$

The numerical values for the limiting cases $\text{Pr} \rightarrow 0$ and $\text{Pr} \rightarrow \infty$ correspond to the formulae in Table 9.1, but can also be obtained in part from Eqs. (9.33), (9.35) and (9.39). Explicit formulae for arbitrary values of m and n can also be stated in both limiting cases, cf. K. Gersten; H. Körner (1968). Here, for $\text{Pr} \rightarrow \infty$, we have to distinguish between cases where $\tau_w \neq 0$ ($f''_w \neq 0$) and those where the wall shear stress vanishes ($\tau_w = 0, f''_w = 0$). The dependence of the Nusselt number on the Prandtl number is different for these two cases. For $\tau_w \neq 0$ we find $\text{Nu}_x \sim \text{Pr}^{1/3}$, while for $\tau_w = 0$ the dependence is $\text{Nu}_x \sim \text{Pr}^{1/4}$. This latter dependence can therefore not be acquired from the formula for cases $\tau_w \neq 0$ by setting $\tau_w \rightarrow 0$ there. Rather we need to carry out a double limit $\text{Pr} \rightarrow \infty, f''_w \rightarrow 0$, noting that the order of taking the limit is of importance.

Figure 9.3 shows the dependence of the local Nusselt number on the Prandtl number, from numerical work by H.L. Evans (1962). These are cases where the wall temperature is constant ($n = 0$).

Further solutions of Eq. (9.52) have been given by H.L. Evans (1968) and K. Gersten; H. Körner (1968).

Since the energy equation (9.13) is linear, the different solutions for power distributions of the wall temperature in Eq. (9.49) can be *superimposed* on one another to generate solutions for arbitrary temperature distributions which can be expanded as power series.

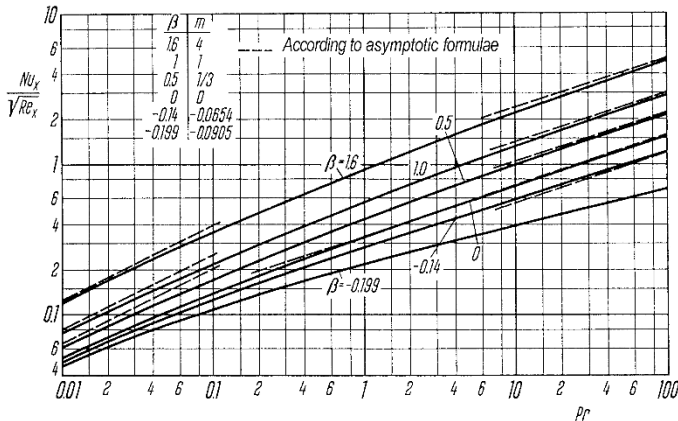


Fig. 9.3. Dependence of the local Nusselt number on the Prandtl number and the flow parameter m for wedge flows, as in Eq. (9.54) ($U \sim x^m$, $T_w = \text{const}$, neglecting dissipation). Dashed lines are asymptotes

Example: Linear temperature distribution at a plate ($\text{Pr} = 0.7$)

For the wall temperature distribution

$$T_w(x) - T_\infty = (T_w - T_\infty)_{x=0} \left(1 - 2 \frac{x}{l} \right)$$

and the quantities from Eq. (9.54)

$$\vartheta'_w(0; 0; 0.7) = -0.414; \quad \vartheta'_w(0; 1; 0.7) = -0.675$$

we obtain the distribution of the wall heat flux

$$\widetilde{\text{Nu}} = \frac{q_w(x)l}{\lambda T_\infty} = \sqrt{\text{Re}} \frac{(T_w - T_\infty)_{x=0}}{T_\infty} \left(\frac{x}{l} \right)^{-1/2} \left(0.293 - 0.954 \frac{x}{l} \right).$$

Here the Nusselt number $\widetilde{\text{Nu}}$ was formed with the temperature T_∞ . It would not be particularly sensible in this example to form the Nusselt number as usual with the temperature difference $T_w(x) - T_\infty$, because this difference vanishes at $x = l/2$, although the wall heat flux is indeed non-zero at this position. Since in the general case $q_w(x)$ is not proportional to $T_w(x) - T_\infty$, the Nusselt number should be formed with either one temperature (e.g. T_∞) or else a non-vanishing temperature difference (here for example with $(T_w(x) - T_\infty)_{x=0}$).

In this example, heat is removed from the flow in the region $0.307 < x/l < 0.5$ for $(T_w(x) - T_\infty)_{x=0}$ (heat is transferred from the fluid to the wall), even though $T_w > T_\infty$. The explanation for this is as follows: since the fluid close to the wall comes from boundary-layer regions further upstream with higher temperatures, it has attained a temperature which is higher than the local wall temperature in that particular region.

1.2 Wedge flow in reverse ($\alpha_1 = -1, \alpha_2 = \alpha_3 = -\beta, \alpha_4 = -r(2 - \beta)$)**1.3 Flow in a convergent channel ($\alpha_1 = 0, \alpha_2 = \alpha_3 = 1, \alpha_4 = -r$)**

Example: $r\text{Pr} = -2 : \vartheta'_w = -1/f''_w = -0.866$.

1.4 Moving flat plate ($\alpha_1 = 1, \alpha_2 = \alpha_3 = 0, \alpha_4 = 2r$)

Example: $r = 0, \text{Pr} = 0.7 : \vartheta'_w = -0.494$.

1.5 Wall jet ($\alpha_1 = 1, \alpha_2 = 0, \alpha_3 = -2, \alpha_4 = 4n$)

Numerical values for the wall jet can be found in K. Gersten; S. Schilawa (1978) and S. Schilawa (1981).

As well as the solution of the energy equation for the wall jet

$$\vartheta'' + \text{Pr}(f\vartheta' - 4nf'\vartheta) = 0 \quad (9.56)$$

with the inhomogeneous boundary condition (9.48) (for $q_w = \text{const}$ we have $n = 3/4$), an “eigen-solution” of Eq. (9.56) with homogeneous boundary conditions $\eta = 0 : \vartheta = 0; \eta \rightarrow \infty : \vartheta = 0$ also exists. The eigenvalue of this solution is

$$n = -\frac{3\text{Pr} + 1}{8\text{Pr}}. \quad (9.57)$$

This is the case of the “hot wall jet” which is blown along the wall with temperature $T_w = T_\infty$, cf. W.H. Schwartz; B. Caswell (1961).

2. Boundary layers without a wall**2.1 Mixing layer ($\alpha_1 = 1, \alpha_2 = \alpha_3 = 0, \alpha_4 = 0$)**

With the boundary conditions

$$\eta \rightarrow \infty : \vartheta = 1; \quad \eta \rightarrow +\infty : \vartheta = 0,$$

ΔT_R in Eq. (9.41) is the temperature difference between the two parallel jets.

2.1 Free jet ($\alpha_1 = 1, \alpha_2 = 0, \alpha_3 = -1, \alpha_4 = 2n$)

As in the case of the wall jet, we must distinguish between two cases here. If the fluid on each sides of the free jet has a different temperature, the boundary conditions

$$\eta \rightarrow -\infty : \vartheta = 1; \quad \eta \rightarrow +\infty : \vartheta = 0$$

can be satisfied for $n = 0$. In addition there exists an “eigen-solution”, that of the “hot free jet”. This has the eigenvalue $n = -1/2$ with the general solution

$$\vartheta = (f')^{\text{Pr}}. \quad (9.58)$$

The eigenvalue emerges from the demand that the thermal energy in the free jet must be independent of the distance along the jet.

9.5 Integral Methods for Computing the Heat Transfer

In Chap. 8 we looked at the integral methods to compute the velocity boundary layer. These were useful whenever one was interested in approximate solutions for the wall shear stress distribution.

An analogous integral method for the approximate calculation of the heat transfer can also be developed. The basis of this is the integral relation obtained from the thermal energy equation. If we integrate Eq. (9.13) from $y = 0$ to $y \rightarrow \infty$, we find the *thermal-energy-integral equation*:

$$\frac{d}{dx} \{ [T_w(x) - T_\infty] U(x) \delta_T(x) \} = \frac{q_w}{\rho c_p} \quad (9.59)$$

with the *thermal energy thickness*

$$\delta_T(x) = \int_0^\infty \frac{T(x, y) - T_\infty}{T_w(x) - T_\infty} \frac{u(x, y)}{U(x)} dy . \quad (9.60)$$

Since Eq. (9.59) is constructed in a similar manner to the momentum-integral equation (8.1), it seems natural to exploit this formal similarity in order to obtain a quadrature formula corresponding to Eq. (8.23).

To this end, we first, in analogy to Eqs. (8.12) and (8.13), define the following quantities:

$$Z_T(x) = \frac{\delta_T^2}{\nu} U , \quad (9.61)$$

$$\Gamma_T(x) = -\frac{\delta_T^2}{U} \left(\frac{\partial^2 u}{\partial y^2} \right)_w = \frac{\delta_T^2}{\nu} \frac{dU}{dx} . \quad (9.62)$$

Corresponding to Eq. (8.19), the thermal-energy-integral equation (9.59) then yields

$$\frac{dZ_T}{dx} = F_{T2}(\Gamma_T) \quad (9.63)$$

with

$$F_{T2} = \frac{2\delta_T q_w}{\mu c_p (T_w - T_\infty)} - \left(1 + 2 \frac{U}{dU/dx} \frac{dT_w/dx}{T_w - T_\infty} \right) \Gamma_T . \quad (9.64)$$

If we now approximate F_{T2} by the linear relation

$$F_{T2}(\Gamma_T) = a_T - b_T \Gamma_T \quad (9.65)$$

in analogy to Eq. (8.20), and, with $Z_T(0) = 0$, we obtain the following quadrature formula for $Z_T(x)$:

$$Z_T(x) = \frac{a_T}{[U(x)]^{b_T}} \int_0^x [U(x)]^{b_T} dx . \quad (9.66)$$

Table 9.2. Constants in the quadrature formula (9.66)

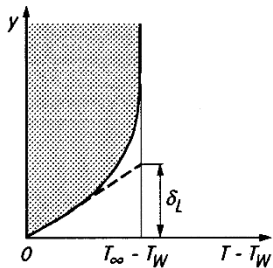
Pr	$T_w = \text{const}$		$q_w = \text{const}$	
	a_T	b_T	a_T	b_T
$\rightarrow 0$	$4/(\text{Pr} \pi)$	1	$\pi/(4\text{Pr})$	0.234
0.01	106.58	0.845	60.170	0.042
0.1	7.841	0.627	4.027	-0.164
0.7	0.699	0.393	0.336	-0.330
1	0.441	0.355	0.211	-0.353
5	0.053	0.222	0.025	-0.425
7	0.034	0.202	0.016	-0.435
10	0.011	0.183	0.010	-0.445
100	0.001	0.108	0.000	-0.481
$\rightarrow \infty$	$0.459\text{Pr}^{-4/3}$	0.051	$0.215\text{Pr}^{-4/3}$	-0.508

The constants a_T and b_T are now dependent on the Prandtl number and the thermal boundary condition. They can be determined by the demand that Eq. (9.66) yield exact results for the plate flow and for the stagnation-point flow. The numerical values $a_T(\text{Pr})$ and $b_T(\text{Pr})$ found in this manner are shown in Table 9.2. From the solutions for $Z_T(x)$ we find for the Nusselt number

$$T_w = \text{const} : \quad \frac{\text{Nu}}{\sqrt{\text{Re}}} = \frac{\text{Pr}}{2} \sqrt{\frac{Ul}{Z_TV}} \left[a_T + \frac{Z_T}{U} \frac{dU}{dx} (1 - b_T) \right], \quad (9.67a)$$

$$q_w = \text{const} : \quad \frac{\text{Nu}}{\sqrt{\text{Re}}} = \frac{\text{Pr}}{x} \sqrt{\frac{U Z_T l}{V}}. \quad (9.67b)$$

As is to be expected, the integral method yields very good results close to the stagnation point of a body in a flow. On the other hand, the deviations from the exact solution of the thermal boundary layer in regions where the pressure increases become large, more particularly so close to separation. This could be improved by another choice of a_T and b_T , however, in practice, the transition to the turbulent boundary layer takes place in the region of increasing pressure, so that it is mainly the laminar boundary layer close to the stagnation point which is of importance.

Fig. 9.4. The conduction thickness δ_L

Note. In the literature the quantity $\delta_L(x)$, called the *conduction thickness*, is frequently used instead of $\delta_T(x)$, cf. A.G. Smith; D.B. Spalding (1958). The definition reads

$$\delta_L = \frac{\lambda(T_w - T_\infty)}{q_w} . \quad (9.68)$$

From Fig. 9.4, with $q_w = -\lambda(\partial T / \partial y)_w$, the meaning of δ_L is clear. In analogy to Eq. (9.61), the quantity $Z_L = \delta_L^2 U / \nu$ can again be given by a quadrature formula such as that in Eq. (9.66). The constants a_L and b_L which appear in this have a simple relationship with the constants a_T and b_T in Table 9.2, cf. K. Gersten; H. Herwig (1992), p. 174.

Example: Heat transfer at a circular cylinder

Figure 9.5 shows the Nusselt number on the circumference of a circular cylinder. Here the empirical velocity distribution from Eq. (8.41), obtained from a measured pressure distribution, was used. The calculation was carried out for a Prandtl number of $\text{Pr} = 0.7$, for the standard case $T_w = \text{const}$. As well as the numerical solution

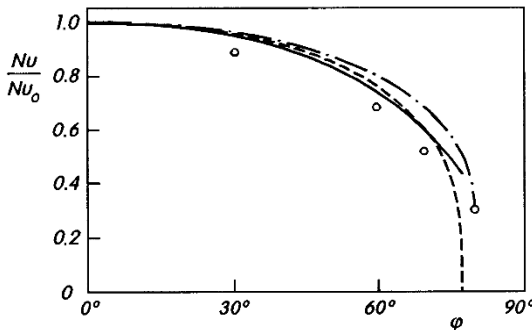


Fig. 9.5. Distribution of the local Nusselt number at a circular cylinder for $\text{Pr} = 0.7$. Velocity distribution $U(x)$ from Eq. (8.41)

- - - numerical solution
- integral method from Eq. (9.66)
- - - asymptotic formula (9.39) with the τ_w distribution according to the quadrature formula (8.23)
- measurements by E. Schmidt; K. Wenner (1941), see H. Schlichting (1982), p. 317, $\text{Re} = 4 \cdot 10^4 - 10^5$

of the energy equation (9.10), the results from the integral method, Eq. (9.66), and from the asymptotic formula (9.39) are given. The results of the quadrature formula (8.23) have been used for the wall shear stress in Eq. (9.39). Apart from directly close to separation, the agreement is very good. Possible effects of variable physical properties are discussed in Sect. 10.3.2.

9.6 Effect of Dissipation; Distribution of the Adiabatic Wall Temperature

The considerations up to now regarding thermal boundary layers were generally carried out with the dissipation neglected. We now propose to treat the effects of dissipation in detail. In this case the distribution of the so-called *adiabatic wall temperature* T_{ad} is important. As a consequence of the dissipation in the boundary layer, even if there is no heat transfer to a body in a flow, a thermal boundary layer forms at the body. If the surface of the body is impermeable to heat, i.e. adiabatic, the dissipation means that the distribution of the wall temperature is such that it is above the surrounding temperature.

For the temperature field at an adiabatic body

$$\Theta = \frac{T - T_\infty}{V^2/(2c_p)} = \frac{\vartheta}{Ec/2} \quad (9.69)$$

we have, from Eq. (9.6), the energy equation

$$u^* \frac{\partial \Theta}{\partial x^*} + \bar{v} \frac{\partial \Theta}{\partial \bar{y}} = \frac{1}{Pr} \frac{\partial^2 \Theta}{\partial \bar{y}^2} + 2 \left(\frac{\partial u^*}{\partial \bar{y}} \right)^2 \quad (9.70)$$

with the boundary conditions

$$\bar{y} = 0 : \quad \frac{\partial \Theta}{\partial \bar{y}} = 0, \quad \bar{y} \rightarrow \infty : \quad \Theta = 0 .$$

From the solution $\Theta_w(x^*, Pr)$ we obtain the adiabatic wall temperature

$$\frac{T_{ad} - T_\infty}{V^2/(2c_p)} = \Theta_w(x^*, Pr) . \quad (9.71)$$

The dependence of the adiabatic wall temperature on the Prandtl number can be given exactly for the two limiting cases of small and large Prandtl numbers.

Small Prandtl numbers. If we set $\bar{\Theta} = \Theta/Pr$ in Eq. (9.70) it follows that

$$Pr \left(u^* \frac{\partial \bar{\Theta}}{\partial x^*} + \bar{v} \frac{\partial \bar{\Theta}}{\partial \bar{y}} \right) = \frac{\partial^2 \bar{\Theta}}{\partial \bar{y}^2} + 2 \left(\frac{\partial u^*}{\partial \bar{y}} \right)^2 . \quad (9.72)$$

For the limiting case $Pr \rightarrow 0$, this equation reduces to

$$\frac{\partial^2 \bar{\Theta}}{\partial \bar{y}^2} = -2 \left(\frac{\partial u^*}{\partial \bar{y}} \right)^2 \quad (9.73)$$

with the solution

$$\frac{1}{\text{Pr}} \left(\frac{\partial \Theta}{\partial \bar{y}} \right)_w = \left(\frac{\partial \bar{\Theta}}{\partial \bar{y}} \right)_w = 2 \int_0^\infty \left(\frac{\partial u^*}{\partial \bar{y}} \right)^2 d\bar{y}. \quad (9.74)$$

Therefore, since the convective terms vanish in this limiting case, the internal energy produced by dissipation is transferred *locally* to the wall. The adiabatic wall temperature distribution must now (neglecting the dissipation) compensate precisely this wall heat flux given by Eq. (9.74). From Eq. (9.20) we then obtain the adiabatic wall temperature as

$$T_{\text{ad}}(x) - T_\infty = \int_0^x g(x, x_0) \cdot \text{Pr} \cdot \frac{\lambda}{c_p} \frac{d}{dx_0} \left(\int_0^\infty \left(\frac{\partial u}{\partial y} \right)^2 dy \right) dx_0. \quad (9.75)$$

Since the distribution $g(x, x_0)$ of the standard solution is proportional to $\text{Pr}^{-1/2}$, we finally obtain

$$\frac{T_{\text{ad}}(x^*) - T_\infty}{V^2/(2c_p)} = \text{Pr}^{1/2} F(x^*) \quad (\text{Pr} \rightarrow 0). \quad (9.76)$$

Large Prandtl numbers. If, in analogy to Eq. (9.36), we set

$$u^* = \tau_w^*(x^*) \bar{y}, \quad \bar{v} = - \frac{d\tau_w^*}{dx^*} \frac{\bar{y}^2}{2}, \quad (9.77)$$

we obtain, from Eq. (9.70)

$$\tau_w^* \bar{y} \frac{\partial \Theta}{\partial x^*} - \frac{1}{2} \frac{d\tau_w^*}{dx^*} \bar{y}^2 \frac{\partial \Theta}{\partial \bar{y}} = \frac{1}{\text{Pr}} \frac{\partial^2 \Theta}{\partial \bar{y}^2} + 2\tau_w^{*2}. \quad (9.78)$$

Using the transformation

$$\Theta(x^*, \bar{y}) = \bar{\Theta}(x^*, Y) \text{Pr}^{1/3}, \quad \bar{y} = \text{Pr}^{-1/3} Y \quad (9.79)$$

we get the following equation which is independent of the Prandtl number:

$$\tau_w^* Y \frac{\partial \bar{\Theta}}{\partial x^*} - \frac{1}{2} \frac{d\tau_w^*}{dx^*} Y^2 \frac{\partial \bar{\Theta}}{\partial Y} = \frac{\partial^2 \bar{\Theta}}{\partial Y^2} + 2\tau_w^{*2}. \quad (9.80)$$

From the solution $\bar{\Theta}_w(x^*)$ it then follows that the adiabatic wall temperature is

$$\frac{T_{\text{ad}} - T_\infty}{V^2/(2c_p)} = \text{Pr}^{1/3} \bar{\Theta}_w(x^*) \quad (\text{Pr} \rightarrow \infty). \quad (9.81)$$

It can be seen from this formula that, for large Prandtl numbers, the temperature increase via dissipation can be considerable, even for moderate velocities.

Flat plate. Using the solutions

$$u^* = \frac{u}{U_\infty} = f'(\eta), \quad \bar{v} = \frac{1}{\sqrt{2x^*}}(\eta f' - f), \quad \eta = \frac{\bar{y}}{\sqrt{2x^*}} \quad (9.82)$$

from Eq. (6.45), (6.47) and (6.48), we obtain the following differential equation from Eq. (9.70)

$$\frac{1}{Pr} \Theta'' + f\Theta' = -2f'^2 \quad (9.83)$$

with the boundary conditions

$$\eta = 0 : \quad \Theta' = 0, \quad \eta \rightarrow \infty : \quad \Theta = 0 .$$

The following quadrature formula can be given for the solution:

$$\Theta(\eta, Pr) = 2 Pr \int_{\eta}^{\infty} [f''(\xi)]^{Pr} \left(\int_0^{\xi} [f''(\tau)]^{2-Pr} d\tau \right) d\xi . \quad (9.84)$$

This yields, e.g. for $Pr = 1$:

$$\Theta(\eta, 1) = 1 - f'^2(\eta) . \quad (9.85)$$

For the adiabatic wall temperature it thus follows that, for arbitrary Prandtl number

$$r(Pr) = \frac{T_{ad} - T_\infty}{U_\infty^2 / (2c_p)} = \Theta_w(Pr) . \quad (9.86)$$

In the case of the flat plate, the adiabatic wall temperature is constant, i.e. independent of x . It is also called the eigen-temperature.

The dimensionless temperature increase of an adiabatic wall as a consequence of dissipation given by Eq. (9.86) is also called the *recovery factor*, since the denominator

$$(\Delta T)_{ad} = T_0 - T_\infty = \frac{U_\infty^2}{2c_p} \quad (9.87)$$

is the temperature increase due adiabatic compression of an ideal gas at constant specific heat capacity. Here T_0 is the *total temperature* of the outer flow. For $Pr = 1$, from Eq. (9.85), we have $r = 1$, i.e. the increase of the wall temperature due to dissipation is precisely the temperature increase due to adiabatic compression.

Figure 9.6 shows $r(Pr)$ as a function of the Prandtl number. From this, the recovery factor for $Pr < 1$ is less than one, while that for $Pr > 1$ is greater than one. The asymptotes Eqs. (9.76) and (9.81) can be written down. From K. Gersten; H. Körner (1968) we have

$$r = 0.9254 Pr^{1/2} \quad (Pr \rightarrow 0) \quad (9.88)$$

while R. Narasimha; S.S. Vasantha (1966) have shown

$$r = 1.9222 Pr^{1/3} - 1.341 \quad (Pr \rightarrow \infty) . \quad (9.89)$$

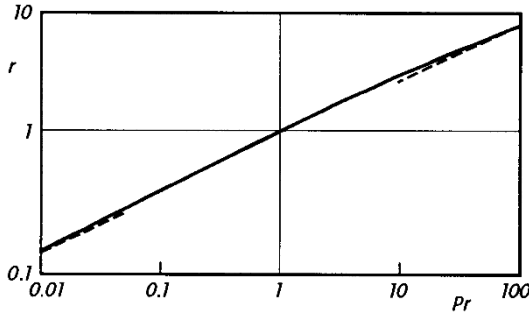


Fig. 9.6. Dependence of the recovery factor of a flat plate at zero incidence on the Prandtl number; asymptotes from Eqs. (9.88) and (9.89)

Figure 9.7 shows the measured adiabatic wall temperature of a flat plate at zero incidence at different Reynolds numbers $U_\infty x/\nu$. In the laminar region it agrees well with the theory ($r = 0.85$ for $\text{Pr} = 0.72$). As will be shown in Sect. 10.3.1, Eq. (10.25), the temperature dependence of the physical properties has practically no effect on the recovery factor. In the transition to turbulent flow, the eigen-temperature increases, cf. Sect. 18.6.

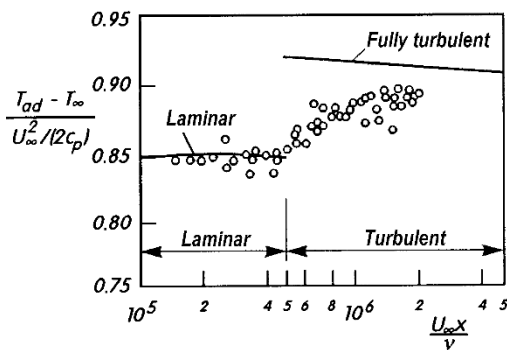


Fig. 9.7. Measurement of the adiabatic wall temperature of a flat plate at zero incidence in air, after E. Eckert; W. Weise (1942).
theory: $\text{Pr} = 0.72$
turbulent: from Eq. (18.160)

Wedge flows. $U \sim x^m$, $\beta = 2m/(m+1)$.

Using the solutions

$$\begin{aligned}
 u^* &= \frac{u}{V} = \frac{U(\bar{x})}{V} f'(\eta), \\
 \bar{v} &= -\sqrt{\frac{2}{(m+1)\bar{x}} \frac{U(\bar{x})}{V}} \left[\frac{m+1}{2} f + \frac{m+1}{2} \eta f' \right], \\
 \eta &= \frac{\bar{y}}{\sqrt{\frac{2\bar{x}}{m+1} \frac{V}{U(x)}}} = y \sqrt{\frac{m+1}{2} \frac{U(x)}{\nu x}}, \\
 \Theta &= \frac{T - T_\infty}{U^2(x)/(2c_p)}, \tag{9.90}
 \end{aligned}$$

cf. Eq. (9.41) to (9.44), we obtain, from Eq. (9.70), the following differential equation

$$\frac{1}{\text{Pr}} \Theta'' + f\Theta' - 2\beta f'\Theta = -2f''^2 \quad (9.91)$$

with the boundary conditions

$$\eta = 0 : \quad \Theta' = 0; \quad \eta \rightarrow \infty : \quad \Theta = 0.$$

From the solution $\Theta_w(\text{Pr}, m)$ we obtain the adiabatic wall temperature, or the recovery factor, as

$$r(\text{Pr}, m) = \frac{T_{\text{ad}} - T_{\infty}}{U'^2(x)/(2c_p)} = \Theta_w(\text{Pr}, m). \quad (9.92)$$

Therefore if the temperature increase due to dissipation is related to the *local* velocity (or its decrease due to adiabatic compression), we obtain a value independent of x , i.e. $T_{\text{ad}}(x) - T_{\infty} \sim x^{2m}$. Numerical values for $r(\text{Pr}, m)$ can be found in K. Gersten; H. Körner (1968). The effect of m is very small, so that Fig. 9.6 also holds for values $m \neq 0$, cf. B. Le Fur (1960).

Wall jet. It can easily be shown that the adiabatic wall temperature for a wall jet is $T_{\text{ad}} - T_{\infty} \sim x^{-1}$. Since the maximum velocity is $u_{\text{max}} \sim x^{-1/2}$, the recovery factor formed with the maximum velocity is

$$r = \frac{T_{\text{ad}} - T_{\infty}}{u_{\text{max}}^2/(2c_p)} = r(\text{Pr}), \quad (9.93)$$

yet again independent of x , cf. N. Riley (1958). For $\text{Pr} = 1$ we have $r = 0$, i.e. $T_{\text{ad}} = T_{\infty}$. In this case the wall jet transports away the total energy produced by dissipation. For $\text{Pr} = 0.72$ we have $r = 0.0029$.

Nusselt number when the dissipation is taken into account. If we take the dissipation into account, heat transfer can only occur if the actual wall temperature differs from the adiabatic wall temperature. Since the energy equation is linear, the temperature fields due to dissipation and due to a temperature difference $T_w - T_{\text{ad}}$ are superimposed on one another. A measure of the heat transfer is therefore the following Nusselt number:

$$\text{Nu} = \frac{q_w l}{\lambda(T_w - T_{\text{ad}})}. \quad (9.94)$$

If the wall temperature is in between the surrounding temperature and the adiabatic wall temperature, i.e. $T_{\infty} < T_w < T_{\text{ad}}$, heat is transferred to the body, even though its temperature is higher than that of the surroundings!

10. Thermal Boundary Layers with Coupling of the Velocity Field to the Temperature Field

10.1 Remark

In the treatment of thermal boundary layers until now, we assumed constant physical properties and so the velocity field was independent of the temperature field. In this chapter we will investigate the effect of variable physical properties. These properties are the density ϱ , the viscosity μ , the isobaric specific heat capacity c_p and the thermal conductivity λ . In the most general case, the properties can depend on the temperature and the pressure. A consequence of the dependence of the density and the viscosity on the temperature is that there is a coupling of the velocity field to the temperature field. In addition, the temperature dependence of the density means that buoyancy forces in the gravity field appear in the momentum equation. These buoyancy forces alone can produce flows called *natural convection* (or *free convection*). If buoyancy forces due to gravity also occur alongside the forced convection discussed in the last chapter, we speak of *mixed convection*.

In many practical cases (flows of liquids, constant pressure flows), it suffices to consider only the temperature dependence of the physical properties.

If we consider only moderate heat fluxes at the wall, or only moderate temperature differences, we can describe the temperature dependence of the physical properties to good approximation by linear functions of the temperature. The calculation of the boundary layers is therefore considerably simplified and leads to quite general statements about the effect of temperature dependent physical properties. This will be demonstrated in what now follows.

This is followed by the treatment of the boundary layers of compressible flows, where, in principle, arbitrary dependencies of the physical properties can be taken into account. Finally natural convection and mixed convection will be treated again. This treatment is based on a density distribution which is linearly dependent on the temperature.

10.2 Boundary-Layer Equations

In order to derive the boundary-layer equations we start with the dimensionless form of the equations of motion (4.3) to (4.5). For large values of the

Reynolds number $\text{Re} = \varrho_{\text{R}} V l / \mu_{\text{R}}$, the solution domain can be divided into two regions: the inviscid outer flow and the frictional boundary layer. The equations of motion for the boundary-layer region are simplified compared to the full equations. This is done using the boundary-layer transformation, cf. Eq. (6.6)

$$\bar{y} = y^* \sqrt{\text{Re}}, \quad \bar{v} = v^* \sqrt{\text{Re}}. \quad (10.1)$$

Taking the limit $\text{Re} \rightarrow \infty$ according to the boundary-layer transformation, Eqs. (4.3) to (4.5) yield the boundary-layer equations. They then do not contain the Reynolds number, but only the following four dimensionless characteristic numbers:

Froude number	$\text{Fr} = \frac{V}{\sqrt{gl}}$	(10.2)
Eckert number	$\text{Ec} = \frac{V^2}{c_{p\text{R}} T_{\text{R}}}$	
Prandtl number	$\text{Pr} = \frac{\mu_{\text{R}} c_{p\text{R}}}{\lambda_{\text{R}}} = \frac{\nu_{\text{R}}}{a_{\text{R}}}$	
thermal expansion number	$K_{\varrho} = \beta_{\text{R}} T_{\text{R}}$	

The two last characteristic numbers are pure physical properties. The Froude number is a measure of the effect of gravity, while the Eckert number characterises the effect of the dissipation. The index R denotes a reference state.

As was already explained in Chap. 6, the coordinate system in the boundary-layer equations follows the contour of the body. If the local angle of inclination to the horizontal at position x is $\alpha(x)$, as in Fig. 10.1, we have

$$g_x = -g \sin \alpha, \quad g_y = -g \cos \alpha. \quad (10.3)$$

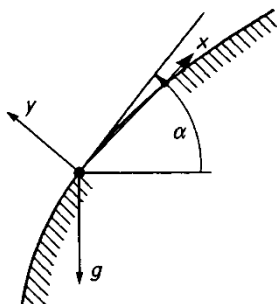


Fig. 10.1. Coordinate system in gravitational field with the local contour angle α to the horizontal

Thus the equations of motion for steady, plane boundary-layer flows in dimensional form read:

$$\frac{\partial(\varrho u)}{\partial x} + \frac{\partial(\varrho v)}{\partial y} = 0, \quad (10.4)$$

$$\varrho \left(u \frac{\partial u}{\partial x} + v \frac{\partial u}{\partial y} \right) = -\varrho g \sin \alpha - \frac{dp}{dx} + \frac{\partial}{\partial y} \left(\mu \frac{\partial u}{\partial y} \right), \quad (10.5)$$

$$\varrho c_p \left(u \frac{\partial T}{\partial x} + v \frac{\partial T}{\partial y} \right) = \frac{\partial}{\partial y} \left(\lambda \frac{\partial T}{\partial y} \right) + \beta T u \frac{dp}{dx} + \mu \left(\frac{\partial u}{\partial y} \right)^2. \quad (10.6)$$

For constant physical properties, Eqs. (10.4) and (10.5) reduce to Eqs. (6.30) and (6.31), if we interpret $p = p_{\text{mot}}$ as the pressure due only to the motion, cf. Eq. (4.19). In the same manner, Eq. (10.6) reduces to Eq. (9.12).

Instead of Eq. (10.6), another form of the energy equation is frequently used. With the generally valid relation

$$c_p \frac{DT}{Dt} = \frac{Dh}{Dt} - \frac{1 - \beta T}{\varrho} \frac{Dp}{Dt},$$

cf. Eq. (3.66), Eq. (10.6) yields the integral equation for the specific enthalpy $h(T, p)$:

$$\varrho \left(u \frac{\partial h}{\partial x} + v \frac{\partial h}{\partial y} \right) = \frac{\partial}{\partial y} \left(\lambda \frac{\partial T}{\partial y} \right) + u \frac{dp}{dx} + \mu \left(\frac{\partial u}{\partial y} \right)^2. \quad (10.7)$$

Note in particular that the geometry of the body appears for the first time in the calculation of the boundary layer via the angle distribution $\alpha(x)$ in the gravity term in the momentum equation (10.5).

10.3 Boundary Layers with Moderate Wall Heat Transfer (Without Gravitational Effects)

10.3.1 Perturbation Calculation

We consider the flow past bodies without the effect of gravity ($\text{Fr} \rightarrow \infty$). Let the outer flow have the temperature T_∞ . Deviations of the temperature from T_∞ as a consequence of the heat transfer at the wall occur only in the boundary layer. These temperature differences should remain small, but still be enough that changes in the physical properties occur compared to the reference properties at $T_R = T_\infty$. We initially assume that the physical properties depend only on the temperature.

As an example of how the temperature dependence of the properties is taken into account in the boundary-layer calculation, we look at the density

function $\varrho(T)$. The function $\varrho(T)$ is expanded at the position $T = T_\infty$ in a Taylor series:

$$\varrho(T) = \varrho_\infty + \left(\frac{d\varrho}{dT} \right)_\infty (T - T_\infty) + \dots . \quad (10.8)$$

We now introduce the dimensionless temperature

$$\vartheta = \frac{T - T_\infty}{\Delta T} . \quad (10.8a)$$

Here ΔT is a reference temperature difference.

For the standard cases we have:

$$\begin{aligned} T_w &= \text{const} : & \Delta T &= T_w - T_\infty \\ q_w &= \text{const} : & \Delta T &= q_w l / \lambda_\infty . \end{aligned} \quad (10.9)$$

For the density we then find

$$\varrho(T) = \varrho_\infty \left(1 + K_\varrho \vartheta \frac{\Delta T}{T_\infty} + \dots \right) \quad (10.10)$$

with the dimensionless physical property

$$K_\varrho = \left(\frac{d\varrho}{dT} \frac{T}{\varrho} \right)_\infty . \quad (10.11)$$

We now assume that $\varepsilon = \Delta T/T_\infty$ is some small value. Carrying out a regular perturbation calculation with ε as the perturbation parameter to find the boundary-layer solution, in analogy to Eq. (10.10), we obtain the other physical properties as:

$$\begin{aligned} \mu(T) &= \mu_\infty (1 + K_\mu \vartheta \varepsilon + \dots) \\ c_p(T) &= c_{p\infty} (1 + K_c \vartheta \varepsilon + \dots) \\ \lambda(T) &= \lambda_\infty (1 + K_\lambda \vartheta \varepsilon + \dots) . \end{aligned} \quad (10.12)$$

The values of K_ϱ , K_μ , K_c and K_λ are given for some substances in Table 3.1.

For the solution functions we use the following trial solutions:

$$\begin{aligned} u(x, y) &= u_0(x, y) + \varepsilon [K_\varrho u_{1\varrho}(x, y) + K_\mu u_{1\mu}(x, y)] \\ v(x, y) &= v_0(x, y) + \varepsilon [K_\varrho v_{1\varrho}(x, y) + K_\mu v_{1\mu}(x, y)] \\ p(x) &= p_0(x) + \varepsilon [K_\varrho p_{1\varrho}(x) + K_\mu p_{1\mu}(x)] \\ \vartheta(x, y) &= \vartheta_0(x, y) + \varepsilon [K_\varrho \vartheta_{1\varrho}(x, y) + K_\mu \vartheta_{1\mu}(x, y) \\ &\quad + K_c \vartheta_{1c}(x, y) + K_\lambda \vartheta_{1\lambda}(x, y)] . \end{aligned} \quad (10.13)$$

Inserting these trial solutions into the boundary-layer equations (10.4) to (10.7), sorting powers of ε , and ignoring terms proportional to ε^2 , we obtain two systems of equations. As well as the system of equations for the boundary

layer with constant physical properties, a system of equations which describes the first approximation to the effect of the temperature dependence of the physical properties arises from the terms proportional to ε . In contrast to the first system, this system of equations is linear. Therefore its complete solution can be additively formed from four partial solutions, each proportional to the quantities K_ϱ to K_λ respectively.

From the complete solution, we finally obtain an expression for the skin-friction coefficient

$$c_f \sqrt{Re} = F_0(x) + \frac{\Delta T}{T_\infty} [K_\varrho F_\varrho(x, Pr, Ec) + K_\mu F_\mu(x, Pr, Ec)], \quad (10.14)$$

where the functions $F_\varrho(x)$ and $F_\mu(x)$ also depend on the type of thermal boundary condition at the wall.

Corresponding formulae are also valid for the wall heat transfer, where terms proportional to K_c and K_λ also appear. Further details are to be found in the comprehensive piece of work by H. Herwig (1985b) and K. Gersten; H. Herwig (1992), p. 86, see also P. Kiš; H. Herwig (2010).

For similar solutions, Eq. (10.14) and the corresponding wall heat transfer relations are simplified in such a way that all functions have the same x dependence, so that instead of the functions F_ϱ, F_μ, \dots , only constants depending on Pr and Ec must be determined.

The representation in Eq. (10.14) has the decisive advantage that the effects of the temperature dependence for the four relevant physical properties are separate, and therefore can be determined singly and independently of the others.

Results of this perturbation calculation for wedge flows ($U \sim x^m$) have been given by H. Herwig (1987).

Example: Flat plate with constant wall temperature

For the flat plate with constant wall temperature at $Pr_\infty = 0.7$, H. Herwig (1985b) has shown that:

$$\begin{aligned} c_f \sqrt{Re_x} &= 0.664 \left[1 + K_{\varrho\mu} \left(0.266 \frac{T_w - T_{ad}}{T_\infty} + 0.149 Ec_\infty \right) \right] \\ &= 0.664 \left[1 + K_{\varrho\mu} \left(0.266 \frac{T_w - T_\infty}{T_\infty} + 0.038 Ec_\infty \right) \right], \end{aligned} \quad (10.15)$$

$$\begin{aligned} \frac{Nu_x}{\sqrt{Re_x}} &= 0.293 \left[1 - K_{\varrho\mu} \left(0.148 \frac{T_w - T_{ad}}{T_\infty} + 0.171 Ec_\infty \right) \right. \\ &\quad \left. + K_{\varrho\lambda} \left(0.397 \frac{T_w - T_{ad}}{T_\infty} + 0.305 Ec_\infty \right) \right. \\ &\quad \left. + K_c \left(0.103 \frac{T_w - T_{ad}}{T_\infty} + 0.113 Ec_\infty \right) \right], \end{aligned} \quad (10.16)$$

$$\begin{aligned} r &= \frac{T_{ad} - T_\infty}{U_\infty^2 / (2c_{p,\infty})} \\ &= 0.836 [1 + Ec_\infty (0.143 K_{\varrho\mu} - 0.134 K_{\varrho\lambda} - 0.075 K_c)]. \end{aligned} \quad (10.17)$$

Here

$$\begin{aligned} c_f &= \frac{2\tau_w(x)}{\varrho_\infty U_\infty^2}, & \text{Re}_x &= \frac{\varrho_\infty U_\infty x}{\mu_\infty}, \\ \text{Ec}_\infty &= \frac{U_\infty^2}{c_p \infty T_\infty}, & \text{Nu}_x &= \frac{q_w(x)x}{\lambda_\infty (T_w - T_{ad})}. \end{aligned} \quad (10.18)$$

It is particularly worth taking note of the fact that, for plate flow, the temperature dependence of the density does not stand alone, but rather appears in combination with the temperature dependencies of the viscosity μ and the thermal conductivity λ . The following relations hold:

$$K_{\varrho\mu} = \left[\frac{d(\varrho\mu)}{dT} \frac{T}{\varrho\mu} \right]_\infty = K_\varrho + K_\mu, \quad K_{\varrho\lambda} = \left[\frac{d(\varrho\lambda)}{dT} \frac{T}{\varrho\lambda} \right]_\infty = K_\varrho + K_\lambda. \quad (10.19)$$

For the adiabatic wall temperature corresponding to Eq. (10.17), Eq. (10.15) for the skin-friction coefficient yields the simple relation

$$\frac{c_f}{c_{f_{c.p.}}} = 1 + 0.149 K_{\varrho\mu} \text{Ec}_\infty \quad (q_w = 0), \quad (10.20)$$

where the index c.p. denotes the case of constant properties. The formulae (10.15) to (10.20) are valid for *arbitrary* substances at $\text{Pr}_\infty = 0.7$.

It is frequently assumed that a gas under consideration is an ideal gas (from $p = \varrho RT$ it follows that $K_\varrho = -1$) with constant c_p ($K_c = 0$) and constant Pr (from $c_p = \text{const}$ it follows that $\lambda \sim \mu$ or $K_\lambda = K_\mu$). Then the Eckert number can be expressed via the Mach number, cf. Eq. (4.14):

$$\text{Ec}_\infty = (\gamma - 1) \text{Ma}_\infty^2 \quad \text{with} \quad \text{Ma}_\infty = \frac{U_\infty}{c_\infty}. \quad (10.21)$$

Thus Eq. (10.20) yields

$$\frac{c_f}{c_{f_{c.p.}}} = 1 - 0.149(\gamma - 1)(1 - K_\mu) \text{Ma}_\infty^2 \quad (10.22)$$

and from Eq. (10.17) we have

$$r = 0.836[1 - 0.009(\gamma - 1)(1 - K_\mu) \text{Ma}_\infty^2]. \quad (10.23)$$

If the viscosity is proportional to the temperature ($K_\mu = 1$, thus $K_{\varrho\mu} = 0$), then $c_f \sqrt{\text{Re}_x}$, $\text{Nu}_x / \sqrt{\text{Re}_x}$ and r remain unaffected by the temperature dependence of the physical properties.

In air ($\gamma = 1.4$), a power law is frequently assumed for the viscosity:

$$\frac{\mu}{\mu_\infty} = \left(\frac{T}{T_\infty} \right)^{K_\mu} \quad (10.24)$$

with $K_\mu = 0.7$. Then Eqs. (10.22) and (10.23) yield

$$\frac{c_f}{c_{f_{c.p.}}} = 1 - 0.018 \text{Ma}_\infty^2, \quad \frac{r}{r_{c.p.}} = 1 - 0.001 \text{Ma}_\infty^2. \quad (10.25)$$

The change in the recovery factor r is therefore very small, as pointed out by H.W. Emmons; J.G. Brainerd (1942). The formula for c_f yields very good results up to Mach numbers of $\text{Ma}_\infty = 3$. This is shown in Fig. 10.6 by comparison with exact solutions, cf. H. Herwig (1985b).

Note (Effect of the pressure dependence of the physical properties)

If the physical properties also depend on the pressure, the perturbation calculation described here can be correspondingly extended. In practice, mostly only the pressure dependence of the density is of importance. The Taylor series (10.8) is extended as follows:

$$\begin{aligned}\varrho(T, p) &= \varrho_\infty + \left(\frac{\partial \varrho}{\partial T} \right)_\infty (T - T_\infty) + \left(\frac{\partial \varrho}{\partial p} \right)_\infty (p - p_\infty) + \dots \\ &= \varrho_\infty \left(1 + K_\varrho \frac{T - T_\infty}{T_\infty} + \tilde{K}_\varrho \frac{p - p_\infty}{p_\infty} + \dots \right),\end{aligned}\quad (10.26)$$

where p_∞ is the pressure at the reference point.

With Eq. (4.22), the speed of sound c_∞ can be introduced. In dimensionless notation Eq. (10.26) then reads:

$$\frac{\varrho(T, p)}{\varrho_\infty} = 1 + K_\varrho \frac{T - T_\infty}{T_\infty} + \gamma \text{Ma}_\infty^2 \frac{p - p_\infty}{\varrho_\infty V^2}. \quad (10.27)$$

Thus the effects of the pressure dependence of the density are proportional to the square of the Mach number.

With this extended Taylor series, the additional perturbation parameter $\text{Ma}_\infty^2 = V^2/c_\infty^2$ appears in the perturbation calculation.

10.3.2 Property Ratio Method (Temperature Ratio Method)

In practice, two methods are frequently used which were initially developed empirically. With their help results obtained under the assumption of constant physical properties can be corrected with respect to the effect of variable properties. These are the *property ratio method*, and, to be treated in the next section, the *reference temperature method*.

According to the property ratio method, the correction formulae read:

$$\frac{c_f}{c_{f_{c.p.}}} = \left(\frac{\varrho_w \mu_w}{\varrho_\infty \mu_\infty} \right)^{m_{\varrho\mu}} \left(\frac{\varrho_w}{\varrho_\infty} \right)^{m_\varrho}, \quad (10.28)$$

$T_w = \text{const}$:

$$\frac{\text{Nu}}{\text{Nu}_{c.p.}} = \left(\frac{\varrho_w \mu_w}{\varrho_\infty \mu_\infty} \right)^{n_{\varrho\mu}} \left(\frac{\varrho_w}{\varrho_\infty} \right)^{n_\varrho} \left(\frac{\text{Pr}_w}{\text{Pr}_\infty} \right)^{n_{\text{Pr}}} \left(\frac{c_{p_w}}{c_{p\infty}} \right)^{0.5}, \quad (10.29)$$

$q_w = \text{const}$:

$$\frac{T_w - T_\infty}{(T_w - T_\infty)_{c.p.}} = \left(\frac{\varrho_w \mu_w}{\varrho_\infty \mu_\infty} \right)^{k_{\varrho\mu}} \left(\frac{\varrho_w}{\varrho_\infty} \right)^{k_\varrho} \left(\frac{\text{Pr}_w}{\text{Pr}_\infty} \right)^{k_{\text{Pr}}} \left(\frac{c_{p_w}}{c_{p\infty}} \right)^{0.5}. \quad (10.30)$$

The particular form of these equations has given this method its name. The type of constitutive relation does not appear explicitly here.

From the results in the last section, the exponents can be determined immediately. For example consider Eq. (10.28) for the case $T_w = \text{const}$. If we insert Eq. (10.12) into Eq. (10.28), using $\vartheta_w = 1$, we obtain

$$\frac{c_f}{c_{f_{\text{c.p.}}}} = [1 + (K_\varrho + K_\mu)\varepsilon]^{m_{\varrho\mu}} [1 + K_\varrho\varepsilon]^{m_\varrho}. \quad (10.31)$$

Expanding the powers in binomial series and taking only the linear terms into account, it follows that

$$\frac{c_f}{c_{f_{\text{c.p.}}}} = 1 + \varepsilon[K_\varrho(m_{\varrho\mu} + m_\varrho) + K_\mu m_{\varrho\mu}],$$

which, after comparison with Eq. (10.14), yields

$$m_{\varrho\mu} = \frac{F_\mu}{F_0}, \quad m_\varrho = \frac{F_\varrho - F_\mu}{F_0}.$$

Therefore the property ratio method is in no way an empirical method. The perturbation calculation of the previous section delivered not only the numerical values of the exponents, but also determined the structure of the correction formulae. Thus it must follow, for example, that the temperature dependence of the physical properties λ and c_p has no effect on the correction to the skin-friction coefficient c_f .

In general the exponents are dependent on x , Pr_∞ , Ec_∞ and on the thermal boundary conditions at the wall. An exception is the exponent of $(c_{pw}/c_{p\infty})$. For boundary layers with similar solutions there is no x dependence.

In Table 10.1, the exponents for plate and stagnation-point flow are given. Here the dissipation was neglected ($\text{Ec}_\infty = 0$). H. Herwig (1985b, 1987) has considered the effect of the Eckert number on the exponents. In Eq. (10.30), the physical properties at the wall temperature $T_{w\text{c.p.}}$ are to be inserted.

It can be read from the table that, in contrast to stagnation-point flow, the temperature dependence of the density in plate flow does not appear separately. For plate flows of fluids with $\text{Pr} = \text{const}$ and $c_p = \text{const}$, the corrections (10.28) to (10.30) are only dependent on a parameter

$$\text{CR} = \frac{\varrho_w \mu_w}{\varrho_\infty \mu_\infty} \quad (10.32)$$

called the Chapman–Rubesin parameter.

For $\text{Pr}_\infty \rightarrow \infty$, there is no correction to the skin-friction coefficient, since the thermal boundary layer is then very thin compared to the velocity boundary layer and thus has no effect.

In contrast, for $\text{Pr}_\infty \rightarrow 0$, the viscosity has no effect on the correction to the wall heat transfer, since then the velocity boundary layer is very thin compared to the thermal boundary layer.

Further numerical values can be found in the work by K. Gersten; H. Herwig (1984) and H. Herwig; G. Wickern (1986).

Table 10.1. Exponents of the property ratio method, from Eqs. (10.28) to (10.30). Plate and stagnation-point flow

Pr_∞	$m_{\varrho\mu}$	$n_{\varrho\mu}$	n_{Pr}	Pr_∞	$m_{\varrho\mu}$	$k_{\varrho\mu}$	k_{Pr}
0	0.500	0.318	-0.318	0	0.667	-0.304	0.304
0.7	0.266	0.249	-0.397	0.7	0.313	-0.255	0.389
1.0	0.241	0.241	-0.399	1.0	0.281	-0.246	0.390
7.0	0.115	0.200	-0.404	7.0	0.132	-0.202	0.392
∞	0.000	0.162	-0.404	∞	0.000	-0.162	0.393

a) flat plate
 $T_w = \text{const}$, $m_\varrho = n_\varrho = 0$

b) flat plate
 $q_w = \text{const}$, $m_\varrho = k_\varrho = 0$

Pr_∞	$m_{\varrho\mu}$	m_ϱ	$n_{\varrho\mu}$	n_ϱ	n_{Pr}
0	0.500	-0.750	0.318	-0.125	-0.318
0.7	0.393	-0.462	0.278	-0.096	-0.379
1.0	0.378	-0.434	0.273	-0.091	-0.382
7.0	0.277	-0.285	0.239	-0.061	-0.394
∞	0.000	0.000	0.162	0.000	-0.404

c) stagnation point, $q_w = \text{const}$ and $T_w = \text{const}$

Note (Difference between heating and cooling?)

The correction formulae (10.28) to (10.30), it has been shown here, are due to a linear dependence of the physical properties on the temperature. Occasionally in the literature, different numerical values for the exponents for “heating” and “cooling” are given, something which is decidedly not recommended. This would mean that the dependence of the physical properties on the temperature runs as two straight lines joined at a sharp bend. This is a useless attempt to take nonlinear effects into account in a linear theory, in which, at a position where the formulae should be exact, a completely *arbitrary* discontinuity is introduced.

Frequently power laws are used for the temperature dependence on the physical properties of fluids (particularly gases). From Eq. (10.28) to (10.30) we then obtain the formulae

$$\begin{aligned} \frac{c_f}{c_{f.c.p.}} &= \left(\frac{T_w}{T_\infty} \right)^m, \\ \frac{\text{Nu}}{\text{Nu}_{c.p.}} &= \left(\frac{T_w}{T_\infty} \right)^n \quad (T_w = \text{const}), \\ \frac{T_w - T_\infty}{(T_w - T_\infty)_{c.p.}} &= \left(\frac{T_w}{T_\infty} \right)^k \quad (q_w = \text{const}), \end{aligned} \quad (10.33)$$

where the exponents are now dependent on the fluid under consideration. The use of formulae (10.33) is called the *temperature ratio method*.

Example: Heat transfer in air

In flow past bodies, the boundary layer commences as a stagnation-point boundary layer and flows through the pressure decrease region generally to a point where the pressure gradient vanishes. Here the boundary layer behaves as a plate boundary layer. In the region of pressure increase following this, either boundary-layer separation or the transition to turbulence generally take place very soon. H. Herwig (1984) has suggested that the formulae (10.28) to (10.30) can also be used for general body contours, i.e. for general distributions $U(x)$. Here, however, the exponents should be approximated as the average of those from stagnation-point flow and plate flow.

In air, as in all gases, the dependence of the Prandtl number on the temperature is often neglected. Then the correction to the Nusselt number for air ($\text{Pr} = 0.70$) would be

$$\frac{\text{Nu}}{\text{Nu}_{\text{c.p.}}} = \left(\frac{\varrho_w \mu_w}{\varrho_\infty \mu_\infty} \right)^{0.265} \left(\frac{\varrho_w}{\varrho_\infty} \right)^{-0.048} \left(\frac{c_{p_w}}{c_{p_\infty}} \right)^{0.5} \quad (\text{Pr} = 0.7). \quad (10.34)$$

The exponent 0.265 corresponds not only to an average of the plate flow and the stagnation-point flow, but also to an average of the cases $T_w = \text{const}$ and $q_w = \text{const}$, whose exponents are only slightly different from each other. Therefore Eq. (10.34) is approximately valid for arbitrary thermal boundary conditions.

It is common to use the following power laws for the physical properties of air, cf. Table 3.1; $\varrho \sim T^{-1}$, $\mu \sim T^{0.78}$, $\lambda \sim T^{0.85}$, $c_p \sim T^{0.07}$. It then follows from Eq. (10.34) that

$$\frac{\text{Nu}}{\text{Nu}_{\text{c.p.}}} = \left(\frac{T_w}{T_\infty} \right)^{0.02}. \quad (10.35)$$

This formula has been confirmed well by experiments, e.g. by W.M. Kays; W.B. Nicoll (1963) in measurements on a circular cylinder.

Therefore the temperature dependence of the physical properties of air has only a very small effect, since clearly the effects of different physical properties directly compensate each other. At $T_\infty = 20^\circ\text{C}$ and $T_w = 100^\circ\text{C}$ the correction is less than 1%. Thus it was justified in Fig. 9.5 to compare the wall heat transfer measurements in air flows with the theory for constant physical properties.

10.3.3 Reference Temperature Method

In discussing the reference temperature method we will formally retain all the results obtained for c_f and Nu under the assumption of constant properties. All the physical properties appearing will now be taken at an initially unknown temperature, the so-called *reference temperature* T_r . This reference temperature is to be chosen so that the results for variable properties are formally reproduced using the relations for constant properties.

The reference temperature T_r can easily be determined from the results from the perturbation calculation in Sect. 10.3.1. We will show this using the example of the skin-friction coefficient at a flat plate for $T_w = \text{const}$.

By definition we have:

$$\frac{2\tau_w}{\varrho_r U_\infty^2} \sqrt{\frac{\varrho_r U_\infty x}{\mu_r}} = 0.664,$$

where ϱ_r and μ_r are physical properties of the fluid at the reference temperature T_r . Hence it follows that

$$\frac{2\tau_w}{\varrho_\infty U_\infty^2} \sqrt{\frac{\varrho_\infty U_\infty x}{\mu_\infty}} \sqrt{\frac{\varrho_\infty \mu_\infty}{\varrho_r \mu_r}} = 0.664$$

or else

$$\frac{c_f \sqrt{\text{Re}}}{(c_f \sqrt{\text{Re}})_{c.p.}} = \left(\frac{\varrho_r \mu_r}{\varrho_\infty \mu_\infty} \right)^{1/2}.$$

If, in analogy to Eq. (10.12), we set

$$\frac{\varrho_r \mu_r}{\varrho_\infty \mu_\infty} = 1 + K_{\varrho \mu} \frac{T_r - T_\infty}{T_\infty}$$

and take only the linear term in the binomial expansion into account, a comparison with Eq. (10.15) yields

$$\frac{T_r - T_\infty}{T_\infty} = 0.532 \frac{T_w - T_\infty}{T_\infty} + 0.076 \text{Ec}_\infty \quad (\text{Pr} = 0.7). \quad (10.36)$$

This formula reproduces the empirical results known from the literature very well, cf. F.M. White (1974), p. 590.

It can be seen immediately that, for plate flow, when the dissipation is neglected ($\text{Ec}_\infty = 0$), we have

$$\frac{T_r - T_\infty}{T_w - T_\infty} = 2m_{\varrho \mu}, \quad (10.37)$$

so that the reference temperature can be read off from Table 10.1. Thus, in the case of $T_w = \text{const}$, the reference temperature is equal to the outer temperature for $\text{Pr} \rightarrow \infty$ and to the wall temperature for $\text{Pr} \rightarrow 0$.

The reference temperatures for the skin-friction coefficient and for the Nusselt number are generally different, and they also depend on the thermal boundary conditions at the wall.

10.4 Compressible Boundary Layers (Without Gravitational Effects)

10.4.1 Physical Property Relations

Consider a plane body in a flow of velocity V . Computing the inviscid flow yields the distributions $u_e(x)$ and $T_e(x)$ at the outer edge of the boundary

layer. (The index e stands for “external” or “edge”.) Boundary-layer theory now aims to calculate the boundary-layer equations (10.4) to (10.7) (with $g = 0$) for given thermal boundary conditions at the wall. In general either the temperature distribution $T_w(x)$ or the distribution of the heat flux $q_w(x)$ at the wall may be given. Special cases are the standard cases $T_w = \text{const}$ or $q_w = \text{const}$. We look for the distributions of the skin-friction coefficient, the adiabatic wall temperature, and the Nusselt number or wall temperature.

The following is assumed regarding the constitutive relations:

1. We consider ideal gases, i.e. we have

$$\frac{p}{\varrho} = RT, \quad (10.38)$$

where R is the specific gas constant (for air: $R = 287 \text{ m}^2/\text{s}^2\text{K}$). For the coefficient of thermal expansion from Eq. (3.67) we then obtain

$$\beta = -\frac{1}{\varrho} \left(\frac{\partial \varrho}{\partial T} \right)_p = \frac{1}{T}. \quad (10.39)$$

This is equivalent to $K_\varrho = -1$. In addition

$$\frac{Dh}{Dt} = c_p \frac{DT}{Dt}, \quad (10.40)$$

as can be seen from Eq. (3.66).

2. We assume constant specific heat capacities:

$$c_p = \text{const}, \quad c_v = \text{const}, \quad \gamma = \text{const}. \quad (10.41)$$

It then follows from Eq. (10.40) that the specific enthalpy is proportional to the (absolute) temperature:

$$h = c_p T. \quad (10.42)$$

3. We assume that the Prandtl number is constant:

$$\text{Pr} = \frac{c_p \mu}{\lambda} = \text{const}. \quad (10.43)$$

Using Eq. (10.41), this implies that the thermal conductivity and the viscosity are proportional:

$$\frac{\lambda}{\mu} = \frac{c_p}{\text{Pr}} = \text{const}. \quad (10.44)$$

4. We assume that the viscosity $\mu(T)$ depends only on the temperature. From Eq. (10.44) we see that the thermal conductivity $\lambda(T)$ then also only depends on the temperature.

The following representations for the law of viscosity $\mu(T)$ are common:

Sutherland formula:

$$\frac{\mu}{\mu_r} = \left(\frac{T}{T_r} \right)^{\frac{3}{2}} \frac{T_r + s}{T + s}. \quad (10.45)$$

Here μ_r is the viscosity value at the reference temperature T_r . The constant s is dependent on the type of gas, and for air $s = 110\text{K}$, cf. F.M. White (1974), p. 29.

Power law:

$$\frac{\mu}{\mu_r} = \left(\frac{T}{T_r} \right)^\omega \quad \frac{1}{2} \leq \omega \leq 1. \quad (10.46)$$

For air $\omega = 0.7$ is used. To see how ω is determined, see J.F. Gross; C.F. Dewey, Jr. (1965).

Linear law:

As will be shown, the boundary-layer equations are considerably simplified if the viscosity is proportional to the temperature, $\omega = 1$, and thus the law of viscosity is occasionally given in the form

$$\frac{\mu}{\mu_r} = b \frac{T}{T_r}. \quad (10.47)$$

Here the constant b is used to approximate the more exact Sutherland formula Eq. (10.45) or the power law Eq. (10.46) close to a desired temperature. For example, for

$$b = \sqrt{\frac{T_w}{T_r}} \frac{T_r + s}{T_w + s}, \quad b = \left(\frac{T_w}{T_r} \right)^{\omega-1}, \quad (10.48)$$

Eq. (10.47) agrees with the Sutherland formula or with the power law at the point $T = T_w$. Here the values μ_r , T_r correspond to the reference point in the Sutherland formula or the power law. Note that this reference point does not lie on the straight line from Eq. (10.47) for $T_w \neq T_r$.

Combining Eq. (10.47) with Eq. (10.38) we obtain

$$\frac{\varrho \mu}{\varrho_r \mu_r} = b \frac{p}{p_r}. \quad (10.49)$$

Since the pressure in the boundary layer is independent of the distance from the wall, applying the law of viscosity in Eq. (10.47) means that the combination in Eq. (10.49) is only a function of the length x .

The four assumptions made lead to a very good description of air at moderate pressures ($p < 1000\text{ bar}$) up to temperatures of about $T = 500\text{K}$. Above this temperature, c_p can no longer be taken to be constant, cf. Sect. 10.4.6. These ideas are also valid for other gases.

10.4.2 Simple Solutions of the Energy Equation

If we use the assumptions met in the previous section, we find a particularly simple equation for the specific total enthalpy (index t):

$$h_t = c_p T_t = h + \frac{1}{2} u^2 = c_p T + \frac{1}{2} u^2. \quad (10.50)$$

Here T_t is the total temperature. In Eq. (10.50), $v^2/2$ was neglected in comparison to $u^2/2$, as is permitted inside the boundary layer.

If we multiply Eq. (10.5) by u and add the resulting equation for the kinetic energy to Eq. (10.7), we obtain

$$\varrho \left(u \frac{\partial h_t}{\partial x} + v \frac{\partial h_t}{\partial y} \right) = \frac{\partial}{\partial y} \left(\frac{\mu}{\text{Pr}} \frac{\partial h_t}{\partial y} \right) + \frac{\partial}{\partial y} \left[\left(1 - \frac{1}{\text{Pr}} \right) \mu u \frac{\partial u}{\partial y} \right]. \quad (10.51)$$

It can be seen immediately from this equation that $h_t = \text{const}$ for inviscid outer flow ($\mu = 0$). Therefore at the outer edge of the boundary layer we have

$$c_p T_e + \frac{1}{2} u_e^2 = h_{te} = c_p T_0 \quad (10.52)$$

with T_0 as the total temperature or stagnation temperature of the outer flow.

Equation (10.51) is greatly simplified for the case $\text{Pr} = 1$. Then two simple solutions of Eq. (10.51) can immediately be written down. These are due to A. Busemann (1931) and L. Crocco (1932) (so-called Busemann–Crocco solutions).

1. Adiabatic wall ($\text{Pr} = 1$).

The solution of Eq. (10.51) reads

$$h_t = h_{te} = \text{const}. \quad (10.53)$$

Differentiating Eq. (10.50), and using $u_w = 0$ we find

$$\left(\frac{\partial h_t}{\partial y} \right)_w = c_p \left(\frac{\partial T}{\partial y} \right)_w = - \frac{c_p}{\lambda_w} q_w$$

and therefore $h_t = \text{const}$ also satisfies the condition $q_w = 0$ for the adiabatic wall. In this case Eq. (10.50) implies that the temperature $T(u)$ is a quadratic function of the velocity. We have:

$$\frac{T_0 - T(u)}{T_0} = \frac{u^2}{2c_p T_0}. \quad (10.54)$$

Because of the no-slip condition ($u_w = 0$), the adiabatic wall temperature is equal to the total temperature T_0 . The recovery factor r from Eq. (9.86) is therefore, for $\text{Pr} = 1$, always $r = 1$.

2. Plate flow ($\text{Pr} = 1$).

In this case there is a linear relation between h_t and u of the form

$$\frac{h_t - h_{te}}{h_{tw} - h_{te}} = 1 - \frac{u}{U_\infty}, \quad (10.55)$$

because the equations (10.51) for h_t and (10.5) for u have the same structure. Thus the dependence of the temperature $T(u)$ on the velocity is again a second order polynomial:

$$\frac{T_0 - T(u)}{T_0} = \frac{u^2}{2c_p T_0} + \frac{T_0 - T_w}{T_0} \left(1 - \frac{u}{U_\infty}\right) \quad (10.56)$$

with the wall temperature assumed constant at T_w . For $T_w = T_0$ this formula is again reduced to Eq. (10.54) for the adiabatic case.

If the Mach number of the free stream (temperature T_∞ in the free stream)

$$\text{Ma}_\infty = \frac{U_\infty}{c_\infty} = \frac{U_\infty}{\sqrt{c_p(\gamma - 1)T_\infty}}$$

is introduced, Eq. (10.56) can also be written as follows:

$$\frac{T - T_\infty}{T_\infty} = \frac{\gamma - 1}{2} \text{Ma}_\infty^2 \left[1 - \left(\frac{u}{U_\infty}\right)^2\right] + \frac{T_w - T_{ad}}{T_\infty} \left(1 - \frac{u}{U_\infty}\right) \quad (10.57a)$$

or

$$\frac{T - T_w}{T_\infty} = \frac{\gamma - 1}{2} \text{Ma}_\infty^2 \frac{u}{U_\infty} \left(1 - \frac{u}{U_\infty}\right) + \frac{T_\infty - T_w}{T_\infty} \frac{u}{U_\infty}, \quad (10.57b)$$

where, for the adiabatic wall temperature we have

$$T_{ad} = T_0 = T_\infty \left(1 + \frac{\gamma - 1}{2} \text{Ma}_\infty^2\right). \quad (10.58)$$

If we form the derivative at the wall from Eq. (10.57a), we obtain

$$q_w = -\lambda_w \left(\frac{\partial T}{\partial y}\right)_w = \frac{(T_w - T_{ad})\lambda_w \tau_w}{U_\infty \mu_w}$$

or in dimensionless form

$$\text{Nu} = \frac{q_w l}{\lambda_\infty (T_w - T_{ad})} = \frac{c_f}{2} \text{Re}, \quad (10.59)$$

where $\text{Re} = \rho U_\infty l / \mu_\infty$.

This simple relation between the Nusselt number Nu and the skin-friction coefficient c_f is called the *Reynolds analogy*. It is only true for plate flows at $\text{Pr} = 1$, but then for arbitrary Mach numbers.

From Eq. (10.59) it follows that

$$\begin{aligned} q_w > 0, \quad T_w > T_{ad} : & \text{ heating: heat from wall to fluid} \\ q_w < 0, \quad T_w < T_{ad} : & \text{ cooling: heat from fluid to wall.} \end{aligned}$$

10.4.3 Transformations of the Boundary-Layer Equations

Dorodnizyn–Howarth transformation

Since compressible boundary layers reduce to boundary layers with constant physical properties at small free stream velocities ($\text{Ma}_\infty \rightarrow 0$) and low wall heat transfer ($\Delta T/T_\infty \rightarrow 0$, cf. Eq. (10.10)), it seems obvious to attempt to transform the equations for the compressible boundary layer in such a manner that they are as similar as possible or even identical to the boundary-layer equations for constant physical properties.

We will use the example of the continuity equation (10.4) to elucidate the basic ideas. Introducing the stream function $\psi(x, y)$

$$\varrho u = \varrho_\infty \frac{\partial \psi}{\partial y}, \quad \varrho v = -\varrho_\infty \frac{\partial \psi}{\partial x} \quad (10.60)$$

with the reference density ϱ_∞ , the continuity equation is satisfied. Using the transformed variable

$$Y = \int_0^y \frac{\varrho}{\varrho_\infty} dy \quad (10.61)$$

we obtain the following relation known from the incompressible boundary layer

$$u = \frac{\partial \psi}{\partial Y}. \quad (10.62)$$

Equation (10.61) is known as the Dorodnizyn–Howarth transformation, cf. K. Stewartson (1964), p. 29.

The following two transformations are extensions to it.

Illingworth–Stewartson transformation

We assume a linear law of viscosity from Eq. (10.47) and constant wall temperature $T_w = \text{const}$. Using the coordinate transformation

$$\tilde{x} = \int_0^x b \frac{p_e c_e}{p_0 c_0} dx, \quad \tilde{y} = \frac{c_e}{c_0} \int_0^y \frac{\varrho}{\varrho_0} dy \quad (10.63)$$

and with Eqs. (10.4), (10.5) and (10.51), we obtain the following system of equations, cf. H. Schlichting (1982) p. 344:

$$\frac{\partial \tilde{u}}{\partial \tilde{x}} + \frac{\partial \tilde{v}}{\partial \tilde{y}} = 0, \quad (10.64)$$

$$\tilde{u} \frac{\partial \tilde{u}}{\partial \tilde{x}} + \tilde{v} \frac{\partial \tilde{u}}{\partial \tilde{y}} = \tilde{u}_e \frac{d\tilde{u}_e}{d\tilde{x}} (1 + S) + \nu_0 \frac{\partial^2 \tilde{u}}{\partial \tilde{y}^2}, \quad (10.65)$$

$$\tilde{u} \frac{\partial S}{\partial \tilde{x}} + \tilde{v} \frac{\partial S}{\partial \tilde{y}} = \nu_0 \left\{ \frac{1}{Pr} \frac{\partial^2 S}{\partial \tilde{y}^2} + \frac{Pr - 1}{Pr} \frac{(\gamma - 1) Ma_e^2}{2 + (\gamma - 1) Ma_e^2} \frac{\partial^2}{\partial \tilde{y}^2} \left[\left(\frac{\tilde{u}}{\tilde{u}_e} \right)^2 \right] \right\}. \quad (10.66)$$

Here

$$u = \frac{c_e}{c_0} \tilde{u}, \quad S = \frac{h_t - h_{te}}{h_{te}} = \frac{T + u^2/(2c_p)}{T_0} - 1. \quad (10.67)$$

The function $S(\tilde{x}, \tilde{y})$ is therefore the dimensionless total enthalpy. The index 0 denotes the stagnation state of the inviscid outer flow; the index e the value at the edge of the boundary layer. The speed of sound is denoted by c . The boundary conditions to the equations (10.64) to (10.66) are

$$\begin{aligned} \tilde{y} = 0 : \quad & \tilde{u} = 0, \quad \tilde{v} = 0, \quad S = S_w \\ & \text{(or : } (\partial S / \partial \tilde{y})_w = 0 \text{ for adiabatic wall)} \\ \tilde{y} \rightarrow \infty : \quad & \tilde{u} = \tilde{u}_e(\tilde{x}), \quad S = 0. \end{aligned}$$

The transformed equation (10.65) differs from the corresponding boundary-layer equation for constant physical properties only by the factor $(S + 1)$ in the pressure term. It is worth noting that the reduction to the equations for constant physical properties can be carried out precisely for those two cases treated in Sect. 10.4.2 ($Pr = 1$: $S = 0$ and $d\tilde{u}_e/d\tilde{x} = 0$). However this is only true for a linear law of viscosity according to Eq. (10.47).

Levy–Lees transformation

This transformation can be interpreted as an extension of the Görtler transformation to compressible flows, cf. Sect. 7.3.1. It reads

$$\xi = \int_0^x \varrho_e \mu_e u_e dx, \quad \eta = \frac{u_e}{\sqrt{2\xi}} \int_0^y \varrho dy. \quad (10.68)$$

For the two functions

$$\frac{u}{u_e} = f'(\xi, \eta), \quad \frac{h_t - h_{te}}{h_{te}} = S = g(\xi, \eta) \quad (10.69)$$

the transformation yields

$$(Cf'')' + ff'' + \beta \left[\frac{\varrho_e}{\varrho} - f'^2 \right] = 2\xi \left(f' \frac{\partial f'}{\partial \xi} - f'' \frac{\partial f}{\partial \xi} \right), \quad (10.70)$$

$$\left[\frac{C}{Pr} g' + C \frac{u_e^2}{h_{te}} \left(1 - \frac{1}{Pr} \right) f' f'' \right]' + fg' = 2\xi \left(f' \frac{\partial g}{\partial \xi} - g' \frac{\partial f}{\partial \xi} \right). \quad (10.71)$$

Here dashes imply partial differentiation with respect to η . For the functions $\beta(\xi)$ and $C(\xi, \eta)$ we have:

$$\beta = \frac{2\xi}{u_e} \frac{du_e}{d\xi}, \quad C = \frac{\varrho \mu}{\varrho_e \mu_e}. \quad (10.72)$$

The boundary conditions read:

$$\eta = 0 : \quad f = 0, \quad f' = 0, \quad g = g_w$$

(or : $g'_w = 0$ for adiabatic wall)

$$\eta \rightarrow \infty : \quad f' = 1, \quad g = 0.$$

For $\beta = \text{const}$, $C = C(\eta)$ and $g_w = \text{const}$, Eqs. (10.70) and (10.71) yield similar solutions.

In the case of constant physical properties ($C = 1, \varrho = \varrho_e = \varrho_\infty$), Eq. (10.70) reduces to Eq. (7.77). From $\text{Ma}_\infty \rightarrow 0$ we obtain

$$g = \frac{T - T_\infty}{T_\infty} \quad (10.73)$$

and $u_e^2/h_{te} \rightarrow 0$, so that from Eq. (10.71) for the variable

$$\vartheta = \frac{g}{g_w} = \frac{T - T_\infty}{T_w - T_\infty}, \quad (10.74)$$

the equation

$$\frac{1}{Pr} \vartheta'' + f \vartheta' = 2\xi \left(f' \frac{\partial \vartheta}{\partial \xi} - \vartheta' \frac{\partial f}{\partial \xi} \right) \quad (10.75)$$

follows, with boundary conditions

$$\eta = 0 : \quad \vartheta = 1, \quad \eta \rightarrow \infty : \quad \vartheta = 0. \quad (10.76)$$

This is the energy equation (9.13) after the Görtler transformation Eq. (7.76) has been applied to it.

In practice, for the numerical calculation of compressible boundary layers, frequently Eqs. (10.70) and (10.71) are used instead of Eqs. (10.4), (10.5) and (10.51). The advantages of doing this include:

1. At the start of the calculation, Eq. (10.70) and (10.71) reduce to ordinary differential equations, i.e. the computation begins with the similar solution for the stagnation point or the flat plate.

2. The growth of the region of computation due to the increase in the boundary-layer thickness is essentially eliminated.
3. The boundary-layer profiles are smoother, change little in the transformed plane, and therefore allow larger numerical steps.

Details will be discussed in Chap. 23.

10.4.4 Similar Solutions

If the boundary-layer equations can be reduced to ordinary differential equations, similar solutions can be found. This similarity can further be related to different coordinate planes depending on which of the two coordinate transformations treated in the last section are used. We therefore have the following possibilities for similar solutions:

1. $\text{Pr} = 1$, linear law of viscosity.

For these flows the Illingworth–Stewartson equations can be used to reduce the boundary-layer equations to those for incompressible boundary layers (up to the factor $(1 + S)$ in the momentum equation). Applying a similarity transformation analogous to Eq. (7.21) for incompressible flows to these equations for $\text{Pr} = 1$

$$\eta = \tilde{y} \sqrt{\frac{(m+1)\tilde{u}_e}{2\nu_0 \tilde{x}}}, \quad \frac{\tilde{u}}{\tilde{u}_e} = f'(\eta), \quad S = \frac{h_t - h_{te}}{h_{te}} = S(\eta), \quad (10.77)$$

we obtain the system of equations

$$f''' + ff'' + \beta(1 + S - f'^2) = 0, \quad (10.78)$$

$$S'' + fS' = 0 \quad (10.79)$$

with the boundary conditions

$$\begin{aligned} \eta = 0 : \quad & f = 0, \quad f' = 0, \quad S = S_w \\ & (\text{or } S'_w = 0 \text{ at adiabatic wall}) \end{aligned} \quad (10.80)$$

$$\eta \rightarrow \infty : \quad f' = 1, \quad S = 0.$$

Here, as in Eqs. (7.17) and (7.19), we have introduced the pressure gradient of the outer flow as a parameter:

$$\beta = \frac{2}{m+1} \frac{\tilde{x}}{\tilde{u}_e} \frac{d\tilde{u}_e}{d\tilde{x}} = \frac{2m}{m+1}. \quad (10.81)$$

In the transformed plane, the outer flow again obeys a power law

$$\tilde{u}_e \sim \tilde{x}^m.$$

The velocity distribution $u_e(x)$ in the original plane is in general no longer a power law. For the special case $m = (\gamma - 1)/(3 - 5\gamma)$ we obtain $u_e \sim x^m$, cf. H. Schlichting (1982), p. 350.

For *adiabatic walls*, we find the solution $S = 0$, so that in this case the momentum equation (10.78) is decoupled from the energy equation and is identical to Eq. (7.15) for the incompressible boundary layer.

For *wall heat transfer*, the solutions of the system Eqs. (10.78) and (10.79), as well as depending on β , also depend on the parameter $S_w = (T_w - T_0)/T_0$. T.Y. Li; H.T. Nagamatsu (1955) and C.B. Cohen; E. Reshotko (1956) have determined solutions for a great number of values of β and S_w .

Figure 10.2 shows the velocity distributions $u/u_e = \tilde{u}/\tilde{u}_e = f'(\eta)$ and the energy distributions $(h_t - h_{te})/h_{te} = S(\eta)$ plotted against the dimensionless distance from the wall for different values of β and S_w . The values of S_w given in the figure correspond to the adiabatic wall ($S_w = 0$), cooling ($S_w = -0.8$; $T_w = 0.2T_0$) and heating ($S_w = 1.0$; $T_w = 2T_0$). For $\beta < 0$ there are two solutions. When multiple solutions are present, the solution with a smaller f''_w value is denoted by a star in Fig. 10.2. It is seen that for heating and pressure decrease ($\beta > 0$), the velocity in a certain region inside the boundary layer can become larger than the velocity u_e of the outer flow. The reason for this lies in the strong increase in volume of the fluid as a consequence of the heating inside the boundary layer. In spite of the decelerating action of the viscosity inside the boundary layer, the gas with lower density will be accelerated by the outer pressure forces more than the outer flow.

The pressure gradient has a much smaller effect on the energy distributions than on the velocity distributions, as seen in Fig. 10.2.

The relation between $S(\eta)$, $f'(\eta)$ and the temperature reads

$$\begin{aligned} \frac{T(\tilde{x}, \eta)}{T_0} &= 1 + S(\eta) - \frac{u^2}{2c_p T_0} \\ &= 1 + S(\eta) - \frac{(\gamma - 1)\text{Ma}_e^2/2}{1 + (\gamma - 1)\text{Ma}_e^2/2} [f'(\eta)]^2. \end{aligned} \quad (10.82)$$

Since $\text{Ma}_e = \text{Ma}_e(\tilde{x})$, there are in general no similar temperature profiles, apart from the special case of the plate ($\text{Ma}_e = \text{const}$).

The skin-friction coefficient related to the local dynamic pressure of the outer flow is

$$c_f = \frac{\tau_w(x)}{\frac{\rho_e}{2} u_e^2} = \frac{f''_w}{\sqrt{\text{Re}_e}} \sqrt{\frac{\varrho_w \mu_w}{\varrho_e \mu_e}} \sqrt{2(m+1) \frac{\tilde{x}}{\tilde{x}} \frac{d\tilde{x}}{dx}}. \quad (10.83)$$

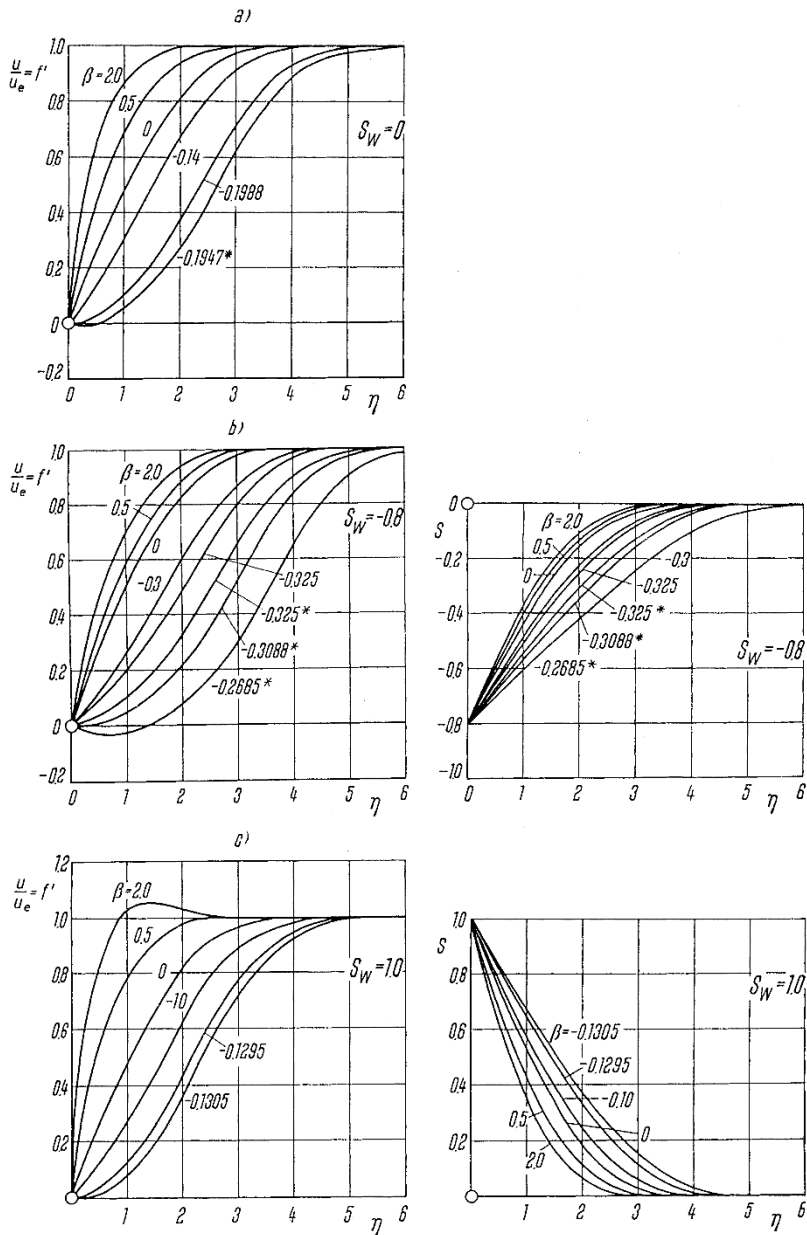


Fig. 10.2. Distribution of the velocity and the total enthalpy in the compressible boundary layer with pressure gradient (β) and wall heat transfer, $\text{Pr} = 1, \omega = 1$. Solutions of Eqs. (10.78) to (10.80) after C.B. Cohen; E. Reshotko (1956)

- (a) $S_w = 0, T_w = T_0$ (adiabatic wall, $S = 0$)
- (b) $S_w = -0.8, T_w = 0.2T_0$ (cooling)
- (c) $S_w = 1.0, T_w = 2T_0$ (heating)

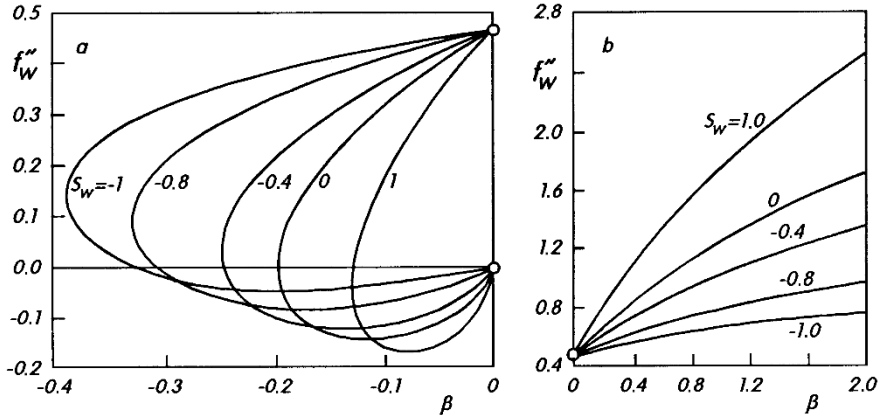


Fig. 10.3. Local skin-friction coefficient in the compressible boundary layer with pressure gradient (β) and wall heat transfer (S_w), $\text{Pr} = 1$, $\omega = 1$. Solutions of Eqs. (10.78) to (10.80)

(a) $\beta < 0$ pressure increase

(b) $\beta > 0$ pressure decrease

Figure 10.3 shows f_w'' plotted against β for various values of S_w . It can be seen that a change of β affects the value f_w'' and therefore the skin-friction coefficient in heating ($S_w > 0$) much more than when cooling occurs ($S_w < 0$). In the region of negative β there are, as already mentioned, two solutions, and therefore two possible wall shear stresses. In the case of the adiabatic wall ($S_w = 0$), the lower branch of the curve corresponds to negative wall shear stress, that is backflow. In heating ($S_w > 0$), if the value of $(\beta - \beta_{\min})$ is small enough, both solutions can yield $f_w'' < 0$ and therefore produce backflow. In cooling ($S_w < 0$), both values of f_w'' can be positive and thus produce a flow without backflow. It can also be seen that heating shifts the separation to smaller pressure increases, cf. H. Herwig, G. Wickern (1986). Heating therefore promotes separation in gas flows.

2. $\text{Ma}_\infty \rightarrow 0$, neglecting the dissipation.

In this case we obtain similar solutions in the ξ - η plane of the Levy-Lees transformation. Because $\text{Ma}_\infty \rightarrow 0$, the temperature of the outer flow is $T_e = T_\infty = \text{const}$. Because $S = (T - T_\infty)/T_\infty$, it follows that $\varrho/\varrho_e = T/T_\infty = S + 1$. Therefore the equations (10.70) and (10.71) reduce to

$$(Cf'')' + ff'' + \beta[1 + S - f'^2] = 0, \quad (10.84)$$

$$\frac{1}{\text{Pr}}(CS')' + fS' = 0. \quad (10.85)$$

The following statements then hold for the viscosity parameter C depending on the law of viscosity:

1. Sutherland formula from Eq. (10.45): (reference temperature T_∞)

$$C(\eta) = (1 + S)^{1/2} \frac{1 + s/T_\infty}{1 + S + s/T_\infty}. \quad (10.86)$$

2. Power law from Eq. (10.46): (reference temperature T_∞)

$$C(\eta) = (1 + S)^{\omega-1}. \quad (10.87)$$

3. Linear law from Eq. (10.47):

$$C = b = \text{const.}$$

If the straight line defined by Eq. (10.47) goes through the reference point, we have $C = b = 1$. On the other hand, if the straight line from Eq. (10.48) is laid to go through the point of the wall temperature, we find

$$C = \frac{\varrho_w \mu_w}{\varrho_\infty \mu_\infty} = CR. \quad (10.88)$$

In this form C is called the *Chapman–Rubesin parameter*, cf. Eq. (10.32).

The boundary conditions for the system of equations (10.84) and (10.85) are again Eq. (10.80).

For $\text{Pr} = 1$ and $C = \text{const.}$, the system (10.84) and (10.85) becomes the system (10.78) and (10.79), if the coordinate transformation

$$\eta = \sqrt{C} \bar{\eta}, \quad f(\eta) = \sqrt{C} \bar{f}(\bar{\eta}) \quad (10.89)$$

is applied.

The system of equations (10.84) and (10.85) has been solved for various values of β , Pr and ω (from Eq. (10.87)) by C.F. Dewey Jr.; J.F. Gross (1967). Further solutions including that of the plate boundary layer can be found in W. Hantzsche; H. Wendt (1940), L. Crocco (1941), E.R. Van Driest (1952), S. Levy (1954) and, for stagnation-point flow ($\beta = 1$), in J.A. Fay; F.R. Riddell (1958).

Example: Stagnation-point flow ($\text{Pr} = 0.7$)

In stagnation-point flow, the velocity u vanishes directly at the stagnation-point streamline, and therefore the effect of the dissipation vanishes. Figure 10.4 shows the dependence of the relative Nusselt number

$$\frac{\text{Nu}_x}{\sqrt{\text{Re}_x}} = \frac{q_w x}{\lambda_0(T_w - T_0)} \sqrt{\frac{\mu_0}{\varrho_0 u_e x}} \quad (10.90)$$

on the temperature ratio T_w/T_0 for $\text{Pr} = 0.7$. For stagnation-point flow, we have $T_e = T_0$, $\mu_e = \mu_0$, $\varrho_e = \varrho_0$. Here the two power laws $\omega = 1$ and $\omega = 0.7$ have been used, and the effect of the exponent ω can be seen clearly. Approximations using

the temperature ratio method from Sect. 10.3.2 are shown in the dashed curves. In the region $0.5 \leq T_w/T_0 \leq 1.5$ these approximations are very good. If we use the linear law of viscosity corresponding to Eq. (10.47), where $T_r = T_0$ and the wall value $\mu_w = \mu(T_w)$ is assumed to be exactly given by the law of viscosity, then $b = \varrho_w \mu_w / \varrho_0 \mu_0 = CR$ is identical to the Chapman–Rubesin parameter.

It can be seen clearly from Fig. 10.4 that, for variable physical properties, the heat flux at the wall q_w is *no longer proportional* to the temperature difference $T_w - T_0$.

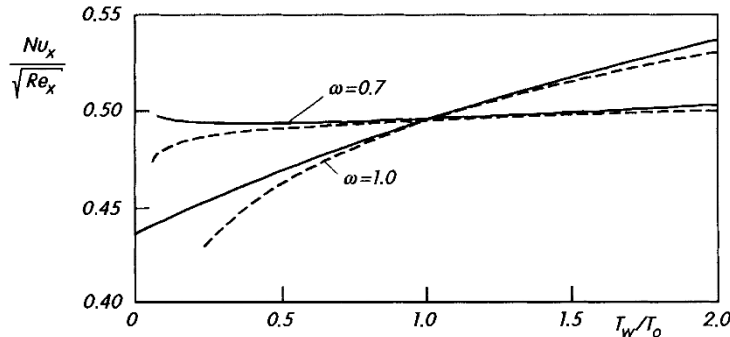


Fig. 10.4. Dependence of the wall heat transfer at plane stagnation-point flow on the temperature ratio T_w/T_0 (ideal gas, $c_p = \text{const}$, $\text{Pr} = 0.7$)

- law of viscosity from Eq. (10.46), $T_r = T_0$
- - - - temperature ratio method, see Sect. 10.3.2
- ($Nu_x/\sqrt{Re_x}$) $_{T_w \approx T_0} = 0.4959$
- $\omega = 1$; $Nu/Nu_{c.p.} = (T_w/T_0)^{0.0960}$
- $\omega = 0.7$; $Nu/Nu_{c.p.} = (T_w/T_0)^{0.0126}$

3. Flat plate with $T_w = \text{const}$ (outer flow with index ∞)

Because of the constant velocity $u_e = U_\infty$ in the outer flow past a plate, Eqs. (10.70) and (10.71) yield similar solutions, even when the dissipation is taken into account. In what follows, we treat the two cases of the adiabatic wall and plate flow with wall heat transfer separately.

Adiabatic wall

Figure 10.5 shows the velocity and temperature distributions for different Mach numbers ($\text{Pr} = 1, \omega = 1$), according to calculations by L. Crocco (1941). Since the viscosity μ is assumed to be proportional to the temperature ($\omega = 1$), the momentum equation (10.70) is decoupled from the energy equation (10.71). The distributions are not plotted against the transformed coordinate η , but rather against a suitable scaled distance from the wall y . The corresponding temperature distribution is used in the conversion from η to $y\sqrt{U_\infty/\nu_\infty x}$. From transformation (10.68) it follows that

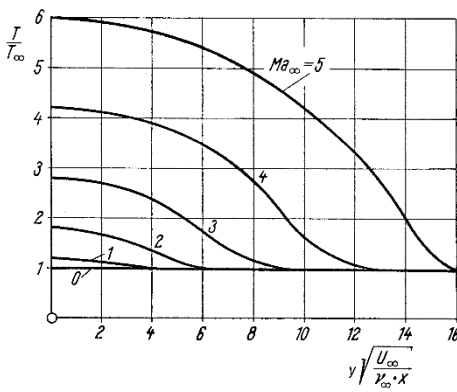
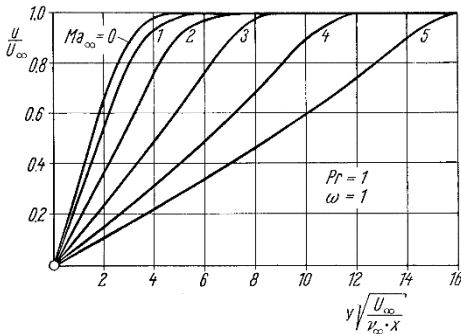


Fig. 10.5. Distribution of the velocity and temperature in the compressible boundary layer on a flat plate at zero incidence, for the *adiabatic wall*, after L. Crocco (1941); $\text{Pr} = 1; \omega = 1; \gamma = 1.4$

$$y\sqrt{\frac{U_\infty}{\nu_\infty x}} = \sqrt{2} \int_0^n \frac{T}{T_\infty} d\eta. \quad (10.91)$$

As the Mach number grows, there is a considerable increase in the boundary-layer thickness. This is due to the increase in volume which is a consequence of the heating of the boundary layer from dissipation. The temperature distributions show temperature increases due to dissipation, and these can take on quite sizable values at large Mach numbers.

The adiabatic wall temperature (also called the eigen-temperature) is usually given by the recovery factor $r = (T_{ad} - T_\infty)/(T_0 - T_\infty)$, cf. Eq. (9.86). In general this is dependent on the Mach number, the Prandtl number and the law of viscosity $\mu(T)$. As has already been mentioned in Sect. 10.3.1, the effects of the Mach number and the law of viscosity on r can be neglected, so that the curve in Fig. 9.6 also approximates that for the compressible plate boundary layer.

Figure 10.6 shows the dependence of the skin-friction coefficient for the adiabatic wall on the Mach number. For $\omega = 1$, the momentum equation (10.71) is decoupled from the energy equation, and therefore the c_f value is independent of the Mach number. For $\omega = 0.8$, the skin-friction coefficient decreases with increasing Mach number. The dashed curves are the results from the perturbation calculation in Sect. 10.3.1 corresponding to Eq. (10.25). They represent a useable approxima-

tion up to Mach number of $\text{Ma}_\infty = 3$. Finally, for comparison, the curve described by the linear law of viscosity through the point $\mu_w = \mu(T_w)$ (Chapman–Rubesin law) is also given.

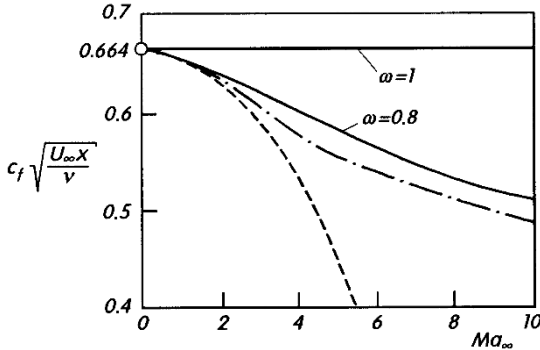


Fig. 10.6. Skin-friction coefficient of the flat plate at zero incidence for an *adiabatic wall*, $\gamma = 1.4$, $\text{Pr} = 1$, $\text{Ec}_\infty = 0.4\text{Ma}_\infty^2$

— solutions for $\omega = 1.0$ and $\omega = 0.8$, after W. Hantzsche; H. Wendt (1940)

- - - solution for $\omega = 0.8$, from the relation analogous to Eq. (10.15):

$$c_f \sqrt{\text{Re}_x} = 0.664(1 + 0.168K_{\varrho\mu}\text{Ec}_\infty)$$

- - - solution for $\omega = 0.8$ with the Chapman–Rubesin parameter

$$c_f \sqrt{\text{Re}_x} = 0.664\sqrt{\text{CR}} = 0.664(1 + 0.5\text{Ec}_\infty)^{-0.1}$$

Plate flow with heat transfer

Many examples of plate flow with heat transfer have been calculated by W. Hantzsche; H. Wendt (1942). Figure 10.7 shows some results for the velocity and temperature distributions, for the special cases $T_w = T_\infty$. Since $T_w < T_{\text{ad}}$, we are here dealing with cooling, i.e. some of the heat generated by dissipation is transferred to the wall. Therefore the boundary-layer thickness is considerably smaller than that at the adiabatic wall, as can be seen by comparing the velocity distributions in Figs. 10.5 and 10.7. The temperature distributions show that in this case the maximum temperature increase in the boundary layer is only about 20% of that at the adiabatic wall.

Figure 10.8 shows the dependence of the skin-friction coefficient and the Nusselt number on the Mach number for three different ratios T_w/T_0 . The dashed lines are the results from the perturbation calculation ($\text{Ma}_\infty \rightarrow 0, T_w \rightarrow T_0$) from Eq. (10.15) and (10.16). These represent a good approximation up to Mach numbers of about 5 and for $|(T_w - T_0)/T_0| < 0.5$.

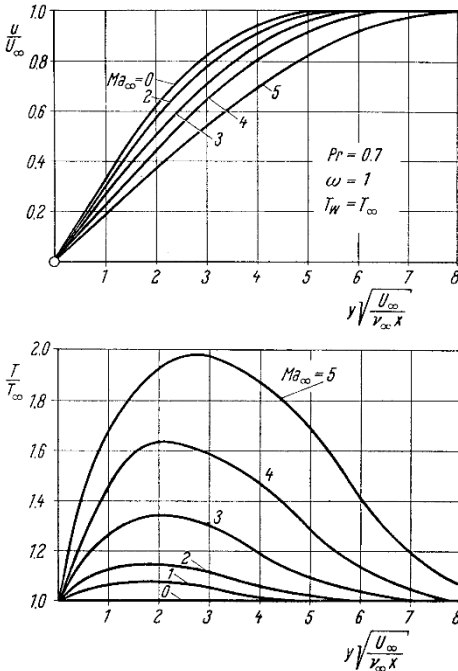


Fig. 10.7. Distribution of the velocity and temperature in the compressible boundary layer on a flat plate at zero incidence, with heat transfer, after W. Hantzsche; H. Wendt (1940);
 $\gamma = 1.4$; $\text{Pr} = 0.7$; $T_w = T_\infty$

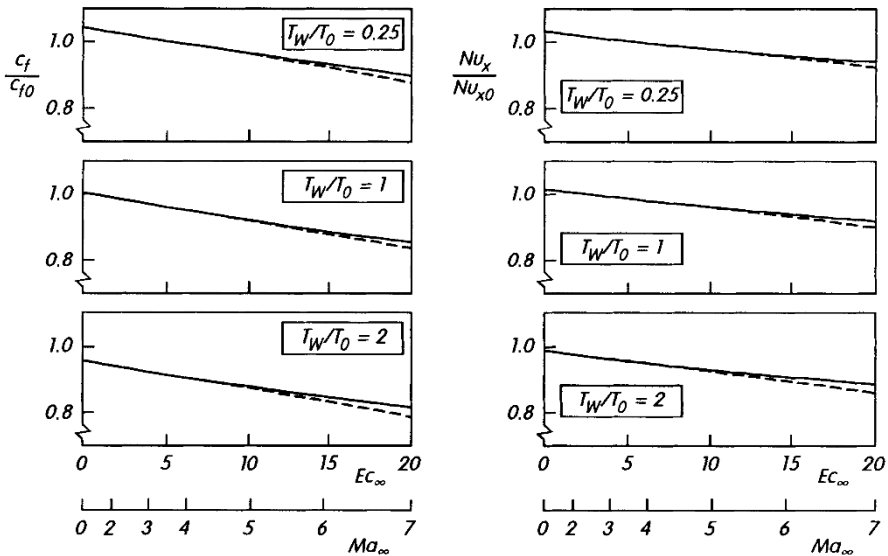


Fig. 10.8. Skin-friction coefficient and Nusselt number for the flat plate at zero incidence with heat transfer, $\text{Pr} = 0.75$; $\gamma = 1.4$; viscosity according to the Sutherland formula (10.45); $s = 110\text{K}$; $T_\infty = 218\text{K}$; $c_{f0}\text{Re}_x^{1/2} = 0.664$; $\text{Nu}_{x0}/\text{Re}_x^{1/2} = 0.30$
— solutions by E.R. Van Driest (1952)
- - - - solutions from equations analogous to Eq. (10.15) and (10.16)

10.4.5 Integral Methods

The approximate methods for calculating incompressible boundary layers described in Chap. 8 can also be extended to compressible boundary layers. An overview of the many different methods is given by H. Schlichting (1982), p. 357. What all these different approximate methods have in common is that they are considerably more complicated than the approximate methods for incompressible boundary layers. Again they are based on the momentum, kinetic-energy and thermal-energy-integral equations.

Integral relations. As in the case of incompressible boundary layers, the integral relations are obtained by integration of the corresponding equation. The following three integral relations emerge:

momentum-integral equation:

$$\frac{d\delta_2}{dx} + \frac{\delta_2}{u_e} \frac{du_e}{dx} \left(2 + \frac{\delta_1}{\delta_2} - Ma_e^2 \right) = \frac{\mu_w}{\rho_e u_e^2} \left(\frac{\partial u}{\partial y} \right)_w = \frac{\tau_w}{\rho_e u_e^2}, \quad (10.92)$$

mechanical-energy-integral equation:

$$\frac{d\delta_3}{dx} + \frac{\delta_3}{u_e} \frac{du_e}{dx} \left[3 + 2 \frac{\delta_h}{\delta_3} - Ma_e^2 \right] = \frac{2D}{\rho_e u_e^3}, \quad (10.93)$$

thermal-energy-integral equation:

$$\frac{d}{dx} (\rho_e h_e u_e \delta_h) + \rho_e u_e^2 \frac{du_e}{dx} \delta_h = D + q_w. \quad (10.94)$$

Here the following thicknesses for the boundary layer were introduced:

$$\delta_1 = \int_0^\delta \left(1 - \frac{\rho u}{\rho_e u_e} \right) dy \quad \text{displacement thickness,} \quad (10.95)$$

$$\delta_2 = \int_0^\delta \frac{\rho u}{\rho_e u_e} \left(1 - \frac{\rho u}{\rho_e u_e} \right) dy \quad \text{momentum thickness,} \quad (10.96)$$

$$\delta_3 = \int_0^\delta \frac{\rho u}{\rho_e u_e} \left[1 - \left(\frac{u}{u_e} \right)^2 \right] dy \quad \text{energy thickness,} \quad (10.97)$$

$$\delta_h = \int_0^\delta \frac{\rho u}{\rho_e u_e} \left(\frac{h}{h_e} - 1 \right) dy \quad \text{enthalpy thickness.} \quad (10.98)$$

In addition, the so-called *dissipation integral* was defined as:

$$D = \int_0^\delta \mu \left(\frac{\partial u}{\partial y} \right)^2 dy. \quad (10.99)$$

Equation (10.92) is obtained from Eqs. (10.4) and (10.5) (with $g = 0$), by integration over y , taking into account the relation for the outer flow

$$\frac{1}{\varrho_e} \frac{d\varrho_e}{dx} = - \frac{\text{Ma}_e^2}{u_e} \frac{du_e}{dx} = \frac{\text{Ma}_e^2}{\varrho_e u_e^2} \frac{dp}{dx}. \quad (10.100)$$

This relation follows from the momentum equation and the condition $T_0 = \text{const}$ at the outer edge of the boundary layer. In the same manner, Eq. (10.93) is obtained from Eq. (10.5) (with $g = 0$) when this latter is multiplied by u and integrated over y . Finally, Eq. (10.94) follows from the integration of Eq. (10.7), again using Eq. (10.100).

For constant physical properties and $\text{Ma}_e \rightarrow 0$, Eqs. (10.92) to (10.94) become the corresponding integral equations (7.100), (7.104) and (9.59). The various thicknesses in Eqs. (10.95) to (10.97) then reduce to the thicknesses given by Eqs. (7.98), (7.99) and (7.102). For this limiting case we also see that

$$\delta_h = \frac{T_w - T_\infty}{T_\infty} \delta_T \quad (\varrho = \varrho_e = \text{const}), \quad (10.101)$$

so that for $(T_w - T_\infty)/T_\infty \rightarrow 0$, Eq. (10.94) becomes Eq. (9.59). Here the dissipation integral may be considered small enough to be neglected, since $\text{Ma}_e \rightarrow 0$.

For the adiabatic wall ($q_w = 0$) we have

$$\delta_h = \frac{\gamma - 1}{2} \text{Ma}_e^2 \delta_3 \quad (q_w = 0), \quad (10.102)$$

and therefore the thermal-energy-integral and mechanical-energy-integral equations deliver identical results.

Walz's integral method for the adiabatic wall

The integral method of A. Walz (1966), p. 118 is one of many integral methods in existence. We shall now apply it to the particular case of the adiabatic wall. This method is based on the use of the two integral equations (10.92) and (10.93). Instead of the variables $\delta_2(x)$ and $\delta_3(x)$, we introduce the new variables

$$Z(x) = \delta_2 \text{Re}_2 = \frac{\varrho_e u_e \delta_2^2}{\mu_w}, \quad H_{32}(x) = \frac{\delta_3}{\delta_2}. \quad (10.103)$$

Equations (10.92) and (10.93) written in terms of these new unknowns become

$$\frac{dZ}{dx} + \frac{F_1}{u_e} \frac{du_e}{dx} Z - F_2 = 0, \quad (10.104)$$

$$\frac{dH_{32}}{dx} + \frac{F_3}{u_e} \frac{du_e}{dx} H_{32} - \frac{F_4}{Z} = 0. \quad (10.105)$$

The auxiliary functions $F_1(H_{32}, \text{Ma}_e)$ to $F_4(H_{32}, \text{Ma}_e)$ are determined using the following assumptions:

1. The velocity profiles are chosen so that the Hartree profile is approximated as precisely as possible for incompressible flow.
2. The power law in Eq. (10.46) is used for the law of viscosity.
3. For the adiabatic wall we have:

$$T_{\text{ad}} = T_e \left(1 + r(\text{Pr}) \frac{\gamma - 1}{2} \text{Ma}_e^2 \right), \quad (10.106)$$

where $r(\text{Pr})$ can be read off from Fig. 9.6, since the pressure gradient and the temperature dependence of the physical properties have essentially no effect on the recovery factor $r(\text{Pr})$.

4. The temperature profile (and thus the density profile) is coupled to the velocity profile via the first Busemann–Crocco solution (10.54). Although this solution is strictly only valid for the plate boundary layer at $\text{Pr} = 1$, it is also a good approximation where pressure gradients do exist and for $\text{Pr} \neq 1$ (but $\text{Pr} \approx 1$). This has been demonstrated in numerous comparisons with exact results.

The analytic representation of the four auxiliary functions $F_1(H_{32}, \text{Ma}_e)$ to $F_4(H_{32}, \text{Ma}_e)$ can be found in A. Walz (1966), p. 264.

In order to perform the calculation, the values γ , c_p , Pr , ω and the distributions $u_e(x)$ and $T_e(x)$ must be prescribed. From these, $r(\text{Pr})$, $\text{Ma}_e(x)$ and $T_{\text{ad}}(x)$ can be determined. With this, the auxiliary functions F_1 to F_4 can be worked out for given H_{32} values. The calculation commences with $Z = 0$ and, depending on the shape of the body, with the H_{32} value of stagnation-point flow or plate flow. The numerical solution of the system (10.104) and (10.105) of ordinary first order differential equations then ends at the separation point, determined by

$$H_{32} = 1.515 \quad (\text{separation}). \quad (10.107)$$

The local skin-friction coefficient is then obtained from the solution function $Z(x)$ as follows:

$$c_f = \frac{2\tau_w}{\rho_e u_e^2} = \frac{F_2}{2} \left(\frac{\rho_e u_e Z}{\mu_w} \right)^{-1/2}. \quad (10.108)$$

It should be noted that the system (10.104) to (10.105) may be rewritten for other independent variables. Instead of Z and H_{32} , H_{21} and H_{31} could also be used, cf. U. Ganzer (1988), p. 297.

The method of Walz, which here was only described for the case of the adiabatic wall, also enables the calculation of boundary layers with heat transfer.

Example 1: Incompressible boundary layer.

For $Mae \rightarrow 0$, the auxiliary functions are considerably simplified. One obtains:

$$\begin{aligned} F_1 &= 3 + 2H_{12}(H_{32}) \\ F_2 &= 2\alpha(H_{32}) \\ F_3 &= 1 - H_{12}(H_{32}) \\ F_4 &= 2\bar{\beta}(H_{32}) - H_{32}\alpha(H_{32}). \end{aligned} \quad (10.109)$$

These functions can be read off from Table 8.1 for the Hartree profiles. Here $\alpha = \beta_2 f_w''$ and $\bar{\beta} = \beta_2 \beta_D$. Analytical approximate formulae for the auxiliary functions $H_{12}(H_{32})$, $\alpha(H_{32})$ and $\bar{\beta}(H_{32})$ have been given by A. Walz (1966), p. 265.

The integral method formulated in this manner yields exact solutions for all wedge flows. For general flows, it is found that the results close to the separation point are more precise compared with those obtained from the quadrature formula (8.23) described in Chap. 8. For example, the integral method described here delivers the position of the separation point for the retarded stagnation-point flow in Eq. (8.37) in almost precise agreement with the exact solution $x_S/l = 0.12$.

Example 2: Compressible decelerated stagnation-point flow.

The effects of the Mach number and the thermal boundary conditions on the retarded stagnation-point flow, which was treated for the incompressible case in Sect. 8.3.1, have been examined by A. Walz (1966), p. 208 using the integral method described. Figure 10.9 shows the dependence of the position of separation on the Mach number Ma_0 for the case of the adiabatic wall. Here Ma_0 is referred to the starting point $x = 0$. As the Mach number increases, separation takes place earlier. The effect of the law of viscosity ($\omega = 0.7$ or $\omega = 1.0$) is not of great importance. Investigations into the effect of heat transfer which are not shown here again confirm that heating (in gas flows) favours separation.

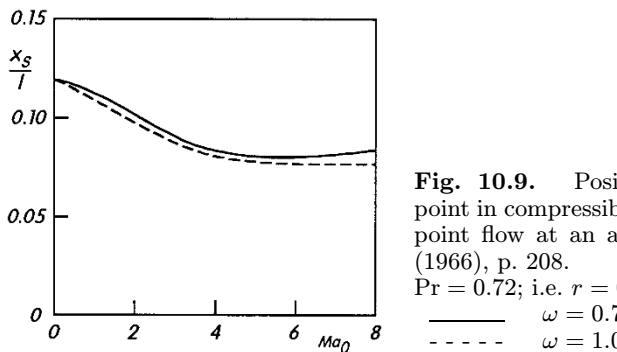


Fig. 10.9. Position of the separation point in compressible retarded stagnation-point flow at an adiabatic wall, A. Walz (1966), p. 208.

$Pr = 0.72$; i.e. $r = 0.85$; $\gamma = 1.4$

— $\omega = 0.7$
- - - $\omega = 1.0$

Example 3: Flow past an airfoil.

The results of a boundary-layer calculation for an airfoil are shown in Fig. 10.10. In this case, the calculation is carried out using the integral method of E. Gruschwitz (1950). It is valid for the adiabatic wall, for $\omega = 1$ and for any Prandtl number. Calculations using this method are simpler to carry out than those using the Walz method, but the results are less exact.

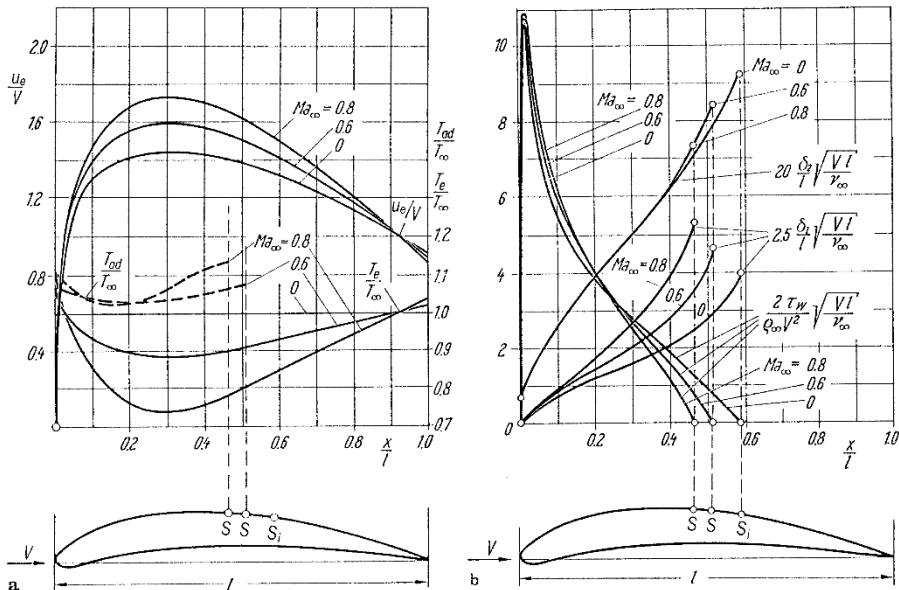


Fig. 10.10. Laminar boundary layer for compressible subsonic flow for the airfoil NACA 8410 at angle of attack $\alpha = 0^\circ$ and with an adiabatic wall. Calculations use the integral method of E. Gruschwitz (1950) for $Pr = 0.725$, S = separation point
 (a) distributions $u_e(x)/V$, T_e/T_∞ and T_{ad}/T_∞
 (b) distributions of the displacement thickness δ_1 , the momentum thickness δ_2 and the wall shear stress τ_w

Figure 10.10a shows the distributions of the velocity and the temperature in the outer flow for the suction side of the airfoil NACA 8410 at angle of attack $\alpha = 0^\circ$, for free stream Mach numbers of $Ma_\infty = 0, 0.6$ and 0.8 . The progression of the adiabatic wall temperature $T_{ad}(x)$ along the airfoil is also shown.

Figure 10.10b shows the momentum thickness δ_2 , the displacement thickness δ_1 and the wall shear stress τ_w along the suction side of the airfoil. As the Mach number increases, the separation point shifts towards the front. The momentum thickness and the wall shear stress are only mildly dependent on the Mach number, while the displacement thickness increases considerably as the Mach number increases.

Interaction of boundary layer and shock wave.

In the example of a boundary layer at an airfoil (Fig. 10.10), the flow is purely subsonic at Mach numbers of $\text{Ma}_\infty = 0.6$. At higher Mach numbers, a typical situation for transonic (close to the speed of sound) flows is that locally supersonic regions form in the outer flow. When the supersonic flow returns to subsonic speed again, this almost always takes place in a shock wave, where the velocity, pressure, temperature and density change in a discontinuous manner (not shown in Fig. 10.10). Since the boundary-layer thickness grows hugely with increasing pressure, the boundary layer experiences a great increase in its thickness at the position of the shock wave. This effect is so large that there are repercussions on the outer flow. These cannot be determined without knowing the displacement effects of the boundary layer. This effect is therefore called a shock-boundary-layer interaction, and cannot be described using the (simple) Prandtl boundary-layer theory discussed up to now. The displacement effect of the boundary layer on the inviscid outer flow is a *higher order boundary-layer effect*. More on this topic is to be found in Chap. 14 where the extensions to the Prandtl boundary-layer theory are treated.

10.4.6 Boundary Layers in Hypersonic Flows

Hypersonic flows occur for Mach numbers above about $\text{Ma}_\infty = 5$, and are important in considering flows past space craft, ballistic missiles and hypersonic aircraft. Summaries of this particular area of aerodynamics can be found in W.D. Hayes; R.F. Probstein (1959), H.W. Dorrance (1962), J.C. Rotta (1962), R.N. Cox; L.F. Crabtree (1965), J. Zierep (1966), G. Koppenwallner (1988), J.D. Anderson Jr. (1989).

At the Mach number $\text{Ma}_\infty = 5$, using $\gamma = 1.4$, Eq. (10.58) yields a total temperature for the outer flow of $T_0 = 6T_\infty$, and so for $T_\infty = 300\text{K}$, we already have $T_0 = 1800\text{K}$. For temperatures this high (and for low pressures of $p_\infty = 10^{-4}\text{ bar}$) the behaviour of air deviates from that of the ideal gas, i.e. Eq. (10.38) is no longer valid.

The reason for this “real gas” behaviour is the onset of dissociation. Instead of Eq. (10.38), the equation $p = \varrho RTZ(T, p)$ is used, where $Z(T, p)$ is called the *compressibility factor*.

Even at low temperatures (for air, above about $T = 500\text{K}$), oscillations in the molecules occur. This leads to a temperature dependent $c_p(T)$. For variable c_p , the specific enthalpy h is no longer proportional to the temperature T .

Hypersonic flows are all those flows where high temperatures mean that the gas can no longer be taken to be an ideal gas with constant specific heat capacity. This is frequently the case for flows above about $\text{Ma}_\infty = 5$.

The following features are typical for hypersonic boundary layers:

1. Real gas effects

Real gas effects occur due to oscillations of molecules, dissociation and, at even higher temperatures, ionisation. If dissociation occurs, the gas is frequently represented as a binary mixture of molecules and atoms. A further integral equation for the concentration of the “atomic gas” can then be added to the existing integral equations, as a measure of the amount of dissociation. In general these are now *non-equilibrium boundary layers*, which have as their two limiting cases *thermodynamic equilibrium* and *frozen flows*. Here the state of the surface is of considerable importance. The wall is called *fully catalytic* if all the atoms recombine at the wall, whereas there is no recombination at a *non-catalytic* wall.

These problems will be discussed more closely in the treatment of binary boundary layers in Sect. 11.3.

2. Thermal protection

When a space craft re-enters the earth’s atmosphere, there is considerable transfer of heat. For this reason, the calculation of wall heat transfer and its reduction via suitable cooling mechanisms is frequently very important, cf. E.R. Van Driest (1956a). In *transpiration cooling*, a (generally light) cooling gas is blown out through the porous surface; in *ablation* the cooling is carried out via the transformation of a thin layer of the surface to a liquid or gaseous state (evaporation cooling, sublimation cooling). In these cases binary boundary layers are found (or boundary layers containing more than two fluids). This will be discussed further in Sect. 11.3. At extremely high temperatures, *radiation cooling* is important. See the overviews of radiation gas dynamics by W. Schneider (1968, 1974a, 1976, 1980), and S.I. Pai (1965).

3. Higher order boundary-layer effects

Frequently a separated curved shock wave will form in front of a hypersonic body. Behind this, the inviscid flow is no longer irrotational. In this case the boundary layer at the outer edge must be matched onto the rotational outer flow. This is a so-called higher order boundary-layer effect, to be treated in Chap. 14. Such effects also occur in hypersonic flows with very low densities (at great heights in the atmosphere) when the no-slip condition no longer holds (so-called *slip flows*) and a *temperature jump* exists between the wall temperature and the gas temperature at the wall, cf. Chap. 14.

4. Interaction of boundary layer and shock wave

When hypersonic airplanes which fly with aerodynamic lift are considered, the configurations found are fairly slender, similar to a slender wedge. Because of the high Mach numbers, the shock wave which forms lies very close to the contour, and there is a strong interaction between the boundary layer and the shock wave at, for example, the leading edge of a plate flow in the hypersonic region. This will be treated in more detail in Sect. 14.3.

10.5 Natural Convection

10.5.1 Boundary-Layer Equations

Natural convection flows arise when buoyancy forces due to density differences occur and these act as “driving forces”. If the density is kept constant, a natural convection flow cannot form. Thus, this is an effect of variable properties, where there is a mutual coupling between momentum and heat transport. (In forced convection this coupling is only one-sided, assuming constant physical properties.)

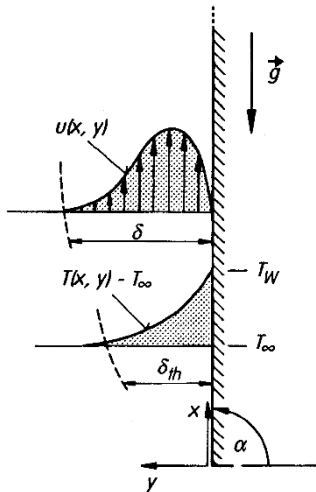


Fig. 10.11. Boundary layer at a heated vertical flat plate

The direct origin of the formation of natural convection flows is a heat transfer via conduction through the fixed walls surrounding the fluid. A simple example is the vertical flat plate, shown in Fig. 10.11, whose temperature T_w is greater than the surrounding temperature T_∞ . The heat transferred from the plate to the fluid leads to an increase of the temperature of the fluid close to the wall and to a change in the density because it is temperature

dependent. If the density decreases with increasing temperature, buoyancy forces arise close to the wall, and warmer fluid moves up along the plate. Obviously the effect of the plate is restricted to a thin layer close to the wall, since the additional internal energy supplied to the fluid through the wall is transported up along the wall by convection and thus cannot reach regions of fluid lying further away. The thickness δ_{th} of the “thermal layer” (region with $T > T_\infty$) is taken to be the distance from the wall at which the temperature has dropped to within a certain percentage (e.g. 1%) of the outer temperature T_∞ . This thickness grows with the length x . This follows from a simple energy balance, according to which the total internal energy supplied through the wall up to a point x must “flow” by convection of the higher temperature fluid over the cross-section $x = \text{const}$. Simple dimensional considerations show that the thickness of the thermal layer is smaller, the smaller the viscosity μ . Therefore the flow has a boundary-layer character, comparable to the flows of free jets and wall jets, where there is also no outer flow.

Thus the fundamental equations again are the boundary-layer equations (10.4) to (10.6) for the coordinate system shown in Fig. 10.1, with an additional buoyancy term in the momentum equation. From this it follows for the static case (no flow) that

$$\frac{dp_{\text{stat}}}{dx} = -\varrho_{\text{stat}} g \sin \alpha. \quad (10.110)$$

In what is discussed next, a static field with constant temperature T_∞ will be assumed, i.e. $\varrho_{\text{stat}} = \varrho_\infty$. Details of natural convection flows where the outer fields are made up of different temperature layers are to be found in C.C. Chen; R. Eichhorn (1976), Y. Jaluria (1980), p. 173, and B.J. Venkat-achala; G. Nath (1981).

Since the outer pressure is imposed on the boundary layer ($\partial p / \partial y = 0$), there is no additional pressure due to the flow, i.e. $p = p_{\text{stat}}$. Therefore

$$-\varrho g \sin \alpha - \frac{dp}{dx} = -(\varrho - \varrho_\infty) g \sin \alpha. \quad (10.111)$$

In what follows, only small temperature differences $\Delta T = T_w - T_\infty$ (or small wall heat fluxes q_w) will be discussed. The density function $\varrho(T)$ can then be expanded in a Taylor series:

$$\varrho(T) = \varrho_\infty - \beta_\infty \varrho_\infty (T - T_\infty) + \dots \quad (10.112)$$

with the coefficient of thermal expansion $\beta_\infty = -[(d\varrho/dT)/\varrho]_\infty$ at temperature T_∞ . If we break off this series after the linear term, combining Eq. (10.111) and (10.112) yields

$$-\varrho g \sin \alpha - \frac{dp}{dx} = \varrho_\infty g \beta_\infty (T - T_\infty) \sin \alpha. \quad (10.113)$$

Using a similar linear expansion for the remaining physical properties, as here for the viscosity

$$\mu(T) = \mu_\infty \left[1 + K_\mu \frac{\Delta T}{T_\infty} \vartheta \right] \quad (10.114)$$

with $\vartheta = (T - T_\infty)/\Delta T$, where ΔT is a characteristic temperature difference, then in the limiting case $\Delta T/T_\infty \rightarrow 0$ all physical properties reduce to their values at T_∞ . This behaviour is called the *Boussinesq approximation*, cf. Sect. 4.2.

Therefore the basic equations for natural convection flows read

$$\frac{\partial u}{\partial x} + \frac{\partial v}{\partial y} = 0, \quad (10.115)$$

$$u \frac{\partial u}{\partial x} + v \frac{\partial u}{\partial y} = \nu_\infty \frac{\partial^2 u}{\partial y^2} + g \beta_\infty (T - T_\infty) \sin \alpha, \quad (10.116)$$

$$u \frac{\partial T}{\partial x} + v \frac{\partial T}{\partial y} = a_\infty \frac{\partial^2 T}{\partial y^2}, \quad (10.117)$$

with $a_\infty = \lambda_\infty / \rho_\infty c_{p\infty}$. Here the dissipation term $\mu_\infty (\partial u / \partial y)^2 / \rho_\infty c_{p\infty}$ has been neglected in the energy equation (10.117). This may be done because the velocities in natural convection flows are small. We will discuss this briefly again in Sect. 10.5.7.

In deriving Eq. (10.116) it was assumed that β_∞ does not vanish. If this does occur (e.g. in water at 4°C), particular steps must be carried out. In the expansion (10.112), the quadratic term must then be taken into account, cf. H. Herwig (1985a).

It is to be recalled that the boundary-layer equations were derived from the Navier–Stokes equations through a limiting process. In forced convection flows this is the limiting case of high Reynolds numbers $Re \rightarrow \infty$. After the boundary-layer transformation, the boundary-layer equations were independent of the Reynolds number (i.e. of the viscosity).

Since there is initially no given reference velocity in natural convection, another characteristic number for these flow must be found instead of the Reynolds number. This is found from dimensional considerations to be

$$Gr = \frac{gl^3 \beta_\infty \Delta T}{\nu_\infty^2} \quad (10.118)$$

and is called the *Grashof number*. Here ΔT is a characteristic temperature difference. From a comparison of the square of the Reynolds number $Re = Vl/\nu$, a characteristic velocity for natural convection flows follows:

$$V_{DN} = (gl\beta_\infty \Delta T)^{1/2}, \quad (10.119)$$

assuming positive $\beta_\infty \Delta T$. The index *DN* in Eq. (10.119) means *direct* natural convection and differs from the characteristic velocity V_{IN} of *indirect* natural

convection which will be treated in Sect. 10.6. The relative thickness $\delta(x)/l$ of the boundary layer decreases with increasing Grashof number.

After the boundary-layer transformation which takes this behaviour into account, the boundary-layer equations become independent of the Grashof number. With the transformation

$$\begin{aligned} x^* &= \frac{x}{l}, & \bar{y} &= \frac{y}{l} \text{Gr}^{1/4}, & u^* &= \frac{u}{V_{DN}}, \\ \bar{v} &= \frac{v}{V_{DN}} \text{Gr}^{1/4}, & \vartheta &= \frac{T - T_\infty}{\Delta T}, \end{aligned} \quad (10.120)$$

we obtain the system of equations

$$\begin{aligned} \frac{\partial u^*}{\partial x^*} + \frac{\partial \bar{v}}{\partial \bar{y}} &= 0 \\ u^* \frac{\partial u^*}{\partial x^*} + \bar{v} \frac{\partial u^*}{\partial \bar{y}} &= \frac{\partial^2 u^*}{\partial \bar{y}^2} + \vartheta \sin \alpha \\ u^* \frac{\partial \vartheta}{\partial x^*} + \bar{v} \frac{\partial \vartheta}{\partial \bar{y}} &= \frac{1}{\text{Pr}_\infty} \frac{\partial^2 \vartheta}{\partial \bar{y}^2} \end{aligned} \quad (10.121)$$

with the boundary conditions

$$\begin{aligned} \bar{y} = 0 : \quad u^* &= 0, \quad \bar{v} = 0, \quad \vartheta = (T_w - T_\infty)/\Delta T \\ \bar{y} \rightarrow \infty : \quad u^* &= 0, \quad \vartheta = 0. \end{aligned} \quad (10.122)$$

Therefore the problem is to solve the system (10.121) with the boundary conditions (10.122) for prescribed body contour $\sin \alpha(x)$, Pr_∞ and distribution of the wall temperature $T_w(x)$.

The solution functions $u^*(x^*, \bar{y})$, $\bar{v}(x^*, \bar{y})$ and $\vartheta(x^*, \bar{y})$ yield the skin-friction coefficient

$$c_f = \frac{2\tau_w}{\rho_\infty V_{DN}^2} = 2 \text{Gr}^{-1/4} \left(\frac{\partial u^*}{\partial \bar{y}} \right)_w, \quad (10.123)$$

the Nusselt number

$$\text{Nu} = \frac{q_w l}{\lambda_\infty \Delta T} = -\text{Gr}^{-1/4} \left(\frac{\partial \vartheta}{\partial \bar{y}} \right)_w \quad (10.124)$$

as well as the entrainment velocity at the edge of the boundary layer

$$\frac{v_\infty}{V_{DN}} = \text{Gr}^{-1/4} \lim_{\bar{y} \rightarrow \infty} \bar{v}(x^*, \bar{y}). \quad (10.125)$$

It is seen from Eq. (10.120) that the thickness of the boundary layer

$$\delta \sim l \text{Gr}^{-1/4} \sim \sqrt{\nu} \quad (10.126)$$

is again proportional to the square root of kinematic viscosity.

Note (when $q_w(x)$ is prescribed) We note that if the wall heat flux $q_w(x)$ is prescribed, then we no longer have $\delta \sim \sqrt{\nu}$ for the boundary-layer thickness. This has

to do with the fact that in this case the reference velocity V_{DN} in Eq. (10.119) is itself dependent on ν . This is very similar to the flows of free jets and wall jets. In those cases $V \sim \nu^{-1}$, cf. Eq. (7.53), and $V \sim \nu^{-2}$, cf. Eq. (7.69), respectively. Since there is also no prescribed velocity in natural convection flow, for a prescribed q_w we find the reference velocity $V_{DN} \sim \nu^{1/4}$. This is required to describe the asymptotic behaviour of the flow for large Grashof numbers via a boundary-layer transformation which yields a system of equations independent of the Grashof number. To this end we formally set ΔT in Eq. (10.119) to

$$\Delta T = \frac{q_{wl} l}{\lambda_\infty} \text{Gr}^{-1/4}, \quad (10.127)$$

where q_{wl} is a characteristic wall heat flux, e.g. that at $x = l$. Equation (10.120) then guarantees that $(\partial\vartheta/\partial\bar{y})_w$ is independent of the Grashof number.

The combination of (10.118) and (10.127) yields

$$\text{Gr} = \frac{gl^4 \beta_\infty q_{wl}}{\lambda_\infty \nu_\infty^2} \text{Gr}^{-1/4}. \quad (10.128)$$

For given q_{wl} we define the Grashof number to be:

$$\text{Gr}_q = \frac{gl^4 \beta_\infty q_{wl}}{\lambda_\infty \nu_\infty^2}. \quad (10.129)$$

Because of Eq. (10.128), the following relation between the Grashof numbers in Eq. (10.118) and (10.129) results:

$$\text{Gr}^{1/4} = \text{Gr}_q^{1/5}. \quad (10.130)$$

With this replacement, the boundary-layer transformation (10.120) again leads to the system of equations (10.121). However the boundary condition for ϑ at $\bar{y} = 0$ now reads

$$\bar{y} = 0 : \left(\frac{\partial \vartheta}{\partial \bar{y}} \right)_w = -\frac{q_w(x)}{q_{wl}}.$$

The boundary-layer thickness in this case is

$$\delta \sim \nu^{2/5}.$$

Compatibility condition at the wall. If we specify Eq. (10.116) for the wall, we find the *compatibility condition at the wall* to be

$$\nu_\infty \left(\frac{\partial^2 u}{\partial y^2} \right)_w = -g\beta_\infty(T_w - T_\infty) \sin \alpha. \quad (10.131)$$

Thus $(\partial^2 u / \partial y^2)_w$ is negative as long as $\beta_\infty(T_w - T_\infty) \sin \alpha$ is positive, i.e. as long as the vertical component of the main flow velocity has the same direction as the buoyancy forces. Since $(\partial^2 u / \partial y^2)_w$ must be positive at the separation point, no separation can occur in the solutions of Eqs. (10.115) to (10.117).

In experiments, however, flow separation for natural convection has indeed been observed. This cannot be described with the above theory. This is a higher order boundary-layer effect, which will be discussed in more detail in Chap. 14.

10.5.2 Transformation of the Boundary-Layer Equations

Saville–Churchill transformation ($T_w = \text{const}$)

In analogy to the Görtler transformation in forced convection flows, cf. Sect. 7.3, D.A. Saville; S.W. Churchill (1967) presented a coordinate transformation for natural convection flows (at $T_w = \text{const}$). Using the transformation

$$\xi = \int_0^{x^*} [\sin \alpha(x^*)]^{1/3} dx^*, \quad \eta = \left(\frac{3}{4}\right)^{1/4} \frac{\bar{y}[\sin \alpha(x^*)]^{1/3}}{\xi^{1/4}} \quad (10.132)$$

for the stream function $F(\xi, \eta)$ with

$$\psi^*(x^*, \bar{y}) = \left(\frac{4}{3}\right)^{3/4} \xi^{3/4} F(\xi, \eta) \quad (10.133)$$

and the temperature $\vartheta(\xi, \eta) = (T - T_\infty)/(T_w - T_\infty)$, the system of equations (10.121) becomes

$$F_{\eta\eta\eta} + F F_{\eta\eta} - \frac{4}{3} \beta(\xi) F_\eta^2 + \vartheta = \frac{4}{3} \xi (F_\eta F_{\xi\eta} - F_\xi F_{\eta\eta}), \quad (10.134)$$

$$\frac{1}{\Pr} \vartheta_{\eta\eta} + F \vartheta_\eta = \frac{4}{3} \xi (F_\eta \vartheta_\xi - F_\xi \vartheta_\eta). \quad (10.135)$$

Here the *principal function* is

$$\beta(\xi) = \frac{1}{2} + \frac{1}{3} \frac{d[\ln \sin \alpha(\xi)]}{d(\ln \xi)}. \quad (10.136)$$

The boundary conditions read:

$$\begin{aligned} \eta = 0 : \quad & F = 0, \quad F_\eta = 0, \quad \vartheta = 1 \\ \eta \rightarrow \infty : \quad & F_\eta = 0, \quad \vartheta = 0. \end{aligned} \quad (10.137)$$

For $\beta = \text{const}$ the system reduces to ordinary differential equations, i.e. similar solutions occur. These will be treated in more detail in Sect. 10.5.4.

Pseudo-similarity transformation

If the \bar{y} coordinate is transformed to the variable

$$\eta = \frac{\bar{y}}{\sqrt{2}x^*} \left[x^{*3} \frac{T_w(x^*) - T_\infty}{\Delta T} \sin \alpha(x^*) \right]^{1/4}, \quad (10.138)$$

we obtain a system of equations for the relative stream function

$$f(x^*, \eta) = 2^{-3/2} \psi^* \left[x^{*3} \frac{T_w(x^*) - T_\infty}{\Delta T} \sin \alpha(x^*) \right]^{-1/4} \quad (10.139)$$

and for the temperature

$$\vartheta(x^*, \eta) = \frac{T(x^*, \bar{y}) - T_\infty}{T_w(x^*) - T_\infty}. \quad (10.140)$$

This system of equations is due to I. Pop; H.S. Takhar (1993) and reads:

$$\begin{aligned} f''' + [3 + P(x^*) + Q(x^*)]ff'' - 2[1 + P(x^*) + Q(x^*)]f'^2 + \vartheta \\ = 4x^* \left(f' \frac{\partial f'}{\partial x^*} - f'' \frac{\partial f}{\partial x^*} \right), \end{aligned} \quad (10.141)$$

$$\begin{aligned} \frac{1}{\text{Pr}}\vartheta'' + [3 + P(x^*) + Q(x^*)]f\vartheta' - 4P(x^*)f'\vartheta \\ = 4x^* \left(f' \frac{\partial \vartheta}{\partial x^*} - \vartheta' \frac{\partial f}{\partial x^*} \right) \end{aligned} \quad (10.142)$$

with the boundary conditions

$$\begin{aligned} \eta = 0 : & \quad f = 0, \quad f' = 0, \quad \vartheta = 1 \\ \eta \rightarrow \infty : & \quad f' = 0, \quad \vartheta = 0. \end{aligned} \quad (10.143)$$

The dashes imply partial differentiation with respect to η . The wall temperature function $P(x^*)$ and the contour function $Q(x^*)$ are defined as follows:

$$\begin{aligned} P(x^*) &= \frac{d[\ln\{(T_w(x^*) - T_\infty)/\Delta T\}]}{d(\ln x^*)} \\ Q(x^*) &= \frac{d[\ln \sin \alpha(x^*)]}{d(\ln x^*)}. \end{aligned} \quad (10.144)$$

It can be seen immediately that the system reduces to ordinary differential equations for constant P and Q values and thus leads to similar solutions. This will be discussed in Sect. 10.5.4. Because of this property, this form of the boundary-layer equations is particularly useful for numerical solutions cf. Sect. 10.4.3.

10.5.3 Limit of Large Prandtl Numbers ($T_w = \text{const}$)

It has been shown by A. Acrivos (1962) that, in the limit of large Prandtl numbers (with $T_w = \text{const}$), the system of equations leads to similar solutions and thus to closed formulae for the skin-friction coefficient and the Nusselt number. This can easily be demonstrated for the transformed system (10.134) and (10.135).

With the further transformation

$$\hat{\eta} = \eta \text{Pr}^{1/4}, \quad \hat{F}(\hat{\eta}) = \text{Pr}^{3/4} F(\eta)$$

this system reduces in the limit $\text{Pr} \rightarrow \infty$ to the following simple ordinary differential equations for the region close to the wall:

$$\hat{F}''' + \vartheta = 0, \quad \vartheta'' + \hat{F}\vartheta' = 0. \quad (10.145)$$

Here the dashes now imply differentiation with respect to the similarity variable $\hat{\eta}$. The boundary conditions read:

$$\begin{aligned}\hat{\eta} = 0 : \quad \widehat{F} = 0, \quad \widehat{F}' = 0, \quad \vartheta = 1 \\ \hat{\eta} \rightarrow \infty : \quad \widehat{F}'' = 0, \quad \vartheta = 0.\end{aligned}$$

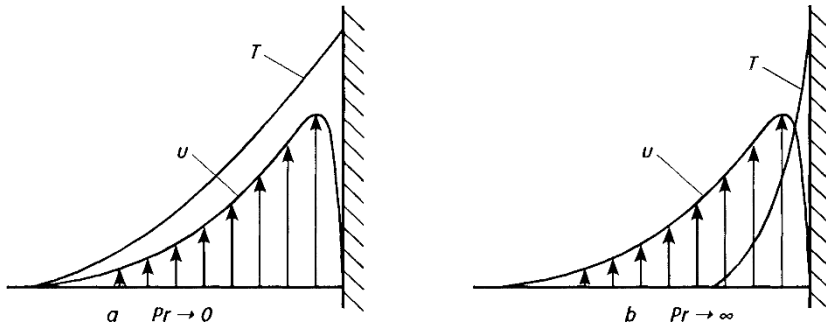


Fig. 10.12 a,b. Natural convection at a heated vertical flat plate. Distributions of velocity and temperature

Worth noting is the condition $\widehat{F}''(\infty) = 0$ instead of, as before, $\widehat{F}'(\infty) = 0$. In fact here $\widehat{F}'(\infty) \neq 0$. This is explained by the fact that the boundary layer in the case $Pr \rightarrow \infty$ consists of two layers, cf. Fig. 10.12b. The system (10.145) only describes the layer close to the wall. However at the outer edge of this layer, the velocity is non-zero. In the outer layer not described here, the velocity then decreases to zero, cf. H.K. Kuiken (1968a). The flow in the outer layer is therefore not directly due to buoyancy forces, but rather due to a “dragging action” of the velocity on the outer edge of the wall layer, comparable to the flow at a moving plate in Sect. 7.2.5.

Therefore the wall layer can be computed without knowledge of the outer layer. We obtain a similar solution which is independent of the geometry $\sin \alpha(x^*)$. The solution of the system (10.145) yields:

$$\widehat{F}_w'' = 1.085, \quad \widehat{F}'(\infty) = 0.884, \quad \vartheta_w' = -0.540.$$

It follows that the Nusselt number is

$$\begin{aligned}\text{Nu} &= \frac{q_w l}{\lambda_w (T_w - T_\infty)} \\ &= 0.503 (\text{Pr Gr})^{1/4} \frac{[\sin \alpha(x)]^{1/3}}{\left\{ \int_0^x [\sin \alpha(x)]^{1/3} d(x/l) \right\}^{1/4}}.\end{aligned}\tag{10.146}$$

Note (Limit of very small Prandtl numbers)

A closed solution can be written down for the limiting case $\text{Pr} \rightarrow 0$. In this limit, the flow also consists of two layers, cf. Fig. 10.12a. For the inner layer close to the wall, we can set $T = T_w$, and hence the velocity field in this layer is independent of the temperature distribution and can be computed immediately. At the outer edge of this layer, the shear stress must vanish. The wall shear stress follows from the solution of the nonlinear differential equation for the wall layer. Although the outer layer is inviscid (viscosity effects vanish), a coupled system of nonlinear differential equations must still be solved, where the velocity has to be matched onto that of the inner flow. The entrainment velocity v_∞ at the outer edge of the boundary layer and the wall heat flux are obtained from this solution, cf. H.K. Kuiken (1969).

10.5.4 Similar Solutions

We start out from the system of equations (10.141) and (10.142). As already mentioned in Sect. 10.5.2, the conditions $P = \text{const}$ and $Q = \text{const}$ lead to similar solutions. This is satisfied for

$$\begin{aligned} T_w(x^*) - T_\infty &= \Delta T \cdot (x^*)^m, & P = m; \\ \sin \alpha(x^*) &= A \cdot (x^*)^n, & Q = n. \end{aligned} \quad (10.147)$$

The wall temperature must therefore obey a power law, where the standard cases are determined by $m = 0$ ($T_w = \text{const}$) and $m = 1/5$ ($q_w = \text{const}$).

Each value n corresponds to a particular body contour. For $n = 0$ we obtain a plate tilted at angle α ($A = \sin \alpha$), while the value $n = 1$ (i.e. $\sin \alpha = x/l$, $A = 1$) corresponds to the *lower “stagnation-point flow”* at a body which is rounded underneath, e.g. a circular cylinder (l is the radius of curvature), cf. Fig. 10.13.

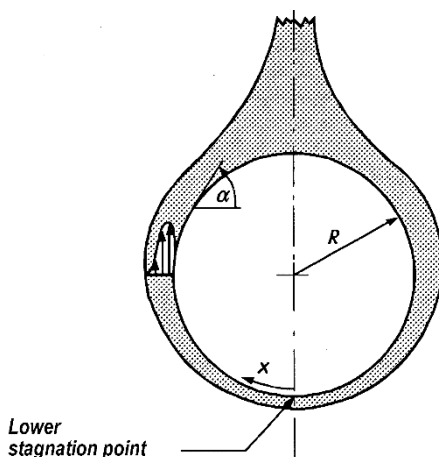


Fig. 10.13. Natural convection at a circular cylinder for $T_w > T_\infty$. Position of “lower stagnation point”

I. Pop; H.S. Takhar (1993) have determined the body contours for values of n between 0 and 1. The system of equations to be solved then has the simple form

$$f''' + (3 + m + n)ff'' - 2(1 + m + n)f'^2 + \vartheta = 0, \quad (10.148)$$

$$\frac{1}{\text{Pr}}\vartheta'' + (3 + m + n)f\vartheta' - 4mf'\vartheta = 0 \quad (10.149)$$

with the boundary conditions (10.143).

The Nusselt number is obtained from the solutions:

$$\frac{\text{Nu}}{\text{Gr}^{1/4}} = -\frac{\vartheta'_w}{\sqrt{2}} A^{1/4} \left(\frac{x}{l}\right)^{(m+n-1)/4}. \quad (10.150)$$

Numerical values of the solutions for the flat plate ($n = 0$) tilted at angle α are given in Table 10.2; those for the “stagnation-point flow” ($n = 1$) from Fig. 10.13 are to be found in Table 10.3. Further numerical values may be found in I. Pop; H.S. Takhar (1993) for $m + n = 0$ and in H. Schlichting (1982), p. 323 for $m = n = 0$. Particular solutions of the system (10.148) and (10.149) have also been investigated by K.T. Yang (1960) and E.M. Sparrow; J.L. Gregg (1958).

For the case of constant wall temperature, we can immediately see from the system (10.134) and (10.135) that body contours of the form $\sin \alpha \sim x^n$ lead to similar solutions. In this case there is, in Eq. (10.134), a constant principal function $\beta = (1/2) + (n/3)$, so that the system reduces to ordinary differential equations.

Table 10.2. Natural convection flow at a flat plate at angle $\alpha \neq 0$. Similar solutions of the system (10.148) and (10.149) with $n = 0$

Pr	$T_w = \text{const } (m = 0)$			$q_w = \text{const } (m = 1/5)$		
	f_w''	$-\vartheta'_w$	f_∞	f_w''	$-\vartheta'_w$	f_∞
$\rightarrow 0$	1.0700	$0.8491\text{Pr}^{\frac{1}{2}}$	$0.4891\text{Pr}^{-\frac{1}{2}}$	1.0116	$1.0051\text{Pr}^{\frac{1}{2}}$	$0.4526\text{Pr}^{-\frac{1}{2}}$
0.01	0.9878	0.0806	4.8480	0.9354	0.0947	4.4790
0.1	0.8592	0.2302	1.5239	0.8136	0.2670	1.4034
0.7	0.6789	0.4995	0.6061	0.6420	0.5701	0.5548
1	0.6422	0.5672	0.5230	0.6070	0.6455	0.4782
7	0.4508	1.0543	0.2752	0.4250	1.1881	0.2509
10	0.4192	1.1693	0.2492	0.3950	1.3164	0.2272
100	0.2517	2.1914	0.1366	0.2367	2.4584	0.1245
$\rightarrow \infty$	$0.8245\text{Pr}^{-\frac{1}{4}}$	$0.7110\text{Pr}^{\frac{1}{4}}$	$0.4292\text{Pr}^{-\frac{1}{4}}$	$0.7743\text{Pr}^{-\frac{1}{4}}$	$0.7964\text{Pr}^{\frac{1}{4}}$	$0.3909\text{Pr}^{-\frac{1}{4}}$

Table 10.3. Natural convection flow at the “lower stagnation point” from Fig. 10.13. Similar solutions of the system (10.148) and (10.149) with $m = 0$ and $n = 1$

Pr	f_w''	$-\vartheta_w'$	f_∞
$\rightarrow 0$	0.8716	$0.8695\text{Pr}^{1/2}$	$0.3864\text{Pr}^{-1/2}$
0.01	0.8275	0.0829	3.8322
0.1	0.7440	0.2384	1.2047
0.7	0.6077	0.5236	0.4770
1	0.5777	0.5960	0.4107
7	0.4133	1.1210	0.2141
10	0.3852	1.2452	0.1937
100	0.2332	2.3474	0.1059
$\rightarrow \infty$	$0.7673\text{Pr}^{-1/4}$	$0.7640\text{Pr}^{1/4}$	$0.3326\text{Pr}^{-1/4}$

Just as forced convection of the free jet and wall jet led to similar solutions, there are also similar solutions for the *buoyant jet* and the *buoyant wall jet* in natural convection.

Buoyant jet

A horizontal line shaped thermal energy source (or in the plane shown, a point source) produces a buoyant jet flow, as sketched in Fig. 10.14a. Since this problem has no characteristic length, the flow is described by a similar solution, analogous to the free jet flow, cf. Sect. 7.2.6. While the momentum in the free jet remained constant, in the buoyant jet it is the power per unit length

$$\dot{Q}_b = \frac{\dot{Q}}{b} = \int_{-\infty}^{+\infty} \rho c_p u(T - T_\infty) dy \quad (10.151)$$

which remains constant ($[\dot{Q}_b] = \text{W/m}$). Since there are no given reference quantities V and ΔT for the velocity or the temperature difference, we acquire these from the condition that \dot{Q} remain constant in the boundary-layer transformation. Therefore the effects of the viscosity are $V \sim \nu^{-1/5}$ and $\Delta T \sim \nu^{-2/5}$. Equations (10.148) and (10.149) are valid with $n = 0$, $m = -3/5$ and corresponding boundary conditions.

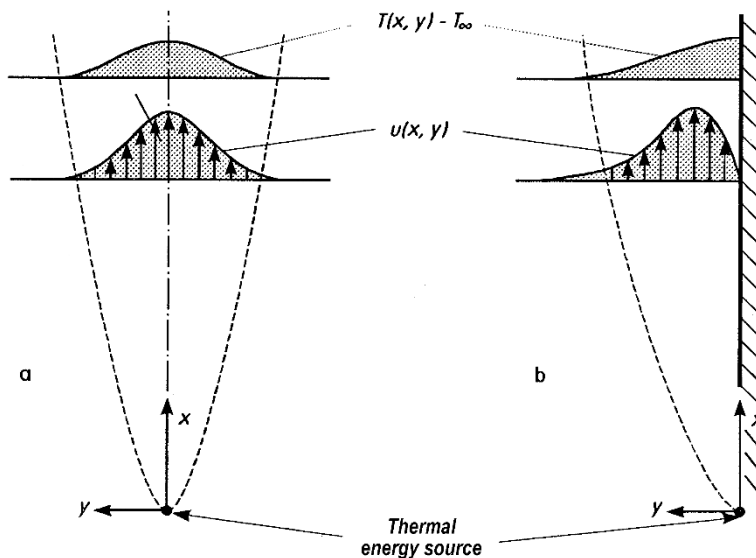


Fig. 10.14. (a) buoyant jet and (b) buoyant wall jet at an adiabatic wall

The maxima of the velocity and the temperature on the jet axis and the width of the jet are found to be

$$\begin{aligned}
 u_{\max} &= 2f'(0) \left(\frac{\dot{Q}_b^2 \beta^2 g^2 x}{\varrho^2 c_p^2 \nu} \right)^{1/5}, \\
 T_{\max} - T_{\infty} &= \vartheta(0) \left(\frac{\dot{Q}_b^4}{\varrho^4 c_p^4 g \beta \nu^2 x^3} \right)^{1/5}, \\
 \delta &\sim \left(\frac{\varrho c_p \nu^3 x^2}{\dot{Q}_b \beta g} \right)^{1/5}.
 \end{aligned} \tag{10.152}$$

The factors $2f'(0)$ and $\vartheta(0)$ are still dependent on the Prandtl number. For $\text{Pr} = 0.7$ we obtain $f'(0) = 0.404$, $\vartheta(0) = 0.373$. Numerical values for other Prandtl numbers are found in K. Gersten; H. Herwig (1992), p. 214, cf. K. Gersten et al. (1980). Simple closed solutions can be given for $\text{Pr} = 2$ and $\text{Pr} = 5/9$, cf. Y. Jaluria (1980), p. 107.

The buoyant jet flow arises in all (direct) natural convection flows at some distance above the hot body. It is comparable with the wake flow in forced convection. Here the value \dot{Q} corresponds to the total thermal energy emitted by the body per unit time.

Buoyant wall jet

The flow sketched in Fig. 10.14b occurs along a vertical wall if an energy source is arranged at the leading edge of the wall. This flow also yields similar solutions. The thermal boundary conditions at the wall of either the adiabatic wall ($q_w = 0$) or the wall with heat transfer ($T_w - T_\infty \sim x^{-3/5}$) may be considered, cf. N. Afzal (1980). In the first case, the adiabatic wall temperature is of interest; in the second case, the heat transfer. The same differential equations as in the buoyant jet are found, but with different boundary conditions at the wall. Results for $\text{Pr} = 0.72$ and $\text{Pr} = 6.7$ can be found in the work of N. Afzal (1980); for large Prandtl numbers in H.S. Takhar; M.H. Whitelaw (1976).

10.5.5 General Solutions

For general body shapes, a system of partial differential equations must be solved to compute the natural convection flow. Here either the system (10.121), or else the transformed system (10.134), (10.135) for $T_w = \text{const}$ or (10.141), (10.142) for any distribution $T_w(x)$ is used as a basis.

Integral methods have also been developed for natural convection flows. They again use equations obtained from the integration of Eqs. (10.115) to (10.117) over the thickness of the boundary layer as follows ($v_w = 0$):

$$\frac{d}{dx} \int_0^\infty u \, dy = -v_\infty, \quad (10.153)$$

$$\frac{d}{dx} \int_0^\infty u^2 \, dy = -\frac{\tau_w}{\varrho_\infty} + g\beta_\infty \int_0^\infty (T - T_\infty) \, dy \sin \alpha, \quad (10.154)$$

$$\frac{d}{dx} \int_0^\infty (T - T_\infty) u \, dy = \frac{q_w}{\varrho_\infty c_{p\infty}}. \quad (10.155)$$

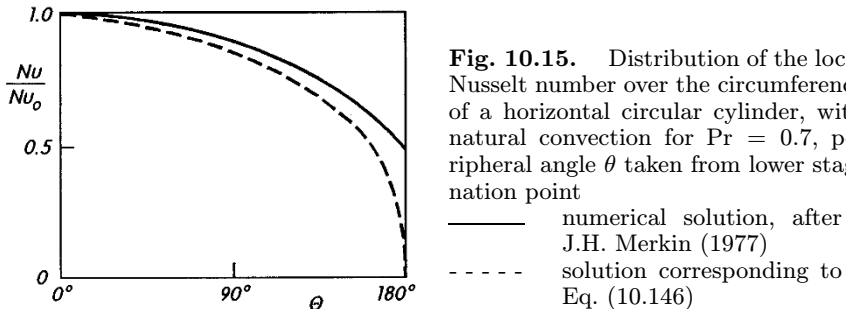
Details of integral methods for natural convection flows are to be found in A.J. Ede (1967) and Y. Jaluria (1980), p. 73.

Example: Horizontal cylinder.

The natural convection flow at a horizontal cylinder with constant wall temperature has been computed numerically by, among others, J.H. Merkin (1977). The distribution of the Nusselt number around the circumference for the Prandtl number $\text{Pr} = 0.7$ is shown in Fig. 10.15. For comparison, the solution according to the asymptotic approximation corresponding to Eq. (10.146) has also been depicted. Although this is valid for the case $\text{Pr} \rightarrow \infty$, it also yields good results for $\text{Pr} = 0.7$.

Integrating the Nusselt number over the circumference yields the average Nusselt number Nu_m . The numerical solution for $\text{Pr} = 0.7$ delivers $\text{Nu}_m \text{Gr}^{-1/4} = 0.372$, with the diameter d of the circular cylinder used as a reference length.

Measurements by K. Jodlbauer (1933) with air ($\text{Pr} = 0.72$; $5 \cdot 10^3 < \text{Gr} < 5 \cdot 10^6$) yield the numerical value 0.395, and are therefore in satisfactory agreement with



the theory, considering the fact that the theory is valid for constant properties, cf. V.T. Morgan (1975).

Natural convection at horizontal elliptic cylinders has also been computed by J.H. Merkin (1977). For the same constant wall temperature and the same surface, the elliptic cylinder with major axis in the vertical direction yields a greater heat transfer than the circular cylinder.

Close to the upper "stagnation point", the solution breaks down, since there it yields finite velocities parallel to the surface, impossible for reasons of symmetry. In reality, the boundary layer separates from the circular cylinder before its highest point and eventually becomes a buoyant jet. Separation in natural convection is, however, a higher order effect, and will be looked into in Chap. 14.

Further examples

The natural convection flow at a vertical plate has been computed for a linear temperature distribution by A. Aziz; T.Y. Na (1984), p. 153 and for a temperature distribution with the form of a ramp function (first linear and then constant) by T. Cebeci; P. Bradshaw (1984), p. 273.

10.5.6 Variable Physical Properties

The natural convection flows treated up until now only occur because the density is temperature dependent. Thus we have been looking at flows with *one* variable property. It was sufficient, within the framework of the Boussinesq approximation, to consider only a linear dependence of the density on the temperature in the buoyancy term.

In this section we will take into account the nonlinear density effects neglected until now, as well as the effect of the temperature dependence of all other physical properties of the fluid. To do this we use the perturbation calculation described in Sect. 10.3.1. This gives the result in the form of the property ratio method, cf. Sect. 10.3.2. If $c_{fc.p.}$, $\text{Nu}_{c.p.}$ and $T_{w c.p.}$ denote results within the framework of the Boussinesq approximation, the correction ratios needed for the different property effects read:

$$\frac{c_f}{c_{fc.p.}} = \left(\frac{\text{Pr}_w}{\text{Pr}_\infty} \right)^{m_{\text{Pr}}} \left(\frac{\varrho_w \beta_\infty}{\varrho_\infty \beta_w} \right)^{m_{\varrho\beta}} \left(\frac{\varrho_w \lambda_w}{\varrho_\infty \lambda_\infty} \right)^{m_{\varrho\lambda}} \left(\frac{c_{pw}}{c_{p\infty}} \right)^{m_c}, \quad (10.156)$$

$T_w = \text{const}$:

$$\frac{\text{Nu}}{\text{Nu}_{\text{c.p.}}} = \left(\frac{\text{Pr}_w}{\text{Pr}_\infty} \right)^{n_{\text{Pr}}} \left(\frac{\varrho_w \beta_\infty}{\varrho_\infty \beta_w} \right)^{n_{\varrho\beta}} \left(\frac{\varrho_w \lambda_w}{\varrho_\infty \lambda_\infty} \right)^{n_{\varrho\lambda}} \left(\frac{c_{pw}}{c_{p\infty}} \right)^{n_c}, \quad (10.157)$$

$q_w = \text{const}$:

$$\frac{T_w - T_\infty}{(T_w - T_\infty)_{\text{c.p.}}} = \left(\frac{\text{Pr}_w}{\text{Pr}_\infty} \right)^{k_{\text{Pr}}} \left(\frac{\varrho_w \beta_\infty}{\varrho_\infty \beta_w} \right)^{k_{\varrho\beta}} \left(\frac{\varrho_w \lambda_w}{\varrho_\infty \lambda_\infty} \right)^{k_{\varrho\lambda}} \left(\frac{c_{pw}}{c_{p\infty}} \right)^{k_c}. \quad (10.158)$$

In the case $q_w = \text{const}$, the physical properties with the index w are taken at the wall temperature obtained from the calculation with the Boussinesq approximation.

The exponents have been computed by H. Herwig et al. (1985) for the whole range of Prandtl numbers for plate flow and stagnation-point flow (both for $T_w = \text{const}$ and $q_w = \text{const}$). Here it was found that the exponents for these two flows differ only minimally from one another. From this it can be concluded that the relations (10.156) to (10.158) are good approximations locally, i.e. independently of x , and therefore can be applied to average values such as the Nusselt number Nu_m . H. Herwig (1984) has determined the averaged exponents, and they are reproduced in Table 10.4.

Table 10.4. Property ratio method for natural convection flows. Exponents in Eqs. (10.156) to (10.158), after H. Herwig (1984)

$T_w = \text{const}$
$m_{\text{Pr}} = 0.5 - 0.305(1 + 1.217\text{Pr}_\infty^{-0.605})^{-0.637}$
$m_{\varrho\beta} = -0.293; m_{\varrho\lambda} = 0.450; m_c = -0.368$
$n_{\text{Pr}} = -0.206(1 + 1.415\text{Pr}_\infty^{-0.7})^{-0.605}$
$n_{\varrho\beta} = -0.070; n_{\varrho\lambda} = 0.308; n_c = 0.202$
$q_w = \text{const}$
$m_{\text{Pr}} = 0.505 - 0.189(1 + 1.304\text{Pr}_\infty^{-0.566})^{-0.66}$
$m_{\varrho\beta} = -0.249; m_{\varrho\lambda} = 0.267; m_c = -0.516$
$k_{\text{Pr}} = 0.163(1 + 1.360\text{Pr}_\infty^{-0.695})^{-0.599}$
$k_{\varrho\beta} = 0.054; k_{\varrho\lambda} = -0.244; k_c = -0.212$

Because of the mutual coupling of the velocity and temperature fields, all physical properties have an effect on the skin-friction coefficient. In addition, because of the nonlinear dependence of the density on the temperature, the coefficient of thermal expansion β now appears as an another “physical property”.

Example 1: Water and oils

Assumptions: $\varrho = \text{const}$, $\lambda = \text{const}$, $c_p = \text{const}$, $\mu(T)$, $\text{Pr}_\infty \rightarrow \infty$

1.1 $T_w = \text{const}$

$$\frac{\text{Nu}}{\text{Nu}_{c.p.}} = \frac{\text{Nu}_m}{\text{Nu}_{m.c.p.}} = \left(\frac{\mu_w}{\mu_\infty} \right)^{-0.21} = \left(\frac{\text{Pr}_w}{\text{Pr}_\infty} \right)^{-0.21}. \quad (10.159)$$

This corresponds to a reference temperature

$$T_r = T_\infty + j(T_w - T_\infty) \quad (10.160)$$

with $j = 0.21/0.5 = 0.42$.

Measurements by T. Fujii et al. (1970) at a vertical plate with water and oils ($\text{Pr} \geq 5$) have delivered exactly the exponent -0.21 .

Measurements by R.M. Fand et al. (1977) at a horizontal cylinder have yielded the exponent -0.25 , corresponding exactly to the exponent n_{Pr} from Table 10.4 for $\text{Pr}_\infty = 7.0$.

1.2 $q_w = \text{const}$

$$\frac{T_w - T_\infty}{(T_w - T_\infty)_{c.p.}} = \left(\frac{\mu_w}{\mu_\infty} \right)^{0.16} = \left(\frac{\text{Pr}_w}{\text{Pr}_\infty} \right)^{0.16} \quad (10.161)$$

or $j = 0.32$, if, in Eq. (10.160), we again use T_w from the calculation with the Boussinesq approximation. Measurements by T. Fujii et al. (1970) produced the value 0.17 for the exponent at the vertical plate.

Example 2: Air, $\text{Pr} = 0.7$, $T_w = \text{const}$

Assumptions: $\varrho \sim T^{-1}$, $\beta \sim T^{-1}$, $\mu \sim T^{0.76}$, $\lambda \sim T^{0.76}$, $c_p = \text{const}$

$$\frac{\text{Nu}}{\text{Nu}_{c.p.}} = \frac{\text{Nu}_m}{\text{Nu}_{m.c.p.}} = \left(\frac{T_w}{T_\infty} \right)^{-0.074}, \quad (10.162)$$

$$j = -0.074/(0.76/2 - 0.75) = 0.62.$$

This is in perfect agreement with the results of E.M. Sparrow; J.L. Gregg (1958) for the vertical plate.

Comparing with the calculations at the horizontal circular cylinder where the correct property laws were used, it follows that Eq. (10.162) for $T_w/T_\infty \leq 1.4$ yields results whose errors are less than 1%, cf. H. Herwig et al. (1985).

10.5.7 Effect of Dissipation

In treating natural convection flows until now, we have neglected the effect of dissipation. In this section we will now examine to what extent this is justified. For simplicity, this will be done by considering the example of the vertical plate with $T_w = \text{const}$. If we also take the dissipation term into account, the thermal energy equation after the boundary-layer transformation (10.120) reads

$$u^* \frac{\partial \vartheta}{\partial x^*} + \bar{v} \frac{\partial \vartheta}{\partial y} = \frac{1}{\text{Pr}_\infty} \frac{\partial^2 \vartheta}{\partial y^2} + \frac{g \beta_\infty l}{c_{p\infty}} \left(\frac{\partial u^*}{\partial y} \right)^2. \quad (10.163)$$

Here a new dimensionless characteristic number $g\beta_\infty l/c_{p\infty}$ appears. Along with the Prandtl number, this additional parameter also affects the solution. According to Table 3.1, this characteristic number has, at 20°C and 1 bar, the values $8 \cdot 10^{-6} l/m$ for water and $3.3 \cdot 10^{-5} l/m$ for air. This shows us that the effect of dissipation can normally be neglected. Because of the transition to turbulent flow, the length l can also not be arbitrarily large, and so the effect of dissipation is only noticeable for gases at extremely low temperatures ($\beta_\infty \sim 1/T_\infty \rightarrow \infty$). The solutions of the equations for the vertical plate when the dissipation is taken into account have been determined by B. Gebhart (1962).

10.6 Indirect Natural Convection

The natural convection flows considered up until now were not able to take place for $\alpha = 0^\circ$ since the buoyancy term then vanishes. However a natural convection flow can indeed occur at $\alpha = 0^\circ$, and this will be described in what follows. Since this comes about in an indirect manner by way of an induced pressure gradient, we differentiate between this and the (direct) natural convection treated until now, and call it *indirect natural convection*.

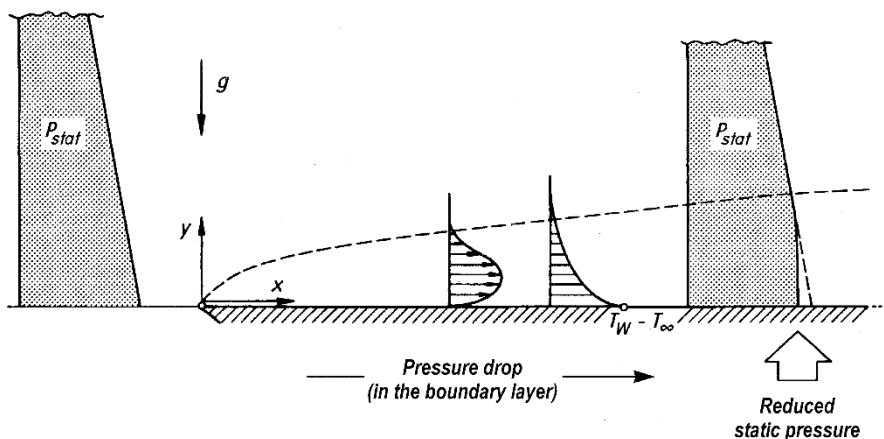


Fig. 10.16. Indirect natural convection. Formation of a pressure gradient $\partial p/\partial x$ in the boundary layer via reduced static pressure above the hot plate

The physical mechanism is depicted in Fig. 10.16. In a fluid whose density decreases with increasing temperature, a boundary-layer flow forms at a horizontal hot plate, as shown in Fig. 10.16. In front of the plate, the temperature is everywhere T_∞ , so that, as in the static field, there is a pressure distribution with the gradient $\partial p/\partial y = \rho_\infty g$. Above the plate, the temperature in

the boundary-layer region is larger than T_∞ and so the density is lower than ϱ_∞ . The decreased pressure gradient $|\partial p/\partial y| = \varrho g < \varrho_\infty g$ leads to a reduced pressure in the boundary-layer region. Hence there is a *pressure drop in the x direction*. This *induced pressure gradient* in the x direction is the origin of the flow parallel to the plate. Just as in the case of direct natural convection, this has a boundary-layer character at high Grashof numbers. It was first shown by K. Stewartson (1958) that such an indirect natural convection flow exists on the upper side of a horizontal flat plate with $T_w > T_\infty$.

Of course, since the pressure gradient $\partial p/\partial y \neq 0$ is of considerable importance for the formation of these flows, the boundary-layer equations (10.4) to (10.6) are no longer sufficient for their description.

If we apply the *boundary-layer transformation*

$$\bar{y} = \frac{y}{l} \text{Gr}^{1/5}, \quad \bar{v} = \frac{v}{V_{IN}} \text{Gr}^{1/5} \quad (10.164)$$

with

$$V_{IN} = (gl^{1/2}\nu^{1/2}\beta_\infty\Delta T)^{2/5}, \quad (10.165)$$

to the complete Navier-Stokes equations (for $\alpha = 0^\circ$), taking the Boussinesq approximation as well as the energy equation into account, we then obtain the boundary-layer equations which can describe indirect natural convection. In dimensional form they read

$$\frac{\partial u}{\partial x} + \frac{\partial v}{\partial y} = 0, \quad (10.166)$$

$$u \frac{\partial u}{\partial x} + v \frac{\partial u}{\partial y} = -\frac{1}{\varrho_\infty} \frac{\partial p}{\partial x} + \nu_\infty \frac{\partial^2 u}{\partial y^2}, \quad (10.167)$$

$$0 = -\frac{1}{\varrho_\infty} \frac{\partial p}{\partial y} + g\beta_\infty(T - T_\infty), \quad (10.168)$$

$$u \frac{\partial T}{\partial x} + v \frac{\partial T}{\partial y} = a_\infty \frac{\partial^2 T}{\partial y^2}. \quad (10.169)$$

The Grashof number is given by Eq. (10.118). In addition, either $\Delta T = T_w - T_\infty$ or Eq. (10.127) is valid.

The powers in Eq. (10.164) were so chosen that the following remain the same after the transformation in the limit $\text{Gr} \rightarrow \infty$: the continuity equation, a friction term in the x momentum equation as well as the pressure and buoyancy terms in the y momentum equations.

Here the velocity field is again dependent on the temperature field. The coupling takes place via the pressure p , which is coupled to the temperature in the y momentum equation.

K. Stewartson (1958) has shown that the system (10.166) to (10.169) leads to similar solutions for the flow above a hot plate ($T_w - T_\infty = \Delta T > 0$). With the similarity transformation

$$\bar{y} = (x^*)^{2/5}\eta, \quad \bar{\psi} = (x^*)^{3/5}f(\eta), \quad \bar{p} = (x^*)^{2/5}g(\eta) \quad (10.170)$$

we obtain

$$\begin{aligned} f''' + \frac{3}{5}ff'' - \frac{1}{5}f'^2 &= \frac{2}{5}(g - \eta g') \\ g' &= \vartheta \\ \vartheta'' + \frac{3}{5}\text{Pr}_\infty f\vartheta' &= 0 \end{aligned} \quad (10.171)$$

with the boundary conditions

$$\begin{aligned} \eta = 0 : \quad f = 0, \quad f' = 0, \quad \vartheta = 1 \\ \eta \rightarrow \infty : \quad f' = 0, \quad \vartheta = 0. \end{aligned} \quad (10.172)$$

The Prandtl number is the only parameter. For $\text{Pr}_\infty = 0.72$ we find $f_w'' = 0.9787$ and $\vartheta'_w = -0.3574$, cf. W.N. Gill et al. (1965). (Unfortunately, the numerical result in K. Stewartson (1958) is incorrect). We find for the heat transfer

$$\text{Nu} = \frac{q_w l}{\lambda_\infty(T_w - T_\infty)} = 0.357 \left(\frac{x}{l} \right)^{-2/5} \text{Gr}^{1/5} \quad (\text{Pr} = 0.72). \quad (10.173)$$

Approximate formulae for arbitrary Prandtl numbers have been given by G. Wickern (1987). The solutions for the limiting cases $\text{Pr} \rightarrow 0$ and $\text{Pr} \rightarrow \infty$ can also be found in this work.

The wall temperature distributions also yield similar solutions for arbitrary power laws. The case $T_w - T_\infty \sim x^{1/3}$ corresponds to constant q_w . Again solutions may be found in G. Wickern (1987). Instead of Gr from Eq. (10.118), Gr_q from Eq. (10.129) is again used, where the relation (10.130) exists between the two characteristic numbers.

The self-similar solution by K. Stewartson (1958) is valid near the leading edge. The flow further downstream leads to flow separation. It is worth mentioning that no singularity appears at the separation point. The separation procedure is completely different from that of forced convection and is connected with the appearance of longitudinal vortices, see L. Pera; B. Gebhard (1973).

Note (Free indirect natural convection flow)

Suppose there is an equivalent flow underneath the flat plate in Fig. 10.16 with $T_\infty - \Delta T$ as the wall temperature at the lower side and suppose the flat plate has a finite length, then a horizontal free jet with an antisymmetric temperature profile develops past the trailing edge of the plate. V. Noshadi;

W. Schneider (1999) have shown that the far field of this jet leads to similar solutions of Eqs. (10.166) to (10.169) for $0.5 < \text{Pr} \leq 1.47$. The analogous axisymmetric case was also treated. Here solutions exist for $\text{Pr} > 1$.

10.7 Mixed Convection

By *mixed convection* we imply *forced convection* where buoyancy forces also exist and thus additional effects occur, such as those known from *natural* (direct and indirect) *convection*. This is therefore a combination of forced and natural convection. The Boussinesq approximation is again taken as the basis of the buoyancy terms.

Since the boundary-layer transformations for forced and natural convection are different, cf. Eqs. (10.1), (10.120) and (10.164), it is in principle impossible to find a boundary-layer transformation such that the resulting boundary-layer equations are independent of the viscosity, i.e. independent of the Reynolds number or the Grashof number, while still describing the effects of indirect natural convection. If we use the boundary-layer transformation in Eq. (10.1), in the limiting case $\text{Re} \rightarrow \infty$ we obtain the following dimensionless system ($\text{Ec} = 0$):

$$\frac{\partial u^*}{\partial x^*} + \frac{\partial \bar{v}}{\partial \bar{y}} = 0, \quad (10.174)$$

$$u^* \frac{\partial u^*}{\partial x^*} + \bar{v} \frac{\partial u^*}{\partial \bar{y}} = - \frac{\partial p^*}{\partial x^*} + \frac{\partial^2 u^*}{\partial \bar{y}^2} + \vartheta P_I \sin \alpha, \quad (10.175)$$

$$0 = - \frac{\partial p^*}{\partial \bar{y}} + \vartheta P_{II} \cos \alpha, \quad (10.176)$$

$$u^* \frac{\partial \vartheta}{\partial x^*} + \bar{v} \frac{\partial \vartheta}{\partial \bar{y}} = \frac{1}{\text{Pr}_\infty} \frac{\partial^2 \vartheta}{\partial \bar{y}^2}. \quad (10.177)$$

Here we set

$$P_I = \frac{\text{Gr}}{\text{Re}^2} = \frac{gl\beta_\infty \Delta T}{V^2}, \quad P_{II} = \frac{\text{Gr}}{\text{Re}^{5/2}} = \frac{gl^{1/2}\nu^{1/2}\beta_\infty \Delta T}{V^{5/2}}. \quad (10.178)$$

We will now differentiate between the following two cases in the limit $\text{Re} \rightarrow \infty$:

1. without indirect natural convection:

$\text{Gr} \sim \text{Re}^2$, therefore $P_{II} \rightarrow 0$ for $\text{Re} \rightarrow \infty$, and the y momentum equation reduces to $\partial p^*/\partial \bar{y} = 0$.

2. with indirect natural convection:

$\text{Gr} \sim \text{Re}^{5/2}$; the product $P_I \sin \alpha$ must remain finite, i.e. we have $\sin \alpha \approx \alpha \sim \text{Re}^{-1/2}$. The angle α therefore tends to zero with increasing Reynolds number.

The two parameters P_I and P_{II} describe the ratio of the different effects:

$$P_I = \left(\frac{V_{DN}}{V} \right)^2 \sim \frac{\text{direct natural convection}}{\text{forced convection}}$$

$P_I \rightarrow 0$: forced convection

$P_I \rightarrow \infty$: pure direct natural convection,

$$P_{II} = \left(\frac{V_{IN}}{V} \right)^{5/2} \sim \frac{\text{indirect natural convection}}{\text{forced convection}}$$

$P_{II} \rightarrow 0$: forced convection

$P_{II} \rightarrow \infty$: pure indirect natural convection.

Example: Mixed convection at an arbitrarily tilted flat plate

The boundary-layer equations (10.174) to (10.177) will now be applied to a flat plate tilted at an arbitrary angle ($0 \leq \alpha < 2\pi$). The aim is to collect together all possible boundary-layer solutions into a whole which includes all special cases (e.g. pure forced convection or pure natural convection). What follows is based essentially on very comprehensive studies by G. Wickern (1987, 1991a, 1991b), in which the momentum and heat transfer for the two thermal boundary conditions $T_w = \text{const}$ and $q_w = \text{const}$ were computed, and where concrete numerical results are given for $\text{Pr} = 0.72$.

Since the three effects involved can both “support” each other and “act against” each other, *separated flows* can occur in different situations, where the approach to the point of vanishing wall shear stress can be either *singular* or *regular*. This means that, in the general solution field spanned by P_I and P_{II} , not all parameter combinations lead to solutions within the framework of the boundary-layer theory presented here. Figure 10.17 shows the region of possible boundary-layer solutions for the thermal boundary condition $T_w = \text{const}$.

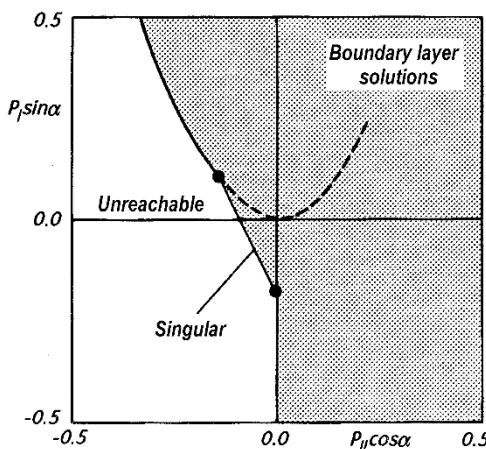


Fig. 10.17. Region of possible boundary-layer solutions for a flat plate at arbitrary angle (thermal boundary condition $T_w = \text{const}$)

Although the flows with only one of the three effects involved will always have a self-similar character (and therefore mathematically will lead to ordinary differential equations), partial differential equations will have to be solved as soon as at least two effects occur together. The physical explanation of this is that the three effects act differently with respect to the length l , and any combination means that a characteristic length is introduced into the problem (e.g. the length from the leading edge to the separation position).

If we interpret the reference velocity for the different effects as a measure of their “strength”, the dependencies on the length l are as follows:

1. pure forced convection: $V \sim (l)^0$
2. pure indirect natural convection: $V_{IN} \sim (l)^{1/5}$
3. pure direct natural convection: $V_{DN} \sim (l)^{1/2}$

This list makes it clear that, if all three effects are present, pure forced convection always dominates for $l \rightarrow 0$, while direct natural convection dominates for $l \rightarrow \infty$. This can be easily understood physically, since close to the leading edge of the plate ($l \rightarrow 0$) there is not yet enough thermal energy supplied to allow any appreciable natural convection effects. On the other hand, the effects of direct natural convection grow with increasing supplied thermal energy ($l \rightarrow \infty$) without limit, and indeed do so more strongly than the effects of indirect natural convection.

If all three effects are present, a calculation must always commence at the leading edge ($x = 0$) with the Blasius solution for forced convection as an initial condition.

Figure 10.18, with axes $P_I \sin \alpha$ and $P_{II} \cos \alpha$, shows all solutions for the Prandtl number $\text{Pr} = 0.72$ in one diagram. One can easily convince oneself that positive values of $P_I \sin \alpha$ or $P_{II} \cos \alpha$ mean that the forced convection is supported by the corresponding natural convection effect, while negative values mean a physical counteraction of effects, with the consequence that separation is “favoured”.

If we imagine a situation where g , β_∞ , ΔT , α , ν and V are all given fixed quantities, the only free variable in P_I and P_{II} is the length l . Different values of l then describe the desired solution at different distances from the leading edge, so that the length l in this interpretation could be replaced by a coordinate x . In this situation imagined here there is then of course a coupling between the parameters. Since $P_I \sim l$ and $P_{II} \sim l^{1/2}$, all solution points at increasing distances from the leading edge (at fixed g , β_∞ , ΔT , α , ν and V) lie on the curve

$$P_I \sin \alpha = C(P_{II} \cos \alpha)^2, \quad (10.179)$$

therefore on a parabola. The constant C in Figs. 10.17 and 10.18 follows as

$$C = -\frac{U^3 \sin \alpha}{g \beta_\infty \Delta T \nu^2 \cos^2 \alpha} = \frac{\text{Re}^3}{\text{Gr}} \frac{\sin \alpha}{\cos^2 \alpha}. \quad (10.180)$$

The lines contained in Fig. 10.18 allow us to read off the values of $c_f \text{Re}^{1/2}(x/l)^{1/2}$ and $\text{Nu} \text{Re}^{-1/2}(x/l)^{1/2}$ for the case $T_w = \text{const}$ and $\text{Pr} = 0.72$. In the origin of the diagram lies the Blasius plate solutions with $c_f \text{Re}^{1/2}(x/l)^{1/2} = 0.664$ and $\text{Nu} \text{Re}^{-1/2}(x/l)^{1/2} = 0.293$, (cf. Sects. 6.5 and 9.4).

The flows in the different quadrants of the diagram have physically very different characters, and will now be described individually.

Quadrant 1: $P_I \sin \alpha > 0$, $P_{II} \cos \alpha > 0$

In these cases the basic flow of forced convection is accelerated by both types of natural convection. For all solutions in this quadrant, both the skin-friction coefficient c_f and the Nusselt number Nu increase monotonically with the length l .

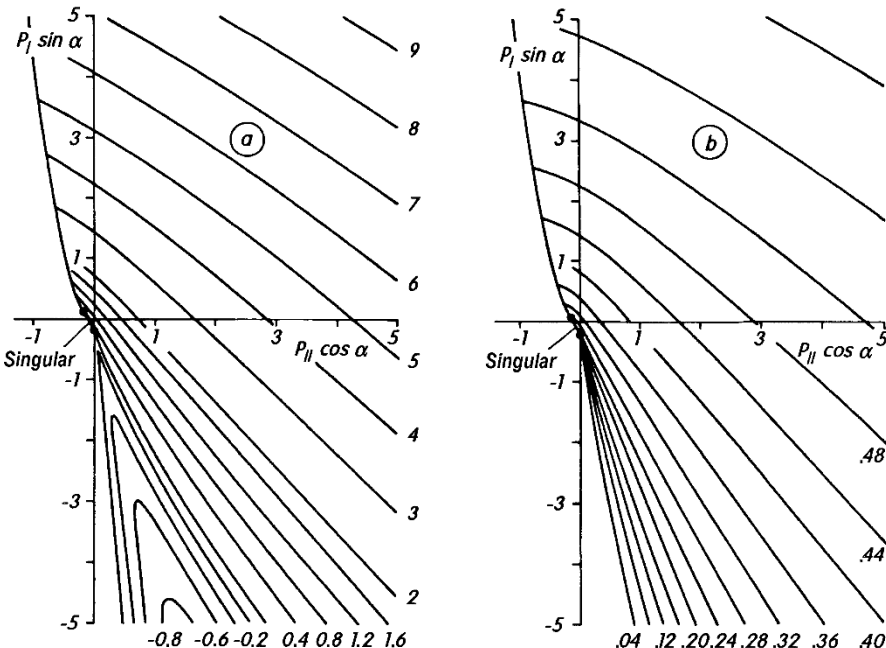


Fig. 10.18. Mixed convection at a tilted flat plate, diagram for $T_w = \text{const}$, $\text{Pr} = 0.72$, after G. Wickern (1987, 1991b)

- (a) lines $c_f \sqrt{\text{Re}_x} = \text{const}$
- (b) lines $\text{Nu}_x / \sqrt{\text{Re}_x} = \text{const}$

Quadrant 2: $P_I \sin \alpha > 0, P_{II} \cos \alpha < 0$

In this quadrant the flow situation is much more complicated. The basic flow is initially decelerated by the indirect natural convection ($P_{II} \cos \alpha < 0$), but is re-accelerated by the direct natural convection ($P_I \sin \alpha > 0$). There is a limiting case, reached precisely on the point of the plate where the wall shear stress satisfies $\tau_w = 0$. For greater lengths l , however, there are again values of $\tau_w > 0$. This case takes place for $C_{\text{crit}} = 4.4366$ and represents a limiting parabola in quadrant 2. Calculations for $C < C_{\text{crit}}$ lead to flatter parabolas, which physically correspond to more strongly acting indirect natural convection, and hence represent cases with separation. As the separation point is approached, the boundary-layer solutions demonstrate singular behaviour and therefore cannot be continued on further. This limit is given in the diagrams by the line marked "singular".

Quadrant 3: $P_I \sin \alpha < 0, P_{II} \cos \alpha < 0$

Both types of natural convection decelerate the forced basic flow, so that separation necessarily occurs with increasing length l . Since singular behaviour is also present here, all calculations corresponding to parabolas along the line "singular" cannot be carried any further. This "singular line" ends precisely on the vertical axis ($\alpha = 90^\circ$).

Quadrant 4: $P_1 \sin \alpha < 0, P_{11} \cos \alpha > 0$

In flows in this quadrant, the forced basic flow is accelerated by the indirect natural convection ($P_{11} \cos \alpha > 0$), but decelerated by the direct natural convection ($P_1 \sin \alpha < 0$). Because of the ideas discussed above, this latter effect always dominates for large lengths l , so that every flow in this quadrant necessarily separates. In contrast to quadrants 2 and 3, the solution at the separation point is completely regular, and therefore can be carried out beyond the point $\tau_w = 0$ within the framework of the boundary-layer approximations. Figure 10.18a therefore also contains results for negative c_f values.

For details of the solutions, as well as for results when $q_w = \text{const}$, which qualitatively correspond to those for $T_w = \text{const}$, refer to the original work by G. Wickern (1987).

Note 1 (“Singular” solutions)

Investigations at the cool horizontal plate ($T_w - T_\infty = \Delta T < 0, P_{11} < 0, \alpha = 0^\circ$) by W. Schneider; M.G. Wasel (1985), W. Schneider et al. (1994) and H. Steinrück (1994) have shown that in this case the boundary-layer equations do not have a unique solution. For this reason, the numerical results of G. Wickern (1987, 1991a) for the “singular” solutions in quadrant 2 with $C < C_{\text{crit}}$ and in quadrant 3 must be treated with caution, cf. also W. Schneider (1991, 1995, 2001). As P.-Y. Lagrée (2001) has shown, the flow can be described without the breakdown of the boundary-layer equations by using the triple-deck concept, see Sect. 14.4.

Note 2 (Heated horizontal flat plate of finite length)

The fluid flow at a heated horizontal flat plate of finite length is quite different at the lower side as compared with the upper side. At the lower side the stratification is stable, because the density increases in upward direction. The removing of the heated fluid takes place quite slowly in the flow over the side edges of the plate. A boundary layer starts developing at the middle of lower plate and is symmetrical with respect to this point. The thickness of the boundary layer at this central point depends on the boundary layer development around the side edges, which means, that there exists an effect on the flow from the upstream area, see T. Schulenberg (1984).

Further solutions

Forced and indirect natural convection

It has been shown by W. Schneider (1979) that mixed convection at a horizontal plate leads to similar solutions when $T_w(x) - T_\infty = \Delta T \sim 1/\sqrt{x}$. The solutions for the hot plate ($\Delta T > 0$) are unique. In the case of the cool plate, initially two similar solutions appear. If the parameter

$$K = g\beta_\infty \Delta T (x\nu)^{1/2} V^{-5/2}$$

falls short of a critical value dependent on the Prandtl number, the solutions no longer exist. A remarkable feature of these similar solutions is that the entire heat transfer is concentrated at the (singular) leading edge, while the rest of the plate is adiabatic. H. Steinrück (1995) has demonstrated that for $K < 0$, apart from the two similar solutions, infinitely many non-similar solutions exist. These represent a relation between the two similar solutions in

the sense that they coincide with one of the similar solutions at the leading edge and downstream eventually turn into the other similar solution. A suitable stability condition can be used to enforce the uniqueness of the solution, cf. also W. Schneider (1995) and V. Noshadi; W. Schneider (1998).

S. Schilawa (1981) has investigated the buoyancy effects in laminar wall jets at horizontal walls. Here it was differentiated between the cases “heated wall jet” and “hot wall jet” according to whether the jet has the surrounding temperature or a temperature different from the surrounding temperature. In both cases, the buoyancy increases the wall shear stress. The heat transfer increases due to the buoyancy forces in the case of the heated wall jet; in the case of the hot wall jet it decreases.

The “cooled wall jet” and the “cool wall jet” have been investigated by F.J. Higuera (1997). In these cases the buoyancy reduces the wall shear stress and leads finally to flow separation. Therefore, an interactive boundary-layer theory must be applied for these flows, as it is mentioned at the end of Sect. 14.2.

Horizontal boundary layers with stable temperature stratification have been investigated by P.G. Daniels; R.J. Gargaro (1993).

The mixed convection at the horizontal flat plate of finite length has been studied by W. Schneider (2000, 2005) for large Peclet numbers and small buoyancy effects. The plate was aligned to the flow. The hydrostatic pressure jump over the plate wake induces a potential flow, which leads to a lateral force (against the thermal lift) and to a suction force (against the drag force). An analogous solution exists also for turbulent flows at high Reynolds numbers. An extension of these studies in a channel of finite width has been presented by M. Müllner; W. Schneider (2010).

Forced and direct natural convection

Wedge flows ($u_e \sim x^m$) in mixed convection have been investigated by E.M. Sparrow et al. (1959) and R.C. Gunness; B. Gebhart (1965). Similar solutions are obtained if the distribution of the wall temperature is proportional to x^{2m-1} . For the stagnation-point flow, this means a linear temperature distribution at the wall, cf. K. Gersten; J. Steinheuer (1967).

As in the case of mixed convection at a plate, backflow can occur if the forced convection and the direct natural convection act against one another.

The (vertical) free jet with buoyancy forces has been considered by S.B. Savage; G.K.C. Chan (1970) and K. Gersten et al. (1980). The free jet starts off initially as a pure “momentum jet” (i.e. no buoyancy effects), and then eventually becomes a pure buoyant jet. In the last work above, the flow is treated using an integral method, in which the start of the jet may lie at any arbitrary angle to the vertical.

The vertical free jet with buoyancy can also start off without initial momentum. This is then the solution for a “fire line”, cf. K. Gersten et al. (1980).

The mixed convection in far wakes above heated or cooled bodies has been considered by P. Ehrhard (2001).

The mixed convection at horizontal cylinders is important for hot-wire technology, cf. Y. Jaluria (1980), p. 151 and V.T. Morgan (1975).

11. Boundary-Layer Control (Suction/Blowing)

11.1 Different Kinds of Boundary-Layer Control

It emerges from the previous discussions of boundary-layer flows that the boundary conditions, i.e. the distributions of the outer velocities $U(x)$ or $u_e(x)$ and the wall temperature $T_w(x)$ or the wall heat flux $q_w(x)$, determine the behaviour of the boundary layer. For example, it turned out that the position of the separation point was quite dependent on how much the velocity of the outer flow was decelerated. Furthermore, in the last chapter we showed that, for temperature dependent physical properties, cooling and heating affected the position of the separation point.

As well as these “natural” ways of controlling the boundary layer through the usual boundary conditions, different methods have also been developed to bring about certain types of behaviour in the boundary layer through *artificial* means. The different measures are as follows:

1. Motion of the solid wall. One optimal method of avoiding separation would be to completely prevent the formation of a boundary layer. Since the boundary layer owes its existence to the velocity difference between the wall and the outer flow (no-slip condition), it could be eliminated altogether by ensuring that the velocity difference is removed. This can be achieved by moving the wall along with the flow.

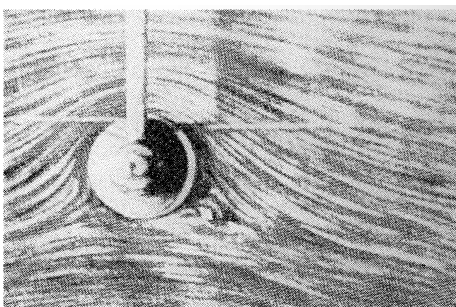


Fig. 11.1. Flow past a rotating circular cylinder

A moving wall can be most simply realised in the rotation of a circular cylinder in a flow. Figure 11.1 shows the flow portrait at a rotating circular cylinder where the flow is perpendicular to its axis. On the upper side where the direction of flow and the direction of rotation are the same, the separation of the boundary layer is completely avoided. The flow field is unsymmetric. The inviscid outer flow corresponds to the cylinder flow with circulation. This flow produces a *transverse force* known as the *Magnus effect*. This effect occurs when a tennis ball is sliced.

There have also been attempts to exploit the transverse force from rotating cylinders in a practical manner to drive ships, cf. the description of the *Flettner rotor* by J. Ackeret (1925).

For other body shapes it is technically difficult to realise this principle, with the result that this method has found little use in practical applications. However the effect of a moving wall at an airfoil has been experimentally investigated in detail by A. Favre (1938). To this end, a wall was set in motion on the upper side of the airfoil in the form of an endless belt moving over two rollers, ensuring that the backwards motion of the tape took place in the interior of the airfoil. This arrangement proved to be very effective, and maximum lift coefficients of about $c_L = 3.5$ were achieved for large angles of attack (about $\alpha = 55^\circ$).

The following investigations into flows with moving walls are also worth mentioning:

- a) The flow past a flat plate where the wall moves as an endless belt has been investigated by J. Siekmann (1962) and J. Steinheuer (1968a). This again yields similar solutions, which even exist when the flow direction is opposite to that of the motion of the wall, up to a velocity $|U_w| < 0.354U_\infty$.
- b) The boundary layer on a flat plate at zero incidence where the part at the back is moved along with the fluid has been investigated by E. Truckenbrodt (1952).
- c) If a body is moved close to the ground a steady flow arises, as seen from the coordinate system fixed to the body. At the ground, moving with the free stream velocity, a boundary layer appears close to the body. This has been considered by E. Beese (1984) and is of importance in, for example, the aerodynamics of motor vehicles.
- d) The usual separation criterion $\tau_w = 0$ can no longer be used at moving walls. Instead the so-called MRS criterion is then valid, see F.K. Moore (1958), N. Rott (1955) and W.R. Sears (1956). According to this criterion, the separation point in the boundary layer appears at the position where $u = 0$ and $\partial u / \partial y = 0$ occur simultaneously. Figure 11.2 shows the flow at a separation point like this.

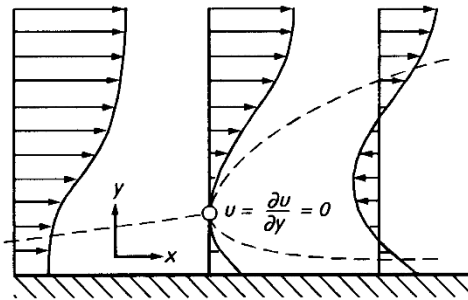


Fig. 11.2. Velocity profiles near the separation point in the boundary layer at a moving wall. MRS criterion: $u = 0$ and $\partial u / \partial y = 0$

2. Slit suction. It was already in the first piece of work by L. Prandtl (1904) on boundary layers that he artificially influenced the boundary layer in order to confirm his fundamental ideas. With this he achieved some quite surprising effects. Figure 11.3 shows the flow past a circular cylinder where suction is applied to one side through a narrow slit. The flow follows along the surface of the body where the suction is applied for a considerable distance thus preventing separation. The consequence of this is that the drag is greatly decreased. Simultaneously, because the flow is not symmetric, a transverse force is produced.

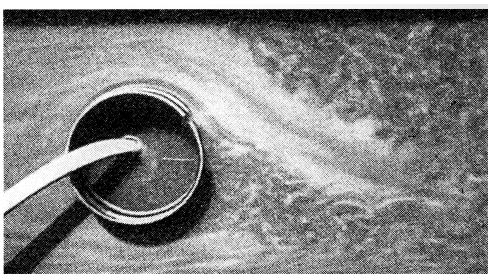


Fig. 11.3. Flow past a circular cylinder with single-sided suction of the boundary layer, after L. Prandtl (1904)

The application of slit suction to a strongly expanding diffuser has been demonstrated in Fig. 2.9. When suction was applied through two slits on each of the two sides, the separation of the flow was completely prevented, cf. Fig. 2.9c.

The effect of slit suction is essentially based on a change in the velocity distribution $U(x)$ of the outer flow. The usual distribution of the inviscid flow is superimposed on the velocity distribution of the sink flow coming from the practically point shaped sink at the suction slit. This accelerates the flow in front of the suction slit and thus prevents separation. Behind the slit, the sink indeed decelerates the outer flow, but now the boundary layer has to start off again from zero thickness, and can therefore withstand greater adverse pressure gradients without separation.

Slit suction was used often in the past in the development of airfoils to reduce the drag, cf. S. Goldstein (1948a), and to increase the lift, cf. O. Schrenk (1935), E.D. Poppleton (1955). However it must be mentioned that, in reducing the drag by suction, both the energy necessary for suction, as well as the so-called *sink drag* must be taken into account.

3. Tangential blowing and suction. A further way of preventing separation consists of supplying additional energy to the fluid elements which are low in energy in the boundary layer. This can be achieved by tangentially blowing higher velocity fluid out from inside the body, as sketched in Fig. 11.4a. The danger of separation is removed by the supply of kinetic energy to the boundary layer.

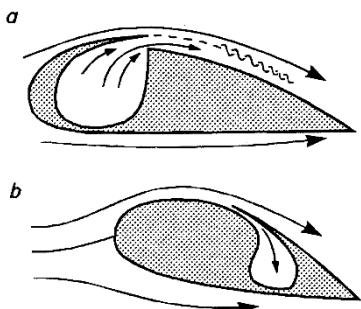


Fig. 11.4. Different ways of influencing the boundary layer
(a) blowing; (b) suction

The effectiveness of wing flaps can be greatly improved if fluid is tangentially blown out just in front of the flap, cf. F. Thomas (1962, 1963), H. Schlichting (1965b). If the intensity of the blown jet is high enough, even the lift predicted by potential theory can be surpassed. The so-called *jet flap effect* then causes *supercirculation*, cf. J. Williams (1958).

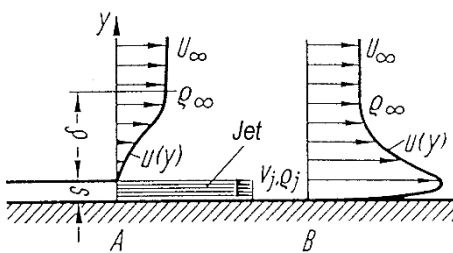


Fig. 11.5. Velocity distribution in the boundary layer directly behind the slit for tangential blowing

Directly behind the position of tangential blowing a wall jet profile forms in the boundary layer, see Fig. 11.5. This profile passes over to the velocity $U(x)$ at the outer edge of the boundary layer. As has already been mentioned in Sect. 7.2.2, such flows have been investigated by J. Steinheuer (1968b), see

also M.B. Glauert (1958) for a contribution by K. Stewartson on the manner in which such a wall jet dies away in constant pressure.

The separation of the boundary layer can also be prevented by *tangential suction*, see Fig. 11.4b. The low energy fluid in the boundary layer is removed by suction before it can separate. Behind the suction slit, a new boundary layer forms which can overcome a certain pressure increase. If the slit is arranged suitably, in certain circumstances the flow will not separate at all.

A so-called *boundary-layer diverter* is also based on the same principle. This is used in the entrance to the engine on the fuselage of an airplane. Here one also ensures that the fluid in the boundary layer which is low in energy does not succeed in entering the engine.

4. Continuous suction and blowing. If the wall is permeable and can therefore let the fluid through, the boundary layer can be controlled by continuous suction or blowing.

Separation can be prevented by suction since the low energy fluid in the boundary layer is removed.

In contrast, the wall shear stress and therefore the friction drag can be reduced by blowing. The most important application of blowing is in so-called *transpiration cooling*. If a different fluid is injected, a *binary boundary layer* occurs. As well as velocity and temperature fields, this boundary layer also has a concentration field.

The stability of the boundary layer and the transition to turbulence are also considerably influenced by continuous suction and blowing. Suction always stabilises the boundary layer, cf. the discussion in Chap. 15.

Because of their particular importance for boundary-layer theory, the next two sections are devoted to continuous suction and blowing. Comprehensive summaries of research in the area of boundary-layer control are to be found in the books by G.V. Lachmann (1961) and P.K. Chang (1976).

11.2 Continuous Suction and Blowing

11.2.1 Fundamentals

Up until now we have always implied that the wall is impermeable to the fluid, and this led to the kinematic boundary condition $v_w = 0$. In this chapter we will take the wall to be permeable, so that fluid can be sucked ($v_w < 0$) or blown ($v_w > 0$). In doing this however, the no-slip condition $u_w = 0$ at the (non-moving) wall shall continue to remain valid; for more on this problem see, for example, G.J. Hokenson (1985).

In deriving the boundary-layer equations in Sect. 6.1, it emerged that the v component of the velocity (relative to V) is a small quantity of the order of magnitude $O(1/\sqrt{Re})$. In what follows we will assume that the velocity v_w has this order of magnitude. The consequence of this is that the outer

flow is independent of v_w (higher order effects will be discussed in Chap. 14). The boundary-layer equations (6.7) to (6.9) remain unchanged, and it is the boundary condition at the wall which now differs. Instead of Eq. (6.16) we now have

$$\bar{y} = 0 : \quad u^* = 0, \quad \bar{v} = \bar{v}_w(x^*) \quad (11.1)$$

with

$$\bar{v}_w = \frac{v_w(x)}{V} \sqrt{\text{Re}}. \quad (11.2)$$

Therefore the boundary-layer equations for constant physical properties read (in dimensional form):

$$\frac{\partial u}{\partial x} + \frac{\partial v}{\partial y} = 0, \quad (11.3)$$

$$u \frac{\partial u}{\partial x} + v \frac{\partial u}{\partial y} = U \frac{dU}{dx} + \nu \frac{\partial^2 u}{\partial y^2}, \quad (11.4)$$

$$u \frac{\partial T}{\partial x} + v \frac{\partial T}{\partial y} = a \frac{\partial^2 T}{\partial y^2} + \frac{\nu}{c_p} \left(\frac{\partial u}{\partial y} \right)^2 \quad (11.5)$$

with the boundary conditions

$$y = 0 : \quad u = 0, \quad v = v_w(x), \quad T = T_w(x) \quad \text{or} \quad q = q_w(x) \quad (11.6)$$

$$y \rightarrow \infty : \quad u = U(x), \quad T = T_\infty.$$

Here the distributions $U(x)$, $v_w(x)$ and $T_w(x)$ or $q_w(x)$ are prescribed.

Suction or blowing causes a double effect with respect to the heat transfer. On the one hand, the temperature profile is influenced by the changed velocity field in the boundary layer, leading to a change in the heat conduction at the wall. On the other hand, convective heat transfer occurs at the wall along with the heat conduction for $v_w \neq 0$. In forming the Nusselt number for the heat transfer $\text{Nu} = q_w l / (\lambda \Delta T)$, it must be noted that q_w is only the conduction part $q_w = -\lambda(\partial T/\partial y)_w$ of the heat flux transferred to the wall, and not the entire heat flux (conduction q_w and convection $\rho c_p T_w v_w$). T_w always implies the temperature of the fluid at $y = 0$, where it is assumed, however, that this is equal to the wall temperature.

The compatibility condition at the wall (7.2) is now extended:

$$\mu \left(\frac{\partial^2 u}{\partial y^2} \right)_w = \frac{dp}{dx} + \frac{\tau_w}{\nu} v_w. \quad (11.7)$$

Furthermore, it follows from this that pressure increase is a necessary condition for separation ($\tau_w = 0$). (The limiting case $\tau_w = 0$, $dp/dx = 0$, $(\partial^2 u/\partial y^2)_w = 0$ will be discussed in Sect. 11.2.4.)

Likewise the integral relations acquire additional terms. The momentum–integral equation Eq. (7.100) reads

$$\frac{d}{dx}(U^2\delta_2) + \delta_1 U \frac{dU}{dx} - v_w U = \frac{\tau_w}{\rho}, \quad (11.8)$$

the energy–integral equation Eq. (7.104)

$$\frac{d}{dx}(U^3\delta_3) - v_w U^2 = \frac{2}{\rho} \int_0^\infty \tau \frac{\partial u}{\partial y} dy = \frac{2D}{\rho}. \quad (11.9)$$

The previous definitions of δ_1 , δ_2 , δ_3 and D (the dissipation integral) hold as before.

By integrating the continuity equation, we now obtain the extension of Eq. (6.35):

$$\lim_{y \rightarrow \infty} (v - V) = \frac{d(U\delta_1)}{dx} + v_w(x). \quad (11.10)$$

This relation shows us that, in principle, the displacement action of the boundary layer can be prevented by suction ($v_w < 0$).

11.2.2 Massive Suction ($v_w \rightarrow -\infty$)

The boundary layer becomes very thin if very strong continuous suction is applied. In order to describe this boundary layer we use, instead of y , the *stretched wall coordinate*

$$N = -\frac{v_w(x)y}{\nu}. \quad (11.11)$$

If we transform the boundary–layer equations (11.3) to (11.5) to the new coordinates x , N and take the limit $v_w \rightarrow -\infty$, we obtain a greatly simplified system (neglecting the dissipation):

$$\frac{\partial v}{\partial N} = 0, \quad (11.12)$$

$$\frac{\partial^2 u}{\partial N^2} + \frac{\partial u}{\partial N} = 0, \quad (11.13)$$

$$\frac{1}{Pr} \frac{\partial^2 T}{\partial N^2} + \frac{\partial T}{\partial N} = 0 \quad (11.14)$$

with the solutions

$$v = v_w(x) < 0, \quad (11.15)$$

$$u = U(x)[1 - \exp(v_w(x)y/\nu)], \quad (11.16)$$

$$T - T_\infty = (T_w - T_\infty) \exp(v_w(x)y/a). \quad (11.17)$$

The solutions are purely *local* solutions and do not depend on the history of the boundary layer. In this limiting case of *massive suction*, the universal distributions of the velocity and temperature are denoted *asymptotic suction profiles*.

For the wall shear stress we obtain

$$\tau_w(x) = \mu \left(\frac{\partial u}{\partial y} \right)_w = \varrho [-v_w(x)] U(x); \quad (11.18)$$

it is therefore independent of the viscosity (!). In spite of this, a “friction drag” can be formally determined from Eq. (6.39) or (6.40). Now, strictly this is not a friction drag, but rather is the so-called *sink drag* which every body in a flow where a certain mass is sucked in experiences. This can easily be shown from the balance of momentum, cf. L. Prandtl; O. Tietjens (1931), Vol. II, p. 140. It emerges from Eq. (11.18) that flow separation can always be prevented by massive suction.

Equation (11.17) yields the wall heat flux to be

$$q_w = -\lambda \left(\frac{\partial T}{\partial y} \right)_w = \varrho [-v_w(x)] c_p [T_w(x) - T_\infty]. \quad (11.19)$$

In order to determine the entire heat flux at the wall, to the part due to “conduction” (which here is dependent on λ and can be said to correspond to a convective heat flux difference) we must add the convective part $\varrho v_w c_p T_w$, so that the total heat flux is given by $q_{w\text{tot}} = \varrho v_w c_p T_\infty$.

Taking the dissipation into account, the recovery factor emerges as

$$r = \frac{T_{ad} - T_\infty}{U^2(x)/(2c_p)} = 1 \quad (11.20)$$

for all Prandtl numbers, cf. K. Gersten et al. (1977).

The different thicknesses of the boundary layer then read

$$\begin{aligned} \delta_1(x) &= \frac{\nu}{[-v_w(x)]}, & \delta_2(x) &= \frac{1}{2} \frac{\nu}{[-v_w(x)]}, & \delta_3(x) &= \frac{5}{6} \frac{\nu}{[-v_w(x)]}, \\ H_{12} &= 2, & H_{32} &= \frac{5}{3}. \end{aligned} \quad (11.21)$$

The solution for massive suction in plane stagnation-point flow has already been discussed in Sect. 5.1.3.

An extension of these solutions to compressible flows has been presented by K. Gersten et al. (1977), cf. also A.D. Young (1948).

Although the limit $v_w \rightarrow -\infty$ was taken, in fact we are strictly still dealing with a small suction velocity compared to the characteristic velocity V of the outer flow, e.g. to the free stream velocity. We find

$$\frac{v_w}{V} = O(1/\text{Re}^n) \quad 0 < n < \frac{1}{2}, \quad (11.22)$$

cf. K. Gersten; J.F. Gross (1974b). For $\text{Re} \rightarrow \infty$, v_w/V tends to zero, whereas $|v_w| \sqrt{\text{Re}}/V$ tends to infinity.

Example: Circular cylinder with massive uniform suction

Starting off with the potential theory velocity distribution for the circular cylinder $U(x) = 2V \sin \varphi$, separation will occur at $\varphi = 104.5^\circ$ if the boundary layer is not controlled, cf. Sect. 8.3.3. This leads to a contradiction in the given $U(x)$ distribution.

If strong enough suction is applied, separation can indeed be prevented. When the suction is uniform, the separation point shifts towards the rear stagnation point, reaching it at about $v_w \sqrt{VR/\nu}/V = -8.5$. The boundary layer is then approximated very well by the asymptotic suction profile, cf. J. Wiedemann (1983). Therefore the drag law, since there is no pressure drag, reads

$$c_D = \frac{2D}{\rho V^2 2Rb} = \int_0^\pi c_f \sin \varphi d\varphi = 2\pi \left(-\frac{v_w}{V} \right) \quad (11.23)$$

and the heat transfer at constant wall temperature, $\bar{q}_w = \int_0^\pi q_w d\varphi / \pi$

$$\text{Nu}_m = \frac{\bar{q}_w R}{\lambda(T_w - T_\infty)} = \left(-\frac{v_w}{V} \right) \text{Pr} \sqrt{\frac{VR}{\nu}}. \quad (11.24)$$

11.2.3 Massive Blowing ($v_w \rightarrow +\infty$)

Massive blowing causes the v component in the boundary layer to become very large, and the boundary layer increases in size compared with the case where there is no blowing.

Therefore we introduce the “compressed” quantities

$$\tilde{v} = \frac{v}{v_{wo}}, \quad \tilde{y} = \frac{y}{v_{wo}}, \quad (11.25)$$

where v_{wo} is the blowing velocity at a reference position $x = x_0$. Taking the limit $v_{wo} \rightarrow \infty$ with these quantities, the boundary-layer equations (11.3) to (11.5) become

$$\frac{\partial u}{\partial x} + \frac{\partial \tilde{v}}{\partial \tilde{y}} = 0, \quad (11.26)$$

$$u \frac{\partial u}{\partial x} + \tilde{v} \frac{\partial u}{\partial \tilde{y}} = U \frac{\partial U}{\partial x}, \quad (11.27)$$

$$u \frac{\partial T}{\partial x} + \tilde{v} \frac{\partial T}{\partial \tilde{y}} = 0. \quad (11.28)$$

The terms proportional to ν or a drop away when the limit is taken. Therefore, to first approximation, massive blowing allows the boundary layer to be described by an “inviscid” theory.

The solution for the velocity field reads

$$u(x, \psi) = \sqrt{2[p(\bar{x}) - p(x)]/\rho}, \quad (11.29)$$

where

$$\psi(\bar{x}) = - \int_0^{\bar{x}} v_w(x) dx = \text{const} \quad (11.30)$$

describes that streamline which begins at the position $x = \bar{x}$ on the wall, cf. Fig. 11.6. Equation (11.29) states that the total pressure $p + \rho u^2/2$ on a streamline is constant (Bernoulli equation).

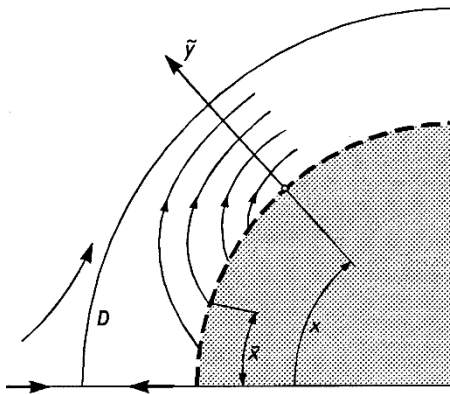


Fig. 11.6. Progression of streamlines in the boundary layer with massive blowing,
D: dividing streamline

The compatibility condition at the wall (Eq. (11.27) for $\tilde{y} \rightarrow 0$) yields the wall shear stress

$$\tau_w = \mu \left(\frac{\partial u}{\partial y} \right)_w = \frac{\mu U(x)}{v_w(x)} \frac{dU}{dx} = - \frac{\nu}{v_w(x)} \frac{dp}{dx}. \quad (11.31)$$

This solution for massive blowing is only possible if there is a pressure drop, since in Eq. (11.29), $p(\bar{x}) > p(x)$ must hold.

The distance from the wall of the *dividing streamline* which divides the blown fluid from the outer flow fluid is obtained from a mass balance:

$$y_D(x) = - \int_0^x \frac{\partial \psi}{u} = \int_0^x \frac{v_w(x') dx'}{u(x, x')}. \quad (11.32)$$

The dividing streamline in this instance is the edge of the boundary layer which therefore has a *finite* distance from the wall in this “compressed” coordinate system x, \tilde{y} . The derivatives of the velocities are not continuous at the dividing streamline between the inviscid rotational boundary-layer flow and the inviscid irrotational outer flow. This discontinuity leads to a frictional layer (a type of mixing layer) close to the dividing streamline which ensures a continuous transition. The differential equation to describe the flow in this free shear layer is independent of the blowing velocity $v_w(x)$, cf. K. Gersten; J.F. Gross (1974b).

The transition from the temperature T_w in the entire boundary layer to the outer temperature T_∞ also takes place in this layer. Many examples have shown that, for $v_w \rightarrow +\infty$, the wall heat flux q_w tends to zero exponentially. For this reason, blowing presents a very effective opportunity to drastically reduce the heat transfer. This is exploited technically in so-called *transpiration cooling*.

Combined blowing and suction

The solution described by Eqs. (11.29) to (11.32) can also be continued on into the region where the pressure rises, as long the distribution $v_w(x)$ is such that its sign changes at the position where the pressure is a minimum. Then massive suction is carried out in the region where the pressure rises. The following example elucidates the physical situation of flow past a circular cylinder.

Example: Flow past a circular cylinder with combined massive suction and blowing

As in Fig. 11.7, the suction or blowing takes place with velocity distribution $v_w(\varphi) = v_{wo} \cos \varphi$ (with $v_{wo} > 0$).

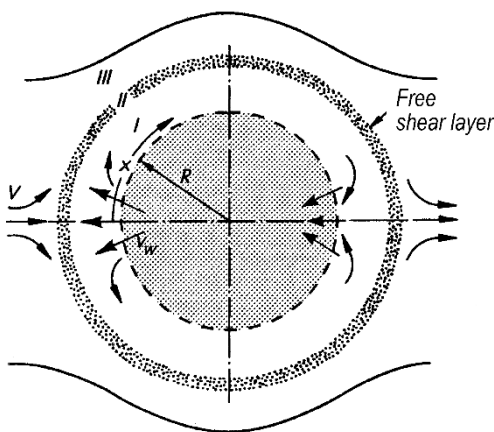


Fig. 11.7. Circular cylinder with massive blowing and suction
 Layer I: boundary layer (inviscid, with vorticity)
 Layer II: mixing layer (viscous)
 Layer III: outer flow (inviscid, irrotational)

The fluid blown out in the front half is precisely that sucked in in the rear half. With the outer velocity $U(\varphi) = 2V \sin \varphi$ in Eq. (11.31), we obtain the distribution of the skin-friction coefficient to be

$$c_f = \frac{2\tau_w}{\rho V^2} = \frac{8\nu}{v_{wo} R} \sin \varphi \quad (11.33)$$

and, after integration, the drag law is

$$c_D = \frac{2D}{\rho V^2 2Rb} = \int_0^\pi c_f \sin \varphi \, d\varphi = \frac{4\pi\nu}{v_{wo} R}. \quad (11.34)$$

Since the flow does not separate, there is no pressure drag. The friction drag from Eq. (11.34) can be reduced by any given amount by increasing v_{wo} .

Thus this example yields an *analytic solution* to the boundary-layer equations for a finite sized body in a flow, cf. K. Gersten (1979).

11.2.4 Similar Solutions

The similar solutions to the boundary-layer equations treated in Sect. 7.2 can very easily be extended to flows with suction or blowing. In order to do this, only the boundary conditions for the ordinary differential equations must in general be changed. The dimensionless stream function $f(\eta)$ now acquires a non-zero value $f_w = f(0)$ at the wall. The blowing velocity at the wall then follows from Eq. (7.11):

$$v_w \sqrt{\text{Re}} = -\frac{d}{d\xi} (U_N \bar{\delta}) f_w. \quad (11.35)$$

Hence, for every similar solution there is a particular distribution $v_w(\xi)$ or $v_w(x)$ whose similarity remains even in the cases of suction and blowing. This is also true of the similar solutions of the temperature field in Sect. 9.4, the compressible boundary layers in Sect. 10.4.4 and the natural convection in Sect. 10.5.4. Examples of similar solutions will now be discussed.

Wedge flows.

The wedge flow with $U(x) = ax^m$ applied to Eq. (7.32) yields the distribution

$$v_w(x) = -\sqrt{\frac{m+1}{2}} \nu a x^{\frac{m-1}{2}} f_w. \quad (11.36)$$

Here $f_w > 0$ implies suction and $f_w < 0$ blowing. The stagnation-point flow ($m = 1$) yields precisely a constant v_w . The system of equations, cf. Eqs. (7.15) and (9.52)

$$f''' + ff'' + \beta(1 - f'^2) = 0, \quad (11.37)$$

$$\frac{1}{\Pr} \vartheta'' + f\vartheta' - \frac{2n}{m+1} f'\vartheta = 0 \quad (11.38)$$

with the boundary conditions

$$\begin{aligned} \eta = 0 : \quad f &= f_w, & f' &= 0, & \vartheta &= 1 \\ \eta \rightarrow \infty : \quad f' &= 1, & \vartheta &= 0 \end{aligned} \quad (11.39)$$

has already been investigated many times.

Figure 11.8 shows f_w'' as a function of $\beta = 2m/(m+1)$ with f_w as a parameter, after K. Nickel (1962). Vanishing wall shear stress is given by the limit $f_w'' = 0$. It is seen from Fig. 11.8 that, even if the flow is strongly decelerated (e.g. $\beta = -1$, i.e. $m = -1/3$), intensive enough suction can enforce a positive wall shear stress. Furthermore it can be seen that there are two solutions for decelerated flow, with one of them exhibiting backflow ($f_w'' < 0$). Solutions of the velocity field have been presented by H. Schlichting (1943/44) and H. Schlichting; K. Bussmann (1943), as have those for $m = 0$ by H.W. Emmons; D.C. Leigh (1954) and J. Steinheuer (1968b).

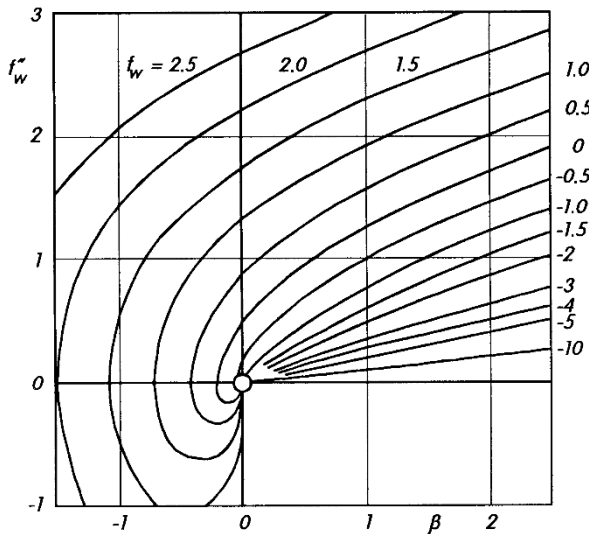


Fig. 11.8. Relation between the wall shear stress $\tau_w \sim f_w''$ and the suction velocity $v_w = f_w$ for wedge flow boundary layers, after K. Nickel (1962)

$$\frac{\tau_w}{\rho U^2} = \sqrt{\frac{m+1}{2}} \sqrt{\frac{\nu}{U_x}} f_w'' \quad \frac{v_w}{U} = -\sqrt{\frac{m+1}{2}} \sqrt{\frac{\nu}{U_x}} f_w \quad \beta = \frac{2m}{m+1} \quad U = ax^m$$

An overview of the solution is to be found in Fig. 11.9. In the β - f_w diagram, each point corresponds to a certain flow. The solutions with $f_w'' = 0$ are given by the bounding curve. This terminates at the plate solution at $f_w = -0.8757$. For blowing of this intensity, the boundary layer lifts off the plate. The solution corresponds exactly to that solution for the jet boundary flow in Sect. 7.2.4 ($\lambda = 0$). Here the blowing velocity $v_w(x)$ takes on the function of the entrainment velocity in Eq. (7.45). The transition $f_w \rightarrow -0.8757$ has been described in more detail by D.R. Kassoy (1970).

The right edge of Fig. 11.9 corresponds to massive suction ($f_w \rightarrow +\infty$); the left edge to massive blowing ($f_w \rightarrow -\infty$). This latter exists only if there is a pressure drop ($\beta > 0$). The solutions without backflow lie above the curve $f_w'' = 0$ ($\tau_w = 0$). It can be seen that cases with $f_w'' = 0$ are shifted to regions of greater pressure rise ($\beta \rightarrow -\infty$) as the suction increases.

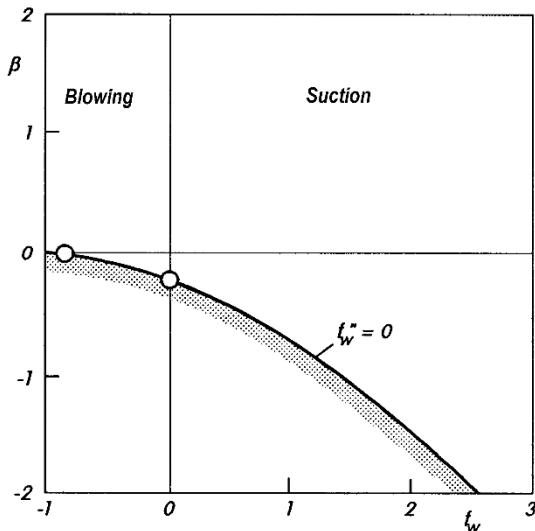


Fig. 11.9. Overview of similar solutions of wedge flows with continuous suction or blowing. Below the limiting curve $f_w'' = 0$, backflow occurs in the boundary layer

Figure 11.10a shows the dependence of the Nusselt number on the Prandtl number for flow at a plate ($m = 0$, $\beta = 0$, $n = 0$). The parameter here is again f_w . The asymptotes for $\text{Pr} \rightarrow 0$ and $\text{Pr} \rightarrow \infty$ are included as dashed lines. Obviously the asymptotic behaviour for $\text{Pr} \rightarrow \infty$ changes as we move closer to $f_w = 0$, i.e. close to the transition from suction to blowing. This has to do with the double limit $\text{Pr} \rightarrow \infty$, $f_w \rightarrow 0$, where the right choice of limits for the two parameters is important

A comprehensive presentation by K. Gersten; H. Herwig (1992), p. 358 has shown that an adequate representation of the function $\text{Nu}_x/\sqrt{\text{Re}_x} = F(\text{Pr}, f_w)$ for $\text{Pr} \rightarrow \infty$ and $f_w \rightarrow 0$ is the so-called “*distinguished limit*”. Here the two limits $\text{Pr} \rightarrow \infty$ and $f_w \rightarrow 0$ are taken so that the *coupling parameter*

$$K = f_w \text{Pr}^{2/3} \quad (11.40)$$

remains constant. This parameter follows from the so-called *principle of minimum degeneracy*, whereby the coupling between Pr and f_w must be just so that the degeneracy of the differential equation resulting from the single-parameter limiting process (due to the coupling) is as small as possible, cf. K. Gersten (1982a). The heat transfer resulting from this is depicted in Fig. 11.10b. In this figure, the solution function is completely “regular” in the region $\text{Pr} \rightarrow \infty$, $f_w \rightarrow 0$. On the other hand, the function in the region $\text{Pr} \rightarrow 0$, $f_w \rightarrow 0$ in this illustration seems singular. Figures 11.10a and 11.10b show the same function. If Prandtl numbers $\text{Pr} < 1$ are being considered it is Fig. 11.10a which is of interest; for $\text{Pr} > 1$ then Fig. 11.10b.

Figure 11.11 shows the dependence of the function from Fig. 11.10b for $\text{Pr} \rightarrow \infty$ on K . The dashed lines are the asymptotes for suction ($K \rightarrow \infty$) and blowing ($K \rightarrow -\infty$). The result for $K = 0$ has already been given in Table 9.1. If we were to start off with a finite f_w and first of all carry out the limit $\text{Pr} \rightarrow \infty$, followed by the limit $f_w \rightarrow 0$, we would get the wrong results. We would follow the asymptotes in Fig. 11.11, which both incorrectly lead to vanishing heat transfer.

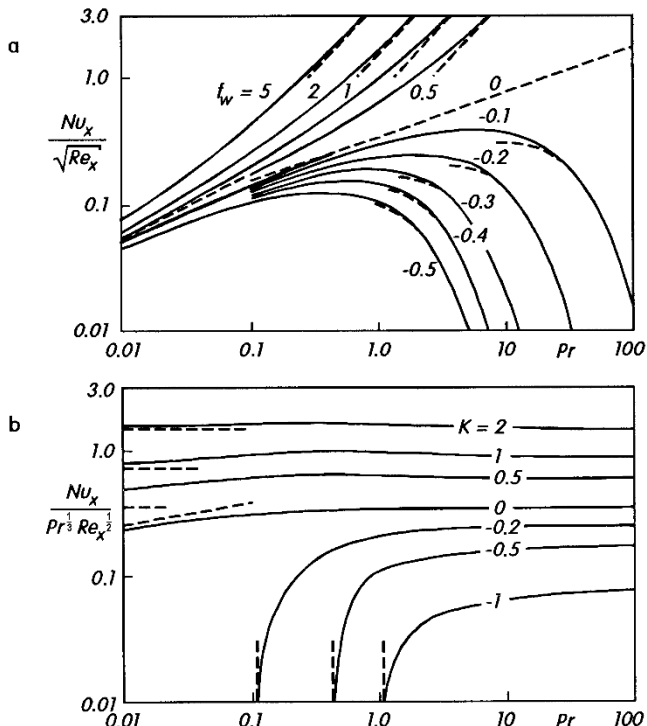


Fig. 11.10. Heat transfer at the flat plate at zero incidence ($T_w = \text{const}$) with continuous suction/blowing as a function of the Prandtl number.

With: $v_w(x)/U_\infty = -\sqrt{\nu/2U_\infty x}f_w$

(a) suitable representation for small Prandtl numbers

(b) suitable representation for large Prandtl numbers, $K = f_w \Pr^{2/3}$

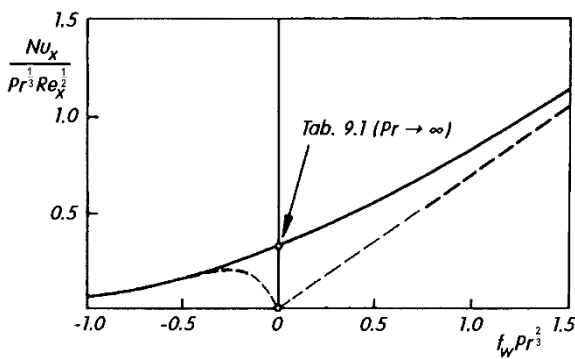


Fig. 11.11. Heat transfer at a flat plate at zero incidence ($T_w = \text{const}$) with continuous suction or blowing, taking the double limit $\Pr \rightarrow \infty$, $f_w \rightarrow 0$ so that $K = f_w \Pr^{2/3}$ remains constant

Note (Double limit)

As the example discussed has shown, taking the double limit can lead to incorrect results in two-parameter problems if it is not carried out correctly. The coupling between the parameters must be taken into account in forming the limit. Hence the following question emerges: because the Prandtl boundary-layer theory arose from the complete equations of motion by means of taking a limit ($\text{Re} \rightarrow \infty$), could it not happen that boundary-layer theory leads to incorrect results if additional (e.g. geometric) parameters describing the behaviour of the boundary layer also reach their limiting values? Unfortunately the answer to this question is affirmative. There are indeed flows which are not sufficiently correctly described by the Prandtl boundary-layer theory in the limit $\text{Re} \rightarrow \infty$. Carrying out the *distinguished limit*, as mentioned above, leads, in these cases, to extensions of boundary-layer theory, as will be seen in Chap. 14.

Further solutions of the thermal boundary-layer equations for wedge flows with suction and blowing can be found in the work by W.E. Stewart; R. Prober (1962), P.L. Donoughe; J.N.B. Livingood (1955) and K. Gersten; H. Körner (1968). The last of these works also treats variable wall temperature distributions ($n = 2m$) and the effect of dissipation. The temperature dependence of the physical properties has also been considered by W.B. Brown; P.L. Donoughe (1951). Details on the effect of dissipation are to be found in K. Gersten; J.F. Gross (1973a).

Diffuser flow

The outer velocity $U(x) = a/x$ ($m = -1$) corresponds to the flow in a diverging channel (source flow). Without suction there is no similar solution for this set up. With a suction distribution

$$v_w(x) = -k\sqrt{\frac{U(x)\nu}{x}} \sim \frac{1}{x} \quad (11.41)$$

similar solutions are found as long as $k \geq 2\sqrt{2}$ is valid, cf. H. Holstein (1943).

Information on the heat transfer for this flow is to be found in K. Gersten; H. Körner (1968).

Wall jet

In Sect. 7.2, we saw that there were similar boundary layers without outer flow for which the following differential equation (cf. (7.29)) holds:

$$f''' + ff'' - \alpha_3 f'^2 = 0. \quad (11.42)$$

We choose the following boundary conditions:

$$\begin{aligned} \eta = 0 : \quad & f = f_w, \quad f' = 0 \\ \eta \rightarrow \infty : \quad & f' = 0. \end{aligned} \quad (11.43)$$

To satisfy the normalisation condition we use

$$\int_0^\infty f'(\eta) d\eta = 1. \quad (11.44)$$

For each given value f_w we must now find an eigenvalue α_3 such that all the boundary and normalisation conditions are satisfied. Therefore the eigenvalue here is dependent on the intensity of blowing or suction.

According to Eq. (11.35), the blowing velocity at the wall is

$$\frac{v_w}{V} = -\frac{f_w}{2-\alpha_3} \left(\frac{Vx}{\nu} \right)^{(\alpha_3-1)/(2-\alpha_3)}. \quad (11.45)$$

This boundary layer can be interpreted as wall jet flow. For $f_w = 0$ we have $\alpha_3 = -2$, corresponding to the wall jet at an impermeable wall, as in Sect. 7.2.7. As the intensity of blowing is increased ($f_w < 0$), α_3 becomes larger, and reaches the limit $\alpha_3 = -1$ for $f_w = -0.5$. This flow describes the free jet as in Sect. 7.2.6. The blowing velocity $v_w \sim x^{-2/3}$ then assumes the function of the entrainment velocity in Eq. (7.55). At this blowing strength, the wall jet lifts off the wall and becomes a free jet. In the limiting case of massive suction ($v_w \rightarrow -\infty$, $f_w \rightarrow +\infty$), the wall jet completely vanishes and only the suction $v_w \sim 1/x$ in surroundings at rest without a viscous shear layer remains. Details of the solutions can be read in J. Steinheuer (1966).

11.2.5 General Solutions

For general prescribed $U(x)$, $v_w(x)$ and $T_w(x)$ or $q_w(x)$, the system of equations (11.3) to (11.6) can be solved in a different manner.

In the past, solutions were carried out using series expansions, cf. R. Iglisch (1944), H. Görtler (1957c), and using approximate methods based on the integral relations (11.8) and (11.9), cf. H. Schlichting (1948). The approximate method of R. Eppler (1963) proved to be successful in practice. E. Truckenbrodt (1956) developed a particularly simple integral method by which the boundary-layer calculation is reduced to the solution of a first order ordinary differential equation. In the special case of the impermeable wall, this becomes the quadrature formula Eq. (8.23).

T.F. Zien (1976) has presented an approximate method for the calculation of the heat transfer in boundary layers with suction or blowing. Integral methods have also been developed for compressible boundary layers, cf. P.A. Libby; A. Pallone (1954), M. Morduchow (1952) and W. Pechau (1963).

In what follows we will discuss some examples of solutions for boundary layers with blowing or suction.

1. Plate Flow with Uniform Suction or Blowing

The boundary layer at a flat plate at zero incidence with uniform suction has been computed by R. Iglisch (1944). Here the boundary layer commences directly at the leading edge with the *Blasius profile* of the solution without suction (with shape factor $H_{12} = 2.59$). Further downstream, the suction acts and leads to a reduction of H_{12} . Finally, the *asymptotic suction profile* in Eq. (11.16) is reached downstream with $H_{12} = 2$ corresponding to Eq. (11.21). In practice, the asymptotic state emerges at about

$$\frac{-v_w}{U_\infty} \sqrt{\frac{U_\infty x}{\nu}} = 2$$

(here $H_{12} < 2.02$). As is shown in Fig. 11.12, the boundary layer grows as usual with distance from the leading edge. As it reaches the asymptotic state for large x values, the boundary layer retains the same thickness given by Eq. (11.21). According to

K. Stewartson (1957), the solution “flows into” the asymptotic value exponentially, i.e. an asymptotic expansion for large x values is not possible since the next term in an approximation is exponentially small compared to the asymptotic suction profile.

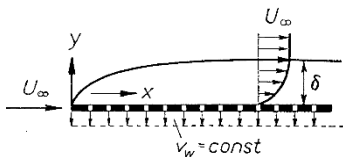


Fig. 11.12. Flat plate at zero incidence with uniform suction

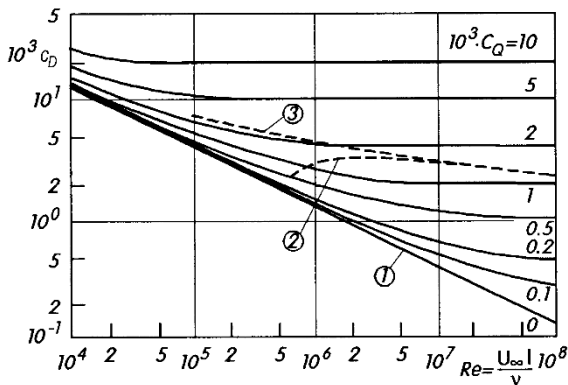


Fig. 11.13. Drag coefficients for the flat plate at zero incidence with uniform suction
 $c_Q = -v_w/U_\infty$: suction volume flux coefficient
curves (1), (2) and (3): without suction
(1) laminar
(2) laminar-turbulent transition
(3) fully turbulent

A point of particular interest in considering the *drag saving* due to forcing the flow to stay laminar as a result of suction is the drag law of the plate with uniform suction shown in Fig. 11.13. For very large Reynolds numbers $\text{Re} = U_\infty l/\nu$ where most of the plate lies within the region of the asymptotic solution, the drag is given by the simple relation (11.18). The drag coefficient then follows as

$$c_D = \frac{2D}{\rho U_\infty^2 bl} = \frac{2}{\rho U_\infty^2 l} \int_0^l \tau_w(x) dx \approx 2c_Q \quad (11.46)$$

with the suction coefficient

$$c_Q = \frac{Q}{U_\infty bl} = \frac{-1}{U_\infty l} \int_0^l v_w(x) dx. \quad (11.47)$$

For uniform suction, $c_Q = -v_w/U_\infty$. The c_D value determined in this manner is therefore independent of the Reynolds number, and thus does not vanish for $\text{Re} \rightarrow \infty$. This again is the *sink drag* experienced by every body, even in inviscid flow, if the volume flux is “swallowed” leading to the momentum flux $I = D = \rho Q U_\infty$ being removed from the flow. The drag is larger for smaller Reynolds numbers since the wall shear stress in the thinner boundary layer on the front part of the plate is larger than that further back.

For comparison, Fig. 11.13 also shows the drag law for the plate with a turbulent boundary layer without suction. This will be discussed later in Sect. 18.2.5. Since suction has a stabilising effect on the boundary layer, the transition from laminar to turbulent behaviour can be suppressed by strong enough suction. As will be shown in Chap. 15, a suction coefficient of

$$c_{Q \text{ crit}} = 1.2 \cdot 10^{-4}$$

is sufficient to keep the boundary layer stable over the entire length of the plate. This critical suction coefficient corresponds to the dashed curve of *most favourable suction*. The region between this curve and the curve for the turbulent boundary layer indicates the amount of drag which can be saved by suction. The drag saving relative to the fully turbulent drag increases somewhat with increasing Reynolds number. It lies between 60% and 80% in the region of Reynolds numbers from $\text{Re} = 10^6$ to 10^8 .

Experimental investigations by J.M. Kay (1948) have confirmed the theoretical results of R. Iglisch (1944).

W. Rheinboldt (1956) investigated the plate boundary layer for the case where the suction only takes place along a finite length of the wall.

In *uniform blowing* from a plate, separation of the boundary layer occurs at

$$x_S = 0.7456 \frac{U_\infty \nu}{v_w^2}.$$

This is a singularity, as D. Catherall et al. (1965) and D.R. Kassoy (1973) have shown. Here, the stronger the blowing is carried out, the earlier separation occurs. The occurrence of a singularity at the separation point implies that the boundary-layer theory would need to be extended to describe this flow, a topic to which we will return in Chap. 14.

Results on heat transfer are to be found in, for example, the work of T.F. Zien (1976). J.B. Klemp; A. Acrivos (1972) have also referred to other blowing distributions.

2. Airfoil

E. Truckenbrodt (1956) has computed the symmetric flow ($\alpha = 0^\circ$) past a symmetric Joukowsky airfoil with uniform suction over the entire surface. One result is shown in Fig. 11.14: the separation point is displaced backwards with increasing suction and, for $c_Q^* = c_Q \sqrt{Vl/\nu} > 1.2$, separation no longer occurs.

Therefore, as well as having a stabilising action in the prevention of the laminar/turbulent transition, which will be discussed in Chap. 15, the effect of greatest importance due to suction is the prevention of separation. For this reason, suction has been applied to airfoils to increase their maximum lift. In doing this, the suction is mostly applied to a narrow area close to the leading edge of the airfoil. See work by E.D. Poppleton (1955), C.A. Holzhauser; R.S. Bray (1956) as well as N. Gregory; W.S. Walker (1955) for more on this topic.

A combination of blowing and suction to reduce the drag of an airfoil has been applied by J. Wiedemann (1983), J. Wiedemann; K. Gersten (1984) and K. Gersten; J. Wiedemann (1982). Blowing was first performed at the front part, i.e. in the pressure drop region, in order to reduce the wall shear stress, while suction was performed in the pressure rise region, in order to prevent separation. Figure 11.15 shows the results of these calculations for the drag as a function of the blowing coefficient. Here the suction volume was only 1/9 of the blowing volume. The dashed line corresponds to the asymptotic solutions of massive blowing (or suction) according to Sect. 11.2.3. We see that the drag can be made arbitrarily small for certain blowing/suction.

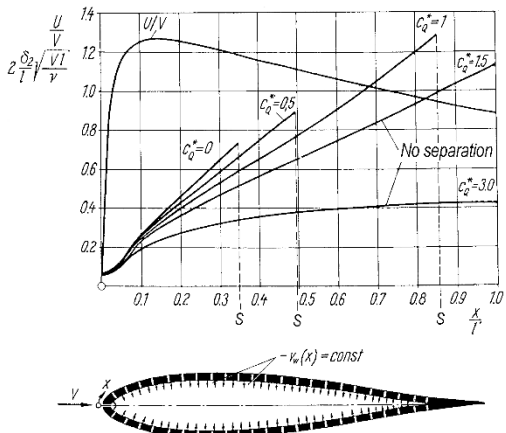


Fig. 11.14. Boundary layer at a symmetric Joukowsky airfoil at zero incidence with uniform suction, computed by E. Truckenbrodt (1956)
 δ_2 momentum thickness; l' half perimeter length; $c_Q^* = c_Q \sqrt{Vl}/\nu$ reduced suction coefficient; U/V velocity distribution from potential theory
 c_Q suction rate

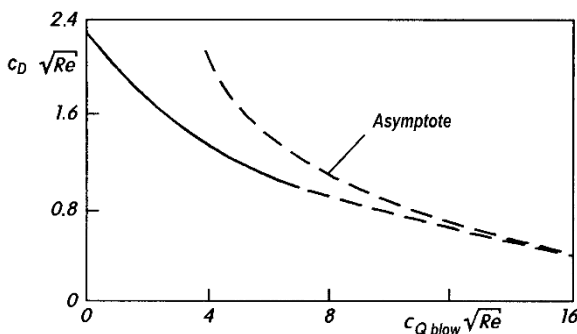


Fig. 11.15. Drag coefficient of a symmetric Joukowsky airfoil (4.4% relative thickness, angle of attack $\alpha = 0^\circ$) with continuous blowing and suction, after J. Wiedemann; K. Gersten (1984).

$v_w \sim dU/dx$, $Q_{\text{blow}} = 9.1 Q_{\text{suct}}$, asymptote $c_D \sqrt{Re} = 8.8/(c_{Q \text{ blow}} \sqrt{Re})$

11.2.6 Natural Convection with Blowing and Suction

Here we will consider the solutions of the system of equations (10.115) to (10.117), where, as well as the body contour $\alpha(x)$ and the wall temperature $T_w(x)$, the blowing velocity $v_w(x)$ is also prescribed. Because of the

boundary-layer transformation (10.120), we are, however, dealing with small velocities

$$v_w/V = O(\text{Gr}^{-1/4}).$$

Again simple solutions for massive suction and massive blowing can be found, cf. J.H. Merkin (1972) and J. Aroesty; J.D. Cole (1965).

Similar solutions can be found from the system of equations (10.148) and (10.149) with the changed boundary condition $f(0) = f_w \neq 0$. The blowing velocity then emerges as

$$\bar{v}_w = \frac{v_w}{V_{DN}} \text{Gr}^{1/4} = -\frac{3+m+n}{\sqrt{2}} A^{-1/4} (x^*)^{(m+n-1)/4} f_w. \quad (11.48)$$

R. Eichhorn (1960) has treated the flat vertical plate. Calculations for the lower stagnation point and for other contour shapes which lead to similar solutions have been presented by J.H. Merkin (1975).

Natural convection with uniform suction and blowing has been investigated for the plate by E.M. Sparrow; R.D. Cess (1961) and J.H. Merkin (1972) as well as for the horizontal cylinder by J.H. Merkin (1975).

11.3 Binary Boundary Layers

11.3.1 Overview

In what we have considered up until now, the injected fluid has been the same as the fluid in the outer flow. If the blown fluid is different from the outer flow, a *binary boundary layer* arises. As well as momentum and heat exchange, there is also exchange of mass through *diffusion*. In addition to the velocity boundary layer and the thermal boundary layer, a further boundary layer for the concentration (of, for example, the injected fluid) forms.

Since blowing out a light gas drastically reduces the heat transfer, this measure is used in practice in heat protection (*transpiration cooling*), cf. J.F. Gross et al. (1961). Binary boundary layers also occur when a layer of liquid evaporates at the wall (*evaporation cooling*), or if the wall material itself melts or sublimates (*sublimation cooling*). If solid wall material is transformed into another aggregate state, this process is known as *ablation*.

Here we will treat quite general binary mixtures of fluids where a concentration boundary layer also forms due to appropriate boundary conditions at the wall (e.g. evaporation). As has already been mentioned in Sect. 10.4.6, binary boundary layers frequently occur in hypersonic flows. In the cooling mechanisms (transpiration cooling, ablation cooling), boundary layers of mixtures of reactive gases are mainly found. One frequently finds such flows in connection with dissociation and ionisation of a gas at high temperatures or with combustion. If dissociation occurs in a flow as a consequence of high temperatures, the gas is frequently represented as a binary mixture

of molecules and atoms. The concentration of the “atomic gas” is then the *degree of dissociation*. The state of the surface of the wall is then used as a boundary condition. The wall is called *fully catalytic* if all the atoms *recombine* at the wall, while there is no recombination of atoms at a *non-catalytic* wall. A further difficulty arises because there is generally a coupling between the three boundary layers mentioned, particularly between the temperature and concentration boundary layers.

Summaries of binary boundary layers can be found in the work of G. Ludwig; M. Heil (1960), R.B. Bird et al. (1960), W. Wuest (1962, 1963) and J.D. Anderson Jr. (1989).

11.3.2 Basic Equations

Let the fluid under consideration now be a mixture of two components. The *mass concentration* of the component i ($i = 1, 2$) is defined as

$$c_i = \frac{\varrho_i}{\varrho} \quad \text{with} \quad \varrho_i = \lim_{\Delta V \rightarrow 0} \frac{\Delta m_i}{\Delta V} \quad \text{and} \quad \sum_i c_i = 1, \quad (11.49)$$

where ϱ_i is the so-called *partial density*.

At any position under consideration, each component can have a velocity \vec{v}_i which may differ somewhat from the velocity of the other. Therefore, in order to characterise the state of the flow, we introduce a *mean velocity* or equivalently a *mass-weighted velocity*. It reads

$$\vec{v} = \sum_i c_i \vec{v}_i \quad \text{or} \quad \varrho \vec{v} = \sum_i \varrho_i \vec{v}_i. \quad (11.50)$$

In practice this velocity is determined using a Pitot tube. This velocity also occurs in the momentum equation and the thermal energy equation.

For each component i , we have a conservation of mass equation (*partial continuity equation*) of the form

$$\operatorname{div}(\varrho_i \vec{v}_i) = \dot{w}_i. \quad (11.51)$$

Here \dot{w}_i is the mass of component i per unit volume and time originating from chemical reactions, $[\dot{w}_i] = \text{kg/m}^3\text{s}$. For a binary mixture we have $\dot{w}_1 + \dot{w}_2 = 0$.

If we sum over all components, Eq. (11.50) yields the global continuity equation

$$\operatorname{div}(\varrho \vec{v}) = 0 \quad (11.52)$$

in the familiar form, cf. Eq. (3.3).

According to Eq. (11.50) therefore, if there is a difference in concentration in the fluid, relative velocities $\vec{v}_i - \vec{v}$ of the individual components i related to the mass-weighted velocity occur, and hence there are corresponding mass flows in a coordinate system moving with the mass-weighted velocity. We obtain the so-called *diffusion flux vector*

$$\vec{j}_i = \varrho_i (\vec{v}_i - \vec{v}). \quad (11.53)$$

Combining Eqs. (11.51) to (11.53), a two-dimensional, steady concentration boundary layer (where $\partial j_{1x}/\partial x$ can be neglected compared to $\partial j_{1y}/\partial y$ in the boundary layer) yields the following partial continuity equation for component 1:

$$\varrho \left(u \frac{\partial c_1}{\partial x} + v \frac{\partial c_1}{\partial y} \right) = - \frac{\partial j_{1y}}{\partial y} + \dot{w}_1. \quad (11.54)$$

The *diffusion law* delivers the relation between the diffusion flux vector \vec{j}_1 and the concentration and temperature fields. For binary mixtures the diffusion law reads

$$\vec{j}_1 = -\varrho D_{12} [\text{grad } c_1 + \bar{\alpha} c_1 (1 - c_1) \text{ grad ln } T]. \quad (11.55)$$

Here, strictly speaking, two diffusion effects have been neglected: the *pressure diffusion* due to pressure gradients, which are however neglected in the y direction in boundary layers, and the *diffusion due to volume forces*, which indeed only acts if the individual components are acted on by different force fields. In the gravity field here, this is not the case.

The diffusion law (11.55) has two parts. The first term describes the diffusion due to concentration gradients. It is known as *Fick's diffusion law* and corresponds to the Fourier heat conduction law in the thermal boundary layer. The binary diffusion coefficient D_{12} is a physical property and has the units $[D_{12}] = \text{m}^2/\text{s}$. Numerical values for some technically important mixtures have been given by K. Gersten; H. Herwig (1992), p. 781.

The second term in Eq. (11.55) describes the *thermodiffusion* (also called the *Soret effect*). This gives rise to an additional mass transfer because of the temperature gradients. Therefore there is a “coupling effect” between heat transfer and mass transfer.

The ansatz is carried out so that the dimensionless *thermal diffusion coefficient* $\bar{\alpha}$ is as far as possible independent of the concentration, and can therefore be considered to be a constant for every specific combination of gases.

There is a further coupling effect which must be taken into account when the thermal energy equation is being set up. This is the so-called *diffusion thermoeffect* or *Dufour effect*. According to this, an additional heat flux occurs because of the concentration gradient. The Fourier heat conduction law can be extended as follows:

$$q = -\lambda \frac{\partial T}{\partial y} + \left[(h_1 - h_2) + \bar{\alpha} RT \frac{\widetilde{M}^2}{\widetilde{M}_1 \widetilde{M}_2} \right] j_{1y}, \quad (11.56)$$

where j_{1y} is the y component of the diffusion flux vector from Eq. (11.55). In addition, R is the specific gas constant of the mixture, \widetilde{M}_1 and \widetilde{M}_2 are the molar masses of the two components and \widetilde{M} is the molar mass of the mixture, given by $1/\widetilde{M} = c_1/\widetilde{M}_1 + c_2/\widetilde{M}_2$. This formulation holds for binary gas mixtures. For general fluids, see, for example, R. Haase (1963), p. 391.

If we assume a mixture of ideal gases, the thermal energy equation can be construed as a balance law for the enthalpy of the mixture

$$h = c_1 h_1 + c_2 h_2. \quad (11.57)$$

We obtain the following system of equations for a plane, steady, binary boundary layer:

$$\frac{\partial(\varrho u)}{\partial x} + \frac{\partial(\varrho v)}{\partial y} = 0, \quad (11.58)$$

$$\varrho \left(u \frac{\partial u}{\partial x} + v \frac{\partial u}{\partial y} \right) = -\varrho g \sin \alpha - \frac{dp}{dx} + \frac{\partial}{\partial y} \left(\mu \frac{\partial u}{\partial y} \right), \quad (11.59)$$

$$\begin{aligned} \varrho c_p \left(u \frac{\partial T}{\partial x} + v \frac{\partial T}{\partial y} \right) &= \frac{\partial}{\partial y} \left(\lambda \frac{\partial T}{\partial y} \right) + \beta T u \frac{dp}{dx} + \mu \left(\frac{\partial u}{\partial y} \right)^2 \\ &\quad + \frac{\partial}{\partial y} \left\{ \varrho D_{12} \left[h_1 - h_2 + \overline{\alpha} RT \frac{\widetilde{M}^2}{\widetilde{M}_1 \widetilde{M}_2} \right] \right. \\ &\quad \times \left. \left[\frac{\partial c_1}{\partial y} + \overline{\alpha} c_1 (1 - c_1) \frac{\partial \ln T}{\partial y} \right] \right\}, \end{aligned} \quad (11.60)$$

$$\begin{aligned} \varrho \left(u \frac{\partial c_1}{\partial x} + v \frac{\partial c_1}{\partial y} \right) &= \frac{\partial}{\partial y} \left[\varrho D_{12} \left(\frac{\partial c_1}{\partial y} + \overline{\alpha} c_1 (1 - c_1) \frac{\partial \ln T}{\partial y} \right) \right] \\ &\quad + \dot{w}_1. \end{aligned} \quad (11.61)$$

If we neglect the coupling effects (proportional to $\overline{\alpha}$), the underlined terms drop away.

In many cases the coupling effects are small enough to be neglected compared to the effects of diffusion or heat conduction. However, there are exceptions. For example, the thermodiffusion is used in separating isotopes. The diffusion thermoeffect can, for example, play a role in mixtures of gases with very different molar masses, cf. R.B. Bird et al. (1960) and E.M. Sparrow et al. (1964).

In the special case $c_1 = 1$, the system (11.58) to (11.61) again reduces to the system (10.4) to (10.6) for single-substance boundary layers. The specific enthalpies h_1 and h_2 of the components are absolute values, i.e. they also contain their formation enthalpies, so that these do not explicitly appear in the balance law for the energy, cf. J.D. Anderson Jr. (1989), p. 616.

The physical properties of a binary mixture are in general not only dependent on the temperature and the pressure, but also on the concentration. If the dependence is small, generally valid statements can be found by using the asymptotic methods described in Sect. 10.3, cf. K. Gersten; H. Herwig (1992), p. 360.

The boundary conditions for the velocity and temperature correspond to those for single-substance boundary layers. There are however two new boundary conditions for the concentration. At large distances from the wall we have $c_1 = c_{1e}$. If only the outer gas is present there, then $c_{1e} = 0$.

Of particular importance is the condition for the concentration at the wall. There are several different possibilities for this:

- 1. Single-sided diffusion.** If, for example, component 1 is blown out through the wall, we can assume that the external component 2 does not penetrate the wall, i.e. that the diffusion velocity of the outer fluid at the wall is equal and opposite to the blowing velocity v_w at the wall. Inserting $\vec{v}_{2w} = 0$ into Eq. (11.53), this leads to

$$j_{2w} = -\varrho_2 v_w = -\varrho v_w (1 - c_1) = -j_{1w}$$

and, using Eq. (11.55) and neglecting the thermodiffusion, eventually to

$$v_w = - \left\{ \frac{D_{12}}{1 - c_1} \frac{\partial c_1}{\partial y} \right\}_w . \quad (11.62)$$

Therefore here, even for constant physical properties, the velocity field is dependent on the concentration and temperature fields.

Equation (11.62) is called the *Eckert-Schneider condition*. This is the boundary condition for single-sided diffusion at semi-permeable bounding surfaces. An example is the flow above a free water surface (film of water). A boundary layer then emerges which is a mixture of air and steam (moist air). Evaporation therefore corresponds to a flow with blowing. In contrast, the condensation of steam at a wall is equivalent to suction. The mass flux in blowing is therefore $\dot{m}_w = \varrho_w v_w$, where it is not the partial density ϱ_{1w} which is used, but the density of the mixture, cf. Eq. (11.50).

- 2. Non-catalytic wall.** Since there is no recombination of atoms at the wall in this case,

$$\left(\frac{\partial c_1}{\partial y} \right)_w = 0 . \quad (11.63)$$

- 3. Fully catalytic wall.** In this case the chemical reactions at the wall take place infinitely fast. Therefore the local values of temperature and pressure at the wall become those pertaining to the equilibrium concentration:

$$c_{1w} = (c_{1w})_{\text{equil.}} . \quad (11.64)$$

From the solutions for the system (11.58) to (11.61), we obtain, in particular, results about the heat and mass transfer. Equation (11.56) yields the heat transfer at the wall. Neglecting the coupling effects ($\bar{\alpha} = 0$), the wall heat flux reads:

$$q_w = - \left[\lambda \frac{\partial T}{\partial y} + \varrho D_{12} (h_1 - h_2) \frac{\partial c_1}{\partial y} \right]_w . \quad (11.65)$$

The diffusion flux at the wall follows from Eq. (11.55):

$$j_{1w} = - \left(\varrho D_{12} \frac{\partial c_1}{\partial y} \right)_w. \quad (11.66)$$

In analogy to the Nusselt number which represents a dimensionless q_w , the so-called *Sherwood number* Sh is introduced as a dimensionless j_{1w} . We have:

$$Nu = \frac{q_w l}{\lambda \Delta T}, \quad Sh = \frac{j_{1w} l}{\varrho D_{12} \Delta c}, \quad (11.67)$$

where Δc is a suitable concentration difference.

Note (Gas mixtures in chemical equilibrium) If the gas mixture is in chemical equilibrium, the concentration $c_1(T, p)$ is a given function of T and p . Then the partial continuity equation for c_1 is superfluous, so that the flow can be treated as a single-substance flow. Examples here are the equilibrium flows of dissociated gases. The *mass action law* then yields the relation for the degree of dissociation $c_1 = f(T, p)$. From this, it emerges that in the boundary layer

$$\frac{\partial c_1}{\partial y} = \frac{\partial c_1}{\partial T} \frac{\partial T}{\partial y},$$

so that for the wall heat flux from Eq. (11.65) we have

$$q_w = - \left(\lambda_T \frac{\partial T}{\partial y} \right)_w, \quad (11.68)$$

where the *total thermal conductivity* is introduced as

$$\lambda_T = \left[\lambda + \varrho D_{12} (h_1 - h_2) \frac{\partial c_1}{\partial T} \right]_w. \quad (11.69)$$

Numerical values for λ_T for air have been given by C.F. Hansen (1959).

11.3.3 Analogy Between Heat and Mass Transfer

If we assume constant physical properties and neglect the coupling effects ($\bar{\alpha} = 0$) as well as both the dissipation and the term due to a concentration gradient in the energy equation, Eqs. (11.60) and (11.61) have the same form:

$$u \frac{\partial T}{\partial x} + v \frac{\partial T}{\partial y} = a \frac{\partial^2 T}{\partial y^2}, \quad (11.70)$$

$$u \frac{\partial c_1}{\partial x} + v \frac{\partial c_1}{\partial y} = D_{12} \frac{\partial^2 c_1}{\partial y^2}. \quad (11.71)$$

The equations for T and c_1 are identical if the *Lewis number*

$$Le = \frac{D_{12}}{a} = \frac{Pr}{Sc} \quad (11.72)$$

has the value one. In Eq. (11.72), in analogy to the Prandtl number $\text{Pr} = \nu/a$, we introduced the *Schmidt number*

$$\text{Sc} = \frac{\nu}{D_{12}} . \quad (11.73)$$

Because Eqs. (11.70) and (11.71) have the same structure under the above conditions, there are far-reaching analogies between heat and mass transfer. For analogous boundary conditions, each relation

$$\frac{\text{Nu}}{\sqrt{\text{Re}}} = f(\text{Pr}, x^*) \quad (11.74)$$

corresponds to an analogous relation

$$\frac{\text{Sh}}{\sqrt{\text{Re}}} = f(\text{Sc}, x^*) . \quad (11.75)$$

In single-sided diffusion, because of the Eckert–Schneider condition, this means that a heat transfer problem with suction or blowing corresponds to the mass transfer problem. Therefore all heat transfer problems treated earlier in Sect. 11.2 can also be interpreted as mass transfer problems using the analogy between Eq. (11.74) and Eq. (11.75).

A. Acrivos (1960a, 1962) has considered, for example, the mass transfer for those cases which correspond to massive suction or blowing. The mass transfer in flows which lead to similar solutions have been investigated particularly thoroughly.

Note however that in practice this analogy is frequently applied by neglecting the finite velocity v_w , meaning the results can only be an approximation, cf. the example in the next section.

11.3.4 Similar Solutions

So-called wedge flows ($U \sim x^m$) lead to similar solutions for the velocity field, and do so likewise for the temperature field if the distribution of the wall temperature obeys a power law. This similarity remains even if suction or blowing is performed, as long as the blowing velocity satisfies $v_w \sim x^{(m-1)/2}$.

Since v_w is used in the Eckert–Schneider condition, the question emerges for which distributions $T_w(x)$ or $c_{1w}(x)$ the solutions for single-sided diffusion (with the additional condition (11.62)) remain similar. With Eqs. (7.32) and (7.33) we obtain the following form of the Eckert–Schneider condition for wedge flows:

$$f_w = \frac{1}{\text{Sc}(1 - c_{1w})} \left(\frac{\partial c_1}{\partial \eta} \right)_w . \quad (11.76)$$

Hence, the concentration boundary layers for all wedge flows with $c_{1w} = \text{const}$ lead to similar solutions. The same is true for the extensions to boundary layers with variable properties and to compressible boundary layers. Here it is mainly the plate boundary layer (or the supersonic flow with attached

shock wave past a wedge) and the boundary layer at a stagnation point which have been examined comprehensively.

Mass transfer and the binary boundary layers with natural convection have been considered by, among others, Y. Jaluria (1980), p. 271 and A. Mersmann (1986), p. 265. The analogy to heat transfer has mostly been exploited here.

Example 1. Mass transfer at a plate

If we approximate by neglecting the finite wall velocity v_w , in analogy to heat transfer, it follows that

$$\text{Sh}_0 = \frac{j_{1w}l}{\rho D_{12}c_{1w}} = \sqrt{\text{Re}} \left(\frac{x}{l} \right)^{-1/2} f(\text{Sc}) \quad (11.77)$$

with the limiting cases for $\text{Sc} \rightarrow 0$ and $\text{Sc} \rightarrow \infty$ taken from Table 9.1. (It was assumed that $c_{1\infty} = c_{1e} = 0$.)

Taking a finite but moderate v_w velocity into account, K. Gersten; H. Herwig (1992), p. 358 have shown the Sherwood number Sh to be

$$\frac{\text{Sh}}{\text{Sh}_0} = 1 - F(\text{Sc}) \frac{c_{1w}}{1 - c_{1w}}, \quad (11.78)$$

where the value of the function $F(\text{Sc})$ can be taken from Table 11.1. This formula can be used to estimate the error made in neglecting the Eckert–Schneider condition, cf. A. Mersmann (1986), p. 162.

Table 11.1. Numerical values of the function $F(\text{Sc})$ in Eq. (11.78), after K. Gersten; H. Herwig (1992), p. 358

Sc	0	0.1	0.6	0.72	1.0	10	∞
$F(\text{Sc})$	1.308	0.948	0.766	0.749	0.724	0.610	0.566

The extension of this formula to larger values of $c_{1w}/(1 - c_{1w})$ has been presented by A. Acrivos (1962) for $\text{Sc} = 1$ and $\text{Sc} \rightarrow \infty$. The extension to arbitrary wedge flows for $\text{Sc} \rightarrow \infty$ has been treated by K. Gersten (1974b).

Solutions of binary boundary layers which arise from adiabatic evaporation of a hydrocarbon film have been given by F. Eisfeld (1971), where variable physical properties have been taken into account.

The reference temperature method (cf. Sect. 10.3.3) also yields good results for mass transfer problems, as Y. Taitel; A. Tamir (1975) have shown.

The system of three coupled boundary layers (momentum, heat and mass transfer) has been computed for evaporation and sublimation processes by W. Splettstösser (1975).

Example 2. Injection of a different gas (transpiration cooling)

If a different gas is blown out for transpiration cooling, a binary boundary layer is at hand. Very light gases (helium, hydrogen) have a particularly good cooling effect. Figure 11.16 shows the Nusselt number as a function of the blowing parameter for helium injected into an air flow at a flat plate (after W. Wuest (1963)). For

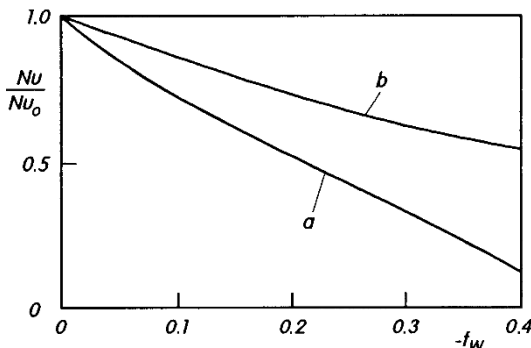


Fig. 11.16. Effect of blowing on the heat transfer at a flat plate at zero incidence (transpiration cooling), after J.R. Baron; P.E. Scott (1960).
 (a) blowing helium into air
 (b) blowing air into air

comparison, the curve for the blowing of air (single-substance boundary layer, see Sect. 11.2) is also drawn. The considerable advantage of blowing a lighter gas can be seen easily.

The influence of different ratios of molecular weights of the two gases involved in the blowing of light gases has been examined by C.R. Faulders (1961).

A method of calculating binary boundary layers at a stagnation point with temperature dependent physical properties has been given by J. Steinheuer (1971) and this has been applied to the example of ablation cooling by pyrolyzing Teflon.

Experimental investigations into the blowing of a foreign gas in supersonic boundary layers concentrate almost exclusively on the measurement of the adiabatic wall temperature.

Example 3. Boundary layer of a dissociated gas

As already mentioned, a dissociated gas is frequently represented as a mixture of a molecular gas and an atomic gas. The concentration c_1 is the degree of dissociation. A fundamental piece of work on boundary layers of dissociated air in the region of the stagnation point is that of J.A. Fay; F.R. Riddell (1958). Here again there are similar solutions to the boundary-layer equations. Figure 11.17 shows, as an example from this work, the heat transfer in the stagnation point as a function of the recombination parameter C_R of the wall surface. If this parameter is very large, the system is in equilibrium (fully catalytic wall). For smaller values of this parameter, this solution is dependent on the catalytic behaviour of the wall. The dashed curve depicts the part of the heat transfer due to heat conduction for the catalytic wall. The remaining part of the heat transfer is due to the diffusion from Eq. (11.56). The curve for the non-catalytic wall is also shown for comparison. This curve shows a considerable reduction in the heat transfer when the recombination parameter is small.

An integral method for the non-equilibrium boundary layer at a flat plate has been developed by M. Jischa (1982).

Boundary layers of dissociated gases have been treated comprehensively by H.W. Dorrance (1962), p. 69 and P.M. Chung (1965).

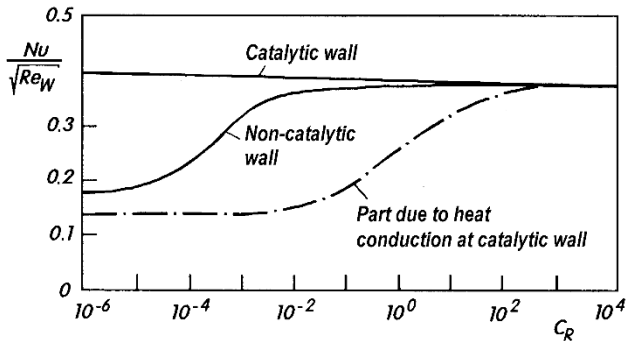


Fig. 11.17. Dependence of the heat transfer at the stagnation point of a gas flow on the recombination parameter C_R of the wall surface, after J.A. Fay; F.R. Riddell (1958)

12. Axisymmetric and Three-Dimensional Boundary Layers

In the previous chapters, the calculation of boundary layers was restricted to the plane case, where the two velocity components depended only on two spatial coordinates. There was no velocity component present in the direction of the third spatial coordinate.

The general case of a boundary layer with velocity components in all three spatial directions dependent on all three spatial coordinates is considerably more complicated than the plane boundary layer.

On the other hand, the calculation of axisymmetric boundary layers presents far fewer difficulties, and is hardly any more complicated than the plane case. Here a third velocity component in the circumferential direction may even be present if the symmetric body rotates about its axis.

Therefore this chapter has two sections: in the first section we will treat axisymmetric boundary layers, both with and without circumferential velocity components; the second section is then dedicated to three-dimensional boundary layers.

12.1 Axisymmetric Boundary Layers

12.1.1 Boundary-Layer Equations

We consider a body of revolution in a flow in the direction of its axis. The curvilinear orthogonal coordinate system shown in Fig. 12.1 is used to describe the boundary layer on such a body. The geometry of the body is described by a function $r_w(x)$, where $r_w(x)$ is the radius of a section of the body perpendicular to its axis. The coordinate x is an arc length measured along a meridian section from the stagnation point. The y coordinate is perpendicular to the surface; z is in the circumferential direction. Let the velocity components be denoted by u (parallel to the wall in the meridian direction), v (perpendicular to the wall) and w (parallel to the wall in the circumferential direction). The velocity of the outer flow (potential flow) $U(x)$ is assumed to be known.

If we assume that the Reynolds number $\text{Re} = Vl/\nu$ is large, the flow again divides into two regions. The radius of curvature at the stagnation point can, for example, be used as a reference length l . If the Navier-Stokes equations

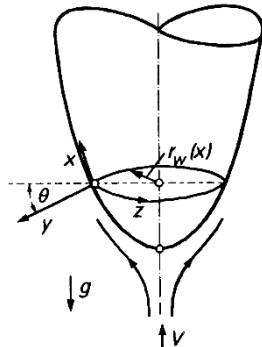


Fig. 12.1. Coordinate system for axisymmetric boundary layers, $\theta = \alpha - \pi/2$

for the coordinate system shown in Fig. 12.1 and the energy equation are submitted to an analogous boundary-layer transformation, the limiting case $\text{Re} \rightarrow \infty$ yields the following system of boundary-layer equations, in dimensional notation. (Initially we consider the case without rotation, cf. E. Boltze (1908) and M. Van Dyke (1962c):

$$\frac{\partial(r_w \varrho u)}{\partial x} + \frac{\partial(r_w \varrho v)}{\partial y} = 0, \quad (12.1)$$

$$\varrho \left(u \frac{\partial u}{\partial x} + v \frac{\partial u}{\partial y} \right) = -\varrho g \sin \alpha - \frac{dp}{dx} + \frac{\partial}{\partial y} \left(\mu \frac{\partial u}{\partial y} \right), \quad (12.2)$$

$$\varrho c_p \left(u \frac{\partial T}{\partial x} + v \frac{\partial T}{\partial y} \right) = \frac{\partial}{\partial y} \left(\lambda \frac{\partial T}{\partial y} \right) + \beta T u \frac{dp}{dx} + \mu \left(\frac{\partial u}{\partial y} \right)^2. \quad (12.3)$$

The pressure gradient obeys

$$\frac{dp}{dx} = -\varrho_e U \frac{dU}{dx}, \quad (12.4)$$

where the index e denotes the outer edge of the boundary layer ($U(x) = u_e(x)$).

It is worth noting that, compared to the plane boundary-layer equations, it is only the continuity equation which has undergone a change. Comparison with the system (10.4) to (10.6) will show this. For this reason one often finds that both plane and axisymmetric boundary layers are treated together in the literature. The continuity equation is then written in the form

$$\frac{\partial(r_w^j \varrho u)}{\partial x} + \frac{\partial(r_w^j \varrho v)}{\partial y} = 0, \quad (12.5)$$

where $j = 1$ is the axisymmetric case and $j = 0$ the plane case.

One particular difference to the plane boundary-layer equations should be emphasised here: whereas the geometry of the body does not enter into

the calculation of plane boundary layers, apart from the buoyancy term proportional to $\sin \alpha$, the geometry of the body $r_w(x)$ now appears explicitly along with the outer velocity $U(x)$ in the system of equations (actually only in the continuity equation). Therefore three functions have to be prescribed for the boundary-layer calculation: $U(x)$, $r_w(x)$ and $T_w(x)$ or $q_w(x)$.

Note too that the boundary layer can also exist on the inner side of a body, as in the case of boundary layers in nozzles or diffusers. The same equations are then valid. This can easily be seen by changing the signs of y and v simultaneously.

Note (Transversal curvature)

For $r_w(x) = \text{const}$, the system (12.1) to (12.3) reduces to the equations for plane boundary layers, and so the boundary layer on a circular cylinder at zero incidence is identical to the plate boundary layer. The system (12.1) to (12.3) is only valid as long as the boundary-layer thickness δ is very small compared to the radius, i.e. for $\delta/r_w \ll 1$. This is satisfied for flow past a cylinder in the region close to the leading edge. Because the thickness of the boundary layer then increases, this condition breaks down further upstream. In the region $\delta/r_w = O(1)$, transversal curvature then comes into play. However this is a higher order boundary-layer effect, and will be discussed in more detail in Chap. 14.

12.1.2 Mangler Transformation

Because the differences from plane boundary layers are so little, the question emerges of whether there is a transformation with which the axisymmetric boundary-layer equations can be reduced to the plane boundary-layer equations. Indeed W. Mangler (1948) presented such a transformation. It basically allows the calculation of the boundary layer at a body of revolution to be reduced to the calculation of the boundary layer at a suitable plane (cylindrical) body.

If l is the reference length, the transformation formulae read:

$$\bar{x} = \frac{1}{l^2} \int_0^x r_w^2(x) dx, \quad \bar{y} = \frac{r_w(x)}{l} y, \quad \sin \bar{\alpha} = \frac{l^2}{r_w^2} \sin \alpha, \quad (12.6)$$

$$\bar{u} = u, \quad \bar{v} = \frac{l}{r_w} \left(v + \frac{1}{r_w} \frac{dr_w}{dx} y u \right), \quad \bar{U} = U, \quad \bar{T} = T. \quad (12.7)$$

If we take the following relation into account:

$$\frac{\partial f}{\partial x} = \frac{r_w^2}{l^2} \frac{\partial f}{\partial \bar{x}} + \frac{1}{r_w} \frac{dr_w}{dx} \bar{y} \frac{\partial f}{\partial \bar{y}}, \quad \frac{\partial f}{\partial y} = \frac{r_w}{l} \frac{\partial f}{\partial \bar{y}}, \quad (12.8)$$

we can easily verify that the formulae (12.6) reduce the system (12.1) to (12.3) to the system (10.4) to (10.6).

This transformation can therefore be used to determine the boundary layer at a body of revolution $r_w(x)$ with the potential theory velocity distribution $U(x)$ in such a manner that one calculates the plane boundary layer

with velocity distribution $\overline{U}(\bar{x})$, where $\overline{U} = U$ must hold, and the relation between x and \bar{x} is given in Eq. (12.6). The transformation equations (12.7) can then be used to compute the velocities u, v for the axisymmetric boundary layer from the velocities \bar{u}, \bar{v} for the plane boundary layer.

Example: Axisymmetric stagnation point

For such boundary layers we have, cf. Sect. 5.2.3

$$r_w(x) = x; \quad U(x) = ax. \quad (12.9)$$

Thus Eq. (12.6) yields

$$\bar{x} = \frac{x^3}{3l^2} \quad \text{or} \quad x = (3l^2\bar{x})^{1/3}.$$

The velocity at the outer edge of the appropriate plane boundary layer is therefore

$$\overline{U}(\bar{x}) = a(3l^2)^{1/3}\bar{x}^{1/3}.$$

This plane potential flow belongs to the wedge flows with $m = 1/3$ and wedge angle $\beta = 2m/(m+1) = 1/2$ treated in Sect. 7.2.2.

The relation between the wedge flow with $\beta = 1/2$ and the axisymmetric stagnation-point flow has already been mentioned in Sect. 7.2.2, cf. Eq. (7.34).

12.1.3 Boundary Layers on Non-Rotating Bodies of Revolution

The numerical methods used to solve plane boundary layers can easily be applied to axisymmetric boundary layers. Similar solutions have been investigated by Th. Geis (1955).

Integral methods have also been developed for axisymmetric boundary layers. These are again based on the integral relations for momentum, kinetic energy and thermal energy. For boundary layers with constant physical properties, neglecting the dissipation in the energy equation, they read:

$$\frac{d}{dx}(U^2\delta_2) + \delta_1 U \frac{dU}{dx} + jU^2 \frac{\delta_2}{r_w} \frac{dr_w}{dx} = \frac{\tau_w}{\varrho}, \quad (12.10)$$

$$\frac{d}{dx}(U^3\delta_3) + jU^3 \frac{\delta_3}{r_w} \frac{dr_w}{dx} = \frac{2}{\varrho} \mathcal{D}, \quad (12.11)$$

$$\frac{d}{dx}[(T_w - T_\infty)U\delta_T] + j(T_w - T_\infty)U \frac{\delta_T}{r_w} \frac{dr_w}{dx} = \frac{q_w}{\varrho c_p}. \quad (12.12)$$

The definitions of $\delta_1, \delta_2, \delta_3$ and δ_T are the same as in plane boundary layers, cf. Eqs. (7.98), (7.99), (9.60). For $j = 0$ the equations become the already known integral equations (7.100), (7.104) and (9.59).

An integral method for axisymmetric boundary layers ($j = 1$) has been developed by, for example, F.W. Scholkmeyer (1949). N. Rott; L.F. Crabtree (1952) have shown that even for these boundary layers, a quadrature formula can be given. It reads:

$$\frac{U\delta_2^2}{\nu} = \frac{a}{r_w^2 U^b} \int_0^x r_w^2 U^b dx. \quad (12.13)$$

As would be expected, this formula reduces to Eq. (8.23) for $r_w = \text{const.}$ The constants a and b may be taken from the plane case. If we demand, however, that both the plate boundary layer (close to the leading edge of the circular cylinder at zero incidence) and the boundary layer at the axisymmetric stagnation point are correctly represented, then for $\Gamma > 0$ we find the numerical values $a = 0.441$ and $b = 4.19$. For the wall shear stress we again have Eq. (8.29), just as Eqs. (8.12) and (8.16) also remain unchanged.

Both F.W. Scholkemeier (1949) and J. Pretsch (1941a) have used the quadrature formula to compute some examples. The calculation of the boundary layer at a sphere has been carried out by S. Tomotika (1935) for both the potential theory pressure distribution (leading to a separation angle of about $\varphi_s = 105^\circ$) and for pressure distributions measured at different Reynolds numbers, cf. the summary by F.M. White (1974), p. 346.

The transformations of H. Görtler (Sect. 7.3.1), Illingworth–Stewartson (Sect. 10.4.3) and Saville–Churchill (Sect. 10.5.2) have been combined with the Mangler transformation and applied to axisymmetric boundary layers, cf. F.M. White (1974), p. 604 and D.A. Saville; S.W. Churchill (1967).

In what follows we will discuss some examples of axisymmetric boundary layers.

Axisymmetric stagnation point. As has been shown in Sect. 5.2.3, this case is an exact solution of the Navier–Stokes equations, since the terms which are neglected in the boundary–layer equations vanish anyway in the momentum equation in the x direction (in Sect. 5.2.3, r was used instead of x) and in the energy equation. (In the stagnation–point plane, the coordinate system shown in Fig. 12.1 is identical to the cylindrical coordinate system used in Sect. 5.2.3 if we set $x = r$ and $y = z$.) The pressure gradient $\partial p / \partial y$ neglected in the boundary–layer theory may then be determined afterwards from the momentum equation in the y direction. The velocity profile is shown in Fig. 5.6. Some important numerical values for the velocity field are to be found in Table 5.1.

H. Herwig; G. Wickern (1986) have presented some numerical values regarding the dependence of the heat transfer on the Prandtl number, for both constant and variable physical properties (method of property ratios), cf. H. Herwig (1987). According to this, for the Prandtl number $\text{Pr}_\infty = 0.7$ we find

$$\frac{\text{Nu}}{\text{Nu}_{c.p.}} = \left(\frac{\varrho_w \mu_w}{\varrho_\infty \mu_\infty} \right)^{0.270} \left(\frac{\varrho_w}{\varrho_\infty} \right)^{-0.075} \left(\frac{\text{Pr}_w}{\text{Pr}_\infty} \right)^{-0.384} \left(\frac{c_{pw}}{c_{p\infty}} \right)^{0.5} \quad (12.14)$$

with

$$\text{Nu}_{c.p.}/\sqrt{\text{Re}} = 0.665, \quad U = ax, \quad V = al. \quad (12.15)$$

Large and small temperature ratios T_w/T_∞ have been investigated by C.F. Dewey Jr.; J.F. Gross (1967), including also the case of blowing. Details on suction and blowing with the limiting cases $v_w \rightarrow +\infty$ and $v_w \rightarrow -\infty$ are to be found in the work by W.E. Stewart; R. Prober (1962) and K. Gersten (1973a). Finally, for details on binary boundary layers at the stagnation point, the work by H.W. Dorrance (1962) is recommended.

Axisymmetric wall jet. If a axisymmetric free jet approaches a flat wall at right angles, a wall jet radially extending on all sides appears at some distance from the

point of impact. With $r_w = x$ and $U = 0$, this obeys the equations (12.1) to (12.3). These again are similar solutions of the boundary-layer equations which lead to the same ordinary differential equation as in the plane case, cf. M.B. Glauert (1956b) and N. Riley (1958). All results can be therefore carried over from the plane wall jet.

Radial jet. A radial jet arises if, for example, fluid is blown out of a hollow tube through a slit in the circumference into an outer region where the fluid is at rest. The fluid then flows as an axisymmetric free jet radially outwards. Again we have $r_w = x$ and $U = 0$ in Eqs. (12.1) and (12.3). Here again it is possible to transfer results from the plane free jet, cf. H.B. Squire (1955).

Supersonic flow at a cone. As long as the shock wave remains attached to the apex of the cone, we have $r_w = \alpha x$, $U = \text{const}$. This flow is related to plate flow and can be reduced to this using the Mangler transformation. Just as for plate flow, we therefore also obtain an adiabatic wall temperature independent of x , as shown in Fig. 12.2. The recovery factor depicted here is also independent of the Mach number (for $\text{Ma} < 5$), and the agreement between theory and measurement is very good, cf. W. Hantzsche; H. Wendt (1941). Further measurements on other cones and also on a *paraboloid* are to be found in the work of B. des Clers; J. Sternberg (1952) and R. Scherrer (1951).

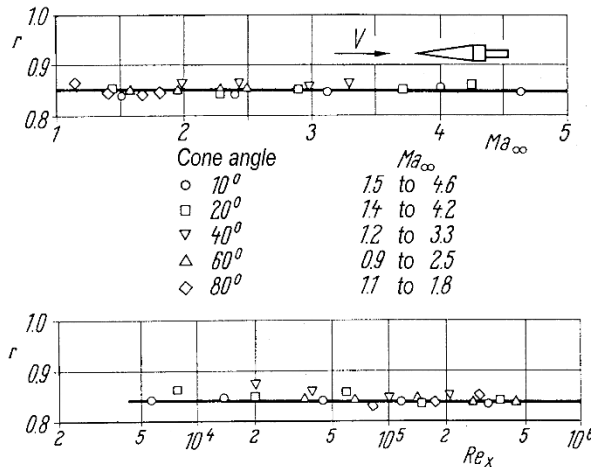


Fig. 12.2. Measured recovery factor for the laminar boundary layer at cones in supersonic flow for different Mach and Reynolds numbers, cf. G.R. Eber (1952). Comparison with the theory from Eq. (9.86), see Fig. 9.6

The binary boundary layer at a cone has also been investigated by W. Wuest (1963). In order to obtain similar solutions of the boundary-layer equations, we must have the same distribution of the blowing velocity $v_w(x)$ as in the case of the plate, i.e. $v_w \sim x^{-1/2}$.

Nozzle flow. An example of a boundary layer on the “inner side” of a body of revolution is the flow in a nozzle with a circular cross-section. A. Michalke (1962) has carried out theoretical and experimental investigations into this topic.

Natural convection. Here too it is possible to reduce the computation of the axisymmetric boundary layer to that of a plane boundary layer by means of the Mangler transformation. W.H. Braun et al. (1961) have considered those body

contours which lead to similar solutions. Among these is also the “lower stagnation point”. Details on the computation of natural convection at bodies of revolution with vertical axes using series expansions and integral methods are to be found in the work by Y. Jaluria (1980), p. 84.

F.N. Lin; B.T. Chao (1974, 1976) have investigated arbitrary body contours, and there are, in particular, many pieces of work on the sphere, e.g. T. Chaing et al. (1964).

A. Acrivos (1960b) has treated the limiting case $\text{Pr} \rightarrow \infty$. The Nusselt number at the sphere with $T_w = \text{const}$ is found to be

$$\text{Nu}_m = 0.589(\text{Gr Pr})^{1/4} \quad (\text{Pr} \rightarrow \infty), \quad (12.16)$$

where the Nusselt number and the Grashof number are formed with the diameter of the sphere.

Details on natural convection may be found as follows: for the case of the paraboloid, see I.C. Walton (1974); for the cone, see R.G. Hering; R.J. Grosh (1962).

12.1.4 Boundary Layers on Rotating Bodies of Revolution

If the body of revolution itself rotates, the no-slip condition produces an additional velocity component in the circumferential direction. Within the boundary layer this tends to zero as one moves outwards. The flow is still axisymmetric, i.e. independent of the circumferential component z , see Fig. 12.1. The boundary-layer equations (12.1) to (12.3) are then extended by a momentum equation in the circumferential direction, and by some additional terms dependent on w in the previous equations. We have:

$$\boxed{\frac{\partial(r_w \varrho u)}{\partial x} + \frac{\partial(r_w \varrho v)}{\partial y} = 0,} \quad (12.17)$$

$$\boxed{\varrho \left(u \frac{\partial u}{\partial x} + v \frac{\partial u}{\partial y} - \underline{\frac{w^2}{r_w} \frac{dr_w}{dx}} \right) = -\varrho g \sin \alpha - \frac{\partial p}{\partial x} + \frac{\partial}{\partial y} \left(\mu \frac{\partial u}{\partial y} \right),} \quad (12.18)$$

$$\boxed{\varrho \left(u \frac{\partial w}{\partial x} + v \frac{\partial w}{\partial y} + \underline{\frac{uw}{r_w} \frac{dr_w}{dx}} \right) = \frac{\partial}{\partial y} \left(\mu \frac{\partial w}{\partial y} \right),} \quad (12.19)$$

$$\boxed{\begin{aligned} \varrho c_p \left(u \frac{\partial T}{\partial x} + v \frac{\partial T}{\partial y} \right) &= \frac{\partial}{\partial y} \left(\lambda \frac{\partial T}{\partial y} \right) \\ &+ \beta T u \frac{\partial p}{\partial x} + \mu \left[\left(\frac{\partial u}{\partial y} \right)^2 + \underline{\left(\frac{\partial w}{\partial y} \right)^2} \right]. \end{aligned}} \quad (12.20)$$

The underlined terms have been added to the previous equations as “coupling terms”.

In computing this boundary layer using an integral method, as well as the momentum-integral equation in the meridian direction (x direction), we also use the momentum-integral equation in the azimuthal direction (z direction).

These two momentum-integral equations (for constant physical properties) read:

$$U^2 \frac{d\delta_{2x}}{dx} + U \frac{dU}{dx} (2\delta_{2x} + \delta_{1x}) + \frac{1}{r_w} \frac{dr_w}{dx} (U^2 \delta_{2x} + w_w^2 \delta_{2z}) = \frac{\tau_{wx}}{\varrho}, \quad (12.21)$$

$$\frac{w_w}{r_w^3} \frac{d}{dx} (U r_w^3 \delta_{2xz}) = -\frac{\tau_{wz}}{\varrho}. \quad (12.22)$$

The components of the wall shear stress are

$$\tau_{wx} = \mu \left(\frac{\partial u}{\partial y} \right)_w; \quad \tau_{wz} = \mu \left(\frac{\partial w}{\partial y} \right)_w \quad (12.23)$$

and the displacement and momentum thicknesses are

$$\delta_{1x} = \int_0^\infty \left(1 - \frac{u}{U} \right) dy; \quad \delta_{2x} = \int_0^\infty \frac{u}{U} \left(1 - \frac{u}{U} \right) dy; \quad (12.24)$$

$$\delta_{2z} = \int_0^\infty \left(\frac{w}{w_w} \right)^2 dy; \quad \delta_{2xz} = \int_0^\infty \frac{u}{U} \frac{w}{w_w} dy, \quad (12.25)$$

where $w_w = r_w \omega$ is the local circumferential velocity.

Integral methods using these integral relations have been developed by H. Schlichting (1953), E. Truckenbrodt (1954a) and O. Parr (1963).

In what follows we shall discuss some different solutions:

Rotating disk in an axial flow. The simplest case of a boundary layer at a rotating body has been treated in Sect. 5.2.4: the disk rotating in a fluid at rest. A generalisation of this case is the rotating disk (radius R , angular velocity ω) in a flow of velocity V in the direction of the axis of rotation. In this case the flow depends not only on the Reynolds number $Re = \omega R^2 / \nu$, but also on the rotation parameter $V/\omega R$ which represents the ratio of the free stream velocity to the circumferential velocity. Exact solutions have been given by D.M. Hannah (1952) and A.N. Tifford; S.T. Chu (1952), while H. Schlichting; E. Truckenbrodt (1952) have presented approximate solutions. Figure 12.3 shows the dependence of the moment coefficient $c_M = 2M/(\varrho \omega^2 R^5)$ obtained from these calculations on the Reynolds number and the rotation parameter. Here M is the moment of the front side of the disk. The special case of $V = 0$ from Sect. 5.2.4 is also depicted. It is seen from Fig. 12.3 that, if the rotation is constant, the moment increases considerably with increasing free stream velocity V .

The turbulent part of this diagram will be discussed more closely in Sect. 20.1.3.

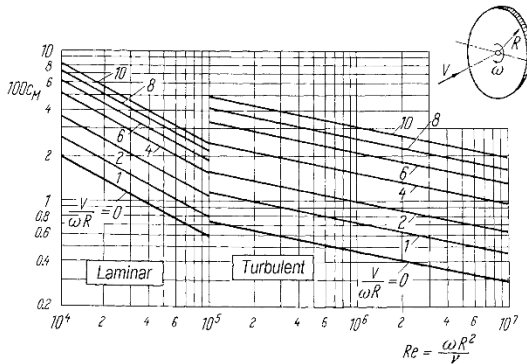


Fig. 12.3. Moment coefficient of a rotating disk in axial flow, after H. Schlichting; E. Truckenbrodt (1952) and E. Truckenbrodt (1954a).
 $c_M = 2M/(\rho\omega^2 R^5)$,
 M = moment of the front side of the disk
 $V = 0$; cf. Fig. 5.10

Rotating flow over the ground. Closely related to the flow at a rotating disk is the flow which arises at a fixed wall when the fluid circulates with constant angular velocity at a great distance from the wall, cf. Fig. 12.4. This case has been treated by U.T. Bödewadt (1940), J.E. Nydahl (1971) and K. Stewartson (1953). As in the case of a rotating disk in surroundings at rest, a *secondary flow* also arises for this flow, but with the opposite sign. The centrifugal force and the radial pressure gradient for circulating particles at great distances from the wall are in equilibrium. Those particles close to the wall whose circumferential velocity is retarded are under the same pressure gradient directed inwards. However the centrifugal force they are subjected to is greatly decreased. In this manner there is a radial flow inwards close to the ground and, for reasons of continuity, a rising flow in the axial direction, as is shown in Fig. 12.4.

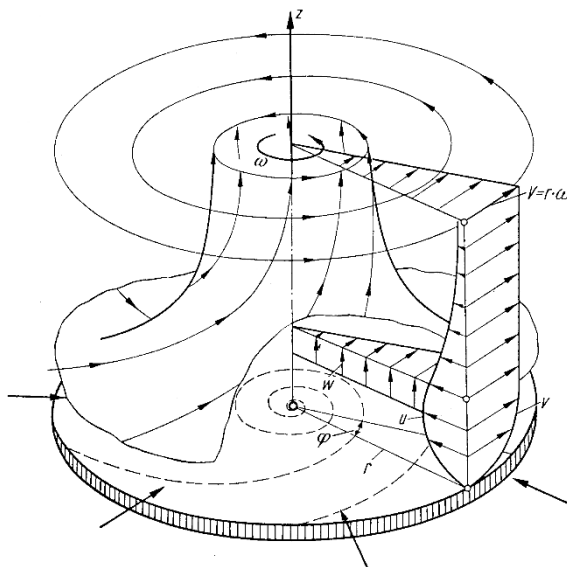


Fig. 12.4. Rotating flow over the ground. Velocity components: u : radial, v : azimuthal, w : axial

A flow which arises in the boundary layer in this manner such that its direction deviates from that of the outer flow is generally called a *secondary flow*.

The secondary flow discussed here can be seen very clearly in a tea cup. Initiating the rotating flow by stirring strongly and then leaving the flow to itself will prove that, after a short time, a radially inwards flow close to the ground is formed. This is the reason why tea leaves collect together in the middle of the base of the cup.

The general outer flow with circular streamlines has been investigated by A. Mager; A.G. Hansen (1952) and E. Becker (1959a). If the outer flow has the form of a vortex source, the kind of boundary layer treated by G. Vogelpohl (1944) emerges.

Swirling radial jet. As already mentioned, a radial jet is obtained when fluid is blown out of a slit arranged over the circumference of a pipe. If this pipe rotates, a swirling radial jet is formed. This has been treated by L.G. Loitsianski (1967), p. 217.

Swirling nozzle flow. The swirling convergent flow through a conical nozzle with angular momentum is shown in Fig. 12.5. This was investigated by K. Garbsch (1956). The potential theory kernel flow is produced by a sink of strength Q in the apex of the cone and a potential vortex on the axis of the cone with vortex strength Γ is formed. Two special cases of this flow have been calculated using integral methods. Pure sink flows ($\Gamma = 0$) have been investigated by A.M. Binnie; D.P. Harris (1950), while G.I. Taylor (1950) and J.C. Cooke (1952) have looked at pure vortex flows ($Q = 0$). In the latter case, a boundary layer forms on the wall of the nozzle, as in Fig. 12.5. This even has velocity components in the direction of the apex of the cone, whereas the inviscid kernel flow, a pure vortex flow, only has circumferential components. The *secondary flow* arising in the boundary layer transports fluid towards the apex of the cone. For comparison, see the work by H.E. Weber (1956).

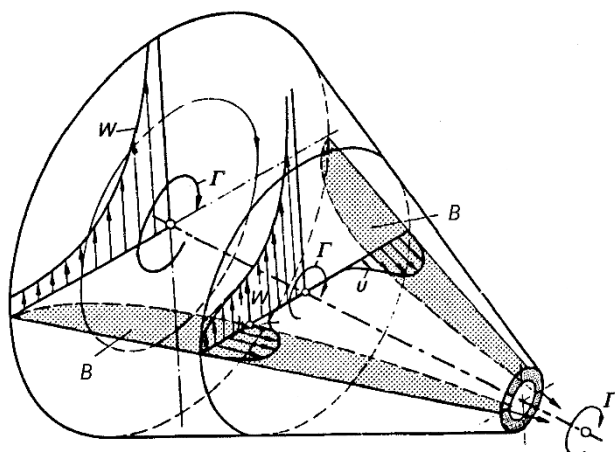


Fig. 12.5. Swirling flow in a convergent conical channel, after G.I. Taylor (1950).
B: boundary layer at the wall of the cone with secondary motion towards the apex

Rotating sphere. A sphere in an axial flow exhibits a considerable increase in the drag if it is rotated. This has been shown by measurements by C. Wieselsberger (1927) and S. Luthander; A. Rydberg (1935) and has to do with the position of the separation point. Figure 12.6 shows the effect of rotation on the separation, after calculations by N.E. Hoskin (1955). For the value $\omega R/V = 5$, the separation point lies about 10° further forwards compared to the case where there is no rotation. The physical origin of this is that the fluid in the boundary layer experiences the effect of the centrifugal force, and this acts towards the equatorial plane as an additional adverse pressure gradient.

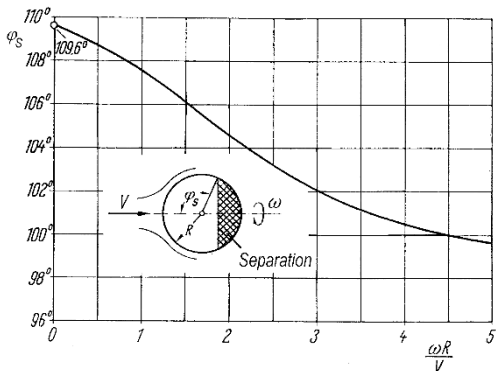


Fig. 12.6. Position of the separation point in the laminar boundary layer at a sphere in a flow in the direction of its axis of rotation

The special case of a rotating sphere in a fluid at rest has been treated by L. Howarth (1951a) and S.D. Nigam (1954). An extension to *ellipsoids of revolution* is due to B.S. Fadnis (1954). At the poles the flow acts as at a rotating disk and close to the equator it acts as at a rotating cylinder. There is a flow of fluid towards the poles and a flow away from the equator. Assuming the equatorial cross-section and the angular velocity remain the same, this flow is larger the more slender the body, cf. W.H.H. Banks (1965).

Extensions to other bodies of revolution in flows in the axial direction are to be found in the literature in H. Schlichting (1982), p. 249. Application to compressible flows is to be found in J. Yamaga (1956).

12.1.5 Free Jets and Wakes

In Sect. 5.2.5 we presented the axisymmetric free jet as an exact solution of the Navier–Stokes equations in spherical polar coordinates. It emerged that for large Reynolds numbers, i.e. for $\nu \rightarrow 0$, the jet flow is restricted to a small area close to the axis. Since we are only interested in this “boundary-layer solution”, the description of the jet flow may be carried out in cylindrical coordinates. Here x is the axial coordinate in the main flow direction (velocity component u) and the radial coordinate is r (with v as the radial velocity component).

Using this system of cylindrical coordinates, the boundary-layer equations for constant pressure flows (with $\partial^2 u / \partial x^2 \ll \partial^2 u / \partial r^2$) read

$$\frac{\partial(r\varrho u)}{\partial x} + \frac{\partial(r\varrho v)}{\partial r} = 0, \quad (12.26)$$

$$\varrho \left(u \frac{\partial u}{\partial x} + v \frac{\partial u}{\partial r} \right) = -\varrho g + \frac{1}{r} \frac{\partial}{\partial r} \left(\mu r \frac{\partial u}{\partial r} \right), \quad (12.27)$$

$$\varrho c_p \left(u \frac{\partial T}{\partial x} + v \frac{\partial T}{\partial r} \right) = +\frac{1}{r} \frac{\partial}{\partial r} \left(\lambda r \frac{\partial T}{\partial r} \right) + \mu \left(\frac{\partial u}{\partial r} \right)^2. \quad (12.28)$$

The boundary conditions read

$$\begin{aligned} r = 0 : \quad v &= 0, \quad \frac{\partial u}{\partial r} = 0, \quad \frac{\partial T}{\partial r} = 0 \\ r \rightarrow \infty : \quad u &= 0, \quad T = T_\infty. \end{aligned} \quad (12.29)$$

When compared to the plane boundary-layer equations for constant pressure, we see that both the continuity equation *and* the terms describing the friction force and the heat conduction have changed.

This system of equations describes the axisymmetric momentum jet, buoyant jet and wake. These will be treated in more detail in what follows.

Momentum jet. The jet emerges from a point shaped opening and is characterised by the fact that, for constant physical properties, its kinematic momentum

$$K_a = 2\pi \int_0^\infty u^2 r dr = \text{const} \quad (12.30)$$

is constant. In this case the system (12.26) to (12.28) yields similar solutions.

With the trial solutions

$$u = \gamma^2 \frac{\nu}{x} \frac{F'}{\eta}, \quad v = \gamma \frac{\nu}{x} \left(F' - \frac{F}{\eta} \right), \quad \eta = \gamma \frac{r}{x} \quad (12.31)$$

we use Eqs. (12.26) and (12.27) to form the following ordinary differential equation for $F(\eta)$:

$$\eta F'' + FF' - F' = 0 \quad (12.32)$$

with the boundary conditions

$$\eta = 0 : \quad F = 0, \quad F' = 0; \quad \eta \rightarrow \infty : \quad F' = 0. \quad (12.33)$$

The solution reads

$$F(\eta) = \frac{4\eta^2}{1 + \eta^2}. \quad (12.34)$$

Therefore the kinematic momentum (see Eq. (5.90) with $\gamma = 1/\theta_0$) is

$$K_a = \frac{64}{3} \pi \gamma^2 \nu^2, \quad (12.35)$$

from which we obtain the solutions for the velocity field:

$$u = \frac{3}{8\pi} \frac{K_a}{\nu x} \frac{1}{(1 + \eta^2)^2}, \quad (12.36)$$

$$v = \frac{1}{2} \sqrt{\frac{3K_a}{\pi}} \frac{\eta}{x} \frac{1 - \eta^2}{(1 + \eta^2)^2}, \quad (12.37)$$

$$\eta = \frac{1}{8} \sqrt{\frac{3K_a}{\pi}} \frac{1}{\nu x}. \quad (12.38)$$

The volume flux in the jet, which grows with increasing distance from the jet outlet because of the side entrainment, is simply

$$Q = 2\pi \int_0^\infty ur dr = 8\pi\nu x. \quad (12.39)$$

This formula is to be compared with Eq. (7.56) for the plane jet. We have the unusual result for the axisymmetric jet that the volume flux is independent of the jet momentum. As can easily be seen from the results Eq. (12.36) and (12.38), a jet with larger K_a remains more slender than a jet with smaller K_a . This latter has a circumferentially large entrainment surface, so that the amount of fluid entrained is the same for both jets (at equal ν).

The axisymmetric jet in compressible flow has been treated by M.Z. Krzywoblocki (1949) and D.C. Pack (1954). For a jet in the subsonic region, the density is larger and the temperature smaller on the jet axis than on the edge of the jet.

If a weak angular momentum is superimposed on the jet, the development of the angular momentum downstream can be calculated (cf. H. Görtler (1954)). He has shown that the maximum circumferential velocity decreases faster than that at the axis of the jet.

Particular emphasis is drawn to the fact that the jet momentum in Eq. (12.30) is only constant if no walls are at hand in the flow field. As has been described in Sect. 5.2.5, the entire flow field consists of the actual jet flow close to the axis and the induced flow caused by the mixing effect. Now if, for example, the jet corresponding to Fig. 7.7 exits a wall at right angles to it, the interaction between the jet flow and the induced flow leads to a slow decrease in the jet momentum, cf. W. Schneider (1985). The decrease in the jet momentum corresponds to the total force on the wall arising from the distribution of the induced pressure on the wall. The induced flow here is not a potential flow as in the case of the plane free jet, but rather is viscous and rotational. Far downstream boundary-layer theory is no longer valid since, as the jet momentum decreases, the radius of the jet flow close to the axis grows without limit. A recirculation region is formed; this has been seen in laboratory experiments and has been computed by means of numerical solution of the Navier-Stokes equations, cf. E. Zauner (1985) and W. Schneider et al. (1987).

Buoyant jet. A buoyant jet will form above a “point-shaped” energy source (e.g. a hot body). This leads to similar solutions in the far field, i.e. at some distance away. The corresponding plane jet has already been treated in Sect. 10.5.4. According to calculations by T. Fujii (1963), with the jet power (energy release per unit time)

$$\dot{Q} = 2\pi \int_0^\infty \varrho c_p u(T - T_\infty) r dr = \text{const}, \quad (12.40)$$

and constant physical properties, it is found that

$$u_{\max} = A(\text{Pr}) \sqrt{\frac{g\beta_\infty \dot{Q}}{2\pi\mu c_p}}, \quad (12.41)$$

$$T_{\max} - T_\infty = B(\text{Pr}) \frac{\dot{Q}}{2\pi\mu c_p x}, \quad (12.42)$$

$$\delta \sim \left(\frac{c_p \varrho \nu^3}{g\beta \dot{Q}} \right)^{1/4} x^{1/2}. \quad (12.43)$$

The factors are still dependent on the Prandtl number. For $\text{Pr} = 0.7$ we have $A = 0.938$ and $B = 0.481$. Up until now we have assumed that the initial momentum of the buoyant jet vanishes. Jets which have a finite initial momentum and which are subjected to buoyancy forces because their temperatures differ from the surrounding temperature have been investigated by J.C. Mollendorf; B. Gebhart (1973) and W. Schneider; K. Potsch (1979). These jets start off initially as momentum jets but with increasing buoyancy, their momentum flux in the direction of flow grows until finally the jets behave asymptotically as pure buoyant jets.

See also the summary on buoyant jets by J.S. Turner (1969, 1973).

Axisymmetric wake. With the help of the system of equations (12.26) to (12.28), we can treat the wake which appears behind a body of revolution in an axial flow. The calculation is carried out just as for the plane wake, cf. Sect. 7.5.1. Let U_∞ be the free stream velocity and $u(x, r)$ be the velocity in the wake, so that corresponding to Eq. (7.86),

$$u_1(x, r) = U_\infty - u(x, r) \quad (12.44)$$

is the velocity defect. This is very small compared to U_∞ at large distances behind the body, so that terms quadratic in u_1 can be neglected. With this simplification, Eqs. (12.26) and (12.27) for $u_1(x, r)$ yield the linear differential equation

$$U_\infty \frac{\partial u_1}{\partial x} = \frac{\nu}{r} \frac{\partial}{\partial r} \left(r \frac{\partial u_1}{\partial r} \right). \quad (12.45)$$

Using the trial solution

$$u_1 = U_\infty C \left(\frac{x}{l} \right)^{-m} F(\eta), \quad \eta = \frac{r}{2} \sqrt{\frac{U_\infty}{\nu x}} \quad (12.46)$$

we obtain the following differential equation for the function $F(\eta)$:

$$(\eta F')' + 2\eta^2 F' + 4m\eta F = 0 \quad (12.47)$$

with the boundary conditions

$$\eta = 0 : \quad F' = 0; \quad \eta \rightarrow \infty : \quad F = 0. \quad (12.48)$$

From the condition that the drag

$$D = 2\pi\rho U_\infty \int_0^\infty u_1 r dr = 8\pi\rho U_\infty^2 C \left(\frac{x}{l}\right)^{-m} \frac{\nu x}{U_\infty} \int_0^\infty F(\eta) \eta d\eta \quad (12.49)$$

is to be independent of x , it follows that $m = 1$. The differential equation determined in this manner has the solution

$$F(\eta) = e^{-\eta^2}, \quad (12.50)$$

which is identical to the solution of the plane wake, cf. (7.93). With the drag coefficient

$$c_D = \frac{2D}{\rho U_\infty^2 \pi l^2} \quad (12.51)$$

and the Reynolds number $\text{Re} = U_\infty l / \nu$, we obtain the velocity distribution in the wake

$$\frac{u_1(x, r)}{U_\infty} = \frac{\pi c_D}{32} \frac{l \text{Re}}{x} e^{-\frac{r^2 U_\infty}{4x\nu}}. \quad (12.52)$$

Experimental results may be found in the work by F.R. Hama; L.F. Peterson (1976).

The extension of this asymptotic solution to finite x values has been described by S.A. Berger (1971), p. 248.

12.2 Three-Dimensional Boundary Layers

12.2.1 Boundary-Layer Equations

Now let us consider a general three-dimensional body on whose surface a boundary layer forms. Edges or extremely strong curvatures of the surface are excluded from this treatment.

In order to describe the flow past these bodies, we use an orthogonal curvilinear coordinate system, as in Fig. 12.7. The coordinate lines $x = \text{const}$ and $z = \text{const}$ form an orthogonal grid on the surface. The y coordinate is perpendicular to the surface and denotes the distance from the wall. Let the velocity components for this x, y, z system again be u, v, w . For this coordinate system, the so-called *Lamé metric coefficients* read $h_x, h_y = 1, h_z$. For an infinitesimal element of arc therefore:

$$(ds)^2 = (h_x dx)^2 + (dy)^2 + (h_z dz)^2.$$

These metric coefficients are in general still functions of x and z and they determine the particular coordinate system of choice.

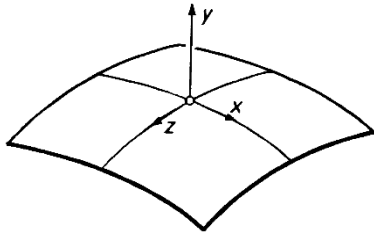


Fig. 12.7. Orthogonal curvilinear coordinate system for an arbitrary body surface

The metric coefficients can be determined by relating the curvilinear x, y, z system to a suitably chosen Cartesian coordinate system X, Y, Z . Then

$$\begin{aligned} h_x^2 &= \left(\frac{\partial X}{\partial x} \right)^2 + \left(\frac{\partial Y}{\partial x} \right)^2 + \left(\frac{\partial Z}{\partial x} \right)^2 \\ &= \left[\left(\frac{\partial x}{\partial X} \right)^2 + \left(\frac{\partial x}{\partial Y} \right)^2 + \left(\frac{\partial x}{\partial Z} \right)^2 \right]^{-1}, \end{aligned} \quad (12.53)$$

$$\begin{aligned} h_z^2 &= \left(\frac{\partial X}{\partial z} \right)^2 + \left(\frac{\partial Y}{\partial z} \right)^2 + \left(\frac{\partial Z}{\partial z} \right)^2 \\ &= \left[\left(\frac{\partial z}{\partial X} \right)^2 + \left(\frac{\partial z}{\partial Y} \right)^2 + \left(\frac{\partial z}{\partial Z} \right)^2 \right]^{-1}. \end{aligned} \quad (12.54)$$

For large Reynolds numbers and after carrying out a boundary-layer transformation, the complete Navier-Stokes equations for the coordinate system chosen in this manner yield the following boundary-layer equations in dimensional form (without gravity, i.e. $g = 0$), cf. for example H.-D. Papenfuß (1975):

$$\frac{1}{h_x h_z} \frac{\partial}{\partial x} (h_z \varrho u) + \frac{\partial}{\partial y} (\varrho v) + \frac{1}{h_x h_z} \frac{\partial}{\partial z} (h_x \varrho w) = 0, \quad (12.55)$$

$$\begin{aligned} \varrho \left[\frac{u}{h_x} \frac{\partial u}{\partial x} + v \frac{\partial u}{\partial y} + \frac{w}{h_z} \frac{\partial u}{\partial z} + \frac{1}{h_x h_z} \left(\frac{\partial h_x}{\partial z} uw - \frac{\partial h_z}{\partial x} w^2 \right) \right] \\ = -\frac{1}{h_x} \frac{\partial p}{\partial x} + \frac{\partial}{\partial y} \left(\mu \frac{\partial u}{\partial y} \right), \end{aligned} \quad (12.56)$$

$$\begin{aligned} \varrho \left[\frac{u}{h_x} \frac{\partial w}{\partial x} + v \frac{\partial w}{\partial y} + \frac{w}{h_z} \frac{\partial w}{\partial z} + \frac{1}{h_x h_z} \left(\frac{\partial h_z}{\partial x} uw - \frac{\partial h_x}{\partial z} u^2 \right) \right] \\ = -\frac{1}{h_z} \frac{\partial p}{\partial z} + \frac{\partial}{\partial y} \left(\mu \frac{\partial w}{\partial y} \right), \end{aligned} \quad (12.57)$$

$$\begin{aligned}
 & \rho c_p \left(\frac{u}{h_x} \frac{\partial T}{\partial x} + v \frac{\partial T}{\partial y} + \frac{w}{h_z} \frac{\partial T}{\partial z} \right) \\
 &= \frac{\partial}{\partial y} \left(\lambda \frac{\partial T}{\partial y} \right) + \beta T \left(\frac{u}{h_x} \frac{\partial p}{\partial x} + \frac{w}{h_z} \frac{\partial p}{\partial z} \right) \\
 &+ \mu \left[\left(\frac{\partial u}{\partial y} \right)^2 + \left(\frac{\partial w}{\partial y} \right)^2 \right]. \tag{12.58}
 \end{aligned}$$

The boundary-layer equations used up until now are special cases of this general system:

- 1) For $h_x = h_z = 1$, $w = 0$, we obtain Eqs. (10.4) to (10.6).
- 2) For $h_x = 1$, $h_z = r_w(x)$, $w = 0$ we obtain Eqs. (12.1) to (12.3).
- 3) For $h_x = 1$, $h_z = r_w(x)$, $w \neq 0$, $\partial/\partial z = 0$ we obtain Eq. (12.17) to (12.20).

With this system of equations we have the following boundary conditions

$$\begin{aligned}
 y = 0 : \quad u = 0, \quad v = v_w(x, z), \quad w = 0, \quad T = T_w(x, z) \\
 \text{or } q = q_w(x, z) \\
 y \rightarrow \infty : \quad u = U(x, z), \quad w = W(x, z), \quad T = T_e(x, z).
 \end{aligned}$$

The solutions yield in particular

$$\tau_{wx} = \left(\mu \frac{\partial u}{\partial y} \right)_w, \quad \tau_{wz} = \left(\mu \frac{\partial w}{\partial y} \right)_w, \quad q_w = \left(-\lambda \frac{\partial T}{\partial y} \right)_w. \tag{12.59}$$

The direction of the resulting wall shear stress generally differs from the direction of the streamlines at the outer edge of the boundary layer (i.e. the inviscid outer flow close of the wall).

As one can easily convince oneself, as before the Busemann–Crocco solution (cf. Sect. 10.4.2) still holds. According to this, the total enthalpy in the boundary layer for an adiabatic wall and $\text{Pr} = 1$ is constant and equal to that of the outer flow.

Similar solutions of three-dimensional boundary layers have been investigated by V.G. Pavlov (1979).

There are many different choices of coordinate system and we consider two different groups:

1. Body-fitting coordinate systems.

Independent of the outer flow, the coordinate system is only determined by the geometry of the body.

If the main lines of curvature of the surface of the body are chosen as coordinate lines, the metric coefficients are related to the main curvatures in the surface in a simple manner, cf. L. Howarth (1951b), see also Fig. 12.14.

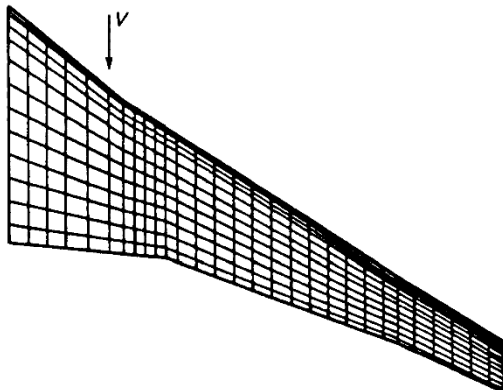


Fig. 12.8. Non-orthogonal coordinate system on a swept-back wing

Frequently such non-orthogonal coordinate systems as that shown in Fig. 12.8 for a swept-back wing are chosen. Here the y axis is still perpendicular to the surface, but the two coordinate lines on the surface generally form an angle which is not 90° . In this case the system of equations (12.55) to (12.58) has to be extended by terms which contain the angle as an additional quantity, cf. Sect. 20.2.1 and J. Cousteix (1987b). Body-fitting coordinate systems have the advantage that they are independent of changes in the flow, i.e. of variations in the angle of attack. On the other hand, singularities can appear in the metric coefficients, and these must be handled using complicated transformations, cf. T. Cebeci et al. (1980b) and T. Cebeci (1987). Such problems also occur in non-orthogonal coordinate systems on fuselage shaped bodies, cf. R. Grundmann (1981), Y.S. Wie; J.E. Harris (1991).

2. Flow-fitting coordinate systems

The streamlines of the inviscid outer flow and their orthogonal trajectories are often chosen as the coordinate lines on the surface of a body, cf. W.D. Hayes (1951) and L. Prandtl (1961). The disadvantage here is that the coordinate system also changes if the angle of attack is varied. But an advantage is that the w component of the velocity vanishes at the outer edge of the boundary layer ($W(x, z) = 0$). Here:

$$\varrho U \frac{\partial U}{\partial x} = - \frac{\partial p}{\partial x}; \quad \frac{\varrho}{h_x} \frac{\partial h_x}{\partial z} U^2 = \frac{\partial p}{\partial z}. \quad (12.60)$$

In this case, the w component describes the *secondary flow*, cf. Fig. 12.9. Equation (12.60) means that, for $\partial h_x / \partial z = 0$, Eq. (12.57) reduces to a ho-

mogeneous equation for w . Because of the homogeneous boundary conditions for w , this has the trivial solution $w = 0$, i.e. in this case there is no secondary flow. R. Sedney (1957) has shown that $\partial h_x / \partial z = 0$ holds (i.e. there are no secondary flows in the boundary layer) if the outer flow streamlines which are close to the wall are *geodetic lines* of the body's surface. A curve on the surface is called a geodetic line if the normal to the surface at all points along the curve is the same as the *main normal* of the curve (e.g. great circles on the sphere are geodetic lines).

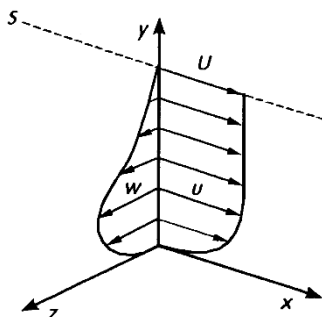


Fig. 12.9. Orthogonal streamline coordinate system, s : streamline at the outer edge of the boundary layer

Numerical methods for the solution of the system of equations (12.55) to (12.58) or else the extended system for non-orthogonal coordinate systems have been described by, for example, E. Krause et al. (1969), E. Krause (1973), W.L. Melnik (1982), T. Cebeci (1987) and V. Iyer; J.E. Harris (1990). Although the equations are parabolic, the directions in which the computation advances have to be chosen very carefully, taking into account the *zone of influence* of a point in the boundary layer. As in Fig. 12.10, this is determined by the region of the boundary layer in which all streamlines which go through the normal AB (with the point P) lie. Analogously, upstream from AB is the *zone of dependence*, in which all points which influence P lie.

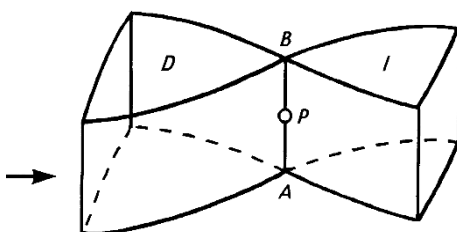


Fig. 12.10. Zone of dependence and zone of influence in three-dimensional boundary layers
D: zone of dependence
I: zone of influence

The numerical computation using a finite difference method requires a particular manner of proceeding if the secondary flow is a backflow. The so-

called zig-zag scheme of E. Krause et al. (1969) has proved successful to this end, cf. T. Cebeci (1987), see also Chap. 23.

Even for three-dimensional boundary layers, coordinate transformations corresponding to the Görtler transformation (7.76) or the pseudo-similarity transformation (10.138) are used to reduce the growth of the boundary layer in the computation region, cf. T. Cebeci (1987).

The definition of separation is of particular importance in three-dimensional boundary layers, cf. the summaries by E.C. Maskell (1955), M.J. Lighthill (1963) and K.C. Wang (1972, 1976), M. Tobak; D.J. Peake (1982), U. Dallmann (1983), H. Hornung; A.E. Perry (1984). According to E.C. Maskell, the separation line is an envelope of the limiting streamlines (i.e. of the wall shear stress lines), cf. Fig. 12.11. Closely related to the separation line is the edge of the so-called *region of accessibility*, which contains all points which can be reached by the boundary-layer computation commencing at the front stagnation point, cf. T. Cebeci et al. (1981).

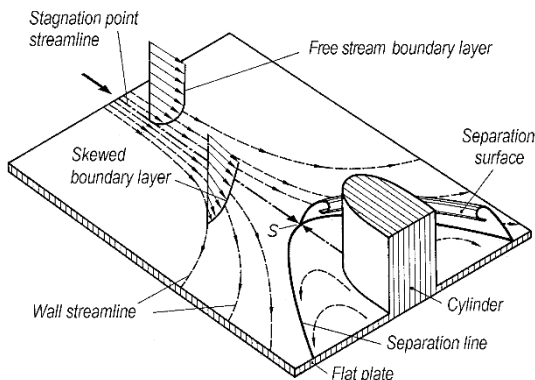


Fig. 12.11. Separation line of a three-dimensional boundary layer as an envelope of the wall streamlines

If separation of a three-dimensional boundary layer occurs, particularly in the case of all general blunt bodies, there is a drastic change in the outer flow, leading to great difficulties in computing the inviscid flow. Because of the complex vortex structure arising in three-dimensional separation, a displacement correction, as is possible in plane flows and as will be described in Chap. 14 as a higher order effect, is also no longer possible. In this case, there are no further advantages to using the asymptotic theory ($\text{Re} \rightarrow \infty$) over the solution of the complete equations of motion. This is particularly true since three-dimensional separated flows frequently tend to become unsteady.

Integral methods have also been used to compute three-dimensional boundary layers, cf. H.-W. Stock; H.P. Horton (1985). Here the definition of the displacement thickness $\delta_1(x, z)$ should be noted. For the two coordi-

nate directions in the system in Fig. 12.9 (i.e. $W = 0$) and for $\varrho = \text{const}$, the value of δ_{1x} is determined by Eq. (12.24) and

$$\delta_{1z} = \int_0^\infty \frac{w}{U} dy . \quad (12.61)$$

Using the partial differential equation

$$\frac{\partial}{\partial x} [h_z U (\delta_1 - \delta_{1x})] + \frac{\partial}{\partial z} [h_x U \delta_{1z}] = 0 , \quad (12.62)$$

the real displacement thickness $\delta_1(x, z)$ can be determined. The *displacement velocity* at the outer edge of the boundary layer is

$$\lim_{y \rightarrow \infty} (v - V) = \frac{1}{h_x h_z} \frac{\partial}{\partial x} (h_z U \delta_1) . \quad (12.63)$$

For plane flows ($h_x = h_z = 1$), this formula becomes Eq. (6.35).

Summaries of three-dimensional boundary layers have been given by W.R. Sears (1954), F.K. Moore (1956), H. Schlichting (1961), J.C. Cooke; M.G. Hall (1962), M.J. Lighthill (1963), L.F. Crabtree et al. (1963), A. Mager (1964), E.A. Eichelbrenner (1973), H.A. Dwyer (1981) and J. Cousteix (1986, 1987a, 1987b). In what follows we will look at some particular examples.

12.2.2 Boundary Layer at a Cylinder

If the surface of the body is a cylindrical surface as in Fig. 12.12, we have $h_x = 1$, $h_z = 1$, so that Eqs. (12.55) to (12.58) are greatly simplified. The functions $U(x, z)$, $W(x, z)$ and $T_w(x, z)$ or $q_w(x, z)$ are prescribed. For $w = 0$ the system then becomes the boundary-layer equations for plane flows, Eq. (10.4) to (10.6).

Th. Geis (1956b) has investigated those flows which yield similar solutions. In analogy to the wedge flows in the two-dimensional case, cf. Sect. 7.2, the velocity profiles in each of the axial directions are similar to one another. This allows the system of equations to be reduced to a system of ordinary differential equations.

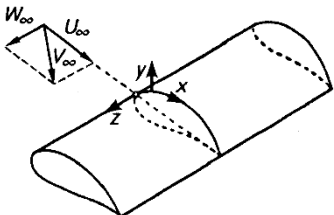


Fig. 12.12. Coordinate system for a three-dimensional boundary layer on cylindrical bodies

A generalisation to compressible boundary layers has been presented by V. Salnikov; U. Dallmann (1989); this also contains further references.

H.G. Loos (1955) has investigated the boundary layer for the outer flow $U = \text{const}$, $W = a_0 + a_1 x$, and an extension to $U = \text{const}$, $W = \sum a_n x^n$ has been given by A.G. Hansen; H.Z. Herzig (1956). Since these outer flows are no longer irrotational, it can happen that the velocity in the boundary layer is greater than that in the outer flow. These excess velocities are due to the secondary flow in the boundary layer, which obtains fluid from zones which are rich in energy. In these flows, the case can occur where the velocity profile in the main flow direction initially demonstrates backflow. However the backflow does not mean flow separation, it rather vanishes further downstream. This behaviour can also be explained by the energy transport of the secondary flow. It can be seen from this example that the definition of separation in three-dimensional flow is not without its difficulties, since the relation between backflow and wall shear stress is no longer as simple as in plane boundary layers, cf. T. Cebeci et al. (1981).

The computation is simpler if the outer flow has the form:

$$U(x, z) = U_0(x) + U_1(x, z) \quad U_1 \ll U_0 ,$$

$$W(x, z) = W_1(x, z) \quad W_1 \ll U_0 ,$$

i.e. for outer flows which consist of a plane basic flow and a weak perturbing flow. The differential equations for the latter can be linearised and the basic flow is independent of the perturbing flow, cf. A. Mager (1954, 1955).

The three-dimensional boundary layer on the moving plate has been investigated by M. Kronast (1992). It is important in the ground effect for motor vehicles.

The three-dimensionality in the plate flow can also come into being via the boundary conditions at the wall, i.e. through appropriate distributions of the suction velocity, cf. K. Gersten; J.F. Gross (1974a), K.D. Singh (1993) and P. Singh et al. (1981), or of the temperature for variable physical properties.

Three-dimensional boundary layers also appear in mixed convection if the buoyancy forces do not act in the direction of the main flow, cf. G.H. Evans; O.A. Plumb (1982a, 1982b).

Natural convection at a cylinder at an angle of attack has been investigated by A. Suwono (1980).

12.2.3 Boundary Layer at a Yawing Cylinder

The boundary layer at an infinitely long yawing cylinder is a special case of the previous section. For the outer flow we then have $W = W_\infty = \text{const}$ and all derivatives with respect to z vanish. The boundary-layer equations reduce to

$$\frac{\partial(\varrho u)}{\partial x} + \frac{\partial(\varrho v)}{\partial y} = 0, \quad (12.64)$$

$$\varrho \left(u \frac{\partial u}{\partial x} + v \frac{\partial u}{\partial y} \right) = -\frac{dp}{dx} + \frac{\partial}{\partial y} \left(\mu \frac{\partial u}{\partial y} \right), \quad (12.65)$$

$$\varrho \left(u \frac{\partial w}{\partial x} + v \frac{\partial w}{\partial y} \right) = \frac{\partial}{\partial y} \left(\mu \frac{\partial w}{\partial y} \right), \quad (12.66)$$

$$\varrho c_p \left(u \frac{\partial T}{\partial x} + v \frac{\partial T}{\partial y} \right) = \frac{\partial}{\partial y} \left(\lambda \frac{\partial T}{\partial y} \right) + \beta T u \frac{dp}{dx} + \mu \left(\frac{\partial u}{\partial y} \right)^2. \quad (12.67)$$

It can be seen that Eqs. (12.64), (12.65) and (12.67) are identical to the system of plane boundary layers in Eqs. (10.4) to (10.6), and are therefore independent of the transverse flow. According to this *principle of independence*, the flow can then be computed as a plane flow straight away. Afterwards the velocity of the transverse flow $w(x, y)$ is determined from the linear differential equation (12.66). Incidentally, this equation for w is the same as that for the temperature distribution, if $\beta = 0$, $\text{Pr} = 1$ and the dissipation is neglected.

The special case $U = U_\infty = \text{const}$ corresponds to the *yawing flat plate*. The pressure terms then drop out of Eqs. (12.65) and (12.67), so that Eq. (12.65) and (12.66) become identical if u is replaced by w . Thus $w/W_\infty = u/U_\infty$. Therefore, the yawing motion of the plate has no effect on the formation of the boundary layer.

C.F. Dewey Jr.; J.F. Gross (1967) have presented numerous results for the outer flow $U \sim x^m$, as well as for the case of blowing. These are similar solutions. The most important special case is the stagnation line with $U = ax$.

For general outer flows $U(x)$, solutions have been determined by series expansion, cf. W.R. Sears (1948) and H. Görtler (1952a) and by integral methods, cf. L. Prandtl (1945), W. Dienemann (1953) and J.M. Wild (1949). As an example of such a calculation, Fig. 12.13 shows the streamline portrait at a yawing elliptical cylinder at an angle of attack (axis ratio 6:1, lift coefficient $c_L = 0.47$). The figure clearly shows the difference between the streamlines of the outer flow and the limiting streamlines (wall shear stress streamlines) on the surface. A secondary flow emerges, due to which the boundary-layer flow is diverted to the back end. The separation line which is also sketched is, as already mentioned above, the envelope of all the limiting streamlines. On it $\tau_{wx} = 0$, but $\tau_{wz} \neq 0$. i.e. the resulting wall shear stress does not vanish on the separation line.

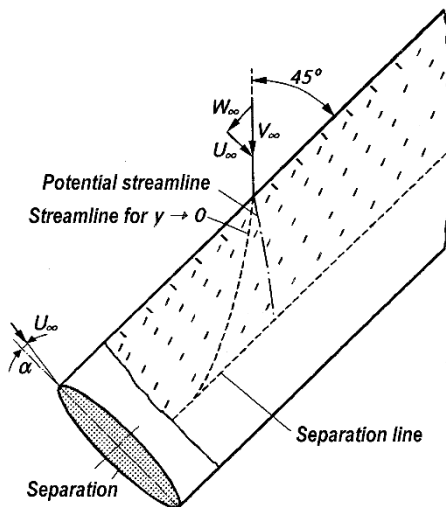


Fig. 12.13. Boundary-layer flow at yawing elliptical cylinder with lift, cf. J.M. Wild (1949)

The semi-ininitely long rotating cylinder in oblique flow has been investigated by L.G. Loitsianski (1967), p. 247.

12.2.4 Three-Dimensional Stagnation Point

In the three-dimensional stagnation point depicted in Fig. 12.14, the outer flow is:

$$U(x) = ax, \quad W(z) = bz = caz. \quad (12.68)$$

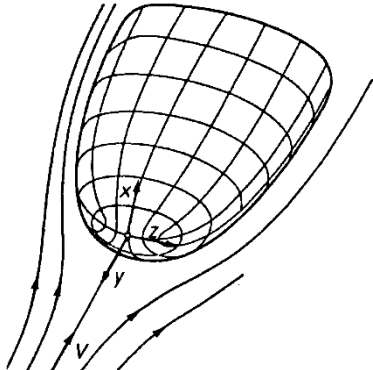


Fig. 12.14. Coordinate system close to a three-dimensional stagnation point.
coordinate lines = main curvature lines

Using the trial solutions

$$\begin{aligned} u &= U(x)f'(\eta), & w &= W(z)g'(\eta), \\ \vartheta(\eta) &= \frac{T}{T_e} = \frac{\rho_e}{\rho}, & \eta &= \sqrt{\frac{a}{\rho_e \mu_e}} \int_0^y \rho dy \end{aligned} \quad (12.69)$$

we obtain the ordinary differential equations

$$\left(\frac{\rho \mu}{\rho_e \mu_e} f'' \right)' + (f + cg)f'' - (f'^2 - \vartheta) = 0, \quad (12.70)$$

$$\left(\frac{\rho \mu}{\rho_e \mu_e} g'' \right)' + (f + cg)g'' - c(g'^2 - \vartheta) = 0, \quad (12.71)$$

$$\left(\frac{\rho \mu}{\rho_e \mu_e} \vartheta' \right)' + \text{Pr}(f + cg)\vartheta' = 0 \quad (12.72)$$

with the boundary conditions

$$\begin{aligned} \eta = 0 : \quad f &= f_w, \quad f' = 0, \quad g = 0, \quad g' = 0, \quad \vartheta = \frac{T_w}{T_e} \\ \eta \rightarrow \infty : \quad f' &= 1, \quad g' = 1, \quad \vartheta = 1. \end{aligned} \quad (12.73)$$

Special cases are the axisymmetric stagnation point ($c = 1, f = g$), cf. Sect. 5.2.3, and the plane stagnation point ($c = 0$), cf. Sect. 5.1.3 and Sect. 10.4.4. In the latter case, the solution $g(\eta)$ corresponds to the velocity distribution along the stagnation line of a yawing cylinder, cf. Sect. 12.2.3.

Many numerical results for the three-dimensional stagnation point for different values of c , also with blowing ($f_w \neq 0$) have been presented by L. Howarth (1951b), E. Reshotko (1958), P.A. Libby (1967), K. Gersten (1973a) and H.-D. Papenfuß (1975).

12.2.5 Boundary Layers in Symmetry Planes

Symmetry planes are characterised by the fact that $w = 0$ holds and all derivatives with respect to z vanish, apart from the term $\partial w / \partial z \neq 0$. The boundary-layer equations are thus considerably simplified. For constant ϱ , Eq. (12.55) yields

$$\frac{1}{h_x} \frac{\partial u}{\partial x} + \frac{u}{h_x h_z} \frac{\partial h_z}{\partial x} + \frac{\partial v}{\partial y} + \frac{1}{h_z} \frac{\partial w}{\partial z} = 0. \quad (12.74)$$

It can be seen that the flow in the symmetry plane corresponds in no way to a plane boundary layer. The last term in Eq. (12.74) is a measure of the convergence or divergence of the streamlines close to the symmetry plane. The equation (12.57) is singular in the symmetry plane, but, for constant physical properties, partial differentiation with respect to z yields

$$\begin{aligned} \varrho & \left[\frac{u}{h_x} \frac{\partial}{\partial x} \left(\frac{\partial w}{\partial z} \right) + v \frac{\partial}{\partial y} \left(\frac{\partial w}{\partial z} \right) + \frac{1}{h_z} \left(\frac{\partial w}{\partial z} \right)^2 + \frac{1}{h_x h_z} \frac{\partial h_z}{\partial x} u \frac{\partial w}{\partial z} \right] \\ &= - \frac{\partial}{\partial z} \left(\frac{1}{h_z} \frac{\partial p}{\partial z} \right) + \mu \frac{\partial^2}{\partial y^2} \left(\frac{\partial w}{\partial z} \right). \end{aligned} \quad (12.75)$$

This equation, together with Eq. (12.74) and the simplified equation (12.56) ($w = 0$), form three equations for the three quantities $u(x, y)$, $v(x, y)$ and $\frac{\partial w}{\partial z}(x, y)$. In the symmetry plane, almost as in a plane boundary layer, the flow can be determined independently of the boundary layer on the rest of the body, cf. K.C. Wang (1970, 1974a), R. Grundmann (1981), G.R. Schneider; Z. Zhu (1982) and H.-W. Stock (1986). The stagnation-point boundary layer treated in the previous section can be used as a starting solution.

12.2.6 General Configurations

Ellipsoids. Numerous boundary-layer investigations have been carried out on axisymmetric ellipsoids and on triple-axis ellipsoids with and without angles of attack, cf. for example, E.A. Eichelbrenner; A. Oudart (1955), W. Geißler (1974a, 1974b), K.C. Wang (1974b, 1974c, 1974d), H.-W. Stock (1980, 1986) and V.C. Patel; J.H. Baek (1985).

One of the reasons for this abundance of literature may be because the potential flows past these bodies are very simple analytical solutions.

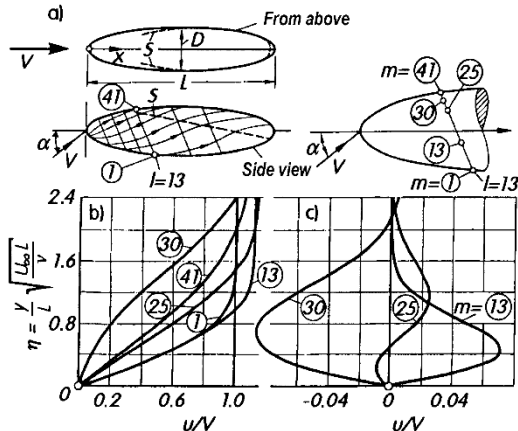


Fig. 12.15. Velocity distribution of the three-dimensional boundary layer at an ellipsoid of revolution of axis ratio $l/D = 4$ at an angle of attack $\alpha = 15^\circ$, after W. Geißler (1974a, 1974b).

- (a) system of potential lines and streamlines of the outer flow; S : separation line
- (b) velocity profile u/V in the direction of the outer flow streamlines
- (c) velocity profile w/V of the secondary flow perpendicular to the direction of the outer flow streamlines

Φ : azimuthal angle

$\Phi = 0^\circ$: windward symmetry line

m	Φ	x/l
(1)	0°	0.300
(13)	71°	0.322
(25)	122°	0.277
(30)	141°	0.264
(41)	180°	0.254

Figure 12.15 shows results for the three-dimensional boundary layer at an axisymmetric ellipsoid at an angle of attack. In Fig. 12.15a, as well as the potential lines and streamlines of the outer flow, the separation line S from the theory is also shown. Figures 12.15b and 12.15c show the velocity distribution in the boundary layer at different positions on a specific potential line. New experiments for this case have been presented by H.U. Meier; H.P. Kreplin (1980).

Fuselages. The three-dimensional boundary layers on fuselages and fuselage-shaped bodies of revolution have been investigated by Y.S. Wie; J.E. Harris (1991) and V.C. Patel; D.H. Choi (1980). The hulls of ships have been treated by T. Cebeci et al. (1980a).

Swept-back wings. Because of their great practical importance, three-dimensional boundary layers on swept-back wings have been examined very intensively, cf. T. Cebeci et al. (1977), D. Schwamborn (1984), J. Cousteix (1987a, 1987b).

The behaviour of the three-dimensional boundary layer plays an essential role in the design of airplane wings. The aim is to reduce the drag by keeping as large a part as possible of the boundary layer laminar. The shape can be altered to yield an appropriately favourable pressure distribution. However suction is also used to stabilise the boundary layer and to keep it laminar. In transonic regions the interaction between shock waves and the boundary layer is particularly important. This will be discussed in Chap. 14.

The start of boundary-layer development close to the stagnation line of wings has been treated by D. Schwamborn (1981).

Comprehensive measurements of the boundary layer on delta wings have been carried out by D. Hummel (1986).

Cones in supersonic flow. The laminar boundary layer at a rotating circular cone at an angle of attack in supersonic flow has been investigated by R. Sedney (1957), cf. also A.N. Pokrovskii et al. (1984).

Boundary layers in rotating systems. Flow in rotating systems are primarily of interest in connection with propellers, helicopter rotors and turbomachinery. G. Jungclaus (1955) developed an integral method and R. Grundmann (1976) computed boundary layers at curved rotating cylinders numerically. Here it was found that the Coriolis forces which additionally occur are extremely important. These forces can ensure that the pressure gradient perpendicular to the boundary layer no longer vanishes. The three-dimensional boundary layer at a rotating cylindrical wing has been investigated by L.E. Fogarty (1951), W.R. Sears (1954) and H.S. Tan (1953). Further investigations into rotating blades have been carried out by Ph.J. Morris (1981) and T. Toyokura et al. (1982).

13. Unsteady Boundary Layers

13.1 Fundamentals

13.1.1 Remark

The examples of solutions of the boundary-layer equations treated up until now have been those for steady flows. Although it is steady flows which are by far of greatest importance in practical applications, in this chapter we will treat some cases of boundary layers which vary in time, that is, unsteady boundary layers.

Unsteady boundary layers are mostly either start-up processes, i.e. motions from rest or transitions from one steady flow to another, or else periodic motions.

We have already described such unsteady flows for which solutions to the complete Navier–Stokes equations can be given in Sects. 5.3 and 5.4. It turned out that the solutions for small viscosities, i.e. for large Reynolds numbers, had boundary-layer character.

Because of the additional variable t , as well as l , V and ν , there is also an additional reference quantity in the form of a characteristic time t_R or a characteristic frequency $n = 1/t_R$. Two dimensionless characteristic numbers can be formed from the four quantities l , V , ν and t_R . The first characteristic number is the dimensionless reference time

$$t_R^* = t_R V/l, \quad (13.1)$$

which, for periodic flows with $t_R = 1/n$, is identical to the inverse of the Strouhal number $Sr = nl/V = 1/t_R^*$ as in Eq. (1.16). The choice of the second characteristic number depends on the flow under consideration. As was already seen in Chap. 5, there are simplifications in the calculation of periodic flows for very small frequencies (quasi-steady flows) and for very high frequencies (Stokes layer). For large times (i.e. small frequencies), the second characteristic number chosen is the Reynolds number $Re = Vl/\nu$

used in the steady case. For small times (i.e. high frequencies), however, the characteristic number

$$t_{R0}^* = \frac{\nu t_R}{l^2} = \frac{\nu}{nl^2} = \frac{t_R^*}{\text{Re}} \quad (13.2)$$

appears (e.g. it follows from Eq. (5.105) that $\eta_s = y/(l\sqrt{2t_{R0}^*})$).

In what follows a coordinate system fixed to the body will always be used. The flow will again be made up of the inviscid, but unsteady, outer flow, and the frictional boundary layer.

Initially we will only treat plane and axisymmetric unsteady boundary layers. The velocity distribution $U(x, t)$ of the inviscid outer flow close the wall can therefore again be assumed to be known.

Start-up processes of bodies in a fluid at rest are carried out so that directly after the motion starts irrotational potential flow is at hand in the entire field, apart from in a thin layer at the body. The thickness of the boundary layer then increases with time. In computing its further development, it is important to state the time when separation first appears. When separation starts, the outer flow is considerably changed by the separating boundary layer. A clean division between the irrotational outer flow and the rotational separated boundary layer is then in general no longer possible. In these cases boundary-layer theory, which requires a clearly defined layered structure in the flow, can no longer be applied. This is not only true for start-up processes of blunt bodies after the onset of separation, but also for all unsteady boundary layers with distinct separation. Therefore, in what follows we shall only consider unsteady boundary layers without separation or with minimal separation (i.e. without strong repercussions on the outer flow). In start-up processes we shall only examine the flow up until the onset of separation.

Summaries and overviews of unsteady flows have been given by K. Stewartson (1960), J.T. Stuart (1963), N. Rott (1964), E.A. Eichelbrenner (1972), N. Riley (1975), R.B. Kinney (1975), D.P. Telionis (1979, 1981), T. Cebeci (1982) and W. Geißler (1993).

13.1.2 Boundary-Layer Equations

Let us consider plane and axisymmetric compressible boundary layers. According to Chap. 3, we obtain the complete Navier-Stokes equations for unsteady flows from those for steady flows by the addition of a few terms. The additional term in the continuity equation reads $\partial\rho/\partial t$, cf. Eq. (3.3), in the x momentum equation $\rho\partial u/\partial t$, cf. Eq. (3.20) and in the thermal energy equation (3.72) on the left hand side of the equation we gain $\rho c_p \partial T / \partial t$ and on

the right hand side $\beta T \partial p / \partial t$. The equations for unsteady boundary layers are obtained in an analogous manner. In dimensional form they read:

$$\frac{\partial \varrho}{\partial t} + \frac{\partial(r_w^j \varrho u)}{\partial x} + \frac{\partial(r_w^j \varrho v)}{\partial y} = 0, \quad (13.3)$$

$$\varrho \left(\frac{\partial u}{\partial t} + u \frac{\partial u}{\partial x} + v \frac{\partial u}{\partial y} \right) = -\varrho g \sin \alpha - \frac{\partial p}{\partial x} + \frac{\partial}{\partial y} \left(\mu \frac{\partial u}{\partial y} \right), \quad (13.4)$$

$$\begin{aligned} \varrho c_p \left(\frac{\partial T}{\partial t} + u \frac{\partial T}{\partial x} + v \frac{\partial T}{\partial y} \right) &= \frac{\partial}{\partial y} \left(\lambda \frac{\partial T}{\partial y} \right) + \beta T \left(\frac{\partial p}{\partial t} + u \frac{\partial p}{\partial x} \right) \\ &\quad + \mu \left(\frac{\partial u}{\partial y} \right)^2. \end{aligned} \quad (13.5)$$

These are valid both for plane boundary layers ($j = 0$) as well as for axisymmetric boundary layers ($j = 1$). The system (13.3) to (13.5) for steady flows becomes Eq. (10.4) to (10.6) ($j = 0$) or else Eq. (12.1) to (12.3) ($j = 1$).

The boundary conditions read:

$$y = 0 : \quad u = 0, \quad v = v_w, \quad T = T_w(x, t),$$

$$y \rightarrow \infty : \quad u = U(x, t), \quad T = T_e(x, t).$$

The velocity of the outer flow $U(x, t)$ is related to the pressure in the boundary layer as follows:

$$-\frac{\partial p}{\partial x} = \varrho_e \left(\frac{\partial U}{\partial t} + U \frac{dU}{dx} \right), \quad (13.6)$$

if the gravity term, cf. Eq. (13.4), is neglected. If the constitutive relations for ϱ , μ , λ and c_p are prescribed, the system of equations is closed, and if the functions $U(x, t)$, $v_w(x, t)$, $T_e(x, t)$, $T_w(x, t)$ are given, the boundary layer can be computed.

A numerical method (field method) for solving the unsteady boundary-layer equations for two-dimensional flows with constant physical properties has been given by M.G. Hall (1969), cf. also Sect. 23.3.

13.1.3 Similar and Semi-Similar Solutions

In steady boundary layers, solutions are called *similar*, cf. Sect. 7.2, if the two independent variables x and y can be reduced to a single variable η by the application of a suitable similarity transformation. In analogy, in the case of unsteady boundary layers we also speak of similar solutions when the three independent variables x , y and t can be reduced to a single variable.

H. Schuh (1955) and Th. Geis (1956a) have indicated all such solutions where a reduction to a single variable is possible. These are of the form

$$u(x, y, t) = U(x, t)H(\eta) \quad \text{with} \quad \eta = \frac{y}{N(x, t)}. \quad (13.7)$$

Among these solutions are outer flows of the form $U(x, t) = cx/t$ or $U(x, t) = ct^m$. The similar solutions for the outer flows $U(x, t) = x/(a + bt)$ with constants a and b have been calculated by K.T. Yang (1958).

If a suitable transformation yields a reduction of the three variables x, y, t to *two* variables, we speak of a *semi-similar solution*, cf. N. Hayasi (1962). If the reduction is specifically to the variables y and x/t , the solutions are called *pseudo-steady*, cf. E. Becker (1962). I. Tani (1958) has presented such a solution for the outer flow $U(x, t) = U_0 - x/(t_0 - t)$ with constants U_0 and t_0 . A wider class of semi-similar solutions has been treated by H.A. Hassan (1960), cf. also N. Hayasi (1962).

13.1.4 Solutions for Small Times (High Frequencies)

The boundary-layer equations (13.4) and (13.5) emerge, as for steady boundary layers, by applying a boundary-layer transformation to the complete Navier-Stokes equations and then by forming the limit for $\nu \rightarrow 0$ (or by taking the limit of a dimensionless characteristic number proportional to ν to zero).

As has already been mentioned in Sect. 13.1.1, different characteristic numbers for unsteady boundary layers are formed depending on whether small times t_R or large times t_R are being considered. For large times the Reynolds number $Re = Vl/\nu$ from the steady case is the characteristic number. For $\nu \rightarrow 0$ this takes the limit $Re \rightarrow \infty$. This yields the known boundary-layer transformation, cf. Eq. (6.6)

$$\bar{y} = y^* \sqrt{Re}, \quad \bar{v} = v^* \sqrt{Re} \quad (t_R^* \rightarrow \infty). \quad (13.8)$$

For small times t_R , however, the characteristic number t_{R0}^* from Eq. (13.2) is used. Instead of the Reynolds number the characteristic number $1/t_{R0}^* = l^2/\nu t_R$ now appears. Therefore the boundary-layer transformation for this case reads

$$\bar{y} = y^* \sqrt{\frac{l^2}{t_R \nu}}, \quad \bar{v} = v^* \sqrt{\frac{l^2}{t_R \nu}} \quad (t_R^* \rightarrow 0). \quad (13.9)$$

If the time t is referred to t_R , (i.e. $t^* = t/t_R$), we apply the boundary-layer transformation and take the limit $t_{R0}^* \rightarrow 0$, and the momentum equation in the x direction assumes the following dimensionless form (constant physical properties):

$$\frac{\partial u^*}{\partial t^*} + t_R^* \left(u^* \frac{\partial u^*}{\partial x^*} + \bar{v} \frac{\partial u^*}{\partial \bar{y}} \right) = \frac{\partial U^*}{\partial t^*} + t_R^* U^* \frac{\partial U^*}{\partial x^*} + \frac{\partial^2 u^*}{\partial \bar{y}^2}. \quad (13.10)$$

For the solution we use an ansatz of a power series in t_R^* :

$$u^*(x^*, \bar{y}, t^*) = u_0(x^*, \bar{y}, t^*) + t_R^* u_1(x^*, \bar{y}, t^*) + \dots \quad (13.11)$$

Inserting this into Eq. (13.10) and ordering the powers of t_R^* successively yields the following differential equations for the different terms in the power series:

$$\frac{\partial u_0}{\partial t^*} - \frac{\partial^2 u_0}{\partial \bar{y}^2} = \frac{\partial U^*}{\partial t^*}, \quad (13.12)$$

$$\frac{\partial u_1}{\partial t^*} - \frac{\partial^2 u_1}{\partial \bar{y}^2} = U^* \frac{\partial U^*}{\partial x^*} - u_0 \frac{\partial u_0}{\partial x^*} - \bar{v}_0 \frac{\partial u_0}{\partial \bar{y}} \quad (13.13)$$

with the boundary conditions

$$\bar{y} = 0 : \quad u_0 = 0, \quad u_1 = 0$$

$$\bar{y} = \infty : \quad u_0 = U^*(x^*, t^*), \quad u_1 = 0.$$

Equations (13.12) and (13.13) are supplemented by the continuity equations for u_0 , v_0 and u_1 , v_1 . In a similar manner, the equations for further terms in the power series u_2 , v_2 etc. can also be written down. Corresponding equations can also be derived for the temperature.

It is worth noting that all differential equations, and therefore also those for u_0 , are linear. Equation (13.12) states that for small values for t_R^* to first approximation, the convective accelerations which lead to nonlinearities in the equations can be neglected, so the local acceleration forces and the friction force are in equilibrium. In addition, Eq. (13.12) does not explicitly contain the variable x^* ; it only appears as a parameter. The solution $u_0(x^*, \bar{y}, t^*)$ is therefore a *local* solution comparable with the solution for massive suction in Sect. 11.2.2. It will be shown that, for simple velocity distributions $U^*(x^*, t^*)$, Eq. (13.12) leads to similar solutions.

13.1.5 Separation of Unsteady Boundary Layers

In steady two-dimensional boundary layers the separation point is defined by the position where the wall shear stress vanishes ($\tau_w = 0$). For a given pressure distribution of the outer flow, a singularity forms at this position (the gradients $d\delta_1/dx$ and $d\tau_w/dx$ become infinite, cf. Eq. (7.84)), so that the boundary-layer computation cannot be carried out beyond this point.

This definition cannot be adopted for unsteady boundary layers. *The separation point is now that point where a singularity occurs* (e.g. if the gradient $d\delta_1/dx \rightarrow \infty$). In contrast, at the position with $\tau_w = 0$, which in general varies in time, the solution of the boundary-layer equations is generally regular.

The position of the separation point for unsteady boundary layers can be determined using the MRS criterion which was initially developed for

steady boundary layers at moving walls, cf. Sect. 11.1 and Fig. 11.2. In a coordinate system which moves with the separation point, the boundary layer close to the separation point appears steady and at a moving wall, so that the MRS criterion may be applied in this coordinate system. Note, however, that the two conditions named in Sect. 11.1 can generally not be controlled in a simple manner in the computation of unsteady boundary layers, cf. W. Geißler (1989).

Further details on the separation of unsteady boundary layers or on the appearance of the singularity have been given by W.R. Sears; D.P. Telionis (1972), S.F. Shen; J.P. Nenni (1975), S.F. Shen (1978), T. Cebeci (1982), L.L. Van Dommelen; S.F. Shen (1982), P.G. Williams (1982), J.C. Williams III (1982), F.T. Smith (1986) and T. Cebeci (1986).

As will be shown in Chap. 14, higher order boundary-layer effects can be taken into account in order to prevent the appearance of the singularity.

13.1.6 Integral Relations and Integral Methods

Just as for steady boundary layers, integral equations can also be derived from the boundary-layer equations for unsteady boundary layers. For boundary layers with constant physical properties and neglecting the dissipation they read:

$$\frac{\partial}{\partial t}(U\delta_1) + \frac{\partial}{\partial x}(U^2\delta_2) + \delta_1 U \frac{\partial U}{\partial x} + jU^2 \frac{\delta_2}{r_w} \frac{dr_w}{dx} = \frac{\tau_w}{\varrho}, \quad (13.14)$$

$$U^2 \frac{\partial \delta_1}{\partial t} + \frac{\partial}{\partial t}(U^2\delta_2) + \frac{\partial}{\partial x}(U^3\delta_3) + jU^3 \frac{\delta_3}{r_w} \frac{dr_w}{dx} = \frac{2}{\varrho} \mathcal{D}, \quad (13.15)$$

$$U \frac{\partial U}{\partial t} \frac{\delta_T}{c_p} + \frac{\partial}{\partial x}[(T_w - T_\infty)U\delta_T] + j(T_w - T_\infty)U \frac{\delta_T}{r_w} \frac{dr_w}{dx} = \frac{q_w}{\varrho c_p} \quad (13.16)$$

with $j = 0$ for plane boundary layers, and $j = 1$ for axisymmetric boundary layers. For steady boundary layers, these equations become Eq. (12.10) to (12.12). An extension of the integral equations to compressible flows of the ideal gas has been given by H. Schlichting (1982), p. 414.

In analogy to the approximate methods for steady boundary layers described in Chap. 8, corresponding methods for unsteady boundary layers have also been developed. H. Schuh (1953), K.T. Yang (1959), L.A. Rozin (1960), M. Holt; W.-K. Chan (1975) and M. Matsushita et al. (1984a, 1984b) have all presented integral methods of this kind, and the method of K.T. Yang also treats the thermal boundary layer. Here the fundamental equations used are the integral relations (13.14) to (13.16). Either polynomials or profiles from similar solutions are used for the profiles of the velocity and the temperature. Since the integration over the boundary-layer thickness only allows one coordinate (the y coordinate) to be eliminated, it is still partial differential equations which have to be solved in integral methods for unsteady boundary layers.

13.2 Unsteady Motion of Bodies in a Fluid at Rest

13.2.1 Start–Up Processes

The motion of body surrounding by fluid moving out of a position at rest is called a *start-up process*. In a coordinate system fixed to the body, a time dependent flow past the body forms. At first this is inviscid. It is only close to the wall that an unsteady boundary layer forms in time. The velocity $U(x, t)$ at the outer edge of the boundary layer is a typical distribution for start-up processes:

$$U(x, t) = \tilde{U}(x)[1 - e^{-t/t_R}]. \quad (13.17)$$

Here the characteristic time t_R is a measure of the duration of the start-up process. The limit $t_R \rightarrow 0$ is that of an impulsively accelerated wall, and this is the case which we will first consider.

Since this is a case with small reference times ($t_R \rightarrow 0$), the solution from Sect. 13.1.4 can be used.

Because of the boundary condition $\bar{y} \rightarrow \infty : u_0 = \tilde{U}^*(x^*)$, Eq. (13.12) reduces to the simple differential equation

$$\frac{\partial u_0}{\partial t^*} - \frac{\partial^2 u_0}{\partial \bar{y}^2} = 0 \quad (13.18)$$

with the similar solution

$$\frac{u_0}{\tilde{U}^*(x^*)} = f'_0(\eta) = \operatorname{erf} \eta \quad (13.19)$$

with

$$\eta = \frac{y}{2\sqrt{\nu t}}, \quad (13.20)$$

cf. also Eq. (5.93) to (5.98). Therefore the boundary layer at each point behaves *locally* as the first Stokes problem from Sect. 5.3.1, i.e. as a flow at a flat wall impulsively set into motion.

The extension of this solution from Sect. 13.1.4 leads to the ansatz

$$\frac{u(x, y, t)}{\tilde{U}(x)} = f'_0(\eta) + \left[\frac{d\tilde{U}}{dx} f'_{10}(\eta) + j \frac{\tilde{U}}{r_w} \frac{dr_w}{dx} f'_{11}(\eta) \right]. \quad (13.21)$$

The functions $f_0(\eta)$, $f_{10}(\eta)$ and $f_{11}(\eta)$ satisfy the differential equations

$$\begin{aligned} f'''_0 + 2\eta f''_0 &= 0 \\ f''_{10} + 2\eta f'_{10} - 4f'_{10} &= 4(f'^2_0 - f_0 f''_0 - 1) \\ f''_{11} + 2\eta f'_{11} - 4f'_{11} &= -4f_0 f''_0 \end{aligned} \quad (13.22)$$

with the boundary conditions:

$$\begin{aligned}\eta = 0 : \quad f_0 &= f_{10} = f_{11} = 0, \quad f'_0 = f'_{10} = f'_{11} = 0 \\ \eta \rightarrow \infty : \quad f' &= 1, \quad f'_{10} = f'_{11} = 0.\end{aligned}$$

The following values are a measure of the wall shear stress

$$f''_{0w} = 2/\sqrt{\pi} = 1.128, \quad f''_{10w} = 1.607, \quad f''_{11w} = 0.169. \quad (13.23)$$

A further term of the expansion (13.11) and thus (13.21) has been computed by E. Boltze (1908) and S. Goldstein; L. Rosenhead (1936).

Differentiating Eq. (13.21) yields the following conditions for vanishing wall shear stress:

$$1.128 + t_0 \left(1.607 \frac{d\tilde{U}}{dx} + 0.169j \frac{\tilde{U}}{r_w} \frac{dr_w}{dx} \right) = 0. \quad (13.24)$$

Therefore, separation occurs in plane flow ($j = 0$) only for negative $d\tilde{U}/dx$. The earliest position at which the wall shear stress vanishes is the point where the absolute value of $d\tilde{U}/dx$ is largest. In what follows we will discuss some examples.

Semi-infinite flat plate. Initially the flow behaves as that at the infinitely extended wall in Sect. 5.3.1. Therefore, at a certain time t , the region downstream from the point with coordinate $x = U_\infty t$ (here $\tilde{U} = U_\infty$) does not yet perceive that the plate has a leading edge. Since $\tilde{U} = U_\infty = \text{const}$, the second term in the expansion (13.21) vanishes.

The unsteady boundary-layer equations with the three dependent variables x , y and t have been solved numerically by both H.A. Dwyer (1968) and by M.G. Hall, see D.P. Telionis (1981), p. 99. Figure 13.1 shows the dimensionless wall shear stress $\tau_w(x, t)$ as a function of a dimensionless time. It can also be concluded from dimensional considerations (because $\tau_w \sim \sqrt{\nu}$) that the results can be shown on one curve. The numerical results deliver the transition from the Stokes solutions for small times to the Blasius solution for large times.

Circular cylinder. Up until the onset of separation, the outer flow is identical to the potential flow:

$$\tilde{U}(x) = 2V \sin \frac{x}{R}.$$

The absolute value of $d\tilde{U}/dx$ is largest at the rear stagnation point, and $d\tilde{U}/dx = -2V/R$. Therefore the wall shear stress first vanishes at the rear stagnation point, and the time until the wall shear stress vanishes is, from Eq. (13.24), given by $t_0 = 0.35R/V$. More precise calculations yield $t_0 = 0.32 R/V$, cf. T. Cebeci (1979) and M. Katagiri (1976). Figure 13.2 shows the dependence of the position of the point where the wall shear stress vanishes on time. For $t > t_0$ an initially very fast forwards movement can be seen.

Separation, i.e. the appearance of a singularity, only takes place later, for $t_S > t_0$. According to L.L. Van Dommelen; S.F. Shen (1982), T. Cebeci (1982), K.C. Wang (1982) and S.J. Cowley (1983), separation occurs at about $t_S = 1.5R/V$, not at the rear stagnation point but rather at the position $x_S/R = 1.94$, ($\varphi_S = 111^\circ$).

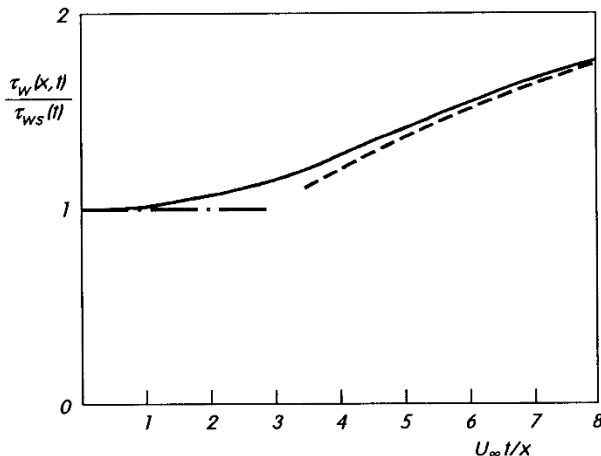


Fig. 13.1. Wall shear stress $\tau_w(x,t)$ for the flat plate impulsively set into motion
 $\tau_{ws}(t)$: wall shear stress according to Eq. (5.100)
— numerical result, after H.A. Dwyer (1968)
- - - asymptote for $U_\infty t/x \rightarrow 0$ (Stokes solution)
- - - asymptote for $U_\infty t/x \rightarrow \infty$ (steady Blasius solution)

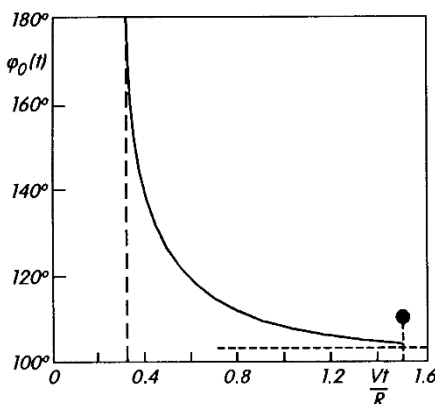


Fig. 13.2. Position of the point where the wall shear stress vanishes $\varphi_0 = \varphi_{\tau_w=0}$ for the circular cylinder impulsively set into motion, after T. Cebeci (1979)
● separation

This singularity manifests itself as an infinitely large increase in the displacement thickness ($d\delta_1/dx \rightarrow \infty$). Figure 13.3 shows calculations by T. Cebeci (1986) on the progression of the skin-friction coefficient $c_f = 2\tau_w/\rho V^2$ and the displacement thickness δ_1/R over the circumference of the cylinder at time $t = 1.5R/V$. The considerable increases of δ_1 at $\varphi = 111^\circ$ can easily be seen. At this time, the position of vanishing wall shear stress is already at $\varphi = 106^\circ$. T. Cebeci (1986)

showed that the boundary-layer calculation may be carried out beyond the time $t = 1.5R/V$, albeit with considerable numerical effort, and it is only at $t \rightarrow \infty$ that the singularity at $\varphi_S = 104.5^\circ$ known from the steady case is formed, cf. also J. Cousteix (1986).

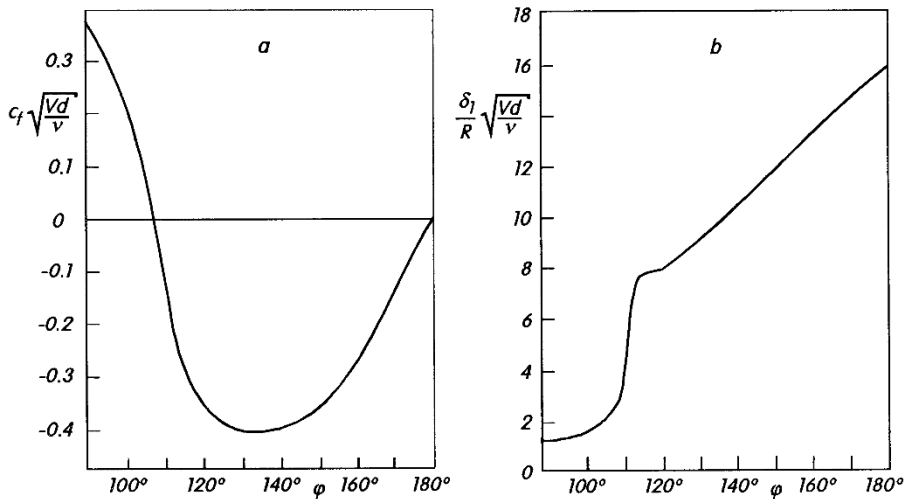


Fig. 13.3. Distributions of wall shear stress and displacement thickness at time $tV/R = 1.5$ at a circular cylinder impulsively set into motion, after T. Cebeci (1986)
 (a) skin-friction coefficient $c_f \sqrt{Vd/\nu}$ with $c_f = 2\tau_w/\rho V^2$
 (b) dimensionless displacement thickness $(\delta_1/R)\sqrt{Vd/\nu}$

As will be explained in Chap. 14, the question of the singularity is superfluous when higher order boundary-layer effects, particularly the interaction between the boundary layer and the outer flow, are taken into account.

A succession of flow portraits at a circular cylinder in start-up from rest are shown in Fig. 13.4. These shots were taken by L. Prandtl. It can be seen from Fig. 13.4a that immediately after start-up the flow portrait is that of potential flow. In Fig. 13.4b, the separation at the rear stagnation point has just begun. In Fig. 13.4c, the separation point has already shifted quite far forwards. A vortex layer develops from the separation point, and this then rolls up and forms two concentrated vortices (Fig. 13.4d). In Fig. 13.4e it is seen that these two vortices have grown further. Later this vortex pair becomes unstable. The vortices are pulled along by the outer flow and swim away (Fig. 13.4f). Finally an irregularly oscillating flow forms with a pressure distribution at the body which differs greatly from that of potential theory, cf. also M. Schwabe (1935). The dividing of the flow field into a boundary layer close to the wall and an inviscid outer flow, the concept which is the basis of boundary-layer theory, is then no longer possible.

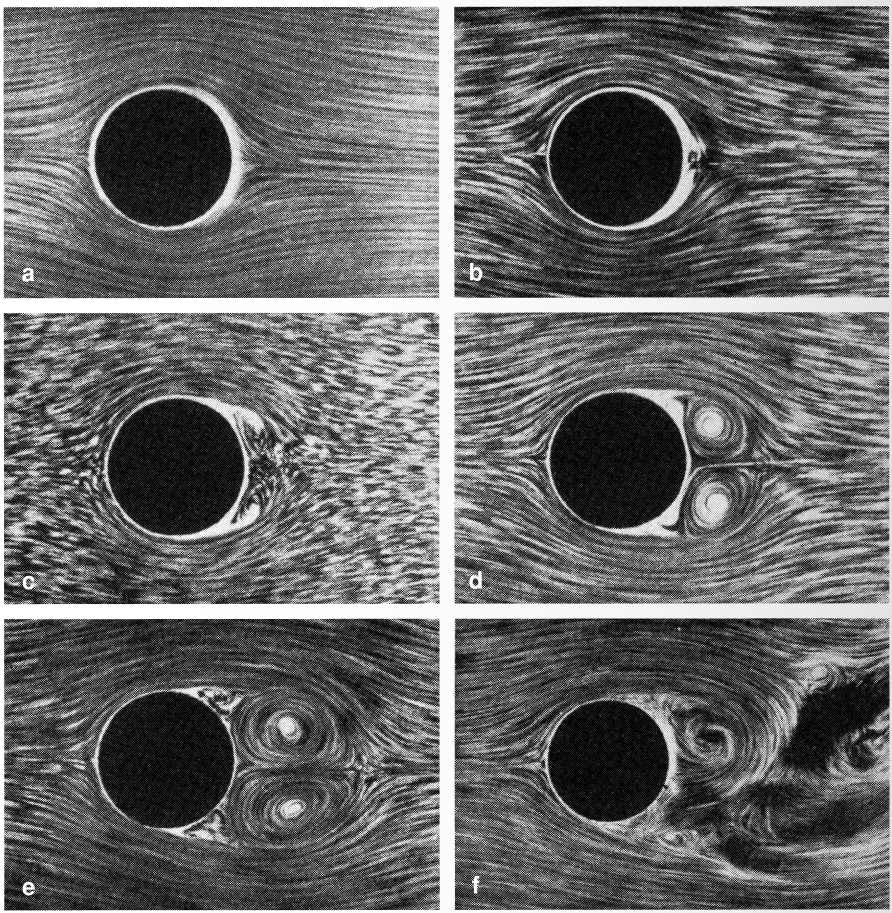


Fig. 13.4 a-f. Formation of vortices in the flow past a circular cylinder after acceleration from rest, after L. Prandtl

Elliptical cylinder. Elliptical cylinders suddenly set into motion out of rest in the direction of the semi-major axis a have been treated by W. Tollmien (1931) and H. Görtler (1948). The maximum of $|d\tilde{U}/dx|$ depends on the axial ratio $k = b/a$. It turns out that $|d\tilde{U}/dx|_{\max}$ only lies at the rear stagnation point as long as $k^2 < 4/3$. For $k^2 \geq 4/3$, the position with $|d\tilde{U}/dx|_{\max}$ is at

$$\frac{y}{b} = \sqrt{1 - \frac{1}{3(k^2 - 1)}}, \quad k^2 \geq \frac{4}{3}.$$

Therefore, for $k^2 \geq 4/3$ the position with $|d\tilde{U}/dx|_{\max}$ is displaced further in the direction of the summit at the end of the semi-minor axis b . For the flat plate ($k^2 \rightarrow \infty$) in a transverse flow, the position with $|d\tilde{U}/dx|_{\max}$ lies at the edge. The time t_0 to the onset of vanishing wall shear stress (or the distance to this point $t_0 V$ in Eq. (13.24)) is shown in Fig. 13.5 as a function of the axial ratio k .

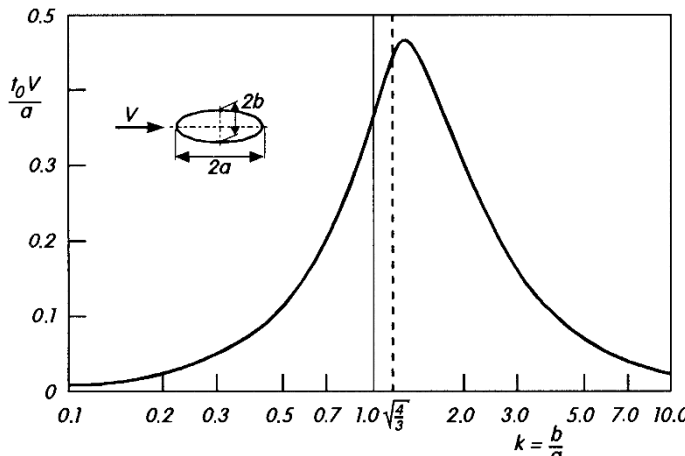


Fig. 13.5. Dimensionless time until the onset of vanishing wall shear stress for an elliptical cylinder impulsively set into motion

The start-up process of elliptical cylinders at an angle of attack has been investigated by D.P. Telionis; D.T. Tsahalis (1974), see also H.J. Lügt; H.J. Haussling (1974) and D.P. Telionis (1981), p. 129.

Sphere. The formation of the boundary layer at a sphere impulsively set into motion out of rest has been calculated by E. Boltze (1908). With the velocity of the outer flow

$$\tilde{U}(x) = \frac{3}{2}V \sin \frac{x}{R},$$

the wall shear stress vanishes at (from Eq. (13.24))

$$1 + 1.573t_0 \frac{3}{2}V \cos \frac{x}{R} = 0$$

or at the rear stagnation point $t_0 V / R = 0.42$. The extension of Eq. (13.24) by two further terms in the expansion has been used by E. Boltze to determine the more exact value of $t_0 V / R = 0.39$. The position with $\tau_w = 0$ is displaced (as with the circular cylinder in Fig. 13.2) away from $\varphi = \pi$ first quickly and then ever more slowly towards the position $\varphi = 110^\circ$ of the steady flow. This is only reached after an infinitely long time. Figure 13.6 shows the streamline portrait and the velocity distributions at an intermediate time. This state corresponds to the time $tV/R = 0.6$. The velocities inside the closed vortex are very small. The velocity gradient and the vorticity are largest outside the dividing streamline $\psi = 0$. Recent investigations into the flow of a sphere set impulsively into motion are presented by L.L. Van Dommelen (1987, 1990).

The boundary layer on a axisymmetric ellipsoid at an angle of attack set impulsively into motion has been computed by T. Wu; S.F. Shen (1992).

Start-up of rotating bodies. The formation of the boundary layer at a rotating disk has been treated by K.H. Thiriot (1950), both for the case where the disk is set impulsively into constant rotation in a fluid at rest, and for the case where the

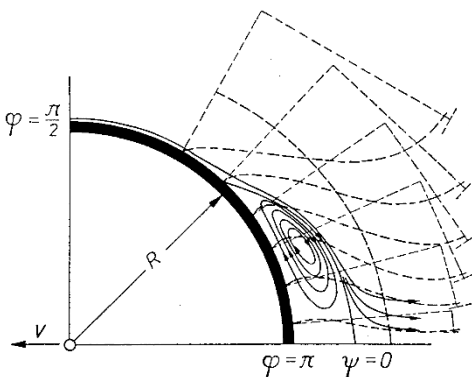


Fig. 13.6. Boundary layer on the downstream side of a sphere accelerated impulsively at time $tV/R = 0.6$, after E. Boltze (1908)

disk rotating with the fluid is impulsively brought to a standstill. The final state of the first case is the solution of the rotating disk in a fluid at rest in Sect. 5.2.4. The final state of the second case is the solution of the rotating flow over fixed ground in Sect. 12.1.4. The first case has also been investigated by S.D. Nigam (1951). The second case has been generalised by K.H. Thiriot (1942) to the case where a disk rotating with the fluid is suddenly brought to another slightly different constant angular velocity: eventually a steady boundary layer will form at the rotating disk.

The boundary layer at a non-uniformly rotating disk has been computed by E.M. Sparrow; J.L. Gregg (1960a) and the growth of the boundary layer at rotating symmetric bodies by C.R. Illingworth (1954) and Y.D. Wadhwa (1958); for the case of the rotating sphere see also L.L. Van Dommelen (1987, 1990).

The formation of the boundary layer at a circular cylinder impulsively set into translational and rotational motion has been investigated by W. Tollmien (1924), see also M.C. Ece et al. (1984).

Start-up processes and natural convection. If a vertical flat plate in a fluid at rest is impulsively brought to a temperature different from that of the fluid, the start-up process for natural convection occurs. This has been computed by S.N. Brown; N. Riley (1973), cf. also C.R. Illingworth (1950) and D.B. Ingham (1977).

Start-up processes with finite acceleration. As well as sudden start-up, start-up processes with finite acceleration have also been investigated. These then have the outer flow of Eq. (13.17). In this case, the motion begins with the finite acceleration $\tilde{U}(x)/t_R$. The formation of the boundary layer for the case of a time independent acceleration of the body has already been presented by H. Blasius (1908). The results are very similar to those of impulsive start-up, see also H. Schlichting (1982), p. 428.

An extension of these investigations to outer flows of the form $U(x, t) = \tilde{U}(x) t^n$ ($n = 0, 1, 2, 3, 4$) has been carried out by H. Görtler (1944). Here $n = 0$ is impulsive start-up, and $n = 1$ is start-up with constant acceleration. Similar investigations are also due to J. Watson (1958) and C.Y. Wang (1967). The start-up process of a rotating sphere under the assumption $U(x, t) \sim t^n$ has also been examined by C. Sozou (1971) and Z. Zapryanov (1977).

13.2.2 Oscillation of Bodies in a Fluid at Rest

An example of a periodic boundary-layer flow is the boundary layer at a body which moves back and forth in the form of a harmonic oscillation with small amplitude in a fluid at rest. This is an extension of the problem of the boundary layer at a flat wall carrying out harmonic oscillations in its own plane which was treated in Sect. 5.3.2.

The ideas in this section will show that high frequency oscillations in a fluid initially at rest cause a *steady secondary flow* through the action of viscosity in the boundary layer. This secondary flow is such that the entire fluid close to the oscillating body is set into steady motion, although the motion of the body is purely periodic. This phenomenon is called “streaming” or “acoustic streaming”. Effects of this kind come into play in the formation of *dust patterns* in a Kundt tube.

In computing the boundary layer we will again use a coordinate system fixed to the body. If the cylindrical body in steady plane flow under consideration has the potential theory velocity distribution $\tilde{U}(x)$, the potential flow for periodic oscillations with frequency n is:

$$U(x, t) = \tilde{U}(x) \cos nt. \quad (13.25)$$

The velocity boundary layer then satisfies the equations (13.3) and (13.4) with $j = 0$, $\varrho = \text{const}$, $\mu = \text{const}$, $g = 0$. The calculation is due to H. Schlichting (1932), cf. also D.P. Telionis (1981), p. 158.

Because of the high frequency n , the solution can be written down in the form of an expansion as in Sect. 13.1.4. For the u component of the velocity, the trial solution reads

$$\begin{aligned} u(x, y, t) = & \tilde{U}(x)[f'_{00}(\eta_s) \cos nt + f'_{01}(\eta_s) \sin nt] \\ & + \frac{\tilde{U}}{n} \frac{d\tilde{U}}{dx} [f'_{10}(\eta_s) \cos 2nt + f'_{11}(\eta_s) \sin 2nt + f'_{12}(\eta_s)] \end{aligned} \quad (13.26)$$

with

$$\eta_s = \sqrt{\frac{n}{2\nu}} y \quad (13.27)$$

according to Eq. (5.105). The term in the first square brackets corresponds to the solution of Eq. (13.12), while that in the second square brackets is the solution of Eq. (13.13). The term $f'_{01}(\eta_s) \sin nt$ takes into account the fact that a phase shift can occur between the oscillation in the boundary layer and the oscillation in the outer flow. Also worth noting in the trial solution is the time independent term $f'_{12}(\eta_s)$. Equation (13.13) contains products of the solution u_0 , \bar{u}_0 . Since these are proportional to $\cos nt$ and $\sin nt$ respectively, products of the trigonometric functions appear. From

$$(\cos nt)^2 = 1 - (\sin nt)^2 = \frac{1}{2} \cos 2nt + \frac{1}{2}, \quad \cos nt \sin nt = \frac{1}{2} \sin 2nt$$

the trial solution with double frequency oscillations and the steady part follows.

The differential equations for the functions dependent on η_s are

$$\begin{aligned} f_{00}''' - 2f'_{01} &= 0 \\ f_{01}''' + 2f'_{00} &= 2 \\ f_{10}''' - 4f'_{11} &= f_{00}^{\prime 2} - f_{01}^{\prime 2} - f_{00}f'_{00} + f_{01}f'_{01} - 1 \\ f_{11}''' + 4f'_{10} &= 2f'_{00}f'_{01} - f_{00}f'_{01} - f_{01}f'_{00} \\ f''_{12} &= f_{00}^{\prime 2} + f_{01}^{\prime 2} - f_{00}f'_{00} - f_{01}f'_{01} - 1 \end{aligned} \quad (13.28)$$

with the boundary conditions:

$$\begin{aligned} \eta_s = 0 : \quad f_i &= 0, \quad f'_i = 0, \quad i = 00, 01, 10, 11, 12 \\ \eta_s \rightarrow \infty : \quad f'_{00} &= 1, \quad f_i = 0, \quad i = 01, 10, 11. \end{aligned} \quad (13.29)$$

The first two solutions are

$$f'_{00} = 1 - e^{-\eta_s} \cos \eta_s, \quad f'_{01} = -e^{-\eta_s} \sin \eta_s. \quad (13.30)$$

For the boundary condition $\eta \rightarrow \infty$ in Eq. (13.29), we expressly did not require that $f'_{12} = 0$. It turns out that the solutions of the differential equation for $f_{12}(\eta_s)$

$$f''_{12} = e^{-2\eta_s} - \eta_s e^{-\eta_s} (\cos \eta_s + \sin \eta_s) + e^{-\eta_s} (\sin \eta_s - 2 \cos \eta_s) \quad (13.31)$$

cannot satisfy this condition. This solution reads:

$$\begin{aligned} f'_{12}(\eta_s) &= -\frac{3}{4} + \frac{1}{4}e^{-2\eta_s} - \frac{1}{2}\eta_s e^{-\eta_s} (\cos \eta_s - \sin \eta_s) \\ &\quad + \frac{1}{2}e^{-\eta_s} (\cos \eta_s + 4 \sin \eta_s). \end{aligned} \quad (13.32)$$

In particular

$$f'_{12}(\eta_s \rightarrow \infty) = -\frac{3}{4}. \quad (13.33)$$

According to the trial solution (13.26), the inviscid outer flow then no longer reads as Eq. (13.25) but rather

$$U(x, t) = \tilde{U}(x) \cos nt - \frac{3}{4} \frac{\tilde{U}}{n} \frac{d\tilde{U}}{dx}. \quad (13.34)$$

The extension of the solution for high frequencies therefore yields, with two terms on the outer edge of the boundary layer, a steady part which is independent of the viscosity and which decreases with increasing frequency. The contribution of the additional term in Eq. (13.34) is therefore directed so that the fluid flows in the direction of decreasing velocity $\tilde{U}(x)$.

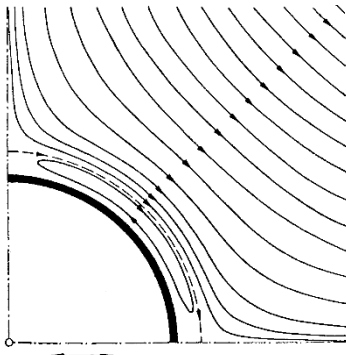


Fig. 13.7. Flow portrait of the secondary flow (streaming) close to an oscillating circular cylinder, after H. Schlichting (1932)

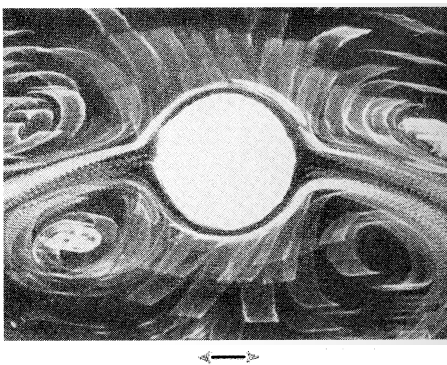


Fig. 13.8. Secondary flow (streaming) close to an oscillating circular cylinder, after H. Schlichting (1932)

Figure 13.7 shows the streamline portrait of this steady additional flow for the example of an oscillating circular cylinder. Figure 13.8 shows a shot of a water flow at a circular cylinder which oscillates back and forth in a tank. The shot was taken by a camera moving with the cylinder. Small metallic particles were scattered on the surface of the water and at this slow shutter speed they describe the oscillating motion with wide bands. The steady flow approaches the cylinder from above and below and moves away from both sides in the direction of oscillation, in good agreement with the theoretical streamline portrait in Fig. 13.7. Similar flow portraits have also been presented by E.N. Andrade (1931), where a circular cylinder was brought to a standing sound wave and the secondary flow was made visible with smoke.

This phenomenon now presents a simple explanation for the appearance of Kundt's dust patterns. Sound waves are longitudinal waves where the amplitude maximum is between two nodes, cf. Fig. 13.9. Because of the above effect we obtain an additional flow which, close to the wall, is directed away from the maxima towards the nodes. At great distances from the wall, for continuity reasons, the flow is in the opposite direction. This steady additional flow is precisely that which transports the dust and heaps it up at the nodes.

It simultaneously becomes clear that the appearance of dust patterns is greatly dependent on the amount of dust present. If there is a lot of dust, this swirls up

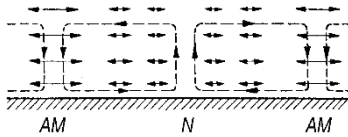


Fig. 13.9. Explanation of the formation of Kundt's dust patterns
AM: amplitude maximum. N: node

and much of it ends up in the inner flow, so that dust cannot be carried away from the maxima. On the other hand, if there is only a little dust present, the action of the wall flow dominates and the maxima are soon free of dust. This question has been extensively discussed in the literature on acoustics, cf. P.J. Westervelt (1953).

A corresponding investigation into flows close to an axisymmetric ellipsoid which carries out oscillations parallel to its axis in a fluid at rest has been made by A. Gosh (1961), cf. also D. Roy (1961, 1962).

13.3 Unsteady Boundary Layers in a Steady Basic Flow

We shall now consider unsteady boundary layers where the outer flow consists of a steady basic flow with an unsteady flow superimposed, thus

$$U(x, t) = \bar{U}(x) + U_1(x, t). \quad (13.35)$$

If $U_1(x, t)$ is a periodic function, then $\bar{U}(x)$ is the time average over one period (i.e. $\bar{U}_1(x, t) = 0$). However $U_1(x, t)$ can be a transition function corresponding to Eq. (13.17).

In practice, the unsteady part $U_1(x, t)$ is frequently much smaller than the steady part. This can lead to considerable simplifications in the calculation, as will be shown in the following examples.

13.3.1 Periodic Outer Flow

The solutions of Eqs. (13.3) and (13.4) with $j = 0$, $\varrho = \text{const}$, $\eta = \text{const}$ and $g = 0$ can also be divided up into a time average and a periodic part:

$$\begin{aligned} u(x, y, t) &= \bar{u}(x, y) + u_1(x, y, t) \\ v(x, y, t) &= \bar{v}(x, y) + v_1(x, y, t) \\ p(x, t) &= \bar{p}(x) + p_1(x, t) \end{aligned} \quad (13.36)$$

with $\bar{u}_1 = \bar{v}_1 = \bar{p}_1 = 0$. If we insert Eq. (13.35) into Eq. (13.6) and form the time average, we obtain

$$-\frac{\partial \bar{p}}{\partial x} = \varrho \left(\bar{U} \frac{d\bar{U}}{dx} + \overline{U_1 \frac{\partial \bar{U}_1}{\partial x}} \right). \quad (13.37)$$

Subtracting this equation from Eq. (13.6) yields

$$-\frac{\partial p_1}{\partial x} = \varrho \left(\frac{\partial U_1}{\partial t} + \overline{U} \frac{\partial U_1}{\partial x} + U_1 \frac{d\overline{U}}{dx} + U_1 \frac{\partial U_1}{\partial x} - \overline{U_1 \frac{\partial U_1}{\partial x}} \right). \quad (13.38)$$

Similarly Eq. (13.4) yields the following equation for the average motion $\overline{u}(x, y), \overline{v}(x, y)$:

$$\overline{u} \frac{\partial \overline{u}}{\partial x} + \overline{v} \frac{\partial \overline{u}}{\partial y} = \overline{U} \frac{d\overline{U}}{dx} + \nu \frac{\partial^2 \overline{u}}{\partial y^2} + F(x, y) \quad (13.39)$$

with

$$F(x, y) = \overline{U_1 \frac{\partial U_1}{\partial x}} - \left(\overline{u_1 \frac{\partial u_1}{\partial x}} + \overline{v_1 \frac{\partial u_1}{\partial y}} \right), \quad (13.40)$$

cf. also Eq. (5.131). Because of the additional term $F(x, y)$, the average motion for the periodic outer flow is *different* from the motion for the steady basic flow. As emerges from Eq. (13.40), $F(x, y)$ can only be determined if the unsteady parts u_1, v_1, p_1 of the flow are known. In addition to Eq. (13.39) we also have the continuity equation

$$\frac{\partial \overline{u}}{\partial x} + \frac{\partial \overline{v}}{\partial x} = 0 \quad (13.41)$$

and the usual boundary conditions.

The oscillating motions satisfy equations which agree with Eqs. (5.132) and (5.133).

As has already been described in Sect. 5.3.5, this system of equations is greatly simplified in the limit of high frequencies, cf. also Sect. 13.1.4. For $u_1(x, y, t)$ we then have the linear equation

$$\frac{\partial u_1}{\partial t} = \frac{\partial U_1}{\partial t} + \nu \frac{\partial^2 u_1}{\partial y^2}, \quad (13.42)$$

which corresponds to Eq. (5.135). If

$$U_1(x, t) = U(x) \cos nt, \quad (13.43)$$

then the addition term $F(x, y)$ from Eqs. (5.138) and (5.139) is found. The function $\overline{F}(\eta_s)$ is shown in Fig. 5.15.

The outer flow of general form

$$U(x, t) = \overline{U}(x) + \sum_{k=1} U_{1k}(x) \cos knt \quad (13.44)$$

possesses the additional function

$$F(x, y) = \frac{1}{2} \sum_{k=1} U_{1k} \frac{dU_{1k}}{dx} \overline{F} \left(\frac{y}{\sqrt{2\nu/kn}} \right), \quad (13.45)$$

cf. C.C. Lin (1957). The special case $U(x) = \bar{U}(x)$ in Eq. (13.43) has been investigated by T.J. Pedley (1972).

As has already been shown in Sect. 5.5, the boundary layer has a *two-layer structure* at high frequencies. As well as the thickness $\delta \sim \sqrt{\nu/Vl} l$ of the steady basic flow boundary layer (*Prandtl layer*), the much thinner *Stokes layer* of thickness $\delta \sim \sqrt{\nu/n}$ also exists. The oscillations due to the unsteady part of the outer flow take place in this Stokes layer.

The position of the point where the wall shear stress vanishes ($\tau_w = 0$) behaves in a manner corresponding to the structure of the flow. The wall shear stress is also an oscillating quantity, so that the position of $\tau_w = 0$ is displaced periodically along the wall. The time average position is therefore generally different from the position in a steady basic flow alone.

13.3.2 Steady Flow with a Weak Periodic Perturbation

If the outer flow has a velocity distribution of the form

$$U(x, t) = \bar{U}(x) + \varepsilon U_1(x, t) \quad (13.46)$$

where ε is a small value, we can use a power series expansion for the solution:

$$u(x, y, t) = u_0(x, y) + \varepsilon u_1(x, y, t) + \varepsilon^2 u_2(x, y, t) + \dots$$

$$v(x, y, t) = v_0(x, y) + \varepsilon v_1(x, y, t) + \varepsilon^2 v_2(x, y, t) + \dots$$

Comparison with Eq. (13.36) yields

$$\bar{u} = u_0 + \varepsilon^2 \bar{u}_2, \quad \bar{v} = v_0 + \varepsilon^2 \bar{v}_2. \quad (13.47)$$

The time independent changes compared to the steady basic flow are therefore of the order of magnitude $O(\varepsilon^2)$. Inserting Eq. (13.47) into Eq. (13.39) and only taking terms $O(\varepsilon^2)$ into account, with $F = \varepsilon^2 \tilde{F}$, we find the following system of equations for $\bar{u}_2(x, y)$, $\bar{v}_2(x, y)$:

$$\begin{aligned} \frac{\partial \bar{u}_2}{\partial x} + \frac{\partial \bar{v}_2}{\partial y} &= 0 \\ u_0 \frac{\partial \bar{u}_2}{\partial x} + \bar{u}_2 \frac{\partial u_0}{\partial x} + \bar{v}_0 \frac{\partial \bar{u}_2}{\partial y} + \bar{v}_2 \frac{\partial u_0}{\partial y} &= \tilde{F}(x, y). \end{aligned} \quad (13.48)$$

Just as for the differential equations for $u_1(x, y, t)$, $v_1(x, y, t)$, these are linear differential equations.

The wedge flow with outer flow of the form

$$U(x, t) = ax^m(1 + \varepsilon \cos nt) \quad (13.49)$$

has been the subject of numerous investigations, cf. N. Rott; M.L. Rosenzweig (1960) and K. Gersten (1965). Special cases are the stagnation-point flow treated in Sect. 5.3.2 and the flow at a flat plate at zero incidence

investigated by A. Gosh (1961) and S. Gibellato (1954, 1956). A. Gosh (1961) and P.G. Hill; A.H. Stenning (1960) have also carried out measurements on unsteady boundary layers. K. Gersten (1965) has determined the heat transfer. He showed that for heat transfer too, there is a time independent change compared to the steady case proportional to ε^2 . However, the heat transfer due to oscillations decreases for stagnation-point flow, for example, while the wall shear stress increases.

Example: Wall shear stress at the flat plate

With the outer flow

$$U(x, t) = U_\infty(1 + \varepsilon \cos nt) \quad (13.50)$$

K. Gersten (1965) showed that the skin-friction coefficient is

$$\begin{aligned} c_f(x, t)\sqrt{\text{Re}_x} &= 0.664 + \varepsilon[f''_{10w}(X) \cos nt + f''_{11w}(X) \sin nt] \\ &\quad + \varepsilon^2[f''_{20w}(X) \cos 2nt + f''_{21w}(X) \sin 2nt + f''_{22w}(X)] \end{aligned} \quad (13.51)$$

with

$$X = \frac{nx}{U_\infty}. \quad (13.52)$$

The functions depending on X can be found in K. Gersten (1965). For $X = 0$ these functions satisfy $f''_{10w} = (3/2)0.664$; $f''_{11w} = 0$; $f''_{20w} = f''_{22w} = (3/16)0.664$; $f''_{21w} = 0$. We obtain a quasi-steady solution, i.e. at any point in time, the solution behaves as the corresponding steady solution with that instantaneous outer flow. The appearance of a term proportional to $\sin nt$ implies that the boundary layer experiences a phase shift compared to the outer flow. The maximum of the wall shear stress leads the maximum of the outer flow velocity, and in the limit $X \rightarrow \infty$, the phase angle is 45° . For $X \rightarrow \infty$ there is again a two-layer structure. In addition it turns out that the amplitude of the wall shear stress oscillation grows infinitely with increasing X .

The solutions $u_2(x, y, t)$, $v_2(x, y, t)$ have a periodic part with double frequency and in addition a part independent of time which changes the basic flow of the boundary layer, but which dies away towards the outer edge of the boundary layer.

The formula for the Nusselt number analogous to Eq. (13.51) can be found in K. Gersten (1965). Numerical results for the velocity field proportional to ε have also been presented by W. Geißler (1993).

Further examples. W. Geißler (1993) has computed the unsteady boundary layer on an oscillating airfoil (airfoil NACA 0012 at a moderate angle of attack of $\alpha = 8^\circ$). The position of vanishing wall shear stress is discussed in great depth here.

M.H. Patel (1975) has investigated the unsteady boundary layer at the flat plate if a travelling wave is exposed to the plate. Here the wavelength must be much longer than the boundary-layer thickness. This problem is of importance for the instability of laminar boundary layers, cf. Chap. 15.

The unsteady heat transfer in the flow on a flat plate at zero incidence has been examined by N. Riley (1963).

13.3.3 Transition Between Two Slightly Different Steady Boundary Layers

We now consider flows where the outer flow changes according to a given transition function from one steady state to a new closely related steady state. An example of such an outer flow is

$$U(x, t) = U(x)[1 - \varepsilon(1 - e^{-t/t_R})]. \quad (13.53)$$

The problem is very closely related to that treated in the previous section. As K. Gersten (1967) has shown, the solutions linear in ε can be determined from those for the harmonically oscillating outer flow via a Laplace transform. This was carried out for wedge flows by K. Gersten (1967), both for the velocity field and the temperature field.

Example: Transition from one plate boundary layer to a slightly different plate boundary layer.

Setting $U(x) = U_\infty$ in Eq. (13.53) yields the simplifications that the initial and final states are now steady similar solutions. Figure 13.10 shows a typical result for the wall shear stress $\tau_w(x, t)$ for $\varepsilon = 0.1$. For $t_R \rightarrow \infty$ i.e. for $x/U_\infty t_R \rightarrow 0$ a *quasi-steady* solution is found. On the other hand, for the Stokes approximation ($t_R \rightarrow 0$) the transition of the wall shear stress is no longer monotonic and we “overshoot” the result. In heat transfer, not shown here, overshooting does not occur.

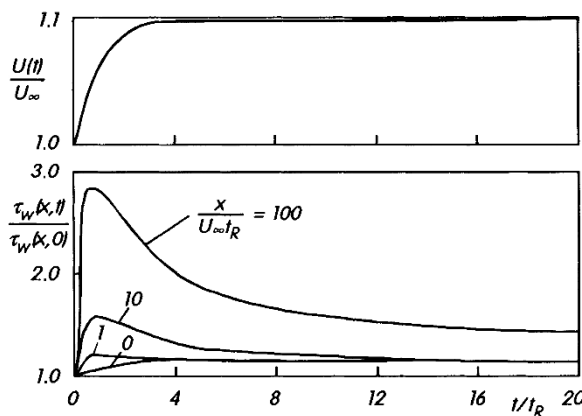


Fig. 13.10. Wall shear stress $\tau_w(x, t)$ in the transition from one plate boundary layer to another only slightly different plate boundary layer, after K. Gersten (1967)

For general unsteady boundary layers, the solution can be written down as a power series expansion in terms of:

$$\frac{x^k}{U^{k+1}} \frac{\partial^k U}{\partial t^k}, \quad \frac{1}{T_w - T_\infty} \left(\frac{x}{U} \right)^k \frac{\partial^k T_w}{\partial t^k}, \quad (13.54)$$

see F.K. Moore (1951), S. Ostrach (1955), F.K. Moore; S. Ostrach (1956) and E.M. Sparrow (1958). We will return to this in Sect. 13.4.3.

13.4 Compressible Unsteady Boundary Layers

13.4.1 Remark

The interest in compressible unsteady boundary layers is on the increase. Such boundary layers appear in shock-tubes and similar experimental set-ups used in thermodynamics behind shock waves or expansion waves. A good knowledge of unsteady compressible boundary layers is also required to determine the friction drag and the heat transfer on airfoils which carry out oscillating and accelerated or decelerated motion and whose wall temperatures possibly change in time.

In what follows we shall consider two simple examples of unsteady compressible boundary layers: the boundary layer behind a shock wave or expansion wave, and the boundary layer on a flat plate at zero incidence in non-uniform motion with a varying wall temperature.

An comprehensive study of unsteady boundary layers has been carried out by E. Becker (1961) and K. Stewartson (1964).

For the sake of simplicity, in what follows we shall assume that the gas is ideal with constant specific heat capacity c_p and constant Prandtl number. In addition we take the viscosity to be proportional to the absolute temperature (i.e. $\omega = 1$ in Eq. (10.46)). We neglect gravity. Using these assumptions we search for the solutions of Eqs. (13.3) to (13.5) for $j = 0$ and the corresponding boundary conditions.

The continuity equation may be satisfied by introducing a stream function $\psi(x, y, t)$. The velocity components are then

$$u = \frac{\varrho_\infty}{\varrho} \frac{\partial \psi}{\partial y}, \quad v = \frac{\varrho_\infty}{\varrho} \left(\frac{\partial \psi}{\partial x} + \frac{\partial Y}{\partial t} \right), \quad (13.55)$$

where the new transverse coordinate

$$Y = \int_0^y \frac{\varrho}{\varrho_\infty} dy \quad (13.56)$$

may be described as an “equivalent incompressible distance from the wall”, cf. Eq. (10.61). The value ϱ_∞ is some suitable constant reference density. Equations (13.55) are extensions to Eq. (10.60) for unsteady flows, where Eq. (13.56) is again the Dorodnizyn–Howarth transformation.

13.4.2 Boundary Layer Behind a Moving Normal Shock Wave

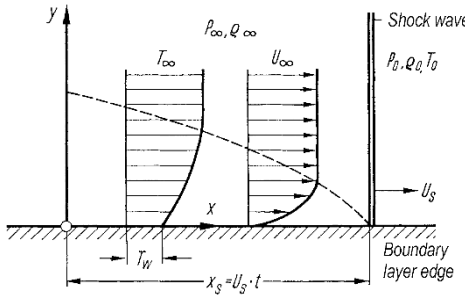


Fig. 13.11. Formation of the boundary layer behind a shock wave moving with velocity U_S

We consider the boundary-layer flow in Fig. 13.11 which forms behind a discontinuous compression wave (shock wave). The state of the gas at rest in front of the shock wave is denoted by the index 0; the gas state behind the shock wave outside the boundary layer with the index ∞ . Let the shock wave have constant velocity U_S . In addition, let us assume that the values of the outer flow behind the shock waves are independent of x and t . This implies that we are neglecting the effect of the boundary layer on the outer flow, as could occur in a shock tube. It turns out that this problem leads to similar solutions, i.e. the solutions are, instead of on the three variables x, y, t , only dependent on the single variable

$$\eta = \frac{Y}{2\sqrt{\nu_\infty \left(t - \frac{x}{U_S} \right)}} = \int_0^y \frac{\varrho}{\varrho_\infty} dy \Bigg/ 2\sqrt{\nu_\infty \left(t - \frac{x}{U_S} \right)} . \quad (13.57)$$

With the stream function ansatz

$$\psi(x, y, t) = 2U_\infty \sqrt{\nu_\infty \left(t - \frac{x}{U_S} \right)} f(\eta) \quad (13.58)$$

we obtain the velocity distribution in the boundary layer

$$u = U_\infty f'(\eta) . \quad (13.59)$$

For the temperature distribution we use the ansatz

$$\frac{T}{T_\infty} = 1 + \frac{\gamma - 1}{2} \text{Ma}_\infty^2 r(\eta) + \frac{T_w - T_{ad}}{T_\infty} s(\eta). \quad (13.60)$$

Inserting the trial solutions (13.58) and (13.60) into Eqs. (13.3) to (13.5), we obtain the following ordinary differential equations for $f(\eta)$, $r(\eta)$ and $s(\eta)$:

$$f''' + 2 \left(\eta - \frac{U_\infty}{U_S} f \right) f'' = 0, \quad (13.61)$$

$$\frac{1}{\text{Pr}} r'' + 2 \left(\eta - \frac{U_\infty}{U_S} f \right) r' = -2 f''^2, \quad (13.62)$$

$$\frac{1}{\text{Pr}} s'' + 2 \left(\eta - \frac{U_\infty}{U_S} f \right) s' = 0 \quad (13.63)$$

with the boundary conditions

$$\begin{aligned} \eta = 0 : \quad & f = 0, \quad f' = 0, \quad r' = 0, \quad s = 1 \\ \eta \rightarrow \infty : \quad & f' = 1, \quad r = 0, \quad s = 0. \end{aligned} \quad (13.64)$$

For $\eta = 0$, Eq. (13.60) yields the *adiabatic wall temperature* T_{ad} .

$$T_{ad} = T_\infty \left[1 + \frac{\gamma - 1}{2} \text{Ma}_\infty^2 r_w \right]. \quad (13.65)$$

The quantity r_w is the *recovery factor*, cf. Eq. (9.86) and (10.106).

For the skin-friction coefficient $c_f = 2\tau_w/\rho_w U_\infty^2$ we obtain

$$c_f \sqrt{\text{Re}} = f_w'' \quad (13.66)$$

and for the local Nusselt number

$$\text{Nu} = \frac{q_w}{T_w - T_{ad}} \frac{U_\infty(t - x/U_S)}{\lambda_w} = \frac{1}{2} \sqrt{\text{Re}} s'_w \quad (13.67)$$

with

$$\text{Re} = U_\infty^2 (t - x/U_S) / \nu_w. \quad (13.68)$$

The recovery factor r_w , the skin-friction coefficient c_f and Nusselt number Nu are shown in Fig. 13.12 plotted against U_∞/U_S for $\text{Pr} = 0.72$. The work of H. Mirels (1956), from which these results are obtained, also contains results for other Prandtl numbers.

The parameter U_∞/U_S is a measure of the strength of the shock. The greatest possible value is $U_\infty/U_S = 2/(\gamma + 1)$ (infinitely strong shock). For $\gamma = 1.4$ this yields the value $U_\infty/U_S = 0.83$. Negative values of U_∞/U_S correspond to fictitious discontinuous expansion waves whose appearance can be thought of as a concentration of continuous expansion waves. The special case

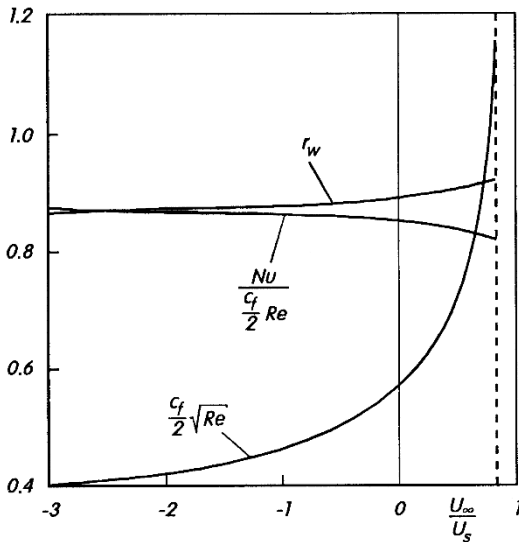


Fig. 13.12. Boundary layer behind a shock wave ($U_\infty > 0$) or an expansion wave ($U_\infty < 0$). Skin-friction coefficient c_f , Nusselt number Nu and recovery factor r_w plotted against U_∞/U_s , after H. Mirels (1956)

$U_\infty/U_s = 0$ is the first Stokes problem (cf. Sect. 5.3.1) of the flat wall impulsively set into motion.

As Fig. 13.12 shows, the skin-friction coefficient and the Nusselt number are smaller, and thus the boundary-layer thickness is smaller, for compression shock waves than for the case $U_\infty/U_s = 0$. The opposite is true for expansion waves.

In the special case $\text{Pr} = 1$ we have $s(\eta) = 1 - f'(\eta)$ yielding simple formulae for the Nusselt number (*Reynolds analogy* cf. Eq. (10.59)) and the recovery factor

$$\text{Nu} = \frac{c_f}{2} \text{Re}, \quad r_w = 1 \quad (\text{Pr} = 1) \quad (13.69)$$

for all values of U_∞/U_s . Then the adiabatic wall temperature is always equal to the total temperature.

The boundary layer behind a shock wave of constant pressure treated here is a simple special case in as much as it can be reduced to a steady problem. This is done by choosing a coordinate system in which the shock wave is at rest. More general solutions behind shock waves and expansion waves can be found in the work by E. Becker (1957, 1959b, 1961, 1962) and H. Mirels; J. Hamman (1962).

13.4.3 Flat Plate at Zero Incidence with Variable Free Stream Velocity and Wall Temperature

In our second example we consider the compressible unsteady boundary layer flow along a flat plate where both the outer flow $U_\infty(t)$ and the wall temperature $T_w(t)$ vary in time.

The stream function ψ in Eq. (13.55) and the dimensionless temperature distribution $\vartheta = (T - T_\infty)/(T_w - T_\infty)$ are written down as series:

$$\psi = \sqrt{\nu_\infty U_\infty x} [f_0(\eta) + \zeta_1 f_1(\eta) + \zeta_2 f_2(\eta) + \dots], \quad (13.70)$$

$$\vartheta = (T - T_\infty)/(T_w - T_\infty) = \vartheta_0(\eta) + \beta_1 \vartheta_1(\eta) + \beta_2 \vartheta_2(\eta) + \dots$$

$$+ \zeta_1 h_1(\eta) + \zeta_2 h_2(\eta) + \dots$$

$$+ \frac{U_\infty^2}{2c_p(T_w - T_\infty)} [s_0(\eta) + \zeta_1 s_1(\eta) + \zeta_2 s_2(\eta) + \dots]. \quad (13.71)$$

Here

$$\eta = \frac{Y}{2x} \sqrt{\frac{U_\infty x}{\nu_\infty}} \quad (13.72)$$

with Y in Eq. (13.56) a new dimensionless coordinate. We have used the following abbreviations:

$$\zeta_1 = \frac{\dot{U}_\infty}{U_\infty} \left(\frac{x}{U_\infty} \right), \quad \zeta_2 = \frac{\ddot{U}_\infty}{U_\infty} \left(\frac{x}{U_\infty} \right)^2, \dots \quad (13.73)$$

$$\beta_1 = \frac{\dot{T}_w}{T_w - T_\infty} \left(\frac{x}{U_\infty} \right), \quad \beta_2 = \frac{\ddot{T}_w}{T_w - T_\infty} \left(\frac{x}{U_\infty} \right)^2, \dots \quad (13.74)$$

Dots refer to differentiation with respect to time. Introducing these trial solutions into Eq. (13.3) to (13.5) yields differential equations for the solutions $f_i(\eta)$, $\vartheta_i(\eta)$ and $s_i(\eta)$ with $i = 0, 1, 2, \dots$. The solutions to these differential equations for $\text{Pr} = 0.72$ have been given by S. Ostrach (1955) and E.M. Sparrow; J.L. Gregg (1957). The functions $f_0(\eta)$, $\vartheta_0(\eta)$ and $s_0(\eta)$ are identical to the solutions for the steady problem for the instantaneous velocity U_∞ (*quasi-steady solution*). The other solutions deliver deviations from the quasi-steady solution.

The ratio of the wall shear stress τ_w to that for quasi-steady flow τ_{ws} is given by

$$\frac{\tau_w}{\tau_{ws}} = 1 + \frac{x}{U_\infty} \left[2.555 \frac{\dot{U}_\infty}{U_\infty} - 1.414 \frac{\ddot{U}_\infty}{U_\infty} \left(\frac{x}{U_\infty} \right) + \dots \right]. \quad (13.75)$$

In analogy the ratio of the wall heat fluxes with $\text{Pr} = 0.72$ can be obtained, cf. E.M. Sparrow (1958):

$$\begin{aligned} \frac{q_w}{q_{ws}} &= 1 + \frac{x}{U_\infty} \left[2.39 \frac{\dot{T}_w}{T_w - T_{\text{adS}}} + \dots \right. \\ &\quad \left. - \frac{\dot{U}_\infty}{U_\infty} \left(0.0692 \frac{T_w - T_\infty}{T_w - T_{\text{adS}}} - 0.0448 \frac{T_\infty - T_{\text{adS}}}{T_w - T_{\text{adS}}} \right) + \dots \right] \end{aligned} \quad (13.76)$$

with the adiabatic wall temperature of the quasi-steady flow

$$T_{\text{adS}} = T_\infty + 0.848 \frac{U_\infty^2}{2c_p}. \quad (13.77)$$

It is to be noted in using this method that the expressions $\zeta_1, \zeta_2 \dots$, $\beta_1, \beta_2 \dots$ for given functions $U_\infty(t)$ and $T_w(t)$ are in general dependent on one another. Compare the work of H. Tsuji (1953), H.D. Harris; A.D. Young (1967) and J.T. Stuart (1963).

14. Extensions to the Prandtl Boundary-Layer Theory

14.1 Remark

In the previous chapters we have already made mention of higher order boundary-layer theory on some different occasions. This theory treats the effects which were not taken into account in the boundary-layer equations used up until now. They will now be included in an extension to the Prandtl boundary-layer theory to a higher order boundary-layer theory. In acquiring this theory we will simultaneously be able to achieve statements about the region of validity of the Prandtl boundary-layer theory.

Already when deriving the Prandtl boundary-layer equations in Chap. 6, we took note of the two most important higher order boundary-layer effects, the *displacement* and the *wall curvature*, cf. Sect. 6.2. At the outer edge of the boundary layer, the v component of the boundary-layer solution does *not* pass over to that of the outer flow. The velocity difference in Eq. (6.35) is the velocity by which the outer flow is displaced outwards.

In addition in Sect. 6.2, we already mentioned that the curvature at the wall along which the boundary layer forms does not enter into the Prandtl boundary-layer equations.

In this chapter we will describe how the Prandtl boundary-layer theory can be systematically generalised and how the higher order effects mentioned can be taken into account.

Because of the displacement, there is a reaction of the boundary layer on the outer flow which changes it correspondingly. This change again leads back to a reaction on the boundary layer and therefore there is an *interaction* between the boundary layer and the outer flow. Here distinction is made between *weak* and *strong interactions*. In a weak interaction, the hierarchy just described exists: it commences with the displacement effect of the boundary layer on the outer flow and then continues with the subsequent action of the outer flow on the boundary layer, and so forth. We then speak of *higher order boundary-layer theory* in its narrowest sense. This is only true as long as there is no flow separation, i.e. no singularity occurs.

If a singularity does appear (e.g. separation) then there is a *strong interaction* at hand which cannot be included in the Prandtl boundary-layer theory in its original format and for this reason leads to the singularity. In strong interactions, the outer flow and the boundary-layer flow must be

computed *simultaneously*. An example is the strong interaction in hypersonic flows ($\text{Ma}_\infty \rightarrow \infty$) at slender bodies.

Frequently the structure of the flow field changes as a result of a strong interaction. Instead of the usual division of the flow field into the outer flow and the boundary-layer flow, in the region of the strong interaction there is a *three-layer structure*, and one speaks of *triple-deck theory* or *asymptotic interaction theory*. A characteristic feature here is that the frictional boundary layer is divided up into two further layers. Examples of strong interactions of this kind are flows at the trailing edge of a flat plate at zero incidence, at walls with obvious dents or humps and at walls in the region of a shock wave.

As has already been mentioned in Sect. 10.4.6, as well as displacement and curvature, there are also further higher order boundary-layer effects. These are of particular importance in hypersonic boundary layers.

In what follows we will treat the extensions to the Prandtl boundary-layer theory first of all for incompressible plane or axisymmetric flows. The generalisation to compressible flows and to hypersonic flows will then be presented.

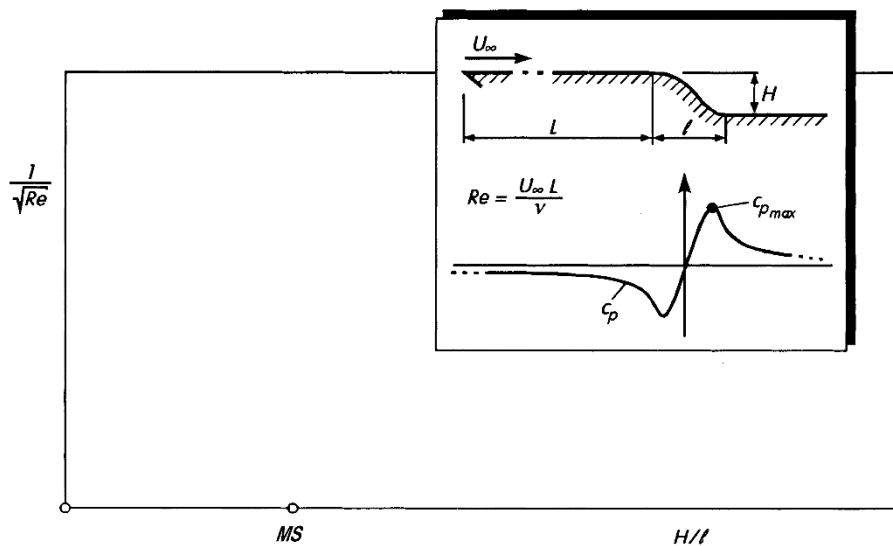


Fig. 14.1. Diagram for step flows. For constant ratio L/ℓ each point in the diagram corresponds to a step flow. MS: marginal separation

The treatment of incompressible plane flows will be carried out in a simple geometric configuration which possesses all essential geometric details in order to produce generally valid results which may be carried over to other geometries. As in Fig. 14.1, we consider the flows past rounded backward-facing steps. The flow is dependent on the following quantities: free stream velocity

U_∞ , kinematic viscosity ν , approach length L , length of the step ℓ and height of the step H . For a fixed step contour, we can form three dimensionless characteristic numbers: $\text{Re} = U_\infty L / \nu$, H/ℓ and L/ℓ . For a fixed characteristic number $L/\ell = \text{const}$, the diagram with axes scaled to $1/\sqrt{\text{Re}}$ and H/ℓ in Fig. 14.1 contains all possible solutions for a rounded backward-facing step. The region close to the H/ℓ axis corresponds to the Prandtl boundary-layer theory, as long as $H/\ell < (H/\ell)_{\text{MS}}$ holds. The Goldstein singularity occurs for $H/\ell = (H/\ell)_{\text{MS}}$.

As the following sections will show, the Prandtl boundary-layer theory can be systematically extended. This is done by taking into account either weak interactions for $(H/\ell) < (H/\ell)_{\text{MS}}$ (higher order boundary-layer theory) or strong interactions for $(H/\ell) \geq (H/\ell)_{\text{MS}}$ (triple-deck theory).

14.2 Higher Order Boundary-Layer Theory

In Sect. 6.1 we obtained the Prandtl boundary-layer equations from the complete equations of motion by estimating the order of magnitude of the different terms. However the boundary-layer equations can also be procured from a more general theory.

In order to acquire asymptotic expansions of the solutions of the Navier-Stokes equations for large Reynolds numbers, we carry out a *perturbation calculation*, where

$$\varepsilon = \frac{1}{\sqrt{\text{Re}}} = \frac{1}{\sqrt{\frac{U_\infty L}{\nu}}} \quad (14.1)$$

is used as the *perturbation parameter*. We obtain a so-called *singular perturbation problem* which leads to the asymptotic expansion desired being split up into an outer expansion (outer flow) and an inner expansion (boundary-layer flow). Using the *method of matched asymptotic expansions*, these yield the total solution.

The first term of the asymptotic expansion won in this manner is precisely the solution of the Prandtl boundary-layer equations. Carrying out the perturbation calculation however allows us to determine further terms in the expansion and thus to extend the Prandtl boundary-layer theory. This is called *higher order boundary-layer theory*. The second term in the expansion is of particular practical importance. This can be taken to yield a correction to the classical boundary-layer theory and thus the so-called second order boundary-layer effects.

Comprehensive descriptions of higher order boundary-layer theory have been given by M. Van Dyke (1969), K. Gersten (1972, 1982a), as well as K. Gersten; J.F. Gross (1976), V.V. Sychev et al. (1998), I.J. Sobey (2000). The method of matched asymptotic expansion is also described by M. Van Dyke (1964b). The essential basic ideas of this method are due to L. Prandtl and

have been made plausible in Sect. 4.7 in the form of a simple mathematical example.

In what follows we will briefly describe the theory used in determining asymptotic solutions for large Reynolds numbers for plane and axisymmetric incompressible flows. The main aim in doing this is the extension of the Prandtl boundary-layer theory and the derivation of the second order boundary-layer equation. The details are to be found in M. Van Dyke (1962a, 1962c).

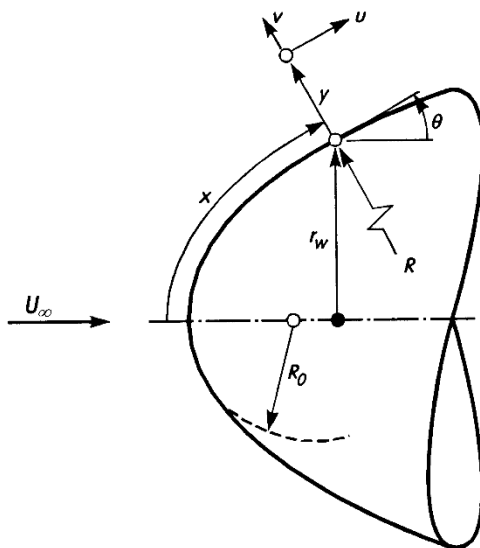


Fig. 14.2. System of natural coordinates for a plane or axisymmetric body

The foundations here are the Navier-Stokes equations in natural coordinates, as in Fig. 14.2. These equations are given in Sect. 3.13 (cf. Fig. 3.6) for plane flows and in M. Van Dyke (1962c) for axisymmetric flows (without velocity components in the circumferential direction).

The lengths are referred to a suitable reference length L , the velocities to U_∞ and the pressure exceeding p_∞ to ϱU_∞^2 . The geometry of the body is given by the local radius of curvature $R(x)$ (along a meridian) as well as by $r_w(x)$ in axisymmetric bodies. For the dimensionless surface curvature we have

$$K(x) = \frac{L}{R(x)}. \quad (14.2)$$

Outer expansions. We use the following asymptotic expansions for the solutions of the Navier–Stokes equations in natural coordinates (for plane flows Eqs. (3.99) to (3.101) with $\varrho = \text{const}$ and $f_x = f_y = 0$):

$$\begin{aligned} u(x, y, \varepsilon) &= U_1(x, y) + \varepsilon U_2(x, y) + \dots \\ v(x, y, \varepsilon) &= V_1(x, y) + \varepsilon V_2(x, y) + \dots \\ p(x, y, \varepsilon) &= P_1(x, y) + \varepsilon P_2(x, y) + \dots \end{aligned} \quad (14.3)$$

Insertion and sorting powers of ε leads to systems of equations for the first order solution $U_1(x, y)$, $V_1(x, y)$, $P_1(x, y)$, the second order solution $U_2(x, y)$, $V_2(x, y)$, $P_2(x, y)$ and so on in succession. Up until the second order solution, the terms proportional to ε^2 are neglected, i.e. the friction terms in the Navier–Stokes equations are not taken into account. The first and second order solutions therefore correspond to inviscid flow. In fact they correspond to potential flow if only homogeneous free streams are taken into account.

The boundary conditions for the *first* order solution are

$$\begin{aligned} y = 0 : \quad V_1(x, 0) &= 0, \\ y \rightarrow \infty : \quad U_1^2 + V_1^2 &= 1. \end{aligned} \quad (14.4)$$

The potential equation solution $U_1(x, y)$, $V_1(x, y)$ yields the velocity at the wall $U_1(x, 0)$ and, from the Bernoulli equation, the pressure at the wall

$$P_1(x, 0) = \frac{1}{2} - \frac{1}{2} U_1^2(x, 0). \quad (14.5)$$

The *second* order solution has the following boundary conditions:

$$\begin{aligned} y = 0 : \quad V_2(x, 0) &= \frac{1}{\varepsilon r_w^j} \frac{d}{dx} [U_1(x, 0) r_w^j \delta_1(x)], \\ y \rightarrow \infty : \quad U_2^2 + V_2^2 &= 0, \end{aligned} \quad (14.6)$$

where $\delta_1(x)$ is the displacement thickness defined in analogy to Eq. (2.4), cf. Eq. (14.12). We have $j = 0$ for plane flow and $j = 1$ for axisymmetric flow.

The solution of the potential equation again delivers the distribution at the wall for the velocity component parallel to the wall $U_2(x, 0)$ and for the pressure

$$P_2(x, 0) = -U_1(x, 0) \cdot U_2(x, 0). \quad (14.7)$$

The solutions in this manner generally do not satisfy the no-slip condition at the wall, and thus are not valid close to the wall. They are therefore called “outer solutions” or “outer asymptotic expansions”.

Inner expansions. The solution close to the wall requires special treatment. Instead of the distance from the wall y , we introduce a new stretched coordinate

$$N = \frac{y}{\varepsilon}. \quad (14.8)$$

This so-called *inner variable* is chosen precisely so that not all the friction terms in the first order theory in the new x, N coordinate system vanish.

We now use the following asymptotic expansion for the solution in the region close to the wall (boundary layer):

$$\begin{aligned} u(x, y, \varepsilon) &= u_1(x, N) + \varepsilon u_2(x, N) + \dots \\ v(x, y, \varepsilon) &= \varepsilon v_1(x, N) + \varepsilon^2 v_2(x, N) + \dots \\ p(x, y, \varepsilon) &= p_1(x, N) + \varepsilon p_2(x, N) + \dots \end{aligned} \quad (14.9)$$

Inserting this into the Navier–Stokes equations (in Eqs. (3.99) to (3.100) for plane flows) and sorting powers of ε leads to the following systems of equations: ($j = 0$: plane, $j = 1$: axisymmetric)

First order boundary layer:

$$\begin{aligned} \frac{\partial}{\partial x}(r_w^j u_1) + \frac{\partial}{\partial N}(r_w^j v_1) &= 0 \\ u_1 \frac{\partial u_1}{\partial x} + v_1 \frac{\partial u_1}{\partial N} + \frac{\partial p_1}{\partial x} - \frac{\partial^2 u_1}{\partial N^2} &= 0 \\ \frac{\partial p_1}{\partial N} &= 0 \end{aligned} \quad (14.10)$$

with the boundary conditions

$$\begin{aligned} N = 0 : \quad u_1 &= 0, v_1 = 0 \\ N \rightarrow \infty : \quad u_1 &= U_1(x, 0). \end{aligned} \quad (14.11)$$

These are precisely the Prandtl boundary-layer equations (6.30) and (6.31) or (12.1) and (12.2) (but without the buoyancy term, i.e. for $g = 0$), if they are suitably transformed to the x, N system. In addition $p_1(x) = P_1(x, 0)$.

The solution $u_1(x, N)$ yields the displacement thickness:

$$\delta_1(x) = \varepsilon \int_0^\infty \left[1 - \frac{u_1(x, N)}{U_1(x, 0)} \right] dN. \quad (14.12)$$

The first order boundary-layer equations (14.10) no longer contain the Reynolds number. Therefore it follows that $u_1(x, N)$ and $v_1(x, N)$ are also independent of the Reynolds number. Thus the position of the point of separation is also not dependent on the Reynolds number as long as higher order effects are neglected.

Second order boundary layer:

$$\begin{aligned}
 & \frac{\partial}{\partial x} \left[r_w^j \left(u_2 + j u_1 N \frac{\cos \theta}{r_w} \right) \right] \\
 & + \frac{\partial}{\partial N} \left[r_w^j \left\{ v_2 + v_1 N \left(K + j \frac{\cos \theta}{r_w} \right) \right\} \right] = 0 \\
 & u_1 \frac{\partial u_2}{\partial x} + u_2 \frac{\partial u_1}{\partial x} + v_1 \frac{\partial u_2}{\partial N} + v_2 \frac{\partial u_1}{\partial N} + \frac{\partial p_2}{\partial x} - \frac{\partial^2 u_2}{\partial N^2} \\
 & = K \left(N \frac{\partial^2 u_1}{\partial N^2} + \frac{\partial u_1}{\partial N} - N v_1 \frac{\partial u_1}{\partial N} - u_1 v_1 \right) + j \frac{\partial u_1}{\partial N} \frac{\cos \theta}{r_w} \\
 & \frac{\partial p_2}{\partial N} = K u_1^2
 \end{aligned} \tag{14.13}$$

with the boundary conditions

$$\begin{aligned}
 N = 0 : \quad u_2 = 0, \quad v_2 = 0, \\
 N \rightarrow \infty : \quad u_2 = U_2(x, 0) - K U_1(x, 0) N \\
 p_2 = P_2(x, 0) + K U_1^2(x, 0) N.
 \end{aligned} \tag{14.14}$$

The outer boundary conditions (i.e. $N \rightarrow \infty$) of the inner solution and the inner boundary conditions ($y = 0$) of the outer solution have been found by matching the outer and inner solutions, cf. M. Van Dyke (1962a).

The system of equations (14.13) and (14.14) for the second order boundary layer again does not contain the Reynolds number. It does, however, contain the solutions of the first order boundary-layer equations and is also more extensive than the system of equations for the first order boundary layer, but it consists of linear differential equations. Therefore the solution can be divided up into partial solutions. It is usual to split up the solution into a curvature part and a displacement part, a subject into which we will, at this juncture, go no further.

Because the wall curvature has been taken into account in the second order boundary-layer theory, a pressure gradient perpendicular to the wall occurs. The pressure at the wall is therefore different from the pressure imposed by the outer flow. Integration over the boundary layer yields the pressure coefficient at the wall:

$$\begin{aligned}
 \frac{1}{2} c_{pw} &= p(x, 0, \varepsilon) \\
 &= P_1(x, 0) + \varepsilon \left[P_2(x, 0) + K \int_0^\infty [U_1^2(x, 0) - u_1^2(x, N)] dN \right] \\
 &\quad + O(\varepsilon^2).
 \end{aligned} \tag{14.15}$$

The pressure at the wall is larger than the pressure imposed from outside if the curvature of the surface is convex ($K > 0$).

The distribution of the local skin-friction coefficient can be obtained by taking the second order boundary layer into account:

$$\frac{1}{2}c_f = \frac{\tau_w(x)}{\rho U_\infty^2} = \varepsilon \left(\frac{\partial u_1}{\partial N} \right)_{N=0} + \varepsilon^2 \left(\frac{\partial u_2}{\partial N} \right)_{N=0} + O(\varepsilon^3). \quad (14.16)$$

The second order boundary layer also has a reaction on the outer flow. The calculation of the second order displacement thickness is given in the work by K. Gersten (1974a).

Examples

Flat plate at zero incidence. In the case of the impermeable flat plate at zero incidence, the displacement thickness satisfies $\delta_1 \sim \sqrt{x}$. This, corresponding to Eq. (14.6), yields the boundary condition for the second order outer flow:

$$V_2(x, 0) = \frac{0.8604}{\sqrt{x}}, \quad (14.17)$$

where the plate length has been used as a reference length. The solution of the plane potential flow with this boundary condition leads precisely to $U_2(x, 0) = 0$. Therefore the solution of the system (14.13), (14.14) is the trivial solution. The second order friction drag then also vanishes at the flat plate.

Note 1 (Optimal coordinates)

Until now we have been using Cartesian coordinates. If we had been using parabolic coordinates instead, the first order outer flow would already be the sum of the first and second order outer flow presented here, so that the matching condition (14.17) for the v component in parabolic coordinates would already be satisfied in the first order. Therefore, for plate flows, parabolic coordinates are the so-called “optimal coordinates”. Optimal coordinates depend on the geometry of the body under consideration, cf. M. Van Dyke (1964b), p. 144. For example, for stagnation-point flow Cartesian coordinates are optimal, since the solution of the first order boundary-layer equation in this case is also the solution of the complete Navier-Stokes equations. For the convergent channel polar coordinates are optimal, cf. Sect. 7.2.3.

Note 2 (Drag coefficient at the semi-infinite plate)

Close to the leading edge, the first order boundary-layer equations are not valid. Since the wall shear stress $\tau_w \sim x^{-1/2}$, the limit $x \rightarrow 0$ produces a singularity. Indeed the flow up to a distance $x = O(\text{Re}^{-1})$ from the leading edge must be described by the complete Navier-Stokes equations. As A.I. Van De Vooren; D. Dijkstra (1970) have shown, integrating the wall shear stress of the complete solution leads to the following extended drag formula for the semi-infinite plate (cf. Eq. (6.59)):

$$c_D = 1.328 \text{Re}^{-1/2} + 2.326 \text{Re}^{-1} + O(\text{Re}^{-3/2}), \quad (14.18)$$

cf. also A.E.P. Veldman (1976). I. Imai (1957) used a global momentum balance to show that the second term in Eq. (14.18) alone can be computed from the Blasius boundary layer. It is found that $\beta_1^2 \pi/2 = 2.326$ with $\beta_1 = 1.2168$ from Eq. (6.52).

The extension of the drag formula to a *finite* flat plate at zero incidence from Eq. (6.59) (trailing edge effect) will be discussed in Sect. 14.4.

Plane symmetric stagnation-point flow. This flow has been treated comprehensively by M. Van Dyke (1962b). It is assumed that the first and second order outer flows yield the following velocity at the convex curved wall ($R = L$, i.e. $K = 1$) in the stagnation point ($x = 0$):

$$U(x, 0) = U_{11}x + \varepsilon U_{21}x + O(\varepsilon^2), \quad (14.19)$$

where U_{11} and U_{21} are constants which are only dependent on the geometry of the body in the flow. (In the cases of massive suction or blowing, U_{21} also depends on v_w .) K. Gersten; H. Herwig (1992), p. 271 have presented these constants for some different geometries.

The skin-friction coefficient for an impermeable wall is (see H. Schlichting (1982), p. 197):

$$\frac{1}{2}c_f = \frac{\tau_w}{\rho U_\infty^2} = \varepsilon x \sqrt{U_{11}} \left[1.2326 U_{11} - \varepsilon \left(1.19133 \sqrt{U_{11}} - 1.8489 U_{21} \right) \right] + O(\varepsilon^3) \quad (14.20)$$

and the pressure coefficient is

$$c_{pw} = 2 \frac{p_w - p_\infty}{\rho U_\infty^2} \\ = 1 - U_{11}^2 x^2 \left[1 - \varepsilon \left(1.8805 \frac{1}{\sqrt{U_{11}}} - 2 \frac{U_{21}}{U_{11}} \right) + O(\varepsilon^2) \right]. \quad (14.21)$$

These results for the skin-friction coefficient and the pressure coefficient are universal. The constants U_{11} and U_{21} to be inserted only depend on the geometry of the body. In all examples known so far, U_{21} is always negative. Therefore, close to the stagnation point of convex curved bodies, the skin-friction coefficient is made smaller and the pressure coefficient at the wall larger by second order boundary-layer effects (curvature and displacement).

Parabola in a symmetric flow. The second order boundary layer for a parabola in a symmetric flow has been computed by M. Van Dyke (1964a). Here $U_{11} = 1$ and $U_{21} = -0.61$. Figure 14.3 shows the distributions of the static pressure and the wall shear stress on the contour of the parabola according to second order boundary-layer theory for the Reynolds number $\text{Re} = U_\infty R_0 / \nu = 100$ (R_0 is the radius of curvature at the apex of the parabola). The distributions for first order boundary-layer theory ($\text{Re} \rightarrow \infty$) are also presented for comparison. Both pressure distributions start in the stagnation point with $c_p = 1$. For inviscid flow ($\text{Re} \rightarrow \infty$) it is found that

$$c_p = \frac{1}{1 + 2x^*}. \quad (14.22)$$

where $x^* = x'/R_0$ is the dimensionless distance from the top of the parabola measured along the axis, cf. Fig. 14.3. For $\text{Re} = 100$ the relation (14.22) holds close to the stagnation point, but here the coefficient 2 must be replaced by the numerical value 1.38, cf. H. Schlichting (1982), p. 198. As would be expected, the higher order boundary-layer effects decrease downstream, since, in particular, the curvature is less here. At about $x^* = 2$, the second order boundary effects have practically died away. A similar situation is also true for the skin-friction coefficient. In the stagnation point the second order boundary effects on the skin-friction coefficient

are strongest. Comparison with numerical solutions of the complete Navier–Stokes equations shows that at $\text{Re} = 100$, second order boundary-layer theory essentially yields the exact solution, cf. H. Schlichting (1982), p. 197.

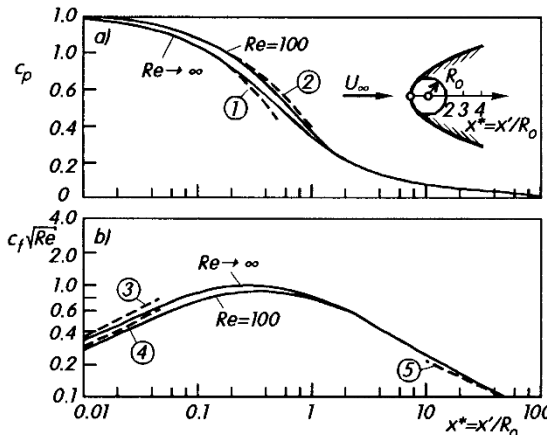


Fig. 14.3. Distribution of the static pressure (a) and the shear stress (b) on the contour of a parabola in a symmetric flow. The curves for $\text{Re} = 100$ are those from second order boundary-layer theory, those for $\text{Re} \rightarrow \infty$ from first order boundary-layer theory.

- (1) c_p for inviscid flow $\text{Re} \rightarrow \infty$, Eq. (14.22)
- (2) $c_p = 1/(1 + 1.38 x^*)$ for $\text{Re} = 100$
- (3) $c_f \sqrt{\text{Re}} = 3.486 \sqrt{x^*}$, stagnation point $\text{Re} \rightarrow \infty$
- (4) $c_f \sqrt{\text{Re}} = 2.63 \sqrt{x^*}$, stagnation point $\text{Re} = 100$
- (5) $c_f \sqrt{\text{Re}} = 0.664/\sqrt{x^*}$, flat plate

While the pressure coefficient increases due to second order boundary-layer effects, the skin-friction coefficient decreases. Therefore, the pressure drag of the parabola is greater than that for $\text{Re} \rightarrow \infty$, while the friction drag is less. In Sect. 5.1.4 we already used Fig. 5.7 to show how well the solution of the Navier–Stokes equations up to a Reynolds number of about $\text{Re} = 100$ is given by second order boundary-layer theory.

Further plane flows. The second order effects for the plane half body have been investigated by L. Devan (1964). The results are similar to those for the parabola. There are further solutions of the second order boundary-layer equations particularly in flows where the first order theory leads to similar solutions, cf. Sect. 7.2. For those flows where the first order outer flow is $U_1(x, 0) \sim x^m$, the second order boundary-layer equations also possess similar solutions if $K(x) \sim x^{(m-1)/2}$ and $U_2(x, 0) \sim x^n$.

Further details on investigations into second order boundary-layer effects can be found in M. Van Dyke (1969), K. Gersten (1972, 1982a, 1989a) and K. Gersten; J.F. Gross (1976). Details on work on second order boundary-layer theory when the boundary layer is influenced through suction or blowing are also to be found in these references, see also K. Gersten; J.F. Gross (1974b), K. Gersten et al. (1972, 1977), K. Gersten (1979) and J. Wiedemann (1983). Heat transfer is also dealt with by F. Schultz–Grunow; H. Henseler (1968), K. Gersten (1982a) and K. Gersten et al. (1991).

The plane free jet has been treated by S.G. Rubin; R. Falco (1968) and K. Mitsotakis et al. (1984) while K. Mörwald et al. (1986) has considered the buoyant jet. In the latter work it has also been shown that good agreement with experiment can only be attained if the temperature dependence of all physical properties is taken into account.

A certain parameter region of the rounded backward-facing step shown in Fig. 14.1 is also covered by higher order boundary-layer theory. For fixed l/L , a certain value of $H/l = (H/l)_{\text{MS}}$ from the first order theory produces a singularity. In principle, solutions for all values $H/l < (H/l)_{\text{MS}}$ for any Reynolds number can be given by this theory. On the other hand, this theory breaks down for $H/l \geq (H/l)_{\text{MS}}$. As already mentioned, *strong* interaction methods have to be applied here. These will be discussed in more detail in the next sections. Beforehand we will now look at some further examples of and extensions to higher order boundary-layer theory.

Axisymmetric flows. The axisymmetric stagnation-point flow and the axisymmetric flow at an axisymmetric paraboloid have been investigated by H.-D. Papenfuß (1974a, 1974b, 1975). As with the analogous plane flows, it was again possible, by comparison with the numerical solutions of the Navier-Stokes equations, to demonstrate that the second order boundary-layer theory yields practically exact results for $\text{Re} > 100$ (Re formed with R_0). While second order boundary effects lower the heat transfer at the stagnation point of the parabola, in the case of the paraboloid the heat transfer is increased.

E. Beese; K. Gersten (1979) have determined the second order boundary layer on a axially moved cylinder in surroundings at rest.

Also worth mentioning are the pieces of work on higher order effects for the axisymmetric momentum jet by K. Mitsotakis et al. (1984) as well as on the buoyant jet by C.A. Hieber; E.J. Nash (1975) and K. Mörwald et al. (1986).

Effects of transversal curvature in natural convection have been investigated by H.K. Kuiken (1968b).

Three-dimensional flows. The theory presented here has been extended to three-dimensional flows in numerous pieces of work. These may be the flow at a yawing plane body, see for example K. Gersten; J.F. Gross (1973b), K. Gersten et al. (1972), K. Gersten (1977), or the flow past a three-dimensional body, such as the three-dimensional paraboloid, investigated by H.-D. Papenfuß (1974a, 1974b, 1975).

Compressible flows. The extension of higher order boundary-layer theory to compressible flows has been carried out by M. Van Dyke (1962c). As well as the displacement and curvature effects appearing in incompressible flows, there are also two further second order effects: the influence of the *vorticity* in the outer flow which could be, for example, a consequence of curved shock waves in front of the body, and *non-continuum effects*. These are effects such as a *slipping* of the flow and a *temperature jump* at the wall. Such effects are consequences of the corresponding boundary conditions at the outer edge (shock wave) of a supersonic flow or at the wall.

There are numerous examples at hand, particularly of calculations of supersonic flows. In Chap. 1, Fig. 1.18, we already presented the results of a second order boundary-layer computation at a circular cylinder by K. Oberländer. This was compared to experimental results. There are further pieces of work on blunt bodies in supersonic and hypersonic flows by R.T. Davis; I. Flügge-Lotz (1964), T.K. Fannelöp; I. Flügge-Lotz (1965, 1966), H.D. Papenfuß (1975), K. Gersten (1977).

H.D. Papenfuß (1975) has shown that the heat transfer in the stagnation point of a paraboloid of revolution at zero incidence, with $\text{Ma}_\infty = 4$, neglecting the displacement effect, is given by

$$\frac{q_w}{q_{w\infty}} = 1 + \left(\underbrace{0.236}_{\text{curvature}} + \underbrace{0.514}_{\text{non-continuum}} + \underbrace{1.092}_{\text{vorticity}} \right) \frac{1}{\sqrt{\text{Re}_\infty}}.$$

Here the Reynolds number Re_∞ is formed with the radius of curvature in the stagnation point and the quantities belonging to the free stream.

The calculation is considerably simplified if massive suction is applied to the body, cf. K. Gersten et al. (1977).

The circular cylinder at zero incidence in supersonic flow has been examined by K. Gersten; J.F. Gross (1973b) and A.E. Wehrum (1975). The generalisation to a cylinder of any cross-section has been presented by V. Vasanta Ram (1975).

Note. (Interacting boundary-layer theory)

In practice, instead of carrying out the four calculations (first order outer flow, first order inner flow, second order outer flow, second order inner flow) in succession, one calculation is performed, and the matching of the inner flow to the outer flow takes place iteratively. Simplified Navier-Stokes equations, which still contain all terms which contribute to the second order boundary-layer equations, are used for the inner solution (boundary layer). For plane ($j = 0$) or axisymmetric ($j = 1$) compressible flows, these read

$$\frac{\partial}{\partial x} [(r_w + y \cos \theta)^j \varrho u] + \frac{\partial}{\partial y} [(1 + Ky)(r_w + y \cos \theta)^j \varrho v] = 0, \quad (14.23)$$

$$\begin{aligned} \varrho \left(\frac{u}{1 + Ky} \frac{\partial u}{\partial x} + v \frac{\partial u}{\partial y} + Ku v \right) &= -\frac{1}{1 + Ky} \frac{\partial p}{\partial x} + \frac{\partial \tau_{xy}}{\partial y} \\ &\quad + \left(2K + \frac{j \cos \theta}{r_w} \right) \tau_{xy}, \end{aligned} \quad (14.24)$$

$$K \varrho u^2 = \frac{\partial p}{\partial y}, \quad (14.25)$$

$$\begin{aligned} \varrho c_p \left(\frac{u}{1 + Ky} \frac{\partial T}{\partial x} + v \frac{\partial T}{\partial y} \right) &= \frac{\partial}{\partial y} \left(\lambda \frac{\partial T}{\partial y} \right) + \left(K + \frac{j \cos \theta}{r_w} \right) \lambda \frac{\partial T}{\partial y} \\ &\quad + \beta T \left(\frac{u}{1 + Ky} \frac{\partial p}{\partial x} + v \frac{\partial p}{\partial y} \right) + \frac{\tau_{xy}^2}{\mu} \end{aligned} \quad (14.26)$$

with

$$\tau_{xy} = \mu \left(\frac{\partial u}{\partial y} - Ku \right). \quad (14.27)$$

The disadvantage in this procedure is that a separate calculation must be carried out for each Reynolds number.

Summaries have been given by R.T. Davis; M.J. Werle (1982), H. McDonald; W.R. Briley (1984), T. Cebeci; J.H. Whitelaw (1986) and J.D. Anderson Jr. (1989), p. 339.

Applying interacting boundary-layer theory to the step flow sketched in Fig. 14.1 means that non-separating solutions can even be found for $(H/l) > (H/l)_{\text{MS}}$ at finite Reynolds numbers. As will be shown later, these equations are also valid for

solutions with backflow, as long as the Reynolds numbers are large enough and the regions with backflow remain inside the boundary layer. A singularity then no longer occurs. This is also true for unsteady boundary layers, cf. Chap. 13.

14.3 Hypersonic Interaction

In the previous section we discussed the interaction between the outer flow and the boundary layer. It was assumed that the mutual interaction was weak, so that reactions were only to be seen in the next highest order. For example, the first order boundary layer had a reaction on the second order outer flow, but not on the first order outer flow.

Frequently, so-called “strong interactions” occur in hypersonic flows past slender bodies. Here the first order outer flow depends on the behaviour of the boundary layer, and the manner in which this behaves is itself a consequence of the outer flow. The outer flow and the (first order) boundary layer therefore have a mutual effect on each other, and must be computed simultaneously.

This strong interaction will be elucidated by following the example of hypersonic flow along a plate. This flow is sketched in Fig. 14.4. The high Mach numbers in hypersonic flow ($Ma_\infty > 5$) produce two effects which lead to the strong interaction. On the one hand there is a considerable increase in the boundary-layer thickness with increasing Mach number, as has already been discussed in connection with Fig. 10.5. On the other hand, as the Mach number increases, the shock angle θ becomes flatter, i.e. the shock front approaches the body more closely. The distances from the wall of the shock and the outer edge of the boundary layer therefore eventually reach the same order of magnitude as the Mach number increases.

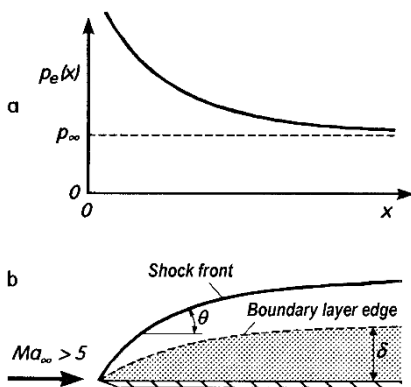


Fig. 14.4. Hypersonic flow at a plate at zero incidence
 (a) induced pressure distribution due to interaction
 (b) sketch of the flow field

In what follows we will consider an ideal gas ($\gamma = 1.4$; $\text{Pr} = 0.7$). It will be seen that the displacement thickness again obeys a power law of the form

$$\delta_1(x) \sim x^n. \quad (14.28)$$

Here, however, the exponent is no longer that of constant pressure $n = 1/2$. According to the theory of inviscid hypersonic flows, slender bodies whose contours conform to power laws yield similar solutions, i.e. the streamlines formed also conform to power laws with the same exponent, see K. Gersten; D. Nicolai (1974). According to this piece of work, the following is the pressure distribution on the fictitious contour:

$$\frac{p_e}{p_\infty} = \lambda^2(n) \text{Ma}_\infty^2 \left(\frac{d\delta_1}{dx} \right)^2, \quad (14.29)$$

where the coefficient λ (at fixed γ) only depends on the exponent n . Therefore the pressure distribution at the outer edge of the boundary layer obeys a power law, and so similar solutions also emerge here, as has already been explained in Sect. 10.4.4. These solutions have been comprehensively tabulated by C.F. Dewey Jr.; J.F. Gross (1967) who showed that the displacement thickness at constant wall temperature T_w is

$$\frac{\delta_1(x)}{x} = \frac{\gamma - 1}{\sqrt{2(2n - 1)}} \frac{\text{Ma}_\infty^2}{\sqrt{\text{Re}_{x\infty}}} \sqrt{\frac{\text{CR}_\infty}{p_e/p_\infty}} I_1(\beta, T_w/T_0) \quad (14.30)$$

with T_0 as the total temperature, cf. Eq. (10.52). A linear law was used for the viscosity, cf. Eq. (10.47):

$$\frac{\mu}{\mu_\infty} = \text{CR}_\infty \frac{T}{T_\infty}, \quad \text{CR}_\infty = \frac{T_\infty \mu_w}{T_w \mu_\infty}. \quad (14.31)$$

CR_∞ is the Chapman–Rubesin parameter from Eq. (10.32). Equations (14.29) and (14.30) are two coupled equations for the desired functions $\delta_1(x)$ and $p_e(x)$. The exponent for the solution $\delta_1(x)$ in Eq. (14.28) is $n = 3/4$, and so Eq. (14.29) yields the pressure distribution $p_e/p_\infty \sim x^{-1/2}$. This pressure distribution furnishes the parameter β in Eq. (10.72) as

$$\beta = \frac{\gamma - 1}{\gamma} = 0.2857 \quad (\gamma = 1.4), \quad (14.32)$$

cf. C.F. Dewey Jr. (1963). Therefore the boundary-layer solution for the adiabatic wall ($\text{Pr} = 0.7$; $T_{ad}/T_0 = 0.819$) delivers the value $I_1 = 0.21$, cf. C.F. Dewey Jr.; J.F. Gross (1967). With $\lambda(n = 3/4) = 1.409$ from K. Gersten; D. Nicolai (1974) we finally obtain the pressure distribution as

$$\frac{p_e(x)}{p_\infty} = \frac{3}{4}(\gamma - 1)\lambda I_1 \bar{\chi} = 0.51 \bar{\chi}, \quad (14.33)$$

with the hypersonic similarity parameter

$$\bar{\chi} = \frac{\text{Ma}_\infty^2}{\sqrt{\text{Re}_{x\infty}}} \sqrt{\text{CR}_\infty} \quad (14.34)$$

Figure 14.5 shows the induced pressure distribution due to strong interaction in Eq. (14.33) compared with experimental results. Here $p_e(x)/p_\infty$ is plotted against $1/\bar{\chi}^2 \sim x$, thus against the dimensionless length x . For about $1/\bar{\chi}^2 < 0.1$ (i.e. $\bar{\chi} > 3$) the agreement between theory and experiment is good. For $1/\bar{\chi}^2 > 0.1$, only a weak interaction is at hand. This is described by the theory in Sect. 14.2. For this case ($\gamma = 1.4$; $Pr = 0.725$), the relation $p_e(x)/p_\infty = 1 + 0.31\bar{\chi} + 0.05\bar{\chi}^2$ holds. This is also depicted in Fig. 14.5.

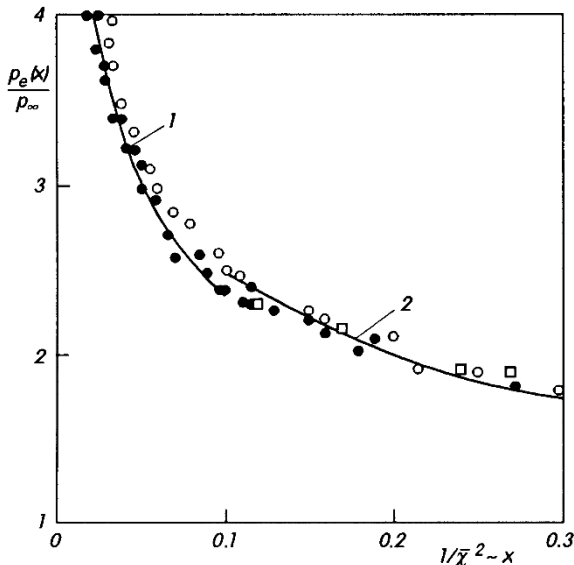


Fig. 14.5. Dependence of the induced pressure distribution on the hypersonic similarity parameter $\bar{\chi}$. Comparison of interaction theory with measurements, cf. W.D. Hayes; R.F. Probstein (1959)

- (1) strong interaction: extension of Eq. (14.33): $p_e/p_\infty = 0.51\bar{\chi} + 0.76$
- (2) weak interaction: $p_e(x)/p_\infty = 1 + 0.31\bar{\chi} + 0.05\bar{\chi}^2$

According to Eq. (14.33), the pressure $p_e(x)$ becomes infinite at the leading edge ($x \rightarrow 0$, $\bar{\chi} \rightarrow \infty$). The theory is based on the concept of a continuum and thus it breaks down here. Very close to the leading edge of the plate, thus at distances of the order of magnitude of the mean free path of the molecules, the Navier–Stokes equations and the no-slip condition are no longer valid. In reality, the non-continuum effects cause the pressure at the leading edge to become finite, cf. G. Koppenwallner (1988) and J.D. Anderson Jr. (1989), p. 314.

The boundary-layer solution for strong interactions yields the wall shear stress

$$c_f \sqrt{\frac{\text{Re}_{x_\infty}}{\text{CR}_\infty}} = 0.517 \sqrt{\bar{\chi}}. \quad (14.35)$$

A more exact analysis of the strong interaction shows that the two solutions (the frictionless solution for the hypersonic flow past slender bodies with contours which obey a power law and the boundary solution) cannot be matched correctly with respect to the temperature or the density. According to W.B. Bush (1966), the flow field behind the shock front consists of *three* layers. A transition solution in the middle allows the two solutions above to be matched correctly.

For details on the strong hypersonic interaction at other slender bodies (plates at an angle of attack, cones at zero incidence or at an angle of attack) see the relevant literature, e.g. W.D. Hayes; R.F. Probstein (1959), p. 363, J.D. Anderson Jr. (1989), p. 315.

14.4 Triple-Deck Theory

Higher order boundary-layer theory breaks down for the step flow sketched in Fig. 14.1 for $H/\ell > (H/\ell)_{\text{MS}}$. At finite Reynolds numbers, interaction theory can be used to find solutions for $H/\ell \geq (H/\ell)_{\text{MS}}$. The question then arises of whether these latter solutions can be found using an asymptotically correct theory. The answer to this question is affirmative. The solutions can be determined using *asymptotic interaction theory*, also called *triple-deck theory*.

Higher order boundary-layer theory breaks down because of the appearance of the Goldstein singularity in the first order theory. Triple-deck theory avoids this singularity using a simple trick. It starts off with the Blasius plate solution as a limiting solution and considers, for example, the step flow as a perturbation to the plate flow. The geometry is therefore coupled together with the Reynolds number, so that for $\text{Re} \rightarrow \infty$, $H/L \rightarrow 0$. The origin in Fig. 14.1 therefore forms the starting point of this particular perturbation theory for large Reynolds numbers.

As further analysis of this perturbation calculation will show, the flow close to the step which represents a deviation from the plate flow has a three-layer structure, see Fig. 14.6. Each of the three *layers* or *decks* has its own physical functions within the interaction region under consideration. Therefore each layer is scaled differently with respect to the Reynolds number.

Let the region of interaction in the direction of flow be scaled as

$$\frac{L_l}{L} = \lambda_L \text{Re}^{-n_L}, \quad n_L > 0. \quad (14.36)$$

Since $L_l/l = O(1)$, the geometry and the Reynolds number are coupled together. The constant λ_L will be determined later so that equations which are as simple as possible are found. The thickness of the lower deck δ_l , for which $\delta_l/H = O(1)$ holds, is set as follows to determine the second coupling:

$$\frac{\delta_l}{L} = \lambda_\Delta \text{Re}^{-n_\Delta}, \quad n_\Delta > 0. \quad (14.37)$$

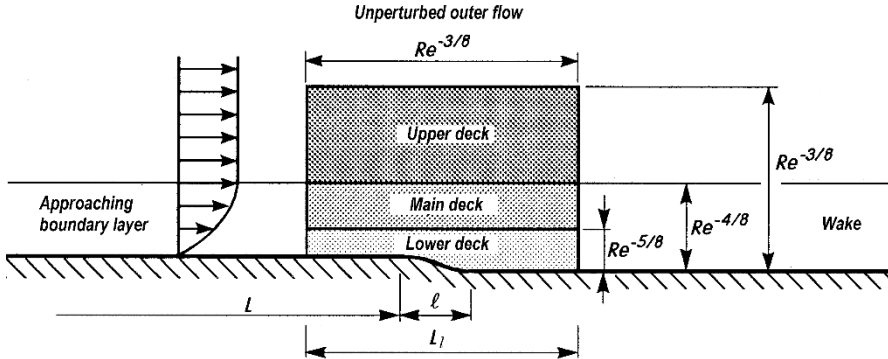


Fig. 14.6. Triple-deck structure at a step flow

Here it was assumed that the change in the velocity profile due to viscosity is restricted to the sublayer. The rest of the velocity profile outside the sublayer moves only in the y direction. Therefore, the midlayer has the passive function of passing on the displacement effects due to viscosity in the sublayer to the upper layer.

The upper deck is where the inviscid outer flow is to be found and therefore is scaled in the same manner in the x and y direction, i.e. its thickness is of order of magnitude L_l . Since only very weak displacement effects are taken into account, the relation between the displacement and the pressure perturbation in the upper deck may be described using the so-called *Hilbert integral*. We set the *reference perturbation pressure* to

$$\frac{(p - p_\infty)_R}{\rho U_\infty^2} = \lambda_p \text{Re}^{-n_p}, \quad n_p > 0. \quad (14.38)$$

The three initially unknown exponents n_L , n_Δ and n_p in Eqs. (14.36) to (14.38) may be determined as follows:

- (1) A characteristic reference velocity u_R is fixed for the lower deck. This is chosen to be the velocity at the start of the interaction region at a distance $y = \delta_l$ from the wall. Since the lower deck is much thinner than the approaching plate boundary layer, this velocity is in that part of the Blasius velocity profile which can be described by a tangent to the wall. According to Eq. (6.54), the reference velocity is then

$$u_R = \left(\frac{\partial u_{BL}}{\partial y} \right)_w \delta_l = c U_\infty \text{Re}^{1/2} \frac{\delta_l}{L}, \quad c = 0.332. \quad (14.39)$$

- (2) The following dimensionless quantities are introduced for the lower deck:

$$x_D = \frac{x - L}{L_l} = \frac{x}{L} \frac{\text{Re}^{n_L}}{\lambda_L},$$

$$y_D = \frac{y - y_C}{\delta_l} = \frac{y - y_C}{L} \frac{\text{Re}^{n_\Delta}}{\lambda_\Delta},$$

$$\begin{aligned}
u_D &= \frac{u}{u_R} = \frac{u}{U_\infty} \frac{\text{Re}^{n_\Delta - 1/2}}{c\lambda_\Delta}, \\
v_D &= \frac{v}{u_R} \frac{L_l}{\delta_l} = \frac{v}{U_\infty} \frac{\lambda_L}{c\lambda_\Delta^2} \text{Re}^{2n_\Delta - n_L - 1/2}, \\
p_D &= \frac{p - p_\infty}{(p - p_\infty)_R} = \frac{p - p_\infty}{\varrho U_\infty^2} \frac{\text{Re}^{n_p}}{\lambda_p}.
\end{aligned} \tag{14.40}$$

The trial solution for v_D ensures that the continuity equation is satisfied.

Inserting the chosen quantities into the momentum equation in the x direction yields

$$\begin{aligned}
&\frac{c^2 \lambda_\Delta^2}{\lambda_L} \text{Re}^{1-2n_\Delta+n_L} \left(u_D \frac{\partial u_D}{\partial x_D} + v_D \frac{\partial u_D}{\partial y_D} \right) \\
&= -\frac{\lambda_p}{\lambda_L} \text{Re}^{n_L-n_p} \frac{\partial p_D}{\partial x_D} \\
&+ \frac{c}{\lambda_\Delta} \text{Re}^{n_\Delta-1/2} \left(\frac{\partial^2 u_D}{\partial y_D^2} + \frac{\lambda_\Delta^2}{\lambda_L^2} \text{Re}^{2n_L-2n_\Delta} \frac{\partial^2 u_D}{\partial x_D^2} \right).
\end{aligned} \tag{14.41}$$

Note (Parallel displacement of the y coordinate)

Strictly speaking, the parallel displacement of the y coordinate contained in the defining equation for y_D yields further terms in Eq. (14.41). However these vanish to leading order for $\text{Re} \rightarrow \infty$ because $y_C(x)/\delta_l = O(1)$, cf. H. Herwig (1981). The parallel shifting implies that on the contour $y_D = 0$.

The condition that the inertial forces, the pressure forces and the leading friction forces must all have the same order of magnitude yields the following two relations for the exponents:

$$1 - 2n_\Delta + n_L = n_L - n_p, \tag{14.42}$$

$$n_L - n_p = n_\Delta - \frac{1}{2}. \tag{14.43}$$

In order that the coefficients in Eq. (14.41) have the value one, it must also hold that

$$\frac{c^2 \lambda_\Delta^2}{\lambda_L} = \frac{\lambda_p}{\lambda_L}, \tag{14.44}$$

$$\frac{\lambda_p}{\lambda_L} = \frac{c}{\lambda_\Delta}. \tag{14.45}$$

- (3) The upper deck “perceives” (in addition to the displacement contour of the flat plate) a displacement contour $\Delta(x)$ which is made up of the real contour $y_C(x)$ and the displacement thickness of the lower deck $D_1(x)$:

$$\Delta(x) = y_C(x) + D_1(x). \tag{14.46}$$

This displacement contour induces a pressure distribution which can be computed using the *Hilbert integral*:

$$\frac{p - p_\infty}{\rho U_\infty^2} = -\frac{1}{\pi} \oint_{-\infty}^{+\infty} \frac{d\Delta/d\bar{x}}{x - \bar{x}} d\bar{x}. \quad (14.47)$$

The “C” inside the integration symbol implies that this is the Cauchy principal value. Because $\bar{x}/L = O(L_l/L)$ and $\Delta_D = \Delta/\delta_l = O(1)$, it follows from Eq. (14.47) that

$$\frac{\lambda_p}{\text{Re}^{n_p}} p_D = -\frac{\lambda_\Delta}{\lambda_L} \text{Re}^{n_L - n_\Delta} \frac{1}{\pi} \oint_{-\infty}^{+\infty} \frac{d\Delta_D}{d\bar{x}_D} \frac{d\bar{x}_D}{x_D S - \bar{x}_D} \quad (14.48)$$

and comparison of the exponents and coefficients yields

$$-n_p = n_L - n_\Delta, \quad (14.49)$$

$$\lambda_p = \lambda_\Delta / \lambda_L. \quad (14.50)$$

Equations (14.42), (14.43) and (14.49) yield the exponents

$$n_L = \frac{3}{8}, \quad n_\Delta = \frac{5}{8}, \quad n_p = \frac{2}{8} \quad (14.51)$$

and Eqs. (14.44), (14.45) and (14.50) the coefficients

$$\lambda_L = c^{-5/4}, \quad \lambda_\Delta = c^{-3/4}, \quad \lambda_p = c^{1/2}. \quad (14.52)$$

Therefore, using $D_{1D} = D_1/\delta_l$, we obtain the following system of equations to compute the interaction:

$$\frac{\partial u_D}{\partial x_D} + \frac{\partial v_D}{\partial y_D} = 0, \quad (14.53)$$

$$u_D \frac{\partial u_D}{\partial x_D} + v_D \frac{\partial u_D}{\partial y_D} = -\frac{dp_D}{dx_D} + \frac{\partial^2 u_D}{\partial y_D^2}, \quad (14.54)$$

$$p_D = -\frac{1}{\pi} \oint_{-\infty}^{+\infty} \frac{d\Delta_D}{d\bar{x}_D} \frac{d\bar{x}_D}{x_D - \bar{x}_D} \quad (14.55)$$

with the boundary conditions

$$\begin{aligned} x_D \rightarrow -\infty : \quad & u_D = y_D \\ y_D = 0 : \quad & u_D = 0, \quad v_D = 0 \\ y_D \rightarrow \infty : \quad & u_D = y_D - D_{1D}. \end{aligned} \quad (14.56)$$

This system of equations (Eqs. (14.53) and (14.54)) for the lower deck is the same as the system of equations for the Prandtl boundary layer; only the initial and boundary conditions are different.

Data specifying the geometry of the wall have to be supplied. For the example of the backward-facing step in Fig. 14.1, we have the following contour equation

$$\begin{aligned} y_C &= H \left[20 \left(\frac{x - L}{\ell} \right)^7 - 70 \left(\frac{x - L}{\ell} \right)^6 \right. \\ &\quad \left. + 84 \left(\frac{x - L}{\ell} \right)^5 - 35 \left(\frac{x - L}{\ell} \right)^4 + 1 \right] \\ &= H \cdot F_C \left(\frac{x - L}{\ell} \right) \end{aligned} \quad (14.57)$$

or else, using lower deck coordinates

$$\frac{y_C(x)}{\delta_l} = H_D F_C \left(\frac{x_D}{\ell_D} \right) \quad (14.58)$$

with

$$\frac{x - L}{\ell} = \frac{x_D}{\ell_D}. \quad (14.59)$$

Therefore the solutions are dependent on the two characteristic numbers

$$\ell_D = \frac{\ell}{L_l} = \frac{\ell c^{5/4} \text{Re}^{3/8}}{L}; \quad H_D = \frac{H}{\delta_l} = \frac{H c^{3/4} \text{Re}^{5/8}}{L}. \quad (14.60)$$

Thus, within the framework of triple-deck theory, the original three parameters L/ℓ , H/ℓ and Re have been reduced to two parameters ℓ_D and H_D . For each solution corresponding to a point in the diagram in Fig. 14.1 with $L/\ell = \text{const}$ there are infinitely many further solutions for other values of L/ℓ . If L/ℓ increases, for the same triple-deck solution i.e. for the same ℓ_D , the Reynolds number must also increase.

In Fig. 14.7, each point corresponds to an infinite number of solutions for, for example, different high Reynolds numbers. The dashed line divides the entire solution region into boundary layers attached to the body and boundary layers with backflow. These latter may be computed without a singularity appearing.

Note (Boundary layers with backflow)

The system of equations (14.53) to (14.56) must be solved simultaneously. This is carried out using iteration. The most obvious way starts with an estimation of the function $p_D(x_D)$. Then, as is usual in boundary-layer theory, Eqs. (14.53) and (14.54) can be solved. The result of the “boundary-layer computation” is the function $D_{1D}(x_D)$ and, from Eq. (14.46), eventually $\Delta_D(x_D)$. The Hilbert integral (14.55) can then be used to confirm the estimation of $p_D(x_D)$.

This iteration scheme breaks down if the wall shear stress τ_w vanishes, since the Goldstein singularity then appears in the solution of Eqs. (14.53) and (14.54). In

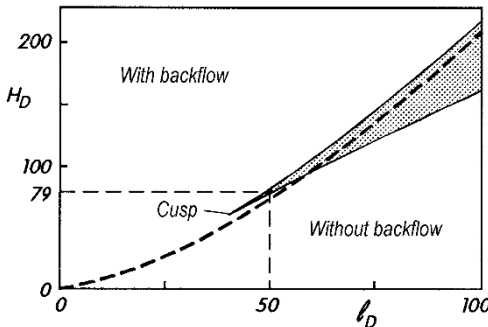


Fig. 14.7. Parameter field of the step flow in Fig. 14.1, cf. P. Schäfer (1995). Definitions of ℓ_D and H_D as in Eq. (14.60). shaded area: two solutions left of dashed line: solutions with backflow right of dashed line: one solution without backflow

this case an *inverse iteration scheme* can lead to success. First of all, the function $D_{1D}(x_D)$ is estimated, and then the pressure distribution $p_D(x_D)$ is computed from Eqs. (14.53) and (14.54) (*inverse boundary-layer computation method*). Inverting the Hilbert integral

$$\frac{d\Delta_D}{dx_D} = \frac{1}{\pi} \oint_{-\infty}^{+\infty} \frac{p_D(\bar{x}_D)}{x_D - \bar{x}_D} d\bar{x}_D \quad (14.61)$$

then yields the function $\Delta_D(x_D)$, and, from Eq. (14.46), $D_{1D}(x_D)$.

If the wall shear stress is positive, the boundary-layer equations (14.53) and (14.54) are parabolic, so that the numerical solution can be carried out stepwise in the flow direction. If backflow occurs, the differential equation changes its type, and this must be taken into account in computing the numerical solution. Two different manners of doing this have proved useful, cf. H. Herwig (1982):

1. DUIT (downstream upstream iteration): The direction of integration follows the direction of flow. Two solution regions are found (main flow, backflow) which must be matched up iteratively, cf. P.G. Williams (1975).
2. FLARE (Flügge-Lotz and Reyhner (1968)): The convective term $u_D \partial u_D / \partial x_D$ is set to zero in the backflow.

It is particularly worth noting that two solutions exist in the shaded area in Fig. 14.7. The second solution always exhibits backflow. Therefore, even on the right hand side of the dashed line, the second solution in the shaded area has a region of backflow.

Figure 14.8 shows the distribution of the wall pressure and the wall shear stress for the two solutions in the shaded area ($H_D = 79$, $\ell_D = 50$). Although both solutions have a region of backflow, that of solution 2 is much further extended.

If we again return to the original representation in Fig. 14.1, Fig. 14.7 adds a few additional curves to Fig. 14.1. These are shown in Fig. 14.9. The (dashed) dividing curve in Fig. 14.7 between attached boundary layers and those with backflow now corresponds to the curve DCA. The shaded areas in Figs. 14.7 and 14.9 are equivalent to each other. Unfortunately the regions close to the H/ℓ axis are not described by triple-deck theory, since, as already mentioned, the plate solution is used as the basic solutions and therefore H/ℓ tends to zero with increasing Reynolds number. In particular,

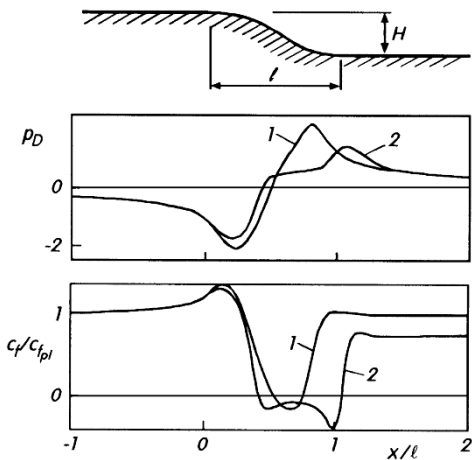


Fig. 14.8. Distributions of the pressure and the shear stress at the wall for step flow with $\ell_D = 50$ and $H_D = 79$, cf. P. Schäfer (1995).
Solution 1: short backflow region
Solution 2: long backflow region

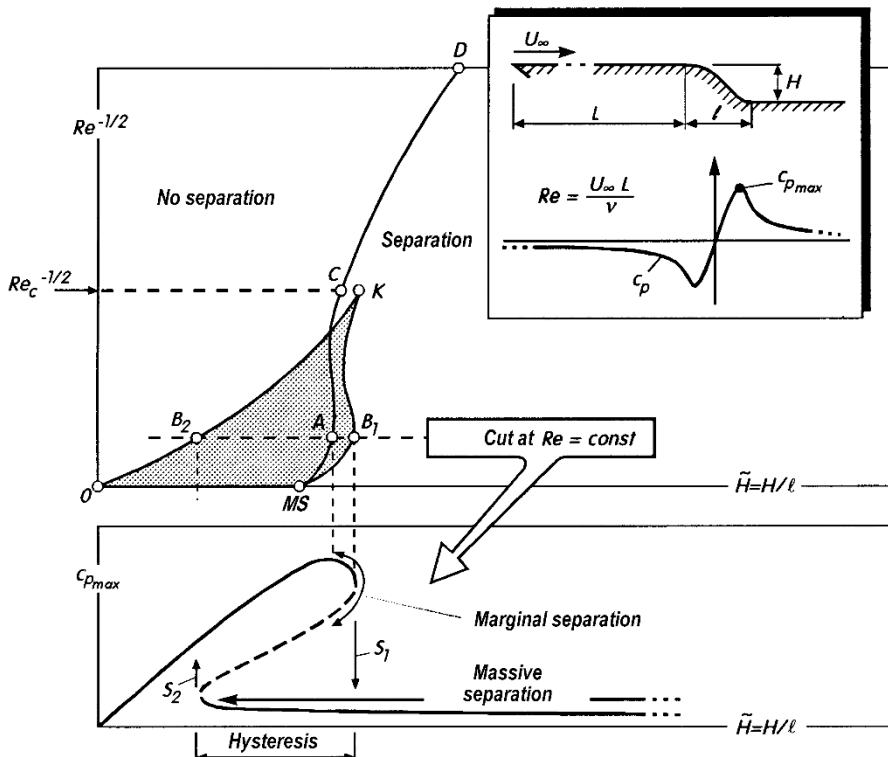


Fig. 14.9. Step flow diagram at constant ratio ℓ/L , cf. Fig. 14.1
 $D - C - A - MS$: limit between attached flow and separated flow
 $K - B_1 - MS$: jump from local to massive separation
 $K - B_2 - O$: jump from massive separation to attached flow
 K : position of the cusp

marginal separation denoted by the point MS can not be reached. For this reason, a special asymptotic theory has been developed for the region close to this point. This will be described in the next section.

A rather clear geometrical interpretation may be made for the shaded region in which (at least) two solutions exist. If we plot the $c_{p\max}$ values against large H/ℓ for constant Reynolds number, we obtain the graph shown in the lower part of Fig. 14.9. The solution surface $c_{p\max}(1/\sqrt{Re}, H/\ell)$ has the shape shown in Fig. 14.10. It is folded in such a manner that several solutions exist above the shaded area. Therefore it becomes clear why a variation of the parameter H/ℓ leads to hysteresis, cf. Fig. 14.9. At the edge point B_1 , the solution jumps from a flow with local separation (small separation region) to a flow with *massive separation* (large separation region). Since this latter is not described by triple-deck theory, special treatment is required. This will be presented in Sect. 14.6.

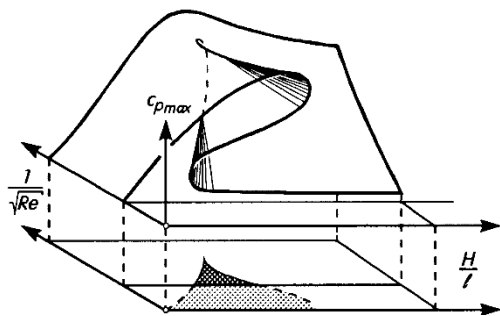


Fig. 14.10. Step flow from Fig. 14.1 for constant ratio l/L . Folded solution surface for the maximal pressure coefficient $c_{p\max}$

The mathematical theory to describe folded solution surfaces is called *catastrophe theory*, cf. for example P.T. Saunders (1980). The case here with the solution surface as in Fig. 14.10 is a so-called *cusp catastrophe*.

Further solutions of triple-deck theory for step flows have been given by F. Sommer (1992) and P. Schäfer (1995). P. Schäfer has also computed the heat transfer.

Summaries of triple-deck theory have been given by K. Stewartson (1974, 1982), A. Kluwick (1979, 1987, 1991, 1998), A.F. Messiter (1983) and F.T. Smith (1986).

In what follows we shall discuss some further applications of triple-deck theory.

1. **Humps and dents on a flat plate.** The plane flow at a flat plate with humps of height H and length ℓ has been computed by F.T. Smith (1973), cf. S.A. Ragab; A.H. Nayfeh (1982). The analogous problem of a flat plate with dents ($H < 0$) has been treated by H. Herwig (1981, 1982). H. Herwig (1983) has also investigated the heat transfer. The solution manifold corresponds to that of the step flow, and the different methods of treating backflow are also used, cf. also F.T. Smith et al. (1981) and I.J. Sobey (2000).

- 2. Flow close to the trailing edge of a plate of finite length.** At some distance (to be precise, at distances $O(\text{Re}^{-3/8})$) from the trailing edge, the solution is the Blasius solution of the Prandtl boundary layer, cf. Sect. 6.5. Very far behind the plate, the flow becomes that of the wake flow discussed in Sect. 7.5.1. In the transition region the flow has a triple-deck structure. Again the processes in the lower deck are important. Because the no-slip condition suddenly drops away at the trailing edge, in front of the trailing edge there is a local acceleration of the outer flow (pressure drop). This leads to an increase of the wall shear stress close to the trailing edge. It follows that the drag coefficient of a plate of finite length L is:

$$c_D = 1.328 \text{Re}^{-1/2} + 2.67 \text{Re}^{-7/8} + O(\text{Re}^{-1}). \quad (14.62)$$

This function is shown in Fig. 1.3. Even at Reynolds numbers $O(1)$ it is in very good agreement with experiment, see R.E. Melnik; R. Chow (1975). Details of the theory have been given by K. Stewartson (1969, 1974) and A.F. Messiter (1970). The coefficient in the additional term in Eq. (14.62) was first computed by C.E. Jobe, cf. C.E. Jobe; O.R. Burggraf (1974). The results of triple-deck theory have been impressively confirmed in a comparison with numerical solutions of the complete Navier-Stokes equations, cf. R.T. Davis; M.J. Werle (1982) and H.C. Chen; V.C. Patel (1987).

Corresponding investigations for supercritical transonic flows have been carried out by R.J. Bodonyi; A. Kluwick (1982) and for supersonic flows by P.G. Daniels (1974). The results have been carried over to axisymmetric flows past slender bodies of finite length by R.J. Bodonyi et al. (1985).

Note (Continuation of the asymptotic expansion)

The discontinuous jump in the boundary condition for u_D at the trailing edge is and remains a singularity in the flow field. It cannot be gotten rid of by triple-deck theory. Therefore the asymptotic expansions of triple-deck theory are not valid arbitrarily close to the trailing edge. There is a region of size $O(\text{Re}^{-3/4})$ in both coordinate directions in the lower deck close to the trailing edge in which the full Navier-Stokes equations must be solved. The contribution to the c_D value is of the order of magnitude $O(\text{Re}^{-5/4})$.

- 3. Other flows at the trailing edge.** For plates at an angle of attack, it is assumed that the angle of attack $\alpha = O(\text{Re}^{-1/16})$. The theory yields a viscosity correction to the lift, cf. K. Stewartson (1974), R. Chow; R.E. Melnik (1976).

For airfoils with a trailing edge angle f this is set at $O(\text{Re}^{-1/4})$, cf. K. Stewartson (1974) and F.T. Smith; J.H. Merkin (1982). Flows at convex and concave corners can be treated in a similar manner.

The corresponding flow problem at axisymmetric bodies has been investigated by A. Kluwick; Ph. Gittler (1994).

- 4. Blowing from a slit.** In applying triple-deck theory to this case, it is assumed that the width of the slit and the blowing velocity are $O(\text{Re}^{-3/8})$, cf. K. Stewartson (1974) and M. Napolitano; R.E. Messick (1980).

- 5. Unsteady flows.** The extension of triple-deck theory to unsteady flows has been carried out by O.S. Ryzhov; V.I. Zhuk (1980). M.-K. Huang; G.R. Inger (1984) have treated the interaction at an oscillating flap, cf. also W. Schneider (1974b) and P.W. Duck (1984).

- 6. Three-dimensional interaction.** Three-dimensional flows at dents of finite width have been investigated by F.T. Smith et al. (1977), R.I. Sykes (1980), O.R. Burggraf; P.W. Duck (1982) and C. Roget et al. (1998). Ph. Gittler (1985)

has considered the swept dent. The flow at a yawing wing with separation is also investigated in this work, cf. also Ph. Gittler; A. Kluwick (1989).

7. **Natural convection.** If there is a “abrupt” change in the boundary condition in natural convection flows, a layered structure is formed in the boundary layer. Because the outer flow is missing, there is no upper deck. Here a *double-deck theory* is used. Because of the displacement action of the lower deck, a pressure distribution is induced in the main deck. This is because the displacement contour of the viscous lower layer displays a *curvature* which can no longer be ignored. Pressure gradients perpendicular to the main flow direction appear and thus a pressure field is induced.

Examples are the natural convection at a vertical flat plate with local wall contour perturbation, cf. J.H. Merkin (1983) and K. Gersten et al. (1991), as well as the processes close to the trailing edge for finite plate lengths, cf. A.F. Messiter; A. Liñán (1976). Discontinuous jumps in the wall temperature distribution are treated in this last work. A strong local drop in the wall temperature can lead to backflow, as A. Exner; A. Kluwick (1999) have shown. Interactions in forced convection without outer flow also lead to a double-deck structure. An example is the wall jet flow at a concave corner, cf. F.T. Smith; P.W. Duck (1977).

8. **Compressible flows.** The formulation for triple-deck theory for compressible flows has been presented by, for example, K. Stewartson (1974). A suitable transformation allows the system of equations to be reduced to the incompressible form, Eqs. (14.53) to (14.56). In supersonic flows, the Hilbert integral for the upper deck in Eq. (14.55) is replaced using linearised supersonic theory by

$$P = -\frac{d\Delta_D}{dx_D}. \quad (14.63)$$

Special treatment it required close to transonic speeds, cf. A.F. Messiter et al. (1971).

The interaction in compressible plate flow close to a discontinuous jump in the wall temperature has been investigated by C. Treviño; F. Méndez (1992). A strong enough discontinuous increase in the wall temperature can even lead to separation ($\tau_w = 0$).

Shock–boundary–layer interaction

In supersonic flows, it is above all the interactions between boundary layers and outer flows with shock waves which are of practical importance. Figure 14.11 shows two important examples: the shock boundary–layer interaction at an oblique shock and the compression ramp (concave corner). It is particularly worth noting that in these examples the interaction begins *in front of* the shock contact point, as well as *in front of* the corner of the ramp.

These processes could not be described using the Prandtl boundary–layer theory, since an attached boundary layer (parabolic differential equation) and supersonic flow (hyperbolic differential equation) cannot be matched up. The matching of these two solutions can only be described using the interaction mechanism. Because of the displacement, the growth of the boundary layer produces a pressure increase which itself leads to further growth in the boundary layer, cf. J. Lighthill (2000). This interaction cycle eventually leads to separation (self-induced separation), cf. K. Stewartson; P.G. Williams (1969). Close to the separation point, the flow has a universal triple-deck structure, providing the scale is chosen correctly. Figure 14.12 shows the universal pressure and wall shear stress distributions by K. Stewartson (1974). These results have been confirmed by experiment, cf. K. Stewartson; P.G. Williams (1969).

As is sketched in Fig. 14.11, the flow at a compression ramp consists of three regions. After the region of self-induced pressure there is a plateau region, and finally a region where the flow reattaches to the wall. O.R. Burggraf (1975) has computed flows at compression ramps using this division. If the ramp angle α is $O(\text{Re}^{-1/4})$, then the entire interaction region close to the corner can be thought of in terms of one triple-deck structure. The solutions found by D.P. Rizzetta et al. (1978) agree with more precise numerical solutions from interaction theory very well for $\text{Re} > 10^8$. This has been shown by O.R. Burggraf et al. (1979).

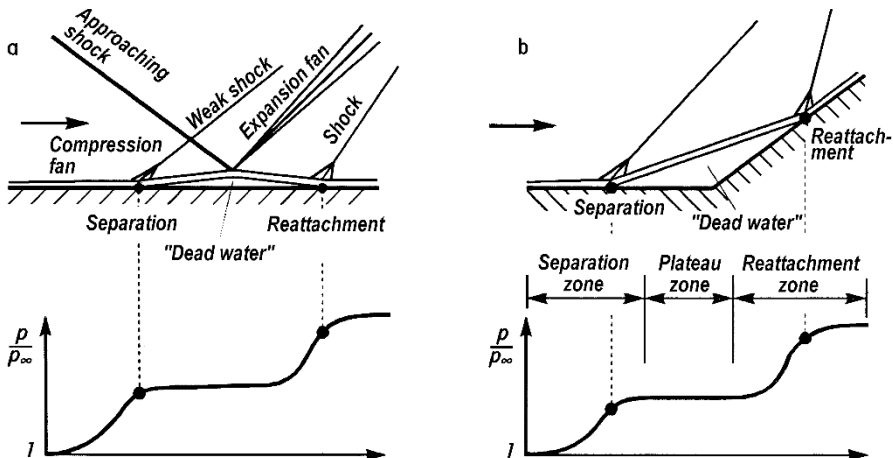


Fig. 14.11. Two examples of shock–boundary–layer interaction
 (a) reflection of an oblique shock wave
 (b) compression ramp in supersonic flow

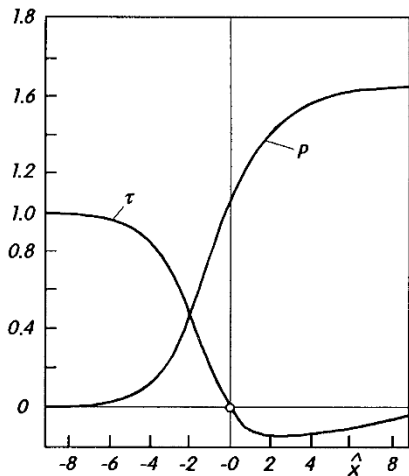


Fig. 14.12. Universal pressure and wall shear stress distributions for free interaction in supersonic flow, after K. Stewartson (1974)

The free interaction between a weak oblique shock and a laminar boundary layer in transonic flow has been investigated by H.M. Brilliant; T.C. Adamson Jr. (1974) for the case without separation and by R.J. Bodonyi; A. Kluwick (1977) for the case with separation.

This theory has been carried over to axisymmetric flows by A. Kluwick et al. (1984, 1985) and Ph. Gittler; A. Kluwick (1987).

Summaries have been presented by T.C. Adamson Jr.; A.F. Messiter (1980) and J. Delery; J.G. Marvin (1986).

Note (Interaction theory)

Since the boundary-layer equations are solved in triple-deck theory in the leading order, interactions can also be computed using the Prandtl boundary-layer theory. Overviews on this have been given in AGARD (1981), and by H. McDonald; W.R. Briley (1984), J. Delery; J.G. Marvin (1986). Here the system of differential equations to be solved simultaneously is no longer independent of the Reynolds number, so that a separate calculation must be carried out for each different Reynolds number. In addition, an inverse formulation must be chosen for the boundary-layer equations when separation occurs in order to avoid the Goldstein singularity. The displacement thickness is given and the velocity of the outer flow is computed, cf. J.E. Carter (1979) and A.E.P. Veldman (1981). The justification for this method can be found in triple-deck theory.

14.5 Marginal Separation

Figure 14.9 has shown that using triple-deck theory means that step flows for $H/\ell > (H/\ell)_{\text{MS}}$ can be computed. Since this theory takes its starting point from the limiting solution of the flat plate ($\text{Re}^{-1/2} \rightarrow 0$, $H/\ell = 0$), it cannot encompass the limiting solutions $\text{Re} \rightarrow \infty$ for finite values of H/ℓ . In particular it cannot deliver solutions for $H/\ell \geq (H/\ell)_{\text{MS}}$ for which the Prandtl boundary-layer theory breaks down because of the appearance of the Goldstein singularity.

We are thus especially interested in the solutions close to the point denoted MS in Figs. 14.1 and 14.9. The name “marginal separation” is used to describe this “limiting point” and the solutions close to it. We need the asymptotic expansion for large Reynolds numbers around the point MS. The solution in this point represents the limiting solution of this expansion. This theory has been described comprehensively by K. Stewartson et al. (1982) and A.I. Ruban (1991). It turns out that the solutions again have a triple-deck structure. However, it is of particular importance that the solutions are no longer unique.

Marginal separation always occurs in flow arrangements which are described by one particular parameter. In what follows, this will be called the *singularity parameter S*. This parameter must be able to take on values where a simple boundary-layer calculation along the entire geometry of the body without the appearance of the Goldstein singularity is possible (attached flows), as well as values where the boundary-layer calculation cannot be carried on any further because of the appearance of the Goldstein singularity.

The limit between these two values is given by the “critical value” S_c . For marginal separation, the flow for $\text{Re} \rightarrow \infty$ is given by this limiting case. The Goldstein singularity has just not appeared. In the example of the step flow treated here, $S = H/\ell$ and $S_c = (H/\ell)_{\text{MS}}$.

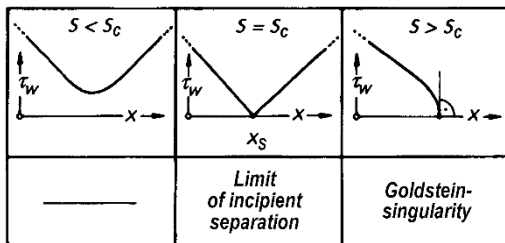


Fig. 14.13. Wall shear stress for $\text{Re} \rightarrow \infty$ (Prandtl boundary-layer theory)

The starting point for the theory of marginal separation is the behaviour of the wall shear stress of a simple Prandtl boundary-layer calculation in the limit $S = S_c$. The central case in Fig. 14.13 shows this behaviour. A particular characteristic is the *linear* distribution of the wall shear stress in front of and behind the point marked with the coordinate x_S , with a jump in the slope of τ_w at x_S . The position x_S is the point on the contour where for $S = S_c$ the wall shear stress goes to zero in the limit $\text{Re} \rightarrow \infty$. Because of the jump in $d\tau_w/dx$ at x_S , there is again an interaction between the outer flow and the boundary layer at x_S . This manifests itself as a triple-deck structure. Again there is a coupling between the Reynolds number and the geometry, with

$$S \rightarrow S_c, \quad \text{Re} \rightarrow \infty, \quad (S - S_c) \text{Re}^{2/5} = O(1). \quad (14.64)$$

This triple-deck here now scales differently from the triple-deck described in Sect. 14.4. For details see the original work.

After formulating the problem in the triple-deck variables, it is possible to write down the wall shear stress close to the position x_S as a function of $S - S_c$. This can be done universally and is independent of the concrete geometry of the body. An asymptotic correction to the wall shear stress distribution close to x_S can therefore be achieved. Figure 14.14 shows the wall shear stress at the position x_S in the form of $\tilde{\tau}_w(x = x_S)$. It also shows the wall shear stress distribution close to x_S in the form of $\tilde{\tau}_w(\tilde{x})$ for some chosen values of the singularity parameter: see the caption of Fig. 14.14 for more details. In each case the distributions are only qualitative. In a concrete case, the factors of proportionality will certainly have to be determined by inverse transformation to the physical variables.

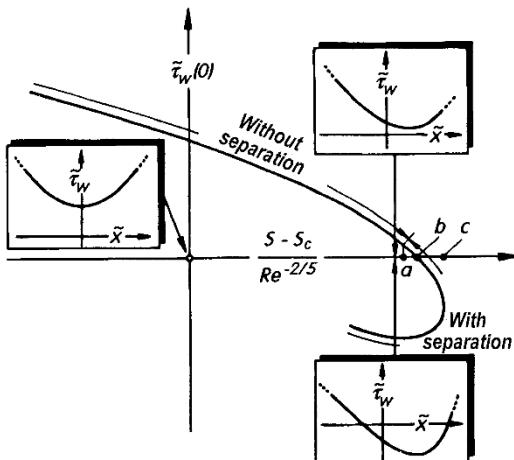


Fig. 14.14. Theory of marginal separation; universal dependence of the wall shear stress at x_S on the singularity parameter S
smaller figures: wall shear stress close to x_S

$$\tilde{x} \sim \frac{x - x_S}{L} Re^{1/5}, \quad \tilde{\tau}_w(\tilde{x}) \sim \frac{\tau_w}{\rho U_\infty^2} Re^{1/5}, \quad Re = \frac{U_\infty L}{\nu}$$

a: start of separation

b: separation point at x_S

c: maximum value of parameter $(S - S_c)Re^{2/5}$

The results in Fig. 14.14 are universal and are therefore independent of the particular geometry of the body. They will be discussed more detail in the next four points:

1. For $S = S_c$ the wall shear stress is always positive, i.e. the effect of the interaction described in triple-deck theory acts to prevent separation.
2. Starting off with a completely attached flow, as $S - S_c$ increases cases with double roots of $\tilde{\tau}_w(\tilde{x})$ occur. This means separation and reattachment (see the smaller figure in Fig. 14.14 below right). The case where $\tilde{\tau}_w(\tilde{x})$ just becomes zero (point a in Fig. 14.14) is mathematically not particularly exciting, but physically is “incipient separation at finite Reynolds numbers”.
3. In certain $(S - S_c)$ regions, the solution is no longer unique. Two solutions exist. An example of such a double solution is shown in Fig. 14.15. S.N. Brown; K. Stewartson (1983) have proved that in certain (small) parameter regions there are even four solutions.
4. Solutions do not exist for arbitrarily large parameters $S - S_c$: there is an upper limit. Since for large parameters $S - S_c$ “massive separation” (as described in the next section) occurs, this implies physically that no continuous transition from marginal separation to massive separation exists!

The question emerges of how the transition from the attached flow for small values of the parameter S to the case of massive separation (for very large values of S) takes place if the theory of marginal separation does not allow a continuous transition.

The only explanation is to be found in the fold of the solution surface, as is sketched in Fig. 14.9 for the maximal value of the pressure at the rounded step. The upper part of the figure is the top elevation onto the “solution hill” of $c_{p\max}$ as a function of H/ℓ and $\text{Re}^{-1/2}$. The lower part is the side elevation for $\text{Re} = \text{const}$ and clarifies the fold of the solution hill. In the shaded region there is more than one solution (fold of the solution region).

The regions with separation are on the right hand side of the curve $D - C - A - MS$. The narrow shaded area between the curves $C - A - MS$ and $K - B_1 - MS$ lies on the upper solution area and belongs to the region of marginal separation. There is no continuous transition from this region to the region of massive separation. Rather there is a discontinuous jump to the lower solution surface, as the arrow S_1 in the lower figure shows.

The inverse transition where a decrease in H/ℓ occurs leads to flow which is attached everywhere. This transition also takes place as a discontinuous jump S_2 . Since S_1 and S_2 are at different values of H/ℓ , there is hysteresis in the behaviour of the solution. This hysteresis only exists above a certain Reynolds number, as the upper part of Fig. 14.9 shows. For increasing Reynolds numbers, more than one solution only occurs at the point K . This is the point where the previously smooth solution surface first starts to fold. In the projection, the angle between the curves $O - K$ and $MS - K$ in the point K is equal to zero and is called the cusp. The mathematical theory concerned with folded solution surfaces is called *catastrophe theory*, cf. P.T. Saunders (1980). The case in point here is a so-called *cusp catastrophe*.

The behaviour of the solution which we have described in a qualitative manner has been impressively confirmed by F. Sommer (1992) with a very thorough numerical study. The flow at a rounded step whose shape is described by the seventh order polynomial in Eq. (14.57) was considered, see Fig. 14.15.

The aim was to confirm the general behaviour of the solution from boundary-layer calculations at finite Reynolds numbers (since there is then no Goldstein singularity) in the region of the folded solution surface. In order to do this, the equations for the outer flow and all terms in the boundary-layer equations which count towards the second order (as described in Sect. 14.2) were taken into account. These describe curvature and displacement effects. However, there was no division made between the first and second order, but rather one system of equations was used (an extended version of the Prandtl boundary-layer equations). In these, the Reynolds number appears explicitly and therefore solutions at finite Reynolds numbers are permitted. The boundary-layer calculations were carried out using the so-called *inverse method*, where the displacement thickness is given as a boundary condition and the pressure is calculated, see for example A.E.P. Veldman (1981).

The relative step height $\tilde{H} = H/\ell$ was systematically varied with fixed ratio $\ell/L = 0.5$. Figure 14.15 shows the maximal value of the pressure coefficient $c_{p\max}$ as a characteristic quantity of the solution for $\text{Re} = U_\infty L/\nu = 10^7$. Starting off

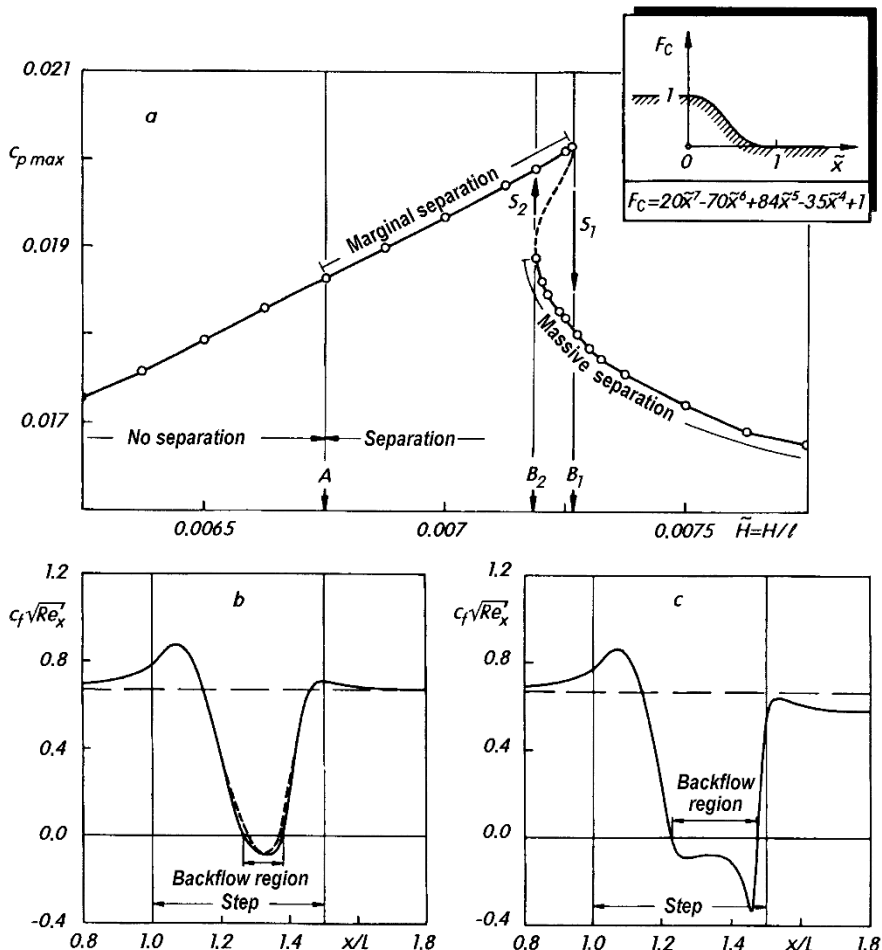


Fig. 14.15. Step flow for $\ell/L = 0.5$ and $Re = 10^7$, after F. Sommer (1992)

- (a) cut of the folded solution surface $c_p \max(H/\ell)$. A, B_1, B_2, S_1, S_2 as in Fig. 14.9.
- (b) example of marginal separation $\tilde{H} = B_2$
 - interaction theory
 - asymptotic theory of marginal separation
- (c) example of massive separation (interaction theory), $\tilde{H} = B_2$
 $Re_x = U_\infty x/\nu$ in figures (b) and (c)

with a low value of H where the flow was attached everywhere, separation first occurs when \tilde{H} is increased to about $6.8 \cdot 10^{-3}$ (point A). Further increase of \tilde{H} shows continuous increase of $c_p \max$. At $\tilde{H} = B_1 = 7.25 \cdot 10^{-3}$, the solution jumps discontinuously to the lower branch. If \tilde{H} is further increased, there is again a continuous (but decreasing) progression.

If we now carry out the same experiment “backwards”, starting off at a high value of \tilde{H} , we move along the lower branch of the solutions, but now on beyond the value $\tilde{H} = B_1$ towards lower values of \tilde{H} ! At $\tilde{H} = B_2 = 7.175 \cdot 10^{-3}$ the solution jumps to the upper branch. The hysteresis region in Fig. 14.9 is shown in Fig. 14.15a between B_2 and B_1 . In contrast to the main behaviour in Fig. 14.9, there is a jump back to a solution with separation in the example computed here. The curve $K - B_2 - O$ lies at $\text{Re} = 10^7$ in this example, still on the right hand side of the curve $C - A - MS$.

Figures 14.15b and 14.15c show the skin-friction coefficient c_f for the two different solutions with the same value $\tilde{H} = B_2$. Figure 14.15b from the domain of marginal separation shows only a small backflow region, whereas Fig. 14.15c demonstrates a considerably larger backflow region from the massive separation domain.

In addition, Fig. 14.15b contains the asymptotic results of the theory of marginal separation. Here this has been worked out at the finite Reynolds number $\text{Re} = 10^7$. This shows rather impressively that the universal result of the asymptotic theory (see Fig. 14.14, lower small figure) agrees very well with the numerical results for a certain geometry.

A further example of marginal separation occurs at the flow past an airfoil at an angle of attack. In this case the angle of attack α serves as a singularity parameter S , cf. K. Stewartson et al. (1982).

The marginal separation at narrow bumps and dents and the extension to three-dimensional obstacles has been investigated by G. Hackmüller; A. Kluwick (1989, 1990, 1991a, 1991b). A. Kluwick (1989b) has also treated the marginal separation of axisymmetric boundary layers.

The blow-up and control of marginally separated boundary layers have been investigated by S. Braun; A. Kluwick (2005). The same authors studied also three-dimensional unsteady perturbations of an incompressible steady two-dimensional marginally separated laminar boundary layer. The flow behavior near the critical value Γ_c of the controlling parameter Γ was of special interest. The integro-differential equation which governs these perturbations reduces to a nonlinear partial differential equation known as Fisher equation. Its interesting solutions show waves with singularities, which can be interpreted as vortex sheets, see S. Braun; A. Kluwick (2004). In the investigation of a singularity solution in the theory of unsteady marginal separation by S. Scheichl; S. Braun; A. Kluwick (2008) it is shown that any blow-up solution finally approaches a unique structure.

14.6 Massive Separation

Massive separation occurs when the boundary layer leaves the wall as one and marks the boundary between the outer flow and a separation region (backflow region) as a free shear layer. First of all we must consider the point where the boundary layer leaves the wall. This is called the *separation point*. Massive separation takes place when the thickness of the boundary layer in front of the separation point is small compared to the dimension of the separation region perpendicular to the main flow direction.

A strong increase in the v component close to separation implies that the reaction on the outer flow is no longer asymptotically small. Again an interaction process is present which must be described using triple-deck theory. However K. Stewartson (1970) was able to show that using the triple-deck

theory can *not* remove the singularity. It turns out that the positive pressure gradient imposed on the boundary layer, which is only modified in an asymptotically small region in triple-deck theory, is the important obstacle.

We are now faced with a dilemma: the positive pressure gradient is a necessary condition for the onset of separation, but is simultaneously the origin of the singular behaviour of the boundary-layer solution. V.V. Sychev (1972) discovered an amazingly simple way out of this dilemma: close to the separation point the pressure gradient is assumed to be asymptotically small; it only exists for finite Reynolds numbers. In the limit of infinite Reynolds number (it is only in this limit that the Goldstein singularity can occur) there is no pressure increase directly in front of the separation point and thus no Goldstein singularity. It has not been removed, but has been avoided!

Three important aspects determine the asymptotically consistent description of flows with massive separation:

1. In the limit $\text{Re}^{-1} = 0$ all (thin, at high Reynolds numbers) shear layers “degenerate” to lines. If we start by assuming that the boundary layer leaves the wall in the separation point, then in the limit $\text{Re}^{-1} = 0$ a so-called *free-streamline* leaves the body. This divides the inviscid outer flow from the backflow region. It is a line of discontinuity, because the velocities on either side are generally different. The limiting solutions on which the perturbation calculation for large Reynolds number is based are therefore no longer potential flows continuous everywhere, but are now solutions of the potential equation with so-called free streamlines and adjoining “dead water regions”.

Figure 14.16 shows the two different limiting solutions for some geometries. The limiting solution in the column on the right corresponds to the so-called *free-streamline theory* of H. Helmholtz (1868) and G. Kirchhoff (1869). There is constant pressure along the free streamlines, namely that in the dead water region. Thus there is constant pressure at the separation point. For step flows, the limiting solution is translation flow.

2. In the near field, the flow for $\text{Re}^{-1} = 0$ is given by the Helmholtz-Kirchhoff solution. For $\text{Re}^{-1} \neq 0$, it must be modified so that a pressure gradient arises which matches the pressure from the triple-deck scaling. It follows from triple-deck theory that, at finite Reynolds numbers, the separation point x_0 shifts downstream with $x_0 - \hat{x}_0 = O(\text{Re}^{-1/16})$ compared to the *break-away point* \hat{x}_0 of the limiting free streamline (for step flows $\hat{x}_0 = L$).

The pressure distribution in front of the separation point x_0 is

$$p - p_0 = -c_0(x_0 - x)^{1/2} + O((x_0 - x)) \quad (14.65)$$

for

$$x < x_0 \quad \text{and} \quad x \rightarrow x_0$$

with

$$c_0 = 0.44 c^{9/8} \text{Re}^{-1/16}, \quad (14.66)$$

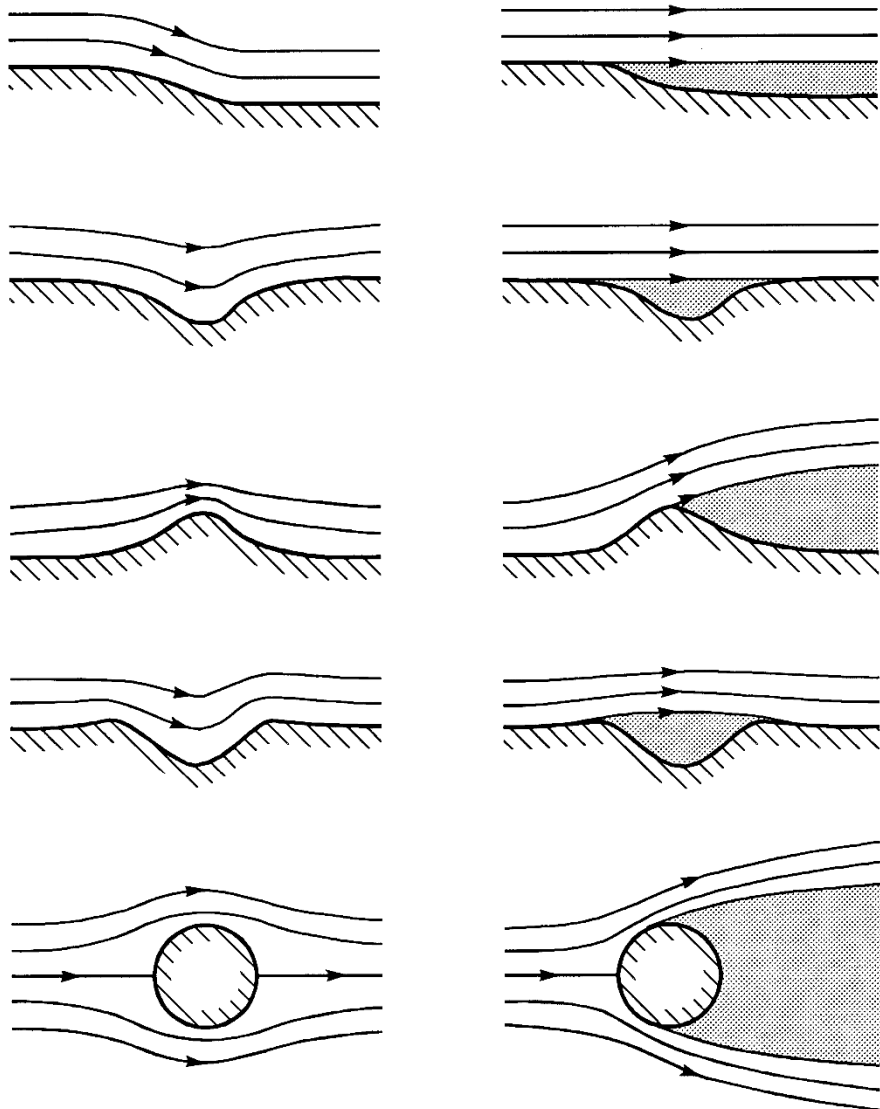


Fig. 14.16. Limiting solution for $\text{Re}^{-1} = 0$ (inviscid flows)
 left column: continuous potential flows
 right column: free-streamline theory solutions by Helmholtz-Kirchhoff

where c describes the wall gradient of the approaching flow boundary layer, cf. F.T. Smith (1977). For step flow $c = 0.332$.

3. F. Sommer (1992) has shown how the curve KB_2O in step flows (Fig. 14.9) can be determined close to the origin. A new inviscid limiting solution has to be determined where the free streamline leaves the body at x_0 (and no longer at \tilde{x}_0). H.K. Cheng; F.T. Smith (1982) have also presented an approximate method to compute this limiting solution, cf. also H.K. Cheng; C.J. Lee (1986).

As yet there is no complete theory for the asymptotic description of the flow in the so-called far field, i.e. for example, close to the reattachment point.

Example: circular cylinder

The (fictitious steady) flow at a circular cylinder for high Reynolds numbers is another example of massive separation. At the circular cylinder there is only one peripheral angle at which the free streamline can leave the wall tangentially so that there is no pressure increase region downstream (Brillouin–Villat condition, see V.V. Sychev (1972)). This angle is about 55° from the front stagnation point. Figure 14.17 shows the limiting solution ($Re^{-1} = 0$). For large values of \tilde{x} , the free streamline takes on a parabolic shape. Close to the separation point, the flow can be described using triple-deck theory, as V.V. Sychev (1972) and F.T. Smith (1977) have shown. A more exact analysis shows that the Helmholtz–Kirchhoff theory is only suitable for describing the near field. F.T. Smith (1979a) has suggested an asymptotic model where an elliptical backflow region of length $O(Re)$ and thickness $O(Re^{1/2})$ exists at the back of the body. This backflow region can be matched up asymptotically to the near field of the body. Problems arise close to the peak of the ellipse lying downstream where the free shear layers which are a continuation of the wall boundary layers coincide. For details, see the work of F.T. Smith (1979a, 1986).

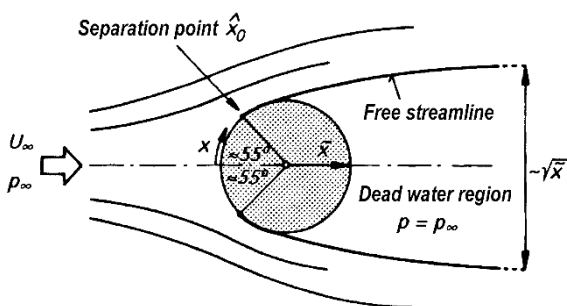


Fig. 14.17. Limiting solution ($Re^{-1} = 0$) for the circular cylinder, according to the free-streamline theory by Helmholtz–Kirchhoff

Part III

Laminar–Turbulent Transition

15. Onset of Turbulence (Stability Theory)

15.1 Some Experimental Results on the Laminar–Turbulent Transition

15.1.1 Transition in the Pipe Flow

In many cases, real flows deviate considerably from the laminar flows treated in the previous chapters. They demonstrate a characteristic feature called *turbulence*. As the Reynolds number is increased, both internal flows through pipes and channels and external boundary–layers flows past bodies exhibit a noticeable change from a laminar flow form to a turbulent flow form. This *transition* from laminar to turbulent flow, also called the *onset of turbulence* is of fundamental importance for the whole science of fluid mechanics.

This phenomenon was first noticed in flows through straight pipes and channels. At small Reynolds numbers, every fluid particle in a long straight pipe with constant cross–section and smooth walls moves with constant velocity on a straight path. Because of the friction forces, the particles close to the wall flow more slowly than those further inside. The flow is one of well–ordered layers moving alongside each other (laminar flow), Fig. 1.6a. However, observation shows that this orderly flow no longer exists at higher Reynolds numbers (Fig. 1.6b). Rather a strong mixing effect occurs. This was made visible by O. Reynolds (1883) in pipe flow using “coloured filaments” added to the flow. As long as the flow is laminar, the coloured fluid particles flow through the pipe as filaments with sharp boundaries. However, as soon as the flow becomes turbulent, the coloured filaments break up and causes the fluid in the pipe to appear evenly coloured. In turbulent flow, *transverse movements* which bring about this mixing are superimposed on the main motion in the direction of the pipe axis. This transverse motion causes an exchange of momentum in the tranverse direction, since each particle essentially retains its momentum in the longitudinal direction while carrying out the mixing motion. A consequence of this is that the velocity distribution over the cross–section of the pipe is much more uniform than in the laminar case. Figure 15.1 shows the measured velocity distribution in pipe flow for laminar and turbulent flow. While the velocity distribution over the cross–section is parabolic for laminar flow, cf. Sect. 5.2.1, in turbulent flow the momentum exchange means that it is much more uniform. A closer analysis of turbu-

lent flow will show that its most striking characteristic is that the velocity and pressure at a fixed point in space are not constant in time, but rather they carry out irregular fluctuations of changing frequency, cf. Fig. 15.16. Only the average of the velocity over a long time interval can be taken to be constant (*quasi-steady motion*). The *quasi-steady* pipe flow which thus has a velocity dependent on position and time may be characterised either by the time averaged volume flux Q or the time averaged pressure gradient $-d\bar{p}/dx$. Figure 15.1 shows this clearly. Curve a shows the time averaged velocity distribution of turbulent pipe flow. The other two distributions correspond to laminar pipe flow, at the same volume flux (curve b) and the same pressure gradient (curve c) as curve a .

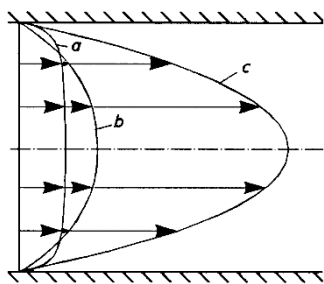


Fig. 15.1. Velocity distribution in a pipe
 (a) turbulent
 (b) laminar, same volume flux as a
 (c) laminar, same pressure gradient as a

The first systematic investigations into these two fundamentally different flow states were carried out by O. Reynolds (1883). He also carried out the coloured filament experiment which bears his name. He discovered the *similarity principle with respect to the Reynolds number* which says that the transition from laminar to turbulent flow forms always takes place at about the same Reynolds number $\text{Re} = u_m d / \nu$, where $u_m = Q/A$ is the mean velocity (Q = volume flux, A = pipe cross-sectional area). The numerical value of the Reynolds number at which the transition occurs (*critical Reynolds number*) was found to be

$$\text{Re}_{\text{crit}} = \left(\frac{u_m d}{\nu} \right)_{\text{crit}} = 2300 . \quad (15.1)$$

Accordingly pipe flows whose Reynolds number is $\text{Re} < \text{Re}_{\text{crit}}$ are laminar, and those for which $\text{Re} > \text{Re}_{\text{crit}}$ are turbulent.

The two laminar pipe flows in Fig. 15.1 (curves b and c) are associated with one and the same turbulent pipe flow, but are described by different Reynolds numbers: these are $\text{Re}_p = -(dp/dx) d^3 / 32\varrho\nu^2$ and $\text{Re}_Q = u_m d / \nu$. For laminar flows, according with Eqs. (5.60) and (5.61), $\text{Re}_p = \text{Re}_Q$. However, Re_p and Re_Q have to be distinguished for turbulent flows and they are a manner of characterising turbulent pipe flows and channel flows, cf. B.L. Rozhdestvensky; L.N. Simakin (1982, 1984) and P.G. Saffman (1983, 1988).

The numerical value of the critical Reynolds number depends quite strongly on the particular conditions of the pipe entrance and in the approach to it. In fact, O. Reynolds already surmised that the critical Reynolds number is larger the smaller the disturbances in the flow before the pipe. This was confirmed in experiments by H.T. Barnes; E.G. Coker (1905) and later by L. Schiller (1922), where values of up to $Re_{crit} = 20\,000$ were obtained. V.W. Ekman (1910), using an entrance particularly free from disturbances, was able to achieve $Re_{crit} = 40\,000$. On the other hand, different experiments have shown that there is a lower limit of Re_{crit} which lies at about $Re_{crit} = 2000$. Below this Reynolds number, even if the disturbances are very strong, the flow remains laminar.

Also connected to the transition from laminar flow to turbulent flow is a noticeable change in the pipe drag law. Whereas in laminar flow the pressure drop which drives the flow is, corresponding to $Re_p = Re_Q$, proportional to the first power of the velocity u_m , cf. Eq. (5.59), this pressure gradient in turbulent flow is almost proportional to the square of the mean velocity. This large flow drag has its origin in the turbulent mixing motion. The change in the drag law with the laminar-turbulent transition can be seen in Fig. 1.4.

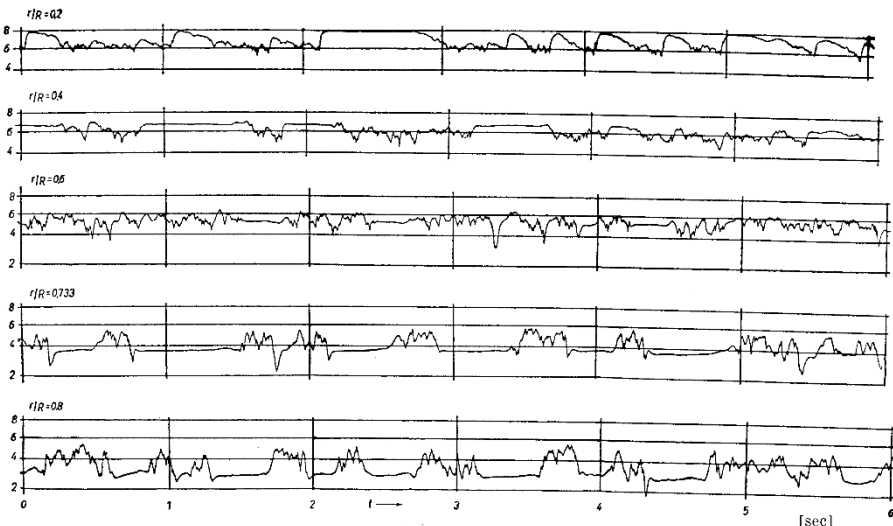


Fig. 15.2. Change in time of the velocity of pipe flow close to the laminar-turbulent transition for various distances r from the center of the pipe, after J.C. Rotta (1956)

Reynolds number $Re = u_m d / \nu = 2550$
 length $x/d = 322$;
 velocity $u(t)$ in m/s, time in s
 $u_m = 4.27$ m/s

Detailed experimental investigations into the laminar–turbulent transition in pipe flow have shown that the flow has an “intermittent character” in a certain region of Reynolds numbers close to the critical Reynolds number. By this we mean that the flow is occasionally laminar and occasionally turbulent. Figure 15.2 depicts measurements from J.C. Rotta (1956) showing the dependence of the velocity on the time at different positions along the radius. The velocity illustration shows that time segments with laminar and turbulent flow occur one after another at irregular intervals. At positions close to the center of the pipe, the velocity in the laminar time segments is greater than the time averaged velocity in the turbulent sections; at positions close to the wall of the pipe it is the reverse. Since in the experiments it was ensured that the volume flux remains constant, we must conclude that the velocity distribution alternates between a corresponding developed laminar and a corresponding fully developed turbulent pipe flow (curve *b* or *a* in Fig. 15.1).

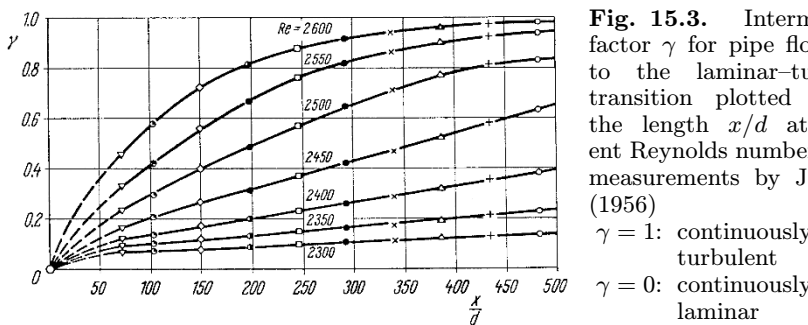


Fig. 15.3. Intermittency factor γ for pipe flow close to the laminar–turbulent transition plotted against the length x/d at different Reynolds numbers, after measurements by J. Rotta (1956)

$\gamma = 1$: continuously turbulent
 $\gamma = 0$: continuously laminar

The physical character of this flow is given by the *intermittency factor* γ . This gives the fraction of time for which there is turbulent flow at a particular position. Therefore $\gamma = 1$ means continuous turbulent flow and $\gamma = 0$ continuous laminar flow. Figure 15.3 shows the intermittency factor at different Reynolds numbers along the length x . For constant Reynolds number, the intermittency factor increases continuously with the distance. The Reynolds numbers in which the transition is carried out are in the region $Re = 2300$ to $Re = 2600$. For Reynolds numbers close to the lower limit, the development from laminar to fully turbulent flow takes place over a very long pipe length, equivalent to thousands of pipe diameters.

The processes described here for the pipe with circular cross-section take place in a similar manner for plane channel flow.

The laminar–turbulent transition is a *stability problem*, based on the idea that laminar flow is acted on by some small perturbations, such as those which could arise in the pipe entrance. At small Reynolds numbers, i.e. at large values of ν , the damping action of the viscosity is large enough to ensure that these small perturbations die away again. It is only at large

enough Reynolds numbers that the damping due to the viscosity is no longer sufficient, so that the disturbances are intensified and thus eventually initiate the transition to turbulence.

It will be seen later that the initial disturbances occurring in plane boundary layers are two-dimensional, but these later develop into three-dimensional perturbations.

Investigations into the parabolic velocity profile in pipe flow, cf. Sect. 5.2.1, using stability theory show that this is stable with respect to two-dimensional perturbations. In contrast to the boundary-layer flows treated in the next section, the laminar–turbulent transition in pipe flow originates with three-dimensional perturbations from the start.

15.1.2 Transition in the Boundary Layer

In comparison to the investigations into pipe flow, it was much later that it was discovered that the boundary layer at a body in a flow can also be either laminar or turbulent. In this case, the entire behaviour of the flow past the body, particularly the force acting on the body, is strongly dependent on whether the boundary layer is laminar or turbulent. The laminar–turbulent transition in the boundary layer on a solid body is affected by many parameters of which the most important apart from the Reynolds number, are the pressure distribution of the outer flow, the nature of the wall (roughness) and the level of disturbance of the outer flow (turbulence intensity). Figure 15.4 shows the laminar–turbulent transition in the boundary layer on a body of revolution. The concentration of the smoke added makes an instantaneous picture of the structural development in the *transition region* visible. The region of laminar flow is replaced downstream by axisymmetric waves, so-called *Tollmien–Schlichting waves*. These initiate the transition to turbulent flow via a subsequent characteristic three-dimensional structure formation.

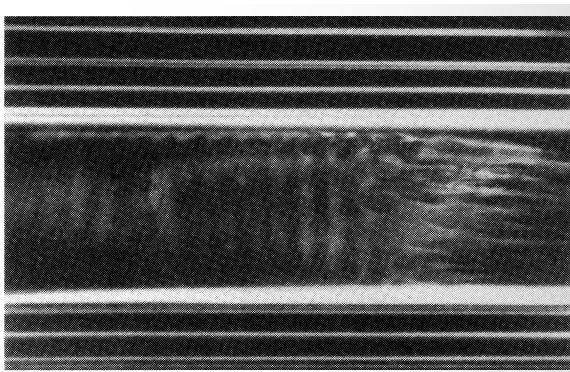


Fig. 15.4. View of the transition process in the boundary layer at a body of revolution, after F.N.M. Brown (1957)

Flat plate at zero incidence. Just as with a body of revolution, the laminar-turbulent transition can be observed for a flat plate at zero incidence. For the laminar boundary layer at a plate, Sect. 6.5 showed us that the boundary-layer thickness grows with \sqrt{x} , where x is the distance from the leading edge. The transition from the laminar to the turbulent boundary layer was first investigated by J.M. Burgers (1924), B.G. Van der Hegge Zijnen (1924), later by M. Hansen (1928) and more comprehensively by H.L. Dryden (1934, 1937, 1939). Close to the leading edge of the plate, the boundary layer is initially always laminar but further downstream it then becomes turbulent. For a plate with a sharp leading edge, the laminar-turbulent transition in a normal air stream takes place at a distance x from the leading edge, given by

$$\text{Re}_x \text{crit} = \left(\frac{U_\infty x}{\nu} \right)_{\text{crit}} = 3.5 \cdot 10^5 \quad \text{to} \quad 10^6.$$

As for a pipe, the critical Reynolds number for a plate at zero incidence can be raised if an outer flow free from perturbations (low turbulence intensity) is ensured.

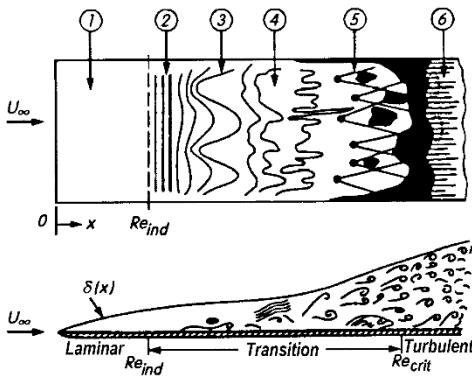


Fig. 15.5. Sketch of laminar-turbulent transition in the boundary layer on a flat plate at zero incidence, after F.M. White (1974)
 (1) stable laminar flow
 (2) unstable Tollmien-Schlichting waves
 (3) three-dimensional waves and vortex formation (Λ -structures)
 (4) vortex decay
 (5) formation of turbulent spots
 (6) fully turbulent flow

The experimental results are shown in the basic sketch in Fig. 15.5. Two-dimensional Tollmien-Schlichting waves are superimposed onto the laminar boundary-layer flow at the *indifference Reynolds number* Re_{ind} . These can be described using *primary stability theory* (cf. Sect. 15.2.2). Because of *secondary instabilities* (cf. Sect. 15.3.2), three-dimensional disturbances are superimposed further downstream. These lead to a characteristic *Λ -structure formation*. The Λ -vortices are replaced by *turbulent spots*, which initiate the transition to fully turbulent boundary-layer flow. At $\text{Re}_x = \text{Re}_x \text{crit}$, the transition process is complete, and further downstream the flow is fully turbulent.

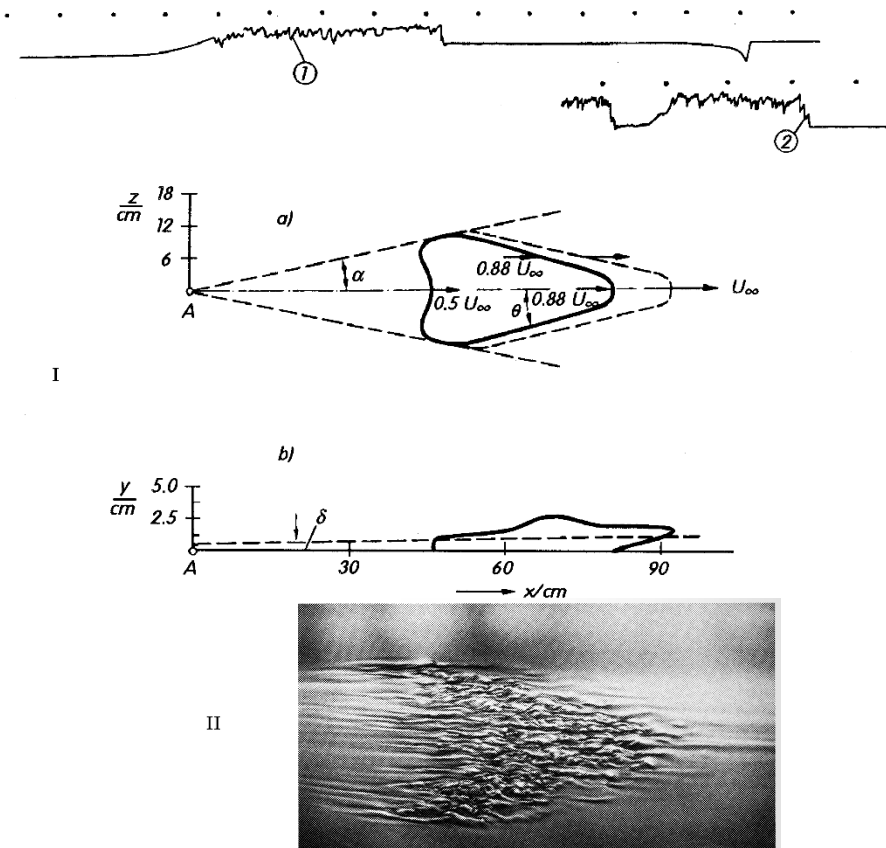


Fig. 15.6. Growth of an artificial turbulent spot in the transition boundary layer on a flat plate at zero incidence.

(I) Measurements by G.B. Schubauer; P.S. Klebanoff (1955), from H.L. Dryden (1956).

(a) ground plan, (b) side view of an artificial turbulent spot produced at position A at a distance of about 70cm from the position of appearance. Position A is about 70cm behind the leading edge of the plate. $\alpha = 11.3^\circ$, $\theta = 15.3^\circ$, δ = thickness of laminar boundary layer, free stream velocity $U_\infty = 10$ m/s

(1) and (2): oscillogram of a hot-wire anemometer moving through an artificially produced turbulent spot and a naturally appearing turbulent spot respectively. Time interval between two marks: s/60.

(II) view due to R. Falco (1980)

Investigations by H.W. Emmons; A.E. Bryson (1951/52) and G.B. Schubauer; P.S. Klebanoff (1955) have shown that the turbulent spots in Fig. 15.6 appear irregularly at arbitrary positions in the boundary layer and wander downstream in a wedge shaped region. Such turbulent spots appear at irregular time intervals at different irregularly distributed positions on the plate.

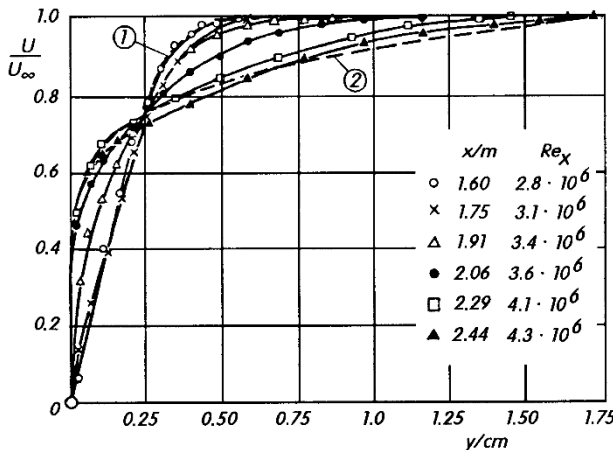
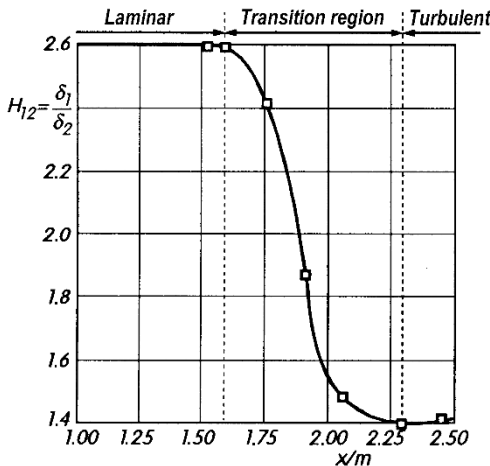


Fig. 15.7. Velocity profile of the plate boundary layer close to the laminar-turbulent transition, after measurements by G.B. Schubauer; P.S. Klebanoff (1955)
(1) laminar, Blasius profile
(2) turbulent, profile from Fig. 18.5, $\delta = 17$ mm
outer velocity $U_\infty = 27$ m/s
outer flow turbulence intensity $Tu = 3 \cdot 10^{-4}$

As can be seen from Fig. 15.5, the transition occurs together with a strong increase in the boundary-layer thickness. In the laminar boundary layer, the dimensionless boundary-layer thickness $\delta/\sqrt{\nu x}/U_\infty$ is constant and approximately equal to 5, cf. Eq. (6.60). Figure 2.4 shows this dimensionless boundary-layer thickness plotted against the Reynolds number formed with the length x , namely $Re_x = U_\infty x / \nu$. For $Re_x \geq 3 \cdot 10^5$ a great increase in the boundary-layer thickness occurs. As well as this, there is also a noticeable change in the form of the time averaged velocity profile. Figure 15.7 shows the velocity profile in a transition region from about $Re_x = 3 \cdot 10^6$ to $4 \cdot 10^6$ for a free stream with very low turbulence intensity, according to measurements by G.B. Schubauer; P.S. Klebanoff (1955). Within this region, the velocity distribution is reshaped from that of the Blasius profile for the laminar plate boundary layer (H. Blasius (1908), cf. Fig. 6.6a and Fig. 6.7) to that of the fully turbulent plate boundary layer, cf. Sect. 18.2.5.

Along with the reforming of the velocity distribution in the transition region, there is a strong decrease in the shape factor $H_{12} = \delta_1/\delta_2$, as is shown in Fig. 15.8. For the plate boundary layer, the shape factor of $H_{12} = 2.59$ in the laminar region decreases to $H_{12} \approx 1.4$ in the turbulent region.



1.19 that at Reynolds numbers of about $\text{Re} = V d/\nu = 3 \cdot 10^5$ a sudden sharp drop in the drag coefficient occurs. This strong drag decrease was first discovered by G. Eiffel (1912) for the sphere and is a consequence of transition in the boundary layer. When the boundary layer is turbulent, the position of separation is shifted further backwards and thus the wake region is made considerably narrower. L. Prandtl (1914) was able to show that this explanation is indeed correct by laying a thin wire loop (*trip wire*) around the sphere just in front of the equator. This artificially forced the laminar boundary layer to become turbulent at a smaller Reynolds number and similarly achieved the same low drag as normally only occurs at higher Reynolds numbers. Figure 2.14 shows flow portraits of a sphere in the subcritical flow state with large wake and drag, and a sphere in the supercritical flow state with small wake and low drag. The second state is produced using *Prandtl's trip wire*. This experiment proved convincingly that the jump in the drag curve of the sphere can only be understood as a boundary-layer effect which has to do with the laminar-turbulent transition.

15.2 Fundamentals of Stability Theory

15.2.1 Remark

Attempts to clarify the striking phenomena of the transition from laminar to turbulent flow theoretically had already begun in the last century, but only led to success in about 1930. These theoretical investigations assume that the laminar flow is acted on by some small disturbances, which, in pipe flow, could come from the pipe entrance, or, in the boundary layer of a body, from the wall roughness or from irregularities in the outer flow. The theory follows the rate of change of such perturbations superimposed on the laminar basic flow. In each individual case their form remains to be determined. The decisive question here is whether the disturbances die away or grow in time. If the disturbances die away in time, the basic flow is considered to be *stable*; if they grow, the basic flow is *unstable*, i.e. it is possible that the laminar-turbulent transition will occur. In this manner, a *stability theory* of laminar flow can be developed. Its aim is to determine the *indifference Reynolds number* for a given laminar flow. The basic idea of stability theory comes from the conjecture by O. Reynolds (1894) that the laminar flow, always a possible solution of the equations of motion, becomes unstable above a certain limit (namely the indifference Reynolds number) and becomes turbulent flow.

O. Reynolds worked for many decades on the mathematical reasoning for this conjecture, as did Lord Rayleigh (1880–1913) later. These theoretical efforts at first were unsuccessful for many years. It was only in about 1930 that the original aim, namely the theoretical calculation of an indifference Reynolds number, was achieved satisfactorily by L. Prandtl's colleagues W. Tollmien and H. Schlichting. The experimental confirmation of stability

theory was accomplished some ten years later by H.L. Dryden and his colleagues. There was a remarkable agreement between theory and experiment.

Summaries of stability theory have been presented by H. Schlichting (1950, 1959), C.C. Lin (1955), R. Betchov; W.O. Criminale (1967), E. Reshotko (1976), L.M. Mack (1977), P.G. Drazin; W.H. Reid (1981) and J.T. Stuart (1986), cf. also V.V. Kozlov (1985), M.V. Morkovin (1988), H.L. Reed et al. (1996), H. Oertel Jr.; J. Delfs (2005), H. Oertel Jr. (2001, 2002, 2010, 2016) and K.R. Sreenivasan; H. Oertel Jr. (2010, 2016).

A new aspect of stability theory has been carried over from the work of R.J. Briggs (1964) and A. Bers (1973) in the area of plasma physics to fluid mechanical stability problems. The overview articles by P. Huerre; P.A. Monkewitz (1990) and H. Oertel Jr. (1990, 1995, 2010) indicate that the temporal and spatial amplification of disturbances in a transitional flow field require the *absolutely unstable* or *absolutely sensitive* regions to be determined. It turned out that precisely these regions of the flow field are of particular importance for the laminar–turbulent transition and efficient ways of controlling it. Fluid mechanical instabilities which commence abruptly, as in the wake flow behind a body for example, are *absolutely unstable*. We define an absolutely unstable region to be that flow region where perturbations added locally are magnified temporally and spatially and, with increasing time, affect the entire absolutely unstable flow region, cf. also M. Gaster (1962, 1965). In *convectively unstable* regions, locally introduced perturbations flow downstream and can, at later times, no longer affect the original position of the perturbation.

The instabilities of the plate boundary layer which lead to the turbulent boundary layer via several discrete instabilities are *convectively unstable*, cf. L. Brevoord (1993).

This determines a division of areas of viscous flows with the basics of stability analysis, one which also differentiates between flow regions of absolute and convective instability above the indifference Reynolds number, cf. H. Oertel Jr. (1995, 2001, 2002, 2010, 2016) and H. Oertel Jr.; J. Delfs (2005).

15.2.2 Fundamentals of Primary Stability Theory

In investigating the stability of laminar flows, the motion is decomposed into the basic flow whose stability is to be examined, and a superimposed perturbation motion. For the basic flow, regarded as being steady, let the Cartesian velocity components be U , V , W and the pressure P . This basic flow is a solution of the Navier–Stokes equations or the boundary–layer equations. Let the corresponding quantities for the time varying disturbance be u' , v' , w' and p' . Therefore the resulting flow has the velocity and pressure

$$u = U + u', \quad v = V + v', \quad w = W + w', \quad (15.2)$$

$$p = P + p'. \quad (15.3)$$

In most cases it is assumed that the perturbation quantities are small compared to those of the basic flow.

The investigation into the stability of such a perturbed motion can be carried out using two different methods. The first method (*energy method*) basically determines the rate of change of the energy of the perturbation. The increase or decrease of the disturbance energy in time allows the stability or instability of the basic flow to be determined. Here an arbitrary form of perturbation is allowed, but it must be compatible with the continuity equation. This energy method which was mainly developed by H.A. Lorentz (1907) proved unsuccessful: therefore we will not discuss it further here.

In the second method, only those perturbations which are consistent with the hydrodynamic equations of motion are allowed and the progression in time of the disturbance is traced, based on these differential equations. This is the *method of small disturbances*. This second method has led to complete success, and therefore will be discussed in detail.

We assume a two-dimensional incompressible basic flow and a two-dimensional disturbance. The resulting flow in Eqs. (15.2) and (15.3) then satisfies the two-dimensional Navier–Stokes equations, cf. Eq. (3.42). In addition we take the assumed basic flow to be particularly simple so that the component U only depends on y , i.e. $U = U(y)$, while the two remaining velocity components vanish $V = W = 0$.¹ Such a shear flow exists exactly in a channel or a pipe of constant cross-section at great enough distances from the entrance cross-section. But the boundary-layer flow can also be regarded as an approximation to such a parallel flow, since here the dependence of the basic flow U on the longitudinal coordinate x is much smaller than on the transverse coordinate y (*parallel-flow assumption*). However, for the pressure $P(x, y)$, a dependence on x must of course be assumed, since it is the pressure gradient $\partial P / \partial x$ which maintains the flow. Therefore the given basic flow has the form

$$U(y), \quad V = W = 0, \quad P(x, y). \quad (15.4)$$

Onto this basic flow, we superimpose a two-dimensional perturbation which is also dependent on the time. For this, the velocity components and the pressure are

$$u'(x, y, t), \quad v'(x, y, t), \quad p'(x, y, t). \quad (15.5)$$

Therefore the resulting motion according to Eqs. (15.2) and (15.3) is

$$u = U + u', \quad v = v', \quad w = 0, \quad p = P + p'. \quad (15.6)$$

The basic flow Eq. (15.4) is a solution of the Navier–Stokes equations by assumption. However the resulting motion in Eq. (15.6) also has to satisfy

¹ G.B. Schubauer; P.S. Klebanoff (1955) showed that it is reasonable to assume that these two velocity components are indeed present in the real flow. Their size can be neglected in most cases, but they seem to play a part in the transition from laminar to turbulent flow.

the Navier–Stokes equations. The superimposed perturbation in Eq. (15.5) will be assumed to be “small” in the sense that all quadratic terms of the perturbation can be neglected compared to the linear terms. Further details on the form of the perturbation will be given in the next section. The aim of the stability investigation is now to determine if, for a given basic flow, the disturbance dies away or is amplified *in time*. The basic flow is then called stable or unstable, respectively.

Inserting Eq. (15.6) into the Navier–Stokes equations of the two-dimensional incompressible unsteady flow Eq. (3.42), and ignoring all terms quadratic in the perturbation velocities, we obtain

$$\begin{aligned}\frac{\partial u'}{\partial t} + U \frac{\partial u'}{\partial x} + v' \frac{dU}{dy} + \frac{1}{\varrho} \frac{\partial P}{\partial x} + \frac{1}{\varrho} \frac{\partial p'}{\partial x} &= \nu \left(\frac{d^2 U}{dy^2} + \Delta u' \right), \\ \frac{\partial v'}{\partial t} + U \frac{\partial v'}{\partial x} + \frac{1}{\varrho} \frac{\partial P}{\partial y} + \frac{1}{\varrho} \frac{\partial p'}{\partial y} &= \nu \Delta v', \\ \frac{\partial u'}{\partial x} + \frac{\partial v'}{\partial y} &= 0.\end{aligned}$$

Here Δ is the operator $\partial^2/\partial x^2 + \partial^2/\partial y^2$.

If we consider that the basic flow must itself satisfy the Navier–Stokes equations (in the case of the boundary layer, approximately) these equations simplify to

$$\frac{\partial u'}{\partial t} + U \frac{\partial u'}{\partial x} + v' \frac{dU}{dy} + \frac{1}{\varrho} \frac{\partial p'}{\partial x} = \nu \Delta u', \quad (15.7)$$

$$\frac{\partial v'}{\partial t} + U \frac{\partial v'}{\partial x} + \frac{1}{\varrho} \frac{\partial p'}{\partial y} = \nu \Delta v', \quad (15.8)$$

$$\frac{\partial u'}{\partial x} + \frac{\partial v'}{\partial y} = 0. \quad (15.9)$$

These are three equations for u' , v' , p' . The appropriate boundary conditions require that the perturbation velocities u' and v' vanish at the walls (no-slip condition). The pressure p' can easily be eliminated from Eqs. (15.7) and (15.8), so that together with the continuity equation, we have two equations for u' and v' . With regard to boundary-layer flows, we could object to the form of the basic flow in Eq. (15.4) (parallel-flow assumption) where the change in the longitudinal velocity component U with x and also the normal component V were neglected. However J. Pretsch (1941b) proved that the resulting terms for the stability investigation of a boundary layer can be neglected, cf. also S.J. Cheng (1953). The small differences between the results with and without the parallel-flow assumption can be seen in Fig. 15.18.

15.2.3 Orr–Sommerfeld Equation

Let the basic flow in the x direction with velocity $U(y)$ be superimposed with a perturbation which is made up of single *partial perturbations* or *modes*,

where each mode is a wave propagating in the x direction. A stream function $\psi(x, y, t)$ can be introduced for the (assumed) two-dimensional perturbation. This allows the continuity equation (15.9) to be integrated. The following trial solution is used for the stream function of one mode in the perturbation:¹

$$\psi(x, y, t) = \varphi(y)e^{i(\alpha x - \beta t)}. \quad (15.10)$$

An arbitrary plane disturbance can be considered to be decomposed into such Fourier modes. Here α is real and $\lambda = 2\pi/\alpha$ is the wavelength of the perturbation. The quantity β is complex

$$\beta = \beta_r + i\beta_i,$$

and β_r is the frequency of the mode, while β_i (amplification factor) determines whether the wave grows or dies away. If $\beta_i < 0$, the wave is damped, and the laminar flow is stable, while for $\beta_i > 0$, there are instabilities present. It is useful, in addition to α and β , to introduce the combined quantity

$$c = \frac{\beta}{\alpha} = c_r + i c_i. \quad (15.11)$$

Here c_r is the phase velocity of the wave in the x direction while again c_i decides between amplification and damping, depending on whether c_i is positive or negative. The amplitude function $\varphi(y)$ of the disturbance is set to be only dependent on y , since the basic flow is only dependent on y . Equation (15.10) yields the components of the perturbation velocity as

$$u' = \frac{\partial \psi}{\partial y} = \varphi'(y)e^{i(\alpha x - \beta t)}, \quad (15.12)$$

$$v' = -\frac{\partial \psi}{\partial x} = -i\alpha\varphi(y)e^{i(\alpha x - \beta t)}. \quad (15.13)$$

Inserting these in Eq. (15.7) and (15.8), and eliminating the pressure, the following fourth order ordinary differential equation is found for the amplitude function $\varphi(y)$:

$$(U - c)(\varphi'' - \alpha^2\varphi) - U''\varphi = -\frac{i}{\alpha \text{Re}}(\varphi''' - 2\alpha^2\varphi'' + \alpha^4\varphi). \quad (15.14)$$

This perturbation differential equation forms the starting point of the stability theory of laminar flow. It is called the Orr–Sommerfeld equation in honour of W.M.F. Orr (1907) and A. Sommerfeld (1908). In the dimensionless quantities introduced into Eq. (15.14), all the lengths have been referred to a suitably chosen reference length b or δ (channel width or boundary-layer thickness) and all velocities to the maximum velocity of the basic flow

¹ Here complex notation is used. Only the real part is physically significant:

$$\text{Re}(\psi) = e^{\beta_i t} [\varphi_r \cos(\alpha x - \beta_r t) - \varphi_i \sin(\alpha x - \beta_i t)],$$

where $\varphi = \varphi_r + i\varphi_i$ is the complex amplitude.

U_e (i.e. to the velocity at the outer edge of the boundary layer). The dash means differentiation with respect to the dimensionless coordinate y/δ or y/b , while

$$\text{Re} = \frac{U_e b}{\nu} \quad \text{or} \quad \text{Re} = \frac{U_e \delta}{\nu}$$

is the characteristic Reynolds number for the given mean flow. The terms on the left hand side of Eq. (15.14) are due to the inertial terms, while those on the right hand side come from the friction terms of the equations of motion. The boundary conditions for a boundary-layer flow where both velocity components or the disturbance vanish at the wall ($y = 0$) and at large distances from the wall (outer flow) are:

$$\begin{aligned} y = 0 : \quad u' &= v' = 0 : \quad \varphi = 0, \quad \varphi' = 0, \\ y = \infty : \quad u' &= v' = 0 : \quad \varphi = 0, \quad \varphi' = 0. \end{aligned} \tag{15.15}$$

The ansatz (15.10) for the perturbation motion was confirmed by H.B. Squire (1933). He was able to show that plane flow only becomes unstable with respect to *three-dimensional* perturbations at higher Reynolds numbers, so that it is *two-dimensional* perturbations which dominate.

The eigenvalue problem. The stability analysis of a laminar flow is now an eigenvalue problem of the perturbation differential equation (15.14) with the boundary conditions (15.15). For a given basic flow $U(y)$, Eq. (15.14) contains four parameters, namely Re , α , c_r and c_i . Of these, the Reynolds number of the basic flow is likewise specified, and in addition the wavelength $\lambda = 2\pi/\alpha$ of the perturbation can be taken as given. Therefore, for every pair α , Re , the differential equation (15.14) with boundary conditions (15.15) yields an eigenfunction $\varphi(y)$ and a complex eigenvalue $c = c_r + i c_i$. Here c_r is the phase velocity of the given perturbation, while the sign of c_i determines the stability ($c_i < 0$) or instability ($c_i > 0$) of the basic flow. The limiting case $c_i = 0$ gives neutral (indifferent) disturbances. These circumstances describe the *temporal* amplification or decay of the disturbance.

Assuming the perturbations develop in time, we can represent the results of the stability computation for a given laminar flow $U(y)$ by assigning a pair of values c_r , c_i to each point in the α , Re plane. In particular, the curve $c_i = 0$ separates the stable from the unstable solutions. It is called the *curve of neutral stability* (Fig. 15.9). The point on this curve where the Reynolds number is smallest (tangent to the curve of neutral stability parallel to the α axis) is of special interest. This gives that Reynolds number below which all modes are damped, while above which some are amplified. This smallest Reynolds number on the curve of neutral stability is the theoretical *indifference Reynolds number* or *limit of stability* of the laminar flow investigated.

Because of the experimental results on the laminar-turbulent transition discussed above, we would expect that at small Reynolds numbers where the flow is laminar, only stable disturbances exist at all wavelengths, while at

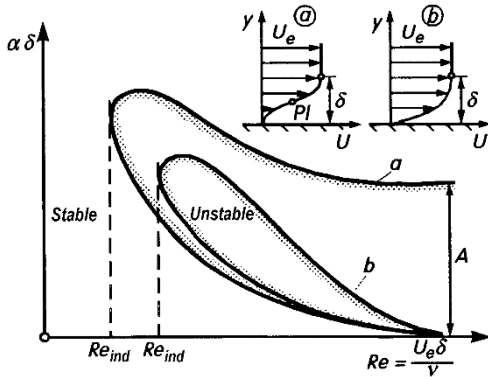


Fig. 15.9. Curves of neutral stability of a plane boundary layer for two-dimensional incompressible perturbations

- (a) “inviscid” instability: for type (a) velocity profiles *with* point of inflection PI , the curve of neutral stability is of type (a).
The asymptotes of the curve of neutral stability (a) for $Re \rightarrow \infty$ are obtained from the inviscid perturbation differential equation (15.16)
 A : inviscid instability
- (b) “viscous” instability: for type (b) velocity profiles *without* point of inflection, the curve of neutral stability is of type (b)

larger Reynolds numbers where the flow is turbulent, there are unstable perturbations for at least some wavelengths. Note now however that it cannot be expected that the theoretical indifference Reynolds number obtained from the stability investigation will be at all the same as the critical Reynolds number at the laminar-turbulent transition determined by experiment. Consider for example, the boundary-layer flow along a wall: the theoretical indifference Reynolds number obtained from the stability analysis gives the position on the wall from which an amplification of the modes takes place downstream. However it takes some time until these modes are amplified enough to produce turbulence. By then, the unstable disturbance will have wandered further downstream. Therefore we would expect that the observed position of the laminar-turbulent transition is always further downstream than the theoretically computed limit of stability. In other words, the experimental critical Reynolds number is larger than the theoretical indifference Reynolds number. This is true for Reynolds numbers formed both with the length along the body and with the boundary-layer thickness.

In what follows, we shall restrict ourselves to sketching the development of stability theory and referring to its most important results, without presenting it comprehensively.

Absolute or convective instabilities and spatially amplified waves. The stability analysis based on the wave ansatz (15.10) is very restricted, because it only permits “monochromatic” waves, i.e. only waves with one fixed wavelength

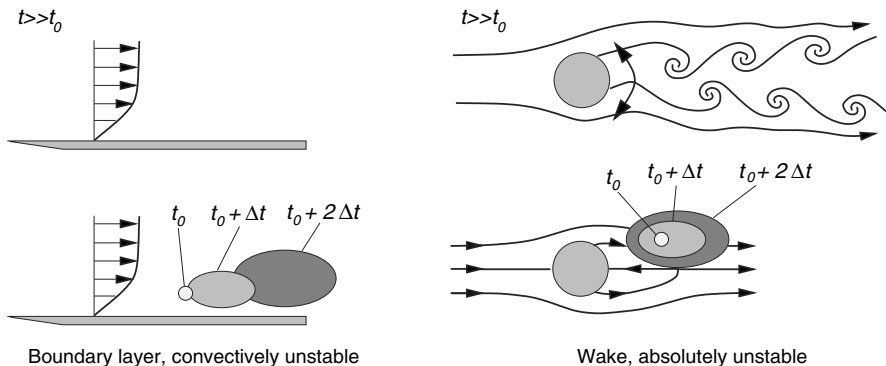


Fig. 15.10. Propagation of convectively and absolutely unstable perturbations

$\lambda = 2\pi/\alpha$. However in many flow problems, the perturbations are fixed in space. This means that, in order to compute realistic linear perturbations in the boundary layer, a suitable initial value and boundary value problem must be solved for the system of equations (15.7) to (15.9).

The analysis of the temporal and spatial development of “wave packets” was developed in plasma physics in the fifties (see R.J. Briggs (1964) and A. Bers (1973)). The stability analysis of R.J. Briggs is based on the investigation of asymptotic solutions of the inverse Laplace–Fourier integral of the wave ansatz which describes the stability theory solution of the problem. L. Brevoord (1988) carried over this analytical formalism to shear flows.

The analytical treatment of unstable wave packets in boundary-layer flows had already been carried out in the sixties by M. Gaster (1968, 1975) and M. Gaster; I. Grant (1975). Here the physical aspect of influencing the flow through a spatially local and temporally limited perturbation is used. If the wave packet then moves downstream, the flow is *convectively* or *spatially unstable*. If the temporal and spatial amplification is such that it can be observed at each point in the flow field, the flow is *absolutely unstable*. The investigation of absolutely and convectively unstable regions in the flow field is particularly important because in the region of absolute instability, the amplification of the disturbance in each point in the flow field means that no final state can be formulated. From this, H. Oertel Jr. (1990, 1995) concluded that these must be the regions where the flow can be influenced particularly effectively.

Meanwhile, R.J. Deissler (1987) was able to show that plane channel flow is absolutely stable, but convectively unstable. The velocity of expansion of the unstable wave packet grows with increasing Reynolds number. A comprehensive analytical and numerical investigation of unstable wave packets in two and three-dimensional boundary layers has been published by H. Oertel jr.; J. Delfs (1995, 1997).

We speak of a laminar–turbulent “sudden change” in the flow field when the instability becomes abruptly *absolutely unstable*, as for example in the wake behind a body in a flow. On the other hand, the *convectively unstable* plate boundary layer is carried out over several stability processes to turbulent boundary-layer flow. This is called a laminar–turbulent “transition” (Fig. 15.10).

General properties of the perturbation differential equation. Since experimental results have shown that the limit of stability $c_i = 0$ is expected at high Reynolds numbers, it seems natural to simplify the general perturbation equation (15.14) by neglecting the friction terms on the right hand side which are multiplied by the small factor $1/\text{Re}$ compared to the inertial terms on the left hand side. We then obtain the so-called inviscid perturbation differential equation, or the *Rayleigh equation*

$$(U - c)(\varphi'' - \alpha^2 \varphi) - U''\varphi = 0. \quad (15.16)$$

Since this equation is of second order, only two of the four boundary conditions Eq. (15.15) can now be satisfied. With respect to the inviscid flow, these are the vanishing of the normal component of the perturbation velocity at both walls in a channel flow, or at one wall and at a great distance from the wall in boundary-layer flow. For the latter case they read

$$y = 0 : \quad \varphi = 0; \quad y = \infty : \quad \varphi = 0. \quad (15.17)$$

Cutting out the friction terms in the Orr–Sommerfeld equation is a rather drastic mathematical operation, since reducing the order of the differential equation from four to two could mean that important properties of the general solution of the complete perturbation equation are lost. Again we have to use the ideas we discussed earlier in Chap. 4 when we looked at the reduction of the Navier–Stokes equations for viscous flows to the Euler equations for inviscid flows.

Earlier work on stability theory mainly used the inviscid perturbation equation (15.16) as a starting point. Lord Rayleigh (1880–1913) was already able to determine some very important theorems regarding the stability of laminar velocity profiles based on this inviscid perturbation equation (15.16). These were confirmed later by the addition of the viscous effects to the perturbation differential equation.

Theorem I: A first important general statement of this kind is the so-called *point of inflection criterion*. This states that velocity profiles with points of inflection are unstable.

Lord Rayleigh (1880–1913) was basically only able to prove that the presence of a point of inflection is a *necessary condition* for the appearance of unstable waves, but W. Tollmien (1935) showed much later that the presence of a point of inflection is a *sufficient condition* for the presence of amplified waves. The point of inflection criterion is of fundamental importance for stability theory, since, provided that we include a correction due to the neglected viscosity effect, it provides a first rough classification of all laminar flows. In practice it is therefore of great importance, because the presence of a point of inflection in the velocity profile is directly related to the pressure gradient of the flow. It was seen from Fig. 5.2 that a flow in a convergent channel with pressure decrease (favourable pressure gradient), the velocity profile is very

flat with no point of inflection; on the other hand, in a divergent channel with pressure increase (adverse pressure gradient), we find a pointed velocity profile with a point of inflection. The laminar boundary layer at a body in a flow also has the same differences in shape. According to boundary-layer theory, the velocity profiles in a pressure drop region have no point of inflection, whereas those in a pressure rise region always have a point of inflection, cf. Sect. 7.1. Therefore the point of inflection criterion is equivalent to the effect of the pressure gradient of the outer flow on the stability of the boundary layer. For boundary-layer flows this means: pressure drops are stabilising, pressure rises are destabilising. This implies that the position of the pressure minimum on a body in a flow has a fundamental influence on the position of completed transition. The following simple rule holds: the position of the pressure minimum determines the position of completed transition roughly in such a way that the position of completed transition lies just behind the pressure minimum.

The effect of viscosity on the solution of the perturbation differential equation which we have neglected here changes the results only very slightly. The instability of the boundary-layer profile with a point of inflection discussed above is also called the *inviscid instability*, since the laminar flow is unstable even if the effect of friction is neglected. The stability diagram in Fig. 15.9 shows the inviscid instability as the curve of neutral stability of type *a*. At $\text{Re} = \infty$ there is already a certain unstable range of perturbation wavelengths; in the direction of smaller Reynolds numbers this range is separated from the stable region by the curve of neutral stability.

In contrast to this, a *viscous instability* with a curve of neutral stability of type *b* appears in Fig. 15.9, for example in the case of laminar boundary-layer profiles without a point of inflection. At infinitely large Reynolds numbers, the region of unstable perturbation wavelengths shrinks to nothing, and it is only for finitely large Reynolds numbers that a region of unstable waves exists. In all, the magnitude of the amplification for inviscid instabilities is much larger than that for viscous instabilities.

The existence of viscous instability can only be discovered if we discuss the complete perturbation differential equation (15.14), and therefore it is more difficult to treat viscous instability than inviscid instability. The simplest boundary-layer flow along a plate wall without pressure gradient is one where only viscous instability arises, and therefore it has been successfully tackled only relatively recently.

Theorem II: A second important general statement says that in boundary-layer profiles the velocity of propagation for neutral perturbations ($c_i = 0$) is smaller than the maximum velocity of the mean flow, $c_r < U_e$.

This law had already been proved by Lord Rayleigh (1880–1913) under certain restricting assumptions and later by W. Tollmien (1935) under more general assumptions. It says that there is a point inside the flow for neutral

perturbations where $U - c = 0$. This fact is also of fundamental importance for stability theory. The position $U - c = 0$ is namely a singular point of the inviscid perturbation differential equation (15.16). At this point φ'' becomes infinite, unless U'' vanishes there simultaneously. The layer $y = y_C$ where $U = c$ is the *critical layer* of the basic flow. If $U_C'' \neq 0$, close to the critical layer where $U - c = U_C'(y - y_C)$ can be set, φ'' becomes infinite as $\frac{U_C''}{U_C'} \frac{1}{y - y_C}$ and therefore the x component of the velocity is:

$$u' = \varphi' \sim \frac{U_C''}{U_C'} \cdot \ln(y - y_C). \quad (15.18)$$

Therefore, according to the inviscid perturbation differential equation, in the critical layer the component of the perturbation velocity parallel to the wall u' becomes infinitely large, unless the curvature of the velocity profile in the critical layer vanishes simultaneously. This mathematical singularity of the inviscid perturbation differential equation indicates that in the critical layer the effect of viscosity must be taken into account in determining the perturbation. Only the effect of viscosity on the perturbation gets rid of this physically meaningless singularity of the inviscid perturbation equation. The discussion of this so-called frictional correction to the solution of the perturbation differential equation is of fundamental importance in the discussion of the stability, cf. also F.T. Smith (1979b).

It follows from these two laws of Lord Rayleigh that the curvature of the velocity profile is very important for the stability of laminar flow. Simultaneously it was shown that, when investigating the stability, the computation of the velocity profile of the basic flow must be done rather precisely: not only $U(y)$ but also d^2U/dy^2 must be known accurately. An overview of the solutions of the Rayleigh equation from a mathematical standpoint is to be found in the summary by P.G. Drazin; L.N. Howard (1966), see also P.G. Drazin; W.H. Reid (1981).

15.2.4 Curve of Neutral Stability and the Indifference Reynolds Number

We remain with time dependent stability theory. In order to integrate the fourth order Orr–Sommerfeld differential equation (15.14), we need a fundamental system of solutions of this equation.

For $y \rightarrow \infty$, where $U(y) = U_e = 1$, this reads:

$$\begin{aligned} \tilde{\varphi}_1 &= e^{-\alpha y}, & \tilde{\varphi}_2 &= e^{+\alpha y}, \\ \tilde{\varphi}_3 &= e^{-\gamma y}, & \tilde{\varphi}_4 &= e^{+\gamma y} \end{aligned} \quad (15.19)$$

with

$$\gamma^2 = \alpha^2 + i \operatorname{Re}(\alpha - \beta). \quad (15.20)$$

Since for neutral waves we generally have

$$|\gamma| \gg |\alpha|, \quad (15.20a)$$

$\tilde{\varphi}_1$ and $\tilde{\varphi}_2$ are the slowly varying and $\tilde{\varphi}_3$ and $\tilde{\varphi}_4$ the quickly varying solutions. For $y \rightarrow \infty$ the solution pair $\tilde{\varphi}_{1,2}$ satisfies both the inviscid perturbation equation (15.16) (Rayleigh equation) and the perturbation equation with viscosity (15.14) (Orr–Sommerfeld equation); the solution pair $\tilde{\varphi}_{3,4}$ only satisfies the perturbation equation with viscosity. Thus $\tilde{\varphi}_{1,2}$ are called the inviscid solution pair and $\tilde{\varphi}_{3,4}$ the viscous solution pair.

In determining the general solution

$$\varphi = C_1\varphi_1 + C_2\varphi_2 + C_3\varphi_3 + C_4\varphi_4,$$

which has to satisfy the boundary conditions Eq. (15.15), we note that φ_2 and φ_4 drop away because φ and φ' must vanish as $y \rightarrow \infty$ and it is

$$\lim_{y \rightarrow \infty} \varphi_2 = \tilde{\varphi}_2, \quad \lim_{y \rightarrow \infty} \varphi_4 = \tilde{\varphi}_4.$$

This general solution is then

$$\varphi = C_1\varphi_1 + C_3\varphi_3; \quad (15.21)$$

it has to satisfy the boundary conditions $\varphi = \varphi' = 0$ at $y = 0$. Since the inviscid solution φ_1 does not satisfy the no-slip condition at the wall ($\varphi'_1 \neq 0$) and in the critical layer ($U - c = 0$) indeed $\varphi'_1 \rightarrow \infty$, the contributions from the viscous solution φ_3 are particularly large at these locations; this implies that both the desired particular solution $\varphi_3(y)$ and the total solution $\varphi(y)$ vary strongly with y at these positions.

A consequence of this behaviour is that for a given pair α , Re the characteristic function $\varphi(y)$ and therefore also the eigenvalue $c = c_r + i c_i$ can only be determined with great difficulty both analytically and numerically. In the numerical solution of the eigenvalue problem, these particular difficulties have to do with the fact that in the Orr–Sommerfeld equation the highest order derivative φ''' is multiplied by the very small factor $1/\text{Re}$. The big difference in the characteristic solutions $\varphi(y)$ close to the wall and in the critical layer according to the inviscid solution (Rayleigh equation) and the viscous solution (Orr–Sommerfeld equation) is due, mathematically, to the fact that neglecting the friction terms in the perturbation differential equation reduces its order from four to two.

A numerical method to compute the eigensolution $\varphi(y)$ of the Orr–Sommerfeld equation (15.14) for numerous given pairs of the reciprocal wavelength α and the Reynolds number Re makes demands on the capacity and speed of a computer that could not be satisfied in the mid twenties when O. Tietjens (1922) and W. Heisenberg (1924) attacked this problem. W. Tollmien, who renewed attempts to treat this problem at the end of the twenties, was forced to limit himself to analytical methods which required considerable effort. However these time consuming *analytical* calculations were of great success. The details are to be found in the original work by W. Tollmien (1929, 1935, 1947) and D. Grohne (1954). It was only about 30

years after the publication of W. Tollmien's (1929) results that the decisive break-through in the *numerical* solution of the Orr–Sommerfeld equation took place in a piece of work by E.F. Kurtz; S.H. Chandrasekhar (1962); this was extended in 1970 in two pieces of work by R. Jordinson (1970, 1971). Certain important earlier work had been carried out by M.R. Osborne (1967) as well as L.H. Lee; W.C. Reynolds (1967). The particular challenges in numerically computing the characteristic solutions and eigenvalues of the Orr–Sommerfeld equation were intensively discussed soon afterwards in work by J.M. Gersting; D.F. Jankowski (1972), as well as A. Davie (1973). The difficulties in the numerical integration of the Orr–Sommerfeld equation have also been summarised in the book by R. Betchov; W.O. Criminale (1967). The latest integration methods are described by H. Oertel Jr.; E. Laurien (2002).

At this point we should note that the stability investigation of a boundary-layer flow is in general more difficult than that of a channel flow. This has to do with the fact that in the boundary layer one of the two boundaries lies at infinity, whereas in the channel flow both boundaries lie at finite distances. Added to this is the fact that the velocity profile of the basic flow $U(y)$ of the boundary layer is not an exact solution of the Navier–Stokes equations, while this indeed is the case for channel flow (e.g. Hagen–Poiseuille flow). Finally here it should also be mentioned that in deriving the Orr–Sommerfeld equation it was assumed that the mean flow $U(y)$ does not change in the longitudinal direction. This is satisfied for channel flow, but not for boundary-layer flow. Investigations on this have been carried out by M.D.J. Barry; M.A.S. Ross (1970), M. Gaster (1974), A.R. Wazzan et al. (1974), A.R. Wazzan (1975), T.L. Van Stijn; A.I. Van de Vooren (1983) and F.P. Bertolotti (1991).

In what follows we shall initially present the results of primary stability theory for the incompressible plate boundary layer. Afterwards we will discuss further important effects on the boundary-layer instability, such as the effect of the pressure gradient and the wall heat transfer for temperature dependent physical properties.

15.2.4a Plate Boundary Layer

The stability of the boundary layer on a flat plate at zero incidence was first investigated by W. Tollmien (1929). The velocity profile of the plate boundary layer by H. Blasius is shown in Fig. 6.6a. The velocity profiles at different positions along the plate are affine with one another, i.e. they coincide if we plot them against $y/\delta(x)$. Here $\delta(x)$ is the boundary-layer thickness, for which, according to Eq. (6.60), $\delta = 5.0\sqrt{\nu x/U_\infty}$. The velocity profile has a point of inflection at the wall. With respect to the point of inflection criterion mentioned in the last section, this profile lies just at the borderline between profiles without a point of inflection which are stable when computed inviscidly, and those with a point of inflection which are unstable.

The results of the stability calculation are shown in Fig. 15.11. The region inside the curves is unstable and that outside the curves is stable, while the curves themselves represent neutral disturbance waves. For very large Reynolds numbers, the two branches of the neutral stability curves go to zero. The smallest Reynolds number at which a neutral perturbation still exists is the indifference Reynolds number¹ with

$$\left(\frac{U_\infty \delta_1}{\nu} \right)_{\text{ind}} = \text{Re}_{1 \text{ ind}} = 520 \quad (\text{indifference point}) \quad (15.22)$$

This is the indifference point for the plate boundary layer. It is worth noting that according to Fig. 15.11 only a very narrow region of perturbation wavelengths and perturbation frequencies becomes unstable. Just as a lower limit exists for the Reynolds number, there is an upper limit for the characteristic magnitudes of the disturbances beyond which no further instabilities occur. From Fig. 15.11, the upper limits are:

$$\frac{c_r}{U_\infty} = 0.39; \quad \alpha \delta_1 = 0.36; \quad \frac{\beta_r \delta_1}{U_\infty} = 0.14.$$

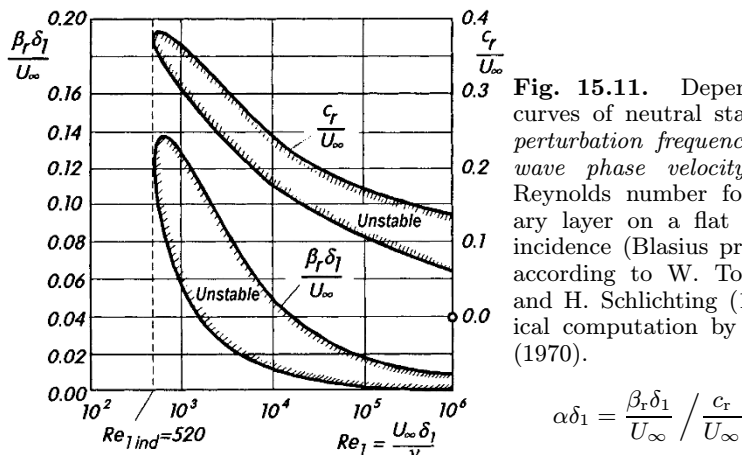


Fig. 15.11. Dependence of the curves of neutral stability for the perturbation frequency β_r and the wave phase velocity c_r on the Reynolds number for the boundary layer on a flat plate at zero incidence (Blasius profile). Theory according to W. Tollmien (1929) and H. Schlichting (1933); numerical computation by R. Jordinson (1970).

$$\alpha \delta_1 = \frac{\beta_r \delta_1}{U_\infty} / \frac{c_r}{U_\infty}$$

It can be seen that the wavelength of the unstable disturbance is quite large compared to the boundary-layer thickness. The smallest unstable wavelength is

$$\lambda_{\min} = \frac{2\pi}{0.36} \delta_1 = 17.5 \delta_1 \approx 6 \delta.$$

¹ In the literature on stability theory, the indifference Reynolds number is frequently called the critical Reynolds number. However, since the transition from laminar to turbulent flow takes place in a region of finite length, in this book we differentiate clearly between the start of transition (indifference point) and the position of completed transition (critical point), see also Fig. 15.5.

A more exact comparison of these theoretical results with experiments is carried out below. In Sect. 15.1.2, older measurements of the position of completed transition with $(U_\infty x/\nu)_{\text{crit}} = 3.5 \cdot 10^5$ to 10^6 were presented. Using the value $\delta_1 = 1.72\sqrt{\nu x/U_\infty}$ from Eq. (6.62), this corresponds to a critical Reynolds number of about

$$\left(\frac{U_\infty \delta_1}{\nu} \right)_{\text{crit}} = 950 \quad (\text{point of completed transition, critical point}),$$

and therefore is considerably larger than the above value for the indifference point of 520.

The distance between the indifference point and the experimentally observed point of completed transition is fundamentally determined by the magnitude of the *amplification* of the unstable perturbations. We can get insight into the strength of the amplification by determining the magnitude of the parameters $c_i = \beta_i/\alpha > 0$ inside the curve of neutral stability. This was first carried out for the plate boundary layer by H. Schlichting (1933) and later repeated by S.F. Shen (1954).

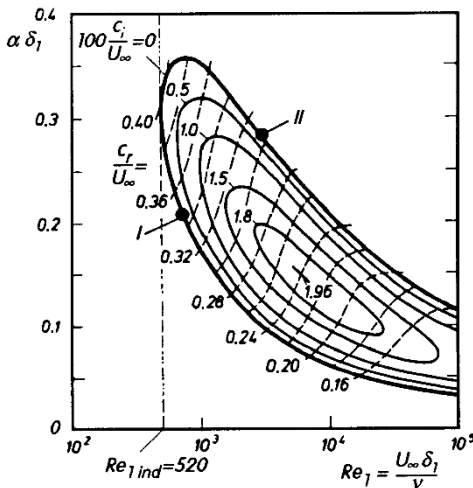


Fig. 15.12. Curves of constant *temporal* amplification c_i for the boundary layer at a flat plate at zero incidence in a large region of Reynolds numbers, after H.J. Obremski et al. (1969)

Figure 15.12 shows the amplification of unstable perturbations for the plate boundary layer in a large region of Reynolds numbers according to a calculation by H.J. Obremski (1969). It turns out that the maximum amplification rate is not that for very large Reynolds numbers ($Re_1 \rightarrow \infty$) but rather that for moderate Reynolds numbers in the region $Re_1 = U_\infty \delta_1 / \nu = 10^3$ to 10^4 .

It follows from this that, for a given sensitivity of the chosen method of measurement, the measured indifference point will basically be determined

downstream of the theoretical indifference point in the region of large amplification. Only methods of measurement where the spatial resolution is high enough allow the theoretically predicted indifference point to be found, see Fig. 15.17.

In order to obtain closer insight into the mechanism of disturbance, H. Schlichting (1935a) determined the characteristic functions $\varphi(y)$ for some neutral waves. With these it is possible to compute the streamline portrait of the perturbed flow for neutral wave disturbances. An example of this is given in Fig. 15.13.

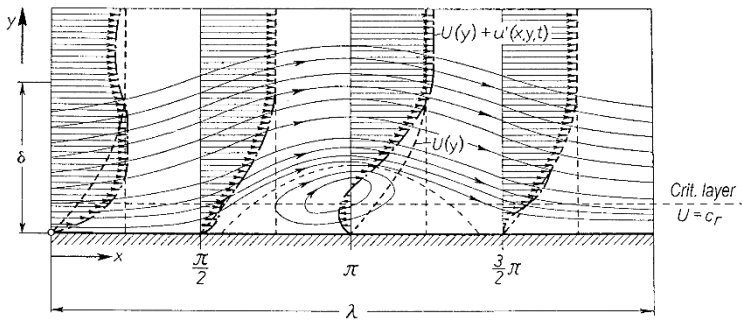


Fig. 15.13. Streamline portrait and velocity distribution for a neutral wave in the boundary layer on a flat plate at zero incidence (perturbation I in Fig. 15.12)

$U(y)$ = basic flow

$U(y) + u'(x, y, t)$ = perturbed velocity distribution

Reynolds number $Re_1 = U_\infty \delta_1 / \nu = 893$

perturbation wave length $\lambda = 40 \delta_1$

wave group velocity $c_r = 0.35 U_\infty$

intensity of perturbation $\int_0^\delta \sqrt{\overline{u'^2}} dy = 0.172 U_\infty \delta$

Later J.T. Stuart (1956) and D. Grohne (1972) attempted to compute the process of amplification of the unstable perturbations taking the nonlinear terms into account. It is important to note here that the basic flow is distorted by the growth of the unstable disturbances. The consequence of this is that the energy carried over from the basic flow (mean flow) to the secondary flow (perturbation flow) is changed, since it is proportional to dU/dy . The basic effect of this is that at a later time the unstable perturbations no longer grow in proportion to $\exp(\beta_i t)$ but rather tend to a finite amplitude which is moreover independent of the value of the (small) initial perturbation.

The experimental verification of the stability theory discussed above took more than a decade. It was then provided by G.B. Schubauer; H.K. Skramstad (1947); this will be discussed later. After this confirmation was already known, the stability theory was recalculated by C.C. Lin (1945–46); this lead to an agreement with the results of W. Tollmien and H. Schlichting in all essential points.

Older measurements of the laminar–turbulent transition. With the above results, stability theory had for the first time delivered a Reynolds number as a limit of stability which had the same order of magnitude as the critical Reynolds number from experimental results. The idea of this theory is that small perturbations which lie in a certain wavelength and frequency range are amplified whereas those with smaller and larger wavelengths are damped, assuming the Reynolds number lies above a certain limit. According to the theory, long wavelength perturbations whose wavelength is equal to a multiple of the boundary-layer thickness are particularly “dangerous”. It is assumed that the amplification of unstable disturbances eventually leads to the transition from laminar to turbulent flow. The process of amplification thus provides the relation between stability theory and the experimentally observed transition.

Already before the first successes of stability theory, L. Schiller (1934) investigated the transition problem for pipe flow particularly incisively. From this a *semi-empirical* theory of transition was developed. This starts off with the premise that the transition is essentially due to the finitely large disturbances which come from the entrance of the pipe or, in the case of the boundary layer, exist in the outer flow. This idea was expanded theoretically in particular by G.I. Taylor (1938).

The decision as to which of these two theories was to be adopted was subject to experiment. Even before stability theory was constructed, the transition at a flat plate at zero incidence had been measured in detail by J.M. Burgers (1924), B.G. Van der Hegge Zijnen (1924) and M. Hansen (1928). This yielded a critical Reynolds number of

$$\text{Re}_{x \text{ crit}} = \left(\frac{U_\infty x}{\nu} \right)_{\text{crit}} = 3.5 \text{ to } 5 \cdot 10^5.$$

Shortly after this, H.L. Dryden (1934, 1937) and his colleagues set up some very detailed and careful investigations into the plate boundary layer. Here the spatial and temporal distributions of the velocity were measured very precisely with the aid of hot-wire methods. However this experiment was not able to prove the *selective* amplification predicted by the theory.

At around the same time, investigations into the plate boundary layer were being carried out by Prandtl in Göttingen and these yielded at least a certain qualitative confirmation of stability theory. Figure 15.14 shows the appearance of turbulence from an initially long wavelength perturbation. The similarity of this photo with the theoretical streamline portrait of a neutral perturbation in Fig. 15.13 is unmistakable.

A very important parameter for the laminar–turbulent transition in the boundary layer is the “degree of disturbance” of the outer flow. This had already been recognised earlier from drag measurements at spheres in different wind tunnels. It was seen that the critical Reynolds number of the sphere, namely the Reynolds number at which the drag coefficient suddenly drops

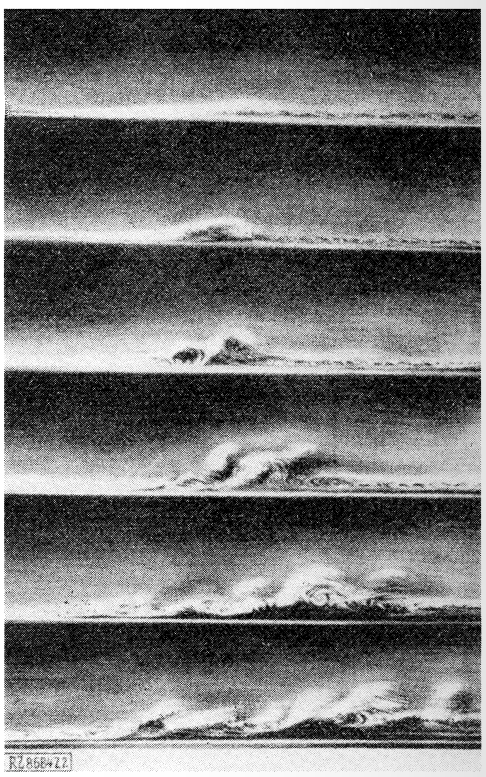


Fig. 15.14. Plate flow: appearance of turbulence from an initially long wavelength perturbation, after L. Prandtl (1933)
The camera is moving with the flow, so that the same group of vortices always remains in the picture. The flow is made visible by aluminium dust scattered on the surface of the water

(Fig. 1.19), depends very strongly on the perturbation intensity of the outer flow. The degree of disturbance of the outer flow can be measured quantitatively via the time average of the turbulent fluctuation velocities as they appear at some distance behind a screen, cf. Chap. 16. Denoting the time averages for the three components of the fluctuation velocity as $\overline{u'^2}$, $\overline{v'^2}$, $\overline{w'^2}$, the *turbulence intensity* of a flow is the quantity

$$\text{Tu} = \sqrt{\frac{1}{3}(\overline{u'^2} + \overline{v'^2} + \overline{w'^2})} / U_\infty,$$

where U_∞ is the velocity of the basic flow (velocity in the wind tunnel). In general in a wind tunnel flow there is so-called *isotropic* flow at some distance behind the screens. An isotropic flow is a turbulent flow for which the average fluctuation velocity is the same in all three coordinate directions:

$$\overline{u'^2} = \overline{v'^2} = \overline{w'^2}.$$

In this case the longitudinal velocity u' alone can be used for the turbulence intensity; thus

$$\text{Tu} = \sqrt{\overline{u'^2}} / U_\infty.$$

Drag measurements at spheres in different wind tunnels show great dependence of the critical Reynolds number on this turbulence intensity Tu ; Re_{crit} increases greatly with decreasing Tu . The turbulence intensity in older wind tunnels was about $Tu = 0.01$.

Confirmation of stability theory through experiment. In the year 1940 H.L. Dryden and his coworkers G.B. Schubauer and H.K. Skramstad in the National Bureau of Standards, Washington, made a renewed start on a comprehensive research program to investigate the laminar-turbulent transition, cf. H.L. Dryden (1946–1948). In the mean time, it was becoming accepted that the turbulence intensity probably had a considerable effect on the transition. They were successful in building a wind tunnel for their investigations in which, due to many suitable screens and a very high contraction ratio, the turbulence intensity was reduced to level which had never before been achieved:

$$Tu = \sqrt{\bar{u'^2}} / U_\infty = 0.0002 .$$

The boundary layer on a flat plate was extensively investigated in this very low turbulence flow. It was found that for small intensities of turbulence, $Tu < 0.001$, the critical Reynolds number formed with the length along the plate, which had previously been measured at $Re_{x crit} = 3.5$ to $5 \cdot 10^5$, had now been raised to

$$Re_{x crit} = \left(\frac{U_\infty x}{\nu} \right)_{crit} \approx 3.9 \cdot 10^6 ,$$

see Fig. 15.15. In addition it turned out, as can be seen in Fig. 15.15, that as the turbulence intensity decreases, the Reynolds number initially grows considerably, but then at about $Tu = 0.001$ reaches the value $Re_{x crit} = 3.9 \cdot 10^6$ and retains this value for even smaller intensities of turbulence. Therefore there is an upper limit for the critical Reynolds number of the plate boundary layer. An earlier measurement carried out by A.A. Hall; G.S. Hislop (1938) fits into Fig. 15.15 very well too.

The measurements discussed in what follows were all carried out at an turbulence intensity of $Tu = 0.0003$. The rate of change in velocity at different positions along the plate was measured, for the normal state of flow (so-called natural perturbations) and then also for artificially aroused perturbations. Such artificial perturbations were generated at a certain frequency by a thin metal strip at a distance 0.15 nm from the wall and whose oscillations were stimulated electromagnetically. The existence of amplified sine waves as a preliminary stage of the transition could easily be proved in the case of *natural disturbances* (without stimulation), see Fig. 15.16. As the indifference point is reached, almost purely sine shaped oscillations appear. Their amplitude is initially small, but it increases greatly downstream. Shortly before the

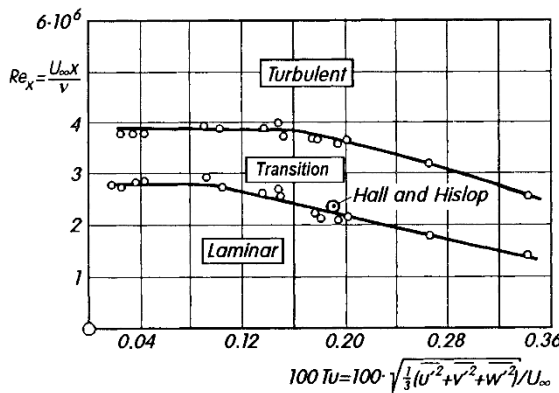


Fig. 15.15. Effect of the turbulence intensity on the critical Reynolds number for a flat plate at zero incidence, after measurements by G.B. Schubauer; H.K. Skramstad (1947)

end of the transition region, very large amplitudes appear. The transition is completed with the sudden disappearance of the regular waves.

These measurements also go some way to explaining why these amplified sine waves were not found in earlier measurements. Namely if we increase the turbulence intensity, here set to $Tu = 0.0003$, to $Tu = 0.01$ as it was commonly encountered in earlier measurements, the transition is immediately caused by the random perturbations, and no selective amplification of sine waves occurs. The existence of Tollmien–Schlichting waves in natural transition has also been experimentally confirmed by D. Arnal et al. (1977).

In the investigation of *artificial disturbances* a thin metal band of thickness 0.05 mm and width 2.5 mm was placed at a distance 0.15 mm from the wall. This was stimulated by an alternating current and a magnetic field to cause oscillations. In this manner the two-dimensional disturbances stipulated in the theory could be generated at a given frequency. Amplified, damped and neutral perturbation waves were found. Figure 15.17 shows the result of such a measurement. The points in the diagram (or the dashed curve) denote the measured neutral waves. The theoretical curve of neutral stability by W. Tollmien (1929) is also given for comparison. The agreement is very good.

Figure 15.18 shows the comparison of the linear stability theory with experimental results. Whereas there is good agreement between theory and experiment for high Reynolds numbers, there are strong deviations visible in the region of the indifference Reynolds number and the higher perturbation frequencies. An initial conjecture that this could be a consequence of the *parallel-flow assumption* has not been confirmed, cf. T. Herbert; F.P. Bertolotti (1987). W.S. Saric (1990) and F.P. Bertolotti (1991) have drawn attention to the high sensitivity of measurement results compared to the experimental conditions, particularly in the region of the indifference Reynolds number and the high frequencies. The effect of controlled disturbance introduction in the form of an oscillating band has been discussed by D.E. Aships; E. Reshotko (1990).

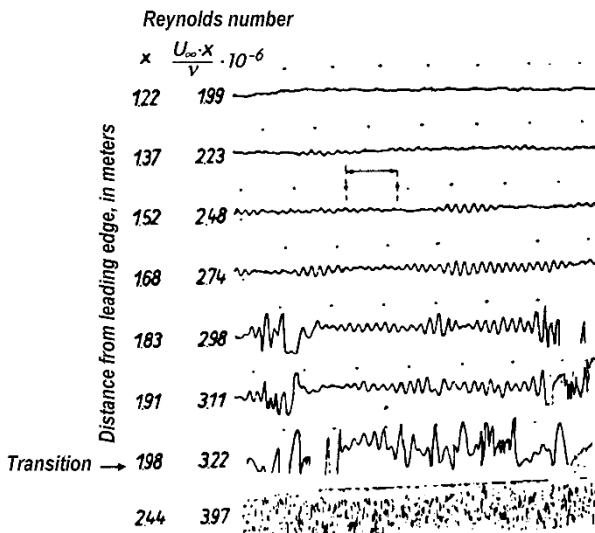


Fig. 15.16. Oscillogram of the u' oscillations of random ("natural") disturbances in the laminar boundary layer on a flat plate at zero incidence in an air flow. Measurements of the laminar-turbulent transition by G.B. Schubauer; H.K. Skramstad (1947)

distance from the wall: 0.57 mm; stream velocity: $U_\infty = 24 \text{ m/s}$
time interval between marks: $\text{s}/30$

The arrow marks the position of completed transition

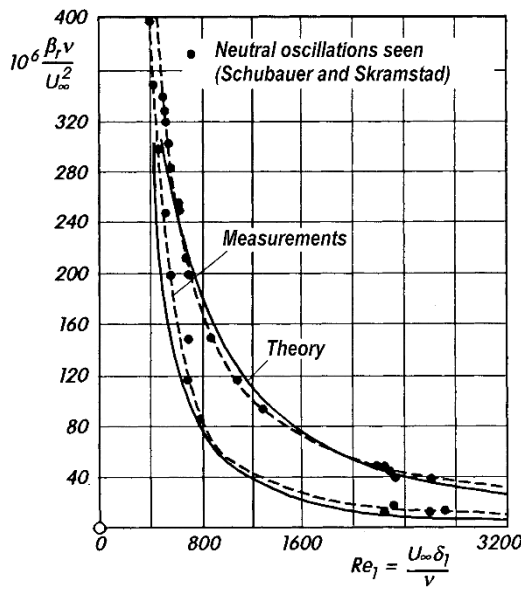


Fig. 15.17. Curves of neutral stability for perturbation frequencies at the flat plate at zero incidence. Measurements according to G.B. Schubauer; H.K. Skramstad (1947). The theoretical curve is based on the original results of W. Tollmien (1929) and shows, due to lack of precision in the calculation, an indifference Reynolds number of $Re_{1\text{ind}} = 420$ in contrast to Eq. (15.22)

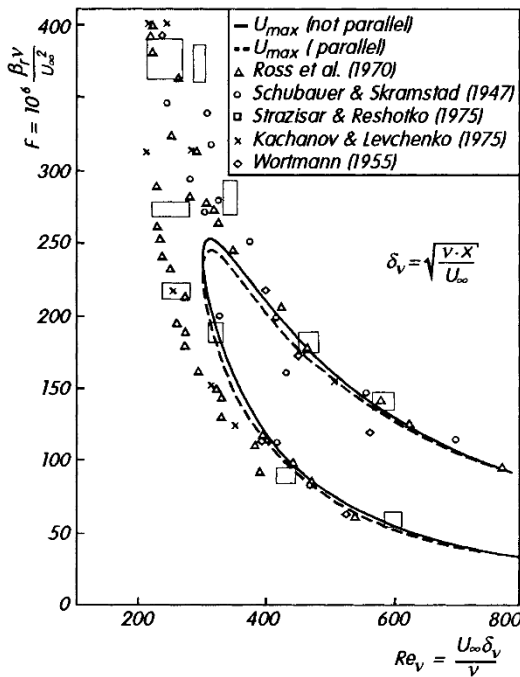


Fig. 15.18. Comparison of the theoretical curve of neutral stability for a flat plate at zero incidence with experiment, and the effect of the parallel-flow assumption, cf. T. Herbert; F.P. Bertolotti (1987)

15.2.4b Effect of Pressure Gradient

The boundary layer at a flat plate at zero incidence whose stability has just been treated is distinguished by the fact that the velocity profiles at different distances from the leading edge of the plate are similar to each other, cf. Sect. 6.5. This similarity is a consequence of the constant pressure in the outer flow. In contrast, the laminar boundary-layer profiles at any cylindrical shaped body, where the pressure gradient along the wall differs from place to place, are in general not similar to one another at different points along the contour of the body. In the pressure drop region there are velocity profiles without a point of inflection and in the pressure increase region those with a point of inflection. Whereas all the velocity profiles for a flat plate at zero incidence have the same limit of stability, namely $Re_{1\text{crit}} = (U_\infty \delta_1 / \nu)_{\text{crit}} = 520$, at an arbitrary body this limit of stability is very different for the individual profiles. Indeed in the pressure drop region the limit of stability is higher, and that in the pressure increase region lower than for the plate boundary layer. Now in order to obtain the position of the indifference point for a given body, we have to carry out the following calculations in succession:

1. Determination of the pressure distribution along the contour of the body in inviscid flow.
2. Calculation of the laminar boundary layer for this pressure distribution.
3. Stability calculation for the individual boundary-layer profiles.

The calculation of the pressure distribution for the body at hand is an exercise for potential theory. Methods for computing the laminar boundary layer were presented in Chap. 8, cf. also Chap. 23. The third step, the stability calculation shall be explained in more detail here.

It is known from the theory of laminar boundary layers (Chap. 6) that the wall curvature at a body in a flow generally has little effect on the formation of the boundary layer, as long as the radius of curvature at the wall is very much larger than the boundary-layer thickness. This boils down to the fact that in the formation of the boundary layer on such bodies, the action of the centrifugal force can be neglected. The boundary layer therefore forms in the same manner as at a *plane* wall under the influence of that pressure gradient as is given by the inviscid flow past the body. The same holds for the investigation into the stability of the laminar boundary layer with pressure gradient.

Whereas the outer flow of the boundary layer is constant for the flat plate at zero incidence, $U_\infty = \text{const}$, we now have an outer flow $U_e(x)$ which varies with the length x . It is related to the pressure gradient along the wall dp/dx via the Bernoulli equation:

$$\frac{dp}{dx} = -\rho U_e \frac{dU_e}{dx}. \quad (15.23)$$

In spite of the dependence of the outer flow on x , it is possible, as J. Pretsch (1942) has shown, to carry out the stability investigation of the laminar flow with pressure gradient in the same manner as for the flat plate at zero incidence (with no pressure gradient), thus with a basic flow $U(y)$ only dependent on the transverse coordinate y . In the stability investigation the effect of the pressure gradient is only expressed in the form of the velocity profile $U(y)$. We already showed in Sect. 15.2.3 that the limit of stability of a boundary-layer profile is strongly dependent on the form of the velocity profile, indeed in a manner such that profiles with a point of inflection have considerably lower limits of stability than those without points of inflection (point of inflection criterion). Since the pressure gradient controls the curvature of the velocity profile according to the equation, cf. Eq. (7.2),

$$\mu \left(\frac{d^2U}{dy^2} \right)_w = \frac{dp}{dx}, \quad (15.24)$$

the strong dependence of the limit of stability on the form of the velocity profile is equivalent to a great influence of the pressure gradient on the stability: it is found that laminar boundary layers in the pressure drop region ($dp/dx < 0$, $dU_e/dx > 0$, accelerated flow) are considerably more stable than those in the pressure increase region ($dp/dx > 0$, $dU_e/dx < 0$, decelerated flow).

The strong influence of the pressure gradient on the stability and on the amplification of small disturbances predicted by theory could be confirmed

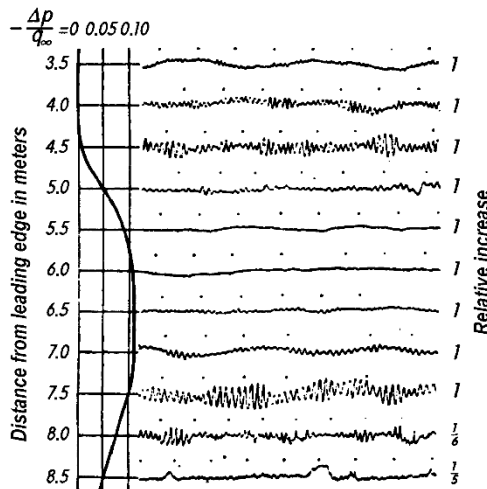


Fig. 15.19. Oscillogram of the velocity fluctuations in a laminar boundary layer with pressure gradient, after measurements by G.B. Schubauer; H.K. Skramstad (1947).

Pressure drop acts to damp, pressure increase to strongly amplify disturbances and leads to the laminar-turbulent transition, distance of the point of measurement from the wall: 0.5 mm, velocity $U_\infty = 29 \text{ m/s}$, $q_\infty = \rho U_\infty^2 / 2$

experimentally very well by G.B. Schubauer; H.K. Skramstad (1947). Figure 15.19 shows an oscillogram of the velocity fluctuations for the boundary layer at a flat wall with pressure gradient. It can be seen in the upper half of the figure that a pressure drop of about 10% of the stagnation pressure completely extinguishes the disturbances, while a consequent pressure increase of only 5% of the stagnation pressure does not only strongly amplify the fluctuations but indeed initiates the transition immediately. (Note the smaller scale of the last two printouts!)

In investigating the stability of the boundary layer with pressure gradient it is useful to describe the effect of the pressure gradient with a shape factor of the velocity profile and then, for simplicity, to use a single parameter family of laminar velocity profiles. An example of such a single parameter family of velocity profiles which are indeed exact solutions of the boundary-layer differential equations are those computed by Hartree for wedge flows:

$$U_e(x) = a \cdot x^m , \quad (15.25)$$

see Fig. 7.3. Here m is the shape factor of the velocity profile and $\beta = 2m/(m+1)$ is the wedge angle. For $m < 0$ (pressure increase), the velocity profiles have a point of inflection, but not for $m > 0$ (pressure decrease). J. Pretsch (1941b, 1942) carried out the stability calculation for a series of velocity profiles of this one parameter family as early as 1941. These calculations have been considerably extended by H.J. Obremski et al. (1969). Here not only was the indifference Reynolds number (neutral perturbations) determined but also the amplification of the unstable perturbations. It turns out that the indifference Reynolds number depends strongly on the shape factor m . Figure 15.20 shows a result of these investigations, namely the curve of constant amplification for the boundary-layer profiles with outer flow given

by Eq. (15.25) for $m = -0.048$: this corresponds to the wedge angle $\beta = -0.1$, cf. also A.R. Wazzan (1975).

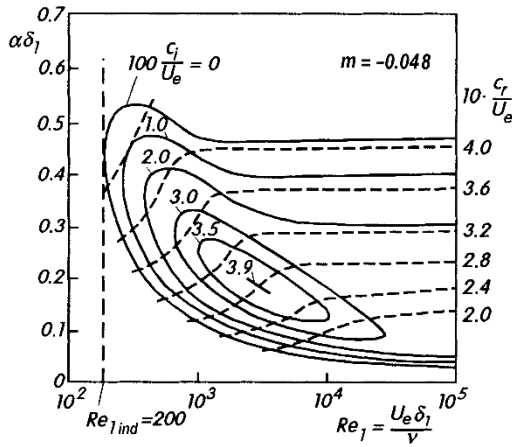


Fig. 15.20. Curves of constant *temporal* amplification c_i for the boundary layer of decelerated outer flow $U_e(x) = ax^m$ in a wide range of Reynolds numbers, after H.J. Obremski et al. (1969)
 $m = \beta/(2 - \beta) = -0.048$;
 $\beta = -0.1$

To first approximation, the velocity profiles in laminar boundary layers can be described by the following fourth order polynomial:

$$\frac{U(y)}{U_e} = 2\eta - 2\eta^3 + \eta^4 + \frac{\Lambda}{6}\eta(1-\eta)^3 \quad \text{with} \quad \eta = \frac{y}{\delta}, \quad (15.26)$$

where the curvature at the wall according to Eq. (7.2) yields the shape factor Λ to be

$$\Lambda = \frac{\delta^2}{\nu} \frac{dU_e}{dx}. \quad (15.27)$$

The shape factor Λ has values between $\Lambda = +12$ and $\Lambda = -12$, where the latter value corresponds to the separation point. At the forward stagnation point $\Lambda = 7.05$ and at the pressure minimum $\Lambda = 0$. $\Lambda > 0$ implies pressure decrease and $\Lambda < 0$ pressure increase. The velocity profiles for $\Lambda < 0$ have a point of inflection.

The stability calculation for this family of velocity profiles was carried out by H. Schlichting; A. Ulrich (1940). Figure 15.21 shows the curves of neutral stability. For the velocity profiles in the pressure drop region ($\Lambda > 0$), both branches of the curve of neutral stability vanish for $Re \rightarrow \infty$ (just as for the plate boundary layer, $\Lambda = 0$). On the other hand, for velocity profiles with pressure increase ($\Lambda < 0$), the upper branch of the curve of neutral stability tends towards a non-zero asymptote, so that a finite wavelength region of amplified disturbances is always present for $Re \rightarrow \infty$. The velocity profile in the pressure drop region ($\Lambda > 0$) and also the profile at equal pressure ($\Lambda = 0$) belong to the type of “viscous” instabilities (curve *b* in Fig. 15.9), while the velocity profiles in the pressure increase region ($\Lambda < 0$) are of the

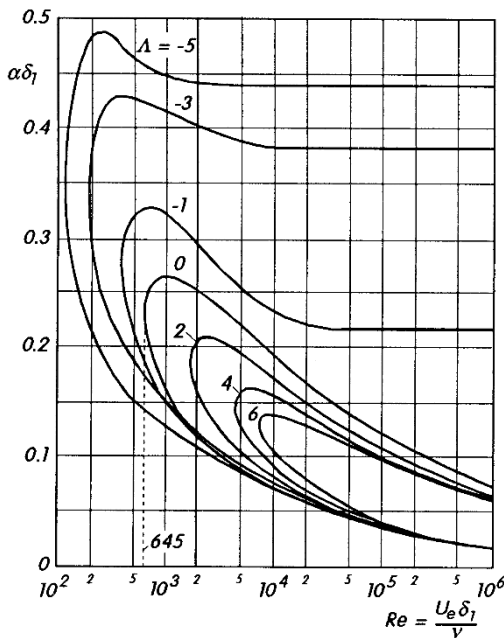


Fig. 15.21. Curves of neutral stability for laminar boundary-layer profiles with pressure drop ($\Lambda > 0$) and pressure increase ($\Lambda < 0$), $\Lambda = (\delta^2/\nu)(dU_e/dx)$: shape factor of the velocity profile

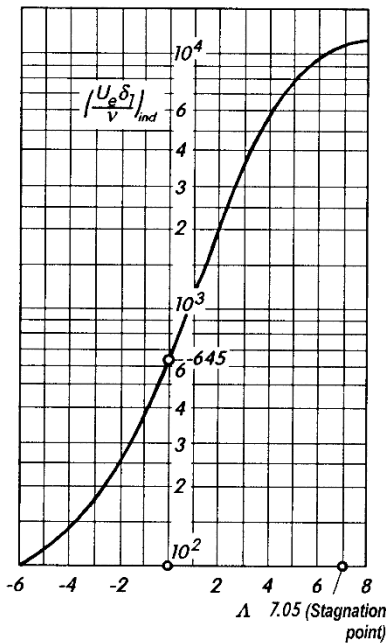


Fig. 15.22. Dependence of the indifference Reynolds number of the boundary-layer profile with pressure drop and pressure increase on the shape factor Λ , see also Fig. 15.21

type characteristic of “inviscid” instability (curve *a* in Fig. 15.9). It can be seen from Fig. 15.21 that the unstable region of perturbations enclosed by the curve of neutral stability for boundary layers with a pressure increase region is much larger than for accelerated flows. Figure 15.22 shows the dependence of the indifference Reynolds number from Fig. 15.21 on the shape factor Λ .¹ This varies very greatly with the shape factor Λ and thus also with the pressure gradient. In addition, Fig. 15.20 shows the curves of constant amplification $c_i/U_e = \text{const}$ for a velocity profile with a small pressure rise $\beta = -0.1$. Comparison with Fig. 15.12 shows that the amplification rate is greatly increased by the weak increase in pressure.

Computation of the position of the indifference point for a given body. The results in Figs. 15.21 and 15.22 can be used to determine the position of the indifference point for a given body (in plane flow) quite easily. The stability computation does not need to be repeated separately for each individual case, but is taken care of once and for all by Fig. 15.21.

Using the potential theory velocity distribution $U_e(x)/U_\infty$, which is assumed to be known, we first determine the laminar boundary layer using the approximate method in Chap. 8. This boundary-layer calculation also yields the dependence of the shape factor Λ in Eq. (15.27) and the displacement thickness δ_1 on the contour length x measured from the front stagnation point. For a given Reynolds number of the body $U_\infty l/\nu$ (l = body length) we follow the laminar boundary layer downstream from the forward stagnation point. Just behind the stagnation point, the strong pressure drop means that the limit of stability $(U_e\delta_1/\nu)_{\text{ind}}$ is high but the boundary-layer thickness is small. Because of this, the local Reynolds number $U_e\delta_1/\nu$ is smaller than the local limit of stability $(U_e\delta_1/\nu)_{\text{ind}}$. Therefore the boundary layer is stable here. Further downstream, the pressure drop is weaker, and beyond the velocity maximum, pressure increase occurs. Because of this the local limit of stability $(U_e\delta_1/\nu)_{\text{ind}}$ decreases downstream, whereas the boundary layer thickness and the local Reynolds number $U_e\delta_1/\nu$ both increase. At a particular point it is found that the two become equal:

$$\frac{U_e\delta_1}{\nu} = \left(\frac{U_e\delta_1}{\nu} \right)_{\text{ind}} \quad (\text{indifference point}). \quad (15.28)$$

The boundary layer is unstable from here on downstream. The point determined by Eq. (15.28) may then be called the indifference point. It clearly still depends on the Reynolds number of the flow past the body $U_\infty l/\nu$ since this influences the local boundary-layer thickness.

¹ For $\Lambda = 0$ here $\text{Re}_{1\text{ind}} = 645$, whereas in Fig. 15.11 the value 520 was given. This is because Fig. 15.21 for the plate boundary layer was calculated with an approximate function, while in Fig. 15.11 the exact solution of H. Blasius was used.

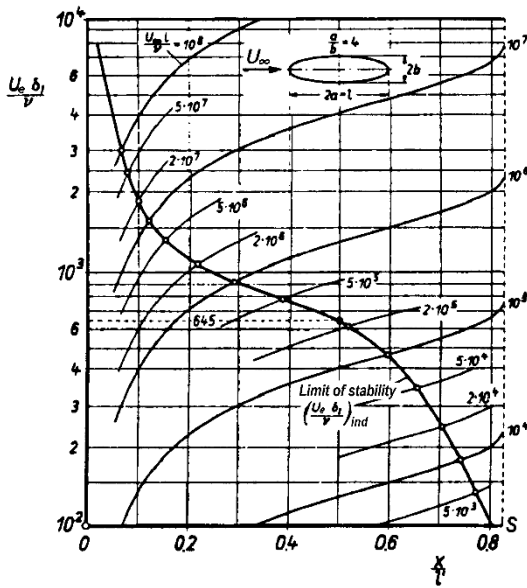


Fig. 15.23. The position of the indifference point dependent on the Reynolds number Re for an elliptical cylinder. axial ratio $a/b = 4$, $2l' = \text{circumference}$, $l = 2a$, $\text{Re} = U_\infty l/\nu$, S : separation

This manner of determining the dependence of the indifference point on the Reynolds number can easily be carried out using the diagram shown in Fig. 15.23. This figure is based on the example of an elliptic cylinder with axial ratio $a/b = 4$ in a flow parallel to its major axis. From the dependence of Λ on x , we can use Fig. 15.22 to determine the progression of the local indifference Reynolds number $\text{Re}_{1\text{ind}} = (U_e \delta_1 / \nu)_{\text{ind}}$, shown in Fig. 15.23 as the *limit of stability*. The computation of the laminar boundary layer yielded the progression of the dimensionless displacement thickness $(\delta_1 / l) \cdot \sqrt{U_\infty l / \nu}$. This allows us, for fixed Reynolds number of the body $U_\infty l / \nu$, to determine the local Reynolds number formed with the displacement thickness $U_e \delta_1 / \nu$ as

$$\frac{U_e \delta_1}{\nu} = \left(\frac{\delta_1}{l} \sqrt{\frac{U_\infty l}{\nu}} \right) \sqrt{\frac{U_\infty l}{\nu}} \frac{U_e}{U_\infty}.$$

The dependence of the curves $U_e \delta_1 / \nu$ on the arc length x/l' is also depicted in Fig. 15.23 for different values of the Reynolds number $U_\infty l / \nu$. The points of intersection of these curves with the limit of stability yield the position of the indifference point $(x/l)_{\text{ind}}$ for that particular Reynolds number.¹

In the same manner we can determine also the position of the indifference point for an airfoil, where not only is the variation with Reynolds number

¹ If we choose a logarithmic scale for the ordinate in Fig. 15.23, and shift the $U_e \delta_1 / \nu$ curves at different $U_\infty l / \nu$ parallel to the ordinate axis, they will all lie on top of each other. This is particularly convenient when determining the position of the indifference point graphically.

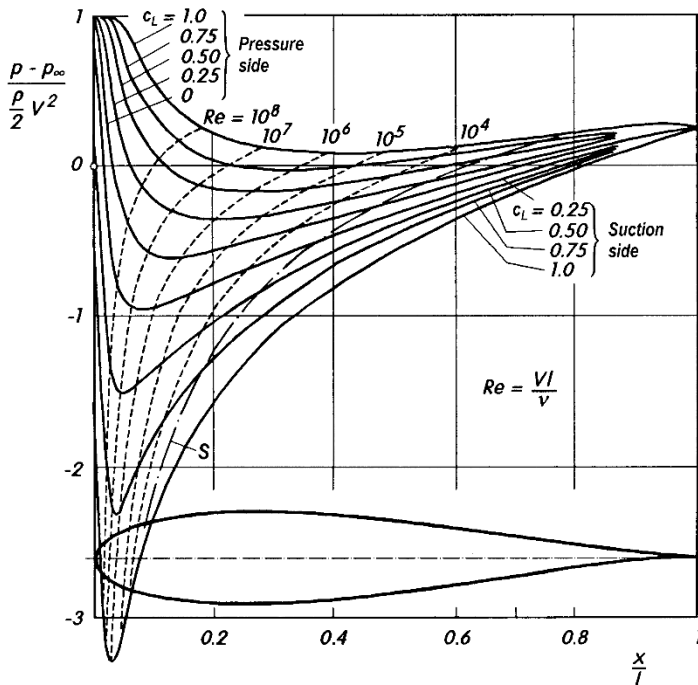


Fig. 15.24. Symmetric Joukowsky profile for different lift coefficients

- pressure distribution
- - - position of indifference point
- · - position of laminar separation point S

important but also the variation with angle of attack. Figure 15.24 shows the result for a symmetric Joukowsky airfoil at different angles of attack or lift coefficients. As the angle of attack is increased, the pressure minimum on the suction side becomes more and more prominent and shifts forwards, while on the pressure side the pressure minimum flattens out more and more and shifts backwards. A consequence of this is that as the angle of attack is increased the indifference point on the suction side moves forwards and that on the pressure side backwards. Because of the steep pressure minimum on the suction side, the indifference points for all Reynolds numbers lie closely together at the pressure minimum, while on the pressure side, where the pressure minimum is flat, they are further spaced out. The dominating role of the pressure distribution on the position of the indifference point can easily be seen from Fig. 15.24. Even at large Reynolds numbers, the indifference point (and therefore also the transition region) rarely shifts in front of the pressure minimum, while behind the minimum, instability and thus also the transition generally occur immediately.

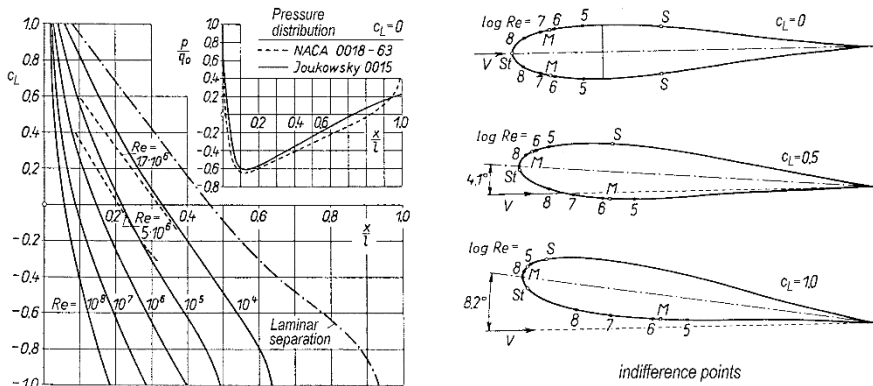


Fig. 15.25. Position of the indifference point and the point of completed transition plotted against the lift coefficient and the Reynolds number

- theoretical indifference point, airfoil J 0015
- - - measured point of completed transition, airfoil NACA 0018
- St: stagnation point
- M: pressure minimum
- S: laminar separation point

Figure 15.25 shows the experimentally determined position of the point of completed transition for a NACA airfoil with almost the same pressure distribution as a Joukowsky airfoil. It can be seen firstly that the transition lies behind the indifference point for all Reynolds numbers and lift coefficients, but in front of the laminar separation point, corresponding to theoretical expectations; secondly we see that the progression of the point of completed transition with the Reynolds number and the lift coefficient is just the same as the progression of the indifference point. Results of further systematic computation of the indifference point for airfoils with different thicknesses and camber can be found in a report by K. Bussmann; A. Ulrich (1943).

As a rough guide in transition calculations, we can use the rule of thumb that for Reynolds numbers between 10^6 and 10^7 , the position of completed transition and the position of the pressure minimum are about the same. However for very large Reynolds numbers, the point of transition can in some cases lie somewhat in front of this position, and for small Reynolds numbers, quite a distance behind, particularly if the pressure drop or pressure increase is only weak. On the other hand, for all Reynolds numbers the position of completed transition lies in front of the laminar separation point. Therefore, apart from at very large Reynolds numbers, the position of the point of completed transition is in between the pressure minimum and the laminar separation point.

How far the point of transition lies behind the indifference point depends on the turbulence intensity of the outer flow and the magnitude of the amplification of the unstable perturbations, which for their part are again affected by

the pressure gradient. A strikingly simple relation between the magnitude of the amplification and the distance of the theoretically determined indifference point from the experimentally determined position of completed transition was determined purely empirically by R. Michel (1951): see the end of this chapter. This was confirmed by A.M.O. Smith (1957) using stability theory. Each unstable perturbation moving downstream in the boundary layer experiences an amplification on entering the instability region in Fig. 15.21. This amplification is proportional to $e^{\int \beta_i dt}$, or, if β_i is time dependent, to

$$e^{\int \beta_i dt}. \quad (15.29)$$

Here the integral is to be taken over those unstable perturbations which the flow carries out after entering the instability region. A.M.O. Smith (1957) determined the amplification factor from Eq. (15.29) for the distance between the theoretical indifference point and the experimental point of completed transition for many different airfoils and bodies of revolution for which transition measurements are at hand. The results are shown in Fig. 15.26. The evaluation of very different kinds of measurements, which are all based on very low intensities of turbulence in the outer flow and very smooth walls, show that the amplification factor of the unstable perturbations throughout the transition region has the value

$$e^{\int \beta_i dt} = e^9 = 8103. \quad (15.30)$$

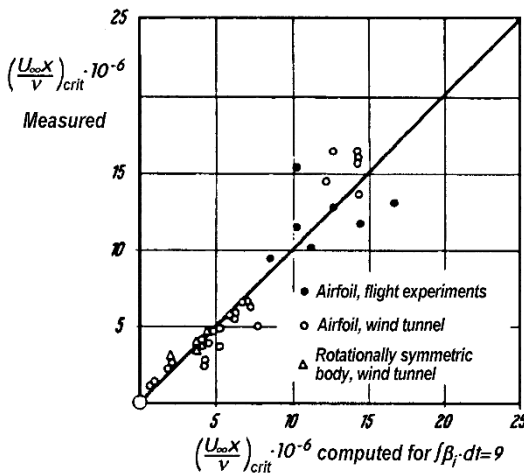


Fig. 15.26. The amplification factor $\exp \int \beta_i dt$ of unstable perturbations along the path from the theoretical indifference point to the point of completed transition, after A.M.O. Smith (1957)

These findings have been confirmed by J.L. Van Ingen (1956); cf. also the work by R. Michel (1952). Later these observations were again able to be confirmed by an even larger number of measurements, where the amplification factor was about $e^{10} = 22026$, cf. N.A. Jaffe et al. (1970).

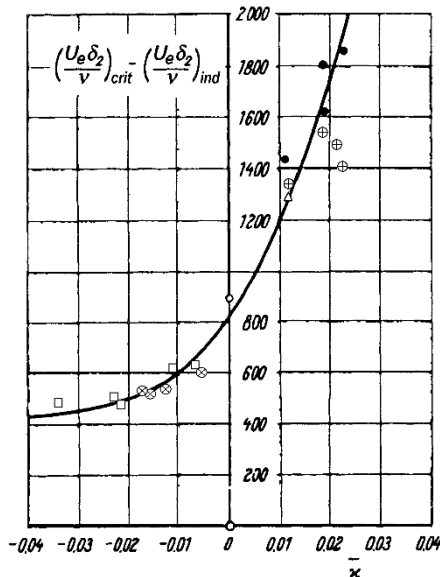


Fig. 15.27. Measurement of the position of completed transition in the boundary layer with pressure gradient, after P.S. Granville (1953). Difference in the Reynolds numbers between the position of completed transition $\text{Re}_2 \text{crit} = (U_e \delta_2 / \nu)_{\text{crit}}$ and the indifference point $\text{Re}_2 \text{ind} = (U_e \delta_2 / \nu)_{\text{ind}}$ against the average pressure gradient $\bar{\kappa}$ from Eq. (15.31)

$\bar{\kappa} > 0$ accelerated flow, $\bar{\kappa} < 0$ decelerated flow

- flat plate, after G.B. Schubauer; H.K. Skramstad (1943)
- ⊗ airfoil NACA 0012, after A.E. von Doenhoff (1940)
- suction side airfoil NACA 65₍₂₁₅₎ — 114,
after A.L. Braslow; F. Visconti (1948)
- ⊕ pressure side airfoil NACA 65₍₂₁₅₎ — 114,
after A.L. Braslow; F. Visconti (1948)
- airfoil 8% relative thickness, after B.M. Jones (1938)
- △ laminar airfoil 14.7% relative thickness,
after J.A. Zalovcik; R.B. Skoog (1945)

Circular symbols denote measurements in wind tunnels weak in turbulence;
other symbols denote flight measurements

The length of the transition region for boundary layers with pressure gradient can also be characterised by the difference between the Reynolds numbers formed with the momentum thickness at the point of completed transition and at the indifference point, that is by $(U \delta_2 / \nu)_{\text{crit}} - (U \delta_2 / \nu)_{\text{ind}}$. Figure 15.27 shows the dependence of this quantity on the average Pohlhausen parameter $\bar{\kappa}$, according to P.S. Granville (1953). Here

$$\bar{\kappa} = \frac{1}{x_{\text{crit}} - x_{\text{ind}}} \int_{x_{\text{ind}}}^{x_{\text{crit}}} \frac{\delta_2^2}{\nu} \frac{dU_e}{dx} dx. \quad (15.31)$$

The measurements are all based on very low intensities of turbulence (flight measurements and measurement in low turbulence wind tunnels). Figure 15.27 shows that the results of different experiments are all satisfactorily ordered onto one curve. The difference $(U_e \delta_2 / \nu)_{\text{crit}} - (U_e \delta_2 / \nu)_{\text{ind}}$ for pressure drop ($\bar{\kappa} > 0$) is considerably larger than that for pressure increase ($\bar{\kappa} < 0$). At constant pressure ($\bar{\kappa} = 0$), the value of $\text{Re}_2 \text{crit} - \text{Re}_2 \text{ind}$ is about 800 and is equal to that for the plate boundary layer at very low turbulence intensities. Compare also E.R. Van Driest; C.B. Blumer (1963).

Laminar airfoils. The stability calculations from Fig. 15.27 demonstrate impressively that the pressure gradient has a prominent influence on the stability and the laminar-turbulent transition in complete agreement with measurements. The construction of the *laminar airfoil* is based on this fact, whereby the longest possible laminar stretch of the boundary layer is achieved. Thus a low airfoil drag can be obtained via a contour where the greatest thickness is far backwards since in doing this the pressure minimum also lies far back towards the trailing edge. However a pressure minimum so far back can only be achieved for a certain small range of angles of attack.

During the Second World War, many measurements on laminar airfoils were carried out, particularly in the USA, cf. J.H. Abbott et al. (1945), after H. Doetsch (1940) published the first experimental results in 1939. Even earlier than this, B.M. Jones (1938) had noted particularly large laminar stretches in flight measurements. Today laminar airfoils have an important application in the construction of gliders. Fundamental investigations of glider wings have been carried out by R. Eppler (1969) and F.X. Wortmann; the latter have been presented under the name of FX airfoils in a piece of work by D. Althaus (1981). Figure 15.28 shows an overview of the drag coefficients of laminar airfoils. There is a drag saving of about 30 to 50% of the drag of a normal airfoil via the “laminar effect” in the Reynolds number region of about $\text{Re} = 2 \cdot 10^6$ to $3 \cdot 10^7$. For very large Reynolds numbers, of about $\text{Re} > 5 \cdot 10^7$, the laminar effect is no more, since here the transition is suddenly shifted forwards on the airfoil. This effect can however be explained by stability theory.

Investigations by those such as W. Pfenninger (1965), as well as H. Körner (1990), G. Redeker et al. (1988, 1990), K.H. Horstmann et al. (1990) have shown that a *transonic laminar wing* can indeed be realised for passenger aircraft under certain conditions. The strong transverse pressure gradient close to the leading edge of a swept-back transonic wing leads to strongly skewed velocity profiles in the boundary layer (see Fig. 15.50). If a critical sweep angle is exceeded, the component of the velocity profile normal to the main stream direction becomes unstable. This leads to *cross-flow instabilities* (see Sect. 15.3.5). These commence abruptly in the region at the front of the wing and, for highly swept-back wings, bring about the laminar-turbulent transition.

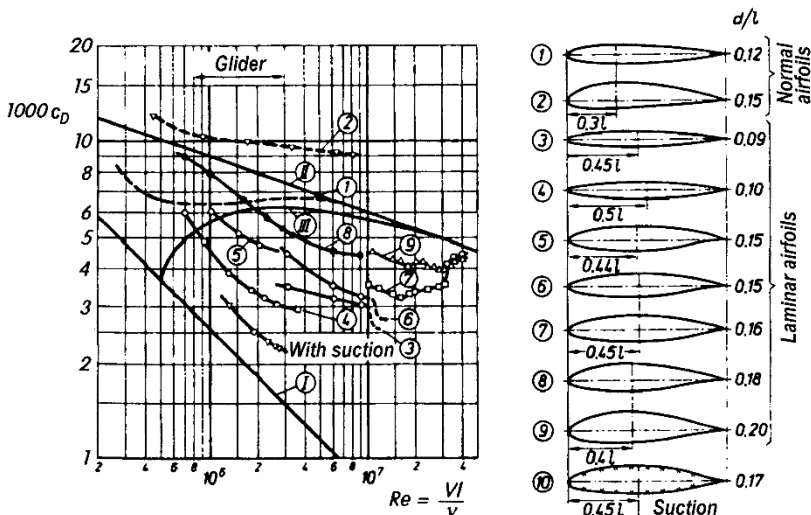


Fig. 15.28. Drag coefficients for laminar airfoils and “normal” airfoils, after H. Schlichting (1982), p. 511
 (I), (II), (III): drag coefficient of the flat plate
 (I): laminar, (II): fully turbulent, (III): laminar–turbulent transition

Empirical method. Numerous measurements have determined that there is a fixed relation between the quantities $Re_2 = U_e \delta_2 / \nu$ and $Re_x = U_e x / \nu$ at the position of completed transition (coordinate x_{crit}). According to R. Michel (see T. Cebeci; P. Bradshaw (1984), p. 189) it reads:

$$(Re_2)_{\text{crit}} = 1.174 \left(1 + \frac{22400}{Re_{x \text{ crit}}} \right) Re_{x \text{ crit}}^{0.46}.$$

If, in computing the laminar boundary layer, we also wish to know if this relation is satisfied, we can determine the position x_{crit} of the point of completed transition. One criterion is also the more simple relation $Re_{2 \text{ crit}} = 1.535 Re_{x \text{ crit}}^{0.444}$. Both of these relations are valid for low intensities of turbulence of the outer flow (free flight condition). For the flat plate ($U_e = \text{const}$) it is found that $Re_{x \text{ crit}} = 2 \cdot 10^6$ or $Re_{x \text{ crit}} = 3 \cdot 10^6$.

More details on the laminar–turbulent transition of a separated laminar boundary layer (e.g. at a separation bubble) are given by C. Gleyzes et al. (1984).

15.2.4c Effect of Suction

It was already pointed out in Chap. 11 that the application of suction of the laminar boundary layer is a very effective means of reducing the friction drag. Suction acts in a similar manner to the effect of a pressure drop to stabilise the boundary layer, and the reduction in drag is achieved by avoiding the laminar–turbulent transition. Therefore the effects of suction are twofold. Firstly suction acts to decrease the boundary-layer thickness, and a thinner boundary layer is less likely to go over to a turbulent flow form than a thick

one. Secondly, however, suction produces a laminar velocity profile which has a higher limit of stability (indifference Reynolds number) than the boundary layer without suction.

The theoretical treatment of the case of continuous suction is relatively accessible. Several solutions for this case have been given in Chap. 11. An important question in relation to retaining a laminar boundary layer is that of the amount of suction required. If the amount of suction is increased, the boundary-layer thickness can be made arbitrarily small, and thus the Reynolds number $Re_1 = U_e \delta_1 / \nu$ can be kept under the limit of stability. However a large amount of suction is uneconomical, since then a considerable part of the energy saved in drag reduction is again required for the suction. Therefore the question of the *minimum amount of suction* needed to retain a laminar boundary layer is important. Now this minimum amount of suction also yields the greatest drag saving which can be achieved by suction. This is because greater amounts of suction produce a thinner boundary layer and therefore also a greater wall shear stress.

A particularly simple solution of the boundary-layer equations is found, as was shown in Chap. 11, for the plate at zero incidence with homogeneous suction at the velocity $-v_w$.¹ In this case, the velocity distribution and thus also the boundary-layer thickness at some distance from the leading edge are independent of the distance along the plate. The displacement thickness of this *asymptotic suction profile* has, according to Eq. (11.21), the value

$$\delta_1 = \frac{\nu}{-v_w}. \quad (15.32)$$

Now in order to investigate the transition of the boundary layer with suction theoretically, a stability calculation was carried out for this airfoil whose velocity distribution is given by the equation

$$u(y) = U_\infty \left(1 - e^{\frac{v_w y}{\nu}} \right),$$

by K. Bussmann; H. Münz (1942). This yields an indifference Reynolds number with the very high value

$$\left(\frac{U_\infty \delta_1}{\nu} \right)_{\text{ind}} = 70\,000. \quad (15.33)$$

The indifference Reynolds number of the asymptotic suction profile is therefore about one hundred times larger than that for the plate boundary layer without pressure gradient and without suction, demonstrating that the stabilising action of suction is considerable. This shows us that not only does suction cause a reduction in the boundary-layer thickness of the laminar case, but also the limit of stability is increased. The curve of neutral stability for the asymptotic suction profile is shown in Fig. 15.29 ($\xi = \infty$). It can be seen that not only is the limit of stability considerably raised compared to the case

¹ Here $v_w < 0$ denotes suction and $v_w > 0$ blowing.

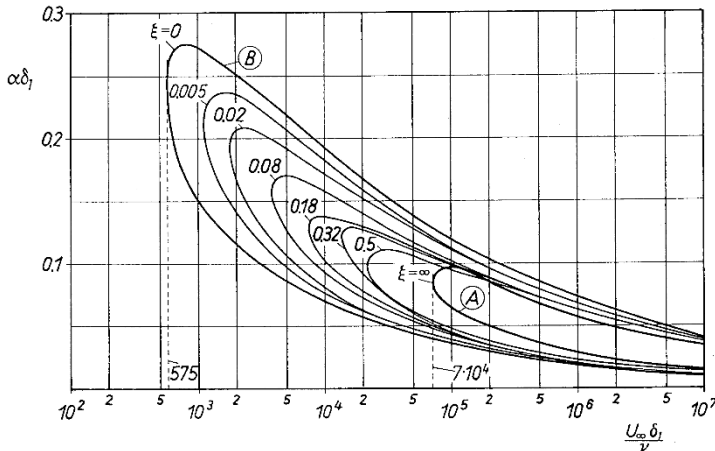


Fig. 15.29. Curves of neutral stability for the boundary-layer profile at the flat plate at zero incidence with homogeneous suction, after K. Bussmann; H. Münz (1942).

dimensionless entrance length $\xi = (-v_w/U_\infty)^2(U_\infty x/\nu) = c_Q^2 \text{Re}_x$
 (A): asymptotic suction profile
 (B): profile without suction (Blasius profile)

without suction, but the region of unstable perturbation waves enclosed by the curve of neutral stability has shrunk greatly compared to the boundary layer without suction.

This result can be used to answer the important question of the amount of suction required for laminar behaviour. Assuming, for simplification, that the asymptotic suction profile is already present at the leading edge of the plate with homogeneous suction, if the Reynolds number formed with the displacement thickness is everywhere under the limit of stability given by Eq. (15.33), then a stable boundary layer along the whole length of the plate is found when

$$\text{stable : } \frac{U_\infty \delta_1}{\nu} < \left(\frac{U_\infty \delta_1}{\nu} \right)_{\text{ind}} = 70000.$$

Inserting the value of δ_1 for the asymptotic profile as in Eq. (15.32), this becomes

$$\text{stable : } \frac{(-v_w)}{U_\infty} = c_Q > \frac{1}{70000}. \quad (15.34)$$

Thus, stability is present if the mass coefficient of suction c_Q is larger than the very small number $1/70000 = 1.4 \cdot 10^{-5}$.

At this point it must be mentioned that we would expect a larger critical mass coefficient than this one from a more precise calculation. This is due to the fact that the asymptotic suction profile used as a basis here is only achieved at a certain distance after the leading edge of the plate. Further

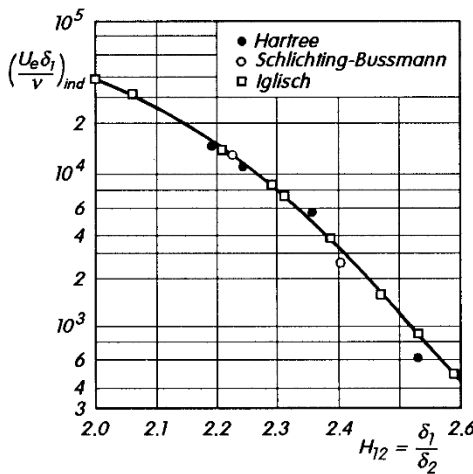


Fig. 15.30. Indifference Reynolds number of laminar boundary layers with suction and pressure gradients plotted against the shape factor $H_{12} = \delta_1 / \delta_2$

fowards, other velocity profiles are present; in fact the velocity profile passes over gradually from the Blasius profile without suction present close to the leading edge to the asymptotic suction profile. The velocity profile of the “approach” has a lower limit of stability than the asymptotic suction profile, and this means that a larger amount of suction is required for a laminar boundary layer along the run-up region than that predicted by Eq. (15.34). The considerable drag savings predicted by theory if the boundary layer is kept laminar by suction have been essentially confirmed by measurements in wind tunnels and by flight experiments, cf. M.R. Head (1955), B.M. Jones; M.R. Head (1951) and J.M. Kay (1948).

The effects of suction and a pressure gradient on the limit of stability can be determined from the plot of the indifference Reynolds number against the shape factor $H_{12} = \delta_1 / \delta_2$ of the velocity profile in Fig. 15.30. The indifference Reynolds numbers for the boundary-layer profiles of a flat plate at zero incidence with homogeneous suction (Igisch profile), with the suction $v_w \sim 1/\sqrt{x}$ (Bussmann profile) and that without suction but with a pressure gradient (Hartree profile) all lie along one curve. For the asymptotic suction profile, $H_{12} = 2$ and for the plate without suction, $H_{12} = 2.59$.

The stabilising effect of suction on the amplitude growth of Tollmien-Schlichting waves under certain suction conditions has been experimentally investigated by G.A. Reynolds; W.S. Saric (1986) and W.S. Saric; H.L. Reed (1986).

15.2.4d Effect of Wall Heat Transfer

As the theoretical and experimental results below will show, in gas flows heat transfer from the boundary layer to the wall (cooling) acts to stabilise the boundary layer, i.e. leads to an increase of the indifference Reynolds

number, while heat transfer from the wall to the boundary layer (heating) is destabilising and gives rise to a lower indifference Reynolds number.

The essential features of the effect of heat transfer from the wall to the flow on the stability of the laminar boundary layer can already be recognised in the case of incompressible flow. Many years ago W. Linke (1942) carried out some experimental investigations on the effect of wall heat transfer on the laminar–turbulent transition. Measurements of the friction drag at a hot flat plate standing vertically in a horizontal flow demonstrated a considerable increase in the friction drag due to heating, for Reynolds numbers of $Re_l = 10^5$ to 10^6 . From this W. Linke rightly concluded that increasing the temperature of the plate reduces the critical Reynolds number, and because of this there is a noticeable increase in the friction drag in the Reynolds number region which represents the laminar–turbulent transition region.

Using the point of inflection criterion discussed in Sect. 15.2.3, it can be seen that for incompressible flow and $T_w \neq T_\infty$, the heat transfer at the wall lowers or raises the limit of stability. The stabilising or destabilising effect of the heat transfer at the wall is essentially due to the dependence of the viscosity μ on the temperature T . Taking the temperature dependence of the viscosity into account, the curvature of the velocity profile at the wall of a flat plate at zero incidence, cf. Eq. (10.5), is

$$\left(\frac{d^2U}{dy^2} \right)_w = -\frac{1}{\mu_w} \left(\frac{d\mu}{dy} \right)_w \left(\frac{dU}{dy} \right)_w. \quad (15.35)$$

Now if the wall is warmer than the gas outside the boundary layer, $T_w > T_\infty$, the temperature gradient at the wall is negative, $(\partial T / \partial y)_w < 0$, and because the viscosity grows with increasing temperature for gases, then also $(d\mu / dy)_w < 0$. Since the velocity gradient at the wall is positive, it therefore follows from Eq. (15.35) that

$$T_w > T_\infty : \left(\frac{d^2U}{dy^2} \right)_w > 0. \quad (15.36)$$

Thus for hot walls, the curvature of the velocity profile at the wall is positive. It immediately follows from this that for hot walls there is a point inside the boundary layer where the curvature vanishes (point of inflection), i.e. where $d^2U/dy^2 = 0$, because the curvature for $y \rightarrow \infty$ is vanishingly small but negative. If heat is transferred from the wall to the flow, the boundary layer is unstable according to the point of inflection criterion. The addition of heat from the wall to a gas flowing past therefore acts to destabilise the boundary layer in the same way that a pressure increase in the flow direction does, while removing heat from the boundary layer stabilises just as a pressure drop does (cf. Fig. 7.1).

A numerical calculation by T. Cebeci; A.M.O. Smith (1968) for air confirms the reduction of the indifference Reynolds number for the onset of instability at a hot plate. A similar reduction in the transition Reynolds number

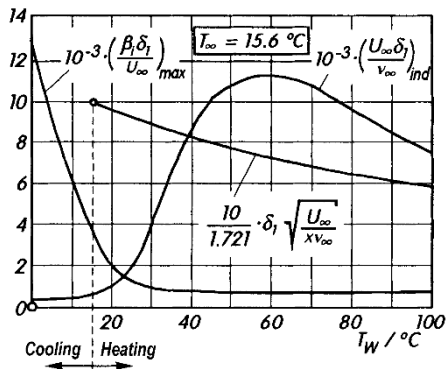


Fig. 15.31. Effect of the wall temperature on the instability and the displacement thickness of the boundary layer on a flat plate in water, after A.R. Wazzan et al. (1970a)
 T_w = wall temperature
 T_∞ = temperature of outer flow

was observed in the experiments by H.W. Liepmann; G.H. Fila (1947) at a vertical plate at zero incidence.

Since the viscosity of liquids decreases as the temperature is increased, the effects of heating and cooling from Eq. (15.35) should be just the opposite. An investigation by A.R. Wazzan et al. (1968, 1970a, 1970b) with water confirms this expectation. The indifference Reynolds number for the onset of instability is shown in Fig. 15.31 for walls with different temperatures. The maximum amplification factor $(\beta_i \delta_1 / U_\infty)_{\max}$ and the ratio of the dimensionless displacement thickness $\delta_1 / \sqrt{U_\infty / x \nu_\infty}$ to its value 1.721 for the wall with $T_w = T_\infty$ are also shown.

A strongly stabilising effect is found when the wall temperature is raised from its initial value of 15.6°C to 60°C , but further heating is then destabilising. Although the dimensionless amplification factor is constant for $T_w > 60^\circ\text{C}$, the dimensional value $(\beta_i)_{\max}$ increases in inverse proportion to δ_1 . The results for cooling show the expected destabilising effect for liquids. In the theory of A.R. Wazzan, the only influence of wall heat transfer, other than in the mean velocity profile, is via the temperature dependence of the viscosity. A complete theory by R.L. Lowell; E. Reshotko (1974) takes the temperature and density variations into account, but leads to almost exactly the same results. An experiment carried out by A. Strazisar et al. (1977) on the stability confirms the predicted shifting of the critical Reynolds number due to light heating.

If only moderate temperature differences $T_w - T_\infty$ are considered, we have the following relation for the indifference Reynolds number valid for all fluids (cf. H. Herwig; P. Schäfer (1992))

$$\text{Re}_{\text{ind}} = (\text{Re}_{\text{ind}})_\infty \left[1 + \frac{T_w - T_\infty}{T_\infty} \left(\frac{d\mu}{dT} \right)_\infty A_\mu(\text{Pr}_\infty) \right].$$

The function $A_\mu(\text{Pr}_\infty)$ is always negative and depends on the flow under consideration. For the flat plate at zero incidence with $T_w = \text{const}$ we have $A_\mu(\text{Pr}_\infty = 8.1) = -1.2$. P. Schäfer et al. (1994) have presented the corresponding formula for $q_w = \text{const}$, and also for temperature dependent densities $\varrho(T)$.

15.2.4e Effect of Compressibility

Of the many transition phenomena met in supersonic and hypersonic boundary layers, we will now concentrate on the effects of the Mach number and the wall heat transfer on boundary layers under constant pressure which form at flat plates or at cones at zero angle of incidence. We will first present a summary of the most important results obtained using the method of small disturbances and then show how the theory explains some experimental observations. Many of the theoretical results given here are taken from a comprehensive investigation into stability theory for compressible flows by L.M. Mack (1969). An extensive summary has also been given by L.M. Mack (1984).

The stability of laminar boundary layers in compressible flow was first investigated by D. Küchemann (1938), neglecting the effect of viscosity on the disturbance. The temperature gradient and the curvature of the velocity profile were first taken into account in the inviscid investigation by L. Lees; C.C. Lin (1946). These authors divided perturbations up into three categories called subsonic, sonic and supersonic perturbations, depending on whether the relative velocity between the outer flow U_∞ and the phase velocity c_r was smaller than, equal to or greater than the speed of sound a_∞ . In particular, L. Lees and C.C. Lin proved that

$$\left[\frac{d}{dy} \left(\varrho \frac{dU}{dy} \right) \right]_{y_s} = 0 \quad (15.37)$$

is a sufficient condition for the existence of an unstable subsonic perturbation, provided that $U(y_s) > U_\infty - a_\infty$.

This law is an extension of the first law in Sect. 15.2.3 to compressible flows, and y_s is the compressible counterpart of the distance of the point of inflection from the wall in incompressible flow. For convenience this is denoted as the distance from the wall of a “generalised” point of inflection. Using this generalised point of inflection, we have a neutral perturbation with $c_r = c_s = U(y_s)$ and also a neutral sonic perturbation moving downstream with the phase velocity $c_r = c_0 = U_\infty - a_\infty$ and $\alpha = 0$, if $\text{Ma}_\infty > 1$. Neutral supersonic perturbations are possible for certain flows, but no general condition has been given for their existence. Figure 15.32 shows the dimensionless phase velocities c_s/U_∞ and c_0/U_∞ of the neutral subsonic perturbation and the sonic perturbation as functions of Ma_∞ for a family of *adiabatic* boundary layers on the flat plate. The boundary-layer profiles of the basic flow used in computing c_s and which will be used throughout this section are exact numerical solutions of the compressible laminar boundary layer for air. Here the viscosity and the Prandtl number are functions of the temperature, at an outer flow stagnation temperature of $T_0 = 311\text{ K}$ with $\text{Ma}_\infty = 5.1$, where $T_\infty = 50\text{ K}$. At higher Mach numbers T_∞ remains at 50 K . These temperature conditions are characteristic for supersonic and hypersonic wind tunnels. Since in Fig. 15.32 we have $c_s > c_0 > 0$, all the boundary layers of this family satisfy the extended law and are unstable with respect to inviscid perturba-

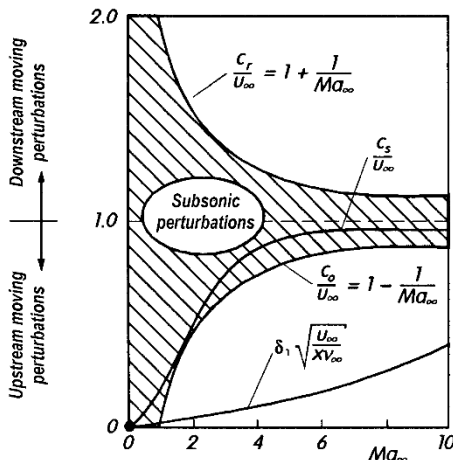


Fig. 15.32. Effect of the Mach number on the phase velocity of two-dimensional neutral perturbations and on the displacement thickness at adiabatic flat plates. Outside the shaded area of subsonic perturbations is the area of supersonic perturbations. The limit $|1 - (c_r/U_\infty)| = 1/\text{Ma}_\infty$ denotes the sonic perturbations

tions. Shifting the generalised point of inflection to greater y/δ with increasing Ma_∞ is similar to shifting the point of inflection with increasing pressure gradient for incompressible flow. Figure 15.32 also displays the dependence of the dimensionless displacement thickness $\delta_1 \sqrt{U_\infty / x \nu}$ on Ma_∞ for the family of adiabatic boundary layers. L. Lees and C.C. Lin were able to prove that, just as in incompressible flows, a single wave number gives the neutral subsonic disturbance, assuming that the basic flow is everywhere under the speed of sound compared to the phase velocity, i.e. $\widehat{\text{Ma}}^2 < 1$ throughout the entire boundary layer, where $\widehat{\text{Ma}} = (U - c_r)/a$ is the local relative Mach number. Although the proof that Eq. (15.37) is a sufficient condition for instability is subject to the same restriction, it is seen from numerous numerical calculations that Eq. (15.37) is a sufficient condition even when $\widehat{\text{Ma}}^2 > 1$. On the other hand, L.M. Mack (1965) has shown using a numerical computation that there is an infinite number of neutral wave numbers or modes with the same phase velocity c_s if a region with $\widehat{\text{Ma}}^2 > 1$ arises in the boundary layer.

These multiple modes are a consequence of the change in the form of the differential equations, for, say, the pressure waves from elliptical at $\widehat{\text{Ma}}^2 < 1$ to hyperbolic at $\widehat{\text{Ma}}^2 > 1$. The first mode is the same as for incompressible flow and was first computed for compressible flow by L. Lees; E. Reshotko (1962). As can be seen from Fig. 15.33, further instabilities occur at higher α values. These further instabilities, also called second partial perturbations or Mack modes, have no counterpart in incompressible flow. With $c_r = c_s$, $\widehat{\text{Ma}}$ first reaches the value 1 in the adiabatic plate boundary layer at $\text{Ma}_\infty = 2.2$. The upper layer of the supersonic flow region is at $y/\delta = 0.16, 0.43$ and 0.59 for $\text{Ma}_\infty = 3, 5$ and 10 respectively.

The multiple neutral perturbations with the phase velocity c_s are not the only ones possible when $\widehat{\text{Ma}}^2 > 1$. There are also many neutral disturbances

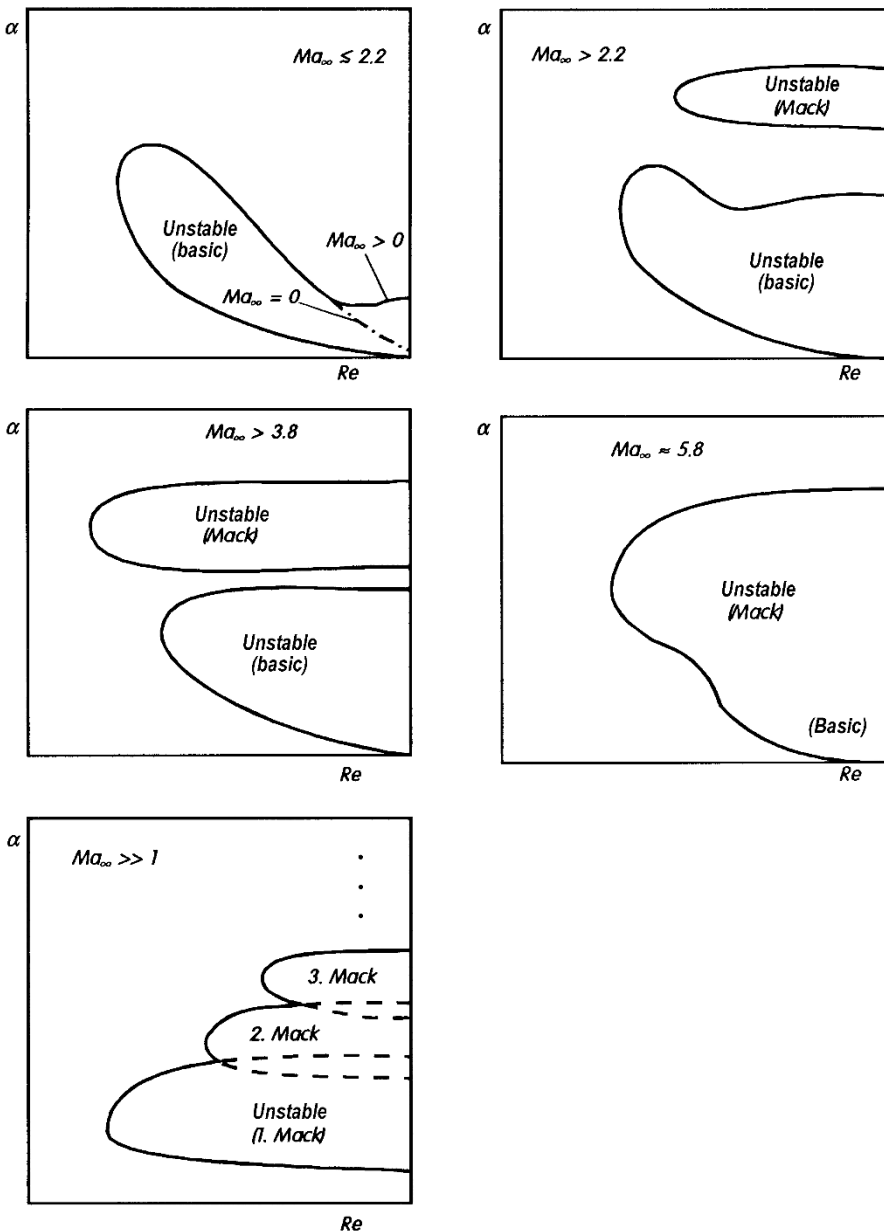


Fig. 15.33. Stability diagram for boundary layers at flat adiabatic plates at different Mach numbers for two-dimensional perturbations. Qualitative presentation of results by L.M. Mack (1969), after E. Reshotko (1976)

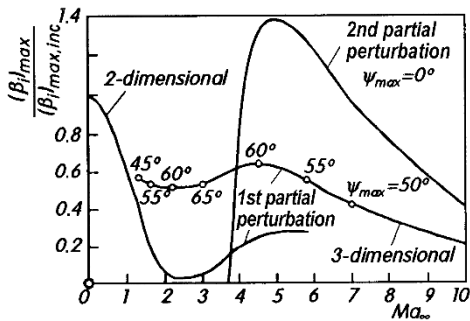


Fig. 15.34. Effect of the Mach number on the amplification parameter of the first and second partial disturbances according to the viscous theory for adiabatic flat-plate boundary layers, after L.M. Mack (1969)
 $\text{Re}_x = U_\infty x / \nu_\infty = 2.25 \cdot 10^6$
 ψ_{\max} = wave angle of greatest instability

with $U_\infty \leq c_r \leq U_\infty + a_\infty$. These perturbations do not depend on whether the boundary layer has a generalised point of inflection. In addition there are always neighbouring amplified perturbations of the same type with phase velocity $c_r < U_\infty$. Therefore the compressible boundary layer is unstable with respect to inviscid perturbations whatever the properties of the velocity and temperature profiles are, as long as there is a region where $\tilde{\text{Ma}}^2 > 1$.

Figure 15.34 qualitatively shows the appearance of the second instability due to the effects of compressibility. As the theory of L.M. Mack (1969) predicts, the instability region of the basic flow merges with the second instability with increasing Mach number. It is worth noting that a disturbance with a given frequency from the second instability region can be amplified without any interaction with the basic flow.

In contrast to the incompressible case, for supersonic Mach numbers oblique, that is three-dimensional basic perturbations, are more unstable than downstream moving two-dimensional perturbations. Thus a more general form of the perturbation must be considered:

$$u'(x, y, z, t) = \hat{u}(y) \exp[i(\alpha_1 x + \alpha_2 z - \beta t)]. \quad (15.38)$$

Equation (15.38) is an oblique wave perturbation whose direction is tilted at an angle to the x direction of

$$\psi = \arctan(\alpha_2 / \alpha_1).$$

On the other hand, the Mack modes are always most strongly amplified as two-dimensional disturbances, see Fig. 15.34.

Theoretical investigations by N.M. El-Hady; A.H. Nayfeh (1980), N.M. El-Hady (1991) and F.P. Bertolotti (1991) show that the parallel-flow assumption has a much greater effect on the amplification of the oblique modes discussed above compared to the two-dimensional modes.

At flat heat insulating plates, if the Mach number increases, one can differentiate between three different Mach number regions with different instability characteristics. Figure 15.34 shows the ratio $(\beta_i)_{\max} / (\beta_i)_{\max, \text{inc}}$ as a function of Ma_∞ for two-dimensional second modes at $\text{Re}_x = U_\infty x / \nu_\infty = 2.25 \cdot 10^6$, where $(\beta_i)_{\max, \text{inc}} = 0.00432 U_\infty / \delta_1$ is the amplification factor for incom-

pressible flow at the same Reynolds number. In the first region up to about $\text{Ma}_\infty \approx 3.8$, cf. Fig. 15.33, only basic disturbances are important. The maximum amplification factor of two-dimensional disturbances decreases strongly, but for $\text{Ma}_\infty > 1$ it is three-dimensional disturbances which are most unstable. At $\text{Ma}_\infty \approx 3.8$ the unstable Mack mode appears and is so greatly unstable for $3.8 \leq \text{Ma}_\infty \leq 5.0$ that it dominates all basic disturbances. Finally the third region above $\text{Ma}_\infty \approx 5.0$ is distinguished by the fact that an increase in the Mach number weakens all the instabilities. The boundaries between the three Mach number regions depend on the Reynolds number. However the Mack mode never occurs for the adiabatic plate boundary layer under $\text{Ma}_\infty = 2.2$.

In compressible flow (gas flow), *heat transfer* between the wall and the flow has a great effect on the stability. Some results on this are shown in Fig. 15.35a for the plate boundary layer at a moderately large Mach number ($\text{Ma}_\infty = 0.7$). The curves of neutral stability for different values of the ratio of the wall temperature to the outer temperature T_w/T_∞ show that at this Mach number heat removal from the boundary layer ($T_w < T_\infty$) greatly increases the stability, whereas the addition of heat to the boundary layer ($T_w > T_\infty$) strongly decreases the limit of stability with respect to two-dimensional disturbances. Completely different relations are seen in Fig. 15.35b for high Mach numbers, where cooling has no stabilising effects (on the second modes), cf. L.M. Mack (1969).

We have already looked at the destabilising effect of heating ($T_w > T_\infty$) and the stabilising effect of cooling ($T_w < T_\infty$) in incompressible gas flows, cf. Sect. 15.2.4d. The compressible basic flow behaves similarly to the incompressible instability. The stability behaviour changes as a consequence of the fact that the point of inflection of the basic profile is so easily affected by wall heat transfer. In contrast to the basic disturbances, Mack modes are not stabilised by cooling ($T_w < T_{\text{ad}}$). Their amplification is affected by an extension of the region with $\widehat{\text{Ma}}^2 = (U - c_r)^2/a^2 > 1$. It is easy to see that cooling reduces the local speed of sound a , and thus increases $\widehat{\text{Ma}}$. M.R. Malik; A.A. Godil (1990) have discussed influencing the Mach modes by cooling with suction.

15.2.4f Effect of Wall Roughness

Remark. The question to be treated in this section of how the laminar-turbulent transition is affected by the roughness of the wall is of considerable practical importance, but is rather inaccessible to theoretical treatment. This question has gained in importance since the appearance of laminar airfoils for aerodynamic applications. The existence of quite extensive experimental data encompasses cylindrical (two-dimensional) and point-like shaped (three-dimensional) single roughness elements as well as roughness elements distributed on the surface. In many of the cases investigated, as well as rough-

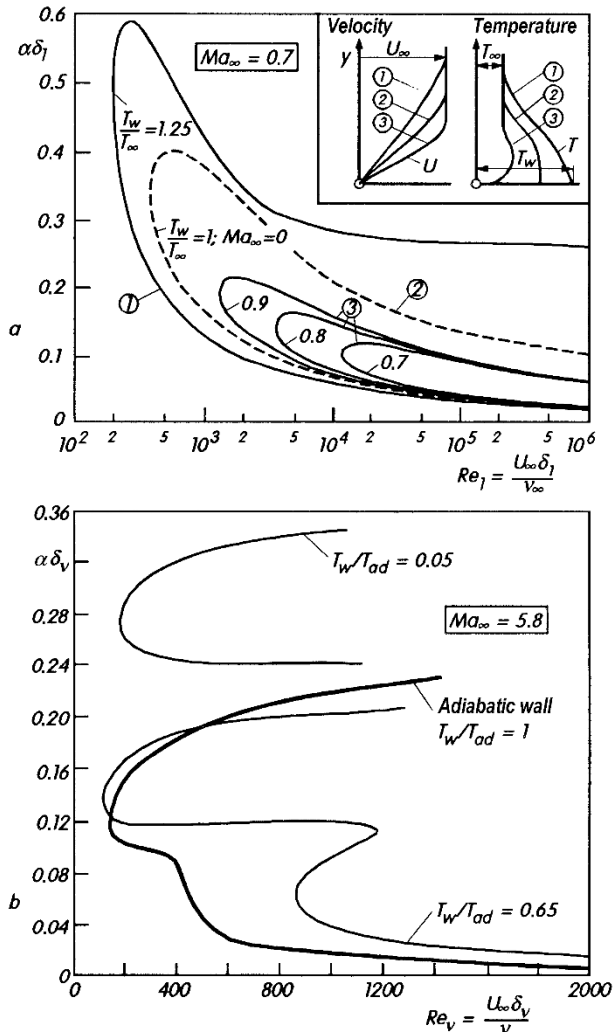


Fig. 15.35. Curves of neutral stability of two-dimensional perturbations for the laminar boundary layer on a flat plate at zero incidence in compressible flow with heat transfer (gas flow)

- (a) subsonic flow, $Ma_\infty = 0.7$, after L. Lees; C.C. Lin (1946),
Prandtl number $Pr = 1$, $T_{ad} = 1.098T_\infty$
 - (1) heating the boundary layer ($T_w > T_{ad}$) lowers the stability
 - (2) heat insulating wall
 - (3) cooling the boundary layer ($T_w < T_{ad}$) raises the stability
- (b) supersonic flow $Ma_\infty = 5.8$, after L.M. Mack (1969)
 $T_\infty = 125 \text{ K}$, $\delta_\nu = (\nu_\infty x / U_\infty)^{1/2}$

ness there is simultaneously an effect of the pressure gradient, the turbulence intensity or the Mach number present.

In general wall roughness favours the laminar-turbulent transition, in the sense that, under otherwise equal conditions, the transition occurs at smaller Reynolds numbers for a rough wall than for a smooth wall. In general the roughness produces additional large amplitude disturbances in the laminar flow. Results from nonlinear perturbation theory show that the critical Reynolds number is reduced.

Cylindrical single roughness elements. By a cylindrical (or two-dimensional) single roughness we mean one such as a wire which lies at the wall perpendicular to the stream direction. Older measurements led S. Goldstein (1936) to deduce the following relation for the *critical roughness height*:

$$\frac{u_{\tau k} k_{\text{crit}}}{\nu} = 7. \quad (15.39)$$

This is the roughness height which just does not affect the transition. Here $u_{\tau k} = \sqrt{\tau_{wk}/\rho}$ is the shear stress velocity with τ_{wk} the wall shear stress of the laminar boundary layer at the position of the roughness. The smallest roughness height where the transition just takes place directly at the roughness element has been given by I. Tani et al. (1940) as $u_{\tau k} k_{\text{crit}}/\nu = 15$, while according to A. Fage; J.H. Preston (1941)

$$\frac{u_{\tau k} k_{\text{crit}}}{\nu} = 20. \quad (15.40)$$

The numerical values apply to wires with circular cross-sections. Flat cupped cross-sections and grooves lead to greater numbers, while sharply edged roughness elements yield smaller numbers.

H.L. Dryden (1953) used dimensional considerations to find an empirical law which gives the dependence of the position of completed transition x_{crit} both on the roughness height k and on the position of the roughness element x_k . H.L. Dryden found that, for incompressible flows, all experimental data where the position of completed transition is not directly dependent on the roughness element, and thus for which $x_{\text{crit}} > x_k$, lies pretty well along *one* curve (about $Uk/\nu \approx 900$). This occurs in the plot of the Reynolds number $Re_{1\text{crit}} = U\delta_{1\text{crit}}/\nu$ formed with the displacement thickness of the boundary layer at the position of the roughness $\delta_{1\text{crit}}$ against k/δ_{1k} (Fig. 15.36), where δ_{1k} is the displacement thickness at the position of the roughness element. The second scale on the vertical axis is $Re_{x\text{crit}} = Ux_{\text{crit}}/\nu$.¹ With increasing k ,

¹ The relation between the two Reynolds numbers on the vertical axis is

$$Re_{1\text{crit}} = \frac{U\delta_{1\text{crit}}}{\nu} = 1.72 \sqrt{\frac{Ux_{\text{crit}}}{\nu}} = 1.72 \sqrt{Re_{x\text{crit}}}.$$

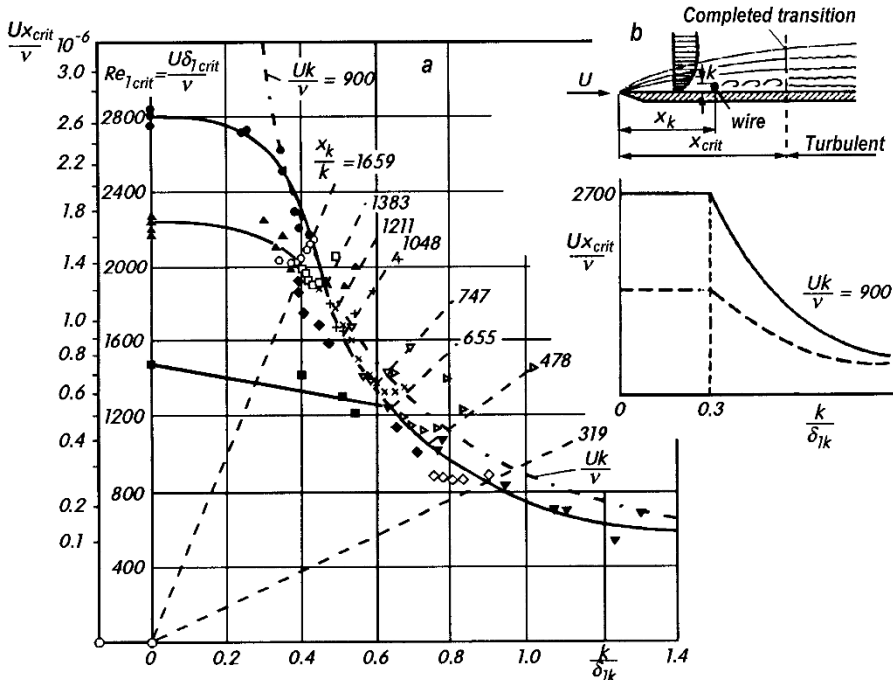


Fig. 15.36. Effect of single roughness elements on transition

(a) Dependence of the critical Reynolds number on the ratio of the roughness height k to displacement thickness of the boundary layer at the position of the roughness element δ_{1k} , for two-dimensional single roughness elements in incompressible flow

Measurements have been interpolated using Eq. (15.41)

$$Re_{1crit} = U\delta_{1crit}/\nu, Re_{xcrit} = Ux_{crit}/\nu$$

$$\text{and } Re_{1crit} = 1.72\sqrt{Re_{xcrit}}$$

The index 0 implies the smooth plate

- - - - computed using Eq. (15.41) for $(Re_{1crit})_0 = 1.7 \cdot 10^6$; $p = \text{const}$, after E.G. Feindt (1956)

▲ $(Re_{1crit})_0 = 1.7 \cdot 10^6$; $p = \text{const}$, after I. Tani

● $(Re_{1crit})_0 = 1.7 \cdot 10^6$; $p = \text{const}$, after I. Tani

◆ $(Re_{1crit})_0 = 2.7 \cdot 10^6$

▼ $p = \text{const}$, after G.B. Schubauer; H.K. Skramstad (1943)

■ $(Re_{xcrit})_0 = 6 \cdot 10^5$; $p = \text{const}$, after I. Tani et al. (1954)

filled measurement points imply $x_{crit} > x_k$

pressure drop $2(p_1 - p_{crit})/\rho U_1^2 = 0.2$ to 0.8, after I. Tani et al. (1954)

(b) basic sketch of the laminar-turbulent transition with individual roughness element (wire) and effect of outer turbulence on the critical Reynolds number Re_{xcrit}

— without outer turbulence

- - - - with outer turbulence

x_{crit} shifts closer to the roughness element, so that as k increases, the straight lines in Fig. 15.36 run from left to right. As soon as the position of completed transition has reached the roughness element, $x_{\text{crit}} = x_k$, the experimental data deviate upwards from this curve.

The family of straight lines dependent on the parameter x_k/k then follows as

$$\frac{U\delta_{1\text{crit}}}{\nu} = 3.0 \frac{k}{\delta_{1k}} \frac{x_k}{k}; \quad (15.41)$$

this is depicted in Fig. 15.36.

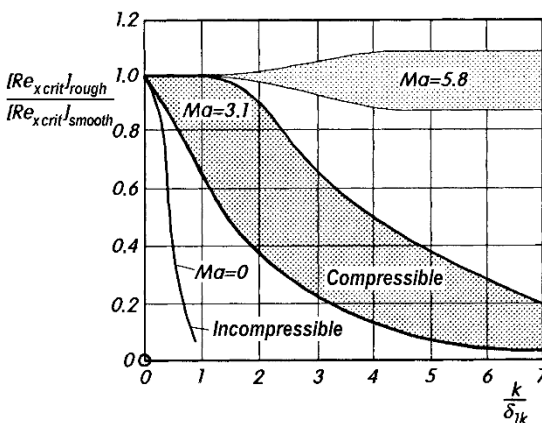


Fig. 15.37. Influence of a two-dimensional single roughness element on the critical Reynolds number on the flat plate at zero incidence in compressible flow, after measurements by P.F. Brinich (1954) and R.H. Korgeki (1956)
 k = height of roughness element
 δ_{1k} = displacement thickness of boundary layer at position of roughness

The effect of roughness on the laminar-turbulent transition in supersonic flows is much less than in incompressible flows. This can be seen from Fig. 15.37 which depicts the situation for a flat plate at zero incidence and, as far as measurements in the supersonic region are concerned, is based on work by P.F. Brinich (1954). The measurements carried out for cylindrical single roughness elements at a Mach number $\text{Ma} = 3.1$ yield a family of curves which lies in the shaded area but which is still strongly dependent on the position of the roughness element x_k . The curve for incompressible flow from Fig. 15.38 which is shown for comparison, shows that the boundary layer at high Mach numbers can “withstand” much greater roughness than incompressible flow. The critical roughness height for supersonic flow is about three to seven times greater than that for incompressible flow. Experiments by R.H. Korgeki (1956) at the even greater Mach number of $\text{Ma} = 5.8$ shows that here a trip wire may introduce no turbulence at all. However, blowing air into the boundary layer even at supersonic velocities does seem to be a functional way of inducing the transition.

Roughness elements distributed on the surface. There are very few transition measurement results pertaining to roughness elements distributed

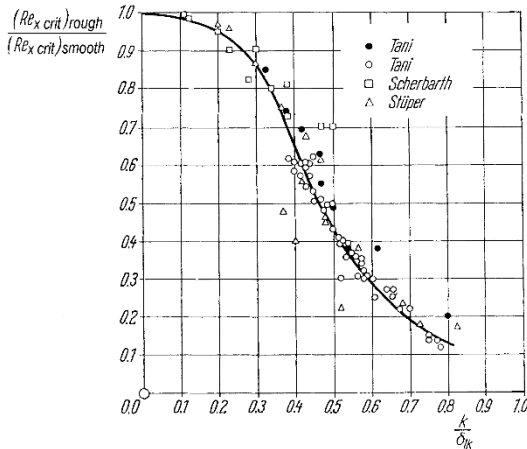


Fig. 15.38. Ratio of the critical Reynolds number at a flat plate at zero incidence with single roughness elements to that of the smooth plate, after H.L. Dryden (1953)

$$Re_x \text{ crit} = U x_{\text{crit}} / \nu$$

k = roughness height

δ_{1k} = displacement thickness of the boundary layer at the roughness element;

measurements by I. Tani et al. (1940) and J. Stüper (1956)

over a surface. Only when the Reynolds number formed with the roughness height k_s exceeds the value

$$\frac{U_1 k_s}{\nu} = 120$$

does the critical Reynolds number drop greatly. Thus this value determines the *critical roughness height*. Above this limit, the roughness height has just as large an effect on the critical Reynolds number as the pressure gradient, cf. E.G. Feindt (1956).

15.2.4g Further Effects

Flexible wall. There are indications that the flexibility of the wall in the flow could affect the stability of the laminar boundary layer. To this end see the work by T.B. Benjamin (1960) and M.T. Landahl (1962). As well as the Tollmien–Schlichting waves, there are also further waves, particularly elastic waves in the wall. The work by G. Zimmermann (1974) refers to further pieces of work on this topic, see also A.E. Dixon et al. (1994).

Oscillating outer flow. Just as the turbulence intensity of the outer flow greatly affects the stability of the boundary layer, so too do regular periodic oscillations in the outer flow. See the summaries by R.J. Loehrke et al. (1975) and S.H. Davis (1976). With reference to the effect of sound waves, see E. Reshotko (1976).

Gravity. The buoyancy forces due to gravity lead to the natural convection flows treated in Sect. 10.5. The transition of these flows to a turbulent state takes place in a similar manner to the forced flows treated until now. Because of the coupling between the velocity and temperature fields, even primary

stability theory yields wave shaped temperature variations which affect the Tollmien–Schlichting waves. There is extensive literature available on this and other nonlinear effects, cf. B. Gebhart (1973), B. Gebhart; R.L. Mahajan (1982) and B. Gebhart et al. (1988), see also J. Severin; H. Herwig (2001).

In this connection we ought to mention horizontal boundary layers with *stratification*, which occur for example in heat transfer when the dependence of the density on the temperature has to be taken into account. There is a stable layering effect if the density decreases upwards, and it is unstable if the density increases upwards. As well as the Reynolds number, the (*gradient*) *Richardson number*

$$\text{Ri} = -\frac{g d\varrho}{\varrho dy} / \left(\frac{\partial U}{\partial y} \right)_w^2,$$

cf. H. Schlichting (1982), p. 520 is also important for the stability of layered boundary layers. According to H. Schlichting (1935b), the horizontal plate flow boundary layer is stable for $\text{Ri} > 1/24$.

15.3 Instability of the Boundary Layer for Three-Dimensional Perturbations

15.3.1 Remark

In the previous section we developed the basis of the primary stability theory which describes the onset of two-dimensional Tollmien–Schlichting waves and their amplification downstream in the boundary layer. In this section we will derive the *secondary stability theory* which treats the onset of three-dimensional perturbations and the formation of Λ -structures in the transition region, corresponding to the sketch in Fig. 15.5. The primary stability analysis (i.e. analysis of the Orr–Sommerfeld equation) starts out with the boundary-layer solution as the fundamental state. The two-dimensional Tollmien–Schlichting waves carry out the transition process downstream. Analogously, the local secondary stability analysis takes the two-dimensional perturbed basic state of the unstable boundary layer and describes the occurrence of three-dimensional perturbations and their development downstream.

Let us look at some experimental and numerical results to extend the overview of the transition process shown in Fig. 15.5. Figure 15.5 described the transition process as a succession of Tollmien–Schlichting waves, Λ -structures, vortex decay and formation of turbulent spots as preliminary stages to fully turbulent boundary-layer flow, cf. H.W. Emmons; A.E. Bryson (1951/52), G.B. Schubauer; H.K. Skramstad (1947), P.S. Klebanoff et al. (1962), L.S.G. Kovasznay et al. (1962), F.R. Hama; J. Nutant (1963), S.A. Orszag; A.T. Patera (1983), T. Herbert (1983), A. Wary; M.Y. Hussaini (1984), P.R. Spalart; K.S. Yang (1987), E. Laurien; L. Kleiser (1989). A summary of the transition processes is given by D. Arnal (1984).

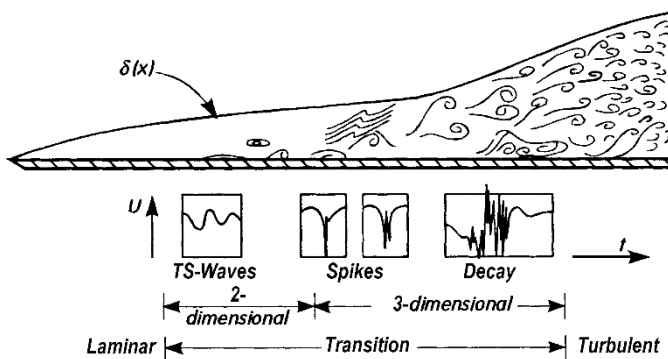


Fig. 15.39. Signals found at different regions in the transition at a plate at zero incidence, after M. Nishioka et al. (1975, 1990)

The stability theory of the “momentum response” by L. Brevoort (1993) shows that the Blasius boundary layer (plate boundary layer) is convectively unstable and therefore a transition process has to take place. This is in contrast to the abrupt onset of instabilities in absolutely unstable flows.

The phenomena observed during the transition process are similar for the plate boundary layer and for the plane channel flow. Figure 15.39 is based on measurements by M. Nishioka et al. (1975) on a channel. In the region of primary instabilities, the velocity fluctuations measured demonstrate the characteristic signal of periodic Tollmien–Schlichting waves. Downstream the signal is characterised by so-called *spikes* which denote the appearance of local high shearing regions together with point of inflection velocity profiles. Further downstream, these spikes appear more and more frequently within a period, until finally an irregular fully turbulent region has developed. The numerical simulation results show that the magnitude of the shearing in the three-dimensional shearing layers grows hugely in the spike state. Many local maxima occur, introducing the decay of the shearing layers and thus the transition to turbulence. Along with this, regions of high shearing appear close to the wall. These are called “*hair-pin structures*”, cf. P.S. Klebanoff et al. (1962). Here the periodic initial perturbations were generated in the boundary layer using an oscillating cord. The growth of the local fluctuations downstream occurs via the formation of the Λ -structures and for increasing Reynolds number the formation of the “*hair-pin structures*” close to the wall (see Fig. 15.40).

Following experimental and theoretical results by P.S. Klebanoff et al. (1962), T. Herbert (1983), S.A. Orszag; A.T. Patera (1983) and F.P. Bertolotti (1991), two types of transition processes can be observed (for discrete superimposed periodic oscillations): the harmonic or fundamental K-type (K for Klebanoff) of the transition and the subharmonic H-type (H for Herbert) corresponding to the chosen initial disturbance. The harmonic perturbations

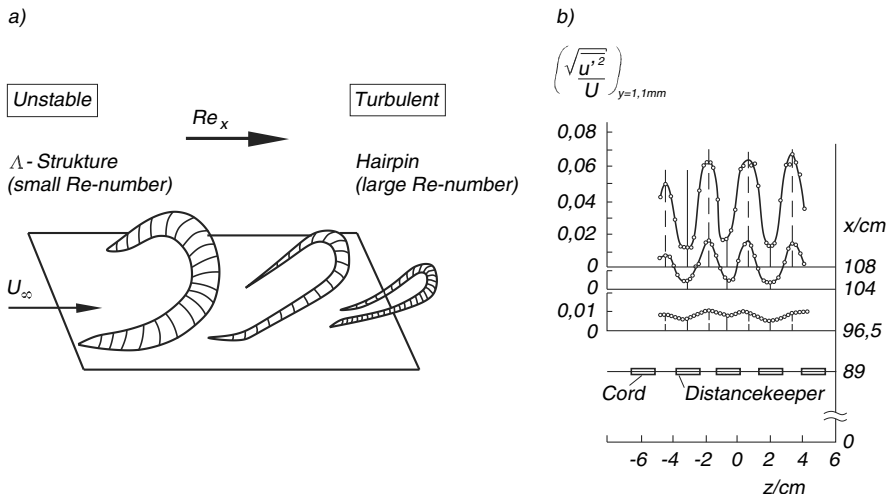


Fig. 15.40. Three-dimensional perturbation to the plate boundary layer
 (a) basic sketch of Λ and “hair-pin” structures for increasing Reynolds number Re_x , after M.R. Head; P. Bandyopadhyay (1981)
 (b) oscillation velocities, produced by local periodic perturbations, after P.S. Klebanoff et al. (1962)

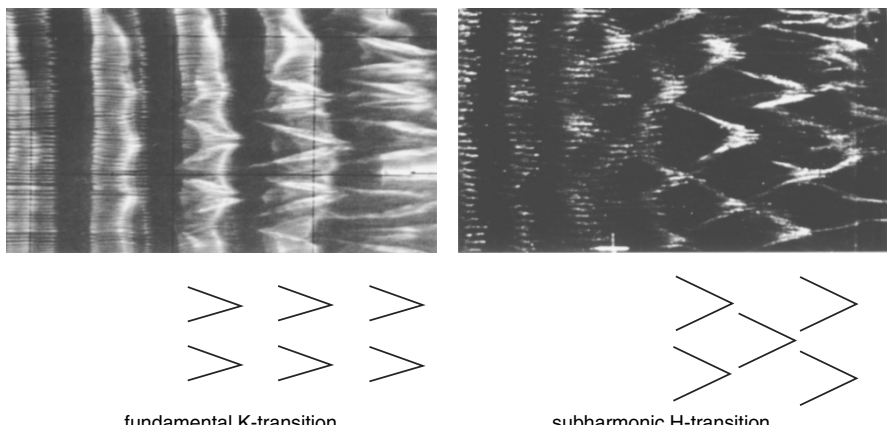


Fig. 15.41. Streaklines of the Λ -structures in the plate boundary layer for harmonic and subharmonic perturbations, after H. Bippes (1972), W.S. Saric (1994)

were first generated and studied by P.S. Klebanoff, hence the name K-type oscillations. Figure 15.41 shows the Λ -vortices ordered one after the other of the harmonic K-structures excited by the Tollmien–Schlichting waves. These are generally superimposed with staggered Λ -vortices of the subharmonic H-structures. Although in this “computer experiment” they have been separated, both transition mechanisms determine the transition process in tech-

nical problems. The onset of these three-dimensional perturbations may be treated using the local secondary Orr–Sommerfeld stability analysis.

15.3.2 Fundamentals of Secondary Stability Theory

In primary stability theory, the two-dimensional Tollmien–Schlichting perturbation was superimposed onto the two-dimensional basic flow. The resulting motion was written as in Eq. (15.6):

$$\begin{aligned} u_P(x, y, t) &= U(y) + u'(x, y, t), \\ v_P(x, y, t) &= v'(x, y, t), \\ w_P &= 0, \\ p_P &= P(x, y) + p'(x, y, t). \end{aligned} \tag{15.42}$$

Secondary stability theory treats the onset of three-dimensional perturbations. The theoretical ansatz starts out from the idea that the solutions of the primary stability analysis can be set as a new basic flow from a local viewpoint. This basic flow is then superimposed with three-dimensional perturbations. Therefore the resulting three-dimensional disturbance motion has the form

$$u_S = u_P + u^*, \quad v_S = v_P + v^*, \quad w_S = w^*, \quad p_S = p_P + p^*. \tag{15.43}$$

In Eq. (15.42), $U(y)$, $P(x, y)$ are solutions of the Navier–Stokes equations (e.g. for fully formed channel flow) or approximations for boundary layers with the parallel-flow assumption. The perturbing quantities u' , v' , p' can be determined using the perturbation differential equations (15.7) to (15.9). Introducing the stream function $\psi(x, y, t)$ from Eqs. (15.12) and (15.13), we obtain the Orr–Sommerfeld equation (15.14).

In order to compute the three-dimensional perturbing quantities u^* , v^* , w^* , p^* from Eq. (15.43), we first have to fix a suitable coordinate system. By describing the new basic flow in a coordinate system (ξ, y, z) moving with the Tollmien–Schlichting waves with phase velocity c_r , where

$$\xi = x - c_r t, \tag{15.44}$$

we can obtain a *steady basic state*. We assume local parallel flow $V = 0$ and neglect terms nonlinear in the perturbing quantities u^* , v^* , w^* , p^* . After eliminating the pressure p^* from the three momentum equations and the continuity equation, we obtain two *linear* partial differential equations for the two perturbing quantities u^* and v^* . These equations contain neither w^* nor p^* , cf. T. Herbert (1988) and A.H. Nayfeh (1987). The two differential equations for u^* and v^* also contain an expansion parameter from the primary Tollmien–Schlichting instabilities. If this is normalised correctly, this assumes the role of the maximum squared average of the perturbation fluctuations. The third velocity component w^* is found from the continuity equation:

$$\frac{\partial u^*}{\partial \xi} + \frac{\partial v^*}{\partial y} + \frac{\partial w^*}{\partial z} = 0. \quad (15.45)$$

For three-dimensional perturbations we use the trial solution:

$$\left. \begin{array}{l} u^* \\ v^* \\ w^* \end{array} \right\} \sim \left. \begin{array}{l} \varphi^*(\xi, y) \\ \psi^*(\xi, y) \\ \zeta^*(\xi, y) \end{array} \right\} \cdot e^{i(\alpha^* z - \beta^* t)} \quad (15.46)$$

with the boundary conditions

$$y = 0 \quad \text{and} \quad y \rightarrow \infty : \quad \varphi^* = 0, \quad \psi^* = 0, \quad \frac{\partial \psi^*}{\partial y} = 0. \quad (15.47)$$

This describes the eigenvalue problem of secondary stability theory. The resulting system of two coupled differential equations for $\varphi^*(\xi, y)$ and $\psi^*(\xi, y)$ is solved numerically. Here α^* denotes the wave number of the secondary perturbations in the perpendicular direction. *Floquet theory* can then be applied to this linear system with coefficients which are periodic in ξ . The eigenfunctions then consist of a function of ξ which is periodic in $2\pi/\alpha^*$, multiplied by some characteristic factor.

According to T. Herbert (1988), the corresponding Fourier series trial solution reads

$$\left. \begin{array}{l} \varphi^* \\ \psi^* \\ \zeta^* \end{array} \right\} \sim e^{-i\delta_r \xi} \cdot \sum_{n=-N}^{+N} \left. \begin{array}{l} \varphi_n^*(y) \\ \psi_n^*(y) \\ \zeta_n^*(y) \end{array} \right\} \cdot e^{i n \alpha^* \xi}. \quad (15.48)$$

Assuming that the phase shift factor δ_r is real, this is the theory of the temporal amplification of those secondary instabilities from experiment which develop downstream spatially. It suffices to consider the interval $0 \leq \delta_r \leq 1/2$ ($\delta_r = 0$: harmonic case; $\delta_r = 1/2$: subharmonic case).

The results by P.S. Klebanoff et al. (1962) and Y.S. Kachanov; V.Y. Levchenko (1984) show that if the amplitude of the primary Tollmien–Schlichting waves is large enough, the harmonic and subharmonic perturbations of the secondary instabilities move downstream in phase with the Tollmien–Schlichting waves. This results in a maximal energy transport from the primary to the secondary perturbations which initiate the transition process. Mathematically, from Eq. (15.46), primary and secondary waves moving synchronously is given by a purely imaginary β^* . Figure 15.42 shows the dependence of the change in temporal amplification of the subharmonic secondary instability on the wave number in the perpendicular direction. For small amplitudes A of the primary Tollmien–Schlichting waves, the amplification of the secondary waves is carried out in a small wave number domain. As the primary perturbation amplitude is increased, e.g. $A = 0.01$, the maximum of the secondary amplification grows by two orders of magnitude within six periods of the Tollmien–Schlichting waves. This occurs along with an extension of the band of amplified waves in the perpendicular direction.

Figure 15.43 shows the comparison of the amplification computed by T. Herbert (1988) with numerical simulations by P.R. Spalart; K.S. Yang

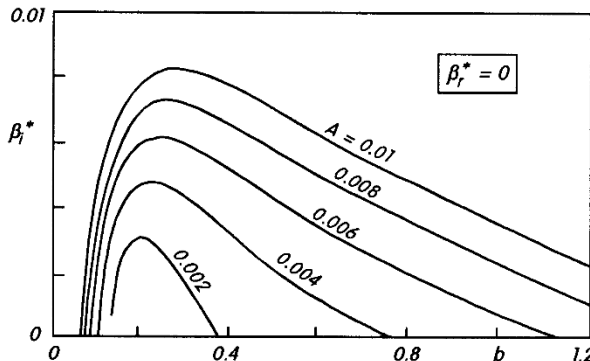


Fig. 15.42. Subharmonic amplification of the secondary instability plotted against the wave number $b = -10^3 \alpha^*/\text{Re} = -2\pi 10^3 / (\text{Re}\lambda^*)$, after T. Herbert (1984)
 $F = 10^6 \alpha^* c_r / \text{Re} = 10^6 \beta_r / \text{Re} = 124$
 $A = \text{amplitude of the Tollmien-Schlichting waves}$

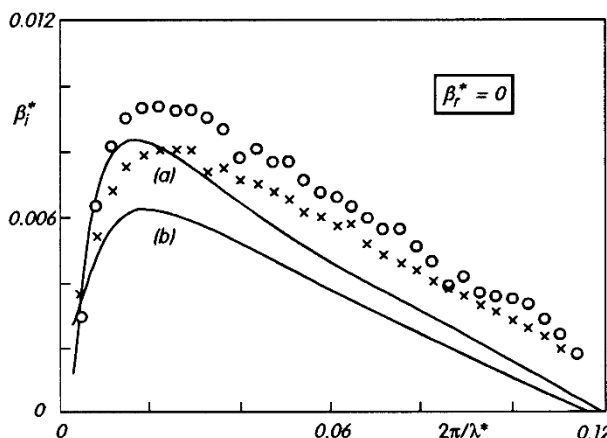


Fig. 15.43. Subharmonic amplification of the secondary instability plotted against the wave number in the perpendicular direction, $F = 58.8$; $\text{Re} = 950$; $A = 0.014$ theory according to T. Herbert (1988)
(a) subharmonic, (b) harmonic
numerical simulations by P.R. Spalart; K.S. Yang (1986):
○ subharmonic, × harmonic

(1986). The results show that the subharmonic secondary instability is more strongly amplified than the harmonic. The differences between the results from stability theory and the numerical simulations can be explained by differing theoretical approaches, although the qualitative dependence on the wave number agrees well. It can be concluded from the results that the subharmonic perturbations are more unstable than the harmonic.

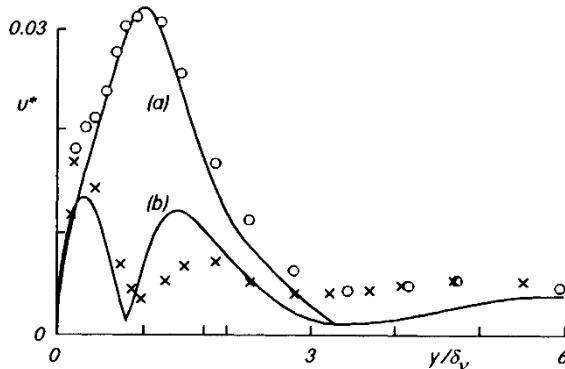


Fig. 15.44. Dimensionless distribution of u^* perturbations for the subharmonic eigenmotion $F = 124$; $b = 0.38$; $\text{Re} = 608$; $A = 0.0122$; $\delta_\nu = \sqrt{x\nu/U}$
Theory, after T. Herbert (1988)
Experiment, after P.S. Klebanoff et al. (1962)
(a) \circ oscillation maximum (b) \times oscillation minimum

The proof of the validity of secondary stability theory is shown in Fig. 15.44 as a comparison with the experimental results of P.S. Klebanoff et al. (1962).

For a more detailed description of laminar-turbulent transition in the boundary layer, reference may also be made to R. Narasimha (1985), V. Boiko et al. (2002) and T. K. Sengupta (2012).

The combination of stability theory and experiment has been able to advance our understanding of the origin of turbulence in certain broad classes of flows, as the boundary layers. However, there are other circumstances for which linear stability is an unsuitable starting point for understanding the onset of turbulence. In those instances the onset of turbulence is sudden, and a fundamentally different sequence of events is involved. In particular, the many scales of turbulence appear more or less at the same time. Flow through pipes is an excellent example of this kind of transition. Typically, flows of this kind are stable to all linear perturbations, and one of their strong characteristics is that the transition has no reproducible critical Reynolds number, as would be characteristic of linear instability.

In shear flows, experiments show that the transition does not usually wait until the critical Reynolds number is reached, but occurs at lower Reynolds numbers. The mechanism of transition in these cases is called subcritical because it occurs below the linear stability value, see S. Grossmann (2000). Linear disturbances of shear flows could grow for some time even if they are stable, since the concept of stability is related to the asymptotic growth of perturbations.

Figure 15.45 shows a schematic plot of subcritical transition. With increasing initial disturbance amplitude A the transition to turbulence occurs at smaller Reynolds numbers Re_{ind} . The transition line should be interpreted as the envelope of all stability lines for possible types of disturbances.

The transition process can be divided into different stages, corresponding to Fig. 15.5.

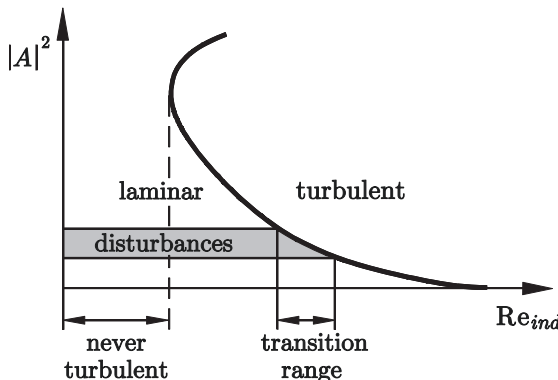


Fig. 15.45. Subcritical transition

The first is usually called the receptivity stage, which is associated with disturbances in the flow. Receptivity is often the most difficult process to conclude the transition prediction for realistic flow situations. It entails knowledge about the ambient disturbance environment and the mechanisms by which disturbances are projected into growing eigenmodes.

The next stage is the linear growth stage of primary instabilities as Tollmien-Schlichting waves in the boundary layer, where small disturbances are amplified until they reach a size where nonlinear interactions become important. This amplification can be in the form of exponential growth of eigenmodes, nonmodal growth of optimal disturbances, or nonmodal response to forcing.

Once a disturbance has reached a finite amplitude, it often saturates and transforms the flow into a new state. Only in a few cases does the primary instability lead the flow directly into a turbulent state. Instead, the new unstable flow becomes a base flow on which secondary instabilities can grow. The secondary instability can be viewed as a new instability of a more complicated flow. This stage of the transition process is in many cases more rapid than the stage where primary instabilities prevail.

The last stage is the breakdown stage where nonlinearities and higher order instabilities excite an increasing number of scales and frequencies in the flow. This stage is often more rapid than both the linear stage and the secondary instability stage.

Dividing the transition process into stages of receptivity, linear growth, nonlinear saturation, secondary instability, and breakdown certainly idealizes the transition process, because all stages cannot always be expected to occur in an unambiguous manner. However, they often provide a good framework to view transition even for complicated flows.

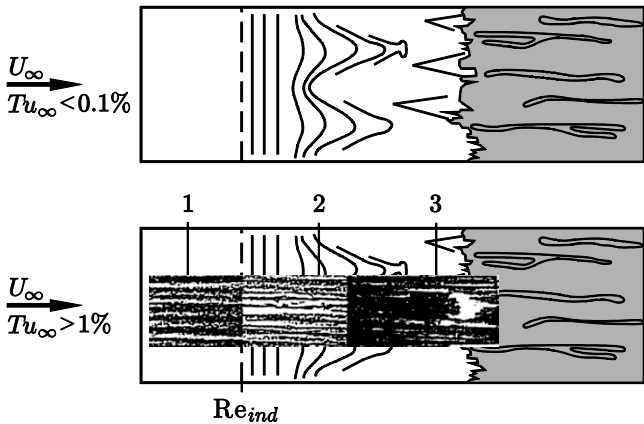


Fig. 15.46. Transition scenario at low and high free-stream turbulence.

Figure 15.46 shows an example of a transition scenario at high free-stream turbulence level in comparison with the flat plate transition process described in Fig. 15.5. In the first stage the formation of streaks by free-stream-localized vortical disturbances in the boundary layer can be observed in experiments, see J.H.M. Franssen et al. (2005). The streaks modulate the boundary layer in the spanwise direction. The second stage includes the following streak development accompanied by the generation of high-frequency wave packets and incipient spots due to different nonlinear mechanisms including the interaction with Tollmien-Schlichting waves and secondary instabilities. The third stage of the transition includes development and interaction of turbulent spots which completes the laminar-turbulent transition in the boundary layer.

15.3.3 Boundary Layers at Curved Walls

Boundary layers at curved walls (centrifugal force). The effect of curvature at the wall is rather important in technical applications. H. Görtler (1940a) presented a generalisation of the Tollmien instability criterion for points of inflection to this end. The Tollmien law which states that in the limit of very large Reynolds numbers (inviscid flow), velocity profiles at flat walls with a sign change of d^2U/dy^2 are unstable, assumes the following form for curved walls: a change of sign of

$$\left(\frac{d^2U}{dy^2} + \frac{1}{R} \frac{dU}{dy} \right) \quad (15.49)$$

causes the inviscid instability. Here R is the radius of curvature of the wall, where $R > 0$ indicates convex and $R < 0$ concave walls. Thus the instability with respect to two-dimensional perturbations occurs just in front of the pressure minimum for convex walls, and just behind the pressure minimum for concave walls (stabilising). In general however, the effect of the

wall curvature in boundary-layer flows where the ratio $\delta/|R| \ll 1$ holds (δ = boundary-layer thickness) is very small. For concave walls a completely different kind of instability with respect to certain three-dimensional perturbations is considerably more important, as will be discussed in what follows.

Boundary layers at concave walls. Although the effect of the centrifugal force at concave walls with respect to two-dimensional disturbances is stabilising, it was shown by H. Görtler (1940b) that the effect of the centrifugal force on the boundary layer at concave walls leads to an instability with respect to three-dimensional disturbances. For a basic flow $U(x, y)$, $V(x, y)$ (y = distance from the wall, z = perpendicular direction to the basic flow in the plane of the wall), we assume a disturbance of the form

$$\begin{aligned} \frac{u}{U_\infty} &= U(x, y) + u'(x, y, z); \\ \frac{v}{U_\infty} &= V(x, y) + \frac{\nu}{\delta_\nu U_\infty} v'(x, y, z); \\ \frac{w}{U_\infty} &= w'(x, y, z); \\ \frac{p}{\rho U_\infty^2} &= P(x, y) + \frac{\nu^2}{\delta_\nu^2 U_\infty^2} p'(x, y, z). \end{aligned} \tag{15.50}$$

This yields the perturbation differential equations (cf. J.M. Floryan; W.S. Saric (1979, 1982))

$$\begin{aligned} \frac{\partial u'}{\partial x} + \frac{\partial v'}{\partial y} + \frac{\partial w'}{\partial z} &= 0 \\ u' \frac{\partial U}{\partial x} + U \frac{\partial u'}{\partial x} + v' \frac{\partial U}{\partial y} + V \frac{\partial u'}{\partial y} &= \frac{\partial^2 u'}{\partial y^2} + \frac{\partial^2 u'}{\partial z^2} \\ u' \frac{\partial V}{\partial x} + U \frac{\partial v'}{\partial x} + v' \frac{\partial V}{\partial y} + V \frac{\partial v'}{\partial y} + 2 \text{Gö}^2 U u' &= -\frac{\partial p'}{\partial y} + \frac{\partial^2 v'}{\partial y^2} + \frac{\partial^2 v'}{\partial z^2} \\ U \frac{\partial w'}{\partial x} + V \frac{\partial w'}{\partial y} &= -\frac{\partial p'}{\partial z} + \frac{\partial^2 w'}{\partial y^2} + \frac{\partial^2 w'}{\partial z^2}. \end{aligned} \tag{15.51}$$

Here the coordinates in the perpendicular direction in the plane and the normal direction to the plane were related to $\delta_\nu = \sqrt{\nu x/U_\infty}$ while the x coordinate, because of the slow downstream development, is related to $\text{Re} \cdot \delta_\nu$. The only parameter in the system of equations (15.51) is the square of the Görtler number

$$\text{Gö} = \frac{U_\infty \delta_\nu}{\nu} \sqrt{\frac{\delta_\nu}{R}}, \tag{15.52}$$

which is a measure of the local radius of curvature $R > 0$ of the concave wall.

Although the parallel-flow assumption $V = 0$ is not permissible here, cf. P. Hall (1982) and J.M. Floryan (1991), assuming that U, V and P are independent of x , we can use a local wave ansatz:

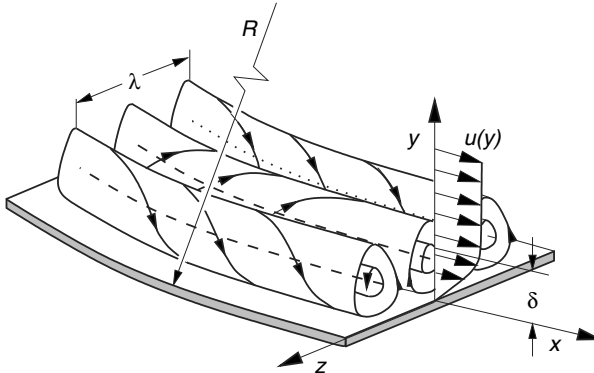


Fig. 15.47. Görtler vortices in the boundary layer at a concavely curved wall

$U(y)$ — basic profile

δ — boundary-layer thickness

λ — wavelength of primary perturbation

$$\begin{aligned} u'(x, y, z) &= U(y) \cos(\alpha z) \cdot e^{\beta x} \\ v'(x, y, z) &= V(y) \cos(\alpha z) \cdot e^{\beta x} \\ p'(x, y, z) &= P(y) \cos(\alpha z) \cdot e^{\beta x} \\ w'(x, y, z) &= w^*(y) \sin(\alpha z) \cdot e^{\beta x}. \end{aligned} \quad (15.53)$$

The real quantity β is the spatial amplification ($\beta > 0$) or damping ($\beta < 0$), while $\lambda = 2\pi/\alpha$ is the wavelength of the perturbation perpendicular to the main flow direction. Thus the perturbation has the form shown in Fig. 15.47, where the vortex axes are parallel to the basic flow. In contrast to Tollmien–Schlichting waves, these waves here are *standing waves*.

The computation of the spatial amplification of these *three-dimensional* disturbances leads to an eigenvalue problem. The first approximate solution to the *temporal* eigenvalue problem was presented by H. Görtler (1940b). Further development of the theory can be found in H. Görtler (1955a). F. Schultz–Grunow; D. Behbahani (1973) constructed a more precise theory by taking all first order terms into account.

Experiments on boundary layers on bodies with both convex and concave walls carried out by F. Clauser (1937) and H.W. Liepmann (1943a, 1945) have verified the transition to turbulent flow. Figure 15.48 shows some results by H.W. Liepmann based on both concave and convex walls. Figure 15.48a confirms the theoretical prediction that the effect of the wall curvature on the critical Reynolds number is small for convex walls, and that the critical Reynolds number is smaller for concave walls than for convex walls. In Fig. 15.48b we see the parameter $(U_\infty \delta_{2 \text{ crit}} / \nu) \sqrt{\delta_{2 \text{ crit}} / R}$, which is equal to the Görtler number up to a numerical factor, plotted against δ_2 / R .

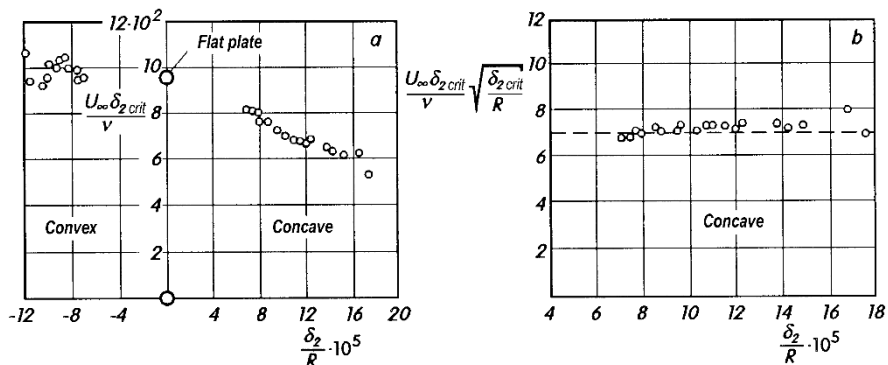


Fig. 15.48. Measurements of the position of completed transition (index crit) at weakly curved walls, after H.W. Liepmann (1943a, 1943b)

- (a) critical Reynolds number $Re_{2\text{crit}} = U_\infty \delta_{2\text{crit}} / \nu$
- (b) Görtler number $G_o2 = (U_\infty \delta_{2\text{crit}} / \nu) \sqrt{\delta_{2\text{crit}} / R}$

The transition occurs for

$$\frac{U_\infty \delta_{2\text{crit}}}{\nu} \sqrt{\frac{\delta_{2\text{crit}}}{R}} > 7. \quad (15.54)$$

See also the experimental investigations by H. Bippes (1972) and A. Ito (1987).

H. Görtler has pointed out that this instability can also occur close to the forward stagnation point of a body in a flow. The condition that the streamlines be concave on the side of increasing velocity is valid here. The calculations carried out by H. Görtler (1955b) and G. Hämmerlin (1955) for plane stagnation point flow did indeed yield unstable perturbations, but no critical Reynolds number as a limit of stability.

The same is also true for the concave streamlines in the region where a separated flow reattaches itself to flat and curved surfaces. In addition J.M. Floryan (1986, 1991) indicates that if a non-monotonic velocity profile is at hand there is also the possibility of Görtler instabilities at convex walls. Secondary instabilities of the primary Taylor-Görtler instabilities at concave curved walls have been investigated experimentally by I. Tani (1962), I. Tani; J. Sakagami (1964), I. Tani; Y. Aihara (1969), F.X. Wortmann (1969) and W.S. Saric (1994).

The theory of secondary Taylor-Görtler instabilities has only been developed in recent years. T. Herbert (1988), M.R. Malik; M.Y. Hussaini (1990), A.H. Nayfeh (1981), K.M. Srivastava (1985), K.M. Srivastava; U. Dallmann (1987) and A.H. Nayfeh; A. Al-Maaitah (1987) have extended the predictions of stability theory with numerical simulations of the transition process. Until now these have been restricted to two-dimensional boundary-layer flows taking concave surface curvature into account. The results indicate that the secondary unstable transition process is initiated via *vortex stretching* of the

primary Taylor–Görtler vortices with a periodically superimposed meander shaped longitudinal structure. These wave instabilities have a similar character to the secondary instabilities in the classic stability problems of *G.I. Taylor* (Couette flow with curvature) and of *Rayleigh–Bénard* (unstable horizontal stratification) which also indicate periodic longitudinal deformation coupled with a vortex stretching.

15.3.4 Boundary Layer at a Rotating Disk

Let us study the extension of the two-dimensional boundary layer as a basic flow to three dimensions in the example of a rotating disk. Figure 5.8 shows a sketch of the three-dimensional basic flow. The instability of this flow is shown in Fig. 15.49 in a photo by N. Gregory et al. (1955). Standing vortices in the form of logarithmic spirals form in a ring shaped region $R_i < r < R_o$ more or less along the streamlines of the basic flow. We shall call these primary instabilities of the three-dimensional boundary-layer flow *cross-flow instabilities*. The inner radius R_i of the unstable ring denotes the position of the onset of turbulence. The outer radius R_o indicates the region of secondary instabilities and thus the laminar–turbulent transition in the three-dimensional boundary layer. J.T. Stuart (see N. Gregory et al. (1955)) has carried out a theoretical stability investigation of this flow. Periodic trial solutions were chosen as three-dimensional disturbances. Special cases of these are the marching plane Tollmien–Schlichting waves and the standing three-dimensional Taylor–Görtler vortices which describe the effect of the centrifugal forces. The results are in qualitative agreement with the experimental discoveries in Fig. 15.49. Newer results of the stability analysis in rotating boundary layers show that the onset of cross flow instability is absolutely unstable (R.J. Lingwood (1995, 1996)).

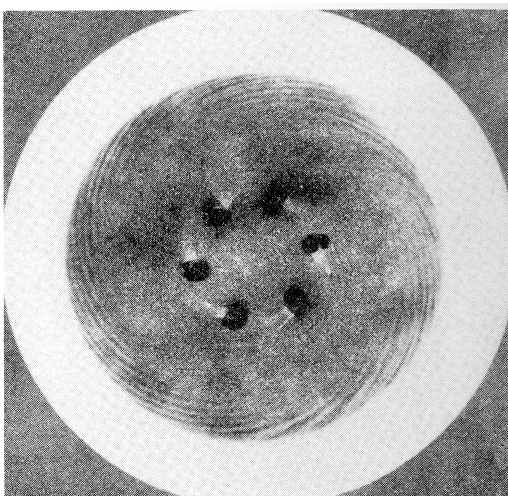


Fig. 15.49. Flow portrait of the laminar–turbulent transition in the boundary layer on a disk rotating in a fluid at rest, after N. Gregory et al. (1955) Anticlockwise motion, $N = 3200$ revs per min; disk radius 15 cm. Standing vortices form in a ring shaped region (inner radius $R_i = 8.7$ cm, outer radius $R_o = 10.1$ cm). Inner radius is the limit of stability at $Re_i = R_i^2 \omega / \nu = 1.9 \cdot 10^5$. Outer radius yields completed transition at $Re_o = R_o^2 \omega / \nu = 2.8 \cdot 10^5$

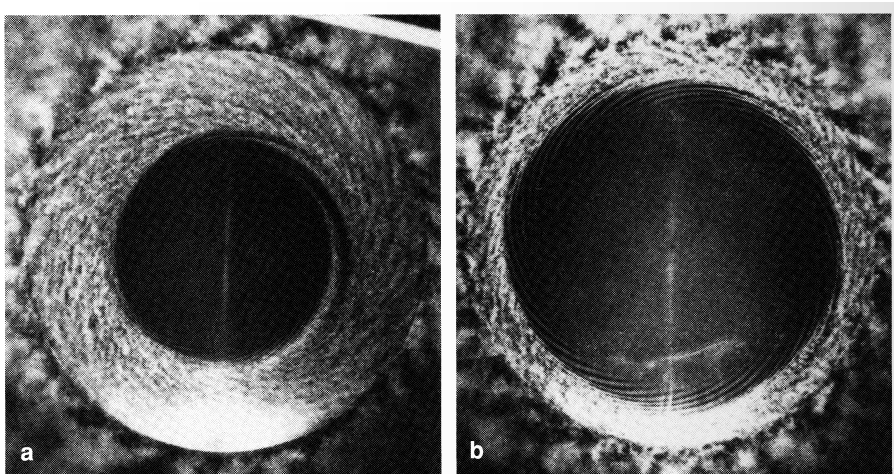


Fig. 15.50. Flow portraits of the transition in the boundary layer on a rotating disk, after Y. Kohama (1987b), $R_o = 200 \text{ mm}$;

(a) $\omega = 524 \text{ s}^{-1}$, (b) $\omega = 199 \text{ s}^{-1}$

Indifference Reynolds number for the onset of primary cross-flow instabilities

$$Re_{ind} = R_o^2 \omega / \nu = 8.8 \cdot 10^4$$

The transition region and the onset of secondary instabilities have been experimentally determined by Y. Kohama (1987b). The centrifugal forces perpendicular to the curved streamlines cause the secondary velocity components, which themselves cause the cross-flow instability. This secondary flow in the boundary layer is observed as an additional velocity component in the direction of the wall. This results in steady vortices rotating in the opposite direction. These are shown in Fig. 15.50 as streaklines produced by

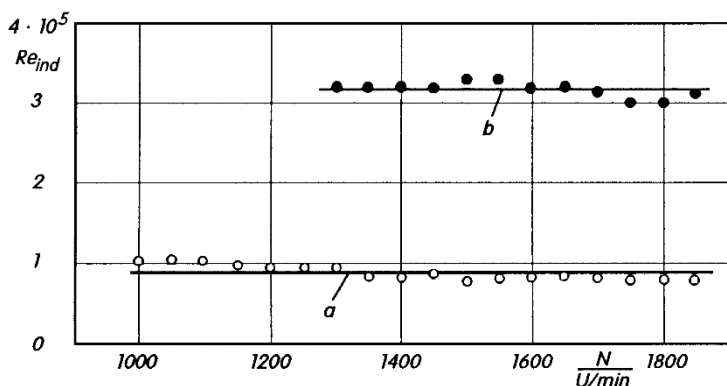


Fig. 15.51. Indifference Reynolds number Re_{ind} for the onset of primary (a) and secondary (b) cross-flow instabilities in the boundary layer on a rotating disk, after R. Kobayashi et al. (1980)

smoke. The experiments show that the transition to turbulent flow in the three-dimensional boundary layer is initiated by secondary ring vortices superimposed on the primary transverse instabilities, cf. Y. Kohama (1987b). The dependence of the indifference Reynolds numbers for primary and secondary cross-flow instabilities on the number of revolutions N is shown in Fig. 15.51.

15.3.5 Three-Dimensional Boundary Layers

The last sections described secondary stability theory for two-dimensional incompressible boundary layers, the effect of curvature and the appearance of cross-flow instabilities in a three-dimensional boundary layer. In this section we will treat the simplest case of secondary stability theory for a general given boundary layer with velocity components $U(y)$, $W(y)$. Again we assume that the classic parallel-flow assumption required for the Orr-Sommerfeld equation is approximately valid at the chosen position of the local stability analysis. This condition is satisfied for boundary layers on high aspect ratio wings to which we will restrict ourselves in this section.

Cross-flow instabilities were first observed experimentally by W.E. Gray (1952). Experimental work on the stability of three-dimensional boundary layers on swept-back wings has been carried out by W.S. Saric; L.G. Yeates (1985) and H. Bippes; P. Nitschke-Kowsky (1987).

The theoretical formulation of the corresponding linear stability problem has been treated by N. Gregory et al. (1955). Further developments have been presented by L.M. Mack (1984, 1988), H. Oertel Jr.; J. Delfs (1995, 2005).

Figure 15.52 shows a basic sketch of the boundary-layer profile under consideration and the region between the primary instabilities and the turbulent boundary-layer flow on the wing. Free flight experiments show that the Tollmien-Schlichting transition (TSI) treated in Sect. 15.2.4 dominates for non-swept-back wings in the subsonic region. Figure 15.52 also shows that local disturbances on the wing in the unstable region of the boundary

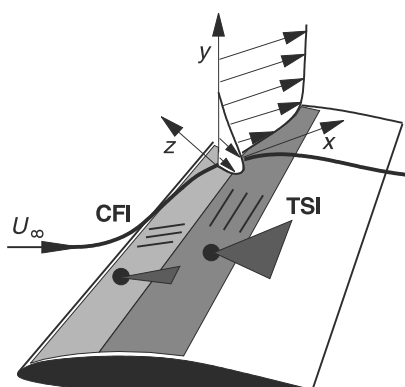


Fig. 15.52. Sketch of the different instabilities in the three-dimensional boundary layer on a swept-back wing
 TSI: Tollmien-Schlichting instabilities
 CFI: cross-flow instabilities

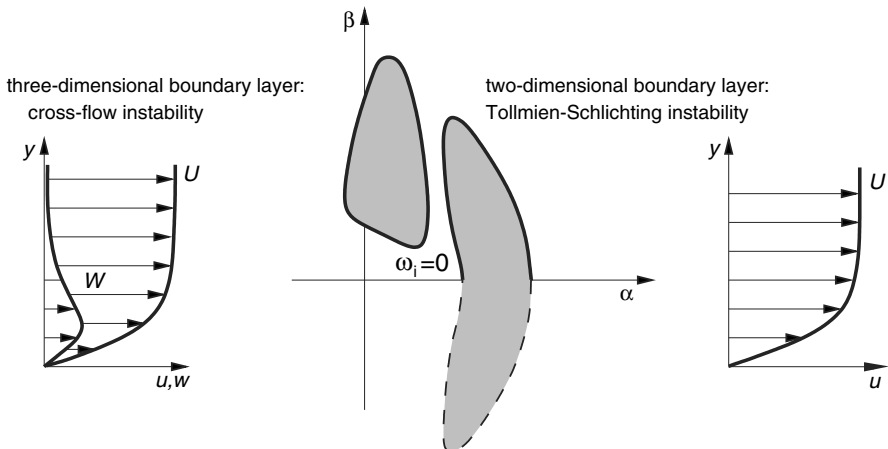


Fig. 15.53. Unstable waves for boundary layers with and without cross-flow component $W(y)$

layer lead to an abrupt laminar-turbulent boundary-layer transition in the form of a wedge of turbulence.

The superposition of cross-flow instabilities (CFI) only occurs on wings in the transonic region which are swept back. This is due to the additional pressure gradient along the wing and the fact that the boundary layer then becomes three-dimensional.

A third kind of instability at the attachment line in the nose region of a wing has been treated experimentally by W. Pfenninger (1965) and D.I.A. Poll (1979) and theoretically by P. Hall et al. (1984).

Which waves have cross-flow instabilities is shown in the wave number diagram, Figure 15.53, using the instability region for fixed Reynolds number. The Tollmien-Schlichting waves occur downstream only when the critical Reynolds number is exceeded. Note, however, that the Reynolds number in this regime is very small, and therefore there is a strong friction effect, in this case dampening. For comparison an instability region for the two-dimensional velocity profile $U(y)$, such as that which occurs for the flat plate boundary layer, is also included. It is typical that in two-dimensional boundary layers instability waves with considerably larger lateral direction angles $\varphi = \arctan(\beta/\alpha)$ exist than in the three-dimensional boundary layer. Because of its characteristic form, the indifference curve $\omega_i = 0$ in the wave number diagram for two-dimensional boundary layers is also called a kidney curve.

Equally typical for cross-flow instabilities is the appearance of standing perturbation vortices. As the angular frequency of these (standing) perturbation waves is $\omega_r = 0$, they are also called *zero-Hertz modes*. Their wave normal is almost perpendicular to the downstream direction at the edge of the boundary layer. In contrast to the Görtler longitudinal vortices, they rotate in the same direction. These standing waves can be made visible in experiment, with, for example, smoke introduced into the flow, and have a clear structure

in the downstream direction (see Fig. 15.54). The perturbation waves which are amplified the most are, however, generally unsteady and travel at a large angle φ , i.e. transverse to the downstream direction x . Figure 15.55 shows the streamlines of the eigensolution of the steady cross-flow vortex of the eigenvalue problem for a given three-dimensional boundary-layer flow. The theoretical results are in good agreement with D. Arnal et al. (1984) and H.L. Reed (1985).

We develop the theory of the secondary instabilities of the primary Tollmien–Schlichting waves (TSI) and the cross-flow instabilities (CFI) from Eq. (15.42) to (15.48). The extension of Eq. (15.42) reads

$$\begin{aligned} u_P(x, y, z, t) &= U(y) + u'(x, y, z, t), \\ v_P(x, y, z, t) &= v'(x, y, z, t), \\ w_P(x, y, z, t) &= W(y) + w'(x, y, z, t), \\ p_P &= P(x, y, z) + p'(x, y, z, t). \end{aligned} \quad (15.55)$$

The index P denotes the perturbations of the primary Tollmien–Schlichting instabilities or cross-flow instabilities. The boundary layer at the perturbation under consideration, which is generally computed numerically, has velocity components $U(y)$ and $W(y)$.

The ansatz for the secondary Tollmien–Schlichting instabilities and the cross-flow instabilities reads, according to Eq. (15.43)

$$u_S = u_P + u^*, \quad v_S = v_P + v^*, \quad w_S = w_P + w^*, \quad p_S = p_P + p^*. \quad (15.56)$$

Again neglecting quadratic terms in the disturbances u^* , v^* , w^* , p^* , we obtain linear perturbation differential equations for these quantities. These are given by T. Herbert (1988), A.H. Nayfeh (1987) and H. Oertel Jr. (1995). Again

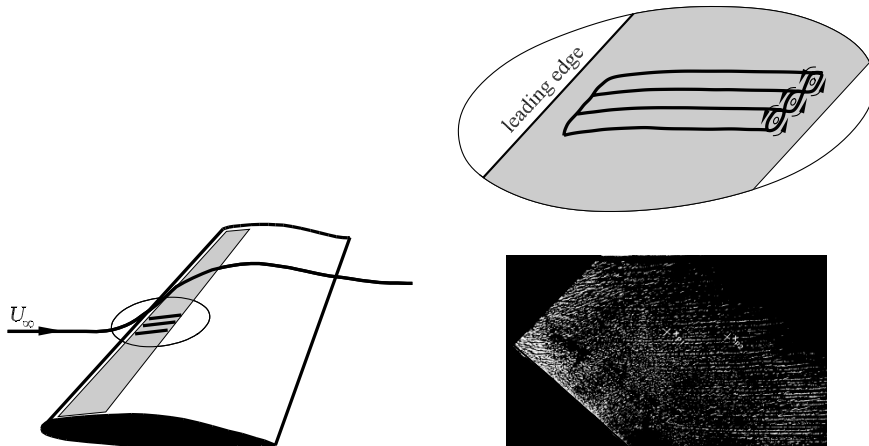


Fig. 15.54. Cross-flow instability in a three-dimensional boundary layer, Y. Ko-hama (1987a)

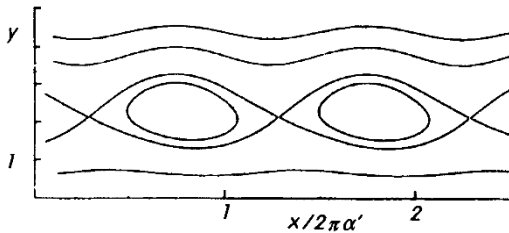


Fig. 15.55. Streamlines of the steady cross-flow vortices in a cut along the direction of expansion of the primary perturbation and perpendicular to the wall.

$$\sigma_r = 1/4, \vec{v} = \vec{V} + \varepsilon' \vec{v}', \varepsilon' = 0.069$$

we use the coordinate ξ from Eq. (15.44), where c can be either the phase velocity c_{TS} of the Tollmien–Schlichting wave or the phase velocity c_{CF} of a mode in a cross-flow instability. In the case of a standing wave, $\xi = x$ is the direction perpendicular to the wave front. Here y is the direction normal to the wave and z the coordinate perpendicular to ξ in the plane of the wall.

The wave ansatz for three-dimensional perturbations in Eq. (15.46) with the given boundary conditions, leads again to an eigenvalue problem which has to be solved numerically. Note that the (weak) spatial amplification of a primary steady cross-flow instability ($c_{CF} = 0$) can approximately represented in time dependent stability theory, cf. A.H. Nayfeh; A. Padhye (1979).

The sequence of instantaneous streamlines of the entire unstable flow field in sections perpendicular to the primary cross-flow vortices is shown in Fig. 15.56. It turns out that the secondary perturbation wave oscillates about the primary cross-flow vortices and periodically waxes and wanes. This periodic fluctuation computed using stability theory is consistent with hot-wire measurements by W.S. Saric; L.G. Yeates (1985). It initiates the laminar–turbulent cross-flow transition in three-dimensional boundary layers just as the Λ -vortices of the Tollmien–Schlichting instabilities do in two-dimensional boundary-layer flows.

In addition to the stability analysis, direct simulation of the transition process up to turbulent boundary-layer flow by numerical solution of the Navier–Stokes equations is also performed. Figure 15.57 shows the simulation results of the *Tollmien–Schlichting transition* and the *transition of the cross-flow vortices* in a three-dimensional wing boundary layer at Mach number $M_\infty = 0.62$ and Reynolds number $Re_L = 26 \cdot 10^6$. Contour surfaces of the rotation $\vec{\omega} = \nabla \times \vec{v}$ are shown. The transition process of the Tollmien–Schlichting waves begins with plane downstream travelling waves. As in Figure 15.5, three-dimensional perturbations are superimposed and Λ -structures (fundamental transition type) form. The Λ -structures are regions of local shearing and excess velocity in the peaks. They are lined up periodically in the span and form several rows ordered periodically behind each other. The occurrence of the Λ -structures is associated with the appearance of high free shear

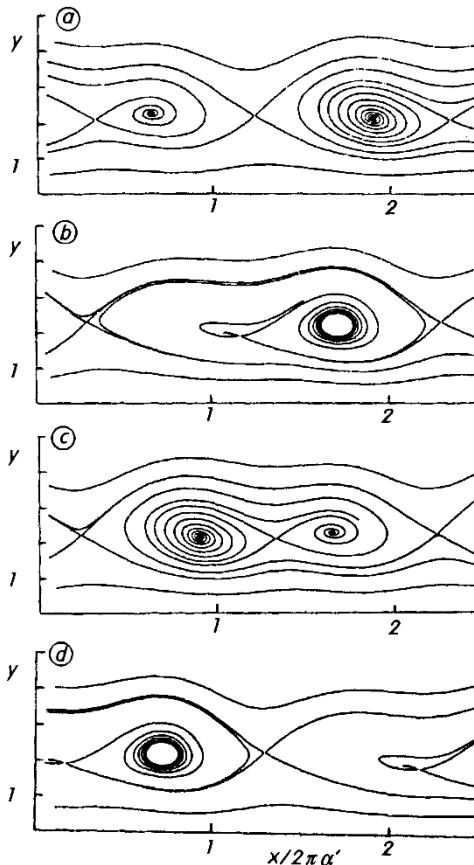


Fig. 15.56 a-d. Instantaneous streamlines of the secondary cross-flow waves in sections along the direction of expansion of the primary disturbances and perpendicular to the wall, after T.M. Fischer; U. Dallmann (1987), $\varepsilon' = 0.069$, $\varepsilon^* = 0.05$
a, b, c, d: sequence of a period along the primary cross-flow vortices
 $\vec{v} = \vec{V} + \varepsilon' \vec{v}' + \varepsilon^* \vec{v}^*$

layers. These are prominent local maxima of the shear stress far from the wall (Fig. 15.41). As the transition proceeds, the high shear rates decay into increasingly smaller structures, leading to the turbulent end state. The decay of the shear layers takes place within wavelengths of the Tollmien-Schlichting waves.

The mechanisms of the transition process of cross-flow vortices are similar. The formation of the Λ -structures are associated with high shear rates and fluctuation in the perturbation quantities in the peaks. In the final state of the transition they decay within a short distance into the turbulent boundary-layer flow.

In addition to transition experiments, direct flow simulation of the transition processes can be exploited to investigate *nonlinear transition processes* such as the effect of initial conditions. The laminar-turbulent transition is influenced by disturbances in the free stream such as sound waves or turbulence. Additional fluctuations are superimposed onto the basic unperturbed boundary layer. These fluctuations accelerate or decelerate the amplification

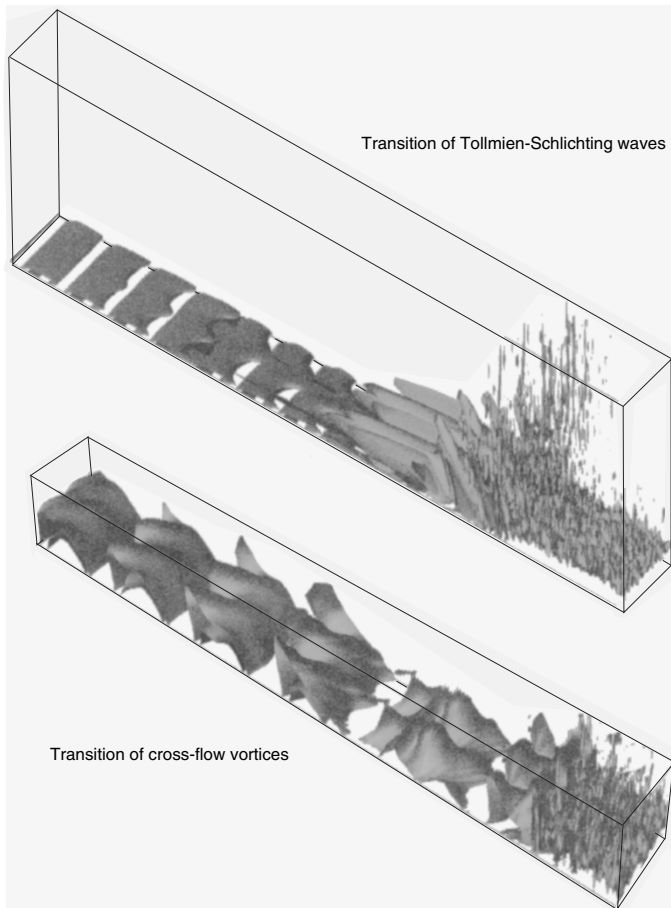


Fig. 15.57. Laminar-turbulent transition in the compressible wing boundary layer, $M_\infty = 0.62$, $Re_L = 26 \cdot 10^6$

of three-dimensional perturbation waves and hence are also a factor in determining the size of the transition region. M.V. Morkovin in H.J. Obremski et al. (1969) and M.V. Morkovin (1988) and E. Reshotko in U. Goldberg; E. Reshotko (1984) have named the influencing of the transition region by perturbations in the free stream *receptivity*. The perturbations in the free stream determine the amplitude, frequency and phase of the initial conditions. Results in this area have been summarized by M.E. Goldstein; L.S. Hultgren (1989) and W.S. Saric et al. (1984, 2003) as well as in AGARD (1994).

If the amplitude of the initial perturbation exceeds a certain value the weakly amplified perturbations of the linear stability theory can be *by-passed*, and three-dimensional perturbations of secondary instabilities or turbulent spots are then directly amplified. M.V. Morkovin (1988) was the first to

refer to this process. U. Goldberg; E. Reshotko (1984), E. Reshotko (1986, 1994, 1997) and others have also discussed the *by-passed transition* caused by surface roughness and turbulence in the free stream.

However, the theory of these nonlinear transition mechanisms is not the subject of this chapter which is restricted to the local linear stability theory of primary and secondary instabilities.

15.4 Local Perturbations

In the previous sections on primary stabilities, we explained in detail how the instabilities in a flow can be investigated using monochromatic wave disturbances as a base. Here we did not consider that every physically realisable perturbation appears as the response to a spatial (and generally temporal) localised stimulus. Since the monochromatic wave disturbances in classical stability analysis are by definition spatially infinitely extended, they do not initially represent the properties of a spatially limited disturbance (or *wave packet*). Rather the localised perturbation consists, according to J.B. Fourier, of a continuum of modes, that is, a group of waves. Hydrodynamic instabilities represent disturbances to the vorticity field, and their phase velocity $c = \omega/\alpha$ depends on the wavelength $\lambda = 2\pi/\alpha$. This so-called dispersive wave expansion obviously implies that a wave packet coming from a local perturbation stimulus “decays” over time.

A very important conceptional advantage of considering wave packets instead of monochromatic single perturbations is that the perturbation energy is localised in the wave packet. Therefore it is possible to determine the transport (directions and velocities) of the perturbation energy as well as the damping of the perturbation. Considering unstable flows in the framework of wave packet dynamics means we are almost forced to divide up the flows as follows. If the perturbation wave packet which is unstable and thus taking in energy leaves the position of stimulation asymptotically in time, the flow is *convectively unstable*. On the other hand, if there are unstable parts of the wave packet which remain at the position of disturbance (i.e. no energy transport) then the flow is *absolutely unstable*.

It is known from the theory of dispersing waves that the perturbation energy is transported with the *group velocity* $c_g = \partial\omega/\partial\alpha$ and not with the phase velocity of the waves. Note that in three-dimensional boundary layers it is not only the magnitude of the group and phase velocities which differs but also the directions.

We will avoid the details of the mathematical description of the dynamics of local perturbations here. The theory is treated comprehensively in connection with instabilities in plasma jets by R.J. Briggs (1964). It has been carried over to shear flows by M. Gaster (1968) (wave packets), W. Koch (1985), P. Huerre; P.A. Monkewitz (1985, 1990), R.J. Deissler (1987), K. Han-

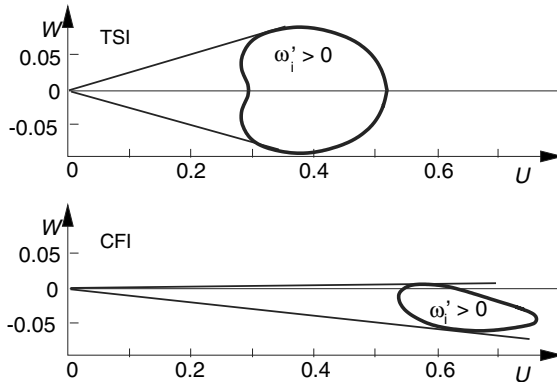


Fig. 15.58. Regions of relative temporal amplification of the Tollmien-Schlichting instabilities (TSI) and cross-flow instabilities (CFI) in the group velocity plane (U, W)

nemann; H. Oertel Jr. (1989), H. Oertel Jr. (1990, 2001, 2002, 2010, 2016), H. Oertel Jr.; J. Delfs (1995, 1996, 1997, 2005) and L. Brevoord (1991, 1993, 1995).

In what follows we will analyze the behavior of three-dimensional wave packets in a three-dimensional compressible boundary layer. In contrast to the investigation into two-dimensional perturbations, the transverse wave number β now also appears in the dispersion relation function $D(\omega, \alpha, \beta)$, whose roots are indeed given by those combinations (ω, α, β) which represent the solutions of the stability eigenvalue problem for complex ω, α, β . We consider the change in amplitude of a perturbation wave packet in the plane reference frame, moving with the group velocity (U, W) . The frequency observed is then

$$\omega' = \omega - \alpha \cdot U - \beta \cdot W . \quad (15.57)$$

As in the two-dimensional case, we again have to find those waves whose group velocity vector $(\partial\Omega/\partial\alpha, \partial\Omega/\partial\beta)$ is real. The complex frequency function $\Omega(\alpha, \beta)$ is then defined by $D(\Omega(\alpha, \beta), \alpha, \beta) = 0$. The relative temporal amplification ω'_i is then plotted, not just as a function of $U = \partial\Omega/\partial\alpha$, but also against the group velocity plane (U, W) . The line of height $\omega'_i = 0$ is of particular interest as it encloses that region in the (U, W) plane in which $\omega'_i > 0$. Therefore this region represents those parts of the perturbation which contribute time-asymptotically to the wave packet. Figure 15.58 contains diagrams with the regions of temporal amplification at two representative positions on a swept wing. The lower diagram in the figure shows a typical curve $\omega'_i = 0$, which is computed for a position close to the leading edge of a swept wing, i.e. in the cross-flow instability region. The upper diagram shows the same curve at a position further downstream on the wing, where Tollmien-Schlichting instabilities are present. We see that both instabilities have convective character, as in both cases the origin $(U, W) = (0, 0)$

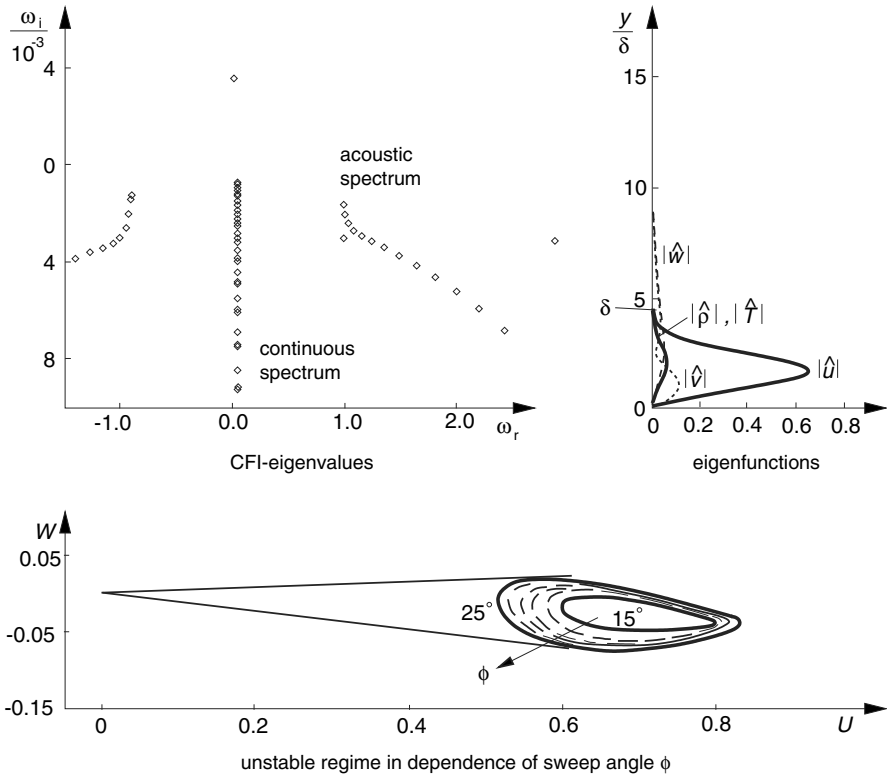


Fig. 15.59. Eigenvalues, eigenfunctions and unstable regions of the cross-flow instability in the compressible boundary layers of swept wings, $M_\infty = 0.87$, $Re_L = 26 \cdot 10^7$

is not contained in the $\omega'_i > 0$ region. The growing perturbation energy is transported downstream in both cases. The tangents at the curves $\omega'_i = 0$ determine the angular region within which these amplified perturbations remain. In the case of the cross-flow instabilities, the angular range is very narrow and lies essentially downstream. Note that the associated instabilities are waves which travel practically perpendicular to the downstream direction. This clearly indicates the fundamental difference between group velocity and phase velocity.

Now that we have determined that the cross-flow instabilities are convective in nature and that they induce a spatially extended transition process downstream, the associated spatial wave packet amplification rates ($g_{\max} = [(\omega_i - \alpha_i \cdot U - \beta_i \cdot W)/\sqrt{U^2 + W^2}]_{\max}$) for the transonic swept-wing boundary layer have been computed. Figure 15.59 shows the eigenvalues, eigenfunctions and unstable regions of wave packet perturbations for angles of sweep from 15° to 25°, H. Oertel Jr.; R. Stank (1999). In developing a swept laminar wing, it is essential to avoid cross-flow instabilities, as they

induce a transition process already directly at the leading edge. Using the methods of stability analysis, the region of the design parameters of a swept wing can be determined within which active influencing measures are not needed (natural laminar behavior). One of these parameters is the angle of sweep. In an otherwise identical free stream, there is a critical range of angle of sweep within which the transition process changes from TSI-dominated to CFI-dominated.

Part IV

Turbulent Boundary Layers

16. Fundamentals of Turbulent Flows

16.1 Remark

Most flows which occur in practical applications are turbulent. This term denotes a motion in which an irregular fluctuation (mixing, or eddying motion) is superimposed on the main stream. Figures 16.1a–d illustrate this. These are photographs of the turbulent flow in a water channel. The flow has been made visible by powder sprinkled on the surface. The flow velocity is the same in all four photos, but the camera is moved at different velocities along the axis of the channel. It can easily be deduced from the figures whether the longitudinal velocity of the fluid particles is larger or smaller than that of the camera. These figures give us a rather impressive idea of the complexity of turbulent flow.

The details of the fluctuating motion superimposed on the main motion are so hopelessly complex that to describe them theoretically seems futile. However the resulting mixing motion is of great importance for the course of the flow and for the balance of the forces. It causes the viscosity to seem tens of thousands of times greater than it actually is. At high Reynolds numbers, energy constantly flows from the basic flow to the large eddies. On the other hand the dissipation of the energy mainly takes place in the small eddies, in a narrow strip in the boundary layer in the neighbourhood of the wall. This is described by P.S. Klebanoff (1955) and will be shown in Sects. 16.3.3 and 17.1.2.

The turbulent mixing motion is important for the great drag of turbulent flows in pipes, for the friction drag encountered by ships and airplanes and for the losses in turbines and turbocompressors. On the other hand, it is only turbulence which makes a large pressure increase in diffusers or along airplane wings and compressor blades at all possible. In a laminar flow, one without turbulence, these flows would exhibit separation. Therefore only small pressure increases in diffusers would occur and the performance of wings and blades would be poor.

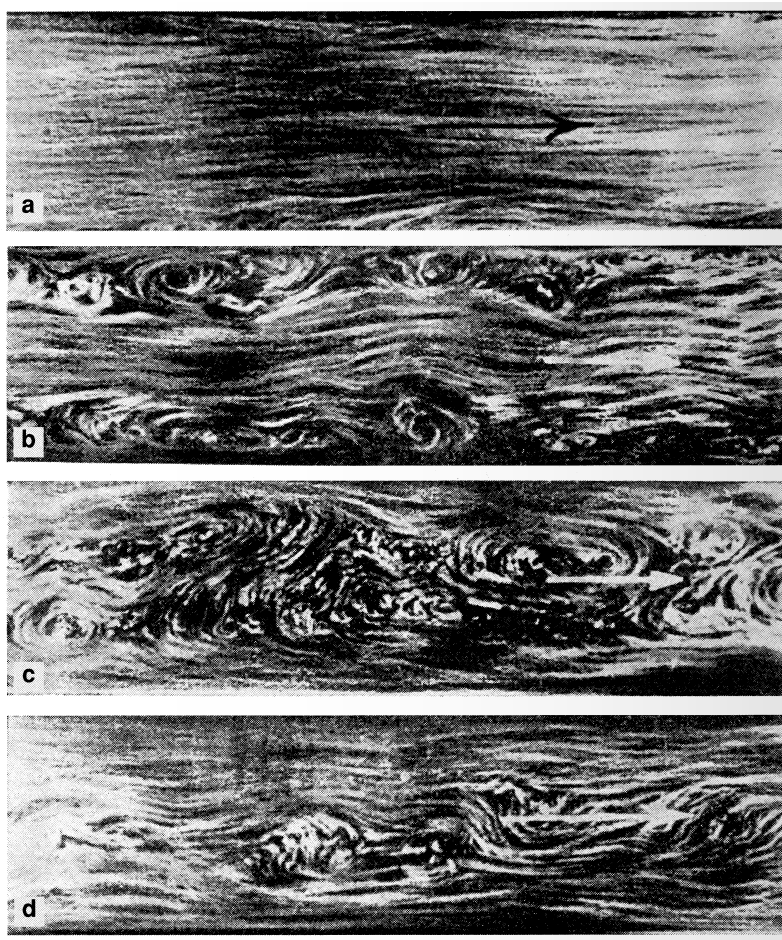


Fig. 16.1. Turbulent flow in a water channel 6 cm wide, shot with cameras moving at varying speeds. Taken by J. Nikuradse (1929), published by W. Tollmien (1931). Camera velocity: (a): 12.2 cm/s; (b): 20 cm/s; (c): 25 cm/s; (d): 27.6 cm/s

In the following chapters we will treat the *laws of fully developed turbulent flow*. Because of the complexity of the fluctuations, a purely numerical computation of turbulent flow has only been possible in a few special cases. Therefore in practice one makes do with determining the time average of the turbulent motion.

However fundamental difficulties arise in setting up equations of motion for the mean motion only. Since the turbulent fluctuations are strongly coupled with the mean motion, when we attempt to write down the basic equations for the mean motion by time averaging the Navier-Stokes equations, additional terms appear. These are determined by the turbulent fluctuations. These additional terms present additional unknowns for the computation of

the mean motion. In forming the time average of the Navier–Stokes equations therefore, we have more unknowns than equations. This will be seen later. In order to *close* the system of equations of motion, we require additional equations. These will connect the additional terms from the fluctuating motion with the velocity field of the mean motion. These equations can no longer be set up purely from the balances of mass, momentum and energy. Rather they are *model equations* which model the relation between the fluctuations and the mean motion. Setting up these model equations to close the system of equations is called *turbulence modelling* and is the central problem in computing the mean motion of turbulent flows.

In the following sections we derive the fundamental equations for the mean motion of turbulent flows. Since a *model* of the turbulent fluctuations is required to close the system of equations, some important basic concepts will be presented in Sect. 16.5.

16.2 Mean Motion and Fluctuations

When turbulent flow is analysed more closely, one striking characteristic noted is that the velocity and pressure at a fixed point in space do not remain constant in time but perform irregular fluctuations (cf. Fig. 15.15). Now the fluid elements which carry out fluctuations both in the direction of main flow and at right angles to this direction are not individual molecules, as assumed in kinetic gas theory, but rather are macroscopic “fluid balls” or “lumps” of varying small size called *eddies*. In the flow in a channel for example, the velocity fluctuations amount to only a very few percent of the average velocity, but they are still the deciding factor in the whole course of the motion. These fluctuations ought to be imagined in the following manner: certain large volumes of fluid are furnished with an intrinsic motion, and this is superimposed on the mean motion. Such eddies can easily be seen in the flow photos in Fig. 16.1b, c, d. These eddies continually appear and then disintegrate, and their size indicates the spatial extent of the eddies. Therefore the size of the eddies is determined by the external conditions of the flow, for example the mesh of a honeycomb through which the fluid flow has been passed. Some quantitative measurements of the magnitudes associated with such fluctuations will be presented in Sect. 16.5.

In natural winds, these fluctuations can easily be recognised as *squalls*. Here they frequently obtain a magnitude of 50% of the mean velocity. The size of the eddies in wind can be seen from the patterns formed in a field of corn for example.

In Chap. 15 we have already indicated that in computing a turbulent motion it is useful to decompose the motion into a *mean motion* and a *fluctuating motion*. If we denote the time average of the velocity components u as \bar{u} , and

the fluctuation velocity as u' , then the velocity components and the pressure may be written down as

$$u = \bar{u} + u'; \quad v = \bar{v} + v'; \quad w = \bar{w} + w'; \quad p = \bar{p} + p', \quad (16.1a,b,c,d)$$

as already given in Eq. (15.2). In compressible turbulent flows (Chap. 19), the density ϱ and the temperature T also fluctuate,

$$\varrho = \bar{\varrho} + \varrho'; \quad T = \bar{T} + T'. \quad (16.1e,f)$$

The average is formed as the time average at a fixed point in space, thus for example

$$\bar{u} = \frac{1}{t_1 - t_0} \int_{t_0}^{t_0+t_1} u dt. \quad (16.2)$$

This integral is to be taken over a sufficiently large time interval t_1 so that the average is independent of the time. The time averages of the fluctuating quantities are then zero by definition:

$$\bar{u}' = 0; \quad \bar{v}' = 0; \quad \bar{w}' = 0; \quad \bar{p}' = 0; \quad \bar{\varrho}' = 0; \quad \bar{T}' = 0. \quad (16.3)$$

Here and in what follows, we first assume that this *mean motion* is independent of the time. Such flows are then called *steady turbulent flows*. We will look at *unsteady turbulent flows* in Chap. 22.

The feature which is of fundamental importance for the course of the turbulent motion is that the fluctuations u' , v' , w' influence the progress of the mean motion \bar{u} , \bar{v} , \bar{w} so that the latter exhibit an apparent increase in the resistance against deformation. In other words, the fluctuating motion acts on the mean motion such that its viscosity is apparently increased. This increased *apparent viscosity* is the central concept of all theoretical considerations on turbulent flow. Therefore our first endeavour will be to acquire some insight into this.

In what follows it will prove useful to briefly present a few rules of computation which the time averages satisfy. If f and g are independent variables whose mean values are to be formed, and s is one of the independent variables x , y , z , t , the following rules apply:

$$\begin{aligned} \bar{\bar{f}} &= \bar{f}, & \overline{f+g} &= \bar{f} + \bar{g}, & \overline{\bar{f} \cdot g} &= \bar{f} \cdot \bar{g}, \\ \frac{\partial \bar{f}}{\partial s} &= \frac{\partial \bar{f}}{\partial s}, & \overline{\int f ds} &= \int \bar{f} ds. \end{aligned} \quad (16.4)$$

Before we derive the relation between the mean motion and the *apparent stresses* caused by the fluctuating motion, we present an illustration of the most important of these apparent stresses using the momentum-integral equation.

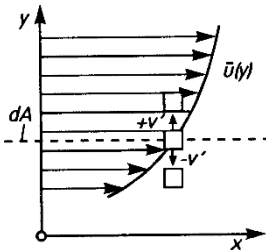


Fig. 16.2. Momentum transfer due to the turbulent fluctuation velocity

We consider a small surface dA in a turbulent stream with velocity components u, v, w . Its normal is parallel to the y axis, cf. Fig. 16.2. The surface dA is spanned by the directions x and z . The fluid mass flowing through this surface in time dt is $dA \rho v dt$. The x component of the momentum is therefore $dA \rho u v dt$. If we form the time average of the momentum, we find the average momentum flux (momentum per unit time) for constant density to be

$$d\bar{I} = dA \cdot \rho \bar{u} \bar{v}.$$

According to Eq. (16.1)

$$uv = (\bar{u} + u')(\bar{v} + v') = \bar{u}\bar{v} + \bar{u}v' + \bar{v}u' + u'v',$$

so that with the rules (16.3) and (16.4) we obtain

$$\bar{u}v = \bar{u}\bar{v} + \bar{u}'v'.$$

Therefore the flux in the y direction of the x momentum is

$$d\bar{I} = dA \cdot \rho(\bar{u}\bar{v} + \bar{u}'v').$$

This expression for the rate of change of the momentum has the dimensions of a force at the surface dA . Dividing by dA yields a force per unit area, that is, a stress. Since the momentum flux is equivalent to an equal but opposite shearing force of the fluid on this surface, a shear stress in the x direction acts on the surface element whose normal is in the y direction. This yields the result that the fluctuation causes the following additional shear stress in the x direction on the surface element perpendicular to the y direction:

$$\tau'_{xy} = -\rho \bar{u}'v'. \quad (16.5)$$

It can easily be shown that additional stresses also occur for the two other coordinate directions (a normal stress in the y direction and a shear stress in the z direction), cf. H. Schlichting (1982), p. 570.

The additional stresses are called “*apparent*” stresses of the turbulent flow and they must be added to the steady flow stresses which we met in connection with laminar flow. Analogous expressions for the stress components can be obtained for surface elements perpendicular to the x and z axes, yielding a complete *stress tensor of the turbulent apparent friction*. Equation (16.5) was first derived by O. Reynolds (1894) from the hydrodynamic equations of motion (see the next section). The apparent stresses are therefore also called *Reynolds stresses*.

It can easily be seen that the time average $\bar{u}'v'$ in Eq. (16.5) does indeed have a non-zero value. Consider the plane shear flow in Fig. 16.2 with

$\bar{u} = \bar{u}(y)$, $\bar{v} = \bar{w} = 0$ and $d\bar{u}/dy > 0$. The transverse motion causes eddies to approach the layer y from below. These eddies ($v' > 0$) come from a region of smaller average velocity \bar{u} . Since they essentially retain their original velocity \bar{u} in the transverse motion, they cause a negative u' in the layer y . In contrast, particles approaching from above ($v' < 0$) produce a positive u' in the layer y . Thus in this flow, a positive v' is “generally” coupled to a negative u' and a negative v' to a positive u' . Thus we expect that the time average $\bar{u}'v'$ is non-zero, and indeed negative. Therefore in this case the shear stress $\tau'_{xy} = -\rho u'v'$ is positive and thus has the same sign as the viscous shear stress for this case $\bar{\tau}_v = \mu d\bar{u}/dy$. One also says that in this case there is a *correlation* between the longitudinal and transverse fluctuations of the velocity at the same position.

16.3 Basic Equations for the Mean Motion of Turbulent Flows

For simplicity, in this section we will initially consider only flows with constant physical properties. The extension to flows with variable physical properties follows in Chap. 19. We will now derive the fundamental equations for the mean motion of turbulent flows from the corresponding balances for mass, momentum and energy of unsteady laminar flows.

16.3.1 Continuity Equation

In the continuity equation

$$\frac{\partial u}{\partial x} + \frac{\partial v}{\partial y} + \frac{\partial w}{\partial z} = 0 \quad (16.6)$$

(cf. Eq. (12.55) with $h_x = h_z = 1$), we decomposed the velocities into their average values and their fluctuating values, as in Eq. (16.1). The time averaging of Eq. (16.6) is carried out term by term. Because $\bar{\partial u'}/\partial x = 0$, etc. this yields

$$\frac{\partial \bar{u}}{\partial x} + \frac{\partial \bar{v}}{\partial y} + \frac{\partial \bar{w}}{\partial z} = 0. \quad (16.7)$$

Using Eq. (16.6) we then also find

$$\frac{\partial u'}{\partial x} + \frac{\partial v'}{\partial y} + \frac{\partial w'}{\partial z} = 0. \quad (16.8)$$

Both the time average values and the fluctuations of the velocity components satisfy the laminar flow continuity equation in the same manner.

16.3.2 Momentum Equations (Reynolds Equations)

The aim of the following calculation is to derive the equations of motion which the time average of the velocity components \bar{u} , \bar{v} , \bar{w} and the pressure \bar{p} must satisfy. We write the incompressible flow Navier–Stokes equations from Eq. (3.42) in the form

$$\varrho \left\{ \frac{\partial u}{\partial t} + \frac{\partial(u^2)}{\partial x} + \frac{\partial(uv)}{\partial y} + \frac{\partial(uw)}{\partial z} \right\} = -\frac{\partial p}{\partial x} + \mu \Delta u, \quad (16.9a)$$

$$\varrho \left\{ \frac{\partial v}{\partial t} + \frac{\partial(vu)}{\partial x} + \frac{\partial(v^2)}{\partial y} + \frac{\partial(vw)}{\partial z} \right\} = -\frac{\partial p}{\partial y} + \mu \Delta v, \quad (16.9b)$$

$$\varrho \left\{ \frac{\partial w}{\partial t} + \frac{\partial(wu)}{\partial x} + \frac{\partial(wv)}{\partial y} + \frac{\partial(w^2)}{\partial z} \right\} = -\frac{\partial p}{\partial z} + \mu \Delta w. \quad (16.9c)$$

Here Δ is the Laplace operator. The gravity term is absent here since the pressure is already that caused by the motion of the fluid as in Eq. (4.19). We decompose the velocity components and the pressure into their time average and fluctuation quantities as in Eq. (16.1), thus forming the time averages term by term in the resulting equations. The rules (16.4) are to be taken note of.

Introducing the trial solutions Eq. (16.1) into the equations of motion (16.9a,b,c) yields expressions such as that in Eq. (16.5). Forming the time averages, while taking the rules (16.4) into account, leaves the barred square terms unchanged since these are already constant in time. The terms which are linear in the fluctuating quantities, such as $\partial u'/\partial t$ and $\partial^2 u'/\partial x^2$, drop away when the time average is formed (see Eq. (16.3)). However the terms which are quadratic in the fluctuating quantities remain; they assume the form \bar{u}'^2 , $\bar{u}'\bar{v}'$, etc. Thus, after taking the time average of Eq. (16.9), using the continuity equation (16.7) to transform the left hand side and bringing the quadratic fluctuating terms to the right hand side, we obtain the following system of equations:

$$\begin{aligned} \varrho \left(\bar{u} \frac{\partial \bar{u}}{\partial x} + \bar{v} \frac{\partial \bar{u}}{\partial y} + \bar{w} \frac{\partial \bar{u}}{\partial z} \right) \\ = -\frac{\partial \bar{p}}{\partial x} + \mu \Delta \bar{u} - \varrho \left(\frac{\partial \bar{u}'^2}{\partial x} + \frac{\partial \bar{u}'\bar{v}'}{\partial y} + \frac{\partial \bar{u}'\bar{w}'}{\partial z} \right) \end{aligned} \quad (16.10)$$

$$\begin{aligned} \varrho \left(\bar{u} \frac{\partial \bar{v}}{\partial x} + \bar{v} \frac{\partial \bar{v}}{\partial y} + \bar{w} \frac{\partial \bar{v}}{\partial z} \right) \\ = -\frac{\partial \bar{p}}{\partial y} + \mu \Delta \bar{v} - \varrho \left(\frac{\partial \bar{u}'\bar{v}'}{\partial x} + \frac{\partial \bar{v}'^2}{\partial y} + \frac{\partial \bar{v}'\bar{w}'}{\partial z} \right) \end{aligned}$$

$$\begin{aligned} \varrho \left(\bar{u} \frac{\partial \bar{w}}{\partial x} + \bar{v} \frac{\partial \bar{w}}{\partial y} + \bar{w} \frac{\partial \bar{w}}{\partial z} \right) \\ = -\frac{\partial \bar{p}}{\partial z} + \mu \Delta \bar{w} - \varrho \left(\frac{\partial \bar{u}'\bar{w}'}{\partial x} + \frac{\partial \bar{v}'\bar{w}'}{\partial y} + \frac{\partial \bar{w}'^2}{\partial z} \right). \end{aligned}$$

As well as these equations we also have the continuity equation (16.7). The left hand side of Eq. (16.10) is formally the same as the steady Navier–Stokes equations (3.42) if u , v , w are replaced by their time averages. The same is true for the pressure and friction terms on the right hand side. However there are also additional terms which are due to the turbulent fluctuating motion.

As can be seen from a comparison of Eq. (16.10) with Eq. (3.17), the additional terms on the right hand side of Eq. (16.10) can be construed as the components of a stress tensor. This yields the resulting surface force per unit volume according to Eq. (3.16):

$$\begin{aligned}\vec{P} = & \vec{e}_x \left(\frac{\partial \sigma'_x}{\partial x} + \frac{\partial \tau'_{xy}}{\partial y} + \frac{\partial \tau'_{xz}}{\partial z} \right) \\ & + \vec{e}_y \left(\frac{\partial \tau'_{xy}}{\partial x} + \frac{\partial \sigma'_y}{\partial y} + \frac{\partial \tau'_{yz}}{\partial z} \right) \\ & + \vec{e}_z \left(\frac{\partial \tau'_{xz}}{\partial x} + \frac{\partial \tau'_{yz}}{\partial y} + \frac{\partial \sigma'_z}{\partial z} \right).\end{aligned}$$

Using Eq. (3.17) as an example, we can rewrite Eq. (16.10) in the form

$$\begin{aligned}\varrho \left(\bar{u} \frac{\partial \bar{u}}{\partial x} + \bar{v} \frac{\partial \bar{u}}{\partial y} + \bar{w} \frac{\partial \bar{u}}{\partial z} \right) &= - \frac{\partial \bar{p}}{\partial x} + \mu \Delta \bar{u} + \left(\frac{\partial \sigma'_x}{\partial x} + \frac{\partial \tau'_{xy}}{\partial y} + \frac{\partial \tau'_{xz}}{\partial z} \right) \\ \varrho \left(\bar{u} \frac{\partial \bar{v}}{\partial x} + \bar{v} \frac{\partial \bar{v}}{\partial y} + \bar{w} \frac{\partial \bar{v}}{\partial z} \right) &= - \frac{\partial \bar{p}}{\partial y} + \mu \Delta \bar{v} + \left(\frac{\partial \tau'_{xy}}{\partial x} + \frac{\partial \sigma'_y}{\partial y} + \frac{\partial \tau'_{yz}}{\partial z} \right) \\ \varrho \left(\bar{u} \frac{\partial \bar{w}}{\partial x} + \bar{v} \frac{\partial \bar{w}}{\partial y} + \bar{w} \frac{\partial \bar{w}}{\partial z} \right) &= - \frac{\partial \bar{p}}{\partial z} + \mu \Delta \bar{w} + \left(\frac{\partial \tau'_{xz}}{\partial x} + \frac{\partial \tau'_{yz}}{\partial y} + \frac{\partial \sigma'_z}{\partial z} \right).\end{aligned}\tag{16.11}$$

Comparison of Eq. (16.11) with Eq. (16.10) then gives the stress tensor due to the turbulent velocity components as

$$\begin{pmatrix} \sigma'_x & \tau'_{xy} & \tau'_{xz} \\ \tau'_{xy} & \sigma'_y & \tau'_{yz} \\ \tau'_{xz} & \tau'_{yz} & \sigma'_z \end{pmatrix} = - \begin{pmatrix} \varrho \overline{u'^2} & \varrho \overline{u'v'} & \varrho \overline{u'w'} \\ \varrho \overline{u'v'} & \varrho \overline{v'^2} & \varrho \overline{v'w'} \\ \varrho \overline{u'w'} & \varrho \overline{v'w'} & \varrho \overline{w'^2} \end{pmatrix}.\tag{16.12}$$

The component τ'_{xy} of the stress tensor is the same as the quantity obtained from momentum considerations in Eq. (16.5).

As already mentioned, the apparent stresses are also called *Reynolds stresses*. Correspondingly the momentum equations (16.11) are also called the *Reynolds equations*.

The result of these deliberations is that the time averages of the velocity components of the turbulent motion in Eq. (16.11) satisfy the same equations as the velocity components of a laminar flow, whereby as well as the friction forces of the laminar flow there are also additional stresses given by the stress tensor Eq. (16.12). This additional stresses are called *apparent stresses of the turbulent flow*. They are due to the turbulent fluctuations and are given by the time averages of the quadratic fluctuation terms. Since these stresses are supplementary to the usual stresses of a flow, they are frequently called the *shear forces of the apparent turbulent friction*. The complete stresses consist of the ordinary viscous stresses in Eqs. (3.37) and (3.38a) and these apparent turbulent stresses, thus

$$\begin{aligned}\sigma_x &= -p + 2\mu \frac{\partial \bar{u}}{\partial x} - \varrho \bar{u'^2}, \\ \tau_{xy} &= \mu \left(\frac{\partial \bar{u}}{\partial y} + \frac{\partial \bar{v}}{\partial x} \right) - \varrho \bar{u'v'}, \dots\end{aligned}\tag{16.13}$$

In general the stresses of the apparent turbulent friction predominate over the viscous stresses, so that these latter can frequently be neglected, apart from in regions directly at the wall.

16.3.3 Equation for the Kinetic Energy of the Turbulent Fluctuations (*k*-Equation)

The balance of the kinetic energy of the fluctuation is very important in understanding the physical processes in turbulent fluctuations and particularly in turbulence modelling. We consider the balance of the quantity

$$k = \frac{1}{2} \bar{q^2} = \frac{1}{2} (\bar{u'^2} + \bar{v'^2} + \bar{w'^2})\tag{16.14}$$

with

$$\bar{q^2} = \bar{u'^2} + \bar{v'^2} + \bar{w'^2}.\tag{16.15}$$

It is for this reason that the name *k-equation* is used. This equation can be derived from the Navier–Stokes equations, as K. Gersten; H. Herwig (1992),

p. 769 have described. For steady flows with constant physical properties it reads:

$$\begin{aligned}
 & \varrho \left(\bar{u} \frac{\partial k}{\partial x} + \bar{v} \frac{\partial k}{\partial y} + \bar{w} \frac{\partial k}{\partial z} \right) && \text{convection} \\
 & = -\frac{\partial}{\partial x} \left[\bar{u}' \left(p' + \frac{\varrho}{2} q^2 \right) \right] && \\
 & -\frac{\partial}{\partial y} \left[\bar{v}' \left(p' + \frac{\varrho}{2} q^2 \right) \right] && \text{turbulent} \\
 & -\frac{\partial}{\partial z} \left[\bar{w}' \left(p' + \frac{\varrho}{2} q^2 \right) \right] && \text{diffusion} \\
 & + \mu \left[\frac{\partial^2}{\partial x^2} (k + \bar{u}'^2) + \frac{\partial^2}{\partial y^2} (k + \bar{v}'^2) \right. && \\
 & + \frac{\partial^2}{\partial z^2} (k + \bar{w}'^2) && \text{viscous} \\
 & \left. + 2 \left(\frac{\partial^2 \bar{u}' v'}{\partial x \partial y} + \frac{\partial^2 \bar{v}' w'}{\partial y \partial z} + \frac{\partial^2 \bar{w}' u'}{\partial z \partial x} \right) \right] && \text{diffusion} \\
 & - \varrho \left(\bar{u}'^2 \frac{\partial \bar{u}}{\partial x} + \bar{u}' \bar{v}' \frac{\partial \bar{v}}{\partial x} + \bar{u}' \bar{w}' \frac{\partial \bar{w}}{\partial x} \right. && \\
 & + \bar{u}' \bar{v}' \frac{\partial \bar{u}}{\partial y} + \bar{v}'^2 \frac{\partial \bar{v}}{\partial y} + \bar{v}' \bar{w}' \frac{\partial \bar{w}}{\partial y} && \text{turbulence} \\
 & \left. + \bar{u}' \bar{w}' \frac{\partial \bar{u}}{\partial z} + \bar{v}' \bar{w}' \frac{\partial \bar{v}}{\partial z} + \bar{w}'^2 \frac{\partial \bar{w}}{\partial z} \right) && \text{production} \\
 & - \varrho \tilde{\varepsilon} && \text{dissipation.}
 \end{aligned} \tag{16.16}$$

The dissipation (cf. Eq. (3.62)) is

$$\begin{aligned}
 \varrho \tilde{\varepsilon} = \mu & \left[2 \left(\frac{\partial u'}{\partial x} \right)^2 + 2 \left(\frac{\partial v'}{\partial y} \right)^2 + 2 \left(\frac{\partial w'}{\partial z} \right)^2 \right. \\
 & \left. + \left(\frac{\partial u'}{\partial y} + \frac{\partial v'}{\partial x} \right)^2 + \left(\frac{\partial u'}{\partial z} + \frac{\partial w'}{\partial x} \right)^2 + \left(\frac{\partial v'}{\partial z} + \frac{\partial w'}{\partial y} \right)^2 \right]. \tag{16.17}
 \end{aligned}$$

Frequently the terms for the viscous diffusion and the dissipation are collected together differently, and we have

$$\mu[\dots] - \varrho \tilde{\varepsilon} = \mu \Delta k - \varrho \varepsilon, \tag{16.18}$$

where Δ is the Laplace operator.

The newly introduced quantity

$$\varrho\varepsilon = \mu \left[\overline{\left(\frac{\partial u'}{\partial x} \right)^2} + \overline{\left(\frac{\partial v'}{\partial x} \right)^2} + \overline{\left(\frac{\partial w'}{\partial x} \right)^2} \right. \\ \left. + \overline{\left(\frac{\partial u'}{\partial y} \right)^2} + \overline{\left(\frac{\partial v'}{\partial y} \right)^2} + \overline{\left(\frac{\partial w'}{\partial y} \right)^2} \right. \\ \left. + \overline{\left(\frac{\partial u'}{\partial z} \right)^2} + \overline{\left(\frac{\partial v'}{\partial z} \right)^2} + \overline{\left(\frac{\partial w'}{\partial z} \right)^2} \right] \quad (16.19)$$

is a kind of *pseudo-dissipation*. Unfortunately in the literature it is frequently wrongly also called dissipation.

The k -equation describes the balance between four contributions to the energy budget of the turbulent fluctuations: convection, diffusion, production and dissipation. The diffusion consists of parts due to viscous diffusion and turbulent diffusion. The diffusion terms are always gradients whose contribution therefore vanishes by integration (e.g. over the flow cross-section) when a global balance is taken.

As can be seen from Eq. (16.17), the dissipation $\tilde{\varepsilon}$ is always positive. In Eq. (16.16) the dissipation term $-\varrho\tilde{\varepsilon}$ is an “*energy sink*”. In contrast to this, the turbulence production in Eq. (16.16) is generally positive. If the terms for turbulence production and dissipation are much larger than the remaining terms in a turbulent flow, we can speak of an *equilibrium region*, since then the turbulence production is approximately equal to the dissipation, cf. Chaps. 17 and 18. Zones can also exist within turbulent flows where the turbulence production is negative, i.e. where energy flows back from the fluctuations to the mean motion. (This occurs for example in the turbulent wall jet, cf. Sect. 22.8.) However in general the change in turbulent energy due to convection is compensated by an “*energy source*” (turbulence production), an “*energy sink*” (dissipation) and energy transport (diffusion). The dissipation means a change from turbulent kinetic energy to internal energy.

16.3.4 Thermal Energy Equation

In order to describe the average temperature field $\bar{T}(x, y, z)$, a corresponding equation can be derived from the thermal energy equation (3.71). For constant physical properties it reads:

$$\begin{aligned}
 & \varrho c_p \left(\bar{u} \frac{\partial \bar{T}}{\partial x} + \bar{v} \frac{\partial \bar{T}}{\partial y} + \bar{w} \frac{\partial \bar{T}}{\partial z} \right) \\
 &= \lambda \left(\frac{\partial^2 \bar{T}}{\partial x^2} + \frac{\partial^2 \bar{T}}{\partial y^2} + \frac{\partial^2 \bar{T}}{\partial z^2} \right) \\
 & - \varrho c_p \left(\frac{\partial \bar{u}' T'}{\partial x} + \frac{\partial \bar{v}' T'}{\partial y} + \frac{\partial \bar{w}' T'}{\partial z} \right) \\
 &+ \mu \left[2 \left(\frac{\partial \bar{u}}{\partial x} \right)^2 + 2 \left(\frac{\partial \bar{v}}{\partial y} \right)^2 + 2 \left(\frac{\partial \bar{w}}{\partial z} \right)^2 \right. \\
 &+ \left(\frac{\partial \bar{u}}{\partial y} + \frac{\partial \bar{v}}{\partial x} \right)^2 + \left(\frac{\partial \bar{u}}{\partial z} + \frac{\partial \bar{w}}{\partial x} \right)^2 \\
 &+ \left. \left(\frac{\partial \bar{v}}{\partial z} + \frac{\partial \bar{w}}{\partial y} \right)^2 \right] \\
 &+ \varrho \tilde{\varepsilon} \quad \left. \begin{array}{l} \text{convection} \\ \text{molecular} \\ \text{heat} \\ \text{transport} \\ \text{turbulent} \\ \text{heat} \\ \text{transport} \\ \text{direct} \\ \text{dissipation} \\ \text{turbulent} \\ \text{dissipation.} \end{array} \right\} \quad (16.20)
 \end{aligned}$$

Thus the same equation holds for the average temperature field as for laminar temperature fields, apart from two additional terms. First of all, as well as the molecular heat conduction, an “apparent” heat conduction occurs. This is due to the turbulent fluctuations of the velocity and the temperature. The correlation between the velocity fluctuations and the temperature fluctuations leads to a “*turbulent heat transfer*” which is characterised by the expression $\operatorname{div}(\bar{v}' T')$. Secondly, as well as the “direct” dissipation corresponding to the dissipation in laminar flows, there is also the “turbulent” dissipation $\varrho \tilde{\varepsilon}$. This already appeared in the balance for the turbulent kinetic energy Eq. (16.16). Thus in turbulent flows mechanical energy is transformed to internal energy in two different ways. In direct dissipation, the transfer is due directly to the viscosity, whereas in turbulent dissipation the transfer takes place indirectly, i.e. via the turbulent fluctuations whereby mechanical energy from the mean motion is initially transformed to the turbulent fluctuations and then finally to internal energy.

16.4 Closure Problem

Equations (16.7), (16.11) and (16.20) are used to compute time averaged fields for the velocity \bar{v} , the pressure \bar{p} and the temperature \bar{T} .

The *boundary conditions* for the time average quantities are the same as those for laminar flows, such as the no-slip condition for the velocity at fixed walls. However at the walls all the fluctuation components of the velocity also vanish and thus also all the Reynolds stresses. Thus in turbulent flows, shear forces at the wall are also only produced by the viscosity. In practice it is also generally assumed that the wall temperature exhibits no fluctuations. This is satisfied if the product $\varrho c_p \lambda$ for the wall material is much larger than that for the fluid, cf. K. Gersten; H. Herwig (1992), p. 461 and 470. The velocity and temperature gradients and thus the shear stress $\tau = \mu(\partial u / \partial y)$ and the heat flux $q = -\lambda(\partial T / \partial y)$ are however still quantities which oscillate in time at the wall, as is the wall pressure.

In computing the average velocity and temperature fields for turbulent flows using the equations (16.7), (16.11) and (16.20), there is a fundamental difficulty. As well as the unknowns \bar{v} , \bar{p} and \bar{T} , these equations also contain further unknowns, namely the Reynolds stresses, the components of the correlation $\bar{v}' \bar{T}'$ and the turbulent dissipation $\varrho \tilde{\epsilon}$. In order to be able to calculate turbulent flows, the system of equations must be supplemented by additional equations for these additional unknowns, i.e. it has to be “closed”. Now balances can also be set up for the additional unknowns which are essentially correlations. The k -equation (16.16) is one example. It is a balance for the sum of the normal stresses of the Reynolds stresses. Analogous balances also exist for all the above mentioned correlations. Unfortunately, as might be guessed from the example of the k -equation, additional unknowns also appear in these balance equations. These are the velocity-pressure correlation $\bar{v}' p'$ and the so-called triple correlation $\bar{v}' q^2 = \bar{v}'(u'^2 + v'^2 + w'^2)$. Therefore adding balances for the unknowns which appear in the system of equations simply does not allow this system of equations to be closed. This so-called “closure problem” is of central importance in turbulence research.

In order to produce the relation between the Reynolds stresses and the quantities of the mean motion, model equations must be developed; thus one speaks of *turbulence models* or *turbulence modelling*. These model equations will contain empirical elements. The balance equations for the Reynolds stresses may be used for this purpose, as for example occurs with the k -equation, but the velocity-pressure correlation or the triple correlations have to be suitably modelled. The different turbulence models will be discussed in Chaps. 17 and 18.

Detailed knowledge of the physical processes of turbulent fluctuations is required in order to develop as good and generally valid model equations as possible. In what follows some of the important properties of turbulent fluctuations will be presented.

16.5 Description of the Turbulent Fluctuations

16.5.1 Correlations

The temporally fluctuating velocity components in turbulent flows can be determined experimentally using *hot-wire anemometry* or *laser-Doppler anemometry*. The temperature fluctuations can also be obtained using (“cold”) hot-wire probes. However it is more difficult to measure the pressure fluctuations, cf. W. Nitsche (1994), p. 14 and W.W. Willmarth (1975). Fluctuations of the wall pressure have been measured by R. Emmerling (1973) and A. Dinkelacker et al. (1977).

As can already be seen for the Reynolds stresses Eq. (16.12), the correlations, i.e. the time averages of the products of fluctuating quantities, are very important in describing turbulent flows.

As well as the correlations of different fluctuating quantities, e.g. different velocity components at the same point, the correlations of the same fluctuation quantities at different times (autocorrelation) or at different positions (space correlation) are also of interest.

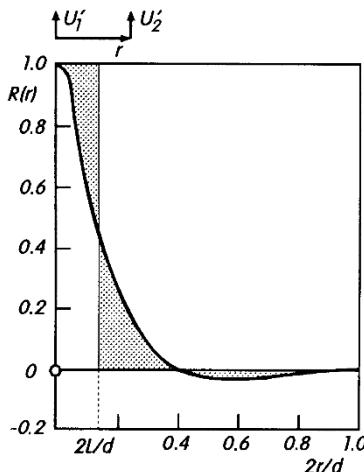


Fig. 16.3. Correlation function for the turbulent longitudinal velocity fluctuations u'_1 in the centre of a pipe related to the velocity fluctuations u'_2 at a distance r , after measurements by L.F.G. Simmons; C. Salter (1938); cf. also G.I. Taylor (1936)

Figure 16.3 shows the normalised correlation function

$$R(r) = \frac{\overline{u'_1 u'_2}}{\sqrt{\overline{u'^2_1}} \cdot \sqrt{\overline{u'^2_2}}} \quad (16.21)$$

for a pipe flow. This was introduced by G.I. Taylor (1935). The point with index 1 is on the axis of the pipe and point 2 is at a variable distance r from the axis. The function shows how much motion at one point (here the longitudinal motion) influences that in the other point. Negative values of the correlation function imply that the time averages of the velocities in the two correlated points have different signs. This is to be expected in the “side correlation” shown in Fig. 16.3 because the volume flux is constant in time.

The integral of R yields a characteristic length of the turbulence structure

$$L = \int_0^{d/2} R(r) dr. \quad (16.22)$$

This length, known as the *turbulence length*, is a measure of the extent of fluid mass which moves as a unit, and thus gives us an idea of the average size of the eddies. In the example shown, $L \approx 0.14 d/2$.

The *space-time correlation* yields far-reaching insights into the structures of the turbulent motion. Here two velocity components at different places and different times are correlated with one another, cf. A.J. Favre et al. (1957, 1958).

Conditioned sampling allows clear coherent structures to be identified in turbulent shear flows. Compare the summaries by A. Roshko (1976), B.J. Cantwell (1981), J.L. Lumley (1981), M.T. Landahl; E. Mollo-Christensen (1986) and H.E. Fiedler (1988).

16.5.2 Spectra and Eddies

Instead of describing the structure using correlation functions, we can also carry out a *frequency analysis* of the motion. Denoting the frequency by n and letting $F(n)dn$ be the percentage of the square average of the longitudinal fluctuation $\overline{u'^2}$ which lies between n and $n + dn$, then $F(n)$ yields the spectral distribution of $\overline{u'^2}$. By definition

$$\int_0^\infty F(n) dn = 1. \quad (16.23)$$

Mathematically, the spectral function $F(n)$ is the *Fourier transform* of the auto-correlation.

The *spectra* shown in Fig. 16.4 were measured by P.S. Klebanoff (1955) in the turbulent boundary layer at a flat plate. The largest value of $F(n)$ was found to belong to the smallest frequency measured. At smaller frequencies (not shown here) and larger frequencies, $F(n)$ then decreases to zero, in order to satisfy the condition (16.23). A *continuous spectrum* is characteristic of turbulent flows, in contrast to the spectra with *discrete frequencies* in unsteady laminar flows. The depiction in Fig. 16.4 is frequently also called the *energy spectrum*, although it refers only to the part $\overline{u'^2}$ of the longitudinal fluctuations and not the entire kinetic energy k from Eq. (16.14). Instead of the frequency n , the so-called wave number with units 1/length is taken along the abscissa. Different eddies with different sizes are then assigned to the corresponding lengths. In Fig. 16.4, eddies with dimensions from some tenths of a millimeter to several centimeters were measured. Thus these latter large eddies are the main carriers of kinetic energy in the fluctuations. They obtain their energy from the mean motion, and then decay, passing on their energy to smaller eddies. This *cascade process* is carried on through ever smaller eddies, until eventually dissipation, i.e. the transfer from mechanical energy to internal energy, occurs in the smallest eddies.

At very large Reynolds numbers, turbulent flows have a *locally isotropic structure*, as has been shown by A.N. Kolmogorov (1941a). Only regions close to the walls and edges are excluded. By this is meant that the fluctuations in a *small* neighbourhood close to a point possess no particular direction, i.e. they are *isotropic*. Since the dissipation occurs in the region of the smallest eddies, it can be computed corresponding to Eq. (16.17) under the assumption of isotropic turbulence, cf. A.N. Kolmogorov (1941b). In this case we have

$$\overline{u'^2} = \overline{v'^2} = \overline{w'^2}, \quad \overline{u'v'} = \overline{u'w'} = \overline{v'w'} = 0, \quad (16.24)$$

and for $\tilde{\varepsilon}$ this can be simplified as follows, cf. J.O. Hinze (1975), p. 219:

$$\varrho\tilde{\varepsilon} = 15\mu \left(\frac{\partial u'}{\partial x} \right)^2. \quad (16.25)$$

Similarity considerations, carried out by A.N. Kolmogorov (1941a) and later independently by C.F. v. Weizsäcker (1948) and W. Heisenberg (1948), revealed further details related to the form of the correlation functions at small distances

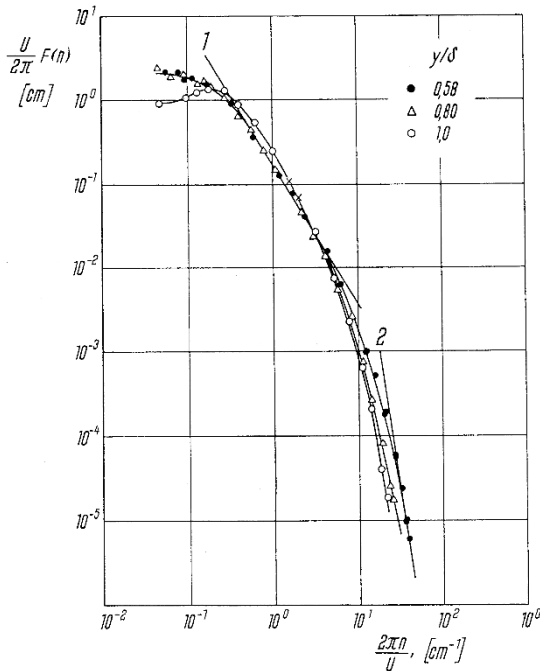


Fig. 16.4. Frequency spectrum of the longitudinal velocity fluctuation in the turbulent boundary layer at a flat plate, after P.S. Klebanoff (1955)
curve (1): $F \sim n^{-5/3}$
curve (2): $F \sim n^{-7}$
Theory due to W. Heisenberg (1948)

r or of the spectrum for high frequencies/small eddies. According to these, in the mid frequency region, $F(n) \sim n^{-5/3}$. This is confirmed well by the measurements in Fig. 16.4. W. Heisenberg (1948) has shown that at very high frequencies ($n \rightarrow \infty$), $F(n) \sim n^{-7}$. These two theoretical progressions are shown in the logarithmic diagram Fig. 16.4 as the straight lines (1) and (2).

The essential aspect in understanding turbulence is that the apparent stresses are mainly produced by the large eddies of order of magnitude L . Because of the instability of the flow, motion of smaller dimensions then follows, until finally such steep velocity gradients $\partial u'/\partial x$, etc. occur in the smallest eddies that a transfer to internal energy takes place. The power carried over from the main flow to the large eddies via the apparent stresses which is independent of the viscosity is therefore passed along to ever smaller eddies step by step, until the energy dissipates. The fact that in turbulent flows the friction drag and the distribution of the average velocity are only slightly dependent on the Reynolds number, even though all energy losses are due to the viscosity, is ascribed to this mechanism.

The dissipation in Eq. (16.17) is also independent of the Reynolds number. Because of the factor μ , we could get the impression that for $Re \rightarrow \infty$, the dissipation tends to zero. However this is not the case. Rather $\tilde{\varepsilon}$ tends towards a finite limit, while $(\partial u'/\partial x)^2$ for $Re \rightarrow \infty$ tends as $\tilde{\varepsilon}/15\nu$ towards arbitrarily large values.

According to A.N. Kolmogorov (1941a), the *locally isotropic turbulence* is uniquely determined by the two quantities ν and $\tilde{\varepsilon}$. They yield as a length scale of the fine structure of the turbulence the *Kolmogorov length*

$$\ell_K = (\nu^3 / \tilde{\varepsilon})^{1/4} \quad (16.26)$$

and the *time scale*

$$t_K = (\nu / \tilde{\varepsilon})^{1/2}. \quad (16.27)$$

Since the velocity gradient is inversely proportional to the time scale, we have $(\partial u'/\partial x)^2 = (1/15t_K^2)$.

16.5.3 Turbulence of the Outer Flow

The appearance of boundary layers is typical for external flows at high Reynolds numbers. Instead of the laminar boundary layers treated up until now, these boundary layers are turbulent. Therefore in the ideal case, the flow field consists of a turbulent boundary layer close to the wall and an inviscid free stream which exhibits no velocity fluctuations at all.

However in practice the outer flow is not completely free from turbulence. A measure of the intensity of fluctuations is the *turbulence intensity*

$$Tu = \frac{\sqrt{\frac{1}{3}(\bar{u'^2} + \bar{v'^2} + \bar{w'^2})}}{U_\infty} = \frac{\sqrt{2k/3}}{U_\infty}. \quad (16.28)$$

Since the turbulence intensity of the outer flow can sometimes have considerable influence on the boundary layer, this quantity is important in considering whether model results in wind tunnels can be carried over to full-scale constructions, and for the comparison of measurements in different wind tunnels. It was already mentioned in Sect. 15.2.4a that the laminar–turbulent transition is greatly dependent on the turbulence intensity of the outer flow. As well as this, the development of the turbulent boundary layer, the position of separation, and the heat transfer are all affected by the turbulence intensity of the outer flow, cf. Sect. 18.5.4.

The turbulence intensity in a wind tunnel is essentially determined by the mesh width in the screens. At some distance behind the screen, the flow is approximately isotropically turbulent. Because of Eq. (16.24), Eq. (16.28) then simplifies to

$$Tu = \frac{\sqrt{\bar{u'^2}}}{U_\infty}. \quad (16.29)$$

If enough finely meshed screens are installed, good wind tunnels can reach values of $Tu = 0.001$, while in extreme cases values of $Tu = 0.0002$ have been achieved, cf. G.B. Schubauer; H.K. Skramstad (1947).

Thorough investigations by G.I. Taylor (1936) and 1938) have shown that as well as the turbulence intensity Tu , the characteristic turbulence length L from Eq. (16.22) can have some effect. The influence of L on turbulent boundary layers has been investigated by H.U. Meier; H.P. Kreplin (1980). The highest values of the wall shear stress were found when L was of the order of magnitude of the boundary-layer thickness. See also Sect. 18.5.4.

16.5.4 Edges of Turbulent Regions and Intermittence

In contrast to laminar boundary layers, additional features occur at the edge of turbulent boundary layers. This is characterised by the transition from the non-fluctuating (or weakly fluctuating) irrotational outer flow to the turbulent and thus rotational boundary-layer flow. The viscosity is of great importance in the transition from non-turbulent to fully turbulent flow. The thickness of the layer in which this transition takes place is proportional to the Kolmogorov length l_K from Eq. (16.26), cf. J.C. Rotta (1972), p. 166 and S. Corrsin; A.L. Kistler (1955).

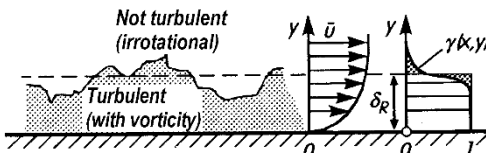


Fig. 16.5. Outer edge of a turbulent boundary layer

Left: instantaneous shot of a section of the boundary layer. The extension in the x direction is so small that the increase of $\delta_e(x)$ with x cannot be seen.

Right: Distributions of the average velocity and the intermittency factor

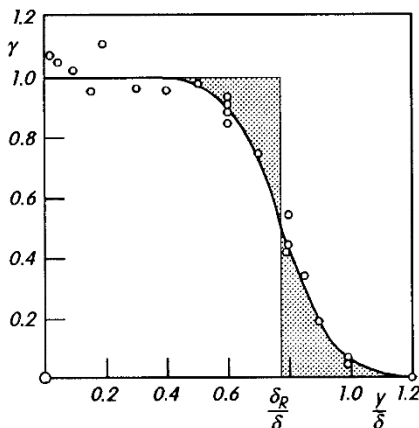


Fig. 16.6. Variation of the intermittency factor γ in the turbulent boundary layer at a flat plate at zero incidence, after measurements by P.S. Klebanoff (1955)

The edge of the turbulent boundary layer is actually a spatially and temporally strongly fluctuating surface, as sketched in Fig. 16.5. At any one point in the transition region, laminar and turbulent flow swaps back and forth at irregular intervals. These processes may be described using the *intervallency factor* $\gamma(x, y)$. The value defines the probability that turbulent flow is met at the position x, y . In experiments, $\gamma(x, y)$ describes the fraction of time for which turbulent flow is observed at this position. In the fully turbulent region $\gamma = 1$. Figure 6.6 shows the progress of γ in the boundary layer plotted against the distance from the wall. This curve can be approximated by

$$\gamma(x, y) = \{1 + 5.5[y/\delta(x)]^6\}^{-1}. \quad (16.30)$$

Analogous distributions of the intermittency can also be found at the edges of free turbulent shear layers, as in for example a free jet or wake, cf. Chap. 22.

The *average position* of the boundary-layer edge can be determined using the distance from the wall

$$\delta_e(x) = \int_0^\infty \gamma(x, y) dy \quad (16.31)$$

This differs from the boundary-layer thickness $\delta(x)$. It describes the time average position of a discrete external boundary-layer edge which represents the limit between the boundary layer and the outer flow. It will be seen later that most turbulent models yield a discrete boundary-layer thickness δ for $Re \rightarrow \infty$. This is fundamentally different from the behaviour of laminar boundary layers, where the transition to the outer flow takes place continuously and therefore such a boundary-layer thickness cannot be defined. The two boundary-layer quantities δ_e and δ are proportional to one another, with about $\delta_e = 0.78\delta$. It will be seen later that for a smooth wall δ_e and δ tend to zero for $Re \rightarrow \infty$.

16.6 Boundary-Layer Equations for Plane Flows

Just as laminar flows, turbulent flows at high Reynolds numbers also have boundary-layer character, i.e. the entire flow field consists of an inviscid outer flow and a thin turbulent boundary layer close to the wall. Again, the fundamental equations for this layer can be considerably simplified. In analogy to

laminar boundary layers, the momentum equation for the y direction reduces to the statement that the pressure at the outer edge of the boundary layer is the same as the wall pressure (neglecting curvature effects). Furthermore, again the changes in the x momentum and the x component of the heat flux can be taken to be small enough to be neglected in the main flow direction.

Equation (16.11) together with the boundary-layer approximation ($\text{Re} \rightarrow \infty, \bar{v} \ll U_\infty, \partial/\partial x \ll \partial/\partial y$) yields the following equation in the y direction:

$$0 = -\frac{\partial \bar{p}}{\partial y} - \frac{\partial(\varrho \bar{v}'^2)}{\partial y}. \quad (16.32)$$

Integrating over the boundary-layer thickness delivers:

$$\bar{p} + \varrho \bar{v}'^2 = \bar{p}_w = p_e, \quad (16.33)$$

if the outer flow is assumed to be free from turbulence. In turbulent boundary layers therefore it is not the pressure \bar{p} which is constant over the boundary layer, but rather the expression $p + \varrho v'^2$. Since the fluctuations vanish at the wall and at the outer edge, as before $\bar{p}_w = p_e$.

Thus we obtain the following equations for plane turbulent boundary layers with constant physical properties:

$$\frac{\partial \bar{u}}{\partial x} + \frac{\partial \bar{v}}{\partial y} = 0, \quad (16.34)$$

$$\varrho \left(\bar{u} \frac{\partial \bar{u}}{\partial x} + \bar{v} \frac{\partial \bar{u}}{\partial y} \right) = -\frac{dp_e}{dx} + \frac{\partial}{\partial y} (\bar{\tau}_v + \tau_t), \quad (16.35)$$

$$\varrho c_p \left(\bar{u} \frac{\partial \bar{T}}{\partial x} + \bar{v} \frac{\partial \bar{T}}{\partial y} \right) = -\frac{\partial}{\partial y} (\bar{q}_\lambda + q_t). \quad (16.36)$$

Here we set

$$\bar{\tau}_v = \mu \frac{\partial \bar{u}}{\partial y}, \quad \tau_t = -\varrho \bar{u}' \bar{v}', \quad (16.37)$$

$$\bar{q}_\lambda = -\lambda \frac{\partial \bar{T}}{\partial y}, \quad q_t = \varrho c_p \bar{v}' \bar{T}'. \quad (16.38)$$

The dissipation was neglected in the equation for the thermal energy.

Comparison with the equations for the laminar boundary layer, Eq. (6.26), (6.27) and (9.13), shows that the transfer from the equations for the laminar boundary layer to those for the turbulent boundary layer is carried out as follows:

- a) The quantities u , v and T are set to the time averages \bar{u} , \bar{v} and \bar{T} and p to p_e .

- b) The shear stress and the heat flux now each consist of two parts. The first part is due to the molecular exchange (index v for viscosity, index λ for thermal conductivity) and is computed from the time average field as in the laminar case; the second part appears additionally and is due to turbulent exchange.

The two additional terms $\tau_t(x, y)$ and $q_t(x, y)$ are new unknowns for which a relation with the average field of the velocity and temperature must be constructed via a turbulence model.

Since the k -equation (16.16) is frequently used for turbulence modelling, we will present it here in the simplified form for boundary layers with constant physical properties:

$$\varrho \left(\bar{u} \frac{\partial k}{\partial x} + \bar{v} \frac{\partial k}{\partial y} \right) = \mu \frac{\partial^2 k}{\partial y^2} - \frac{\partial}{\partial y} \left[\overline{v' \left(p' + \frac{\varrho}{2} q'^2 \right)} \right] + \tau_t \frac{\partial \bar{u}}{\partial y} - \varrho (\overline{u'^2} - \overline{v'^2}) \frac{\partial \bar{u}}{\partial x} - \varrho \varepsilon. \quad (16.39)$$

Here Eqs. (16.15) and (16.18) have been taken into account. The terms on the right hand side are as follows: viscous diffusion, turbulent diffusion, production (two terms) and (pseudo) dissipation. The second production term is frequently neglected compared to the first.

It will be seen later that the turbulent boundary layer at high Reynolds numbers consists of two layers between which again can be clearly differentiated. This is of fundamental importance in turbulence modelling.

The boundary-layer equations (16.34) to (16.39) are also valid (and are indeed exact) for fully developed internal turbulent flows. Since the two-layer character can be particularly easily represented for these much simpler flows and since the knowledge obtained from these flows can effortlessly be carried over to boundary-layer flows, in the following chapter we will treat fully developed internal turbulent flows. As already mentioned, these also possess a boundary-layer character in a general sense. The results achieved in Chap. 17 will then be carried over to turbulent boundary-layer flows in Chap. 18.

17. Internal Flows

17.1 Couette Flow

17.1.1 Two-Layer Structure of the Velocity Field and the Logarithmic Overlap Law

Fully developed Couette flow is a simple shear flow where the shear stress has a constant value everywhere in the flow field. It is our intention to treat turbulent Couette flow particularly comprehensively in this section, since it is of fundamental importance for turbulent flows close to walls in general, far beyond this particular example. It will be seen that the flow regions of the turbulent Couette flow close to the wall have universal importance, so that, up to some yet to be specified conditions, the results can be carried over to the regions close to the wall of general turbulent flows.

Let us consider the turbulent flow between two parallel plates a distance $2H$ apart as in Fig. 17.1. The origin of the chosen coordinate system is on the lower fixed plate, i.e. y is the distance from the lower wall. Our aim is to determine the distribution of the time averaged velocity $\bar{u}(y)$. The upper plate moves parallel to the lower fixed plate with the constant velocity $u_{wu} = 2\bar{u}_c$ where \bar{u}_c is the velocity at the center line $y = H$. Let the flow be fully developed, i.e. independent of the coordinate x . Let the physical properties ϱ and ν be constant.

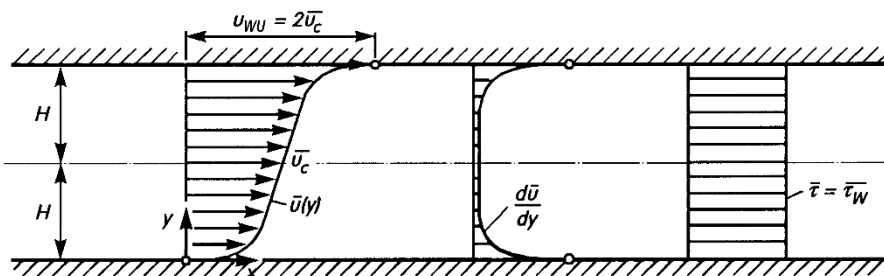


Fig. 17.1. Turbulent Couette flow

A shear stress $\bar{\tau}_w$, i.e. a shear force per unit area, is used to keep the upper plate in motion. The shear force acting is carried over as a constant value through the flow to the lower fixed plate. Therefore the balance of forces for this flow reads:

$$\bar{\tau} = \bar{\tau}_v + \tau_t = \bar{\tau}_w = \text{const} \quad (17.1)$$

with

$$\bar{\tau}_v = \varrho \nu \frac{d\bar{u}}{dy} \quad (17.2)$$

and

$$\tau_t = -\varrho \bar{u}' v', \quad (17.3)$$

cf. also Eq. (16.37). This balance law is obtained from Eq. (16.35). Since the flow is fully developed (i.e. $\partial \bar{u} / \partial x = 0$), it follows from the continuity equation (16.34) that $\bar{v} = 0$. Therefore all inertial terms vanish. Because no external pressure gradient acts, there are also no pressure forces. This is a “pure” shear flow. There are two different mechanisms by which the momentum component (which is parallel to the wall) can be carried over through the flow from one plate to another: molecular momentum transfer due to viscosity (i.e. $\bar{\tau}_v$) and momentum transfer due to turbulent fluctuations (i.e. τ_t).

We will use Eq. (17.1) to solve the following problem: the wall shear stress $\bar{\tau}_w$ and the quantities H , ϱ and ν are prescribed, and we desire the velocity distribution

$$\bar{u} = f(y, H, \nu, \bar{\tau}_w / \varrho) \quad (17.4)$$

and particularly the velocity $u_{wu}(H, \nu, \bar{\tau}_w / \varrho) = 2\bar{u}_c$ of the upper plate for very small kinematic viscosities $\nu \rightarrow 0$.

Since in Eq. (17.1) to (17.3) only the combination $\bar{\tau}_w / \varrho$ appears, Eq. (17.4) is a relation between pure kinematic quantities (with only two basic units m and s). According to the Π theorem from dimensional analysis this can be reduced to a relation between three dimensionless quantities. To this end we introduce the *friction velocity*

$$u_\tau = \sqrt{\frac{\bar{\tau}_w}{\varrho}}$$

(17.5)

(or more correctly the *wall friction velocity*). This is the characteristic velocity for turbulent flows at a given wall shear stress.

Using the dimensionless quantities

$$\eta = \frac{y}{H}, \quad u^+ = \frac{\bar{u}}{u_\tau}, \quad \text{Re}_\tau = \frac{u_\tau H}{\nu}, \quad \tau_t^+ = \frac{\tau_t}{\varrho u_\tau^2} \quad (17.6)$$

instead of Eq. (17.4) we have

$$u^+ = F(\eta, \text{Re}_\tau). \quad (17.7)$$

This satisfies the following differential equation from Eq. (17.1):

$$\frac{1}{\text{Re}_\tau} \frac{du^+}{d\eta} + \tau_t^+ = 1. \quad (17.8)$$

For reasons of symmetry we need only consider the region $0 < \eta < 1$; the boundary conditions for these equations are

$$\begin{aligned} \eta = 0 : \quad u^+ &= 0, \quad \tau_t^+ = 0, \\ \eta = 1 : \quad d^2u^+ / d\eta^2 &= 0. \end{aligned} \quad (17.9)$$

The last boundary condition states that the velocity distribution on the center line has a point of inflection. By changing the coordinate system we can take the upper plate to be fixed and the lower to be moving. This indicates directly that the velocity distribution $\bar{u}(y)$ is antimetric about the velocity \bar{u}_c .

Since turbulent flows occur at large Reynolds numbers, we will now consider Couette flow for $\text{Re}_\tau \rightarrow \infty$.

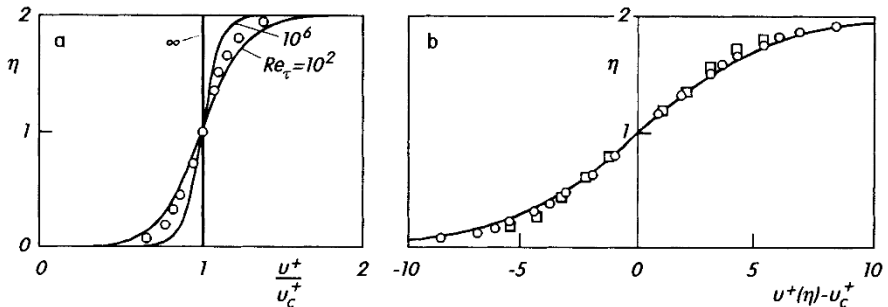


Fig. 17.2. Velocity distributions for turbulent Couette flow

- (a) $u^+(\eta, \text{Re}_\tau)$
- (b) defect velocity $u^+(\eta, \text{Re}_\tau) - u_c^+(\text{Re}_\tau)$, cf. Sect. 17.1.3
- measurements by H. Reichardt (1959), $\text{Re}_\tau = 733$
- △ measurements by M.M.M. El Telbany; A.J. Reynolds (1982), $\text{Re}_\tau = 626$
- curves: $u^+(\eta) - u_c^+ = [\ln \eta - \ln(2-\eta)]/\kappa - 0.41(1-\eta)$, $\bar{C} = 2.1$ (indirect turbulence model)

Figure 17.2a shows the results for the distributions $u^+(\eta, \text{Re}_\tau)$ at different Re_τ values. As $\text{Re}_\tau \rightarrow \infty$, the curves tend to one limiting curve. This curve is however singular. The curves for finite but large Re_τ values can then be considered to be perturbations to this limiting curve. This set-up is a typical example of a *singular perturbation problem*, quite similar to the problem of the Prandtl boundary-layer theory for laminar flows.

Unfortunately the system (17.8) and (17.9) is not closed, since it furnishes only *one* equation for *two* unknown functions $u^+(\eta, \text{Re}_\tau)$ and $\tau_t^+(\eta, \text{Re}_\tau)$. The necessary second equation which will have to yield a further relation between τ_t^+ and the velocity derivatives $du^+/d\eta$, $d^2u^+/d\eta^2$, etc., follows from the *turbulence model*.

Before we discuss turbulence models for Couette flow in Sect. 17.1.4, we will first attempt to obtain as much information as possible about the structure for the desired solution from Eqs. (17.8) and (17.9) alone.

In the limit $1/\text{Re}_\tau = 0$, Eq. (17.8) yields

$$\tau_t^+ = 1 \quad (\text{core layer}). \quad (17.10)$$

This implies that for $\text{Re}_\tau \rightarrow \infty$ the molecular momentum transfer due to viscosity can be neglected compared to the turbulent momentum transfer. This is satisfied well nearly everywhere in the turbulent flow, but it is not valid close to the wall, since the solution (17.10) does not satisfy the boundary condition $\tau_t^+ = 0$ at the wall. For large Reynolds numbers therefore, the turbulent Couette flow has a *two-layer structure*. This is typical for *singular perturbation problems*. The flow consists of a large *core layer* where the molecular momentum transfer can be neglected compared to the turbulent momentum transfer, and a *thin wall layer* (or *sublayer*), where both turbulent and molecular momentum transfer act.

The two layers clearly have thicknesses of different orders of magnitude. Whereas the thickness of the core layer is of the order of magnitude of H , a *wall layer thickness* may be determined from the two characteristic quantities ν and u_τ :

$$\delta_v = \frac{\nu}{u_\tau} = \frac{H}{\text{Re}_\tau}. \quad (17.11)$$

This tends to zero for $\text{Re}_\tau \rightarrow \infty$. The wall layer thickness is therefore small compared to H for $\text{Re}_\tau \rightarrow \infty$. The processes in the wall layer are therefore *independent of H* .

Introducing the characteristic (stretched) wall coordinate for the wall layer

$$y^+ = \frac{y}{\delta_v} = \frac{yu_\tau}{\nu} = \eta \text{Re}_\tau. \quad (17.12)$$

Eq. (17.8) yields

$$\frac{du^+}{dy^+} + \tau_t^+ = 1 \quad (\text{wall layer}) \quad (17.13)$$

with the boundary condition at the wall:

$$y^+ = 0 : \quad \frac{du^+}{dy^+} = 1. \quad (17.14)$$

The velocity distribution in the wall layer therefore has the form $u^+ = f(y^+)$. It will be seen later that this velocity distribution is *universal*, i.e. it is valid for the wall layers of all turbulent flows with finite wall shear stress.

After the solutions for the core layer and the wall layer have been determined, they have to be suitably matched up, i.e. they have to agree in an *overlap layer*. Since this overlap layer is part of two adjacent layers, its velocity distribution can depend on neither H nor ν . Instead of Eq. (17.4), it must then hold for $\text{Re}_\tau \rightarrow \infty$ that

$$\frac{d\bar{u}}{dy} = f(y, \bar{\tau}_w/\varrho) \quad (\text{overlap layer}). \quad (17.15)$$

According to the Π theorem in dimensional analysis this yields

$$\hat{y} \frac{du^+}{d\hat{y}} = \frac{1}{\kappa} = \text{const}, \quad (17.16)$$

where

$$\hat{y} = \eta \text{Re}_\tau^\alpha \quad 0 < \alpha < 1 \quad (17.17)$$

is an *intermediate coordinate* for the overlap layer ($\alpha = 0 : \hat{y} = \eta$; $\alpha = 1 : \hat{y} = y^+$). The constant κ in Eq. (17.16) is called the *Karman constant* after v. Kármán (1930), and has been determined from many experiments to be

$$\kappa = 0.41. \quad (17.18)$$

The *matching condition* (17.16) represents a boundary condition, both for the core layer

$$\lim_{\eta \rightarrow 0} \frac{du^+}{d\eta} = \frac{1}{\kappa \eta} \quad (17.19)$$

and for the wall layer:

$$\lim_{y^+ \rightarrow \infty} \frac{du^+}{dy^+} = \frac{1}{\kappa y^+}. \quad (17.20)$$

Integrating the last equation yields

$$\lim_{y^+ \rightarrow \infty} u^+(y^+) = \frac{1}{\kappa} \ln y^+ + C^+. \quad (17.21)$$

The constant of integration

$$C^+ = \int_0^1 \frac{du^+}{dy^+} dy^+ + \lim_{y^+ \rightarrow \infty} \int_1^{y^+} \left(\frac{du^+}{dy^+} - \frac{1}{\kappa y^+} \right) dy^+ \quad (17.22)$$

has been determined from numerous experiments to be

$$C^+ = 5.0 \quad (\text{smooth wall}). \quad (17.23)$$

As will be shown in the next section, C^+ generally depends on the wall roughness. Equation (17.21) is the *logarithmic overlap law*. It describes how the universal law of the wall $u^+(y^+)$ behaves for $y^+ \rightarrow \infty$. This law, which goes back to C.B. Millikan (1938), is a statement about the solution in a certain region in the flow even without a turbulence model. In the literature Eq. (17.21) is frequently called the “logarithmic law of the wall”. However this name is misleading and should therefore be avoided.

Equation (17.21) together with the boundary conditions (17.9), (17.19) and (17.20) already yield some pretty good information on the solution. In the next two sections we will treat further details of the solution, for the wall layer and the core layer separately.

Note (Derivation of logarithmic law from flow equations)

So far the logarithmic overlap layer has been derived by using only dimensional analysis, the two-layer concept and asymptotic matching. The Reynolds-averaged flow equations have not been involved. M. Oberlack (2001) succeeded obviously for the first time in deriving the logarithmic law directly from the Navier–Stokes equations.

17.1.2 Universal Laws of the Wall

Velocity distribution. The velocity distribution in the wall layer of Couette flow has universal character beyond that particular example, since, as will be shown, in the limit of very large Reynolds numbers, almost all turbulent flows at finite wall shear stress exhibit a thin wall layer with precisely this velocity distribution. One therefore speaks of the *universal law of the wall*.

Numerous measurements of this distribution $u^+(y^+)$ exist. Figure 17.3 shows the distributions $u^+(y^+)$ and $\tau_t^+(y^+)$. In addition, the asymptotes of the functions for $y^+ \rightarrow 0$ and $y^+ \rightarrow \infty$ are depicted. These correspond to Eqs. (17.20) and (17.21). The no-slip condition and the continuity equation yield the asymptote close to the wall

$$\frac{du^+}{dy^+} = 1 - Ay^{+3} + \dots \quad (y^+ \rightarrow 0), \quad (17.24)$$

where here the value $A = 6.1 \cdot 10^{-4}$ is used. In this book the following analytical description for the universal law of the wall is given in the form of an *indirect turbulence model*, cf. K. Gersten; H. Herwig (1992), p. 378:

$$\frac{du^+}{dy^+} = \frac{1}{1 + (A + B)y^{+3}} + \frac{By^{+3}}{1 + \kappa By^{+4}}, \quad (17.25)$$

$$u^+ = \frac{1}{A} \left[\frac{1}{3} \ln \frac{\Lambda y^+ + 1}{\sqrt{(\Lambda y^+)^2 - \Lambda y^+ + 1}} + \frac{1}{\sqrt{3}} \left(\arctan \frac{2\Lambda y^+ - 1}{\sqrt{3}} + \frac{\pi}{6} \right) \right] \\ + \frac{1}{4\kappa} \ln(1 + \kappa By^{+4}) \quad (17.26)$$

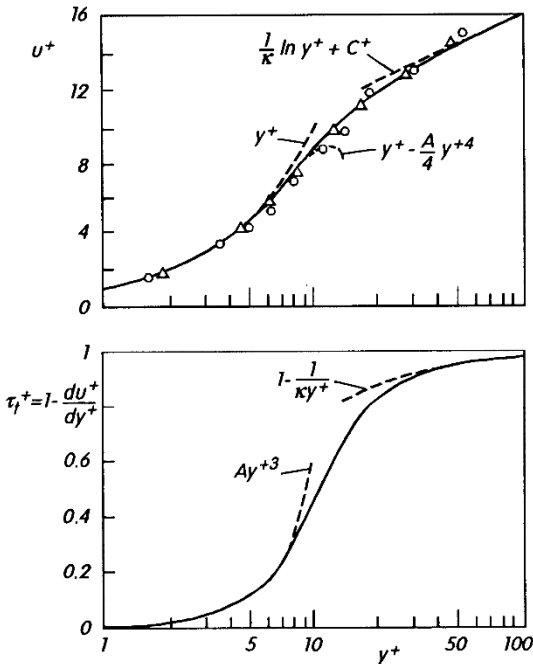


Fig. 17.3. Universal distributions of $u^+(y^+)$ and $\tau_t^+(y^+)$ in the wall layer (smooth wall)
— Eqs. (17.25) and (17.26)
- - - asymptotes from Eq. (17.20), (17.21) and (17.24)
 $\kappa = 0.41; C^+ = 5.0; A = 6.1 \cdot 10^{-4}$
○ measurements collected by J. Kestin; P.D. Richardson (1963)
△ measurements by E.R. Lindgren, cf. F.M. White (1974), p. 476
 $Re_\tau = 1260$

with the numerical values

$$\begin{aligned} \kappa &= 0.41, \quad A = 6.1 \cdot 10^{-4}, \quad B = 1.43 \cdot 10^{-3} \\ \Lambda &= (A + B)^{1/3} = 0.127 \\ C^+ &= \frac{2\pi}{3\sqrt{3}\Lambda} + \frac{1}{4\kappa} \ln(\kappa B) = 5.0. \end{aligned} \tag{17.27}$$

Equations (17.25) and (17.26) satisfy the boundary conditions (17.21) and (17.24). Extensive numerical evaluations by D. Coles (1968) and G.D. Huffman; P. Bradshaw (1972) have yielded the values $\kappa = 0.41$ and $C^+ = 5.0$. The value $A = 6.1 \cdot 10^{-4}$ follows from the condition that the distribution $u^+(y^+)$ from Eq. (17.26) must have the value $u^+ = 10.6$ at $y^+ = 15$. This has emerged from numerous measurements, cf. H. Reichardt (1951) and J. Kestin; P.D. Richardson (1963). For further presentations of the law of the wall see K. Gersten; H. Herwig (1992), p. 380.

According to Fig. 17.3, we can differentiate between the following regions:

$$\begin{aligned} \text{pure viscous sublayer: } &0 \leq y^+ < 5 & u^+ &= y^+, \\ \text{buffer layer: } &5 < y^+ < 70 & \text{Eq. (17.26)}, \\ \text{overlap layer: } &70 < y^+ & u^+ &= \frac{1}{\kappa} \ln y^+ + C^+. \end{aligned}$$

Energy balance of the mean motion. If Eq. (17.13) is multiplied by du^+/dy^+ , the resulting equation

$$\frac{du^+}{dy^+} = \left(\frac{du^+}{dy^+} \right)^2 + \tau_t^+ \frac{du^+}{dy^+}$$

energy supply direct dissipation turbulence production

(17.28)

can be interpreted as the the energy balance of the mean motion. The different terms are shown in Fig. 17.4. The power due to the shear forces is divided into two parts. One part is transformed *directly* to internal energy via viscous dissipation (and it thus called *direct dissipation*) while the second part is used to generate turbulent fluctuation energy, i.e. to produce turbulence. As will be shown, this part is eventually also transformed into internal energy, but this time via the turbulent fluctuations ("indirect" or *turbulent dissipation*). The turbulence production has a maximum of 0.25 at $du^+/dy^+ = 0.5$, i.e. from Eq. (17.25) at $y^+ = 10.6$. At this distance from the wall, the direct dissipation and the turbulence production are equal. For $y^+ < 10.6$ the direct dissipation dominates, and for $y^+ > 10.6$ the turbulence production, and turbulence production eventually provides the entire energy supply for $y^+ \rightarrow \infty$.

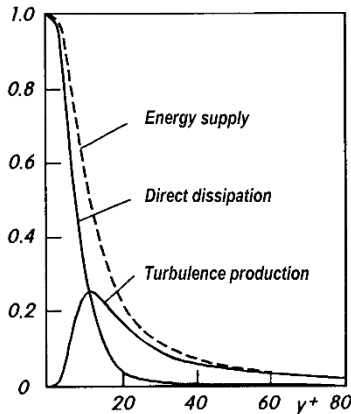


Fig. 17.4. Universal energy balance of the mean motion in the wall layer, from Eq. (17.28)

Energy balance of the turbulent flucutations. The k -equation (16.39) for the wall layer reduces to the relation

$$\tau_t^+ \frac{du^+}{dy^+} + \frac{d^2 k^+}{dy^{+2}} + \frac{dB^+}{dy^+} - \varepsilon^+ = 0.$$

turbulence production viscous diffusion turbulent dissipation

(17.29)

Here the following dimensionless quantities were introduced:

$$k^+ = \frac{k}{u_\tau^2}, \quad B^+ = -\frac{\overline{v'(p' + \varrho q^2/2)}}{u_\tau \bar{\tau}_w}, \quad \varepsilon^+ = \frac{\varepsilon \nu}{u_\tau^4}. \quad (17.30)$$

The universal production, diffusion and dissipation curves corresponding to Eq. (17.29) are shown in Fig. 17.5a. As already mentioned, the maximum of the turbulence production is at about $y^+ = 10.6$. At about this point, the sign of the diffusion also changes. For $y^+ < 10$ energy is transported towards the wall, while for $y^+ > 10$ energy is transported in the direction of the core flow. For $y^+ \rightarrow \infty$ the diffusion tends to zero faster than the production and the dissipation, which behave as $\sim (y^+)^{-1}$. This yields the following statement for the *overlap layer* (i.e. for $y^+ \rightarrow \infty$):

production = dissipation (overlap layer).

This important results is a consequence of matching up the energy terms in the wall layer and the core layer, cf. K. Gersten; H. Herwig (1992), p. 391, and has been confirmed very well by experiment. Because of this “equilibrium” between production and dissipation, the overlap layer is frequently called the *equilibrium layer*.

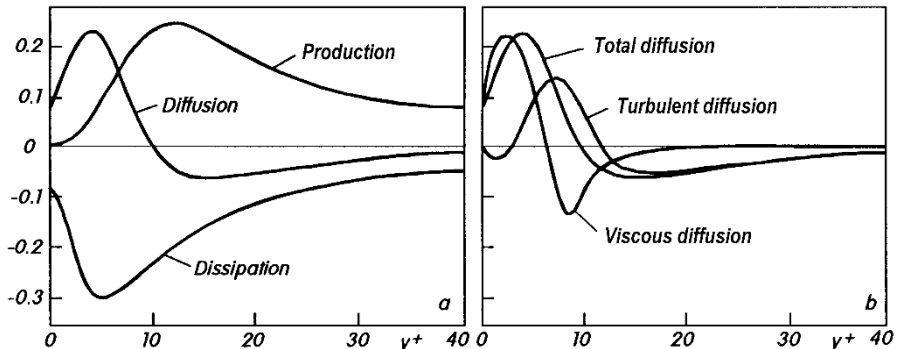


Fig. 17.5. Universal balances of the turbulent fluctuations in the wall layer

(a) kinetic energy corresponding to Eq. (17.29), after L.V. Krishnamoorthy;

R.A. Antonia (1988), see also V.C. Patel et al. (1985)

(b) division of the total diffusion into viscous diffusion and turbulent diffusion

The division of the diffusion into its viscous and turbulent parts is shown in Fig. 17.5b. Here it is seen that the sign of the turbulent diffusion changes twice.

Energy k and normal stresses. Integrating the term for the viscous diffusion twice yields the distribution $k^+(y^+)$. This is depicted in Fig. 17.6, together with the distribution of the normal stresses. From this we see that all quantities in the overlap layer ($y^+ \rightarrow \infty$) attain constant values, e.g. $k^+ \rightarrow 3.3$; $\overline{u'^2}/u_\tau^2 \rightarrow 3.3$; $\overline{v'^2}/u_\tau^2 \approx \overline{w'^2}/u_\tau^2 \rightarrow 1.65$. The different curves can be explained by the balance equations for the normal stresses which are not given here, cf. K. Gersten; H. Herwig (1992), p. 396 and Sect. 18.1.5. These show that the energy $\tau_t^+ du^+/dy^+$ due to the shear forces is initially supplied to the u' component. Because of the continuity equation, it is then carried over to the other components. For this reason, $\overline{v'^2}$ and $\overline{w'^2}$ are smaller than $\overline{u'^2}$. Eventually however at large Reynolds numbers, the three components participate *equally* in the dissipation (*local isotropy* according to A.N. Kolmogorov).

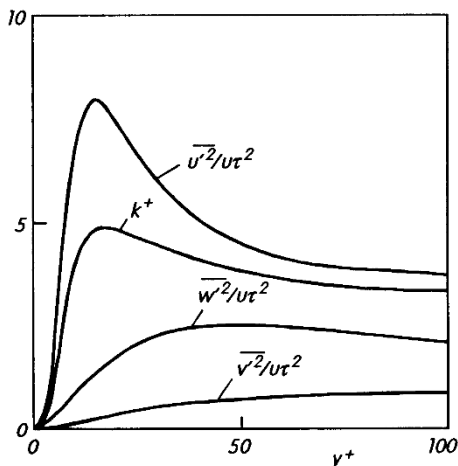


Fig. 17.6. Universal distributions of the Reynolds normal stresses and the kinetic energy of the turbulent fluctuations in the wall layer. Details are given by V.C. Patel et al. (1985), A.A. Townsend (1976), p. 144, D. Coles (1978) and M.M.M. El Telbany; A.J. Reynolds (1981)

Influence of wall roughness. In the deliberations until now, we always implicitly assumed that the surfaces of the walls were smooth. In reality however, the wall surfaces exhibit some roughness. Since there can be an infinite number of possible surface states, a *standard roughness* has been introduced to describe the effect of roughness on a flow. Here it is assumed as in Fig. 17.7 that the wall is covered with a layer of spheres packed together as densely as possible. This is in fact more or less the case for sandpaper. Therefore standard roughness is also called *sand roughness*. The diameter of the spheres is called the *sand roughness height* k_s and is a measure of the surface roughness of the wall.

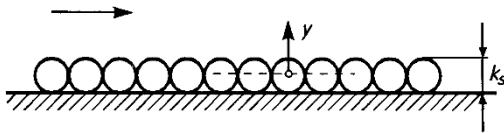


Fig. 17.7. Sand roughness height k_s

Any technical roughness element can be generally assigned to a so-called *equivalent sand roughness*, as shall be shown in what follows. Therefore it is sufficient to consider the effect of sand roughness on the law of the wall.

Using the characteristic length δ_v of the wall layer from Eq. (17.11), we obtain the following dimensionless characteristic number to describe the sand roughness quantitatively:

$$k_s^+ = \frac{k_s}{\delta_v} = \frac{k_s u_\tau}{\nu}. \quad (17.31)$$

The constant of integration C^+ in Eq. (17.21) is now only a function of the roughness characteristic number k_s^+ . The asymptotes for $k_s^+ \rightarrow 0$ and $k_s^+ \rightarrow \infty$ may be written down for this function $C^+(k_s^+)$. For a smooth surface

$$\lim_{k_s^+ \rightarrow 0} C^+(k_s^+) = 5.0 \quad (\text{smooth}). \quad (17.32)$$

It follows for the overlap law (17.21) that

$$\begin{aligned} \lim_{y^+ \rightarrow \infty} u^+(y^+) &= \frac{1}{\kappa} \ln y^+ + C^+(k_s^+) \\ &= \frac{1}{\kappa} \ln \frac{y}{k_s} + \frac{1}{\kappa} \ln k_s^+ + C^+(k_s^+) \end{aligned} \quad (17.33)$$

or

$$\lim_{y \rightarrow 0} u^+(y) = \frac{1}{\kappa} \ln \frac{y}{k_s} + C_r^+(k_s^+) \quad (17.34)$$

with

$$C_r^+(k_s^+) = C^+(k_s^+) + \frac{1}{\kappa} \ln k_s^+. \quad (17.35)$$

If k_s becomes very large, i.e. $k_s \gg \delta_v$, then the roughness elements take up all of the wall layer. In this case the viscosity is of no further importance. The function $C_r^+(k_s^+)$ must then be a constant. It follows from experiments in the so-called *fully rough regime* that

$$\lim_{k_s^+ \rightarrow \infty} C_r^+(k_s^+) = \lim_{k_s^+ \rightarrow \infty} \left[C^+(k_s^+) + \frac{1}{\kappa} \ln k_s^+ \right] = 8.0 \quad (\text{fully rough}). \quad (17.36)$$

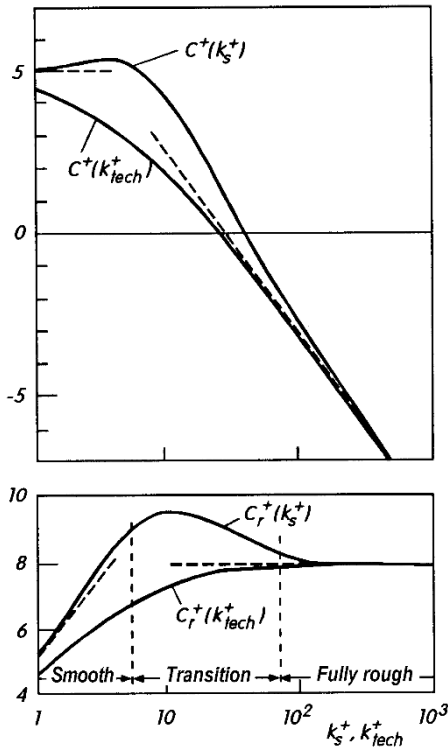


Fig. 17.8. Functions $C^+(k_s^+)$ and $C_r(k_s^+)$, after I. Tani (1988). Curve for technical roughness from Eq. (17.40)

The functions $C^+(k_s^+)$ and $C_r(k_s^+)$ have been determined by I. Tani (1987) and are shown in Fig. 17.8. It is worth noting that for $k_s^+ \leq 5$, the function $C^+(k_s^+)$ lies *above* the value for the smooth wall. For $k_s^+ > 70$ the asymptote from Eq. (17.36) has already been reached.

The overlap law (17.21) is frequently written as

$$\lim_{y^+ \rightarrow \infty} u^+(y^+, k_s^+) = \frac{1}{\kappa} \ln \frac{y}{y_k} \quad (17.37)$$

where

$$y_k = \frac{\nu}{u_\tau} \exp[-\kappa C^+(k_s^+)] \quad (17.38)$$

is the *roughness length*. In the fully rough regime $y_k = k_s \exp(-8.0\kappa) = 0.04 k_s$.

If the surface is rough, it is difficult to determine the origin of the coordinate system $y = 0$. It is usual to choose this origin so that the overlap law (17.21) is satisfied, cf. C.W.B. Grigson (1984) and Fig. 17.7.

The universal velocity distributions $u^+(y^+, k_s^+)$ are shown in Fig. 17.9: the dependence on k_s^+ for the asymptotes for $y^+ \rightarrow \infty$ is seen to be a parallel displacement.

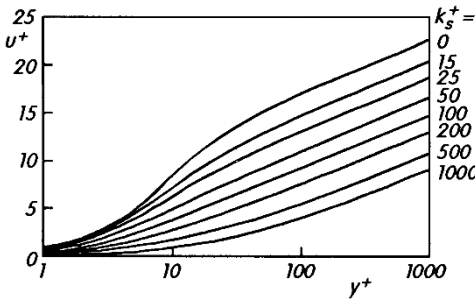


Fig. 17.9. Universal velocity distributions $u^+(y^+, k_s^+)$ in the wall layer

Note. (Influencing the turbulence with “riblets”)

The reduction of the friction drag by small regular roughness elements in the wall surface is clearly due to a damping of the turbulent fluctuations. Recently this effect has been exploited to reduce the friction drag, by forming ripples on the surface. Ripples with depth and width of about $15 \delta_v$ have been used to achieve up to 8% reduction of the friction drag, cf. L. Gaudet (1987), I. Tani (1988) and J.R. Debisschop; F.T.M. Nieuwstadt (1996).

Equivalent sand roughness. As already mentioned, to every *technical roughness* we can assign an *equivalent sand roughness* $k_{s\text{ eq}}$. An experiment must be carried out to determine the velocity distribution $u^+(y)$ in the overlap layer at the technically rough wall. It then follows from Eq. (17.34) and (17.36) that

$$k_{s\text{ eq}} = \exp \left\{ \kappa \lim_{y \rightarrow 0} \left[8.0 + \frac{1}{\kappa} \ln y - u^+(y) \right] \right\}. \quad (17.39)$$

Afterwards it must be checked if the condition $k_{s\text{ eq}}^+ = k_{s\text{ eq}} u_\tau / \nu > 70$ was satisfied in the experiment.

This condition is necessary because it has turned out that the functions $C^+(k_s^+)$ and $C_r^+(k_s^+)$ for technical roughness are different from those for sand roughness in the region $5 < k_s^+ < 70$. A formula from C.F. Colebrook (1938) gives the formula for technical roughness:

$$\begin{aligned} C^+(k_{\text{tech}}^+) &= 8.0 - \frac{1}{\kappa} \ln(3.4 + k_{\text{tech}}^+) \\ &= 5.0 - \frac{1}{\kappa} \ln \left(1 + \frac{k_{\text{tech}}^+}{3.4} \right) \end{aligned} \quad (17.40)$$

and analogously for $C_r^+(k_{\text{tech}}^+)$. These functions are also depicted in Fig. 17.8. They exhibit the same asymptotic behaviour as the sand roughness. The roughness can therefore be divided into the following three regimes:

hydraulically smooth : $0 \leq k_s^+ \leq 5 \quad C^+ \approx 5.0,$

transition region : $5 < k_s^+ < 70 \quad C^+(k_s^+),$

fully rough : $70 \leq k_s^+ \quad C_r^+ \approx 8.0.$

These three regimes correspond approximately to the three layers within the boundary layer mentioned in connection with Fig. 17.3. As long as the roughness elements are still completely within the purely viscous sublayer ($k_s < 5 \delta_v$), there is no difference compared to the ideal smooth surface. However if the roughness elements project out of the purely viscous sublayer, roughness effects start. If the roughness elements project right into the overlap layer, i.e. fill up practically the entire wall layer, the viscosity effects vanish. This is now the fully rough regime for which the flow is independent of the Reynolds number.

Table 17.1 shows the equivalent sand roughness k_{seq} for some technical roughnesses. H. Schlichting (1936) determined the equivalent sand roughness for many different regularly arranged roughness elements. Some results of

Table 17.1. Equivalent sand roughness k_{seq} for technically important wall surfaces, according to DIN 1952

material	state	k_{seq} in mm
brass, copper,	smooth, without deposition	< 0.03
aluminium		
plastic		
glass		
steel	new, seamless, drawn cold	< 0.03
	new, seamless, drawn warm	
	new, seamless, rolled	
	new, welded longitudinally	
	new, welded spirally	0.10
	slightly rusted	0.10 to 0.20
	rusted	0.20 to 0.30
	encrusted	0.50 to 2
	greatly encrusted	> 2
	bituminized, new	0.03 to 0.05
	bituminized, normal	0.10 to 0.20
	galvanized	0.13
cast iron	new	0.25
	rusted	1.0 to 1.5
	encrusted	> 1.5
	bituminized, new	0.03 to 0.05
asbestos cement	coated or not, new	< 0.03
	not coated, used	0.05

these measurements are presented in Fig. 17.10. Measurements of a similar type on pipes drawn in different forms and thus made artificially rough have been carried out by V.L. Streeter (1935) and H. Möbius (1940).

No.	Type	Dimension	D [cm]	d [cm]	k [cm]	k_s [cm]	Photo
1	Spheres		4	0.41	0.41	0.093	
2			2	0.41	0.41	0.344	
3			1	0.41	0.41	1.26	
4			0.6	0.41	0.41	1.56	
5			Tightest packing	0.41	0.41	0.257	
6			1	0.21	0.21	0.172	
7			0.5	0.21	0.21	0.759	
8	Hemispherical caps		4	0.8	0.26	0.031	
9			3	0.8	0.26	0.049	
10			2	0.8	0.26	0.149	
11			Tightest packing	0.8	0.26	0.365	
12	Cones		4	0.8	0.375	0.059	
13			3	0.8	0.375	0.164	
14			2	0.8	0.375	0.374	
15	"Short" angles		4	0.8	0.30	0.291	
16			3	0.8	0.30	0.618	
17			2	0.8	0.30	1.47	

Fig. 17.10. Results from roughness measurements on regularly placed roughness elements, after H. Schlichting (1936)

k : geometric roughness height

$k_{s\text{ eq}}$: equivalent roughness height

Whereas $k_{s\text{ eq}}$ is a geometrical quantity, $k_{s\text{ eq}}^+ = k_{s\text{ eq}} u_\tau / \nu$ is a flow quantity. Depending on the flow, i.e. depending on u_τ and ν , hydraulically smooth, fully rough or transition conditions can occur for the same $k_{s\text{ eq}}$. The larger the Reynolds number, the stronger the roughness effects.

The name "smooth surface" is used to imply that the flow is in the hydraulically smooth regime. The roughness may then not exceed a so-called admissible roughness $k_{s\text{ adm}}$, for which

$$k_{s\text{ adm}}^+ = \frac{k_{s\text{ adm}} u_\tau}{\nu} = 5. \quad (17.41)$$

The equivalence between a technical roughness element and the corresponding sand roughness is an approximation which can mainly describe global values of the flow well. Details of the wall layer flow can of course

not be described in this manner. For details on the limits to this equivalence principle see the literature, for example the work by I. Tani (1987) as well as M.R. Raupach et al. (1991), N. Afzal (2008b), R. Seiferth; W. Krüger (1950), V.C. Patel (1998), J. Jiménez (2004).

Note (Profilometer roughness)

It is worth mentioning that the technical roughness k is obviously proportional to heights which can be derived from the microgeometry of the surface obtained by profilometer traces (“profilometer roughness”). K. Gersten (2004) found

$$k_{\text{tech}} = 3.5R_a ,$$

where R_a is the centerline average roughness height

$$R_a = \frac{1}{L} \int_0^L |y| dx .$$

Here y is the height relative to the mean roughness level over the length L .

Drag reduction by addition of polymers. The friction drag of turbulent water flows can be greatly reduced by the addition of small quantities of *polymers*. The experiments which have been carried out to this end indicate that the drag reduction is due to a change in the turbulence structure. The long chain of polymer molecules mainly damp the small scaled turbulence (small eddies) in the transition zone $5 < y^+ < 70$. To first approximation this acts to increase the constant C^+ , while the Karman constant κ remains unchanged. The increase in C^+ depends on the molecular weight of the polymer and its concentration.

Since only a part of the turbulence is damped by the molecular chain of polymers, no matter how much the polymer concentration is increased, laminar flow can still not be produced. P.S. Virk (1971) has determined the maximum possible drag reduction, while further details are to be found in the following summaries: J.L. Lumley (1969, 1978b), M.T. Landahl (1973), B. Gampert (1985).

Wall layer of the temperature field. If there is also heat transfer present in addition to the previously treated turbulent flow, a universal wall layer also forms for the temperature field. The kinematic viscosity ν in the flow field corresponds to the thermal diffusivity $a = \lambda/(\rho c_p)$ of the temperature field. The wall layer of the temperature field is that region where a is important. If a and ν are of the same order of magnitude, the velocity and temperature field wall layers have about the same thickness. The thermal wall layer only has universal properties if it is within the flow wall layer. This is the case for about $\text{Pr} = \nu/a > 0.5$.

If the two plates in the Couette flow in Fig. 17.1 have different temperatures, this implies that there is a constant heat flux in the entire flow, as long as the dissipation can be neglected.

Let the constant heat flux \bar{q}_w in the *thermal wall layer* be given. Then, in analogy to Eq. (17.1), we have

$$\bar{q} = \bar{q}_\lambda + q_t = \bar{q}_w = \text{const} \quad (17.42)$$

with

$$\bar{q}_\lambda = -\lambda \frac{\partial \bar{T}}{\partial y} \quad (17.43)$$

and

$$q_t = \varrho c_p \bar{T}' v'. \quad (17.44)$$

The physical properties λ , ϱ , c_p and ν are again assumed to be constant.

In analogy to the friction velocity u_τ in Eq. (17.5), we can introduce the *friction temperature*:

$$T_\tau = -\frac{\bar{q}_w}{\varrho c_p u_\tau}. \quad (17.45)$$

Introducing the dimensionless quantities

$$\Theta^+ = \frac{\bar{T} - T_{wl}}{T_\tau}, \quad q_t^+ = \frac{q_t}{\bar{q}_w}, \quad (17.46)$$

we have, in analogy to Eq. (17.13), the following relation for the wall layer:

$$\frac{1}{\text{Pr}} \frac{d\Theta^+}{dy^+} + q_t^+ = 1 \quad (17.47)$$

with the boundary condition

$$y^+ = 0 : \quad q_t^+ = 0 \quad \left(\text{i.e. } \frac{d\Theta^+}{dy^+} = \text{Pr} \right). \quad (17.48)$$

After matching up the wall layer and the core layer, we again obtain the temperature distribution in the overlap layer as

$$\lim_{y^+ \rightarrow \infty} \Theta^+(y^+, \text{Pr}) = \frac{1}{\kappa_\theta} \ln y^+ + C_\theta^+(\text{Pr}). \quad (17.49)$$

Here we chose the constant $\kappa_\theta = 0.47$, cf. M. Wier; L. Römer (1987). For a smooth wall, the constant of integration C_θ^+ is now a function of the Prandtl number $\text{Pr} = \nu/a$. It can be approximated well by

$$C_\theta^+(\text{Pr}) = 13.7 \text{Pr}^{2/3} - 7.5 \quad (\text{Pr} > 0.5). \quad (17.50)$$

For other ways of representing this function see K. Gersten; H. Herwig (1992), p. 473. In this piece of work an *analytical* representation of the temperature distribution $\Theta^+(y^+, \text{Pr})$ is also given. This describes the asymptotes for

$y^+ \rightarrow 0$, $y^+ \rightarrow \infty$ and $\text{Pr} \rightarrow \infty$ correctly. In addition, details on the effect of roughness on $C_\theta^+(\text{Pr}, k_s^+)$ (p. 486), on the balance of the temperature fluctuations (p. 479) and on the extension of Eq. (17.49) taking the dissipation into account (p. 495) are all to be found there.

17.1.3 Friction Law

Seeing as the velocity distribution u^+ in the wall layer is known (Eq. (17.26)), we must now determine it in the core layer. If the distribution of the velocity gradient $du^+/d\eta$ is known, we can obtain $u^+(\eta)$ by integration. It is natural to integrate outwards from the center line $\eta = 1$. Using

$$u_c^+ - u^+(\eta) = \int_{\eta}^1 \frac{du^+}{d\eta} d\eta \quad (17.51)$$

we then obtain the *defect* of the velocity compared to the velocity u_c^+ on the center line. Because of this manner of representing the velocity, the core layer is also called the *defect layer*. It is independent of the wall layer and therefore also independent of the Reynolds number. This has been confirmed very well by experiments, see Fig. 17.2b.

The desired velocity on the center line $u_c^+(\text{Re}_\tau)$ and thus the friction law can then be obtained from the matching condition

$$\lim_{\eta \rightarrow 0} u^+(\eta) = \lim_{y^+ \rightarrow \infty} u^+(y^+), \quad (17.52)$$

i.e. the velocity of the wall layer in Eq. (17.26) and of the defect layer in Eq. (17.51) must be the same in the overlap layer. With $y^+ = \eta \text{Re}_\tau$, Eq. (17.52) yields

$$u_c^+ - \lim_{\eta \rightarrow 0} \int_{\eta}^1 \frac{du^+}{d\eta} d\eta = \frac{1}{\kappa} \ln \eta + \frac{1}{\kappa} \ln \text{Re}_\tau + C^+. \quad (17.53)$$

If we split up the singularity of the integrand according to Eq. (17.19), the logarithmic term cancels out and we obtain the *friction law* $u_c^+(\text{Re}_\tau)$ as

$$u_c^+ = \frac{1}{\kappa} \ln \text{Re}_\tau + C^+ + \bar{C}$$

(17.54)

with

$$\bar{C} = \lim_{\eta \rightarrow 0} \int_{\eta}^1 \left(\frac{du^+}{d\eta} - \frac{1}{\kappa \eta} \right) d\eta. \quad (17.55)$$

This is an *analytical formula* for the asymptotic behaviour of the plate velocity $u_{wu} = 2\bar{C}_c$ at large Reynolds which has been obtained without using a turbulence model. Since κ and C^+ are universal constants, the result from

a turbulence model is only to be found in the constant \bar{C} via the integral (17.55). This has a value of about 2.1. Only the solution in the defect layer is required to determine \bar{C} and this solution is independent of the Reynolds number. Turbulence models are therefore only concerned with the flow in the defect layer. However, when setting up the model it must be ensured that the flow in the overlap regime satisfies the matching conditions (17.19) and (17.52) with Eq. (17.21).

Turbulent Couette flows only exist for about $\text{Re}_\tau > 100$. Therefore the effect of a turbulence model on the result for u_c^+ which comes about via the constant $\bar{C} \approx 2.1$ is maximally 11%, and this tends to decrease for increasing Reynolds numbers.

Inversion of the friction law. The friction law (17.54) is an explicit formula for the center velocity u_c as long as the wall shear stress $\bar{\tau}_w$ is given. Frequently the problem is to determine the wall shear stress for a prescribed center velocity. Dimensionlessly, this means that we need to represent the skin-friction coefficient

$$c_f = \frac{2\bar{\tau}_w}{\varrho u_c^2} = \frac{2}{u_c^{+2}} \quad (17.56)$$

as a function of the Reynolds number formed with \bar{u}_c

$$\text{Re}_c = \frac{\bar{u}_c H}{\nu}. \quad (17.57)$$

Because $\text{Re}_c = u_c^+ \text{Re}_\tau$, Eq. (17.54) yields the *implicit representation*

$$\sqrt{\frac{2}{c_f}} = \frac{1}{\kappa} \ln \left(\sqrt{\frac{c_f}{2}} \text{Re}_c \right) + C^+ + \bar{C}. \quad (17.58)$$

This allows us to derive the following *explicit* form of the friction law:

$$c_f = 2 \left[\frac{\kappa}{\ln \text{Re}_c} G(\Lambda; D) \right]^2. \quad (17.59)$$

The newly introduced function $G(\Lambda; D)$ is defined by

$$\frac{\Lambda}{G} + 2 \ln \frac{\Lambda}{G} - D = \Lambda \quad (17.60)$$

and is tabulated in K. Gersten; H. Herwig (1992), p. 782. It satisfies the asymptotic condition

$$\lim_{\Lambda \rightarrow \infty} G(\Lambda; D) = 1. \quad (17.61)$$

In the case above, it was set

$$\Lambda = 2 \ln \text{Re}_c, \quad D = 2 [\ln(2\kappa) + \kappa(C^+ + \bar{C})]. \quad (17.62)$$

Therefore c_f is a function of $\ln \text{Re}_c$ which tends to zero as $c_f = 2\kappa^2/(\ln \text{Re}_c)^2$ for $\text{Re}_c \rightarrow \infty$.

17.1.4 Turbulence Models

Now that the structure of the friction law (17.54) or (17.59) has been laid down, we now have to determine the constant \bar{C} in Eq. (17.55). To do this it will be sufficient to compute the velocity gradient distribution $du^+/d\eta$ in the defect layer. We require a turbulence model which will relate τ_t to $du^+/d\eta$. In what follows we will first describe turbulence models in quite general terms and only then specify to Couette flows with Eq. (17.10).

Eddy viscosity. J. Boussinesq (1872) suggested that, in analogy to Newton's law of friction (1.2), the following ansatz should be used for τ_t :

$$\tau_t = \mu_t \frac{\partial \bar{u}}{\partial y} = \varrho \nu_t \frac{\partial \bar{u}}{\partial y}. \quad (17.63)$$

Here $\mu_t(x, y)$ and $\nu_t(x, y)$ are not physical properties, but rather are functions of position, i.e. they are dependent on the flow under consideration. They are called the *eddy viscosity* and the *kinematic eddy viscosity* respectively. Frequently, but not really correctly, ν_t is also simply called an eddy viscosity. The word "eddy" indicates that the momentum transfer takes place because of the irregular turbulent fluctuations, i.e. because of a strongly "eddied" flow field.

At first glance it may seem as if not much has been gained from this ansatz, since now instead of τ_t we still have to model ν_t . However the latter is easier to model. From Eqs. (17.10) and (17.19) it follows from the Couette flow that

$$\lim_{\eta \rightarrow 0} \nu_t = \kappa \eta u_\tau H \quad (17.64)$$

and analogously for the upper wall that

$$\lim_{\eta \rightarrow 2} \nu_t = \kappa(2 - \eta) u_\tau H. \quad (17.65)$$

The function $\nu_t(\eta)$ is therefore a symmetric function with its maximum on the center line and its two tangents given by Eqs. (17.64) and (17.65).

Example: Parabolic or sinusoidal distribution for Couette flow

If we choose a parabolic shape for $\nu_t(\eta)$:

$$\nu_t = \kappa u_\tau H \eta(2 - \eta)/2, \quad (17.66)$$

Eq. (17.55) yields the value $\bar{C} = (\ln 2)/\kappa = 1.7$ in good agreement with experiments ($\bar{C} \approx 2.1$). If a sinusoidal shape is chosen for $\nu_t(\eta)$:

$$\nu_t = 2\kappa u_\tau H \cdot \sin(\pi\eta/2)/\pi \quad (17.67)$$

we obtain $\bar{C} = [\ln(4/\pi)]/\kappa = 0.59$, which is in less good agreement with experiment.

Mixing length. A simple relation between τ_t and $\partial \bar{u} / \partial y$ has been constructed by L. Prandtl (1925). Consider the velocity profile in Fig. 17.11. Following the molecular motion of gases, Prandtl assumes a greatly simplified model of the fluctuations, according to which the individual fluid elements are displaced by the fluctuations by a mean distance ℓ , the *mixing length*, perpendicular to the main flow direction, but still retain their momentum. The mixing length corresponds roughly to the mean free path in kinetic gas theory. According to Fig. 17.11, the element which was initially at y , and is now at $y + \ell$, has a higher velocity than its new surroundings. The velocity difference is a measure of the fluctuation velocity in the x direction:

$$\Delta u = \bar{u}(y + \ell) - \bar{u}(y).$$

If $\bar{u}(y + \ell)$ is expanded in a Taylor series up to the linear term only, we obtain

$$\Delta u = \ell \frac{\partial \bar{u}}{\partial y}.$$

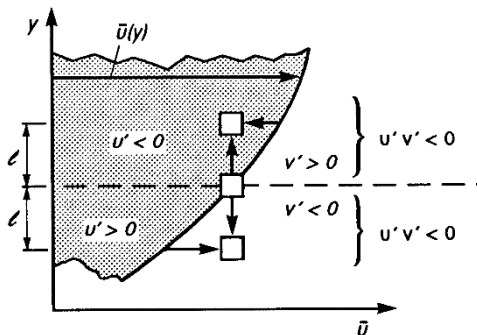


Fig. 17.11. Mixing length ℓ

Following Prandtl we assume that u' and v' have the same order of magnitude and set:

$$-\bar{u}'v' = (\Delta u)^2.$$

This yields the turbulence model of the mixing length

$$\tau_t = \varrho \ell^2 \left| \frac{\partial \bar{u}}{\partial y} \right| \left| \frac{\partial \bar{u}}{\partial y} \right|. \quad (17.68)$$

The absolute value has been taken to ensure that negative $d\bar{u}/dy$ also implies negative τ_t . The mixing length $\ell(x, y)$ can be construed as a characteristic *turbulence length* and thus is like $\nu_t(x, y)$ and must still be modelled. If we

compare the formulae for eddy viscosity and mixing length, we obtain the relation

$$\nu_t = \ell^2 \left| \frac{\partial \bar{u}}{\partial y} \right|. \quad (17.69)$$

Since for Couette flow $\tau_t = \bar{\tau}_w > 0$, Eqs. (17.63) and (17.69) for this special case yield

$$\ell = \nu_t / u_\tau, \quad (17.70)$$

i.e. the distributions for $\nu_t(y)$ and $\ell(y)$ are proportional to one another. All statements about the eddy viscosity are therefore also valid for the mixing length. In particular for the overlap layer it is found that

$$\lim_{y \rightarrow 0} \ell = \kappa y, \quad \lim_{y \rightarrow 2H} \ell = \kappa(2H - y). \quad (17.71)$$

Further turbulence models. Th. v. Kármán (1930) developed a model based on a similarity hypothesis. According to this model

$$\tau_t = \varrho \kappa^2 \left(\frac{\partial \bar{u}}{\partial y} \right)^4 / \left(\frac{\partial^2 \bar{u}}{\partial y^2} \right)^2. \quad (17.72)$$

This equation which also satisfies Eqs. (17.16) or (17.19) has yielded the name *Karman constant* for κ . A generalisation of this similarity hypothesis by K. Gersten; H. Herwig (1992), p. 404 leads, when applied to Couette flow, to the following differential equation for $\ell(y) = \nu_t(y)/u_\tau$

$$\ell \ell'' - \frac{n}{2} (\ell'^2 - \kappa^2) = 0 \quad (17.73)$$

with the boundary conditions (17.71). In order to ensure that the solution behaves regularly for $y \rightarrow 0$, n may only be one of the natural numbers. For $n = 1$ the solution is the parabola from Eq. (17.66) and for $n = 2$ we obtain the sine distribution from Eq. (17.67). Solutions for higher values of n deviate rapidly from the experimental results.

As already mentioned, more demanding turbulence models use the k -equation (16.39). Most models yield vanishing diffusion in the core region in Couette flow, so that throughout this region the turbulence production and diffusion are equal. However this has not been confirmed by experiment. W. Schneider (1989b) has suggested an improved model of the diffusion term in Eq. (16.39).

In Chap. 18 we will discuss the so-called *two-equation models* in detail. In this case, a second model equation is used in addition to the k -equation. In the following models, this second equation reduces to Eq. (17.73): the $k-L$ model by Rotta with $n = 1$, the $k-\varepsilon$ model and the $k-\omega$ model with $n = 2$, cf. K. Gersten; H. Herwig (1992), p. 409.

17.1.5 Heat Transfer

The problem is now to determine the temperature distribution $\bar{T}(y)$ between the walls and particularly the center temperature $\bar{T}_c = (T_{wu} + T_{wl})/2$ for a given heat flux \bar{q}_w . The heat transfer law is obtained in the same manner as the friction law (17.54), whereby the dimensionless temperature from Eq. (17.46) in the core layer is matched up to that in the wall layer with Eq. (17.49). We then obtain

$$\Theta_c^+(\text{Re}_\tau, \text{Pr}) = \frac{\bar{T}_c - T_{wl}}{T_\tau} = \frac{1}{\kappa_\theta} \ln \text{Re}_\tau + C_\theta^+(\text{Pr}) + \bar{C}_\theta \quad (17.74)$$

with

$$\bar{C}_\theta = \lim_{\eta \rightarrow 0} \int_{\eta}^1 \left(\frac{d\Theta^+}{d\eta} - \frac{1}{\kappa_\theta \eta} \right) d\eta. \quad (17.75)$$

The function $C_\theta^+(\text{Pr})$ is given in Eq. (17.50) for smooth walls.

Turbulence model. In order to determine \bar{C}_θ for the core layer, we require a turbulence model. Almost all known turbulence models for the temperature field are based on the concept of the *constant turbulent Prandtl number*. In analogy to Eq. (17.63), we set the turbulent heat flux from Eq. (17.44) to

$$q_t = \varrho c_p \bar{T}' v' = -\lambda_t \frac{\partial \bar{T}}{\partial y} = -\varrho c_p a_t \frac{\partial \bar{T}}{\partial y}, \quad (17.76)$$

where a_t is the *turbulent thermal diffusivity*. The definition of the *turbulent Prandtl number* then reads:

$$\text{Pr}_t = \frac{\nu_t}{a_t} = -\tau_t c_p \frac{\partial \bar{T}}{\partial y} \Big/ \left(q_t \frac{\partial \bar{u}}{\partial y} \right). \quad (17.77)$$

The laws (17.21) and (17.49) for $\text{Pr} > 0.5$ yield the following relation in the overlap layer:

$$\text{Pr}_t = \frac{\kappa}{\kappa_\theta} = \frac{0.41}{0.47} = 0.87. \quad (17.78)$$

According to this turbulence model, the turbulent Prandtl number is not only constant in the overlap layer, but also in the entire core layer. This yields $\bar{C}_\theta = (\kappa/\kappa_\theta)\bar{C} = 0.87\bar{C}$.

Again the effect of the turbulence model on Θ_c^+ is only of a few percent, and it decreases as the Reynolds number increases.

Nusselt number. Frequently the temperature difference is prescribed and the heat flux is desired. Using the Nusselt number

$$\text{Nu} = \frac{-\bar{q}_w H}{\lambda(\bar{T}_c - T_{wl})} \quad (17.79)$$

Eq. (17.74) delivers the heat transfer law

$$\text{Nu} = \frac{\frac{1}{2} c_f \text{Re}_c \text{Pr}}{\frac{\kappa}{\kappa_\theta} + \sqrt{\frac{c_f}{2}} D_\theta(\text{Pr})} \quad (17.80)$$

with

$$D_\theta(\text{Pr}) = C_\theta^+(\text{Pr}) + \bar{C}_\theta - \frac{\kappa}{\kappa_\theta}(C^+ + \bar{C}). \quad (17.81)$$

In turbulence models where the turbulent Prandtl number is constant, the function $D_\theta(\text{Pr})$ is independent of the velocity field from the model. This only affects the result via the friction law, here in the form of $c_f(\text{Re}_c)$ from Eq. (17.59).

Large Prandtl numbers. If we take Eq. (17.50) for $C_\theta^+(\text{Pr})$ into account, Eq. (17.80) may be simplified in the limit $\text{Pr} \rightarrow \infty$ to

$$\tilde{\text{Co}}_\tau = 0.073 \frac{\bar{T}_c - T_{wl}}{T_{wl}} \quad (\text{Pr} \rightarrow \infty). \quad (17.82)$$

Here we have introduced the *Colburn number* which is only formed with quantities at the wall:

$$\tilde{\text{Co}}_\tau = \frac{-\bar{q}_w \text{Pr}^{2/3}}{\rho c_p u_\tau T_{wl}}. \quad (17.83)$$

Since the formula (17.82) is independent of the core layer and thus of the turbulent model too, it is valid for *all* turbulent flows at high Reynolds numbers, as long as c_f is non-zero. Here \bar{T}_c is generally the temperature outside the thermal boundary layer. Instead of the factor 0.073, one frequently finds somewhat different numerical values in the literature, cf. K. Gersten; H. Herwig (1992), p. 478.

17.2 Fully Developed Internal Flows ($A = \text{const}$)

17.2.1 Channel Flow

In plane channel flow (also called *Poiseuille flow*), both plates in Fig. 17.1 are fixed and a constant pressure gradient $d\bar{p}_w/dx < 0$ causes a flow in the x direction. Equation (16.35) yields the fundamental equation

$$\frac{d\bar{\tau}}{dy} = \frac{d\bar{p}_w}{dx} \quad (17.84)$$

and after integration, using Eq. (17.1),

$$\bar{\tau} = \varrho\nu \frac{d\bar{u}}{dy} + \tau_t = \bar{\tau}_{wl} + \frac{d\bar{p}_w}{dx} y. \quad (17.85)$$

The shear stress $\bar{\tau}(y)$ is therefore a linear function and for reasons of symmetry it must hold that

$$\bar{\tau}(y = H) = 0, \quad \bar{\tau}_{wl} = -\bar{\tau}_{wu} = -(d\bar{p}_w/dx)H > 0.$$

Using the dimensionless quantities

$$\eta = \frac{y}{H}, \quad u^+ = \frac{\bar{u}}{u_\tau}, \quad \tau_t^+ = \frac{\tau_t}{\bar{\tau}_{wl}}, \quad u_\tau = \sqrt{\frac{\bar{\tau}_{wl}}{\varrho}}, \quad \text{Re}_\tau = \frac{u_\tau H}{\nu} \quad (17.86)$$

Eq. (17.85) delivers

$$\frac{1}{\text{Re}_\tau} \frac{du^+}{d\eta} + \tau_t^+ = 1 - \eta. \quad (17.87)$$

In contrast to the corresponding equation (17.8) for Couette flow, here there is also a term proportional to η which is due to the pressure gradient.

Introducing the wall coordinate y^+ as in Eq. (17.12), Eq. (17.87) yields

$$\frac{du^+}{dy^+} + \tau_t^+ = 1 - \frac{y^+}{\text{Re}_\tau}. \quad (17.88)$$

For $\text{Re}_\tau \rightarrow \infty$ this becomes the universal equation (17.13). Therefore at large Reynolds numbers the pressure gradient has *no* effect on the wall layer flow, so that the results for the wall layer of Couette flow may be carried over to any turbulent flows with the same wall shear stress.

As before, Eqs. (17.54) and (17.55) are still valid for the velocity on the center line u_c^+ (= maximum velocity). In order to determine the volume flux, we need the mean velocity

$$u_m^+ = \lim_{\eta \rightarrow 0} \int_{\eta}^1 u^+(\eta) d\eta = u_c^+ + \bar{C} \quad (17.89)$$

with

$$\overline{\overline{C}} = \lim_{\eta \rightarrow 0} \int_{\eta}^1 [u^+(\eta) - u_c^+] d\eta. \quad (17.90)$$

The constant $\overline{\overline{C}}$ is, as an integral over the velocity defect just as \overline{C} , independent of the Reynolds number. Therefore the friction law reads

$$u_m^+ = \frac{1}{\kappa} \ln \text{Re}_\tau + C^+ + \overline{C} + \overline{\overline{C}} \quad (17.91)$$

or

$$c_f = \frac{2\overline{\tau}_{wl}}{\rho u_m^2} = \frac{\lambda}{4} = 2 \left[\frac{\kappa}{\ln \text{Re}_{dh}} G(A; D) \right]^2 \quad (17.92)$$

with

$$A = 2 \ln \text{Re}_{dh}$$

and

$$D = 2 \left[\ln(2\kappa) + \kappa \left(C^+ + \overline{C} + \overline{\overline{C}} - \frac{1}{\kappa} \ln 4 \right) \right],$$

cf. Eq. (17.60). Measurements have yielded $\overline{C} = 0.94$, $\overline{\overline{C}} = -2.64$ and $\overline{C} + \overline{\overline{C}} = -1.7$, and thus $D = -4.56 + 0.82C^+$. The Reynolds number $\text{Re}_{dh} = d_h u_m / \nu$ has been formed with the hydraulic diameter $d_h = 4H$. Equations (17.91) and (17.92) are valid for both smooth and rough channel walls (as long as the roughness on both walls is the same, cf. K. Hanjalić; B.E. Launder (1972b)).

The ansatz for the eddy viscosity

$$\nu_t / (u_\tau H) = (\kappa/6)[1 - (1 - \eta)^2][1 + 2(1 - \eta)^2] \quad (17.93)$$

delivers good agreement with measurements, yielding $\overline{C} + \overline{\overline{C}} = -1.6$; cf. K. Gersten; H. Herwig (1992), p. 593. This piece of work also contains results of other turbulence models and details on the functions $k(\eta)$ and $\varepsilon(\eta)$, cf. also M.M.M. El Telbany; A.J. Reynolds (1980).

Information regarding the heat transfer can also be found in K. Gersten; H. Herwig (1992), and also in M. Voigt (1994).

17.2.2 Couette–Poiseuille Flows

Consider the fully developed turbulent flow between two parallel plates as in Fig. 17.12. Here, as in Couette flow, the upper plate moves with u_{wu} , and there is additionally, as in channel flow, a constant pressure gradient $d\bar{p}_w/dx$. The flows which take place in this manner are called *Couette–Poiseuille flows*, because they yield the Couette flow ($d\bar{p}_w/dx = 0$) and the Poiseuille flow (channel flow, $u_{wu} = 0$) as special cases.

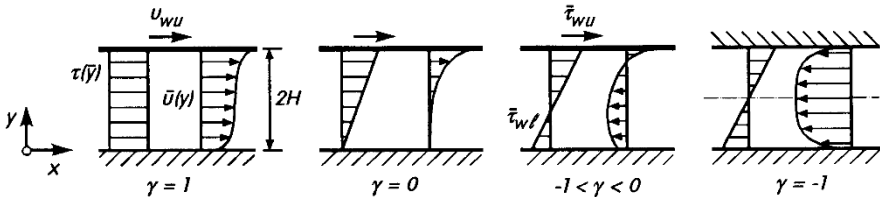


Fig. 17.12. Couette–Poiseuille flows, $\gamma = \bar{\tau}_{wl}/\bar{\tau}_{wu}$

Balance of forces. If the frictional velocity of the lower plate $u_\tau = \sqrt{\bar{\tau}_{wl}/\rho}$ is chosen as the reference velocity, and the dimensionless quantities

$$\gamma = \frac{\bar{\tau}_{wl}}{\bar{\tau}_{wu}}, \quad \gamma_R = \text{sign}(\gamma) \sqrt{|\gamma|} \quad (17.94)$$

introduced, the momentum equation in the x direction becomes

$$\frac{1}{Re_\tau} \frac{du^+}{d\eta} + \tau_t^+ = 1 + \frac{1-\gamma}{2\gamma} \eta. \quad (17.95)$$

This equation reduces to Eq. (17.8) for $\gamma = 1$ (Couette flow) and to Eq. (17.87) for $\gamma = -1$ (channel flow). As long as $\bar{\tau}_{wl}$ and $\bar{\tau}_{wu}$ are non-zero, matching up the wall layer is carried out via the logarithmic overlap law (17.21). Special treatment is required for the case $\gamma = \gamma_R = 0$ (i.e. $\bar{\tau}_{wl} = 0$) however.

Vanishing wall shear stress ($\bar{\tau}_{wl} = 0$). Equation (17.84) is also valid for this case, and after integration it yields

$$\frac{\bar{\tau}}{\rho} = \nu \frac{d\bar{u}}{dy} + \frac{\tau_t}{\rho} = \frac{1}{\rho} \frac{d\bar{p}_w}{dx} y \quad (17.96)$$

with

$$\frac{1}{\rho} \frac{d\bar{p}_w}{dx} = \frac{\bar{\tau}_{wu}}{2\rho H} > 0. \quad (17.97)$$

Therefore the shear stress is proportional to the distance from the wall y .

Since the friction velocity at the lower wall vanishes, another reference velocity must be chosen. The flow in the viscous wall layer must be independent of H . There we have the following dependence

$$f \left(\frac{d\bar{u}}{dy}, y, \nu, \frac{1}{\rho} \frac{d\bar{p}_w}{dx} \right) = 0. \quad (17.98)$$

From dimensional analysis we then obtain the *universal* relation

$u^\times = F(y^\times)$

(17.99)

with

$$u^x = \frac{\bar{u}}{u_s}; \quad y^x = \frac{yu_s}{\nu}, \quad (17.100)$$

where

$$u_s = \left(\frac{\nu}{\varrho} \frac{dp_w}{dx} \right)^{1/3} \quad (17.101)$$

is the new reference velocity. This corresponds to the friction velocity u_τ at finite wall shear stresses.

The condition that $d\bar{u}/dy$ must also be independent of ν in the overlap regime yields the *overlap law for vanishing wall shear stress*

$$\lim_{y^x \rightarrow \infty} \frac{du^x}{dy^x} = \frac{1}{\kappa_\infty \sqrt{y^x}} \quad (17.102)$$

or, after integration

$$\lim_{y^x \rightarrow \infty} u^x = \frac{2}{\kappa_\infty} \sqrt{y^x} + C^x. \quad (17.103)$$

Therefore there is a *square root law* for the velocity in the overlap layer instead of the logarithmic law for non-vanishing wall shear stress.

The two constants κ_∞ and C^x are again universal, since the law of the wall (17.99) is valid at points of vanishing wall shear stress (separation or reattachment points) for arbitrary turbulent flows. The numerical values for κ_∞ and C^x found in the literature do vary somewhat: $0.41 \leq \kappa_\infty \leq 0.8$; $-3.2 \leq C^x \leq 2.2$, cf. J. Klauer (1989). In what follows we will use the values $\kappa_\infty = 0.6$ and $C^x = 0$ which were obtained from the measurements by R. Kiel (1995).

The universal velocity distribution (17.99) is shown in Fig. 17.13. Since u^x is plotted against $\sqrt{y^x}$, Eq. (17.103) is a straight line here.

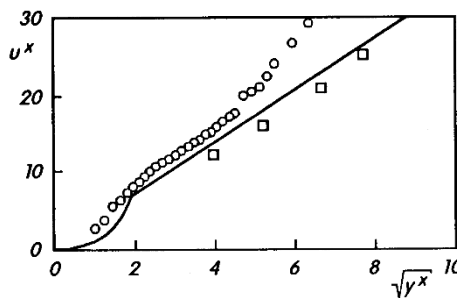


Fig. 17.13. Universal velocity distribution $u^x = F(y^x)$ in the wall layer for vanishing wall shear stress, from Eq. (17.99)

- measurements by R. Kiel (1995)
- measurements by P. Dengel, H.H. Fernholz (1990)

asymptote for $y^x \rightarrow \infty$: Eq. (17.103), $\kappa_\infty = 0.59$, $C^x \approx 0$
asymptote for $y^x \rightarrow 0$: $u^x = y^{x/2}$

Generalised law of the wall. The question emerges as to how the transition from logarithmic overlap law to the square root law takes place as the case of vanishing wall shear stress is approached. This is a case of a *singular distinguished limit* with $1/\text{Re}_\tau \rightarrow 0$ and $\gamma_R \rightarrow 0$, cf. K. Gersten; H. Herwig (1992), p. 584 and K. Gersten et al. (1993). The two limiting processes must be coupled together so that the *coupling parameter*

$$K = \frac{\nu}{u_{\tau l} \bar{\tau}_{wl}} \frac{d\bar{p}_w}{dx} = \left(\frac{u_s}{u_{\tau l}} \right)^3 \sim (\text{Re}_{\tau l} \gamma)^{-1} \quad (17.104)$$

is kept constant. Cases with finite wall shear stress are denoted by $K \rightarrow 0$, while $K \rightarrow \infty$ corresponds to the case of vanishing wall shear stress. The coupling parameter K is frequently denoted $-p^+$ or p_\times^+ in the literature, cf. T. Cebeci; P. Bradshaw (1984), p. 357 and T.B. Nickels (2004). The balance of forces (17.95) may then be written down in wall coordinates:

$$\tau^+(y^+) = \frac{|\tau_w|}{\tau_w} \frac{du^+}{dy^+} + \tau_t^+ = 1 + Ky^+. \quad (17.105)$$

Thus the generalised law of the wall has the form:

$$\frac{du^+}{dy^+} = F'(y^+, K); \quad u^+ = F(y^+, K). \quad (17.106)$$

The overlap layer between the viscous wall layer and the adjoining fully turbulent layer is denoted by vanishing viscosity effect at constant K . Here

$$\frac{d\bar{u}}{dy} = f \left(y, \frac{\tau_t}{\varrho}, K \right) \quad (17.107)$$

and using Eq. (17.105) it is found that

$$\tau_t^+ = 1 + Ky^+. \quad (17.108)$$

According to the Π theorem in dimensional analysis, it follows from Eqs. (17.107) and (17.108) that

$$\lim_{y \rightarrow 0} \frac{y}{\sqrt{\tau_t / \varrho}} \frac{d\bar{u}}{dy} = \lim_{y^+ \rightarrow \infty} \left(\frac{y^+}{\sqrt{1 + Ky^+}} \frac{du^+}{dy^+} \right) = \frac{1}{\kappa(K)} \quad (17.109)$$

or, after integration over the wall layer

$$\begin{aligned} \lim_{y^+ \rightarrow \infty} u^+(y^+, K) &= \frac{1}{\kappa(K)} \left[\ln y^+ + 2(\sqrt{1 + Ky^+} - 1) \right. \\ &\quad \left. + 2 \ln \left(\frac{2}{\sqrt{1 + Ky^+} + 1} \right) \right] + C(K) \quad . \end{aligned} \quad (17.110)$$

This is the *generalised overlap law* with the two universal functions $\kappa(K)$ and $C(K)$. For the limiting cases we find:

attached flow ($\bar{\tau}_w \neq 0$) : $K \rightarrow 0$

$$C(0) = C^+, \quad \kappa(0) = \kappa_0 = 0.41$$

Eq. (17.110) reduces to Eq. (17.21),

separation (reattachment) ($\bar{\tau}_w = 0$) : $K \rightarrow \infty$

$$C(\infty) = K^{1/3} C^\times + \frac{1}{\kappa_\infty} \ln K, \quad \kappa(\infty) = \kappa_\infty$$

Eq. (17.110) reduces to Eq. (17.103).

Figure 17.14 shows the functions $\kappa(K)$ and $C(K)$ in comparison with measurements.

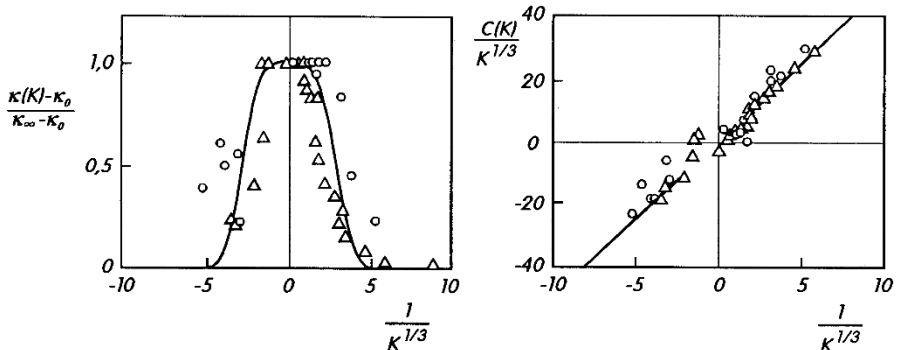


Fig. 17.14. The functions $\kappa(K)$ and $C(K)$ from Eq. (17.110), after D. Vieth (1996). Comparison with measurements

If the core layer and the wall layer are matched up using the generalised overlap law, we eventually obtain the velocity at the upper wall as

$$u_{wu}^+(\gamma) = u_c^+ + \frac{1}{\kappa} \ln \text{Re}_\tau + C^+ + \hat{C}_2(\gamma) \quad (17.111)$$

and the friction law becomes

$$u_m^+(\gamma, K) = u_c^+ + \overline{\overline{C}}(\gamma) \quad (17.112)$$

with

$$u_c^+(\gamma, K) = \gamma_R C(K) + \frac{1}{\kappa(K)} \left[W(\gamma) + \gamma_R \ln \frac{4}{|K|} \right] + \hat{C}_1(\gamma). \quad (17.113)$$

The functions $W(\gamma)$, $\hat{C}_1(\gamma)$, $\hat{C}_2(\gamma)$ and $\bar{C}(\gamma)$ depend on the turbulence model used. They are continuous at the point $\gamma = 0$, as can be seen from Fig. 17.15, cf. K. Gersten et al. (1993).

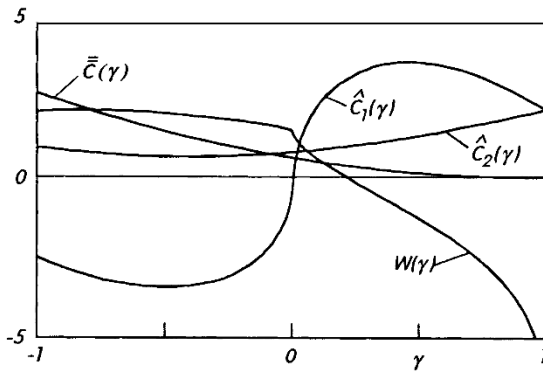


Fig. 17.15. The functions $\hat{C}_1(\gamma)$, $\hat{C}_2(\gamma)$, $\bar{C}(\gamma)$ and $W(\gamma)$ from Eq. (17.111) to (17.113) for Couette–Poiseuille flow, $\gamma = \bar{\tau}_{wl}/\bar{\tau}_{wu}$

Turbulence models for $\gamma \leq 0$. In the region $-1 < \gamma < 0$ “backflow” occurs. This means that the sign of the velocity and the shear stress changes. Since τ_t and $d\bar{u}/dy$ are proportional for the turbulence models of the eddy viscosity from Eq. (17.63) and the mixing length from Eq. (17.68), according to these models τ_t and $d\bar{u}/dy$ vanish at the same distance from the wall. However this has not been confirmed by experiment. In addition, $\ell(\eta)$ becomes singular at the points $du^+/d\eta = 0$, also for channel flow ($\gamma = -1$). Apart from the *indirect* turbulence model in Fig. 17.15, there is still no model in existence which describes the region $-1 < \gamma \leq 0$ properly.

17.2.3 Pipe Flow

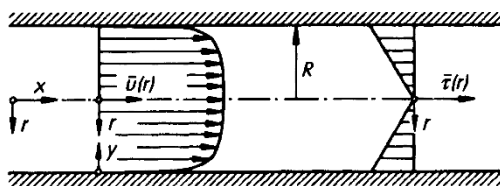


Fig. 17.16. Turbulent pipe flow. Distributions $\bar{u}(r)$ and $\bar{\tau}(r)$, v is the velocity component in the r direction

We consider fully developed turbulent pipe flow, as in Fig. 17.16. In order to describe this flow we will use cylindrical coordinates x, r, φ with the velocities u, v, w . Initially we will assume the physical properties to be constant.

The momentum equation in the x direction is

$$\frac{1}{r} \frac{d}{dr}(r \bar{\tau}) = \frac{dp_w}{dx} \quad (17.114)$$

with

$$\bar{\tau} = \varrho\nu \frac{d\bar{u}}{dr} - \varrho \overline{u'v'} = \varrho\nu \frac{d\bar{u}}{dr} + \tau_t. \quad (17.115)$$

This corresponds to Eq. (17.84) and (17.85) for channel flow. Integration of Eq. (17.114) over the radius yields

$$\bar{\tau} = \frac{dp_w}{dx} \frac{r}{2} = \frac{r}{R} \bar{\tau}_w. \quad (17.116)$$

Therefore the shear stress is proportional to the local radius r . Here the gradient $d\bar{\tau}/dr$ is equal to half the pressure gradient. Using the dimensionless quantities

$$\eta = \frac{r}{R}, \quad u^+ = \frac{\bar{u}}{u_\tau}, \quad \tau_t^+ = \frac{\tau_t}{\bar{\tau}_w}, \quad u_\tau = \sqrt{\frac{-\bar{\tau}_w}{\varrho}}, \quad \text{Re}_\tau = \frac{Ru_\tau}{\nu}, \quad (17.117)$$

combining Eqs. (17.114) to (17.116) yields

$$-\frac{1}{\text{Re}_\tau} \frac{du^+}{d\eta} + \tau_t^+ = \eta. \quad (17.118)$$

Again we look for the function $u^+(\eta, \text{Re}_\tau)$ for $\text{Re}_\tau \rightarrow \infty$.

Friction law. For $\text{Re}_\tau \rightarrow \infty$, the velocity distribution $u^+(\eta, \text{Re}_\tau)$ is again made up of two parts. Introducing the wall layer coordinate

$$y^+ = (1 - \eta) \text{Re}_\tau \quad (17.119)$$

and then carrying out the limit $\text{Re}_\tau \rightarrow \infty$, Eq. (17.118) again yields the universal equation (17.13) for the wall layer. The universal wall solution $u^+(y^+)$ such as that in Eq. (17.26) can therefore be carried over to this case. For the core layer, Eq. (17.118) yields $\tau_t^+ = \eta$. Here the equation to determine $u^+(\eta)$ must be obtained from a turbulence model. The overlap law reads

$$\lim_{\eta \rightarrow 1} \frac{du^+}{d\eta} = -\frac{1}{\kappa(1 - \eta)}. \quad (17.120)$$

If $du^+/d\eta$ is known, this can be integrated to obtain the velocity distribution in the form of a *velocity defect law* as follows

$$u^+(\eta) - u_c^+ = \int_0^\eta \frac{du^+}{d\eta} d\eta. \quad (17.121)$$

Here u_c^+ is the velocity on the axis (the maximum velocity).

The matching condition in the overlap layer

$$\lim_{\eta \rightarrow 1} u^+(\eta) = \lim_{y^+ \rightarrow \infty} u^+(y^+) = \frac{1}{\kappa} \ln y^+ + C^+ \quad (17.122)$$

yields the axial velocity

$$u_c^+ = \frac{1}{\kappa} \ln \text{Re}_\tau + C^+ + \bar{C} \quad (17.123)$$

with

$$\bar{C} = -\lim_{\eta \rightarrow 1} \int_0^\eta \left[\frac{du^+}{d\eta} + \frac{1}{\kappa(1-\eta)} \right] d\eta. \quad (17.124)$$

For the velocity averaged over the cross-section of the pipe we obtain

$$u_m^+ = \frac{u_m}{u_\tau} = \frac{2}{u_\tau R^2} \int_0^R \bar{u} r dr = 2 \int_0^1 u^+ \eta d\eta = u_c^+ + \bar{\bar{C}} \quad (17.125)$$

with

$$\bar{\bar{C}} = -2 \lim_{\eta \rightarrow 1} \int_0^\eta (u_c^+ - u^+) \eta d\eta. \quad (17.126)$$

Therefore the friction law reads

$$u_m^+ = \frac{1}{\kappa} \ln \text{Re}_\tau + C^+ + \bar{C} + \bar{\bar{C}}. \quad (17.127)$$

Since the wall shear stress over the pressure drop can be determined very precisely by experiment for pipe flow, reliable data are available for the constants \bar{C} and $\bar{\bar{C}}$. It is found that $\bar{C} + \bar{\bar{C}} = -3.04$.

Frequently the friction law is taken to be the dependence of the skin-friction coefficient c_f or the pipe friction factor λ

$$c_f = \frac{\lambda}{4} = \frac{-2\bar{\tau}_w}{\varrho u_m^2} = \frac{2}{u_m^{+2}} \quad (17.128)$$

on the Reynolds number

$$\text{Re} = \frac{u_m d}{\nu} = 2 \text{Re}_\tau \sqrt{\frac{2}{c_f}}. \quad (17.129)$$

For smooth surfaces ($C^+ = 5.0$), Eq. (17.127) yields the *implicit* form

$$\frac{1}{\sqrt{\lambda}} = 2 \log(\text{Re} \sqrt{\lambda}) - 0.80 \quad (17.130)$$

given by L. Prandtl (1933). (Recent measurements at high Reynolds numbers by M.V. Zagarola; A.J. Smits (1998) have yielded the constants instead of 2.0 and -0.8 as 1.93 and -0.554 respectively.) The explicit form of the friction law for smooth pipes reads

$$c_f = \frac{\lambda}{4} = 2 \left[\frac{\kappa}{\ln \text{Re}} G(\Lambda; D) \right]^2 \quad (17.131)$$

with the G-function as in Eq. (17.60) and $\Lambda = 2 \ln \text{Re}$, $D = -0.17$. See also K. Gersten (2004).

Figure 17.17 shows the resistance diagram according to H. Rouse (1943). It includes both the implicit as well as the explicit representation. In particular, the asymptotic behaviour for the turbulent region can be seen easily. For rough pipes, Eq. (17.40) was used. In the *fully rough* regime ($k_{\text{tech}}^+ > 70$), instead of Eq. (17.130), one uses

$$\frac{1}{\sqrt{\lambda}} = 2 \log \frac{R}{k_{\text{tech}}} + 1.74. \quad (17.132)$$

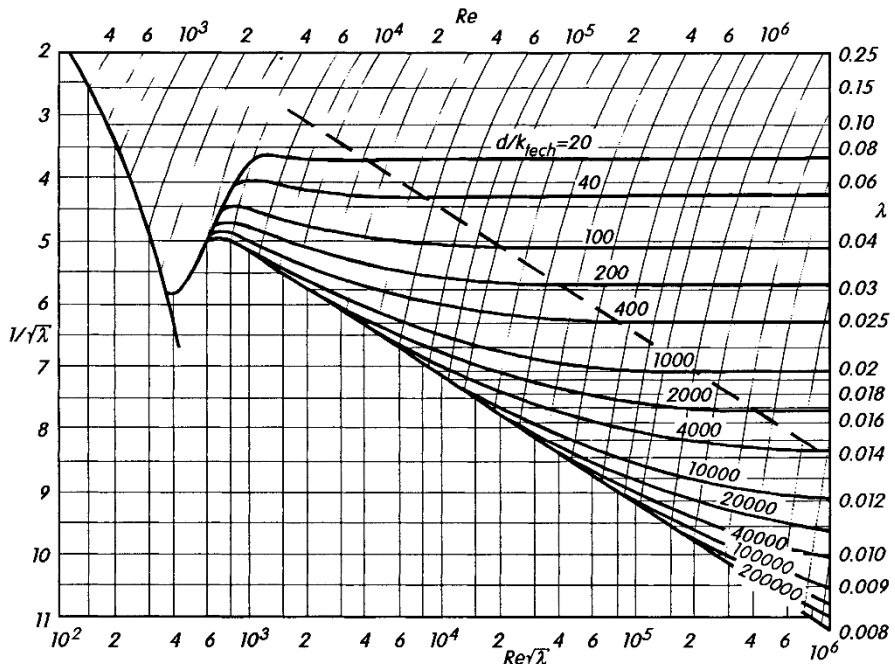
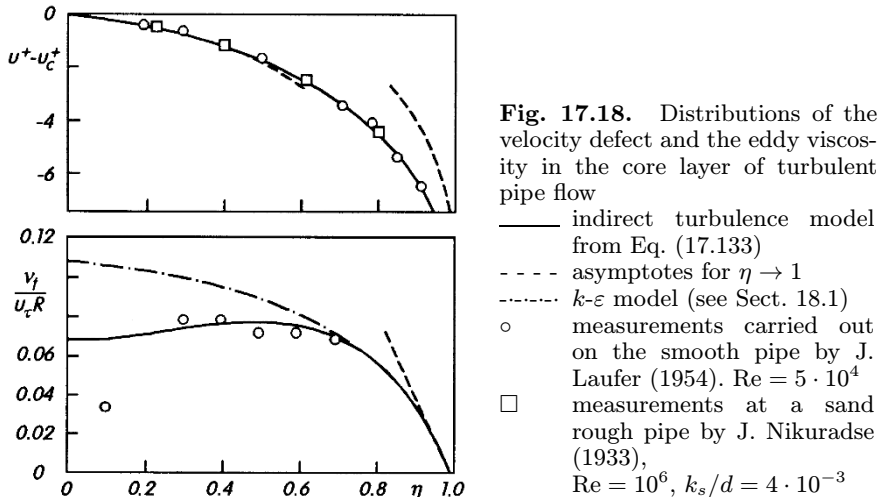


Fig. 17.17. Pipe resistance diagram according to H. Rouse (1943). On the right hand side of the curve — · — is the fully rough regime. Each point on this diagram is determined by the pair (Re, λ) . The horizontal lines are those where $\lambda = \text{const}$, and λ may be read off the right edge, or $1/\sqrt{\lambda}$ off the left edge. The vertical lines are those where $Re\sqrt{\lambda}$ is constant (reading off the lower edge). In addition, in the upper half of the diagram the lines $Re = \text{const}$ have been drawn in (reading Re off the upper edge). The curves shown are those where $d/k_{\text{tech}} = \text{const}$

Eddy viscosity. If we choose the following distribution of the eddy viscosity for the turbulence model:

$$\frac{\nu_t}{u_\tau R} = -\frac{\tau_t^+}{du^+/d\eta} = -\frac{\eta}{du^+/d\eta} = \frac{\kappa}{6}(1 - \eta^2)(1 + 2\eta^2), \quad (17.133)$$

cf. also Eq. (17.93), it follows that $\overline{C} + \overline{\bar{C}} = -3.03$, in very good agreement with the experimental value. Figure 17.18 shows this distribution $\nu_t(\eta)$ in comparison with measurements. The distribution of the velocity defect which is also shown is in good agreement with experimental data too. The distributions for the kinetic energy, the diffusion and the dissipation in a pipe and the results with other turbulence models have been presented by K. Gersten; H. Herwig (1992), p. 531.



Wall heat transfer. In analogy to Eq. (17.80) we obtain the heat transfer law for the pipe

$$\text{Nu} = \frac{-\bar{q}_w d}{\lambda(T_w - T_m)} = \frac{\frac{1}{2} c_f \text{Re Pr}}{\frac{\kappa}{\kappa_\theta} + \sqrt{\frac{c_f}{2} D_\theta(\text{Pr})}}. \quad (17.134)$$

Here the bulk temperature (or mean temperature) has been defined as

$$T_m = \frac{1}{\pi R^2 u_m} \int_0^R \bar{T}(r) \bar{u}(r) 2\pi r dr. \quad (17.135)$$

The function $D_\theta(\text{Pr})$ depends on the given thermal boundary condition (e.g. $\bar{q}_w = \text{const}$ or $T_w = \text{const}$) and a turbulence model is required to be able to compute it, cf. K. Gersten; H. Herwig (1992), p. 540. This work also contains information on the fact that the dissipation which is generally neglected can indeed be of great importance at high Prandtl numbers, cf. K. Gersten (1997).

Variable physical properties. If we take the temperature dependence of the physical properties into account, the heat transfer law (17.134) changes. The temperature field then generally has an effect on the velocity field, and thus too on the friction law. According to K. Gersten; H. Herwig (1992), p. 558:

$$\frac{c_f}{c_{f_{c.p.}}} = \left(\frac{\varrho_w}{\varrho_m} \right)^{m_\varrho} \left(\frac{\mu_w}{\mu_m} \right)^{m_\mu}. \quad (17.136)$$

Here the indices w imply the wall temperature, m the mean temperature and c.p. constant physical properties. If the mean temperature is chosen as a reference temperature, i.e. c_f and Re are formed with physical properties at T_m , then

$$m_\varrho = \frac{1}{2} - 4.9 \sqrt{\frac{c_{f_{c.p.}}}{2}}, \quad m_\mu = 4.9 \sqrt{\frac{c_{f_{c.p.}}}{2}}. \quad (17.137)$$

If the density is variable, additional buoyancy forces due to the effect of gravity arise in the flow. These are particularly noticeable in vertical pipes, cf. K. Gersten; H. Herwig (1992), p. 568.

17.3 Slender–Channel Theory

All the internal flows considered until now had layered structures in common. The flows could be divided up into the core flow with a velocity defect which was independent of the viscosity and a viscous wall layer. This structure is also present in channels or pipes which are slightly widened (diffusers) or narrowed (nozzles). When the double limit $\text{Re} \rightarrow \infty$ (or $c_f \rightarrow 0$) and angle of inclination of the contour $\alpha \rightarrow 0$ is studied, the simplifications compared to the complete fundamental equations are considerable. This is *slender-channel theory*, and was described for laminar flows in Sect. 5.1.2 already.

Plane nozzles and diffusers. Slender–channel theory will now be applied to plane nozzle and diffuser flows where the walls are straight. In this case self-similar solutions are found, i.e. computing these flows is reduced to the solutions of ordinary differential equations.

If we choose a system of polar coordinates r, φ , the equation of motion in the core region reads

$$\varrho \bar{u} \frac{\partial \bar{u}}{\partial r} = - \frac{d \bar{p}_w}{dr} + \frac{1}{r} \frac{\partial \tau_t}{\partial \varphi}. \quad (17.138)$$

The inviscid flow ($\text{Re} \rightarrow \infty, \tau_t = 0$) satisfies the equation

$$\varrho U \frac{dU}{dr} = - \frac{dp_0}{dr} \quad (17.139)$$

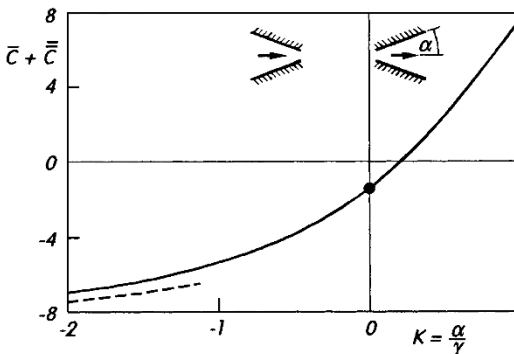


Fig. 17.19. \bar{C} and $\bar{\bar{C}}$ as functions of K for slender plane channels (straight walls), from Eq. (17.149)

diffusers: $\alpha > 0, u_{\max} > 0,$

$$\bar{\tau}_w(\eta = 1) < 0$$

nozzles: $\alpha < 0, u_{\max} < 0,$

$$\bar{\tau}_w(\eta = 1) > 0$$

with the solution

$$U = \text{sign} \left(\frac{dp_0}{dr} \right) \sqrt{\frac{r^3}{\varrho} \left| \frac{dp_0}{dr} \right|} \frac{1}{r}. \quad (17.140)$$

The desired solution is a small perturbation of this solution for $c_f \rightarrow 0$.

Using the trial solutions

$$\frac{\bar{u}(r, \varphi)}{U(r)} = 1 - \gamma F'(\eta), \quad \eta = \frac{\varphi}{\alpha}, \quad \gamma = \frac{u_\tau}{U}, \quad (17.141)$$

$$\frac{\tau_t(r, \varphi)}{\varrho U(r)^2} = \gamma^2 S(\eta), \quad u_\tau = \text{sign } \alpha \sqrt{\frac{-\bar{\tau}_w(\eta = 1)}{\varrho}}, \quad (17.142)$$

$$\frac{d\bar{p}_w}{dr} = \frac{dp_0}{dr} + \gamma^2 \frac{\varrho U^2}{r \alpha} P \quad (17.143)$$

Eq. (17.138) yields the ordinary differential equation

$$2K F'(\eta) = S'(\eta) - P \quad (17.144)$$

with the boundary conditions

$$\begin{aligned} \eta = 0 : \quad F' &= 0, \quad F'' = 0, \quad S = 0 \\ \eta \rightarrow 1 : \quad F'' &= \frac{1}{\kappa(1 - \eta)}, \quad S = 1. \end{aligned} \quad (17.145)$$

Here the *slender-channel parameter*

$$K = \frac{\alpha}{\gamma} = \frac{\alpha U}{u_\tau} \quad (17.146)$$

was introduced. This is kept constant in performing the double limit $u_\tau \rightarrow 0, \alpha \rightarrow 0$.

The friction law is again

$$c_{f_m} = \frac{2|\bar{\tau}_w|}{\varrho u_m^2} = 2 \left[\frac{\kappa}{\ln \text{Re}_{dh}} G(\Lambda; D) \right]^2, \quad (17.147)$$

with the Reynolds number

$$\text{Re}_{\text{dh}} = \frac{4u_m r \alpha}{\nu} \quad (17.148)$$

formed with the hydraulic diameter. The function $G(\Lambda; D)$ from Eq. (17.60) contains the parameters

$$\Lambda = 2 \ln \text{Re}_{\text{dh}}, \quad D(K) = 2[\ln(\kappa/2) + \kappa(C^+ + \bar{C} + \bar{\bar{C}})]. \quad (17.149)$$

The dependence of the quantity $\bar{C} + \bar{\bar{C}}$ on K is shown in Fig. 17.19. A turbulence model was required to compute this; it is described in K. Gersten; B. Rocklage (1994). The straight channel corresponds to $K = 0$.

In the limiting case $K \rightarrow -\infty$, the flow has boundary-layer character, i.e. as well as the inviscid turbulence-free core flow, a turbulent flow forms close to the wall as a boundary layer. This will be discussed more closely in Sect. 18.2.4. The limiting case $K \rightarrow +\infty$ with the transition to separation has been treated by B. Rocklage (1996). The heat transfer law for plane nozzles and diffusers has also been presented by B. Rocklage (1995).

Entrance flows for channels and pipes. The transition from a homogeneous velocity profile in the entrance cross-section of a channel or pipe to the fully developed velocity profile takes place in an entry flow. This flow can also be computed using slender-channel theory, i.e. it again has a layered structure, with a core layer and a wall layer.

M. Voigt (1994) has carried out these calculations according to slender-channel theory for channels and pipes, also for the case of thermal entrance flows, cf. H. Herwig; M. Voigt (1995, 1996).

18. Turbulent Boundary Layers without Coupling of the Velocity Field to the Temperature Field

18.1 Turbulence Models

18.1.1 Remark

In this chapter we will look at turbulent plane flows with constant physical properties. As has already been explained in Sect. 16.6, turbulent flows also have boundary-layer character at high Reynolds numbers, i.e. the entire flow field consists of the inviscid outer flow and the thin turbulent boundary layer close to the wall, for which the boundary-layer equations (16.34) to (16.36) hold. However these equations do not form a closed system. A turbulence model is required for the so-called closure problem; this presents additional equations which connect the turbulent shear stress τ_t (and the turbulent heat flux q_t) with the mean motion (or with the mean temperature field).

In general this relation is a partial differential equation. If the equation contains new unknowns, for example the turbulent dissipation $\varepsilon(x, y)$, further model equations are required. Depending on how many partial differential equations are used, the model is called a *one-equation model*, a *two-equation model*, etc. If an ordinary differential equation for a quantity which is only dependent on x , for example $\tau_{t\max}(x)$, is used instead of a second partial differential equation, we are dealing with a *one-and-a-half-equation model*. If the relation between τ_t and the quantities of the mean motion are given by algebraic equations, this *algebraic turbulence model* is also called a *zero-equation model*. Examples of this are the models of the *eddy viscosity* and the *mixing length* mentioned in Sect. 17.1.4.

In what follows we will discuss typical examples from the different turbulence model categories. Here the model equations will be presented in the simplified form for the boundary layer (e.g. neglecting the variation in the diffusion flux in the x direction).

At high Reynolds numbers, turbulent boundary layers also have a layered character. They essentially consist of two layers, the *viscous wall layer* and the *fully turbulent outer flow*, in which the viscosity effects may be neglected.

At finite wall shear stress $\bar{\tau}_w(x)$, the thickness of the viscous wall layer is proportional to $\delta_v = \nu/u_\tau(x)$ with the local shear stress velocity $u_\tau(x) = \sqrt{\bar{\tau}_w(x)/\rho}$ from Eq. (17.5). It can be shown, cf. K. Gersten; H. Herwig (1992), p. 669, that the viscous wall layer is so thin for $\text{Re} \rightarrow \infty$ (i.e. $\nu \rightarrow 0$) that the

inertial and pressure forces may be neglected compared to the friction forces. Therefore the viscous wall layer is locally identical to that of a Couette flow with the same $\bar{\tau}_w$ and ν . In this wall layer the universal laws of the wall described in Sect. 17.1.2 hold.

Therefore in order to compute turbulent boundary layers at high Reynolds numbers we do not need a detailed description of the flow in the viscous wall layer. It suffices to compute the outer fully turbulent layer and the wall shear stress $\bar{\tau}_w(x)$. The matching condition (17.16) or (17.19) is then the boundary condition for the outer flow. We find that

$$\lim_{y \rightarrow 0} \frac{\partial \bar{u}}{\partial y} = \frac{u_\tau(x)}{\kappa y} \quad (18.1)$$

or, after integration, the logarithmic overlap law

$$\lim_{y \rightarrow 0} \bar{u} = u_\tau(x) \left[\frac{1}{\kappa} \ln \frac{y u_\tau(x)}{\nu} + C^+ \right], \quad (18.2)$$

cf. also Eq. (17.21). As in the case of Couette flow, here again

$$\lim_{y \rightarrow 0} \bar{v} = 0, \quad \lim_{y \rightarrow 0} \tau_t = \bar{\tau}_w. \quad (18.3)$$

Computing the outer fully turbulent layer with the boundary conditions (18.1) to (18.3) for the velocity components is called the *method of wall functions*. The turbulence model is only required in the outer fully turbulent layer, still taking Eqs. (18.1) to (18.3) into account. Since the effects of viscosity may be neglected in this layer, the fundamental equations contain no friction terms ($\nu = 0$). The effect of viscosity is only via the boundary condition (18.2).

On the other hand, if the entire turbulent boundary layer including the viscous wall layer is computed using the boundary condition (no-slip condition)

$$y = 0 : \quad \bar{u} = 0, \quad \bar{v} = 0, \quad \tau_t = 0, \quad (18.4)$$

this is then called a *low-Reynolds-number model*.

Note (Overlap power law)

The overlap law is logarithmic only for attached boundary layers with small pressure gradients. The overlap laws can also be power laws. The Stratford flow, see Sect. 18.31, and the natural convection flow, see Sect. 19.3, are examples, cf. K. Gersten (2001).

Note (Viscous superlayer)

Strictly speaking, the turbulent boundary layer consists of *three* layers. As well as the two layers mentioned above, there is also another layer between the fully turbulent outer layer and the inviscid outer flow, known as the *viscous superlayer*. The viscosity is very important in this layer. The thickness of this layer is, as was

mentioned in Sect. 16.5.4, proportional to the Kolmogorov length in Eq. (16.26), thus proportional to $\nu^{3/4}$, so that it may be neglected for large Reynolds numbers. In this case the solution for the fully turbulent outer layer may be matched up directly onto the inviscid outer flow. A consequence of this is that the solution of the inviscid equations generally has a singularity at the discrete transition $y = \delta$. At finite Reynolds numbers this is avoided by the viscous superlayer.

B. Jeken (1992) has investigated the asymptotic behaviour of the superlayer for large Reynolds numbers. He showed that, as for the viscous wall layer, universal solutions can be found which are independent of the pressure gradient and the curvature and whose essential parameter is the entrainment velocity, see Eq. (18.127).

18.1.2 Algebraic Turbulence Models

The two most common algebraic turbulence models have already been described in Sect. 17.1.4.

The *eddy viscosity* ν_t is given by

$$\boxed{\tau_t = \varrho \nu_t \frac{\partial \bar{u}}{\partial y}} \quad (18.5)$$

and the *mixing length* ℓ by

$$\boxed{\tau_t = \varrho \ell^2 \left| \frac{\partial \bar{u}}{\partial y} \right| \frac{\partial \bar{u}}{\partial y}.} \quad (18.6)$$

The relation $\nu_t = \ell^2 |\partial \bar{u} / \partial y|$ holds.

The models are only complete when the spatial functions $\nu_t(x, y)$ and $\ell(x, y)$ can be given. In order to do this we relate them to functions with local values of the boundary layer, such as the boundary-layer thickness δ and the displacement thickness δ_1 , as the following examples show:

1. Model by T. Cebeci; A.M.O. Smith (1974), p. 255:

$$\begin{aligned} \nu_t &= \kappa^2 y^2 \left| \frac{\partial \bar{u}}{\partial y} \right| & 0 < y < y_c \\ \nu_t &= \alpha U(x) \delta_1(x) \gamma(x, y) & y_c \leq y \end{aligned} \quad (18.7)$$

with $\alpha = 0.016$. Here $\gamma(x, y)$ is the intermittency factor from Eq. (16.30) and y_c is the coordinate of the crossing point of the two ν_t functions which is closest to the wall. A very similar model has been formulated by B.S. Baldwin; H. Lomax (1978); this differs only in the ν_t function for $y \geq y_c$.

2. Model by R. Michel et al. (1968):

$$\frac{\ell}{\delta} = \lambda \tanh \left(\frac{\kappa y}{\lambda \delta} \right) \quad (18.8)$$

with $\lambda = 0.085$. For $y > 0.6 \delta$ the mixing length is then practically independent of y , i.e. $\ell = \ell_\delta \approx \lambda \delta(x)$.

3. Model by M.P. Escudier (1966):

$$\begin{aligned}\ell &= \kappa y & 0 < y \leq \frac{\lambda}{\kappa} \delta \\ \ell &= \lambda \delta & \frac{\lambda}{\kappa} \delta \leq y \leq \delta\end{aligned}\quad (18.9)$$

with $\lambda = 0.09$.

The last two models are very similar. For all three models, the limit

$$\lim_{y \rightarrow 0} \ell = \kappa y, \quad (18.10)$$

as has already been seen in Eq. (17.71), holds.

Extensions of these models to so-called *one-half-equation models* are obtained when the quantities $\nu_t(x)$ in Eq. (18.7) or $\ell(x)$ in Eqs. (18.8) and (18.9) have to satisfy an ordinary differential equation. An overview of such models has been given by D.A. Anderson et al. (1984), p. 229.

In the model by D.A. Johnson; L.S. King (1985), an ordinary differential equation has been used for $\tau_{t \max}(x)$. F.R. Menter (1992) has also used this model to compute separated boundary layers.

It will be seen later, cf. Sect. 18.2.4, that boundary layers exist where the relation between $\nu_t(x, y)$ or $\ell(x, y)$ and the local boundary-layer quantities $\delta(x)$ or $\delta_1(x)$ is exact. These are called *equilibrium boundary layers*. The algebraic turbulence models are only an approximation for all other boundary layers. One or more equation models are then more precise.

18.1.3 Turbulent Energy Equation

All non-algebraic turbulence models use the equation for the kinetic energy of the turbulent fluctuations (*k*-equation) from Eq. (16.39). This is originally based on work by L. Prandtl (1945).

The turbulent diffusion is commonly modelled using the following gradient ansatz:

$$\overline{v'} \left(p' + \frac{\varrho}{2} q^2 \right) = - \frac{\varrho \nu_t}{Pr_k} \frac{\partial k}{\partial y}, \quad (18.11)$$

whereby the terms for viscous and turbulent diffusion in Eq. (16.39) have practically the same form. The eddy viscosity ν_t is defined by Eq. (18.5).

The model equation for the fully turbulent outer region of the boundary layer in which the viscous diffusion may be neglected compared to the turbulent diffusion then reads

$$\overline{u} \frac{\partial k}{\partial x} + \overline{v} \frac{\partial k}{\partial y} = \frac{\partial}{\partial y} \left(\frac{\nu_t}{Pr_k} \frac{\partial k}{\partial y} \right) + \frac{\tau_t}{\varrho} \frac{\partial \overline{u}}{\partial y} - \varepsilon. \quad (18.12)$$

The model constant is frequently set to $\text{Pr}_k = 1$.

If we interpret this equation as the defining equation for the turbulent shear stress $\tau_t(x, y)$, where ν_t may be replaced by τ_t using Eq. (18.5), two further equations for the unknown functions $k(x, y)$ and $\varepsilon(x, y)$ are then required to close the system of equations. This leads us then to two and more equation models.

If we assume that the eddy viscosity $\nu_t = f(k, \varepsilon)$ is only a function of k and ε , it follows from the Π theorem from dimensional analysis that

$$\nu_t = c_\mu \frac{k^2}{\varepsilon} \quad (c_\mu \approx 0.09). \quad (18.13)$$

Dimensional considerations also allow a turbulence length L to be obtained from ν_t and k and defined as

$$\nu_t = c_P L \sqrt{k} \quad (c_P \approx 0.55). \quad (18.14)$$

The index P indicates that this formula is due to L. Prandtl (1945).

Combining Eqs. (18.13) and (18.14) yields the *Prandtl–Kolmogorov* formula

$$L = c_\varepsilon \frac{k^{3/2}}{\varepsilon} \quad \left(c_\varepsilon = \frac{c_\mu}{c_P} \approx 0.168 \right). \quad (18.15)$$

The ansatz (18.11) is deceptively simple and delivers good results in many cases. However it does have its limits. Therefore W. Schneider (1989a, 1989b) and W. Schneider et al. (1990) have presented an extension to the ansatz (18.11) of one additional term. Using this, better agreement was found with experiments in one particular flow (Couette flow).

Note (Turbulence model by P. Bradshaw et al. (1967))

In this one-equation model, the turbulent energy equation is taken to be the defining equation for the shear stress τ_t . The ansatz

$$\tau_t = a \varrho k \quad (a \approx 0.3) \quad (18.16)$$

is used. This is exactly valid for the overlap layer between the fully turbulent outer region of the boundary layer and the viscous wall layer. The proportionality between τ_t/ϱ and k in this model was assumed for the entire outer region of the boundary layer. In analogy to Eq. (18.15), a turbulence length is introduced for the dissipation. The differential equation for τ_t then reads

$$\begin{aligned} \bar{u} \frac{\partial}{\partial x} \left(\frac{\tau_t}{a \varrho} \right) + \bar{v} \frac{\partial}{\partial y} \left(\frac{\tau_t}{a \varrho} \right) &= - \left(\frac{\tau_{t \max}}{\varrho} \right)^{1/2} \frac{\partial}{\partial y} \left(G \frac{\tau_t}{\varrho} \right) \\ &+ \frac{\tau_t}{\varrho} \frac{\partial \bar{u}}{\partial y} - \frac{(\tau_t/\varrho)^{3/2}}{L}. \end{aligned} \quad (18.17)$$

The turbulence length L is assumed to be a function of y/δ :

$$L = \delta f_1(y/\delta). \quad (18.18)$$

The turbulent diffusion is proportional to $(\tau_{t \max} / \varrho)^{1/2}$, where $\tau_{t \max}$ is the maximum value of τ_t in the region $0.25 \delta \leq y < \delta$. The function G in Eq. (18.17) is defined by

$$G = (\tau_{t \max} / \varrho U^2)^{1/2} f_2(y/\delta). \quad (18.19)$$

Here $f_1(y, \delta)$ and $f_2(y, \delta)$ are universal functions.

Note that in the overlap region to the viscous wall layer, Eq. (18.17) becomes the mixing length formula for L . This is because production = dissipation in this layer. It is interesting that the system of equations which appears is not parabolic but rather hyperbolic. The numerical computation is described in detail by P. Bradshaw et al. (1967). This computation method has been used frequently and it is judged to be good in practice, cf. S.J. Kline et al. (1968).

Note (One and one-and-a-half equation models)

As well as the model by P. Bradshaw et al. (1967), one-equation models have also been developed by M.W. Rubesin (1976) and U.C. Goldberg (1991). In the models by B.S. Baldwin; T.J. Barth (1990) and P.R. Spalart; S.R. Allmaras (1992), the k -equation is not used but rather each has formulated an equation for $\nu_t(x, y)$.

In the one-and-a-half-equation model by R.H. Pletcher (1978), as well as the k -equation, an ordinary differential equation for the turbulence length $\ell_\delta(x)$ at the outer edge of the boundary layer has been used, cf. Eq. (18.8) and (18.9)

18.1.4 Two-Equation Models

As was already mentioned in the last section, in order to close the system of equations, two further equations are required as well as the turbulent energy equation and Eq. (18.5). If one of these equations is a partial differential equation and the other an algebraic equation, the model is a two-equation model.

Summaries of two-equation models have been given by W.C. Reynolds (1976), V.C. Patel et al. (1985), C.G. Speziale et al. (1990), D.C. Wilcox (1998) and C.J. Chen; S.Y. Jaw (1998).

In what follows we will look at some important examples:

1. $k-\varepsilon$ model by W.P. Jones; B.E. Launder (1972a).

The second partial differential equation used in this model is the following heuristic balance equation for the dissipation ε :

$$\bar{u} \frac{\partial \varepsilon}{\partial x} + \bar{v} \frac{\partial \varepsilon}{\partial y} = \frac{\partial}{\partial y} \left(\frac{\nu_t}{\text{Pr}_\varepsilon} \frac{\partial \varepsilon}{\partial y} \right) + c_{\varepsilon 1} \frac{\varepsilon}{k} \frac{\tau_t}{\varrho} \frac{\partial \bar{u}}{\partial y} - c_{\varepsilon 2} \frac{\varepsilon^2}{k} \quad (18.20)$$

with the model constants

$$c_{\varepsilon 1} = 1.44, \quad c_{\varepsilon 2} = 1.87, \quad \text{Pr}_\varepsilon = 1.3.$$

As well as this, Eq. (18.13) is used.

In order that the velocity distribution passes over to the logarithmic law (18.2) in the transition to the viscous wall layer, the following relation must hold between

the four model constants:

$$\text{Pr}_\varepsilon \sqrt{c_\mu} (c_{\varepsilon 2} - c_{\varepsilon 1}) = \kappa^2. \quad (18.21)$$

Since in Eq. (18.12) we set $\text{Pr}_k = 1$, when $\kappa = 0.41$ is given, there are still three models constants which have to be determined empirically.

Equation (18.20) for the dissipation has the same structure as the k -equation (18.12). The analogous terms to those for production and dissipation in Eq. (18.12) were formed by multiplication with $c_i \varepsilon / k$, $i = 1$ or 2.

The six equations (16.34), (16.35) with $\bar{\tau}_v = 0$, (18.5), (18.12), (18.13) and (18.20) determine the six unknown functions $\bar{u}(x, y)$, $\bar{v}(x, y)$, $\tau_t(x, y)$, $\nu_t(x, y)$, $k(x, y)$ and $\varepsilon(x, y)$ which describe the outer fully turbulent region of the boundary layer.

The matching conditions at the viscous wall layer yield the following boundary conditions for the solution functions (here it is assumed that the wall shear stress is finite, $\bar{\tau}_w \neq 0$ and the wall is impermeable, $v_w = 0$):

$$\begin{aligned} \lim_{y \rightarrow 0} \bar{u}(x, y) &= \frac{1}{\kappa} \ln y^+ + C^+, \quad \lim_{y \rightarrow 0} \bar{v}(x, y) = 0, \\ \lim_{y \rightarrow 0} \tau_t(x, y) &= \bar{\tau}_w(x), \quad \lim_{y \rightarrow 0} \nu_t(x, y) = \kappa y \sqrt{\bar{\tau}_w / \varrho} = \kappa y u_\tau, \\ \lim_{y \rightarrow 0} k(x, y) &= u_\tau^2 / \sqrt{c_\mu}, \quad \lim_{y \rightarrow 0} \varepsilon(x, y) = u_\tau^3 / \kappa y. \end{aligned} \quad (18.22)$$

These boundary conditions are the same as those for the Couette flow treated in Sect. 17.1 (see Eq. (17.21) and (17.64)). The boundary condition for ε follows from Eq. (18.13), since at high Reynolds numbers the viscous wall layer locally obeys the same equations as those for the Couette flow with the same wall shear stress $\bar{\tau}_w$.

The corresponding boundary conditions at the outer edge of the boundary layer ($y = \delta$) read:

$$\bar{u} = U, \quad \tau_t = 0, \quad \nu_t = 0, \quad k = 0, \quad \varepsilon = 0. \quad (18.23)$$

The velocity defect $U - \bar{u}$ and the remaining four functions tend linearly to zero for $y \rightarrow \delta$. This discontinuity compared to the inviscid turbulence free outer flow is dealt with at finite Reynolds numbers by a continuous transition in the viscous superlayer, cf. B. Jeken (1992).

In solving the system of equations numerically, it is advantageous to introduce the coordinate $\eta = y/\delta(x)$, since the region of computation then becomes rectangular. J.C. Rotta (1983) has suggested that the singular behaviour of $\bar{u}(x, y)$ and $\varepsilon(x, y)$ for $y \rightarrow 0$ can be dealt with by placing the lower edge not at $y = 0$ but rather at a small positive distance from the wall y_l . If we set $\ln y_l^+ = -\kappa C^+$, following Rotta, at the lower edge of the region of computation $\bar{u}(x, y_l) = 0$ and $\varepsilon(x, y_l) = u_\tau^3 / \kappa y_l$.

The k - ε model has been extended to a k - ε - γ model where γ is the intermittency factor according to Eq. (16.30), cf. R. Radespiel (1986) and A. Dewan; J.H. Arakeri (2000).

2. k - ω model by D.C. Wilcox (1998).

This model is based on ideas by A.N. Kolmogorov (1942). Further extensions and the version used today are described in detail by D.C. Wilcox (1998). Here the second equation used is the balance equation for ω :

$$\bar{u} \frac{\partial \omega}{\partial x} + \bar{v} \frac{\partial \omega}{\partial y} = \frac{\partial}{\partial y} \left(\frac{\nu_t}{\text{Pr}_\omega} \frac{\partial \omega}{\partial y} \right) + \alpha \frac{\omega}{k} \frac{\tau_t}{\varrho} \frac{\partial \bar{u}}{\partial y} - \beta \omega^2 \quad (18.24)$$

with the model constants

$$\alpha = \frac{5}{9}, \quad \beta = \frac{3}{40}, \quad \text{Pr}_\omega = 2.$$

Here ω is defined by

$$\omega = \frac{1}{c_\mu} \frac{\varepsilon}{k} \quad (18.25)$$

with $c_\mu = 0.09$. This is the dissipation per unit turbulent kinetic energy and has the units 1/s. Equation (18.25) means that instead of Eq. (18.13) we have

$$\nu_t = \frac{k}{\omega}. \quad (18.26)$$

Again the transition requirements when passing over to the viscous wall layer yield a relation between the constants:

$$\text{Pr}_\omega \sqrt{c_\mu} \left(\frac{\beta}{c_\mu} - \alpha \right) = \kappa^2. \quad (18.27)$$

The boundary condition for ω reads

$$\lim_{y \rightarrow 0} \omega(x, y) = u_\tau / \sqrt{c_\mu} \kappa y. \quad (18.28)$$

At the outer edge of the boundary layer ω attains a constant value. In the k -equation, the value $\text{Pr}_k = 2$ is set.

3. SST $k-\omega$ model by F.R. Menter (1994)

The **shear stress turbulence** model by F.R. Menter is a combination of the $k - \varepsilon$ model and the $k - \omega$ model. It utilizes the original $k - \omega$ model in the inner region of the boundary layer and switches to the standard $k - \varepsilon$ model in the outer region.

4. $k-L$ model by J.C. Rotta (1986).

The second equation used in this model is a balance for the product kL , where L is the turbulence length defined in Eq. (18.14). This balance equation is derived using the exact transport equations for the correlation functions $R(r)$ from Eq. (16.21) and reads

$$\begin{aligned} \bar{u} \frac{\partial(kL)}{\partial x} + \bar{v} \frac{\partial(kL)}{\partial y} &= \frac{\partial}{\partial y} \left[\sqrt{kL} \left(k_q L \frac{\partial k}{\partial y} + k_{qL} k \frac{\partial L}{\partial y} \right) \right] + L \frac{\tau_t}{\varrho} \frac{\partial \bar{u}}{\partial y} \\ &\quad + L^2 \frac{\partial^2 \bar{u}}{\partial y^2} \left(\zeta_2 L \frac{\partial(\tau_t/\varrho)}{\partial y} + \zeta_{2L} \frac{\tau_t}{\varrho} \frac{\partial L}{\partial y} \right) - c_L c_\varepsilon k^{3/2} \end{aligned} \quad (18.29)$$

using

$$k_q = 0.25 + 0.55 \left[1 - \left(\frac{1}{\kappa} \frac{\partial L}{\partial y} \right)^2 \right]^2 \quad (18.30)$$

with the model constants

$$k_{qL} = 0.3; \quad \zeta_2 = 1.2; \quad \zeta_{2L} = 3.0; \quad c_L = 0.8; \quad c_\varepsilon = c_P^3 = 0.165.$$

Matching at the viscous sublayer again yields a relation between the model constants:

$$1 - c_L = (c_\varepsilon \zeta_{2L} - k_{qL}) \kappa^2 / c_\varepsilon. \quad (18.31)$$

Thus Eqs. (16.34), (16.35) with $\tau_v = 0$, (18.5), (18.12), (18.14), (18.15) and (18.29) determine the seven unknown functions $\bar{u}(x, y)$, $\bar{v}(x, y)$, $\tau_t(x, y)$, $\nu_t(x, y)$, $k(x, y)$, $\varepsilon(x, y)$ and $L(x, y)$. The boundary condition for L reads

$$\lim_{y \rightarrow 0} L(x, y) = \kappa y. \quad (18.32)$$

Numerous worked examples using this method have been performed by H. Vollmers; J.C. Rotta (1977) and R. Voges (1978), cf. also K. Gersten; H. Herwig (1992), pp. 410, 457, 619.

18.1.5 Reynolds Stress Models

The Reynolds stress models, which are also called *second-moment closure models*, use the balance equations for the Reynolds stresses from Eq. (16.12). For each term in the stress tensor, balance equations can be determined from the Navier–Stokes equations, cf. K. Gersten; H. Herwig (1992), p. 396. The sum of the balance equations for the three normal stresses \bar{u}'^2 , \bar{v}'^2 and \bar{w}'^2 again yield the k -equation (16.16).

For plane flows there are four balance equations for \bar{u}'^2 , \bar{v}'^2 , \bar{w}'^2 and $\bar{u}'\bar{v}'$. They have the general form:

$\bar{u} \frac{\partial \bar{u}_i \bar{u}_j}{\partial x}$	$+ \bar{v} \frac{\partial \bar{u}_i \bar{u}_j}{\partial y}$	$= D_{ij} + P_{ij} - \varepsilon_{ij} + \Phi_{ij}$	(18.33)
convection	diffusion	production	dissipation
			pressure-shear correlation

where the indices i and j can take on the values 1, 2 and 3. Here $u_1 = u'$, $u_2 = v'$ and $u_3 = w'$, see Table 18.1. The modelled terms of the four equations are presented in Table 18.1.

The boundary conditions read:

$$\begin{aligned} \lim_{y \rightarrow 0} \frac{\bar{u}'^2}{k} &= A [c_1(2 + c_1 - 2c_2 + c_{2w}) + 3c_{1w}(1 + c_1 - c_2)] \approx 1.1 \\ \lim_{y \rightarrow 0} \frac{\bar{v}'^2}{k} &= Ac_1(-1 + c_1 + c_2 - 2c_{2w}) \approx 0.2 \\ \lim_{y \rightarrow 0} \frac{\bar{w}'^2}{k} &= A [c_1(-1 + c_1 + c_2 + c_{2w}) + 3c_{1w}(-1 + c_1 + c_2)] \approx 0.7 \\ \lim_{y \rightarrow 0} \frac{k}{u_\tau^2} &= \sqrt{\frac{(c_1 + 2c_{1w})(3c_1 + 2c_{1w})}{(-1 + c_1 + c_2 - 2c_{2w})(2 - 2c_2 + 3c_{2w})}} \approx 3.1 \\ \lim_{y \rightarrow 0} \frac{\bar{u}'\bar{v}'}{u_\tau^2} &= -1 \\ \text{with } A &= 2/[3c_1(c_1 + 2c_{1w})] \approx 0.13. \end{aligned} \quad (18.34)$$

Table 18.1. Model equations for Reynolds stress models as in Eq. (18.33)

$$2P = P_{11} + P_{22}, \quad f_w = k^{3/2}/(c_L \varepsilon y)$$

$$c_1 = 1.8; \quad c_2 = 0.6; \quad c_s = 0.22; \quad c_{1w} = 0.5; \quad c_{2w} = 0.3; \quad c_L = 2.5$$

i	j	$\overline{u'_i u'_j}$	P_{ij}	ε_{ij}	Φ_{ij}	D_{ij}
1	1	$\overline{u'^2}$	$-2\overline{u'v'}\frac{\partial \overline{u}}{\partial y} - 2\overline{u'^2}\frac{\partial \overline{u}}{\partial x}$	$\frac{2}{3}\varepsilon$	$-c_1\varepsilon\left(\frac{\overline{u'^2}}{k} - \frac{2}{3}\right) - c_2\left(P_{11} - \frac{2}{3}P\right) + \left[c_{1w}\varepsilon\frac{\overline{v'^2}}{k} - c_{2w}\left(P_{22} - \frac{2}{3}P\right)\right]f_w$	$\frac{\partial}{\partial y}\left(c_s \frac{k}{\varepsilon} \overline{v'^2} \frac{\partial \overline{u'^2}}{\partial y}\right)$
2	2	$\overline{v'^2}$	$-2\overline{v'^2}\frac{\partial \overline{v}}{\partial y}$	$\frac{2}{3}\varepsilon$	$-c_1\varepsilon\left(\frac{\overline{v'^2}}{k} - \frac{2}{3}\right) - c_2\left(P_{22} - \frac{2}{3}P\right) + \left[-2c_{1w}\varepsilon\frac{\overline{v'^2}}{k} + 2c_{2w}\left(P_{22} - \frac{2}{3}P\right)\right]f_w$	$\frac{\partial}{\partial y}\left(c_s \frac{k}{\varepsilon} \overline{v'^2} \frac{\partial \overline{v'^2}}{\partial y}\right)$
3	3	$\overline{w'^2}$	0	$\frac{2}{3}\varepsilon$	$-c_1\varepsilon\left(\frac{\overline{w'^2}}{k} - \frac{2}{3}\right) + c_2\frac{2}{3}P + \left[c_{1w}\varepsilon\frac{\overline{v'^2}}{k} - c_{2w}\left(P_{22} - \frac{2}{3}P\right)\right]f_w$	$\frac{\partial}{\partial y}\left(c_s \frac{k}{\varepsilon} \overline{v'^2} \frac{\partial \overline{w'^2}}{\partial y}\right)$
1	2	$\overline{u'v'}$	$-\overline{v'^2}\frac{\partial \overline{u}}{\partial y}$	0	$-c_1\varepsilon\frac{\overline{u'v'}}{k} - c_2P_{12} + \left[-\frac{3}{2}c_{1w}\varepsilon\frac{\overline{u'v'}}{k} + \frac{3}{2}c_{2w}P_{12}\right]f_w$	$\frac{\partial}{\partial y}\left(c_s \frac{k}{\varepsilon} \overline{v'^2} \frac{\partial \overline{u'v'}}{\partial y}\right)$

The following improvements can be stated about Reynolds stress models compared to simpler turbulence models:

1. The simple proportionality between τ_t and the velocity gradient $\partial\bar{u}/\partial y$ from Eq. (18.5) has been replaced by differential equations which can be better justified physically. According to Eq. (18.5) the velocity must possess an extremum at the position $\tau_t = 0$. However, according to experimental knowledge, this is not the case for many important flows, e.g. wall jets, separated flows, annular flows.
2. Turbulence modelling is highly dependent on the wall curvature. In the Reynolds stress model one differentiates between the stresses parallel and perpendicular to the centrifugal forces and so this effect can be taken into account. This is not the case in two-equation models. Details on the extension of Eq. (18.33) to include curvature effects have been given by B. Jeken (1992). Similarly, the effects of gravity can also be taken into account in a better way.
3. It is now possible to take all relevant production terms into account. With Eq. (16.14), the sum of the equations for the normal stresses yields the k -equation. Now added to Eq. (16.39) is the additional production term $\varrho(\bar{v}^2 - \bar{u}^2)\partial\bar{u}/\partial x$. This has the same order of magnitude as the term $\tau_t\partial\bar{u}/\partial y$, see B. Jeken (1992). Because of the defect formulation, to be described in the next sections, the velocity $\bar{u}(x, y)$, see Eq. (18.56), is to first approximation equal to the outer velocity $U(x)$. This means that $\tau_t\partial\bar{u}/\partial y$ is only non-zero when higher order terms are taken into account and it then has the order of magnitude of $\varrho(\bar{v}^2 - \bar{u}^2)dU/dx$. The importance of the additional term increases as the pressure gradient increases, and may especially not be neglected close to separation, a fact already mentioned by R.L. Simpson (1975). However this additional term can strictly speaking only be taken into account with the help of Reynolds stress models.

As well as the three effects of diffusion, production and dissipation which already appeared in the k -equation, a fourth effect Φ_{ij} appears in Eq. (18.33). This is due to correlation of the fluctuation of the pressure and the shear velocities $p'\partial u'/\partial y$, etc, and is therefore called the *pressure–shear correlation*. It takes care of the exchange of turbulence energy between the velocity components of different directions which endeavours to bring about an equal distribution of the fluctuation intensities in all directions. Because of the continuity equation (16.8), the pressure–shear correlations do not appear in the k -equation. It is particularly difficult to model the pressure–shear correlations, since the relevant experimental data are practically non-existent, cf. J.C. Rotta (1980b, 1991).

In order to close the model, a further equation for $\varepsilon(x, y)$ or for the turbulence length $L(x, y)$ is necessary. Then the equations (16.14), (16.34), (16.35), (18.20) with (18.13) together with the four equations from Table 18.1 determine the eight desired functions \bar{u} , \bar{v} , τ_t , ε , k , \bar{u}'^2 , \bar{v}'^2 and w'^2 .

Summaries of the Reynolds stress models have been given by, for example, K. Hanjalić; B.E. Launder (1972a, 1976), B.E. Launder (1984), C.G. Speziale (1991), K. Hanjalić (1994a).

Note (Algebraic Reynolds stress models)

Because of the derivatives in the convection and diffusion terms, Eq. (18.33) are differential equations. If these terms are approximated by algebraic expressions of the form

$$\bar{u} \frac{\partial \bar{u}' \bar{u}'_j}{\partial x} + \bar{v} \frac{\partial \bar{u}' \bar{u}'_j}{\partial y} - D_{ij} = \frac{\bar{u}' \bar{u}'_j}{k} (P - \varepsilon), \quad (18.35)$$

we then have an *algebraic Reynolds stress model*, see W. Rodi (1976). The Reynolds stresses $\bar{u}' \bar{u}'_j / k$ then become the algebraic functions P_{11}/ε , P_{22}/ε and

$$f_w = \frac{k^{3/2}}{c_L \varepsilon y}.$$

The equation for the turbulent shear stress then has the form

$$\tau_t = \varrho c_\mu \frac{k^2}{\varepsilon} \frac{\partial \bar{u}}{\partial y} \quad (18.36)$$

obtained from Eqs. (18.12) and (18.13). Here c_μ is not a constant but rather a function of the above three variables. This dependence is used in extensions to the $k-\varepsilon$ model, for example.

18.1.6 Heat Transfer Models

Just as in the case of momentum transfer, turbulence models for the temperature field essentially deal with the outer fully turbulent region of the boundary layer. Here we require that the Prandtl number, cf. Eq. (4.8), satisfy $\text{Pr} > 0.5$, because then neither the viscosity μ nor the thermal conductivity λ has any effect in the fully turbulent region. Thus the turbulence models for $\text{Pr} > 0.5$ will also be independent of the Prandtl number.

Since the thermal energy equation (16.36) contains the turbulent heat flux $q_t(x, y)$ as an unknown, the aim of the turbulence model is to construct a relation between $q_t(x, y)$ and the quantities of the mean temperature field or possibly even the mean velocity field.

Turbulence models for the temperature field can again be algebraic models, one-equation models or many-equation models. In what follows we will consider some of the more typical and frequently used models.

1. Turbulent thermal diffusivity and turbulent Prandtl number

In analogy to the eddy viscosity ν_t and (18.5), we introduce the *turbulent thermal diffusivity* a_t , via the equation

$$q_t = \varrho c_p \bar{v}' \bar{T}' = -\lambda_t \frac{\partial \bar{T}}{\partial y} = -\varrho c_p a_t \frac{\partial \bar{T}}{\partial y}. \quad (18.37)$$

Matching to the viscous wall layer, in analogy to Eq. (17.64) we find that a_t is linear close to the wall. Thus

$$\lim_{y \rightarrow 0} \nu_t = \kappa u_\tau y, \quad \lim_{y \rightarrow 0} a_t = \kappa_\theta u_\tau y \quad (18.38)$$

with a new universal constant $\kappa_\theta \approx 0.47$.

In analogy to the molecular Prandtl number $\text{Pr} = \nu/a$ we define the *turbulent Prandtl number*

$$\text{Pr}_t = \frac{\nu_t}{a_t} = -c_p \frac{\tau_t}{q_t} \frac{\partial \bar{T}}{\partial y}. \quad (18.39)$$

cf. Eq. (17.77). As we approach the viscous wall layer this assumes the constant value

$$\text{Pr}_t = \frac{\kappa}{\kappa_\theta} = 0.87. \quad (18.40)$$

Frequently this value is assumed for the entire fully turbulent outer layer (for $\text{Pr} > 0.5$). As long as the boundary layer is attached, the results are very good, cf. J.C. Rotta (1964). In boundary layers with backflow, where $\partial \bar{u} / \partial y$ vanishes in the field, the ansatz (18.39) breaks down.

2. Mixing length for the heat transfer

Assuming the relation

$$\frac{q_t}{\varrho c_p} = F \left(\frac{\partial \bar{T}}{\partial y}, \frac{\tau_t}{\varrho}, \ell_\theta \right)$$

for the thermal mixing length ℓ_θ , the Π theorem then yields

$$q_t = -\varrho c_p \ell_\theta \sqrt{\frac{\tau_t}{\varrho}} \frac{\partial \bar{T}}{\partial y}. \quad (18.41)$$

Comparison with Eq. (18.37) delivers $a_t = \ell_\theta \sqrt{\tau_t / \varrho}$. As the viscous wall layer is approached ($\tau_t \rightarrow \bar{\tau}_w$) we obtain

$$\lim_{y \rightarrow 0} \ell_\theta = \kappa_\theta y \quad (18.42)$$

in analogy to Eq. (17.71).

Corresponding to Eq. (17.68), H.U. Meier; J.C. Rotta (1971) have defined the length ℓ_{MR} via

$$q_t = -\varrho c_p \ell_{MR}^2 \frac{\partial \bar{u}}{\partial y} \frac{\partial \bar{T}}{\partial y}, \quad (18.43)$$

and $\ell_{MR} = \sqrt{\ell \ell_\theta}$.

3. Balance equation for temperature fluctuations (k_θ -equation)

As a measure of the variance of the temperature $\overline{T'^2}$ and in analogy to k we introduce the quantity

$$k_\theta = \frac{1}{2} \overline{T'^2}. \quad (18.44)$$

The balance equation for this quantity reads:

$$\overline{u} \frac{\partial k_\theta}{\partial x} + \overline{v} \frac{\partial k_\theta}{\partial y} = \frac{\partial}{\partial y} \left(\frac{a_t}{\text{Pr}_{k\theta}} \frac{\partial k_\theta}{\partial y} \right) + \frac{q_t}{\varrho c_p} \frac{\partial \overline{T}}{\partial y} - \varepsilon_\theta, \quad (18.45)$$

where the “diffusion term” has already been modelled as in the k -equation. The boundary condition, cf. K. Gersten; H. Herwig (1992), p. 481 is

$$\lim_{y \rightarrow 0} k_\theta \approx \frac{1}{2} \left(\frac{\overline{q}_w}{\varrho c_p u_\tau} \right)^2. \quad (18.46)$$

4. Further models

Y. Nagano; C. Kim (1988) have developed a two-equation model for the heat transfer (k_θ - ε_θ model), which corresponds to the k - ε model for momentum transfer, cf. also K. Hanjalić (1994b).

A balance equation may also be written down for $q_t = \varrho c_p \overline{v' T'}$. It reads, cf. B.E. Launder (1988), Y.G. Lai; R.M.C. So (1990):

$$\begin{aligned} \overline{u} \frac{\partial q_t}{\partial x} + \overline{v} \frac{\partial q_t}{\partial y} &= \frac{\partial}{\partial y} \left(c_0 \overline{v'^2} k \frac{\partial q_t}{\partial y} \right) - \varrho c_p \overline{v'^2} \frac{\partial \overline{T}}{\partial y} + q_t \frac{\partial \overline{u}}{\partial x} \\ &\quad + \varrho c_p \tau_t \frac{\partial \overline{T}}{\partial x} - c_{1\theta} \frac{\varepsilon}{k} q_t - c_{2\theta} q_t \frac{\partial \overline{u}}{\partial x} \end{aligned} \quad (18.47)$$

with $c_\theta \approx 0.15$; $c_{1\theta} \approx 3.0$; $c_{2\theta} \approx 0.4$.

This equation corresponds to that for $\tau_t = -\varrho \overline{u' v'}$ from Table 18.1. For details on a term for the wall reflection proportional to f_w , see Y.G. Lai; R.M.C. So (1990).

18.1.7 Low-Reynolds-Number Models

In these models the entire boundary layer including the viscous wall layer is computed. They are therefore extensions to the models treated up until now which include the viscous wall layer. Instead of having *prescribed* wall functions as boundary conditions, in principle these are now computed along with the rest as the solution region extends to the wall. In determining the friction law (e.g. Eq. (17.91) for the plane channel), as well as calculating the constant

$\overline{C} + \overline{\overline{C}}$ from the outer fully turbulent layer, we also work out C^+ from the viscous wall layer, cf. D.C. Wilcox (1998), p. 190. The additional numerical effort required to obtain this result is quite considerable (because there are large gradients in the viscous wall layer of, for example, the velocity). One advantage is the particularly simple boundary conditions at the wall (all velocities vanish). The transition to the inviscid outer flow takes place continuously, as for laminar flows, since the molecular diffusion terms have to be taken into account in all balance equations.

If we use the algebraic model of the mixing length, the wall layer is described by the equation

$$\ell = \kappa y D(y^+)$$

instead of Eq. (18.10). Here

$$D(y^+) = 1 - \exp\left(-\frac{y^+}{A}\right)$$

with $A^+ = 25$ is called the *damping function*, cf. E.R. Van Driest (1956b).

A low-Reynolds-number version of a Reynolds stress model has been presented by S. Jakirlić; K. Hanjalić (1995)

Summaries have been given by V.C. Patel et al. (1985), W. Rodi (1991), D.C. Wilcox (1998), p. 185, K. Hanjalić (1994a) and B. Launder; B. Sandham (2002).

18.1.8 Large-Eddy Simulation and Direct Numerical Simulation

All the turbulence models up to now have started out with the time averaged equations of motion. In carrying out the time average over products of fluctuating quantities, terms such as the Reynolds stresses appeared. These had to be coupled to quantities from the mean motion by corresponding turbulence models.

It would be desirable to solve the general unsteady equations of motion without previous time average. In this case one speaks of *direct simulation*.

Since the numerical effort required is extraordinarily high only very few such computations have been carried out until now. Those that have are for very simple flows and at low Reynolds numbers, cf. U. Schumann; R. Friedrich (1986), R.S. Rogallo; P. Moin (1984), P.R. Spalart; A. Leonard (1987). The value of such calculations is that they furnish fundamental insight into and understanding of turbulence. In particular, all correlations of fluctuations can be computed, even those which it has not yet been possible to measure. This provides a base for the improvement of traditional turbulence models.

So-called *large-eddy simulations* require numerically less effort, but the computational costs are still quite high. In this technique, the time dependent equations of motion are also solved numerically, but the equations are first *filtered*. This filtering can be carried out by, for example, integrating the equations of motion over a grid volume in the computation lattice. The

large-eddy quantities (three velocity components and the pressure) are then constant within one volume, but change from one grid volume to the next, and also with the time, and thus are instantaneous values. The effect of the turbulent fine structure has to be modelled onto this coarse structure. Modelling the fine structure takes place in a similar manner to the turbulence modelling described in the previous sections. However approximation errors are less serious since the contribution of the motion of the fine structure turbulence to the total turbulent kinetic energy and to the momentum flux is only very small. The finer the grid size of the computation lattice and thus the filtering, the smaller the part of the turbulence which has to be modelled. Certain universal properties of the fine structure (e.g. isotropy) simplify the modelling.

As already mentioned, the computational costs for large-eddy simulation are also high. Therefore this method, just as for direct simulation, has only been used until now to deliver fundamental information for turbulence research. The effort required for both methods is too great to allow them to be used for practical engineering problems. Summaries of these two methods have been presented by U. Schumann; R. Friedrich (1986, 1987).

18.2 Attached Boundary Layers ($\bar{\tau}_w \neq 0$)

18.2.1 Layered Structure

We have already presented the basic equations (16.34) and (16.35) for plane turbulent boundary layers with constant physical properties in Sect. 16.6. In the limit $Re^{-1} = 0$, i.e. $\nu = 0$, the solution reduces to $\bar{u} = U(x)$, $\bar{v} = 0$. Therefore the inviscid and irrotational outer flow stretches all the way to the wall and the boundary layer vanishes. Since the no-slip condition is then not satisfied, we require a special treatment for the wall layer at large but finite Reynolds numbers. Therefore boundary layers, just as the flows in Chap. 17, also have a two-layer structure. They consist of a *thin wall layer* where both turbulent and molecular momentum transfer act, and a much larger fully turbulent layer, where the molecular momentum transfer may be neglected compared to that due to turbulence. The system of equations presented above, supplemented and closed by means of equations from a turbulence model, are again a case of a *singular perturbation problem*, for which the layered structure described is typical, cf. G.L. Mellor (1972).

As in Chap. 17, in order to describe the viscous wall layer, we introduce the wall coordinate

$$y^+ = \frac{u_\tau(x)y}{\nu} \quad (18.48)$$

with the local shear stress velocity

$$u_\tau(x) = \sqrt{\frac{\bar{\tau}_w(x)}{\varrho}}. \quad (18.49)$$

Using the dimensionless variables (l and V as reference lengths)

$$\begin{aligned} x^* &= \frac{x}{l}, & \text{Re} &= \frac{Vl}{\nu}, & u_\tau^* &= \frac{u_\tau}{V} \\ p_e^* &= \frac{p_e - p_\infty}{\varrho V^2}, & u^+ &= \frac{\bar{u}}{u_\tau}, & v^+ &= \frac{\bar{v}}{u_\tau}, & \tau^+ &= \frac{\bar{\tau}_v + \tau_t}{\varrho u_\tau^2}, \end{aligned} \quad (18.50)$$

Eqs. (16.34) and (16.35) yield the boundary-layer equations for the viscous wall layer:

$$\frac{1}{\text{Re } u_\tau^*} \left(\frac{\partial u^+}{\partial x^*} + \frac{u^+}{u_\tau^*} \frac{du_\tau^*}{dx^*} + \frac{y^+}{u_\tau^*} \frac{\partial u^+}{\partial y^+} \frac{du_\tau^*}{dx^*} \right) + \frac{\partial v^+}{\partial y^+} = 0, \quad (18.51)$$

$$\begin{aligned} \frac{1}{\text{Re } u_\tau^*} \left(u^+ \frac{\partial u^+}{\partial x^*} + \frac{u^{+2}}{u_\tau^*} \frac{du_\tau^*}{dx^*} + \frac{u^+ y^+}{u_\tau^*} \frac{\partial u^+}{\partial y^+} \frac{du_\tau^*}{dx^*} \right. \\ \left. + \frac{1}{u_\tau^{*2}} \frac{dp_e^*}{dx^*} \right) + v^+ \frac{\partial u^+}{\partial y^+} = \frac{\partial \tau^+}{\partial y^+}. \end{aligned} \quad (18.52)$$

For $\text{Re} \cdot u_\tau^* \rightarrow \infty$, Eq. (18.4) yields $v^+ = 0$ and thus from Eq. (18.52), $\tau^+ = \text{const}$. This corresponds to the fundamental equations for the wall layer of turbulent Couette flow, indeed of that flow with the *local* shear stress velocity $u_\tau(x)$ at the position x . All results from the Couette wall layer can therefore be carried over from Sect. 17.1. In particular, the logarithmic overlap law (17.21) is valid. As a measure of the local wall layer thickness we have, from Eq. (17.11), $\delta_v = \nu/u_\tau(x)$.

Note (k -equation for the wall layer)

In the k -equation (16.39) too, all the convective terms (and the production terms proportional to the normal stresses) in the wall layer drop out. Using Eq. (18.11) we find

$$\frac{d}{dy^+} \left[\left(1 + \frac{\nu_t^+}{\text{Pr}_k} \right) \frac{dk^+}{dy^+} \right] + \nu_t^+ \left(\frac{du^+}{dy^+} \right)^2 - \varepsilon^+ = 0 \quad (18.53)$$

with

$$v_t^+ = \frac{\nu_t}{\nu}, \quad k^+ = \frac{k}{u_\tau^2}, \quad \varepsilon^+ = \frac{\varepsilon \nu}{u_\tau^4}. \quad (18.54)$$

From Eq. (16.18), the dimensionless *pseudo-dissipation* ε^+ depends on the dissipation $\tilde{\varepsilon}^+ = \tilde{\varepsilon}\nu/u_\tau^4$ as follows

$$\varepsilon^+ = \tilde{\varepsilon}^+ - \frac{d^2}{dy^{+2}} \left(\frac{\overline{v'^2}}{u_\tau^2} \right) = \tilde{\varepsilon}^+ + D^+. \quad (18.55)$$

Here the additional term D^+ also has to be modelled, cf. K. Gersten; H. Herwig (1992), p. 415 and V.C. Patel et al. (1985).

Since the solution for the viscous wall layer is assumed to be known, we therefore restrict the calculation to the outer part of the boundary layer where the viscosity effects in the balance equations may be neglected.

18.2.2 Boundary-Layer Equations Using the Defect Formulation

In the limiting case $\text{Re}^{-1} = 0$, the velocity $\bar{u}(x, y)$ in the boundary layer takes on the value $U(x)$ of the free stream (homogeneous velocity distribution). Therefore it would seem natural to write down the velocity in the form of a defect law:

$$\bar{u}(x, y) = U(x) - u_\tau(x)F'(x, \eta) = U(x)[1 - \gamma(x)F'(x, \eta)], \quad (18.56)$$

$$\bar{v}(x, y) = u_\tau \left[\frac{d\delta}{dx}(F - \eta F') + \frac{\delta}{u_\tau} \frac{du_\tau}{dx} F - \frac{\delta}{u_\tau} \frac{dU}{dx} \eta + \delta \frac{\partial F}{\partial x} \right], \quad (18.57)$$

$$\tau_t = \varrho u_\tau^2(x)S(x, \eta) = \varrho U^2(x)\gamma^2(x)S(x, \eta) \quad (18.58)$$

with

$$\eta = \frac{y}{\delta(x)}, \quad \gamma(x) = \frac{u_\tau(x)}{U(x)}. \quad (18.59)$$

Here dashes indicate differentiation with respect to the variable η . The boundary-layer thickness is denoted by $\delta(x)$, and $u_\tau(x)$ is the local shear stress velocity according to Eqs. (17.5) or (18.49).

Because of this defect formulation, the outer part of the boundary layer is also called the *defect layer*. Equation (18.56) can be construed as a perturbation ansatz with γ as the perturbation parameter.

The continuity equation is satisfied by the trial solutions (18.56) and (18.57). The momentum equation (16.35) becomes:

$$\begin{aligned} & \frac{1}{u_\tau} \frac{d(U\delta)}{dx} \eta F'' - \frac{\delta}{u_\tau^2} \frac{d(Uu_\tau)}{dx} F' - S' + \frac{\delta}{u_\tau} \frac{du_\tau}{dx} F'^2 - \frac{1}{u_\tau} \frac{d(u_\tau\delta)}{dx} FF'' \\ &= \delta \frac{\partial F}{\partial x} F'' + \frac{\partial F'}{\partial x} \left(\frac{U\delta}{u_\tau} - F'\delta \right). \end{aligned} \quad (18.60)$$

As the Reynolds number $\text{Re} = Vl/\nu$ increases, u_τ (or γ) and δ tend to zero. It will be shown later (see Eq. (18.76)) that $\gamma = O(\delta/l) = O(1/\ln \text{Re})$. If, in Eq. (18.60), we neglect the terms $O(\gamma)$ compared to the terms $O(1)$, we obtain

$$A(x)\eta F'' + B(x)F' - S' = \frac{\partial F'}{\partial x} \frac{U\delta}{u_\tau} \quad (18.61)$$

with

$$A(x) = \frac{1}{u_\tau} \frac{d(U\delta)}{dx}, \quad B(x) = -\frac{\delta}{u_\tau^2} \frac{d(U u_\tau)}{dx}. \quad (18.62)$$

Equation (18.61) is a *linear* partial differential equation for the dimensionless velocity defect $F'(x, \eta) = (U - \bar{u})/u_\tau$ and the dimensionless turbulent shear stress $S(x, \eta)$. In order to close the system of equations we require a further relation between $F'(x, \eta)$ and $S(x, \eta)$. This will be furnished by the turbulence model.

For example, according to the algebraic turbulence model by R. Michel et al. (1968) (cf. also Eq. (18.8)):

$$S = \ell_\delta^2 F'^2, \quad \ell_\delta = \frac{\ell}{\delta} = c_\ell \tanh\left(\frac{\kappa}{c_\ell} \eta\right). \quad (18.63)$$

As this example shows, the turbulence model generally delivers a nonlinear relation between $F'(x, \eta)$ and $S(x, \eta)$. Therefore, in spite of the fact that the momentum equation (18.61) is linear, the boundary-layer calculation is still a nonlinear problem.

The boundary conditions read:

$$\begin{aligned} \lim_{\eta \rightarrow 0} F &= 0, & \lim_{\eta \rightarrow 0} F'' &= -\frac{1}{\kappa\eta}, & \lim_{\eta \rightarrow 0} S &= 1, \\ \eta = 1 : \quad F' &= 0, & S &= 0. \end{aligned} \quad (18.64)$$

These are obtained for $\eta \rightarrow 0$ by matching to the viscous wall layer, cf. Eq. (17.19) and $\tau_t^+ = 1$ from Eq. (18.52). Using the condition $F = 0$ for $\eta \rightarrow 0$, Eq. (18.51) guarantees that $v^+ = 0$ in the wall layer (this only holds for impermeable walls).

Equation (18.61), supplemented by a turbulence model such as Eq. (18.63) with boundary conditions (18.64), yields, for a given $U(x)$, not only $F'(x, \eta)$ and $S(x, \eta)$, but also the x dependent function

$$\tilde{\Delta}(x) = \frac{U\delta}{u_\tau l} = \frac{\delta}{\gamma l}, \quad (18.65)$$

cf. also Eq. (18.68).

Using Eq. (18.74) to be derived in the next section, it follows that $d\gamma/dx = O(\gamma^2)$ and thus

$$\frac{du_\tau}{dx} = \gamma \frac{dU}{dx} + O(\gamma^2) = \frac{u_\tau}{U} \frac{dU}{dx} + O(\gamma^2). \quad (18.66)$$

The functions in Eq. (18.62) therefore only depend on $U(x)$ and $\tilde{\Delta}(x)$:

$$\begin{aligned} A(x) &= \frac{d}{dx} \left(\frac{U\delta}{u_\tau} \right) + \frac{\delta}{u_\tau} \frac{dU}{dx} = \frac{d\tilde{\Delta}}{dx^*} + \frac{\tilde{\Delta}}{U} \frac{dU}{dx^*} \\ B(x) &= -2 \frac{\delta}{u_\tau} \frac{dU}{dx} = -2 \frac{\tilde{\Delta}}{U} \frac{dU}{dx^*}. \end{aligned} \quad (18.67)$$

Here the dimensionless coordinate $x^* = x/l$ was used.

Integrating Eq. (18.61) over the boundary-layer thickness yields

$$\frac{d(F_e \tilde{\Delta})}{dx^*} + \frac{3}{U} \frac{dU}{dx^*} F_e \tilde{\Delta} = 1 \quad \text{or} \quad \frac{d}{dx^*} \left(F_e \tilde{\Delta} U^3 \right) = U^3$$

with the following quadrature formula as the solution:

$$\tilde{\Delta} = F_e \tilde{\Delta} = \frac{2\delta_1}{c_f l} = \left(C + \int_0^{x^*} U^3 dx^* \right) / U^3. \quad (18.68)$$

If we specify Eq. (18.61) to the boundary-layer edge $\eta = 1$, we obtain the following equation

$$A = \frac{d\tilde{\Delta}}{dx^*} + \frac{\tilde{\Delta}}{U} \frac{dU}{dx^*} = \frac{S'_e}{F''_e}.$$

This may be construed as the defining equation for $\tilde{\Delta}(x^*)$. In case the turbulence model used yields $F''_e = 0$, as for example Eq. (18.63) does, l'Hôpital's rule must be applied to the right hand side of this equation, replacing it by S''_e/F'''_e .

The solution $F(x^*, \eta)$ yields the following boundary-layer global values: edge value:

$$F_e(x^*) = F(x^*, 1) = \frac{\delta_1}{\delta \sqrt{c_f/2}}, \quad (18.69)$$

wake parameter:

$$\Pi(x^*) = \frac{\kappa}{2} \lim_{\eta \rightarrow 0} \left[F'(x^*, \eta) + \frac{1}{\kappa} \ln \eta \right], \quad (18.70)$$

shape factor:

$$G(x^*) = \frac{\lim_{y \rightarrow 0} \int_y^\delta (U - \bar{u})^2 dy}{u_\tau \lim_{y \rightarrow 0} \int_y^\delta (U - \bar{u}) dy} = \frac{1}{F_e} \lim_{\eta \rightarrow 0} \int_\eta^1 F'^2 d\eta. \quad (18.71)$$

Equation (18.69) follows from Eqs. (7.98) and (18.56), see also Eqs. (18.79) and (18.77).

It is worth noting that the boundary-layer calculation described is *independent* of the Reynolds number and the roughness of the wall surface. Therefore *one* calculation determines the global values of the boundary layer given by Eqs. (18.69) to (18.71). It is only when the function $\gamma(x) = \sqrt{c_f/2}$ is determined that the Reynolds number comes into play, as will be shown in the next section. If $\gamma(x)$ is known, then the function $\delta(x)$ from Eq. (18.65), which also depends on the Reynolds number, can also be determined.

K. Gersten; D. Vieth (1995) have presented an integral method whereby only one ordinary differential equation for the shape factor $G(x)$ has to be solved.

18.2.3 Friction Law and Characteristic Quantities of the Boundary Layer

In order to compute the wall shear stress distribution, the velocity of the defect layer and the viscous wall layer are matched up:

$$\lim_{y \rightarrow 0} \frac{\bar{u}(x, y)}{u_\tau(x)} = \lim_{y^+ \rightarrow \infty} u^+(y^+). \quad (18.72)$$

Together with this result, Eqs. (17.21) and (18.56) then yield:

$$\frac{U}{u_\tau} - \lim_{\eta \rightarrow 0} F'(x^*, \eta) = \frac{1}{\kappa} \ln \frac{yu_\tau}{\nu} + C^+$$

or else, using Eq. (18.70)

$$\frac{1}{\gamma} = \frac{U}{u_\tau} = \frac{1}{\kappa} \ln \frac{u_\tau \delta}{\nu} + C^+ + \frac{2\Pi(x^*)}{\kappa}. \quad (18.73)$$

Splitting up the logarithm of the solution function $\tilde{\Delta}(x)$, we obtain the friction law for $\gamma(x^*, \text{Re})$:

$$\boxed{\frac{1}{\gamma} = \frac{1}{\kappa} \ln(\gamma^2 \text{Re}) + C^+ + \tilde{C}(x^*)} \quad (18.74)$$

with

$$\tilde{C}(x^*) = \frac{1}{\kappa} \left[2\Pi(x^*) + \ln \left\{ \frac{U(x^*)}{V} \tilde{\Delta}(x^*) \right\} \right]. \quad (18.75)$$

The function $G(\Lambda; D)$ from Eq. (17.60) may be used to obtain the friction law in explicit form

$$\boxed{\gamma = \frac{u_\tau}{U} = \sqrt{\frac{c_f}{2}} = \frac{\kappa}{\ln \text{Re}} G(\Lambda; D)} \quad (18.76)$$

with

$$c_f(x^*) = \frac{2\tau_w}{\varrho U^2(x^*)} \quad (18.77)$$

and

$$\Lambda = \ln \text{Re}; \quad D(x^*) = 2 \ln \kappa + \kappa [C^+ + \tilde{C}(x^*)]. \quad (18.78)$$

This confirms the order of magnitude for $\gamma = O(1/\ln \text{Re})$ which was assumed in the previous section. In addition, differentiation of Eq. (18.73) with respect to x^* yields Eq. (18.66).

The first two terms on the right hand side of Eq. (18.74) are due to the viscous wall layer and therefore contain the universal constants κ and C^+ . These terms dominate in the friction law. If the surface of the wall is rough, $C^+(k_{\text{tech}}^+)$ is the universal distribution given in Eq. (17.40). The term $\tilde{C}(x^*)$ characterises the effect of the defect layer and is therefore dependent on the turbulence model. However its effect is small, and decreases with increasing Reynolds number.

The characteristic quantities of the boundary layer, which have already been used for laminar boundary layers, cf. Eqs. (7.98), (7.99) and (7.102), may be determined from the solution functions as follows:

$$\begin{aligned} \delta_1(x^*) &= \gamma \delta F_e = \gamma^2 \hat{\Delta} l \\ \delta_2(x^*) &= \gamma \delta F_e (1 - \gamma G) = \delta_1 (1 - \gamma G) \\ \delta_3(x^*) &= \gamma \delta F_e (2 - 3\gamma G) = \delta_1 (2 - 3\gamma G). \end{aligned} \quad (18.79)$$

In contrast to laminar boundary layers where δ_1 , δ_2 and δ_3 all have the same order of magnitude as the boundary-layer thickness δ , these thicknesses in turbulent boundary layers are all one order of magnitude smaller than δ .

In obtaining Eq. (18.79), the integration was only carried out over the defect layer, since the part due to the wall layer is of the order $O(\text{Re}^{-1})$ and can therefore be neglected, cf. D. Coles (1968), I. Tani; T. Motohashi (1985) and K. Gersten; H. Herwig (1992), p. 629.

The ratio of the thickness of the wall layer, cf. Eq. (17.11) to that of the defect layer is

$$\frac{\delta_v(x^*)}{\delta(x^*)} = \frac{\nu}{u_* \delta} = O\left(\frac{\ln \text{Re}}{\text{Re}}\right), \quad (18.80)$$

i.e. as the Reynolds number increases, the thickness of the wall layer decreases much faster than the thickness of the defect layer.

The shape factors for the boundary layer follow from Eq. (18.79) as

$$H_{21} = \frac{\delta_2}{\delta_1} = 1 - \gamma G; \quad H_{31} = \frac{\delta_3}{\delta_1} = 2 - 3\gamma G. \quad (18.81)$$

Eliminating γ , we obtain a relation independent of the Reynolds number:

$$2 - H_{31} = 3(1 - H_{21}) \quad \text{or} \quad 2 - H_{32} = H_{12} - 1. \quad (18.82)$$

This has also been confirmed very well by experiment, see also Fig. 18.9.

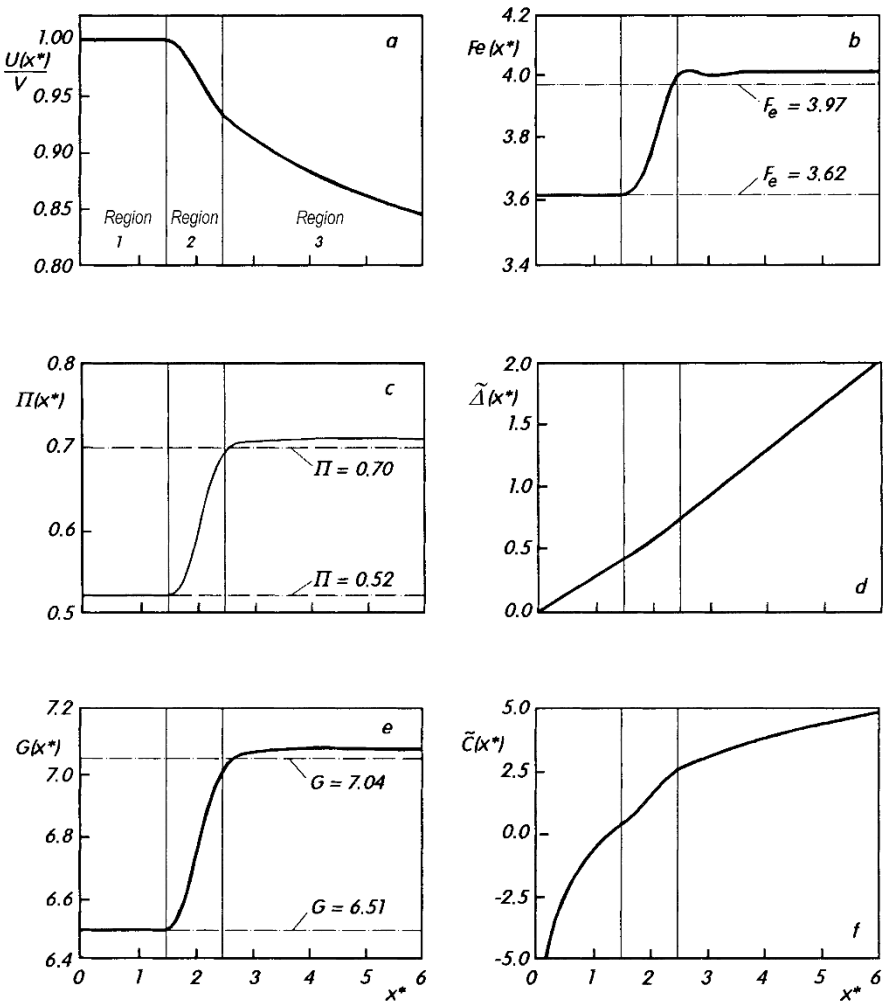


Fig. 18.1a-f. Results of a boundary-layer calculation using Eqs. (18.61), (18.63) and (18.64) by K. Gersten; D. Vieth (1995) for the velocity distribution:
 region 1: $0 \leq x^* \leq 1.5$; $U/V = 1$
 region 2: $1.5 \leq x^* \leq 2.5$; $U/V = 0.087x^{*3} - 0.547x^{*2} + 1.052x^* + 0.354$
 region 3: $2.5 \leq x^*$; $U/V = (x^* - 0.5)^{-0.1}$
 In Eq. (18.63): $c_\ell = 0.078$

Example: Boundary-layer calculations have been carried out for the velocity distribution $U(x^*)$ shown in Fig. 18.1a using the turbulence model by R. Michel et al. (1968), see Eq. (18.63). The distributions $F_e(x^*)$, $\Pi(x^*)$, $\tilde{\Delta}(x^*)$, $G(x^*)$ and $\tilde{C}(x^*)$ obtained are shown in Figs. 18.1b to 18.1f. They are independent of the Reynolds number. Although the velocity distribution $U(x^*)$ obeys a power law in region 3 ($x^* > 2.5$), the boundary layer in the regime shown ($x^* \leq 6$) has not yet reached the equilibrium state (dashed-dotted line). This can be seen in the plots of $F_e(x^*)$, $\Pi(x^*)$ and $G(x^*)$. The skin-friction coefficient $c_f(x^*, \text{Re})$ and the shape factor $H_{12}(x^*, \text{Re})$ are dependent on the Reynolds number and tend to the limits $c_f = 0$ and $H_{12} = 1$ as $\text{Re} \rightarrow \infty$.

18.2.4 Equilibrium Boundary Layers

Equilibrium boundary layers are found when the distributions of the related velocity defect are *similar*, i.e. when the function $F'(\eta)$ in Eq. (18.56) is independent of x . In these cases Eq. (18.61) reduces to the *ordinary* differential equation

$$A\eta F'' + B F' = S', \quad (18.83)$$

where A and B must now be constants. Integrating this equation with respect to η over the defect layer and taking the boundary conditions (18.64) into account, we obtain

$$F_e(A - B) = 1. \quad (18.84)$$

It is usual to introduce the Rotta–Clauser parameter

$$\beta = \frac{\delta_1}{\bar{\tau}_w} \frac{dp_e}{dx} = -\frac{\delta}{u_\tau} \frac{dU}{dx} F_e \quad (18.85)$$

named after J.C. Rotta (1950) and F.H. Clauser (1956). Equations (18.85) and (18.84) then yield

$$F_e B = 2\beta; \quad F_e A = 1 + 2\beta. \quad (18.86)$$

The equations of motion for equilibrium boundary layers then read

$$(1 + 2\beta)\eta F'' + 2\beta F' = F_e S'. \quad (18.87)$$

Equilibrium boundary layers are therefore characterised by $\beta = \text{const.}$

The solution of Eq. (18.87) has to satisfy the boundary conditions (18.64).

Note (Changed coordinate)

In the literature, the coordinate $\hat{\eta} = y/\Delta(x)$ with $\Delta(x) = F_e \delta$ is frequently used instead of the coordinate $\eta = y/\delta(x)$. The edge of the boundary layer ($y = \delta$) is then found at $\hat{\eta}_e = 1/F_e$. There the function $\hat{F}(\hat{\eta})$ is subject to the new boundary condition $\hat{F}(\hat{\eta} = \hat{\eta}_e) = 1$. The differential equation for $\hat{F}(\hat{\eta})$ has the same

appearance as Eq. (18.87), but without the factor F_e on the right hand side, cf. K. Gersten; H. Herwig (1992), p. 604. The quantities defined in Eq. (18.69) to (18.71) are independent of the choice of coordinate. It is found that

$$F_e = \frac{1}{\hat{\eta}_e}, \quad 2\Pi = \lim_{\hat{\eta} \rightarrow 0} (\kappa \hat{F}' + \ln \hat{\eta} - \ln \hat{\eta}_e), \quad G = \lim_{\hat{\eta} \rightarrow 0} \int_{\hat{\eta}}^{\hat{\eta}_e} \hat{F}'^2 d\hat{\eta}.$$

The equations (18.67) and (18.86) yield

$$\frac{d\tilde{\Delta}}{dx^*} = A + \frac{1}{2}B = \frac{1}{F_e}(1 + 3\beta) \quad (18.88)$$

and thus

$$\hat{\Delta}(x^*) = F_e \tilde{\Delta}(x^*) = (1 + 3\beta)x^*. \quad (18.89)$$

In the same way, Eq. (18.67) delivers

$$U(x^*) = U_1 \cdot (x^*)^m, \quad (18.90)$$

where

$$m = -\frac{\beta}{1 + 3\beta}, \quad \beta = -\frac{m}{1 + 3m}. \quad (18.91)$$

Here $U_1 = U(x^* = 1)$ is a free coefficient. Therefore outer flows with *power laws* for $U(x^*)$ lead to equilibrium boundary layers. One of these is the boundary layer at a flat plate at zero incidence ($\beta = 0, m = 0$), which will be discussed in more detail in the next section.

The differential equation (18.87) has been solved using very many different turbulence models, cf. K. Gersten; H. Herwig (1992), p. 638 and D.C. Wilcox (1998), p. 155. Figure 18.2 shows the functions $\Pi(\beta)$ for different turbulence models, and a comparison with measurements is also presented. According to the figure, the k - ε model fares less well than the other models, cf. D.C. Wilcox (1998), p. 165.

In the limit $\beta \rightarrow \infty$ ($\bar{\tau}_w \rightarrow 0$), the assumption $\bar{\tau}_w \neq 0$ breaks down. The defect formulation from Eqs. (18.56) to (18.58) is then no longer valid, and another description is necessary. This will be discussed in Sect. 18.3.

The region $(-1/3 < \beta < \infty)$ corresponds to the interval $(\infty > m > -1/3)$. In the limit $\beta = -1/3$ ($m \rightarrow \infty$), instead of Eq. (18.90) we have $U(x^*) = U_1 \exp(\mu x^*)$, yielding $\gamma = 3\mu\delta$. The constant μ may be compared to m in Eq. (18.90).

Note (Region $-\infty < m < -1/3, \beta < -1/3$)

According to Eq. (18.89), for $\beta < -1/3$ and $x^* > 0$, $\tilde{\Delta}$ becomes negative. But even the solutions for $\beta < -1/3$ can be interpreted physically. In these cases, the outer flow has the velocity distribution $U(x) = U_1 \cdot (-x^*)^m$. Here only the negative x^* regime is taken into account, so that according to Eq. (18.89), $\tilde{\Delta}$ is positive. These are strongly *accelerated outer flows*, where $\tilde{\Delta}$ actually decreases downstream.

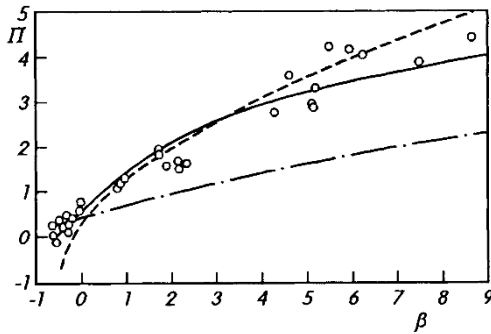


Fig. 18.2. Equilibrium boundary layers: the quantity $\Pi(\beta)$ defined in Eq. (18.70) for different turbulence models and from experiment, cf. D.C. Wilcox (1998), R. Michel et al. (1968), I.E. Alber (1968).

○ experiments
 - - - turbulence model by R. Michel et al. (1968), $c_\ell = 0.085$
 —— $k-\omega$ model by D.C. Wilcox (1998)
 - - - $k-\varepsilon$ model

One interesting example is the case $m = -1$, ($\beta = -0.5$). This is plane *sink flow* (nozzle flow). For this flow: $F' = -F_e S'$ or $F = F_e(1 - S)$. Furthermore, Eq. (18.75) implies that \tilde{C} is constant, and from Eq. (18.74), so too is γ . Therefore this flow has *similar* velocity profiles over the entire boundary-layer thickness, including the wall layer (i.e. H_{12} and H_{31} are constant according to Eq. (18.81), while $\delta_v(x^*)$, according to Eq. (17.11), and $\tilde{\Delta}(x^*)$ are both proportional to $(-x^*)$). This flow has been investigated experimentally in detail by W.P. Jones; B.E. Launder (1972b) and M.B. Jones et al. (2001). The latter investigation supports the proposition of D.E. Coles (1957) that $F = \eta(1 - \ln \eta)/\kappa$, $F' = -\ln \eta/\kappa$, and hence $F_e = 1/\kappa$, $\Pi = 0$ and $G = 2/\kappa$ according to Eqs. (18.69) to (18.71).

It can happen in strongly accelerated flow that the turbulent boundary layer returns to the laminar state again. This is called *relaminarisation*, cf. R. Narasimha; K.R. Sreenivasan (1979). According to this work, the boundary layer becomes laminar again when the quantity

$$K(x) = \frac{\nu}{U^2} \frac{dU}{dx} = 3.5 \cdot 10^{-6} \quad \text{relaminarisation} \quad (18.92)$$

exceeds the given value. It can then be seen from the velocity distribution $U(x)$ already if relaminarisation is expected. In sink flow, $K = \nu/|U_1|l$ is precisely a constant.

18.2.5 Boundary Layer on a Plate at Zero Incidence

As has already been mentioned, the boundary layer on a flat plate at zero incidence is an equilibrium boundary layer ($\beta = 0$, $m = 0$, $U = V = U_\infty$). Generally the Reynolds number is formed with the length along the plate x :

$$\text{Re}_x = \frac{U_\infty x}{\nu} = \text{Re} \cdot x^*.$$

Then Eq. (18.74), (18.75) and (18.89) yield the friction law

$$\frac{1}{\gamma} = \frac{1}{\kappa} \ln(\gamma^2 \text{Re}_x) + C^+ + \frac{1}{\kappa} (2\pi - \ln F_e). \quad (18.93)$$

For a plate of breadth b and depth x which is wetted on one side, the drag coefficient reads

$$c_D = \frac{2D}{\rho U_\infty^2 bx} = \frac{1}{x} \int_0^x c_f(x) dx. \quad (18.94)$$

Differentiation with respect to x yields

$$\frac{d}{dx}(c_D x) = c_f$$

or

$$c_D = c_f - x \frac{dc_D}{dx} = c_f - x \frac{dc_f}{dx} + O(c_f^2). \quad (18.95)$$

If we differentiate Eq. (18.93) with respect to x , then Eq. (18.95) delivers

$$c_D = c_f \left(1 + \frac{2}{\kappa} \sqrt{\frac{c_f}{2}} \right)$$

or

$$\sqrt{\frac{2}{c_D}} = \sqrt{\frac{2}{c_f}} - \frac{1}{\kappa} + O\left(\sqrt{\frac{c_f}{2}}\right). \quad (18.96)$$

Experiments have produced the following values, cf. T. Cebeci; A.M.O. Smith (1974), p. 190:

$$F_e = 3.78, \quad \pi = 0.55, \quad G = 6.6. \quad (18.97)$$

Combining Eq. (18.93) and (18.96) together with the numerical values (18.97) delivers the law for the total resistance of the plate (the drag coefficient is now referred to the plate length l):

$$\sqrt{\frac{2}{c_D}} = \frac{1}{\kappa} \ln \left(\frac{c_D}{2} \text{Re} \right) + C^+ - 3.0. \quad (18.98)$$

Explicitly the law reads

$$c_D = 2 \left[\frac{\kappa}{\ln \text{Re}} G(\Lambda; D) \right]^2 \quad (18.99)$$

with

$$\Lambda = \ln \text{Re}, \quad D = 2 \ln \kappa + \kappa(C^+ - 3.0),$$

where $G(\Lambda; D)$ is again defined by Eq. (17.60).

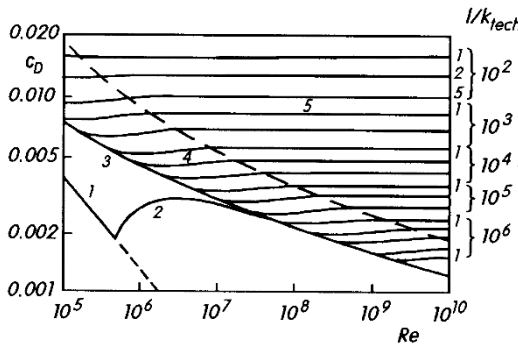


Fig. 18.3. Resistance diagram for the flat plate at zero incidence (one side)

- (1) laminar, from Eq. (6.59)
- (2) turbulent, with laminar starting region, $Re_{crit} = 5 \cdot 10^5$
- (3) turbulent, hydraulically smooth, from Eq. (18.98), with $C^+ = 5.0$
- (4) turbulent with roughness, from Eq. (18.98), with C^+ from Fig. 17.8
- (5) turbulent, fully rough, with $C_r^+ = 8.0$
- - - boundary between 4 and 5, $k_s^+ = 70$

The friction law (18.98) or (18.99) holds for both smooth and rough surfaces. It is shown for smooth surfaces ($C^+ = 5.0$) in Fig. 1.3. For rough surfaces, the function $C^+(k_{tech}^+)$ where $k_{tech}^+ = k_{tech} u_\tau / \nu$ from Sect. 17.1.2 has to be used. One then obtains the complete resistance diagram as in Fig. 18.3.

The roughness only has an effect on the drag when the *admissible roughness* $k_{tech\,adm} = 5\nu/u_\tau(x=l)$ is exceeded. The boundary between region 4 and the so-called *fully rough* region 5 is denoted by $k_{tech} = 70\nu/u_\tau(x=l)$. In the fully rough region, c_D is independent of the Reynolds number and depends only on the relative roughness k_{tech}/l . Curve 2 corresponds to those flows where a laminar boundary layer forms first of all, but where this becomes turbulent at $Re_{crit} = U_\infty x_{crit}/\nu = 5 \cdot 10^5$. Although this transition actually takes place along a certain length (cf. Chap. 15), it is assumed here that it occurs abruptly in one point.

Using Eq. (18.94), the momentum-integral equation yields

$$c_D = 2 \frac{\delta_2}{l}. \quad (18.100)$$

The momentum thickness $\delta_2(x)$ is therefore a measure of the friction drag up to the point x , and therefore (in contrast to $\delta_1(x)$ and $\delta_3(x)$) is not discontinuous at the point of completed transition. The function $\delta_2(Re_x)$ is sketched in Fig. 18.4. According to this figure, the boundary layer behaves as if it had commenced at a virtual leading edge (point A at Re_A). Using Eq. (6.64) for δ_2 for laminar boundary layers, we find that in the transition point Re_{crit} :

$$0.664 \sqrt{Re_{crit}} = (Re_{crit} - Re_A) \left[\frac{\kappa}{\ln(Re_{crit} - Re_A)} G(\Lambda; D) \right]^2 \quad (18.101)$$

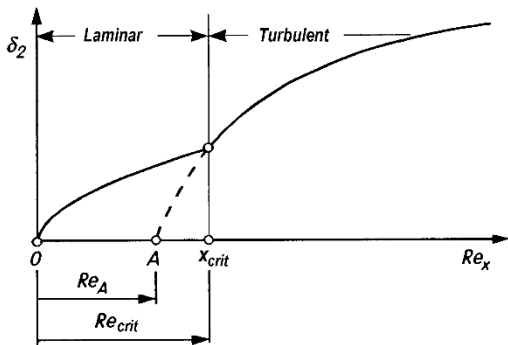


Fig. 18.4. Momentum thickness for a turbulent plate boundary layer with laminar starting region

with

$$A = \ln(\text{Re}_{\text{crit}} - \text{Re}_A), \quad D = 2 \ln \kappa + \kappa(C^+ - 3.0).$$

For a given Re_{crit} , this is a defining equation for Re_A . Because of the laminar starting region, in the turbulent part $\text{Re}_2 = U_\infty \delta_2 / \nu$ and c_D are smaller, and c_f larger than the corresponding values in the case without approach. At the transition point, δ_1 and H_{12} drop abruptly, and δ_3 and H_{32} increase abruptly. H_{12} jumps from 2.59 to values between 1.4 and 1.0, and H_{32} from 1.57 to values between 1.7 and 2.0. Therefore determining the shape factors in experiments allows one to ascertain if the boundary layer is laminar or turbulent.

Table 18.2 shows the characteristic numbers F_e , Π and G for different turbulence models. Comparison with experimental data gives an indication of the precision of the computational method. The agreement with experiment can be improved by changing the model constants.

Table 18.2. Global values from Eqs. (18.69) to (18.71) of the turbulent plate boundary layer. Comparison of the results from various turbulence models with experiment

Authors		F_e	Π	G
K. Wiegardt (1968)	measurements: $\text{Re}_1 > 19\,000$	3.9	0.59	6.8
model by R. Michel et al. (1968)	Eq. (18.8)	3.3	0.38	6.2
model by T. Cebeci; A.M.O. Smith (1974)	Eq. (18.7)	3.8	0.55	6.6
$k-\varepsilon$ model, Eqs. (18.12) and (18.20)		2.9	0.29	5.7

Measurements at higher Reynolds numbers ($\text{Re}_1 > 50\,000$) by Fernholz et al. (1995) resulted in $G = 6.5$.

Figure 18.5 shows some important boundary-layer quantities for different turbulence models and equations.

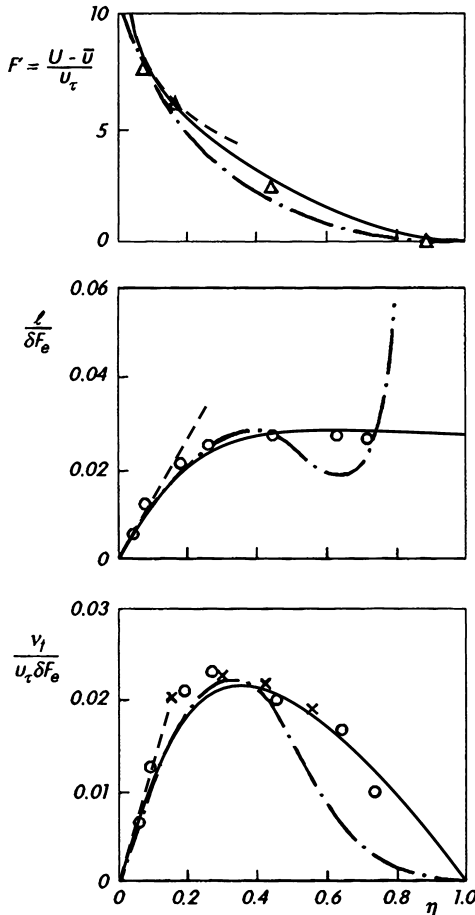


Fig. 18.5. Turbulent plate boundary layer: distributions of the relative velocity defect $F'(\eta)$, mixing length $\ell(\eta)$ and eddy viscosity $\nu_t(\eta)$ according to two turbulence models.

— · · · · · eddy viscosity model $\nu_t(\eta) = \nu_{t\infty} \gamma(x, y) [1 - \exp(-\kappa u_\tau y / \nu_{t\infty})]$
with $\gamma(x, y)$ from Eq. (16.31) and $\nu_{t\infty}/u_\tau \delta = 0.10$, $F_e = 3.6$, $\Pi = 0.46$,
 $G = 6.3$

— — — indirect turbulence model

$$F'(\eta) = \frac{1}{\kappa} [-\ln \eta + 2\Pi - (1+6\Pi)\eta^2 + (1+4\Pi)\eta^3]$$

$$S(\eta) = 1 - \frac{1}{\kappa F_e} \left[\eta + \frac{2}{3}(1+6\Pi)\eta^3 - \frac{3}{4}(1+4\Pi)\eta^4 \right]$$

$$\frac{\ell}{\delta F_e} = -\frac{\sqrt{S}}{F_e F''}; \quad \frac{\nu_t}{u_\tau \delta F_e} = -\frac{S}{F_e F''}; \quad F_e = \frac{1}{\kappa} \left(\frac{11}{12} + \Pi \right); \quad \kappa = 0.41$$

$$\Pi = 0.37 \text{ (given)}; \quad F_e = 3.1; \quad G = 6.1$$

— · · · · asymptote for $\eta \rightarrow 0$

○ × △ measurements, see T. Cebeci; A.M.O. Smith (1974), p. 108 and J.O. Hinze (1975), pp. 631, 645

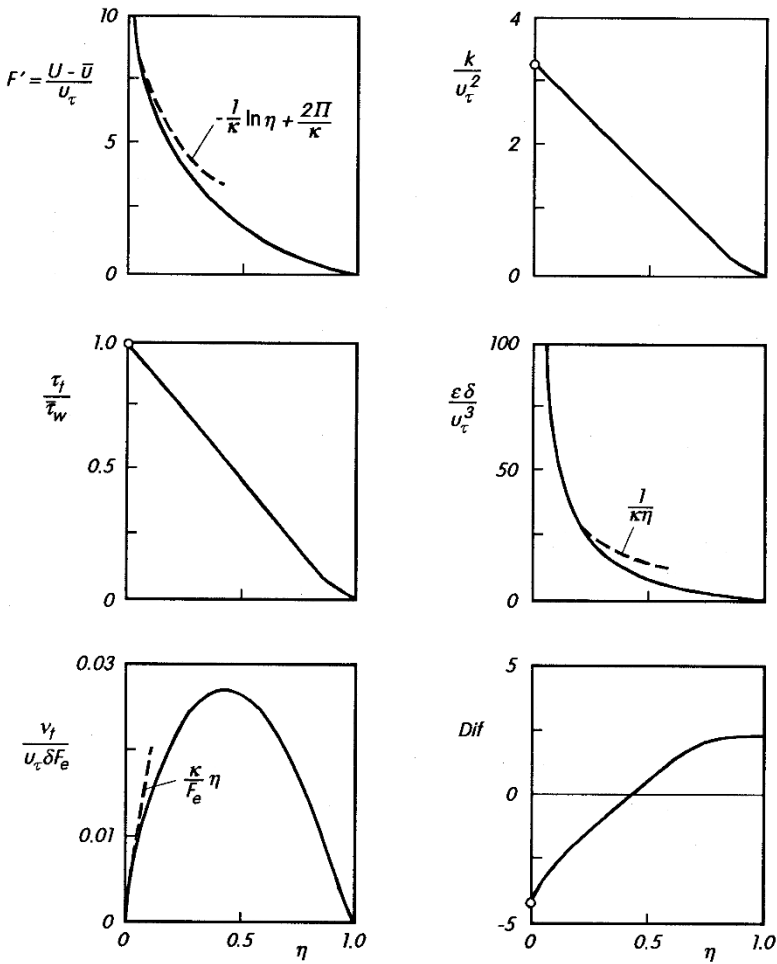


Fig. 18.6. Distributions of the most important characteristic quantities in the defect layer of a turbulent plate flow: calculations using the k - ε model:

$$F_e = 2.94; \quad \Pi = 0.29; \quad G = 5.7; \quad F''(\eta = 1) = -1.7$$

$$Dif = \frac{\delta}{\kappa u_\tau^3} \frac{\partial}{\partial y} \left(\nu_t \frac{\partial k}{\partial y} \right)$$

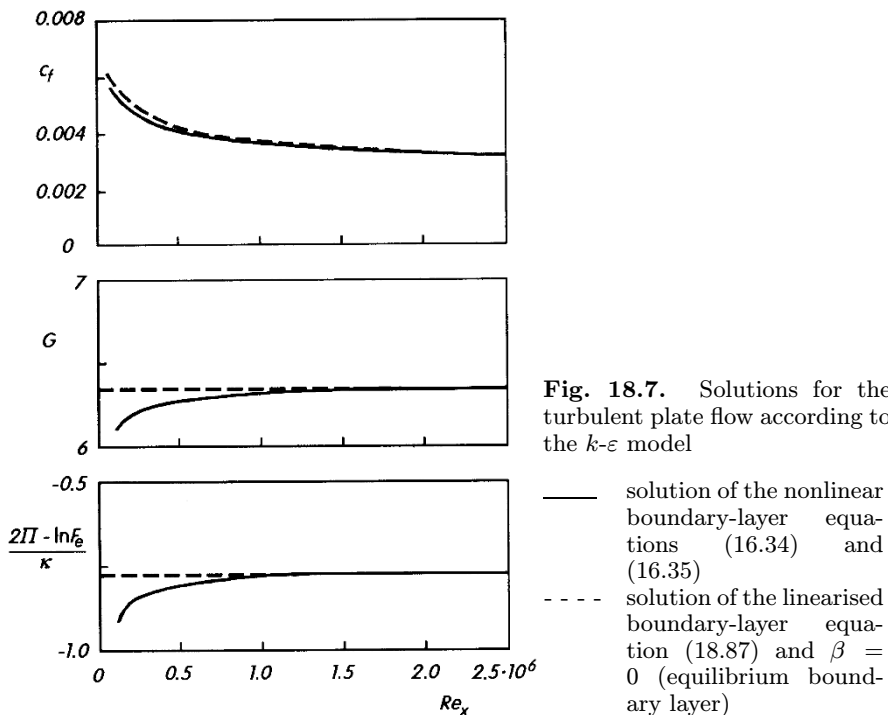


Fig. 18.7. Solutions for the turbulent plate flow according to the k - ε model

Finally Fig. 18.6 compares the different terms in the turbulent energy equation obtained using distributions from the k - ε model with measurements. Calculations using the k - L model by J.C. Rotta (1975, 1986) have been carried out by R. Voges (1978).

If the complete nonlinear boundary-layer equations (16.34) and (16.35) are used, the k - ε model yields the results shown in Fig. 18.7. The plots of the functions G and Π show that the asymptotic solution considered until now is only valid for $Re_x > 2 \cdot 10^6$ (this corresponds to about $Re_2 = U_\infty \delta_2 / \nu > 2 \cdot 10^3$), cf. T. Cebeci; A.M.O. Smith (1974), p. 125 and L.P. Erm et al. (1987). The differences in Fig. 18.7 have to do with the fact that on the one hand the complete, nonlinear equations of motion were used and on the other hand the linearisation by means of the defect formulation.

In the region $Re_x < 2 \cdot 10^6$, the model constants of the algebraic model (i.e. α in Eq. (18.7); λ in Eq. (18.8) and (18.9)) are clearly dependent on the Reynolds number $Re_2 = U(x) \delta_2(x) / \nu$, cf. T. Cebeci; A.M.O. Smith (1974), p. 221.

A comprehensive collection of data regarding the turbulent constant pressure boundary layer has been presented and evaluated by H.H. Fernholz; P.J. Finley (1996).

The turbulent flow along a moving plate (cf. Sect. 17.2.5 for the laminar case) has been investigated by N. Afzal (1996).

18.3 Boundary Layers with Separation

18.3.1 Stratford Flow

The flow where the wall shear stress vanishes everywhere was experimentally investigated by B.S. Stratford (1959b) and is therefore called *Stratford flow*. A more recent investigation of this flow has been carried out by K. Elsberry et al. (2000).

As has already been mentioned, the defect formulation for describing this flow breaks down, since the shear stress velocity cannot be used as a reference quantity. The homogeneous velocity therefore no longer represents the limiting solution $\text{Re}^{-1} = 0$.

However there is a second limiting solution for vanishing wall shear stress. Since the viscosity is no longer required to transmit the wall shear stress at $\bar{\tau}_w = 0$, a boundary layer of *finite* thickness δ exists for $\text{Re}^{-1} = 0$.

In order to determine the velocity \bar{u} for this limiting solution, a similarity trial solution is chosen, just as in the case of laminar boundary layers, cf. Eq. (7.9):

$$\begin{aligned}\bar{u} &= U f'(\eta), \quad \bar{v} = -\frac{d}{dx}(U \delta) f(\eta) + U \frac{d\delta}{dx} \eta f'(\eta), \\ \tau_t &= \varrho U^2 s(\eta), \quad \eta = \frac{y}{\delta}.\end{aligned}\tag{18.102}$$

The momentum equation (16.35) with $\bar{\tau}_v = 0$ then yields an ordinary differential equation if $U(x)$ obeys a power law as in Eq. (18.90) and $\delta = \alpha x$ increases linearly along the plate. The differential equation reads

$$f'^2 - 1 - \frac{m+1}{m} f f'' = \frac{1}{\alpha m} s'\tag{18.103}$$

with the boundary conditions

$$\begin{aligned}\eta = 0 : \quad f &= 0, \quad f' = 0 \\ \eta = 1 : \quad f' &= 1, \quad f'' = 0.\end{aligned}\tag{18.103a}$$

It was shown in Sect. 17.2.2 that if the wall shear stress vanishes, the velocity distribution close to the wall obeys the square root law

$$\bar{u} = \frac{2}{\kappa_\infty} \sqrt{\frac{1}{\varrho} \frac{dp}{dx}} \sqrt{y} + u_s C^\times \quad \text{or} \quad f'(\eta) = \frac{2}{\kappa_\infty} \sqrt{-\alpha m} \sqrt{\eta} + \frac{u_s}{U} C^\times,\tag{18.104}$$

where

$$u_s = \frac{\nu}{\varrho} \left(\frac{dp}{dx} \right)^{1/3}.\tag{18.104a}$$

The solution of Eq. (18.103) does not obey this condition. Therefore, an intermediate layer (also called “lower outer layer”) is necessary. The coordinate in this layer is

$$\tilde{\eta} = \frac{1}{\alpha^n} \frac{y}{x-x_0} = \alpha^{n-1} \eta \quad n \geq 1. \quad (18.105)$$

The exponent n depends on the turbulence model. It is $n = 4/3$ for the eddy viscosity model, see K. Gersten; H. Herwig (1992), and $n = 3/2$ for the mixing-length model, see B. Scheichl (2001). More details of the Stratford flow can be found in K. Gersten; H. Herwig (1992).

The effect of the Reynolds number in this flow is clearly minimal. It is described by the integration constant C^\times in the square root law of the wall (17.103). Unfortunately in the literature, the value given to C^\times varies greatly, although it seems likely that C^\times is negative, cf. P.R. Spalart; A. Leonard (1987).

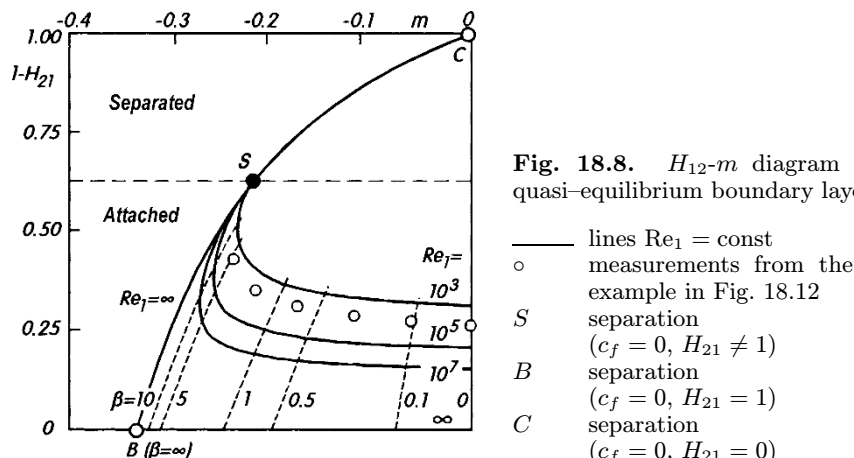


Fig. 18.8. H_{12} - m diagram for quasi-equilibrium boundary layers

- lines $Re_1 = \text{const}$
- measurements from the example in Fig. 18.12
- S separation ($c_f = 0, H_{21} \neq 1$)
- B separation ($c_f = 0, H_{21} = 1$)
- C separation ($c_f = 0, H_{21} = 0$)

The outer flow which obeys a power law from Eq. (18.90) leads to equilibrium boundary layers for $\bar{\tau}_w \neq 0$ and to Stratford flow for $\bar{\tau}_w = 0$. Figure 18.8 presents an overview of these flows in the form of an H_{12} - m diagram. The points on the abscissa ($H_{21} = 1$) correspond to the limiting solution ($Re^{-1} = 0$) for equilibrium boundary layers. The curve BSC satisfies the equation

$$1 - H_{21} = \frac{3m + 1}{2m + 1}. \quad (18.106)$$

This is obtained from the momentum-integral equation (7.100) with $\bar{\tau}_w = 0$ and from Eq. (18.90) (δ_1 and δ_2 are proportional to x). On this curve lies the point S from Eq. (18.105) which corresponds to Stratford flow. In the next section we will show how this diagram can be used to establish a relation between Stratford flow and equilibrium boundary layers.

18.3.2 Quasi-Equilibrium Boundary Layers

We assume that the wake parameter $\Pi(x)$ introduced in Eq. (18.70) changes only weakly with the distance x . Thus, if its variation in x may be neglected compared to the logarithmic term in Eq. (18.73), differentiating Eq. (18.73) with respect to x delivers

$$\frac{U}{\gamma} \frac{d\gamma/dx}{dU/dx} = -\frac{\gamma}{\kappa + \gamma} \frac{m+1}{m} \quad (18.107)$$

with

$$m(x) = \frac{\delta dU/dx}{U d\delta/dx}. \quad (18.108)$$

In addition, if we also neglect the terms on the right hand side of Eq. (18.60), that is, the partial derivatives $\partial F/\partial x$ and $\partial F'/\partial x$, as being small, and take Eqs. (18.107) and (18.108) into account, we obtain the following differential equation for $F(x, \eta)$:

$$\begin{aligned} & \frac{m+1}{m} \left\{ \eta F'' - \gamma F F'' + \frac{\gamma}{\kappa + \gamma} [F' + \gamma(F F'' - F'^2)] \right\} - 2F' + \gamma F'^2 \\ &= -\frac{F_e S'}{\beta} \end{aligned} \quad (18.109)$$

with the boundary conditions (18.64). Here β is the Rotta–Clauser parameter from Eq. (18.85). The function $F(x, \eta)$ can be determined once a turbulence model, such as Eq. (18.63), has been supplied. Since $\gamma(x)$ and also $m(x)$ and $\beta(x)$ are functions of x , the solution $F(x, \eta)$ depends on x too. Now Eq. (18.109) contains no partial derivatives with respect to x , i.e. x only appears as a parameter via the functions $\gamma(x)$, $m(x)$ and $\beta(x)$. Therefore at every point $x = \text{const}$ it is only an ordinary differential equation which has to be solved, just as in the case of equilibrium boundary layers. Such situations are thus called *quasi-equilibrium boundary layers* or are a case of *local equilibrium* or *pseudo-equilibrium*, cf. B.A. Kader; A.M. Yaglom (1978). The velocity profiles obtained in this manner are only dependent on the *local* values $\gamma(x)$, $m(x)$ and $\beta(x)$. In the limit $\gamma \rightarrow 0$, Eq. (18.109) reduces to the ordinary differential equation (18.87), i.e. in this case the profile becomes that of the equilibrium boundary layer.

Integrating Eq. (18.109) with respect to η from $\eta \rightarrow 0$ to $\eta = 1$ yields the momentum-integral equation in the form:

$$\frac{m+1}{m} = - \left[1 + H_{12} \left(1 + \frac{1}{\beta} \right) \right] \frac{1 + \gamma/\kappa}{1 + (H_{12} - 1)\gamma/\kappa}. \quad (18.110)$$

This coupling of m , γ and β means that we have a family of velocity profiles with *two* parameters. In what follows we shall assume that $F'(\eta; \gamma, \beta)$ describes all possible velocity defect profiles in turbulent boundary layers.

The solutions then again yield the boundary-layer parameters defined in Eqs. (18.69) to (18.71), and thus eventually lead to the thicknesses from

Eq. (18.79) and the shape factor from Eq. (18.81). The Reynolds number formed with the local velocity $U(x)$ and the displacement thickness $\delta_1(x)$:

$$\text{Re}_1 = \frac{U(x) \delta_1(x)}{\nu} \quad (18.111)$$

also depends on β and $\gamma = \sqrt{c_f/2}$. This lead to the relations

$$c_f = c_f(\text{Re}_1, H_{12}), \quad H_{32} = H_{32}(\text{Re}_1, H_{12}). \quad (18.112)$$

Equilibrium boundary layers are found in the limits $c_f = c_f(\text{Re}_1, H_{12} \rightarrow 1)$ and $H_{32} = H_{32}(H_{12}, \text{Re}_1 \rightarrow \infty)$.

A.W.M. Henkes (1998) applied four commonly used turbulence models to investigate quasi-equilibrium boundary layers although he did not use the expression ‘quasi-equilibrium’.

See also R.W. Barnwell et al. (1989).

Note (Connection to empirical relations)

Comprehensive analyses of many different kinds of turbulence boundary layers have also led to empirical relations such as Eq. (18.112).

One very well known empirical relation is due to H. Ludwieg; W. Tillman (1949)

$$c_f(\text{Re}_1, H_{12}) = 0.246 \cdot 10^{-0.678 H_{12}} \left(\frac{\text{Re}_1}{H_{12}} \right)^{-0.268}. \quad (18.113)$$

However this formula is incorrect for $\text{Re}_1 \rightarrow \infty$; the asymptotically correct formula for $\text{Re}_1 \rightarrow \infty$ is Eq. (18.74) or (18.76).

Analysis of the measurements has also delivered a relation between the shape factors which is almost independent of Re_1 . One finds the following formula

$$H_{12} - 1 = 1.48(2 - H_{32}) + 104(2 - H_{32})^{6.7}. \quad (18.114)$$

For $H_{32} \rightarrow 2$ this formula becomes Eq. (18.82), disregarding the factor 1.48.

Figure 18.8 shows the relations between the different boundary-layer parameters. Here $C^\times = 0$ was set, so that all the $\text{Re}_1 = \text{const}$ lines run through the point A . Then, using the transformation

$$f'(\hat{\eta}) = 1 - \gamma F'(x), \quad \hat{\eta} = \frac{\eta}{\gamma}, \quad (18.115)$$

Eq. (18.109) for $\gamma \rightarrow 0$ becomes Eq. (18.103). Numerous measurements have shown that many turbulent boundary layers are quasi-equilibrium boundary layers in the pressure increase region. The development of a boundary layer from an initial plate boundary layer on to separation is displayed as a curve rising from a point on the ordinate ($\beta = 0$) to the separation point S in Fig. 18.8. This is indicated by the experimental data from the example in Fig. 18.12.

For every Re_1 there is a minimum m . According to A.P. Härtl (1989), this minimum value of m lies approximately on the line

$$1 - H_{21} = 5 \left(m_{\min} + \frac{1}{3} \right). \quad (18.116)$$

Since, according to Eq. (18.108), m is a measure of the pressure gradient, the minimum value m_{\min} corresponds to boundary layers with the greatest possible pressure rise. These are of great importance in optimising diffuser flows, cf. J. Klauer (1989), A.P. Härtl (1989). The view frequently held in the literature that the boundary layer undergoing incipient separation can withstand the greatest pressure rise, i.e. $m \approx -0.22$, is therefore untrue.

For every given Re_1 and $m > m_{\min}$ two solutions exist, whereby for $m > m_s \approx -0.22$, one is a solution for an attached flow and one for a separated boundary layer, cf. J. Klauer (1989).

The approximation considered here for describing the velocity in a boundary layer is better the closer the boundary layer is to an equilibrium boundary layer. Because very good agreement with experiments on boundary layers in pressure rise regions has been achieved with the two parameter profile family, this shows us that these boundary layers tend towards local equilibrium very quickly, so that a turbulence model using only local parameters of the boundary layers is indeed possible (algebraic turbulence models).

Note (Indirect turbulence model: law of the wake)

Following the analysis of numerous experimental data, D. Coles (1956) presented the following expression for the solution $F'(x, y)$ of Eq. (18.109):

$$\frac{U(x) - \bar{u}(x, y)}{u_\tau(x)} = F'(x, \eta) = \frac{1}{\kappa} \{\Pi(x)[2 - W(\eta)] - \ln \eta\}, \quad (18.117)$$

where $W(\eta)$ is called the *wake function* and Π is defined by Eq. (18.70). This representation is called the *law of the wake*. The three free parameters $\delta(x)$, $u_\tau(x)$ and $\Pi(x)$ are determined in order that the measured velocity profiles are approximated as well as possible (*indirect turbulence model*). The wake function $W(\eta)$ is subject to the boundary conditions

$$\begin{aligned} W(0) &= 0, & W'(0) &= 0, & W(1) &= 2, & W'(1) &= 0 \\ \int_0^1 W(\eta) d\eta &= 1. \end{aligned} \quad (18.118)$$

If we choose

$$W(\eta) = 1 - \cos \pi \eta = 2 \sin^2 \left(\frac{\pi}{2} \eta \right), \quad (18.119)$$

we obtain the following expressions for the quantities defined in Eq. (18.69) and (18.71):

$$F_e = \int_0^1 F' d\eta = \frac{1}{\kappa} (1 + \Pi), \quad (18.120)$$

$$G(x) = \frac{1}{F_e \kappa^2} (2 + 3.179 \Pi + 1.5 \Pi^2). \quad (18.121)$$

The expression obtained for H_{31} is an extension to Eq. (18.81):

$$H_{31} = 2 - 3\gamma G + \gamma^2 I_3 \quad (18.122)$$

with

$$I_3 = \int_0^1 F'^3(\eta) d\eta = \frac{1}{\kappa^3} (6 + 11.14\pi + 8.5\pi^2 + 2.56\pi^3). \quad (18.123)$$

The results change only a little if the wake function is replaced by the power law $W(\eta) = 2\eta^2(3 - 2\eta)$.

Corrections to the law of the wake with improvements at the outer edge of the boundary layer have been presented by P.J. Finley et al. (1966) and A.K. Lewkowicz (1982), see J. Klauer (1989).

If the relation $G(\beta)$ of the equilibrium boundary layer is adopted for all boundary layers, for a given π and γ one can consecutively determine F_e , G , β , H_{21} , Re_1 (from Eq. (18.73)) and m (from Eq. (18.110)). Using these, a diagram such as Fig. 18.8 can again be constructed. For the limit $\gamma \rightarrow 0$, $\pi \rightarrow \infty$ with $\gamma\pi = \kappa/2$ a pure sine profile is again found in the separation point, although now $1 - H_{21} = 0.75$ ($m = -0.167$), a figure in less good agreement with experiments.

The law of the wake (18.117) is therefore an approximation for the velocity distributions of quasi-equilibrium boundary layers.

Note (Stratford's separation criterion)

Analogous to the separation criterion for laminar boundary layers given in Sect. 8.2, B.S. Stratford (1959a) also developed a separation criterion for turbulent boundary layers. The criterion is based on the two-layer structure of the turbulent boundary layer. Again the location of the separation point can in principle be determined directly from the given pressure distribution.

18.4 Computation of Boundary Layers Using Integral Methods

18.4.1 Direct Method

In Sect. 8.1 we already treated an integral method for calculating laminar boundary layers. In integral methods it is sufficient to determine the global characteristic values of the boundary layer. For example, for a given velocity distribution $U(x)$, the functions $Re_1(x)$ and $H_{21}(x)$ are computed.

The basis of integral methods are the momentum-integral and, for example, (mechanical) energy-integral equations. These are obtained by integrating the momentum and energy equations respectively over the boundary-layer thickness. The two parameter profiles described in the previous section are used to evaluate the integrals which appear. This will guarantee that asymptotically exact solutions are obtained in the special case of equilibrium boundary layers.

The integral method described in what follows is based on the momentum-integral equation (7.100) and the energy-integral equation (7.104). We introduce the dimensionless *dissipation integral coefficient*

$$c_D = \frac{2\mathcal{D}}{\varrho U^3} = \frac{2}{\varrho U^3} \int_0^\delta \bar{\tau}_t \frac{\partial \bar{u}}{\partial y} dy. \quad (18.124)$$

The two integral equations can then be written as differential equations for the quantities $\text{Re}_1(X)$ and H_{21} . Introducing the independent variable

$$X = \frac{x - x_0}{l} \text{Re} = \frac{(x - x_0)V}{\nu}$$

with an arbitrarily chosen point x_0 as the origin and $\text{Re} = Vl/\nu$, after some manipulation we obtain

$$\frac{d\text{Re}_1}{dX} = \frac{1}{A} \left[BU + C \frac{\text{Re}_1}{U} \frac{dU}{dX} \right], \quad (18.125)$$

$$\frac{dH_{21}}{dX} = -\frac{1}{A} \left[DU + E \frac{H_{21}}{U} \frac{dU}{dX} \right]. \quad (18.126)$$

Here the auxilliary functions $A(H_{21})$, $B(H_{21}, \text{Re}_1)$, $C(H_{21})$, $D(H_{21}, \text{Re}_1)$ and $E(H_{21})$ were determined using the quasi-equilibrium boundary-layer equations. These functions are shown in Fig. 18.9. With the help of these functions, $\text{Re}_1(X)$ and $H_{21}(X)$ may be determined from Eq. (18.125) and (18.126) for a given $U(X)$. If the computation begins at the transition point, then $H_{21} \cdot \text{Re}_1 = \text{Re}_2 = (\text{Re}_2)_{\text{lam}}$ holds, as does $dp/dx = 0$ ($\beta = 0$, $G = 6.6$) approximately. Therefore the starting value may be read off from Fig. 18.9 using Eq. (18.81).

The function $c_f(X)$ from Fig. 18.9 can then be obtained from $\text{Re}_1(X)$ and $H_{21}(X)$. This is again valid for quasi-equilibrium boundary layers. In the previous section it was described how all the other boundary-layer characteristic parameters and also the velocity profiles may be obtained from Re_1 and H_{21} . The computation breaks down at $H_{21} = 0.4$, since there the function A vanishes. If the velocity profile $U(X)$ is given, the boundary-layer calculation can only be carried on as far as the separation point, because these equations have a singularity there. This corresponds to the Goldstein singularity in laminar boundary layers.

Example: Symmetric Joukowsky airfoil

(relative thickness $d/l = 0.2$; angle of attack $\alpha = 0^\circ$; $\text{Re} = 10^7$)

The transition point is assumed to be in the pressure minimum ($x/l = 0.15$). The laminar boundary layer from the stagnation point to the transition point is calculated using the quadrature formula (8.23). The skin-friction coefficient c_f along the chord of the airfoil is shown in Fig. 18.10.

Integrating c_f along the chord yields the drag coefficient c_D , see Eqs. (1.5) and (6.40). One obtains the value $c_D = 5.9 \cdot 10^{-3}$. For comparison, the field method (turbulence model by Cebeci-Smith, Eq. (18.7)) delivers the value $c_D = 6.0 \cdot 10^{-3}$. Note

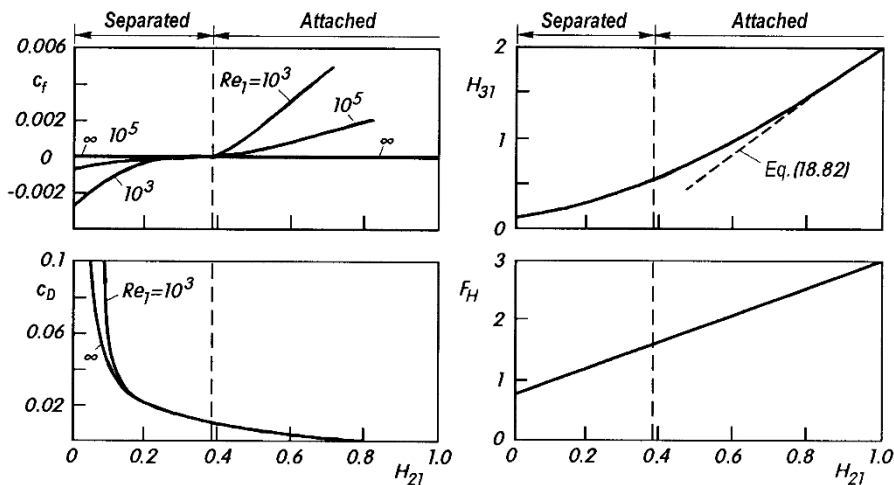


Fig. 18.9. Quasi-equilibrium auxilliary functions
 $H_{31}(H_{21})$, $F_H(H_{21})$, $c_f(H_{21}, Re_1)$, $c_D(H_{21}, Re_1)$

The functions in Eq. (18.125) and (18.126) are:

$$\begin{aligned} A(H_{21}) &= H_{21}F_H - H_{31} & D(H_{21}, Re_1) &= (\frac{1}{2}c_f H_{31} - c_D H_{21})/Re_1 \\ B(H_{21}, Re_1) &= \frac{1}{2}F_H c_f - c_D & E(H_{21}) &= -(1 - H_{21})H_{31}/H_{21} \\ C(H_{21}) &= 2H_{31} - F_H - H_{21}F_H \end{aligned}$$

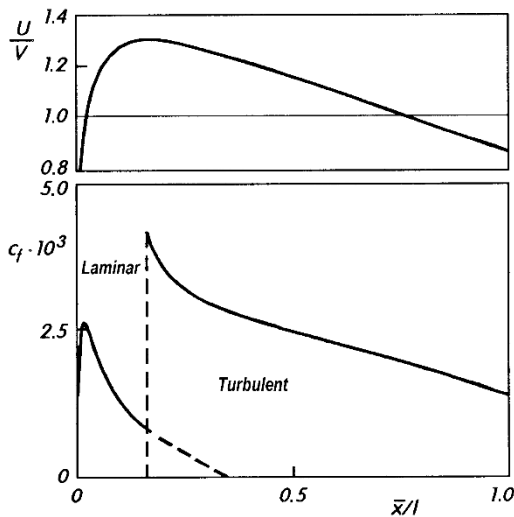


Fig. 18.10. Outer flow velocity $U(\bar{x})$ and skin-friction coefficient $c_f(\bar{x})$ on a Joukowsky airfoil in a symmetric flow, with $d/l = 0.2$, $Re = 10^7$, transition at $\bar{x}/l = 0.15$. Coordinate \bar{x} runs along the chord of the airfoil

that the drag coefficient of the flat plate at zero incidence at the same Reynolds number has the somewhat larger (!) value of $c_D = 6.2 \cdot 10^{-3}$.

Note (Correction for nonequilibrium boundary layers)

The integral method described delivers exact solutions for equilibrium boundary layers. If the boundary layer deviates from equilibrium, the solutions are approximations. Some integral methods contain corrections which take this into account, cf. J. Klauer (1989).

Note (Further integral methods)

Numerous different integral methods are to be found in the literature, and that described here is only one example. An overview has been given by S.J. Kline et al. (1968) and J. Delery; J.G. Marvin (1986). Practically all methods use the momentum-integral equation. Instead of the energy-integral equation, the *moment-of-momentum-integral equation* is frequently used as the second equation. This is obtained by multiplying the momentum equation by y and integrating over the boundary-layer thickness, cf. Eq. (7.106).

A relation involving the *entrainment* can also serve as a second equation. According to M.R. Head (1960), the boundary-layer thickness δ grows because the boundary layer entrains irrotational fluid from the outer flow, cf. Sect. 16.5.4. The entrainment velocity is

$$v_E = \frac{dQ_b}{dx} = \frac{d}{dx} \int_0^{\delta(x)} \bar{u} dy = \frac{d}{dx} [U(\delta - \delta_1)] = U \frac{d\delta}{dx} - v_e . \quad (18.127)$$

According to Fig. 18.11, v_E can be interpreted as the velocity of the outer flow perpendicular to the edge of the boundary layer.

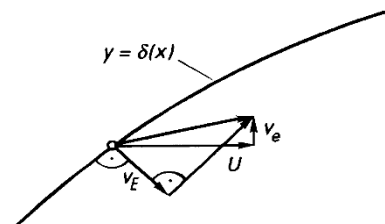


Fig. 18.11. Entrainment velocity v_E

The quantity $c_E(H_{21}, \text{Re}_1) = v_E/U$ may again be determined for equilibrium boundary layers, cf. J. Klauer (1989). Then Eq. (18.127) can be transformed into a differential equation for H_{21} and Re_1 .

18.4.2 Inverse Method

Frequently it is the inverse of the problem discussed up until now which has to be dealt with. A displacement thickness distribution $\delta_1(x)$ is given and the

outer velocity $U(x)$ and the shape factor H_{21} are desired. For example, this problem arises when interactions between the outer flow and the boundary layer have to be taken into account. This is particularly true if separation takes place, but can also occur in flows through bodies where the “outer flow” depends on the displacement action of the boundary layer.

Using the quantity

$$\Delta_1(X) = \frac{\delta_1(x)}{l} \text{Re} \quad (18.128)$$

the momentum–integral equation (7.100) and the energy–integral equation (7.104) can be converted into

$$\frac{dH_{21}}{dX} + \frac{1+2H_{21}}{\text{Re}_1} \frac{d\text{Re}_1}{dX} = \frac{c_f}{2\Delta_1} + \frac{1+H_{21}}{\Delta_1} \frac{d\Delta_1}{dX}, \quad (18.129)$$

$$F_H \frac{dH_{21}}{dX} + \frac{3H_{31}}{\text{Re}_1} \frac{d\text{Re}_1}{dX} = \frac{c_D}{\Delta_1} + \frac{2H_{31}}{\Delta_1} \frac{d\Delta_1}{dX} \quad (18.130)$$

with the auxilliary functions

$$H_{31} = 2 - 3(1 - H_{21}) + 1.19(1 - H_{21})^2, \quad (18.131)$$

$$F_H = 3 - 2.38(1 - H_{21}) \quad (18.132)$$

as well as $c_f(H_{21}, \text{Re}_1)$ and $c_D(H_{21}, \text{Re}_1)$ from Fig. 18.9.

This system possesses no singularity in the region $0 \leq H_{21} \leq 1$.

Example: Comparison with measurements by R.L. Simpson et al. (1981)

An experiment carried out by R.L. Simpson et al. (1981) was also checked theoretically by J. Klauer (1989). Because flow separation occurred in the measurements, the inverse method was chosen. Figure 18.12 shows plots of the most important flow parameters. The measured δ_1 distribution and the initial values of Re_1 and H_{21} were given. The computed plots of $U(x)$, $c_f(x)$ and $H_{21}(x)$ agree well with the experimental results.

18.5 Computation of Boundary Layers Using Field Methods

18.5.1 Attached Boundary Layers ($\bar{\tau}_w \neq 0$)

The aim of field methods is to compute the flow field with the velocity components $\bar{u}(x, y)$ and $\bar{v}(x, y)$ as well as the shear stress $\bar{\tau}(x, y)$. Additional fields such as the turbulent kinetic energy field $k(x, y)$ and the dissipation field $\varepsilon(x, y)$ can come into play via the choice of turbulence model. In contrast to integral methods where only the boundary–layer characteristic quantities

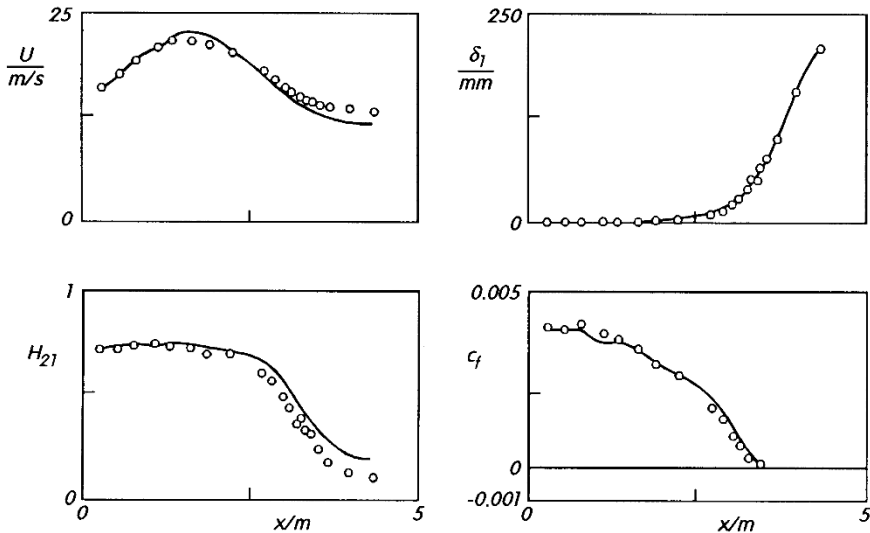


Fig. 18.12. Computation of a turbulent boundary layer using the inverse integral method by J. Klauer (1989). The experimentally determined δ_1 distribution and the initial values of Re_1 and H_{21} were given

which are dependent on x are determined and thus only ordinary differential equations have to be solved, in field methods it is partial differential equations which are to be solved.

Again it is boundary layers at high Reynolds numbers which are of interest. We shall only consider the outer layer of the boundary layer, since the (viscous) wall layer is asymptotically thin in comparison. The outer layer is that part of the boundary layer where the viscous transport processes (viscous shear stress, viscous diffusion) can be neglected compared to the turbulent transport processes. The fundamental equations for the outer layer are Eqs. (16.34) and (16.35) with $\bar{\tau}_v = 0$. The distribution $U(x)$ of the outer flow is given, while $\bar{u}(x, y)$, $\bar{v}(x, y)$, $\tau_t(x, y)$ and further field functions of the turbulence model are to be found. At the outer edge of the boundary layer, $\bar{u}(x, y)$ passes over to $U(x)$ and $\tau_t(x, y)$ tends to zero. The boundary conditions for $y \rightarrow 0$ are obtained from matching up the outer layer to the viscous sublayer. This manner of considering the asymptotic behaviour for high Reynolds numbers is called the *method of wall functions*.

In what follows, the $k-\varepsilon$ turbulence model by W.P. Jones; B.E. Launder (1972a), cf. Eqs. (18.12), (18.20) to (18.23), will be used. The entire system of equations for calculating the boundary layer then reads:

$$\frac{\partial \bar{u}}{\partial x} + \frac{\partial \bar{v}}{\partial y} = 0, \quad (18.133)$$

$$\bar{u} \frac{\partial \bar{u}}{\partial x} + \bar{v} \frac{\partial \bar{u}}{\partial y} = U \frac{dU}{dx} + \frac{\partial}{\partial y} \left(\nu_t \frac{\partial \bar{u}}{\partial y} \right), \quad (18.134)$$

$$\bar{u} \frac{\partial k}{\partial x} + \bar{v} \frac{\partial k}{\partial y} = \frac{\partial}{\partial y} \left(\frac{\nu_t}{\text{Pr}_k} \frac{\partial k}{\partial y} \right) + \nu_t \left(\frac{\partial \bar{u}}{\partial y} \right)^2 - \varepsilon, \quad (18.135)$$

$$\bar{u} \frac{\partial \varepsilon}{\partial x} + \bar{v} \frac{\partial \varepsilon}{\partial y} = \frac{\partial}{\partial y} \left(\frac{\nu_t}{\text{Pr}_\varepsilon} \frac{\partial \varepsilon}{\partial y} \right) + c_{\varepsilon 1} \frac{\varepsilon}{k} \nu_t \left(\frac{\partial \bar{u}}{\partial y} \right)^2 - c_{\varepsilon 2} \frac{\varepsilon^2}{k}, \quad (18.136)$$

$$\nu_t = c_\mu \frac{k^2}{\varepsilon} \quad (18.137)$$

with the model constants

$$\begin{aligned} \text{Pr}_k &= 1; & \text{Pr}_\varepsilon &= 1, 3; \\ c_{\varepsilon 1} &= 1.44, & c_{\varepsilon 2} &= 1.87, & c_\mu &= 0.09. \end{aligned} \quad (18.138)$$

The boundary conditions (for outer flow which is free from turbulence and an impermeable wall) are:

$$\begin{aligned} y = \delta : \quad &\bar{u} = U, \quad k = 0, \quad \varepsilon = 0 \quad \nu_t = 0 \\ y \rightarrow 0 : \quad &\bar{u} = u_\tau \left[\frac{1}{\kappa} \ln \left(\frac{yu_\tau}{\nu} \right) + C^+ \right], \\ &\bar{v} = -\frac{\bar{u}}{u_\tau} \frac{du_\tau}{dx} y, \\ &k = \frac{u_\tau^2}{\sqrt{c_\mu}}, \quad \varepsilon = \frac{u_\tau^3}{ky}, \quad \nu_t = u_\tau \kappa y \end{aligned} \quad (18.139)$$

with $u_\tau = \sqrt{\tau_w/\rho}$ as the local shear stress velocity. For $y \rightarrow \delta$, k , ε and ν_t tend linearly to zero.

For prescribed $U(x)$ and ν , Eqs. (18.133) to (18.137) determine the five unknown functions $\bar{u}(x, y)$, $\bar{v}(x, y)$, $k(x, y)$, $\varepsilon(x, y)$ and $\nu_t(x, y)$. Here the functions $\delta(x)$ and $u_\tau(x)$ must be chosen in order that the boundary conditions (18.139) are satisfied.

The initial conditions (approximately at the transition point) can then be taken from the solutions from equilibrium boundary layers (e.g. the plate boundary layer). However an initial profile can also be obtained by using the velocity profiles of the quasi-equilibrium boundary layers from Eq. (18.117), whereby ℓ and τ_t are determined from Eqs. (18.8) and (18.6), k from Eq. (18.16) and ε from Eq. (18.15) with $L = \ell$. The $\bar{v}(y)$ distribution may be determined from

$$\frac{\partial}{\partial y} \left(\frac{\bar{v}}{\bar{u}} \right) = -\frac{1}{\bar{u}^2} \left[U \frac{dU}{dx} + \frac{\partial}{\partial y} \left(\nu_t \frac{\partial \bar{u}}{\partial y} \right) \right]. \quad (18.140)$$

The relation is found by combining Eqs. (18.133) and (18.134), cf. P. Bradshaw et al. (1981), p. 96.

Because we are dealing with a system of parabolic differential equations, if the initial distributions and the boundary conditions are prescribed, the solution can be determined using a differencing method in the form of a marching procedure, cf. Chap. 23.

Numerous boundary-layer calculations have been performed using this system of equations, see for example B.E. Launder; D.B. Spalding (1972), R. Voges (1978).

E. Deriat; J.-P. Guiraud (1986) and E. Deriat (1987) have carried out an asymptotic analysis of the $k-\varepsilon$ model. Details on the mathematical basis have been presented by B. Mohammadi; O. Pironneau (1994).

Other computation methods

Of the many different methods in existence, here is a list of those most frequently used in practice for calculating turbulent boundary layers:

1. method by T. Cebeci; A.M.O. Smith (1974) (algebraic model)
2. method by P. Bradshaw et al. (1967) (one-equation model)
3. method by D.C. Wilcox (1998) (two-equation model)
4. method by J.C. Rotta (1986, 1991) (two-equation model);
examples of this to be found in H. Vollmers; J.C. Rotta (1977) and R. Voges (1978)
5. method by B.E. Launder et al. (1975) (Reynolds stress model, i.e. second-moment closure model);
examples are to be found in B.E. Launder (1984), C.G. Speziale (1991), K. Hanjalić (1994a).

Summaries of computational methods applied to turbulent boundary layers have been given by W.C. Reynolds (1976), J.L. Lumley (1978a), W. Rodi (1991), C.G. Speziale (1991), J.C. Rotta (1991).

18.5.2 Boundary Layers with Separation

The calculation method described in the previous section is unable to describe flows with vanishing wall shear stress. In particular, the square root law in the overlap layer in Eq. (17.103) for the separation point ($\bar{\tau}_w = 0$) cannot be obtained by simply varying the model constants and the boundary conditions.

In the development of the boundary layer from the attached state to the separation point, the parameter

$$K = \frac{\nu}{\varrho(\bar{\tau}_w/\varrho)^{3/2}} \frac{dp_e}{dx} \quad (18.141)$$

is particularly important, cf. Eq. (17.104).

The boundary conditions (18.139) for $y \rightarrow 0$ are changed as follows. The velocity is subject to the general law of the wall (17.110) and $\bar{v} = 0$. For the remaining quantities

$$k = \frac{|\tau_t/\varrho|}{C_k(K)}, \quad \varepsilon = \frac{C_\varepsilon(K)|\tau_t/\varrho|^{3/2}}{y}, \quad \nu_t = \sqrt{\left| \frac{\tau_t}{\varrho} \right|} \kappa(K)y \quad (18.142)$$

with $c_\mu = \kappa C_k^2 C_\varepsilon$ and

$$\tau_t = \bar{\tau}_w + \frac{dp_e}{dx} y = \bar{\tau}_w(1 + Ky^+). \quad (18.143)$$

As well as $\kappa(K)$ and $C(K)$ in Eq. (17.110), the quantities $C_k(K)$ and $C_\varepsilon(K)$ from the boundary conditions and all the model constants are now dependent on K . D. Vieth (1996) has presented these dependencies on K according to experimental results by R. Kiel (1995) and has carried out sample calculations with this generalised k - ε model. Instead of the relation $\tau_t = \varrho v_t \partial \bar{u} / \partial y$, the balance law for $\tau_t = -\varrho \bar{u}' \bar{v}'$ from Eq. (18.33) and Table 18.1 was used. This is necessary because when backflow regions appear in the boundary layer, the positions with large backflow velocity ($\partial \bar{u} / \partial y = 0$) and the positions with $\tau_t = 0$ are not the same, i.e. in general τ_t and $\partial \bar{u} / \partial y$ are no longer proportional.

As has already been discussed in Sect. 18.4.2, boundary layers with separation can only be calculated using an inverse method. Here the distribution of the displacement thickness $\delta_1(x)$ (or the distribution of $\bar{\tau}_w(x)$) is given and the distribution of the outer velocity $U(x)$ is looked for. The interaction between the boundary layer and the outer flow then yields the total solution.

A summary of turbulent boundary layers with separation is given by R.L. Simpson (1985), see also N. Afzal (2008a).

In recent years several contributions to a rational asymptotic theory for turbulent boundary layers subjected to strong adverse pressure gradients have been published. It started with B. Scheichl (2001), where a slenderness parameter was chosen as the basic limit process aside from the sufficiently high global Reynolds number. A self-consistent description shows how the classical logarithmic law of the wall (two-tiered boundary layer) is gradually transformed into the well-known square root law that holds at the point of zero skin friction (three-tiered boundary layer). Adopting the concept of locally interacting boundary layers results in a closure-free and uniformly valid asymptotic description of boundary layers that exhibit small closed reverse-flow regimes. This situation is associated with *turbulent marginal separation*, see B. Scheichl; A. Kluwick (2007a). By including effects due to high but finite values of the Reynolds number the gradual transformation of the so-called wall functions can be clarified, see B. Scheichl; A. Kluwick (2007b). Investigation by B. Scheichl et al. (2008) led to the tentative but rather remarkable conclusion that the boundary layer along the smooth surface of a bluff body never attains a fully developed state, even in the limit $Re \rightarrow \infty$. A self-consistent flow description in the vicinity of separation is derived by B. Scheichl et al. (2011), where the predominantly turbulent region is included. A criterion is established that acts to select the position of separation. The basic analysis which appears physically feasible and rational is carried out without needing a specific turbulence closure.

18.5.3 Low–Reynolds–Number Turbulence Models

In contrast to the method of wall functions, in low–Reynolds–number turbulence models the entire boundary layer including the viscous wall layer is calculated, cf. Sect. 18.1.7. In order to do this, the turbulence model must be extended to include the viscous wall layer. The particularly simple boundary condition at the wall (no-slip condition) is advantageous. Since the fundamental equations now also contain viscous terms, the transition to the inviscid outer flow now takes place continuously as with laminar boundary layers.

The equations for the low–Reynolds–number version of the k – ε model read, cf. V.C. Patel et al. (1985):

$$\frac{\partial \bar{u}}{\partial x} + \frac{\partial \bar{v}}{\partial y} = 0, \quad (18.144)$$

$$\bar{u} \frac{\partial \bar{u}}{\partial x} + \bar{v} \frac{\partial \bar{v}}{\partial y} = U \frac{dU}{dx} + \frac{\partial}{\partial y} \left[(\nu + \nu_t) \frac{\partial \bar{u}}{\partial y} \right], \quad (18.145)$$

$$\bar{u} \frac{\partial k}{\partial x} + \bar{v} \frac{\partial k}{\partial y} = \frac{\partial}{\partial y} \left[\left(\nu + \frac{\nu_t}{Pr_k} \right) \frac{\partial k}{\partial y} \right] + \nu_t \left(\frac{\partial \bar{u}}{\partial y} \right)^2 - \tilde{\varepsilon} - D, \quad (18.146)$$

$$\begin{aligned} \bar{u} \frac{\partial \tilde{\varepsilon}}{\partial x} + \bar{v} \frac{\partial \tilde{\varepsilon}}{\partial y} &= \frac{\partial}{\partial y} \left[\left(\nu + \frac{\nu_t}{Pr_\varepsilon} \right) \frac{\partial \tilde{\varepsilon}}{\partial y} \right] + c_{\varepsilon 1} f_1 \frac{\tilde{\varepsilon}}{k} \nu_t \left(\frac{\partial \bar{u}}{\partial y} \right)^2 \\ &\quad - c_{\varepsilon 2} f_2 \frac{\tilde{\varepsilon}^2}{k} + E, \end{aligned} \quad (18.147)$$

$$\nu_t = c_\mu f_\mu \frac{k^2}{\tilde{\varepsilon}}. \quad (18.148)$$

The two new functions D and E are proportional to ν and are simply related to the field functions \bar{u} , k or $\tilde{\varepsilon}$. The so-called *damping functions* f_1 , f_2 and f_μ are dependent on the turbulent Reynolds number

$$Re_T = \frac{k^2}{\nu \tilde{\varepsilon}}. \quad (18.149)$$

For $Re_T \rightarrow \infty$ these functions tend to one. Details on the functions D , E , f_1 , f_2 and f_μ are given in V.C. Patel et al. (1985).

The boundary conditions read:

$$\begin{aligned} y = 0 : \quad \bar{u} &= 0, \quad \bar{v} = 0, \quad k = 0, \quad \tilde{\varepsilon} = 0 \\ y \rightarrow \infty : \quad \bar{u} &= U, \quad k = 0, \quad \tilde{\varepsilon} = 0. \end{aligned} \quad (18.150)$$

In the article last mentioned, it is also described how suitable initial values can be determined and how the numerical solution of the system of equations can be carried out. The examples given relate only to attached boundary layers. For large Reynolds numbers the system reduces to Eq. (18.133) to (18.137).

When applying this model to boundary layers with separation, particular attention should be paid to the following two aspects:

1. If the model is also to be correct for large Reynolds numbers, then the model constants and functions should also depend on the parameter K in a suitable manner.
2. Since the zero of the shear stress generally does not coincide with the position of $\partial \bar{u} / \partial y = 0$ in backflow, the proportionality between τ_t and $\partial \bar{u} / \partial y$ assumed in Eqs. (18.144) and (18.145) is no longer given. This can be put right using a balance law for τ_t , cf. D. Vieth (1996).

The main difficulty in low-Reynolds-number models lies in modelling the wall layer as effectively as possible, cf. R.M.C. So et al. (1991). Research in this is still very much underway, particularly when additional effects such as blowing, cf. R.M.C. So; G.J. Yoo (1987), or strong curvature at the wall are to be taken into account. The effect of the roughness of the wall cannot be included by these models.

Note (Computation of the laminar–turbulent transition)

The equations of turbulence models can also be used to compute the transition from laminar to turbulent boudary layers, see D.C. Wilcox (1998), p. 193. Here both $k_e(x)$ and the turbulent length scale $\ell_e = c_\mu k_e^{3/2} / \varepsilon_e$ of the external stream affect the length and position of the transition region.

This method yields particularly good results at high intensities of turbulence ($Tu > 1\%$) of the outer flow, as is always the case for example in turbomachinery, cf. W. Rodi (1991).

18.5.4 Additional Effects

Effect of outer turbulence

Until now we have always assumed that the inviscid outer flow is also free from turbulence. In many practical applications (e.g. in the flow past blades in turbomachinery) the flow outside the boundary layer has a not inconsiderable turbulence intensity. This can be taken into account in turbulence models which work with the k -equation by changing the outer boundary condition for k . At the boundary–layer edge Eqs. (18.135) and (18.136) then reduce to

$$U \frac{dk_e}{dx} = -\varepsilon_e, \quad U \frac{d\varepsilon_e}{dx} = -c_{\varepsilon 2} \frac{\varepsilon_e^2}{k_e}, \quad (18.151)$$

from which, for a given $U(x)$, the functions $k_e(x)$ and $\varepsilon_e(x)$ may be determined.

J.C. Rotta (1980a) has carried out such calculations for the flat plate. An increase of the outer turbulence leads to an increase of the momentum transfer, i.e. of the skin-friction coefficient. According to experiments by H.U. Meier; H.P. Kreplin (1980), in addition to the turbulence intensity, the turbulence length scale also has an effect on the wall shear stress, cf. also D.M. Bott; P. Bradshaw (1998).

M. Champion; P.A. Libby (1991, 1996) have treated the turbulent stagnation-point flow for a turbulent free stream. This problem is of great practical importance in computing the heat transfer in the stagnation point in turbulent flow (i.e. impinging jets), cf. also J. Kestin (1966c), L. Kayalar (1969), G.W. Lowery; R.J. Vachon (1975).

The effects of sudden disturbances on turbulent flows have been described by A.J. Smits; D.H. Wood (1985).

The Reynolds stress closure for turbulent boundary layers in turbulent freestream has been evaluated by J.C. Mackinnon et al. (1998).

Note (Effect of screens)

Frequently screens are used to control the turbulence in experiments. Turbulent boundary layers undergo drastic changes if they flow through screens, cf. P. Bradshaw (1965) and R.D. Mehta (1985). In particular, the boundary-layer thickness is reduced and the danger of separation decreased. This is exploited in wide angle diffusers (short diffusers) by installing screens, see R.D. Mehta (1977).

Effect of wall curvature

The boundary-layer equations used until now are only valid for boundary layers at curved walls if the radius of curvature of the wall $R(x) = 1/\kappa(x)$ is large compared to the boundary-layer thickness $\delta(x)$. If, however, $R(x)$ and $\delta(x)$ are of the same order of magnitude, the following additional effects due to curvature occur:

1. The boundary-layer equations have to be extended by curvature terms, as are seen in Eq. (3.98) to (3.105).

We emphasise that the gradient $(\partial U / \partial y)_w$ of the outer flow does not vanish for boundary layers at curved walls. From the condition that the flow be irrotational, see Eq. (3.98), it follows that

$$\left(\frac{\partial U}{\partial y} \right)_w = -\kappa(x) U(x) \quad (18.152)$$

and therefore the velocity $U(x, y)$ of the outer flow is dependent on y . This must be taken into account in computing the boundary-layer characteristic quantities δ_1 , δ_2 and δ_3 .

2. The curvature has a considerable influence on the turbulence model. The centrifugal forces due to the curvature act preferentially on the fluctuations in the y direction. For this reason, it is only the Reynolds stress models in Sect. 18.1.5 which allow the curvature effects to be represented correctly. This is because here separate balance equations are used for the three normal stresses and therefore the different curvature effects in the three directions can be included.

A systematic investigation into curvature effects for turbulent boundary layers at high Reynolds numbers has been carried out by B. Jeken

(1992). This showed that the viscous wall layer and the overlap layer are free from curvature effects.

For corrections to the two-equation models, see the work by B. Lakshminarayana (1986). A new scalar quantity for the influence of curvature and rotation on turbulence models which is Galilean-invariant has been proposed by P.R. Spalart; M. Shur (1997).

Effect of displacement (interaction with the outer flow)

The effect of displacement of the boundary layer on the outer flow has already been comprehensively treated for laminar boundary layers in Chap. 14. The displacement action of turbulent boundary layers is completely analogous. Here too, one differentiates between direct and indirect methods depending on whether $U(x)$ is prescribed and $\delta_1(x)$ is to be determined or vice versa, cf. Sects. 18.4.1 and 18.4.2. Summaries on turbulent interaction theory have been given, by, for example, H. McDonald; W.R. Briley (1984), J. Delery; J.G. Marvin (1986) and R.C. Lock; B.R. Williams (1987).

Effect of blowing or suction

If fluid is blown through a permeable wall, the blowing velocity v_w ($v_w < 0$ for suction) appears as an additional (given) quantity. The characteristic blowing parameter for the viscous wall layer and the overlap layer is $v_w^+ = v_w/u_\tau$. If this is a small quantity ($|v_w^+| < 0.1$), as in many practical applications, general valid statements can be formulated, cf. K. Gersten; H. Herwig (1992), pp. 448, 497, 625. The logarithmic law of the wall is then extended by terms proportional to v_w^+ , whereby a term with $(\ln y^+)^2$ also appears.

According to K. Gersten; H. Herwig (1992), p. 627, for the plate boundary layer with blowing, the following friction law is an extension to Eq. (18.93):

$$\frac{1}{\gamma} = \frac{1}{\kappa} \ln(\gamma^2 \text{Re}_x) + C^+ + \frac{1}{\kappa} (2\pi - \ln F_e) + v_w^+ \left[\frac{1}{4\gamma^2} + \frac{F_{v0}}{\kappa} \ln(\gamma^2 \text{Re}_x) + C_v^+ + \bar{C}_v - \frac{1}{4} C^{+2} \right] \quad (18.153)$$

with $F_{v0} \approx 6.5$ and $C_0^+ + \bar{C}_v \approx -31$. This formula has also already been presented by J.C. Rotta (1970) using the simplification $F_{v0} = C_v^+ = 0$, cf. also T.N. Stevenson (1963) and T. Cebeci; A.M.O. Smith (1974), p. 137.

Turbulent boundary layers with blowing or suction have also been investigated by J. Wiedemann (1983), J. Wiedemann; K. Gersten (1984).

A different way of influencing the boundary layer is tangential blowing, cf. Sect. 11.1. In this case the velocities in the boundary can be higher than in the outer flow, see Fig. 11.5. This wall jet in an external stream has a region of negative production of turbulent kinetic energy between the points of maximum velocity and vanishing shear stress. Hence, turbulence models

using the eddy viscosity concept fail. R. Tangemann; W. Gretler (2000) have extended the k - ε model to cover this flow, see also the turbulent wall jet without external stream in Sect. 22.8.

18.6 Computation of Thermal Boundary Layers

18.6.1 Fundamentals

The basic equation used for thermal boundary layers is the thermal energy equation

$$\begin{aligned} \bar{u} \frac{\partial \bar{T}}{\partial x} + \bar{v} \frac{\partial \bar{T}}{\partial y} &= -\frac{1}{\varrho c_p} \frac{\partial}{\partial y} (\bar{q}_\lambda + q_t) \\ &= \frac{\partial}{\partial y} \left[\left(\frac{\nu}{\text{Pr}} + \frac{\nu_t}{\text{Pr}_t} \right) \frac{\partial \bar{T}}{\partial y} \right] \end{aligned} \quad (18.154)$$

with

$$\bar{q}_\lambda = -\lambda \frac{\partial \bar{T}}{\partial y}; \quad q_t = \varrho c_p \bar{v}' \bar{T}' = -\lambda_t \frac{\partial \bar{T}}{\partial y}. \quad (18.155)$$

The dissipation has been neglected here. A turbulence model is again required to compute the temperature field with this equation. This model should construct a relation between the turbulent heat flux $q_t(x, y)$ and the mean temperature field $\bar{T}(x, y)$. Some turbulence models for the heat transfer have already been given in Sect. 18.1.6.

At high Reynolds numbers, the thermal boundary layer has a layered character just as the velocity boundary layer, i.e. the thermal boundary layer consists of a layer close to the wall in which the molecular thermal conductivity λ and the turbulent thermal conductivity $\lambda_t(x, y)$ are of the same order of magnitude, and a fully turbulent outer layer in which λ may be neglected compared to $\lambda_t(x, y)$. When heat transfer takes place, as well as the viscous wall layer, there is also a thermal wall layer which is affected by λ . The ratio of the thicknesses of these two wall layers depends (for boundary layers with the same starting point) on the Prandtl number $\text{Pr} = \mu c_p / \lambda = \nu/a$. For $\text{Pr} = O(1)$, the thicknesses are of the same order of magnitude, and for $\text{Pr} \gg 1$ the thermal wall layer is much smaller than the viscous wall layer.

As has already been shown in Sect. 17.1.2, there is a universal temperature distribution in the thermal wall layer which does however depend on the Prandtl number. In the overlap layer, the temperature distribution satisfies the universal logarithmic law of the wall given in Eq. (17.49), as long as $\text{Pr} > 0.5$.

In analogy to the friction law (18.64), we obtain the following heat transfer law for attached boundary layers:

$$\frac{T_\infty - T_w(x)}{T_\tau(x)} = \frac{1}{\kappa_\theta} \ln(\gamma^2 \text{Re}) + C_\theta(\text{Pr}) + \tilde{C}_\theta(x) \quad (18.156)$$

with $C_\theta^+(\text{Pr})$ from Eq. (17.50) and $T_\tau(x)$ from Eq. (17.45).

Eliminating Re with the help of Eq. (18.74), we find the Stanton number

$$\boxed{\text{St} = \frac{\text{Nu}_x}{\text{Re}_x \text{Pr}} = \frac{\bar{q}_w}{\varrho c_p(T_w - T_\infty)U} = \frac{c_f/2}{\frac{\kappa}{\kappa_\theta} + \sqrt{\frac{c_f}{2}} D_\theta(x^*, \text{Pr})}} \quad (18.157)$$

with

$$D_\theta(x^*, \text{Pr}) = C_\theta^+(\text{Pr}) + \tilde{C}_\theta(x^*) - \frac{\kappa}{\kappa_\theta}[C^+ + \tilde{C}(x^*)]. \quad (18.158)$$

For large Reynolds numbers, i.e. for $c_f \rightarrow 0$, or for $\text{Pr} \approx 1$, i.e. for $D_\theta \approx 0$, Eq. (18.157) reduces to $\text{St} = (\kappa_\theta/\kappa)c_f/2$. For $\kappa = \kappa_\theta$ this relation is called the *Reynolds analogy*.

For large Prandtl numbers, $D_\theta \approx C_\theta^+ \approx 13.7 \cdot \text{Pr}^{2/3}$. Then Eq. (18.157) simplifies to

$$\lim_{\text{Pr} \rightarrow \infty} \text{Co} = \lim_{\text{Pr} \rightarrow \infty} \frac{\text{Nu}_x}{\text{Re}_x \text{Pr}^{1/3}} = 0.073 \sqrt{\frac{c_f}{2}}, \quad (18.159)$$

where Co is the *Colburn number*.

The function $D_\theta(x^*, \text{Pr})$ also depends on the thermal boundary conditions. As already explained in Sect. 9.2, the standard boundary conditions $T_w = \text{const}$ and $\bar{q}_w = \text{const}$ are frequently met.

In equilibrium boundary layers, both of these boundary conditions lead to similar distributions of the relative temperature defect. Different values of the Rotta–Clauser parameter β of the distributions of the temperature defect and the turbulent heat flux, as well as the quantity $D_\theta(x^*, \text{Pr})$ in Eq. (18.157) are given by K. Gersten; H. Herwig (1992), p. 639. Here the constant turbulent Prandtl number $\text{Pr}_t = \kappa/\kappa_\theta = 0.87$ was used as a turbulence model. Indeed for attached boundary layers this is a fairly useful model. J.C. Rotta (1964) has shown that suitable distributions $\text{Pr}_t(y)$ along the defect region exhibit only slight changes in the heat transfer compared to the $\text{Pr}_t = \text{const}$ model. For the plate boundary layer, the solution for $T_w = \text{const}$ also satisfies the boundary condition $\bar{q}_w = \text{const}$. The constant in Eq. (18.157) then is about $D_\theta \approx C_\theta^+ - 4.5$. If the wall surface is rough, C_θ^+ is also a function of the parameter k_s^+ from Eq. (17.31), see K. Gersten; H. Herwig (1992), p. 486.

Note (Adiabatic wall temperature)

If the dissipation is taken into account in Eq. (18.154), see Eq. (16.20), then a heat insulating wall takes on the so-called adiabatic wall temperature T_{ad} , also called eigen-temperature. This lies above the temperature of the surroundings. For the flat plate, the *recovery factor* is

$$r = \frac{T_{\text{ad}} - T_\infty}{U_\infty^2/(2c_p)} = \frac{\kappa}{\kappa_\theta} \left[1 + 1.2 \sqrt{\frac{c_f}{2}} + O\left(\frac{c_f}{2}\right) \right]. \quad (18.160)$$

Therefore, to leading order, r is independent of the Reynolds number and the Prandtl number. This has been confirmed by experiments. In the second term in the formula a Reynolds number dependent factor appears. The Prandtl number does not appear until the term $O(c_f/2)$, as K. Gersten; H. Herwig (1992), p. 634 have shown. At high Prandtl numbers, this term increases strongly, so that the recovery factor noticeably increases and may take on values above one.

Do note that the adiabatic wall temperature is *not* a compressibility effect, but rather is due to the dissipation and therefore also occurs for constant physical properties.

Until now we have assumed that the velocity boundary layer and the thermal boundary layer start at the same point x .

We will now consider the case where the velocity boundary layer has an unheated approach and only at the position x_0 does the wall temperature (or wall heat flux) jump discontinuously to a constant value. The thermal boundary layer then starts at this point, cf. Fig. 9.1. At small distances from x_0 , it lies within the wall layer of the velocity boundary layer, while at greater distances it reaches into the overlap layer and eventually as far as the defect layer.

As long as the thermal boundary layer is still inside the overlap layer and the wall layer, the temperature profiles are again similar, as has been shown by A.A. Townsend (1976), p. 361, see also K. Gersten; H. Herwig (1992), p. 636 and H. Klick (1992).

As with laminar boundary layers, cf. Sect. 9.2, the thermal boundary layer with arbitrary $T_w(x)$ or $\bar{q}_w(x)$ may be determined by superposition of solutions with unheated approaches, cf. T. Cebeci; P. Bradshaw (1984), p. 181.

Note (Quadrature formula for heat transfer)

The Reynolds analogy can be used to develop a simple integral method for the thermal boundary layer whose approximation eventually leads to a quadrature formula for the Stanton number, cf. W.M. Kays; M.E. Crawford (1980), p. 219 and P.M. Moretti; W.M. Kays (1965).

18.6.2 Computation of Thermal Boundary Layers Using Field Methods

As in the field methods to calculate velocity boundary layers, here too we differentiate between methods of wall functions and the low-Reynolds-number versions of two and more equation models.

Equation (17.49) serves as a wall function for attached boundary layers. If separation and backflow occur, the dependence on K from Eq. (18.141) causes the wall functions to change, as R. Kiel (1995) and D. Vieth (1996) have shown. In the separation point itself ($\bar{\tau}_w = 0$), the temperature distribution in the overlap layer obeys a $1/\sqrt{y}$ law, cf. K. Gersten (1989a).

The model of the constant Prandtl number Pr_t from Eq. (17.77) can no longer be used for boundary layers with backflow, since in general $\partial \bar{u} / \partial y$ vanishes for $\bar{\tau} \neq 0$ and therefore Pr_t becomes singular. Instead of this, a balance law for $q_t(x, y)$ may be used, as for example in the method given by D. Vieth (1996).

For details on heat transfer in separated flows, see the summarising essay by W. Merzkirch et al. (1988).

A low-Reynolds-number version of a two-equation model for computing thermal boundary layers has been presented by Y. Nagano; C. Kim (1988), cf. also Y.G. Lai; R.M.C. So (1990) and P.G. Huang; P. Bradshaw (1995).

Numerous sample calculations of turbulent boundary layers have been given by T. Cebeci; P. Bradshaw (1984), pp. 189, 201. One example here concerns boundary layers with excess velocities close to the wall (“wall jet” profiles). These play a role in so-called *film cooling*. For details on heat transfer at circular cylinders, see A. Žukauskas; J. Zingžda (1985).

Heat transfer in turbulent boundary layers with blowing has been treated in the work of R.J. Baker; B.E. Launder (1974).

C. Benocci (1991), S. Ramadhyani (1997) and K. Hanjalić (2002) have presented the state of research in turbulence modelling with heat transfer.

19. Turbulent Boundary Layers with Coupling of the Velocity Field to the Temperature Field

19.1 Fundamental Equations

19.1.1 Time Averaging for Variable Density

As Sect. 10.1 showed for laminar boundary layers, the velocity field is coupled to the temperature field if the physical properties are no longer constant but rather depend on the temperature. These physical properties are the density ϱ , the viscosity μ , the isobaric specific heat capacity c_p and the thermal conductivity λ . In the most general case they may depend on both the temperature and the pressure.

If the density is variable, there are two different ways of forming the time average and thus two different ways of decomposing the flow into the mean motion and the fluctuations. We will demonstrate this using the continuity equation; for an arbitrary time dependent three-dimensional flow it reads:

$$\frac{\partial \varrho}{\partial t} + \frac{\partial(\varrho u)}{\partial x} + \frac{\partial(\varrho v)}{\partial y} + \frac{\partial(\varrho w)}{\partial z} = 0, \quad (19.1)$$

cf. Eq. (3.2).

Conventional time averaging

As has been done until now, the time dependent quantities are decomposed into the time averaged value and the fluctuation value. For a steady two-dimensional mean flow this reads:

$$\begin{aligned} \varrho &= \bar{\varrho}(x, y) + \varrho'(t, x, y, z) & \bar{\varrho}' &= 0 \\ u &= \bar{u}(x, y) + u'(t, x, y, z) & \bar{u}' &= 0 \\ v &= \bar{v}(x, y) + v'(t, x, y, z) & \bar{v}' &= 0 \\ &\vdots \end{aligned} \quad (19.2)$$

Inserting Eq. (9.2) and then forming the time average yields

$$\frac{\partial(\bar{\varrho}\bar{u})}{\partial x} + \frac{\partial(\bar{\varrho}\bar{v})}{\partial y} + \frac{\partial(\bar{\varrho}'\bar{u}')}{\partial x} + \frac{\partial(\bar{\varrho}'\bar{v}')}{\partial y} = 0. \quad (19.3)$$

Therefore the mean turbulent flow alone no longer satisfies the continuity equation which is valid for laminar variable density flows, and so no stream function of the mean flow can be formed. If we define the streamlines as usual to be those lines to which the flow density vector $(\bar{\varrho}\bar{u}, \bar{\varrho}\bar{v})$ is tangent, then the mass flux between two streamlines is no longer constant.

Mass-weighted time averaging (Favre averaging)

In order to avoid the difficulties described and to ensure that the mean flow satisfies the continuity equation, we carry out a *mass-weighted* time average. This is also called *Favre averaging* after A. Favre (1965). Here the density, the pressure, the temperature and the physical properties μ , λ and c_p are still averaged in the conventional manner. The mass-weighted averaging is applied to the velocities and the specific enthalpies. Instead of Eq. (9.2) we now have:

$$\begin{aligned} \varrho &= \bar{\varrho}(x, y) + \varrho'(t, x, y, z) & \overline{\varrho'} &= 0 \\ p &= \bar{p}(x, y) + p'(t, x, y, z) & \overline{p'} &= 0 \\ T &= \bar{T}(x, y) + T'(t, x, y, z) & \overline{T'} &= 0 \\ u &= \tilde{u}(x, y) + u''(t, x, y, z) & \overline{\varrho u''} &= 0 \\ v &= \tilde{v}(x, y) + v''(t, x, y, z) & \overline{\varrho v''} &= 0 \\ w &= w''(t, x, y, z) & \overline{\varrho w''} &= 0 \\ h &= \tilde{h}(x, y) + h''(t, x, y, z) & \overline{\varrho h''} &= 0 \\ h_t &= \tilde{h}_t(x, y) + h''_t(t, x, y, z) & \overline{\varrho h''_t} &= 0. \end{aligned} \tag{19.4}$$

For a plane (steady) mean flow we obtain

$$\frac{\partial(\bar{\varrho}u)}{\partial x} + \frac{\partial(\bar{\varrho}v)}{\partial y} = 0 \quad \text{or} \quad \frac{\partial(\bar{\varrho}\tilde{u})}{\partial x} + \frac{\partial(\bar{\varrho}\tilde{v})}{\partial y} = 0. \tag{19.5}$$

The differences between the two average values of the velocity are

$$\begin{aligned} \overline{u''} &= \bar{u} - \tilde{u} = -\frac{\overline{\varrho' u'}}{\bar{\varrho}} = -\frac{\overline{\varrho' u'}}{\bar{\varrho}}, \\ \overline{v''} &= \bar{v} - \tilde{v} = -\frac{\overline{\varrho' v'}}{\bar{\varrho}} = -\frac{\overline{\varrho' v'}}{\bar{\varrho}}; \end{aligned} \tag{19.6}$$

similar relations hold for the remaining quantities. Both averages are identical if the density is constant.¹

Note (Choice of time average)

A consequence of mass-weighted averaging is that the balance laws take on a particularly simple form, i.e. only comparatively few additional terms due to the fluctuations appear. In spite of this, many authors consistently use conventional averaging. There are different opinions on the type of averaging which should be preferred, cf. P. Chassaing (1985) and S.K. Lele (1994). The difference between the average values obtained with the two different methods grows with the Mach number, so that the advantages of Favre averaging only really become clear for hypersonic flows, cf. P. Bradshaw (1977) and E.F. Spina et al. (1994).

19.1.2 Boundary-Layer Equations

If we take the above averages into account we can extend the boundary-layer equations for plane flows given in Sect. 16.6 to those with variable physical properties.

The momentum equation in the y direction is no longer Eq. (16.33) but rather

$$\bar{p} + \overline{\rho v''^2} = \bar{p}_w = p_e = \bar{p} + \widetilde{\overline{\rho v''^2}}, \quad (19.7)$$

i.e. the inertial terms and the viscosity effects have been neglected.

The balances for mass, momentum in the x direction and specific total enthalpy of the mean motion yield the following boundary-layer equations for flows with variable physical properties:

$$\frac{\partial(\widetilde{\rho u})}{\partial x} + \frac{\partial(\widetilde{\rho v})}{\partial y} = 0, \quad (19.8)$$

$$\overline{\rho} \left(\widetilde{u} \frac{\partial \widetilde{u}}{\partial x} + \widetilde{v} \frac{\partial \widetilde{u}}{\partial y} \right) = - \frac{dp_e}{dx} + \frac{\partial}{\partial y} (\overline{\tau}_v + \tau_t), \quad (19.9)$$

$$\overline{\rho} \left(\widetilde{u} \frac{\partial \widetilde{h}_t}{\partial x} + \widetilde{v} \frac{\partial \widetilde{h}_t}{\partial y} \right) = \frac{\partial}{\partial y} \left(\overline{\lambda} \frac{\partial \overline{T}}{\partial y} - \overline{\rho h''_t v''} + \widetilde{u} \overline{\tau}_v \right). \quad (19.10)$$

The extensions of the k and ε equations, Eqs. (18.135) and (18.136) to flows with variable physical properties read:

$$\overline{\rho} \left(\widetilde{u} \frac{\partial k}{\partial x} + \widetilde{v} \frac{\partial k}{\partial y} \right) = \frac{\partial}{\partial y} \left(\frac{\mu_t}{Pr_k} \frac{\partial k}{\partial y} \right) + \tau_t \frac{\partial \widetilde{u}}{\partial y} - \overline{\rho} \widetilde{\varepsilon}, \quad (19.11)$$

$$\overline{\rho} \left(\widetilde{u} \frac{\partial \widetilde{\varepsilon}}{\partial x} + \widetilde{v} \frac{\partial \widetilde{\varepsilon}}{\partial y} \right) = \frac{\partial}{\partial y} \left(\frac{\mu_t}{Pr_\varepsilon} \frac{\partial \widetilde{\varepsilon}}{\partial y} \right) + c_{\varepsilon 1} \frac{\widetilde{\varepsilon}}{k} \tau_t \frac{\partial \widetilde{u}}{\partial y} - c_{\varepsilon 2} \frac{\overline{\rho} \widetilde{\varepsilon}^2}{k} = 0 \quad (19.12)$$

¹ Unfortunately the fluctuation quantities are not consistently denoted in the literature. Accordingly, in contrast to this book, the fluctuation quantities in Favre averaging are sometimes indicated with *one* dash, e.g. T. Cebeci; A.M.O. Smith (1974) and K. Gersten; H. Herwig (1992), while two dashes are used for conventional averages.

with

$$\mu_t = c_\mu \bar{\varrho} k^2 / \tilde{\varepsilon}. \quad (19.13)$$

Here the following abbreviations were used:

$$\begin{aligned} \bar{\tau}_v &= \bar{\mu} \frac{\partial \tilde{u}}{\partial y}, & \tau_t &= -\overline{\varrho u'' v''} = -\widetilde{\overline{\varrho u'' v''}}, \\ \tilde{h}_t &= \tilde{h} + \frac{1}{2} \tilde{u}^2 + k, & \overline{\varrho h''_t v''} &= \overline{\varrho h'' v''} + \frac{\bar{\varrho}}{2} q^2 v'' - \tilde{u} \tau_t, \\ q^2 &= u''^2 + v''^2 + w''^2, & k &= \frac{\overline{\varrho q^2}}{2 \bar{\varrho}} = \frac{1}{2} \widetilde{q^2}. \end{aligned} \quad (19.14)$$

As before, in the k -equation (19.11), the turbulent diffusion was modelled using a gradient ansatz, cf. Eq. (18.11):

$$\frac{\mu_t}{\text{Pr}_k} \frac{\partial k}{\partial y} = - \overline{\left(p' + \frac{\varrho q^2}{2} \right) v''}. \quad (19.15)$$

The quantity $\tilde{\varepsilon}$ in Eq. (19.11) to (19.13) is the real dissipation. It has been denoted with a tilde to distinguish it from the pseudo-dissipation ε , cf. Eq. (16.17) to (16.19). Here

$$\begin{aligned} \overline{\varrho \tilde{\varepsilon}} &= \overline{\tau_{xx} \frac{\partial u''}{\partial x}} + \overline{\tau_{xy} \frac{\partial v''}{\partial x}} + \overline{\tau_{xz} \frac{\partial w''}{\partial x}} \\ &\quad + \overline{\tau_{yx} \frac{\partial u''}{\partial y}} + \overline{\tau_{yy} \frac{\partial v''}{\partial y}} + \overline{\tau_{yz} \frac{\partial w''}{\partial y}} \\ &\quad + \overline{\tau_{zx} \frac{\partial u''}{\partial z}} + \overline{\tau_{zy} \frac{\partial v''}{\partial z}} + \overline{\tau_{zz} \frac{\partial w''}{\partial z}}. \end{aligned}$$

If Eq. (19.9) is multiplied by \tilde{u} , we obtain a balance law for the mean kinetic energy $\tilde{u}^2/2$ in the boundary layer. Then subtracting this equation and Eq. (19.11) from Eq. (19.10), we obtain the boundary-layer equation for the mean specific enthalpy \tilde{h} (thermal boundary layer):

$$\overline{\varrho} \left(\tilde{u} \frac{\partial \tilde{h}}{\partial x} + \tilde{v} \frac{\partial \tilde{h}}{\partial y} \right) = \frac{\partial}{\partial y} \left(\bar{\lambda} \frac{\partial \bar{T}}{\partial y} - \overline{\varrho v'' h''} \right) + \tilde{u} \frac{dp_e}{dx} + \bar{\tau}_v \frac{\partial \tilde{u}}{\partial y} + \overline{\varrho \tilde{\varepsilon}}. \quad (19.16)$$

Here $\overline{p' v''}$ has been neglected compared to $\overline{\varrho v'' h''}$.

Equations (19.7) to (19.16) are obtained from the complete balance laws, cf. K. Gersten; H. Herwig (1992), p. 764, as long as the following assumptions are used:

1. The diffusion terms in the x direction (e.g. variation of the x momentum flux in the x direction) are neglected compared to those in the y direction (all divergence terms only consist of the term $\partial \cdots / \partial y$). Thus, for example, $|\partial \tilde{u} / \partial x| \ll |\partial \tilde{u} / \partial y|$.

2. The velocity component \tilde{v} is much smaller than the velocity component \tilde{u} . This yields, for example, $|\partial\tilde{v}/\partial x| \ll |\partial\tilde{u}/\partial x| \ll |\partial\tilde{u}/\partial y|$. Therefore, in the formula for \tilde{h}_t in Eq. (19.14), the term $\tilde{v}^2/2$ was neglected compared to $\tilde{u}^2/2$. The reduced y momentum equation (19.7) is a consequence of this assumption.
3. The normal stresses $\overline{\rho u''^2}$ and $\overline{\rho v''^2}$ are neglected compared to the pressure \overline{p} . Then, for example, Eq. (19.7) yields $\partial\overline{p}/\partial x = dp_e/dx$ and $\partial\overline{p}/\partial y = 0$. This is generally satisfied well in boundary layers. Close to separation however, the normal stresses can become more important (in Eqs. (19.7), (19.9), (19.11) and (19.12)), as R.L. Simpson (1975) has shown.
4. In the equations for \tilde{h}_t , k and $\tilde{\varepsilon}$, the viscous diffusion has been neglected compared to the turbulent diffusion. This is permissible if we ignore the region directly at the wall. In the method of wall functions, for example, the viscous wall layer is not even involved.
5. In the boundary-layer equation for the specific enthalpy \tilde{h} , the energy flux $\overline{p'u''}$ has been neglected compared to the heat flux $\overline{\rho v''h''}$. It is known from measurements on boundary layers that the pressure fluctuations are considerably smaller than the fluctuations of the temperature or the specific enthalpy, cf. T. Cebeci; A.M.O. Smith (1974), p. 72.
6. The following approximations have been used:

$$\overline{\mu \frac{\partial u}{\partial y}} \approx \overline{\mu} \frac{\partial \tilde{u}}{\partial y}, \quad \overline{\lambda \frac{\partial T}{\partial y}} = \overline{\lambda} \frac{\partial \overline{T}}{\partial y}.$$

This is equivalent to using the assumptions

$$\left| \overline{\mu \frac{\partial u''}{\partial y}} \right| \ll \left| \overline{\mu} \frac{\partial \tilde{u}}{\partial y} \right|, \quad \left| \overline{\lambda' \frac{\partial T'}{\partial y}} \right| \ll \left| \overline{\lambda} \frac{\partial \overline{T}}{\partial y} \right|;$$

these have also been confirmed by experiment for boundary layers at $\text{Ma} < 5$, cf. T. Cebeci; A.M.O. Smith (1974), p. 73.

7. In the k -equation (and therefore also in the $\tilde{\varepsilon}$ -equation) the terms on the right hand side

$$\overline{p'} \left(\frac{\partial u''}{\partial x} + \frac{\partial v''}{\partial y} + \frac{\partial w''}{\partial z} \right) - \overline{u''} \frac{dp_e}{dx} \quad (19.17)$$

have been neglected. The first term is called the *pressure dilatation*; the second *pressure work* (actually it is power per unit volume). Both terms vanish at constant densities, cf. Eq. (16.8). However they only become important in hypersonic boundary layers, i.e. for about $\text{Ma} > 5$. In spite of different suggestions, a generally accepted model has not been achieved, cf. D.C. Wilcox (1998), p. 241.

8. For variable densities, the dissipation $\tilde{\varepsilon}$ can be decomposed into the *solenoidal dissipation* (divergence free fluctuations) and *dilatation dissipation*. The second part vanishes at constant densities, but can also be neglected for boundary layers at $\text{Ma} < 5$, cf. D.C. Wilcox (1998), p. 239.
9. Gravity effects are neglected: these will be discussed in Sect. 19.3.

Assumptions 1 to 5 have already been used in discussing boundary layers with constant physical properties; assumptions 6 to 9 are added for variable physical properties. As already mentioned, assumptions 6 to 8 are satisfied well for boundary

layers with $\text{Ma} < 5$. For hypersonic boundary layers ($\text{Ma} > 5$), see the relevant literature, e.g. S.K. Lele (1994), J.D. Anderson Jr. (1989) and S. Catris; B. Aupoix (2000).

Because of $\overline{u''} = 0$ in assumption 7, Eq. (19.6) implies that $\tilde{u} \approx \bar{u}$. Since, for boundary layers with $\text{Ma} < 5$, both $\tilde{h}_t \approx \bar{h}_t$ and $\tilde{h} \approx \bar{h}$ hold, the system of equations (19.8) to (19.16) can also be written using conventional averaging. Only the \tilde{v} component remains unchanged: because of

$$\overline{\tilde{v}} = \overline{\varrho v} = \overline{\varrho} \bar{v} + \overline{\varrho' v'}, \quad (19.17a)$$

the quantity $\overline{\varrho' v'}$ cannot be neglected compared to the equally small quantity $\overline{\varrho} \bar{v}$. The turbulent shear stress is then set to

$$\tau_t = -\overline{\varrho u'' v''} = -\overline{\varrho} \widetilde{u'' v''} \approx -\overline{\varrho} \overline{u' v'}. \quad (19.18)$$

This is equivalent to the assumption

$$|\overline{\varrho' u' v'}| \ll |\overline{\varrho} \overline{u' v'}|.$$

This is an example of the so-called *Morkovin hypothesis* which states that for boundary layers with $\text{Ma} < 5$, the effect of density fluctuations on the turbulence is small, cf. M.V. Morkovin (1962). Correspondingly, because of $|\overline{\varrho' v' h'}| \ll \overline{\varrho} \overline{v' h'}$, the turbulent heat flux can be approximated by $\overline{\varrho v' h'} \approx \overline{\varrho} \overline{v' h'}$. Analogously $\overline{\varrho v' h'_t} \approx \overline{\varrho} \overline{v' h'_t}$. Therefore the additional terms due to turbulence in Eqs. (19.9) to (19.16) are the same as those for constant physical properties. Equation (19.9) is formally identical to Eq. (16.35) for constant physical properties, just as Eqs. (19.11) to (19.13) are to Eqs. (18.135) to (18.137). If the dissipation terms in Eq. (19.16) are neglected and we take into account that for a fluid with constant density, cf. Eq. (3.66),

$$\frac{Dh}{Dt} = c_p \frac{DT}{Dt} + \frac{1}{\varrho} \frac{Dp}{Dt},$$

then Eq. (19.8) becomes Eq. (16.34) and Eq. (19.16) passes over to Eq. (16.36). Note too that for laminar boundary layers Eq. (19.8) to (19.16) become the boundary-layer equations already used in Chap. 10, cf. Eq. (10.4) to Eq. (10.7).

According to M.V. Morkovin (1962), the turbulence structure with variable physical properties is essentially the same as that for constant physical properties, as long as the fluctuation Ma' of the local Mach number remains well below 1. This is the case for adiabatic plate boundary layers for Mach numbers of $\text{Ma} < 5$.

However changes in the turbulence structure can indeed occur for $\text{Ma} < 5$ if there are strong pressure gradients, strong longitudinal wall curvature, and particularly shock-boundary-layer interactions at hand, cf. E.F. Spina et al. (1994).

19.2 Compressible Turbulent Boundary Layers

19.2.1 Temperature Field

Throughout all of Sect. 19.2 we will consider ideal gas flows with constant specific heat capacity. Thus

$$p = R\varrho T, \quad h = c_p T, \quad h_t = c_p T_t \quad (19.19)$$

with $R = \text{const}$ and $c_p = \text{const}$. Time averaging applied to the equation of state $p = R\varrho T$ yields

$$\frac{p'}{\bar{p}} = \frac{\varrho'}{\bar{\varrho}} + \frac{T'}{\bar{T}} \quad \text{with} \quad |\varrho' T'| \ll \bar{\varrho} \bar{T}. \quad (19.20)$$

As has already been mentioned, experiments on turbulent boundary layers with $\text{Ma} < 5$ have demonstrated that the relative pressure fluctuations are very small compared to the relative density fluctuations, cf. T. Cebeci; A.M.O. Smith (1974), p. 72. Therefore Eq. (19.20) yields

$$\frac{\varrho'}{\bar{\varrho}} \approx -\frac{T'}{\bar{T}} \quad (19.21)$$

and, because of $|\varrho' T'| \ll \bar{\varrho} \bar{T}$, also $\bar{T}'^2 \ll \bar{T}^2$. This last condition is satisfied well, cf. T. Cebeci; P. Bradshaw (1984), p. 52. With Eqs. (19.6) and (19.21) we have:

$$\tilde{h} = c_p \bar{T}, \quad \tilde{h}_t = c_p \bar{T}_t, \quad h'' = c_p T'. \quad (19.22)$$

Using Eq. (19.10), the total temperature satisfies

$$c_p \bar{\varrho} \left(\tilde{u} \frac{\partial \bar{T}_t}{\partial x} + \tilde{v} \frac{\partial \bar{T}_t}{\partial y} \right) = \frac{\partial}{\partial y} \left(\bar{\lambda} \frac{\partial \bar{T}}{\partial y} - c_p \bar{\varrho} \bar{T}_t v'' + \tilde{u} \bar{\tau}_v \right) \quad (19.23)$$

and, using Eq. (19.16), the temperature satisfies

$$c_p \bar{\varrho} \left(\tilde{u} \frac{\partial \bar{T}}{\partial x} + \tilde{v} \frac{\partial \bar{T}}{\partial y} \right) = -\frac{\partial}{\partial y} (\bar{q}_\lambda + q_t) + \tilde{u} \frac{dp_e}{dx} + (\bar{\tau}_v + \tau_t) \frac{\partial \tilde{u}}{\partial y} \quad (19.24)$$

with

$$\bar{q}_\lambda = -\bar{\lambda} \frac{\partial \bar{T}}{\partial y}, \quad q_t = c_p \bar{\varrho} \bar{T}' v''. \quad (19.25)$$

Here the dissipation $\bar{\varrho} \tilde{\varepsilon}$ in Eq. (19.24) has been replaced by the turbulence production $\tau_t \partial \tilde{u} / \partial y$, see Eq. (19.11). Although this assumption is only valid in the overlap layer of attached boundary layers, in the literature it is frequently used to form the boundary-layer equations, cf. also J.C. Rotta (1959).

In extending Eqs. (16.37) and (16.38) we set:

$$\begin{aligned} \tau_t &= -\bar{\varrho} \bar{u}'' v'' = \bar{\varrho} \nu_t \frac{\partial \tilde{u}}{\partial y}, \\ q_t &= c_p \bar{\varrho} \bar{T}' v'' = -c_p \bar{\varrho} a_t \frac{\partial \bar{T}}{\partial y} = -\lambda_t \frac{\partial \bar{T}}{\partial y}. \end{aligned} \quad (19.26)$$

Therefore, from Eq. (19.23), the total temperature $\bar{T}_t = \bar{T} + \tilde{u}^2/(2c_p)$ satisfies

$$\begin{aligned}\bar{\rho} \left(\tilde{u} \frac{\partial \bar{T}_t}{\partial x} + \tilde{v} \frac{\partial \bar{T}_t}{\partial y} \right) &= \frac{\partial}{\partial y} \left[\left(\frac{\bar{\mu}}{\text{Pr}} + \frac{\mu_t}{\text{Pr}_t} \right) \frac{\partial \bar{T}_t}{\partial y} \right] \\ &+ \frac{\partial}{\partial y} \left\{ \left[\bar{\mu} \left(1 - \frac{1}{\text{Pr}} \right) + \mu_t \left(1 - \frac{1}{\text{Pr}_t} \right) \right] \frac{\partial}{\partial y} \left(\frac{\tilde{u}^2}{2c_p} \right) \right\}\end{aligned}\quad (19.27)$$

with

$$\text{Pr} = \frac{\bar{\mu}}{c_p \bar{\lambda}} = \frac{\bar{\nu}}{\bar{a}}, \quad \text{Pr}_t = \frac{\mu_t}{c_p \lambda_t} = \frac{\nu_t}{a_t} \quad (19.28)$$

and the boundary conditions

$$y = 0 : \quad \bar{T}_t = T_w, \quad y = \delta : \quad \bar{T}_t = \bar{T}_{te} = T_0.$$

For the special case $\text{Pr} = 1$ and $\text{Pr}_t = 1$, Eq. (19.27) again delivers two simple *Busemann–Crocco solutions*, cf. Sect. 10.4.2:

1. Adiabatic wall ($\text{Pr} = \text{Pr}_t = 1$)

The solution reads $\bar{T}_t = T_0 = \text{const}$ (T_0 is the total temperature or rest temperature of the outer flow). The temperature is a quadratic function of the velocity, cf. Eq. (10.54), and the adiabatic wall temperature is equal to the total temperature of the outer flow.

2. Plate flow ($\text{Pr} = \text{Pr}_t = 1$)

A linear relation exists between \bar{T}_t and \tilde{u} of the form:

$$\frac{\bar{T}_t - \bar{T}_{te}}{\bar{T}_{tw} - \bar{T}_{te}} = 1 - \frac{\tilde{u}}{u_e}. \quad (19.29)$$

This is because Eq. (19.27) for \bar{T}_t and Eq. (19.9) for \tilde{u} now have the same form. Therefore the dependence of the temperature $\bar{T}(\tilde{u})$ on the velocity is again a second order polynomial, cf. Eq. (10.57):

$$\frac{\bar{T} - T_w}{T_e} = \frac{T_{ad} - T_w}{T_e} \frac{\tilde{u}}{u_e} - \frac{T_{ad} - T_e}{T_e} \left(\frac{\tilde{u}}{u_e} \right)^2 \quad (19.30)$$

with the adiabatic wall temperature

$$T_{ad} = T_e + r(T_0 - T_e) = T_e \left[1 + r \frac{\gamma - 1}{2} \text{Ma}_e^2 \right]. \quad (19.31)$$

Here r is the recovery factor; because of Eq. (19.29), we have $r = 1$. The analysis of numerous measurements by H.H. Fernholz; P.J. Finley (1980) has demonstrated that Eq. (19.30) is also a good approximation if the Prandtl number Pr deviates from 1 ($0.7 \leq \text{Pr} \leq 1$) and if moderate

pressure gradients are present. Here the recovery factor is generally set to $r = \kappa/\kappa_\theta = 0.87$. Equation (19.30) yields the Reynolds analogy between the Nusselt number and the skin-friction coefficient corresponding to Eq. (10.59), cf. also Eq. (18.157) for $\text{Pr} \approx 1$.

19.2.2 Overlap Law

In Sect. 17.1.2 we showed that the velocity and temperature distributions in the viscous wall layer are universal, cf. Eqs. (17.26) and (17.47). In particular, it was possible to write down these distributions a priori in the overlap layer between the viscous wall layer and the fully turbulent outer flow, without having to use a turbulence model, cf. Eqs. (17.21) and (17.49).

These results can be extended to flows with variable physical properties. For attached boundary layers, the inertial and pressure terms as well as the convective change of the total enthalpy are neglected in the viscous wall layer. According to Eqs. (19.9), (19.24) and (19.25), in the viscous wall layer:

$$\bar{\mu} \frac{d\tilde{u}}{dy} + \tau_t = \bar{\tau}_w, \quad -\bar{\lambda} \frac{dT}{dy} + q_t - \tilde{u} \left(\bar{\mu} \frac{d\tilde{u}}{dy} + \tau_t \right) = \bar{q}_w. \quad (19.32)$$

Therefore the velocity depends on the following quantities:

$$\tilde{u} = f(y, \bar{\tau}_w, \mu_w, \varrho_w, T_w, \bar{q}_w, c_p, \lambda_w). \quad (19.33)$$

It seems natural to replace the wall temperature T_w by the speed of sound at the wall $c_w = \sqrt{(\gamma - 1)c_p T_w}$. According to the Π theorem, Eq. (19.33) then yields the universal wall law for the velocity

$$u^+ = \frac{\tilde{u}}{u_\tau} = F(y^+, B_q, Ma_\tau, Pr_w) \quad (19.34)$$

with

$$u_\tau = \sqrt{\frac{\bar{\tau}_w}{\varrho_w}}, \quad T_\tau = -\frac{-\bar{q}_w}{\varrho_w c_p u_\tau}, \quad B_q = \frac{T_\tau}{T_w}, \\ Ma_\tau = \frac{u_\tau}{c_w}, \quad Pr_w = \frac{\mu_w c_p}{\lambda_w}. \quad (19.35)$$

Here T_τ is called the friction temperature, B_q the heat flux number and Ma_τ the friction Mach number. The dimensionless temperature $\Theta^+ = (\bar{T} - T_w)/T_\tau$ or $(\bar{T} - T_w)/T_w$ satisfies a relation corresponding to Eq. (16.34). Examples of these universal distributions of velocity and temperature can be found in the work by J.C. Rotta (1959), P. Bradshaw (1977) and H.H. Fernholz; P.J. Finley (1980).

The overlap layer is the outer part of the wall layer in which the effects of the viscosity and the thermal conductivity can already be neglected. Then Eq. (19.32) reduces to

$$\tau_t = \bar{\tau}_w, \quad q_t = \bar{q}_w + \tilde{u} \tau_t. \quad (19.36)$$

The turbulent Prandtl number for the overlap layer with constant physical properties was found to be $\text{Pr}_t = \kappa/\kappa_\theta$ from Eq. (17.77), cf. Eq. (17.78). Measurements have shown that this is also true for variable physical properties. If we take Eq. (19.36) into account, Eqs. (17.77) and (17.78) yield

$$\frac{d\bar{T}}{d\tilde{u}} = -\frac{\kappa}{\kappa_\theta} \frac{\bar{q}_w + \tilde{u}\bar{\tau}_w}{c_p\bar{\tau}_w} \quad (19.37)$$

or, after integrating the temperature distribution in the overlap layer:

$$\frac{\bar{T}}{T_w} = \frac{\kappa}{\kappa_\theta} B_q \frac{\tilde{u}}{u_\tau} - R^2 \left(\frac{\tilde{u}}{u_\tau} \right)^2 + C_1(B_q, \text{Ma}_\tau) \quad (19.38)$$

with

$$R = \sqrt{\frac{\kappa}{\kappa_\theta} \frac{\gamma - 1}{2} \text{Ma}_\tau^2}. \quad (19.39)$$

Similarity considerations for the velocity gradient similar to Eq. (17.15) deliver:

$$\frac{d\tilde{u}}{dy} = \sqrt{\frac{\bar{\tau}_w}{\bar{\rho}}} \frac{1}{\kappa y} = \frac{u_\tau}{\kappa y} \sqrt{\frac{\varrho_w}{\bar{\rho}}}. \quad (19.40)$$

Because of $\varrho_w/\bar{\rho} = \bar{T}/T_w$, combining Eq. (19.40) and (19.38) furnishes a differential equation for $\tilde{u}(y)$, which, after integration of the velocity distribution in the overlap layer, yields

$$u^+ = \frac{\tilde{u}}{u_\tau} = \frac{\sqrt{C_1}}{R} \sin \left[R \left(\frac{1}{\kappa} \ln y^+ + C_2 \right) \right] + \frac{\kappa_\theta}{\kappa} \frac{B_q}{2R^2} \left\{ 1 - \cos \left[R \left(\frac{1}{\kappa} \ln y^+ + C_2 \right) \right] \right\}. \quad (19.41)$$

The two constants of integration with respect to y , C_1 and C_2 , are still functions of B_q and Ma_τ . They depend on the model for the viscous wall layer. In particular, C_2 is also affected by the viscosity law, thus, for example, by ω in Eq. (10.46). In addition, C_2 is generally a function of the Prandtl number, cf. K. Gersten; H. Herwig (1992), p. 506. According to P. Bradshaw (1977):

$$C_1 = 1, \quad C_2 = 5.2 + 95 \text{Ma}_\tau^2 - 30.7 B_q + 226 B_q^2. \quad (19.42)$$

The constants have also been computed with the help of two-equation models, cf. D.C. Wilcox (1998), p. 248. For $B_q = 0$, the $k-\omega$ model yields $C_1 = 1 + 0.87 \text{Ma}_\tau^2$ and the $k-\varepsilon$ model $C_1 = 1 + 3.07 \text{Ma}_\tau^2$. In both models, C_2 is not a true constant, but is still a function of $\bar{\rho}/\varrho_w$, see also P.G. Huang et al. (1994).

The effect of Ma_τ is generally very small. For $\text{Ma} < 5$, we find $\text{Ma}_\tau < 0.1$. For small values of Ma_τ ($R \rightarrow 0$ from Eq. (19.39)), Eq. (19.41) simplifies to

$$u^+ = \frac{\tilde{u}}{u_\tau} = \sqrt{C_1} \left(\frac{1}{\kappa} \ln y^+ + C_2 \right) + \frac{\kappa_\theta B_q}{\kappa} \left(\frac{1}{\kappa} \ln y^+ + C_2 \right)^2. \quad (19.43)$$

Strictly speaking, the term proportional to B_q still contains the factor $-\beta_w T_w$, but for ideal gases this is just equal to 1. Therefore for fluids with constant densities ($\beta_w = 0$), the second term vanishes, even for $B_q \neq 0$, and therefore $C_1 = 1$ and $C_2 = 5.2$ or $C_2 = C^+ = 5.0$.

K. Gersten (1989b) and K. Gersten; H. Herwig (1992), p. 505 have shown that for variable densities, the viscous wall layer strictly does not have universal velocity and temperature distributions. Rather, in matching onto the fully turbulent outer flow, the solution of the outer layer and thus the turbulence model influence the wall layer. This coupling between the turbulent outer layer and the viscous wall layer due to variable densities generally produces only very small effects. This has been shown by K. Gersten; H. Herwig (1992), p. 696 for the flat plate with heat transfer at moderate velocities.

19.2.3 Skin-Friction Coefficient and Nusselt Number

Based on the overlap law described in the previous section, K. Gersten; H. Herwig (1992), p. 695 have also determined the skin-friction coefficients and Nusselt numbers for moderate velocities ($\text{Ma}_\tau = 0$) and moderate heat transfer (B_q small). This is a regular perturbation calculation for the solution for constant physical properties, where B_q is the perturbation parameter. The results may be represented particularly simply in the form of the *property ratio method*, cf. Sect. 10.3.2. With constant values c_p and Pr , $c_f = 2\bar{\tau}_w / (\varrho_\infty U_\infty^2)$ and $\text{Nu} = \bar{q}_w l / [\lambda_\infty (T_w - T_\infty)]$ satisfy:

$$\frac{c_f}{c_{f_{c.p.}}} = \left(\frac{\varrho_w}{\varrho_\infty} \right)^{m_\varrho} \left(\frac{\mu_w}{\mu_\infty} \right)^{m_\mu}, \quad \frac{\text{Nu}}{\text{Nu}_{c.p.}} = \left(\frac{\varrho_w}{\varrho_\infty} \right)^{n_\varrho} \left(\frac{\mu_w}{\mu_\infty} \right)^{n_\mu}. \quad (19.44)$$

Again the index c.p. refers to constant physical properties. For variable c_p and Pr , the corresponding powers of these physical properties would be added to the formula for the Nusselt number. There have been frequent attempts in the literature to determine empirically the exponents in Eq. (19.44), which can be ascertained from the solution with constant physical properties. They are functions of the Reynolds number and the Prandtl number:

$$m_\varrho = \frac{1}{2} - M_\varrho(\text{Pr}) \sqrt{\frac{c_{f_{c.p.}}}{2}}, \quad m_\mu = \frac{2}{\kappa} \sqrt{\frac{c_{f_{c.p.}}}{2}}, \quad (19.45)$$

$$n_\varrho = \frac{1}{2} - N_\varrho(\text{Pr}) \sqrt{\frac{c_{f_{c.p.}}}{2}}, \quad n_\mu = \frac{2}{\kappa} \sqrt{\frac{c_{f_{c.p.}}}{2}}. \quad (19.46)$$

The functions $M_\varrho(\text{Pr})$ and $N_\varrho(\text{Pr})$ have been determined by K. Gersten; H. Herwig (1992), p. 696. For $\text{Pr} = 0.72$ it is found that $M_\varrho = 4.6$ and $N_\varrho = 3.3$. The results for constant physical properties are Eqs. (18.76), (18.93) and

(18.157). In the limit $\text{Re} \rightarrow \infty$, as expected, the effect of the viscosity vanishes ($m_\mu \rightarrow 0, n_\mu \rightarrow 0$), and the simple result $m_\varrho = n_\varrho = 1/2$ is obtained. The formulae (19.44) can also be used if the wall heat flux is given. The quantities ϱ_w and μ_w are then determined at $T_{w.c.p.}$. Since Eq. (19.44) are purely local correction formulae, they can be used for any attached boundary layers, cf. Sect. 18.2. Here only the functions $M_\varrho(\text{Pr})$ and $N_\varrho(\text{Pr})$ are only mildly dependent on the quantity \tilde{C} in Eq. (18.74).

The results also deliver the reference temperatures for the *reference temperature method* described in Sect. 10.3.3. These are generally dependent of the Reynolds number and the Prandtl number. In the limit $\text{Re} \rightarrow \infty$, because $m_\varrho = n_\varrho = 1/2$, the reference temperature is precisely the so-called *film temperature*, the arithmetic mean of the wall and outer temperatures.

Example: Skin-friction coefficient of the flat plate with an adiabatic wall

According to the method of reference temperatures, in the limit $\text{Re} \rightarrow \infty$ one obtains

$$\frac{c_f}{c_{f.c.p.}} \approx \frac{\bar{\varrho}_r}{\varrho_\infty}, \quad (19.47)$$

since, according to Eq. (18.76), $\bar{\tau}_w$ is proportional to $\bar{\varrho}$. In addition, since the reference temperature T_r is equal to the film temperature, we use $\bar{\varrho}_r/\varrho_\infty = T_\infty/T_r$ and Eq. (19.33) to obtain

$$\frac{c_f}{c_{f.c.p.}} = \left(1 + r \frac{\gamma - 1}{4} \text{Ma}^2\right)^{-1}. \quad (19.48)$$

Figure 19.1 compares this function with experimental results. As the Reynolds number decreases, the reference temperature approaches the outer temperature, and $c_f/c_{f.c.p.}$ increases, cf. T. Cebeci; P. Bradshaw (1984), p. 355.

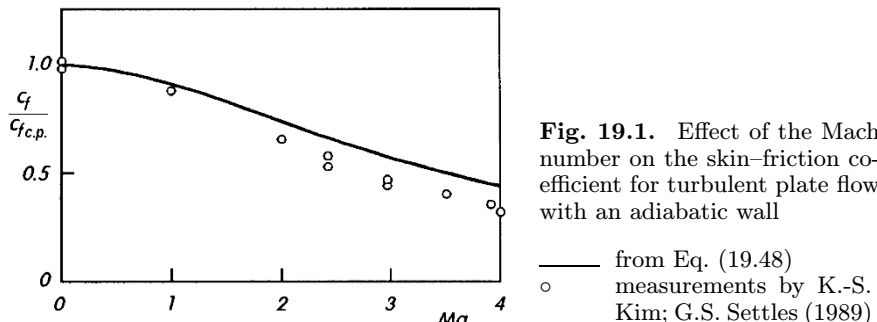


Fig. 19.1. Effect of the Mach number on the skin-friction coefficient for turbulent plate flow with an adiabatic wall

— from Eq. (19.48)
 ○ measurements by K.-S. Kim; G.S. Settles (1989)

D.B. Spalding; S.W. Chi (1964) have presented a semi empirical method to determine the ratio $c_f/c_{f.c.p.}$ of plate flow at $\text{Pr} = 0.72$ at arbitrary ratios T_w/T_∞ and arbitrary Mach numbers. For $\text{Ma} = 0$ and moderate heat transfer, this agrees with Eq. (19.44).

E.R. Van Driest (1951) has given a formula for the dependence of c_f for plate flow on T_w/T_∞ and Ma . This is known as the Van-Driest-II formula, see T. Cebeci; P. Bradshaw (1984), p. 345. This formula follows from a turbulence model which uses the mixing length. For $\text{Ma} = 0$ and moderate heat transfer it yields:

$$\sqrt{\frac{2}{c_f}} = \frac{\sqrt{\varrho_\infty/\varrho_w} + 1}{2} \left[\frac{1}{\kappa} \ln \left(\text{Re}_x \frac{c_f}{2} \frac{\mu_\infty}{\mu_w} \right) + C^+ + \frac{1}{\kappa} (2\pi - \ln F_e) \right]. \quad (19.49)$$

In the isothermal case ($T_w = T_\infty$) this becomes Eq. (18.93). Note that Eq. (19.49) contains no further constants compared to the isothermal case. Eq. (19.45) can be used to rewrite this formula as Eq. (19.44), where $M_\varrho = 1/\kappa = 2.44$. Since C^+ is also a function of the wall roughness, Eq. (19.49) is also valid for rough plates.

A method of calculating the skin-friction coefficient for compressible plate boundary layers with and without heat transfer has also been presented by P.G. Huang et al. (1993).

Note also that at finite Mach numbers the Nusselt number and Stanton number ought to be formed with the difference between wall temperature and adiabatic wall temperature:

$$\text{St} = \frac{\text{Nu}_x}{\text{Re}_x \text{Pr}_\infty} = \frac{\bar{q}_w}{\varrho_\infty c_p (T_w - T_{ad}) U}; \quad \text{Nu}_x = \frac{\bar{q}_w x}{\lambda_\infty (T_w - T_{ad})}, \quad (19.50)$$

cf. Eq. (18.157).

19.2.4 Integral Methods for Adiabatic Walls

Just as for constant physical property boundary layers, numerous integral methods also exist for compressible boundary layers (see the overview by J. Delery; J.G. Marvin (1986)). Here we will describe the extension of the integral method described in Sect. 18.4.1 using the boundary condition which appears most frequently in practice, namely the adiabatic wall ($\bar{q}_w = 0$).

The aim is to determine the skin-friction coefficient $c_f(x)$ and the adiabatic wall temperature $T_{ad}(x)$ (eigen-temperature) for given distributions $u_e(x)$, $p_e(x)$, $\varrho_e(x)$ and $T_e(x)$.

The integral method uses the momentum-integral and mean-kinetic-energy-integral equations. These are the same as the equations (10.92) and (10.93) for laminar compressible boundary layers if the quantities of the mean motion are inserted into the formula for the boundary-layer thicknesses. Because of Eq. (10.102), δ_h in Eq. (10.93) can be replaced by δ_3 , so that only the three thicknesses δ_1 , δ_2 and δ_3 appear in the integral equations. Equation (19.30) is used for the temperature distribution, so that, because of $\bar{\varrho}/\varrho_e = T_e/\bar{T}$, the density distribution is also at hand. Therefore the boundary-layer thicknesses δ_i ($i = 1, 2, 3$) can be reduced to the

corresponding *kinematic thicknesses* δ_{iu} ($i = 1, 2, 3$) by suitable choice of a velocity profile family. The kinematic thicknesses can be determined from the δ_i formula by setting $\overline{\varrho} = \varrho_e$. The same is true for the quantities

$$c_f = \frac{2\overline{\tau}_w}{\varrho_e u_e^2}, \quad c_D = \frac{2D}{\varrho_e u_e^3} = \frac{2}{\varrho_e u_e^3} \int_0^\delta \overline{\tau} \frac{\partial \tilde{u}}{\partial y} dy. \quad (19.51)$$

It is found that, cf. U. Ganzer (1988), p. 298:

$$\frac{\delta_1}{\delta_{1u}} = 1 + r \frac{\gamma - 1}{2} Ma_e^2 H_{31u} F, \quad \frac{\delta_2}{\delta_{2u}} = \frac{\delta_3}{\delta_{3u}} = \frac{c_f}{c_{fu}} = \frac{c_D}{c_{Du}} = F \quad (19.52)$$

with

$$F = \left[1 + r \frac{\gamma - 1}{2} Ma_e^2 \Phi(H_{32u}) \right]^{-1}, \quad (19.53)$$

where $\Phi(H_{32u})$ depends on the choice of the velocity profile family. M. Jischa (1982), p. 307 has presented the relation

$$\Phi(H_{32u}) = H_{32u}(2 - H_{32u}). \quad (19.54)$$

The “kinematic” quantities (index u) are practically independent of the Mach number, so that the relations $c_{fu}(Re_{1u}, H_{21u})$, $c_{Du}(Re_{1u}, H_{21u})$ and $H_{31u}(H_{21u})$ from Sect. 18.4.1, Fig. 18.9, can be used.

This reduces the integral method for compressible boundary layers at adiabatic walls to that for incompressible boundary layers.

For given values γ , c_p , Pr , $u_e(x)$, $T_e(x)$ and initial values Re_1 and H_{21} , we proceed as follows:

First of all, the adiabatic wall temperature $T_{ad}(x)$ can be determined from Eq. (19.31) with $r = \kappa/\kappa_\theta = 0.87$. Then H_{31u} or H_{32u} are estimated at the starting point, and the associated values of Re_{1u} and H_{21u} may be determined iteratively. In computing $Re_1(x)$ and $H_{21}(x)$ from Eqs. (10.92) and (10.93), combined with Eq. (10.102), the “kinetic” quantities serve as auxiliary values. The desired distribution of the skin-friction coefficient c_f is finally obtained from Eqs. (18.74) and (19.52).

Integral methods of this kind have proved to be very useful in practice. Summaries and worked examples have been presented by A. Walz (1966), p. 230, M. Jischa (1982), p. 204, U. Ganzer (1988), p. 298 and J. Delery; J.G. Marvin (1986). J. Cousteix et al. (1974) have also given an integral method for compressible boundary layers with heat transfer.

Note (Velocity distribution)

For boundary layers with constant physical properties, Eqs. (18.117), (18.120) and (18.69) yield the following general form of the velocity distribution:

$$\frac{u(x, y)}{u_e(x)} = 1 + \frac{u_\tau(x)}{\kappa u_e(x)} \ln \frac{y}{\delta(x)} - \left[\frac{\delta_{1u}(x)}{\delta(x)} - \frac{u_\tau(x)}{\kappa U_e(x)} \right] \left[2 - W \left(\frac{y}{\delta(x)} \right) \right]. \quad (19.55)$$

In fact it turns out that this velocity distribution is also valid for compressible boundary layers, if the wall is adiabatic and $\text{Ma}_e < 2$ holds, cf. J. Delery; J.G. Marvin (1986). Here, $\delta_1(x)$ must be replaced by the kinematic displacement thickness $\delta_{1u}(x)$.

19.2.5 Field Methods

In field methods, the balance equations (19.8), (19.9) and (19.24), extended by model equations for the turbulent transport quantities τ_t and q_t , are solved numerically.

In practice, the method given by T. Cebeci; A.M.O. Smith (1974), p. 255 has proved useful. Here the eddy viscosity ν_t from the incompressible boundary layer according to Eq. (18.7) can be used, as long as δ_1 is replaced by δ_{1u} . Providing no flow separation occurs, the temperature field may be computed with $\text{Pr}_t = \kappa/\kappa_\theta = 0.87$. Worked examples using this method have been presented by T. Cebeci; A.M.O. Smith (1974), p. 364 and T. Cebeci; P. Bradshaw (1984), p. 357.

The method by P. Bradshaw et al. (1967), see Sect. 18.1.3, has been extended to compressible boundary layers at adiabatic walls, see P. Bradshaw; D.H. Ferris (1971).

For details on methods with two-equation turbulence models, see D.C. Wilcox (1998), p. 254, see also S. Catris; B. Apoix (2000).

19.2.6 Shock–Boundary–Layer Interaction

If the velocity of the free stream is supersonic, compression shock waves can occur. There is then locally a *strong interaction* between the shock wave and the boundary layer. This is called *shock–boundary–layer interaction*. The usual *weak interaction* in boundary layers is then no longer at hand, but rather a *strong interaction* where the outer layer depends locally on the development of the boundary layer.

These processes are of great practical importance in transonic flows ($\text{Ma}_\infty \approx 1$). Summaries have been given by R.E. Melnik (1981), T.C. Adamson Jr.; A.F. Messiter (1981), J.M. Delery (1985), J. Delery; J.G. Marvin (1986), G.S. Settles; L.J. Dodson (1994). To be precise, shock–boundary–layer interaction for transonic flows is a case of a double limit. As well as the high Reynolds number limit, characterised by $\sqrt{c_{fR}/2} \rightarrow 0$, the limit $\text{Ma}_\infty \rightarrow 1$ also takes place. The limiting process is therefore characterised by the new characteristic number (transonic similarity parameter)

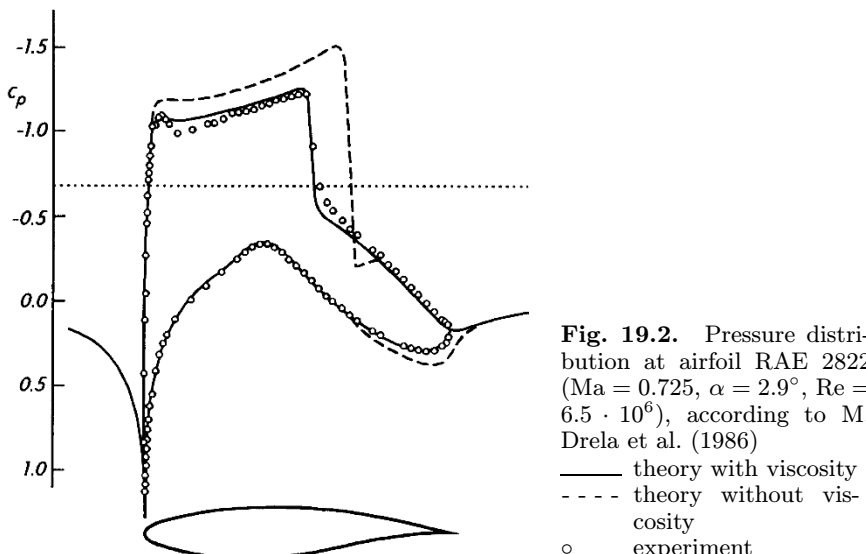
$$\chi = \frac{\text{Ma}_\infty^2 - 1}{\sqrt{c_{fR}/2}}. \quad (19.56)$$

We differentiate between three different cases:

- (1) $\chi \rightarrow 0$: very weak shock,
- (2) $\chi = O(1)$: weak shock,
- (3) $\chi \rightarrow \infty$: strong shock.

Each of these cases requires different mathematical treatment. In shock-boundary-layer interaction, the boundary layer generally has a three-layer structure (not counting the viscous sublayer). For details on this see the work by R. Bohning; J. Zierep (1981). U. Ganzer (1988), p. 332 discusses controlling the boundary layer by suction or blowing, both important in practice, cf. also S. Raghunathan (1988).

Boundary layers under the influence of strong vertical compression shocks can be described to good approximation by neglecting the friction forces. The existing integral methods are then greatly simplified (e.g. $c_f = c_D = 0$) and they deliver global statements about changes in the boundary-layer thicknesses and shape factors as dependent on the strength of the shock and the boundary-layer quantities in front of the shock. A corresponding separation criterion then allows one to determine which shock strengths lead to boundary-layer separation, cf. J. Delery; J.G. Marvin (1986), p. 110.



Shock-boundary-layer interference is particularly important in flows past airfoils close to the speed of sound. This is shown in Fig. 19.2, which depicts the pressure distribution at the airfoil RAE 2822 at $Ma = 0.725$ ($\alpha = 2.9^\circ$, $Re = 6.5 \cdot 10^6$). The large influence of boundary-layer effects on the pres-

sure distribution is easily seen in the difference between the two theoretical distributions, one without viscosity and one with viscosity.

D.S. Dolling (2001) has described the state of the art and a future outlook of the shock-wave/boundary-layer interaction research. The shock wave-boundary layer interaction control by wall ventilation has been investigated by P.P. Doerffer; R. Bohning (2003).

19.3 Natural Convection

The fundamental equations are analogous to those for laminar natural convection which have already been derived in Sect. 10.5.1, with only the turbulent transport quantities added to them. If we again use the *Boussinesq approximation*, the fundamental equations read

$$\frac{\partial \tilde{u}}{\partial x} + \frac{\partial \tilde{v}}{\partial y} = 0, \quad (19.57)$$

$$\varrho_\infty \left(\tilde{u} \frac{\partial \tilde{u}}{\partial x} + \tilde{v} \frac{\partial \tilde{u}}{\partial y} \right) = \frac{\partial}{\partial y} (\tau_v + \tau_t) + \varrho_\infty g \beta_\infty (\bar{T} - T_\infty) \sin \alpha, \quad (19.58)$$

$$\varrho_\infty c_{p\infty} \left(\tilde{u} \frac{\partial \bar{T}}{\partial x} + \tilde{v} \frac{\partial \bar{T}}{\partial y} \right) = \frac{\partial}{\partial y} (\bar{q}_\lambda + q_t), \quad (19.59)$$

where α is the angle between the x axis and the horizontal, as in Fig. 10.1. In what follows, we will initially set $\alpha = 90^\circ$ (vertical wall).

For a given wall heat flux \bar{q}_w , as well as the reference length l , we use the reference velocity

$$U_R = \left(\frac{\bar{q}_w g \beta_\infty l}{\varrho_\infty c_{p\infty}} \right)^{1/3}, \quad (19.60)$$

since the flow possesses no characteristic velocity. The Reynolds number formed using these

$$\frac{U_R l}{\nu_\infty} = \left(\frac{\bar{q}_w g \beta_\infty l^4}{\varrho_\infty c_{p\infty} \nu_\infty^3} \right)^{1/3} = \frac{\text{Ra}_q^{1/3}}{\text{Pr}_\infty^{2/3}} = \frac{\text{Gr}_q}{\text{Pr}_\infty^{1/3}} \quad (19.61)$$

can also be expressed using the Rayleigh number

$$\text{Ra}_q = \frac{\bar{q}_w g \beta_\infty l^4}{a_\infty \lambda_\infty \nu_\infty} = \frac{\bar{q}_w g \beta_\infty \varrho_\infty^2 c_{p\infty} l^4}{\lambda_\infty^2 \mu_\infty} \quad (19.62)$$

or the Grashof number

$$\text{Gr}_q = \frac{\text{Ra}_q}{\text{Pr}_\infty} = \frac{\bar{q}_w g \beta_\infty l^4}{\lambda_\infty \nu_\infty^2}. \quad (19.63)$$

For large Rayleigh numbers, or Grashof numbers, the flow is again subdivided into a viscous wall layer and the remaining fully turbulent outer layer.

Again universal wall laws hold for the viscous wall layer, cf. K. Gersten; H. Herwig (1992), p. 711, see also M. Wosnik; W.K. George (1995). With $\text{Pr}_\infty = \text{Pr}$ they read:

$$u^\times = \frac{\tilde{u}}{u_q} = f_N(y_N^\times, \text{Pr}), \quad \lim_{y^\times \rightarrow \infty} u^\times = \kappa_1 \cdot (y_N^\times)^{1/3} - C_N^\times(\text{Pr}), \quad (19.64)$$

$$\Theta^\times = \frac{\bar{T} - T_w}{T_q} = g_N(y_N^\times, \text{Pr}), \quad \lim_{y^\times \rightarrow \infty} \Theta^\times = \kappa_2 \cdot (y_N^\times)^{-1/3} - C_{N\theta}^\times(\text{Pr}) \quad (19.65)$$

$$\tau^\times = \frac{\bar{\tau}}{\varrho u_q^2} = s_N(y_N^\times, \text{Pr}), \quad \lim_{y^\times \rightarrow \infty} \tau^\times = -\kappa_3 \cdot (y_N^\times)^{2/3}, \quad (19.66)$$

$$q^\times = \frac{\bar{q}}{\bar{q}_w} = 1 \quad (19.67)$$

with

$$y^\times = \frac{yu_q}{\nu}, \quad u_q = \left(\frac{\bar{q}_w \beta g \nu}{\varrho c_p} \right)^{1/4}, \quad T_q = \frac{\bar{q}_w}{\varrho c_p u_q}. \quad (19.68)$$

Here, according to K. Gersten; H. Herwig (1992), p. 710, $\kappa_1 = 27$, $\kappa_2 = 5.6$ and $\kappa_3 = 8.4$. The “constants of integration” $C_N^\times(\text{Pr})$ and $C_{N\theta}^\times(\text{Pr})$ are universal functions of the Prandtl number.

S.W. Churchill (1983) has presented the formulae

$$C_{N\theta}^\times(\text{Pr}) = \frac{\text{Pr}^{1/2}}{0.24[\Psi(\text{Pr})]^{1/4}}, \quad \Psi(\text{Pr}) = \left[1 + \left(\frac{C_{ch}}{\text{Pr}} \right)^{9/16} \right]^{-16/9}. \quad (19.69)$$

According to Churchill, the constant C_{ch} lies between 0.43 and 0.49. Here $C_{ch} = 0.46$ has been used. Note that $\Psi(\text{Pr} \rightarrow \infty) = 1$ and $\Psi(\text{Pr} \rightarrow 0) = 2.2 \text{Pr}$ hold.

As before, the overlap laws can be determined from the general matching conditions, which here read:

$$\lim_{y \rightarrow 0} \frac{y}{\sqrt{-\tau_t/\varrho}} \frac{d\tilde{u}}{dy} = \frac{1}{\kappa_N}, \quad \lim_{y \rightarrow 0} \frac{\sqrt{-\tau_t/\varrho y}}{-q_t/(\varrho c_p)} \frac{dT}{dy} = \frac{1}{\kappa_{N\theta}}, \quad (19.70)$$

where the constants κ_N and $\kappa_{N\theta}$ correspond to the constants κ and κ_θ for forced convection. According to W.K. George; S.P. Capp (1979) their values are $\kappa_N = 0.32$ and $\kappa_{N\theta} = 0.18$. The fact that the law for the overlap layer is now a power law and no longer a logarithmic law has to do with the variable shear stress distribution $\tau_t(y)$.

Matching the temperature in the overlap layer leads to the relation:

$$\frac{T_w - T_\infty}{T_q} = C_{N\theta}^\times(\text{Pr}). \quad (19.71)$$

Therefore the wall temperature is also constant. There is therefore a *purely local* relation between the wall heat flux \bar{q}_w and the temperature difference,

and thus the solution for the two boundary conditions $\bar{q}_w = \text{const}$ and $T_w = \text{const}$ is the same. A length does not appear in Eq. (19.71).

Two different formulae follow for the Nusselt number, depending on whether \bar{q}_w or $T_w - T_\infty$ is given:

$$\text{Nu}_x = 0.24(\Psi \text{Pr})^{1/4} \text{Gr}_{qx}^{1/4} = 0.24(\Psi \text{Ra}_{qx})^{1/4}, \quad (19.72)$$

$$\text{Nu}_x = 0.15(\Psi \text{Pr})^{1/3} \text{Gr}_x^{1/3} = 0.15(\Psi \text{Ra}_x)^{1/3}, \quad (19.73)$$

with

$$\text{Ra}_x = \text{Gr}_x \text{Pr} = \frac{g\beta(T_w - T_\infty)x^3}{\nu a} \quad (19.74)$$

and

$$\text{Gr}_x = \frac{g\beta(T_w - T_\infty)x^3}{\nu^2}. \quad (19.75)$$

Figure 19.3 shows the heat transfer law for natural convection at a vertical flat plate for air ($\text{Pr} = 0.72$), according to R.A.W.M. Henkes (1990). Good agreement between theory and experiment can be seen.

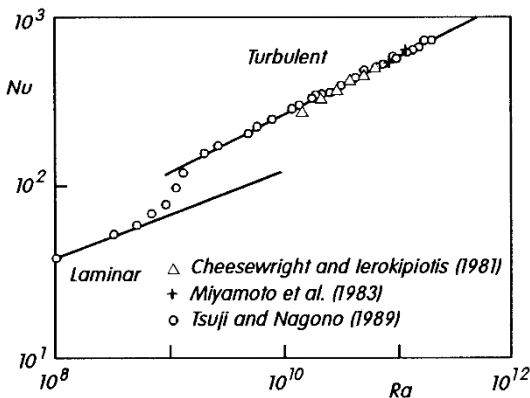


Fig. 19.3. Heat transfer law for natural convection at a vertical flat plate for air ($\text{Pr} = 0.72$), according to R.A.W.M. Henkes (1990)

laminar from Eq. (10.150)
 $\text{Nu} = 0.39 \text{Ra}^{1/4} (T_w = \text{const})$
turbulent from Eq. (19.73)
 $\text{Nu} = 0.11 \text{Ra}^{1/3}$

If the x axis deviates from the vertical ($\alpha \neq 90^\circ$), the formulae given may still be used, as long as g is replaced by $g \sin \alpha$ (but $\alpha \neq 0$).

A turbulence model is needed to be able to discuss the fully turbulent outer region of the boundary layer in detail. Since the velocity maximum in the outer layer is found at finite shear stress, turbulence models involving the eddy viscosity or the mixing length cannot be used.

Formulae for further characteristic quantities of the flow, such as the wall shear stress, thickness of the boundary layer, entrainment and so on have been given by K. Gersten; H. Herwig (1992), p. 718. See also M. Hölling; H. Herwig (2005), P. Kiš; H. Herwig (2012) and the overview articles by D.D. Papailiou (1991) and K. Hanjalić (2002).

Details on mixed convection have been presented by K. Gersten; H. Herwig (1992), p. 719.

20. Axisymmetric and Three-Dimensional Turbulent Boundary Layers

In Chap. 12 we treated axisymmetric and three-dimensional laminar boundary layers. The boundary-layer equations given there are also valid for turbulent boundary layers, as long as the friction terms are extended by corresponding terms of the Reynolds stresses. Therefore, compared to Chap. 12, we have to deal with the additional problem of turbulence modelling.

As in Chap. 12, this chapter will also be divided up into axisymmetric boundary layers and three-dimensional boundary layers.

20.1 Axisymmetric Boundary Layers

20.1.1 Boundary-Layer Equations

We consider a body of revolution which can also rotate about its axis with angular velocity ω in an axial flow. In order to describe the boundary layer, we use the coordinate system shown in Fig. 12.1. Equations (12.17) to (12.20) for the boundary layer are extended to:

$$\frac{\partial(r_w \bar{\varrho} \tilde{u})}{\partial x} + \frac{\partial(r_w \bar{\varrho} \tilde{v})}{\partial y} = 0, \quad (20.1)$$

$$\begin{aligned} \bar{\varrho} \left(\tilde{u} \frac{\partial \tilde{u}}{\partial x} + \tilde{v} \frac{\partial \tilde{u}}{\partial y} - \frac{\tilde{w}^2}{r_w} \frac{dr_w}{dx} \right) &= -\bar{\varrho} g \sin \alpha - \frac{dp_e}{dx} \\ &+ \frac{\partial}{\partial y} \left(\bar{\mu} \frac{\partial \tilde{u}}{\partial y} - \widetilde{\bar{\varrho} u'' v''} \right), \end{aligned} \quad (20.2)$$

$$\bar{\varrho} \left(\tilde{u} \frac{\partial \tilde{w}}{\partial x} + \tilde{v} \frac{\partial \tilde{w}}{\partial y} + \frac{\tilde{u} \tilde{w}}{r_w} \frac{dr_w}{dx} \right) = \frac{\partial}{\partial y} \left(\bar{\mu} \frac{\partial \tilde{w}}{\partial y} - \widetilde{\bar{\varrho} v'' w''} \right), \quad (20.3)$$

$$\boxed{c_p \bar{\varrho} \left(\tilde{u} \frac{\partial \bar{T}}{\partial x} + \tilde{v} \frac{\partial \bar{T}}{\partial y} \right) = \frac{\partial}{\partial y} \left(\bar{\lambda} \frac{\partial \bar{T}}{\partial y} - c_p \bar{\varrho} v''' T' \right) + \beta \bar{T} \tilde{u} \frac{dp_e}{dx} + \left(\bar{\mu} \frac{\partial \tilde{u}}{\partial y} - \widetilde{\bar{\varrho} u'' v''} \right) \frac{\partial \tilde{u}}{\partial y} + \left(\bar{\mu} \frac{\partial \tilde{w}}{\partial y} - \widetilde{\bar{\varrho} v'' w''} \right) \frac{\partial \tilde{w}}{\partial y}.} \quad (20.4)$$

Here we have used assumptions which are analogous to those for Eqs. (19.8), (19.9) and (19.24). In the literature, \tilde{u} , \tilde{w} , $\widetilde{u''v''}$, $\widetilde{v''w''}$ are frequently replaced by the conventional averages \bar{u} , \bar{w} , $\overline{u''v''}$, $\overline{v''w''}$. However Eq. (19.17a) remains valid.

For a low-Reynolds-number turbulence model, the boundary conditions read:

$$\begin{aligned} y = 0 : \quad \tilde{u} = 0, \quad \tilde{v} = 0, \quad \tilde{w} = w_w = \omega r_w, \quad \bar{T} = T_w, \\ y = \delta : \quad \tilde{u} = u_e, \quad \tilde{w} = 0, \quad \bar{T} = T_e. \end{aligned} \quad (20.5)$$

The geometry of the body $r_w(x)$, the angular velocity ω , the physical properties and the functions $u_e(x)$, $T_w(x)$ and $T_e(x)$ are all prescribed. The momentum-integral equations (12.21) and (12.22) remain unchanged for the turbulent boundary layer. For details on these integral relations for compressible flows, see the work by J. Cousteix (1987a, 1987b).

20.1.2 Boundary Layers without Body Rotation

If the body does not rotate ($\omega = 0$, $\tilde{w} = 0$), the boundary-layer equations (20.2) and (20.4) are identical to those for plane boundary layers, and it is only the continuity equation (20.1) which differs. Therefore in this case, the turbulence models are also identical to those for plane boundary layers.

Thus the boundary layer at bodies of revolution in axial flows also possesses a two-layer structure with the logarithmic velocity law in the overlap region.

For $\tilde{w} = 0$, Eqs. (20.1) to (20.4) contain no effects of the *transversal curvature*. This can be seen immediately when we look at the simple example of the boundary layer along a circular cylinder. Because of $r_w = \text{const}$, this is identical to that for the flat plate at zero incidence.

The boundary-layer equations must therefore be appropriately extended to be able to include the effects of transversal curvature. For the laminar case, the extended boundary-layer equations were given in Sect. 14.2, Eqs. (14.23) to (14.27). These are also valid for turbulent boundary layers as long as they are suitably extended by terms for the Reynolds stresses. If the longitudinal curvature of the body of revolution is neglected ($K = 0$), we obtain the boundary-layer equations

$$\frac{\partial}{\partial x} (\bar{\varrho} r \tilde{u}) + \frac{\partial}{\partial y} (\bar{\varrho} r \tilde{v}) = 0, \quad (20.6)$$

$$\bar{\varrho} \left(\tilde{u} \frac{\partial \tilde{u}}{\partial x} + \tilde{v} \frac{\partial \tilde{u}}{\partial y} \right) = - \frac{dp_e}{dx} + \frac{1}{r} \frac{\partial}{\partial y} \left[r \left(\bar{\mu} \frac{\partial \tilde{u}}{\partial y} - \widetilde{\bar{\varrho} u'' v''} \right) \right], \quad (20.7)$$

$$\bar{\varrho} c_p \left(\tilde{u} \frac{\partial \bar{T}}{\partial x} + \tilde{v} \frac{\partial \bar{T}}{\partial y} \right) = \frac{1}{r} \frac{\partial}{\partial y} \left[r \left(\bar{\lambda} \frac{\partial \bar{T}}{\partial y} - c_p \bar{\varrho} \widetilde{T' v''} \right) \right] \quad (20.8)$$

with

$$r = r_w + y \cos \theta. \quad (20.9)$$

Therefore, compared to the simple boundary-layer equations, only the terms for the momentum and heat transport have been changed. For the circular cylinder at zero incidence ($r_w = \text{const}$, $\Theta = 0^\circ$), these are the equations of motion in cylindrical coordinates, where the terms for the momentum and heat transport in the axial direction and the dissipation in the energy equation are neglected.

For $\delta/r_w = O(1)$, i.e. according to F.M. White (1974), p. 555 for about $u_e(x) r_w(x)/\nu < 1000$, the effects of the transversal curvature have to be taken into account.

In the overlap layer between the viscous wall layer and the fully turbulent outer layer, the logarithmic velocity law is still valid:

$$u^+ = A(R^+) \ln y^+ + B(R^+). \quad (20.10)$$

Here A and B depend on $R^+ = r_w u_\tau / \nu$. For $R^+ > 250$ one obtains the known values $A = 1/\kappa$, $B = C^+ = 5.0$, cf. N. Afzal; R. Narasimha (1985).

For details on turbulence models, see Th.T. Huang; M.-Sh. Chang (1986).

Examples

Cone in supersonic flow. There is constant pressure at the outer edge of the boundary layer if the shock cone is attached, and so the situation is similar to the boundary layer on a plate. E.R. Van Driest (1952) has shown that the two boundary layers are approximately related by means of the Mangler transformation described in Sect. 12.1.2. Therefore the skin-friction coefficients c_f are the same for $(Re_x)_{\text{cone}} = 2(Re_x)_{\text{plate}}$.

Waisted body of revolution. K.G. Winter et al. (1965) investigated a waisted body of revolution which has both concave and convex curvature. As T. Cebeci; A.M.O. Smith (1974), p. 370 show, the transversal curvature also has a considerable effect on the momentum thickness.

Circular cylinder at zero incidence. This flow illustrates the effect of transversal curvature. Without taking it into account, there would be no difference between this situation and the boundary layer at a flat plate. Numerous experimental and theoretical pieces of work discuss this flow, compare F.M. White (1974), p. 555 and N. Afzal; R. Narasimha (1976). F.M. White has also computed the skin-friction coefficient $c_f(Re_x, U_\infty R/\nu)$. Transversal curvature raises c_f considerably.

Body of revolution with wake. T.T. Huang; M.-S. Chang (1986) have computed the flow at a body of revolution as in Fig. 20.1. Here the transversal curvature was taken into account but the longitudinal curvature neglected. In addition, the interaction with the inviscid outer flow was included. In order to do this, the axisymmetric wake and its effect (entrainment) on the outer flow had to be determined. In spite

of the fairly thick boundary layer at the back of the body (the pressure gradient perpendicular to the wall inside the boundary layer is neglected) the agreement with experiment is very good.

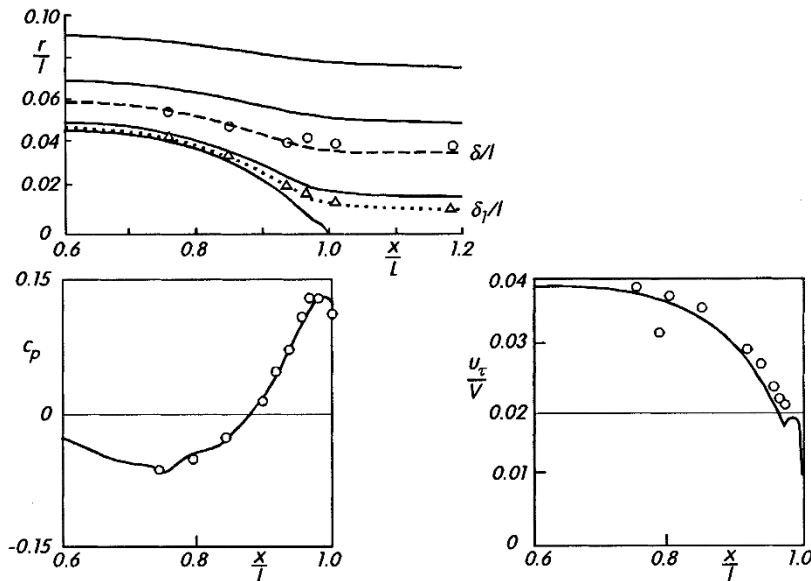


Fig. 20.1. Streamlines, pressure coefficient and skin-friction coefficient at the back end of a body of revolution at zero incidence, after Th.T. Huang; M.-Sh. Chang (1986)

○ △ experiment
— boundary-layer theory taking the transversal curvature and the interaction with the outer flow into account

Turbulent sink flows. We consider the axisymmetric flow due to a line sink of constant strength, where the flow field is bounded by an infinite plane wall perpendicular to the line-sink axis. This interesting flow has been investigated by S. Haas; W. Schneider (1996) for the limit of large Reynolds numbers. The flow field has a three-layer structure, consisting of a viscous sublayer, a defect layer and a non-turbulent core layer. The logarithmic overlap law between the viscous sublayer and the defect layer is valid. The defect layer exhibits the peculiarity of negative entrainment.

It is shown that the solution to this problem is non-unique. A second solution exists which has a two-layer structure, the mean velocity near the wall exhibits a square-root law and the wall shear stress vanishes in the first order.

Nozzles and diffusers. As we have already mentioned in Chap. 12, the boundary-layer equations (20.1) to (20.4) are also valid inside bodies of revolution. Examples of axisymmetric inner flows are those in nozzles and diffusers. In order to optimise wind tunnel nozzles and hence avoid separation, boundary-layer calculations are necessary, cf. G.-G. Börger (1975) and M.N. Mikhail (1979). In diffusers too, the flow can be divided up into an inviscid core flow and a wall boundary layer, as long as the inlet flow only has a thin boundary layer, cf. K. Gersten; H. Herwig (1992), p. 680, A.P. Härtl (1989), H.-W. Stock (1985). In diffusers, the boundary-layer

thickness can assume the order of magnitude of the radius. Then the interaction of the boundary layer with the core flow and the transversal curvature must be taken into account in the boundary-layer equations, see H. Schlichting, K. Gersten (1961).

Natural convection. Results on heat transfer at vertical cylinders, vertical cones and spheres have been collected by S.W. Churchill (1983). The transversal curvature at the outside of a vertical cylinder leads to an increase in the heat transfer.

20.1.3 Boundary Layers with Body Rotation

If the axisymmetric body rotates about its axis, in spite of the axial symmetry a three-dimensional boundary layer occurs where all three velocity components are in general non-zero. These are known as *shear-driven boundary layers*, in contrast to the *pressure-driven boundary layers* which will be discussed in Sect. 20.2.

According to E. Truckenbrodt (1954b), the velocity distribution in the circumferential direction can be written as

$$\frac{\bar{w}(x, y)}{w_w(x)} = 1 - \frac{\bar{u}(x, y)}{\bar{u}_e}. \quad (20.11)$$

If the transversal curvature is to be taken into account, according to Y. Furuya et al. (1978) this relation must be extended to

$$\frac{r_w(x)}{r(x, y)} \frac{\bar{w}(x, y)}{w_w(x)} = 1 - \frac{\bar{u}(x, y)}{\bar{u}_e(x)}. \quad (20.12)$$

Measurements by O. Parr (1963) and I. Nakamura; S. Yamashita (1982) confirm Eqs. (20.11) and (20.12) respectively very well. In the latter work it is shown that the velocity distribution in the circumferential direction satisfies the logarithmic law, cf. also Y. Furuya et al. (1978).

Integral methods to compute the turbulent boundary layer on rotating bodies have been developed by several authors including E. Truckenbrodt (1954b), O. Parr (1963) and I. Nakamura et al. (1980).

In field methods, an *isotropic eddy viscosity* is frequently used. This is the same for both velocity distributions:

$$\frac{\tau_{tx}}{\bar{\rho}} = -\widetilde{u''v''} = \nu_t \frac{\partial \tilde{u}}{\partial y}, \quad \frac{\tau_{tz}}{\bar{\rho}} = -\widetilde{v''w''} = \nu_t \frac{\partial \tilde{w}}{\partial y}. \quad (20.13)$$

In algebraic turbulence models, the eddy viscosity ν_t is related to the resulting velocity profile. If we use the mixing length ℓ , it follows that

$$\nu_t = D^2 \ell^2 \sqrt{\left(\frac{\partial \tilde{u}}{\partial y} \right)^2 + \left(\frac{\partial \tilde{w}}{\partial y} \right)^2}. \quad (20.14)$$

Here $D(y^+)$ is a damping function, cf. Sect. 18.1.7. In the overlap layer it is found that

$$\lim_{y^+ \rightarrow \infty} D = 1, \quad \lim_{y \rightarrow 0} \ell = \kappa y, \quad (20.15)$$

cf. Eq. (18.10). The functions $\ell(y)$ and $\nu_t(y)$ given in Sect. 18.1.2 are similarly valid. The displacement thickness for the Cebeci-Smith model then reads:

$$\delta_1 = \int_0^\delta \left(1 - \frac{\sqrt{\tilde{u}^2 + \tilde{w}^2}}{u_e} \right) dy. \quad (20.16)$$

The wall shear stress has the two components

$$\bar{\tau}_{wx} = \left(\bar{\mu} \frac{\partial \tilde{u}}{\partial y} \right)_w, \quad \bar{\tau}_{wz} = \left(\bar{\mu} \frac{\partial \tilde{w}}{\partial y} \right)_w. \quad (20.17)$$

Examples

Rotating bodies. Many different bodies have been investigated by O. Parr (1963), Y. Furuya et al. (1978), I. Nakamura et al. (1980) and I. Nakamura et al. (1981).

One special case is the *rotating disk* in an axial flow. This case has been treated by E. Truckenbrodt (1954a). Results on the moment coefficient are shown in Fig. 12.3. This is dependent on the Reynolds number $Re = \omega R^2 / \nu$ and the rotation parameter $V/\omega R$. It can be seen from Fig. 12.3 that, for constant rate of revolution, the moment increases considerably with increasing free stream velocity V . The special case $V = 0$ (rotating disk without free stream) is also sketched in this figure. S. Goldstein (1935) computed the moment coefficient for this case, and the result reads:

$$\frac{1}{\sqrt{c_M}} = \frac{1}{\kappa \sqrt{8}} \ln (Re \sqrt{c_M}) + 0.03. \quad (20.18)$$

This is also shown in Fig. 12.3. The effects of roughness and addition of polymers on the moment have been investigated by P.S. Granville (1973).

Rotating cylinder. Numerous flow investigations have been carried out on axisymmetric bodies such as those in Fig. 20.2, where the front part is fixed and a cylindrical part further aft rotates, cf. L.R. Bissonnette; G.L. Mellor (1974), R.P. Lohmann (1976), L. Fulachier et al. (1982). At the transition from the fixed to the rotating wall, a new boundary layer forms inside an already developed boundary-layer flow. All three velocity components are present in this new boundary layer. The extension of the velocity profile in the circumferential direction is initially very much smaller than in the median direction. Therefore Eq. (20.12) and (20.13) and other statements which assumed the same extension for both velocity distributions are no longer valid. The problems of finding turbulence models for this flow have been comprehensively discussed by L. Fulachier et al. (1982). M.S. Ölçmen; R.L. Simpson (1993) have tested how well this flow can be described by algebraic models.

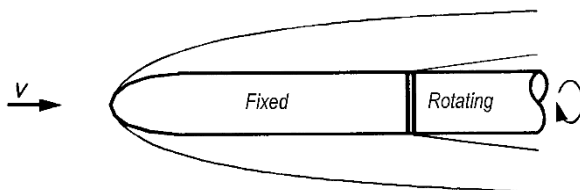


Fig. 20.2. Body of revolution with rotating cylindrical end

Diffuser with swirling flow. This flow appears frequently in practice (turbo-machinery, combustion chambers). Here the velocity in the boundary layer in the circumferential direction is not driven by a rotating wall but by the swirling inviscid core flow. For details see the work by F. Liepe (1960, 1962).

20.2 Three-Dimensional Boundary Layers

20.2.1 Boundary-Layer Equations

In Sect. 12.2 we discussed laminar three-dimensional boundary-layer equations in great detail. Many of the results obtained there can be carried over to turbulent boundary layers quite simply.

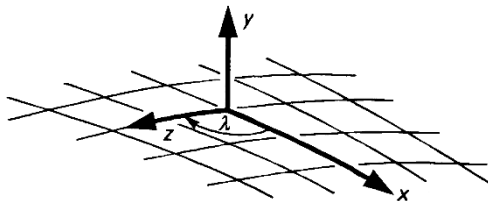


Fig. 20.3. Non-orthogonal curvilinear coordinate system

For a non-orthogonal curvilinear coordinate system as in Fig. 20.3, the boundary-layer equations read:

$$\frac{\partial}{\partial x}(\bar{\rho}\tilde{u}h_z \sin \lambda) + \frac{\partial}{\partial y}(\bar{\rho}\tilde{v}h_x h_z \sin \lambda) + \frac{\partial}{\partial z}(\bar{\rho}\tilde{w}h_x \sin \lambda) = 0, \quad (20.19)$$

$$\begin{aligned} & \bar{\rho} \left(\frac{\tilde{u}}{h_x} \frac{\partial \tilde{u}}{\partial x} + \tilde{v} \frac{\partial \tilde{u}}{\partial y} + \frac{\tilde{w}}{h_z} \frac{\partial \tilde{u}}{\partial z} + K_{12}\tilde{u}\tilde{w} - K_1 \frac{\cos \lambda}{\sin \lambda} \tilde{u}^2 + \frac{K_2}{\sin \lambda} \tilde{w}^2 \right) \\ &= -\frac{1}{h_x \sin^2 \lambda} \frac{\partial p_e}{\partial x} + \frac{\cos \lambda}{h_z \sin^2 \lambda} \frac{\partial p_e}{\partial z} + \frac{\partial}{\partial y} \left(\bar{\mu} \frac{\partial \tilde{u}}{\partial y} - \widetilde{\bar{\rho} u'' v''} \right), \end{aligned}$$

(20.20)

$$\begin{aligned} & \bar{\rho} \left(\frac{\tilde{u}}{h_x} \frac{\partial \tilde{w}}{\partial x} + \tilde{v} \frac{\partial \tilde{w}}{\partial y} + \frac{\tilde{w}}{h_z} \frac{\partial \tilde{w}}{\partial z} + K_{21}\tilde{u}\tilde{w} + \frac{K_1}{\sin \lambda} \tilde{u}^2 - K_2 \frac{\cos \lambda}{\sin \lambda} \tilde{w}^2 \right) \\ &= \frac{\cos \lambda}{h_x \sin^2 \lambda} \frac{\partial p_e}{\partial x} - \frac{1}{h_z \sin^2 \lambda} \frac{\partial p_e}{\partial z} + \frac{\partial}{\partial y} \left(\bar{\mu} \frac{\partial \tilde{w}}{\partial y} - \widetilde{\bar{\rho} v'' w''} \right), \end{aligned}$$

(20.21)

$$\begin{aligned}
c_p \bar{\varrho} \left(\frac{\tilde{u}}{h_x} \frac{\partial \bar{T}}{\partial x} + \tilde{v} \frac{\partial \bar{T}}{\partial y} + \frac{\tilde{w}}{h_z} \frac{\partial \bar{T}}{\partial z} \right) &= \frac{\partial}{\partial y} \left(\bar{\lambda} \frac{\partial \bar{T}}{\partial y} - c_p \bar{\varrho} \widetilde{v'' T'} \right) \\
&+ \beta \bar{T} \left(\frac{\tilde{u}}{h_x} \frac{\partial p_e}{\partial x} + \frac{\tilde{w}}{h_z} \frac{\partial p_e}{\partial z} \right) \\
&+ \left(\bar{\mu} \frac{\partial \tilde{u}}{\partial y} - \bar{\varrho} \widetilde{u'' v''} \right) \left(\frac{\partial \tilde{u}}{\partial y} + \frac{\partial \tilde{w}}{\partial y} \cos \lambda \right) \\
&+ \left(\bar{\mu} \frac{\partial \tilde{w}}{\partial y} - \bar{\varrho} \widetilde{v'' w''} \right) \left(\frac{\partial \tilde{w}}{\partial y} + \frac{\partial \tilde{u}}{\partial y} \cos \lambda \right).
\end{aligned} \tag{20.22}$$

It was assumed for the thermal energy equation that $c_p = \text{const.}$ Otherwise, analogous conditions hold as for Eq. (19.8), (19.9) and (19.24). Frequently in the literature, for Mach numbers $\text{Ma}_\infty < 5$, the quantities \tilde{u} , \tilde{w} , $\widetilde{u'' v''}$, $\widetilde{v'' w''}$ are replaced by \bar{u} , \bar{w} , $\widetilde{u'' v''}$, $\widetilde{v'' w''}$, while $\bar{\varrho} \tilde{v}$ satisfies Eq. (19.17a).

The Lamé metric coefficients $h_x(x, z)$, $h_z(x, z)$ and the angle $\lambda(x, z)$ between the coordinate lines on the surface are given by the choice of coordinate system, cf. J. Cousteix (1987b).

The following abbreviations are used:

$$\begin{aligned}
K_1 &= \left[\frac{\partial}{\partial x} (h_z \cos \lambda) - \frac{\partial h_x}{\partial z} \right] / (h_x h_z \sin \lambda) \\
K_2 &= \left[\frac{\partial}{\partial z} (h_x \cos \lambda) - \frac{\partial h_z}{\partial x} \right] / (h_x h_z \sin \lambda),
\end{aligned} \tag{20.23}$$

$$\begin{aligned}
K_{12} &= \left[- \left(K_1 + \frac{1}{h_x} \frac{\partial \lambda}{\partial x} \right) + \cos \lambda \left(K_2 + \frac{1}{h_z} \frac{\partial \lambda}{\partial z} \right) \right] / \sin \lambda \\
K_{21} &= \left[- \left(K_2 + \frac{1}{h_z} \frac{\partial \lambda}{\partial z} \right) + \cos \lambda \left(K_1 + \frac{1}{h_x} \frac{\partial \lambda}{\partial x} \right) \right] / \sin \lambda.
\end{aligned} \tag{20.24}$$

For $\lambda = 90^\circ$, this is an orthogonal coordinate system. If the turbulent correlations drop away, this then reduces to Eqs. (12.55) to (12.58). The boundary conditions given there are also valid, as is Eq. (12.59).

At high Reynolds numbers, the method of wall functions again has to be used. In order to do this we have to consider the velocity distributions in detail. Figure 20.4 shows the velocity profile in a flow-adapted orthogonal coordinate system, where the x coordinate lines are the wall streamlines of the outer flow. Therefore $w_e(x, z) = 0$. Here (x, z) are called streamline coordinates. In this case the flow belonging to the \tilde{w} component is called the *secondary flow*. It follows the pressure drop $\partial p_e / \partial z$ imprinted by the outer flow. (In Fig. 20.4, $\partial p_e / \partial z < 0$.) If the outer streamline has a point of inflection, the \tilde{w} component inside the boundary layer can change its sign, cf. E.H. Hirschel (1987).

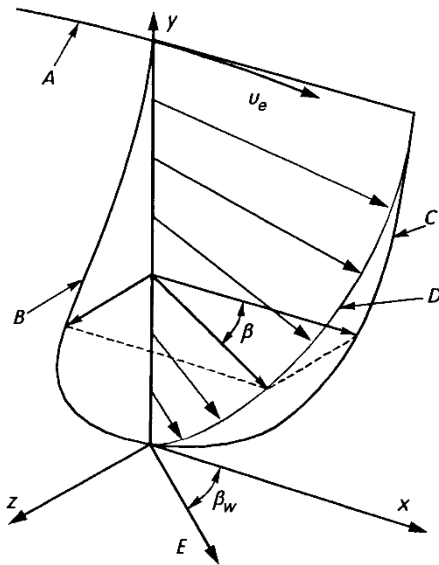


Fig. 20.4. Skewed velocity profile of a three-dimensional boundary layer (streamline coordinate system)
A: outer streamline
B: distribution $\tilde{w}(y)$
C: distribution $\tilde{u}(y)$
D: distribution of resulting velocity
E: direction of wall streamline

In the *skewed* velocity profile we differentiate between the following angles:

$$\beta(y) = \arctan \frac{\tilde{w}}{\tilde{u}} \quad \text{angle between the velocity vector } (\tilde{u}, \tilde{w}) \text{ and the } x \text{ direction}$$

$$\beta_g(y) = \arctan \frac{\partial \tilde{w} / \partial y}{\partial \tilde{u} / \partial y} \quad \text{angle between the velocity gradient vector } (\partial \tilde{u} / \partial y, \partial \tilde{w} / \partial y) \text{ and the } x \text{ direction}$$

$$\beta_\tau(y) = \arctan \frac{\widetilde{v''w''}}{\widetilde{u''v''}} \quad \text{angle between the turbulent shear stress vector } (\widetilde{u''v''}, \widetilde{v''w''}) \text{ and the } x \text{ direction}$$

The direction of the resulting wall shear stress is the same as the direction of the wall streamline. This forms the angle

$$\beta_w = \beta_{gw} = \arctan \frac{\bar{\tau}_{wz}}{\bar{\tau}_{wx}} \quad (20.25)$$

with the *x* direction, with

$$\bar{\tau}_{wx} = \left(\bar{\mu} \frac{\partial \tilde{u}}{\partial y} \right)_w, \quad \bar{\tau}_{wz} = \left(\bar{\mu} \frac{\partial \tilde{w}}{\partial y} \right)_w. \quad (20.26)$$

The velocity profile is *skewed* about this angle β_w .

There is also a subdivision into a viscous wall layer and a fully turbulent outer layer for three-dimensional turbulent boundary layers. This is demonstrated in the asymptotic analyses by U. Goldberg; E. Reshotko (1984) and A.T. Degani et al. (1992, 1993). At high Reynolds numbers, the viscous wall layer is characterised by the resulting wall shear stress

$$\bar{\tau}_w = \sqrt{\bar{\tau}_{wx}^2 + \bar{\tau}_{wz}^2}. \quad (20.27)$$

Therefore, here the velocity profile has, to first approximation, the direction of the wall streamline, i.e. we have $\beta = \beta_w = \text{const}$, and for the resulting shear stress $\bar{\tau} = \bar{\tau}_w = \text{const}$. It is only in the fully turbulent outer layer that the velocity vector is “twisted” from β_w to $\beta_e = 0$ at the outer edge of the boundary layer. This can be seen from the *hodograph* of the skewed velocity profile shown in Fig. 20.5.

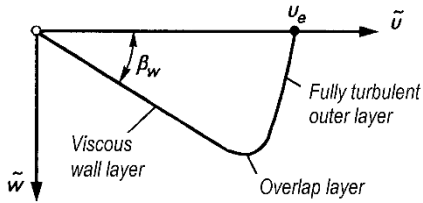


Fig. 20.5. Hodograph of the skewed velocity profile in the streamline coordinate system

For attached boundary layers ($\bar{\tau}_w \neq 0$), the \tilde{u} component of the fully turbulent outer layer can again be described using the defect formulation, cf. A.T. Degani et al. (1993).

In the overlap layer, where the viscous wall layer and the fully turbulent outer layer meet, it is found that:

$$\lim_{y^+ \rightarrow \infty} \tilde{u} = u_\tau \cos \beta_w \left(\frac{1}{\kappa} \ln y^+ + C^+ \right), \quad (20.28)$$

$$\lim_{y^+ \rightarrow \infty} \tilde{w} = u_\tau \sin \beta_w \left(\frac{1}{\kappa} \ln y^+ + C^+ \right) \quad (20.29)$$

with $u_\tau = \sqrt{\bar{\tau}_w / \rho}$ and $y^+ = y u_\tau / \nu$, or else

$$\lim_{\eta \rightarrow 0} \tilde{u} = u_e + u_\tau \cos \beta_w \left(\frac{1}{\kappa} \ln \eta - \frac{2}{\kappa} \Pi \right), \quad (20.30)$$

$$\lim_{\eta \rightarrow 0} \tilde{w} = u_e \tan \beta_w + u_\tau \sin \beta_w \left(\frac{1}{\kappa} \ln \eta - \frac{2}{\kappa} \Pi \right) \quad (20.31)$$

with $\eta = y / \delta$.

Matching the two velocity components then yields

$$\frac{1}{\gamma \cos \beta_w} = \frac{u_e}{u_\tau \cos \beta_w} = \frac{1}{\kappa} \ln \frac{u_\tau \delta}{\nu} + C^+ + \frac{2H}{\kappa}; \quad (20.32)$$

an extension to Eq. (18.73).

Both velocity components therefore obey a logarithmic distribution in the overlap layer. The \tilde{u} component of the boundary layer behaves very similarly to the velocity of plane boundary layers. The \tilde{w} component has the same order of magnitude as the defect velocity, namely $O(u_\tau/u_e)$. With Eq. (20.31) this then yields $\tan \beta_w = O(u_\tau/u_e)$. The skew angle β_w therefore decreases with increasing Reynolds number, and vanishes, as would be expected, in the inviscid limit.

At high Reynolds numbers, Eqs. (20.30) and (20.31) can be used as wall functions and therefore as boundary conditions for the boundary-layer equations.

At moderately large Reynolds numbers, higher order effects can cause the pressure gradient $\partial p_e / \partial z$ to act in the viscous wall layer and already there to lead to a skewed velocity profile, as A.T. Degani et al. (1993) have shown. The near wall similarity of three-dimensional turbulent boundary layers has been investigated by M.S. Ölçmen; R.L. Simpson (1992).

As for laminar three-dimensional boundary layers, cf. Sect. 12.2.5, turbulent boundary layers can also be computed in *symmetry planes* independently of the rest of the boundary layer, see A.T. Degani et al. (1992), W.R. Pauley et al. (1993).

If u_e satisfies a power law $\sim x^m$, similar solutions are found for the defect velocity. This is an extension to the *equilibrium boundary layers* for plane flows, cf. A.T. Degani et al. (1993). In the special case $m = -1$, we obtain similar solutions for the entire velocity profile, including the viscous wall layer, cf. M.A. Takullu; J.C. Williams III (1985).

20.2.2 Computation Methods

Summaries of the computation methods for three-dimensional turbulent boundary layers have been presented by J.F. Nash; V.C. Patel (1972), H.H. Fernholz; E. Krause (1982), J. Cousteix (1986), AGARD-R-741 (1987), D.A. Humphreys; J.P.F. Lindhout (1988), B. van den Berg et al. (1988), AGARD-AR-255 (1990). Here the different methods are generally compared to selected experiments.

D. Arnal (1987) has reported on the ways of determining the laminar-turbulent transition for three-dimensional boundary layers.

The separation of three-dimensional boundary layers is considerably more complicated than in the plane case, cf. AGARD-AR-255 (1990). One distinguishes between *open* and *closed* separation. The latter leads to closed regions of separation (“separation bubbles”), such as those which appear behind a shock wave at swept-back wings. In these cases the boundary-layer calculation must be carried out using an inverse formalism, cf. Sect. 18.5.2, and the

interaction with the outer flow must be taken into account, cf. J.C. Wai et al. (1986). Open separation occurs when the separated boundary layer forms rolled up free shear layers. This can occur at bodies of revolution at large angles of attack. In these cases, the boundary-layer concept breaks down, since the “free stream” can no longer be computed as an inviscid flow.

The methods will again be divided into integral methods and field methods.

Integral methods

The integral relations are used here as a basis, see for example P.D. Smith (1982). The profile families of plane boundary layers are generally used for the \tilde{u} component. The \tilde{w} component can be determined from these using an analytical representation for the hodographs, as in Fig. 20.5.

There are numerous integral methods for three-dimensional turbulent boundary layers in the literature, such as those by: D.F. Myring (1970), P.D. Smith (1974), P.D. Smith (1982), J. Cousteix (1974), T. Okuno (1976), H.-W. Stock (1978), J.-C. Le Balleur; M. Lazareff (1985).

Field methods

D.A. Humphreys; J.P.F. Lindhout (1988) have presented an overview of the different field methods. Here are some examples:

1. algebraic turbulence models

T. Cebeci (1987), T.K. Fannelöp; D.A. Humphreys (1975),
J.P.F. Lindhout et al. (1979), L.J. Johnston (1988)

2. $k-\varepsilon$ model

A.K. Rastogi; W. Rodi (1978)

3. Reynolds stress models

J.C. Rotta (1979), M.M. Gibson et al. (1981)

In turbulence models, instead of the eddy viscosity from Eq. (20.13), an *anisotropic eddy viscosity* is frequently used, where the ν_t values are different for each of the two coordinate directions. J.C. Rotta (1980b) has described a model with anisotropic eddy viscosity, tested by M.S. Ölçmen; R.L. Simpson (1993), cf. also S.F. Radwan; S.G. Lekondis (1986).

Interactive boundary-layer theory

The interactive boundary-layer theory is based on the solutions of the reduced Navier-Stokes equations and involves Euler equations and boundary-layer equations. The numerical solutions of inviscid and viscous flow equations are coupled by an interaction law. For this iteration process the prediction of transition and the modelling of transitional turbulent flow as well as the prediction of flow separation and the development of separated

flow are required. The interactive boundary-layer theory is not an asymptotic theory, because for each given Reynolds number a characteristic solution has to be found. The books by T. Cebeci (1999) and E.H. Hirschel et al. (2014) present good descriptions of the interactive boundary-layer theory.

20.2.3 Examples

Yawing wings. This test case has been investigated many times, cf. B. van den Berg et al. (1988). In spite of the use of inverse methods, the turbulence models frequently have to be modified close to the separation line in order to achieve good agreement with experiments, cf. L.J. Johnston (1988), J.-C. Le Balleur (1984).

Swept-back wings. There are numerous worked examples at hand, including those by M. Lazareff; J.-C. Le Balleur (1983), T. Cebeci et al. (1986), J.C. Wai et al. (1986), AGARD-AR-255 (1990), p. 125

Plates with imposed pressure field. Three-dimensional boundary layers occur when a cylindrical body (circular cylinder, wing), cf. H.G. Hornung; P.N. Joubert (1963) and B. van den Berg et al. (1988), or a guiding surface is set at right angles to a plate, see the example by W.R. Schwarz; P. Bradshaw (1993). Frequently such configurations are used to test turbulence models.

Slender bodies. Because of their practical importance, bodies of revolution at moderate angles of attack are frequently investigated, particularly slender ellipsoids of revolution: cf. V.C. Patel; D.H. Choi (1980), D. Barberis (1986), S.F. Radwan; S.G. Lekondis (1986), AGARD-AR-255 (1990), pp. 39,77,130, R. Stäger (1993).

If these bodies of revolution at an angle of attack also rotate about their axes, a side force occurs. This is called the *Magnus effect*; it is a pure boundary-layer effect due to the asymmetric displacement thickness, cf. W.B. Sturek et al. (1978).

We also mention the investigations on three-dimensional hulls of airplanes, cf. E.H. Hirschel (1982), and ships, cf. J. Piquet; M. Visonneau (1986) and I. Tanaka (1988).

Motor vehicles. Boundary-layer theory can also be used to great success in the aerodynamics of motor vehicles, cf. K. Gersten; H.-D. Papenfuß (1992) and H.-D. Papenfuß (1997). In order to compute the outer flow, the displacement action of the wake must be taken into account. However, this does not require great precision, since the action of the wake on the pressure distribution of the vehicle drops greatly as one moves away from the vehicle. As P.G. Dilgen (1995) has shown, the coefficients for drag and lift can be computed with good accuracy. This method is eminently suitable in optimizing aerodynamically favourable shapes, where the three-dimensional boundary layer should separate nowhere except at the sharp edge at the back.

Rotating systems. Boundary layers in rotating systems are very important in discussing propellers, helicopter rotors and turbomachinery, cf. Y. Senoo (1982). The rotation here is also important for turbulence modelling, cf. J.M. Galmes; B. Lakshminarayana (1984) and B. Lakshminarayana (1986).

21. Unsteady Turbulent Boundary Layers

21.1 Averaging and Boundary-Layer Equations

Turbulent flows are by definition unsteady, and so we need to explain what is meant by “unsteady turbulent flows”. Up until now, turbulent flows were decomposed into the flow obtained after time averaging (which was therefore time independent), and the fluctuations which varied in time. Now, the “mean” motion is also dependent on the time. It is generally made up of a time independent part and a time dependent *ordered* part.

The instantaneous value of the velocity component in the x direction can therefore be written as

$$u(\vec{x}, t) = \bar{u}(\vec{x}) + \tilde{u}(\vec{x}, t) + u'(\vec{x}, t). \quad (21.1)$$

Here \bar{u} and \tilde{u} form the “mean” motion, and u' is again the disordered turbulent fluctuation.¹

Turbulent flows with time dependent “mean” motion occur very frequently in practice. All start-up and shut-down processes belong to this group, as do the transitions from one steady flow to another. These are called *transient flows*. In addition to these we have the *periodic flows*. Examples of periodic flows are the flows at helicopter rotor blades, in the blades of turbomachines and at oscillating airfoils.

Even if the free stream is steady, unsteady processes can take place in the flow field. This frequently occurs in so-called *pressure-induced boundary-layer separation*. Examples of this are the periodic wakes behind blunt bodies (such as circular cylinders) or at airfoils at large angles of attack (“*dynamic stall*”), and the shock oscillations which occur at airfoils in the region close to the speed of sound and are due to shock-induced oscillations, cf. J.-C. Le Balleur; P. Girodroux-Lavigne (1986).

The quantities of the “mean” motion are determined by *ensemble averaging*. The same experiment is carried out on the flow N times, and each time the velocity $u_i(\vec{x}, t)$, $i = 0, 1, 2, \dots, N$ is measured.

¹ Quantities denoted with a tilde \sim here should not be confused with the mass-averaged quantities in the two previous chapters.

The *ensemble average* is then:

$$\langle u(\vec{x}, t) \rangle = \bar{u}(\vec{x}) + \tilde{u}(\vec{x}, t) = \frac{1}{N} \sum_{i=0}^N u_i(\vec{x}, t). \quad (21.2)$$

If the flow is periodic, the $u_i(\vec{x}, t)$ are measured at the same phase within the period and then averaged. This is called *phase averaging*:

$$\langle u(\vec{x}, t) \rangle = \frac{1}{N} \sum_{i=0}^N u(\vec{x}, t + i\tau), \quad (21.3)$$

if τ is the length of the period.

The turbulent fluctuation is then obtained from Eqs. (21.1) and (21.2) as

$$u'(\vec{x}, t) = u(\vec{x}, t) - \langle u(\vec{x}, t) \rangle. \quad (21.4)$$

The usual time average, cf. Eq. (16.2) is still

$$\bar{u}(\vec{x}) = \lim_{t_1 \rightarrow \infty} \frac{1}{t_1} \int_{t_0}^{t_0+t_1} u(\vec{x}, t) dt. \quad (21.5)$$

The following relations hold

$$\langle u' \rangle = 0, \quad \bar{\tilde{u}} = 0, \quad \bar{u'} = 0, \quad \overline{\langle u \rangle} = \bar{u} = \langle \bar{u} \rangle, \quad (21.6)$$

$$\langle \tilde{u}\tilde{v} \rangle = \tilde{u}\langle v \rangle, \quad \langle \bar{u}\bar{v} \rangle = \bar{u}\langle v \rangle, \quad \overline{\langle \tilde{u}\tilde{v}' \rangle} = \overline{\langle \tilde{u}\tilde{v}' \rangle} = 0. \quad (21.7)$$

Balance laws can be written down for each of the three different motions into which unsteady boundary-layer flow can be divided up corresponding to Eq. (21.1). However these balance laws are coupled to one another, cf. D.P. Telionis (1981), p. 226.

The boundary-layer equations for the *time-averaged* motion of incompressible two-dimensional flow read:

$$\frac{\partial \bar{u}}{\partial x} + \frac{\partial \bar{v}}{\partial y} = 0, \quad (21.8)$$

$$\bar{u} \frac{\partial \bar{u}}{\partial x} + \bar{v} \frac{\partial \bar{u}}{\partial y} = \bar{u}_e \frac{d\bar{u}_e}{dx} + \frac{\partial}{\partial y} \left(\nu \frac{\partial \bar{u}}{\partial y} - \bar{u}'\bar{v}' - \bar{u}\bar{v}' \right), \quad (21.9)$$

$$y = 0 : \quad \bar{u} = 0, \quad \bar{v} = 0, \quad (21.10)$$

$$y = \bar{\delta} : \quad \bar{u} = \bar{u}_e(x).$$

It can be seen from Eq. (21.9) that there are now *two* additional (apparent) shear stresses on the right hand side. The first one is due to the disordered turbulent fluctuation velocities and also appeared for steady flows. The second term, which is formed in a similar way, corresponds to the nonlinear influence of the time dependent ordered motion.

If we assume that the given outer flow $u_e(x, t)$ differs only slightly from its time-averaged value $\bar{u}_e(x)$, a perturbation calculation will show that the term $\bar{u}\bar{v}$ is small compared to $u'v'$, and therefore the flow is identical to the *steady* flow for $\bar{u}_e(x)$, cf. D.P. Telionis (1981), p. 228. Nevertheless locally strong unsteady viscous effects can exist, cf. L.W. Carr (1981a).

For the “mean” motion, we use

$$U = \bar{u} + \tilde{u}, \quad V = \bar{v} + \tilde{v}, \quad P = \bar{p} + \tilde{p} \quad (21.11)$$

to form the boundary-layer equations

$$\frac{\partial U}{\partial x} + \frac{\partial V}{\partial y} = 0, \quad (21.12)$$

$$\frac{\partial U}{\partial t} + U \frac{\partial U}{\partial x} + V \frac{\partial U}{\partial y} = \frac{\partial U_e}{\partial t} + U_e \frac{\partial U_e}{\partial x} + \frac{\partial}{\partial y} \left(\nu \frac{\partial U}{\partial y} + \frac{\tau_t}{\varrho} \right) \quad (21.13)$$

with

$$\tau_t = \langle u'v' \rangle \quad (21.14)$$

and the boundary conditions

$$\begin{aligned} y = 0 : \quad & U = 0, \quad V = 0, \\ y = \delta(x, t) : \quad & U = U_e(x, t). \end{aligned} \quad (21.15)$$

Apart from the additional term given in Eq. (21.14), these are formally the same as the boundary-layer equations for unsteady laminar boundary layers, cf. Eqs. (13.3) and (13.4), with $\varrho = \text{const}$, $j = 0$, $\alpha = 0$.

Again we need a turbulence model to be able to close the system of equations. However, in this model the interaction of the turbulent fluctuations and the time dependent “mean” motion must be taken into account.

Sometimes U , V and P are interpreted as time averages, whereby the time interval t_1 in Eq. (21.5) has to be chosen to be large enough to include all turbulent fluctuations, but still small enough to contain no effect from the transient, or periodic, part. However this assumes that the transient process occurs very slowly, or that the frequency of the oscillation is very small and lies outside the turbulent spectrum.

Frequently turbulence models from steady flows are used; these are then called *quasi-steady turbulence models*. The only difference from the steady equations is then the additional terms for the local accelerations $\partial U_e / \partial t$ and $\partial U / \partial t$. If the given outer velocity $u_e(x, t)$ varies only very slowly in time (small frequencies in periodic motion), the local acceleration can be neglected compared to the convective acceleration. In this case the flow is *quasi-steady*. At any instant in time t_0 it behaves just like the corresponding steady flow for the outer flow $u_e(x, t_0)$.

As already mentioned, the flow is also quasi-steady if the unsteady part of the outer velocity is very small. This is only true for periodic flows if the frequency of the outer flow is below the so-called *burst frequency* f_B . At this frequency, the eddy structures in the boundary layer begin to react to the forces from the outer flow. For a flat plate with oscillating outer flow, the burst velocity is $f_B = U/5\delta$, cf. K.N. Rao et al. (1971). Figure 21.1 is a frequency–amplitude diagram of the limit between quasi-steady boundary layers (shaded) and true unsteady boundary layers.

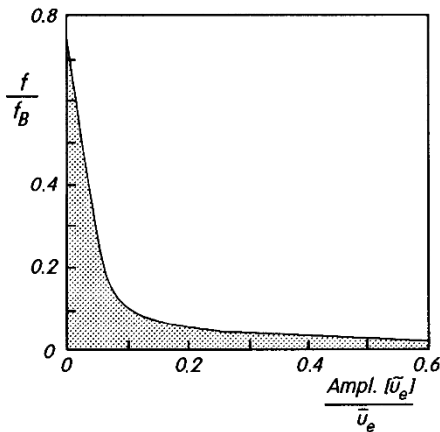


Fig. 21.1. Frequency–amplitude diagram for unsteady turbulent boundary layers, according to L.W. Carr (1981a). The boundary layer is quasi-steady in the shaded area. f_B : burst frequency

When unsteady effects do play a role, they are generally restricted to the viscous wall layer, while the outer region of the boundary layer remains widely unaffected, cf. L.W. Carr (1981a). J. Cousteix, R. Houdeville (1985) have shown that the unsteady effects are restricted to the viscous wall layer for $\sqrt{2\nu/\omega u_\tau}/\nu < 8$. A review of turbulence modeling for time-dependent flows has been given by C.G. Speziale (1998).

21.2 Computation Methods

Most practical applications are based on periodic flows. Again we differ between integral methods and field methods. The computational difficulty of the latter is dependent on the turbulence model used, whereby frequently, as already mentioned, quasi-steady turbulence models are used.

a) Integral methods

- J. Cousteix et al. (1981)
- A. Desopper (1981)
- A.A. Lyrio et al. (1981)
- J.-C. Le Balleur (1984)
- R. Houwink (1984)

b) Field methods

algebraic turbulence models

T. Cebeci; H.B. Keller (1972)

one-equation models

V.C. Patel; J.F. Nash (1975)

two-equation models (including low-Reynolds-number versions)

P. Justesen; P.R. Spalart (1990)

R.R. Mankbadi; A. Mobark (1991)

S. Fan et al. (1993)

Reynolds stress models

K. Hanjalić; N. Stosic (1983)

H. Ha Minh et al. (1989), low-Reynolds number version

Deviations between theoretical and experimental results are frequently due to inadequate modelling of the viscous wall layer, cf. S. Fan et al. (1993).

For details on numerical methods, see Sect. 23.3.

21.3 Examples

A summary of experimental data on unsteady turbulent boundary layers has been presented by L.W. Carr (1981a, 1981b). This deals mainly with flows past a flat plate (oscillating, with a vibrating flap or approached by a travelling wave), at airfoils and at cascades in turbomachinery.

Flat plate

J. Cousteix; R. Houdeville (1983) have carried out measurements of the unsteady turbulent boundary layers with the following outer flow velocity, see also J. Cousteix et al. (1981):

$$u_e(x, t) = u_0[1 + A(x) \sin\{\omega t + \varphi_e(x)\}] \quad (21.16)$$

with

$$u_0 = 16.8 \text{ m/s}, \quad f = 62 \text{ Hz}, \quad \omega = 2\pi f = 390/\text{s},$$

$$A(x) = 0.118 - 0.114(x - 0.047),$$

$$\varphi_e(x) = 1.55(x - 0.047)^2 + 0.116(x - 0.047),$$

where t is measured in seconds and x in meters. Figure 21.2 shows the displacement thickness δ_1 and the skin-friction coefficient c_f , both their amplitude and phase shift. For comparison, the theoretical results by S. Fan et al. (1993) are also depicted. The displacement thickness undergoes a slightly damped spatial *pseudo-periodicity*; according to J. Cousteix; R. Houdeville (1983), this follows from the combination of the turbulent convection in the outer region and the externally enforced oscillation. The skin-friction coefficient, which essentially depends on the

processes in the viscous wall layer, is also described quite well by the theory. As in the laminar case, cf. Sect. 13.3.2, the skin-friction coefficient leads the outer velocity, and for large values of $\omega x/u_0$, a phase shift of 45° is clearly reached.

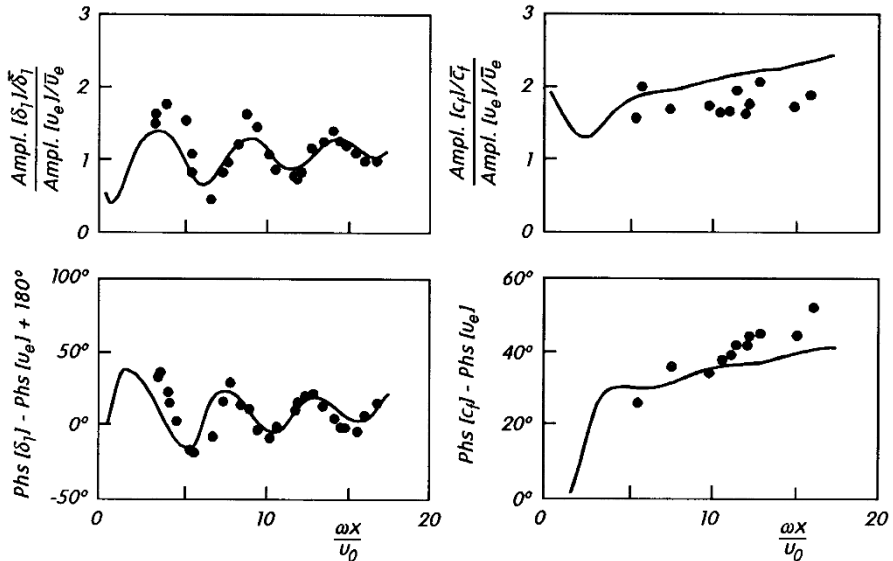


Fig. 21.2. Displacement thickness δ_1 and skin-friction coefficient c_f : amplitude and phase shift of each, for the outer velocity corresponding to Eq. (21.16), according to S. Fan et al. (1993)

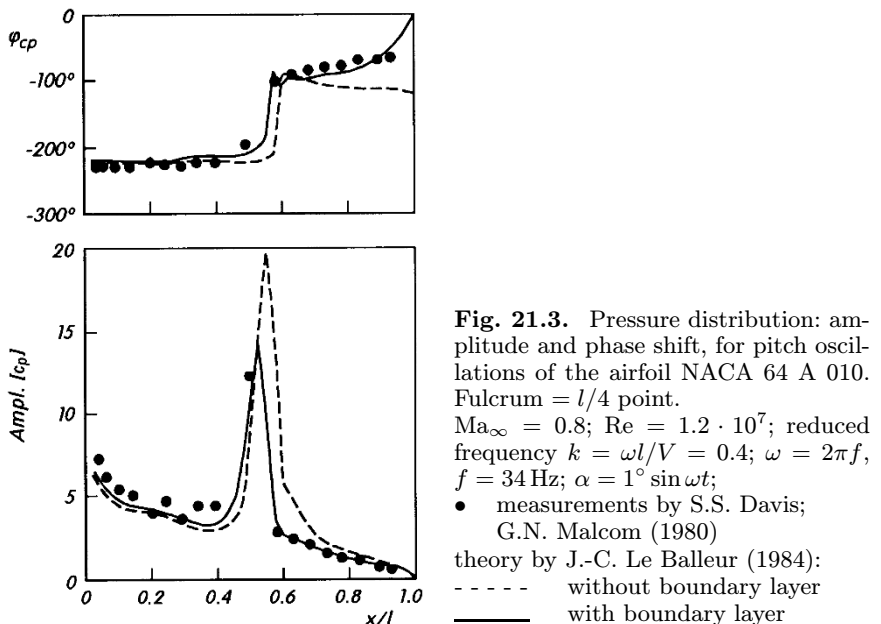
Oscillating airfoil

Figure 21.3 shows the comparison between theory and experiment for the airfoil NACA 64 A 010 which carries out pitch oscillations about the $l/4$ point. The amplitude and the phase shift for the pressure distribution are shown. The effect of the boundary layer can be seen from the difference between the two theoretical curves. If the boundary layer is taken into account, the comparison between theory and experiment is greatly improved.

Unsteady separation

Shock-induced separation, where the separation region is spatially restricted, can occur if airfoils carry out pitch oscillations in regimes close to the speed of sound. This can be described very well by boundary-layer calculations (in interference with the outer flow), as, for example, J.-C. Le Balleur; P. Girodroux-Lavigne (1986) have shown. The self-induced oscillating flow at a transonic airfoil in a steady flow is also computed in this work. Such flows tend to occur when the shock-induced separation and a separation close to the trailing edge interfere with one another.

If *massive separation* occurs, and with it the formation of large eddies in the wake, as for example at a circular cylinder, the flow field can no longer be divided into an inviscid outer flow and the frictional boundary layer. The complete Navier-



Stokes equations must now be solved numerically, cf. for example G.S. Deiwert; H.E. Bailey (1984). If an airfoil carries out pitch oscillations, *deep dynamic stall* then occurs. On the other hand, *light dynamic stall* can indeed be described using the boundary-layer concept, cf. for example W. Geißler (1993).

22. Turbulent Free Shear Flows

22.1 Remark

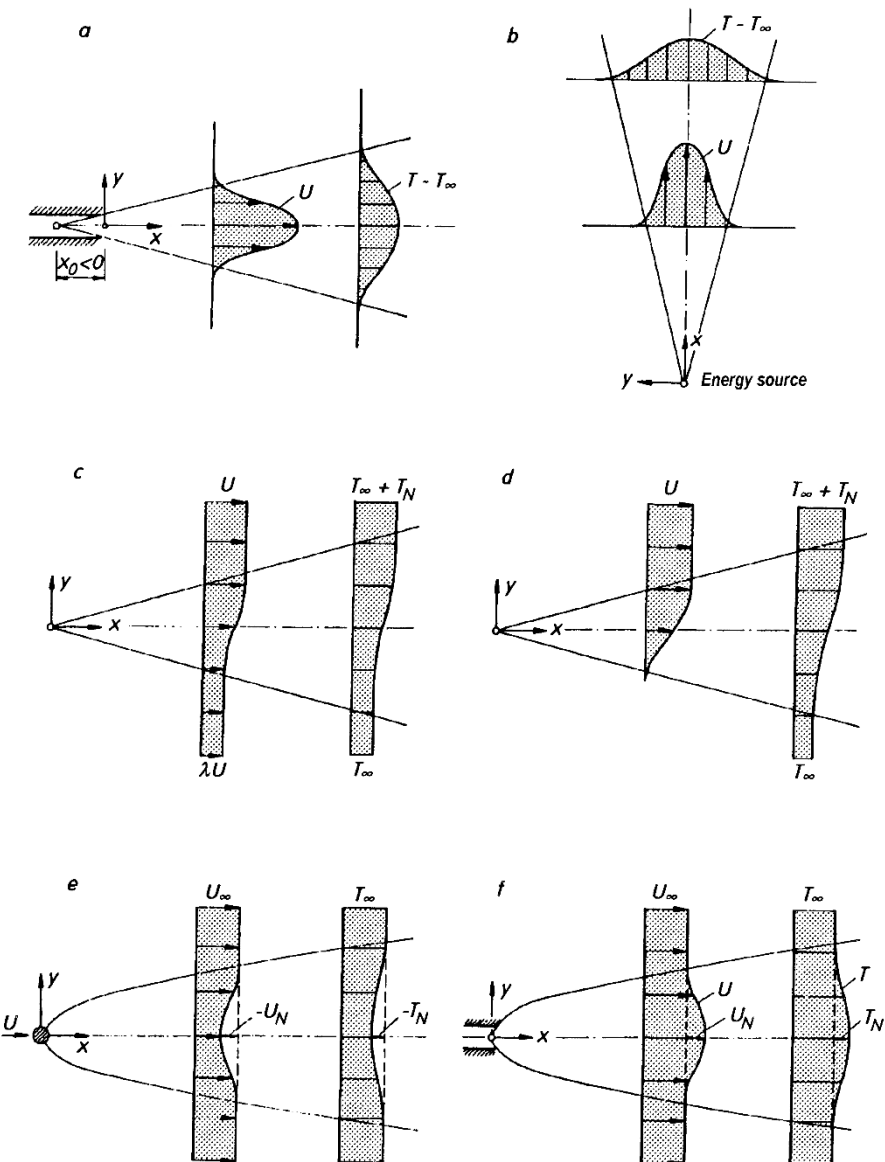
Turbulent *free shear flows* occur if there are no walls directly at the flow. Figure 22.1 shows some examples: a free jet, a buoyant jet, a mixing layer with the free jet–boundary flow as a special case, and a wake flow. The corresponding laminar flows are treated in Sects. 7.2, 7.5, 10.5.4 and 12.1.5.

The momentum transfer directly at the wall for turbulent flows also takes place via viscosity (viscous wall layer). Since there are no walls present in free shear flows, the viscosity effects can be neglected. This is because the turbulent friction is always much greater than the viscous friction. The viscosity is only important at the edges when we consider the mean motion of turbulent free shear layers. Here the situation is similar to that at the outer edge of turbulent boundary layers, as discussed in Sect. 18.1 (viscous superlayers). The thicknesses of the viscous superlayers are of the order of magnitude $O(\text{Re}^{-3/4})$ and therefore do not have to be taken into account for large Reynolds numbers.

It is usual in discussing free shear flows to use the boundary–layer equations (at large Reynolds numbers, without viscous shear stresses) instead of the Navier–Stokes equations. The reason for this is experimental: free shear flows are *slender*, i.e. the region of space in which a solution is sought does not extend far in a transversal direction. They are therefore called *free boundary layers* or *free shear layers*. The question of why turbulent free shear flows are slender has not yet been conclusively answered, cf. W. Schneider (1991) and K. Gersten; H. Herwig (1992), p. 725.

The boundary–layer equations without the friction terms are therefore used to compute turbulent free shear layers. For plane flows (without buoyancy terms), these are Eqs. (16.34) to (16.36). Just as for wall boundary layers, depending on the turbulence model there is a continuous or discontinuous description of the outer edge of free shear layers, cf. Sect. 18.1. If constant eddy viscosity is used, a continuous transition to the outer region is found, whereas using the mixing length yields a discrete edge of the free shear layer.

Algebraic turbulence models are not complete for free shear layers, since a slenderness parameter α (still to be defined) has to be fitted to the experiments. Overviews on complete turbulence models (e.g. two–equation models)

**Fig. 22.1.** Examples of turbulent free shear flows

(a): free jet (momentum jet)

(b): buoyant jet

(c): mixing layer

(d): jet boundary

(e): wake

(f): free jet in parallel flow

for turbulent free shear layers have been presented by W. Rodi (1972) and B.E. Launder et al. (1973). The state of research in the year 1972 is detailed in the conference proceedings NASA SP-321 (1973).

An asymptotically correct treatment of turbulent free shear layers at high Reynolds numbers again leads to a layered flow structure. Details are to be found in the work by W. Schneider; K. Mörwald (1987), K. Mörwald (1988), W. Schneider (1991).

22.2 Equations for Plane Free Shear Layers

No pressure forces appear in the examples in Fig. 22.1. Therefore in what follows we will only treat free turbulent shear flows at constant pressure. The equations read:

$$\frac{\partial \bar{u}}{\partial x} + \frac{\partial \bar{v}}{\partial y} = 0, \quad (22.1)$$

$$\varrho \left(\bar{u} \frac{\partial \bar{u}}{\partial x} + \bar{v} \frac{\partial \bar{u}}{\partial y} \right) = \frac{\partial \tau_t}{\partial y}, \quad (22.2)$$

$$\varrho c_p \left(\bar{u} \frac{\partial \bar{T}}{\partial x} + \bar{v} \frac{\partial \bar{T}}{\partial y} \right) = - \frac{\partial q_t}{\partial y}, \quad (22.3)$$

cf. Eq. (16.34), (16.35) and (16.36). Equations (22.2) and (22.3) are simpler than the complete Navier–Stokes equations, because free shear layers are “slender” flows where the extension $\Delta = O(\alpha)$ in the transversal direction (y direction) is small compared to the extension $O(1)$ in the main flow direction (x direction). This slenderness condition also appeared for wall boundary layers and a posteriori justified the simplification of the fundamental equations to the boundary-layer equations.

The boundary conditions will be treated later for each example as it is met.

The flows shown in Fig. 22.1 are characterised by the fact that they lead to similar solutions. Therefore for these flows, the partial differential equations (22.1) to (22.3) reduce to ordinary differential equations.

We will first look at the simple turbulence models involving the concepts of eddy viscosity ν_t and constant turbulent Prandtl number Pr_t . Then we obtain, cf. Eq. (17.63) and (17.76)

$$\tau_t = \varrho \nu_t \frac{\partial \bar{u}}{\partial y}, \quad q_t = - \frac{\varrho c_p \nu_t}{\text{Pr}_t} \frac{\partial \bar{T}}{\partial y}. \quad (22.4)$$

With the trial solutions

$$\bar{u} = U_\infty + U_N(x)f'(\eta), \quad (22.5)$$

$$\bar{v} = - \frac{d(\Delta U_N)}{dx} f(\eta) + \frac{d\Delta}{dx} U_N \eta f'(\eta), \quad (22.6)$$

$$\bar{T} = T_\infty + T_N(x)g'(\eta), \quad (22.7)$$

$$\eta = \frac{y}{\Delta}, \quad (22.8)$$

Eq. (22.1) to (22.4) yield the two differential equations

$$(U_\infty + U_N f') \Delta \frac{dU_N}{dx} f' - U_\infty U_N \frac{d\Delta}{dx} \eta f'' - U_N \frac{d(U_N \Delta)}{dx} f f'' \\ = \frac{U_N}{\Delta} (\nu_t f''), \quad (22.9)$$

$$(U_\infty + U_N f') \Delta \frac{dT_N}{dx} g' - U_\infty T_N \frac{d\Delta}{dx} \eta g'' - T_N \frac{d(U_N \Delta)}{dx} f g'' \\ = \frac{T_N}{\Pr_t \Delta} (\nu_t g''). \quad (22.10)$$

The dashes imply differentiation with respect to η .

We first assume that the eddy viscosity ν_t is independent of η . Dimensional analysis then yields the ansatz

$$\nu_t(x) = \alpha |U_N(x)| \Delta(x). \quad (22.11)$$

This trial solution is simultaneously the defining equation for the *slenderness parameter* α , which can be interpreted as the inverse of a characteristic *turbulent Reynolds number*

$$\text{Re}_t = \frac{|U_N| \Delta}{\nu_t} = \frac{1}{\alpha}. \quad (22.12)$$

The numerical value of α depends on the choice of $U_N(x)$ and $\Delta(x)$ and is therefore different for each flow.

Using the power trial solutions

$$U_N(x) = B(x - x_0)^m, \quad (22.13)$$

$$T_N(x) = B_\theta(x - x_0)^n$$

the two following groups of flows reduce to ordinary differential equations, i.e. to self-similar solutions:

(1) $U_\infty = 0$:

$$\Delta = \alpha a(x - x_0) \quad (22.14)$$

$$\frac{1}{a} f''' + (m+1)f f'' - m f'^2 = 0, \quad (22.15)$$

$$\frac{1}{a \Pr_t} g''' + (m+1)f g'' - n f' g' = 0. \quad (22.16)$$

These flows include examples a to d in Fig. 22.1.

(2) $U_\infty \neq 0$, small perturbations of the outer flow:

$$|U_N| \ll U_\infty, \quad \Delta = \alpha a(x - x_0)^{m+1}, \quad (22.17)$$

$$\frac{|B|}{U_\infty a} f''' + (m+1)\eta f'' - mf' = 0, \quad (22.18)$$

$$\frac{|B|}{U_\infty a \Pr_t} g''' + (m+1)\eta g'' - ng' = 0. \quad (22.19)$$

The flows include the examples e and f in Fig. 22.1. In contrast to Eq. (22.15), Eq. (22.18) is linear, since this is a regular perturbation calculation with $U_N/U_\infty \rightarrow 0$.

The condition of similarity yields the form of the width scale $\Delta(x)$, where α now appears clearly as the slenderness parameter. In what follows, the factor $a = O(1)$ will be chosen so that the differential equations have coefficients which are as simple as possible.

The dependence of the functions $\Delta(x)$, $U_N(x)$, $\nu_t(x)$ and $T_N(x)$ on $x - x_0$ for the eight examples considered is summarised in Table 22.1; x_0 denotes the position of the *virtual origin* of the flow, cf. Fig. 22.1a. If ν_t also depends on y (or r), the value of ν_t on the axis ($y = 0$, or $r = 0$) is implied. The table also contains information on the velocity $v_e(x)$.

For completeness, we also present the equations for the turbulent kinetic energy

$$\bar{u} \frac{\partial k}{\partial x} + \bar{v} \frac{\partial k}{\partial y} = \frac{\partial}{\partial y} \left(\frac{\nu_t}{\Pr_k} \frac{\partial k}{\partial y} \right) + \frac{\tau_t}{\varrho} \frac{\partial \bar{u}}{\partial y} - \varepsilon = 0 \quad (22.20)$$

and for the variance of the temperature fluctuations

$$\bar{u} \frac{\partial k_\theta}{\partial x} + \bar{v} \frac{\partial k_\theta}{\partial y} = \frac{\partial}{\partial y} \left(\frac{a_t}{\Pr_{k\theta}} \frac{\partial k_\theta}{\partial y} \right) - \varepsilon_\theta = 0. \quad (22.21)$$

Here the usual turbulence models were used for the diffusion terms.

The extension of Eq. (22.2) to the case where buoyancy forces due to the effects of gravity are taken into account will be treated in Sect. 22.7.

The equations for the turbulent quantities are given by W. Rodi (1975) within the framework of an overview of experimental results. Further experimental results have been given by A.A. Townsend (1976) p. 188 and J.O. Hinze (1975) p. 483.

Table 22.1. Dependence of the most important characteristic values of free turbulent shear layers on the x coordinate.
The quantities $\ell(x)$ and $y_e(x)$ have the same x dependence as $\Delta(x)$

	$\Delta(x)$ $\sim (x - x_0)^a$	$U_N(x)$ $\sim (x - x_0)^a$	$\nu_t(x)$ $\sim (x - x_0)^a$	$T_N(x)$ $\sim (x - x_0)^a$	$v_e(x)$ $\sim (x - x_0)^a$	$y_{0.5u}$ $= A(x - x_0)^a$	$y_{0.5T}$ $= A(x - x_0)^a$
	a	a	a	a	a	A	A
plane free jet	1	$-\frac{1}{2}$	$\frac{1}{2}$	$-\frac{1}{2}$	$-\frac{1}{2}$	0.11	0.14
axisymmetric free jet	1	-1	0	-1	-1	0.09	0.11
plane buoyant jet	1	0	1	-1	0	0.12	0.13
axisymmetric buoyant jet	1	$-\frac{1}{3}$	$\frac{2}{3}$	$-\frac{5}{3}$	$-\frac{1}{3}$	0.11	0.10
plane mixing layer	1	0	1	0	0		
axisymmetric mixing layer	1	0	1	0	0		
plane wake (jet)	$\frac{1}{2}$	$-\frac{1}{2}$	0	$-\frac{1}{2}$	-1	$0.2l\sqrt{c_D}$	$\frac{1}{2}$
axisymmetric wake (jet)	$\frac{1}{3}$	$-\frac{2}{3}$	$-\frac{1}{3}$	$-\frac{2}{3}$	$-\frac{1}{3}$	$0.6lc_D^{1/3}$	$\frac{1}{3}$
						$0.84lc_D^{1/3}$	$\frac{1}{3}$

Note (Mixing length)

If, instead of the eddy viscosity ν_t from Eq. (22.4), we use the mixing length $\ell(x)$, from

$$\tau_t = \varrho \ell^2 \frac{\partial \bar{u}}{\partial y} \left| \frac{\partial \bar{u}}{\partial y} \right| \quad (22.22)$$

we obtain the relation

$$\nu_t = \ell^2 \left| \frac{\partial \bar{u}}{\partial y} \right| = \frac{\ell^2(x)}{\Delta(x)} |U_N(x) f''(\eta)|. \quad (22.23)$$

The eight examples given have all been computed using this model. In each case, a mixing length $\ell(x)$ which is independent of η was assumed. As can be seen from Eq. (22.23), this is not the same as assuming that ν_t is independent of η . The two algebraic models (ν_t and $\ell(x)$) therefore differ in their treatment of the transverse direction.

When written in terms of the mixing length, the right hand side of Eq. (22.9) reads $\ell^2 U_N^2(f'^2)' / \Delta^2$, while the right hand side of Eq. (22.10) is then $T_N \ell^2 U_N(f''g'')' / (\Pr_t \Delta^2)$. Equations (22.11) and (22.23) yield

$$\ell(x) = \sqrt{\frac{\alpha}{f''(0)}} \Delta(x), \quad (22.24)$$

if α in Eq. (22.11) is defined by ν_t on the axis. The x dependence of $\ell(x)$ and $y_e(x)$ corresponds to that of $\Delta(x)$, cf. Table 22.1.

We emphasise that the solutions of these differential equations is that the solutions already satisfy the conditions at the outer edge at *discrete* values $\eta = \eta_e$. The transition to the outer region at rest or to the outer flow does therefore not take place continuously, but rather “abruptly” at a discrete edge line. This edge line $y = y_e$ divides the turbulent from the non-turbulent flow.

The discontinuities in the higher derivatives of the velocity distributions at the edge are “compensated” by the viscosity effects in the superlayer. If the mixing length ℓ is used, singularities also appear at positions where the velocity has a maximum or minimum (on the axis for jets and wakes). If $\ell(x)$ is independent of η , the velocity close to the axis has the form $\bar{u}(x, y) = \bar{u}(x, 0) + A(x) y^{3/2}$, i.e. $\partial^2 \bar{u} / \partial y^2$ becomes infinite on the axis. In a regular velocity distribution, $\ell(x, y)$ would have to behave like $1/\sqrt{y}$ as $y \rightarrow 0$. Therefore the mixing length is unsuitable as a turbulence model close to the axis. D.H. Rudy; D.M. Bushnell (1973) have presented an overview.

22.3 Plane Free Jet

22.3.1 Global Balances

We consider a plane jet as in Fig. 22.1a in surroundings at rest whose temperature differs from the surrounding temperature. Noting Eq. (22.1), we integrate Eq. (22.2) and (22.3) over the cross-section of the jet, and obtain the global balances

$$K = \int_{-\infty}^{+\infty} \bar{u}^2 dy = U_N^2(x) \Delta(x) \int_{-\infty}^{+\infty} f'^2 d\eta = \text{const}, \quad (22.25)$$

$$\begin{aligned}
E_T &= \frac{\dot{Q}}{\varrho c_p b} = \int_{-\infty}^{+\infty} \bar{u}(\bar{T} - T_\infty) dy \\
&= U_N(x)T_N(x)\Delta(x) \int_{-\infty}^{+\infty} f'g' d\eta = \text{const.}
\end{aligned} \tag{22.26}$$

The momentum (because the density is absent, K is called the *kinematic momentum*) and the thermal energy are independent of the length along the jet x . These are the two characteristic parameters of a (non-isothermal) free jet.

In free jet flow the velocity and temperature distributions change in the direction of flow. The distributions are almost homogeneous at the nozzle outlet and then assume a bell shape further downstream.

The flow processes close to the nozzle outlet are particularly simple, in the so-called *near field*, and in the *far field* very far downstream. We will now treat these two regimes separately.

22.3.2 Far Field

It is to be expected that very far downstream the effect of the dimension of the nozzle dies away and, since a length scale is no longer at hand, similar solutions occur. Inserting the trial solutions from Eq. (22.13) for $U_N(x)$ and $T_N(x)$ into the conditions (22.25) and (22.26), we obtain the values $m = n = -1/2$. With the choice $a = 4$, the differential equations (22.15) and (22.16) read

$$f''' + 2(f f')' = 0, \tag{22.27}$$

$$\frac{1}{Pr_t} g''' + 2(f g')' = 0 \tag{22.28}$$

with the boundary conditions

$$\eta = 0 : \quad f = 0, \quad g = 0 \tag{22.29}$$

$$\eta \rightarrow \pm\infty : \quad f' = 0, \quad g' = 0.$$

As well as the trivial solutions $f = 0, g = 0$, there are also so-called *eigen-solutions*. They are so named because Eq. (22.15) and (22.16) with the boundary conditions (22.29) only have non-trivial solutions for the *eigenvalues* $m = -1/2$ and $n = -1/2$. They read

$$f(\eta) = \tanh \eta \tag{22.30}$$

$$f'(\eta) = 1 - \tanh^2 \eta, \tag{22.31}$$

$$g'(\eta) = [f'(\eta)]^{Pr_t}. \tag{22.32}$$

Therefore $U_N(x)$ and $T_N(x)$ are the maximum values on the symmetry line. Note that the same solutions are found for laminar free jets, although the functions $\Delta(x)$, $U_N(x)$ and $T_N(x)$ are different, cf. Sect. 7.2.6.

A measure of the jet width is the *half-value width*, i.e. the local distance of the points with half the maximum velocity.

The half-value widths are found to be

$$y_{0.5u} = 0.881\Delta = 0.881 \cdot 4\alpha(x - x_0), \quad (22.33)$$

$$y_{0.5T} = \Delta \operatorname{arctanh} \sqrt{1 - (0.5)^{1/\Pr_t}}. \quad (22.34)$$

Here x_0 corresponds to the virtual origin which in general is not the same as the position of the nozzle outlet, cf. Fig. 22.1a.

Measurements have yielded

$$y_{0.5u} = 0.11(x - x_0), \quad (22.35)$$

$$y_{0.5T} = 1.27 y_{0.5u} = 0.14(x - x_0). \quad (22.36)$$

If the turbulence model for ν_t according to Eq. (22.11) is used, we obtain $\alpha = 0.033$ and $\Pr_t = 0.84$.

The width of a jet grows linearly with the length along the jet, independently of the momentum and the thermal energy of the jet. The straight lines on which the half values lie form the angles 6.6° and 8.5° with the symmetry line for all plane free jets. Therefore the temperature field extends about 30% further sideways than the velocity field.

The conditions (22.25) and (22.26) yield the following formulae for the maximum values of the velocity and temperature with $\alpha = 0.033$:

$$\bar{u}_{\max}(x) = U_N(x) = \sqrt{\frac{3K}{4\Delta}} = \frac{1}{4} \sqrt{\frac{3K}{\alpha(x - x_0)}} = 2.4 \sqrt{\frac{K}{x - x_0}}, \quad (22.37)$$

$$\bar{T}_{\max}(x) - T_\infty = T_N(x) = 2.6 \frac{E_T}{\sqrt{K(x - x_0)}}. \quad (22.38)$$

These values decrease with distance along the jet. If we form the volume flux $Q_b(x)$ and the kinetic energy of the mean motion $E(x)$ (referred to the density), we obtain

$$Q_b(x) = \int_{-\infty}^{+\infty} \bar{u} dy = U_N \Delta \int_{-\infty}^{+\infty} f' d\eta = 2U_N \Delta = 0.63 \sqrt{K(x - x_0)}, \quad (22.39)$$

$$E(x) = \frac{1}{2} \int_{-\infty}^{+\infty} \bar{u}^3 dy = \frac{U_N^3 \Delta}{2} \int_{-\infty}^{+\infty} f'^3 d\eta = 0.48 \sqrt{\frac{K^3}{x - x_0}}. \quad (22.40)$$

The increase of the volume flux with the distance along the jet is particularly worth noting. It is based on an important action of the turbulent fluctuations called the *turbulent mixing*. Because of the turbulent fluctuations on the edge of the jet, there is a sideways exchange of momentum with which ever larger regions of the surroundings which are initially at rest get caught up and carried along. This *dragging action* of the jet is the origin of the *entrainment* of the fluid at rest in the surroundings; compare also Sect. 18.1.1. The entrainment is exploited by the *water jet pump*.

The v component of the velocity therefore does not vanish at the edges of the jet. According to Eqs. (22.6) and (22.30) with $\alpha = 0.033$, we obtain

$$\pm \bar{v}(y = \mp\infty) = v_e(x) = 0.87 \sqrt{\frac{K\alpha}{x - x_0}} = 0.16 \sqrt{\frac{K}{x - x_0}}. \quad (22.41)$$

The surroundings of the free jet are therefore not at rest, but, because of the entrainment from Eq. (22.41), a velocity field is *induced* around the jet. The reaction of this induced outer flow on the jet flow is a higher order effect which will be treated in Sect. 22.3.4.

The decrease of the kinetic energy of the mean motion corresponds to the turbulence production, as can be seen from the corresponding energy-integral equation

$$\frac{dE}{dx} = \int_{-\infty}^{+\infty} \frac{\bar{u}}{\varrho} \frac{\partial \tau_t}{\partial y} dy = - \int_{-\infty}^{+\infty} \frac{\tau_t}{\varrho} \frac{\partial \bar{u}}{\partial y} dy. \quad (22.42)$$

Equation (22.42) is found when Eq. (22.2) is multiplied by \bar{u} and integrated over the cross-section of the jet.

Integrating Eq. (22.20) over the cross-section of the jet yields the balance equation for the turbulent energy in the jet

$$\frac{d}{dx} \int_{-\infty}^{+\infty} k \bar{u} dy = \int_{-\infty}^{+\infty} \frac{\tau_t}{\varrho} \frac{\partial \bar{u}}{\partial y} dy - \int_{-\infty}^{+\infty} \varepsilon dy. \quad (22.43)$$

Therefore the change in the turbulent energy is the difference between turbulence production and dissipation.

Combining Eq. (22.42) and (22.43)

$$\frac{d}{dx} \int_{-\infty}^{+\infty} \left(\frac{\bar{u}^2}{2} + k \right) \bar{u} dy = - \int_{-\infty}^{+\infty} \varepsilon dy \quad (22.44)$$

states that the dissipation, i.e. the increase of internal energy, corresponds to the decrease of mechanical energy. The change in the temperature field due to dissipation is proportional to $\bar{E}_c = U_N^2 / (c_p T_\infty)$ and is in general small, so that this effect was neglected in Eq. (22.3).

Considering the orders of magnitude with respect to the slenderness parameter α ($y = O(\alpha)$, $\bar{u} = O(\alpha^{-1/2})$, $\nu_t = O(\alpha^{3/2})$, $\tau_t = O(1)$, $k = O(1)$), we find for the turbulent energy

$$\frac{k(x, y)}{U_N^2(x)} = O(\alpha), \quad (22.45)$$

cf. W. Schneider (1991), K. Mörwald (1988). Therefore the parameter α can also be interpreted as the ratio of the kinetic energy of the turbulent fluctuations to the kinetic energy of the mean motion. Equations (22.37) and (22.41) deliver $v_e/U_N = 2\alpha$, so that α is a measure of the *entrainment*.

We emphasise that α is a *fixed* constant for all free jets. In the turbulence model where ν_t is independent of y , α is the only empirical quantity necessary to describe the flow. If $U_N = \bar{u}_{\max}$ and $y_{0.5u}$ are both measured at two positions x_1 and x_2 , Eq. (22.33) and (22.37) deliver the parameter α as

$$\alpha = \left[\frac{y_{0.5u}}{3.524(x - x_0)} \right]_1 = \left[\frac{y_{0.5u}}{3.524(x - x_0)} \right]_2 \quad (22.46)$$

with

$$x_0 = \frac{(U_N^2 x)_1 - (U_N^2 x)_2}{U_{N1}^2 - U_{N2}^2}. \quad (22.47)$$

The agreement of the α values determined at the two positions is a measure of how well the self-similarity is satisfied.

Figure 22.2 shows the measured distributions of some characteristic values of a free jet and compares them with theoretical results. This figure shows that deviations appear at the edge of the jet when the model of constant eddy viscosity is used.

Better agreement can be achieved if, as for boundary layers, cf. Sect. 16.5.4, an intermittency function is introduced with which the eddy viscosity decreases to zero towards the edge of the jet, cf. K. Gersten; H. Herwig (1992) p. 737.

Furthermore, it can be seen from Fig. 22.2 that there is no proportionality between k and τ_t , so that the turbulence model by P. Bradshaw et al. (1967) cannot be applied, cf. Eq. (18.16) and (18.19).

The computation of plane free jets using the mixing length has been carried out by W. Tollmien (1926), while numerical values pertaining to this model have been presented by N. Rajaratnam (1976), p. 17. This model describes the velocity distribution at the outer edge somewhat better, cf. H. Schlichting (1982), p. 766.

The plane free jet has been computed by B.E. Launder et al. (1973) with the $k-\varepsilon$ model and by H. Vollmers; J.C. Rotta (1977) with the Rotta model. The agreement with measurements is good, since the constants of the models are determined by matching onto the measurements of free jet flow. E. Meineke (1977) has, along with other free shear flows, computed the free jet with a three-equation turbulence model by J.C. Rotta.

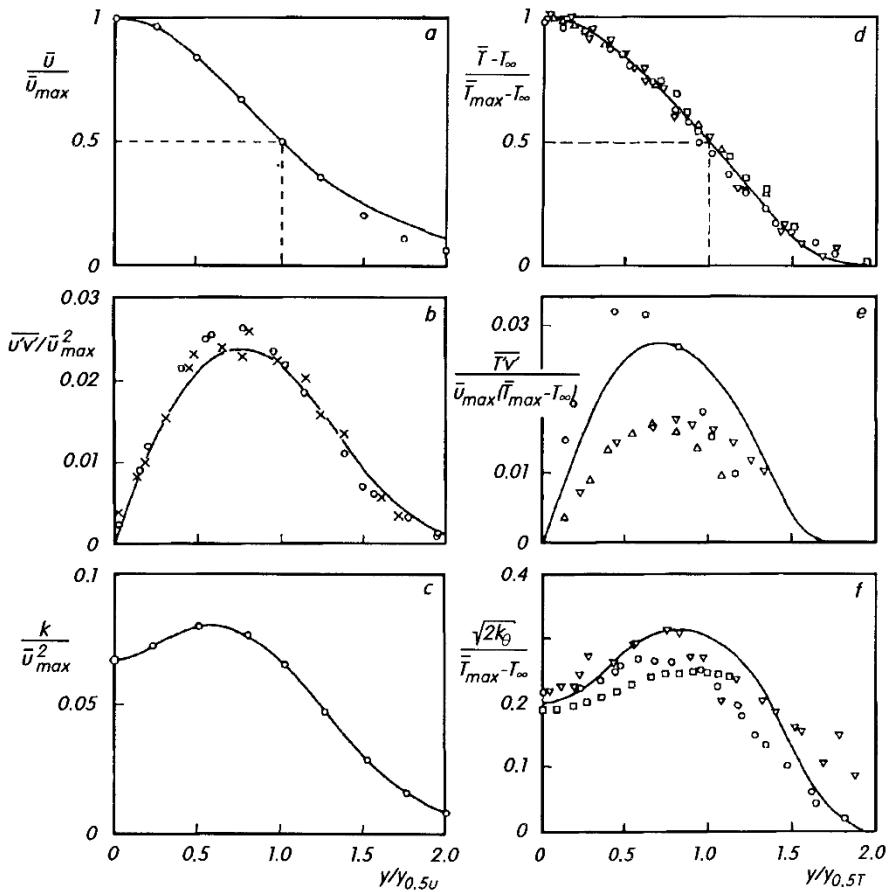


Fig. 22.2a–f. Turbulent plane free jet: most important flow quantities in the far field. Theoretical results (—) and experimental data (\circ , ∇ , \square , \dots) according to T.-H. Shih et al. (1990)

If there are different temperatures on the two sides of a free jet, there is heat transfer perpendicular to the free jet. This is of importance for *air curtains*, cf. K. Gersten; H. Herwig (1992), p. 736.

If the velocity of the free jet is large, the dissipation must also be taken into account. Since calculations have to be performed with temperature dependent physical properties at excess temperatures, there is a mutual coupling between the velocity field and the temperature field (“compressible” free jet), cf. NASA SP-321 (1973). Strictly speaking, the pressure is not constant throughout the free jet, but, because of Eq. (16.33), there is a weak pressure deficiency in the free jet.

22.3.3 Near Field

The *near field* of the free jet, i.e. the flow directly at the nozzle outlet, is quite different from the far field. A simple description is possible for the ideal special case in which there is a homogeneous velocity distribution at the outlet of the nozzle, and this case again leads to *similar* solutions. Figure 22.3 shows the flow in the near field. In this figure we see that two jet-boundary zones form. These commence at the edges of the nozzle outlet and in them the velocity decreases from the constant value $\bar{u}(x, 0) = \bar{u}(0, 0)$ to zero as we move further outwards. The two jet-boundary flows lead to similar solutions, as will be shown in Sect. 22.4. Their width also increases linearly along the length of the jet. The length of the near field is about five times the height of the nozzle outlet ($2H$), cf. F.K. v.Schulz-Hausmann (1985). After this, i.e. for $x > 10H$, the velocity on the axis decreases in a transition field, until the distribution $\bar{u}(x, 0)$ eventually becomes that of the far field $\sim (x - x_0)^{-1/2}$. F.K. v. Schulz-Hausmann (1985) has presented an integral method to compute the near field.

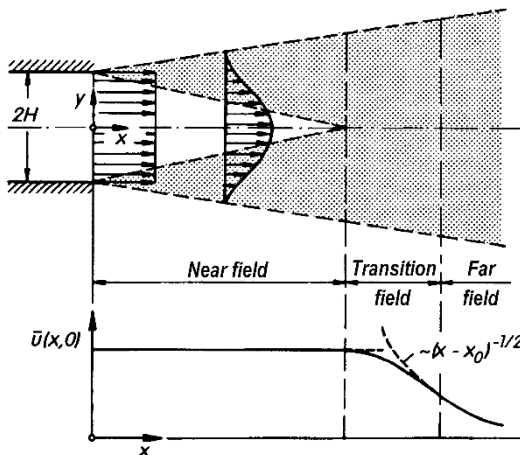


Fig. 22.3. Turbulent plane free jet: near field and transition field

If a fully developed channel flow is already at hand at the outlet, there is no near field. The flow at the nozzle outlet then begins directly with the transition field.

22.3.4 Wall Effects

We have already indicated many times that the v component of the velocity does not vanish at the edge of the jet, but rather is directed inwards towards the jet (entrainment). However the magnitude of the velocity in the far field decreases downstream in proportion to $(x - x_0)^{-1/2}$, cf. Eq. (22.41). This

entrainment causes the jet to *induce* a flow about it, and this has an effect on the jet. If there are walls in the outer region or at the jet outlet, pressure forces are formed on them, which then change the balance of momentum. The integral in Eq. (22.25) is no longer a constant, but is rather a slowly varying function of x . W. Schneider (1985) has shown how the momentum of a jet which exits a wall at right angles decreases downstream. According to this work

$$\frac{K(x)}{K_0} = \left(\frac{2H}{x - x_0} \right)^{\frac{3}{2}\alpha \cot(\Theta_w/2)}, \quad (22.48)$$

where Θ_w is the angle between the wall and the jet in Fig. 22.4. Furthermore, according to Eq. (22.48), K_0 is the kinematic momentum at the position $x - x_0 = 2H$. Since α is very small, according to Eq. (22.48) K changes only very slowly. For $x/2H = 40$, Eq. (22.48) yields a momentum decrease of 17%, in good agreement with measurements by D.R. Miller; E.W. Comings (1957).

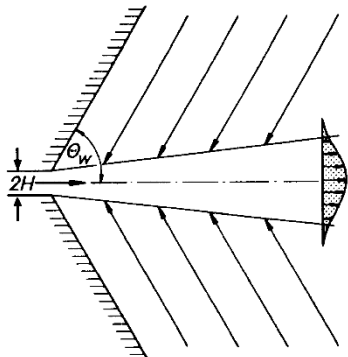


Fig. 22.4. Turbulent plane free jet with induced outer field

Inviscid flows with or without walls (potential flows) which have been induced by turbulent free jets have been computed by H. Reichardt (1942), G.I. Taylor (1958), I. Wygnanski (1964) and K. Kraemer (1971). Whereas strong asymmetries require numerical treatment, cf. F.K. v.Schulz-Hausmann (1985), an analytic solution can be written down for small angular differences, cf. W. Schneider (1991). If, for example, the angle at the lower wall in Fig. 22.4 is greater than that at the upper wall, or if there is no lower wall, the induced outer flow leads to a curvature of the free jet. Curved free jets require an extended turbulence model, cf. P. Bradshaw (1973). For angles of the upper wall of about $\Theta_w \leq 64^\circ$, after a certain distance x_R , the jet attaches to the wall. This phenomenon is named after the Romanian aeronautical engineer H.O. Coanda as the *Coanda effect*. R.A. Sawyer (1963) has computed the reattachment length $x_R(\Theta_w)$. In the region $50^\circ < \Theta_w < 64^\circ$, *hysteresis* occurs, i.e. the jet either attaches to the wall or not depending on whether the current state comes from an increase or decrease in Θ_w . The Coanda effect

has very many technical applications, cf. R. Wille; H. Fernholz (1965), as well as H.H. Fernholz (1964). The action of *fluidic elements* is based on this effect, cf. H.M. Schaadel (1979).

22.4 Mixing Layer

We will now consider the mixing layer shown in Fig. 22.1c between two parallel flows with the two velocities U and λU ($0 \leq \lambda < 1$), and the two temperatures $T_\infty + T_N$ and T_∞ . If we choose $U_\infty = 0$, $U_N = U$, and $m = 0$, $n = 0$ and $a = 1$ in Eq. (22.5), Eqs. (22.15) and (22.16) yield the differential equations

$$f''' + f f'' = 0, \quad (22.49)$$

$$\frac{1}{\Pr_t} g''' + f g'' = 0 \quad (22.50)$$

with the boundary conditions

$$\eta \rightarrow +\infty : \quad f' = 1, \quad g' = 1 \quad (22.51)$$

$$\eta \rightarrow -\infty : \quad f' = \lambda, \quad g' = 0.$$

This system is identical to that for the laminar mixing layer, where \Pr_t corresponds to \Pr , cf. Sect. 7.2.4. However the meaning of η and therefore the x dependence of $\Delta(x)$ are different (turbulent: $\Delta \sim (x - x_0)$, laminar: $\Delta(x) \sim (x - x_0)^{1/2}$).

For the two-sided plane mixing layer, Figure 22.1c, with $0 < \lambda < 1$ a third boundary condition is missing. As for the laminar mixing layer, cf. Section 7.2.4, the location of the dividing streamline remains indeterminate, if both streams are subsonic and semi-infinite in extent, see also K. Mörwald (1988) and W. Schneider (1991).

Experiments have shown, that mixing layers are not symmetric. They spread preferentially into the low-speed stream and they entrain fluid. The entrainment velocities at the outer edges of the mixing layers are independent of x . Therefore, the free stream on both sides is uniform. Consequentially the two free streams are not exactly parallel. In experiments, the free streams can be maintained at approximately uniform velocities by adjusting the inclination of the wind-tunnel walls, cf. S.B. Pope (2000).

We emphasise that the x -axis is not the dividing streamline. Rather it is a straight line. The system (22.49) - (22.51) for $0 < \lambda < 1$ can be used to find the asymptotic solution of the mixing layer far downstream. When the flow field within the leading-edges region in close proximity of the origin has been considered, this solution would then lead to a third boundary condition for the asymptotic solution far downstream.

The parameter $\alpha(\lambda)$ in Eq. (22.14) is a function of the velocity ratio λ . C.M. Sabin (1963), see also S.F. Birch; J.M. Eggers (1972), has produced the empirical equation

$$\alpha(\lambda) = \alpha_0 \frac{1 - \lambda}{\sqrt{1 + \lambda}} \quad (22.52)$$

with $\alpha_0 = 0.045$. In the literature one frequently finds information on

$$\sigma(\lambda) = \frac{\sqrt{1 + \lambda}}{2\alpha(\lambda)} = \sigma_0 \frac{1 + \lambda}{1 - \lambda} \quad (22.53)$$

with $\sigma_0 = (2\alpha_0)^{-1} = 11$. These trial solutions are equivalent to the model

$$\nu_t = \frac{\alpha^2(\lambda)}{1 - \lambda} (U - \lambda U)(x - x_0) = \frac{1}{4\sigma_0 \sigma(\lambda)} (U - \lambda U)(x - x_0). \quad (22.54)$$

The angle of inclination of the dividing streamline can be determined from these relations and the distributions of velocity and temperature.

The special case $\lambda = 0$ is frequently called *jet-boundary flow*, since it occurs in the near field of a free jet, as has already been explained in Sect. 22.3.3. In this case the third boundary-layer condition for the differential equation (22.49) is

$$f''(\eta \rightarrow +\infty) = 0. \quad (22.55)$$

This implies that the entrainment only takes place from the region of fluid which is at rest. The straight-lined dividing streamline forms the angle

$$\varphi_{DS} = -0.374 \cdot 0.045 = -0.017 (-1^\circ) \quad (22.56)$$

with the x-axis. Table 22.2 shows results from the solutions. For the mixing-layer flow, one frequently sets $\text{Prt} = 0.5 = \text{const}$.

Table 22.2. Numerical results for the jet-boundary flow (mixing layer with $\lambda = 0$), $\text{Prt} = 0.5$. Position of the dividing streamline at $\eta = -0.3740$

η	f	f'	f''	g'	g''
$\rightarrow \infty$	η	1	0	1	0
0	0.2392	0.6914	0.2704	0.6937	0.1823
-0.3740	0	0.5872	0.2825	0.6246	0.1863
$\rightarrow -\infty$	-0.8757	0	0	0	0

The mixing layer flow and the jet-boundary flow have been computed by W. Tollmien (1926), only $\lambda = 0$, using the mixing length model, by B.E. Launder et al. (1973) using the k - ε model and by H. Vollmers; J.C. Rotta (1977) using the Rotta model (but only $\lambda = 0$). All cases exhibit good agreement with experiments.

If large temperature differences appear (e.g. if the dissipation is also taken into account), temperature dependent physical properties have to be considered. This leads to a mutual coupling of the velocity field and the temperature

field (“compressible” mixing layer), cf. S.F. Birch; J.M. Eggers (1972). Details on the changes to the turbulence models due to this effect are found in, for example, S. Sarkar; B. Lakshmanan (1991).

22.5 Plane Wake

Very far downstream in the flow past a plane body a wake flow, as sketched in Fig. 22.1e, appears. The homogeneous free stream has the velocity U_∞ . The *depth* of the *wake depression* is denoted by $(-U_N(x))$. Because of *turbulent mixing*, the width of the depression continually increases downstream, and $U_N(x)$ tends towards zero with x . Here we will consider the flow so far downstream that $|U_N(x)| \ll U_\infty$ holds (*far field*). If the body in the flow has a lower temperature than the free stream, a similar *temperature wake depression* with depth $(-T_N(x))$ forms, as is shown in Fig. 22.1e. A global momentum balance yields the relation between the drag D of the body (width b and characteristic length l) and the momentum loss in the wake depression, cf. Sect. 7.5.1. The *drag coefficient* is then

$$c_D = \frac{2D}{\varrho U_\infty^2 bl} = \frac{2}{U_\infty^2 l} \int_{-\infty}^{+\infty} \bar{u}(U_\infty - \bar{u}) dy \quad (22.57)$$

or, with (22.5), (22.8) and $|U_N| \ll U_\infty$

$$c_D = -2 \frac{U_N(x)\Delta(x)}{U_\infty l} \int_{-\infty}^{+\infty} f'(\eta) d\eta. \quad (22.58)$$

Similarly, a thermal energy balance yields

$$c_Q = \frac{2\dot{Q}}{\varrho c_p T_\infty U_\infty bl} = 2 \frac{T_N(x)\Delta(x)}{T_\infty l} \int_{-\infty}^{+\infty} g'(\eta) d\eta. \quad (22.59)$$

Therefore the products $U_N(x)\Delta(x)$ and $T_N(x)\Delta(x)$ must be independent of x . According to Eqs. (22.13) and (22.17), this is the case for $m = n = -1/2$. Therefore, according to Eq. (22.11), ν_t is also independent of x . In this case laminar and turbulent flows are identical, if ν is replaced by ν_t . Furthermore, it follows from Eq. (22.6), that the entrainment velocity v_e vanishes. If we fix the width scale by $a = 4|B|/U_\infty$, we obtain the differential equations

$$f''' + 2(\eta f'' + f') = 0, \quad (22.60)$$

$$\frac{1}{Pr_t} g''' + 2(\eta g'' + g') = 0 \quad (22.61)$$

with the boundary conditions:

$$\eta = 0 : \quad f' = 1, \quad g' = 1, \quad (22.62)$$

$$\eta = \pm\infty : \quad f' = 0, \quad g' = 0.$$

The solutions read:

$$f'(\eta) = \exp(-\eta^2), \quad (22.63)$$

$$g'(\eta) = \exp(-\text{Pr}_t \eta^2) = [f'(\eta)]^{\text{Pr}_t}. \quad (22.64)$$

This yields

$$-\frac{U_N(x)}{U_\infty} = \frac{1}{\sqrt{8\alpha}\pi^{1/4}} \left(\frac{c_D l}{x - x_0} \right)^{1/2} = 1.15 \left(\frac{c_D l}{x - x_0} \right)^{1/2}, \quad (22.65)$$

$$\frac{T_N(x)}{T_\infty} = \frac{1}{\sqrt{8\alpha}} \left(\frac{\text{Pr}_t}{\pi} \right)^{1/4} \left(\frac{c_Q l}{x - x_0} \right)^{1/2} = 0.97 \left(\frac{c_Q l}{x - x_0} \right)^{1/2}. \quad (22.66)$$

Here the values $\alpha = 0.055$ and $\text{Pr}_t = 0.5$ were chosen from measurements, cf. K.R. Sreenivasan; R. Narasimha (1982) and H. Schlichting (1982), pp. 760,773. We emphasise that, because of the assumption $|U_N| \ll U_\infty$, Eq. (22.61) does not contain the function $f(\eta)$, and so the temperature field is independent of the velocity field. For details on the changes to the turbulence models due to “compressibility”, see the piece of work by S. Sarkar; B. Lakshmanan (1991).

Note in particular that the x dependence of $\bar{v}(x)$ ($\sim (x - x_0)^{-1}$) and of $\bar{u} - U_\infty$ ($\sim (x - x_0)^{-1/2}$) are different. This is a case of *incomplete similarity*, cf. J.O. Hinze (1975), pp. 499 and 503. Computations using the mixing length model have been carried out by H. Schlichting (1930), using the k - ε model by B.E. Launder et al. (1973) and using the Rotta model by H. Vollmers; J.C. Rotta (1977). A.A. Townsend (1976), p. 206 has presented details on the balance of the turbulent energy which can also be determined using the two-equation models.

Investigations into the *near field* of wakes have generally been carried out behind the flat plate, cf. R. Chevray; L.S.G. Kovasznay (1969) and N. Subaschandar; A. Prabhu (1999). The flow field behind an airfoil is much more complicated, because the near field is then within the pressure field of the airfoil, cf. V.C. Patel; G. Scheuerer (1982). There is considerable practical importance attached to this problem, since the total drag of an airfoil can be determined if the flow can be computed from the trailing edge into the far field. There are therefore numerous investigations which aim to determine the total drag from the boundary-layer quantities close to the trailing edge of the airfoil, cf. A.D. Young (1989), p. 227, H. Schlichting (1982), p. 780.

The drag coefficient of an airfoil (free stream velocity V , airfoil chord length l) is

$$c_D = \frac{2D}{\rho V^2 bl} = 2 \frac{\delta_{2TE}}{l} \left(\frac{U_{TE}}{V} \right)^{(H_{12}+5)_{TE}/2}, \quad (22.67)$$

where the index TE indicates the trailing edge. Therefore the drag coefficient can be determined if the momentum thickness δ_2 and the shape factor H_{12} have been worked out from the boundary-layer calculation. The potential theory velocity at the trailing edge U_{TE} can be determined, for example, from measurements of the static pressure at the trailing edge. In Eq. (22.67), δ_{2TE} is the sum of the momentum thickness δ_2 on the upper and lower sides of the airfoil. Several examples have been computed using this formula by H.B. Squire; A.D. Young (1939), and these yielded the effect of the profile thickness, the Reynolds number and the position of the laminar-turbulent transition. Extensions to this method are due to N. Scholz (1951), who also treated the axisymmetric case, see also A.D. Young (1939) and P.S. Granville (1953, 1977).

The flow close to the trailing edges of plates or profiles has, as in the laminar case, a multi-layer structure, cf. R.E. Melnik; B. Grossmann (1981).

Note (Free jet in parallel flow)

The equations of the far field of a wake are also valid for the far field of a heated free jet which is injected into a translation flow parallel to the flow direction with the velocity U_j (width $2l$), cf. N. Rajaratnam (1976), p. 63, cf. Fig. 22.1f. Instead of the drag coefficient, one then obtains a coefficient for the momentum surplus in the jet

$$c_\mu = \frac{2\varrho U_j(U_j - U_\infty)2lb}{\varrho U_\infty^2 lb} = \frac{4U_j(U_j - U_\infty)}{U_\infty^2}.$$

This yields

$$\frac{U_N(x)}{\sqrt{U_j(U_j - U_\infty)}} = 1.9 \left(\frac{c_\mu l}{x - x_0} \right)^{1/2}. \quad (22.68)$$

Here the near field consists of two mixing layers, cf. Sect. 22.4.

22.6 Axisymmetric Free Shear Flows

22.6.1 Basic Equations

Important axisymmetric free shear flows are the free jet and the wake. Here we use cylindrical coordinates x, r with velocity components \bar{u}, \bar{v} . If we assume *slenderness* as in the plane case, we obtain the following equations (at equal pressure):

$$\frac{\partial(r\bar{u})}{\partial x} + \frac{\partial(r\bar{v})}{\partial r} = 0, \quad (22.69)$$

$$\varrho \left(\bar{u} \frac{\partial \bar{u}}{\partial x} + \bar{v} \frac{\partial \bar{u}}{\partial r} \right) = \frac{1}{r} \frac{\partial(r\tau_t)}{\partial r}, \quad (22.70)$$

$$\varrho c_p \left(\bar{u} \frac{\partial \bar{T}}{\partial x} + \bar{v} \frac{\partial \bar{T}}{\partial r} \right) = -\frac{1}{r} \frac{\partial(rq_t)}{\partial r} \quad (22.71)$$

with

$$\tau_t = \varrho \nu_t \frac{\partial \bar{u}}{\partial r}, \quad q_t = -\frac{\varrho c_p \nu_t}{Pr_t} \frac{\partial \bar{T}}{\partial r}. \quad (22.72)$$

For similar solutions, in analogy to Eq. (22.5), (22.7) and (22.11), we use the following trial solutions

$$\bar{u} = U_\infty + U_N(x) \frac{f'(\eta)}{\eta}, \quad (22.73)$$

$$\bar{T} = T_\infty + T_N(x)g'(\eta), \quad (22.74)$$

$$\nu_t = \alpha U_N(x) \Delta(x) = \frac{1}{\text{Re}_t} U_N(x) \Delta(x) \quad (22.75)$$

with

$$\eta = \frac{r}{\Delta(x)}. \quad (22.76)$$

The conditions for similarity again depend on the flow under consideration.

22.6.2 Free Jet ($U_\infty = 0$, $\Delta = 8\alpha(x - x_0)$)

With the conditions (cf. Eq. (22.25) and (22.26))

$$K_a = 2\pi \int_0^\infty \bar{u}^2 r dr = 2\pi U_N^2(x) \Delta^2(x) \int_0^\infty \frac{f'^2}{\eta} d\eta = \text{const}, \quad (22.77)$$

$$\begin{aligned} E_{Ta} &= \frac{\dot{Q}}{\varrho c_p} = 2\pi \int_0^\infty \bar{u}(\bar{T} - T_\infty) r dr \\ &= 2\pi U_N(x) T_N(x) \Delta^2(x) \int_0^\infty g' f' d\eta = \text{const} \end{aligned} \quad (22.78)$$

Eqs. (22.69) to (22.76) for $f(\eta)$ and $g(\eta)$ yield the differential equations

$$\begin{aligned} \eta f'' + 8fg' - f' &= 0 \\ \frac{1}{\text{Pr}_t} \eta g'' + 8fg' &= 0 \end{aligned}$$

(22.79)

with the solutions

$$f(\eta) = \frac{\eta^2}{2(1+\eta^2)}, \quad \frac{f'(\eta)}{\eta} = \frac{1}{(1+\eta^2)^2}, \quad g'(\eta) = \left(\frac{f'}{\eta}\right)^{\text{Pr}_t}. \quad (22.80)$$

This eventually yields

$$\begin{aligned} \bar{u} &= \frac{1}{8\alpha} \sqrt{\frac{3K_a}{\pi}} \frac{1}{x-x_0} \frac{1}{(1+\eta^2)^2} \\ \bar{v} &= \frac{1}{2} \sqrt{\frac{3K_a}{\pi}} \frac{1}{x-x_0} \frac{\eta(1-\eta^2)}{(1+\eta^2)^2}, \end{aligned} \quad (22.81)$$

$$\bar{T} - T_\infty = \frac{(2\text{Pr}_t + 1)E_{Ta}}{8\alpha\sqrt{3\pi K_a}} \frac{1}{x-x_0} \frac{1}{(1+\eta^2)^{2\text{Pr}_t}}, \quad (22.82)$$

$$\nu_t = \alpha \sqrt{\frac{3K_a}{\pi}}, \quad (22.83)$$

$$Q = 2\pi \int_0^\infty \bar{u} r dr = 8\alpha \sqrt{3\pi K_a} (x - x_0) \quad (22.84)$$

with the empirical constant $\alpha = 0.017$.

It is worth noting that ν_t is constant in the entire field and the jet behaves like a laminar axisymmetric free jet in this manner. However in the turbulent jet, ν_t depends on the kinematic jet momentum K_a . If we use Eq. (22.83) to eliminate α in Eqs. (22.81), (22.82) and (22.84) and replace ν_t and Pr_t by the corresponding molecular values ν and Pr , we obtain the solutions for the laminar axisymmetric free jet, cf. Sect. 12.1.5.

The half expansion angles at the positions of half maximal velocity are of magnitude (for $\text{Pr}_t = 0.5$)

$$\begin{aligned} \frac{r_{0.5u}}{x - x_0} &= 8\alpha\eta_{0.5u} = 0.086 \quad (4.9^\circ); \\ \frac{r_{0.5T}}{x - x_0} &= 8\alpha\eta_{0.5T} = 0.13 \quad (7.4^\circ). \end{aligned} \quad (22.85)$$

The free jet has also been computed by W. Tollmien (1926) using the mixing length model, by B.E. Launder et al. (1973) using the $k-\varepsilon$ model and by H. Vollmers; J.C. Rotta (1977) using the Rotta model.

We point out that the mixing length model in the outer region of the free jet delivers better results than the model with constant ν_t . A ν_t which dies away as one moves outwards would yield better agreement with experiments, cf. F. Thiele (1975). The entrainment action of the free jet corresponds to a sink line on the jet axis with an intensity independent on x , i.e. $\lim_{r \rightarrow \infty} (\bar{v}r)$ does not depend on x .

Note (Radial jets)

Radial jets are formed when fluid is blown out of a peripheral slit in a tube. The main flow direction is radial (in the r direction). Because of the slenderness of these jets, their general equations of motion can also be simplified to boundary-layer equations. Again these lead to similar solutions, cf. N. Rajaratnam (1976), p. 50. If there is a wall (whose normal is the axis of the jet) close to a radial jet, the jet is sucked onto the wall. This process is similar to the Coanda effect for plane jets. Depending on the exit angle of the radial jet, pressure or suction forces may act on the wall. A theory of this flow which is based on the ideas of boundary-layer theory has been presented by R.H. Page et al. (1989) and R.H. Page (1993).

22.6.3 Wake ($|U_N| \ll U_\infty$, $\Delta = \lambda(x - x_0)^{1/3}$)

Using the conditions

$$\begin{aligned} c_D &= \frac{2D}{\varrho U_\infty^2 \frac{\pi}{4} l^2} = \frac{16}{U_\infty^2 l^2} \int_0^\infty \bar{u}(U_\infty - \bar{u})r dr \\ &= -16 \frac{U_N(x)\Delta^2(x)}{U_\infty l^2} \int_0^\infty f' d\eta = \text{const}, \end{aligned} \quad (22.86)$$

$$\begin{aligned}
c_Q &= \frac{2\dot{Q}}{\varrho c_p T_\infty U_\infty \frac{\pi}{4} L^2} = \frac{16}{T_\infty U_\infty l^2} \int_0^\infty \bar{u}(T_\infty - \bar{T}) r dr \\
&= -16 \frac{T_N(x) \Delta^2(x)}{T_\infty l^2} \int_0^\infty g' d\eta = \text{const}
\end{aligned} \tag{22.87}$$

Eqs. (22.69) to (22.76) yield the following differential equations for $f(\eta)$ and $g(\eta)$:

$$\boxed{f' + 2\eta f = 0,} \quad \boxed{\frac{1}{\text{Pr}_t} g'' + 2\eta g' = 0} \tag{22.88}$$

with the solutions

$$\begin{aligned}
f(\eta) &= -\frac{1}{2} \exp(-\eta^2), \quad \frac{f'(\eta)}{\eta} = \exp(-\eta^2), \\
g'(\eta) &= \left(\frac{f'}{\eta} \right)^{\text{Pr}_t} = \exp(-\text{Pr}_t \eta^2).
\end{aligned} \tag{22.89}$$

This eventually delivers

$$\begin{aligned}
\bar{u} &= U_\infty - \frac{U_\infty c_D l^2}{8\lambda^2} (x - x_0)^{-2/3} \exp(-\eta^2), \\
\bar{v} &= -\frac{U_\infty c_D l^2}{24\lambda} (x - x_0)^{-4/3} \eta \exp(-\eta^2),
\end{aligned} \tag{22.90}$$

$$\begin{aligned}
\bar{T} &= T_\infty - T_\infty \frac{c_Q \text{Pr}_t l^2}{8\lambda^2} (x - x_0)^{-2/3} \exp(-\text{Pr}_t \eta^2), \\
\nu_t &= \alpha |U_N| \Delta = \frac{4}{3} \frac{\lambda^3}{c_D l^2} |U_N| \Delta = \frac{\lambda^2}{6} U_\infty (x - x_0)^{-1/3}
\end{aligned} \tag{22.91}$$

with

$$\alpha = \frac{4}{3c_D} \frac{\lambda^3}{l^2}. \tag{22.92}$$

We emphasise particularly that Δ grows nonlinearly with $x - x_0$. According to an assessment of experimental data by W. Rodi (1975), the constant α lies in the region $0.06 < \alpha < 0.56$ (1.67α is identical to the spreading parameter S given by Rodi). Here the calculations have been carried out with a value of $\alpha = 0.3$. The radial expansion $r_{0.5u}$ or $r_{0.5T}$ of the axisymmetric wake is proportional to $c_D^{1/3}$, cf. Table 22.1. Note also that J.O. Hinze (1975), p. 510 has set the value $\lambda = 0.76$, whereby the expansion of the axisymmetric wake is, in contrast to the plane wake, independent of c_D .

For details on calculations using other models and on experimental results, see H. Schlichting (1982), p. 763 and J.O. Hinze (1975), pp. 502, 509, 519. As with the plane wake, cf. Sect. 22.5, the axisymmetric wake also possesses *incomplete similarity*, since \bar{u} and \bar{v} obey different powers of $x - x_0$. The far field of a free jet into which a translation flow is injected in parallel can also be

described using this solution, providing the drag coefficient is again replaced by a coefficient for the momentum excess of the jet, cf. A.A. Townsend (1976), pp. 226, 255.

22.7 Buoyant Jets

22.7.1 Plane Buoyant Jet

A buoyant jet or plume is the flow above an energy source with power E_T , as shown in Fig. 22.1b. In the plane case this is a “line source”. There is a certain similarity between buoyant jets and the free jets treated in Sect. 22.3. (These free jets are also called *momentum jets*). The buoyancy forces cause the flow to accelerate upwards, i.e. with increasing x , the kinematic “jet momentum” $K(x)$ and, because of the entrainment effect, also the volume flux $Q(x)$, increase continually. On the other hand, the maximum temperature decreases with increasing x .

Equations (22.1) to (22.3) can be used to describe the buoyant jet, as long as the term for the buoyancy force is added to Eq. (22.2). With the Boussinesq approximation, the momentum equation reads

$$\bar{u} \frac{\partial \bar{u}}{\partial x} + \bar{v} \frac{\partial \bar{u}}{\partial y} = g\beta_\infty(\bar{T} - T_\infty) + \frac{1}{\varrho} \frac{\partial \tau_t}{\partial y}. \quad (22.93)$$

Again similar solutions can be found. Here we will present only the most important results.

Using the trial solutions

$$\bar{u} = U_N(x)f'(\eta), \quad \bar{T} - T_\infty = T_N(x)g'(\eta) \quad (22.94)$$

and the condition (cf. Sect. 10.5.4 for the laminar case)

$$\begin{aligned} E_T &= \frac{\dot{Q}}{\varrho c_p b} = \int_0^{+\infty} (\bar{T} - T_\infty) \bar{u} dy \\ &= T_N(x)U_N(x)\Delta \int_{-\infty}^{+\infty} f'g' d\eta = \text{const} \end{aligned} \quad (22.95)$$

we obtain the results

$$U_N(x) = 1.7(g\beta_\infty E_T)^{1/3}, \quad (22.96)$$

$$T_N(x) = 2.5E_T(g\beta_\infty E_T)^{-1/3}(x - x_0)^{-1}, \quad (22.97)$$

$$\Delta(x) = y_{0.5u} = 0.135(x - x_0) \approx 0.92y_{0.5T}, \quad (22.98)$$

$$Q_b(x) = 0.52(g\beta_\infty E_T)^{1/3}(x - x_0), \quad (22.99)$$

$$K(x) = 0.63(g\beta_\infty E_T)^{2/3}(x - x_0), \quad (22.100)$$

$$\nu_t = 0.062U_N(x)\Delta(x). \quad (22.101)$$

Since $f'(0) = g'(0) = 1$ holds, $U_N(x)$ and $T_N(x)$ are the maximum values on the axis. Here the turbulent Prandtl number was set to $\text{Pr}_t = 0.74$. The numerical values were fitted to experiments, cf. C.J. Chen; W. Rodi (1980) and K. Gersten et al. (1980).

Whereas the maximal velocity is independent of x , the volume flux Q and the kinematic momentum K grow in proportion to x . This flow has been computed using an extended $k-\varepsilon$ model by M.S. Hossain; W. Rodi (1982).

An extension is the *buoyant momentum jet* or *forced plume*. In this case there is a transition from the momentum jet (near field) to the buoyant jet (far field), whereby there is no similarity in the transition region. This flow has been computed by K. Gersten et al. (1980) with an integral method. Here an inclination of the initial momentum away from the vertical was also taken into account.

If the outer field does not have a constant temperature, but rather is in the form of temperature stratification, the buoyant jet flow changes correspondingly, cf. J.S. Turner (1973) and H. Schlichting (1982), p. 774.

Note (Surface fire)

The system of equations (22.1), (22.93) and (22.3) also has a similar solution where no entrainment occurs, i.e. the volume flux is constant. The flow starts off with infinite width $\Delta \sim x^{-1/2}$, whereas the velocity $U \sim x^{1/2}$ and the kinematic momentum $K \sim x^{1/2}$ commence at zero. The maximum temperature is independent of x . Such a flow occurs to good approximation in a superficially extended fire (such as a burning oil surface) directly above the burning surface (near field). At greater distances (in the far field) this flow again becomes a buoyant jet, cf. K. Gersten et al. (1980).

22.7.2 Axisymmetric Buoyant Jet

In analogy to the plane buoyant jet, the axisymmetric buoyant jet can also be computed. If the dimensionless power of the energy source is

$$E_{Ta} = \frac{\dot{Q}}{\varrho c_P} = 2\pi \int_0^{\infty} (\bar{T} - T_{\infty}) \bar{u} r dr, \quad (22.102)$$

the following distributions of velocity and temperature are obtained (cf. J.S. Turner (1973))

$$\bar{u} = 4.3(g\beta_{\infty} E_{Ta})^{1/3} (x - x_0)^{-1/3} e^{-\frac{96r^2}{(x-x_0)^2}}, \quad (22.103)$$

$$\bar{T} - T_{\infty} = 9.4E_{Ta}(g\beta_{\infty} E_{Ta})^{-1/3} (x - x_0)^{-5/3} e^{-\frac{71r^2}{(x-x_0)^2}}. \quad (22.104)$$

Somewhat different numerical values have been presented in the work by C.J. Chen; W. Rodi (1980), cf. Table 22.1. The extension to buoyant momentum jets has been carried out in the work of W. Schneider (1975) and G. Fleischhacker; W. Schneider (1980), and the case of inclined initial momentum is treated by W. Schneider (1991). The results have also been compared with experiments; see the summaries by E.J. List (1982) and B. Gebhart et al. (1984).

22.8 Plane Wall Jet

Wall jets are jets which are bounded on one side by a wall. This flow type is a mixture of free turbulence in the outer region and boundary layer in the wall region. Wall jets have many practical applications, for example in ventilation, for heating, cooling or drying.

The following analysis is not valid for wall jets that emerge from a second wall perpendicular to the inlet velocity vector. The reason for this restriction will be given at the end of this section.

Corresponding to the two constituents of the flow (free turbulence and boundary layer), the turbulent wall jet flow depends on two parameters: the slenderness parameter α (for the outer region) and a suitably formed Reynolds number Re (for the wall region). Consequently, this gives rise to a two-parameter problem. The wall jet flow has a *three-layer structure*, as being demonstrated in Fig. 22.5.

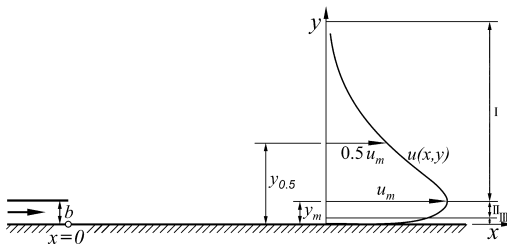


Fig. 22.5. Plane turbulent wall jet (far field)

For large Reynolds numbers, the two lower layers fade away, so that asymptotically a so-called *half jet*, i.e. half a free jet, remains. This (slender) half jet flow is the basic solution and is perturbed by the no-slip condition at the wall. The half jet is characterised by the constant kinematic momentum flux

$$K_\infty = \lim_{Re_x \rightarrow \infty} \int_0^\infty \bar{u}^2(y) dy . \quad (22.105)$$

The maximum velocity far downstream becomes according to Eq. (22.37):

$$U_N(x) = \sqrt{\frac{3K_\infty}{8\alpha(x - x_0)}} . \quad (22.106)$$

The asymptotic kinematic momentum flux K_∞ is therefore a characteristic quantity of the wall jet flow.

The maximum velocity u_m of the turbulent wall jet with the asymptotic kinematic momentum flux $K_\infty(m^3 s^{-2})$ has the form

$$u_m = f(x - x_0, v, K_\infty) , \quad (22.107)$$

where x_0 is the coordinate of a virtual origin and v is the kinematic viscosity. The asymptotic formula is by definition independent of the slot width b , the inlet mean velocity U_j and the inlet momentum flux K_j . Dimensional analysis leads to

$$\frac{u_m V}{K_\infty} = F(\text{Re}_x) , \quad (22.108)$$

where the Reynolds number Re_x is defined as

$$\text{Re}_x = \frac{\sqrt{(x-x_0) K_\infty}}{\nu} . \quad (22.109)$$

The one and only curve representing (22.108) is universal and valid for all plane turbulent wall jets (without perpendicular wall).

The following dimensionless combinations depend also only on the Reynolds number:

$$\frac{y_m}{y_{0.5}}, \frac{u_m y_{0.5}}{\nu}, \frac{\sqrt{(x-x_0) K_\infty}}{\nu}, \text{Re}_m = \frac{u_m y_m}{\nu}, \frac{K}{K_\infty}, \gamma_G^2 = \frac{\tau_w}{\rho U_N^2}, \frac{\tau_w V^2}{\rho K_\infty^2} . \quad (22.110)$$

Diagrams showing these dimensionless combinations as functions of the Reynolds number, can be used to determine the characteristic momentum flux K_∞ for a given wall jet. This will lead to the same value K_∞ at all stations $x-x_0$ of the wall jet flow. An iterative process is necessary to determine K_∞ for combinations that contain K_∞ .

In analogy to equilibrium boundary layers, we introduce a perturbation parameter:

$$\gamma_G(x) = \frac{u_\tau(x)}{U_N(x)} . \quad (22.111)$$

The description of the wall jet flow field is based on a three-layer structure. In addition it is assumed that the velocity distribution is self-similar, however separately in each of the three layers.

According to Fig. 22.5 the following three layers are found:

(I) Outer layer $y \geq y_m$

no viscous friction

$$u(x, y) = u_m(x) \dot{F}(\bar{\eta}) \\ \bar{\eta} = [x - y_m(x)] / \Delta(x), \Delta(x) = [y_{0.5}(x) - y_m(x)] / k, \dot{F}(k) = 0.5 \quad (22.112)$$

(II) Defect layer $0 < y < y_m$

no viscous friction, $y_m(x) / y_{0.5}(x) = O(\gamma_G)$

$$u(x, y) = u_m(x) - u_\tau(x) \cdot f'(\eta), \quad \eta = y / y_m(x) \quad (22.113)$$

(III) Viscous wall layer $0 \leq y < 70\nu/u_\tau$

constant shear stress perpendicular to the wall, $\tau(x) = \tau_w(x) = u_\tau^2(x) / \rho$

$$u(x, y) = u_\tau(x) \cdot u^+(y^+), \quad y^+ = y u_\tau(x) / \nu \quad (22.114)$$

Details of the calculation are described in K. Gersten (2015). The matching of defect layer and wall layer occurs in an overlap layer. Hence, in K. Gersten (2015) the turbulent wall jet is considered as a flow with a four-layer structure. In the overlap layer the logarithmic velocity law is valid. To match the velocity in the overlap layer yields the friction law in the following form:

$$\frac{1}{\gamma_G} = \frac{1}{\kappa} \ln(\text{Re}_x \gamma_G^2) + \hat{D} + \hat{E} \gamma_G + \dots \quad (22.115)$$

or explicitly

$$\gamma_G = \frac{\kappa}{\ln \text{Re}_x} G(\Lambda; D, E) \quad (22.116)$$

with $\Lambda = \ln \text{Re}_x$, $D = 2 \ln \kappa + \kappa \hat{D}$, $E = \kappa^2 \hat{E}$

$$\frac{\Lambda}{G} + 2 \ln \frac{\Lambda}{G} - D = \Lambda + E \frac{G}{A} . \quad (22.117)$$

At the border between the outer layer and the defect layer $y = y_m$ ($\eta = 1, \bar{\eta} = 0$) the functions $u(x, y), v(x, y), \tau(x, y), \partial u / \partial y$ and $\partial^2 u / \partial y^2 (\gamma_G \rightarrow 0)$ are continuous (“patching”).

Assuming an eddy viscosity independent of $\bar{\eta}$ leads to the well-known free-jet solution:

$$\dot{F}(\bar{\eta}) = 1 - \left(\tanh \bar{\eta} \right)^2 , \quad (22.118)$$

see Eq. (22.31). An indirect turbulence model in the defect layer yields

$$f'(\eta) = \frac{1}{\kappa} \left(-\ln \eta - \frac{5}{6} + \frac{3}{2} \eta^2 - \frac{2}{3} \eta^3 \right) , \quad (22.119)$$

see K. Gersten (2015, page 360).

By using these functions the following formulae can be obtained ($\kappa = 0.41$; $k = 0.8814$):

$$Q_b(x) = \int_0^\infty u(x, y) dy = 1.135 u_m y_{0.5} \left[1 - \frac{y_m}{y_{0.5}} \left(0.119 + 1.075 \frac{u_\tau}{u_m} \right) \right] \quad (22.120)$$

$$K(x) = \int_0^\infty u^2(x, y) dy = 0.756 u_m^2 y_{0.5} \left[1 + \frac{y_m}{y_{0.5}} \left(0.322 - 3.226 \frac{u_\tau}{u_m} \right) \right] . \quad (22.121)$$

The momentum flux $K(x)$ must satisfy the momentum-integral equation:

$$K(x) = K_\infty + \int_0^x \frac{\tau_w(x)}{\rho} dx . \quad (22.122)$$

Using the friction law (22.116) and integration lead to the final formula:

$$K(x) = K_\infty \left\langle 1 + \frac{3\kappa}{4\alpha} \left[\gamma_G(x) + \frac{1}{\kappa} \gamma_G^2(x) + O(\gamma_G^3) \right] \right\rangle . \quad (22.123)$$

This is a universal function for all turbulent wall jets. The function contains no empirical constants except the Karman constant $\kappa (= 0.41)$ and the slenderness parameter $\alpha (= 0.021)$. The slenderness parameter for the half-free jet is smaller than that for the free jet ($\alpha = 0.033$). The reason is that presence of the wall reduces the entrainment and hence the spreading rate of the jet.

Further global values are:

Wall jet thickness:

$$y_{0.5}(x) = 4\alpha k(x - x_0) \quad (22.124)$$

Maximum velocity:

$$u_m(x) = U_N(x) [1 + B_1 \gamma_G + B_2 \gamma_G^2 + \dots] \quad (22.125)$$

Wall distance of point with maximum velocity:

$$y_m(x) = A_1 y_{0.5}(x) \gamma_G [1 + A_2 \gamma_G + \dots] \quad (22.126)$$

Equation (22.123) can be applied to determine K_∞ , when the experimental values $y_{0.5}(x)$, $u_m(x)$ and $K(x)$ are given and the combination of (22.106), (22.111) and (22.124) is used:

$$\gamma_G(x) = u_m(x) \sqrt{\frac{2y_{0.5}(x)}{3k K_\infty}} . \quad (22.127)$$

The universal constants A_1 , A_2 , B_1 , and B_2 defined in (22.125) and (22.126) have been determined in such a way that the analysis is concordant with existing experiments. In K. Gersten (2015) data of two wall jets, investigated by Tailland and Mathieu, have been used.

It is worth mentioning that τ_t changes sign in the defect layer. Between the zero of $\tau_t(y = y_{\tau_t=0})$ and the velocity maximum ($y = y_m$) the turbulence production ($\sim \tau_t \partial \bar{u} / \partial y$) is negative, i.e. energy is transferred from the turbulent fluctuations to the mean motion. Examples with equal behaviour are the Couette - Poiseuille flow in Sect. 17.2.2 and the natural convection in Sect. 19.3. The concepts of eddy viscosity and mixing length fail here.

Overviews on experimental results on wall jets are given by B.E. Launder; W. Rodi (1981) and M.E. Schneider; R.J. Goldstein (1994).

As has been mentioned at the beginning of this section, the preceding analysis is not valid for wall jets emerging from a wall perpendicular to the inflow velocity vector. As W. Schneider (1985) has shown, the momentum flux of turbulent free jets emerging from orifices of plane walls decreases to zero far downstream. The same is, of course, true for turbulent half-free jets.

Part V

Numerical Methods in Boundary-Layer Theory

23. Numerical Integration of the Boundary-Layer Equations

23.1 Laminar Boundary Layers

23.1.1 Remark

Numerical solutions of the boundary-layer equations are based on the assumption that the differential expressions in the partial differential equations can be approximated by difference expressions. This approximation, called *discretisation* can be obtained from a series expansion for the velocity components in the coordinate directions. These series expansions do not necessarily have to consist of Taylor series. Since only a certain number of terms in any expansion can be taken, there is a *discretisation or truncation error*, and this is dependent on the number and size of the terms neglected.

In order to derive the difference expressions, a *grid* must be placed over the boundary layer. This grid is formed by coordinate lines. The unknown velocity components are then determined in the solution for the crossing points of the coordinate coordinate lines, the grid points. The spacing between coordinate lines may be chosen to be constant or variable. If there are large local variations in the velocity components, the spacing between the grid points must be small enough so that the discretisation error remains small.

The discretisation can yield linear but also nonlinear difference equations to determine the unknown velocity components defined at the grid points. The number of unknowns is obtained from the number of grid points. Since the spacing between them must be small in order for the model to be as accurate as possible, the number of unknowns is always large. For this reason, computers must be used to solve the difference equations.

Because of the nonlinearities which appear in the differential equations, the solution of the difference equations must generally be *iterated*. The accuracy of the results therefore depends on the solution method used. Since there are many different ways of discretising a field and also several solution methods, the numerical solutions are not uniquely defined. There are many variations in the formulation of the difference equations and also in their solution. The order of the discretisation error is of primary importance in setting up the difference equations. If the order of the error is increased, or also if the number of grid points is increased, the accuracy is generally improved, but the computational effort also becomes greater. For this reason

a compromise has to be found between accuracy and computational effort. Therefore when constructing a numerical solution, one of the most important goals is to achieve the greatest accuracy with the least computational cost.

The accuracy of a numerical solution of the boundary–layer equations also depends on the choice of the independent and dependent variables. There are many different possibilities here too, and this increases the number of trial solutions even more. The choice of the variables can categorically influence the accuracy of a solution: we will discuss this angle in more detail later.

Numerical solutions of the boundary–layer equations can today be constructed using standard methods (field methods). One of the first computer solutions was designed by F.G. Blottner; I. Flügge-Lotz (1963). Almost concurrently, A.M.O. Smith; D.W. Clutter (1963) published a different numerical solution for the boundary–layer equations. As time went on and the capacities of computers increased, these solutions were extended to larger areas of application: compressible boundary layers, cf. A.M.O. Smith; D.W. Clutter (1965); binary gases, cf. F.G. Blottner (1964); perturbed boundary layers, cf. E. Krause (1967, 1969, 1972); three–dimensional boundary layers, cf. E. Krause et al. (1968). A new variant in the solution methods was introduced by H.B. Keller (1971): this is the “box scheme” and is frequently used today. It involves transforming the momentum equation, a second order partial differential equation, into two first order differential equations. The solution is only one of many which are in use today. A summary of solution methods has been presented by F.G. Blottner (1975). A second overview based on the “box scheme” has been published by H.B. Keller (1978).

23.1.2 Note on Boundary–Layer Transformations

The boundary–layer equations for steady, incompressible, two–dimensional laminar boundary layers were presented in Chaps. 6 and 7 in three different forms.

In the form of Eqs. (6.14) to (6.16), the dependence on the Reynolds number has been already removed via the boundary–layer transformation. The great advantage in integrating these equations numerically is that both dimensionless velocity components and their derivatives are of the order of magnitude $O(1)$. This guarantees that the discretisation error does not grow arbitrarily and the solution become distorted. The numerical solution of Eqs. (6.14) to (6.16) is obtained by discretising the two differential equations using a suitable grid and then solving the resulting difference equations for the given initial and boundary conditions.

The second form of the boundary–layer equations is Eq. (7.77); this was obtained by means of the Görtler transformation. Introducing both a dimensionless stream function and a scale function $g(\xi) = \sqrt{2\xi}$ to the momentum and continuity equations yields only one equation for the dimensionless relative stream function $f(\xi, \eta)$. If we replace the partial derivatives with respect to ξ in Eq. (7.77) by difference quotients, the resulting difference–differential

equation, which only contains derivatives with respect to η , can be solved using numerical methods for nonlinear ordinary differential equations. The truncation error for this approach can grow rapidly if the quotient $g^2(\xi)/\Delta\xi$ becomes large. However, the advantage in using this similarity transformation is that variations in the boundary-layer thickness are essentially compensated by the scale function $g(\xi)$. This means that solutions of Eq. (7.77) hardly need a search algorithm to locate the edge of the boundary layer, such as that required for numerical solutions of Eqs. (6.14) and (6.15).

The third form of the boundary-layer equations which was presented in Sect. 7.3.2 is due to v.Mises transformation. Here the coordinates x and y are transformed to the independent variables ξ and ψ , where ξ is identical to x and ψ is again the stream function. The total pressure is used as a dependent variable; the term $\varrho v^2/2$ in the total pressure is small within the boundary layer and hence is neglected. The equation resulting from this transformation is Eq. (7.80) and it has the form of the heat conduction equation; by discretising both differential expressions it can be transformed to a difference equation. The advantage of the v.Mises transformation is similar to that of the similarity transformation: the number of dependent variables is reduced from two to one. Lack of accuracy can occur in the inverse transformation from the computational space to the real space close to the wall where u tends to zero and the numerical evaluation of the integral $y = \int(1/u) d\psi$ can yield an incorrect velocity profile $u(y)$.

Numerical solutions have been developed and successfully tested using all three forms of the boundary-layer equations.

23.1.3 Explicit and Implicit Discretisation

We will now demonstrate how the difference equations for the boundary-layer equations in the form of the differential equations (6.14) and (6.15) are obtained. For simplicity, we will neglect the stars and bars in these equations. They now read:

$$u \frac{\partial u}{\partial x} + v \frac{\partial u}{\partial y} = -\frac{dp}{dx} + \frac{\partial^2 u}{\partial y^2}, \quad (23.1)$$

$$\frac{\partial u}{\partial x} + \frac{\partial v}{\partial y} = 0. \quad (23.2)$$

Only the momentum equation (23.1) has to be considered for the moment, because it is this which delivers the tangential component $u(x, y)$ of the velocity. If this is known on the initial slice or has just been calculated on another cross-section $x = \text{const}$, the normal component can be determined.

This becomes clear if we insert the continuity equation (23.2) into the momentum equation (23.1). We obtain:

$$u \frac{\partial v}{\partial y} - v \frac{\partial u}{\partial y} = \frac{dp}{dx} - \frac{\partial^2 u}{\partial y^2}. \quad (23.3)$$

If the tangential component of the velocity u and the pressure gradient dp/dx is known, Eq. (23.3) is an ordinary linear differential equation for v , whose formal solution reads

$$v(x_0, y) = \exp(-F) \left[\int_0^y [\exp(F)] g \, dy' + v(x_0, 0) \right] \quad (23.4)$$

with

$$F(y) = - \int_0^y \left(\frac{1}{u} \frac{\partial u}{\partial y'} \right) \, dy', \quad g(y) = \frac{1}{u} \left(\frac{dp}{dx} - \frac{\partial^2 u}{\partial y^2} \right). \quad (23.5)$$

In Eq. (23.4), x_0 is the coordinate of the initial slice on which the boundary-layer calculation is to be commenced. The quantity $v(x_0, 0)$ denotes the value of the normal component at the wall ($y = 0$). If the wall is impermeable, $v(x_0, 0) = 0$.

Since the initial distribution $u(x_0, y)$ is generally not given as a function but rather as a table of values, Eq. (23.3) is usually numerically integrated, using, for example, a Runge–Kutta method. The normal component of the velocity may therefore not be arbitrarily given but must always be computed for each cross-section in the boundary layer so that it is compatible with the tangential component. From a mathematical point of view, therefore, the continuity equation is a compatibility condition which guarantees that the flow is source-free, cf. L. Ting (1965).

In order to derive the difference equation for Eq. (23.1), the partial derivatives of u and v are replaced by difference quotients. A coordinate grid is superimposed on the boundary layer: the coordinates used are those tangential and normal to the surface of the body. For simplicity, we choose Cartesian coordinates x and y here. Defining the spacing between two coordinate lines by Δx and Δy , and denoting the grid points in the x direction by i and those in the y direction by j , we can replace the partial derivatives with respect to y at any point P , characterised by i and j (Fig. 23.1), by the following so-called *centered space* difference expressions:

$$\left(\frac{\partial u}{\partial y} \right)_{i,j} = \frac{u_{i,j+1} - u_{i,j-1}}{2\Delta y} + O[(\Delta y)^2], \quad (23.6)$$

$$\left(\frac{\partial^2 u}{\partial y^2} \right)_{i,j} = \frac{u_{i,j+1} - 2u_{i,j} + u_{i,j-1}}{(\Delta y)^2} + O[(\Delta y)^2]. \quad (23.7)$$

The truncation error in both approximations is of the order of magnitude $O[(\Delta y)^2]$. If only the data $u(x_0, y)$ is known on the initial slice, the partial

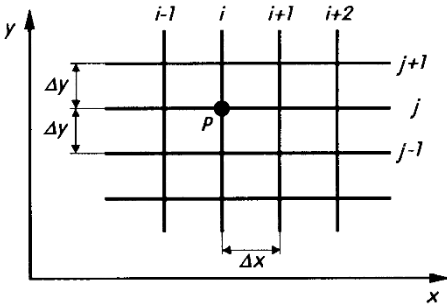


Fig. 23.1. Grid layout for difference equations

derivative with respect of x can only be approximated with a truncation error of the order of magnitude $O(\Delta x)$. The approximation is known as *forward space differencing*:

$$\left(\frac{\partial u}{\partial x} \right)_{i,j} = \frac{u(i+1,j) - u(i,j)}{\Delta x} + O(\Delta x). \quad (23.8)$$

Now, if the grid points with indices i and $1 \leq j \leq J$ are those on the initial slice, where $P_{i,j=1}$ denotes a grid point on the wall ($y = 0$) and $P_{i,j=J}$ a point on the edge of the boundary layer, all values of the two velocity components u and v in all grid points $P_{i,j}$ can be assumed to be known. Inserting the series expansions Eqs. (23.6), (23.7) and (23.8) into the momentum equation (23.1), all values of the velocity component u at all grid points $P_{i+1,j}$ can be determined directly:

$$u_{i+1,j} = u_{i,j} + (u_{i,j+1} - 2u_{i,j} + u_{i,j-1}) \frac{\Delta x}{u_{i,j}(\Delta y)^2} - (u_{i,j+1} - u_{i,j-1}) \frac{v_{i,j}}{u_{i,j}} \frac{\Delta x}{2\Delta y} - \left(\frac{\partial p}{\partial x} \right)_i \frac{\Delta x}{u_{i,j}} + O[(\Delta x)^2, (\Delta x)(\Delta y)^2]. \quad (23.9)$$

Now that the values $u_{i+1,j}$ are known, the values $v_{i+1,j}$ for all points $P_{i+1,j}$ can also be determined using Eq. (23.4). This means that the cross-section which lies a distance Δx downstream from the initial slice has been calculated fully. In the formulation chosen here, all values of the desired velocity component $u_{i+1,j}$ are obtained directly from the difference equations, and so this approach is called *explicit*. If the normal components of the velocity $v_{i+1,j}$ are computed using Eq. (23.4), all the data required for the next integration step Δx is known, and the velocity components $u_{i+2,j}$ and $v_{i+2,j}$ can be determined. In this manner, the integration can be continued as many times as desired in the direction of flow.

The advantage of explicit solutions is that the algebraic effort required is minimal. However a disadvantage is that the step size in the flow direction Δx cannot be chosen arbitrarily. In order that errors do not grow without limit, Δx may not exceed a certain value. The following condition must be met so that the solution is numerically stable:

$$\Delta x \leq \frac{1}{2}[u_{i,j}(\Delta y)^2]. \quad (23.10)$$

According to Eq. (23.10), the value of the tangential component of the grid point closest to the wall $u_{i,j=2}$ with $u \rightarrow 0$ for $y \rightarrow 0$ will have considerable influence on the step size in the main direction of flow. Because of this restriction to the step size, explicit solutions are only used for boundary-layer calculations when the boundary conditions require extremely small step sizes for reasons of accuracy. We will not discuss the question of numerical stability any further here. Details on the formulation of difference equations are to be found in R.D. Richtmyer; K.W. Morton (1967) and E. Isaacson; H.B. Keller (1966), and with particular reference to fluid mechanical problems, in C. Hirsch (1988).

In deriving the difference equation (23.9), the derivatives $\partial u / \partial y$ and $\partial^2 u / \partial y^2$ were replaced by the centered difference expressions Eqs. (23.6) and (23.7). In order to increase the accuracy, the difference equations for the point $P_{i+1/2,j}$ can also be formulated. We form the following averages:

$$\left(\frac{\partial u}{\partial y} \right)_{i+1/2,j} = \frac{1}{2} \left[\left(\frac{\partial u}{\partial y} \right)_{i,j} + \left(\frac{\partial u}{\partial y} \right)_{i+1,j} \right] + O[(\Delta x)^2], \quad (23.11)$$

$$\left(\frac{\partial^2 u}{\partial y^2} \right)_{i+1/2,j} = \frac{1}{2} \left[\left(\frac{\partial^2 u}{\partial y^2} \right)_{i,j} + \left(\frac{\partial^2 u}{\partial y^2} \right)_{i+1,j} \right] + O[(\Delta x)^2]. \quad (23.12)$$

In these expressions, the differential expressions are replaced with difference expressions:

$$\begin{aligned} \left(\frac{\partial u}{\partial y} \right)_{i+1/2,j} &= \frac{u_{i+1,j+1} - u_{i+1,j-1} + u_{i,j+1} - u_{i,j-1}}{4 \Delta y} \\ &\quad + O[(\Delta x)^2, (\Delta y)^2], \end{aligned} \quad (23.13)$$

$$\begin{aligned} \left(\frac{\partial^2 u}{\partial y^2} \right)_{i+1/2,j} &= \frac{u_{i+1,j+1} - 2u_{i+1,j} + u_{i+1,j-1} + u_{i,j+1} - 2u_{i,j} + u_{i,j-1}}{2(\Delta y)^2} \\ &\quad + O[(\Delta x)^2, (\Delta y)^2]. \end{aligned} \quad (23.14)$$

If we insert the difference expressions Eq. (23.8), (23.13) and (23.14) into the momentum equation (23.1), we obtain the difference equations according to the *Crank–Nicolson scheme*:

$$\begin{aligned} A_{i+1/2,j} u_{i+1,j+1} + B_{i+1/2,j} u_{i+1,j} + C_{i+1/2,j} u_{i+1,j-1} \\ + D_{i+1/2,j} + O[(\Delta x), (\Delta y)^2] = 0 \quad 2 \leq j \leq J-1 \end{aligned} \quad (23.15)$$

with

$$A_{i+1/2,j} = \frac{1/\Delta y - v_{i,j}/2}{2\Delta y}, \quad B_{i+1/2,j} = -[1/(\Delta y)^2 + u_{i,j}/\Delta x], \quad (23.16)$$

$$C_{i+1/2,j} = \frac{1/\Delta y + v_{i,j}/2}{2\Delta y}, \quad \bar{B}_{i+1/2,j} = -[1/(\Delta y)^2 - u_{i,j}/\Delta x], \quad (23.17)$$

$$\begin{aligned} D_{i+1/2,j} = A_{i+1/2,j} u_{i,j+1} + \bar{B}_{i+1/2,j} u_{i,j} + C_{i+1/2,j} u_{i,j-1} \\ - \left(\frac{dp}{dx} \right)_{i+1/2}. \end{aligned} \quad (23.18)$$

Strictly speaking in Eqs. (23.16) and (23.17) the values $u_{i,j}$ and $v_{i,j}$ should be replaced by the values $u_{i+1/2,j}$ and $v_{i+1/2,j}$. We will consider this in more detail in the next section, cf. Eq. (23.25).

In contrast to the explicit formulation Eq. (23.9), the difference equation (23.15) contains the unknown values of the tangential component of the velocity at three neighbouring points, and $u_{i+1,j}$ cannot be given directly. This formulation of the difference equations is therefore known as *implicit*; its solution will be described in the next section.

23.1.4 Solution of the Implicit Difference Equations

The coefficient matrix of the system of equations (23.15) is *tridiagonal*, i.e. only the main diagonal and the two neighbouring diagonals are occupied. The solution of this system of equations can be acquired using the *Thomas recursion algorithm*. Just as was done earlier in the case of the explicit solution, we assume that the velocity components $u_{i,j}$ and $v_{i,j}$ are known, and so we can determine the following quantities, using the no-slip condition $u(x, 0) = 0$ for the point closest to the wall $P_{i+1/2,j=2}$:

$$E_{i+1/2,j=2} = -\frac{A_{i+1/2,j=2}}{B_{i+1/2,j=2}}, \quad F_{i+1/2,j=2} = -\frac{D_{i+1/2,j=2}}{B_{i+1/2,j=2}}. \quad (23.19)$$

Thus $u_{i+1,j=2}$ can be expressed in terms of $u_{i+1,j=3}$:

$$u_{i+1/2,j=2} = E_{i+1/2,j=2} u_{i+1,j=3} + F_{i+1/2,j=2}. \quad (23.20)$$

Inserting Eq. (23.20) into the difference equation (23.15) for $j = 3$, the value of the tangential component of the velocity for the next point $u_{i+1,j=3}$ can be expressed in terms of $u_{i+1,j=4}$:

$$u_{i+1/2,j=3} = E_{i+1/2,j=3} u_{i+1,j=4} + F_{i+1/2,j=3}. \quad (23.21)$$

This recursion may be repeated as often as desired; one obtains

$$u_{i+1,j} = E_{i+1/2,j} u_{i+1,j+1} + F_{i+1/2,j} \quad 2 < j \leq J - 1 \quad (23.22)$$

with

$$E_{i+1/2,j} = -\frac{A_{i+1/2,j}}{B_{i+1/2,j} + C_{i+1/2,j} + E_{i+1/2,j-1}}, \quad (23.23)$$

$$F_{i+1/2,j} = -\frac{C_{i+1/2,j} F_{i+1/2,j-1} + D_{i+1/2,j}}{B_{i+1/2,j} + C_{i+1/2,j} E_{i+1/2,j-1}}. \quad (23.24)$$

According to R.D. Richtmyer; K.W. Morton (1967), p. 199, this solution has been used by many authors independently. It represents an adaptation of the Gauss elimination method to the parabolic form of the momentum equation and is known as the *Thomas algorithm*, cf. L.H. Thomas (1949).

Therefore, in order to compute the velocity profile for the cross-section $i+1$, first all quantities $E_{i+1/2,j}$ and $F_{i+1/2,j}$ for $2 \leq j \leq J-1$ are determined. Then $u_{i+1,J}$ is set equal to the value of the external boundary condition $U(x_{i+1})$ and the velocity profile at the position x_{i+1} can be computed in full.

Since the difference equations are formulated for the point $P_{i+1/2,j}$, but the four quantities $A_{i+1/2,j}$, $B_{i+1/2,j}$, $C_{i+1/2,j}$ and $\bar{B}_{i+1/2,j}$ in Eqs. (23.16) and (23.17) have been computed with the values $u_{i,j}$ and $v_{i,j}$, an error of the order of magnitude $O(\Delta x)$ arises. This may be reduced to $O[(\Delta x)^2]$ via an iteration of the computation of the $u(x_{i+1})$ profile, if $u_{i,j}$ and $v_{i,j}$ in the expressions $A_{i+1/2,j}$, $B_{i+1/2,j}$, $C_{i+1/2,j}$ and $\bar{B}_{i+1/2,j}$ are replaced by the following average values:

$$u_{m,i+1/2,j} = \frac{u_{i,j} + u_{i+1,j}}{2}, \quad v_{m,i+1/2,j} = \frac{v_{i,j} + v_{i+1,j}}{2}. \quad (23.25)$$

The values $u_{i,j+1}$, $u_{i,j}$ and $u_{i,j-1}$ which appear in Eq. (23.18) remain unaffected by this averaging. Further iterations cannot improve the accuracy of the solution. The implicit integration of the boundary-layer equations has the advantage that the solution of the difference equations is numerically unconditionally stable and although the step size Δx must be small, it is not subject to any restriction to maintain the numerical stability, cf. R.D. Richtmyer; K.W. Morton (1967) and E. Isaacson; H.B. Keller (1966).

23.1.5 Integration of the Continuity Equation

If the implicit solution is iterated, the computation of the normal component v can be incorporated into the iteration process. Instead of forming the average from Eq. (23.25), we then determine $v_{i+1/2,j}$ with a difference approximation of the continuity equation. In order to do this, the centered space difference form of the continuity equation is formulated for the point $P_{i+1/2,j-1/2}$. The normal component of the velocity is then computed, not for x_i and x_{i+1} , but for $x_{i+1/2}$. Equation (23.2) yields:

$$\begin{aligned} v_{i+1/2,j} &= v_{i+1/2,j-1} + (u_{i,j} - u_{i+1,j} + u_{i,j-1} - u_{i+1,j-1}) \frac{\Delta y}{2\Delta x} \\ &\quad + O[(\Delta x)^2, (\Delta y)^2]. \end{aligned} \quad (23.26)$$

The numerical integration of Eqs. (23.15) and (23.26) is commenced by first setting the values in the initial slice $v_{i+1/2,j}$ to zero. Using Eq. (23.15), we obtain a first approximation for the profile $u_{i+1,j}$ which is to be determined. These values are then inserted into Eq. (23.26), from which $v_{i+1/2,j}$ is then computed. The computation for the initial slice is repeated as often as is required until the difference between two consecutive iteration values $v_{i+1/2,j}$ lies within some given error constraint of order of magnitude $O[(\Delta x)^2, (\Delta y)^2]$. This query only has to be carried out for some chosen values j of the profile $v_{i+1/2,j}$.

At all subsequent positions, the computation of the normal components of the velocity only has to be repeated once, because after the v profile has been determined in the initial slice, $v_{i+1/2,j}$ can be used as a first approximation with an error of order $O(\Delta x)$. This calculation is carried out together with the formation of the averages in Eq. (23.25).

23.1.6 Boundary-Layer Edge and Wall Shear Stress

After the velocity components $u_{i+1,j}$ and $v_{i+1/2,j}$ have been calculated, we then have to check if the thickness of the boundary layer has changed. The growth and decline of the boundary-layer thickness depends on the form of the initial profile and on the boundary conditions. The inquiry into whether it has changed can be carried out using a simple error constraint: we determine the value of the tangential component of the velocity at the next to last point at the edge of the boundary layer $u_{i+1,J-1}$ and then investigate whether:

$$|u_{i+1,J-1} - U(x_{i+1})| \leq \varepsilon. \quad (23.27)$$

If Eq. (23.27) is satisfied for a given limit ε , e.g. 10^{-4} , the profile $u(y)$ can be computed for the cross-section $i+1$. If the velocity difference in Eq. (23.27) is greater than the given limit, the number of grid points for the y direction is increased by one, i.e. $J_{\text{new}} = J_{\text{old}} + 1$. This point must now also be occupied for x_i with the known edge value $U(x_i)$, so that the new value $u_{i+1,J_{\text{new}}-1}$

can be computed. The query in Eq. (23.27) is then repeated. In this manner, the edge of the boundary layer can be easily determined.

In order to compute the friction drag, the local wall shear stress and thus the derivative $(\partial u / \partial y)_{y=0}$ have to be determined. Since no symmetry condition in the differencing process can be used in discretising differentials at an edge point, the truncation error is relatively large. Therefore the aim is to improve the accuracy by including further grid points. One frequently used *four-point-formula* (valid for the edge point $u_{i+1,j=1} = 0$) reads:

$$\left[\left(\frac{\partial u}{\partial y} \right)_{y=0} \right]_{i+1} = \frac{18u_{i+1,j=2} - 9u_{i+1,j=3} + 2u_{i+1,j=4}}{6 \Delta y} + O[(\Delta y)^3]. \quad (23.28)$$

The increase of the grid points used can be avoided if we take the curvature at the wall from Eq. (7.2) into account in carrying out the discretisation. In the Taylor series, using the dimensionless representation, the derivative $(\partial^2 u / \partial y^2)_{y=0}$ is replaced by the pressure gradient dp/dx . This then leads to the *three-point-formula*:

$$\left[\left(\frac{\partial u}{\partial y} \right)_{y=0} \right]_{i+1} = \frac{8u_{i+1,j=2} - u_{i+1,j=3}}{6 \Delta y} - \left(\frac{dp}{dx} \right)_{i+1} \frac{\Delta y}{3} + O[(\Delta y)^3]. \quad (23.29)$$

For details of a *five-point formula* for the wall shear stress which is also valid for non-equidistant y steps, see H. Schlichting (1982), p. 193.

23.1.7 Integration of the Transformed Boundary–Layer Equations Using the Box Scheme

Equations (23.15) and (23.26) represent one of many known difference equations for the boundary–layer equations (23.1) and (23.2). In what now follows we shall show how the transformed boundary–layer equation (7.77) can be numerically integrated using the *box scheme* due to H.B. Keller (1971). The use of Eq. (7.77) has the advantage that the change in the boundary–layer thickness in the transformed ξ – η plane is only small, and one therefore does not need to inquire into the position of the boundary–layer edge for every integration step Δx . Furthermore, integration using the box scheme by H.B. Keller has the advantage that the difference equations can be formulated within *one* grid box $\Delta A = \Delta x \Delta y$, while for the previous set up we required two boxes. This means that the step size in the direction normal to the wall can also be formed in a variable manner without lowering the order of the truncation error. By controlling Δy , the computing time can be greatly reduced and the integration method generally made more efficient.

The solution of the boundary–layer equations using the box scheme has been described in detail in more recent literature, see, for example

H.B. Keller; T. Cebeci (1972a). The flexibility of the solution method has also been demonstrated by numerous examples. For instance, the inverse problem had also already been solved by H.B. Keller; T. Cebeci (1972b), i.e. they determined the pressure gradient for a given distribution of the wall shear stress. The computation of turbulent boundary layers is presented in H.B. Keller; T. Cebeci (1972a). Boundary layers undergoing separation can be safely calculated using the box scheme, cf. T. Cebeci et al. (1979).

One of the many transformed momentum equations which can be used to derive the box scheme reads:

$$f_{\eta\eta\eta} + f f_{\eta\eta} + \beta(\xi)(1 - f_\eta^2) = 2\xi(f_\eta f_{\xi\eta} - f_\xi f_{\eta\eta}), \quad (23.30)$$

cf. Eq. (7.77). This third order partial differential equation for the relative stream function $f(\xi, \eta)$ is transformed into three first order partial differential equations. Using the notation of H.B. Keller (1978), we define the derivatives $\partial f / \partial \eta$ and $\partial^2 f / \partial \eta^2$ via new variables U and V , such that

$$\frac{\partial f}{\partial \eta} = U, \quad \frac{\partial^2 f}{\partial \eta^2} = \frac{\partial U}{\partial \eta} = V. \quad (23.31)$$

Thus Eq. (23.30) assumes the following form:

$$\frac{\partial V}{\partial \eta} + fV + \beta(1 - U^2) = 2\xi \left(U \frac{\partial U}{\partial \xi} - V \frac{\partial f}{\partial \xi} \right). \quad (23.32)$$

Only first derivatives, for whose discretisation only two grid points are required, appear in the system (23.31) and (23.32). If we formulate the difference expressions for the midpoint of a grid box, the four edge points of one cell are needed for the discretisation (Fig. 23.2).

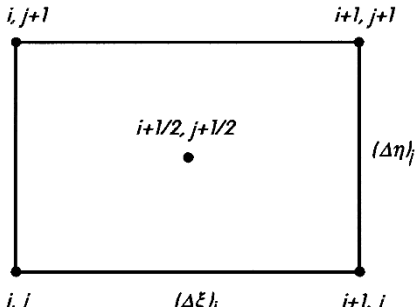


Fig. 23.2. The box scheme

Note (Reduction to a difference-differential equation)

The system (23.31) and (23.32) can be discretised in any number of ways. If we discretise, for example, the nonlinear expressions $U(\partial U / \partial \xi)$ and $V(\partial f / \partial \xi)$, where U and V are given by their average values, we obtain a first order difference-differential equation. This can be interpreted as a two point boundary value problem and can be solved using a numerical solution method for nonlinear ordinary differential equations, cf. H.B. Keller (1978).

In order to discretise the system (23.31) and (23.32) according to the box scheme of H.B. Keller (1978), averages and space centered difference schemes are used. If w denotes one of the three dependent variables U , V and f , the following relations hold for the discretisation:

$$\begin{aligned} [w]_{i+1,j+1/2} &= \frac{w_{i+1,j+1} + w_{i+1,j}}{2} \\ \left[\frac{\partial w}{\partial \eta} \right]_{i+1,j+1/2} &= \frac{w_{i+1,j+1} - w_{i+1,j}}{(\Delta \eta)_j} \\ \left[\frac{\partial w}{\partial \xi} \right]_{i+1/2,j+1/2} &= \frac{[w]_{i+1,j+1/2} - [w]_{i,j+1/2}}{(\Delta \xi)_i} \\ \left[\frac{\partial w}{\partial \eta} \right]_{i+1/2,j+1/2} &= \frac{\left[\frac{\partial w}{\partial \eta} \right]_{i+1,j+1/2} + \left[\frac{\partial w}{\partial \eta} \right]_{i,j+1/2}}{2} \\ [w]_{i+1/2,j+1/2} &= \frac{[w]_{i+1,j+1/2} + [w]_{i,j+1/2}}{2}, \end{aligned} \quad (23.33)$$

The discretised form of Eq. (23.31) and (23.32) is then:

$$\begin{aligned} \left[\frac{\partial f}{\partial \eta} \right]_{i+1,j+1/2} &= [U]_{i+1,j+1/2} \\ \left[\frac{\partial U}{\partial \eta} \right]_{i+1,j+1/2} &= [V]_{i+1,j+1/2}. \end{aligned} \quad (23.34)$$

$$\begin{aligned} \left[\frac{\partial V}{\partial \eta} \right]_{i+1/2,j+1/2} &= 2(\xi)_{i+1/2} \left([U]_{i+1/2,j+1/2} \left[\frac{\partial U}{\partial \xi} \right]_{i+1/2,j+1/2} \right. \\ &\quad \left. - [V]_{i+1/2,j+1/2} \left[\frac{\partial f}{\partial \xi} \right]_{i+1/2,j+1/2} \right) \\ &\quad - [fV + \beta(1 - U^2)]_{i+1/2,j+1/2}. \end{aligned} \quad (23.35)$$

The system of difference equations (23.34) and (23.35) is nonlinear and is therefore solved using an *iteration method*. H.B. Keller has suggested that the Newton method may be used. If the iteration values are denoted by k , they can be formulated as follows:

$$\begin{aligned} (f_{i+1,j}^{k+1}, U_{i+1,j}^{k+1}, V_{i+1,j}^{k+1}) &= (f_{i+1,j}^k, U_{i+1,j}^k, V_{i+1,j}^k) \\ &\quad + (\delta f_{i+1,j}^k, \delta U_{i+1,j}^k, \delta V_{i+1,j}^k). \end{aligned} \quad (23.36)$$

The system can be linearised using Eq. (23.36) and we obtain a *block tridiagonal* system of equations of the form:

$$\boxed{\mathbf{A}_{i,j}\delta_{i+1,j-1}^{k+1} + \mathbf{B}_{i,j}\delta_{i+1,j}^{k+1} + \mathbf{C}_{i,j}\delta_{i+1,j+1}^{k+1} = r_{i,j}}, \quad (23.37)$$

in which the quantity $\delta := (\delta f, \delta U, \delta V)^T$ and \mathbf{A} , \mathbf{B} and \mathbf{C} correspond to 3×3 matrices.¹ A solution is possible for given boundary conditions using the known algorithms, such as that given by E. Isaacson; H.B. Keller (1966). Details of the required transformations of the difference equations can be found in H.B. Keller; T. Cebeci (1971) and H.B. Keller (1974). Here we only indicate that the system Eq. (23.34) and (23.35) can be brought to the form

$$\mathbf{F}_{i+1,j} = \mathbf{D}_{i+1/2,j+1/2} \mathbf{F}_{i+1,j+1} + \mathbf{R}_{i+1/2,j+1/2}. \quad (23.38)$$

Here $\mathbf{F} = (f, U, V)^T$, while \mathbf{D} denotes a 3×3 matrix which along with the vector \mathbf{R} can be determined with Eq. (23.33) from Eqs. (23.34) and (23.35). According to Eq. (23.38), \mathbf{F} can be determined for all points $P_{i+1,j}$ as long as $\mathbf{F}_{i+1,j=J}$ is known on the edge of the boundary layer. For $j = J$ however only U is known from the boundary conditions. The boundary conditions at the wall for $y = 0$ corresponding to the formulation of the given two point boundary value problem must be satisfied by the quantities f and V . Equation (23.38) can also be used to construct an iterative solution in which the two unknown components of the solution vector $\mathbf{F}_{i+1,j=J}$ at the edge of the boundary layer are estimated and varied until the boundary conditions at the wall are satisfied to within some given error constraint. The required number of iterations is small since the data to be computed at the position x_{i+1} are already known to within an error of $O(\Delta x)$ from the previously computed velocity profile. As already indicated earlier there are several different ways of solving the difference equations. One very efficient method of solution is that by H.B. Keller (1974).

23.2 Turbulent Boundary Layers

23.2.1 Method of Wall Functions

In Sect. 18.5.1 we described the method of wall functions for attached boundary layers. Leaving off the bars denoting the time average, the system of equations to be solved reads:

$$u \frac{\partial u}{\partial x} + v \frac{\partial u}{\partial y} = -\frac{1}{\varrho} \frac{dp}{dx} + \frac{\partial}{\partial y} \left(\nu_t \frac{\partial u}{\partial y} \right), \quad (23.39)$$

$$\frac{\partial u}{\partial x} + \frac{\partial v}{\partial y} = 0 \quad (23.40)$$

¹ $(\delta f, \delta U, \delta V)^T$ denotes the *transposed matrix* which is obtained from the original matrix by swapping rows and columns.

with the boundary conditions

$$y \rightarrow 0 : \quad u = u_\tau \left(\frac{1}{\kappa} \ln \frac{yu_\tau}{\nu} + C^+ \right), \quad v = 0, \quad (23.41)$$

$$y = \delta : \quad u = u_e. \quad (23.42)$$

For $\nu_t = \text{const}$ and after introducing dimensionless quantities (related to the quantities $l, V, \nu_{tR} = lV$), Eqs. (23.39) and (23.40) formally become the boundary–layer equations (23.1) and (23.2) for laminar flows. This means that the numerical methods described for laminar boundary layers can be used to a great extent for turbulent boundary layers too.

Equation (23.39) can be used to derive the following behaviour of the solutions $u(x, y)$ and $\nu_t(x, y)$ close to the edge of the boundary layer, i.e. for $y \rightarrow \delta$:

$$\lim_{y \rightarrow \delta} (u_e - u) = a(x) (\delta - y)^n, \quad (23.43)$$

$$\lim_{y \rightarrow \delta} \nu_t = b(x) (\delta - y). \quad (23.44)$$

The exponent n is dependent on the turbulence model chosen. For example, $n = 2$ is the exponent for the model by R. Michel et al. (1968) and $n = 1$ that for the k - ε model. With Eq. (23.43) and (23.44), we take the limit $y \rightarrow \delta$ ($v = v_e, u = u_e$) of Eq. (23.39):

$$\frac{d\delta}{dx} = \frac{v_e}{u_e} + \frac{bn}{u_e}. \quad (23.45)$$

It has been suggested by J.C. Rotta (1983) that if one applies the coordinate shift

$$\hat{y} = y - y_0(x), \quad y_0(x) = (\nu/u_\tau) \exp(-\kappa C^+) \quad (23.46)$$

to the boundary condition (23.41) for $u(x, y)$, it simplifies to

$$u(x, \hat{y} = 0) = 0. \quad (23.47)$$

The shift $y_0(x)$ is small compared to the boundary–layer thickness and can in general be neglected. For smooth walls, with $C^+ = 5.0$, the value $y_0^+ = y_0 u_\tau / \nu = 0.124$ holds, i.e. the shift takes place in the purely viscous region ($y^+ < 1$) of the wall layer.

Using the dimensionless coordinate

$$\eta = \frac{\hat{y}}{\delta} = \frac{y - y_0}{\delta - y_0}, \quad \hat{\delta} = \delta - y_0 \approx \delta \quad (23.48)$$

the system of equations reads

$$u \frac{\partial u}{\partial x} + m_{II} \frac{\partial u}{\partial \eta} + \frac{1}{\varrho} \frac{dp}{dx} - m_I^2 \nu_t \frac{\partial^2 u}{\partial \eta^2} = 0, \quad (23.49)$$

$$\frac{\partial u}{\partial x} + m_I \frac{\partial v}{\partial \eta} - m_{III} \frac{\partial u}{\partial \eta} = 0 \quad (23.50)$$

with the boundary conditions

$$\begin{aligned}\eta = 0 : \quad u = 0, \quad v = 0, \\ \eta = 1 : \quad u = u_e.\end{aligned}\tag{23.51}$$

Here:

$$\begin{aligned}m_I(x) &= \frac{1}{\hat{\delta}}, \\ m_{II}(x, \eta) &= m_I v - m_{III} u - m_I^2 \frac{\partial \nu_t}{\partial \eta}, \\ m_{III}(x, \eta) &= m_I \eta \frac{d\hat{\delta}}{dx},\end{aligned}\tag{23.52}$$

where $m_{III}(x, \eta)$ can be determined using Eq. (23.45) from $d\hat{\delta}/dx \approx d\delta/dx$.

Introducing the coordinate η from Eq. (23.48) has the benefit that the region of integration is restricted to a slice of constant height $0 \leq \eta \leq 1$. In this slice, one can carry out a fixed grid division with respect to η ; this is advantageous and time saving for the numerical computation.

The structure of Eq. (23.49) corresponds to that of Eq. (23.1), and so the discretisation may be carried out in analogy to Sect. 23.1.3.

Implicit discretisation using the Crank–Nicolson scheme for the point $P_{i+1/2,j}$ again yields Eq. (23.15) with

$$A_{i+1/2,j} = -\frac{m_{II}}{4\Delta\eta} + \frac{m_I^2\nu_t}{2(\Delta\eta)^2},\tag{23.53}$$

$$B_{i+1/2,j} = -\frac{u}{\Delta x} - \frac{m_I^2\nu_t}{(\Delta\eta)^2},\tag{23.54}$$

$$C_{i+1/2,j} = -\frac{m_{II}}{4\Delta\eta} + \frac{m_I^2\nu_t}{2(\Delta\eta)^2},\tag{23.55}$$

$$\bar{B}_{i+1/2,j} = \frac{u}{\Delta x} - \frac{m_I^2\nu_t}{2(\Delta\eta)^2},\tag{23.56}$$

$$D_{i+1/2,j} = A_{i+1/2,j} U_{i+1/2,j} + \bar{B}_{i+1/2,j} u_{i,j} + C_{i+1/2,j} u_{i,j-1},$$

$$-\frac{1}{\varrho} \left(\frac{dp}{dx} \right)_{i+1/2}.\tag{23.57}$$

Here, the values m_{II} , $m_I^2\nu_t$ and u in Eqs. (23.53) to (23.56) are again determined in point $P_{i,j}$ instead of point $P_{i+1/2,j}$ and are then replaced by the average values using iteration in analogy to Eq. (23.25).

The quantity b in Eq. (23.45) can be determined from the ν_t distribution at the outer edge of the boundary layer according to Eq. (23.44), using the difference equation

$$b_i = \frac{(m_I)_i (\nu_t)_{i,J-1}}{1 - \eta_{J-1}} \quad (23.58)$$

with $\eta_J = 1$.

If we integrate the continuity equation (23.50), we obtain the following expression, in analogy to Eq. (23.26):

$$\begin{aligned} v_{i+1/2,j} &= v_{i+1/2,j-1} (u_{i+1,j} - u_{i,j} + u_{i+1,j-1} - u_{i,j-1}) \frac{\Delta\eta}{2(m_I)_{i+1/2} \Delta x} \\ &\quad - (u_{i,j} - u_{i,j-1} + u_{i+1,j} - u_{i+1,j-1}) \frac{(m_{III})_{i+1/2,j-1/2}}{(m_I)_{i+1/2}}. \end{aligned} \quad (23.59)$$

In order to close the system (23.49) to (23.51) we need to include a turbulence model. Algebraic models consist of simple relations between ν_t and the velocity field, for example Eq. (18.8) with $\nu_t = (\ell^2/\delta)(\partial u/\partial\eta)$. In one and more equation models, the differential equations have the same structure as Eq. (23.49), so that if implicit discretisation according to Crank–Nicolson is carried out, they yield algebraic equations similar to Eq. (23.15). The solution of the extended system of implicit difference equations can be obtained using the method in Sect. 23.1.4. Numerical details have been given by authors such as R. Voges (1978). Here the solution of the system of equations is carried out (using a tridiagonal matrix) by means of the Thomas algorithm.

The initial conditions may be taken approximately from the solutions of equilibrium boundary layers or the profiles of quasi-equilibrium boundary layers, cf. Sect. 18.5.1.

Variable step size in the η direction

Because of the large velocity gradients in turbulent boundary layers close to the wall, a coordinate system with variable step size in the η direction is recommended; such as system was introduced in the form of the box scheme in Sect. 23.1.7. If the box scheme is not used, the approximations for the differential quotients $\partial u/\partial y$ and $\partial^2 u/\partial\eta^2$ shown below can be used. Neighbouring step sizes are denoted by $(\Delta\eta)_{i,j} = \eta_{i,j} - \eta_{i,j-1}$ and $(\Delta\eta)_{i,j+1} = \eta_{i,j+1} - \eta_{i,j}$.

$$\begin{aligned} \left(\frac{\partial u}{\partial\eta} \right)_{i+1,j} &= (g_1)_{i,j} u_{i+1,j+1} - [(g_1)_{i,j} - (g_2)_{i,j}] u_{i+1,j} \\ &\quad - (g_2)_{i,j} u_{i+1,j-1} + O[(\Delta\eta)_{i,j} (\Delta\eta)_{i,j+1}], \end{aligned} \quad (23.60)$$

$$\begin{aligned} \left(\frac{\partial^2 u}{\partial\eta^2} \right)_{i+1,j} &= 2 \{ (g_3)_{i,j} u_{i+1,j+1} - [(g_3)_{i,j} - (g_4)_{i,j}] u_{i+1,j} \\ &\quad + (g_4)_{i,j} u_{i+1,j-1} \} + O[(\Delta\eta)_{i,j+1} - (\Delta\eta)_{i,j}]. \end{aligned} \quad (23.61)$$

The quantities g_1 , g_2 , g_3 and g_4 are defined as follows:

$$\begin{aligned}(g_1)_{i,j} &= \frac{[(\Delta\eta)^2]_{i,j}}{h_{i,j}}, & (g_2)_{i,j} &= \frac{[(\Delta\eta)^2]_{i,j+1}}{h_{i,j}}, \\ (g_3)_{i,j} &= \frac{[(\Delta\eta)]_{i,j}}{h_{i,j}}, & (g_4)_{i,j} &= \frac{[(\Delta\eta)]_{i,j+1}}{h_{i,j}}\end{aligned}\quad (23.62)$$

with

$$h_{i,j} = (\Delta\eta)_{i,j}(\Delta\eta)_{i,j+1}[(\Delta\eta)_{i,j} + (\Delta\eta)_{i,j+1}]. \quad (23.63)$$

If the errors in Eqs. (23.60) and (23.61) are to be of the same order of magnitude for reasons of accuracy, the ratio of two neighbouring step sizes may only be of magnitude $O[1 + (\Delta\eta)_{i,j}]$. The step size $(\Delta\eta)_{i,j}$ can therefore not be varied arbitrarily.

Using this discretisation we again obtain the difference equations (23.15) with the abbreviations:

$$A_{i+1/2,j} = \left[m_I^2 \nu_t g_3 - \frac{1}{2} m_{II} g_1 \right]_{i,j}, \quad (23.64)$$

$$B_{i+1/2,j} = - \left[m_I^2 \nu_t (g_3 + g_4) + \frac{u}{\Delta x} - \frac{1}{2} m_{II} (g_1 - g_2) \right]_{i,j}, \quad (23.65)$$

$$C_{i+1/2,j} = \left[m_I^2 \nu_t g_4 - \frac{1}{2} m_{II} g_2 \right]_{i,j}, \quad (23.66)$$

$$\bar{B}_{i+1/2,j} = - \left[m_I^2 \nu_t (g_3 + g_4) - \frac{u}{\Delta x} - \frac{1}{2} m_{II} (g_1 - g_2) \right]_{i,j}. \quad (23.67)$$

Again $D_{i+1/2,j}$ is defined by Eq. (23.57). For constant step sizes, Eqs. (23.64) to (23.67) become Eqs. (23.53) to (23.56).

The integration of the continuity equation again delivers Eq. (23.59), if $\Delta\eta$ is replaced by $\Delta\eta_{i,j}$.

Example: Grid definition using a geometric series

Frequently a grid is used where the step size grows according to a geometric series. Then

$$\eta_1 = 0, \quad \eta_j = \eta_2 \frac{K^{j-1} - 1}{K - 1}, \quad \eta_J = 1, \quad \Delta\eta_{i,j} = \eta_2 K^{j-2}, \quad (23.68)$$

where K has a value of about 1.1. The number J of grid points in the η direction fixes $\eta_2 = (K - 1)/(K^{J-1} - 1)$. The quantities in Eq. (23.62) are then:

$$\begin{aligned}(g_1)_{i,j} &= \frac{1}{\eta_2} \frac{K}{1 + K}, & (g_2)_{i,j} &= K^2 (g_1)_{i,j}, \\ (g_3)_{i,j} &= \frac{1}{\eta_2^2} \frac{K^{3-2j}}{1 + K}, & (g_4)_{i,j} &= K^2 (g_3)_{i,j}.\end{aligned}\quad (23.69)$$

Note (logarithmic coordinate)

Because of the boundary condition (23.41) for $u(x, y)$, the solution $u(x, y)$ for $\eta \rightarrow 0$ has the form

$$\lim_{\eta \rightarrow 0} u(x, \eta) = \frac{u_\tau}{\kappa} \left[\ln \left(\eta + \frac{y_0}{\hat{\delta}} \right) - \ln \frac{y_0}{\hat{\delta}} \right]. \quad (23.70)$$

The difference formulae used in the numerical method for the partial derivatives are based on the fact that the function which is to be differenced can be approximated by a second order polynomial at three neighbouring grid points. The logarithmic function in Eq. (23.70) which the velocity distribution close to the wall is, however, not described particularly well by a second order polynomial.

This difficulty can be avoided by following J.C. Rotta (1983) and introducing the logarithmic coordinate

$$\zeta = \ln \left(\eta + \frac{y_0}{\hat{\delta}} \right) \quad (23.71)$$

and forming the differentials $\partial u / \partial \zeta$ and $d^2 u / d\zeta^2$ with the difference formulae. If the distribution of u over η is logarithmic, these differentials are then exact. But even further outwards where the velocity distribution deviates from the logarithmic distribution, they can be determined fairly exactly. This is because the grid spacing on the ζ axis becomes ever narrower as the distance from the wall increases and it approximates an equidistant distribution if the spacing on the η axis grows according to a geometric series.

Of course introducing the logarithmic coordinate requires additional computational effort. However, this is not considerable and the gain in accuracy is great, cf. J.C. Rotta (1983).

J.C. Rotta (1983) has used this numerical method to compute turbulent boundary layers, with the turbulence model by R. Michel et al. (1968).

In the same way, a more demanding turbulent model can be chosen. Examples would be the $k-\varepsilon$ model for large Reynolds numbers which has been presented by W.P. Jones; B.E. Launder (1972a), or the Reynolds stress model by K. Hanjalić; B.E. Launder (1972a). The work by B. Jeken (1992) also contains information on this latter type of model. The extension to turbulent boundary layers with separation has been treated by D. Vieth (1996), with the heat transfer also taken into account.

23.2.2 Low–Reynolds–Number Turbulence Models

Low–Reynolds–number turbulence models are all those turbulence models where the friction terms are taken into account and both the viscous wall layer and the viscous superlayer are brought into the calculation. Then the boundary conditions at the wall (no-slip condition) are particularly simple and the transition to the inviscid outer flow takes place continuously as for laminar boundary layers, cf. Sect. 18.5.3. Since the equations have practically the same structure as those for laminar boundary layers, the numerical

methods for laminar boundary layers can be quite simply extended to turbulent boundary layers. Because of the much larger wall gradients in turbulent boundary layers, these must be computed using variable step sizes in the y direction. Since the boundary-layer thickness of turbulent boundary layers grows strongly, a suitable boundary-layer transformation analogous to the Görtler transformation is frequently used.

We emphasise that low-Reynolds-number turbulence models deliver no higher order improvements to the solution compared to the method of wall functions. The results from both methods (for example, with respect to the distribution of the skin-friction coefficient) are of the same order of magnitude, cf. for example K. Gersten; H. Herwig (1992), p. 668 and D.C. Wilcox (1998), p. 190.

Examples

Algebraic turbulence models

Again the system of equations (23.1) and (23.2) is valid, if the term $\partial^2 u / \partial y^2$ in Eq. (23.1) is replaced by $\partial [N \partial u / \partial y] / \partial y$, with $N = 1 + \nu_t / \nu$. In the same way, Eq. (23.30) holds, if $f_{\eta\eta\eta}$ is replaced by $(N f_{\eta\eta})_\eta$.

A numerical method of solving Eq. (23.30) thus changed is described in detail by H. Schlichting (1982), p. 188. The same equation is also used in the numerical method given by T. Cebeci; P. Bradshaw (1984), p. 185. This method is also valid for compressible boundary layers and works with the box method. The $k - \omega$ model has the advantage of a better description of the near-wall area compared to the other models. In the SST model (**s**hear **s**tress **t**ransport model) by F.R. Menter (1994) the advantages of the $k - \omega$ model and the $k - \varepsilon$ model have been combined.

The Falkner–Skan transformation from Eq. (7.7) and (7.18) is sometimes used instead of the Görtler transformation, cf. T. Cebeci; P. Bradshaw (1984), p. 195, and T. Cebeci; P. Bradshaw (1977), p. 237.

Many-equation turbulent models

An overview of low-Reynolds-number versions of two-equation turbulence models has been given by, for example, V.C. Patel et al. (1985) and D.C. Wilcox (1998), p. 185. Clearly the $k-\omega$ model has advantages compared to the other models.

A low-Reynolds-number version of a Reynolds stress model has been presented by S. Jakirlić; K. Hanjalić (1995).

23.3 Unsteady Boundary Layers

Boundary-layer flows can become unsteady when the initial and boundary conditions are time dependent, as was shown in Chaps. 13 and 21. For two-dimensional incompressible flows, the momentum equation contains a term which describes the local acceleration $\partial u / \partial t$, while the continuity equation remains unchanged. In order to analyse the time dependence more closely, we write down Eq. (13.4) in the following dimensionless form, with $\varrho = \text{const}$, $\mu = \text{const}$ and $g = 0$:

$$\frac{\partial u}{\partial t} + u \frac{\partial u}{\partial x} = - \frac{\partial p}{\partial x} + \frac{\partial^2 u}{\partial y^2} - v \frac{\partial u}{\partial y}. \quad (23.72)$$

Characteristic lines for constant distance from the wall $y = \text{const}$ can be defined for the two acceleration terms on the left hand side of Eq. (23.72). Their slope is given by projection onto the x - t plane:

$$\left(\frac{dx}{dt} \right)_{y=\text{const}} = u. \quad (23.73)$$

Using Eq. (23.73), Eq. (23.72) can be written as follows:

$$\frac{\partial u}{\partial t} + u \frac{\partial u}{\partial x} = \left(\frac{du}{dt} \right)_{y=\text{const}} = -\frac{\partial p}{\partial x} + \frac{\partial^2 u}{\partial y^2} - v \frac{\partial u}{\partial y}. \quad (23.74)$$

The numerical integration of Eq. (23.74) then has to be carried out along the characteristic lines which are defined by Eq. (23.73). For one time step Δt we obtain

$$x_{i+1,k+1} = x_{P,k} + u_m \Delta t. \quad (23.75)$$

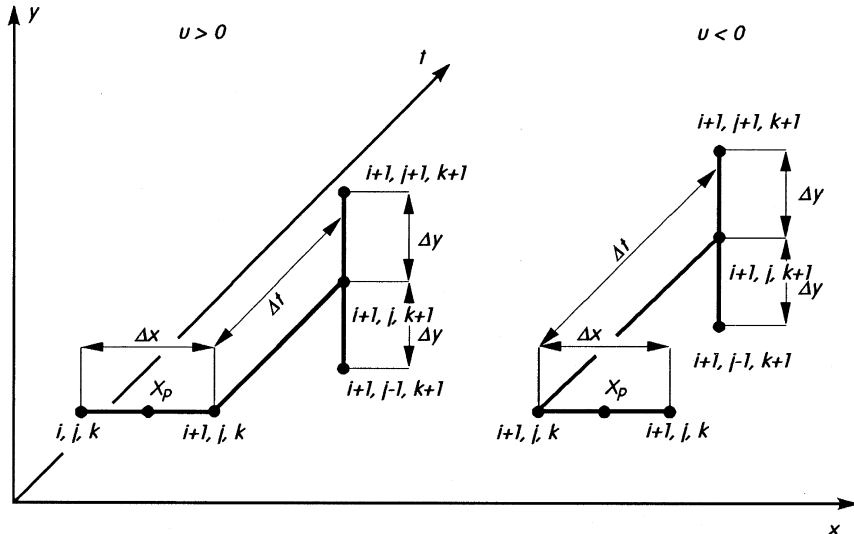


Fig. 23.3. Discretisation for unsteady boundary layers

According to Fig. 23.3, $x_{i+1,k+1}$ in Eq. (23.75) represents the x coordinate of the point in the grid in the x - t plane for which u and v are to be computed. As before, the index i counts the integration steps in the x direction, j those in the y direction while k denotes the number of time steps Δt . The index j is not required and so will not be included in the following derivation. The point with the coordinate $x_{P,k}$ generally lies between two grid points, so that either $x_{i,k} \leq x_{P,k} \leq x_{i+1,k}$ or $x_{i+1,k} \leq x_{P,k} \leq x_{i+2,k}$, depending on whether

$u_m \geq 0$ or $u_m \leq 0$. The average u_m is formed with the values $u_{i+1,k+1}$ and $u_{P,k}$. The velocity in the point $x_{P,k}$ can be determined by discretising the left hand side of Eq. (23.74), taking the position of the point $x_{P,k}$ into account:

$$u_{P,k} = \left(1 - u \frac{\Delta t}{\Delta x}\right) u_{i+1,k} + \left(u \frac{\Delta t}{\Delta x}\right) u_{i,k} \quad \text{for } u \geq 0 \quad (23.76)$$

and

$$u_{P,k} = \left(1 + u \frac{\Delta t}{\Delta x}\right) u_{i+1,k} - \left(u \frac{\Delta t}{\Delta x}\right) u_{i+2,k} \quad \text{for } u \leq 0. \quad (23.77)$$

In order that the error in the approximations Eq. (23.76) and (23.77) remains of order $O(\Delta x)$, Δt has to satisfy the following condition

$$|u| \frac{\Delta t}{\Delta x} \leq 1. \quad (23.78)$$

This condition is the Courant–Friedrichs–Lewy condition, cf. E. Isaacson; H.B. Keller (1966), and it guarantees numerical stability for difference solutions of hyperbolic differential equations if the differencing domain of dependency is larger than that of the partial differential equation. This rule can now be used to discretise the boundary-layer equations with the formulae given. One only has to ascertain whether u is larger than or smaller than zero. One way of setting up the difference quotients is shown in Fig. 23.3. The solution of the implicit difference equations can be carried out using the Thomas algorithm for the initial conditions formulated earlier. In integration using the box scheme is given by H.B. Keller (1978).

The deliberations above show that backflows can also be computed with the momentum equation for unsteady boundary layers. However this is not true for the case where the characteristics run back into the initial slice, since the initial data can then not be chosen freely. If the numerical solution is known, the distribution of the wall shear stress for unsteady as well as for steady boundary layers can be given. Details on the numerical computation of unsteady turbulent boundary layers are given by W. Geißler (1993).

23.4 Steady Three-Dimensional Boundary Layers

The many different three-dimensional boundary layers were presented in Sect. 12.2 and in Chap. 20. Here we will only discuss the discretisation of the boundary-layer equations for three-dimensional flows and the solution of the resulting difference equations. We will not consider the formulation of the problem in the otherwise usual curvilinear non-orthogonal coordinates, cf. E. Krause et al. (1976). According to Eq. (12.55) to (12.57), the boundary-layer

equations in Cartesian coordinates in dimensionless form read ($h_x = h_z = 1$, $\varrho = \text{const}$, $\mu = \text{const}$):

$$\begin{aligned} u \frac{\partial u}{\partial x} + v \frac{\partial u}{\partial y} + w \frac{\partial u}{\partial z} &= -\frac{\partial p}{\partial x} + \frac{\partial^2 u}{\partial y^2}, \\ u \frac{\partial w}{\partial x} + v \frac{\partial w}{\partial y} + w \frac{\partial w}{\partial z} &= -\frac{\partial p}{\partial z} + \frac{\partial^2 w}{\partial y^2}, \\ \frac{\partial u}{\partial x} + \frac{\partial v}{\partial y} + \frac{\partial w}{\partial z} &= 0. \end{aligned} \quad (23.79)$$

Initial and boundary conditions are needed to integrate Eq. (23.79). If we wish to compute the boundary layer on a flat plate for the rectangle $x_I \leq x \leq x_E$ and $z_I \leq z \leq z_E$, the boundary conditions at the wall are given by the no-slip condition:

$$y = 0 : \quad u(x, 0, z) = v(x, 0, z) = w(x, 0, z) = 0 \quad (23.80)$$

and those at the edge of the boundary layer by the velocity components of the inviscid outer flow $U(x, z)$ and $W(x, z)$:

$$y = \delta : \quad u(x, y, z) = U(x, z), \quad w(x, y, z) = W(x, z). \quad (23.81)$$

The velocity components $U(x, z)$ and $W(x, z)$ satisfy the Euler equation for two-dimensional flows, so that the pressure $p = p(x, z)$ is known in the region of integration $x_I \leq x \leq x_E$, $z_I \leq z \leq z_E$. Furthermore, the velocity profile of the two tangential components must be given in the initial slice:

$$\begin{aligned} x = x_I, \quad z_I \leq z \leq z_E, \quad 0 \leq y \leq \delta; \\ u(x_I, y, z) = u_{xI}(y, z) \quad w(x_I, y, z) = w_{xI}(y, z), \end{aligned} \quad (23.82)$$

$$\begin{aligned} z = z_I, \quad x_I \leq x \leq x_E, \quad 0 \leq y \leq \delta; \\ u(x, y, z_I) = u_{zI}(x, y) \quad w(x, y, z_I) = w_{zI}(y, z). \end{aligned} \quad (23.83)$$

As in the case of unsteady two-dimensional boundary layers, characteristic lines can be identified here too. The momentum equations are again rewritten as:

$$\begin{aligned} u \frac{\partial u}{\partial x} + w \frac{\partial u}{\partial z} &= -\frac{\partial p}{\partial x} + \frac{\partial^2 u}{\partial y^2} - v \frac{\partial u}{\partial y} \\ u \frac{\partial w}{\partial x} + w \frac{\partial w}{\partial z} &= -\frac{\partial p}{\partial z} + \frac{\partial^2 w}{\partial y^2} - v \frac{\partial w}{\partial y}. \end{aligned} \quad (23.84)$$

The slope of the characteristics at constant distance from the wall $y = \text{const}$ is found to be

$$\left(\frac{dz}{dx} \right)_{y=\text{const}} = \frac{w}{u}. \quad (23.85)$$

This equation is the projection of the streamlines onto the x - z plane. The left hand side of Eq. (23.84) can be transformed using Eq. (23.85) to

$$\begin{aligned} u \frac{\partial u}{\partial x} + w \frac{\partial u}{\partial z} &= u \left(\frac{du}{dx} \right)_{y=\text{const}} \\ u \frac{\partial w}{\partial x} + w \frac{\partial w}{\partial z} &= u \left(\frac{dw}{dx} \right)_{y=\text{const}}. \end{aligned} \quad (23.86)$$

The integration of the right hand side of Eq. (23.84) must again, as was done for unsteady flows, be carried out along the characteristics defined by Eq. (23.85). If a Cartesian grid is placed on the integration region, it can be carried out in the x and z directions. If the index k numbers the grid points in the z direction, Eq. (23.85) delivers the relations:

$$z_{i+1,k+1} = z_{i,P} + \left(\frac{w}{u} \right)_m \Delta x, \quad x_{i+1,k+1} = x_{P,k} + \left(\frac{u}{w} \right)_m \Delta z. \quad (23.87)$$

Figure 23.4 shows $x_{i+1,k+1}$ and $z_{i+1,k+1}$, the coordinates of the grid points in the x - z plane for which u and w are to be computed. The points $x_{P,k}$ and $z_{k,P}$ again generally lie between two grid points. If $0 \leq (w/u)_m$, then it follows that $z_{i,k} \leq z_{i,P} \leq z_{i,k+1}$, while if $(w/u)_m \leq 0$, then $z_{i,k+1} \leq z_{i,P} \leq z_{i,k+2}$. The two other possible locations of the point P with respect to the coordinate $x_{P,k}$ are $x_{i,k} \leq x_{i,P} \leq x_{i,k+1}$ for $0 \leq (w/u)_m$ and $x_{i,k+1} \leq x_{i,P} \leq x_{i,k+2}$ for $(w/u)_m \leq 0$. The velocity components u and w of the point with coordinates $x_{P,k}$ and $z_{i,P}$ are found by discretising Eq. (23.86):

$$u_{i,P} = \left(1 - \frac{w}{u} \frac{\Delta x}{\Delta z} \right) u_{i,k+1} + \left(\frac{w}{u} \frac{\Delta x}{\Delta z} \right) u_{i,k}, \quad \frac{w}{u} \geq 0 \quad (23.88)$$

and

$$u_{i,P} = \left(1 - \frac{w}{u} \frac{\Delta x}{\Delta z} \right) u_{i,k+1} - \left(\frac{w}{u} \frac{\Delta x}{\Delta z} \right) u_{i,k+2}, \quad \frac{w}{u} \leq 0. \quad (23.89)$$

In the corresponding expressions for w , $u_{i,P}$ is replaced by $w_{i,P}$, $u_{i,k+1}$ by $w_{i,k+1}$ and $u_{i,k+2}$ by $w_{i,k+2}$. For the point with coordinate $x_{P,k}$ we obtain the relations

$$u_{P,k} = \left(1 - \frac{u}{w} \frac{\Delta z}{\Delta x} \right) u_{i+1,k} + \left(\frac{u}{w} \frac{\Delta z}{\Delta x} \right) u_{i,k}, \quad \frac{u}{w} \geq 0 \quad (23.90)$$

and

$$u_{P,k} = \left(1 + \frac{u}{w} \frac{\Delta z}{\Delta x} \right) u_{i+1,k} - \left(\frac{u}{w} \frac{\Delta z}{\Delta x} \right) u_{i+2,k}, \quad \frac{u}{w} \leq 0 \quad (23.91)$$

and corresponding relations for w . The Courant–Friedrichs–Lowy condition for Eq. (23.88) and (23.89) has the following form:

$$\left| \frac{w}{u} \right| \frac{\Delta x}{\Delta z} \leq 1 \quad (23.92)$$

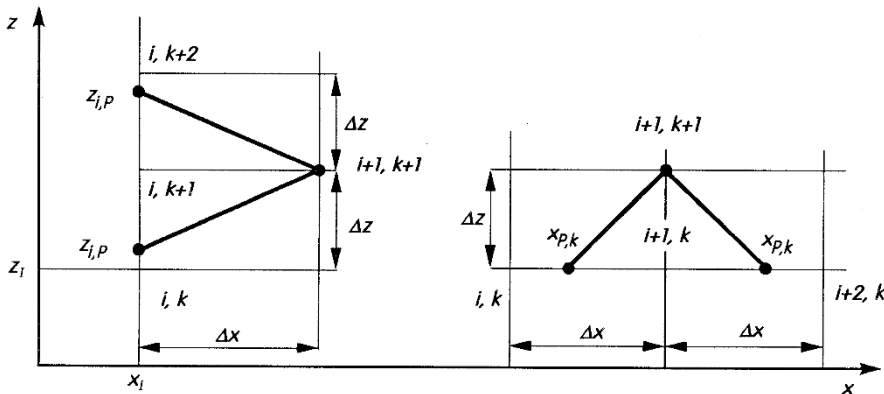


Fig. 23.4. Discretisation for three-dimensional boundary layers

and for Eq. (23.90) and (23.91):

$$\left| \frac{u}{w} \right| \frac{\Delta z}{\Delta x} \leq 1. \quad (23.93)$$

The momentum equations and the continuity equation (23.79) can now be discretised explicitly or implicitly (for example, using the box scheme). The different possible schemes are given in E. Krause et al. (1969). The accuracy of the schemes depends on the number of grid points used for the discretisation in the x - z plane. If four grid points are used, the accuracy of order $O[(\Delta x)^2, (\Delta z)^2]$ can always be achieved, whereas if three grid points are used the accuracy is only $O(\Delta x, \Delta z)$. Figure 23.5 shows two differencing schemes with second order accuracy.

Since three-dimensional boundary layers frequently exhibit large changes of direction of the cross flow as one moves along the coordinate normal to the wall, it is advantageous to choose the domain of dependency to be as large as possible, so that numerical instabilities are avoided. If the second scheme shown in Fig. 23.5 is used for four grid points in the x - z plane for $\Delta x/\Delta z = 1$, it allows a change of direction in the cross flow of 135° before the computation becomes unstable. The rapid growth in the error outside the region of stability is shown in Fig. 23.6.

The integration of the momentum equations can be carried out in both the x direction and the z direction. Details of the computation of three-dimensional turbulent boundary layers, also for compressible fluids, can be found in the overviews presented by H.H. Fernholz; E. Krause (1982) and D.A. Humphreys; J.P.F. Lindhout (1988).

The problem of solving the three-dimensional boundary-layer equations has not yet lost its actuality. In the past the numerical methods have been investigated and extended in great detail. E.H. Hirschel; J. Cousteix and W. Kordulla (2013) have presented a comprehensive description of the state of the research.

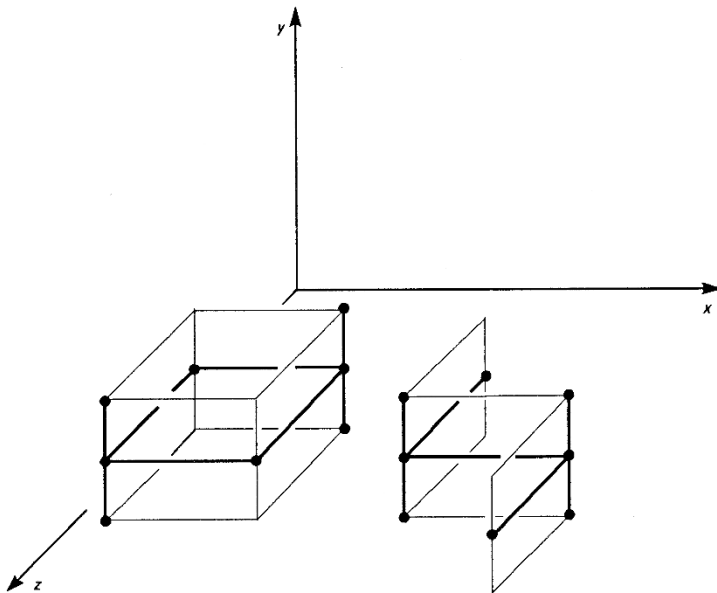


Fig. 23.5. Differencing schemes for three-dimensional boundary layers

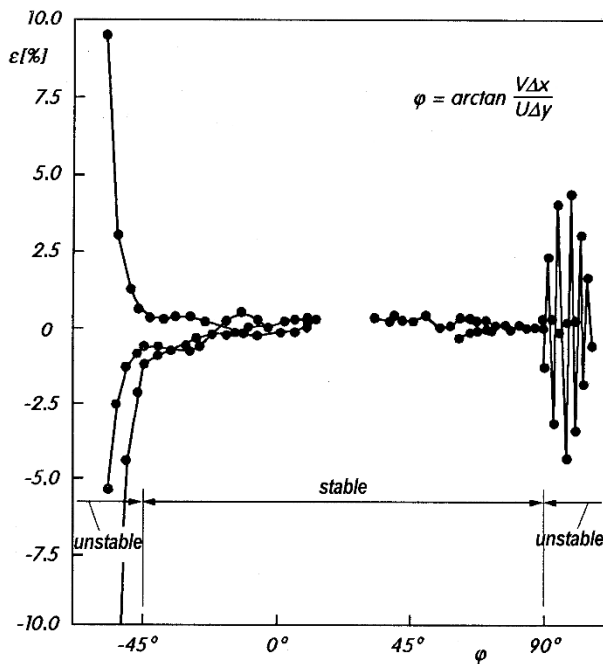


Fig. 23.6. Numerically stable region of the second differencing scheme in Fig. 23.5, according to E. Krause et al. (1969)

List of Frequently Used Symbols

a	m^2/s	thermal diffusivity, Eq. (4.12)
A	m^2	cross-sectional area
Ar	—	Archimedes number, Eq. (4.32)
b	m	span, breadth, width
B	—	blockage, Eq. (1.17)
B_q	—	heat flux number, wall Stanton number, Eq. (19.35)
c	m/s	speed of sound
c, c_p, c_v	$\text{J}/\text{kg K}$	specific heat capacity
c_D	—	drag coefficient, Eq. (1.5)
$c_{\mathcal{D}}$	—	dissipation integral coefficient, Eq. (19.51)
c_f	—	skin-friction coefficient, Eq. (2.8), (18.77)
c_g	m/s	group velocity
c_i	—	concentration of component i
c_L	—	lift coefficient, Eq. (1.5)
c_M	—	moment coefficient, Eq. (5.84)
c_p	—	pressure coefficient, $= 2(p - p_\infty)/(\rho V^2)$
c_Q	—	volume flux coefficient, Eq. (11.47)
$c_{\dot{Q}}$	—	thermal-energy coefficient, Eq. (22.59), (22.87)
c_r	m/s	wave speed
c_s	m/s	wave speed of a neutral subsonic disturbance
C	—	viscosity function, Eq. (10.72)
Co	—	Colburn number, Eq. (18.159)
CR	—	Chapman–Rubesin parameter, Eq. (10.32)
C^+, C_r^+, C_θ^+	—	universal quantities of the turbulent wall layer, Eq. (17.22), (17.35), (17.49)
d	m	diameter, airfoil thickness
d_h	m	hydraulic diameter, Eq. (5.11)
D, D_f, D_p	N	drag, friction drag, pressure drag
\mathcal{D}	kg/s^3	dissipation integral, Eq. (19.51)

D_{12}	m^2/s	diffusion coefficient, Eq. (11.55)
e	m^2/s^2	specific internal energy, Eq. (3.51)
e_t	m^2/s^2	specific total energy, Eq. (3.51)
$\vec{e}_x, \vec{e}_y, \vec{e}_z$	—	unit vectors along coordinate axes
E	m^4/s^3	“kinematic” kinetic energy, Eq. (7.57)
E_t	J	total energy, Eq. (3.48)
E_T	$\text{m}^2\text{K}/\text{s}$	“kinematic” thermal energy for plane flows, Eq. (22.26)
E_{T_a}	$\text{m}^3\text{K}/\text{s}$	“kinematic” thermal energy for axisymmetric flows, Eq. (22.78)
Ec	—	Eckert number, Eq. (4.9) or Eq. (9.8)
f	$1/\text{s}, \text{Hz}$	frequency, $f = \omega/2\pi$
\vec{f}	N/m^3	force per unit volume
F	N	force
F_e	—	characteristic quantity of turbulent boundary layers, Eq. (18.69)
g	m/s^2	gravitational acceleration
g	N/m^2	total pressure, Eq. (7.79)
G	—	shape factor, Eq. (18.71)
$G(\Lambda; D)$	—	G-function, Eq. (17.60)
Ga	—	Galilei number, Eq. (4.44)
Gö	—	Görtler number, Eq. (15.52)
Gr	—	Grashof number, $T_w - T_\infty$ prescribed, Eq. (4.48)
Gr_q	—	Grashof number, q_w prescribed, Eq. (4.51)
h	m	distance between plates, Fig. 1.1
h	m^2/s^2	specific enthalpy, Eq. (3.64)
h_t	m^2/s^2	specific total enthalpy, Eq. (10.50)
h_x, h_z	—	Lamé metric coefficients, Eq. (12.53), (12.54)
H	m	half distance between plates, Fig. 17.1
H_{12}, H_{32}	—	shape factors, Eq. (8.26), (8.27)
\dot{I}	N	momentum flux, Eq. (7.52)
\vec{j}	$\text{kg}/\text{m}^2\text{s}$	diffusion flux vector, Eq. (11.53)
k	m	roughness (height)
k	m^2/s^2	kinetic energy of turbulent fluctuation, Eq. (16.14)
k_s	m	sand roughness (height)
$k_{s\text{ eq}}$	m	equivalent roughness (height), Eq. (17.39)
$k_{s\text{ ad}}$	m	admissible roughness (height), Eq. (17.41)
k_{tech}	m	technical roughness (height), Eq. (17.40)
k_θ	K^2	variance of temperature fluctuation, Eq. (18.44)

K	m^3/s^2	kinematic momentum for plane flows, Eq. (7.52)
K	–	dimensionless contour curvature, Eq. (14.2)
K	–	coupling parameter, Eq. (17.104), (18.141)
K	–	relaminarisation parameter, Eq. (18.92)
K	–	slender channel parameter, Eq. (17.146)
K_a	m^4/s^2	kinematic momentum for axisymmetric flows, Eq. (12.30)
$K_\mu, K_\varrho, K_\lambda, K_c$	–	isobaric variation parameters, Eq. (10.11), (10.12), also Table 3.1
Kn	–	Knudsen number, $\text{Kn} = \ell_0/\ell$, ℓ_0 : mean free path
l	m	length
ℓ	m	mixing length, Eq. (17.68), step length, Fig. 14.1
ℓ_K	m	Kolmogorov length, Eq. (16.26)
$\ell_\theta, \ell_{\text{MR}}$	m	mixing lengths for the temperature field, Eq. (18.41), (18.43)
L	m	turbulence length, Eq. (16.22), (18.14), (18.29)
L	N	lift
Le	–	Lewis number, Eq. (11.72)
M	kg	mass
M	Nm	moment, torque, Eq. (5.64)
\tilde{M}_i	kg/kmol	molar mass of component i
Ma	–	Mach number, Eq. (10.21)
Ma_τ	–	viscous Mach number, Eq. (19.35)
n	1/s	angular frequency
Nu	–	Nusselt number, Eq. (9.22) or Eq. (9.94), also p. 221
Nu_m	–	mean Nusselt number
Nu_x	–	local Nusselt number, Eq. (9.53)
p	N/m^2	pressure
P_M	J/s	mechanical power
Pe	–	Peclet number, Eq. (4.14)
Pr	–	Prandtl number, Eq. (4.8)
Pr_t	–	turbulent Prandtl number, Eq. (17.77)
$\text{Pr}_k, \text{Pr}_\varepsilon, \text{Pr}_\omega$	–	model constants, Eq. (18.12), (18.20), (18.24)
q	m/s	magnitude of instantaneous turbulent fluctuation velocity, Eq. (16.15)

\vec{q}	W/m^2	heat flux
q_t	W/m^2	turbulent heat flux, Eq. (16.38)
q_λ	W/m^2	molecular heat flux, Eq. (16.38)
Q	m^3/s	volume flux, Eq. (22.84)
Q_b	m^2/s	volume flux per unit span, Eq. (7.56)
\dot{Q}	J/s	thermal energy flux, Eq. (3.48), (22.95)
\dot{Q}_b	J/ms	thermal energy flux per unit span, Eq. (10.151)
r	m	radial coordinate
r	—	recovery factor, Eq. (9.86)
R	m	radius
R	$\text{m}^2/\text{s}^2\text{K}$	specific gas constant, Eq. (10.38)
$R(r)$	—	correlation function, Eq. (16.21)
Ra, Ra_q	—	Rayleigh number, Eq. (19.74), (19.61)
Re, Re_x	—	Reynolds number, Eq. (1.4), (18.93)
Re_1, Re_2	—	Reynolds number, formed with δ_1, δ_2 respectively, Eq. (18.111)
Re_T, Re_t	—	turbulent Reynolds number, Eq. (18.149), (22.12)
Re_τ	—	Reynolds number, formed with u_τ , Eq. (17.6)
s	$\text{m}^2/\text{s}^2\text{K}$	specific entropy, Eq. (3.69)
Sc	—	Schmidt number, Eq. (11.73)
Sh	—	Sherwood number, Eq. (11.67)
Sr	—	Strouhal number, Eq. (1.16)
St	—	Stanton number, Eq. (19.50)
t	s	time
T	K	(absolute) temperature
T_0	K	total temperature of outer flow, Eq. (9.87), (10.52)
T_m	K	mean temperature, Eq. (17.135)
T_q	K	reference temperature, Eq. (19.68)
T_t	K	total temperature, stagnation temperature, Eq. (10.50)
T_τ	K	friction temperature, Eq. (17.45)
Tu	—	turbulence intensity, Eq. (16.28)
u	m/s	velocity component in x -direction
u_m	m/s	average velocity, Eq. (17.125)
u_τ	m/s	friction velocity, Eq. (17.5)
u_q, u_s	m/s	reference velocities, Eq. (19.68), (17.101)
U	m/s	velocity at boundary-layer edge, in the free stream
U_N, U_R	m/s	reference velocities, Eq. (7.10), (19.60)

U_P	m	wetted circumference of flow cross-section
v	m/s	velocity component in y -direction
\vec{v}	m/s	velocity vector, Eq. (3.1)
v_E	m/s	entrainment velocity, Eq. (18.127)
V	m/s	free stream velocity, y component of velocity in the outer flow
w	m/s	velocity component in the z -direction
\dot{w}_i	kg/m ³ s	mass (per unit volume and time) of component i arising from chemical reaction, Eq. (11.51)
W	—	wake function, Eq. (18.117)
\dot{W}	J/s	power
x, y, z	m	Cartesian coordinates
\bar{y}	—	boundary-layer coordinate, Eq. (6.6)
\hat{y}	—	intermediate coordinate, Eq. (17.17)
y^+, y^\times	—	coordinate in viscous wall layer, Eq. (17.12), (17.100)
Y	m	transformed y coordinate, Eq. (10.61)
Z, Z_T	m	thickness parameter, Eq. (8.12), (9.61)
$Z(T, p)$	—	compressibility factor
α	—	angle of attack, half diffuser angle, contour angle with respect to horizontal, Fig. 10.1
α	W/m ² K	heat transfer coefficient, Eq. (9.17)
α	1/m	wave number, Eq. (15.10)
$\overline{\alpha}$	—	thermal diffusion coefficient, Eq. (11.55)
β	1/K	heat expansion coefficient, Eq. (3.67)
β	—	similarity parameter, Eq. (7.15), Fig. 15.19
β	—	Rotta–Clauser parameter, Eq. (18.85)
$\beta(\xi)$	—	principal function, Eq. (7.78)
β_r, β_r^*	1/s	angular frequency of mode
β_i, β_i^*	1/s	amplification of mode
γ	—	ratio of the specific heat capacities, $\gamma = c_p/c_v$
γ	—	intermittency factor, Eq. (16.30)
γ	—	dimensionless friction velocity, Eq. (17.141)
Γ, Γ_T	—	shape factors, Eq. (8.13), (9.62)
$\delta, \delta_{99}, \delta_R$	m	boundary-layer thicknesses, Eq. (16.31)
$\delta_1, \delta_2, \delta_3, \delta_h, \delta_{th}, \delta_T, \delta_L$	m	boundary-layer thicknesses, Eq. (10.95) – (10.98), (9.60), (9.68), Fig. 9.2

δ_{iu}	m	kinematic thicknesses, Eq. (10.95) – (10.97), with $\varrho = \varrho_e$
δ_N	m	thickness scale for laminar boundary layers, Eq. (8.2)
δ_s	m	thickness of Stokes layer, Eq. (5.117)
δ_v	m	thickness of viscous wall layer, Eq. (17.11)
δ_ν	m	$= \sqrt{x\nu/U}$
Δ	m	width measure, Eq. (22.8)
$\tilde{\Delta}, \hat{\Delta}$	–	dimensionless boundary-layer thicknesses, Eq. (18.65), (18.68)
Δ_1	–	dimensionless displacement thickness, Eq. (18.128)
ε	–	small quantity
ε	m^2/s^3	pseudo-dissipation, Eq. (16.19)
$\tilde{\varepsilon}$	m^2/s^3	(turbulent) dissipation, Eq. (16.17)
η	–	dimensionless y coordinate, similarity coordinate, Eq. (18.59), (7.21)
η_s	–	Stokes coordinate, Eq. (5.105), (13.27)
ϑ	–	dimensionless excess temperature, Eq. (4.27), (9.3)
θ	–	angle
Θ	–	dimensionless excess temperature, Eq. (9.69)
Θ^+	–	dimensionless excess temperature, Eq. (17.46)
$\kappa(x)$	1/m	curvature of body contour, Eq. (3.98)
κ	–	Karman constant, Eq. (17.17)
$\kappa_N, \kappa_{N\theta}, \kappa_0, \kappa_\theta$	–	universal constants, Eq. (19.70), (17.102), (17.74)
λ	J/msK	thermal conductivity, Eq. (3.70)
λ	–	pipe friction factor, Eq. (1.9)
λ	m	wave length, $\lambda = 2\pi/\alpha$
Λ	–	shape factor, Eq. (15.27)
μ	kg/ms	viscosity, Eq. (1.2)
μ_t	kg/ms	eddy viscosity, Eq. (17.63)
ν	m^2/s	kinematic viscosity, Eq. (1.3)
ν_t	m^2/s	(kinematic) eddy viscosity, Eq. (17.63)
ξ	–	dimensionless x coordinate, Eq. (7.7)
ξ	–	Görtler-transformed coordinate, Eq. (7.76)
Π	–	wake parameter, Eq. (18.70)
ϱ, ϱ_i	kg/m^3	density, partial density of component i , Eq. (11.49)

$\sigma_x, \sigma_y, \sigma_z$	N/m ²	normal stresses, Eq. (3.13)
$\tau_{ij}, \bar{\tau}_v$	N/m ²	viscous stresses, Eq. (3.22), (16.37)
τ_t	N/m ²	turbulent shear stress, Eq. (16.37)
φ, Φ	—	angles
Φ	J/m ³ s	dissipation function, Eq. (3.62), (9.2)
$\overline{\chi}$	—	hypersonic similarity parameter, Eq. (14.34)
χ	—	transonic similarity parameter, Eq. (19.56)
ψ	m ² /s	stream function, Eq. (4.58)
$\vec{\omega}$	1/s	angular velocity vector, Eq. (3.27), (18.25)
ω	1/s	angular velocity, angular frequency

Indices

ad	adiabatic wall
adm	admissible
c	center line
c.p.	constant properties
crit	critical, point of completed transition
C	contour, critical layer
CFI	cross-flow instability
DN	direct natural convection
e	outer edge of the boundary layer, outer flow
eq	equivalent
E	entrance
i	imaginary part of a complex number
<i>i</i>	component <i>i</i> , running index
inc	incompressible
ind	indifference point
IN	indirect natural convection
<i>j</i>	running index
<i>k</i>	single rough element
l	lower
max	maximum value
mot	motion
MS	marginal separation
O	reference point, virtual origin, stagnation point, start ($t = 0$)
P	primary stability
r	real part of a complex number
r	reference temperature
R	reference value

s	quasi-steady
S	separation
S	shock wave, secondary stability
St	stagnation point
tech	technical
TS	Tollmien–Schlichting wave
0.5T	half maximum temperature difference
u	upper
0.5u	half maximum velocity
w	wall
x, y, z	in x, y, z -directions
∞	unperturbed by body, free stream, far downstream

Other Symbols

*	dimensionless, perturbation quantity, Eq. (15.56)
—	conventionally time averaged
~	mass weighted time averaged, difference between ensemble average and time average, Eq. (21.2)
()	ensemble average, phase average, Eq. (21.2), (21.3)
/	fluctuation quantity, conventional averaging
//	fluctuation quantity, mass weighted averaging
+	wall layer at $\bar{\tau}_w \neq 0$, formed with $\delta_v = \nu/u_\tau, u_\tau, T_\tau$
×	wall layer at $\bar{\tau}_w = 0$, formed with $\nu/u_s, u_s$

References and Index of Authors

The numbers in square brackets refer to the pages in the book where the author is mentioned.

- Abbott, J.H.; Doenhoff von, A.E.; Stivers, L.S. (1945): Summary of airfoil data. NACA-R-824. [456]
- Abid, R. /s.: Speziale, C.G.; Abid, R.; Anderson, E.C. (1990)
- Achenbach, E. (1968): Distribution of local pressure and skin friction around a circular cylinder in cross-flow up to $Re = 5 \times 10^6$. *J. Fluid Mech.*, Vol. 34, 625–639. [19, 23, 24, 206]
- Achenbach, E. (1971): Influence of surface roughness on the cross-flow around a circular cylinder. *J. Fluid Mech.*, Vol. 46, 321–335. [24]
- Achenbach, E. (1972): Experiments on the flow past spheres at very high Reynolds numbers. *J. Fluid Mech.*, Vol. 54, 565–575. [25]
- Achenbach, E. (1974a): Vortex shedding from spheres. *J. Fluid Mech.*, Vol. 62, 209–221. [25]
- Achenbach, E. (1974b): The effects of surface roughness and tunnel blockage on the flow past spheres. *J. Fluid Mech.*, Vol. 65, 113–125. [25]
- Achenbach, E., Heinecke, E. (1981): On the vortex shedding from smooth and rough cylinders in the range of Reynolds numbers 6×10^3 to 5×10^6 . *J. Fluid Mech.*, Vol. 109, 239–251. [24]
- Ackeret, J. (1925): Das Rotorschiff und seine physikalischen Grundlagen, Vandenhoeck und Ruprecht, Göttingen. 2. Auflage. [292]
- Ackeret, J. (1952): Über exakte Lösungen der Navier-Stokes-Gleichungen inkompressibler Flüssigkeiten bei veränderten Grenzbedingungen. *Z. angew. Math. Phys. (ZAMP)*. Bd. 3, 259–271. [93]
- Acrivos, A. (1960a): Mass-transfer in laminar-boundary-layer flows with finite interfacial velocities. *A.I.Ch.E. Journal*, Vol. 6, 410–414. [317]
- Acrivos, A. (1960b): A theoretical analysis of laminar natural convection heat transfer to non-Newtonian fluids. *A.I.Ch.E. Journal*, Vol. 6, 584–590. [327]
- Acrivos, A. (1962): The asymptotic form of the laminar boundary-layer mass-transfer rate for large interfacial velocities. *J. Fluid Mech.*, Vol. 12, 337–357. [271, 317, 318]
- Acrivos, A. /s.: Klemp, J.B.; Acrivos, A. (1972)
- Adamson Jr., T.C. /s.: Brilliant, H.M.; Adamson Jr., T.C. (1974)
- Adamson Jr., T.C.; Messiter, A.F. (1980): Analysis of two-dimensional interactions between shock waves and boundary layers. *Annu. Rev. Fluid Mech.*, Vol. 12, 103–138. [403]
- Adamson Jr., T.C.; Messiter, A.F. (1981): Simple approximations for the asymptotic description of the interaction between a normal shock wave and a turbulent boundary layer at transonic speeds. In: AGARD-CP-291, 16-1 to 16-14. [625]

- Afzal, N.; Narasimha, R. (1976): Axisymmetric turbulent boundary layer along a circular cylinder. *J. Fluid Mech.*, Vol. 74, part 1, 113–128. [633]
- Afzal, N. (1980): Convective wall plume: Higher order analysis. *Int. J. Heat Mass Transfer*. Vol. 23, 505–513. [277]
- Afzal, N.; Narasimha, R. (1985): Asymptotic analysis of thick axisymmetric turbulent boundary layers. *AIAA Journal*, Vol. 23, 963–965. [633]
- Afzal, N. (1996): Turbulent boundary layer on a moving continuous plate. *Fluid Dynamics Research*, Vol. 17, 181–194. [588]
- Afzal, N. (2008a): Turbulent boundary layer with negligible wall stress. *Journal of Fluids Engineering*. Vol. 130, 051205-1-15. [602]
- Afzal, N. (2008b): Alternate scales for turbulent boundary layer on transitional rough walls: Universal log laws. *Journal of Fluids Engineering*. Vol. 130, 041202-1-16. [534]
- AGARD (1981): Computation of Viscous-Inviscid Interactions. AGARD-CP-291. [403]
- AGARD (1987): Computation of Three-Dimensional Boundary Layers Including Separation. AGARD-R-741. [641]
- AGARD (1990): Report of the Fluid Dynamics Panel Working Group 10 on Calculation of 3D Separated Turbulent Flows in Boundary Layer Limit. AGARD-AR-255. [641, 643]
- AGARD (1994): Progress in Transition Modelling. AGARD-R-793. [490]
- Aihara, Y. /s.: Tani, I.; Aihara, Y. (1969)
- Akamatsu, T. /s.: Matsushita, M.; Murata, S.; Akamatsu, T. (1984a)
- Akamatsu, T. /s.: Matsushita, M.; Murata, S.; Akamatsu, T. (1984b)
- Akamnov, N.I. (1953): Development of a two-dimensional laminar fluid jet along a solid surface (in russian). *Proc. LPI, Technical Hydrodynamics*, No. 5, 24-31. [181]
- Alber, I.E. (1968): Application of an exact expression for the equilibrium dissipation integral to the calculation of turbulent nonequilibrium flows. In: S.J. Kline et al. (Eds.): *Proc. Computation of Turbulent Boundary Layers-1968*, AFOSR-IFP-Stanford Conference, Vol. I, 126–135. [582]
- Alfredsson, P.H. /s.: Hallbäck, M.; Henningson, D.S.; Johansson, A.V., Alfredsson, P.H. (Eds.) (1996)
- Alfredsson, P.H. /s.: Franssen, J.H.M.; Matsubara, M.; Alfredsson, P.H. (2005)
- Alletto, M. /s.: Scheichl, B.; Kluwick, A.; Alletto, M. (2008)
- Allmaras, S.R. /s.: Spalart, P.R.; Allmaras, S.R. (1992)
- Al-Maaitah, A. /s.: Nayfeh, A.H.; Al-Maaitah, A. (1987)
- Althaus, D.; Wortmann, F.X. (1981): *Stuttgarter Profilkatalog 1. Messergebnisse aus dem Laminarwindkanal des Instituts für Aerodynamik und Gasdynamik der Universität Stuttgart*. Vieweg-Verlag, Braunschweig/Wiesbaden. [456]
- Anderson Jr., J.D. (1989): *Hypersonic and High Temperature Gas Dynamics*. McGraw-Hill Book Co., New York. [263, 312, 314, 388, 391, 392, 616]
- Anderson, D.A.; Tannehill, J.C.; Pletcher, R.H. (1984): *Computational Fluid Mechanics and Heat Transfer*. McGraw-Hill Book Company, New York. [560]
- Anderson, E.C. /s.: Speziale, C.G.; Abid, R.; Anderson, E.C. (1990)
- Andrade, E.N. (1931): On the circulation caused by the vibration of air in a tube. *Proc. Roy. Soc. London A*, Vol. 134, 447–470. [364]
- Andrade, E.N. (1939): The velocity distribution in a liquid-into-liquid jet. The plane jet. *Proc. Phys. Soc. London*, Vol. 51, 784–793. [180]
- Andre, G. /s.: Schneider, W.; Steinrück, H.; Andre, G. (1994)
- Antonia, R.A. /s.: Krishnamoorthy, L.V.; Antonia, R.A. (1988)
- Antonia, R.A. /s.: Raupach, M.R.; Antonia, R.A.; Rajagopalan, S. (1991)
- Arakeri, J.H. /s.: Dewan, A.; Arakeri, J.H. (2000)

- Arnal, D.; Juillen, J.C.; Michel, R. (1977): Analyse experimentale et calcul de l'appartition et du developpement de la transition de la couche limite. In: AGARD-CP-224, 13-1 to 13-17. [443]
- Arnal, D. (1984): Description and prediction of transition in two-dimensional incompressible flow. In: AGARD-R-709: Special course on stability and transition of laminar flows. 2-1 to 2-71. [473]
- Arnal, D.; Coustols, E.; Juillen, J.C. (1984): Etude experimentale et theorique de la transition sur une aile en fletche infinie. Rech. Aerosp. No. 1984-4, 275-290. Engl. ed.: 1984-4, 39-54. [489]
- Arnal, D. (1987): Three-dimensional boundary layers: Laminar-turbulent transition. In: AGARD-R-741, 4-1 to 4-34. [641]
- Arnal, D. /s.: Reed, H.L.; Saric, W.S.; Arnal, D. (1996)
- Aroestey, J.; Cole, J.D. (1965): Boundary layer flow with large injection rates. RAND Corp. Memorandum RM-4620, ARPA. [311]
- Arzoumanian, E. /s.: Fulachier, L.; Arzoumanian, E.; Dumas, R. (1982)
- Asai, M. /s.: Nishioka, M.; Asai, M.; Iida, S. (1990)
- Aships, D.E.; Reshotko, E. (1990): The vibrating ribbon problem revisited. J. Fluid Mech., Vol. 213, 531-547. [443]
- Atwell, N.P. /s.: Bradshaw, P.; Ferriss, D.H.; Atwell, N.P. (1967)
- Aupoix, B. /s.: Catris, S.; Aupoix, B. (2000)
- Aziz, A.; Na, T.Y. (1984): Perturbation Methods in Heat Transfer. Hemisphere Publishing Corp., Washington, D.C.. [278]
- Badri Narayanan, M.A. /s.: Rao, K.N.; Narasimha, R.; Badri Narayanan, M.A. (1971)
- Baek, J.H. /s.: Patel, V.C.; Baek, J.H. (1985)
- Bailey, H.E. /s.: Deiwert, G.S.; Bailey, H.E. (1984)
- Baillie, J.C. /s.: Wai, J.C.; Baillie, J.C.; Yoshihara, H. (1986)
- Baker, R.J.; Launder, B.E. (1974): The turbulent boundary layer with foreign gas injection. I. Measurements in zero pressure gradient. Int. J. Heat Mass Transfer, Vol. 17, 275-291. [610]
- Baldwin, B.S.; Lomax, H. (1978): Thin layer approximation and algebraic model for separated turbulent flows. AIAA Paper 78-257. [559]
- Baldwin, B.S.; Barth, T.J. (1990): A one-equation turbulence transport model for high Reynolds number wall-bounded flows. NASA-TM-102847. [562]
- Bandyopadhyay, P. /s.: Head, M.R.; Bandyopadhyay, P. (1981)
- Bandyopadhyay, P.R. /s.: Gad-el-Hak, M.; Bandyopadhyay, P.R. (1994)
- Banks, W.H.H. (1965): The boundary layer on a rotating sphere. Quart. J. Mech. Appl. Math., Vol. 18, 443-454. [331]
- Banks, W.H.H.; Drazin, P.G.; Zaturska, M.B. (1988): On perturbation of Jeffery-Hamel flow. J. Fluid Mech., Vol. 186, 559-581. [109]
- Barberis, D. (1986): 3-D boundary layer computation on arbitrary obstacles with direct and inverse methods. Rech. Aerosp., No. 186-3, 1-27. [643]
- Barche, J. (1979) (Editor): Experimental Data Base for Computer Program Assessment. AGARD-AR-138. [16, 18]
- Barker, M. (1922): On the use of very small pitot-tubes for measuring wind velocity. Proc. Roy. Soc. London A, Vol. 101, 435-445. [112]
- Barnes, H.T.; Coker, E.G. (1905): The flow of water through pipes. Proc. Roy. Soc. London, Vol. 74, 341. [417]
- Barnett, M. /s.: Fan, S.; Lakshminarayana, B.; Barnett, M. (1993)
- Barnwell, R.W.; Wahls, R.A.; De Jarnette, F.R. (1989): Defect stream function, law-of-the-wall/wake method for turbulent boundary layers. AIAA Journal, Vol. 27, 1707-1713. [592]
- Baron, J.R.; Scott, P.E. (1960): Some mass-transfer results with external-flow pressure gradients. J. Aero/Space Sci., Vol. 27, 625-626. [319]

- Barry, M.D.J.; Ross, M.A.S. (1970): The flat plate boundary layer. Part 2: The effect of increasing thickness on stability. *J. Fluid Mech.*, Vol. 43, 813–818. [436]
- Barth, T.J. /s.: Baldwin, B.S.; Barth, T.J. (1990)
- Bartlmä, F. (1975): Gasdynamik der Verbrennung. Springer-Verlag, Wien, New York. [70]
- Batchelor, G.K. (1951): Note on a class of solutions of the Navier-Stokes equations representing steady non rotationally symmetric flow. *Quart. J. Mech. Appl. Math.*, Vol. 4, 29–41. [124]
- Batchelor, G.K. (1956): A proposal concerning laminar wakes behind bluff bodies of large Reynolds number. *J. Fluid Mech.*, Vol. 1, 388–398. [93]
- Batchelor, G.K. (1974): An Introduction to Fluid Dynamics. Cambridge University Press, Cambridge. [82, 124]
- Becker, E. (1957): Das Anwachsen der Grenzschicht in und hinter einer Expansionswelle. *Ing.-Arch.*, Bd. 25, 155–163. [373]
- Becker, E. (1959a): Berechnung der Reibungsschichten mit schwacher Sekundärströmung nach dem Impulsverfahren. *Z. Flugwiss.*, Bd. 7, 163–175 (1959); cf. also: Mitteilg. aus dem Max-Planck-Institut für Strömungsforschung Nr. 13 (1956) and ZAMM. *Z. angew. Math. Mech.*, S3–S8. [330]
- Becker, E. (1959b): Instationäre Grenzschichten hinter Verdichtungsstößen und Expansionswellen. *Z. Flugwiss.*, Bd. 7, 61–73. [373]
- Becker, E. (1960): Eine einfache Verallgemeinerung der Rayleigh-Grenzschicht. *Z. angew. Math. Phys. (ZAMP)*, Bd. 11, 146–152. [128]
- Becker, E. (1961): Instationäre Grenzschichten hinter Verdichtungsstößen und Expansionswellen. *Progress in Aeronautical Sciences*, Vol. 1, Pergamon Press, N.Y., 104–173. [370, 373]
- Becker, E. (1962): Anwendung des numerischen Fortsetzungsverfahrens auf die pseudostationäre, kompressible laminare Grenzschicht in einem Stoßwellenrohr, *Z. Flugwiss.*, Bd. 10, 138–147. [352, 373]
- Beese, E.; Gersten, K. (1979): Skin friction and heat transfer on a circular cylinder moving in a fluid at rest. *Z. angew. Math. Phys. (ZAMP)*, Vol. 30, 117–127. [387]
- Beese, E. (1984): Die von einem Tragflügelprofil induzierte Grenzschichtströmung an der Bodenebene. *Z. Flugwiss. Weltraumforsch.*, Bd. 8, 17–27. [190, 191, 299]
- Behbahani, D. /s.: Schultz-Grunow, F.; Behbahani, D. (1973)
- Benjamin, T.B. (1960): Effects of a flexible boundary on hydrodynamic stability. *J. Fluid Mech.*, Vol. 9, 513–532. [472]
- Benocci, C. (1991): Modelling of turbulent heat transport – A state-of-the-art. von Karman Institute for Fluid Dynamics, Technical Memorandum 47. [610]
- Berg, B. van den /s.: Lindhout, J.P.F.; Berg, B. van den (1979)
- Berg, B. van den; Humphreys, D.A.; Krause, E.; Lindhout, J.P.F. (1988): Three-Dimensional Turbulent Boundary Layers – Calculations and Experiments. Notes on Numerical Fluid Mechanics, Vol. 19, Vieweg-Verlag, Braunschweig. [641, 643]
- Berger, E.; Wille, R. (1972): Periodic flow phenomena. *Annu. Rev. Fluid Mech.*, Vol. 4, 313–340. [47]
- Berger, S.A. (1971): Laminar Wakes. American Elsevier Publ. Co., New York. [190, 335]
- Berker, R. (1963): Integration des équations du mouvements d'un fluide visqueux incompressible. In: S. Flügge (Ed.): *Handbuch der Physik*, Bd. VIII/2, Springer-Verlag, Berlin, 1–384. [101]
- Bers, A. (1973): Theory of absolute and convective instabilities. Intern. Congress on Waves and Instabilities in Plasmas (G. Auer and F. Cap, Hg.). Innsbruck, Austria, B1-B52. [425, 431]

- Bertolotti, F.P. /s.: Herbert, T.; Bertolotti, F.P. (1987)
- Bertolotti, F.P. (1991): Linear and Nonlinear Stability of Boundary Layers with Streamwise Varying Properties. Ph.D. thesis, The Ohio State University. [436, 443, 466, 474]
- Betchov, R.; Criminale, W.O. (1967): Stability of Parallel Flows. Academic Press, New York, London. [425, 436]
- Betz, A. (1949): Ziele, Wege und konstruktive Auswertung der Strömungsforschung. Z-VDI, Bd. 91, 253–258. [XXIII]
- Bieler, H. /s.: Horstmann, K.-H.; Redeker, G.; Quast, A.; Dreßler, U.; Bieler, H. (1990)
- Binnie, A.M.; Harris, D.P. (1950): The application of boundary layer theory to swirling liquid flow through a nozzle. Quart. J. Mech. Appl. Math., Vol. 3, 89–106. [330]
- Bippes, H. (1972): Experimentelle Untersuchung des laminar-turbulenten Um- schlages an einer parallel angeströmten konkaven Wand. Sitzungsberichte der Heidelberger Akademie der Wissenschaften, Math.-Naturwiss. Klasse, 103–180, Jahrg. 1972, 3. Abhandlung (English translation: Experimental study of the laminar-turbulent transition of a concave wall in a parallel flow. NASA-TM-75243, March 1978); see also: H. Bippes and H. Görtler, Acta Mech., Vol. 14, 251–267. [475, 484]
- Bippes, H.; Nitschke-Kowsky, P. (1987): Experimental study of instability modes in a three-dimensional boundary layer. AIAA Paper 87-1336. [487]
- Birch S.F.; Eggers J.M. (1972): A critical review of the experimental data for de- veloped free turbulent shear layers. In: Free Turbulent Shear Flows, Conf. Proc., NASA-SP-321, Vol. I, 11–40. [668]
- Bird, R.B.; Stewart, W.E.; Lightfoot, E.N. (1960): Transport Phenomena. John Wiley, New York. [312, 314]
- Bissonnette, L.R.; Mellor, G.L. (1974): Experiments on the behaviour of an axisym- metric turbulent boundary layer with a sudden circumferential strain. J. Fluid Mech., Vol. 63, 369–413. [636]
- Blasius, H. (1908): Grenzschichten in Flüssigkeiten mit kleiner Reibung. Z. Math. Physik, Bd. 56, 1–37. Engl. translation in NACA-TM-1256. [31, 156, 159, 184, 361, 422]
- Blasius, H. (1910): Laminare Strömung in Kanälen wechselnder Breite. Z. Math. Physik, Bd. 58, 225–233. [117]
- Blottner, F.G.; Flügge-Lotz, I. (1963): Finite-difference computation of the bound- ary layer with displacement thickness interaction. Journal de Mécanique, Vol. 2, 397–423. [684]
- Blottner, F.G. (1964): Nonequilibrium laminar boundary-layer flow of ionized air. AIAA Journal, Vol. 2, 1921–1927. [684]
- Blottner, F.G. (1975): Investigation of some finite-difference techniques for solving the boundary layer equations. Computer Meth. Appl. Mech. Eng., Vol. 6, 1–30. [684]
- Blumer, C.B. /s: Van Driest, E.R.; Blumer, C.B. (1963)
- Bodonyi, R.J.; Kluwick, A. (1977): Freely interacting transonic boundary layers. The Physics of Fluids, Vol. 20, 1432–1437. [403]
- Bodonyi, R.J.; Kluwick, A. (1982): Supercritical transonic trailing-edge flow. Q. J. Mech. Appl. Math., Vol. 35, 265–277. [400]
- Bodonyi, R.J. /s.: Kluwick, A.; Gittler, Ph.; Bodonyi, R.J. (1984)
- Bodonyi, R.J. /s.: Kluwick, A.; Gittler, Ph.; Bodonyi, R.J. (1985)
- Bodonyi, R.J.; Smith, F.T. Kluwick, A. (1985): Axisymmetric flow past a slender body of finite length. Proc. Roy. Soc. London A, Vol. 400, 37–54. [400]
- Bödewadt, U.T. (1940): Die Drehströmung über festem Grund. ZAMM. Z. angew. Math. Mech., Bd. 20, 241–253. [329]

- Böhm, H. /s.: Schneider, W.; Zauner, E.; Böhm, H. (1987)
- Böhle, M. /s.: Oertel Jr., H.; Böhle, M. (2002)
- Böhle, M. /s.: Oertel Jr., H.; Böhle, M.; Reviol, T. (2015)
- Börger, G.-G. /s.: Gersten, K.; Gross, J.F.; Börger, G.-G. (1972)
- Börger, G.-G. (1975): Optimierung von Windkanaldüsen für den Unterschallbereich. Z. Flugwiss., Bd. 23, 45–50 and 282. [634]
- Bohning, R.; Zierep, J. (1981): Normal shock-turbulent boundary layer interaction at a curved wall. In: AGARD-CP-291, 17-1 to 17-8. [626]
- Bohning, R. /s.: Doerffer, P.P.; Bohning, R. (2003)
- Boiko, A.V.; Grek, G.R.; Dovgal, A.V.; Kozlov, V.V. (2002): The Origin of Turbulence in Near Wall Flows. Springer, Berlin, Heidelberg. [479 a]
- Boltze, E. (1908): Grenzschichten an Rotationskörpern in Flüssigkeiten mit kleiner Reibung. Diss. Göttingen. [322, 356, 360]
- Bonnet, J.L. /s.: Gleyzes, C.; Cousteix, J.; Bonnet, J.L. (1984)
- Bothmann, Th. /s.: Krause, E.; Hirschel, E.H.; Bothmann, Th. (1968)
- Bothmann, Th. /s.: Krause, E.; Hirschel, E.H.; Bothmann, Th. (1969)
- Bott, D.M.; Bradshaw, P. (1998): Effect of high free-stream turbulence on boundary-layer skin friction and heat transfer. AIAA Paper 98-0531. [604]
- Botta, E.F.F.; Dijkstra, D.; Veldman, A.E.P. (1972): The numerical solution of the Navier-Stokes equations for laminar, incompressible flow past a parabolic cylinder. J. Eng. Math., Vol. 6, 63–81. [115]
- Boussinesq, J. (1872): Essai sur la théorie des eaux courantes. Mémoires Acad. des Sciences, Vol. 23, No. 1, Paris. [538]
- Boussinesq, J. (1903): Théorie Analytique de la chaleur. Vol. 2, Gauthier-Villars, Paris. [89]
- Bradshaw, P. (1965): The effect of wind tunnel screens on nominally two-dimensional boundary layers. J. Fluid Mech., Vol. 22, 679–687. [605]
- Bradshaw, P.; Ferriss, D.H.; Atwell, N.P. (1967): Calculation of boundary-layer development using the turbulent energy equation. J. Fluid Mech., Vol. 28, 593–616. [XXIV, 561, 562, 601, 625, 663]
- Bradshaw, P.; Ferriss, D.H. (1971): Calculation of boundary-layer development using the turbulent energy equation: Compressible flow on adiabatic walls. J. Fluid Mech., Vol. 46, 83–110. [625]
- Bradshaw, P. /s.: Huffmann, G.D.; Bradshaw, P. (1972)
- Bradshaw, P. (1973): Effects of Streamline Curvature on Turbulent Flow. AGARD-AG-169. [666]
- Bradshaw, P. (1977): Compressible turbulent shear layers. Annu. Rev. Fluid Mech., Vol. 9, 33–54. [613, 619, 620]
- Bradshaw, P. /s.: Cebeci, T.; Bradshaw, P. (1977)
- Bradshaw, P.; Cebeci, T.; Whitelaw, J.H. (1981): Engineering Calculation Methods for Turbulent Flow. Academic Press, London. [600]
- Bradshaw, P. /s.: Cebeci, T.; Bradshaw, P. (1984)
- Bradshaw, P. /s.: Huang, P.G.; Bradshaw, P.; Coakley, T.J. (1993)
- Bradshaw, P. /s.: Schwarz, W.R.; Bradshaw, P. (1993)
- Bradshaw, P. /s.: Huang, P.G.; Bradshaw, P.; Coakley, T.J. (1994)
- Bradshaw, P. /s.: Huang, P.G.; Bradshaw, P. (1995)
- Bradshaw, P. /s.: Bott, D.M.; Bradshaw, P. (1998)
- Brainerd, J.G. /s.: Emmons, H.W.; Brainerd, J.G. (1942)
- Braslow, A.L.; Visconti, F. (1948): Investigation of boundary layer Reynolds-number for transition on a NACA 65₍₂₁₅₎ – 114 airfoil in the Langley two-dimensional low-turbulence pressure tunnel. NACA-TN-1704. [455]
- Braun, S.; Kluwick, A. (2004): Unsteady three-dimensional marginal separation caused by surface-mounted obstacles and/or local suction. J. Fluid Mech., Vol. 514, 121–152. [408]

- Braun, S.; Kluwick, A. (2005): Blow-up and control of marginally separated boundary layers. *Phil. Trans. Roy. Soc. Lond. A* 363 (1830), 1057–1067. [408]
- Braun, S./s.: Scheichl, S.; Braun, S.; Kluwick, A. (2008)
- Braun, W.H.; Ostrach, S.; Heighway, J.E. (1961): Free-convection similarity flows about two-dimensional and axisymmetric bodies with closed lower ends. *Int. J. Heat Mass Transfer*, Vol. 2, 121–135. [326]
- Bray, R.S. /s.: Holzhauser, C.A.; Bray, R.S. (1956)
- Brazier, J. /s.: Roget, C.; Brazier, J.Ph.; Cousteix, J.; Mauss, J. (1998)
- Brenner, H. /s.: Happel, J.; Brenner, H. (1973)
- Brevdo, L. (1988): A study of absolute and convective instabilities with an application to the Eady model. *Geophys. Astrophys. Fluid Dyn.*, Vol. 40, 1–92. [431]
- Brevdo, L. (1991): Three-dimensional absolute and convective instabilities and spatially amplifying waves in parallel shear flows. *Z. angew. Math. Phys. (ZAMP)*, Vol. 42, 911–942. [494]
- Brevdo, L. (1993): Instabile Wellenpakete in der Blasius'schen Grenzschichtströmung. TU Braunschweig, Habil.-Schrift; also: ZLR-Forschungsbericht; 92-2. [425, 474, 494]
- Brevdo, L. (1995): Convectively unstable wave packets in the Blasius boundary layer. *ZAMM. Z. angew. Math. Mech.*, Vol. 75, 423–436. [494]
- Briggs, R.J. (1964): Electron-Stream Interactions in Plasmas. MIT Press. [425, 431, 493]
- Brighton, P.W.M. /s.: Smith, F.T.; Sykes, R.I.; Brighton, P.W.M. (1977)
- Brighton, P.W.M. /s.: Smith, F.T.; Brighton, P.W.M.; Jackson, P.S.; Hunt, J.C.R. (1981)
- Briley, W.R. /s: McDonald, H.; Briley, W.R. (1984)
- Brilliant, H.M.; Adamson Jr., T.C. (1974): Shock-wave boundary-layer interactions in laminar transonic flow. *AIAA Journal*, Vol. 12, 323–329. [403]
- Brinich, P.F. (1954): Boundary-layer transition at Mach 3.12 with and without single roughness elements. *NACA-TN-3267*. [471]
- Brown, F.N.M. (1957): ... Dept. Aerospace & Mech. Eng., Univ. Notre Dame, Notre Dame, Indiana; cf. also: Knapp, C.F.; Roache, P.J. (1968): A combined visual and hot-wire anemometer investigation of boundary-layer transition, *AIAA Journal*, Vol. 6, No. 1, 29–36. [419]
- Brown, S.N. (1966): A differential equation occurring in boundary-layer theory. *Mathematika*, Vol. 13, 140–146. [173]
- Brown, S.N.; Stewartson, K. (1966): On the reversed flow solutions of the Falkner-Skan equation. *Mathematika*, Vol. 13, 1–6. [173]
- Brown, S.N.; Riley, N. (1973): Flow past a suddenly heated vertical plate. *J. Fluid Mech.*, Vol. 59, 225–237. [361]
- Brown, S.N.; Stewartson, K. (1983): On an integral equation of marginal separation. *SIAM J. Appl. Math.*, Vol. 43, 1119–1126. [405]
- Brown, W.B.; Donoughe, P.L. (1951): Tables of exact laminar-boundary-layer solutions when the wall is porous and fluid properties are variable. *NACA-TN-2479*. [306]
- Bryson, A.E. /s.: Emmons, H.W.; Bryson, A.E. (1951–52)
- Bühler, K. /s.: Zierep, J.; Bühler, K. (1993)
- Burgers, J.M. (1924): The motion of a fluid in the boundary layer along a plain smooth surface. *Proceedings of the First International Congress for Applied Mechanics*, Delft, 113–128. [33, 162, 420, 440]
- Burggraf, O.R. /s.: Jobe, C.E.; Burggraf, O.R. (1974)
- Burggraf, O.R. (1975): Asymptotic theory of separation and reattachment of a laminar boundary-layer on a compression ramp. In: AGARD-CP-168, 10-1 to 10-9. [402]

- Burggraf, O.R. /s.: Rizzetta, D.P.; Burggraf, O.R.; Jenson, R. (1978)
- Burggraf, O.R.; Rizzetta, D.P.; Werle, M.J.; Vatsa, V.N. (1979): Effects of Reynolds number on laminar separation of a supersonic stream. AIAA Journal, Vol. 17, 336–343. [402]
- Burggraf, O.R.; Duck, P.W. (1982): Spectral computation of triple-deck flows. In: T. Cebeci (Ed.): Numerical and Physical Aspects of Aerodynamics Flows. Springer-Verlag, New York, 145–158. [400]
- Busemann, A. (1931): Gasdynamik. Handbuch der Exp.-Physik, Bd. IV, 1. Akad. Verlag, Leipzig. [244]
- Bush, W.B. (1966): Hypersonic strong-interaction similarity solutions for flow past a flat plate. J. Fluid Mech., Vol. 25, 51–64. [392]
- Bushnell, D.M. /s.: Rudy, D.H.; Bushnell, D.M. (1973)
- Bussmann, K.; Münz, H. (1942): Die Stabilität der laminaren Reibungsschicht mit Absaugung. Jb. dt. Luftfahrtforschung I, 36–39. [458, 459]
- Bussmann, K.; Ulrich, A. (1943): Systematische Untersuchungen über den Einfluß der Profilform auf die Lage des Umschlagpunktes. Preprint Jb. dt. Luftfahrtforschung 1943 in Techn. Berichte 10, Heft 9. [453]
- Cantwell, B.J. (1981): Organized motion in turbulent flow. Annu. Rev. Fluid Mech., Vol. 13, 457–515. [513]
- Cantwell, B.J. /s.: Kline, S.J.; Cantwell, B.J.; Lilley, G.M. (1981)
- Capp, S.P. /s.: George, W.K.; Capp, S.P. (1979)
- Carpenter, P.W. /s.: Dixon, A.E.; Lucey, A.D.; Carpenter, P.W. (1994)
- Carr, L.W. (1981a): A review of unsteady turbulent boundary layer experiments. In: R. Michel; J. Cousteix; R. Houdeville (Eds.): Unsteady Turbulent Shear Flows. Springer-Verlag, Berlin, 3–34. [647, 648, 649]
- Carr, L.W. (1981b): A Compilation of Unsteady Turbulent Boundary Layer Experimental Data. AGARD-AG-265. [649]
- Carslaw, H.S.; Jaeger, J.C. (1959): Conduction of Heat in Solids. Oxford University Press. [127]
- Carter, J.E. (1979): A new boundary-layer inviscid iteration technique for separated flow. AIAA Paper 79-1450. [403]
- Caswell, B. /s.: Schwartz, W.H.; Caswell, B. (1961)
- Catherall, D.; Stewartson, K.; Williams, P.G. (1965): Viscous flow past a flat plate with uniform injection. Proc. Roy. Soc. London A, Vol. 284, 370–396. [309]
- Catris, S.; Aupoix, B. (2000): Density corrections for turbulence models. Aerosp. Sci. Technol. Vol. 4, 1–11. [616, 625]
- Cebeci, T.; Smith, A.M.O. (1968): Investigation of heat transfer and of suction for tripping laminar boundary layer. J. Aircraft, Vol. 5, 450–454. [461]
- Cebeci, T. /s.: Keller, H.B.; Cebeci, T. (1971)
- Cebeci, T. /s.: Keller, H.B.; Cebeci, T. (1972a)
- Cebeci, T. /s.: Keller, H.B.; Cebeci, T. (1972b)
- Cebeci, T.; Keller, H.B. (1972): On the computation of unsteady turbulent boundary layers. In: E.A. Eichelbrenner (Ed.): Recent Research on Unsteady Boundary Layers, Vol. 1, Les Presses de l'Université Laval, Québec. 1072–1105. [649]
- Cebeci, T.; Smith, A.M.O. (1974): Analysis of Turbulent Boundary Layers. Academic Press, New York. [207, 559, 583, 585, 601, 606, 613, 615, 617, 625, 633]
- Cebeci, T.; Bradshaw, P. (1977): Momentum Transfer in Boundary Layers. Hemisphere Publ. Corp., Washington, D.C.. [701]
- Cebeci, T.; Kaups, K.; Ramsey, J.A. (1977): A general method for calculating three-dimensional compressible laminar and turbulent boundary layers on arbitrary wings. NASA-CR-2777. [346]
- Cebeci, T. (1979): The laminar boundary layer on a circular cylinder started impulsively from rest. J. Comput. Phys., Vol. 31, 153–172. [356, 357]

- Cebeci, T.; Keller, H.B.; Williams, P.G. (1979): Separating boundary-layer flow calculations. *J. Comp. Phys.*, Vol. 31, 363–378. [693]
- Cebeci, T.; Chang, K.C.; Kaups, K. (1980a): General method for calculating three-dimensional laminar and turbulent boundary layers on ship hulls. *Ocean Eng.*, Vol. 7, 229–280. [346]
- Cebeci, T.; Khattab, A.K.; Stewartson, K. (1980b): On nose separation. *J. Fluid Mech.*, Vol. 97, 435–454. [338]
- Cebeci, T. /s.: Bradshaw, P.; Cebeci, T.; Whitelaw, J.H. (1981)
- Cebeci, T.; Khattab, A.K.; Stewartson, K. (1981): Three-dimensional laminar boundary layers and the o.k. of accessibility. *J. Fluid Mech.*, Vol. 107, 57–87. [340, 342]
- Cebeci, T. (1982): Unsteady Separation. In: T. Cebeci (Ed.): *Numerical and Physical Aspects of Aerodynamic Flows*. Springer-Verlag, New York, 265–277. [350, 354, 356]
- Cebeci, T.; Bradshaw, P. (1984): *Physical and Computational Aspects of Convective Heat Transfer*. Springer-Verlag, New York. [213, 278, 457, 547, 609, 609, 617, 622, 623, 625, 701]
- Cebeci, T. (1986): Unsteady boundary layers with an intelligent numerical scheme. *J. Fluid Mech.*, Vol. 163, 129–140. [354, 357]
- Cebeci, T.; Chen, L.T.; Chang, K.C. (1986): An interactive scheme of three-dimensional transonic flows. In: T. Cebeci (Ed.): *Numerical and Physical Aspects of Aerodynamic Flows III*. Springer-Verlag, New York, 412–431. [643]
- Cebeci, T.; Whitelaw, J.H. (1986): Calculation methods for aerodynamic flows – a review. In: T. Cebeci (Ed.): *Numerical and Physical Aspects of Aerodynamic Flows III*. Springer-Verlag, New York, 1–19. [388]
- Cebeci, T. (1987): An approach to practical aerodynamic calculations. In: AGARD-R-741, 6-1 to 6-40. [338, 340, 642]
- Cebeci, T. (1999): *An Engineering Approach to the Calculation of Aerodynamic Flows*. Horizons Publishing, Long Beach, and Springer, Berlin. [XXV, 643]
- Cebeci, T. (2004): *Turbulence models and Their Application*. Springer, Berlin. [XXV]
- Cebeci, T.; Cousteix, J. (2005): *Modeling and Computation of Boundary-Layer Flows*. 2nd Edn. Horizons Publ., Springer, Long Beach, Heidelberg (2005). [XXV]
- Cess, R.D. /s.: Sparrow, E.M.; Cess, R.D. (1961)
- Cess, R.D. /s.: Sparrow, E.M.; Cess, R.D. (1966)
- Chaing, T.; Ossin, A.; Tien, C.L. (1964): Laminar free convection from a sphere. *J. Heat Transfer*, Vol. 86, 537–542. [327]
- Chambré, P.L. /s.: Schaad, S.A.; Chambré, P.L. (1958)
- Champion, M.; Libby, P.A. (1991): Asymptotic analysis of stagnating turbulent flows. *AIAA Journal*, Vol. 29, 16–24. [605]
- Champion, M.; Libby, P.A. (1996): Asymptotic and computational results for a turbulent jet impinging on a nearby wall. In: K. Gersten (Ed.): *Asymptotic Methods for Turbulent Shear Flows at High Reynolds Numbers*. Kluwer Academic Publ., Dordrecht, 133–140. [605]
- Chan, G.K.C. /s.: Savage, S.B.; Chan, G.K.C. (1970)
- Chan, W.-K. /s.: Holt, M.; Chan, W.-K. (1975)
- Chang, K.C. /s.: Cebeci, T.; Chang, K.C.; Kaups, K. (1980)
- Chang, K.C. /s.: Cebeci, T.; Chen, L.T.; Chang, K.C. (1980)
- Chang, M.-Sh. /s.: Huang, Th.T.; Chang, M.-Sh. (1986)
- Chang, P.K. (1970): *Separation of Flow*, Pergamon Press, Oxford. [48]

- Chang, P.K. (1976): Control of Flow Separation. Hemisphere Publ. Corp., Washington, D.C.. [48, 295]
- Chao, B.T. /s: Lin, F.N.; Chao, B.T. (1974)
- Chao, B.T. /s: Lin, F.N.; Chao, B.T. (1976)
- Chapman, D.R. (1949): Laminar mixing of a compressible fluid. NACA-TN-1800. [176]
- Chapman, D.R. (1979): Computational aerodynamics. Development and outlook. AIAA Journal, Vol. 17, 1293–1313. [XXIV]
- Chapple, P.J. /s.: Mellor, G.L.; Chapple, P.J.; Stokes, V.K. (1968)
- Chassaing, P. (1985): Une alternative à la formulation des équations du mouvement turbulent d'un fluide à masse volumique variable. Journal de Mécanique Théorique et Appliquée, Vol. 4, 375–389. [613]
- Chen, C.C.; Eichhorn, R. (1976): Natural convection from a vertical surface to a thermally stratified fluid. Journal of Heat Transfer, Vol. 98, 446–451. [266]
- Chen, C.J.; Rodi, W. (1980): Vertical Turbulent Buoyant Jets – A Review of Experimental Data. HTM, Vol. 4, Pergamon Press, Oxford. [676]
- Chen, C.J.; Jaw, S.Y. (1998): Fundamentals of Turbulence Modeling. Taylor & Francis, Washington DC. [562]
- Chen, H.C.; Patel, V.C. (1987): Laminar flow at the trailing edge of a flat plate. AIAA Journal, Vol. 25, 920–928. [400]
- Chen, J.-Y. /s.: Shih, T.-H.; Lumley, J.L.; Chen, J.-Y. (1990)
- Chen, L.T. /s.: Cebeci, T.; Chen, L.T.; Chang, K.C. (1986)
- Cheng, H.K.; Smith, F.T. (1982): The influence of airfoil thickness and Reynolds number on separation. Z. angew. Math. Phys. (ZAMP), Vol. 33, 151–180. [411]
- Cheng, H.K.; Lee, C.J. (1986): Laminar separation studied as an airfoil problem. In: T. Cebeci (Ed.): Numerical and Physical Aspects of Aerodynamics Flows III, Springer-Verlag, New York, 102–125. [411]
- Cheng, S.J. (1953): On the stability of laminar boundary layer flow. Quart. Appl. Math., Vol. 11, 346–350. [427]
- Chevray, R.; Kovasznay L.S.G. (1969): Turbulence measurements in the wake of a thin flat plate. AIAA Journal Vol. 7, 1641–1643. [670]
- Chew, Y.-T. /s.: Simpson, R.L.; Chew, Y.-T.; Shivaprasad, B.G. (1981)
- Chi, S.W. /s.: Spalding, D.B.; Chi, S.W. (1964)
- Choi, D.H. /s.: Patel, V.C.; Choi, D.H. (1980)
- Chow, R. /s.: Melnik, R.E.; Chow, R. (1975)
- Chow, R.; Melnik, R.E. (1976): Numerical solutions of the triple-deck equations for laminar trailing-edge stall. Lecture Notes in Physics, Vol. 59, 135–144. [400]
- Chung, P.M. (1965): Chemically reacting nonequilibrium boundary layers. Advances in Heat Transfer, Vol. 2, Academic Press, New York, 109–270. [319]
- Churchill, S.W. /s.: Saville, D.A.; Churchill, S.W. (1967)
- Churchill, S.W. (1983): Free convection around immersed bodies. In: Heat Exchanger Design Handbook, Chapter 2.5.7., Hemisphere Publ. Corp., Washington D.C.. [628, 635]
- Churchill, S.W. /s.: Galante, S.R.; Churchill, S.W. (1990)
- Clauser, F. /s.: Clauser, L.M.; Clauser, F. (1937)
- Clauser, F.H. (1956): The turbulent boundary layer. Advances in Applied Mechanics, Vol. 4, 1-51. [580]
- Clauser, L.M.; Clauser, F. (1937): The effect of curvature on the transition from laminar to turbulent boundary layer. NACA-TN-613. [483]
- Clers des, B.; Sternberg, J. (1952) : On the boundary layer temperature recovery factors. J. of the Aeronautical Sciences, Vol. 19, 645–646. [326]
- Clutter, D.W. /s.: Smith, A.M.O.; Clutter, D.W. (1963)
- Clutter, D.W. /s.: Smith, A.M.O.; Clutter, D.W. (1965)

- Coakley, T.J. /s.: Huang, P.G.; Bradshaw, P.; Coakley, T.J. (1993)
- Coakley, T.J. /s.: Huang, P.G.; Bradshaw, P.; Coakley, T.J. (1994)
- Cochran, W.G. (1934): The flow due to a rotating disk. Proc. Cambr. Phil. Soc., Vol. 30, 365–375. [121]
- Cockrell, D.J. /s.: Kline, S.J.; Morkovin, M.V.; Sovran, G.; Cockrell, D.J. (Eds.) (1968)
- Cohen, C.B.; Reshotko, E. (1956): Similar solutions for the compressible laminar boundary layer with heat transfer and pressure gradient. NACA-TR-1293. [250]
- Coker, E.G. /s.: Barnes, H.T.; Coker, E.G. (1905)
- Cole, J.D. /s.: Aroesty, J.; Cole, J.D. (1965)
- Cole, J.D. /s.: Kevorkian, J.; Cole, J.D. (1981)
- Colebrook, C.F. (1938): Turbulent flow in pipes, with particular reference to the transition region between the smooth and rough pipe laws. J. Inst. Civil Eng., Vol. 11, 133. [531]
- Coles, D. (1956): The law of the wake in the turbulent boundary layer. J. Fluid Mech., Vol. 1, 191–226. [593]
- Coles, D. (1968): The young person's guide to the data. In: Coles, D.; Hirst, E.A. (Eds.): Proceedings Computation of Turbulent Boundary Layers-1968 AFOSR-IFP-Stanford Conference, Vol. II, 1–45. [525, 578]
- Coles, D. (1978): A model for flow in the viscous sublayer. In: Smith, C.R.; Abbott, D.E. (Eds.): Workshop on Coherent Structure of Turbulent Boundary Layers. Lehigh University, Bethlehem, Pa., 462–475. [528]
- Coles, D.E. (1957): Remarks on the equilibrium turbulent boundary layer. J. Aero. Sci., Vol. 24, 495–506. [582]
- Comings, E.W. /s.: Miller, D.R.; Comings, E.W. (1957)
- Cooke, J.C. (1952): On Pohlhausen's method with applications to a swirl problem of Taylor. J. of the Aeronautical Sciences, Vol. 19, 486–490. [330]
- Cooke, J.C.; Hall, M.G. (1962): Boundary layers in three dimensions. Progress in Aeronautical Sciences, Vol. 2, Pergamon Press, London, 221–282. [341]
- Corrsin, S.; Kistler, A.L. (1955): Free-stream boundaries of turbulent flows. NACA TR 1244. [516]
- Cosart, W.P. /s.: Gersten, K.; Cosart, W.P. (1980)
- Cousteix, J. (1974): Theoretical analysis and prediction method for a three-dimensional turbulent boundary layer. ONERA N.T. 157 Engl. Transl. ESA TT-238. [642]
- Cousteix, J.; Houdeville, R.; Michel, R. (1974): Couches limites turbulentes avec transfert de chaleur. La Rech. Aéosp., No. 174-6, 327–338. [624]
- Cousteix, J.; Houdeville, R.; Javelle, J. (1981): Response of a turbulent boundary layer to a pulsation of the external flow with and without adverse pressure gradient. In: R. Michel, J. Cousteix, R. Houdeville (Eds.): Unsteady Turbulent Shear Flows. Springer-Verlag, Berlin, 120–144. [648]
- Cousteix, J.; Houdeville, R. (1983): Effects of unsteadiness on turbulent boundary layers. VKI Lecture Series 1983-03. [649]
- Cousteix, J. /s.: Gleyzes, C.; Cousteix, J.; Bonnet, J.L. (1984)
- Cousteix, J.; Houdeville, R. (1985): Couche limite turbulente instationnaire: investigations experimentale et numerique. In: AGARD-CP-386, 11-1 to 11-12. [648]
- Cousteix, J. (1986): Three-dimensional and unsteady boundary-layer computations. Annu. Rev. Fluid Mech., Vol. 18, 173–196. [341, 358, 641]
- Cousteix, J. (1987a) (Ed.): Computation of Three-Dimensional Boundary Layers Including Separation. AGARD-R-741. [341, 346, 632]
- Cousteix, J. (1987b): Three-dimensional boundary layers. Introduction to calculation methods. In: AGARD-R-741, 1-1 to 1-49. [338, 341, 346, 632, 638]
- Cousteix, J. /s.: Roget, C.; Brazier, J.Ph.; Cousteix, J.; Mauss J. (1998)
- Cousteix, J. /s.: Cebeci, T.; Cousteix, J. (1999)

- Cousteix, L. /s: Cebeci, T.; Cousteix, J. (2005) [XXV]

Cousteix, J. /s.: Hirschel, E.H., Cousteix, J.; Kordulla, W. (2014)

Cousteix, J.; Mauss, J. (2005): Rational basis of the interactive boundary layer theory. In: G.E.A. Meier (Ed.): One Hundred Years of Boundary Layer Research. Springer, Berlin, Heidelberg. [XXV]

Coustols, E. /s.: Arnal, D.; Coustols, E.; Juillen, J.C. (1984)

Cowley, S.J. (1983): Computer extension and analytic continuation of Blasius expansion for impulsive flow past a circular cylinder. *J. Fluid Mech.*, Vol. 135, 389–405. [356]

Cox, R.N.; Crabtree, L.F. (1965): Elements of Hypersonic Aerodynamics. The English Universities Press, London. [263]

Crabtree, L.F. /s.: Rott, N.; Crabtree, L.F. (1952)

Crabtree, L.F.; Küchemann, D.; Sowerby, L. (1963): Three-dimensional boundary layers. In L. Rosenhead (Ed.): Laminar Boundary Layers, Clarendon Press, Oxford, 409–491. [341]

Crabtree, L.F. /s.: Cox, R.N.; Crabtree, L.F. (1965)

Crandall, S.H. /s.: Kurtz, E.F.; Crandall, S.H. (1962)

Crawford, M.E. /s.: Kays, W.M.; Crawford, M.E. (1980)

Criminale, W.O. /s.: Betchov, R.; Criminale, W.O. (1967)

Crocco, L. (1932): Sulla trasmissione del calore da una lamina piana a un fluido scorrente ad alta velocità. *L'Aerotecnica*. Vol. 12, 181–197. [244]

Crocco, L. (1941): Sulla strato limite laminaire nei gas lungo una lamina plana. *Rend. Mat. Univ. Roma* V2, 138. [253, 254]

Crocco, L. (1946): Lo strato laminare nei gas. *Mon. Sci. Aer. Roma*. [184]

Cutler, A.D. /s.: Pauley, W.R.; Eaton, J.K.; Cutler, A.D. (1993)

Dallmann, U. (1983): Topological structures of three-dimensional vortex flow separation. DFVLR-AVA-Bericht: 221; 82A07. [340]

Dallmann, U. /s.: Fischer, T.M.; Dallmann, U. (1987)

Dallmann, U. /s.: Saljnikov, V.; Dallmann, U. (1989)

Dallmann, U. /s.: Schulte-Werning, B.; Dallmann, U. (1991)

Dallmann, U.; Gebing, H.; Vollmers, H. (1993): Unsteady three-dimensional separated flows around a sphere-analysis of vortex chain formation. In: H. Eckelmann et al. (Eds.): Bluff-Body Wakes, Dynamics and Instabilities. Springer-Verlag, Berlin, 27–30. [24, 25]

Daniels, P.G. (1974): Numerical and asymptotic solutions for the supersonic flow near the trailing edge of a flat plate. *Q. J. Mech. appl. Math.*, Vol. 27, 175–191. [400]

Daniels, P.G.; Gargaro, R.J. (1993): Buoyancy effects in stably stratified horizontal boundary-layer flow. *J. Fluid Mech.*, Vol. 250, 233–251. [289]

Davie, A. (1973): A simple numerical method for solving Orr-Sommerfeld problems. *Q. J. Mech. Appl. Math.*, Vol. 26, 401–411. [436]

Davis, R.T.; Flügge-Lotz, I. (1964): The laminar compressible boundary-layer in the stagnation-point region of an axisymmetric blunt body including the second-order effect of vorticity interaction. *Int. J. Heat Mass Transfer*, Vol. 7, 341–370. [387]

Davis, R.T. (1972): Numerical solution of the Navier-Stokes equations for symmetric laminar incompressible flow past a parabola. *J. Fluid Mech.*, Vol. 15, 1224–1230. [115]

Davis, R.T.; Werle, M.J. (1972): Numerical solutions for laminar incompressible flow past a paraboloid of revolution. *AIAA Journal*, Vol. 10, 1224–1230. [119]

Davis, R.T.; Werle, M.J. (1982): Progress in interacting boundary-layer computations at high Reynolds number. In: T. Cebeci (Ed.): Numerical and Physical Aspects of Aerodynamic Flows. Springer-Verlag, New York, 187–210. [388, 400]

Davis, S.H. (1976): The stability of time-periodic flows. *Annu. Rev. Fluid Mech.*, Vol. 8, 57–74. [472]

- Davis, S.S.; Malcolm, G.N. (1980): Transonic shock-wave/boundary-layer interactions on an oscillating airfoil. AIAA Journal, Vol. 18, 1306–1312. [651]
- De Groot, S.R.; Mazur, P. (1962): Non-equilibrium Thermodynamics. North-Holland Publ. Co. [53, 67]
- De St.Venant, B. (1843): Note à joindre une mémoire sur la dynamique des fluides. Comptes Rendus, Vol. 17, 1240–1244. [68]
- Debisschop, J.R.; Nieuwstadt, F.T.M. (1996): Turbulent boundary layer in an adverse pressure gradient: effectiveness of riblets. AIAA Journal, Vol. 34, 932–937. [531]
- Degani, A.T.; Smith, F.T.; Walker, J.D.A. (1992): The three-dimensional turbulent boundary layer near a plane of symmetry. J. Fluid Mech., Vol. 234, 329–360. [640, 641]
- Degani, A.T.; Smith, F.T.; Walker, J.D.A. (1993): The structure of a three-dimensional turbulent boundary layer. J. Fluid Mech., Vol. 250, 43–68. [640, 641]
- Deissler, R.J. (1987): The convective nature of instability in plane Poiseuille flow. Phys. Fluids, Vol. 30(8), 2303–2305. [431, 493]
- Deiwert, G.S.; Bailey, H.E. (1984): Time-dependent finite-difference simulation of unsteady interactive flows. In: T. Cebeci (Ed.): Numerical and Physical Aspects of Aerodynamic Flows II. Springer-Verlag, New York, 63–78. [651]
- De Jarnette, F.R. /s.: Barnwell, R.W.; Wahls, R.A.; De Jarnette, F.R. (1989)
- Del Casal, E. /s.: Gill, W.N.; Zeh, D.W.; Del Casal, E. (1965)
- Delery, J.; Marvin, J.G. (1986): Shock-wave boundary layer interaction. AGARD-AG-280. [403, 597, 606, 623, 624, 625]
- Delery, J.M. (1985): Shock-wave/turbulent boundary layer interaction and its control. Prog. Aerospace Sci., Vol. 22, 209–280. [625]
- Delfs, J. /s.: Oertel Jr., H.; Delfs, J. (2005)
- Dengel, P.; Fernholz, H.H. (1990): An experimental investigation of an incompressible turbulent boundary layer in the vicinity of separation. J. Fluid Mech., Vol. 212, 615–639. [546]
- Deriat, E.; Guiraud, J.-P. (1986): On the asymptotic description of turbulent boundary layers. Journal de Mécanique Théorique et Appliquée, Numéro spécial, 109–140. [601]
- Deriat, E. (1987): Asymptotic analysis of the k - ε model for a turbulent boundary layer. Rech. Aérospace, No. 1987-5, 1–17. [601]
- Desopper, A. (1981): Influence of the laminar and turbulent boundary layers in unsteady two-dimensional viscous-inviscid coupled calculations. In: R. Michel, J. Cousteix, R. Houdeville (Eds.): Unsteady Turbulent Shear Flows. Springer-Verlag, Berlin, 171–184. [648]
- Devan, L. (1964): Second order incompressible laminar boundary layer development on a two-dimensional semi-infinite body. Ph.D. Thesis, University of California, Los Angeles. [386]
- Dewan, A.; Arakeri, J.H. (2000): Use of k - ε - γ model to predict intermittency in turbulent boundary layers. J. Fluids Engineering, Vol. 122, 542–546. [563]
- Dewey Jr., C.F. (1963): Use of local similarity concepts in hypersonic viscous interaction problems. AIAA Journal, Vol. 1, 20–33. [390]
- Dewey Jr., C.F. /s.: Gross, J.F.; Dewey Jr., C.F. (1965)
- Dewey Jr., C.F.; Gross, J.F. (1967): Exact similar solutions of the laminar boundary-layer equations. Advances in Heat Transfer, Vol. 317–446. [253, 325, 343, 390]
- Dhawan, S. /s.: Liepmann, H.W.; Dhawan, S. (1951)
- Dhawan, S. (1953): Direct measurements of skin friction. NACA-TR-1121. [164]
- Dienemann, W. (1953): Berechnung des Wärmeüberganges an laminar umströmten Körpern mit konstanter und ortsveränderlicher Wandtemperatur. ZAMM. Z. angew. Math. Mech., Bd. 33, 89–109. [343]
- Dijkstra, D. /s.: Van de Vooren, A.I.; Dijkstra, D. (1970)

- Dijkstra, D. /s: Botta, E.F.F.; Dijkstra, D.; Veldmann, A.E.P. (1972)
- Dijkstra, D. /s: Zandbergen, P.J.; Dijkstra, D. (1987)
- Dilgen, P.G. (1995): Berechnung der abgelösten Strömung um Kraftfahrzeuge: Simulation des Nachlaufes mit einem inversen Panelverfahren. Fortschritt-Berichte VDI: Reihe 7; 258, VDI-Verl., Düsseldorf, 1995, also: Bochum, Univ., Diss., (1995). [643]
- Dinkelacker, A.; Hessel, M.; Meier, G.E.A.; Schewe, G. (1977): Investigation of pressure fluctuations beneath a turbulent boundary layer by means of an optical method. *Phys. Fluids*, Vol. 20 (10, part 2), S216–S224. [512]
- Dixon, A.E.; Lucey, A.D.; Carpenter, P.W. (1994): Optimization of viscoelastic compliant walls for transition delay. *AIAA Journal*, Vol. 32, 256–267. [472]
- Dodson, L.J. /s: Settles, G.S.; Dodson, L.J. (1994)
- Doenhoff von, A.E. (1940): Investigation of the boundary layer about a symmetrical airfoil in a windtunnel of low turbulence. NACA Wartime Report L-507. [455]
- Doenhoff von, A.E. /s: Abbott, J.H.; Doenhoff von, A.E.; Stivers, L.S. (1945)
- Doerffer, P.P.; Bohning, R. (2003): Shock wave-boundary layer interaction control by wall ventilation. *Aerospace Science and Technology*. Vol. 7, 171–179. [627]
- Doetsch, H. (1940): Untersuchungen an einigen Profilen mit geringem Widerstand im Bereich kleiner c_a -Werte. *Jb. dt. Luftfahrtforschung* I, 54–57. [456]
- Doligalski, T.L. /s: Ece, M.C.; Walker, J.D.A.; Doligalski, T.L. (1984)
- Dolling, D.S. (2001): Fifty years of shock-wave/boundary-layer interaction research: what next? *AIAA Journal*, Vol. 39, 1517–1531. [627]
- Donoughe, P.L. /s: Brown, W.B.; Donoughe, P.L. (1951)
- Donoughe, P.L.; Livingood, J.N.B. (1955): Exact solutions of laminar boundary layer equations with constant property values for porous wall with variable temperature. NACA-TR-1229. [306]
- Dorrance, H.W. (1962): Viscous Hypersonic Flow. Theory of Reacting and Hypersonic Boundary Layers. McGraw-Hill, New York. [263, 319, 325]
- Dovgal, A.V./s: Boiko, A.V.; Grek, G.R.; Dovgal, A.V.; Kozlov, V.V. (2002)
- Drazin, P.G.; Howard, L.N. (1966): Hydrodynamic stability of parallel flow of inviscid fluid. *Advances in Appl. Mech.*, Vol. 9, 1–89. [434]
- Drazin, P.G.; Reid, W.H. (1981): Hydrodynamic Stability. Cambridge University Press, Cambridge. [425, 434]
- Drazin, P.G. /s: Banks, W.H.H.; Drazin, P.G.; Zaturska, M.B. (1988)
- Drela, M.; Giles, M. Thompson Jr., W.T. (1986): Newton solution of coupled Euler and boundary-layer equations. In: T. Cebeci (Ed.): Numerical and Physical Aspects of Aerodynamic Flow III, Springer-Verlag, New York, 143–167. [626]
- Dreßler, U. /s: Horstmann, K.-H.; Redeker, G.; Quast, A.; Dreßler, U.; Bieler, H. (1990)
- Dryden, H.L. (1934): Boundary layer flow near flat plates. Proc. Fourth Internat. Congress for Appl. Mech., Cambridge, 175. [420, 440]
- Dryden, H.L. (1937): Airflow in the boundary layer near a plate. NACA-TR-562. [420, 440]
- Dryden, H.L. (1938): Turbulence investigations at the National Bureau of Standards. Proc. Fifth Internat. Congress of Appl. Mechanics, 362. [515]
- Dryden, H.L. (1939): Turbulence and the boundary layer. *J. of the Aeronautical Sciences*, Vol. 6, 85–100 and 101–105. [420]
- Dryden, H.L. (1946–48): Some recent contributions to the study of transition and turbulent boundary layers (Papers presented at Sixth Internat. Congress for Appl. Mech., Paris, Sept. 1946; NACA-TN-1168 (1947)): cf. also; Recent Advances in the mechanics of boundary layer flow. *Advances Appl. Mech.*, New York, Vol. 1, 1–40 (1948). [XXIII, 442]
- Dryden, H.L. (1953): Review of published data on the effect of roughness on transition from laminar to turbulent flow. *J. of the Aeronautical Sciences*, Vol. 20, 477–482. [469, 472]

- Dryden, H.L. (1955): Fifty years of boundary layer theory and experiments. *Science* 121, 375–380. [XXV]
- Dryden, H.L. (1956): Recent investigation of the problem of transition. *Z. Flugwiss., Bd.* 4, 89–95. [421]
- Dubs, W. (1939): Über den Einfluß laminarer und turbulenter Strömungen auf das Röntgenbild von Wasser und Nitrobenzol. Ein röntgengraphischer Beitrag zum Turbulenzproblem. *Helv. Phys. Acta*, Vol. 12, 169–228. [13]
- Duck, P.W. /s.: Smith, F.T.; Duck, P.W. (1977)
- Duck, P.W. /s.: Burggraf, O.R.; Duck, P.W. (1982)
- Duck, P.W. (1984): The interaction between a steady laminar boundary layer and an oscillating flap: The condensed problem. In: T. Cebeci (Ed.): *Numerical and Physical Aspects of Aerodynamics Flows II*, Springer-Verlag, New York, 369–380. [400]
- Dumas, R. /s.: Fulachier, L.; Arzoumanian, E.; Dumas, R. (1982)
- Dumas, R.J. /s.: Favre, A.J.; Gaviglio, J.J.; Dumas, R.J. (1957)
- Dumas, R.J. /s.: Favre, A.J.; Gaviglio, J.J.; Dumas, R.J. (1958)
- Durant, R. /s.: Michel, R.; Quémard, C.; Durant, R. (1968)
- Dutzler, G. /s.: Gretler, W.; Meile, W.; Dutzler, G. (1995)
- Dwyer, H.A. (1968): Calculation of unsteady leading-edge boundary layers. *AIAA Journal*, Vol. 6, 2447–2448. [357]
- Dwyer, H.A. /s.: Sturek, W.B.; Dwyer, H.A.; Kayser, L.D.; Nietubicz, Ch.J.; Reklis, R.P.; Opalka, K.O. (1978)
- Dwyer, H.A. (1981): Some aspects of three-dimensional laminar boundary layers. *Annu. Rev. Fluid Mech.*, Vol. 13, 217–229. [341]
- Eaton, J.K. /s.: Pauley, W.R.; Eaton, J.K.; Cutler, A.D. (1993)
- Eber, G.R. (1952): Recent investigations of temperature recovery and heat transmission on cones and cylinders in axial flow in the NOL aeroballistics wind tunnel. *J. of the Aeronautical Sciences*, Vol. 19, 1–6. [326]
- Ece, M.C.; Walker, J.D.A.; Doligalski, T.L. (1984): The boundary layer on an impulsively started rotating and translating cylinder. *Phy. Fluids.*, Vol. 27, 1077–1089. [361]
- Eckert, E.; Weise, W. (1942): Messung der Temperaturverteilung auf der Oberfläche schnell angeströmter unbeheizter Körper. *Forschg. Ing.-Wes.*, Bd. 13, 246–254. [229]
- Eckert, E.R.G. /s.: Sparrow, E.M.; Minkowycz, W.J.; Eckert, E.R.G.; Ibele, W.E. (1964)
- Ede, A.J. (1967): Advances in free convection. *Advances in Heat Transfer*. Vol. 4, 1–64. [277]
- Eder, R. /s.: Schneider, W.; Eder, R.; Schmidt, J. (1990)
- Eggers, J.M. /s.: Birch, S.F.; Eggers, J.M. (1972)
- Ehrenstein, U. /s.: Fischer, T.M.; Ehrenstein, U.; Meyer, F. (1988)
- Ehrhard, P. (2001): Laminar mixed convection in two-dimensional far wakes above heated/cooled bodies: model and experiments. *J. Fluid Mech.*, Vol. 439, 165–198. [290]
- Eichelbrenner, E.A.; Oudart, A. (Ed.) (1955): Méthode de calcul de la couche limite tridimensionnelle. Application à un corps fuselé incliné sur le vent. ONERA-Publication Nr. 76, Chatillon. [345]
- Eichelbrenner, E.A. (Ed.) (1972): Recent research on unsteady boundary layers. *IUTAM Symposium 1971*, Part 1 and 2, Les Presses de l'Université Laval, Québec. [350]
- Eichelbrenner, E.A. (1973): Three-dimensional boundary layers. *Annu. Rev. Fluid Mech.*, Vol. 5, 339–360. [341]
- Eichhorn, R. /s.: Sparrow, E.M.; Eichhorn, R.; Gregg, J.L. (1959)
- Eichhorn, R. (1960): The effect of mass transfer on free convection. *J. Heat Transfer*, Vol. 82, 260–263. [311]

- Eichhorn, R. /s.: Chen, C.C.; Eichhorn, R. (1976)
- Eiffel, G. (1912): Sur la résistance des sphères dans l'air en mouvement. Comptes Rendus, Vol. 155, 1597–1599. [46, 424]
- Eisfeld, F. (1971): Die Berechnung der Grenzschichten für gekoppelten Wärmeübergang und Stoffaustausch bei Verdunstung eines Flüssigkeitsfilms über einer parallel angeströmten Platte unter Berücksichtigung veränderlicher Stoffwerte. Int. J. Heat Mass Transfer, Vol. 14, 1537–1550. [318]
- Ekman, V.W. (1910): On the change from steady to turbulent motion of liquids. Ark. f. Mat. Astron. och. Fys., Vol. 6, Nr. 12. [417]
- Elsberry, K.; Loeffler, J.; Zhou, M.D.; Wygnanski, I. (2000): An experimental study of a boundary layer that is maintained on the verge of separation. J. Fluid Mech., Vol. 423, 227–261. [589]
- El Telbany, M.M.M.; Reynolds, A.J. (1980): Velocity distributions in plane turbulent channel flows. J. Fluid Mech., Vol. 100, 1–29. [544]
- El Telbany, M.M.M.; Reynolds, A.J. (1981): Turbulence in plane channel flows. J. Fluid Mech., Vol. 111, 283–318. [528]
- El Telbany, M.M.M.; Reynolds, A.J. (1982): The empirical description of turbulent channel flows. Int. J. Heat Mass Transfer, Vol. 25, 77–86. [521]
- El-Hady, N.M.; Nayfeh, A.H. (1980): Nonparallel instability of compressible boundary layer flows. AIAA Paper 80-0277. [466]
- El-Hady, N.M. (1991): Nonparallel instability of supersonic and hypersonic boundary layers. Phys. Fluids, A: Fluid Dynamics, Vol. 3(9), 2164–2178. [466]
- Emmerling, R. (1973): Die momentane Struktur des Wanddruckes einer turbulenten Strömung. Mitt. Max-Planck-Institut für Strömungsforschung und AVA Göttingen, Nr. 56. [512]
- Emmons, H.W.; Brainerd, J.G. (1942): Temperature effects in a laminar compressible fluid boundary layer along a flat plate. J. Appl. Mech., Vol. 8, A 105 (1941) and J. Appl. Mech., Vol. 9, 1. [236]
- Emmons, H.W.; Bryson, A.E. (1951–52): The laminar-turbulent transition in a boundary layer. Part I: J. of the Aeronautical Sciences, Vol. 18, 490–498 (1951); Part II: Proc. First US National Congress Appl. Mech., 859–868 (1952). [422, 473]
- Emmons, H.W.; Leigh, D.C. (1954): Tabulation of Blasius function with blowing and suction. ARC-CP-157. [303]
- Eppler, R. (1963): Praktische Berechnung laminarer und turbulenter Absaug-Grenzschichten. Ing.-Arch., Bd. 32, 221–245. [307]
- Eppler, R. (1969): Laminarprofile für Reynolds-Zahlen größer als $4 \cdot 10^6$. Ing.-Arch., Bd. 38, 232–240. [456]
- Erm, L.P.; Smits, A.J.; Joubert, P.N. (1987): Low Reynolds number turbulent boundary layers on a smooth flat surface in a zero pressure gradient: In: F. Durst et al. (Eds.): Turbulent Shear Flows 5, Springer-Verlag, Berlin, 186–196. [588]
- Escudier, M.P. (1966): The distribution of mixing-length in turbulent flows near walls. Imperial College, Heat Transfer Section, Rep. TWF/TN/1. [560]
- Evans, G.H.; Plumb, O.A. (1982a): Laminar mixed convection from a vertical heated surface in a crossflow. J. Heat Transfer, Vol. 104, 554–558. [342]
- Evans, G.H.; Plumb, O.A. (1982b): Numerical and approximate numerical solutions to a three-dimensional mixed convection boundary layer flow. Numerical Heat Transfer, Vol. 5, 287–298. [342]
- Evans, H.L. (1962): Mass transfer through a laminar boundary layer. Further similar solutions to the b-equation for the case $B = 0$. Int. J. Heat Mass Transfer, Vol. 5, 35–57. [220]
- Evans, H.L. (1968): Laminar Boundary-Layer Theory. Addison-Wesley Publ. Co., Reading/Mass. [207, 220]

- Exner, A.; Kluwick, A. (1999): Locally cooled free-convection boundary layer on the verge of separation. ZAMM. Z. angew. Math. Mech., Bd. 79, S711–S712. [401]
- Exner, A. /s.: Kluwick, A.; Exner, A. (2001)
- Fadnis, B.S. (1954): Boundary layer on rotating spheroids. Z. angew. Math. Phys. (ZAMP), Bd. 5, 156–163. [331]
- Fage, A.; Preston, J.H. (1941): On transition from laminar to turbulent flow in the boundary layer. Proc. Roy. Soc. London A, Vol. 178, 201–227. [469]
- Falco, R. /s.: Rubin, S.G.; Falco, R. (1968)
- Falco, R. (1980): The production of turbulence near a wall. AIAA Paper 80-1356, cf. also: Van Dyke, M. (1982): An Album of Fluid Motion. Parabolic Press. [421]
- Falkner, V.M.; Skan, S.W. (1931): Some approximate solutions of the boundary layer equations. Phil. Mag. 12, 865–896 (1931); ARC-Report 1314. [169]
- Fan, S.; Lakshminarayana, B.; Barnett, M. (1993): Low-Reynolds-number k - ε model for unsteady turbulent boundary-layer flows. AIAA Journal, Vol. 31, 1777–1784. [649, 650]
- Fand, R.M.; Morris, E.W.; Lum, M. (1977): Natural convection heat transfer from horizontal cylinders to air, water and silicone oils for Rayleigh numbers between $3 \cdot 10^2$ and $2 \cdot 10^7$. Int. J. Heat Mass Transfer, Vol. 20, 1173–1184. [280]
- Fannelöp, T.K.; Flügge-Lotz, I. (1965): Two-dimensional hypersonic stagnation flow at low Reynolds numbers. Z. Flugwiss., Bd. 13, 282–296. [387]
- Fannelöp, T.K.; Flügge-Lotz, I. (1966): Viscous hypersonic flow over simple blunt bodies. Comparison of a second-order theory with experimental results. J. de Mécanique, Vol. 5, 69–100. [387]
- Fannelöp, T.K.; Humphreys, D.A. (1975): The solution of the laminar and turbulent three-dimensional boundary layer equations with a simple finite difference technique. FFA Report 126, Stockholm. [642]
- Faulders, C.R. (1961): A note on laminar layer skin friction under the influence of foreign gas injection. J. of the Aero/Space Sciences, Vol. 28, 166–167. [319]
- Favre, A. (1938): Contribution à l'étude expérimentale des mouvement hydrodynamiques à deux dimensions. Thèse Université de Paris, 1–192. [292]
- Favre, A. (1965): Équations des gaz turbulents compressibles. J. de Mécanique, Vol. 4, 361–390 (part I), 391–421 (part II). [612]
- Favre, A.J.; Gaviglio, J.J.; Dumas, R.J. (1957) Space-time correlations and spectra in a turbulent boundary layer. J. Fluid Mech., Vol. 2, 313–342. [513]
- Favre, A.J.; Gaviglio, J.J.; Dumas, R.J. (1958) Further space-time correlations and spectra in a turbulent boundary layer. J. Fluid Mech., Vol. 3, 344–356. [513]
- Fay, J.A.; Riddell, F.R. (1958): Theory of stagnation point heat transfer in dissociated air. J. Aeron. Sci., Vol. 25, 73–85. [253, 319, 320]
- Feindt, E.G. (1956): Untersuchungen über die Abhängigkeiten des Umschlages laminar-turbulent von der Oberflächenrauhigkeit und der Druckverteilung. Dissertation Braunschweig, cf. also: Jb. 1956 der Schiffbautechn. Gesellschaft, Bd. 50, 180–203. [470, 472]
- Fejer, A.A. /s.: Loehrke, R.J.; Morkovin, M.V.; Fejer, A.A. (1975)
- Feo, A. /s.: Messiter, A.F.; Feo, A.; Melnik, R.E. (1971)
- Fernholz, H.H. (1964): Umlenkung von Freistrahlen an gekrümmten Wänden (Übersicht über den Stand der Technik). Jahrbuch 1964 der WGLR, 149–157. [667]
- Fernholz, H.H. /s.: Wille, R.; Fernholz, H.H. (1965)
- Fernholz, H.H.; Finley, P.J. (1980): A critical commentary on mean flow data for two-dimensional compressible turbulent boundary layer. AGARD-AG-253. [618, 619]
- Fernholz, H.H.; Krause, E. (Eds.) (1982): Three-Dimensional Turbulent Boundary Layers. Springer-Verlag, Berlin. [641, 706]

- Fernholz, H.H. /s.: Dengel, P.; Fernholz, H.H. (1990)
- Fernholz, H.H.; Krause, E.; Nockemann, M.; Schober, M. (1995): Comparative measurements in the canonical boundary layer at $Re_{\delta_2} \leq 6 \times 10^4$ on the wall of the German-Dutch windtunnel. *Phys. Fluids*, Vol. 7, 1275–1281. [585]
- Fernholz, H.H.; Finley, P.J. (1996): The incompressible zero-pressure-gradient turbulent boundary layer: on assessment of the data. *Progr. Aerospace Sci.*, Vol. 32, 245–311. [588]
- Ferriss, D.H. /s.: Bradshaw, P.; Ferriss, D.H.; Atwell, N.P. (1967)
- Ferriss, D.H. /s.: Bradshaw, P.; Ferriss, D.H. (1971)
- Ferziger, J.H. /s.: Lyrio, A.A.; Ferziger, J.H.; Kline, S.J. (1981)
- Fiedler, H.E. (1988): Coherent structures in turbulent flows. *Prog. Aerospace Sci.*, Vol. 25, 231–269. [513]
- Fila, G.H. /s.: Liepmann, H.W.; Fila, G.H. (1947)
- Finley, P.J.; Phoe, K.C.; Poh, C.J. (1966): Velocity measurements in a thin turbulent water layer. *La Houille Blanche*, Vol. 21, 713–720. [594]
- Finley, P.J. /s.: Fernholz, H.H.; Finley, P.J. (1980)
- Finley, P.J. /s.: Fernholz, H.H.; Finley, P.J. (1996)
- Fischer, T.M.; Dallmann, U. (1987): Theoretical Investigation of Secondary Instability of Three-Dimensional Boundary-Layer Flows with Application to the DFVLR-F5 Model Wing. DFVLR-FB 87-44. [491]
- Fischer, T.M.; Ehrenstein, U.; Meyer, F. (1988): Theoretical investigation of instability and transition in the DFVLR-F5 swept-wing flow. In: Zierep, J.; Oertel Jr., H. (Eds.): IUTAM Symposium Transsonicum III, Göttingen (1988), Springer-Verlag, Berlin, 243–252.
- Flachsbart, O. (1927): Neuere Untersuchungen über den Luftwiderstand von Kugeln. *Phys. Z.*, Bd. 28, 461–469. [25]
- Fleischhacker, G.; Schneider, W. (1980): Experimentelle und theoretische Untersuchungen über den Einfluß der Schwerkraft auf anisotherme, turbulente Freistrahlen. *Gesundheits-Ing.* Bd. 101, 129–140. Corrigendum: Bd. 104 (1983), 56, see also: *Int. J. Heat Mass Transfer*, Vol. 26 (1983), 1263–1264. [676]
- Fletcher, L.S. /s.: Merzkirch, W.; Page, R.H.; Fletcher, L.S. (1988)
- Floryan, J.M.; Saric, W.S. (1979): Stability of Görtler vortices in boundary layers with suction. In: AIAA Paper 79-1497; see also: *AIAA Journal*, Vol. 20 (1982), 316–324. [482]
- Floryan, J.M.; Saric, W.S. (1982): Stability of Görtler vortices in boundary layers. *AIAA Journal*, Vol. 20, 316–324. [482]
- Floryan, J.M. (1986): Görtler instability of boundary layers over concave and convex walls. *Phys. Fluids*, Vol. 29, 2380–2387. [482]
- Floryan, J.M. (1991): On the Görtler instability of boundary layers. *Prog. Aerospace Sci.*, Vol. 28, 235–271. [482, 484]
- Flügge-Lotz, I. /s.: Blottner, F.G.; Flügge-Lotz, I. (1963)
- Flügge-Lotz, I. /s.: Davis, R.T.; Flügge-Lotz, I. (1964)
- Flügge-Lotz, I. /s.: Fannelöp, T.K.; Flügge-Lotz, I. (1965)
- Flügge-Lotz, I. /s.: Fannelöp, T.K.; Flügge-Lotz, I. (1966)
- Flügge-Lotz, I.; Reyhner, T.A. (1968): The interaction of a shock wave with a laminar boundary layer. *Int. J. Nonlinear Mech.*, Vol. 3, 173–179. [397]
- Försching, H.W. (1978): Prediction of the unsteady air loads on oscillating lifting systems and bodies for aeroelastic analyses. *Prog. Aerospace Sci.*, Vol. 18, Pergamon Press, London, 211–269. [47]
- Föttinger, H. (1939): Strömungen in Dampfkesselanlagen, Mitteilungen der Vereinigung der Groß-Kesselbesitzer, Heft 73, 151. [43]
- Fogarty, L.E. (1951): The laminar boundary layer on a rotating blade. *J. of the Aeronautical Sciences*, Vol. 18, 247–252. [347]

- Fornberg, B. (1980): A numerical study of steady viscous flow past a circular cylinder. *J. Fluid Mech.*, Vol. 98, 819–855. [115]
- Fornberg, B. (1985): Steady viscous flow past a circular cylinder up to Reynolds number 600. *J. Computational Physics*, Vol. 61, 297–320. [19, 115]
- Fornberg, B. (1987): Steady viscous flow past a cylinder and a sphere at high Reynolds numbers. In: F.T. Smith, S.N. Brown (Eds.): *Boundary-Layer Separation*, Springer-Verlag, Berlin, 3–18. [21]
- Fornberg, B. (1988): Steady viscous flow past a sphere at high Reynolds numbers. *J. Fluid Mech.* Vol. 190, 471–489. [24]
- Fourier, J.B. (1822): *Théorie Analytique de la Chaleur*. Didot, Paris. [73]
- Fraenkel, L.E. (1962/63): Laminar flow in symmetric channels with slightly curved walls. I. On the Jeffery-Hamel solutions for flow between plane walls, *Proc. Roy. Soc. London A*, Vol. 267, 119–138 (1962). II. An asymptotic series for the stream-function, *Proc. Roy. Soc. London A*, Vol. 272, 406–428 (1963). [109]
- Franke, R.; Schöning, B. (1988): Die numerische Simulation der laminaren Wirbelablösung an Zylindern mit quadratischen oder kreisförmigen Querschnitten. Bericht SFB 210/T/39. [19, 24]
- Franssen, J.H.M.; Matsubara, M.; Alfredsson, P.H. (2005): Transition induced by free-stream turbulence. *J. Fluid Mech.* Vol. 527, 1–25. [481]
- Friedrich, R. /s.: Schumann, U.; Friedrich, R. (Eds.) (1986)
- Friedrich, R. /s.: Schumann, U.; Friedrich, R. (1987)
- Frössling, N. (1940): Verdunstung, Wärmeübertragung und Geschwindigkeitsverteilung bei zweidimensionaler und rotationssymmetrischer laminarer Grenzschichtströmung. *Lunds. Univ. Arsskr. N.F. Avd. 2*, 35, Nr. 4. [119]
- Froude, W. (1872): Experiments of the surface friction. *Brit. Ass. Rep.* [9, 84]
- Fujii, M. /s: Fujii, T.; Takeuchi, M.; Fujii, M.; Suzuki, K.; Uehara, H. (1970)
- Fujii, T. (1963): Theory of the steady laminar convection above a horizontal line heat source. *Int. J. Heat Mass Transfer*, Vol. 6, 597–606. [334]
- Fujii, T.; Takeuchi, M.; Fujii, M.; Suzuki, K.; Uehara, H. (1970): Experiments on natural convection heat transfer from the outer surface of a vertical cylinder to liquids. *Int. J. Heat Mass Transfer*, Vol. 13, 753–787. [280]
- Fulachier, L.; Arzoumanian, E.; Dumas, R. (1982): Effect on a developed turbulent boundary layer of sudden local wall motion. In: H.H. Fernholz; E. Krause (Eds.) (1982): *Three-Dimensional Turbulent Boundary Layers*, Springer-Verlag, Berlin, 188–198. [636]
- Furuya, Y.; Nakamura, I.; Yamashita, S. (1978): The laminar and turbulent boundary layers on some rotating bodies in axial flows. *Memoirs of the Faculty of Engineering, Nagoya University*, Vol. 30, 1–58. [635, 636]
- Gad-el-Hak, M.; Bandyopadhyay, P.R. (1994): Reynolds number effects in wall-bounded turbulent flows. *Appl. Mech. Rev.*, Vol. 8, 307–365. [XXIV]
- Galante, S.R.; Churchill, S.W. (1990): Applicability of solutions for convection in potential flow. *Advances in Heat Transfer*, Vol. 20, 353–388. [216]
- Galmes, J.M.; Lakshminarayana, B. (1984): Turbulence modeling for three-dimensional shear flows over curved rotating bodies. *AIAA Journal*, Vol. 22, 1420–1428. [643]
- Gampert, B. (Ed.) (1985): *The Influence of Polymer Additives on Velocity and Temperature Fields*. Springer-Verlag, Berlin. [534]
- Ganzer, U. (1988): *Gasdynamik*, Springer-Verlag, Berlin. [260, 624, 624, 626]
- Garbsch, K. (1956): Über die Grenzschicht an der Wand eines Trichters mit innerer Wirbel- und Radialströmung. In: H. Görtler; W. Tollmien (Hrsg.): *Fünfzig Jahre Grenzschichtforschung, Braunschweig 1955*, 471–486; cf. also: *ZAMM. Z. angew. Math. Mech.*, S11–S17. [330]
- Gargaro, R.J. /s.: Daniels, P.G.; Gargaro, R.J. (1993)

- Gaster, M. (1962): A note on the relation between temporally-increasing and spatially-increasing disturbances in hydrodynamic stability. *J. Fluid Mech.*, Vol. 14, 222–224. [425]
- Gaster, M. (1965): The role of spatially growing waves in the theory of hydrodynamic stability. *Prog. Aeronautical Sciences*, Vol. 6, 251–270. [425]
- Gaster, M. (1968): The development of three-dimensional wave packets in a boundary layer. *J. Fluid Mech.*, Vol. 32, 173–184. [431, 493]
- Gaster, M. (1974): On the effect of boundary layer growth on flow stability. *J. Fluid Mech.*, Vol. 66, part 3, 465–480. [436]
- Gaster, M. (1975): A theoretical model for the development of a wave packet in a laminar boundary layer. *Proc. Roy. Soc. London A.*, Vol. 347, 271–289. [431]
- Gaster, M.; Grant, I. (1975): An experimental investigation for the formation and development of a wave packet in a laminar boundary layer. *Proc. Roy. Soc. London A.*, Vol. 347, 253–269. [431]
- Gaudet, L. (1987): An assessment of the drag reduction properties of riblets and the penalties of off design conditions. *RAE Tech. Memo Aero* 2113. [531]
- Gaviglio, J.J. /s: Favre, A.J.; Gaviglio, J.J.; Dumas, R.J. (1957)
- Gaviglio, J.J. /s: Favre, A.J.; Gaviglio, J.J.; Dumas, R.J. (1958)
- Gazley Jr., C. /s.: Gross, J.F.; Hartnett, J.P.; Masson, D.J.; Gazley Jr., C. (1961)
- Gebhart, B. (1962): Effects of viscous dissipation in natural convection. *J. Fluid Mech.*, Vol. 14, 225–232. [281]
- Gebhart, B. /s.: Gunness, R.C.; Gebhart, B. (1965)
- Gebhart, B. (1973): Instability, transition and turbulence in buoyancy-induced flows. *Annu. Rev. Fluid Mech.*, Vol. 5, 213–246. [473]
- Gebhart, B. /s.: Mollendorf, J.C.; Gebhart, B. (1973)
- Gebhard, B. /s.: Pera, L.; Gebhard, B. (1973)
- Gebhart, B.; Mahajan, R.L. (1982): Instability and transition in buoyancy-induced flows. *Advances in Appl. Mech.*, Vol. 22, 231–315. [473]
- Gebhart, B.; Hilder, D.S.; Kelleher, M. (1984): The diffusion of turbulent buoyant jets. *Advances in Heat Transfer*, Vol. 16, 1–57. [676]
- Gebhart, B.; Jaluria, Y.; Mahajan, R.L.; Sammakia, B. (1988): *Buoyancy-Induced Flows and Transport*. Hemisphere Publ. Corp., New York. [473]
- Gebing, H. /s.: Dallmann, U.; Gebing, H.; Vollmers, H. (1993)
- Geis, Th. (1955): Ähnliche Grenzschichten an Rotationskörpern. In: H. Görtler; W. Tollmien (Hrsg.): *Fünfzig Jahre Grenzschichtforschung*, Braunschweig, 294–303. [324]
- Geis, Th. (1956a): Bemerkung zu den “ähnlichen” instationären laminaren Grenzschichtströmungen. *ZAMM. Z. angew. Math. Mech.*, Bd. 36, 396–398. [352]
- Geis, Th. (1956b): “Ähnliche” dreidimensionale Grenzschichten. *J. Rat. Mech. Analysis*, Vol. 5, 643–686. [341]
- Geißler, W. (1974a): Berechnung der dreidimensionalen laminaren Grenzschicht an schrägangeströmten Rotationskörpern mit Ablösung. *Ing.-Arch.*, Bd. 43, 413–425. [345, 346]
- Geißler, W. (1974b): Three-dimensional laminar boundary layer over a body of revolution at incidence and with separation. *AIAA Journal*, Vol. 12, 1743–1745. [345, 346]
- Geißler, W. (1989): Numerical calculation of the unsteady separating flow on oscillating airfoils (Dynamic stall). *Notes on Numerical Fluid Mechanics*, Vol. 25, 125–141. [354]
- Geißler, W. (1993): Verfahren in der instationären Aerodynamik. *DLR-FB* 93-21. [350, 368, 651, 703]
- George, W.K.; Capp, S.P. (1979): A theory for natural convection turbulent boundary layers next to heated vertical surfaces. *Int. J. Heat Mass Transfer*, Vol. 22, 813–826. [628]

- George, W.K. /s.: Wosnik, M.; George, W.K. (1995)
- Gerbers, W. (1951): Zur instationären, laminaren Strömung einer inkompressiblen zähen Flüssigkeit in kreiszylindrischen Rohren. *Z. angew. Physik*, Bd. 3, 267–271. [141]
- Gersten, K. /s.: Schlichting, H.; Gersten, K. (1961)
- Gersten, K. (1965): Heat transfer in laminar boundary layers with oscillating outer flow. In: AGARDograph 97, Part I, 423–475. [133, 136, 367]
- Gersten, K. (1967): Die instationäre laminare Grenzschicht für den Übergang zwischen zwei nur wenig verschiedenen stationären Strömungen. *ZAMM. Z. angew. Math. Mech.*, Bd. 47, T109–T110. [133, 137, 369, 369]
- Gersten, K.; Steinheuer, J. (1967): Untersuchungen im Institut für Aerodynamik auf dem Gebiet der Grenzschichtströmungen. DFL-Mitteilungen, Heft 7, 311–325. [289]
- Gersten, K.; Körner, H. (1968): Wärmeübergang unter Berücksichtigung der Reibungswärme bei laminaren Keilströmungen mit veränderlicher Temperatur und Normalgeschwindigkeit entlang der Wand. *Int. J. Heat Mass Transfer*, Vol. 11, 655–673. [115, 119, 216, 220, 228, 230, 306]
- Gersten, K. (1972): Grenzschichteffekte höherer Ordnung. Lecture on the occasion of the 65th birthday of Prof. Dr.-Ing. E.h. Dr. phil. H. Schlichting on 30.09.1972. Report 72/5 of the Institut für Strömungsmechanik der T.U. Braunschweig, 29–53. [XXIV, 379, 386]
- Gersten, K.; Gross, J.F.; Börger, G.-G. (1972): Die Grenzschicht höherer Ordnung an der Staulinie eines schiebenden Zylinders. *Z. Flugwiss.*, Bd. 20, 330–341. [113, 386, 387]
- Gersten, K. (1973a): Die kompressible Grenzschichtströmung am dreidimensionalen Staupunkt bei starkem Absaugen oder Ausblasen. *Wärme- und Stoffübertrag.*, Bd. 6, 52–61. [119, 325, 345]
- Gersten, K. (1973b): Über die Lösung der Grenzschichtgleichung bei extrem starkem Ausblasen bzw. Absaugen. *ZAMM. Z. angew. Math. Mech.*, Bd. 53, T99–T101. [119]
- Gersten, K.; Gross, J.F. (1973a): Increase of boundary-layer heat transfer by mass injection. *AIAA Journal*, Vol. 11, 738–739. [306]
- Gersten, K.; Gross, J.F. (1973b): The second-order boundary layer along a circular cylinder in supersonic flows. *Int. J. Heat Mass Transfer*, Vol. 16, 2241–2260. [387, 388]
- Gersten, K. (1974a): Die Verdrängungsdicke bei Grenzschichten höherer Ordnung. *ZAMM. Z. angew. Math. Mech.*, Bd. 54, 165–171. [384]
- Gersten, K. (1974b): Wärme- und Stoffübertragung bei großen Prandtl- bzw. Schmidtzahlen. *Wärme-Stoffübertrag.*, Bd. 7, 65–70. [318]
- Gersten, K., Gross, J.F. (1974a): Flow and heat transfer along a plane wall with periodic suction. *Z. angew. Math. Phys. (ZAMP)*, Bd. 25, 399–408. [342]
- Gersten, K., Gross, J.F. (1974b): The flow over a porous body; a singular perturbation problem with two parameters. *l'Aerotecnica Missili e Spazio*, Vol. 4, 238–250. [298, 300, 386]
- Gersten, K.; Nicolai, D. (1974): Die Hyperschallströmung um schlanke Körper mit Konturen der Form $\bar{R} \sim x^n$. DLR-FB 64-19. [390]
- Gersten, K., Gross, J.F. (1976): Higher order boundary layer theory. *Fluid Dynamic Transactions*, Polish Academy of Science, Vol. 7, Part II, 7–36. [XXIV, 379, 386]
- Gersten, K. (1977): Grenzschichteffekte höherer Ordnung an der Staulinie eines Pfeilflügels. "Festschrift" on the occasion of the 60th birthday of Prof. Dr.-Ing. E. Truckenbrodt, Munich, 134–148. [387]
- Gersten, K.; Papenfuß, H.-D.; Gross, J.F. (1977): Second-order boundary-layer flow with hard suction. *AIAA Journal*, Vol. 15, 1750–1755. [298, 386, 388]

- Gersten, K.; Schilawa, S. (1978): Buoyancy effects on forced-convection heat transfer in horizontal boundary layers. In: Proceedings 6th Intern. Heat Transfer Conference, Toronto, Vol. I, MC 13, 73–78. [222]
- Gersten, K. (1979): Second-order boundary-layer effects for large injection or suction. In: U. Müller et al. (Eds.): Recent Developments in Theoretical and Experimental Fluid Mechanics, Springer-Verlag, Berlin, 1979, 446–456. [302, 386]
- Gersten, K. /s.: Beese, E.; Gersten, K. (1979)
- Gersten, K.; Cosart, W.P. (1980): Heat transfer about a rotating disk with strong blowing. J. Math. Phys. Sci., Vol. 14, 57–70. [124]
- Gersten, K.; Schilawa, S.; Schulz-Hausmann, F.K. von (1980): Nichtisotherme ebene Freistrahlen unter Schwerkrafteinfluß. Wärme-Stoffübertrag., Bd. 13, 145–162. [276, 290, 676]
- Gersten, K. (1982a): Advanced boundary-layer theory in heat transfer. In: Proc. 7th Int. Heat Transfer Conf., Munich, Vol. 1, 159–172. [304, 379, 386]
- Gersten, K. (1982b): Two-dimensional separated flows. In: Eighth Int. Conference on Numerical Methods in Fluid Dynamics. Lecture Notes in Physics, Vol. 170, 43–54. [21]
- Gersten, K.; Wiedemann, J. (1982): Widerstandsverminderung umströmter Körper durch kombiniertes Ausblasen und Absaugen an der Wand. Forschungsbericht des Landes Nordrhein-Westfalen, Nr. 3103, Westdeutscher Verlag, Opladen. [309]
- Gersten, K.; Pagendarm, H.G. (1983): Wirkungsgrad von Diffusoren. Forschungsberichte aus dem Gebiet der Luft- und Trocknungstechnik, Heft 14, p.56–76. [25]
- Gersten, K. /s.: Wiedemann, J.; Gersten, K. (1984)
- Gersten, K.; Herwig, H. (1984): Impuls- und Wärmeübertragung bei variablen Stoffwerten für die laminare Plattenströmung. Wärme-Stoffübertrag., Bd. 18, 25–35. [238]
- Gersten, K. /s.: Herwig, H.; Wickern, G.; Gersten, K. (1985)
- Gersten, K. (1987): Some contributions to asymptotic theory for turbulent flows. In: Proceedings 2nd Int. Symposium on Transport Phenomena in “Turbulent Flows”, Tokyo, 201–214. [XXIV]
- Gersten, K. (1989a): Die Bedeutung der Prandtlschen Grenzschichttheorie nach 85 Jahren. Z. Flugwiss. Weltraumforsch., Bd. 13, 209–218. [XXV, 386, 609]
- Gersten, K. (1989b): Some open questions in turbulence modelling from viewpoint of asymptotic theory. In: Proc. of the Tenth Australian Fluid Mechanics Conference, Melbourne, Vol. II, 12.1–12.4. [621]
- Gersten, K. (1989c): Introduction to asymptotic theory for turbulent flows. ZAMM. Z. angew. Math. Mech., Vol. 69, T555–T558. [XXIV]
- Gersten, K.; Grobel, M.; Klick, H.; Merzkirch, W. (1991): Flow separation in laminar natural convection. Int. J. Heat and Fluid Flow, Vol. 12, 331–335. [386, 401]
- Gersten, K.; Herwig, H. (1992): Strömungsmechanik. Grundlagen der Impuls-, Wärme- und Stoffübertragung aus asymptotischer Sicht. Vieweg-Verlag, Braunschweig/Wiesbaden. [XXIV, 94, 176, 214, 225, 235, 276, 304, 313, 314, 318, 385, 507, 511, 524, 527, 535, 537, 540, 542, 544, 547, 553, 553, 554, 557, 565, 570, 574, 578, 581, 581, 590, 606, 608, 613, 614, 620, 621, 628, 629, 634, 633, 663, 701]
- Gersten, K.; Papenfuß, H.-D. (1992): Separated flows behind bluff bodies at low speeds including ground effects. In: Proceedings 2nd Caribbean Conference in Fluid Dynamics, 115–122. [643]
- Gersten, K.; Klauer, J.; Vieth, D. (1993): Asymptotic analysis of two-dimensional turbulent separating flows. In: K. Gersten (Ed.): Physics of Separated Flows – Numerical, Experimental and Theoretical Aspects. Notes on Numerical Fluid Mechanics, Vol. 40, Vieweg-Verlag, Braunschweig, 125–132. [547, 549]

- Gersten, K.; Rocklage, B. (1994): Self-similar solutions for two-dimensional slender-channel flows. *Acta Mechanica* [Suppl.], Vol. 4, 325–334. [556]
- Gersten, K.; Vieth, D. (1995): Berechnung anliegender Grenzschichten bei hohen Reynolds-Zahlen. “Festschrift” on the occasion of the 70th birthday of Prof. Dr. J. Siekmann, Universität-GH Essen. [577, 579]
- Gersten, K. (Ed.) (1996): Asymptotic Methods for Turbulent Shear Flows at High Reynolds Numbers. Kluwer Academic Publishers, Dordrecht, Boston, London. [XXV]
- Gersten, K. (1997): Einfluß der Dissipation auf das Rohrreibungsgesetz. In: M.S. Kim (Hrsg.): Turbulenz in Strömungsmechanik, Shaker Verlag, Aachen, 61–68. [553]
- Gersten, K. (2000): Ludwig Prandtl und die asymptotische Theorie für Strömungen bei hohen Reynolds-Zahlen. In: G.E.A. Meier (Hrsg.): Ludwig Prandtl, ein Führer in der Strömungslehre. Vieweg-Verlag, Braunschweig/Wiesbaden, 125–138. [XXIV]
- Gersten, K. (2001): Asymptotic theory for turbulent shear flows at high Reynolds numbers. *ZAMM, Z. Angew. Math. Mech.*; Vol. 81, S73–S76. [558]
- Gersten, K. (2004): Fully developed turbulent pipe flow. In: W. Merzkirch (Ed.): Fluid Mechanics of Flow Metering. Springer, Berlin, 1–22. [534]
- Gersten, K. (2015): The asymptotic downstream flow of plane turbulent wall jets without external stream. *J. Fluid Mech.* Vol. 779, 351–370. [679]
- Gersting, J.M.; Jankowski, D.F. (1972): Numerical methods for Orr-Sommerfeld problems. *Int. J. Numerical Methods in Engineering*, Vol. 4, 195–206. [436]
- Gibellato, S. (1954): Strato limite attorno ad una lastra piana investita da un fluido incompressibile clotato di una velocità che è somma di una parte costante e di una parete alternata. *Atti della Accademia della Scienze di Torino* 89, 180–192 (1954–1955) and 90, 13–24 (1955–1956). [368]
- Gibellato, S. (1956): Strato limite termico attorno a una lastra piano investita da una corrente lievemente pulsante di fluido incompressibile. *Atti della Accademia della Scienze di Torino* 91, 152–170. [368]
- Gibson, M.M.; Jones, W.P.; Younis, B.A. (1981): Calculation of turbulent boundary layers on curved surface. *Phys. Fluids*, Vol. 24, 386–395. [642]
- Giedt, W.H. /s.: Tewfik, O.K.; Giedt, W.H. (1959)
- Giles, M. /s.: Drela, M.; Giles, M.; Thompkins Jr., W.T. (1986)
- Gill, W.N.; Zeh, D.W.; Del Casal, E. (1965): Free convection on a horizontal plate. *Z. angew. Math. Phys. (ZAMP)*, Bd. 16, 539–541. [283]
- Girodroux-Lavigne, P. /s.: Le Balleur, J.-C.; Girodroux-Lavigne, P. (1986)
- Gittler, Ph. /s.: Kluwick, A.; Gittler, Ph.; Bodonyi, R.J. (1984)
- Gittler, Ph. (1985): Dreidimensionale Wechselwirkungsvorgänge bei laminaren Grenzschichten. Dissertation, Technische Universität Wien. [400]
- Gittler, Ph. /s.: Kluwick, A.; Gittler, Ph.; Bodonyi, R.J. (1985)
- Gittler, Ph.; Kluwick, A. (1987): Triple-deck solutions for supersonic flows past flared cylinders. *J. Fluid Mech.*, Vol. 179, 469–487. [403]
- Gittler, Ph.; Kluwick, A. (1989): Interacting laminar boundary layers in quasi-two-dimensional flow. *Fluid Dynamics Research*, Vol. 5, 29–47. [401]
- Gittler, Ph. /s.: Kluwick, A.; Gittler, Ph. (1994)
- Glauert, M.B. (1956a): The laminar boundary layer on oscillating plates and cylinders. *J. Fluid Mech.*, Vol. 1, 97–110. [132]
- Glauert, M.B. (1956b): The wall jet. *J. Fluid Mech.*, Vol. 1, 625–643. [181, 326]
- Glauert, M.B. (1958): On laminar wall jets. In: H. Görtler (Hrsg.): Grenzschichtforschung, Springer-Verlag, Berlin, 72–78. [295]
- Gleyzes, C.; Cousteix, J.; Bonnet, J.L. (1984): A calculation method of leading-edge separation bubbles. In: T. Cebeci (Ed.): Numerical and Physical Aspects of Aerodynamic Flows II. Springer-Verlag, New York, 173–192. [457]

- Gloss, D. /s.: Herwig, H.; Gloss, D.; Wenterdt, T. (2008)
- Gloss, D.; Herwig, H. (2010): Wall roughness effects in laminar flows: an often ignored though significant issue. *Exp. Fluids*, Vol. 49, 461–470. [534]
- Godil, A.A. /s.: Malik, M.R.; Godil, A.A. (1990)
- Görtler, H. (1940a): Über den Einfluß der Wandkrümmung auf die Entstehung der Turbulenz. *ZAMM. Z. angew. Math. Mech.*, Bd. 20, 138–147. [479]
- Görtler, H. (1940b): Über eine dreidimensionale Instabilität laminarer Grenzschichten an konkaven Wänden. *Nachr. Wiss. Ges. Göttingen, Math. Phys. Klasse, Neue Folge* 2, Nr. 1, see also *ZAMM. Z. angew. Math. Mech.*, Bd. 21, 250–252, 1941. [480, 481]
- Görtler, H. (1944): Verdrängungswirkung der laminaren Grenzschicht und Druckwiderstand. *Ing.-Arch.*, Bd. 14, 286–305. [361]
- Görtler, H. (1948): Grenzschichtentstehung an Zylindern bei Anfahrt aus der Ruhe. *Arch. d. Math.*, Bd. 1, 138–147. [359]
- Görtler, H. (1952a): Die laminare Grenzschicht am schiebenden Zylinder. *Arch. d. Math.*, Bd. 3, Fasc. 3, 216–231. [343]
- Görtler, H. (1952b): Eine neue Reihenentwicklung für laminare Grenzschichten. *ZAMM., Z. angew. Math. Mech.*, Bd. 32, 270–271. [182, 186]
- Görtler, H. (1954): Decay of swirl in an axial symmetrical jet far from the orifice. *Revista matematica hispano-americana*, 4. Ser., Vol. 14, 143–178. [333]
- Görtler, H. (1955a): Dreidimensionales zur Stabilitätstheorie laminarer Grenzschichten. *ZAMM., Z. angew. Math. Mech.*, Vol. 35, 362–364. [481]
- Görtler, H. (1955b): Dreidimensionale Instabilität der ebenen Staupunktströmung gegenüber wirbelartigen Störungen. In: H. Görtler; W. Tollmien (Hrsg): *Fünfzig Jahre Grenzschichtforschung*. Vieweg Verlag, Braunschweig, 304–314. [482]
- Görtler, H. (1957a): A new series for the calculation of steady laminar boundary layer flows. *J. Math. Mech.*, Vol. 6, 1–66. [186]
- Görtler, H. (1957b): Bericht Nr. 34 der Deutschen Versuchsanstalt für Luftfahrt 1957: Zahlentafel universeller Funktionen zur neuen Reihe für die Berechnung laminarer Grenzschichten. [186]
- Görtler, H. (1957c): On the calculation of steady laminar boundary layer flows with continuous suction. *J. Math. Mech.*, Vol. 6, 323–340. [307]
- Goldberg, U.; Reshotko, E. (1984): Scaling and modeling of three-dimensional, pressure-driven turbulent boundary layers. *AIAA Journal*, Vol. 22, 914–920. [490, 491, 640]
- Goldberg, U.C. (1991): Derivation and testing of a one-equation model based on two time scales. *AIAA Journal*, Vol. 29, 1337–1340. [562]
- Goldstein, M.E.; Hultgren, L.S. (1989): Boundary layer receptivity to long-wave disturbances. *Annu. Rev. Fluid Mech.*, Vol. 21, 137–166. [490]
- Goldstein, R.J. /s.: Schneider, M.E.; Goldstein, R.J. (1994)
- Goldstein, S. (1935): On the resistance to the rotation of a disk immersed in a fluid. *Proc. Cambr. Phil. Soc.*, Vol. 31, Pt. 2, 232. [636]
- Goldstein, S. (1936): A note on roughness. *ARC RM 1763*. [469]
- Goldstein, S.; Rosenhead, L. (1936): Boundary layer growth. *Proc. Cambr. Phil. Soc.*, Vol. 32, 392–401. [356]
- Goldstein, S. (1939): A note on the boundary layer equations. *Proc. Cambr. Phil. Soc.*, Vol. 35, 338–340. [167]
- Goldstein, S. (1948a): Low-drag and suction airfoils. *J. of the Aeronautical Sciences*, Vol. 15, 189–220. [294]
- Goldstein, S. (1948b): On laminar-boundary layer flow near a position of separation. *Quart. J. Mech. Appl. Math.*, Vol. 1, 43–69. [186, 205]
- Goldstein, S. (Ed.) (1965): *Modern Developments in Fluid Dynamics* (Two Vols.). Dover, New York. [75]

- Gosh, A. (1961): Contribution à l'étude de la couche limite laminaire instationnaire. Publications Scientifiques et Techniques du Ministère de l'Air. No. 381. [365, 368]
- Grant, I. /s.: Gaster, M.; Grant, I. (1975)
- Granville, P.S. (1953): The calculation of viscous drag of bodies of revolution. Navy Department. The David Taylor Model Basin. Report No. 849. [455, 455, 671]
- Granville, P.S. (1973): The torque and turbulent boundary layer of rotating disks with smooth and rough surfaces, and in drag-reduction polymer solutions. J. Ship. Res., Vol. 17, 181–195. [636]
- Granville, P.S. (1977): A prediction method for the viscous drag of ships and underwater bodies with surface roughness and/or reducing polymer solutions. David W. Taylor Naval Ship Res. Developm. Center, Report SPD-797-01. [671]
- Gray, W.E. (1952): The effect of wing sweep on laminar flow. RAE-TM Aero 255. [485]
- Gregg, J.L. /s.: Sparrow, E.M.; Gregg, J.L. (1957)
- Gregg, J.L. /s.: Sparrow, E.M.; Gregg, J.L. (1958)
- Gregg, J.L. /s.: Sparrow, E.M.; Eichhorn, R.; Gregg, J.L. (1959)
- Gregg, J.L. /s.: Sparrow, E.M.; Gregg, J.L. (1960a)
- Gregg, J.L. /s.: Sparrow, E.M.; Gregg, J.L. (1960b)
- Gregory, N.; Stuart, J.T.; Walker, W.S. (1955): On the stability of three-dimensional boundary layers with applications to the flow due to a rotating disk. Philos. Trans. Roy. Soc. London A, Vol. 248, 155–199. [485, 485, 487]
- Gregory, N.; Walker, W.S. (1955): Wind-tunnel tests on the NACA 63 A 009 aerofoil with distributed suction over the nose. ARC-RM-2900. [309]
- Grek, G.R./s.: Boiko, A.V.; Grek, G.R.; Dovgal, A.V.; Kozlov, V.V. (2002):
- Gretler, W. /s.: Tangemann, R.; Gretler, W. (2000)
- Grigson, C.W.B. (1984): Nikuradse's experiment. AIAA Journal, Vol. 22, 999–1001. [530]
- Grigull, U.; Sandner, H. (1986): Wärmeleitung, Springer-Verlag, Berlin/Heidelberg. [127]
- Grobel, M. /s.: Gersten, K.; Grobel, M.; Klick, H.; Merzkirch, W. (1991)
- Grohne, D. (1954): Über das Spektrum bei Eigenschwingungen ebenen Laminarströmungen. ZAMM. Z. angew. Math. Mech., Vol. 34, 344–357. [435]
- Grohne, D. (1972): Ein Beitrag zur nicht-linearen Stabilitätstheorie von ebenen Laminarströmungen. ZAMM. Z. angew. Math. Mech., Vol. 52, 256–257. [439]
- Grosh, R.J. /s.: Hering, R.G.; Grosh, R.J. (1962)
- Gross, J.F.; Hartnett, J.P.; Masson, D.J.; Gazley Jr., C. (1961): A review of binary boundary layer characteristics. Int. J. Heat Mass Transfer, Vol. 3, 198–221. [311]
- Gross, J.F.; Dewey, Jr. C.F. (1965): Similar solutions of the laminar boundary-layer equations with variable fluid properties. In: W. Fizdon (Ed.): Fluid Dynamic Transactions, Vol. 2, Pergamon Press, New York, 529–548. [243]
- Gross, J.F. /s.: Dewey Jr., C.F.; Gross, J.F. (1967)
- Gross, J.F. /s.: Gersten, K; Gross, J.F.; Börger, G.-G. (1972)
- Gross, J.F. /s.: Gersten, K; Gross, J.F. (1973a)
- Gross, J.F. /s.: Gersten, K; Gross, J.F. (1973b)
- Gross, J.F. /s.: Gersten, K; Gross, J.F. (1974a)
- Gross, J.F. /s.: Gersten, K; Gross, J.F. (1974b)
- Gross, J.F. /s.: Gersten, K; Gross, J.F. (1976)
- Gross, J.F. /s.: Gersten, K; Papenfuß, H.-D.; Gross, J.F. (1977)

- Grossman, B. /s.: Melnik, R.E.; Grossman, B. (1981)
- Grossmann, S. (2000): The onset of shear flow turbulence. Rev. Mod. Phys., Vol.72, 603–618. [479]
- Grundmann, R. (1976): Two-dimensional, laminar, compressible boundary layer calculations in turbomachines. DLR-FB 76–38. [347]
- Grundmann, R. (1981): Dreidimensionale Grenzschichtberechnungen entlang Symmetrielinien auf Körpern. Z. Flugwiss. Weltraumforsch., Bd. 5, 389–395. [338, 345]
- Gruschwitz, E. (1931): Die turbulente Reibungsschicht in ebener Strömung bei Druckabfall und Druckanstieg. Ing.-Arch., Bd. 2, 321–346. [192]
- Gruschwitz, E. (1950): Calcul approché de la couche limite la laminaire en écoulement compressible sur une paroi non-conductrice de la chaleur. ONERA (Office National d'Etudes et de Recherche Aéronautiques), Publication No. 47, Paris. [262]
- Guiraud, J.-P. /s: Deriat, E.; Guiraud, J.-P. (1986)
- Gulcat, U. /s.: Wu, J.C.; Gulcat, U. (1981)
- Gunness, R.C.; Gebhart, B. (1965): Combined forced and natural convection flow for the wedge geometry. Int. J. Heat Mass Transfer, Vol. 8, 43–53. [289]
- Ha Minh, H.; Viegas, J.R.; Rubesin, M.W.; Vandromme, D.D.; Spalart, P.R. (1989): Physical analysis and second-order modeling of an unsteady turbulent flow: the oscillating boundary layer on a flat plate. In: F. Durst et al. (Eds.): Seventh Symposium on Turbulent Shear Flows, Stanford University, 1989. – Springer-Verlag, Berlin – Session 11-5. [649]
- Haas, S.; Schneider, W. (1996): Axisymmetric turbulent sink flows. In: K.Gersten (Ed.): Asymptotic Methods for Turbulent Shear Flows at High Reynolds Numbers. Kluwer Academic Publishers, Dordrecht/Boston/London, 81-94. [634]
- Haas, S.; Schneider, W. (1997): Wall-bounded laminar sink flows. Acta Mechanica, Vol. 125, 211–215. [171]
- Haase, R. (1963): Thermodynamik der irreversiblen Prozesse. Dr. D. Steinkopff-Verlag, Darmstadt. [313]
- Hackmüller, G.; Kluwick, A. (1989): The effect of a surface mounted obstacle on marginal separation. Z. Flugwiss. Weltraumforsch., Bd. 13, 365–370. [408]
- Hackmüller, G.; Kluwick, A. (1990): Marginale Ablösung an ebenen schlanken Hügeln und Dellen. ZAMM. Z. angew. Math. Mech., Bd. 70, T478–479. [408]
- Hackmüller, G.; Kluwick, A. (1991a): Effects of 3-D surface mounted obstacles on marginal separation. In: V.V. Kozlov; A.V. Dovgal (Eds.): Separated Flows and Jets. Springer-Verlag, Berlin, 55–65. [408]
- Hackmüller, G.; Kluwick, A. (1991b): Marginal separation in quasi-two-dimensional flow. In: W. Schneider; H. Troger; F. Ziegler (Eds.): Trends in Applications of Mathematics to Mechanics, Interactions of Mechanics and Mathematics Series. Longman Scientific and Technical, New York, 143–149. [408]
- Hadden, L.L. /s.: Page, R.H.; Hadden, L.L.; Ostowari, C. (1989)
- Hämmerlin, G. (1955): Zur Instabilitätstheorie der ebenen Staupunktströmung. In: H. Görtler; W. Tollmien (Hrsg.): Fünfzig Jahre Grenzschichtforschung, 315–327, Vieweg-Verlag, Braunschweig. [484]
- Härtl, A.P. (1989): Optimierung von Diffusoren durch Konturierung der Wände auf der Basis des Grenzschichtkonzeptes. Dissertation, Ruhr-Universität Bochum, also as Fortschr.-Ber. VDI Reihe 7, Nr. 159, VDI-Verlag, Düsseldorf. [592, 593, 634]
- Hagen, G. (1839): Über die Bewegung des Wassers in engen zylindrischen Röhren. Pogg. Ann. Bd. 46, 423–442. [11]
- Hall, A.A.; Hislop, G.S. (1938): Experiments on the transition of the laminar boundary layer on a flat plate. ARC-RM-1843. [442]

- Hall, M.G. /s.: Cooke, J.C.; Hall, M.G. (1962)
- Hall, M.G. (1969): A numerical method for calculating unsteady two-dimensional laminar boundary layers. *Ing.-Archiv*, Bd. 38, 97–106. [351]
- Hall, P. (1982): Taylor-Görtler vortices in fully developed or boundary-layer flows: Linear theory. *J. Fluid Mech.*, Vol. 124, 475–494. [480]
- Hall, P.; Malik, M.R.; Poll, D.I.A. (1984): On the stability on an infinite swept attachment line boundary layer. *Proc. Roy. Soc. London A*, Vol. 395, 229–245. [488]
- Hallbäck, M.; Henningson, D.S.; Johansson, A.V.; Alfredsson, P.H. (Eds.) (1996): *Turbulence and Transition Modelling*. Kluwer Academic Publishers, Dordrecht, Boston, London. [XXV]
- Hama, F.R.; Nutant, J. (1963): Detailed flow-field observations in the transition process in a thick boundary layer. In: Roshko, A; Sturtevant, B.; Bartz, D.R.: Proc. of the 1963 Heat Transfer and Fluid Mechanics Institute, Stanford Univ. Press, 77–93. [473]
- Hama, F.R.; Peterson, L.F. (1976): Axisymmetric laminar wake behind a slender body of revolution. *J. Fluid Mech.*, Vol. 76, 1–15. [335]
- Hama, R. /s.: Tani, I.; Hama, R.; Mituisi, S. (1940)
- Hamel, G. (1916): Spiralförmige Bewegung zäher Flüssigkeiten. *Jahresber. d. Dt. Mathematiker-Vereinigung* 25, 34–60. [104, 139]
- Hamel, G. (1941): Über die Potentialströmung zäher Flüssigkeiten. *ZAMM. Z. angew. Math. Mech.*, Bd. 21, 129–139. [93]
- Hamielec, A.E.; Raal, J.D. (1969): Numerical studies of viscous flow around circular cylinders. *Phys. Fluids*, Vol. 12, 11–17. [19]
- Hamman, J. /s.: Mirels, H.; Hamman, J. (1962)
- Hanjalić, K.; Launder, B.E. (1972a): A Reynolds stress model of turbulence and its application to thin shear flows. *J. Fluid Mech.*, Vol. 52, 609–638. [567, 700]
- Hanjalić, K.; Launder, B.E. (1972b): Fully developed asymmetric flow in a plane channel. *J. Fluid Mech.*, Vol. 51, 301–335. [544]
- Hanjalić, K.; Launder, B.E. (1976): Contribution towards a Reynolds stress closure for low-Reynolds-number turbulence. *J. Fluid Mech.*, Vol. 74, 593–610. [XXIV, 567]
- Hanjalić, K.; Stosic, N. (1983): Hysteresis of turbulent stresses in wall flows subjected to periodic disturbances. In: L.J.S. Bradbury et al. (Eds.): *Fourth Symposium on Turbulent Shear Flows*. Springer-Verlag, Berlin, 287–300. [649]
- Hanjalić, K. (1994a): Advanced turbulence closure models: a view of current status and future prospects. *Int. J. Heat and Fluid Flow*, Vol. 15, 178–203. [567, 571, 601]
- Hanjalić, K. (1994b): Achievements and limitations in modelling and computation of buoyant turbulent flow and heat transfer. In: Proc. 10th Int. Heat Transfer Conference, August 1994, Brighton, UK, Vol. 1, SK-1, 1–18. [570]
- Hanjalić, K. /s.: Jakirlić, S.; Hanjalić, K. (1995)
- Hanjalić, K. (2002): One-point closure models for buoyancy-driven turbulent flows. *Annu. Rev. Fluid Mech.* Vol. 34, 321–348. [610]
- Hannah, D.M. (1952): Forced flow against a rotating disc. ARC-RM-2772. [328]
- Hannemann, K.; Oertel Jr., H. (1989): Numerical simulation of the absolutely and convectively unstable wake. *J. Fluid Mech.*, Vol. 199, 55–88. [494]
- Hansen, A.G. /s.: Mager, A.; Hansen, A.G. (1952)
- Hansen, A.G.; Herzig, H.Z. (1956): Cross flows in laminar incompressible boundary layers.. NASA-TN-3651. [342]
- Hansen, C.F. (1959): Approximation for the thermodynamic and transport properties of high-temperature air. NASA-TR-R-50. [316]

- Hansen, M. (1928): Die Geschwindigkeitsverteilung in der Grenzschicht an einer eingetauchten Platte. ZAMM. Z. angew. Math. Mech., Bd. 8, 185–199 (1928); NACA-TM-585. [33, 34, 162, 163, 420, 440]
- Hantzsch, W.; Wendt, H. (1940): Zum Kompressibilitätseinfluß bei der laminaren Grenzschicht der ebenen Platte. Jb. dt. Luftfahrtforschung I, 517–521. [253, 256]
- Hantzsch, W.; Wendt, H. (1941): Die laminare Grenzschicht an einem mit Überschallgeschwindigkeit angeströmten nicht angestellten Kreiskegel. Jb. dt. Luftfahrtforschung I, 76–77. [326]
- Hantzsch, W.; Wendt, H. (1942): Die laminare Grenzschicht an der ebenen Platte mit und ohne Wärmeübergang unter Berücksichtigung der Kompressibilität. Jb. dt. Luftfahrtforschung I, 40–50. [256]
- Happel, J.; Brenner, H. (1973): Low Reynolds Number Hydrodynamics with Special Applications to Particulate Media. 2nd Edition, Noordhoff, Leyden. [94]
- Harris, D.P. /s.: Binnie, A.M.; Harris, D.P. (1950)
- Harris, H.D.; Young, A.D. (1967): A set of similar solutions of the compressible laminar boundary layer equations for the flow over a flat plate with unsteady wall temperature. Z. Flugwiss., Bd. 15, 295–301. [375]
- Harris, J.E. /s.: Iyer, V.; Harris, J.E. (1990)
- Harris, J.E. /s.: Wie, Y.-S.; Harris, J.E. (1991)
- Hartnett, J.P. /s.: Gross, J.F.; Hartness, J.P.; Masson, D.J.; Gazley Jr., C. (1961)
- Hartree, D.R. (1937): On an equation occurring in Falkner and Skan's approximate treatment of the equations of the boundary layer. Proc. of the Cambridge Philosophical Society. Vol. 33, part 2, 223–239. [169, 172]
- Hassan, H.A. (1960): On unsteady laminar boundary layers. J. Fluid Mech., Vol. 9, 300–304 (1960); cf. also J. of the Aero/Space Sciences, Vol. 27, 474–476. [352]
- Haussling, H.J. /s.: Lugt, H.J.; Haussling, H.J. (1974)
- Hayasi, N. (1962): On similar solutions of the unsteady quasi-two-dimensional incompressible laminar boundary-layer equations. J. Phys. Soc., Japan, Vol. 17, 194–203. [352]
- Hayes, W.D. (1951): The three-dimensional boundary layer. NAVORD-Rep. 1313. [338]
- Hayes, W.D.; Probstein, R.F. (1959): Hypersonic Flow Theory. Academic Press, New York. [24, 263, 391, 392]
- Head, M.R. /s.: Jones, B.M.; Head, M.R. (1951)
- Head, M.R. (1955): The boundary layer with distributed suction. ARC-RM-2783. [460]
- Head, M.R. (1960): Entrainment in the turbulent boundary layer. ARC-RM-3152. [597]
- Head, M.R.; Bandyopadhyay, P. (1981): New aspects of turbulent boundary-layer structure. J. Fluid Mech., Vol. 107, 297–338. [475]
- Heighway, J.E. /s.: Braun, W.H.; Ostrach, S.; Heighway, J.E. (1961)
- Heil, M. /s.: Ludwig, G.; Heil, M. (1960)
- Heinecke, E. /s.: Achenbach, E.; Heinecke, E. (1981)
- Heisenberg, W. (1924): Über Stabilität und Turbulenz von Flüssigkeitsströmen. Annu. d. Phys., Bd. 74, 577–627. [435]
- Heisenberg, W. (1948): Zur statistischen Theorie der Turbulenz. Z. Phys., Bd. 124, 628–657. [514, 514]
- Helmholtz, H. (1868): Über diskontinuierliche Flüssigkeits-Bewegungen. Monatsberichte der Königlich Preussischen Akademie der Wissenschaften zu Berlin, Berlin Akad. 215–228. [409]
- Henkes, R. A. M.; Hoogendoorn, C.J. (1990): Numerical determination of wall functions for the turbulent natural convection boundary layer. Int. J. Heat Mass Transfer, Vol. 33, 1087–1097. [628]

- Henkes, R.A.W.M. (1990): Natural-convection boundary layers. Dissertation, Technische Universität Delft. [629]
- Henkes, R.A.W.M. (1998): Scaling of equilibrium boundary layers under adverse pressure gradient using turbulence models. AIAA Journal, Vol. 36, 320–326. [592]
- Henningson, D.S. /s.: Hallbäck, M.; Henningson, D.S.; Johansson, A.V.; Alfredsson, P.H. (Eds.) (1996)
- Henningson, D.S. /s.: Schmidt, P.J.; Henningson, D.S (2000)
- Henseler, H. /s.: Schultz-Grunow, F.; Henseler, H. (1968)
- Herbert, T. (1983): Subharmonic three-dimensional disturbances. AIAA Paper 83-1759. [473, 474]
- Herbert, T. (1984): Analysis of the subharmonic route to transition in boundary layers. AIAA Paper 84-0009. [478]
- Herbert, T.; Bertolotti, F.P. (1987): Stability analysis of nonparallel boundary layers. Bull. Amer. Phys. Soc. 32, 2079. [443, 445]
- Herbert, T. (1988): Secondary instability of boundary layers. Annu. Rev. Fluid Mech., Vol. 20, 487–526. [476, 477, 477, 478, 484, 489]
- Hering, R.G.; Grosh, R.J. (1962): Laminar free convection from a non-isothermal cone. Int. J. Heat Mass Transfer. Vol. 5, 1059–1068. [327]
- Herwig, H. (1981): Die Anwendung der Methode der angepaßten asymptotischen Entwicklungen auf laminare, zweidimensionale Strömungen mit endlichen Ablösegebieten. Dissertation, Ruhr-Universität Bochum. [394, 399]
- Herwig, H. (1982): Die Anwendung der asymptotischen Theorie auf laminare Strömungen mit endlichen Ablösegebieten. Z. Flugwiss. Weltraumforsch., Bd. 6, 266–279. [397, 399]
- Herwig, H. (1983): Wärmeübertragung in laminaren Grenzschichten mit starker Wechselwirkung zwischen Grenzschicht und Außenströmung. Z. angew. Math. Phys. (ZAMP), Bd. 34, 899–913. [399]
- Herwig, H. (1984): Näherungsweise Berücksichtigung des Einflusses variabler Stoffwerte bei der Berechnung ebener laminarer Grenzschichtströmungen um zylindrische Körper. Forsch. Ing.-Wes., Bd. 50, 160–166. [240, 279]
- Herwig, H. /s.: Gersten, K.; Herwig, H. (1984)
- Herwig, H. (1985a): An asymptotic approach to free-convection flow at maximum density. Chem. Engng. Sci., Vol. 40, 1709–1715. [267]
- Herwig, H. (1985b): Asymptotische Theorie zur Erfassung des Einflusses variabler Stoffwerte auf Impuls- und Wärmeübertragung. Fortschr.-Ber. VDI Reihe 7, Nr. 93, VDI-Verlag, Düsseldorf. [235, 235, 236, 238]
- Herwig, H.; Wickern, G.; Gersten, K. (1985): Der Einfluß variabler Stoffwerte auf natürliche laminare Konvektionsströmungen. Wärme-Stoffübertrag., Bd. 19, 19–30. [279, 280]
- Herwig, H.; Wickern, G. (1986): The effect of variable properties on laminar boundary layer flow. Wärme-Stoffübertrag., Bd. 20, 47–57. [238, 252, 325]
- Herwig, H. (1987): An asymptotic approach to compressible boundary layer flow. Int. J. Heat Mass Transfer, Vol. 30, 59–68. [235, 238, 325]
- Herwig, H. /s.: Gersten, K.; Herwig, H. (1992)
- Herwig, H. /s.: Hölling, M.; Herwig, H. (2005)
- Herwig, H. /s.: Gloss, D.; Herwig, H. (2010)
- Herwig, H. /s.: Kis, P.; Herwig, H. (2012)
- Herwig, H.; Schäfer, P. (1992): Influence of variable properties on the stability of two-dimensional boundary layers. J. Fluid Mech., Vol. 243, 1–14. [462]

- Herwig, H. /s.: Schäfer, P.; Severin, J.; Herwig, H. (1994)
- Herwig, H.; Voigt, M. (1995): Turbulent entrance flow in a channel: An asymptotic approach. In: P.-A. Bois; E. Dériat; R. Gatignol; A. Rigolot (Eds.): Asymptotic Modelling in Fluid Mechanics. Springer-Verlag, Berlin, Heidelberg, 51–58. [556]
- Herwig, H.; Voigt, M. (1996): A high Reynolds number analysis of turbulent heat transfer in the entrance region of a pipe or channel. In: K. Gersten (Ed.): Asymptotic Methods for Turbulent Shear Flows at High Reynolds Numbers. Kluwer Academic Publishers. Dordrecht, Boston, London, 33–44. [556]
- Herwig, H. /s.: Severin, J.; Herwig, H. (2001)
- Herzig, H.Z. /s.: Hansen, A.G.; Herzig, H.Z. (1956)
- Hessel, M. /s.: Dinkelacker, A.; Hessel, M.; Meier, G.E.A.; Schewe, G. (1977)
- Hieber, C.A.; Nash, E.J. (1975): Natural convection above a line heat source: Higher-order effects and stability. Int. J. Heat Mass Transfer, Vol. 18, 1473–1479. [387]
- Hiemenz, K. (1911): Die Grenzschicht an einem in den gleichförmigen Flüssigkeitsstrom eingetauchten geraden Kreiszylinder. Diss. Göttingen 1911, Dingl. Polytech. J. 326, 321–324, 344–348, 357–362, 372–376, 391–393, 407–410. [112, 185, 206]
- Higuera, F.J. (1997): Opposing mixed convection flow in a wall jet over a horizontal plate. J. Fluid Mech., Vol. 342, 355–375. [288]
- Hilder, D.S. /s.: Gebhart, B.; Hilder, D.S.; Kelleher, M. (1984)
- Hill, P.G.; Stenning, A.H. (1960): Laminar boundary layers in oscillatory flow. J. Basic Engg., Vol. 82, 593–608. [368]
- Hinze, J.O. (1975): Turbulence, 2nd Edition, McGraw-Hill, New York. [514, 586, 657, 670, 675]
- Hirsch, C. (1988): Numerical Computation of Internal and External Flows. Vol. I: Fundamentals of Numerical Discretization. John Wiley, New York. [688]
- Hirschel, E.H. /s.: Krause, E.; Hirschel, E.H.; Bothmann, Th. (1968)
- Hirschel, E.H. /s.: Krause, E.; Hirschel, E.H.; Bothmann, Th. (1969)
- Hirschel, E.H. /s.: Krause, E.; Hirschel, E.H.; Kordulla, W. (1976)
- Hirschel, E.H.; Kordulla, W. (1981): Shear Flow in Surface-Oriented Coordinates. Notes on Numerical Fluid Mechanics, Vol. 4, Vieweg, Braunschweig/Wiesbaden. [82]
- Hirschel, E.H. (1982): Three-dimensional boundary-layer calculations in design aerodynamics. In: H.H. Fernholz; E. Krause (Eds.): Three-Dimensional Turbulent Boundary-Layers. Springer-Verlag, Berlin, 353–365. [643]
- Hirschel, E.H. (1987): Evaluation of results of boundary-layer calculations with regard to design aerodynamics. In: AGARD-R-741, 5-1 to 5-29. [638]
- Hirschel, E.H.; Cousteix, J.; Kordulla, W. (2014): Three-Dimensional Attached Viscous Flow. Springer, Berlin, Heidelberg. [XXV, 643]
- Hislop, G.S. /s.: Hall, A.A.; Hislop, G.S. (1938)
- Hokenson, G.J. (1985): Boundary conditions for flow over permeable surfaces. Journal of Fluids Engineering, Vol. 107, 430–432. [113, 295]
- Hölling, M.; Herwig, H. (2005): Asymptotic analysis of the near wall region of turbulent natural convection flows. J. Fluid Mech., VOL. 541, 383–397. [629]
- Holstein, H. (1943): Ähnliche laminare Reibungsschichten an durchlässigen Wänden. ZWB-VM 3050. [306]
- Holt, M.; Chan, W.-K. (1975): An integral method for unsteady laminar boundary layers. In: R.B. Kinney (Ed.): Unsteady Aerodynamics, Proceedings of a Symposium, held at The University of Arizona, 1975, Arizona, Vol. 1, 283–298. [354]
- Holzhauser, C.A.; Bray, R.S. (1956): Wind-tunnel and flight investigations of the use of leading-edge area suction for the purpose of increasing the maximum lift coefficient of a 35° swept-wing airplane. NACA-TR-1276. [309]

- Homann, F. (1936): Der Einfluß großer Zähigkeit bei der Strömung um den Zylinder und um die Kugel. ZAMM., Z. angew. Math. Mech., Bd. 16, 153–164 (1936); and Forschg. Ing.-Wes., Bd. 7, 1–10. [119]
- Hoogendoorn, C.J. /s.: Henkes, R.A.M.; Hoogendoorn, C.J. (1990)
- Hopf, L. (1927): Zähe Flüssigkeiten. In: H. Geiger (Hrsg.): Handbuch der Physik, Bd. VII, 91–172, Springer-Verlag, Berlin. [62, 64]
- Hopkins, E.J. /s.: Jillie, D.W.; Hopkins, E.J. (1961)
- Hornung, H.; Perry, A.E. (1984): Some aspects of three-dimensional separation – Part I: Streamsurface bifurcations. Z. Fluswiss. Weltraumforsch., Bd. 8, 77–87. [340]
- Hornung, H.G.; Joubert, P.N. (1963): The mean velocity profile in three-dimensional turbulent boundary layers. J. Fluid Mech., Vol. 15, 368–384. [643]
- Horstmann, K.-H. /s.: Redeker, G.; Horstmann, K.-H.; Köster, H.; Quast, A. (1988)
- Horstmann, K.-H. /s.: Redeker, G.; Horstmann, K.-H.; Köster, H.; Thiede, P.; Szodruch, J. (1990)
- Horstmann, K.-H.; Redeker, G.; Quast, A.; Dreßler, U.; Bieler, H. (1990): Flight tests with a natural laminar flow glove on a transport aircraft. AIAA Paper 90–3044. [456]
- Horton, H.P. /s.: Stock, H.-W.; Horton, H.P. (1985)
- Hoskin, N.E. (1955): The laminar boundary layer on a rotating sphere. In: H. Görtler; W. Tollmien (Hrsg.): Fünfzig Jahre Grenzschichtforschung. Braunschweig, 127–131. [331]
- Hossain, M.S.; Rodi, W. (1982): A turbulence model for buoyant flows and its application to vertical buoyant jets. In: Rodi W. (Ed.): Turbulent Buoyant Jets and Plumes, HMT, Vol. 6, Pergamon Press, Oxford, 121–178. [676]
- Houdeville, R. /s.: Cousteix, J.; Houdeville, R.; Michel, R. (1974)
- Houdeville, R. /s.: Cousteix, J.; Houdeville, R.; Javelle, J. (1981)
- Houdeville, R. /s.: Cousteix, J.; Houdeville, R. (1983)
- Houdeville, R. /s.: Cousteix, J.; Houdeville, R. (1985)
- Houwink, R. (1984): Unsteady viscous transonic flow computations using LTRAN 2-NLR code coupled with Green's lag-entrainment method. In: T. Cebeci (Ed.): Numerical and Physical Aspects of Aerodynamic Flows II, Springer-Verlag, New York, 297–311. [648]
- Howard, L.N. /s.: Drazin, P.G.; Howard, L.N. (1966)
- Howarth, L. (1935): On the calculation of the steady flow in the boundary layer near the surface of a cylinder in a stream. ARC-RM-1632. [112, 185, 186, 202]
- Howarth, L. (1938): On the solution of the laminar boundary layer equations. Proc. Roy. Soc. London A, Vol. 164, 547–579. [158, 186]
- Howarth, L. (1951a): Note on the boundary layer on a rotating sphere. Phil. Mag. VII, 42, 1308–1315. [331]
- Howarth, L. (1951b): The boundary layer in three-dimensional flow. Part I: Phil. Mag. VII, 42, 239–243. Part II: The flow near a stagnation point. Phil. Mag. VII, 42, 1433–1440. [338, 345]
- Huang, M.-K.; Inger, G.R. (1984): Application of unsteady laminar triple-deck theory to viscous-inviscid interactions from an oscillating flap in supersonic flow. In: T. Cebeci (Ed.): Numerical and Physical Aspects of Aerodynamics Flows II, Springer-Verlag, New York, 381–391. [400]
- Huang, P.G.; Bradshaw, P.; Coakley, T.J. (1993): Skin friction and velocity profile family for compressible turbulent boundary layers. AIAA Journal, Vol. 31, 1600–1604. [623]
- Huang, P.G.; Bradshaw, P.; Coakley, T.J. (1994): Turbulence models for compressible boundary layers. AIAA Journal, Vol. 32, 735–740. [620]
- Huang, P.G.; Bradshaw, P. (1995): Law of the wall for turbulent flows in pressure gradients. AIAA Journal, Vol. 33, 624–632. [610]

- Huang, Th.T.; Chang, M.-Sh. (1986): Computation of velocity and pressure variation across axisymmetric thick turbulent stern flows. In: T. Cebeci (Ed.): Numerical and physical Aspects of Aerodynamic Flows III. Springer-Verlag, New York, 341–359. [633, 634]
- Hucho, W.H. (1972): Einfluß der Vorderwagenform auf Widerstand, Giermoment und Seitenkraft von Kastenwagen. Z. Flugwiss., Bd. 20, 341–351. [43]
- Hucho, W.H. (1981) (Ed.): Aerodynamik der Automobils. Vogel-Verlag, Würzburg. [43]
- Huerre, P.; Monkewitz, P.A. (1985): Absolute and convective instabilities in free shear layers. J. Fluid Mech., Vol. 159, 151–168. [493]
- Huerre, P.; Monkewitz, P.A. (1990): Local and global instabilities in spatially developing flows. Annu. Rev. Fluid Mech., Vol. 22, 473–537. [425, 493]
- Huffman, G.D.; Bradshaw, P. (1972): A note on von Kármán's constant in low Reynolds number turbulent flows. J. Fluid Mech., Vol. 53, 45–60. [525]
- Hultgren, L.S. /s.: Goldstein, M.E., Hultgren, L.S. (1989)
- Hummel, D. (1986): Experimentelle Untersuchung dreidimensionaler laminarer Grenzschichten an einem schlanken Deltaflügel. Z. Flugwiss. Weltraumforsch., Bd. 10, 133–145. [347]
- Humphreys, D.A. /s.: Fannelöp, T.K.; Humphreys, D.A. (1975)
- Humphreys, D.A. /s.: Berg, B. van den; Humphreys, D.A.; Krause, E.; Lindhout, J.P.F. (1988)
- Humphreys, D.A.; Lindhout, J.P.F. (1988): Calculation methods for three-dimensional turbulent boundary layers. Prog. Aerospace Sci., Vol. 25, 107–129. [641, 642, 706]
- Hunt, J.C.R. /s.: Smith, F.T.; Brighton, P.W.M.; Jackson, P.S.; Hunt, J.C.R. (1981)
- Hussaini, M.Y. /s.: Wary, A.; Hussaini, M.Y. (1984)
- Hussaini, M.Y. /s.: Malik, M.R.; Hussaini, M.Y. (1990)
- Hwang, B.C. /s.: So, R.M.C.; Lai, Y.G.; Zhang, H.S.; Hwang, B.C. (1991)
- Ibele, W.E. /s.: Sparrow, E.M.; Minkowycz, W.J.; Eckert, E.R.G.; Ibele, W.E. (1964)
- Iglisch, R. (1944): Exakte Berechnung der laminaren Reibungsschicht an der längsangeströmten ebenen Platte mit homogener Absaugung. Schriften d. dt. Akad. Luftfahrtforschung, 8B, Nr. 1, translation: NACA-RM-1205 (1949). [307, 309]
- Iida, S. /s.: Nishioka, M.; Iida, S.; Ichikawa, Y. (1975)
- Iida, S. /s.: Nishioka, M.; Asai, M.; Iida, S. (1990)
- Illingworth, C.R. (1950): Unsteady laminar flow of gas near an infinite flat plate. Proc. Camb. Phil. Soc., Vol. 46, 603–613. [128, 361]
- Illingworth, C.R. (1954): Boundary layer growth on a spinning body. Phil Mag. 45 (7), 1–8. [361]
- Imai, I. (1957): Second approximation to the laminar boundary-layer flow over a flat plate. J. Aeron. Sci., Vol. 24, 155–156. [384]
- Inger, G.R. /s.: Huang, M.-K.; Inger, G.R. (1984)
- Ingham, D.B. (1977): Singular parabolic partial differential equations that arise in impulsive motion problems. J. Appl. Mech., Vol. 44, 396–400. [361]
- Isaacson, E.; Keller, H.B. (1966): Analysis of Numerical Methods. John Wiley, New York. [688, 690, 695, 703]
- Ito, A. (1987): Visualization of boundary layer transition along a concave wall. In: Proc. 4th Int. Symp. Flow Visualization, Paris 1986, 339–344, Hemisphere, Washington. [484]
- Iyer, V.; Harris, J.E. (1990): Fourth-order accurate three-dimensional compressible boundary layer calculations. J. Aircraft, Vol. 27, 253–261. [339]
- Jackson, P.S. /s.: Smith, F.T.; Brighton, P.W.M.; Jackson, P.S.; Hunt, J.C.R. (1981)
- Jaeger, J.C. /s.: Carslaw, H.S.; Jaeger, J.C. (1959)

- Jaffe, N.A.; Okamura, T. Smith, A.M.O. (1970): Determination of spatial amplification factors and their application to predicting transition. *AIAA Journal*, Vol. 8, 301–308. [454]
- Jakirlić, S.; Hanjalić, K. (1995): A second-moment closure for non-equilibrium and separating high and low Re-number flows. In: *Proceedings 10th Symposium of Turbulent Shear Flows*. The Pennsylvania State University, USA, August 14–16. [571, 701]
- Jaluria, Y. (1980): *Natural convection heat and mass transfer*. Pergamon Press, Oxford. [266, 276, 277, 290, 318, 327]
- Jaluria, Y. /s.: Gebhart, B.; Jaluria, Y.; Mahajan, R.L.; Sammakia, B. (1988)
- Jankowski, D.F. /s.: Gersting, J.M.; Jankowski, D.F. (1972)
- Janour, Z. (1951): Resistance of a plate in parallel flow at low Reynolds numbers. *NACA-TM-1316*. [10]
- Javelle, J. /s.: Cousteix, J.; Houdeville, R.; Javelle, J. (1981)
- Jaw, S.Y. /s.: Chen, C.J.; Jaw, S.Y. (1998)
- Jeffery, G.B. (1915): The two-dimensional steady motion of a viscous fluid. *Phil. Mag.*, Vol. 29, 455–465. [104]
- Jeken, B. (1992): Asymptotische Analyse ebener turbulenter Strömungen an gekrümmten Wänden bei hohen Reynolds-Zahlen mit einem Reynolds-Spannungs-Modell. *Fortschritt-Berichte VDI*: Reihe 7; 215, VDI-Verl., Düsseldorf, 1992, also: Bochum, Univ., Diss., 1992. See also: *ZAMM. Z. angew. Math. Mech.*, Vol. 72, T 308–312. [559, 563, 567, 606, 700]
- Jenson, R. /s.: Rizzetta, D.P.; Burggraf, O.R.; Jenson, R. (1978)
- Jiménez, J. (2004): Turbulent flows over rough walls. *Annu. Rev. Fluid Mech.*, Vol. 36, 173–196. [534]
- Jischka, M. (1982): Konvektiver Impuls-, Wärme- und Stoffaustausch. Vieweg & Sohn, Braunschweig. [319, 624]
- Jobe, C.E.; Burggraf, O.R. (1974): The numerical solution of the asymptotic equations of trailing-edge flow. *Proc. Roy. Soc. London A*, Vol. 340, 91–111. [400]
- Jodlbauer, K. (1933): Das Temperatur- und Geschwindigkeitsfeld um ein geheiztes Rohr bei freier Konvektion. *Forsch. Ing.-Wes.*, Bd. 4, 157–172. [277]
- Johansson, A.V. /s.: Hallbäck, M.; Henningson, D.S.; Johansson, A.V., Alfredsson, P.H. (Eds.) (1996)
- Johnson, D.A.; King, L.S. (1985): A mathematically simple turbulence closure model for attached and separated turbulent boundary layers. *AIAA Journal*, Vol. 23, 1684–1692. [560]
- Johnston, L.J. (1988): A calculation method for compressible three-dimensional turbulent boundary layer flows. von Karman Institute for Fluid Dynamics, Technical Note 167. [642, 643]
- Jones, B.M. (1938): Flight experiments on the boundary layer (Wright Brothers Lecture). *J. of the Aeronautical Sciences*, Vol. 5, 81–101; also: *Aircraft Eng.*, Vol. 10, 135–141. [455, 456]
- Jones, B.M.; Head, M.R. (1951): The reduction of drag by distributed suction. In: *Proc. Third Anglo-American Aeron. Conference*, Brighton, 199–230. [460]
- Jones, M.B.; Marusic, I.; Perry, A.E. (2001): Evolution and structure of sink-flow turbulent boundary layers. *J. Fluid Mech.*, Vol. 428, 1–27. [582]
- Jones, W.P.; Launder, B.E. (1972a): The prediction of laminarization with a two-equation model of turbulence. *Int. J. Heat Mass Transfer*, Vol. 15, 301–314. [562, 599, 700]
- Jones, W.P.; Launder, B.E. (1972b): Some properties of sink-flow turbulent boundary layers. *J. Fluid Mech.*, Vol. 56, 337–351. [582]
- Jones, W.P.; Launder, B.E. (1973): The calculation of low-Reynolds-number phenomena with a two-equation model of turbulence. *Int. J. Heat Mass Transfer*, Vol. 16, 1119–1130. [XXIV]

- Jones, W.P. /s.: Gibson, M.M.; Jones, W.P.; Younis, B.A. (1981)
- Jordinson, R. (1970): The flat plate boundary layer. Part 1: Numerical integration of the Orr-Sommerfeld equation. *J. Fluid Mech.*, Vol. 43, 801–811; cf. also: Ph.D. thesis, Edinburgh University 1968. [436, 437]
- Jordinson, R. (1971): Spectrum of eigenvalues of the Orr-Sommerfeld equation for Blasius flow. *Phys. Fluids*, Vol. 14, 2535–2537. [436]
- Joseph, D.D. (1976): Stability of Fluid Motions Vol. 1 and 2, Springer-Verlag, Berlin. [90]
- Joubert, P.N. /s.: Hornung, H.G.; Joubert, P.N. (1963)
- Joubert, P.N. /s.: Erm, L.P.; Smits, A.J.; Joubert, P.N. (1987)
- Juchi, M. /s.: Tani, I.; Juchi, M.; Yamamoto, K. (1954)
- Juillen, J.C. /s.: Arnal, D.; Coustols, E.; Juillen, J.C. (1984)
- Juillen, J.C. /s.: Arnal, D.; Juillen, J.C.; Michel, R. (1977)
- Jungclaus, G. (1955): Grenzschichtuntersuchungen in rotierenden Kanälen und bei scherenden Strömungen. Mitteilg. aus dem Max-Planck-Institut für Strömungsforschung, Nr. 11, Göttingen. [347]
- Justesen, P.; Spalart, P.R. (1990): Two-equation turbulence modeling of oscillatory boundary layers. AIAA Paper 90-0496. [649]
- Kachanov, Y.S.; Levchenko, V.Y. (1984): The resonant interaction of disturbances at laminar-turbulent transition in a boundary layer. *J. Fluid Mech.*, Vol. 138, 209–247. [477]
- Kader, B.A.; Yaglom, A.M. (1978): Similarity treatment of moving-equilibrium turbulent boundary layers in adverse pressure gradients. *J. Fluid Mech.*, Vol. 89, 305–342. [591]
- Kaplun, S. (1954): The role of coordinate systems in boundary layer theory. *Z. angew. Math. Phys. (ZAMP)*, Bd. 5, 111–135. [XXIII]
- Kaplun, S.; Lagerstrom, P.A. (1957): Asymptotic expansions of Navier-Stokes solutions for small Reynolds numbers. *J. Math. Mech.*, Vol. 6, 585–593. [XXIII]
- Kármán, Th. von (1921): Über laminare und turbulente Reibung. *ZAMM. Z. angew. Math. Mech.*, Bd. 1, 233–252. English translation: On laminar and turbulent friction. NACA-TM-1092. See also: Collected Works II, 70–97. [121, 196]
- Kármán, Th. von (1930): Mechanische Ähnlichkeit und Turbulenz. *Nachr. Ges. Wiss. Göttingen, Math. Phys. Klasse* 58–76 (1930) and *Verhandl. d. III. Intern. Kongresses für Techn. Mechanik, Stockholm, Teil 1*, 85–93 (1930); NACA-TM-611 (1931); cf. *Collect. Works II*, 337–346. [540]
- Kassoy, D.R. (1970): On laminar boundary layer blowoff. *SIAM J. Appl. Math.*, Vol. 18, 29–40. [303]
- Kassoy, D.R. (1973): The singularity at boundary layer separation due to mass injection. *SIAM J. Appl. Math.*, Vol. 25, 105–123. [309]
- Katagiri, M. (1976): Unsteady boundary-layer flows past an impulsively started circular cylinder. *J. Phys. Soc. Japan*, Vol. 40, 1171–1177. [356]
- Kaups, K. /s.: Cebeci, T.; Kaups, K.; Ramsey, J.A. (1977)
- Kaups, K. /s.: Cebeci, T.; Chang, K.C.; Kaups, K. (1980)
- Kaups, K. /s.: Stewartson, K.; Smith, F.T.; Kaups, K. (1982)
- Kay, J.M. (1948): Boundary layer along a flat plate with uniform suction. ARC-RM-2628. [309, 460]
- Kayalar, L. (1969): Experimentelle und theoretische Untersuchungen über den Einfluß des Turbulenzgrades auf den Wärmeübergang in der Umgebung eines Staupunktes eines Kreiszylinders. Dissertation, Braunschweig 1968, Forsch. Ing.-Wes., Bd. 35, 157–167 (abridged form of dissertation). [605]
- Kays, W.M.; Nicoll, W.B. (1963): Laminar flow heat transfer to a gas with large temperature differences. *J. Heat Transfer*, Vol. 85, 329–338. [240]
- Kays, W.M. /s.: Moretti, P.M.; Kays, W.M. (1965)

- Kays, W.M.; Crawford, M.E. (1980): Convective Heat and Mass Transfer. McGraw-Hill Book Co., New York. [609]
- Kayser, L.D. /s.: Sturek, W.B.; Dwyer, H.A.; Kayser, L.D.; Nietubicz, Ch.J.; Reklis, R.P.; Opalka, K.O. (1978)
- Kelleher, M. /s.: Gebhart, B.; Hilder, D.S.; Kelleher, M. (1984)
- Keller, H.B. /s.: Isaacson, E.; Keller, H.B. (1966)
- Keller, H.B. (1971): A new difference scheme for parabolic problems. In: B. Hubbard (Ed.): Numerical Solution of Partial Differential Equations II. Academic Press, New York, 327–350. [684, 692]
- Keller, H.B.; Cebeci, T. (1971): Accurate numerical methods for boundary-layer flows. II: Two-dimensional laminar flows. Proc. 2nd Int. Conf. Numer. Meth. Fluid Dyn., in: Lecture Notes in Physics, Vol. 8, Springer-Verlag, Berlin 92–100. [695]
- Keller, H.B. /s.: Cebeci, T.; Keller, H.B. (1972)
- Keller, H.B.; Cebeci, T. (1972a): Accurate numerical methods for boundary-layer flows. II: Two-dimensional turbulent flows. AIAA Journal, Vol. 10, 1193–1199. [693]
- Keller, H.B.; Cebeci, T. (1972b): An inverse problem in boundary-layer flows: Numerical determination of pressure gradient for a given wall shear. J. Comput. Phys., Vol. 10, 151–161. [693]
- Keller, H.B. (1974): Accurate difference methods for nonlinear two-point boundary value problems. SIAM, J. Num. Anal., Vol. II, 305–320. [695]
- Keller, H.B. (1978): Numerical methods in boundary-layer theory. Annu. Rev. Fluid Mech., Vol. 10, 417–433. [684, 693, 703]
- Keller, H.B. /s.: Cebeci, T.; Keller, H.B.; Williams, P.G. (1979)
- Keltner, G. /s.: Wazzan, A.R.; Taghavi, H.; Keltner, G. (1974)
- Kempf, G. (1924): Über Reibungswiderstand rotierender Scheiben. Vorträge auf dem Gebiet der Hydro- und Aerodynamik, Innsbrucker Kongr. 1922, p.168, Berlin. [123]
- Kerschen, E.J. /s.: Saric, W.S.; Reed, H.L.; Kerschen, E.J. (1994)
- Kerschen, E.J. /s.: Saric, W.S.; Reed, H.L.; Kerschen, E.J. (2002)
- Kestin, J.; Richardson, P.D. (1963): Heat transfer across turbulent, incompressible boundary layers. Int. J. Heat Mass Transfer, Vol. 6, 147–189. Also: Forsch. Ing.-Wes., Bd. 29, 93–104. [525, 525]
- Kestin, J. (1966a): A Course in Thermodynamics. Vol. I, Blaisdell. [63, 72]
- Kestin, J. (1966b): Etude thermodynamique des phénomènes irréversibles. Rep. No. 66-7, Lab. d'Aérothermique, Meudon. [53, 67]
- Kestin, J. (1966c): The effect of freestream turbulence on heat transfer rates. Advances in Heat Transfer, Vol. 3, 1–32. [605]
- Kestin, J. (1968): A Course in Thermodynamics. Vol. II, Blaisdell. [74]
- Kevorkian, J.; Cole, J.D. (1981): Perturbation Methods in Applied Mathematics, Springer-Verlag, New York. [14]
- Khattab, A.K. /s.: Cebeci, T.; Khattab, A.K.; Stewartson, K. (1980)
- Kiel, R. (1995): Experimentelle Untersuchung einer Strömung mit beheiztem lokalen Ablösewirbel an einer geraden Wand. Dissertation, Ruhr-Universität Bochum; also: Fortschrittsbericht, VDI Reihe 7, Nr. 281, VDI-Verlag, Düsseldorf. [546, 602, 609]
- Kim, C. /s.: Nagano, Y.; Kim, C. (1988)
- Kim, K.-S.; Settles, G.S. (1989): Skin-friction measurements by laser interferometry. In: AGARD-AG-315, 4-1 to 4-8. [622]
- Kimoto, Y. /s.: Toyokura, T.; Kurokawa, J.; Kimoto, Y. (1982)
- King, L.S. /s.: Johnson, D.A.; King, L.S. (1985)
- Kinney, R.B. (Ed.) (1975): Unsteady Aerodynamics. Proceedings of a Symposium, held at The University of Arizona, 1975, Arizona (Two Vols.) [350]

- Kippenhan, Ch.J. /s.: Reeves, B.L.; Kippenhan, Ch.J. (1962)
- Kirchhoff, G. (1869): Zur Theorie freier Flüssigkeitsstrahlen. *J. reine angew. Math.*, Bd. 70, 289–298. [409]
- Kirde, K. (1962): Untersuchungen über die zeitliche Weiterentwicklung eines Wirbels mit vorgegebener Anfangsverteilung. *Ing.-Arch.*, Bd. 31, 385–404. [139]
- Kiš, P.; Herwig, H. (2010): A systematic derivation of a consistent set of “Boussinesq equations”. *Int. J. Heat Mass Transfer*, Vol. 46, 1111–1119. [235]
- Kiš, P.; Herwig, H. (2012): The near wall physics and wall functions for turbulent natural convection. *Int. J. Heat Mass Transfer*, Vol. 55, 2625–2635. [629]
- Kistler, A.L. /s.: Corrsin, St.; Kistler, A.L. (1955)
- Klauer, J. (1989): Berechnung ebener turbulenter Scherschichten mit Ablösung und Rückströmung bei hohen Reynoldszahlen. Dissertation, Ruhr-Universität Bochum; also: *Fortschritt-Ber. VDI Reihe 7*, Nr. 155, VDI-Verlag, Düsseldorf. [546, 593, 594, 597, 598]
- Klauer, J. /s.: Gersten, K.; Klauer, J.; Vieth, D. (1993)
- Klebanoff, P.S. (1955): Characteristics of influence in a boundary layer with zero pressure gradient. NACA-R-1247; also: NACA-TN-3178 (1954). [499, 514, 515]
- Klebanoff, P.S. /s.: Schubauer, G.B.; Klebanoff, P.S. (1955)
- Klebanoff, P.S.; Tidstrom, K.D.; Sargent, L.M. (1962): The three-dimensional nature of boundary layer instability. *J. Fluid Mech.*, Vol. 12, 1–34. [473, 474, 475, 477, 479, 479]
- Kleiser, L.S. /s.: Laurien, E.; Kleiser, L. (1989)
- Klemp, J.B.; Acrivos, A. (1972): A method for integrating the boundary-layer equations through a region of reverse flow. *J. Fluid Mech.*, Vol. 53, 177–191. [309]
- Klemp, J.B.; Acrivos, A. (1972): A note on the laminar mixing of two uniform parallel semi infinite streams. *J. Fluid Mech.*, Vol. 55, 25–30. [175]
- Klick, H. /s.: Gersten, K.; Grobel, M.; Klick, H.; Merzkirch, W. (1991)
- Klick, H. (1992): Einfluß variabler Stoffwerte bei der turbulenten Plattenströmung. *Fortschritt-Berichte VDI*: Reihe 7; 213, VDI-Verlag, Düsseldorf, 1992; also: Bochum, Univ. Diss., 1992. [609]
- Kline, S.J.; Morkovin, M.V.; Sovran, G.; Cockrell, D.J. (Eds.) (1968): Proceedings: Computation of Turbulent Boundary Layers – 1968. AFOSR-IFP-Stanford Conference, Vol. 1: Methods, Predictions, Evaluations and Flow Structures; Vol. 2: Compiled Data (Coles, D.E.; Hirst, A.E. (Eds.)), Stanford University, Stanford, California. [XXIV, 562, 597]
- Kline, S.J. /s.: Lyrio, A.A.; Ferziger, J.H.; Kline, S.J. (1981)
- Kline, S.J.; Cantwell, B.J.; Lilley, G.M. (1981): The 1980-81 AFOSR-HTTM-Stanford Conference of Complex Turbulent Flows: Comparison of Computation and Experiment, Vol. 1 – Vol. 3, Stanford University, Stanford, California. [XXV]
- Kluwick, A. /s.: Bodonyi, R.J.; Kluwick, A. (1977)
- Kluwick, A. (1979): Stationäre, laminare wechselwirkende Reibungsschichten. *Z. Flugwiss. Weltraumforsch.*, Bd. 3, 157–174. [399]
- Kluwick, A. /s.: Bodonyi, R.J.; Kluwick, A. (1982)
- Kluwick, A.; Gittler, Ph.; Bodonyi, R.J. (1984): Viscous-inviscid interactions on axisymmetric bodies of revolution in supersonic flow. *J. Fluid Mech.*, Vol. 140, 281–301. [403]
- Kluwick, A. /s.: Bodonyi, R.J.; Smith, F.T. Kluwick, A. (1985)
- Kluwick, A.; Gittler, Ph.; Bodonyi, R.J. (1985): Freely interacting axisymmetric boundary layers on bodies of revolution. *Q. J. Mech. appl. Math.*, Vol. 38, 575–588. [403]
- Kluwick, A. (1987): Interacting boundary layers. *ZAMM. Z. angew. Math. Mech.*, Vol. 67, T3–T13. [399]

- Kluwick, A. /s.: Gittler, Ph.; Kluwick, A. (1987)
- Kluwick, A. (1989a): Interacting turbulent boundary layers. ZAMM. Z. angew. Math. Mech., Vol. 69, T560–T561. [XXIV]
- Kluwick, A. (1989b): Marginale Ablösung laminarer achsensymmetrischer Grenzschichten. ZAMM. Z. angew. Math. Mech., Vol. 69, T606–T607. [408]
- Kluwick, A. /s.: Gittler, Ph.; Kluwick, A. (1989)
- Kluwick, A. /s.: Hackmüller, G.; Kluwick, A. (1989)
- Kluwick, A. /s.: Hackmüller, G.; Kluwick, A. (1990)
- Kluwick, A. (1991): Axisymmetric laminar interacting boundary layers. Arch. Mech., Vol. 43, 623–651. [399]
- Kluwick, A. /s.: Hackmüller, G.; Kluwick, A. (1991a)
- Kluwick, A. /s.: Hackmüller, G.; Kluwick, A. (1991b)
- Kluwick, A.; Gittler, Ph. (1994): Zur Strömung in der Nähe des Hinterendes achsensymmetrischer Körper bei großen Reynoldszahlen. ZAMM. Z. angew. Math. Mech., Vol. 74, T389–T391. [400]
- Kluwick, A. (Ed.) (1998): Recent Advances in Boundary Layer Theory. Springer-Verlag, Wien, New York. [XXV, 399]
- Kluwick, A. /s.: Exner, A.; Kluwick, A. (1999)
- Kluwick, A. ; Exner, A. (2001): On thermally induced separation of free-convection flows. Phys. Fluids. Vol. 13, 1691–1703. [401]
- Kluwick, A. /s.: Braun, S.; Kluwick, A. (2004)
- Kluwick, A. /s.: Braun, S.; Kluwick, A. (2005)
- Kluwick, A. /s.: Scheichl, B.; Kluwick, A. (2007a)
- Kluwick, A. /s.: Scheichl, B.; Kluwick, A. (2007b)
- Kluwick, A. /s.: Scheichl, B.; Kluwick, A.; Alletto, M. (2008)
- Kluwick, A. /s.: Scheichl, S.; Braun, S.; Kluwick, A. (2008)
- Kluwick, A. /s.: Scheichl, B.; Kluwick, A.; Smith, F.T. (2011)
- Kobayashi, R.; Kohama, Y.; Takamadate, Ch. (1980): Spiral vortices in boundary layer transition regime on a rotating disk. Acta Mechanica, Vol. 35, 71–82. [486]
- Koch, W. (1985): Local instability characteristics and frequency determination of self-excited wake flows. J. Sound Vib., Vol. 99, 53–83. [493]
- Körner, H. /s.: Gersten, K.; Körner, H. (1968)
- Körner, H. (1990): Natural laminar flow research for subsonic transport aircraft in the FRG. Z. Flugwiss. Weltraumforsch., Bd. 14, 223–232. [456]
- Köster, H. /s.: Redeker, G.; Horstmann, K.-H.; Köster, H.; Quast, A. (1988)
- Köster, H. /s.: Redeker, G.; Horstmann, K.-H.; Köster, H.; Thiede, P.; Szodruch, J. (1990)
- Kohama, Y. /s.: Kobayashi, R.; Kohama, Y.; Takamadate, Ch. (1980)
- Kohama, Y. (1987a): Some expectation on the mechanism of cross-flow instability in a swept wing flow. Acta Mechanica, Vol. 66, 21–38. [489]
- Kohama, Y. (1987b): Cross-flow instability in rotating disc boundary layer. AIAA Paper, 87–1340. [486, 487]
- Kolmogorov, A.N. (1941a): Die lokale Struktur der Turbulenz in einer inkompressiblen zähen Flüssigkeit bei sehr großen Reynoldsschen Zahlen. Dokl. Akad. Wiss. USSR, Bd. 30, 301–305. [513, 515]
- Kolmogorov, A.N. (1941b): Die Energiedissipation für lokalisotrope Turbulenz. Dokl. Akad. Wiss. USSR, Bd. 32, 16–18. [514]
- Kolmogorov, A.N. (1942): Equations of turbulent motion of an incompressible fluid. Izvestiya AN SSR Ser. fiz. 6, No. 1–2, 56–58. [563]
- Komoda, H. /s.: Kovasznay, L.S.G.; Komoda, H.; Vasudeva, B.R. (1962)

- Koppenwallner, G. (1988): Aerothermodynamik – Ein Schlüssel zu neuen Transportgeräten der Luft- und Raumfahrt. *Z. Flugwiss. Weltraumforsch.*, Bd. 12, 6–18. [263, 391]
- Kordulla, W. /s.: Krause, E.; Hirschel, E.H.; Kordulla, W. (1976)
- Kordulla, W. /s.: Hirschel, E.H.; Kordulla, W. (1981)
- Kordulla, W. /s.: Hirschel, E.H.; Cousteix, J.; Kordulla, W. (2014)
- Korkegi, R.H. (1956): Transition studies and skin-friction measurements on an insulated flat plate at a Mach number of 5.8. *J. of the Aeronautical Sciences*, Vol. 23, 97–107, 192. [471]
- Korolev, G.L. /s.: Sychev, V.V.; Ruban, A. I.; Sychev, V.V.; Korolev, G. L. (1998)
- Kovasznay, L.S.G.; Komoda, H.; Vasudeva, B.R. (1962): Detailed flow field in transition. In: Ehlers, F.E.; Kauzlarich, J.J.; Sleicher Jr., C.A.; Street, R.E. (Eds.): *Proc. of the 1962 Heat Transfer and Fluid Mechanics Institute*, Stanford Univ. Press, Stanford, California, 1–26. [473]
- Kovasznay, L.S.G. /s.: Chevray, R.; Kovasznay, L.S.G. (1969)
- Kozlov, V.V. /s.: Saric, W.S.; Kozlov, V.V.; Levchenko, V.Y. (1984)
- Kozlov, V.V. (Ed.) (1985): Laminar-Turbulent Transition. *IUTAM Symposium on Laminar-Turbulent Transition* (2, 1984, Novosibirsk), Springer-Verlag, Berlin. [425]
- Kozlov, V.V. /s.: Boiko, A.V.; Grek, G.R.; Dovgal, A.V.; Kozlov, V.V. (2002)
- Kraemer, K. (1971): Die Potentialströmung in der Umgebung von Freistrahlen. *Zeitschr. für Flugwiss.*, Bd. 19, 93–104. [666]
- Krause, E. (1967): Numerical solution of the boundary-layer equations. *AIAA Journal*, Vol. 5, 1231–1237. [684]
- Krause, E.; Hirschel, E.H.; Bothmann, Th. (1968): Numerische Stabilität dreidimensionaler Grenzschichtlösungen. *ZAMM. Z. angew. Math. Mech.*, Bd. 48, T205–T208. [684]
- Krause, E.; Hirschel, E.H.; Bothmann, Th. (1969): Die numerische Integration der Bewegungsgleichungen dreidimensionaler laminarer kompressibler Grenzschichten. In: *Fachtagung Aerodynamik*, Berlin 1968, DGLR Fachbuchreihe Bd. 3, 03-1 to 03-49. [339, 340, 706]
- Krause, E. (1972): Numerical treatment of boundary-layer and Navier-Stokes equations. In: VKI Lecture Series: “Numerical Methods in Fluid Dynamics”. Von Kármán Institute for Fluid Dynamics. Rhode-Saint Genèse, Belgium. [684]
- Krause, E. (1973): Numerical treatment of boundary-layer problems. In: *Advances in Numerical Fluid Dynamics*. In: AGARD Lecture Series 64, 4-1 to 4-21. [339]
- Krause, E.; Hirschel, E.H.; Kordulla, W. (1976): Fourth order “Mehrstellen”-Integration for the three-dimensional turbulent boundary layers. *Computers and Fluids*, Vol. 4, 77–92. [703]
- Krause, E. /s.: Fernholz, H.H.; Krause, E. (1982)
- Krause, E. /s.: Berg, B. van den; Humphreys, D.A.; Krause, E.; Lindhout, J.P.F. (1988)
- Krause, E. /s.: Fernholz, H.H.; Krause, E.; Nockemann, M.; Schober, M. (1995)
- Krause, E. (2014): The Millennium-Problem of Fluid Mechanics - the Solution of the Navier-Stokes Equations. In: E. Stein (Ed.): *Lecture Notes in Applied Mathematics and Mechanics*. Springer, 317 – 341. [76]
- Krishnamoorthy, L.V.; Antonia, R.A. (1988): Turbulent kinetic energy budget in the near-wall region. *AIAA Journal*, Vol. 26, 300–302. [527]
- Kronast, M. (1992): Einfluß eines ruhenden und bewegten Bodens auf die Umströmung zweidimensionaler Fahrzeugmodelle. *Fortschritt-Berichte VDI*: Reihe 7; 205, VDI-Verlag, Düsseldorf, 1992; also: Bochum, Univ., Diss., 1992. [342]
- Kruse, A. /s.: Wagner, W.; Kruse, A. (1998)

- Krzywoblocki, M.Z. (1949): On steady, laminar round jets in compressible viscous gases far behind the mouth. *Österr. Ing.-Arch.*, Bd. 3, 373. [333]
- Küchemann, D. (1938): Störungsbewegungen in einer Gasströmung mit Grenzschicht. *ZAMM. Z. angew. Math. Mech.*, Vol. 18, 207–222 (1938); see also a comment on this by H. Görtler, *ZAMM. Z. angew. Math. Mech.*, Vol. 23, 179–183 (1943). [463]
- Küchemann, D. /s.: Crabtree, L.F.; Küchemann, D.; Sowerby, L. (1963)
- Kuiken, H.K. (1968a): An asymptotic solution for large Prandtl number free convection. *J. Eng. Math.*, Vol. 2, 355–371. [272]
- Kuiken, H.K. (1968b): Axisymmetric free convection boundary layer flow past slender bodies. *Int. J. Heat Mass Transfer*, Vol. 11, 1141–1153. [387]
- Kuiken, H.K. (1969): Free convection at low Prandtl numbers. *J. Fluid Mech.*, Vol. 37, 785–798. [273]
- Kuiken, H.K. (1971): The effect of normal blowing on the flow near a rotating disk of infinite extent. *J. Fluid Mech.*, Vol. 47, 789–798. [124]
- Kurokawa, J. /s.: Toyokura, T.; Kurokawa, J.; Kimoto, Y. (1982)
- Kurtz, E.F.; Candler, S.H. (1962): Computer-aided analysis of hydrodynamic stability. *J. Math. Phys.*, Vol. 44, 264–279. [436]
- Lachmann, G.V. (1961) (Ed.): *Boundary layer and flow control*. Vol. I and II, Pergamon Press, London. [295]
- Lagerstrom, P.A. /s.: Kaplun, S.; Lagerstrom, P.A. (1957)
- Lagrée, P.-Y. (2001): Removing the marching breakdown of the boundary-layer equations for mixed convection above a horizontal plate. *Int. J. Heat Mass Transfer*, Vol. 44, 3359–3372 [288]
- Lai, Y.G.; So, R.M.C. (1990): Near-wall modeling of turbulent heat fluxes. *Int. J. Heat Mass Transfer*, Vol. 33, 1429–1440. [570, 610]
- Lai, Y.G. /s.: So, R.M.C.; Lai, Y.G.; Zhang, H.S.; Hwang, B.C. (1991)
- Lakshmanan, B. /s.: Sarkar, S.; Lakshmanan, B. (1991)
- Lakshminarayana, B. /s.: Galmes, J.M.; Lakshminarayana, B. (1984)
- Lakshminarayana, B. (1986): Turbulence modeling for complex shear flows. *AIAA Journal*, Vol. 24, 1900–1917. [606, 643]
- Lakshminarayana, B. /s.: Fan, S.; Lakshminarayana, B.; Barnett, M. (1993)
- Lamb, H. (1932): *Hydrodynamics*, 6th edition, Cambridge, also: Dover, 1945. [64]
- Lance, G.N. /s.: Rogers, M.G.; Lance, G.N. (1960)
- Landahl, M. /s.: Obremski, H.J.; Morkovin, M.V.; Landahl, M. (1969)
- Landahl, M.T. (1962): On the stability of a laminar incompressible boundary layer over a flexible surface. *J. Fluid Mech.*, Vol. 13, 609–632. [472]
- Landahl, M.T. (1973): Drag reduction by polymer addition. In: Becker, E.; Mikhailov, G.K. (Eds.): *Proc. 13th Int. Congr. Theor. Appl. Mech.*, Springer-Verlag, Berlin, 177–199. [534]
- Landahl, M.T.; Mollo-Christensen, E. (1986): *Turbulence and Random Processes in Fluid Mechanics*. Cambridge University Press, Cambridge. [513]
- Landau, L. (1944): A new exact solution of Navier-Stokes equations. *Akademija Nauk SSSR (Moscow): Doklady Akademie Nauk SSSR (Moscow)*, Vol. 43, 286–288. [124]
- Landau, L.D.; Lifschitz, E.M. (1966): *Lehrbuch der Theoretischen Physik*, Band VI: *Hydrodynamik*, Akademie-Verlag, Berlin. [67]
- Langlois, W.E. (1964): *Slow viscous flow*. Macmillan, New York. [94]
- Laufer, J. (1954): The structure of turbulence in fully developed pipe flow. *NACA Report 1174*. [553]
- Launder, B.E. /s.: Hanjalić, K.; Launder, B.E. (1972a)
- Launder, B.E. /s.: Hanjalić, K.; Launder, B.E. (1972b)
- Launder, B.E. /s.: Jones, W.P.; Launder, B.E. (1972a)

- Launder, B.E. /s.: Jones, W.P.; Launder, B.E. (1972b)
- Launder, B.E.; Spalding, D.B. (1972): Lectures in Mathematical Models of Turbulence, Academic Pr., London. [601]
- Launder, B.E. /s.: Jones, W.P.; Launder, B.E. (1973)
- Launder, B.E.; Morse, A.; Rodi, W.; Spalding, D.B. (1973): Prediction of free shear flows. A comparison of the performance of six turbulence models. In: Free Turbulent Shear Flows, NASA-SP-321, Vol. 1, 361–426. [655, 663, 668, 670, 673]
- Launder, B.E. /s.: Baker, R.J.; Launder, B.E. (1974)
- Launder, B.E.; Reece, G.J.; Rodi, W. (1975): Progress in the development of a Reynolds-stress turbulence closure. *J. Fluid Mech.*, Vol. 68, 537–566. [601]
- Launder, B.E. /s.: Hanjalić, K.; Launder, B.E. (1976)
- Launder, B.E.; Rodi, W. (1981): The turbulent wall jet. *Progress in Aerospace Sciences*, Vol. 19, 81–128. [679]
- Launder, B.E.; Rodi, W. (1983): The turbulent wall jet – measurements and modelling. *Annu. Rev. Fluid Mech.*, Vol. 15, 429–459. [679]
- Launder, B.E. (1984): Second-moment closure: Methodology and practice. In: B.E. Launder et al. (Eds.): *Turbulence Models and their Applications*, Vol. 2, Editions Eyrolles, Saint-Germain, Paris, 1–147. [567, 601]
- Launder, B.E. (1988): On the computation of convective heat transfer in complex turbulent flows. *J. Heat Transfer*, Vol. 110, 1112–1128. [570]
- Launder, B.; Sandham, N. (Eds.) (2002): *Closure Strategies for Turbulent and Transitional Flows*. Cambridge University Press, Cambridge, UK. [571]
- Laurien, E.; Kleiser, L. (1989): Numerical simulation of boundary-layer transition and transition control. *J. Fluid Mech.*, Vol. 199, 403–440. [473]
- Laurien, E. /s.: Oertel Jr., H.; Laurien, E. (2013)
- Lazareff, M.; Le Balleur, J.-C. (1983): Computation of three-dimensional viscous flows on transonic wings by boundary layer-inviscid flow interaction. *La Recherche Aérospatiale*, No. 1983-3, 11–29. [643]
- Lazareff, M. /s.: Le Balleur, J.-C.; Lazareff, M. (1985)
- Le Balleur, J.-C. /s.: Lazareff, M.; Le Balleur, J.-C. (1983)
- Le Balleur, J.-C. (1984): Numerical viscous-inviscid interaction in steady and unsteady flows. In: T. Cebeci (Ed.): *Numerical and Physical Aspects of Aerodynamic Flow II*. Springer-Verlag, New York, 259–284. [643, 648, 651]
- Le Balleur, J.-C.; Lazareff, M. (1985): A multi-zonal-marching integral method for three-dimensional boundary layer with viscous-inviscid interaction. *Lecture Notes in Physics*, Vol. 218, Springer-Verlag, Berlin, 351–364. [642]
- Le Balleur, J.-C.; Girodroux-Lavigne, P. (1986): A viscous-inviscid interaction method for computing unsteady transonic separation. In: T. Cebeci (Ed.): *Numerical and Physical Aspects of Aerodynamic Flows III*. Springer-Verlag, New York, 252–271. [645, 650]
- Le Fur, B. (1960): Convection de la chaleur en régime laminaire dans le cas d'un gradient de pression et d'un température de paroi quelconques, le fluide étant à propriétés physiques constantes, *Int. J. Heat Mass Transfer*, Vol. 1, 68–80. [230]
- Lee, C.J. /s.: Cheng, H.K.; Lee, C.J. (1986)
- Lee, L.H.; Reynolds, W.C. (1967): On the approximate and numerical solution of Orr-Sommerfeld problems. *Quart. J. Mech. Appl. Math.*, Vol. 20, 1–22. [436]
- Lees, L.; Lin, C.C. (1946): Investigation of the stability of the laminar boundary layer in a compressible fluid. *NACA-TN-1115*. [463, 468]
- Lees, L.; Reshotko, E. (1962): Stability of the compressible laminar boundary layer. *J. Fluid Mech.*, Vol. 12, 555–590. [464]
- Leigh, D.C. /s.: Emmons, H.W.; Leigh, D.C. (1954)
- Lekondis, S.G. /s.: Radwan, S.F.; Lekondis, S.G. (1986)
- Lele, S.K. (1994): Compressibility effects on turbulence. *Annu. Rev. Fluid Mech.*, Vol. 26, 211–254. [613, 616]

- Leonard, A. /s.: Spalart, P.R.; Leonard, A. (1987)
- Lessen, M. (1948): On the stability of the laminar free boundary layer between parallel streams. NACA-R-979 (1950); see also Sc.D. Thesis, MIT. [176]
- Levchenko, V.Y. /s.: Kachanov, Y.S.; Levchenko, V.Y. (1984)
- Levchenko, V.Y. /s.: Saric, W.S.; Kozlov, V.V.; Levchenko, V.Y. (1984)
- Lévêque, M.A. (1928): Les lois de la transmission de chaleur par convection. Ann. Mines 13, 201–239. [217]
- Levy, S. (1954): Effect of large temperature changes (including viscous heating) upon laminar boundary layers with variable free-stream velocity. J. of the Aeronautical Sciences, Vol. 21, 459–474. [253]
- Lewkowicz, A.K. (1982): An improved universal wake function for turbulent boundary layers and some of its consequences. Z. Flugwiss. Weltraumforsch., Bd. 6, 261–266. [594]
- Li, T.Y.; Nagamatsu, H.T. (1955): Similar solutions of compressible boundary layer equations. J. of the Aeronautical Sciences, Vol. 22, 607–616. [250]
- Libby, P.A.; Pallone, A. (1954): A method for analyzing the heat insulating properties of the laminar compressible boundary layer. J. of the Aeronautical Sciences, Vol. 21, 825–834. [307]
- Libby, P.A. (1967): Heat and mass transfer at a general three-dimensional stagnation point. AIAA Journal, Vol. 5, 507–517. [345]
- Libby, P.A.; Liu, T.M. (1967): Further solutions of the Falkner-Skan equation. AIAA Journal, Vol. 5, 1040–1042. [173]
- Libby, P.A.; Williams, F.A. (Eds.) (1980): Turbulent Reacting Flows. (Topics in Appl. Physics, Vol. 44). Springer-Verlag, Berlin (1980). [70]
- Libby, P.A. /s.: Champion, M.; Libby, P.A. (1996)
- Libby, P.A. (1998): Introduction to Turbulence. Taylor & Francis, Washington D.C.. [XXIV]
- Liepe, F. (1960): Wirkungsgrade von schlanken Kegeldiffusoren bei drallbehafteten Strömungen. Maschinenbau Technik, Bd. 9, 405–412. [637]
- Liepe, F. (1962): Untersuchungen über das Verhalten von Drallströmungen in Kegeldiffusoren. Dissertation, T.U. Dresden. [637]
- Liepmann, H.W. (1943a): Investigations on laminar boundary layer stability and transition on curved boundaries. NACA Wartime Rep. W-107. [483, 484]
- Liepmann, H.W. (1943b): Investigations on laminar boundary layer stability and transition on curved boundaries. ARC-RM-7302. [484]
- Liepmann, H.W. (1945): Investigation of boundary layer transition on concave walls. NACA Wartime Rep. W-87. [483]
- Liepmann, H.W.; Fila, G.H. (1947): Investigations of effects of surface temperature and single roughness elements on boundary-layer transition. NACA-TN-1196. [462]
- Liepmann, H.W.; Dhawan, S. (1951): Direct measurements of local skin friction in low-speed and high-speed flow. In: Proc. First US Nat. Congr. Appl. Mech., 869. [164]
- Liepmann, H.W. (1958): A simple derivation of Lighthill's heat transfer formula. J. Fluid Mech., Vol. 3, 357–360. [217]
- Lifschitz, E.M. /s.: Landau, L.D.; Lifschitz, E.M. (1966)
- Lightfoot, E.N. /s.: Bird, R.B.; Stewart, W.E.; Lightfoot, E.N. (1960)
- Lighthill, M.J. (1950): Contributions to the theory of heat transfer through a laminar boundary layer. Proc. Roy. Soc. London A, Vol. 202, 359–377. [217]
- Lighthill, M.J. (1954): The response of laminar skin friction and heat transfer to fluctuations in the stream velocity. Proc. Roy. Soc. London A, Vol. 224, 1–23. [140]
- Lighthill, M.J. (1963): Introduction. Boundary Layer Theory. In: L. Rosenhead (Ed.): Laminar Boundary Layers. Oxford University Press, Oxford, 46–113. [340, 341]

- Lighthill, J. (1978): Waves in Fluids. Cambridge University Press, Cambridge. [52]
- Lighthill, J. (2000): Upstream influence in boundary layers 45 years ago. Phil. Trans. R. Soc. Lond. A, Vol. 358, 3047–3061. [401]
- Lilley, G.M. /s.: Kline, S.J.; Cantwell, B.J.; Lilley, G.M. (1981)
- Lin, C.C. (1945–46): On the stability of two-dimensional parallel flows. Quart. Appl. Math., Vol. 3, 117–142 (July 1945); Vol. 3, 213–234 (Oct. 1945); Vol. 3, 277–301 (Jan. 1946). [439]
- Lin, C.C. /s.: Lees, L.; Lin, C.C. (1946)
- Lin, C.C. (1955): The Theory of Hydrodynamic Stability. Cambridge University Press, Cambridge. [425]
- Lin, C.C. (1957): Motion in the boundary layer with a rapidly oscillating external flow. In: Proc. 9th Intern. Congress Appl. Mech. Brussels, Vol. 4, 155–167. [135, 367]
- Lin, F.N.; Chao, B.T. (1974): Laminar free convection over two-dimensional and axisymmetric bodies of arbitrary contour. J. Heat Transfer, Vol. 96, 435–442. [327]
- Lin, F.N.; Chao, B.T. (1976): Addendum to laminar free convection over two-dimensional and axisymmetric bodies of arbitrary contour. J. Heat Transfer, Vol. 98, 344. [327]
- Liñán, A. /s.: Messiter, A.F.; Liñán, A. (1976)
- Lindhout, J.P.F.; Berg, B. van den (1979): Design of a calculation method for 3D turbulent boundary layers. Notes on Numerical Fluid Mechanics, Vol. 2, Vieweg-Verlag, Braunschweig, 174–185. [642]
- Lindhout, J.P.F. /s.: Humphreys, D.A.; Lindhout, J.P.F. (1988)
- Lindhout, J.P.F. /s.: Berg, B. van den; Humphreys, D.A.; Krause, E.; Lindhout, J.P.F. (1988)
- Lingwood, R.J. (1995): Absolute instability of the boundary layer on a rotating disk. J. Fluid Mech., Vol. 299, 17–33. [485]
- Lingwood, R.J. (1996): An experimental study of absolute instability of the rotating disk boundary layer flow. J. Fluid Mech., Vol. 314, 373–405. [485]
- Linke, W. (1942): Über den Strömungswiderstand einer beheizten ebenen Platte. Luftfahrtforschung 19, 157–160. [461]
- List, E.J. (1982): Turbulent jets and plumes. Annu. Rev. Fluid Mech., Vol. 14, 189–212. [676]
- Livingood, J.N.B. /s.: Donoughe, P.L.; Livingood, J.N.B. (1955)
- Liu, T.M. /s.: Libby, P.A.; Liu, T.M. (1967)
- Lock, R.C. (1951): The velocity distribution in the laminar boundary layer between parallel streams. Quart. J. Mech. Appl. Math., Vol. 4, 42–63. [176, 176]
- Lock, R.C.; Williams, B.R. (1987): Viscous-inviscid interactions in external aerodynamics. Prog. Aerospace Sci., Vol. 24, 51–171. [606]
- Loeffler, J. /s.: Elsberry, K.; Loeffler, J.; Zhou, M.D.; Wygnanski, I. (2000)
- Loehrke, R.J.; Morkovin, M.V.; Fejer, A.A. (1975): Review. Transition in nonreversing oscillating boundary layers. J. Fluids Eng., Vol. 97, 534–549. [472]
- Lohmann, R.P. (1976): The response of a developed turbulent boundary layer to local transverse surface motion. J. Fluids Eng., Vol. 98, 354–363. [636]
- Loitsianski, L.G. (1967): Laminare Grenzschichten. Akademie-Verlag, Berlin. [330, 344]
- Lomax, H. /s.: Baldwin, B.S.; Lomax, H. (1978)
- London, A.L. /s.: Shah, R.K.; London, A.L. (1978)
- Long, R.R. (1972): Finite amplitude disturbances in the flow of inviscid rotating and stratified fluids over obstacles. Annu. Rev. Fluid Mech., Vol. 4, 69–92. [52]
- Loos, H.G. (1955): A simple laminar boundary layer with secondary flow. J. of the Aeronautical Sciences, Vol. 22, 35–40. [342]

- Lord Rayleigh (1880–1913): On the stability or instability of certain fluid motions. Proc. London Math. Soc., Vol. 11 (1880), 57 and Vol. 19 (1887), 67; Scientific Papers, Vol. 1 (1880), 474–487; Vol. 3 (1887), 17–23, Vol. 4 (1895), 203–219; Vol. 6 (1913), 197–204. [424, 432, 433]
- Lord Rayleigh (1911): On the motion of solid bodies through viscous liquids. Phil. Mag., Vol. 21, 697–711 (1911); cf. also: Scientific Papers, Vol. 6 (1913), 29. [126, 129]
- Lorentz, H.A. (1907): Abhandlung über theoretische Physik I, 43–71, Leipzig 1907; revision of a paper published by Zittingsverlag Akad. v. Wet. Amsterdam 6, 28 (1897); cf. also L. Prandtl. The mechanics of viscous fluids. In: W.F. Durand (Ed.): Aerodynamic Theory, Vol. 3, Dover, New York, 34–208 (1935). [426]
- Love, A.E.H. (1952): The Mathematical Theory of Elasticity. 4th edition, Cambridge University Press, Cambridge. [62, 64]
- Lowell, R.L.; Reshotko, E. (1974): Numerical study of the stability of heated, water boundary layer. Div. Fluid, Thermal and Aero. Sci., Case Western Reserve Univ., Cleveland, Ohio, Rep. 73–93. [462]
- Lowery, G.W.; Vachon, R.J. (1975): The effect of turbulence on heat transfer from heated cylinders. Int. J. Heat Mass Transfer, Vol. 18, 1229–1242. [605]
- Lucey, A.D. /s.: Dixon, A.E.; Lucey, A.D.; Carpenter, P.W. (1994)
- Luckert, H.J. (1933): Über die Interation der Differentialgleichung einer Gleitschicht in zäher Flüssigkeit. Diss. Berlin 1933. Printed in Schriften d. math. Seminars u. Inst. f. angew. Math. d. Universität Berlin 1, 245. [184]
- Ludwieg, H.; Tillman, W. (1949): Untersuchung über die Wandschubspannung in turbulenten Reibungsschichten. Ing.-Archiv, Bd. 17, 288–299. [592]
- Ludwig, G.; Heil, M. (1960): Boundary layer theory with dissociation and ionization. Adv. Appl. Mechanics, Vol. 6, 39–118. [312]
- Lugt, H.J.; Haussling, H.J. (1974): Laminar flow past an abruptly accelerated elliptic cylinder at 45° incidence. J. Fluid Mech., Vol. 65, 711–734. [360]
- Lum, M. /s.: Fand, R.M.; Morris, E.W.; Lum, M. (1977)
- Lumley, J.L. (1969): Drag reduction by additives. Annu. Rev. Fluid Mech.; Vol. 1, 367–384. [534]
- Lumley, J.L. (1978a): Computational modeling of turbulent flows. Adv. Appl. Mech., Vol. 18, 123–176. [601]
- Lumley, J.L. (1978b): Drag reduction in turbulent flow by polymer additives. J. Polym. Sci. Macromol. Rev., Vol. 7, 263–290. [534]
- Lumley, J.L. (1981): Coherent structures in turbulence. In: R.E. Meyer (Ed.): Transition and Turbulence. Academic Press, 215–242. [513]
- Lumley, J.L. /s.: Shih, T.-H.; Lumley, J.L.; Chen, J.-Y. (1990)
- Luthander, S.; Rydberg, A. (1935): Experimentelle Untersuchungen über den Luftwiderstand bei einer um eine mit der Windrichtung parallelen Achse rotierenden Kugel. Physikal. Z., Bd. 36, 552–558. [331]
- Lyrio, A.A.; Ferziger, J.H.; Kline, S.J. (1981): An integral method for the computation of steady and unsteady turbulent boundary layers, including the transitory stall regime in diffusers. PD-23, Thermosciences Division, Department of Mechanical Engineering, Stanford University, Stanford, Calif.; also: Stanford Univ., Ph.D. Thesis, 1981. [648]
- Mack, L.M. (1965): The stability of the compressible laminar boundary layer according to a direct numerical solution. In: AGARDograph 97, Part 1, 329–362. [464]
- Mack, L.M. (1969): Boundary layer stability theory. Jet Propulsion Lab., Pasadena, Calif., Rep. 900-277. [463, 465, 466, 467, 468]
- Mack, L.M. (1977): Transition and laminar instability. JPL Publ. 77-15, Pasadena, Calif., also in NASA-CR-153203. [425]

- Mack, L.M. (1984): Boundary-layer linear stability theory. In: AGARD-R-709, 3-1 to 3-81. [463, 487]
- Mack, L.M. (1988): Stability of Three-Dimensional Boundary Layers on Swept Wings at Transonic Speeds. In: Zierep, J.; Oertel Jr., H. (1988). IUTAM Symposium Transsonicum III, Göttingen (1988), Springer-Verlag, Berlin, 209–223. [487]
- Mackinnon, J.C.; Renksizbulut, M.; Strong, A.B. (1998): Evaluation of Reynolds stress closure for turbulent boundary layer in turbulent freestream. AIAA Journal, Vol. 36, 936–945. [605]
- Mager, A.; Hansen, A.G. (1952): Laminar boundary layer over flat plate in a flow having circular streamlines. NACA-TN-2658. [330]
- Mager, A. (1954): Three-dimensional laminar boundary layer with small cross-flow. J. of the Aeronautical Sciences, Vol. 21, 835–845. [342]
- Mager, A. (1955): Thick laminar boundary layer under sudden perturbation. In: H. Görtler; W. Tollmien (Hrsg.): Fünfzig Jahre Grenzschichtforschung. Braunschweig, 21–33. [342]
- Mager, A. (1964): Three-dimensional laminar boundary layers. In: F.K. Moore (Ed.): Theory of Laminar Flows. High Speed Aerodynamics and Jet Propulsion, Vol. IV, Princeton University Press, Princeton, 286–394. [341]
- Mahajan, R.L. /s.: Gebhart, B.; Mahajan, R.L. (1982)
- Mahajan, R.L. /s.: Gebhart, B.; Jaluria, Y.; Mahajan, R.L.; Sammakia, B. (1988)
- Malcolm, G.N. /s.: Davis, S.S.; Malcolm, G.N. (1980)
- Malik, M.R. /s.: Hall, P.; Malik, M.R.; Poll, D.I.A. (1984)
- Malik, M.R.; Godil, A.A. (1990): Effect of wall suction and cooling on the second mode instability. In: Hussaini, M.Y.; Voigt, R.G. (Eds.): Instability and Transition, Vol. 2, 235–245, Springer-Verlag, Berlin. [467]
- Malik, M.R.; Hussaini, M.Y. (1990): Numerical simulation of interactions between Görtler vortices and Tollmien-Schlichting waves. J. Fluid Mech., Vol. 210, 183–199. [482]
- Mangler, W. (1943): Die “ähnlichen” Lösungen der Prandtlschen Grenzschichtgleichungen. ZAMM. Z. angew. Math. Mech., Bd. 23, 241–251. [167]
- Mangler, W. (1948): Zusammenhang zwischen ebenen und rotationssymmetrischen Grenzschichten in kompressiblen Flüssigkeiten. ZAMM. Z. angew. Math. Mech., Bd. 28, 97–103. [323]
- Mankbadi, R.R.; Mobark, A. (1991): Quasisteady turbulence modeling of unsteady flows. International Journal of Heat and Fluid Flow, Vol. 12, 122–129. [649]
- Marusic, I. /s.: Jones, M.B.; Marusic, I.; Perry, A.E. (2001)
- Marvin, J.G. /s.: Delery, J.; Marvin, J.G. (1986)
- Maskell, E.C. (1955): Flow separation in three dimensions. RAE Rep. Aero 2565. [340]
- Masson, D.J. /s.: Gross, J.F.; Hartnett, J.P.; Masson, D.J.; Gazley Jr., C. (1961)
- Matsubara, M. /s.: Franssen, J.H.M.; Matsubara, M.; Alfredsson, P.H. (2005)
- Matsushita, M.; Murata, S.; Akamatsu, T. (1984a): Studies on boundary layer separation in unsteady flows using an integral method. J. Fluid Mech., Vol. 149, 477–501. [354]
- Matsushita, M.; Murata, S.; Akamatsu, T. (1984b): Numerical computation of unsteady laminar boundary layers with separation using two-parameter integral method. Bull. JSME, Vol. 28, No. 245, 2630–2638. [354]
- Mauss, J. /s.: Roget, C.; Brazier, J.Ph.; Cousteix, J.; Mauss, J. (1998)
- Mauss, J. /s.: Cousteix, J.; Mauss, J. (2005)
- Mazur, P. /s.: De Groot, S.R.; Mazur, P. (1962)
- McCroskey, W.J. (1977): Some current research in unsteady fluid dynamics – The 1976 Freeman Scholar Lecture. J. Fluids Eng., Vol. 99, 8–39. [47]

- McDonald, H.; Briley, W.R. (1984): A survey of recent work on interacted boundary-layer theory for flow with separation. In: T. Cebeci (Ed.): Numerical and Physical Aspects of Aerodynamic Flows II. Springer-Verlag, New York, 141–162. [388, 403, 606]
- Mehta, R.D. (1977): Aerodynamic design of blower tunnels with wide-angle diffusers. *Progress in Aerospace Sciences*, Vol. 18, 59–120. [605]
- Mehta, R.D. (1985): Turbulent boundary layer perturbed by a screen. *AIAA Journal*, Vol. 23, 1335–1342. [605]
- Meier, G.E.A. /s.: Dinkelacker, A.; Hessel, M.; Meier, G.E.A.; Schewe, G. (1977)
- Meier, G.E.A.; Sreenivasan, K. R. (Eds.); Heinemann, H.-J. (Managing Ed.) (2006): One Hundred Years of Boundary Layer Research. IUTAM Symposium. Springer. [XXV]
- Meier, H.U.; Rotta, J.C. (1971): Temperature distributions in supersonic turbulent boundary layers. *AIAA Journal*, Vol. 9, 2149–2156. [569]
- Meier, H.U.; Kreplin, H.P. (1980): Experimental investigation of the boundary layer transition and separation on a body of revolution. *Z. Flugwiss. Weltraumforsch.*, Bd. 4, 65–71. [346, 514, 605]
- Meile, W. /s.: Gretler, W.; Meile, W.; Dutzler, G. (1995)
- Meineke, E. (1977): Berechnung freier turbulenter Scherströmungen mit einem 3-Gleichungs-Turbulenz-Modell von J.C. Rotta. DLR-FB 77–60. [663]
- Meixner, J.; Reik, H.G. (1959): Thermodynamik der irreversiblen Prozesse. In: S. Flügge (Hrsg.): *Handbuch der Physik*, Bd. III/2, 413–523. [53, 67]
- Mellor, G.L.; Chapple, P.J.; Stokes, V.K. (1968): On the flow between a rotating and a stationary disk. *J. Fluid Mech.*, Vol. 31, 95–112. [124]
- Mellor, G.L. (1972): The large Reynolds number asymptotic theory of turbulent boundary layers. *Int. J. Engng. Sci.*, Vol. 10, 851–873. [XXIV, 572]
- Mellor, G.L. /s.: Bissonnette, L.R.; Mellor, G.L. (1974)
- Melnik, R.E. /s.: Messiter, A.F.; Feo, A.; Melnik, R.E. (1971)
- Melnik, R.E.; Chow, R. (1975): Asymptotic theory of two-dimensional trailing edge flows. Grumman Research Department Rep. RE-510. [400]
- Melnik, R.E. (1981): Turbulent interactions on airfoils at transonic speeds – Recent developments. In: AGARD-CP-291, 10-1 to 10-34. [625]
- Melnik, R.E.; Grossmann B. (1981): On the turbulent viscid-inviscid interaction at a wedge-shaped trailing edge. In: Cebeci, T. (Ed.): Numerical and Physical Aspects of Aerodynamic Flows I. Springer-Verlag, New York, 211–235. [671]
- Melnik, R.E.; Rubel, A. (1983): Asymptotic theory of turbulent wall jets. Grumman Research Dept. Rep. RE-654 J. [679]
- Melnik, W.L. (1982): Solution-adaptive grid for the calculation of three-dimensional laminar and turbulent boundary layers. In: E. Krause (Ed.): Eighth International Conference on Numerical Methods in Fluid Dynamics, Springer-Verlag, Berlin, 377–382. [339]
- Menter, F.R. (1992): Performance of popular turbulence models for attached and separated adverse pressure gradient flows. *AIAA Journal*, Vol. 30, 2066–2072. [560]
- Menter, F.R. (1994): Two-equation eddy-viscosity turbulence models for engineering applications. *AIAA I*, Vol. 32, 1598–1605. [564]
- Merker, G.P. (1987): Konvektive Wärmeübertragung, Springer-Verlag, Berlin. [90]
- Merkin, J.H. (1972): Free convection with blowing and suction. *Int. J. Heat Mass Transfer*, Vol. 15, 989–999. [311]
- Merkin, J.H. (1975): The effects of blowing and suction on free convection boundary layers. *Int. J. Heat Mass Transfer*, Vol. 18, 237–244. [311]
- Merkin, J.H. (1977): Free convection boundary layers on cylinders of elliptic cross section. *J. Heat Transfer*, Vol. 99, 453–457. [277, 278]

- Merkin, J.H. /s.: Smith, F.T.; Merkin, J.H. (1982)
- Merkin, J.H. (1983): Free convection boundary layers over humps and indentations. Quart. J. Mech. Appl. Math., Vol. 36, 71–85. [401]
- Mersmann, A. (1986): Stoffübertragung. Springer-Verlag, Berlin. [318, 318]
- Merzkirch, W.; Page, R.H.; Fletcher, L.S. (1988): A survey of heat transfer in compressible separated and attached flows. AIAA Journal, Vol. 26, 144–150. [610]
- Merzkirch, W. /s.: Gersten, K.; Grobel, M.; Klick, H.; Merzkirch, W. (1991)
- Messick, R.E. /s.: Napolitano, M.; Messick, R.E. (1980)
- Messiter, A.F. (1970): Boundary layer flow near the trailing edge of a flat plate. SIAM J. Appl. Math., Vol. 18, 241–257. [400]
- Messiter, A.F.; Feo, A.; Melnik, R.E. (1971): Shock-wave strength for separation of a laminar boundary layer at transonic speeds. AIAA Journal, Vol. 9, 1197–1198. [401]
- Messiter, A.F.; Liñán, A. (1976): The vertical plate in laminar convection: Effects of leading and trailing edges and discontinuous temperature. Z. angew. Math. Phys. (ZAMP), Bd. 27, 633–651. [401]
- Messiter, A.F. /s.: Adamson Jr., T.C.; Messiter, A.F. (1980)
- Messiter, A.F. /s.: Adamson Jr., T.C.; Messiter, A.F. (1981)
- Messiter, A.F. (1983): Boundary-layer interaction theory. Journal of Applied Mechanics, Vol. 50, 1104–1113. [399]
- Meyer, F. /s.: Fischer, T.M.; Ehrenstein, U.; Meyer, F. (1988)
- Michalke, A. (1962): Theoretische und experimentelle Untersuchung einer rotationssymmetrischen laminaren Düsengrenzschicht. Ing.-Arch., Bd. 31, 268–279. [326]
- Michel, R. (1951): Etude de la transition sur les profiles d'aile-établissement d'un critère de détermination du point de transition et calcul de la traînée de profil en incompressible. ONERA Rapport 1/1578 A. [454]
- Michel, R. (1952): Détermination du point de transition et calcul de la traînée des profiles en incompressible. ONERA Publ. Nr. 58. [454]
- Michel, R.; Quémard, C.; Durant, R. (1968): Hypotheses on the mixing length and application to the calculation of the turbulent boundary layers. In: Kline, S.J. et al. (Eds.): Proceedings Computation of Turbulent Boundary Layers-1968. AFOSR-IFP-Stanford Conference, Vol. I, 195–207. [559, 575, 580, 582, 585, 589, 696, 700]
- Michel, R. /s.: Cousteix, J.; Houdeville, R.; Michel, R. (1974)
- Michel, R. /s.: Arnal, D.; Juillen, J.C.; Michel, R. (1977)
- Mikhail, M.N. (1979): Optimum design of wind tunnel contractions. AIAA Journal, Vol. 17, 471–477. [634]
- Miller, D.R.; Comings, E.W. (1957): Static pressure distribution in the free turbulent jet. J. Fluid Mech., Vol. 3, 1–16. [666]
- Millikan, C.B. (1938): A critical discussion of turbulent flows in channels and circular tubes. Proc. 5th Int. Congr. Applied Mechanics. New York, J. Wiley, New York, 386–392. [524]
- Millsaps, K.; Pohlhausen, K. (1953): Thermal distribution in Jeffery-Hamel flows between nonparallel plane walls. J. of the Aeronautical Sciences, Vol. 20, 187–196. [105, 109]
- Minkowycz, W.J. /s.: Sparrow, E.M.; Minkowycz, W.J.; Eckert, E.R.G.; Ibele, W.E. (1964)
- Mirels, H. (1956): Boundary layer behind shock or thin expansion wave moving into stationary fluid. NACA-TN-3712. [372]
- Mirels, H.; Hamman, J. (1962): Laminar boundary layer behind strong shock moving with non-uniform velocity. Physics of Fluids, Vol. 5, 91–96. [373]

- Mises, R. v. (1927): Bemerkungen zur Hydrodynamik, ZAMM. Z. angew. Math. Mech., Bd. 7, 425–431. [183]
- Misra, U.N. /s.: Singh, P.; Sharma, V.P.; Misra, U.N. (1981)
- Mitchell, A.R.; Thomson, J.Y. (1958): Finite difference methods of solution of the von Mises boundary layer equation with special reference to conditions near the singularity. Z. angew. Math. Phys. (ZAMP), Bd. 9, 26–37. [184]
- Mitsotakis, K.; Schneider, W.; Zauner, E. (1984): Second-order boundary-layer theory of laminar jet flows. Act. Mech., Vol. 53, 115–123. [387, 387]
- Mitsotakis, K. /s.: Mörwald, K.; Mitsotakis, K.; Schneider, W. (1986)
- Mituisi, S. /s.: Tani, I.; Hama, R.; Mituisi, S. (1940)
- Méndez, F. /s.: Treviño, C.; Méndez, F. (1992)
- Mobark, A. /s.: Mankbadi, R.R.; Mobark, A. (1991)
- Möbius, H. (1940): Experimentelle Untersuchungen des Widerstandes und der Geschwindigkeitsverteilung in Rohren mit regelmäßig angeordneten Rauhigkeiten bei turbulenten Strömung. Phys. Z., Bd. 41, 202–225. [533]
- Möller, E. (1951): Luftwiderstandsmessungen am Volkswagen-Lieferwagen. Automobiltechnische Z., Bd. 53, Heft 6, 153–156. [43]
- Mörwald, K.; Mitsotakis, K.; Schneider, W. (1986): Higher-order analysis of laminar plumes. Proc. 8th Int. Heat Transfer Conf. (Eds. C.L. Tien et al.), Hemisphere, 1335–1340. [387, 387]
- Mörwald, K. /s.: Schneider, W.; Mörwald, K. (1987)
- Mörwald, K. (1988): Asymptotische Theorie freier turbulenter Scherströmungen. Dissertation, T.U. Wien. [655, 663]
- Mohammadi, B.; Pironneau, O. (1994): Analysis of the K-Epsilon Turbulence Model. Wiley & Sons, Chichester, etc. [601]
- Moin, P. /s.: Rogallo, R.S.; Moin, P. (1984)
- Mollendorf, J.C.; Gebhart, B. (1973): Thermal buoyancy in round laminar vertical jets. Int. J. Heat Mass Transfer, Vol. 16, 735–745. [334]
- Monkewitz, P.A. /s.: Huerre, P.; Monkewitz, P.A. (1985)
- Monkewitz, P.A. /s.: Huerre, P.; Monkewitz, P.A. (1990)
- Moore, F.K. (1951): Unsteady laminar boundary-layer flow. NACA-TN-2471. [370]
- Moore, F.K. (1956): Three-dimensional laminar boundary layer theory. Advances in Appl. Mech., Vol. 4, 159–228. [341]
- Moore, F.K.; Ostrach, S. (1956): Average properties of compressible laminar boundary layer on a flat plate with unsteady flight velocity. NACA-TN-3886. [370]
- Moore, F.K. (1958): On the separation of the unsteady laminar boundary layer. In: H. Görtler (Hrsg.): Grenzschichtforschung, Springer-Verlag, Berlin, 296–311. [292]
- Morduchow, M. (1952): On heat transfer over a sweat-cooled surface in laminar compressible flow with pressure gradient. J. of the Aeronautical Sciences, Vol. 19, 705–712. [307]
- Moretti, P.M.; Kays, W.M. (1965): Heat transfer to a turbulent boundary layer with varying freestream velocity and varying surface temperature – an experimental study. Int. J. Heat Mass Transfer, Vol. 8, 1187–1202. [609]
- Morgan, V.T. (1975): The overall convective heat transfer from smooth circular cylinders. Advances in Heat Transfer, Vol. 11, 199–264. [278, 290]
- Morkovin, M.V. (1962): Effects of compressibility on turbulent flows. In: A. Favre (Ed.): Méchanique de la Turbulence. Centre National de la Recherche Scientific, Paris, 367–380. [616]
- Morkovin, M.V. (1964): Flow around circular cylinder – A kaleidoscope of challenging fluid phenomena. In: Hansen, A.G. (Ed.): Symposium on Fully Separated Flows. American Society of Mechanical Engineers, 102–118. [21, 47]

- Morkovin, M.V. /s.: Kline, S.J.; Morkovin, M.V.; Sovran, G.; Cockrell, D.J. (Eds.) (1968)
- Morkovin, M.V. /s.: Obremski, H.J.; Morkovin, M.V.; Landahl, M. (1969)
- Morkovin, M.V. /s.: Loehrke, R.J.; Morkovin, M.V.; Fejer, A.A. (1975)
- Morkovin, M.V. (1988): Recent insights into instability and transition to turbulence in open-flow systems – Final Report, NASA-CR-181693. [425, 492, 492]
- Morris, E.W. /s.: Fand, R.M.; Morris, E.W.; Lum, M. (1977)
- Morris, Ph.J. (1981): Three-dimensional boundary layer on a rotating helical blade. *J. Fluid Mech.*, Vol. 112, 283–296. [347]
- Morse, A. /s.: Launder, B.E.; Morse, A.; Rodi, W.; Spalding, D.B. (1973)
- Morton, K.W. /s.: Richtmyer, R.D.; Morton, K.W. (1967)
- Motohashi, T. /s.: Tani, I.; Motohashi, T. (1985)
- Müller, I. (1973): Thermodynamik. Die Grundlagen der Materialtheorie. Bertelsmann Universitätsverlag. [55]
- Müller, W. (1936): Zum Problem der Anlaufströmung einer Flüssigkeit im geraden Rohr mit Kreisring- und Kreisquerschnitt. *ZAMM. Z. angew. Math. Mech.*, Bd. 16, 227–238. [117, 141]
- Müllner, M.; Schneider, W. (2010): Laminar mixed convection on a horizontal plate of finite length in a channel of finite width. *Int. J. Heat Mass Transfer*, Vol. 46, 1097–1110. [289]
- Murata, S. /s.: Matsushita, M.; Murata, S.; Akamatsu, T. (1984a)
- Murata, S. /s.: Matsushita, M.; Murata, S.; Akamatsu, T. (1984b)
- Myring, D.F. (1970): An integral prediction method for three-dimensional turbulent boundary layers. *RAE-TR 70147*. [642]
- Na, T.Y. /s.: Aziz, A.; Na, T.Y. (1984)
- Nagamatsu, H.T. /s.: Li, T.Y.; Nagamatsu, H.T. (1955)
- Nagano, Y.; Kim, C. (1988): A two-equation model for heat transport in wall turbulent shear flows. *Journal of Heat Transfer*, Vol. 110, 583–589. [570, 610]
- Nakamura, I. /s.: Furuya, Y.; Nakamura, I.; Yamashita, S. (1978)
- Nakamura, I.; Yamashita, S.; Yamamoto, K. (1980): On the turbulent boundary layer on a spinning tail body in an axial flow. *Memoirs of the Faculty of Eng., Nagoya University*, Vol. 32, 282–297. [635, 636]
- Nakamura, I.; Yamashita, S.; Watanabe, T.; Sawaki, Y. (1981): Three-dimensional turbulent boundary layer on a spinning thin cylinder in an axial uniform stream. In: *International Symposium on Turbulent Shear Flows* (3, 1981, Univ. of California, Davis). [636]
- Nakamura, I.; Yamashita, S. (1982): Boundary layers on bodies of revolution spinning in axial flows. In: H.H. Fernholz; E. Krause (Eds.): *Three-Dimensional Turbulent Boundary Layers*, Springer-Verlag, Berlin, 177–187. [635]
- Napolitano, M.; Messick, R.E. (1980): On strong slot-injection into a subsonic laminar boundary layer. *Computers and Fluids*, Vol. 8, 199–212. [400]
- Narasimha, R.; Vasantha, S.S. (1966): Laminar boundary layer on a flat plate at high Prandtl number. *Z. angew. Math. Phys. (ZAMP)*, Bd. 17, 585–592. [228]
- Narasimha, R. /s.: Rao, K.N.; Narasimha, R.; Badri Narayanan, M.A. (1971)
- Narasimha, R. /s.: Afzal, N.; Narasimha, R. (1976)
- Narasimha, R.; Sreenivasan, K.R. (1979): Relaminarization of fluid flows. *Advances in Applied Mechanics*, Vol. 19, 221–309. [582]
- Narasimha, R. /s.: Afzal, N.; Narasimha, R. (1985)
- Narasimha, R. (1985): The laminar-turbulent transition zone in the boundary layer. *Prog. Aero. Sci.*, Vol. 22, 29–80. [479]
- NASA SP-321 (1973): Free Turbulent Shear Flows. Conference Proceedings. [655, 664]
- Nash, E.J. /s.: Hieber, C.A.; Nash, E.J. (1975)

- Nash, J.F.; Patel, V.C. (1972): Three-Dimensional Turbulent Boundary Layers. SBC Technical Books, Atlanta. [641]
- Nash, J.F. /s.: Patel, V.C.; Nash, J.F. (1975)
- Nath, G. /s.: Venkatachala, B.J.; Nath, G. (1981)
- Naumann, A. (1953): Luftwiderstand von Kugeln bei hohen Unterschallgeschwindigkeiten. Allgem. Wärmetechnik., Bd. 4, 217–221. [12]
- Naumann, A.; Pfeiffer, H. (1962): Über die Grenzschichtströmung am Zylinder bei hohen Geschwindigkeiten. Advances in Aeronautical Sciences, Vol. 3, 185–206. [24]
- Navier, M. (1827): Mémoire sur les lois du mouvement des fluides. Mém. de l'Acad. d. Sci., Vol. 6, 389–416. [68]
- Nayfeh, A.H.; Padhye, A. (1979): Relation between temporal and spatial stability in three-dimensional flows. AIAA Journal, Vol. 17, 1084–1090. [488]
- Nayfeh, A.H. /s.: El-Hady, N.M.; Nayfeh, A.H. (1980)
- Nayfeh, A.H. (1981): Effects of streamwise vortices on Tollmien-Schlichting waves. J. Fluid Mech., Vol. 107, 441–453. [484]
- Nayfeh, A.H. /s.: Ragab, S.A.; Nayfeh, A.H. (1982)
- Nayfeh, A.H. (1987): Nonlinear stability of boundary layers. AIAA Paper 87-0044. [476, 489]
- Nayfeh, A.H.; Al-Maaitah, A. (1987): Influence of streamwise vortices in Tollmien-Schlichting waves. AIAA Paper 87-1206. [484]
- Nenni, J.P. /s.: Shen, S.F.; Nenni, J.P. (1975)
- Nickel, K. (1962): Eine einfache Abschätzung für Grenzschichten, Ing.-Arch., Bd. 31, 85–100. [303]
- Nickel, K. (1973): Prandtl's boundary-layer theory from the view point of a mathematician. Annu. Rev. Fluid Mech., Vol. 5, 405–428. [173]
- Nickels, T.B. (2004): Inner scaling for wall-bounded flows subject to large pressure gradients. J. Fluid Mech., Vol. 521, 217–239. [146]
- Nicolai, D. /s.: Gersten, K.; Nicolai, D. (1974)
- Nicoll, W.B. /s.: Kays, W.M.; Nicoll, W.B. (1963)
- Nietubicz, Ch.J. /s.: Sturek, W.B.; Dwyer, H.A.; Kayser, L.D.; Nietubicz, Ch.J.; Reklis, R.P.; Opalko, K.O. (1978)
- Nieuwstadt, F.T.M. /s.: Debisschop, J.R.; Nieuwstadt, F.T.M. (1996)
- Nigam, S.D. (1951): Zeitliches Anwachsen der Grenzschicht an einer rotierenden Scheibe bei plötzlichem Beginn der Rotation. Quart. Appl. Math., Vol. 9, 89–91. [361]
- Nigam, S.D. (1954): Note on the boundary layer on a rotating sphere. Z. angew. Math. Phys. (ZAMP), Bd. 5, 151–155. [331]
- Nikuradse, J. (1929): Kinematographische Aufnahme einer turbulenten Strömung. ZAMM Bd. 9, 495–496. [500]
- Nikuradse, J. (1932): Gesetzmäßigkeit der turbulenten Strömungen in glatten Rohren. VDI-Forsch.-Heft 356, VDI-Verl., Berlin. [15]
- Nikuradse, J. (1933): Strömungsgesetze in rauhen Rohren. VDI-Forsch.-Heft 361, VDI-Verl., Berlin. [553]
- Nikuradse, J. (1942): Laminare Reibungsschichten an der längsangeströmten Platte. Monographie, Zentrale f. wiss. Berichtswesen, Berlin. [162]
- Nishioka, M.; Iida, S.; Ichikawa, Y. (1975): An experimental investigation of the stability of plane Poiseuille flow. J. Fluid Mech., Vol. 72, 731–751. [474]
- Nishioka, M.; Asai, M.; Iida, S. (1990): An experimental investigation of the secondary instability. In: R. Eppler; H. Fasel (Eds.): Laminar-Turbulent Transition. Springer-Verlag, Berlin, 37–46. [474]
- Nitsche, W. (1994): Strömungsmeßtechnik. Springer-Verlag, Berlin. [510]
- Nitschke-Kowsky, P. /s.: Bippes, H.; Nitschke-Kowsky, P. (1987)
- Nockemann, M. /s.: Fernholz, H.H.; Krause, E.; Nockemann, M.; Schober, M. (1995)

- Noshadi, V.; Schneider, W. (1998): A numerical investigation of mixed convection on a horizontal semi-infinite plate. In: H.J. Roth; Ch. Egbers (Eds.): Advances in Fluid Mechanics and Turbomachinery. Springer-Verlag, Berlin, 87–97. [289]
- Noshadi, V.; Schneider, W. (1999): Natural convection flow far from a horizontal plate. *J. Fluid Mech.*, Vol. 387, 227–254. [283]
- Nutant, J. /s.: Hama, F.R.; Nutant, J. (1963)
- Nydholt, J.E. (1971): Heat transfer for the Bödewadt problem. Dissertation, Colorado State Univ., Fort Collins, Colorado. [329]
- Oberbeck, A. (1876): Über die Wärmeleitung der Flüssigkeiten bei Berücksichtigung der Strömung infolge von Temperaturdifferenzen. *Annalen der Physik und Chemie*, Bd. 7, 271–292. [89]
- Oberlack, M. (2001): A unified approach for symmetries in plane parallel turbulent shear flows. *J. Fluid Mech.*, Vol. 427, 299–328. [524]
- Oberländer, K. (1974): Überschallströmungen um stumpfe Körper mit Ausblasen. Dissertation, Ruhr-Universität Bochum. [23, 24, 387]
- Obremski, H.J.; Morkovin, M.V.; Landahl, M. (1969): A portfolio of stability characteristics of incompressible boundary layers. AGARDograph 134. [438, 447, 448, 492]
- Ölçmen, M.S.; Simpson, R.L. (1992): Perspective: On the near wall similarity of three-dimensional turbulent boundary layers. *Journal of Fluid Engineering*. Vol. 114, 487–495 [641]
- Ölçmen, M.S.; Simpson, R.L. (1993): Evaluation of algebraic eddy-viscosity models in three-dimensional boundary layer flows. *AIAA Journal*, Vol. 31, 1545–1554. [636, 642]
- Oertel Jr., H. /s.: Hanneman, K.; Oertel Jr., H. (1989)
- Oertel Jr., H. (1990): Wakes behind blunt bodies. *Annu. Rev. Fluid Mech.*, Vol. 22, 539–564. [425, 431, 494]
- Oertel Jr., H. (1995): Bereiche der reibungsbehafteten Strömung. *Z. Flugwiss. Weltraumforsch.*, Bd. 19, 119–128. [425, 431, 489]
- Oertel Jr., H.; Delfs, J. (1995): Mathematische Analyse der Bereiche reibungsbehafteter Strömungen. *ZAMM. Z. angew. Math. Mech.*, Bd. 75, 491–505. [431, 487, 494]
- Oertel Jr., H.; Delfs, J. (1997): Dynamics of localized disturbances in engineering flows: a report on Euromech Colloquium 353. *J. Fluid Mech.*, Vol. 347, 369–374. [431, 492]
- Oertel Jr., Stank, R. (1999): Dynamics of Localized Disturbances in Transonic Wing Boundary Layers. *AIAA 99-0551*, 1–11. [495]
- Oertel Jr., H. (2001): Stabilitätstheorie. In: Prandtl - Führer durch die Strömungslehre, 10. Auflage, Vieweg-Verlag, Braunschweig, Wiesbaden, (2002): 11. Auflage. [425, 494]
- Oertel Jr., H. (2002): Stability Theory. In: Prandtl - Essentials of Fluid Mechanics, 10. edition, Springer-Verlag, New York. [425, 494]
- Oertel Jr., H.; Delfs, J. (2005): Strömungsmechanische Instabilitäten. Universitätsverlag Karlsruhe. [425, 487, 494]
- Oertel Jr., H. (2010): Flow Control – Theoretical Concept of Absolute Instability. KIT Science Publishing. Karlsruhe. [425]
- Oertel Jr., H. /s.: Sreenivasan, K.R.; Oertel Jr., H. (2010).
- Oertel Jr., H.; Laurin, E. (2013): Numerische Strömungsmechanik, 5. Auflage. Springer Vieweg Verlag, Wiesbaden. [436]
- Oertel Jr., H.; Böhle, M.; Reviol, T. (2015): Strömungsmechanik, 7. Auflage. Springer Vieweg-Verlag, Wiesbaden. [425, 494]
- Oertel Jr., H. /s.: Sreenivasan, K.R.; Oertel Jr., H. (2016).

- Okamura, T. /s.: Wazzan, A.R.; Okamura, T.; Smith, A.M.O. (1968)
- Okamura, T. /s.: Jaffe, N.A.; Okamura, T.; Smith, A.M.O. (1970)
- Okamura, T. /s.: Wazzan, A.R.; Okamura, T.; Smith, A.M.O. (1970a)
- Okamura, T. /s.: Wazzan, A.R.; Okamura, T.; Smith, A.M.O. (1970b)
- Okuno, T. (1976): Distribution of wall shear stress and crossflow in three-dimensional turbulent boundary layer on ship hull. *Journ. Soc. Nav. Arch., Japan*, Vol. 139, 1–12 [in Japanese]. [642]
- Opalka, K.O. /s.: Sturek, W.B.; Dwyer, H.A.; Kayser, L.D.; Nietubicz, Ch.J.; Reklis, R.P.; Opalka, K.O. (1978)
- Orr, W.M.F. (1907): The stability or instability of steady motions of a perfect liquid and of a viscous liquid. Part I: A perfect liquid; Part II: A viscous liquid. *Proc. Roy. Irish Acad.*, Vol. 27, 9–38 and 69–138. [428]
- Orszag, S.A.; Patera, A.T. (1983): Secondary instability of wall-bounded shear flows. *J. Fluid Mech.*, Vol. 128, 347–385. [473, 474]
- Osborne, M.R. (1967): Numerical methods for hydrodynamic stability problems. *SIAM J. Appl. Math.*, Vol. 15, 539–557. [436]
- Oseen, C.W. (1911): Über die Stokes'sche Formel und über eine verwandte Aufgabe in der Hydrodynamik. In: *Arkiv foer Matematik, Astronomi och Fysik*, Vol. 6, Nr. 29. [24, 139]
- Ossin, A. /s.: Chaing, T.; Ossin, A.; Tien, C.L. (1964)
- Ostowari, C. /s.: Page, R.H.; Hadden, L.L.; Ostowari, C. (1989)
- Ostrach, S. (1955): Compressible laminar boundary layer and heat transfer for unsteady motions of a flat plate. *NACA-TN-3569*. [370, 374]
- Ostrach, S. /s.: Moore, F.K.; Ostrach, S. (1956)
- Ostrach, S. /s.: Braun, W.H.; Ostrach, S.; Heighway, J.E. (1961)
- Oudart, A. /s.: Eichelbrenner, E.A.; Oudart, A. (1955)
- Pack, D.C. (1954): Laminar flow in an axially symmetrical jet of compressible fluid, far from the orifice. *Proc. Cambr. Phil. Soc.*, Vol. 50, 98–104. [333]
- Padhye, A. /s.: Nayfeh, A.H.; Padhye, A. (1979)
- Page, R.H. /s.: Merzkirch, W.; Page, R.H.; Fletcher, L.S. (1988)
- Page, R.H.; Hadden, L.L.; Ostowari, C. (1989): Theory of radial jet reattachment flow. *AIAA Journal*, Vol. 27, 1500–1505. [674]
- Page, R.H. (1993): Axisymmetric gas jets: Surface impingement phenomena. *Proceedings of 14th Canadian Congress of Applied Mechanics*, Vol. 1, 10–19. [674]
- Pagendarm, H.-G. /s.: Gersten, K.; Pagendarm, H.-G. (1983)
- Pai, S.I. (1965): Radiation Gasdynamics, Springer-Verlag, Berlin. [69, 264]
- Panton, R.L. (1984): Incompressible Flow. John Wiley & Sons, New York. [82, 92, 131]
- Papailiou, D.D. (1991): Turbulence models for natural convection flows along a vertical heated plane. In: AGARD-AR-291, 4-1 to 4-5. [629]
- Papenfuß, H.-D. (1974a): Higher-order solutions for the incompressible three-dimensional boundary-layer flow at the stagnation point of a general body. *Archives of Mechanics*, Vol. 26, 981–994. [387]
- Papenfuß, H.-D. (1974b): Mass-transfer effects on the three-dimensional second order boundary-layer flow at the stagnation point of blunt bodies. *Mech. Res. Comm.*, Vol. 1, 285–290. [387]
- Papenfuß, H.-D. (1975): Die Grenzschichteffekte 2. Ordnung bei der kompressiblen dreidimensionalen Staupunktströmung. Dissertation, Ruhr-Universität Bochum. [336, 345, 387]
- Papenfuß, H.-D. /s.: Gersten, K.; Papenfuß, H.-D.; Gross, J.F. (1977)
- Papenfuß, H.-D. /s.: Gersten, K.; Papenfuß, H.-D. (1992)
- Papenfuß, H.-D. (1997): Theoretische Kraftfahrzeug-Aerodynamik – Die Struktur des Strömungsfeldes bestimmt das Konzept. *ATZ Automobiltechnische Zeitschrift*, Bd. 99, 100–107. [643]

- Parr, O. (1963): Untersuchungen der dreidimensionalen Grenzschicht an rotierenden Drehkörpern bei axialer Anströmung. *Ing.-Arch.*, Bd. 32, 393–413. [328, 635, 636]
- Patel, M.H. (1975): On laminar boundary layers in oscillatory flow. *Proc. Roy. Soc. London A*, Vol. 347, 99–123. [368]
- Patel, V.C. /s.: Nash, J.F.; Patel, V.C. (1972)
- Patel, V.C.; Nash, J.F. (1975): Unsteady turbulent boundary layers with flow reversal. In: R.B. Kinney (Ed.): *Unsteady Aerodynamics, Proceedings of a Symposium, held at The University of Arizona, 1975, Arizona*, Vol. 1, 191–219. [649]
- Patel, V.C.; Choi, D.H. (1980): Calculation of three-dimensional laminar and turbulent boundary layers on bodies of revolution at incidence. In: L.J.S. Bradbury et al. (Eds.): *Turbulent Shear Flows II*. Springer-Verlag, New York, 199–217. [346, 643]
- Patel, V.C.; Scheuerer, G. (1982): Calculation of two-dimensional near and far wakes. *AIAA Journal*, Vol. 20, 900–907. [670]
- Patel, V.C.; Baek, J.H. (1985): Boundary layers and separation on a spheroid at incidence. *AIAA Journal*, Vol. 23, 55–63. [345]
- Patel, V.C.; Rodi, W.; Scheuerer, G. (1985): Turbulence models for near-wall and low Reynolds number flows: A review. *AIAA Journal*, Vol. 23, 1308–1319. [XXIV, 527, 562, 571, 574, 603, 701]
- Patel, V.C. /s.: Chen, H.C.; Patel, V.C. (1987)
- Patel, V.C. (1998): Perspective: Flow at high Reynolds number and over rough surfaces – Achilles heel of CFD. *Journal of Fluid Engineering*, Vol. 120, 434–444. [534]
- Patera, A.T. /s.: Orszag, S.A.; Patera, A.T. (1983)
- Pauley, W.R.; Eaton, J.K.; Cutler, A.D. (1993): Diverging boundary layers with zero streamwise pressure gradient and no wall curvature. *AIAA Journal*, Vol. 31, 2212–2219. [641]
- Pavlov, V.G. (1979): Three-dimensional self-similar laminar boundary layer with longitudinal and transverse pressure gradient. *Sov. Aeronaut.*, Vol. 22, 43–48. [337]
- Peake, D.J. /s.: Tobak, M.; Peake, D.J. (1982)
- Pechau, W. (1963): Ein Näherungsverfahren zur Berechnung der kompressiblen laminaren Grenzschicht mit kontinuierlich verteilter Absaugung. *Ing.-Arch.*, Bd. 32, 157–186. [307]
- Pedley, T.J. (1972): Two-dimensional boundary layers in a free stream which oscillates without reversing. *J. Fluid Mech.*, Vol. 55, 359–383. [367]
- Pera, L.; Gebhard, B. (1973): Natural convection boundary layer flow over horizontal and slightly inclined surfaces. *Int. Journ. Heat Mass Transfer*, Vol. 16, 1131–1146. [283]
- Peregrine, D.H. (1985): A note on the steady high-Reynolds-number flow about a circular cylinder. *J. Fluid Mech.*, Vol. 157, 493–500. [21]
- Perry, A.E. /s.: Jones, M.B.; Marusic, I.; Perry, A.E. (2001)
- Persh, J. (1956): A study of boundary-layer transition from laminar to turbulent flow. U.S. Naval Ordnance Lab. Rep. 4339. [423]
- Peterson, L.F. /s.: Hama, F.R.; Peterson, L.F. (1976)
- Pfeiffer, H. /s.: Naumann, A.; Pfeiffer, H. (1962)
- Pfenninger, W. (1946–49): Untersuchungen über Reibungsverminderung an Tragflügeln, insbesondere mit Hilfe von Grenzschichtabsaugung. Mitteilungen aus dem Institut für Aerodynamik, ETH Zürich, Nr. 13 (1946); cf. also *J. of the Aeronautical Sciences*, Vol. 16, 227–236 (1949); Investigations on reductions of friction on wings, in particular by means of boundary layer suction. NACA-TM-1181 (1947). [456]
- Pfenninger, W. (1965): Some results from the X-21A program. Part I. Flow phenomena at the leading edge of swept wings. In: AGARDograph 97, Part IV, 1–41. [456, 488]

- Phillips, O.M. (1966): The Dynamics of the Upper Ocean, Cambridge University Press. [52]
- Phoe, K.C. /s.: Finley, P.J.; Phoe, K.C.; Poh, C.J. (1966)
- Pinkerton, R.M. (1936): Calculated and measured pressure distributions over the midspan section of the NACA 4412 airfoil. NACA Report No. 563. [17]
- Piquet, J.; Visonneau, M. (1986): Inverse-mode solution of the three-dimensional boundary-layer equations about a shiplike hull: In: T. Cebeci (Ed.): Numerical and Physical Aspects of Aerodynamic Flows III, Springer-Verlag, New York, 360–379. [643]
- Pironneau, O. /s.: Mohammadi, B.; Pironneau, O. (1994)
- Pletcher, R.H. (1978): Prediction of incompressible turbulent separating flow. *J. Fluids Eng.*, Vol. 100, 427–433. [562]
- Pletcher, R.H. /s.: Anderson, D.A.; Tannehill, J.C.; Pletcher, R.H. (1984)
- Plumb, O.A. /s.: Evans, G.H.; Plumb, O.A. (1982a)
- Plumb, O.A. /s.: Evans, G.H.; Plumb, O.A. (1982b)
- Poh, C.J. /s.: Finley, P.J.; Phoe, K.C.; Poh, C.J. (1966)
- Pohlhausen, K. (1921): Zur näherungsweisen Integration der Differentialgleichung der laminaren Grenzschicht. *ZAMM. Z. angew. Math. Mech.*, Bd. 1, 252–268. [171, 196]
- Pohlhausen, K. /s.: Millsaps, K.; Pohlhausen, K. (1953)
- Poiseuille, J.L.M. (1840): Recherches expérimentelles sur le mouvement des liquides dans les tubes de très petits diamètres. *Comptes Rendus*, Vol. 11, 961–967 and 1041–1048 (1840); Vol. 12, 112–115 (1841); in more detail: *Mémoires des Savants Etrangers*, Vol. 9 (1846). [11, 103]
- Poisson, S.D. (1831): Mémoire sur les Equations générales de l'Equilibre et du Mouvement des Corps solides élastique et des Fluides. *J. de l'Ecole polytechn.*, Vol. 13, 139–186. [68]
- Pokrovskii, A.N.; Shmanenkov, V.N.; Skuchuchinov, V.M. (1984): Determination of the parameters of the boundary layer on rotating axisymmetric cones. *Fluid Dynamics*, Vol. 19, 367–372. [347]
- Poll, D.I.A. (1979): Transition in the infinite swept attachment line boundary layer. *Aeronaut. Q.*, Vol. 30, 607–629. [488]
- Poll, D.I.A. /s.: Hall, P.; Malik, M.R.; Poll, D.I.A. (1984)
- Pop, I.; Takhar, H.S. (1993): Free convection from a curved surface. *ZAMM. Z. angew. Math. Mech.*, Bd. 73, T534–T539. [271, 274]
- Pope, S.B. (2000): Turbulent Flows. Cambridge University Press. [667]
- Poppleton, E.D. (1955): Boundary layer control for high lift by suction at the leading-edge of a 40 degree swept-back wing. ARC-RM-2897. [294, 309]
- Potsch, K. (1981): Laminare Freistrahlen im Kegelraum. *Z. Flugwiss., Weltraumforsch.*, Bd. 5, 44–52. [125]
- Potsch, K. /s.: Schneider, W.; Potsch, K. (1979)
- Prabhu, A. /s.: Subaschandar, N.; Prabhu, A. (1999)
- Prager, W. (1961): Einführung in die Kontinuumsmechanik. Birkhäuser-Verlag, Basel and Stuttgart. [64, 64]
- Prahl, J.M. /s.: Starzisar, A.J.; Reshotko, E.; Prahl, J.M. (1977)
- Prandtl, L. (1904): Über Flüssigkeitsbewegungen bei sehr kleiner Reibung. *Verhandl. III. Intern. Math. Kongr. Heidelberg*, 484–491. See also: L. Prandtl: *Gesammelte Abhandlungen zur angewandten Mechanik, Hydro- und Aerodynamik*, in 3 Teilen (1961). [XXI, 29, 95, 145, 293]
- Prandtl, L. (1914): Der Luftwiderstand von Kugeln, *Nachr. Ges. Wiss. Göttingen, Math. Phys. Klasse*, 177–190; cf. also: L. Prandtl: *Gesammelte Abhandlungen zur angewandten Mechanik, Hydro- und Aerodynamik*, Bd. 2, 597–608 (1961). [XXIII, 46, 424]

- Prandtl, L. (1925): Bericht über Untersuchungen zur ausgebildeten Turbulenz. ZAMM. Z. angew. Math. Mech., Bd. 5, 136–139. [XXII, XXIV, 539]
- Prandtl, L. (1927): The generation of vortices in fluids of small viscosity. (15th Wilbur Wright Memorial Lecture 1927). Journal of the Royal Aeronautical Society, Vol. 31, 720–743. [XXIII]
- Prandtl, L.; Tietjens, O. (1929/31): Hydro- und Aeromechanik nach Vorlesungen von L. Prandtl. Bd. I: Gleichgewicht und reibungslose Bewegung (1929), Bd. II: Bewegung reibender Flüssigkeiten und technische Anwendungen (1931), Berlin. [30, 40, 42, 48, 298]
- Prandtl, L. (1933): Neuere Ergebnisse der Turbulenzforschung. Z. VDI, Bd. 77, 105–114. [441, 551]
- Prandtl, L. (1935): The mechanics of viscous fluids. In: W.F. Durand (Ed.): Aerodynamics Theory. Vol. III, Springer-Verlag, Berlin, 34–208. [XXV]
- Prandtl, L. (1938): Zur Berechnung der Grenzschichten, ZAMM. Z. angew. Math. Mech., Bd. 18, 77–82; cf. also: L. Prandtl: Gesammelte Abhandlungen zur angewandten Mechanik, Hydro- und Aerodynamik, Bd. 2, 663–672 (1961), as well as Journal of the Royal Aeronautical Society, Vol. 45, 35–40 (1941) and NACA-TM-959 (1940). [184]
- Prandtl, L. (1945): Über ein neues Formelsystem für die ausgebildete Turbulenz. Nachr. Akad. Wiss. Göttingen, Math. Phys. Klasse, 6–19. [XXIV, 343, 560, 561]
- Prandtl, L. (1961): Über Reibungsschichten bei dreidimensionalen Strömungen. Betz-Festschrift 1945, 134–141, also: L. Prandtl: Gesammelte Abhandlungen zur angewandten Mechanik, Hydro- und Aerodynamik, Bd. 2, 679–686 (1961). [338]
- Preston, J.H. /s.: Fage, A.; Preston, J.H. (1941)
- Pretsch, J. (1941a): Die laminare Reibungsschicht an elliptischen Zylindern und Rotationsellipsoiden bei symmetrischer Anströmung. Luftfahrtforschung 18, 397–402. [325]
- Pretsch, J. (1941b): Die Stabilität einer ebenen Laminarströmung bei Druckgefälle und Druckanstieg. Jb. dt. Luftfahrtforschung I, 58–75. [427, 447]
- Pretsch, J. (1942): Die Anfachung instabiler Störungen in einer laminaren Reibungsschicht. Jb. dt. Luftfahrtforschung I, 54–71. [446, 447]
- Prigogine, I. (1947): Etude thermodynamique des phénomènes irréversibles. Dunod-Desoeer. [53, 67]
- Prober, R. /s.: Stewart, W.E.; Prober, R. (1962)
- Probstein, R.F. /s.: Hayes, W.D.; Probstein, R.F. (1959)
- Quast, A. /s.: Redeker, G.; Horstmann, K.-H.; Köster, H.; Quast, A. (1988)
- Quast, A. /s.: Horstmann, K.-H.; Redeker, G.; Quast, A.; Dreßler, U.; Bieler, H. (1990)
- Quast, A. /s.: Horstmann, K.-H.; Quast, A.; Redeker, G. (1990)
- Quémard, C. /s.: Michel, R.; Quémard, C.; Durant, R. (1968)
- Raal, J.D. /s.: Hamielec, A.E.; Raal, J.D. (1969)
- Radespiel, R. (1986): Ein Berechnungsverfahren für den Triebwerksstrahl und dessen aerodynamische Wechselwirkung mit einem Heckkörper. DFVLR-FB 86–29. [563]
- Radwan, S.F.; Lekondis, S.G. (1986): Inverse mode calculations of incompressible turbulent boundary layer on an ellipsoid. AIAA Journal, Vol. 24, 1628–1635. [642, 643]
- Ragab, S.A.; Nayfeh, A.H. (1982): A comparison of the second-order triple-deck theory with interacting boundary layers. In: Cebeci, T. (Ed.): Numerical and Physical Aspects of Aerodynamic Flows, Springer-Verlag, New York, 237–258. [399]
- Raghunathan, S. (1988): Passive control of shock-boundary layer interaction. Prog. Aerospace Sci., Vol. 25, 271–296. [626]

- Rajagopalan, S. /s.: Raupach, M.R.; Antonia, R.A.; Rajagopalan, S. (1991) Rajaratnam, N. (1976): *Turbulent Jets*. Elsevier Scientific Publishing Company, Amsterdam. [663, 671, 673]
- Ramadhyani, S. (1997): Two-equation and second-moment turbulence models for convective heat transfer. In: W.J. Minkowycz; E.M. Sparrow (Eds.): *Advances in Numerical Heat Transfer*. Taylor & Francis, Washington D.C., 171–199. [610]
- Ramsey, J.A. /s.: Cebeci, T.; Kaups, K.; Ramsey, J.A. (1977)
- Rao, K.N.; Narasimha, R.; Badri Narayanan, M.A. (1971): The ‘bursting’ phenomenon in a turbulent boundary layer. *J. Fluid Mech.*, Vol. 48, 339–352. [648]
- Rastogi, A.K.; Rodi, W. (1978): Calculation of general three-dimensional turbulent boundary layers. *AIAA Journal*, Vol. 16, 151–159. [642]
- Raupach, M.R.; Antonia, R.A.; Rajagopalan, S. (1991): Rough-wall turbulent boundary layers. *Appl. Mech. Rev.*, Vol. 44, 1–25. [534]
- Rayleigh: see Lord Rayleigh.
- Reece, G.J. /s.: Launder, B.E.; Reece, G.J.; Rodi, W. (1975)
- Redeker, G.; Horstmann, K.-H.; Köster, H.; Quast, A. (1988): Investigations of high Reynolds number laminar flow airfoils. *ICAS Proceedings*, 1986, 73–85; cf. also: *Journ. Aircraft*, Vol. 25 (1988), 583–590. [456]
- Redeker, G. /s.: Horstmann, K.-H.; Quast, A.; Redeker, G. (1990)
- Redeker, G. /s.: Horstmann, K.-H.; Redeker, G.; Quast, A.; Dreßler, U.; Bieler, H. (1990)
- Redeker, G.; Horstmann, K.-H.; Köster, H.; Thiede, P.; Szodruch, J. (1990): Design for a natural flow glove for a transport aircraft. *AIAA Paper 90–3043*. [456]
- Reed, H.L. (1985): Disturbance-wave interactions in flows with crossflow. *AIAA Paper 85-0494*. [489]
- Reed, H.L. /s.: Saric, W.S.; Reed, H.L. (1986)
- Reed, H.L.; Saric, W.S. (1989): Stability of three-dimensional boundary layers. *Annu. Rev. Fluid Mech.*, Vol. 21, 235–284.
- Reed, H.L. /s.: Saric, W.S.; Reed, H.L.; Kerschen, E.J. (1994)
- Reed, H.L.; Saric, W.S.; Arnal, D. (1996): Linear stability theory applied to boundary layers. *Annu. Rev. Fluid Mech.*, Vol. 28, 389–428. [425]
- Reed, H.L. /s.: Saric, W.S.; Reed, H.L.; Kerschen, E.J. (2002)
- Reed, H.L. /s.: Saric, W.S.; Reed, H.L.; White, E.B. (2003)
- Reeves, B.L.; Kippenhan, Ch.J. (1962): On a particular class of similar solutions of the equations of motion and energy of a viscous fluid. *J. of the Aero/Space Sciences*, Vol. 29, 38–47. [109]
- Reichardt, H. (1942): Gesetzmäßigkeiten der freien Turbulenz. *VDI-Forschungsheft 414*. [666]
- Reichardt, H. (1951): Vollständige Darstellung der turbulenten Geschwindigkeitsverteilung in glatten Leitungen. *ZAMM. Z. angew. Math. Mech.*, Bd. 31, 208–219. [525]
- Reichardt, H. (1959): Gesetzmäßigkeiten der geradlinigen turbulenten Couette-Strömung. Mitteilungen aus dem Max-Planck-Institut für Strömungsforschung. Nr. 22, Göttingen. [521]
- Reid, W.H. /s.: Drazin, P.G.; Reid, W.H. (1981)
- Reik, H.G. /s.: Meixner, J.; Reik, H.G. (1959)
- Reklis, R.P. /s.: Sturek, W.B.; Dwyer, H.A.; Kayser, L.D.; Nietubicz, Ch.J.; Reklis, R.P.; Opalka, K.O. (1978)
- Renksizbulut, M. /s.: Mackinnon, J.C.; Renksizbulut, M.; Strong, A.B. (1998)
- Reshotko, E. (1958): Heat transfer at a general three-dimensional stagnation point. *Jet Propulsion*, Vol. 28, 58–60. [345]
- Reshotko, E. /s.: Lees, L.; Reshotko, E. (1962)
- Reshotko, E. /s.: Lowell, R.L.; Reshotko, E. (1974)

- Reshotko, E. (1976): Boundary layer stability and transition. *Annu. Rev. Fluid Mech.*, Vol. 8, 311–349. [425, 465, 472]
- Reshotko, E. /s.: Strazisar, A.J.; Reshotko, E.; Prahl, J.M. (1977)
- Reshotko, E. /s.: Goldberg, U.; Reshotko, E. (1984)
- Reshotko, E. (1986): Stability and Transition: What do we know? *Proc. US Congress Appl. Mech.*, 421–424. [493]
- Reshotko, E. /s.: Aships, D.E.; Reshotko, E. (1990)
- Reshotko, E. (1994): Boundary layer instability, transition and control. *AIAA Paper 94-01*. [493]
- Reshotko, E. (1997): Progress, accomplishments and issues in transition research. *AIAA Paper 97-1815*. [493]
- Reviot, T. /s.: Oertel Jr., H.; Böhle, M.; Reviot, T. (2015)
- Reynolds, A.J. /s.: El Telbany, M.M.M.; Reynolds, A.J. (1980)
- Reynolds, A.J. /s.: El Telbany, M.M.M.; Reynolds, A.J. (1981)
- Reynolds, A.J. /s.: El Telbany, M.M.M.; Reynolds, A.J. (1982)
- Reynolds, G.A.; Saric, W.S. (1986): Experiments on the stability of the flat plate boundary layer with suction. *AIAA Journal*, Vol. 24, 202–207. [460]
- Reynolds, O. (1883): An experimental investigation of the circumstances which determine whether the motion of water shall be direct or sinuous, and of the law of resistance in parallel channels. *Phil. Trans. Roy. Soc. London A*, Vol. 174, 935–982; cf. also: *Collected papers II*, 51. [XXIII, 7, 13, 415, 416]
- Reynolds, O. (1894): On the dynamic theory of incompressible viscous fluids and the determination of the criterion. *Phil. Trans. Roy. Soc. London A*, Vol. 186, 123–164; cf. also: *Collected papers I*, 355. [XXII, 424, 503]
- Reynolds, W.C. (1976): Computation of turbulent flows. *Annu. Rev. Fluid Mech.*, Vol. 8, 183–208. [XXIV, 562, 601]
- Rheinboldt, W. (1956): Zur Berechnung stationärer Grenzschichten bei kontinuierlicher Absaugung mit unstetig veränderlicher Absaugegeschwindigkeit, *J. Rat. Mech. Analysis*, Vol. 5, 539–596. [309]
- Riabouchinsky, D. (1935): Bull. de l'Institute Aerodyn. de Koutchino 5, 5-34, Moscow (1914); cf.: *Journal of the Royal Aeronautical Society*, Vol. 39, 340–348 and 377–379. [123]
- Riabouchinsky, D. (1951): Sur la résistance de frottement des disques tournant dans un fluide et les équations intégrales appliquées à ce problème. *Comptes Rendus*, Vol. 233, 899–901. [123]
- Richardson, E.G.; Tyler, E. (1929): The transverse velocity gradient near the mouths of pipes in which an alternating or continuous flow of air is established. *Proc. Phys. Soc. London*, Vol. 42, 1–15. [139]
- Richardson, P.D. /s.: Kestin, J.; Richardson, P.D. (1963)
- Richtmyer, R.D.; Morton, K.W. (1967): *Difference Methods for Initial Value Problems*. John Wiley, New York. [688, 690]
- Riddell, F.R. /s.: Fay, J.A.; Riddell, F.R. (1958)
- Riley, N. (1958): Effects of compressibility on a laminar wall jet. *J. Fluid Mech.*, Vol. 4, 615–628. [230, 326]
- Riley, N. (1963): Unsteady heat transfer for flow over a flat plate. *J. Fluid Mech.*, Vol. 17, 97–104. [368]
- Riley, N. /s.: Brown, S.N.; Riley, N. (1973)
- Riley, N. (1975): Unsteady laminar boundary layers. *SIAM Review*, Vol. 17, 274–297. [350]
- Rizzetta, D.P. /s.: Burggraf, O.R.; Rizzetta, D.P.; Werle, M.J.; Vatsa, V.N. (1979)
- Rizzetta, D.P.; Burggraf, O.R.; Jenson, R. (1978): Triple-deck solutions for viscous supersonic and hypersonic flow past corners. *J. Fluid Mech.*, Vol. 89, 535–552. [402]

- Robinson, S.K. /s.: Spina, E.; Smits, A.J.; Robinson, S.K. (1994)
- Rocklage, B. /s.: Gersten, K.; Rocklage, B. (1994)
- Rocklage, B. (1995): Selbstähnliche Lösungen für die turbulente Strömung und für den Wärmeübergang in ebenen schlanken Kanälen. ZAMM. Z. angew. Math. Mech., Bd. 75, S363–S364. [556]
- Rocklage, B. (1996): Asymptotic analysis of fully turbulent flows in slender convergent and divergent channels. In: K. Gersten (Ed.): Asymptotic Methods for Turbulent Shear Flows at High Reynolds Numbers. Kluwer Academic Publ., Dordrecht, 141–154. [556]
- Rodi, W. (1972): The prediction of free turbulent boundary layers by use of a two-equation model of turbulence. Ph.D. Thesis, Univ. of London. [655]
- Rodi, W. /s.: Launder, B.E.; Morse, A.; Rodi, W.; Spalding, D.B. (1973)
- Rodi, W. (1975): A review of experimental data of uniform density free turbulent boundary layers. In: Launder, B.E. (Ed.): Studies in Convection, Vol. 1, Academic Press, London, 79–165. [657, 675]
- Rodi, W. /s.: Launder, B.E.; Reece, G.J.; Rodi, W. (1975)
- Rodi, W. (1976): A new algebraic relation for calculating the Reynolds stresses. ZAMM. Z. angew. Math. Mech., Bd. 56, T219–T221. [568]
- Rodi, W. /s.: Rastogi, A.K.; Rodi, W. (1978)
- Rodi, W. /s.: Chen, C.J.; Rodi, W. (1980)
- Rodi, W. /s.: Launder, B.E.; Rodi, W. (1981)
- Rodi, W. /s.: Hossain, M.S.; Rodi, W. (1982)
- Rodi, W. /s.: Launder, B.E.; Rodi, W. (1983)
- Rodi, W. /s.: Patel, V.C.; Rodi, W.; Scheuerer, G. (1985)
- Rodi, W. (1991): Some current approaches in turbulence modelling. In: AGARD-R-291, 3-1 to 3-10. [571, 601, 604]
- Römer, L. /s.: Wier, M.; Römer, L. (1987)
- Rogallo, R.S.; Moin, P. (1984): Numerical simulation of turbulent flows. Annu. Rev. Fluid Mech., Vol. 16, 99–138. [571]
- Rogers, M.G.; Lance, G.N. (1960): The rotationally symmetric flow of a viscous fluid in the presence of an infinite rotating disk. J. Fluid Mech., Vol. 7, 617–631. [124]
- Roget, C.; Brazier, J.Ph.; Cousteix, J.; Mauss, J. (1998): A contribution to the physical analysis of separated flows past three-dimensional humps. Eur. J. Mech. B/Fluids, Vol. 17, 307–329. [400]
- Rosenhead, L. (1931/32): The formation of vortices from a surface of discontinuity. Proc. Roy. Soc. London A, Vol. 134, 170–192. [47]
- Rosenhead, L. /s.: Goldstein, S.; Rosenhead, L. (1936)
- Rosenhead, L.; Simpson, J.H. (1936): Note on the velocity distribution in the wake behind a flat plate placed along the stream. Proc. Cambr. Phil. Soc., Vol. 32, 285–291. [184]
- Rosenzweig, M.L. /s.: Rott, N.; Rosenzweig, M.L. (1960)
- Roshko, A. (1967): A review of concepts in separated flow. Proceedings of Canadian Congress of Applied Mechanics, Vol. 1, 3-81 to 3-115. [18]
- Roshko, A. (1976): Structure of turbulent shear flows – A new look. AIAA Journal, Vol. 14, 1349–1357. [513]
- Ross, M.A.S. /s.: Barry, M.D.J.; Ross, M.A.S. (1970)
- Rothmayer, A.P. (1987): A new interaction boundary-layer formulation for flows past bluff bodies. In: F.T. Smith, S.N. Brown (Eds): Boundary-Layer Separation, Springer-Verlag, Berlin, 197–214. [21]
- Rott, N.; Crabtree, L.F. (1952): Simplified laminar boundary layer calculations for bodies of revolution and for yawed wings. J. of the Aeronautical Sciences, Vol. 19, 553–565. [324]

- Rott, N. (1955): Unsteady viscous flow in the vicinity of a stagnation point. Quart. Appl. Math., Vol. 13, 444–451. [132, 292]
- Rott, N.; Rosenzweig, M.L. (1960): On the response of the laminar boundary layer to small fluctuations of the free-stream velocity. J. of the Aeronautical Sciences, Vol. 27, 741–747, 787. [367]
- Rott, N. (1964): Theory of time-dependent laminar flows. Princeton Univ. Series, High Speed Aerodynamics and Jet Propulsion, Vol. 4, Princeton Univ. Press, 395–438. [350]
- Rotta, J.C. (1950): Über die Theorie der turbulenten Grenzschichten. Mitteilungen aus dem Max-Planck-Institut für Strömungsforschung, Nr. 1, Göttingen. [580]
- Rotta, J.C. (1956): Experimenteller Beitrag zur Entstehung turbulenter Strömung im Rohr, Ing.-Arch., Bd. 24, 258–281. [417, 418]
- Rotta, J.C. (1959): Über den Einfluß der Machschen Zahl und des Wärmeübergangs auf das Wandgesetz turbulenter Strömung. Z. Flugwiss., Bd. 7, 264–274. [617, 619]
- Rotta, J.C. (1962): Wärmeübergangsprobleme bei hypersonischen Grenzschichten. Jb. WGLR 1962, 190–196. [263]
- Rotta, J.C. (1964): Temperaturverteilungen in der turbulenten Grenzschicht an der ebenen Platte. Int. J. Heat Mass Transfer, Vol. 7, 215–228. [569, 608]
- Rotta, J.C. /s.: Winter, K.G.; Smith, K.G.; Rotta, J.C. (1965)
- Rotta, J.C. (1970): Control of turbulent boundary layers by uniform injection and suction of fluid. Jahrbuch der DGLR, 91–104. [606]
- Rotta, J.C. /s.: Meier, H.U.; Rotta, J.C. (1971)
- Rotta, J.C. (1972): Turbulente Strömungen. B.G. Teubner Stuttgart. [515]
- Rotta, J.C. (1973): Turbulent shear layer prediction on the basis of the transport equations for the Reynolds stresses. In: E. Becker, G.Y. Mikhailov (Eds.): Theoretical and Applied Mechanics. Proc. XIII, Int. Congr. Theor. Appl. Mech., Springer-Verlag, Berlin, 295–308. [XXIV]
- Rotta, J.C. (1975): Prediction of turbulent shear flows using the transport equations for turbulence energy and turbulence length scale. VKI Lecture Series No. 76. [588]
- Rotta, J.C. /s.: Vollmers, H.; Rotta, J.C. (1977)
- Rotta, J.C. (1979): A family of turbulence models for three-dimensional boundary layers. In: F. Durst et al. (Eds.): Turbulent Shear Flows 1, Springer-Verlag, Berlin, 267–278. [642]
- Rotta, J.C. (1980a): A theoretical treatment of the free stream turbulence effects on the turbulent boundary layer, DFVLR IB 251 80 A 06. [604]
- Rotta, J.C. (1980b): On the effect of the pressure strain correlation on the three-dimensional turbulent boundary layers, In: F. Durst et al. (Eds.): Turbulent Shear Flows 2, Springer-Verlag, Berlin, 17–24. [567, 642]
- Rotta, J.C. (1983): Einige Gesichtspunkte zu rationeller Berechnung turbulenter Grenzschichten. Z. Flugwiss. Weltraumforsch., Bd. 7, 417–429. [563, 696, 700]
- Rotta, J.C. (1986): Experience of second order turbulent flow closure models. Z. Flugwiss. Weltraumforsch., Bd. 10, 401–407. [564, 588, 601]
- Rotta, J.C. (1991): Über die Entwicklung der Berechnungsmethoden für turbulente Strömungen. Z. Flugwiss. Weltraumforsch., Bd. 15, 275–284. [567, 601]
- Rouse, H. (1943): Evaluation of boundary roughness. Proc. of the II Hydraulics Conf.; Univ. of Iowa (Iowa City), Univ. of Iowa studies in engineering, Vol. 27, 105–116. [552, 552]
- Roy, D. (1961): Non-steady periodic boundary layer. Z. angew. Math. Phys. (ZAMP), Vol. 12, 363–366. [365]
- Roy, D. (1962): On the non-steady boundary layer. ZAMM. Z. angew. Math. Mech., Bd. 42, 255–256. [365]

- Rozhdestvensky, B.L.; Simakin, L.N. (1982): Nonstationary flows in a plane channel and stability of the Poiseuille flow with respect to finite disturbances. Dokl. Acad. Nauk USSR, Vol. 266, 1337–1340, [in Russian]. [416]
- Rozhdestvensky, B.L.; Simakin, L.N. (1984): Secondary flows in a plane channel: their relationship and comparison with turbulent flows. J. Fluid Mech., Vol. 147, 261–289. [416]
- Rozin, L.A. (1960): An approximation method for the integration of the equations of a nonstationary laminar boundary layer in an incompressible fluid. NASA Techn. Transl. 22. [354]
- Ruban, A. /s.: Sychev, V. V.; Ruban, A. I.; Sychev, V. V.; Korolev, G. L. (1998)
- Ruban, A.I. (1991): Marginal separation theory. In: V.V. Kozlov; A.V. Dovgal (Eds.): Separated Flows and Jets. Springer-Verlag, New York, 47–54. [403]
- Ruban, A.I. /s.: Sychev, V.V. et al. (1998)
- Rubel, A. /s.: Melnik, R.E.; Rubel, A. (1983)
- Rubesin, M.W. (1976): A one-equation model of turbulence for use with the compressible Navier-Stokes equations. NASA-TM-X-73128. [562]
- Rubesin, M.W. /s.: Ha Minh, H.; Viegas, J.R.; Rubesin, M.W.; Vandromme, D.D.; Spalart, P.R. (1989)
- Rubin, S.G.; Falco, R. (1968): Plane laminar jet. AIAA Journal, Vol. 6, 186–187. [387]
- Rudy, D.H.; Bushnell,D.M. (1973): A rational approach to the use of Prandtl's mixing length model in free turbulent shear flow calculations. In: Free Turbulent Shear Flows, NASA-SP-321, 67–137. [659]
- Rydberg, A. /s.: Luthander, S.; Rydberg, A. (1935)
- Ryzhov, O.S.; Zhuk, V.I. (1980): Internal waves in the boundary layer with the self-induced pressure. Jurnal de Mecanique, Vol. 19, 561–580. [400]
- Sabin C.M. (1963): An analytical and experimental study of the plane, incompressible turbulent shear layer with arbitrary velocity ratio and pressure gradient. Dept. Mech. Eng. Stanford Univ. Report MD-9. [668]
- Saffman, P.G. (1983): Vortices, stability and turbulences. Annals of the New York Academy of Sciences, Vol. 404, 12-24. [416]
- Saffman, P.G. (1988): Two dimensional superharmonic stability of finite-amplitude waves in plane Poiseuille flow. J. Fluid Mech., Vol. 194, 295–307. [416]
- Sakagami, J. /s.: Tani, I.; Sakagami, J. (1964)
- Saljnikov, V.; Dallmann, U. (1989): Verallgemeinerte Ähnlichkeitslösungen für dreidimensionale, laminare, stationäre, kompressible Grenzschichtströmungen an schiebenden profilierten Zylindern. DLR-FB 89-34. [342]
- Salter, C. /s.: Simmons, L.F.G.; Salter, C. (1938)
- Sammakia, B. /s.: Gebhart, B.; Jaluria, Y.; Mahajan, R.L.; Sammakia, B. (1988)
- Sandham, N. /s.: Launder, B.; Sandham, N. (2002)
- Sandner, H. /s.: Grigull, U.; Sandner, H. (1986)
- Sargent, L.M. /s.: Klebanoff, P.S.; Tidstrom, K.D.; Sargent, L.M. (1962)
- Saric, W.S. /s.: Floryan, J.M.; Saric, W.S. (1979)
- Saric, W.S. /s.: Floryan, J.M.; Saric, W.S. (1982)
- Saric, W.S.; Kozlov, V.V.; Levchenko, V.Y. (1984): Forced and unforced subharmonic resonance in boundary-layer transition. AIAA Paper No. 84-0007. [492]
- Saric, W.S.; Yeates, L.G. (1985): Generation of crossflow vortices in a three-dimensional flat-plate flow. In: Kozlov, V.V. (Ed.) (1985): Laminar-Turbulent Transition. Springer-Verlag, Berlin, 429–437. [487, 490]
- Saric, W.S. /s.: Reynolds, G.A.; Saric, W.S. (1986)
- Saric, W.S.; Reed, H.L. (1986): Effect of suction and weak mass injection on boundary layer transition. AIAA Journal, Vol. 24, 383–389. [460]

- Saric, W.S. (1990): Low-speed experiments: Requirements for stability measurements. In: Hussaini, M.Y.; Voigt, R.G. (Eds.): Instability and Transition, Vol. 1, Springer-Verlag, New York, 162–174. [443]
- Saric, W.S. (1994): Görtler vortices. Annu. Rev. Fluid Mech., Vol. 26, 379–409. [475, 484]
- Saric, W.S.; Reed, H.L.; Kerschen, E.J. (1994): Leading-edge receptivity to sound: experiments, DNS, theory. AIAA Paper 94-2222. [492]
- Saric, W.S. /s.: Reed, H.L.; Saric, W.S.; Arnal, D. (1996)
- Saric, W.S.; Reed, H.L.; Kerschen, E.J. (2002): Boundary-layer receptivity to freestream disturbances. Annu. Rev. Fluid Mech., Vol. 34, 291–319. [492]
- Saric, W.S.; Reed, H.L.; White, E.B. (2003): Stability and transition of three-dimensional boundary layers. Annu. Rev. Fluid Mech. Vol. 35, 413-440. [492]
- Sarkar S.; Lakshmanan B. (1991): Application of a Reynolds stress turbulence model to the compressible shear layer. AIAA Journal, Vol. 29, 743–749. [669, 670]
- Sarpkaya, T. (1975): An inviscid model of two-dimensional vortex shedding for transient and asymptotically steady separated flow over an inclined plate. Z. Flugtech. Motor-Luftschiffahrt: ZFM, Vol. 68, 109–128. [47]
- Saunders, P.T. (1980): An Introduction to Catastrophe Theory. Cambridge University Press, Cambridge. [399, 406]
- Savage, S.B.; Chan, G.K.C. (1970): The buoyant two-dimensional laminar vertical jet. Q. J. Mech. Appl. Math., Vol. 23, 413–430. [289]
- Saville, D.A.; Churchill, S.W. (1967): Laminar free convection in boundary layers near horizontal cylinders and vertical axisymmetric bodies. J. Fluid Mech., Vol. 29, 391–399. [270, 325]
- Sawaki, Y. /s.: Nakamura, I.; Yamashita, S.; Watanabe, T.; Sawaki, Y. (1981)
- Sawyer, R.A. (1963): Two-dimensional reattaching jet flows including the effects of curvature on entrainment. J. Fluid Mech., Vol. 17, 481–498. [666]
- Schaaf, S.A. (1958): Mechanics of rarefied gases. In: S. Flügge (Hrsg.): Handbuch der Physik. Bd. VIII/2. Strömungsmechanik II, Springer-Verlag, Berlin, 591–624. [51]
- Schaaf, S.A.; Chambré, P.L. (1958): Flow of rarefied gases. In: H.W. Emmons (Ed.): High Speed Aerodynamics and Jet Propulsion, Vol. 3, Princeton Univ. Press, Princeton, N.J.. 687–739. [75]
- Schäfer, P. /s.: Herwig, H.; Schäfer, P. (1992)
- Schäfer, P.; Severin, J.; Herwig, H. (1994): The effect of heat transfer on the stability of laminar boundary layers. Int. J. Heat Mass Transfer, Vol. 38, 1855–1863. [462]
- Schäfer, P. (1995): Untersuchungen von Mehrfachlösungen bei laminaren Strömungen. Dissertation, Ruhr Universität Bochum. [397, 398, 399]
- Schaedel H.M. (1979): Fluidische Bauelemente und Netzwerke. Vieweg-Verlag, Braunschweig. [667]
- Scheichl, B. (2001): Asymptotic theory of marginal turbulent separation. Ph.D. thesis, Technical University Vienna. [602]
- Scheichl, B.; Kluwick, A. (2007a): On turbulent marginal boundary layer separation: how the half-power law supersedes the logarithmic law of the wall. Int. J. Computing Science and Mathematics, Vol. 1, 343-359. [602]
- Scheichl, B.; Kluwick, A. (2007b): Turbulent marginal separation and the turbulent Goldstein problem. AIAA Journal, Vol. 45, 20-36. [602]
- Scheichl, B.; Kluwick, A.; Alletto, M. (2008): “How turbulent” is the boundary layer separating from a bluff body for arbitrarily large Reynolds Numbers? Acta Mechanica, Vol. 201, 131-151. [602]

- Scheichl, B.; Kluwick, A.; Smith, F.T. (2011): Break-away separation for high turbulence intensity and large Reynolds number. *J. Fluid Mech.* Vol. 670, 260–300. [602]
- Scheichl, B.; Kluwick, A.; Alletto, M. (2008): “How turbulent” is the boundary layer separating from a bluff body for arbitrarily large Reynolds Numbers? *Acta Mechanica*, Vol. 201, 131–151. [602]
- Scheichl, B.; Kluwick, A.; Smith, F.T. (2011): Break-away separation for high turbulence intensity and large Reynolds number. *J. Fluid Mech.* Vol. 670, 260–300. [602]
- Scheichl, S.; Braun, S.; Kluwick, A. (2008): On a similarity solution in the theory of unsteady marginal separation. *Acta Mechanica*, Vol. 201, 153–170. [409]
- Scherrer, R. (1951): Comparison of theoretical and experimental heat transfer characteristics of bodies of revolution of supersonic speeds. NACA-TR-1055. [326]
- Scheuerer, G. /s.: Patel, V.C.; Scheuerer, G. (1982)
- Scheuerer, G. /s.: Patel, V.C.; Rodi, W.; Scheuerer, G. (1985)
- Schewe, G. /s.: Dinkelacker, A.; Hessel, M.; Meier, G.E.A.; Schewe, G. (1977)
- Schilawa, S. /s.: Gersten, K.; Schilawa, S. (1978)
- Schilawa, S. /s.: Gersten, K.; Schilawa, S.; Schulz-Hausmann, F.K. von (1980)
- Schilawa, S. (1981): Auftriebseffekte in laminaren Grenzschichten an horizontalen Wänden. Dissertation, Ruhr-Universität Bochum. [222, 289]
- Schiller, L. (1922): Untersuchungen über laminare und turbulente Strömung. *Forschg. Ing.-Wes.*, Heft 428, or *ZAMM. Z. angew. Math. Mech.*, Bd. 2, 96–106, or *Physikal. Z.*, Bd. 33, 14. [417]
- Schiller, L. (1934): Neue quantitative Versuche zur Turbulenzentstehung. *ZAMM. Z. angew. Math. Mech.*, Bd. 14, 36–42. [440]
- Schllichting, H. (1930): Über das ebene Windschattenproblem. *Ing.-Archiv*, Bd. 1, 533–571. [670]
- Schllichting, H. (1932): Berechnung ebener periodischer Grenzschichtströmungen. *Physikal. Z.*, Bd. 33, 327–335. [362, 364]
- Schllichting, H. (1933): Zur Entstehung der Turbulenz bei der Plattenströmung. *Nachr. Ges. Wiss. Göttingen, Math. Phys. Klasse*, 182–208; cf. also: *ZAMM. Z. angew. Math. Mech.*, Bd. 13 (1933), 171–174. [XXIII, 438]
- Schllichting, H. (1935a): Amplitudenverteilung und Energiebilanz der kleinen Störungen bei der Plattenströmung. *Nachr. Ges. Wiss. Göttingen. Math. Phys. Klasse, Fachgruppe I*, 1, 47–78. [439]
- Schllichting, H. (1935b): Turbulenz bei Wärmeschichtung. *ZAMM. Z. angew. Math. Mech.*, Bd. 15, 313–338. [473]
- Schllichting, H. (1936): Experimentelle Untersuchungen zum Rauhigkeitsproblem. *Ing.-Arch.*, Bd. 7, 1–34. [532, 533]
- Schllichting, H.; Ulrich, A. (1940–42): Zur Berechnung des Umschlages laminar-turbulent. *Jb. dt. Luftfahrtforschung I*, 8–35. Preisausschreiben 1940 der Lilienthal-Gesellschaft für Luftfahrtforschung, Flugzeugbau. Complete version in report S10 of the Lilienthal-Gesellschaft 75–135 (1940). [448]
- Schllichting, H.; Bussmann, K. (1943): Exakte Lösungen für die laminare Reibungsschicht mit Absaugung und Ausblasen. *Schriften der dt. Akad. d. Luftfahrtforschung 7B*, Nr. 2. [303]
- Schllichting, H. (1943/44): Die Beeinflussung der Grenzschicht durch Absaugen und Ausblasen. *Jb. dt. Akad. d. Luftfahrtforschung*, p. 90–108. [303]
- Schllichting, H. (1948): Ein Näherungsverfahren zur Berechnung der laminaren Reibungsschicht mit Absaugung. *Ing.-Arch.* Bd. 16, 201–220, cf. also NACA TM 1216 (1949). [307]
- Schllichting, H. (1950): Über die Theorie der Turbulenzentstehung. Zusammenfassender Bericht. *Forsch. Ing.-Wes.*, Bd. 16, 65–78. [425]
- Schllichting, H.; Truckenbrodt, E. (1952): Die Strömung an einer angestromten rotierenden Scheibe. *ZAMM. Z. angew. Math. Mech.*, Bd. 32, 97–111. [328, 329]

- Schlichting, H. (1953): Die laminare Strömung um einen axial angestromten rotierenden Drehkörper. *Ing.-Arch.*, Bd. 21, 227–244. [328]
- Schlichting, H. (1954): Aerodynamische Untersuchungen an Kraftfahrzeugen, Berichtsband der Technischen Hochschule Braunschweig, 130–139. [43]
- Schlichting, H. (1959): Entstehung der Turbulenz. In: S. Flügge (Hrsg.): Handbuch der Physik, Bd. VIII/1: Strömungsmechanik 1, Springer-Verlag, Berlin, 351–450. [425]
- Schlichting, H. (1960): Some developments of boundary layer research in the past thirty years (The Third Lanchester Memorial Lecture 1959). *Journal of the Royal Aeronautical Society*. Vol. 64, 63–80. [XXV]
- Schlichting, H. (1961): Three-dimensional boundary layer flow. Lecture at the IX. Convention of the International Association for Hydraulic Research at Dubrovnik/Yugoslavia, Sept. 1961. Proceedings of the “Neuvième Assemblée Générale de l’Association Internationale de Recherches Hydrauliques” Dubrovnik, 1262–1290; see also: DFL-Bericht Nr. 195. [341]
- Schlichting, H.; Gersten K. (1961): Berechnung der Strömung in rotationssymmetrischen Diffusoren mit Hilfe der Grenzschichttheorie. *Z. Flugwiss.*, Bd. 9, 135–140. [634]
- Schlichting, H. (1965a): Grenzschicht-Theorie. Braun-Verlag, Karlsruhe, 5. Auflage. [185]
- Schlichting, H. (1965b): Aerodynamische Probleme des Höchstauftriebes. *Z. Flugwiss.*, Bd. 13, 1–14. [294]
- Schlichting, H.; Truckenbrodt, E. (1979): Aerodynamics of the Airplane. McGraw-Hill, New York. [16]
- Schlichting, H. (1982): Grenzschicht-Theorie. Braun-Verlag, Karlsruhe, 8. Auflage. [10, 11, 19, 24, 47, 117, 182, 201, 225, 247, 250, 258, 274, 331, 354, 361, 385, 457, 473, 508, 663, 670, 675, 676, 692, 701]
- Schmatz, M.A. (1986): Calculation of strong viscous/inviscid interactions on airfoils by zonal solutions of the Navier-Stokes equations. In: D. Rues; W. Kordulla (Eds.): Proceedings 6th GAMM-Conference on Numerical Methods in Fluid Mechanics – Notes on Numerical Fluid Mechanics, Vol. 13, Vieweg, Braunschweig-Wiesbaden, 335–342. [18]
- Schmidt, E.; Wenner, K. (1941): Wärmeabgabe über den Umfang eines angeblasenen geheizten Zylinders. *Forschg. Ing.-Wes.*, Bd. 12, 65–73. [225]
- Schmidt, J. /s.: Schneider, W.; Eder, R.; Schmidt, J. (1990)
- Schmidt, P.J.; Henningson, D.S (2000): Stability and Transition. Springer, New York.
- Schmidt, W. (1921): Ein einfaches Meßverfahren für Drehmomente, *Z. VDI*, Bd. 65, 411–444. [123]
- Schneider, G.R.; Zhu, Z. (1982): The calculation of incompressible three-dimensional laminar and turbulent boundary layers in the plane of symmetry of a prolate spheroid at incidence. DFVLR-FB 82-16. [345]
- Schneider, M.E.; Goldstein, R.J. (1994): Laser Doppler measurement of turbulence parameters in a two-dimensional plane wall jet. *Phys. Fluids* Vol. 6, 3116-3129. [677]
- Schneider, W. (1968): Grundlagen der Strahlungsgasdynamik. *Acta Mechanica*, Vol. 5, 87–117. [69, 264]
- Schneider, W. (1974a): Radiation gasdynamics of planetary entry. *Astronautica Acta*, Vol. 18 (Suppl.), 193–213. [264]
- Schneider, W. (1974b): Upstream propagation of unsteady disturbances in supersonic boundary layers. *J. Fluid Mech.*, Vol. 63, 465–485. [400]
- Schneider, W. (1975): Über den Einfluß der Schwerkraft auf anisotherme, turbulente Freistrahlen. *Abhandl. Aerodyn. Inst. RWTH Aachen*, Heft 22, 59–65. [676]
- Schneider, W. (1976): Strahlungseffekte in Ein- und Mehrphasenströmungen. *ZAMM. Z. angew. Math. Mech.*, Bd. 56, T21–T36. [264]

- Schneider, W. (1978): Mathematische Methoden der Strömungsmechanik. Vieweg-Verlag, Braunschweig. [XXIII]
- Schneider, W. (1979): A similarity solution for combined forced and free convection flow over a horizontal plate. Int. J. Heat Mass Transfer, Vol. 22, 1401–1406. [288]
- Schneider, W.; Potsch, K. (1979): Weak buoyancy in laminar vertical jets. In: U. Müller; K.G. Roesner; B. Schmidt (Eds.): Recent Developments in Theoretical and Experimental Fluid Mechanics. Springer-Verlag, Berlin, Heidelberg, 501–510. [334]
- Schneider, W. (1980): Radiation effects in single-phase and multiphase flow. In: F.P.J. Rimrott; B. Tabarrok (Eds.): Proceedings of the 15th International Congress of Theoretical and Applied Mechanics, North Holland Publ. Comp., Amsterdam, etc., 175–188. [264]
- Schneider, W. /s.: Fleischhacker, G.; Schneider, W. (1980)
- Schneider, W. (1981): Flow induced by jets and plumes. J. Fluid Mech., Vol. 108, 55–65. [125]
- Schneider, W. /s.: Mitsotakis, K.; Schneider, W.; Zauner, E. (1984)
- Schneider, W. (1985): Decay of momentum flux in submerged jets. J. Fluid Mech., Vol. 154, 91–110. [333, 666]
- Schneider, W.; Wasel, M.G. (1985): Breakdown of the boundary-layer approximation for mixed convection above a horizontal plate. Int. J. Heat Mass Transfer, Vol. 28, 2307–2313. [288]
- Schneider, W. /s.: Mörwald, K.; Mitsotakis, K.; Schneider, W. (1987)
- Schneider, W.; Mörwald, K. (1987): Asymptotic analysis of turbulent free shear layers. In: Proc. Int. Conf. Fluid Mech., Beijing Univ. Press, 50–55. [655]
- Schneider, W.; Zauner, E.; Böhm, H. (1987): The recirculatory flow induced by a laminar axisymmetric jet issuing from a wall. J. Fluids Engineering, Vol. 109, 237–241. [333]
- Schneider, W. (1989a): On Reynolds stress transport in turbulent Couette flow. Z. Flugwiss. Weltraumforsch., Bd. 13, 315–319. [561]
- Schneider, W. (1989b): On modelling the transport of turbulent kinetic energy in Couette flow. ZAMM. Z. angew. Math. Mech., Bd. 69, T627–T629. [540, 561]
- Schneider, W.; Eder, R. Schmidt, J. (1990): Turbulent Couette flow: Asymptotics vs. experimental data. In: Proc. 3rd Intl. Congress Fluid Mech., Cairo, Vol. IV, 1593–1599. [561]
- Schneider, W. (1991): Boundary-layer theory of free turbulent shear flows. Z. Flugwiss. Weltraumforsch. Bd. 15, 143–158. [XXIV, 653, 655, 663, 666, 676]
- Schneider, W.; Steinrück, H.; Andre, G. (1994): The breakdown of boundary layer computations in the case of the flow over a cooled horizontal flat plate. ZAMM. Z. angew. Math. Mech., Bd. 74, T402–404. [288]
- Schneider, W. (1995): Laminar mixed convection flows on horizontal surfaces. Proc. 3rd Caribbean Congress on Fluid Dynamics, Vol. II, Bolivar University, Caracas. [289]
- Schneider, W. /s.: Haas, S.; Schneider, W. (1996)
- Schneider, W. /s.: Haas, S.; Schneider, W. (1997)
- Schneider, W. /s.: Noshadi, V.; Schneider, W. (1998)
- Schneider, W. /s.: Noshadi, V.; Schneider, W. (1999)
- Schneider, W. (2000): Mixed convection at a finite horizontal plate. In E.W.P. Hahne et al. (Eds.), Proc. 3rd European Thermal Sciences Conf. Edizioni ETS, Pisa, 195–198. [289]
- Schneider, W. (2001): Peculiarities of boundary layer flows over horizontal plates. In: I.C. Misra (Ed.): Applicable mathematics, Narosa Publ. House, New Delhi, 118–123. [288]
- Schneider, W. (2005): Lift, Thrust and heat transfer due to mixed convection flow past a horizontal plate of finite length. J. Fluid Mech., Vol. 529, 51–69. [289]

- Schneider, W. /s.: Müllner, M.; Schneider, W. (2010)
- Schober, M. /s.: Fernholz, H.H.; Krause, E.; Nockemann, M.; Schober, M. (1995)
- Schoenherr, K.E. (1932): Resistance of plates. Transactions Society Naval Architects Marine Eng., Vol. 40. [10]
- Schönauer, W. (1963): Die Lösung der Crocco'schen Grenzschichtdifferentialgleichung mit dem Differenzenverfahren für stationäre, laminare, inkompressible Strömung. Dissertation der TH Karlsruhe. [184, 203, 205]
- Schönung, B.E. /s.: Franke, R.; Schönung, B.E. (1988)
- Schönung, B.E. (1990): Numerische Strömungsmechanik. Springer-Verlag, Berlin/Heidelberg. [101]
- Scholkemeyer, F.W. (1949): Die laminare Reibungsschicht an rotationssymmetrischen Körpern. Diss. Braunschweig 1943. Excerpt in Arch. d. Math., Bd. 1, 270–277. [324]
- Scholz, N. (1951): Über eine rationelle Berechnung des Strömungswiderstandes schlanker Körper mit beliebig rauher Oberfläche. Jb. Schiffbautechn. Ges., Bd. 45, 244–259. [671]
- Schrenk, O. (1935): Versuche mit Absaugeflügeln. Luftfahrtforschung, Bd. 12, 10–27. [48, 294]
- Schubauer, G.B.; Skramstad, H.K. (1943–48): Laminar-boundary-layer oscillations and transition on a flat plate. National Bureau of Standards Research Paper 1772. Reprint of a confidential NACA report from April 1943 (later released as NACA-WR-W-8); H.K. Skramstad (1943): Laminar-boundary-layer oscillations and transition on a flat plate; see also: J. of the Aeronautical Sciences, Vol. 14, 69–78 (1947); cf. also NACA-TR-909 (1948). [439, 443, 444, 447, 455, 470, 473, 515]
- Schubauer, G.B.; Klebanoff, P.S. (1955): Contributions on the mechanics of boundary layer transition. NACA-TN-3489 (1955) and NACA-TR-1289 (1956); cf. also: Proc. Symposium on Boundary Layer Theory. Nat. Phys. Lab. England 1955. [421, 422, 422, 423, 426]
- Schuh, H. (1953): Calculation of unsteady boundary layers in two-dimensional laminar flow. Z. Flugwiss., Bd. 1, 122–131. [354]
- Schuh, H. (1955): Über die “ähnlichen” Lösungen der instationären laminaren Grenzschichtgleichungen in inkompressibler Strömung. In: H. Görtler; W. Tollmien (Hrsg.): Fünfzig Jahre Grenzschichtforschung, Braunschweig, 147–152. [352]
- Schulenberg, T. (1984): Natural convection heat transfer below downward facing horizontal surfaces. Int. J. Heat Mass Transfer, Vol. 28, 467–477. [288]
- Schulte-Werning B.; Dallmann U. (1991): Numerical simulation of the vortex chain formation by vorticity shedding from a sphere into the wake. In: V.V. Kozlov, A.V. Dorgal (Eds.): Separated Flows and Jets. Springer-Verlag, Berlin, 167–170. [25]
- Schultz-Grunow, F.; Henseler, H. (1968): Ähnliche Grenzschichtlösungen zweiter Ordnung für Strömungs- und Temperaturgrenzschichten an longitudinal gekrümmten Wänden mit Grenzschichtbeeinflussung. Wärme- und Stoffübertrag., Bd. 1, 214–219. [386]
- Schultz-Grunow, F.; Behbahani, D. (1973): Boundary layer stability at longitudinally curved walls. Z. angew. Math. Phys. (ZAMP), Vol. 24, 499–506 (1973); Z. angew. Math. Phys. (ZAMP), Vol. 26, 493–495 (1975). [483]
- Schulz-Hausmann, F.K. von /s.: Gersten, K.; Schilawa, S.; Schulz-Hausmann, F.K. von (1980)
- Schulz-Hausmann, F.K. von (1985): Wechselwirkung ebener Freistrahlen mit der Umgebung. Fortschr.-Ber. VDI Reihe 7, Nr. 100, VDI-Verlag, Braunschweig. [665, 666]

- Schumann, U.; Friedrich, R. (Eds.) (1986): Direct and Large Eddy Simulation of Turbulence. Notes on Numerical Fluid Mechanics, Vol. 15., Vieweg-Verlag, Braunschweig. [571, 572]
- Schumann, U.; Friedrich, R. (1987): On direct and large eddy simulation of turbulence. In: Comte-Bellot, G.; Mathieu, J. (Eds.): Advances in Turbulence, Springer-Verlag, Berlin, 88–104. [572]
- Schwabe, M. (1935): Über Druckermittlung in der instationären ebenen Strömung. Ing.-Arch., Bd. 6, 34–50; NACA-TM-1039 (1943). [358]
- Schwamborn, D. (1981): Laminare Grenzschichten in der Nähe der Anlegelinie an Flügeln und flügelähnlichen Körpern mit Anstellung. DFVLR-FB 81-31. [347]
- Schwamborn, D. (1984): Boundary layers on wings. In: Notes on Numerical Fluid Mechanics, Vol. 7, Vieweg-Verlag, Braunschweig, 315–323. [346]
- Schwartz, W.H.; Caswell, B. (1961): Some heat transfer characteristics of the two-dimensional laminar incompressible wall jet. Chemical Engineering Science, Vol. 16, 338–351. [222]
- Schwarz, W.R.; Bradshaw, P. (1993): Measurements in a pressure-driven three-dimensional turbulent boundary layer during development and decay. AIAA Journal, Vol. 31, 1207–1214. [643]
- Scott, P.E. /s.: Baron, J.R.; Scott, P.E. (1960)
- Sears, W.R. (1948): The boundary layer of yawed cylinders. J. of the Aeronautical Sciences, Vol. 15, 49–52. [343]
- Sears, W.R. (1954): Boundary layers in three-dimensional flow. Appl. Mech. Rev., Vol. 7, 281–285. [341, 347]
- Sears, W.R. (1956): Some recent developments in airfoil theory. Journal of the Royal Aeronautical Society, Vol. 23, 490–499. [292]
- Sears, W.R.; Telionis, D.P. (1972): Unsteady boundary-layer separation. In: E.A. Eichelbrenner (Ed.): Recent Research of Unsteady Boundary Layers, Vol. 1, Les Presses de l'Université Laval, Quebec, 1972, 404–447. [354]
- Sedney, R. (1957): Laminar boundary layer on a spinning cone at small angles of attack in a supersonic flow. J. of the Aeronautical Sciences, Vol. 24, 430–436, 455. [339, 347]
- Seiferth, R.; Krüger, W. (1950): Überraschend hohe Reibungsziffer einer Fernwasserleitung. Z. VDI, Bd. 92, 189–191. [534]
- Sengupta, T.K. (2012): Instabilities of Flows and Transition to Turbulence. CRC Press Taylor & Francis Group. [XXV, 479]
- Senoo, Y. (1982): Three-dimensional boundary layers in turbomachines. In: H.H. Fernholz, E. Krause (Eds.): Three-Dimensional Turbulent Boundary Layers. Springer-Verlag, Berlin, 149–164. [643]
- Settles, G.S. /s.: Kim, K.-S.; Settles, G.S. (1989)
- Settles, G.S.; Dodson, L.J. (1994): Supersonic and hypersonic shock/boundary-layer interaction database. AIAA Journal, Vol. 32, 1377–1383. [625]
- Severin, J. /s.: Schäfer, P.; Severin, J.; Herwig, H. (1994)
- Severin, J.; Herwig, H. (2001): Higher order stability effects in natural convection boundary layer over a vertical heated wall. Heat and Mass Transfer, Vol. 38, 97–110. [473]
- Shah, R.K.; London, A.L. (1978): Laminar Flow Forced Convection in Ducts. Advances in Heat Transfer, Supplement 1, Academic Press, New York. [117]
- Sharma, V.P. /s.: Singh, P.; Sharma, V.P.; Misra, U.N. (1981)
- Shen, S.F. (1954): Calculated amplified oscillations in plane Poiseuille and Blasius flows. J. of the Aeronautical Sciences, Vol. 21, 62–64. [438]
- Shen, S.F.; Nenni, J.P. (1975): Asymptotic solution of the unsteady two-dimensional incompressible boundary layer and its implications on separation. In: R.B. Kinney (Ed.): Unsteady Aerodynamics, Proceedings of a Symposium, held at the University of Arizona 1975, Arizona, Vol. I, 245–259. [354]

- Shen, S.F. (1978): Unsteady separation according to the boundary layer equation. Advances in Applied Mechanics, Vol. 18, 177–220. [354]
- Shen, S.F. /s.: Van Dommelen, L.L; Shen, S.F. (1982)
- Shen, S.F. /s.: Wu, T.; Shen, S.F. (1992)
- Shercliff, J.A. (1965): A Textbook of Magnetohydrodynamics, Pergamon Press, Oxford. [70]
- Sherman, F.S. (1990): Viscous Flow, McGraw-Hill Publ. Comp., New York. [124]
- Shih, T.-H.; Lumley, J.L.; Chen, J.-Y. (1990): Second-order modeling of a passive scalar in a turbulent shear flow. AIAA Journal, Vol. 28, 610–617. [664]
- Shivaprasad, B.G. /s.: Simpson, R.L.; Chew, Y.-T.; Shivaprasad, B.G. (1981)
- Shmanenkov, V.N. /s.: Pokrovskii, A.N.; Shmanenkov, V.N.; Skchuchinov, V.M. (1984)
- Shur, M. /s.: Spalart, P.R., Shur, M. (1997)
- Siekmann, J. (1962): The laminar boundary layer along a flat plate. Z. Flugwiss., Bd. 10, 278–281. [292]
- Simakin, L.N. /s.: Rozhdestvensky, B.L.; Simakin, L.N. (1982)
- Simakin, L.N. /s.: Rozhdestvensky, B.L.; Simakin, L.N. (1984)
- Simmons, L.F.G.; Salter, C. (1938): An experimental determination of the spectrum of turbulence. Proc. Roy. Soc. London A 165, 73–89. [512]
- Simpson, J.H. /s.: Rosenhead, L.; Simpson, J.H. (1936)
- Simpson, R.L. (1975): Characteristics of a separating incompressible turbulent boundary layer. In: Flow Separation. In: AGARD-CP-168, 14-1 to 14-14. [567, 615]
- Simpson, R.L.; Chew, Y.-T.; Shivaprasad, B.G. (1981): The structure of a separating turbulent boundary layer. Part 1. Mean flow and Reynolds stresses. J. Fluid Mech., Vol. 113, 23–51. [598]
- Simpson, R.L. (1985): Two-Dimensional Turbulent Separated Flow. AGARD-AG-287. [602]
- Simpson, R.L. /s.: Ölçmen, M.S.; Simpson, R.L. (1992)
- Simpson, R.L. /s.: Ölçmen, M.S.; Simpson, R.L. (1993)
- Singh, K.D. (1993): Three-dimensional viscous flow and heat transfer along a porous plate. ZAMM. Z. angew. Math. Mech., Bd. 73, 58–61. [342]
- Singh, P.; Sharma, V.P.; Misra, U.N. (1981): Transient three-dimensional flow along a porous plate. Acta Mechanica, Vol. 38, 183–190. [342]
- Skan, S.W. /s.: Falkner, V.M.; Skan, S.W. (1930)
- Skchuchinov, V.M. /s.: Pokrovskii, A.N.; Shmanenkov, V.N.; Skchuchinov, V.M. (1984)
- Skoog, R.B. /s.: Zalovcik, J.A.; Skoog, R.B. (1945)
- Skramstad, H.K. /s.: Schubauer, G.B.; Skramstad, H.K. (1943–47)
- Smith, A.G.; Spalding, D.B. (1958): Heat transfer in a laminar boundary layer with constant fluid properties and constant wall temperature. Journal of the Royal Aeronautical Society, Vol. 62, 60–64. [225]
- Smith, A.M.O. (1957–59): Transition pressure gradient and stability theory. Paper presented at the IX. Intern. Congress of Appl. Mech., Vol. 4, 234–244, Brussels; cf. also: J. of the Aero/Space Sciences, Vol. 26, 229–245 (1959). [454, 454, 454]
- Smith, A.M.O.; Clutter, D.W. (1963): Solution of the incompressible laminar boundary layer equations. AIAA Journal, Vol. 1, 2062–2071. [684]
- Smith, A.M.O.; Clutter, D.W. (1965): Machine calculation of compressible boundary layers. AIAA Journal, Vol. 3, 639–647. [684]
- Smith, A.M.O. /s.: Cebeci, T.; Smith, A.M.O. (1968)
- Smith, A.M.O. /s.: Wazzan, A.R.; Okamura, T.; Smith, A.M.O. (1968)
- Smith, A.M.O. /s.: Jaffe, N.A.; Okamura, T.; Smith, A.M.O. (1970)
- Smith, A.M.O. /s.: Wazzan, A.R.; Okamura, T.; Smith, A.M.O. (1970a)

- Smith, A.M.O. /s.: Wazzan, A.R.; Okamura, T.; Smith, A.M.O. (1970b)
- Smith, A.M.O. /s.: Cebeci, T.; Smith, A.M.O. (1974)
- Smith, F.T. (1973): Laminar flow over a small hump on a flat plate. *J. Fluid Mech.*, Vol. 57, 803–824. [399]
- Smith, F.T. (1977): The laminar separation of an incompressible fluid streaming past a smooth surface. *Proc. Roy. Soc. London A*, Vol. 30, 143–156. [411, 411]
- Smith, F.T.; Duck, P.W. (1977): Separation of jets or thermal boundary layers from a wall. *Quart. J. Mech. Appl. Math.*, Vol. 30, 143–156. [401]
- Smith, F.T.; Sykes, R.I.; Brighton, P.W.M. (1977): A two-dimensional boundary layer encountering a three-dimensional hump. *J. Fluid Mech.*, Vol. 83, 163–176. [400]
- Smith, F.T. (1979a): Laminar flow of an incompressible fluid past a bluff body: the separation, reattachment, eddy properties and drag. *J. Fluid Mech.*, Vol. 92, 171–205. [116, 411]
- Smith, F.T. (1979b): On the non-parallel flow stability of the Blasius boundary layer. *Proc. Roy. Soc. London A*, Vol. 366, 91–109. [434]
- Smith, F.T.; Brighton, P.W.M.; Jackson, P.S.; Hunt, J.C.R. (1981): On boundary-layer flow past two-dimensional obstacles. *J. Fluid Mech.*, Vol. 113, 123–152. [399]
- Smith, F.T. /s.: Cheng, H.K.; Smith, F.T. (1982)
- Smith, F.T. /s.: Stewartson, K.; Smith, F.T.; Kaups, K. (1982)
- Smith, F.T.; Merkin, J.H. (1982): Triple-deck solutions for subsonic flow past humps, steps, concave or convex corners, and wedged trailing edges. *Computers and Fluids*, Vol. 10, 7–25. [400]
- Smith, F.T. (1985): A structure for laminar flow past a bluff body at high Reynolds numbers. *J. Fluid Mech.*, Vol. 155, 175–191. [21, 116]
- Smith, F.T. /s.: Bodonyi, R.J.; Smith, F.T.; Kluwick, A. (1985)
- Smith, F.T. (1986): Steady and unsteady boundary-layer separation. *Annu. Rev. Fluid Mech.*, Vol. 18, 197–220. [354, 399, 411]
- Smith, F.T. /s.: Degani, A.T.; Smith, F.T.; Walker, J.D.A. (1992)
- Smith, F.T. /s.: Degani, A.T.; Smith, F.T.; Walker, J.D.A. (1993)
- Smith, F.T. /s.: Scheichl, B.; Kluwick, A.; Smith, F.T. (2011):
- Smith, K.G. /s.: Winter, K.G.; Smith, K.G.; Rotta, J.C. (1965)
- Smith, P.D. (1974): An integral prediction method for three-dimensional compressible turbulent boundary layers. ARC-RM-3739. [642]
- Smith, P.D. (1982): The numerical computation of three-dimensional boundary layers. In: H.H. Fernholz; E. Krause (Eds.): *Three-Dimensional Turbulent Boundary Layers*, Springer-Verlag, Berlin, 265–285. [642]
- Smits, A.J.; Wood, D.H. (1985): The response of turbulent boundary layers to sudden perturbations. *Annu. Rev. Fluid Mech.*, Vol. 17, 321–358. [605]
- Smits, A.J. /s.: Erm, L.P.; Smits, A.J.; Joubert, P.N. (1987)
- Smits, A.J. /s.: Spina, E.; Smits, A.J.; Robinson, S.K. (1994)
- Smits, A.J. /s.: Zagarola, M.V.; Smits, A.J.; Orszag, S.A.; Yakhot, V. (1996)
- So, R.M.C.; Yoo, G.J. (1987): Low-Reynolds-number modeling of turbulent flows with and without wall transpiration. *AIAA Journal*, Vol. 25, 1556–1564. [604]
- So, R.M.C. /s.: Lai, Y.G.; So, R.M.C. (1990)
- So, R.M.C.; Lai, Y.G.; Zhang, H.S.; Hwang, B.C. (1991): Second-order near-wall turbulence closures: a review. *AIAA Journal*, Vol. 29, 1819–1835. [604]
- Sobey, I.J. (2000): *Introduction to Interactive Boundary Layer Theory*. Oxford University Press, Oxford. [XXIV, 379, 399]

- Sommer, F. (1992): Mehrfachlösungen bei laminaren Strömungen mit druckinduzierter Ablösung: eine Kuspen-Katastrophe. VDI-Fortschritt-Bericht, Reihe 7, Nr. 206, VDI-Verlag, Düsseldorf; also: Bochum, Univ., Diss. [399, 406, 411]
- Sommerfeld, A. (1908): Ein Beitrag zur hydrodynamischen Erklärung der turbulenten Flüssigkeitsbewegungen. Atti del 4. Congr. Internat. dei Mat., Vol. III, 116–124, Roma. [428]
- Southwell, R.V.; Vaisey, G. (1948): Relaxation methods applied to engineering problems. XII. Fluid motions characterized by “free” stream-lines. Royal Society (London): Philosophical Transc. of the Roy. Soc. London A. Vol. 240, 117–161. [23]
- Sovran, G. /s.: Kline, S.J.; Morkovin, M.V.; Sovran, G.; Cockrell, D.J. (Eds.) (1968)
- Sowerby, L. /s.: Crabtree, L.F.; Küchemann, D.; Sowerby, L. (1963)
- Sozou, C. (1971): Boundary layer growth on a spinning sphere. J. Inst. Maths. Applies., Vol. 7, 251–259. [361]
- Spalart, P.R.; Yang, K.S. (1986): Numerical simulation of boundary layers: Part 2: Ribbon-induced transition in Blasius flow, NASA-TM-88221. [478, 478]
- Spalart, P.R.; Leonard, A. (1987): Direct numerical simulation of equilibrium turbulent boundary layers. In: F. Durst et al. (Eds.): Turbulent Shear Flows 5, Springer-Verlag, Berlin, Heidelberg, 234–252. [571, 590]
- Spalart, P.R.; Yang, K.S. (1987): Numerical study of ribbon-induced transition in Blasius flow. J. Fluid Mech., Vol. 178, 345–365. [473]
- Spalart, P.R. /s.: Ha Minh, H.; Viegas, J.R.; Rubesin, M.W.; Vandromme, D.D.; Spalart, P.R. (1989)
- Spalart, P.R. /s.: Justesen, P.; Spalart, P.R. (1990)
- Spalart, P.R.; Allmaras, S.R. (1992): A one-equation turbulence model for aerodynamic flows. AIAA Paper 92-0439. [562]
- Spalart, P.R.; Shur, M. (1997): On the sensitisation of turbulence models to rotation and curvature. Aerospace and Technology, Vol. 1, 297–302. [606]
- Spalding, D.B. (1958): Heat transfer from surfaces of nonuniform temperature. J. Fluid Mech., Vol. 4, 22–32. [218]
- Spalding, D.B. /s.: Smith, A.G.; Spalding, D.B. (1958)
- Spalding, D.B.; Chi, S.W. (1964): The drag of a compressible turbulent boundary layer on a smooth flat plate with and without heat transfer. J. Fluid Mech., Vol. 18, 117–143. [622]
- Spalding, D.B. /s.: Launder, B.E.; Morse, A.; Rodi, W.; Spalding, D.B. (1973)
- Sparrow, E.M.; Gregg, J.L. (1957): Nonsteady surface temperature effects on forced convection heat transfer. J. of the Aeronautical Sciences, Vol. 24, 776–777. [374]
- Sparrow, E.M. (1958): Combined effects of unsteady flight velocity and surface temperature on heat transfer. Jet Propulsion, Vol. 28, 403–405. [370, 374]
- Sparrow, E.M.; Gregg, J.L. (1958): Similar solutions for free convection from a nonisothermal vertical plate. Trans. ASME, Vol. 80, 379–386. [274, 280]
- Sparrow, E.M.; Eichhorn, R.; Gregg, J.L. (1959): Combined forced and free convection in a boundary layer flow. Physics of Fluids, Vol. 2, 319–328. [289]
- Sparrow, E.M.; Gregg, J.L. (1960a): Flow about an unsteadily rotating disc. J. of the Aero/Space Sciences, Vol. 27, 252–257. [361]
- Sparrow, E.M.; Gregg, J.L. (1960b): Mass transfer, flow and heat transfer about a rotating disk. J. Heat Transfer, Vol. 82, 294–302. [124]
- Sparrow, E.M.; Cess, R.D. (1961): Free convection with blowing or suction. J. Heat Transfer, Vol. 83, 387–389. [311]
- Sparrow, E.M.; Minkowycz, W.J.; Eckert, E.R.G.; Ibele, W.E. (1964): The effect of thermo and thermal diffusion for helium injection into plane and axisymmetric stagnation flow of air. J. Heat Transfer, Vol. 86, 311–319. [314]
- Sparrow, E.M.; Cess, R.D. (1966): Radiation Heat Transfer. Brooks/Cole, Belmont, Cal. [69]

- Speziale; C.G.; Abid, R.; Anderson, E.C. (1990): A critical evaluation of two-equation models for near-wall turbulence. In: AIAA Paper 90-1481; see also: AIAA Journal, Vol. 30 (1992), 324–331. [562]
- Speziale; C.G. (1991): Analytical methods for the development of Reynolds-stress closures in turbulence. Annu. Rev. Fluid Mech., Vol. 23, 107–157. [567, 601]
- Speziale, C.G. (1998): Turbulence modelling for time-dependent RANS and VLES: a review. AIAA Journal, Vol. 36, 173–184. [648]
- Spina, E.F.; Smits, A.J.; Robinson, S.K. (1994): The physics of supersonic turbulent boundary layers. Annu. Rev. Fluid Mech., Vol. 26, 287–319. [613, 616]
- Splettstösser, W. (1975): Untersuchung der laminaren Zweistoffgrenzschichtströmung längs eines verdunstenden Flüssigkeitsfilms. Diss. Braunschweig 1974. Wärme- und Stoffübertrag., Bd. 8, 71–86. [318]
- Spurk, J.H. (1997): Fluid Mechanics, Springer-Verlag, Berlin. [82]
- Squire, H.B. (1933): On the stability of three-dimensional distribution of viscous fluid between parallel walls. Proc. Roy. Soc. London A, Vol. 142, 621–628. [429]
- Squire, H.B.; Young, A.D. (1939): The calculation of the profile drag of aerofoils. ARC-RM-1838. [671]
- Squire, H.B. (1951): The round laminar jet. Quart. J. Mech. Appl. Math., Vol. 4, 321–329. [124]
- Squire, H.B. (1955): Radial jets. In: H. Görtler, W. Tollmien (Hrsg.): Fünfzig Jahre Grenzschichtforschung, Braunschweig, 47–54. [125, 326]
- Sreenivasan, K.R. /s.: Narasimha, R.; Sreenivasan, K.R. (1979)
- Sreenivasan, K.R.; Narasimha, R. (1982): Equilibrium parameters for two-dimensional turbulent wakes. Journal of Fluids Engineering, Vol. 104, 167–170. [670]
- Sreenivasan, K.R. /s.: Meier, G.E.A.; Sreenivasan, K. R. (Eds.); Heinemann, H.-J. (Managing Ed.) (2006).
- Sreenivasan, K.R.; Oertel Jr., H. (2010): Instabilities and Turbulent Flows. In: Prandtl – Essentials of Fluid Mechanics, 3. Edition, Springer, New York. [425]
- Sreenivasan, K.R.; Oertel Jr., H. (2016): Instabilitäten und turbulente Strömungen. In: Prandtl – Führer durch die Strömungslehre, 14. Auflage, Springer, Berlin, Heidelberg. [425]
- Srivastava, K.M. (1985): Effect of streamwise vortices on Tollmien-Schlichting waves in growing boundary layers. DFVLR-IB 221-85 A 07. [484]
- Srivastava, K.M.; Dallmann, U. (1987): Effect of streamwise vortices on Tollmien-Schlichting waves in growing boundary layers. Phys. Fluids, Vol. 30, 1005–1016. [484]
- Stäger, R. (1993): Turbulenzmessungen in der dreidimensionalen Grenzschicht eines angestellten Rotationsellipsoides. DLR-FB 93-37. [643]
- Steinheuer, J. (1965): Eine exakte Lösung der instationären Couette-Strömung. Abhandl. der Braunschweigischen Wiss. Ges., Bd. 17, 154–164. [131]
- Steinheuer, J. (1966): Die laminare Wandstrahl mit Absaugung und Ausblasen. DLR-FB 66-87. [307]
- Steinheuer, J. /s.: Gersten, K.; Steinheuer, J. (1967)
- Steinheuer, J. (1968a): Die Lösung der Blasiusschen Grenzschichtdifferentialgleichung. Abhandl. der Braunschweigischen Wiss. Ges., Bd. 20, 96–125. [176, 292]
- Steinheuer, J. (1968b): Similar solutions for the laminar wall jet in a decelerating outer flow. AIAA Journal, Vol. 6, 2198–2200. [173, 294, 303]
- Steinheuer, J. (1971): Berechnung der laminaren Zweistoff-Grenzschicht in der hypersonischen Staupunktströmung mit temperaturabhängigen Stoffbeiwerten. ZAMM. Z. angew. Math. Mech., Bd. 51, 209–223. [319]

- Steinrück, H. (1994): Mixed convection over a cooled horizontal plate. Nonuniqueness and numerical instabilities of the boundary layer equations. *J. Fluid Mech.*, Vol. 278, 251–265. [288]
- Steinrück, H. /s.: Schneider, W.; Steinrück, H.; Andre, G. (1994)
- Steinrück, H. (1995): Mixed convection over a horizontal plate: self-similar and connecting boundary-layer flows. *Fluid Dynamics Research*, Vol. 15, 113–127. [288]
- Steinrück, H. (Ed.) (2010): Asymptotic Methods in Fluid Mechanics: Survey and Recent Advances (CISM Courses and Lectures 523). Springer, Wien, New York. [XXV]
- Stenning, A.H. /s.: Hill, P.G.; Stenning, A.H. (1960)
- Sternberg, J. /s.: Clers des, B.; Sternberg, J. (1952)
- Stevenson, T.N. (1963): A law of the wall for turbulent boundary layer with suction or injection. *The College of Aeronautics, Cranfield, Rep. Aero.*, 166. [606]
- Stewart, W.E. /s.: Bird, R.B.; Stewart, W.E.; Lightfoot, E.N. (1960)
- Stewart, W.E.; Prober, R. (1962): Heat transfer and diffusion in wedge flows with rapid mass transfer. *Int. J. Heat Mass Transfer*, Vol. 5, 1149–1163. [119, 306, 325]
- Stewartson, K. (1953): On the flow between two rotating coaxial disks. *Proc. of the Cambridge Phil. Soc. Math. and Phys. Sciences*, Vol. 49, 333–341. [124, 329]
- Stewartson, K. (1954): Further solutions of the Falkner-Skan equation. *Proc. of the Cambridge Phil. Soc. Math. and Phys. Sciences*, Vol. 50, 454–465. [173]
- Stewartson, K. (1957): On asymptotic expansion in the theory of boundary layers. *J. Math. Phys.*, Vol. 36, 173–191. [308]
- Stewartson, K. (1958): On the free convection from a horizontal plate. *Z. angew. Math. Phys. (ZAMP)*, Vol. 9a, 276–282. [282, 283]
- Stewartson, K. (1960): The theory of unsteady laminar boundary layers. *Advances in Applied Mechanics*. Vol. 6, 1–37. [350]
- Stewartson, K. (1964): The Theory of Laminar Boundary Layers in Compressible Fluids. Clarendon Press, Oxford. [246, 370]
- Stewartson, K. /s.: Catherall, D.; Stewartson, K.; Williams, P.G. (1965)
- Stewartson, K. (1969): On the flow near the trailing edge of a flat plate, II. *Mathematika*, Vol. 16, 106–121. [400]
- Stewartson, K.; Williams, P.G. (1969): Self-induced separation. *Proc. Roy. Soc. London A*, Vol. 312, 181–206. [401]
- Stewartson, K. (1970): Is the singularity at separation removable? *J. Fluid Mech.*, Vol. 44, 347–364. [408]
- Stewartson, K. (1974): Multistructured boundary layers on flat plates and related bodies. *Advances in Applied Mechanics*, Vol. 14, 145–239. [XXIV, 399, 400, 401]
- Stewartson, K. /s.: Cebezi, T.; Khattab, A.K.; Stewartson, K. (1980)
- Stewartson, K. /s.: Cebezi, T.; Khattab, A.K.; Stewartson, K. (1981)
- Stewartson, K. (1982): Some recent studies in triple-deck theory. In: T. Cebezi (Ed.): *Numerical and Physical Aspects of Aerodynamic Flows*. Springer-Verlag, New York, 129–143. [399]
- Stewartson, K.; Smith, F.T.; Kaups, K. (1982): Marginal separation. *Studies in Appl. Math.*, Vol. 67, 45–61. [403, 408]
- Stewartson, K. /s.: Brown, S.N.; Stewartson, K. (1983)
- Stivers, L.S. /s.: Abbott, J.H.; Doenhoff von, A.E.; Stivers, L.S. (1945)
- Stock, H.-W. (1978): Integral method for the calculation of three-dimensional laminar and turbulent boundary layers – Final report. NASA-TM-75320. [642]
- Stock, H.-W. (1980): Laminar boundary layers on inclined ellipsoids of revolution. *Z. Flugwiss. Weltraumforsch.*, Bd. 4, 217–224. [345]
- Stock, H.-W. (1985): Compressible turbulent flows in long circular cross-section diffusers of large area ratio. *Z. Flugwiss. Weltraumforsch.*, Bd. 9, 143–155. [634]

- Stock, H.-W.; Horton, H.P. (1985): Ein Integralverfahren zur Berechnung dreidimensionaler, laminarer, kompressibler, adiabater Grenzschichten. *Z. Flugwiss. Weltraumforsch.*, Bd. 9, 101–110. [340]
- Stock, H.-W. (1986): Laminares Grenzschichtverfahren für Strömungen in Symmetrieebenen und Anwendung auf angestellte Rotationsellipsoide. *Z. Flugwiss. Weltraumforsch.*, Bd. 10, 146–157. [345]
- Stokes, G.G. (1849): On the theories of the internal friction of fluids in motion, and of the equilibrium and motion of elastic solids. *Trans. Cambr. Phil. Soc.*, Vol. 8, 287–319. [65, 68]
- Stokes, G.G. (1856): On the effect of the internal friction of fluids on the motion of pendulums. *Trans. Cambr. Phil. Soc.*, Vol. 9, Part II. 8–106, or *Collected Papers III*, 55. [24, 94, 126, 129]
- Stokes, V.K. /s.: Mellor, G.L.; Chapple, P.J.; Stokes, V.K. (1968)
- Stosic, N. /s.: Hanjalić, K.; Stosic, N. (1983)
- Stratford, B.S. (1957): Flow in the laminar layer near separation. In: *ARC-RM-3002*, 1–27. [202]
- Stratford, B.S. (1959a): The prediction of separation of the turbulent boundary layer. *J. Fluid Mech.*, Vol. 5, 1–16. [594]
- Stratford, B.S. (1959b): An experimental flow with zero skin friction throughout its region of pressure rise. *J. Fluid Mech.*, Vol. 5, 17–35. [589]
- Strazisar, A.; Reshotko, E.; Prahla, J.M. (1977): Experimental study of the stability of heated laminar boundary layers in water. *J. Fluid Mech.*, Vol. 83, 225–247. [462]
- Streeter, V.L. (1935): Frictional resistance in artificially roughened pipes. *Proc. Amer. Soc. Civil Engr.*, Vol. 61, 163. [533]
- Strong, A.B. /s.: Mackinnon, J.C.; Renksizbulut, M.; Strong, A.B. (1998)
- Stuart, J.T. (1954): On the effects of uniform suction on the steady flow due to a rotating disk. *Quart. J. Mech. Appl. Math.*, Vol. 7, 446–457. [124]
- Stuart, J.T. (1955): A solution of the Navier-Stokes and energy equations illustrating the response of skin friction and temperature of an infinite plate thermometer to fluctuations in the stream velocity. *Proc. Roy. Soc. London A*, Vol. 231, 116–130. [131]
- Stuart, J.T. /s.: Gregory, N.; Stuart, J.T.; Walker, W.S. (1955)
- Stuart, J.T. (1956): On the effects of the Reynolds stress on hydrodynamic stability. *ZAMM. Z. angew. Math. Mech.*, Bd. 36, S32–S38. [439]
- Stuart, J.T. (1963): Unsteady boundary layers. In: L. Rosenhead (Ed.): *Laminar Boundary Layers*, Clarendon Press, Oxford, 349–408. [350, 375]
- Stuart, J.T. (1986): Instability of flows and their transition to turbulence. *Z. Flugwiss. Weltraumforsch.*, Bd. 10, 379–392. [425]
- Stüper, J. (1956): Der Einfluß eines Stolperdrahtes auf den Umschlag der Grenzschicht an einer ebenen Platte. *Z. Flugwiss.*, Bd. 4, 30–34. [472]
- Sturek, W.B.; Dwyer, H.A.; Kayser, L.D.; Nietubicz, Ch.J.; Reklis, R.P.; Opalka, K.O. (1978): Computation of Magnus effects for a yawed, spinning body of revolution. *AIAA Journal*, Vol. 16, 687–692. [643]
- Subaschandar, N.; Prabhu, A. (1999): Turbulent near-wake development behind a flat plate. *Aerosp. Sci. Technol.*, Vol. 3, 61–70. [670]
- Suwono, A. (1980): Laminar free convection boundary layer in three-dimensional systems. *Int. J. Heat Mass Transfer*, Vol. 23, 53–61. [342]
- Suzaki, K. /s.: Fujii, T.; Takeuchi, M.; Fujii, M.; Suzaki, K.; Uehara, H. (1970)
- Sychev, V.V. (1972): Laminar separation. *Izv. Akad. Nauk SSSR, Mekh. Zhid. i Gaza*, Vol. 3, 47–59; Engl. translation: *Fluid Dynamics*, Vol. 7, 407–417. [409, 411]
- Sychev, V. V.; Ruban, A. I.; Sychev, V. V.; Korolev, G. L. (1998): *Asymptotic Theory of Separated Flow*. Cambridge University Press. [XXV]

- Sychev, V.V.; Ruban, A.I.; Sychev, Vic. V.; Korolev, G.L. (1998): Asymptotic Theory of Separated Flows. Cambridge University Press, Cambridge. [XXIV, 379]
- Sychev, Vic. V. /s.: Sychev, V.V. et al. (1998)
- Sykes, R.I. /s.: Smith, F.T.; Sykes, R.I.; Brighton, P.W.M. (1977)
- Sykes, R.I. (1980): On three-dimensional boundary layer flow over surface irregularities. Proc. Roy. Soc. London A, Vol. 373, 311–329. [400]
- Szodruch, J. /s.: Redeker, G.; Horstmann, K.-H.; Köster, H.; Thiede, P.; Szodruch, J. (1990)
- Szymansky, F. (1932): Quelques solutions exactes des équations de l'hydrodynamique de fluide visqueux dans le cas d'un tube cylindrique. J. de math. pures et appliquées, series 9, 11, 67 (1932); see also: Proc. III. Intern. Mech. Kongr. Stockholm I, 249. [140]
- Taghavi, H. /s.: Wazzan, A.R.; Taghavi, H.; Keltner, G. (1974)
- Taitel, Y.; Tamir, A. (1975): Multicomponent boundary layer characteristics. Use of the reference state. Int. J. Heat Mass Transfer, Vol. 18, 123–129. [318]
- Takamadate, Ch. /s.: Kobayashi, R.; Kohama, Y.; Takamadate, Ch. (1980)
- Takeuchi, M. /s.: Fujii, T.; Takeuchi, M.; Fujii, M.; Suzuki, K.; Uehara, H. (1970)
- Takhar, H.S.; Whitelaw, M.H. (1976): Asymptotic free convection from an insulated vertical flat plate at high Prandtl number. Indian J. Pure & Appl. Math., Vol. 7, 1122–1136. [277]
- Takhar, H.S. /s.: Pop, I.; Takhar, H.S. (1993)
- Takullu, M.A.; Williams, J.C. III (1985): Similar solutions to the three-dimensional turbulent boundary layer equations. AIAA Paper 85–1658. [641]
- Tan, H.S. (1953): On laminar boundary layer over a rotating blade. J. of the Aeronautical Sciences, Vol. 20, 780–781. [347]
- Tanaka, I. (1988): Three-dimensional ship boundary layer and wake. Advances in Applied Mechanics, Vol. 26, 311–359. [643]
- Tangemann, R.; Gretler, W. (2000): Numerical simulation of a two-dimensional turbulent wall jet in an external stream. Forschung im Ingenieurwesen, Vol. 66, 31–39. [607]
- Tani, I.; Hama, R.; Mituisi, S. (1940): On the permissible roughness in the laminar boundary layer. Aero. Res. Inst. Tokyo, Imp. Univ. Rep. 199. [469, 472]
- Tani, I. (1949): On the solution of the laminar boundary layer equations. J. Phys. Soc. Japan, Vol. 4, 149–154; cf. also: H. Görtler; W. Tollmien (Hrsg.): Fünfzig Jahre Grenzschichtforschung. Braunschweig 1955, 193–200. [186]
- Tani, I.; Juchi, M.; Yamamoto, K. (1954): Further experiments on the effect of a single roughness element on boundary layer transition. Rep. Inst. Sci. Technol. Tokyo Univ. 8. [470]
- Tani, I. (1958): An example of unsteady laminar boundary layer flow. Inst. Univ. of Tokyo Report No. 331, also in H. Görtler (Ed.): Grenzschichtforschung. Springer-Verlag, Berlin, 1958. [352]
- Tani, I. (1962): Production of longitudinal vortices in a boundary layer along a curved wall. J. Geophys. Res., Vol. 67, 3075–3080. [484]
- Tani, I.; Sakagami, J. (1964): Boundary layer instability at subsonic speeds. In: Proc. Int. Council Aero. Sci., Third Congress, Stockholm, 1962, 391–403, Spartan, Washington, D.C.. [484]
- Tani, I.; Aihara, Y. (1969): Görtler vortices and boundary layer transition. Z. angew. Math. Phys. (ZAMP), Vol. 20, 609–618. [484]
- Tani, I. (1977): History of boundary layer theory. Annu. Rev. Fluid Mech., Vol. 9, 87–111. [XXV]
- Tani, I.; Motohashi, T. (1985): Non-equilibrium behavior of turbulent boundary layer flows. Proc. Japan Acad., Ser. B, Vol. 61, 333–340. [578]

- Tani, I. (1987): Turbulent boundary layer development over rough surfaces. In: H.U. Meier; P. Bradshaw (Eds.): Perspectives in Turbulence Studies. Springer-Verlag, Berlin, 223–249. [530, 534]
- Tani, I. (1988): Drag reduction by riblet viewed as roughness problem. Proc. Japan Acad., Ser. B, Vol. 64, 21–24. [531]
- Tannehill, J.C. /s.: Anderson, D.A.; Tannehill, J.C.; Pletcher, R.H. (1984)
- Tanner, M. (1973): Theoretical prediction of base pressure for steady base flow. Progr. Aerospace Sci., Vol. 14, 177–225. [176]
- Taylor, G.I. (1935): Statistical theory of turbulence, Parts 1–4, Proc. Roy. Soc. London A, Vol. 151, 421–478. [512]
- Taylor, G.I. (1936): Correlation measurements in a turbulent flow through a pipe. Proc. Roy. Soc. London A, Vol. 157, 537–546. [512, 515]
- Taylor, G.I. (1936–38): Some recent developments on the study of turbulence. Proc. of the Fifth Internat. Congress for Appl. Mech., New York, 294 (1938); see also: Statistical Theory of Turbulence, V. Effect of turbulence on boundary layer. Proc. Roy. Soc. London A, Vol. 156, 307–317 (1936); cf. also Scientific Paper II, 356–364. [440]
- Taylor, G.I. (1950): The boundary layer in the converging nozzle of a swirl atomizer. Quart. J. Mech. Appl. Math., Vol. 3, 129–139. [330]
- Taylor, G.I. (1958): Flow induced by jets. J. Aero/Space Sci., Vol. 25, 464–465. [666]
- Telionis, D.P.; Tsahalis, D.T. (1974): Unsteady laminar separation over impulsively moved cylinders. Acta Astron., Vol. 1, 1487–1505. [360]
- Telionis, D.P. (1979): Review – Unsteady boundary layers, separated and attached. J. Fluids Eng., Vol. 101, 29–43. [350]
- Telionis, D.P. (1981): Unsteady Viscous Flows. Springer-Verlag, New York. [47, 350, 356, 360, 362, 646]
- Terrill, R.M. (1960): Laminar boundary layer flow near separation with and without suction. Trans. Phil. Roy. Soc. London A, Vol. 253, 55–100. [205]
- Tewfik, O.K.; Giedt, W.H. (1959): Heat transfer, recovery factor, and pressure distributions around a cylinder normal to a supersonic rarefied-air stream. Part I: Experimental Data. University of California, Institute of Engineering, Research Report HE-150-162. [23]
- Theodorsen, Th.; Regier, A. (1944): Experiments on drag of revolving disks, cylinders, and streamline rods at high speeds, NACA-TR-793. [123]
- Thiede, P. /s.: Redeker, G.; Horstmann, K.-H.; Köster, H.; Thiede, P.; Szodruch, J. (1990)
- Thiele, F. (1975): Die numerische Berechnung turbulenter rotationssymmetrischer Freistrahlen und Freistrahldiffusionsflammen. Dissertation, Universität Karlsruhe. [673]
- Thiriot, K.H. (1942): Untersuchungen über die Grenzschicht einer Flüssigkeit über einer rotierenden Scheibe bei kleiner Winkelgeschwindigkeitsänderung. ZAMM. Z. angew. Math. Mech., Bd. 22, 23–28. [361]
- Thiriot, K.H. (1950): Grenzschichtströmung kurz nach dem plötzlichen Anlauf bzw. Abstoppen eines rotierenden Bodens. ZAMM. Z. angew. Math. Mech., Bd. 30, 390–393. [360]
- Thomas, F. (1962): Untersuchungen über die Erhöhung des Auftriebes von Tragflügeln mittels Grenzschichtbeeinflussung durch Ausblasen. Z. Flugwiss., Bd. 10, 46–65. [294]
- Thomas, F. (1963): Untersuchungen über die Grenzschicht an einer Wand stromabwärts von einem Ausblasespalt. Abhandl. Braunschweig. Wiss. Ges., Bd. 15, 1–17. [294]
- Thomas, L.H. (1949): Elliptic problems in linear difference equations over a network. Watson Sci. Comput. Lab. Rept., Columbia University, New York. [690]

- Thompkins Jr., W.T. /s.: Drela, M.; Giles, M.; Thompkins Jr., W.T. (1986)
- Thomson, J.Y. /s.: Mitchell, A.R.; Thomson, J.Y. (1958)
- Tidstrom, K.D. /s.: Klebanoff, P.S.; Tidstrom, K.D.; Sargent, L.M. (1962)
- Tien, C.L. /s.: Chaing, T.; Ossin, A.; Tien, C.L. (1964)
- Tietjens, O. (1922): Beiträge zur Entstehung der Turbulenz. Dissertation Göttingen (1922) and ZAMM. Z. angew. Math. Mech., Bd. 5, 200–217 (1925). [435]
- Tietjens, O. /s.: Prandtl, L.; Tietjens, O. (1929/31)
- Tifford, A.N.; Chu, S.T. (1952): On the flow around a rotating disc in a uniform stream. J. of the Aeronautical Sciences, Vol. 19, 284–285. [328]
- Tifford, A.N. (1954): Heat transfer and frictional effects in laminar boundary layers. Universal series solutions. WADC Techn. Rep., 53–288, Part 4. [185]
- Tillmann, W. /s.: Ludwig, H.; Tillmann, W. (1949)
- Timme, A. (1957): Über die Geschwindigkeitsverteilung in Wirbeln, Ing.-Arch., Bd. 25, 205–225. [139]
- Ting, L. (1959): On the mixing of two parallel streams. J. Math. Phys., Vol. 38, 153–165. [175, 667]
- Ting, L. (1965): On the initial conditions for the boundary layer equations. J. Math. Phys., Vol. 44, 353–367. [686]
- Tobak, M.; Peake, D.J. (1982): Topology of three-dimensional separated flows. Annu. Rev. Fluid Mech., Vol. 14, 61–85. [340]
- Tollmien, W. (1924): Die zeitliche Entwicklung der laminaren Grenzschicht am rotierenden Zylinder. Dissertation Göttingen. [361]
- Tollmien, W. (1926): Berechnung turbulenter Ausbreitungsvorgänge. ZAMM. Z. angew. Math. Mech., Bd. 6, 468–478. [663, 668, 673]
- Tollmien, W. (1929): Über die Entstehung der Turbulenz. 1. Mitteilung, Nachr. Ges. Wiss. Göttingen, Math. Phys. Klasse 21–44; English translation in NACA-TM-609 (1931). [XXIII, 435, 436, 437, 443, 444]
- Tollmien, W. (1931): Grenzschicht-Theorie (239–237). Turbulente Strömungen (289–339). In: W. Wien; F. Harms (Hrsg.): Handbuch der Experimentalphysik, Leipzig, Bd. 4, Teil 1. [XXV, 187, 359, 500]
- Tollmien, W. (1935): Ein allgemeines Kriterium der Instabilität laminarer Geschwindigkeitsverteilungen. Nachr. Ges. Wiss. Göttingen, Math. Phys. Klasse, Fachgruppe I, 1, 79–114 (1935); English translation in NACA-TM-792 (1936). [432, 433, 435]
- Tollmien, W. (1947): Asymptotische Integration der Störungsdifferentialgleichungen ebener laminarer Strömungen bei hohen Reynoldsschen Zahlen. ZAMM. Z. angew. Math. Mech., Vol. 25, 33–50 and Vol. 27, 70–83. [435]
- Tomotika, S. (1935): Laminar boundary layer on the surface of a sphere in a uniform stream. ARC-Report 1678. [325]
- Townsend, A.A. (1956 and 1976): The Structure of Turbulent Shear Flows. Cambridge University Press, First Edition; 1956; Second Edition: 1976. [528, 608, 657, 670, 675]
- Toyokura, T.; Kurokawa, J.; Kimoto, Y. (1982): Three dimensional boundary layer on rotating blades. Bull. JSME, Vol. 25, 513–520. [347]
- Traugott, S.C. /s.: Vincenti, W.G.; Traugott, S.C. (1971)
- Treviño, C.; Méndez, F. (1992): Boundary layer separation by a step in surface temperature. In: Proc. Second Caribbean Conference on Fluid Dynamics, 57–64. [401]
- Truckenbrodt, E. (1952): Die laminare Reibungsschicht an einer teilweise mitbewegten längsangeströmten ebenen Platte. Abhdlg. Braunschweig. Wiss. Ges., Bd. 4, 181–195. [292]
- Truckenbrodt, E. /s.: Schlichting, H.; Truckenbrodt, E. (1952)

- Truckenbrodt, E. (1954a): Die turbulente Strömung an einer angeblasenen rotierenden Scheibe. ZAMM. Z. angew. Math. Mech., Bd. 34, 150–162. [328, 329, 636]
- Truckenbrodt, E. (1954b): Ein Quadraturverfahren zur Berechnung der Reibungsschicht an axial angeströmten rotierenden Drehkörpern. Ing.-Arch., Bd. 22, 21–35. [635]
- Truckenbrodt, E. /s.: Schlichting, H.; Truckenbrodt, E. (1979)
- Truesdell, C. (1954): The present status of the controversy regarding the bulk viscosity of fluids. Proc. Roy. Soc. London A, Vol. 226, 59–65, see also: J. Rational Mech. Analysis, Vol. 1, 228–231. [67]
- Tsahalis, D.T. /s.: Telionis, D.P.; Tsahalis, D.T. (1974)
- Tsien, H.S. (1958): The equations of gas dynamics, in fundamentals of gas dynamics. High Speed Aerodynamics and Jet Propulsion, Vol. 3, Princeton University Press, Princeton, N.J., 3–63. [82]
- Tsuji, H. (1953): Note on the solution of the unsteady laminar boundary layer equations. J. of the Aeronautical Sciences, Vol. 20, 295–296. [375]
- Turner, J.S. (1969): Buoyant plumes and thermals. Annu. Rev. Fluid Mech., Vol. 1, 29–44. [334]
- Turner, J.S. (1973): Buoyancy Effects in Fluids. Cambridge University Press, Cambridge. [334, 676, 677]
- Tyler, E. /s.: Richardson, E.G.; Tyler, E. (1929)
- Uchida, S. (1956): The pulsating viscous flow superposed on the steady laminar motion of incompressible fluid in a circular pipe. Z. angew. Math. Phys. (ZAMP), Bd. 7, 403–422. [141]
- Uehara, H. /s.: Fujii, T.; Takeuchi, M.; Fujii, M.; Suzuki, K.; Uehara, H. (1970)
- Ulrich, A. /s.: Schlichting, H.; Ulrich, A. (1940–42)
- Ulrich, A. /s.: Bussmann, K.; Ulrich, A. (1943)
- Vachon, R.J. /s.: Lowery, G.W.; Vachon, R.J. (1975)
- Vaisey, G. /s.: Southwell, R.V.; Vaisey, G. (1948)
- Van De Vooren, A.I.; Dijkstra, D. (1970): The Navier-Stokes solution for laminar flow past a semi-infinite flat plate. Journal of Engineering Math., Vol. 4, 9–27. [384]
- Van De Vooren, A.I. /s.: Van Stijn, T.L.; Van De Vooren, A.I. (1983)
- van den Berg, B.: see Berg, B. van den
- Van der Hegge Zijnen, B.G. (1924): Measurements of the velocity distribution in the boundary layer along a plane surface. Thesis, Delft. [33, 162, 420, 440]
- Van Dommelen, L.L.; Shen, S.F. (1982): The genesis of separation. In: T. Cebeci (Ed.): Numerical and Physical Aspects of Aerodynamic Flows. Springer-Verlag, New York, 293–311. [354, 356]
- Van Dommelen, L.L. (1987): Computation of unsteady separation using Lagrangian procedures. In: F.T. Smith; S.N. Brown (Eds.): Boundary-Layer Separation. Springer-Verlag, Berlin, 73–87. [360]
- Van Dommelen, L.L. (1990): On the Lagrangian description of unsteady boundary layer separation, Part 2: The spinning sphere. J. Fluid Mech., Vol. 210, 627–645. [360]
- Van Driest, E.R. (1951): Turbulent boundary layer in compressible fluids. J. of the Aeronautical Sciences, Vol. 18, 145–160. [623]
- Van Driest, E.R. (1952): Turbulent boundary layer on a cone in a supersonic flow at zero angle of attack. J. of the Aeronautical Sciences, Vol. 19, 55–57, 72. [253, 257, 633]
- Van Driest, E.R. (1956a): The problem of aerodynamic heating. Aero. Eng. Review, Vol. 15, 26–41. [264]

- Van Driest, E.R. (1956b): On turbulent flow near a wall. *J. Aeron. Sci.*, Vol. 23, 1007–1011. [571]
- Van Driest, E.R.; Blumer, C.B. (1963): Boundary layer transition: Freestream turbulence and pressure gradient effects. *AIAA Journal*, Vol. 1, 1303–1306. [456]
- Van Dyke, M. (1962a): Higher approximations in boundary-layer theory. Part 1: General analysis. *J. Fluid Mech.*, Vol. 14, 161–177. [380, 383]
- Van Dyke, M. (1962b): Higher approximations in boundary-layer theory. Part 2: Application to leading edges. *J. Fluid Mech.*, Vol. 14, 481–495. [385]
- Van Dyke, M. (1962c): Second-order compressible boundary layer theory with application to blunt bodies in hypersonic flow. In: Riddell, F.R. (Ed.): *Hypersonic Flow Research. Progress in Astronautics and Rocketry*, Vol. 7, 37–76, Academic Press, New York. [65, 82, 322, 380, 380, 387]
- Van Dyke, M. (1964a): Higher approximations in boundary-layer theory. Part 3: Parabola in uniform stream. *J. Fluid Mech.*, Vol. 19, 145–159. [385]
- Van Dyke, M. (1964b): *Perturbation Methods in Fluid Mechanics*. Academic Press, New York. New edition 1975, The Parabolic Press, Stanford, California. [XXIII, 24, 379, 384]
- Van Dyke, M. (1969): Higher-order boundary layer theory. *Annu. Rev. Fluid Mech.*, Vol. 1, 265–292. [XXIV, 379, 386]
- Van Ingen, J.L. (1956): A suggested semi-empirical method for the calculation of the boundary layer transition region. *Technische Hochschule, Luftfahrtabteilung, Delft, Report V.T.H. 74*. [454]
- Van Stijn, T.L.; Van de Vooren, A.I. (1983): On the stability of almost parallel boundary layer flows. *Computers and Fluids*, Vol. 10, 223–241. [436]
- Vandromme, D.D. /s.: Ha Minh, H.; Viegas, J.R.; Rubesin, M.W.; Vandromme, D.D.; Spalart, P.R. (1989)
- Vasantha, S.S. /s.: Narasimha, R.; Vasantha, S.S. (1966)
- Vasanta Ram, V. (1975): Grenzschichttheorie höhere Ordnung für die Strömung an einer transversal gekrümmten Zylinderfläche beliebiger Gestalt. *Habilitationsschrift Ruhr-Universität Bochum*. [388]
- Vasudeva, B.R. /s.: Kovasznay, L.S.G.; Komoda, H.; Vasudeva, B.R. (1962)
- Vatsa, V.N. /s.: Burggraf, O.R.; Rizzetta, D.P.; Werle, M.J.; Vatsa, V.N. (1979)
- Veldman, A.E.P. /s.: Botta, E.F.F.; Dijkstra, D.; Veldman, A.E.P. (1972)
- Veldman, A.E.P. (1976): Boundary layer flow past a finite flat plate. *Dissertation, Rijksuniversiteit Groningen, Holland*. [10, 384]
- Veldman, A.E.P. (1981): The calculation of incompressible boundary layers with strong viscous-inviscid interaction. In: AGARD-CP-291, 12.1–12.12. [403, 406]
- Venkatachala, B.J.; Nath, G. (1981): Nonsimilar laminar natural convection in a thermally stratified fluid. *Int. J. Heat Mass Transfer*, Vol. 24, 1848–1850. [266]
- Viegas, J.R. /s.: Ha Minh, H.; Viegas, J.R.; Rubesin, M.W.; Vandromme, D.D.; Spalart, P.R. (1989)
- Vieth, D. /s.: Gersten, K.; Klauer, J.; Vieth, D. (1993)
- Vieth, D. /s.: Gersten, K.; Vieth, D. (1995)
- Vieth, D. (1996): Berechnung der Impuls- und Wärmeübertragung in ebenen turbulenten Strömungen mit Ablösung bei hohen Reynolds-Zahlen. *Dissertation, Ruhr-Universität Bochum*. [548, 602, 604, 610, 700]
- Vincenti, W.G.; Traugott, S.C. (1971): The coupling of radiative transfer and gas motion. *Annu. Rev. Fluid Mech.*, Vol. 3, 89–116. [69]
- Vinokur, M. (1974): Conservation equations of gas-dynamics in curvilinear coordinate systems. *J. Comp. Phys.*, Vol. 14, 105–125. [78]
- Virk, P.S. (1971): An elastic sublayer model for drag reduction by dilute solutions of linear macromolecules. *J. Fluid Mech.*, Vol. 45, 417–440. [534]
- Visconti, F. /s.: Braslow, A.L.; Visconti, F. (1948)

- Visonneau, M. /s.: Piquet, J.; Visonneau, M. (1986)
- Viviand, H. (1974): Conservative forms of gas dynamic equations. *Rech. Aéosp.* 1974-1, 65–68. [78]
- Vogelpohl, G. (1944): Die Strömung der Wirbelquelle zwischen ebenen Wänden mit Berücksichtigung der Wandreibung. *ZAMM. Z. angew. Math. Mech.*, Bd. 24, 289–293. [330]
- Voges, R. (1978): Berechnung turbulenter Wandgrenzschichten mit Zweigleichungs-Turbulenzmodellen. Dissertation, TU München. [565, 588, 601, 698]
- Voigt, M. (1994): Die Entwicklung von Geschwindigkeits- und Temperaturfeldern in laminaren und turbulenten Kanal- und Rohrströmungen aus asymptotischer Sicht. *Fortschritt-Berichte VDI: Reihe 7*; 262, VDI-Verl., Düsseldorf, 1995; also: Bochum, Univ., Diss., 1994. [544, 556]
- Voigt, M. /s.: Herwig, H.; Voigt, M. (1995)
- Voigt, M. /s.: Herwig, H.; Voigt, M. (1996)
- Vollmers, H.; Rotta, J.C. (1977): Similar solutions of the mean velocity, turbulent energy and length scale equation. *AIAA Journal*, Vol. 15, 714–720. [565, 601, 663, 668, 670, 673]
- Vollmers, H. /s.: Dallmann, U.; Gebing, H.; Vollmers, H. (1993)
- von Kármán, Th.: see Kármán, Th. von
- von Schulz-Hausmann, F.K.: see Schulz-Hausmann, F.K. von
- Wadhwa, Y.D. (1958): Boundary layer growth on a spinning body; accelerated motion, *Phil. Mag.*, Vol. 3 (8), 152–158. [361]
- Wagner, W.; Kruse, A. (1998): Properties of Water and Steam. The Industrial Standard IAPWS-IF97 for the Thermodynamic Properties and Supplementary Equations for Other Properties. Springer, Berlin, Heidelberg. [76]
- Wahls, R.A. /s.: Barnwell, R.W.; Wahls, R.A.; De Jarnette, F.R. (1989)
- Wai, J.C.; Baillie, J.C.; Yoshihara, H. (1986): Computation of turbulent separated flows over wings. In: T. Cebeci (Ed.): *Numerical and Physical Aspects of Aerodynamic Flows III*. Springer-Verlag, New York, 397–411. [642, 643]
- Walker, J.D.A. /s.: Ece, M.C.; Walker, J.D.A.; Doligalski, T.L. (1984)
- Walker, J.D.A. /s.: Degani, A.T.; Smith, F.T.; Walker, J.D.A. (1992)
- Walker, J.D.A. /s.: Degani, A.T.; Smith, F.T.; Walker, J.D.A. (1993)
- Walker, W.S. /s.: Gregory, N.; Stuart, J.T.; Walker, W.S. (1955)
- Walker, W.S. /s.: Gregory, N.; Walker, W.S. (1955)
- Walton, I.C. (1974): Second-order effects in free convection. *J. Fluid Mech.*, Vol. 62, 793–809. [327]
- Walz, A. (1966): *Strömungs- und Temperaturgrenzschichten*. Braun-Verlag, Karlsruhe; English translation: *Boundary Layers of Flow and Temperature*. The M.I.T. Press, Cambridge (1969). [194, 196, 198, 201, 204, 206, 259, 260, 261, 624]
- Wang, C.Y. (1967): The flow past a circular cylinder which is started impulsively from rest. *J. Math. Phys.*, Vol. 46, 195–202. [361]
- Wang, C.Y. (1989): Exact solutions of the unsteady Navier-Stokes equations. *Appl. Mech. Rev.*, Vol. 42, S269–S282. [101]
- Wang, C.Y. (1991): Exact solutions of the steady-state Navier-Stokes equations. *Annu. Rev. Fluid Mech.*, Vol. 23, 159–177. [101]
- Wang, K.C. (1970): Three-dimensional boundary layer near the plane of symmetry of a spheroid at incidence. *J. Fluid Mech.*, Vol. 43, 187–209. [345]
- Wang, K.C. (1972): Separation patterns of boundary layer over an inclined body of revolution. *AIAA Journal*, Vol. 10, 1044–1050. [340]
- Wang, K.C. (1974a): Laminar boundary layer near the symmetry plane of a prolate spheroid. *AIAA Journal*, Vol. 12, 949–958. [345]
- Wang, K.C. (1974b): Boundary layer over a blunt body at low incidence with circumferential reversed flow. *J. Fluid Mech.*, Vol. 72, 49–65. [345]

- Wang, K.C. (1974c): Boundary layer over a blunt body at high incidence with an open type of separation. Proc. Roy. Soc. London A, Vol. 340, 33–55. [345]
- Wang, K.C. (1974d): Laminar boundary layer over a body of revolution at extremely high incidence. Phys. Fluids, Vol. 17, 1381–1385. [345]
- Wang, K.C. (1976): Separation of three-dimensional flow. In: Proc. of the Lockheed-Georgia Company Viscous Flow Symposium (1976), Lockheed-Georgia Company, Marietta, Georgia, 341–414. [340]
- Wang, K.C. (1982): On the current controversy about unsteady separation. In: T. Cebeci (Ed.): Numerical and Physical Aspects of Aerodynamic Flows. Springer-Verlag, New York, 279–291. [356]
- Wary, A.; Hussaini, M.Y. (1984): Numerical experiments in boundary-layer stability. Proc. Roy. Soc. London A, Vol. 392, 373–389. [473]
- Wasel, M.G. /s.: Schneider, W.; Wasel, M.G. (1985)
- Watanabe, T. /s.: Nakamura, I.; Yamashita, S.; Watanabe, T.; Sawaki, Y. (1981)
- Watson, J. (1958): A solution of the Navier-Stokes equations illustrating the response of a laminar boundary layer to a given change in the external stream velocity. Quart. J. Mech. Appl. Math., Vol. 11, 302–325. [131, 361]
- Watson, J. (1959): The two-dimensional laminar flow near the stagnation point of a cylinder which has an arbitrary, transverse motion. Quart. J. Mech. Appl. Math., Vol. 12, 175–190. [132, 133]
- Wazzan, A.R.; Okamura, T.; Smith, A.M.O. (1968): The stability of water flow over heated and cooled flat plates. J. Heat Transfer, Vol. 90, 109–114. [462]
- Wazzan, A.R.; Okamura, T.; Smith, A.M.O. (1970a): The stability of incompressible flat plate laminar boundary layer in water with temperature dependent viscosity. In: Proc. Sixth South-Eastern Seminar on Thermal Sciences, Raleigh, N.C., 184–202. [462]
- Wazzan, A.R.; Okamura, T.; Smith, A.M.O. (1970b): The stability and transition of heated and cooled incompressible laminar boundary layers. In: U. Grigull, E. Hahne (Eds.): Fourth Intern. Heat Transfer Conf., Vol. 2, Sessions FC 1.4, Elsevier Publ. Comp., Amsterdam. [462]
- Wazzan, A.R.; Taghavi, H.; Keltner, G. (1974): Effect of boundary layer growth on stability of incompressible flat plate boundary layer with pressure gradient. Phys. Fluids., Vol. 17, 1655–1670. [436]
- Wazzan, A.R. (1975): Spatial stability of Tollmien-Schlichting waves. Progr. Aerospace Sciences, Vol. 16, 99–127. [436, 448]
- Weber, H.E. (1956): The boundary layer inside a conical surface due to swirl. J. Appl. Mech., Vol. 23, 587–592. [330]
- Wehrum, A.E. (1975): Die laminare Grenzschicht 2. Ordnung längs eines Kreiszylinders mit poröser Oberfläche in einer Überschallströmung. Dissertation, Ruhr-Universität Bochum. [388]
- Weise, W. /s.: Eckert, E.; Weise, W. (1942)
- v. Weizsäcker, C.F. (1948): Das Spektrum der Turbulenz bei großen Reynoldsschen Zahlen. Z. Phys., Bd. 124, 614–627. [514]
- Wendt, H. /s.: Hantzche, W.; Wendt, H. (1940)
- Wendt, H. /s.: Hantzche, W.; Wendt, H. (1941)
- Wendt, H. /s.: Hantzche, W.; Wendt, H. (1942)
- Wenner, K. /s.: Schmidt, E.; Wenner, K. (1941)
- Wenterodt, T. /s.: Herwig, H.; Gloss, D.; Wenterodt, T. (2008)
- Werle, M.J. /s.: Davis, R.T.; Werle, M.J. (1972)
- Werle, M.J. /s.: Burggraf, O.R.; Rizzetta, D.P.; Werle, M.J.; Vatsa, V.N. (1979)
- Werle, M.J. /s.: Davis, R.T.; Werle, M.J. (1982)
- Westervelt, P.J. (1953): The theory of steady rotation flow generated by a sound field. J. Acoust. Soc. Amer., Vol. 25, 60–67. [365]

- White, E.B. /s.: Saric, W.S.; Reed, H.L.; White, E.B. (2003)
- White, F.M. (1974): Viscous Fluid Flow. McGraw-Hill, New York. [67, 104, 171, 173, 217, 241, 243, 325, 420, 525, 633]
- Whitelaw, J.H. /s.: Bradshaw, P.; Cebeci, T.; Whitelaw, J.H. (1981)
- Whitelaw, J.H. /s.: Cebeci, T.; Whitelaw, J.H. (1986)
- Wickern, G. /s.: Herwig, H.; Wickern, G.; Gersten, K. (1985)
- Wickern, G. /s.: Herwig, H.; Wickern, G. (1986)
- Wickern, G. (1987): Untersuchung der laminaren gemischten Konvektion an einer beliebig geneigten ebenen Platte mit besonderer Berücksichtigung der Strömungsablösung. Fortschritt-Berichte VDI: Reihe 7; 129, VDI-Verl., Düsseldorf; also: Bochum Univ., Diss., 1987. [283, 285, 287, 288]
- Wickern, G. (1991a): Mixed convection from an arbitrarily inclined semi-infinite flat plate – I. The influence of the inclination angle. Int. J. Heat Mass Transfer, Vol. 34, 1935–1945. [285, 288]
- Wickern, G. (1991b): Mixed convection from an arbitrarily inclined semi-infinite flat plate – II. The influence of the Prandtl number. Int. J. Heat Mass Transfer, Vol. 34, 1947–1957. [285, 287]
- Wie, Y.S.; Harris, J.E. (1991): Numerical solution of the boundary layer equations for a general aviation fuselage. J. Aircraft, Vol. 28, 861–868. [338, 346]
- Wiedemann, J. /s.: Gersten, K.; Wiedemann, J. (1982)
- Wiedemann, J. (1983): Der Einfluß von Ausblasen und Absaugen an durchlässigen Wänden auf Strömungen bei großen Reynolds-Zahlen. Dissertation, Ruhr-Universität Bochum. [299, 309, 386, 606]
- Wiedemann, J.; Gersten, K. (1984): Drag reduction due to boundary-layer control by combined blowing and suction. In: AGARD-CP-365, 14-1 to 14-10. [309, 606]
- Wieghardt, K. (1948): Über einen Energiesatz zur Berechnung laminarer Grenzschichten. Ing.-Arch., Bd. 16, 231–242. [192]
- Wieghardt, K. (1968), see Kline, S.J. et al. (1968), Vol. 2, p. 98. [585]
- Wier, M.; Römer, L. (1987): Experimentelle Untersuchung von stabil und instabil geschichteten turbulenten Plattengrenzschichten mit Bodenrauhigkeit. Z. Flugwiss. Weltraumforsch., Bd. 11, 78–86. [535]
- Wieselsberger, C. (1914): Der Luftwiderstand von Kugeln. Z. Flugtech. Motor-Luftschiffahrt: ZFM, Bd. 5, 140–144. [46]
- Wieselsberger, C. (1927): Über den Luftwiderstand bei gleichzeitiger Rotation des Versuchskörpers. Physikal. Z., Bd. 28, 84–88. [331]
- Wilcox, D.C. (1998): Turbulence Modeling for CFD, Second Edition, DCW Industries, Inc., La Cañada, California. [562, 563, 571, 571, 581, 601, 604, 615, 620, 625, 701]
- Wild, J.M. (1949): The boundary layer of yawed infinite wings. J. of the Aeronautical Sciences, Vol. 16, 41–45. [343]
- Wille, R. /s.: Berger, E.; Wille, R. (1972)
- Wille, R.; Fernholz, H. (1965): Report on the first European Mechanics Colloquium on the Coanda effect. J. Fluid Mech., Vol. 23, 801–819. [667]
- Wille, R. (1966): On unsteady flows and transient motions. Progress in Aeronautical Sciences, Vol. 7, Pergamon Press, London, 195–207. [47]
- Williams, B.R. /s.: Lock, R.C.; Williams, B.R. (1987)
- Williams, F.A. /s.: Libby, P.A.; Williams, F.A. (Eds.) (1980)
- Williams, J.C. III (1982): Unsteady development of the boundary layer in the vicinity of a rear stagnation point. In: T. Cebeci (Ed.): Numerical and Physical Aspects of Aerodynamic Flows, Springer-Verlag, New York, 347–364. [354]
- Williams, J.C. III /s.: Takullu, M.A.; Williams, J.C. III (1985)
- Williams, J. (1958): British research on boundary layer control for high lift by blowing. Z. Flugwiss., Bd. 6, 143–160. [294]

- Williams, P.G. /s.: Catherall, D.; Stewartson, K.; Williams, P.G. (1965)
- Williams, P.G. /s.: Stewartson, K.; Williams, P.G. (1969)
- Williams, P.G. (1975): A reverse flow computation in the theory of self-induced separation. Lecture Notes in Physics No. 35, Springer-Verlag, 445–451. [397]
- Williams, P.G. /s.: Cebeci, T.; Keller, H.B.; Williams, P.G. (1979)
- Williams, P.G. (1982): Large-time boundary layer computations at a rear stagnation point using the asymptotic structure. In: T. Cebeci (Ed.): Numerical and Physical Aspects of Aerodynamic Flows, Springer-Verlag, New York, 325–335. [354]
- Willmarth, W.W. (1975): Pressure fluctuations beneath turbulent boundary layers. Annu. Rev. Fluid Mechanics, Vol. 7, 13–38. [512]
- Winter, K.G.; Smith, K.G.; Rotta, J.C. (1965): Turbulent boundary-layer studies on a waisted body of revolution in subsonic and supersonic flow. In: AGARDograph 97, Part 1, 933–962. [633]
- Wood, D.H. /s.: Smits, A.J.; Wood, D.H. (1985)
- Woods, L.C. (1955): Two-dimensional flow of a compressible fluid past given curved obstacles with infinite wakes. Proc. Roy. Soc. London A, Vol. 227, 367–386. [23]
- Wortmann, F.X. (1969): Visualization of transition. J. Fluid Mech., Vol. 38, 473–480. [484]
- Wosnik, M.; George, W.K. (1995): Another look at the turbulent natural convection boundary layer. In: Proc. Of Turbulence, Heat and Mass Transfer, ICHMT Symposium, Lisbon, Portugal. [428]
- Wu, J.C.; Gulcat, U. (1981): Separate treatment of attached and detached flow regions in general viscous flows. AIAA Journal, Vol. 19, 20–27. [116]
- Wu, T.; Shen, S.F. (1992): Multizone time-marching technique for unsteady separating three-dimensional boundary layers and its application to the symmetry-plane solution of an impulsively started prolate spheroid. J. Fluids Engineering, Vol. 113, 228–239. [360]
- Wuest, W. (1952): Grenzschichten an zylindrischen Körpern mit nichtstationärer Querbewegung. ZAMM. Z. angew. Math. Mech., Bd. 32, 172–178. [133]
- Wuest, W. (1962): Laminare Grenzschichten bei Ausblasen eines anderen Mediums (Zweistoffgrenzschichten). Ing.-Arch., Bd. 31, 125–143. [312]
- Wuest, W. (1963): Kompressible laminare Zweistoffgrenzschichten. Z. Flugwiss., Bd. 11, 398–409. [312, 318, 326]
- Wygnanski, I. (1964): The flow induced by two-dimensional and axisymmetric turbulent jets issuing normally from an infinite plane surface. Aeron. Quart. Vol. 15, 373–380, cf. also Aeron. Quart. Vol. 17 (1966), 31–52. [666]
- Wygnanski, I. /s.: Elsberry, K.; Loeffler, J.; Zhou, M.D.; Wygnanski, I. (2000)
- Yaglom, A.M. /s.: Kader, B.A.; Yaglom, A.M. (1978)
- Yajnik, K.S. (1970): Asymptotic theory of turbulent shear flows. J. Fluid Mech., Vol. 42, 411–427. [XXIV]
- Yamaga, J. (1956): An approximate solution of the laminar boundary layer on a rotating body of revolution in uniform compressible flow. In: Proc. 6th Japan. Nat. Congr. Appl. Mech., 295–298. [331]
- Yamamoto, K. /s.: Tani, I.; Juchi, M.; Yamamoto, K. (1954)
- Yamamoto, K. /s.: Nakamura, I.; Yamashita, S.; Yamamoto, K. (1980)
- Yamashita, S. /s.: Furuya, Y.; Nakamura, I.; Yamashita, S. (1978)
- Yamashita, S. /s.: Nakamura, I.; Yamashita, S.; Yamamoto, K. (1980)
- Yamashita, S. /s.: Nakamura, I.; Yamashita, S.; Watanabe, T.; Sawaki, Y. (1981)
- Yamashita, S. /s.: Nakamura, I.; Yamashita, S. (1982)
- Yang, K.S. /s.: Spalart, P.R.; Yang, K.S. (1986)
- Yang, K.S. /s.: Spalart, P.R.; Yang, K.S. (1987)
- Yang, K.T. (1958): Unsteady laminar boundary layers in an incompressible stagnation flow. J. Appl. Mech., Vol. 25, 421–427. [352]

- Yang, K.T. (1959): Unsteady laminar boundary layers over an arbitrary cylinder with heat transfer in an incompressible flow. *J. Appl. Mech.*, Vol. 26, 171–178. [354]
- Yang, K.T. (1960): Possible similarity solutions for laminar free convection on vertical plates and cylinders. *J. Appl. Mech.*, Vol. 28, 230–236. [274]
- Yeates, L.S. /s.: Saric, W.S.; Yeates, L.S. (1985)
- Yih, C.S. (1965): Dynamics of Nonhomogeneous Fluids. The Macmillan Company, New York. [52]
- Yoo, G.J. /s.: So, R.M.C.; Yoo, G.J. (1987)
- Yoshihara, H. /s.: Wai, J.C.; Baillie, J.C.; Yoshihara, H. (1986)
- Young, A.D. (1939): The calculation of the total and skin friction drags of bodies of revolution at 0° incidence. *ARC-RM-1947*. [671]
- Young, A.D. /s.: Squire, H.B.; Young, A.D. (1939)
- Young, A.D. (1948): Note on the velocity and temperature distributions attained with suction on a flat plate of infinite extent in compressible flow. *Quart. J. Mech. Appl. Math.*, Vol. 1, 70–75. [298]
- Young, A.D. /s.: Harris, H.D.; Young, A.D. (1967)
- Young, A.D. (1989): Boundary Layers, BSP Professional Books, Oxford. [XXV, 670]
- Younis, B.A. /s.: Gibson, M.M.; Jones, W.P.; Younis, B.A. (1981)
- Zagarola, M.V.; Smits, A.J. (1998): Mean-flow scaling of turbulent pipe flow. *J. Fluid Mech.*, Vol. 373, 33–79. Corrected data due to private communication. [551]
- Zalovcik, J.A.; Skoog, R.B. (1945): Flight investigation of boundary-layer transition and profile drag of an experimental low-drag wing installed on a fighter-type airplane. *NASA-TM-79833*. [455]
- Zandbergen, P.J.; Dijkstra, D. (1987): von Kármán swirling flows. *Annu. Rev. Fluid Mech.*, Vol. 19, 465–491. [124]
- Zapryanov, Z. (1977): Boundary layer growth on a spinning sphere. *ZAMM. Z. angew. Math. Mech.*, Bd. 57, 41–46. [361]
- Zaturska, M.B. /s.: Banks, W.H.H.; Drazin, P.G.; Zaturska, M.B. (1988)
- Zauner, E. /s.: Mitsotakis, K.; Schneider, W.; Zauner, E. (1984)
- Zauner, E. (1985): Visualization of the viscous flow induced by a round jet. *J. Fluid Mech.*, Vol. 154, 111–119. [333]
- Zauner, E. /s.: Schneider, W.; Zauner, E.; Böhm, H. (1987)
- Zeh, D.W. /s.: Gill, W.N.; Zeh, D.W.; Del Casal, E. (1965)
- Zhang, H.S. /s.: So, R.M.C.; Lai, Y.G.; Zhang, H.S.; Hwang, B.C. (1991)
- Zhou, M.D. /s.: Elsberry, K.; Loeffler, J.; Zhou, M.D.; Wygnanski, I. (2000)
- Zhu, Z. /s.: Schneider, G.R.; Zhu, Z. (1982)
- Zien, T.F. (1976): Approximate analysis of heat transfer in transpired boundary layers with effects of Prandtl number. *Int. J. Heat Mass Transfer*, Vol. 19, 513–521. [307, 309]
- Zierep, J. (1966): Theorie der schallnahen und der Hyperschallströmungen. Verlag G. Braun, Karlsruhe. [263]
- Zierep, J. /s.: Bohning, R.; Zierep, J. (1981)
- Zierep, J. (1983): Einige moderne Aspekte der Strömungsmechanik. *Z. Flugwiss. Weltraumforschung*, Bd. 7, 357–361. [93]
- Zierep, J.; Bühler, K. (1993): Beschleunigte/verzögerte Platte mit homogenem Ausblasen/Absaugen. *ZAMM. Z. angew. Math. Mech.*, Bd. 73, T527–T529. [131]
- Zimmermann, G. (1974): Wechselwirkungen zwischen turbulenten Wandgrenzschichten und flexiblen Wänden. Bericht 10/1974 des Max-Planck-Instituts für Strömungsforschung, Göttingen. [472]
- Zingžda, J. /s.: Žukauskas, A; Zingžda, J. (1985)
- Žukauskas, A; Zingžda, J. (1985): Heat Transfer of a Cylinder in Crossflow. Hemisphere Publ. Co., Washington. [610]

Index

- ablation 311
- absolutely unstable 431, 493
- accessibility
 - region of 340
- addition of polymers 534
- adiabatic wall temperature 115, 210, 226, 244, 259, 372, 608
- air curtain 664
- airfoil 16, 38, 41, 46, 207, 309, 341, 423, 452, 650, 670
- amplification 428, 438
- angular-momentum-integral equation 597
- annulus 117
- apparent stresses 502, 507
- apparent viscosity 502
- Archimedes number 89
- asymptotic theory 602
- autocorrelation 512
- average
 - time 500, 645
- averaging 500, 645
 - conventional 502, 611
 - ensemble 645
 - Favre *see* mass-weighted averaging
 - mass-weighted 612
 - phase 646
 - time 611
- Barker effect 112
- binary boundary layer 295, 311, 326
- Blasius series 184
- blowing 48, 113, 400, 606, 626
 - combined 301
 - continuous 295, 606, 627
 - massive 114, 299
 - tangential 294, 606
 - up 408
- body of revolution 324, 633
- boundary layer
 - binary 295, 311, 326
 - compressible 241, 370, 463, 617
 - equilibrium 560, 580, 641, 698
 - interactive XXV, 289, 388, 602
 - quasi-equilibrium 591, 698
 - thermal 209, 231, 607, 614
 - three-dimensional 335, 487, 637, 703
 - unsteady 349, 645, 701
- boundary-layer control 291, 457, 605, 626
- boundary-layer diverter 295
- boundary-layer effects
 - higher order 263, 264, 379, 598, 605
- boundary-layer equations 145, 152, 209, 231, 265, 282, 284, 314, 321, 327, 350, 517, 613, 631, 637, 655, 671
- boundary-layer thickness 31, 196, 516
- boundary-layer transformation 148, 210, 232, 268, 352, 684
- Boussinesq approximation 88, 267, 627
- box scheme 684, 692, 706
- bulk viscosity 66
- buoyancy 265, 289, *see also* gravitational effect
- buoyant jet 275, 334, 387, 675
- buoyant wall jet 277
- burst frequency 648
- Busemann-Crocco solution 618
- bypass transition 493
- cascade process 513
- catastrophe theory 399, 406
- centrifugal force 481
- channel 103, 137, 543
- Chapman-Rubesin parameter 238, 253
- circular cylinder
 - at zero incidence 388, 633
 - in a cross flow 18, 39, 115, 205, 225, 277, 280, 289, 299, 301, 356, 364, 388, 411, 423, 609
 - rotating 117, 293, 356, 636
- closure problem 511
- Coanda effect 666

- coefficient of thermal expansion 72, 242
- coherent structure 513
- Colburn number 542, 608
- coloured filament experiment 13
- completed transition 420, 438, 444, 453, 584
- computation method 594, 601, 641, 648, 685
 - implicit 689
 - inverse 597, 605
- conditioned sampling 511
- cone 326, 330, 347, 392, 633
- continuity equation 52, 312, 504, 691
- convection 508
 - forced 211
 - free *see* natural convection
 - indirect natural 281
 - mixed 86, 284, 288, 629
 - natural 90, 310, 326, 361, 401, 627, 635
- convectively unstable 431, 493
- cooling
 - ablation 311
 - evaporation 311
 - film 610
 - sublimation 311
 - transpiration 295, 301, 311, 318
- coordinates
 - arbitrary 73
 - body-fitting 337
 - Cartesian 76
 - curvilinear 637
 - cylindrical 79
 - flow-fitting 338
 - logarithmic 700
 - natural 81
 - optimal 384
 - orthogonal 638
 - rotating 347
 - special 79
 - streamline 638
- core layer 522
- correlation 504
 - pressure-shear 567
 - space 512
 - space-time 513
 - triple 511
- Couette flow 4, 130, 519
- Couette–Poiseuille flow 101, 544
- coupling parameter 89, 304, 547
- Courant–Friedrichs–Lowy condition 703
- Crank–Nicolson scheme 689, 697, 698
- criterion
 - point of inflection 432, 446
- cross-flow vortex 489
- curvature 377, 481, 567, 604, 828
 - concave 480, 481, 633
 - convex 481, 633
 - longitudinal 616, 632
 - transversal 323, 632
- curve of neutral stability 434, 437
- cusp catastrophe 399, 406
- cylinder *see* circular cylinder, 341
 - elliptical 343, 359
 - rotating 117, 291, 344, 636
 - yawing 342
- damping function 571, 603
- defect layer 536, 574
- deformation 57
- dent 399
- dependence
 - zone of 339
- diffuser 26, 41, 104, 117, 204, 306, 554, 593, 605, 634, 637
- diffusion 311, 313, 315
- diffusion thermoeffect 313
- dimensional analysis 7, 520, 523, 545, 547, 569, 656
- direct simulation 571
- discretisation 683, 685
- displacement 151, 297, 377, 606
- displacement thickness 31
- dissipation 72, 226, 280, 506, 526, 595, 608, 614, 615
- dissociation 311, 319
- dividing streamline 300, 667
- double limit 304, 547, 625
- double-deck theory 401
- drag coefficient 9, 33, 35, 160, 669
- Dufour effect 313
- dynamic stall 645, 651
- Eckert number 84, 210, 236
- Eckert–Schneider condition 315
- eddy 511
- eddy viscosity 538, 552, 635, 642
- eigenvalue 178, 180, 429
- ellipsoid 345, 365
 - of revolution 331, 643
- elliptical cylinder 359
- energy equation 69, 244
 - thermal 69, 210, 233, 244, 510, 607
- energy spectrum 513

- energy–integral equation 192, 258
 - thermal 223, 258
- ensemble averaging 645
- entrainment 176, 177, 179, 268, 559, 597, 629, 634, 662, 663, 667
- entrance flow 556
- equilibrium
 - chemical 316
 - local 591
- equilibrium boundary layer 560, 580, 641, 698
- equilibrium layer 509, 527
- Falkner–Skan equation 169
- Fick’s diffusion law 313
- field method 598, 609, 625, 649, 684
- film temperature 622
- fire 676
- Floquet theory 477
- fluctuation 499, 501, 512
- fold 406
- free convection *see* natural convection
- free jet 124, 177, 222, 331, 659, 672, 680
- free stream turbulence 481, 493, 515, 605
- free-streamline theory 409
- frequency analysis 513
- friction drag 155
- friction law 537, 551, 577, 584
 - inversion of 537, 551, 555, 584, 678
- friction temperature 535
- friction velocity 520
- fully rough 529, 532, 584
- fuselage 346
- G–function 537
- Galilean invariance 606
- Galilei number 90
- Görtler number 480
- Görtler series 186
- Görtler transformation 182, 684, 701
- Görtler vortices 481
- Goldstein singularity 186, 204, 403, 595
- Grashof number 91, 267, 269, 627
- gravitational effect 52, 83, 472
- grid 683
- group velocity 493
- Hagen–Poiseuille flow 116
- hair–pin structure 474
- half body 386
- half jet 677
- half-value width 661
- heat transfer 510, 541
- Hilbert integral 393
- hodograph 640
- hot-wire anemometry 512
- hump 399
- hydraulically smooth 532
- hypersonic boundary layer 615
- hypersonic interaction 389
- hysteresis 406, 666
- independence
 - principle of 343
- indifference Reynolds number 424, 434
- induced outer flow 666
- influence
 - zone of 339
- instability 431
 - absolute 431, 493
 - convective 431, 493
 - cross-flow 456, 485, 488, 489
 - secondary 480, 484
 - Tollmien–Schlichting 425, 487
- integral method 196, 223, 258, 277, 324, 340, 354, 577, 594, 623, 642, 648
 - inverse 597
- integral relation 191, 258, 297, 324, 328, 354
- interaction 377, 388, 403, 606
 - hypersonic 389
 - shock–boundary-layer 263, 264, 401, 625
 - strong 377, 403, 625
 - weak 377, 388, 605, 625
- interaction theory 378, 392
- interactive boundary-layer theory XXV, 403, 642, 706
- interference *see* interaction
- intermediate coordinate 523
- intermittence 418, 516, 559, 563, 663
- inverse method 397, 406, 597, 605, 641
- isotropic turbulence (local) 513, 514, 528
- iteration method 694
- jet
 - buoyant 275, 334, 387, 675, 676
 - buoyant wall 277
 - free 124, 171, 177, 659, 672
 - impinging 605
 - in parallel flow 190
 - momentum 387, 675
 - radial 326, 330, 673
 - wall 171, 180, 218, 222, 230, 295, 306, 325, 606, 677

- wall effects 125, 171, 333, 665
- jet flap 294
- jet-boundary flow 175, 668
- Joukowsky airfoil 207, 310, 452, 595
- k*-equation 507, 518, 526, 560
- Karman constant 523, 540
- kinematic thicknesses 624
- Kolmogorov length 514, 559
- Kundt's dust patterns 362
- Lamé metric coefficients 335, 638
- Λ -structure 420, 474
- laminar airfoil 423, 456
- laminar starting region 584
- laminar-turbulent transition 415, 419, 604
- large-eddy simulation 571
- laser-Doppler anemometry 512
- layer
 - buffer 525
 - critical 434
 - defect 536, 574
 - equilibrium 509, 527
 - external outer 678
 - fully turbulent outer 557, 572
 - overlap 525, 527, 619
 - Prandtl 367
 - pure viscous sub- 525
 - Stokes 367
 - viscous sub- 522
 - viscous super- 558, 563, 653
 - viscous wall 522, 535, 557, 607
- LES, Large eddy simulation XXV
- Lewis number 316
- limit 96
 - distinguished 87, 88, 304, 547, 625
 - double 87, 304, 547, 625
- limiting solution 14, 93
- logarithmic overlap law 524, 558
- Mach number 9, 85, 245
- Mack mode 464
- Magnus effect 292, 643
- Mangler transformation 323
- marginal separation 27, 403, 408, 602
- mass transfer 318
- massive separation 408, 650
- matching condition 523
- method
 - of small disturbances 426
 - of wall functions 558, 599, 615, 638, 695
 - property ratio 237, 621
 - reference temperature 240, 622
- temperature ratio 240
- metric coefficients 335, 638
- mixed convection 86, 284, 288, 289, 629
- mixing layer 175, 667
- mixing length
 - for heat transfer 569
 - for momentum transfer 539, 559, 571, 659
- mode 428
- moment of momentum 597
- momentum
 - jet 125
 - kinematic 178, 660, 673, 676
- momentum equation 52, 505
- momentum thickness 192
- momentum-integral equation 191, 258, 297, 328, 354
- Morkovin hypothesis 616
- motor vehicle 292, 643
- moving wall 129, 177, *see also* plate
- MRS criterion 292, 353
- natural convection 90, 265, 310, 326, 361, 401, 558, 627, 635
- Navier-Stokes equations XXV, 68, 76
- neutral stability
 - curve of 434, 437
- non-continuum effects 387
- non-uniqueness 99
- normal stresses 528
- nozzle 104, 171, 222, 326, 330, 554, 582, 634
- Nusselt number 86, 214, 230, 542, 621
- Orr-Sommerfeld equation 427
- oscillating body 129, 362
- oscillating outer flow 133, 365, 367, 472
- outer turbulence 513, 604
- overlap law 519, 619
 - generalised 548
 - logarithmic 524, 607
 - power law 558
 - square root 546, 589
- parabola 115, 385
- paraboloid 326, 388
- parallel-flow assumption 426, 483
- periodic flow 129, 131, 137, 140, 362, 365, 645, 649
- perturbation
 - harmonic 477
 - local 493
 - partial 427, 466
 - subharmonic 477
- perturbation problem 379

- regular 234
- singular 379, 521, 572
- phase averaging 646
- phase velocity 428, 493
- physical properties 77, 241, 278, 554, 611
- Π theorem 520, 523, 545, 547, 569, 656
- pipe 11, 15, 36, 116, 139, 415, 549
- pitch oscillations 650
- plate 11, 30, 33, 156, 245, 254, 307, 373, 436, 582
 - moving 131, 172, 177, 588
- point of inflection criterion 432, 446
- Poiseuille flow *see* channel
- polymer addition 534
- Prandtl layer 367
- Prandtl number 84, 210, 215
- Prandtl–Kolmogorov formula 561
- pressure dilatation 615
- pressure–shear correlation 567
- principle of minimum degeneracy 304
- pseudo-dissipation 509, 574, 614
- pseudo-equilibrium 591
- pseudo-periodicity 649
- pseudo-steady 352
- quadrature formula 200, 224, 576, 609
- quasi-equilibrium boundary layer 591, 698
- quasi-steady 374, 416, 647
- radial jet 330, 673
- RANS, Reynolds-averaged Navier-Stokes equations XXV
- Rayleigh equation 432
- Rayleigh number 627
- Rayleigh–Bénard convection 485
- real gas effects 264
- receptivity 480, 492
- recovery factor 228, 298, 372, 608, 618
- region of accessibility 340
- relaminarisation 582
- Reynolds analogy 219, 608
- Reynolds equations 505, 507
- Reynolds number 6, 84
 - critical 416
 - indifference 424, 434
- Reynolds stress model 565, 649, 701
- Reynolds stresses 503, 507
- riblets 531
- Richardson number 473
- rotating flow over the ground 329
- rotation 360, 636
 - of a body of revolution 327, 331, 636
- of a cylinder 117, 636
- of a disk 119, 328, 485, 636
- of a sphere 331
- of coordinate system 82, 347, 643
- Rotta–Clauser parameter 580
- rough
 - fully 529, 532, 584
 - roughness 467, 493, 528, 531, 536, 584
 - admissible 533
 - equivalent 529, 531, 533
 - profilometer 534
 - technical 531
- sand roughness 528, 532
- Schmidt number 317
- screen 605
- secondary flow 329, 338, 362, 364, 638
- secondary instabilities 420
- secondary stability theory 476
- self-similar solution *see* similar solution 283
- semi-similar solution 351
- separation 39, 150, 589, 594, 601
 - closed 641
 - marginal 27, 403, 602
 - massive 408, 650
 - open 641
 - pressure-induced 645
 - shock-induced 645, 650
 - unsteady 353, 650
- separation bubble 457
- separation criterion 40, 202, 292, 353, 594
- series expansion 184
- shape factor 198, 576
- Sherwood number 316
- shock wave 371
- shock–boundary-layer interaction 401, 616, 626
- shut-down flow 126, 131
- similar solutions 167, 218, 249, 273, 302, 317, 351, 655, 665
 - incomplete 670
- similarity law 6, 83, 416
- singularity 354
- sink drag 294, 298, 308
- sink flow 171, 582, 634
- skin-friction coefficient 86, 621
- slender-channel theory 108, 554
- slenderness 643, 656, 671, 677
- slip flow 387
- solution
 - quasi-steady 374
- Soret effect 313
- space correlation 512

- spectrum 513
- speed of sound 85, 245
- sphere 12, 25, 46, 331, 360, 423
- spikes 474
- spreading parameter 674
- square root law 546, 589
- stability theory 295
 - primary 420, 424, 425, 436
 - secondary 476
- stagnation-point flow 41, 110, 118, 131, 202, 344, 385
- standard roughness 528
- Stanton number 608
- start-up flow 126, 130
- start-up process 355, 361
- step flow 379
- step size 698
- Stokes hypothesis 65
- Stokes layer 367
- Stratford flow 558, 589
- stratification 473
- stream function 154
- stresses 54
- Strouhal number 21, 349
- structure
 - coherent 513
 - hair-pin 474
 - layered 572
 - three-layer 392, 677
 - two-layer 367, 522
- sublimation cooling 311
- suction 48, 113, 291, 457, 606, 626
 - asymptotic 114, 131, 297
 - combined 301
 - continuous 295, 605, 627
 - massive 297, 299
 - tangential 294
- swept-back wing 643
- symmetry-plane flow 345, 641
- Taylor-Görtler vortices 485
- temperature jump 387
- temperature stratification 676
- thermal conductivity 316
- thermal diffusion coefficient 313
- thermal protection 264
- thermal wall layer 535, 607
- thermodiffusion 313
- Thomas algorithm 689, 698
- three-dimensional boundary layer 335, 487, 637, 703
- three-layer model 679
- three-layer structure 378, 392
- time average 502
- Tollmien-Schlichting transition 487, 490
- Tollmien-Schlichting waves 419
- total pressure 183
- total temperature 244, 617
- trailing edge 400
- transformation
 - Crocco 184
 - Dorodnizyn-Howarth 246
 - Falkner-Skan 701
 - Görtler 182
 - Illingworth-Stewartson 246
 - Levy-Lees 247
 - Mangler 323
 - pseudo-similarity 270
 - Saville-Churchill 270
 - v. Mises 183, 685
- transient flow 645
- transition 415, 419, 490
 - by separation bubble 457
 - completed 420, 438, 443, 453, 584
 - e^n -method 454
 - nonlinear process 491
 - subcritical 479
- transpiration cooling 295, 301
- tridiagonal matrix 689, 695, 698
- triple correlation 511
- triple-deck theory 288, 378, 392
- trough 399
- turbomachinery 604
- turbulence intensity 441, 515
- turbulence length 539
- turbulence model 501, 511, 522, 538, 556
 - algebraic 557, 649, 701
 - indirect 524, 586, 593
 - $k-\varepsilon$ 562
 - $k-\varepsilon-\gamma$ 563
 - $k-L$ 564
 - $k-\omega$ 563
 - $k_\theta-\varepsilon_\theta$ 570
 - large-eddy simulation 571
 - low-Reynolds-number 558, 570, 603, 700
 - one-and-a-half-equation 557, 562
 - one-equation 557, 562
 - one-half-equation 560
 - Reynolds stress 565
 - second-moment closure 565
 - two-equation 540, 557, 562, 649
 - zero-equation 557
- turbulent fluctuation 512

- turbulent mixing 662, 669
turbulent Prandtl number 541, 569
turbulent Reynolds number 603, 656
turbulent spot 420, 492
turbulent thermal diffusivity 541
two-layer structure 367, 522
universal law of the wall 607
unstable
– absolutely 425, 431, 493
– convectively 425, 431, 493
velocity-pressure correlation 511
virtual origin 657
viscosity 4
– apparent *see* eddy
– bulk 66
– kinematic 5
vortex decay 139
vortex stretching 484
vortices 283
vorticity transport equation 91
wake 47, 187, 331, 334, 576, 593, 669,
 674
wall
– adiabatic 115, 210, 226, 244, 259,
 372, 608, 623
– compatibility condition at 166, 296
– curved 323, 377, 481, 567, 605, 616,
 632
– flexible 472
– fully catalytic 312, 315
– law of the 524, 547
– moving 48, 126, 129, 190, 222, 291,
 387
– non-catalytic 312, 315
– rough 467, 528
wall heat transfer 233, 460, 553
wall jet 171, 180, 218, 222, 230, 289, 295,
 306, 325, 607, 677
wall shear stress formula 692
water jet pump 662
wave 428, 483
wave packet 431, 493
wedge 169, 172, 220, 229, 302, 317, 367
wing 347, 484, 643
zero-Hertz modes 488
zone of dependence 339
zone of influence 339